東京帝國大學

地震研究所彙報

第十一號

昭和八年

BULLETIN

OF THE

EARTHQUAKE RESEARCH INSTITUTE

TOKYO IMPERIAL UNIVERSITY

Vol. XI.

1933.

目　　次

第十一號

第一册（昭和八年三月）

			頁
1.	等方不均一球内の一點より起る彈性波(第一報)(英文)	吉山良一	1
2.	固體摩擦の振動倍率に及ぼす影響(英文)	萩原尊禮	14
3.	淺間山麓に於ける地表傾斜變化の觀測(英文)	高橋龍太郎	25
4.	和歌山縣に於ける土地潛動の測定(英文)	岸上冬彦	38
5.	地震の時間的及空間的分布に就いて(英文)	山口生知	46
6.	筑波山に於ける加速度地震計に依る地震觀測報告(英文)	井上宇胤	69
7.	昭和 7 年 10 月草津白根山の爆發(英文)	津屋弘達	82
8.	振動の知覺限界測定(佛文)	石本巳四雄 大塚實	113
9.	東京市及其附近と板橋町・富士見村間一等水準線檢測成果報告(邦文)		122

第二册（昭和八年六月）

10.	不連續面が彈性波の傳播に及ぼす影響(I)(英文)	西村源六郎 金井清	123
11.	表面層のある場合の表面に於けるレーリー波の振幅（英文）	鈴木武夫	187
12.	重力の働ける半無限彈性體内に存在する球狀填充物附近の應力(I)(英文)	西村源六郎 高山威雄	196
13.	重力の働ける半無限彈性體内に存在する回形填充物附近の應力(I)(英文)	西村源六郎 高山威雄	229
14.	地殻變動と震源における地震波發生(佛文)	石本巳四雄	254
15.	地殻の强さに就いて(英文)	坪井忠二	275
16.	興津・串本間に於ける地殻の變動(英文)	宮部直巳	278
17.	濃尾震災地及び其の他の地方に於ける檢測水準測量の調査(邦文)	武藤勝彦 川畑幸夫	315
18.	或火山彈の飛行速度(獨文)	松澤武雄	329

19. 噴火の時のガスの壓力(獨文)…… 松澤武雄 347
20. 關東地方の地震(英文)…… 小平孝雄 350
21. 加速度地震計の製作及び研究(邦文)…… 田丸卓郎 362
22. 本邦火山岩の石基に産する珪酸鑛物に就いて(英文)…… 久野久 382
23. 伊豆網代産玄武岩に就いて(豫報)(英文)…… 久野久 391

第三册 (昭和八年九月)

24. 地震波の傳播(第二報) 發震機巧, 地殻構造と地震波の振幅に就て(英文)…… 河角廣 403
25. 重力の働ける半無限彈性體内に存在する圓形填充物附近の應力(II)(英文)…… 西村源六郎・高山威雄・金井清 454
26. 伊豆伊東地方に於ける地殻の垂直移動(英文)…… 坪井忠二 488
27. 日本に於ける地震の分布(英文)…… 山口生知 500
28. 地震初動に關した二三の統計的問題(英文)…… 福富孝治 510
29. 北伊豆の地形及び地質構造と昭和五年十一月二十六日伊豆地震の際にその地域に生じた地變及び地殻變形との關係(英文)…… 大塚彌之助 530
30. 信濃國淺間火山の二三の熔岩の岩石學的研究(英文)…… 津屋弘達 575

第四册 (昭和八年十二月)

31. 不連續面が彈性波の傳播に及ぼす影響(II)(英文)…… 西村源六郎・金井清 595
32. 日本の重力に最もよく適合する式(英文)…… 坪井忠二 632
33. 關東地方に於ける地塊運動(英文)…… 宮部直巳 639
34. 筑波山に於ける傾斜變化觀測報告(英文)…… 井上宇胤 693
35. 地震發生前の氣壓勾配に就いて(第二報)(英文)…… 井上宇胤・稻葉佳 704
36. 地震と漁獲(第二報)(英文)…… 寺田寅彦 714
37. 上下成分加速度地震計の製作(佛文)…… 石本巳四雄 717
38. 中部新第三紀以來の日本島の收縮(英文)…… 大塚彌之助 724
39. 火山彈の飛行速度の訂正(獨文)…… 松澤武雄 732

Contents.

Vol. XI.

Part 1.—March, 1933.

Page

1. R. Yosiyama, Elastic Waves from a Point in an Isotropic Heterogeneous Sphere. Part 1. (in English) 1
2. T. Hagiwara, Influence of Solid Friction on Dynamical Magnification. (in English) 14
3. R. Takahasi, Tilt of the Earth's Crust observed at the Asama Volcano. (in English) 25
4. F. Kishinouye, Measurement of a Land-creep in Wakayama Prefecture. (in English) 38
5. S. Yamaguti, On Time and Space Distribution of Earthquakes. (in English) 46
6. W. Inouye, Observations of Near Earthquakes on Mt. Tukuba with an Ishimoto Acceleration Seismograph. (in English) .. 69
7. H. Tsuya, Explosive Activity of Volcano Kusatu-Siranê in October, 1932. (in English) 82
8. M. Ishimoto et M. Ootuka, Détermination de la limite perceptible des secousses. (en français) 113
9. Relative Vertical Displacements of Bench Marks along Routes in Tôkyô and the Environs and from Itabasi to Huzimi. (in Japanese) 122

Part 2.—June, 1933.

10. G. Nishimura and K. Kanai, On the Effects of Discontinuity Surfaces upon the Propagation of Elastic Wave. (I). (in English) 123

11. T. Suzuki, Amplitude of Rayleigh Waves on the Surface of a Stratified Medium. (in English) 187
12. G. Nishimura and T. Takayama, On Stresses in the Interior in the Vicinity of a Spherical Inclusion in a Gravitating Semi-infinite Elastic Solid. (I). (in English) 196
13. G. Nishimura and T. Takayama, On the Stresses in the Interior and in the Vicinity of a Horizontal Cylindrical Inclusion of Circular Section in a Gravitating Semi-infinite Elastic Solid. (I). (in English) 229
14. M. Ishimoto, La déformation de la croûte terrestre et la production des ondes sismique au foyer. (en français) 254
15. C. Tsuboi, Notes on the Mechanical Strength of the Earth's Crust. (in English) 275
16. N. Miyabe, The Crust Deformations in the District between Okitu and Kusimoto, along the Pacific Coast of the Main Island of Japan. (in English) 278
17. K. Muto and Y. Kawabata, Vertical Displacements of Bench Marks in the Nôbi and other Districts. (in Japanese) 315
18. T. Matuzawa, Fluggeschwindigkeit einiger vulkanischen Bomben. (in deutsch) 329
19. T. Matuzawa, Gasdruck bei einigen vulkanischen Ausbrüchen in Japan. (in deutsch) 347
20. T. Kodaira, Earthquakes of the Kwantô District. (in English) 350
21. T. Tamaru, The Construction and Study of an Acceleration Seismograph. (in Japanese) 362
22. H. Kuno, On Silica Minerals Occurring in the Groundmass of Common Japanese Volcanic Rocks. (in English) 382
23. H. Kuno, Preliminary Note on Basalt from Aziro, Idu. (in English) 391

Part 3.—September, 1933.

24. H. Kawasumi, Study on the Propagation of Seismic Waves. (The second paper). Amplitude of Seismic Waves with the

Structure of the Earth's Crust and Mechanisms of their Origin. (in English) 403

25. G. Nishimura, T. Takayama and K. Kanai, On Stresses in the Interior and in the Vicinity of a Horizontal Cylindrical Inclusion of Circular Section in a Gravitating Semi-infinite Elastic Solid. (II). (in English) 454

26. C. Tsuboi, Vertical Crustal Displacement in the Seismic Region of Itô, on the East Coast of the Idu Peninsula. (in English) 488

27. S. Yamaguti, Distribution of Earthquakes in Japan. (in English) 500

28. T. Fukutomi, Some Statistical Problems concerning Initial Earthquake Motion. (The First Report). (in English)..... 510

29. Y. Ôtuka, The Geomorphology and Geology of Northern Idu Peninsula, the Earthquake Fissures of Nov. 26, 1930, and the Pre- and Post-Seismic Crust Deformations. (in English) 530

30. H. Tsuya, Petrology of Some Lavas of Volcano Asama, Sinano Province, Japan. (in English) 575

Part 4.—December, 1933.

31. G. Nishimura and K. Kanai, On the Effects of Discontinuity Surfaces upon the Propagation of Elastic Waves. (II). (in English) 595

32. C. Tsuboi, The Most Suitable Formula for the Japanese Gravity Values. (in English) 632

33. N. Miyabe, Block Movements of the Earth's Crust in the Kwantô Districts. (The Crustal-Blocks and Their Movements. Part III.) (in English)..... 639

34. W. Inouye, Earth-tilts observed at Mt. Tukuba, Japan. (in English) 693

35. W. Inouye and Y. Inaba, On Barometric Gradients at Times of Earthquakes, in Japan (2nd paper). (in English) 704

36. T. Terada, Earthquake and Fisheries. II. (in English)..... 714

37. M. Ishimoto, Construction d'un sismographe accélérométrique

pour la composante verticale. (en français) 717
38. Y. Ôtuka, Contraction of the Japanese Islands since the Middle Neogene (advanced paper). (in English) 724
39. T. Matuzawa, Berichtigung zu meiner Arbeit „Fluggeschwindigkeit einiger vulkanischen Bomben". (in deutsch) 732

1. *Elastic Waves from a Point in an Isotropic Heterogeneous Sphere. Part I.*

AERONAUTICAL RESEARCH INSTITUTE
LIBRARY
APR 28 1933
TOKYO

By Ryoiti YOSIYAMA,

Seismological Institute.

(Read Sept. 20, 1932.—Received Dec. 20, 1932.)

1. In 1921, E. Meissner[1] found that a kind of surface waves resembling Love wave can be propagated along a semi-infinite elastic body, in which rigidity and density vary with depth. This is perhaps the first paper concerning the wave propagated in an isotropic heterogeneous medium. But the equation of motion, on which his treatments are based, lacks a term depending on the gradient of rigidity, and, because of being based on this equation, even the detailed calculations executed in the next year by K. Aiti[2] left something to be added. The correction of the equation was made by E. Meissner[3] himself in 1926, and the problem was reduced to a boundary value problem and numbers of dispersion-curves were obtained, though full discussion of this equation was not executed.

The investigations by these two authors were confined to a one-dimensional problem, but, in 1931, K. Sezawa[4] obtained a rigorous solution in cylindrical co-ordinates of the surface wave of the kind first mentioned, which diverges from a point, has no components of displacement perpendicular to the surface and involves no dilatation. The effect of heterogenuity in the lower medium was also discussed by H. Jeffreys[5] and T. Matuzawa.[6] Rayleigh-wave propagated in a heterogenous medium was also discussed by H. Honda[7]. As to the bodily wave through a heterogeneous medium, the solution has been obtained by T. Matuzawa only for a plane wave propagated in the direction in which the elastic constants vary.

1) E. MEISSNER, *Vierteljahr. Nat. Forsch. Ges.*, Zurich, **67** (1921), 181.
2) K. AITI, *Proc. Phys.-Math. Soc.*, Japan, [3], **4** (1922), 137-142.
3) E. MEISSNER, *Verh. 2. Int. Kongr. f. Tech. Mech.*, (Zurich, 1926), 3-11.
4) K. SEZAWA, *Bull. Earthq. Res. Inst.*, **9** (1931), 310-315.
5) H. JEFFREYS, *Geophys. Suppl. Month. Not. Astr. Soc.*, London, **2** (1928), 110.
6) T. MATUZAWA, *Bull. Earthq. Res. Inst.*, **6** (1929), 225-228.
7) H. HONDA, *Kisyô-syûsi*, [9], **6** (1931), 237.

It is hoped by the author to obtain general solutions of waves divergeing from a point in an isotropic heterogeneous sphere in which elastic constants and density are certain functions of a radial distance only from the centre of the sphere. And one of the special cases is solved in this paper.

2. K. Uller[8] investigated the velocity of propagation of wave-front in an isotropic heterogeneous medium, and gave an expression, essentially equall to the following, as an equation of motion,

$$\left.\begin{aligned} \rho\frac{\partial^2 \boldsymbol{D}}{\partial T^2} &= (\lambda+2\mu)\,\mathrm{grad}\,\Delta - 2\mu\,\mathrm{rot}\,\boldsymbol{W} + \Delta\cdot\mathrm{grad}\lambda \\ &\quad -2[\boldsymbol{W}, \mathrm{grad}\,\mu] + 2(\mathrm{grad}\,\mu\ \nabla)\boldsymbol{D}, \\ \Delta &= \mathrm{div}\,\boldsymbol{D},\quad \boldsymbol{W} = \frac{1}{2}\,\mathrm{rot}\,\boldsymbol{D}, \end{aligned}\right\} \quad \ldots\ldots \quad (1)$$

where $\boldsymbol{D}$ and T stand for a vector of displacement and time-co-ordinate respectively, and the density and two Lame's constants in the medium are respectively denoted by ρ, λ and μ. The vector $(\mathrm{grad}\,\mu\ \nabla)\boldsymbol{D}$ can be considered as an inner product of $\mathrm{grad}\,\mu$ and an asymmetrical tensor τ, where

$$\tau = \begin{bmatrix} \frac{\partial u}{\partial x} & \frac{\partial u}{\partial y} & \frac{\partial u}{\partial z} \\ \frac{\partial v}{\partial y} & \frac{\partial v}{\partial y} & \frac{\partial v}{\partial z} \\ \frac{\partial w}{\partial x} & \frac{\partial w}{\partial y} & \frac{\partial w}{\partial z} \end{bmatrix}$$

in Cartesian co-ordinate, in which u, v and w denote respectively x-, y- and z-component of displacement $\boldsymbol{D}$. This tensor (τ) can be decomposed into two parts, the one symmetrical and the other skew symmetrical, and the former is so-called strain-tensor and the latter consists of components equal to those of rotation.

A system of orthogonal curvilinear co-ordinates α, β and γ being now considered, three components of displacement $\boldsymbol{D}$ are expressed with u_α, u_β and u_γ; three components of rotation $\boldsymbol{W}$ with ϖ_α, ϖ_β and ϖ_γ; six componenents of strain with $e_{\alpha\alpha}$, $e_{\beta\beta}$, $e_{\gamma\gamma}$, $e_{\beta\gamma}$, $e_{\gamma\alpha}$ and $e_{\alpha\beta}$. Then the two tensors, into which the asymmetrical tensor, mentioned above, can be decomposed, are expressed in the following form,

8) K. ULLER, *Beitr. z. Geophys.*, **15** (1926), 219–238.

$$\begin{bmatrix} e_{\alpha\alpha} & \frac{1}{2}e_{\alpha\beta} & \frac{1}{2}e_{\gamma\alpha} \\ \frac{1}{2}e_{\alpha\beta} & e_{\beta\beta} & \frac{1}{2}e_{\beta\gamma} \\ \frac{1}{2}e_{\gamma\alpha} & \frac{1}{2}e_{\beta\gamma} & e_{\gamma\gamma} \end{bmatrix}, \quad \begin{bmatrix} 0 & -\varpi_\gamma & \varpi_\beta \\ \varpi_\gamma & 0 & -\varpi_\alpha \\ -\varpi_\beta & \varpi_\alpha & 0 \end{bmatrix}$$

and, in what follows, the former, symmetrical tensor, shall be denoted by $\mathfrak{E}$.

Thus the equation of motion (1) is transformed as follows[9]:

$$\rho\frac{\partial^2 \boldsymbol{D}}{\partial T^2} = \operatorname{grad}\{(\lambda+2\mu)\Delta\} - 2\operatorname{rot}\mu\boldsymbol{W} + 2[\operatorname{grad}\mu, \boldsymbol{W}]$$
$$-2\Delta\operatorname{grad}\mu + 2(\mathfrak{E}\operatorname{grad}\mu). \quad \cdots\cdots\cdots\cdots\cdots\cdots (2)$$

In order to discuss a wave propagated from a point in a heterogeneous medium which has a spherical symmetry, we first take an auxiliary co-ordinates system r, θ, φ taking its origin at the centre (O) of the spherical symmetry, and let us introduce a new system of curvilinear co-ordinates t, β, φ; t and β being defined by the following relations, and φ remaining the same in both systems. The origin of the new co-ordinates is at $r=h$, $\theta=\varphi=0$, denoted by O'.

$$t = \int^r \frac{g^2(r)dr}{r\sqrt{g^2(r)-\kappa^2}}, \quad \cdots\cdots\cdots\cdots\cdots\cdots (3)$$

$$\theta = \int^r \frac{\kappa dr}{r\sqrt{g^2(r)-\kappa^2}}, \quad \cdots\cdots\cdots\cdots\cdots\cdots (4)$$

$$g(r) = r\cdot\boldsymbol{\nu}(r), \quad \kappa = g(h)\sin\beta, \quad \cdots\cdots\cdots\cdots (5)$$

where $\boldsymbol{\nu}(r)$, consequently $g(r)$ also, is a given function of r only.

Then we have,

$$\frac{\partial r}{\partial t} = \frac{r\sqrt{g^2(r)-\kappa^2}}{g^2(r)}, \quad \cdots\cdots\cdots\cdots\cdots\cdots\cdots\cdots (6)$$

$$\frac{\partial r}{\partial \beta} = -\kappa^2\cot\beta\cdot\frac{r\sqrt{g^2(r)-\kappa^2}}{g^2(r)}\int^r \frac{g^2(r)dr}{r\{g^2(r)-\kappa^2\}^{\frac{3}{2}}}, \quad \cdots\cdots (7)$$

$$\frac{\partial\theta}{\partial t} = \frac{\kappa}{g^2(r)}, \quad \cdots\cdots\cdots\cdots\cdots\cdots\cdots\cdots\cdots (8)$$

$$\frac{\partial\theta}{\partial\beta} = \kappa\cdot\cot\beta\,\frac{g^2(r)-\kappa^2}{g^2(r)}\int^r \frac{g^2(r)dr}{r\{g^2(r)-\kappa^2\}^{\frac{3}{2}}}, \quad \cdots\cdots (9)$$

9) This equation of motion was independently derived by the author without knowing the investigations by K. Uller.

$$\frac{\partial r}{\partial \varphi}=\frac{\partial \theta}{\partial \varphi}=\frac{\partial \varphi}{\partial t}=\frac{\partial \varphi}{\partial \beta}=0, \quad \frac{\partial \varphi}{\partial \varphi}=1, \quad \cdots\cdots\cdots\cdots (10)$$

and, since Cartesian co-ordinates,

$$x=r\sin\theta\cos\varphi, \quad y=r\sin\theta\sin\varphi, \quad z=r\cos\theta, \quad \cdots\cdots\cdots (11)$$

we obtain the following quantities necessary to the transformation of co-ordinates,

$$\frac{1}{h_1^2}=\left(\frac{\partial x}{\partial t}\right)^2+\left(\frac{\partial y}{\partial t}\right)^2+\left(\frac{\partial z}{\partial t}\right)^2=\left(\frac{\partial r}{\partial t}\right)^2+r^2\left(\frac{\partial \theta}{\partial t}\right)^2=\frac{1}{\nu^2(r)}, \quad \cdots\cdots (12)$$

$$\frac{1}{h_2^2}=\left(\frac{\partial x}{\partial \beta}\right)^2+\left(\frac{\partial y}{\partial \beta}\right)^2+\left(\frac{\partial z}{\partial \beta}\right)^2=\left(\frac{\partial r}{\partial \beta}\right)^2+r^2\left(\frac{\partial \theta}{\partial \beta}\right)^2$$

$$=\kappa^2\cot^2\beta\,\frac{g^2(r)-\kappa^2}{\nu^2(r)}\left\{\int^r\frac{g^2(r)dr}{r\{g^2(r)-\kappa^2\}^{\frac{3}{2}}}\right\}^2, \quad (13)$$

$$\frac{1}{h_3^2}=\left(\frac{\partial x}{\partial \varphi}\right)^2+\left(\frac{\partial y}{\partial \varphi}\right)^2+\left(\frac{\partial z}{\partial \varphi}\right)^2=r^2\sin^2\theta, \quad \cdots\cdots\cdots\cdots (14)$$

and, since we have nine formulae for direction cosines as follows:

$$\left.\begin{aligned}
&\cos(t,x)=h_1\frac{\partial x}{\partial t}, \quad \cos(t,y)=h_1\frac{\partial y}{\partial t}, \quad \cos(t,z)=h_1\frac{\partial z}{\partial t},\\
&\cos(\beta,x)=h_2\frac{\partial x}{\partial \beta}, \quad \cos(\beta,y)=h_2\frac{\partial y}{\partial \beta}, \quad \cos(\beta,z)=h_2\frac{\partial z}{\partial \beta},\\
&\cos(\varphi,x)=h_3\frac{\partial x}{\partial \varphi}, \quad \cos(\varphi,y)=h_3\frac{\partial y}{\partial \varphi}, \quad \cos(\varphi,z)=h_3\frac{\partial z}{\partial \varphi},
\end{aligned}\right\} \quad \cdots (15)$$

we can easily prove that the families of surfaces ($t=$const., $\beta=$const. and $\varphi=$const.) cut one another at right angles everywhere. Thus t, β and φ form a system of orthogonal curvilinear co-ordinates.

The curve, determined by

$$\beta=\text{const.}, \quad \varphi=\text{const.}, \quad \cdots\cdots\cdots\cdots\cdots (16)$$

has notable characteristics, that

$$r\cdot\nu(r)\cdot\sin i=h\cdot\nu(h)\cdot\sin\beta=\kappa, \quad \cdots\cdots\cdots\cdots (17)$$

where i is an angle considered at any point between radius vector r and tangent at the point to the curve, and β is equal to the value of i at the origin of the co-ordinates system. (See Fig. 1).

Though nothing has been assumed to the physical meaning of the above quantities, we can easily prove by the Fermat's Principle that t and θ become equal to travel time and epicentral distance of an earthquake originating at the origin O' of co-ordinates, provided $\nu(r)$

represents reciprocal of velocity of wave. Therefore the surface, $t=$const., respresents wave-front and the curve given by (16) gives a path of the wave, which is one of orthogonal trajectories to the wave-front. From such a point of view, it seems quite natural that t, β and φ form a system of orthogonal curvilinaer co-ordinates, and we can easily see that one set of values of t, β and φ corresponds to a point in space, provided

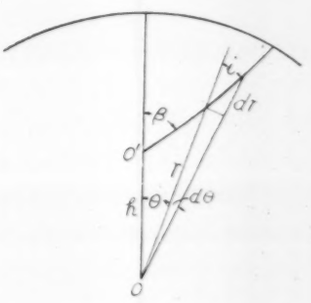

Fig. 1.

$$t>0, \quad 0\leqq\beta\leqq\pi, \quad 0\leqq\varphi\leqq 2\pi. \qquad (18)$$

The strain components refered to such a co-ordinate system are expressed as follows:

$$e_{tt}=\nu\frac{\partial u_t}{\partial t}-\frac{\kappa}{r}\frac{d}{dr}\left(\frac{1}{\nu}\right)\cdot u_\beta,$$

$$e_{\beta\beta}=\frac{1}{\kappa\cot\beta\cdot r\cos i\cdot f}\frac{\partial u_\beta}{\partial\beta}+\frac{1}{r\cos i}\left\{1-\frac{\kappa^2}{g(r)}\frac{d}{dr}\left(\frac{1}{\nu}\right)+\frac{1}{f\cdot g(r)\cos i}\right\}u_t,$$

$$e_{\varphi\varphi}=\frac{1}{r\sin\theta}\frac{\partial u_\varphi}{\partial\varphi}+\frac{\sin(\theta+i)}{r\sin\theta}u_t+\frac{\cos(\theta+i)}{r\sin\theta}u_\beta,$$

$$e_{\beta\varphi}=\frac{1}{\kappa\cot\beta\cdot r\cos i\cdot f}\frac{\partial u_\varphi}{\partial\beta}-\frac{\cos(\theta+i)}{r\sin\theta}u_\varphi+\frac{1}{r\sin\theta}\frac{\partial u_\beta}{\partial\varphi},$$

$$e_{\varphi t}=\frac{1}{r\sin\theta}\frac{\partial u_t}{\partial\varphi}+\nu\frac{\partial u_\varphi}{\partial t}-\frac{\sin(\theta+i)}{r\sin\theta}u_\varphi,$$

$$e_{t\beta}=\nu\frac{\partial u_\beta}{\partial t}-\frac{1}{r\cos i}\left\{1-\frac{\kappa^2}{g(r)}\frac{d}{dr}\left(\frac{1}{\nu}\right)+\frac{1}{f\cdot g(r)\cos i}\right\}u_\beta+\frac{1}{\kappa\cot\beta\cdot r\cos i\cdot f}\frac{\partial u_t}{\partial\beta}+\frac{\kappa}{r}\frac{d}{dr}\left(\frac{1}{\nu}\right)u_t,$$

where

$$f\equiv\int^r\frac{g^2(r)dr}{r\{g^2(r)-\kappa^2\}^{\frac{3}{2}}}.$$

3. Now in this paper, the discussion shall be confined to a special case, where the density (ρ) and the rigidity (μ) in the medium are constant, and λ alone is a function of r only,

$$\sqrt{\frac{\lambda+2\mu}{\rho}}=a-br^2, \qquad (19)$$

in which a and b are constants. The author hopes to treat the more general cases in future occasions.

Then the equation of motion (1) or (2) reduces to

$$\left.\begin{aligned} \rho\frac{\partial^2\boldsymbol{D}}{\partial T^2}&=\operatorname{grad}\{(\lambda+2\mu)\Delta\}-2\mu\operatorname{rot}\boldsymbol{W},\\ \Delta&=\operatorname{div}\boldsymbol{D},\quad \boldsymbol{W}=\frac{1}{2}\operatorname{rot}\boldsymbol{D},\end{aligned}\right\}\quad\cdots\cdots\cdots\quad(20)$$

and evidently from this equation it follows,

$$\frac{\partial^2\Delta}{\partial T^2}=\nabla^2\left(\frac{\lambda+2\mu}{\rho}\cdot\Delta\right),\quad\cdots\cdots\cdots\cdots\quad(21)$$

and

$$\frac{\partial^2\boldsymbol{W}}{\partial T^2}=\frac{\mu}{\rho}\nabla^2\boldsymbol{W}.\quad\cdots\cdots\cdots\cdots\cdots\quad(22)$$

Thus we see that dilatational wave and distortional wave can be propagated independently each other, never exciting the other on the way of propagation. And it is remarkable that the distortional wave given by (22) is not affected by the heterogenuity in this case. Since the distortional wave given by (22) has been fully discussed by many senior authorities, the author confines himself in this paper to the study of the dilatational wave.

From (19) and (21) we have

$$\frac{\partial^2\Delta}{\partial T^2}=\nabla^2\{(a-br^2)^2\Delta\}.\quad\cdots\cdots\cdots\cdots\quad(23)$$

Putting now

$$v(r)=\frac{1}{a-br^2}\quad\cdots\cdots\cdots\cdots\cdots\cdots\quad(24)$$

in the equations of co-ordinates transformation (3) and (4), we get

$$t=\frac{1}{2\sqrt{ab}}\left\{\sinh^{-1}\frac{2\sqrt{ab}\cdot r\cos i}{\sqrt{1+4ab\kappa^2}\cdot(a-br^2)}-\sinh^{-1}\frac{2\sqrt{ab}\cdot h\cos\beta}{\sqrt{1+4ab\kappa^2}\cdot(a-bh^2)}\right\},\quad(25)$$

$$\theta=\sin^{-1}\frac{\cos i}{\sqrt{1+4ab\kappa^2}}-\sin^{-1}\frac{\cos\beta}{\sqrt{1+4ab\kappa^2}},\quad\cdots\cdots\quad(26)$$

$$\frac{1}{h_1}=a-br^2,\quad\cdots\cdots\cdots\cdots\cdots\cdots\quad(27)$$

$$\frac{1}{h_2}=\frac{\sinh 2\sqrt{ab}t}{2\sqrt{ab}}(a-br^2),\quad\cdots\cdots\cdots\cdots\quad(28)$$

$$\frac{1}{h_3}=\frac{\sinh 2\sqrt{ab}t}{2\sqrt{ab}}(a-br^2)\sin\beta.\quad\cdots\cdots\cdots\quad(29)$$

Then by the relation,

$$\nabla^2\phi=h_1h_2h_3\left\{\frac{\partial}{\partial t}\left(\frac{h_1}{h_2h_3}\frac{\partial\phi}{\partial t}\right)+\frac{\partial}{\partial\beta}\left(\frac{h_2}{h_3h_1}\frac{\partial\phi}{\partial\beta}\right)+\frac{\partial}{\partial\gamma}\left(\frac{h_3}{h_1h_2}\frac{\partial\phi}{\partial\gamma}\right)\right\},\quad\cdots\quad(30)$$

and the substitution,

$$\Delta=\frac{2\sqrt{ab}}{(a-br^2)^{\frac{5}{2}}\sinh 2\sqrt{abt}}\cdot\Delta'\cdot e^{ipT}, \quad \ldots\ldots\ldots (31)$$

the following equation for Δ' is obtained from (23),

$$\frac{\partial^2\Delta'}{\partial t^2}+\frac{4ab}{\sinh^2 2\sqrt{abt}}\frac{\partial^2\Delta'}{\partial\beta^2}+\frac{4ab}{\sinh^2 2\sqrt{abt}\cdot\sin^2\beta}\frac{\partial^2\Delta'}{\partial\varphi^2}$$
$$+\frac{4ab\cot\beta}{\sinh^2 2\sqrt{abt}}\frac{\partial\Delta'}{\partial\beta}+(p^2-ab)\Delta'=0. \quad \ldots\ldots\ldots (32)$$

This equation can be satisfied by a function of the form

$$\Delta'=X(t)\,Y(\beta)\,Z(\varphi), \quad \ldots\ldots\ldots (33)$$

if

$$\frac{\partial^2 Z}{\partial\varphi^2}+m^2Z=0, \quad \ldots\ldots\ldots (34)$$

$$\frac{\partial^2 Y}{\partial\beta^2}+\cot\beta\frac{\partial Y}{\partial\beta}+\left\{n(n+1)-\frac{m^2}{\sin^2\beta}\right\}Y=0, \quad \ldots\ldots\ldots (35)$$

$$\frac{\sinh^2 2\sqrt{abt}}{4ab}\frac{\partial^2 X}{\partial t^2}+\left\{\frac{\sinh^2 2\sqrt{abt}}{4ab}(p^2-ab)-n(n+1)\right\}X=0 \quad (36)$$

where m and n are positive integers.

Thus (34) is satisfied by

$$Z=\begin{cases}\sin\ m\varphi\\ \cos\ m\varphi,\end{cases} \quad \ldots\ldots\ldots (37)$$

and (35) by

$$Y=\begin{cases}P_n^m(\cos\beta)\\ Q_n^m(\cos\beta),\end{cases} \quad \ldots\ldots\ldots (38)$$

where $P_n^m(\cos\beta)$ and $Q_n^m(\cos\beta)$ are the associated Legendre's functions.

Since the function X depends not only on t, but also on n, the letter n is hereafter suffixed to X in the equation (36),

$$\frac{\sinh^2 2\sqrt{abt}}{4ab}\frac{d^2X_n}{dt^2}+\left\{\frac{\sinh^2 2\sqrt{abt}}{4ab}(p^2-ab)-n(n+1)\right\}X_n=0. \quad (36')$$

Assuming

$$X_n=A\sin\sqrt{p^2-ab}\,t+B\cos\sqrt{p^2-ab}\,t, \quad \ldots\ldots\ldots (39)$$

substitute in (36'), and we obtain the following simultaneous differential equation to determine A and B.

$$\frac{d^2A}{dt^2}-2\sqrt{p^2-ab}\frac{dB}{dt}-\frac{4abn(n+1)}{\sinh^2 2\sqrt{abt}}A=0, \quad \ldots\ldots\ldots (40)$$

$$\frac{d^2B}{dt^2}+2\sqrt{p^2-ab}\,\frac{dA}{dt}-\frac{4abn(n+1)}{\sinh^2 2\sqrt{ab}t}B=0, \quad \cdots\cdots\cdots (41)$$

As the equation (36′) is of the second degree, two particular solutions are necessary, one is analytic at $t=0$, and the other is convergent for a large absolute value of t. The former shall be denoted by $X_n^{(1)}$ and the latter by $X_n^{(2)}$.

When $n=0$, 1 and 2, the solutions of (40) and (41) are easily obtained.

$$\left.\begin{aligned}
n=0&\begin{cases} X_0^{(1)}=\sin\sqrt{p^2-ab}\,t, \\ X_0^{(2)}=\cos\sqrt{p^2-ab}\,t, \end{cases} \\
n=1&\begin{cases} X_1^{(1)}=\dfrac{u}{\sqrt{p^2-ab}}\sin\sqrt{p^2-ab}\,t-\cos\sqrt{p^2-ab}\,t, \\ X_1^{(2)}=-\sin\sqrt{p^2-ab}\,t-\dfrac{u}{\sqrt{p^2-ab}}\cos\sqrt{p^2-ab}\,t, \end{cases} \\
n=2&\begin{cases} X_2^{(1)}=\left\{3\dfrac{u^2}{\sqrt{p^2-ab}}-\dfrac{(p^2-ab)+4ab}{p^2-ab}\right\}\sin\sqrt{p^2-ab}\,t \\ \qquad\qquad -3\dfrac{u}{\sqrt{p^2-ab}}\cos\sqrt{p^2-ab}\,t, \\ X_2^{(2)}=3\dfrac{u}{\sqrt{p^2-ab}}\sin\sqrt{p^2-ab}\,t+\left\{3\dfrac{u^2}{p^2-ab}\right. \\ \qquad\qquad \left.-\dfrac{(p^2-ab)+4ab}{p^2-ab}\right\}\cos\sqrt{p^2-ab}\,t, \end{cases}
\end{aligned}\right\} \cdots (42)$$

where
$$u\equiv 2\sqrt{ab}\coth 2\sqrt{ab}\,t. \quad \cdots\cdots\cdots\cdots (43)$$

If we introduce a function $R_n^{(i)}$ defined by

$$\sqrt{\frac{2}{\pi p}}\sqrt{2\sqrt{ab}\operatorname{cosech} 2\sqrt{ab}\,t}\,X_n^{(i)}=R_n^{(i)}, \quad (i=1,2), \quad \cdots\cdots (44)$$

following recurrence formulae are obtained by means of mathematical induction from (36′), (42) and (44).

$$\frac{(p^2-ab)+4n^2ab}{p^2-ab}R_{n-1}^{(i)}+R_{n+1}^{(i)}=(-1)^{i+1}\frac{(2n+1)2\sqrt{ab}\coth 2\sqrt{ab}t}{\sqrt{p^2-ab}}R_n^{(i)}, \quad \cdots (45)$$

$$\frac{(p^2-ab)+4n^2ab}{p^2-ab}R_{n-1}^{(i)}-R_{n+1}^{(i)}=(-1)^{i+1}\frac{2}{\sqrt{p^2-ab}}\frac{dR_n^{(i)}}{dt}, (i=1,2). \quad \cdots\cdots (46)$$

The solution are therefore,

$$R_n^{(1)}=\sqrt{\frac{2}{\pi p}}(2\sqrt{ab}\operatorname{cosech} 2\sqrt{ab}t)^{-n-\frac{1}{2}}\left(\frac{-2ab}{\sqrt{p^2-ab}}\right)^n$$

$$\cdot\left(\frac{d}{d(\sinh^2\sqrt{ab}t)}\right)^n\left(\frac{2\sqrt{ab}\sin\sqrt{p^2-abt}}{\sinh 2\sqrt{ab}t}\right), \quad \ldots\ldots (47)$$

$$R_n^{(2)}=\sqrt{\frac{2}{\pi p}}(2\sqrt{ab}\,\mathrm{cosech}\,2\sqrt{ab}t)^{-n-\frac{1}{2}}\left(\frac{2ab}{\sqrt{p^2-ab}}\right)^n$$

$$\cdot\left(\frac{d}{d(\sinh^2\sqrt{abt})}\right)^n\left(\frac{2\sqrt{ab}\cos\sqrt{p^2-abt}}{\sinh 2\sqrt{abt}}\right)\ldots\ldots (48)$$

It is remarkable that the R-functions depend not only on t and n, but also on p and ab. And, when b approaches zero, R-functions tend to the Bessel's functions of the first and the second kind. The differences between R-functions and the Bessel's functions increase with n and the difference between t and $\frac{\sinh 2\sqrt{ab}t}{2\sqrt{ab}}$. Both of the functions are oscillatory, and their phase-difference depends on the ratio of p to ab.

Though the earth may be assumed to be isotropic sphere having a spherical symmetry with respect to its centre, the assumption that the density and rigidity are uniform, as is adopted in this section, is evidently different from what it is. But the author dared to use the values of a and b, obtained by H. Kawasumi[10] by means of analysis of time-distance curves in earthquakes, and calculated the values of R-functions and compared them with the Bessel's functions by which the R-functions are to be replaced when the earth is considered homogeneous.

According to the investigations by H. Kawasumi,

$$\sqrt{ab}\fallingdotseq 2\cdot 82.10^{-3}, \quad b\fallingdotseq 2\cdot 35.10^{-3},$$

the radius of the earth being taken as unit.

Remark: A precise investigation of velocity of wave, especially, of shocks, which is not executed by the author, is necessary to use the value of a and b obtained by H. Kawasumi. But, if the origin of

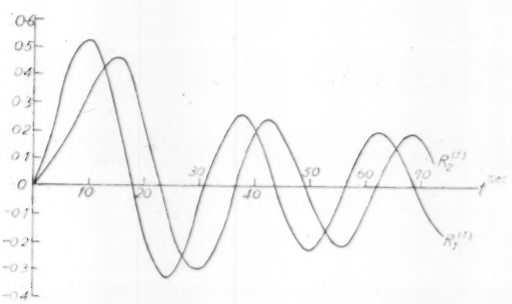

Fig. 2. $R_1^{(1)}, R_2^{(1)}\left(p=\frac{1}{4}\right)$

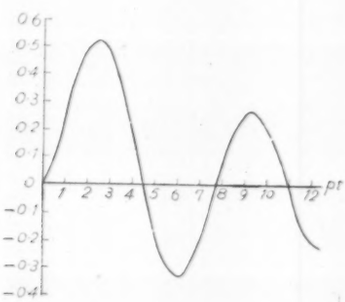

Fig. 3.

10) H. Kawasumi, *Bull. Earthq. Res. Inst.*, 10 (1932), 94-129.

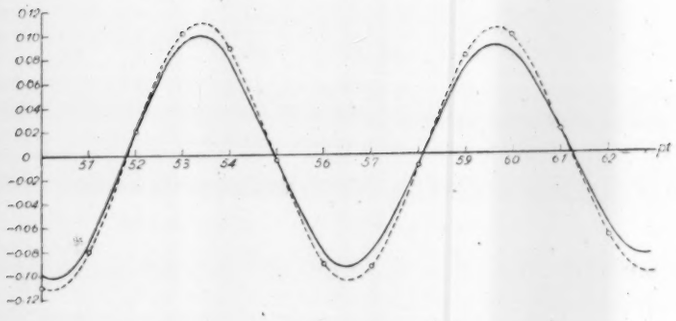

------ $J_{\frac{3}{2}}$

Fig. 4. ○ $R_1^{(1)}(p=3)$

—— $R_1^{(1)}\left(p=\frac{1}{4}\right)$

earthquake is considered as a point, we can deduce from the discussion of the velocity of surface of discontinuity in "Mathematical Theory of Elasticity" by A. E. H. Love that a and b can be calculated by means of analysis of time-distance curves of earthquakes.

$R_1^{(1)}$ and $R_2^{(1)}$ as functions of t, when $p=\frac{1}{4}$, are shown in Fig. 2. As functions of pt, $J_{\frac{3}{2}}$ and $R_1^{(1)}$, when $p=\frac{1}{4}$ and also $p=3$, are compared in Fig. 3 and 4. The former is for smaller values of t while the latter is for larger ones and is given in larger scale than the former. So far as pt is less than 15, the differences between these functions are negligible, as we see from Fig. 3, but when pt become greater than 50, as shown in Fig. 4, $(R_1^{(1)})_{p=\frac{1}{4}}$ is noticeably small than any of the other two, while the differences between $J_{\frac{3}{2}}$ and $(R_1^{(1)})_{p=3}$ are still negligible.

$R_n^{(i)} \cdot e^{ipT}$, as well as $J_n \cdot e^{ipT}$, expresses a standing wave. For the progressive waves, the following functions are introduced.

For a converging wave,

$$U_n^{(1)} = R_n^{(1)} - (-1)^n i R_n^{(2)} \quad \cdots\cdots\cdots\cdots\cdots (49)$$

For a diverging wave,

$$U_n^{(2)} = R_n^{(1)} + (-1)^n i R_n^{(1)} \quad \cdots\cdots\cdots\cdots\cdots (50)$$

The relation of the U-function to the R-function is just that of the Hankel's function to the Bessel's function, and

$$U_n^{(1)} = \sqrt{\frac{2}{\pi p}}\left(\frac{2ab}{\sqrt{p^2-ab}}\right)^n (2\sqrt{ab}\,\mathrm{cosech}\,2\sqrt{ab}t)^{-n-\frac{1}{2}} \cdot \left(\frac{d}{d(\sinh^2\sqrt{ab}t)}\right)^n \left(\frac{2\sqrt{ab}\,e^{i\left(\sqrt{p^2-ab}t-\frac{2n+1}{2}\pi\right)}}{\sinh 2\sqrt{ab}t}\right) \quad \cdots\cdots (51)$$

$$U_n^{(2)}=\sqrt{\frac{2}{\pi p}}\left(\frac{2ab}{\sqrt{p^2-ab}}\right)^n(2\sqrt{ab}\,\mathrm{cosech}\,2\sqrt{ab}t)^{-n-\frac{1}{2}}$$
$$\cdot\left(\frac{d}{d(\sinh^2\sqrt{ab}t)}\right)^n\left(\frac{2\sqrt{ab}\,e^{-i\left(\sqrt{p^2-ab}t-\frac{2n+1}{2}\pi\right)}}{\sinh 2\sqrt{ab}t}\right) \quad \ldots\ldots (52)$$

Recurrence formulae are obtained for U-functions as follows:

$$\frac{(p^2-ab)+4n^2ab}{p^2-ab}U_{n-1}^{(i)}+U_{n+1}^{(i)}=\frac{(2n+1)2\sqrt{ab}\coth 2\sqrt{ab}t}{\sqrt{p^2-ab}}U_n^{(i)}, \quad \ldots (53)$$

$$\frac{(p^2-ab)+4n^2ab}{p^2-ab}U_{n-1}^{(i)}-U_{n+1}^{(i)}=\frac{2}{\sqrt{p^2-ab}}\frac{dU_n^{(i)}}{dt}. \quad \ldots\ldots\ldots\ldots (54)$$
$$(i=1,\ 2.)$$

From what has been stated, follows the solution of the equation (21) for a diverging wave,

$$\Delta=\frac{\sqrt{2\sqrt{ab}\,\mathrm{cosech}\,2\sqrt{ab}t}}{(a-br^2)^{\frac{5}{2}}}U_n^{(2)}\cdot P_n^m(\cos\beta)\begin{matrix}\sin\\ \cos\end{matrix}m\varphi\, e^{ipT} \quad \ldots\ldots\ldots (55)$$

Roughly speaking, the surface given by $t=$const. is a wave-front, and, in such case as adopted in this section, this surface is a sphere, though the proof is omitted here. And it is worthy of note that the solution of the equation of motion involves a factor $P_n^m(\cos\beta)$, as in the similar case when the medium is homogeneous, quite concordantly with the fact the surface expressed by $t=$const. is a sphere.

Thus we can discuss the distribution of "pull and push" of the motion on any surface quite similarly to the case when the medium is homogeneous.

The components of displacement derived from Δ under the condition that rotation vanishes are,

$$u_t=-\frac{1}{p^2}\frac{1}{(a-br^2)^{\frac{3}{2}}}P_n^m(\cos\beta)\begin{matrix}\sin\\ \cos\end{matrix}m\varphi\cdot e^{ipT}\left\{\frac{d}{dt}\left(\sqrt{2\sqrt{ab}\,\mathrm{cosech}\,2\sqrt{ab}t}\,U_n^{(2)}\right)\right.$$
$$\left.+br\cos i\sqrt{2\sqrt{ab}\,\mathrm{cosech}\,2\sqrt{ab}t}\,U_n^{(2)}\right\},$$

$$u_\beta=-\frac{1}{p^2}\frac{(2\sqrt{ab}\,\mathrm{cosech}\,2\sqrt{ab}t)^{\frac{3}{2}}}{(a-br^2)^{\frac{1}{2}}}U_n^{(2)}\begin{matrix}\sin\\ \cos\end{matrix}m\varphi\cdot e^{ipT}\left\{\frac{1}{a-br^2}\frac{dP_n^m(\cos\beta)}{d\beta}\right.$$
$$\left.-\frac{bh\sin\beta}{a-bh^2}\frac{P_n^m(\cos\beta)}{2\sqrt{ab}\,\mathrm{cosech}\,2\sqrt{ab}t}\right\},$$

$$u_\varphi=-\frac{m}{p^2}\frac{(2\sqrt{ab}\,\mathrm{cosech}\,2\sqrt{ab}t)^{\frac{3}{2}}}{(a-br^2)^{\frac{1}{2}}}U_n^{(2)}\cdot\frac{P_n^m(\cos\beta)}{\sin\beta}\begin{matrix}\cos\\ -\sin\end{matrix}m\varphi e^{ipT}.$$

Asymptotic expansions of U-functions being respectively,

$$U_n^{(1)} \approx \frac{(p^2-ab)+4(n-1)^2ab}{p^2-ab} \cdot \sqrt{\frac{2}{\pi p}}(2\sqrt{ab}\,\mathrm{cosech}\,2\sqrt{ab}t)^{\frac{1}{2}} e^{i\left(\sqrt{p^2-ab}\,t-\frac{n+1}{2}\pi\right)},$$

$$U_n^{(2)} \approx \frac{(p^2-ab)+4(n-1)^2ab}{p^2-ab} \cdot \sqrt{\frac{2}{\pi p}}(2\sqrt{ab}\,\mathrm{cosech}\,2\sqrt{ab}t)^{\frac{1}{2}} e^{-i\left(\sqrt{p^2-ab}\,t-\frac{n+1}{2}\pi\right)},$$

if amplitude of displacement be observed on any surface expressed by $r=$const., the component parallel to the direction of propagation, or, to the direction of the tangent at the point of observation to the path of wave determined by the Fermat's Principle of trajectory, is proportional to the reciprocal of $\frac{\sinh 2\sqrt{ab}t}{2\sqrt{ab}}$, and the other components transversal to the same direction are to the square of the same factor.

And we have from the equations (3) and (4),

$$t=\int^r \frac{ds}{a-br^2},$$

provided ds is elementary distance along the curve determined by (16). For a large value of t, the phase-velocity V is determined by

$$\frac{\partial}{\partial T}(pT-\sqrt{p^2-ab}\,t)=0,$$

therefore

$$V=\frac{\partial S}{\partial T}=(a-br^2)\frac{p}{\sqrt{p^2-ab}}.$$

As the ratio of p to ab is a number of a order of 10^{-6}, the dispersion may be negligible compared with that due to the effect of gravity, which was investigated by Bromwich and others.

In conclusion, the author desires to express his sincere thanks to Professor T. Matuzawa and Dr. H. Kawasumi for their kind Guidance.

1. 等方不均一球内の一點より起る彈性波 (第一報)

地震學教室 吉 山 良 一

密度及び彈性的性質が一點からの距離によりて定つてゐる様な等方彈性體内を傳る波動の研究への緒として先づ密度及び剛性率が一様であつて唯ラーメの彈性常數の中 λ のみが a, b を二つの常數とし r を球の中心からの距離とする時

$$\sqrt{\frac{\lambda+2\mu}{\rho}}=a-br^2$$

で表はさるゝ場合を少しく計算した.

斯る場合に著しいことは先づ密度と剛性率が變はらなければ所謂縦波と横波とは各獨立に傳播することである。更に横波に就いてはこれまで均質な媒質の中の問題として研究された結果に何等附け加ふべきことがない.

縦波に就いては,

(1) 震原に於いて, 振幅の分布が其の點に於ける震波線の射出角の餘弦を變數とする表面球函數で與へられた場合には其振幅分布は震波線に沿つて其のま保存される.

(2) 距離による減衰程度は今迄ベツセル乃至ハンケルの函數がこれを表はしてゐたが此處に述べる様な場合には少しく異つた新しい函數が必要である. 筆者はこれを R-函數又は U-函數と名附けたがこれが今迄果して研究されなかつた函數であるか否かについては確言することが出來ない. 二三の場合について此の函數の値を計算して圖示した. 又斯る物理學的の問題に必要なる範圍に於いて此等の函數の一般の形及び漸近級數の最も重要なる項を求めた

斯る媒質の中では波は一般に分散するが地球がもし斯るものであるとすればその分散程度は非常に小さいものである.

震原から相當離れた所で大體の所を考ふれば振動の成分の中傳播の方向への成分は $(a-br^2)^{\frac{3}{2}}$ と $\frac{\sinh 2\sqrt{ab}t}{2\sqrt{ab}}$ に逆比例する. これに垂直な成分は二つ共 $(a-br^2)^{\frac{3}{2}}$ と $\left(\frac{\sinh 2\sqrt{ab}t}{2\sqrt{ab}}\right)^2$ とに逆比例する. 但し地震の様に勝手な形の衝撃の傳播に就いては上述の諸函數の性質が未だ究めてないので嚴密なことは論じ得られない.

2. *Influence of Solid Friction on Dynamical Magnification.*

By Takahiro HAGIWARA,

Seismological Institute.

(Read Nov. 15, 1932.—Received Dec. 20, 1932.)

1. Seismographs with mechanical registration are subject to solid friction acting upon the recording index and the pivots supporting the magnifying lever. Even when the seismograph has been constructed so rigidly that there is no such disturbance as bending of lever caused by the resisting force, existence of solid friction varies the dynamical magnification[1] of the seismograph and in an extreme case the motion of the index can never start unless the earth movement exceeds a certain amount of its amplitude and frequency. Therefore investigation of this effect becomes very important when we study seismographs and seismograms.

The solid friction can be generally considered to be constant in value and only changes its sign according to the direction of velocity of the index. Galitzin,[2] Reid,[3] and Nakamura[4] discussed a case where the effective value of solid friction is affected by the velocity of recording paper. Even if such a matter has to be considerd, the other effects such as caused by the varying pressure of index upon the recording paper due to the centrifugal force acting upon it, and by the deviation of ratio of the major arm of lever to the minor one due to deflection of lever from its medial line, etc., must be taken into account at the

1) There can be several definitions for the magnification used in seismometry, and these were fully discussed by M. Ishimoto. (M. ISHIMOTO, *Disin*, 4 (1932), 119.)

"The dynamical magnification" is defined as a magnifying power of a seismograph considered as a system of oscillating bodies with only liquid friction which can be mathematically treated with a simple linear differential equation. The magnification, when the seismograph is affected by solid friction or other physical disturbances, is called "the physical magnification."

2) B. GALITZIN, "*Vorlesungen über Seismometrie*," (1914), 493.

3) H. F. REID, *Bull. Seism. Soc. Am.*, 4 (1925), 222.

4) S. NAKAMURA, *Proc. Imp. Aca.*, Japan, 8 (1932), 155.

same time, and the problem becomes very complicated. Nevertheless the variation caused by these effects is so small that it can be neglected in ordinary case.

The influence of solid friction with a constant value upon the dynamical magnifiction was studied approximately by Reid[5] and Nakamura[6] who solved the problem under the assumption that the motion of index is simple harmonic as well as the earth movement. But even in the case where the earth movement is simple harmonic, the motion of index can not be simple harmonic when the solid friction exists. In the present paper the writer has attempted to give a general expression for the magnification under the assumption that the solid friction has a constant numerical value.

2. When the earth movement is a stationary simple harmonic motion, the equation of motion of a seismograph subject to the solid friction can be written by

$$\left.\begin{aligned} &\frac{d^2a}{dt^2}+2\varepsilon\frac{da}{dt}+n^2(a\pm\rho)=-Vp^2x_m\cos(pt-\delta),\\ &\quad +\rho \qquad \text{when} \qquad \frac{da}{dt}>0,\\ &\quad -\rho \qquad \text{,,} \qquad \frac{da}{dt}<0, \end{aligned}\right\} \quad \ldots\ldots(1)$$

where a is displacement of index,

ε : constant of the liquid friction,

T_n : natural period of the pendulum without liquid and solid friction,

n : $\dfrac{2\pi}{T_n}$,

ρ : constant of the solid friction,

V : dynamical magnification for infinitely rapid oscillation,

T_p : period of oscillation of the ground,

p : $\dfrac{2\pi}{T_p}$

x_m : the maximum amplitude of oscillation of the ground,

δ : phase difference.

The double sign of frictional term makes it more tedious to solve

5) H. F. Reid, "*The California earthquake of April 18, 1906*", 2 (1910), 166.

6) S. Nakamura, *loc. cit.*

the equation than the case where no solid friction exists. If we derive the general solution in confining our attention to one of these singns, and determine integrating constants according to conditions for stationary state, then the problem can be solved mathematically. But the expression obtained by such a way becomes so complicated that it is not available for the numerical calculation. For this reason, it becomes necessary to give an expression of more convenient form for practical use.

When motion of the ground is of a simple harmonic type with the period $\frac{2\pi}{p}$, that of index must be also a periodic motion with the same period $\frac{2\pi}{p}$ in a stationary state, though it is not a simple harmonic one. Moreover it must have the relation $a(pt+\pi)=-a(pt)$; so that we can express a in Fourier's series

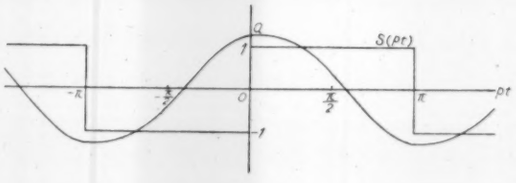

Fig. 1.

$$a=A_1\cos pt+\sum_{N=1}^{\infty}A_{2N+1}\cos(2N+1)pt+B_1\sin pt$$
$$+\sum_{N=1}^{\infty}B_{2N+1}\sin(2N+1)pt. \quad \ldots\ldots\ldots\ldots \quad (2)$$

We assume that a is monotonic within time interval of its half period. Then if we choose the origin of time at the instant when the index is at one of its maximum displacements in the positive direction, we can write the equation of motion as follows:

$$\frac{d^2a}{dt^2}+2\varepsilon\frac{da}{dt}+k^2a-n^2\rho\cdot S(pt)=-Vp^2\cos(pt-\delta), \quad \ldots\ldots\ldots\ldots (3)$$

where $S(pt)$ is a function with period $\frac{2\pi}{p}$ and its numerical values are expressed in the form (cf. Fig. 1).

$$\left.\begin{aligned} S(pt)&= \quad 1 \quad 2N\pi<pt<(2N+1)\pi \\ &=-1 \quad (2N+1)\pi<pt<(2N+2)\pi, \end{aligned}\right\} \quad \ldots\ldots (4)$$

where N is integer including zero.

Representing $S(pt)$ in Fourier's series

$$S(pt)=\frac{4}{\pi}\sum_{N=0}^{\infty}\frac{\sin(2N+1)pt}{2N+1} \quad \ldots\ldots\ldots\ldots\ldots (5)$$

Integrating the equation (3) twice with respect to t,

$$a+2\varepsilon\int a\,dt+n^2\int dt\int a\,dt-n^2\rho\int dt\int S(pt)dt=Vx_m\cos(pt-\delta). \quad \ldots\ldots(6)$$

The two integrating constants vanish because the other terms are all odd harmonic functions of pt.

Substituting (2) and (5) in this equation,

$$\begin{aligned}
&A_1\cos pt+\sum_{N=1}^{\infty}A_{2N+1}\cos(2N+1)pt+B_1\sin pt\\
&\qquad+\sum_{N=1}^{\infty}B_{2N+1}\sin(2N+1)pt\\
&+\frac{2\varepsilon}{p}\Big\{A_1\sin pt+\sum_{N=1}^{\infty}\frac{A_{2N+1}}{2N+1}\sin(2N+1)pt-B_1\cos pt\\
&\qquad-\sum_{N=1}^{\infty}\frac{B_{2N+1}}{2N+1}\cos(2N+1)pt\Big\}\\
&+\frac{n^2}{p^2}\Big\{-A_1\cos pt-\sum_{N=1}^{\infty}\frac{A_{2N+1}}{(2N+1)^2}\cos(2N+1)pt\\
&\qquad-B_1\sin pt-\sum_{N=1}^{\infty}\frac{B_{2N+1}}{(2N+1)^2}\sin(2N+1)pt\Big\}\\
&+\frac{4n^2\rho}{\pi p^2}\Big\{\sin pt+\sum_{N=1}^{\infty}\frac{\sin(2N+1)pt}{(2N+1)^3}\Big\}\\
&=Vx_m\cos(pt-\delta). \quad \ldots\ldots\ldots\ldots\ldots\ldots(7)
\end{aligned}$$

We may determine the coefficients of the series so as to satisfy this equation. Thus

$$\left.\begin{aligned}
&A_{2N+1}-\frac{2\varepsilon}{p}\frac{B_{2N+1}}{2N+1}-\frac{n^2}{p^2}\frac{A_{2N+1}}{(2N+1)^2}=0,\\
&B_{2N+1}+\frac{2\varepsilon}{p}\frac{A_{2N+1}}{2N+1}-\frac{n^2}{p^2}\frac{B_{2N+1}}{(2N+1)^2}+\frac{4n^2\rho}{\pi p^2(2N+1)^3}=0.
\end{aligned}\right\}\quad\ldots\ldots(8)$$

Then

$$\left.\begin{aligned}
A_{2N+1}&=-\frac{4u^2\rho}{\pi}\frac{2hu}{\{u^2-(2N+1)^2\}^2+4h^2u^2(2N+1)^2},\\
B_{2N+1}&=\frac{4u^2\rho}{\pi(2N+1)}\frac{u^2-(2N+1)^2}{\{u^2-(2N+1)^2\}^2+4h^2u^2(2N+1)^2},
\end{aligned}\right\}\quad\ldots\ldots(9)$$

where[7]

7) h has the following relation with the damping ratio v;

$$h=\frac{\log_e v}{\sqrt{\pi^2+(\log_e v)^2}}.$$

$$u=\frac{n}{p}=\frac{T_p}{T_n},\quad h=\frac{\varepsilon}{n}.$$

As N tends to infinity, A_{2N+1} and B_{2N+1} tend to zero by the order of $\frac{1}{N^4}$ and $\frac{1}{N^3}$ respectively; so that the series (2) converges absolutely.

It should be noticed that we have expanded $S(pt)$ in Fourier's series but, strictly speaking, this series has no more discontinuities and there exists so called Gibbs's phenomenon[8] at $pt=N\pi$, that is, the function expressed by the series oscillates infinitly with certain finite amplitudes arround unity in the neighbourhood of $pt=N\pi$. But this is a finite deviation within infintesimal time intervel so that in integrating over time this effect does not affect the result. And because we have not employed such a point when we determined the coefficients of the series (2), we can leave the effect of Gibbs's phenomenon out of consideration.

Differentiating (2),

$$\frac{da}{dt}=p\Big\{-A_1\sin pt-\sum_{N=1}^{\infty}(2N+1)A_{2N+1}\sin(2N+1)pt$$
$$+B_1\cos pt+\sum_{N=1}^{\infty}(2N+1)B_{2N+1}\cos(2N+1)pt\Big\}\quad\ldots\ldots\ (10)$$

The series on the right hand side converges absolutely for a similar reason.

By the first assumption,

$$\left(\frac{da}{dt}\right)_{t=0}=0;$$

hence

$$\left.\begin{aligned}B_1&=-\sum_{N=1}^{\infty}(2N+1)B_{2N+1}\\&=-\frac{4u^2\rho}{\pi}\sum_{N=1}^{\infty}\frac{u^2-(2N+1)^2}{\{u^2-(2N+1)^2\}^2+4h^2u(2N+1)^2}.\end{aligned}\right\}\quad\ldots\ldots(11)$$

Then, the equation (7) takes the form

8) For example, H. S. CARSLAW, "*Introduction to the Theory of Fourier's Series and Integrals*," (1906).

$$-\{(u^2-1)A_1+2huB_1\}\cos pt-\left\{(u^2-1)B_1-2huA_1-\frac{4u^2\rho}{u}\right\}\sin pt$$
$$=Vx_m\cos(pt-\delta)\quad\cdots\cdots(12)$$

If we denote the maximum displacement of the index by a_0 and its corrected value by A, then

$$\left.\begin{aligned} a_0&=A_1+\sum_{N=1}^{\infty}A_{2N+1},\\ A&=Vx_m. \end{aligned}\right\}\quad\cdots\cdots(13)$$

Thus we can obtain the following relation from (12) and (13),

$$\left.\begin{aligned} A&=a_0\sqrt{\{(u^2-1)A_1'+2huB_1'\}^2+\left\{(u^2-1)B_1'-2huA_1'-\frac{4u^2}{\pi}\frac{\rho}{a_0}\right\}^2},\\ \tan\delta&=\frac{(u^2-1)B_1'-2huA_1'-\frac{4u^2}{\pi}\frac{\rho}{a_0}}{(u^2-1)A_1'+2huB_1'},\\ A_1'&=1+S_A\frac{\rho}{a_0},\\ B_1'&=S_B\frac{\rho}{a_0},\\ S_A&=\frac{4u^2}{\pi}\cdot 2hu\sum_{N=1}^{\infty}\frac{1}{\{u^2-(2N+1)^2\}^2+4h^2u^2(2N+1)^2},\\ S_B&=-\frac{4u^2}{\pi}\sum_{N=1}^{\infty}\frac{u^2-(2N+1)^2}{\{u^2-(2N+1)^2\}^2+4h^2u^2(2N+1)^2}. \end{aligned}\right\}\quad(14)$$

Employing these relation, we can calculate the corresponding amplitude of the motion of ground from measurement of a maximum displacement in the actual seismogram.

If we put $S_A=S_B=0$ in the above relation, it agrees with the approximate expression given by Reid and Nakamura. And if $\rho=0$ it becomes the oridinary expression for the dynamicnal magnification without solid friction.

Each term of the series in the above expression resembles the ordinary expression for the magnification of seismograph; so that we can evaluate it easily employing the tables used in seismometry with small modification.

The values of the sums of these series are given in Table I and II.

Table I.

Value of $\sum_{N=1}^{\infty} \frac{1}{\{u^2-(2N+1)^2\}^2+4h^2u^2(2N+1)^2}$.

h \ u	0·0	0·2	0·4	0·6	0·8	1·0	1·2	1·4	1·6	1·8	2·0
0·0	0·0147	0·0148	0·0152	0·0158	0·0168	0·0181	0·0201	0·0229	0·0270	0·0330	0·0431
0·2	147	148	152	157	167	177	194	215	250	294	348
0·4	147	148	150	154	160	168	177	190	203	220	236
0·6	147	147	148	149	151	153	155	158	159	158	154
0·8	147	146	146	144	140	138	132	130	124	117	110
1·0	147	146	143	138	130	123	114	105	095	087	078

Table II.

Value of $\sum_{N=1}^{\infty} \frac{u^2-(2N+1)^2}{\{u^2-(2N+1)^2\}^2+4h^2u^2(2N+1)^2}$.

h \ u	0·0	0·2	0·4	0·6	0·8	1·0	1·2	1·4	1·6	1·8	2·0
0·0	-0·234	-0·234	-0·236	-0·238	-0·244	-0·249	-0·256	-0·268	-0·284	-0·303	-0·333
0·2	234	234	236	237	242	246	252	259	270	289	313
0·4	234	234	234	235	236	237	238	239	238	235	227
0·6	234	234	233	232	229	226	220	214	206	195	182
0·8	234	233	231	238	220	212	200	190	179	165	152
1·0	234	233	229	222	210	197	183	168	155	142	130

It will be seen that when the recorded maximum amplitude a_0 is large compared with the frictional term ρ or when u is small, that is, the forced oscillation is very rapid, the effect of solid friction is small, but in the contrary case its effect becomes very large.

3. We have already obtained a general expression which can be used to find the amplitude of motion of the ground from a seismographic record. Now we will examine to what extent the displacement on record depends upon the feature of the given earth movement. For this purpose the following form is convenient which is given by transforming the relation (14).

$$\left.\begin{aligned}
&\{(u^2-1)^2+(2hu)^2\}\left(\frac{a_0}{\rho}\right)^2+2\{(u^2-1)X+2huY\}\frac{a_0}{\rho}+X^2+Y^2-\left(\frac{A}{\rho}\right)^2=0,\\
&X=(u^2-1)S_A+2huS_B,\\
&Y=2huS_A-(u^2-1)S_B+\frac{4u^2}{\pi}.
\end{aligned}\right\} \quad (15)$$

The positive root $\frac{a_0}{\rho}$ of this equation gives the required amplitude on the record for a given amplitude of the eath movement.

4. At the outset we have assumed that friction takes always a constant value. But when the amplitude of earth movement does not exceed a certain limit, the index can not move continuously but its movement and rest occur alternately. (cf. Fig. 6.)

In such circumstances when the force setting the index in motion is smaller than the full value of solid friction, the frictional resistance balances with this force and the index remains at rest; so that the value of solid friction does not attain to the value which so far assumed to be constant. And after the force exceeds the full value of friction the index starts on. Therefore the first assumption is no more available in such a case and we must deal with the equation under another condition. But in practice it is not so much important to treat such a case because

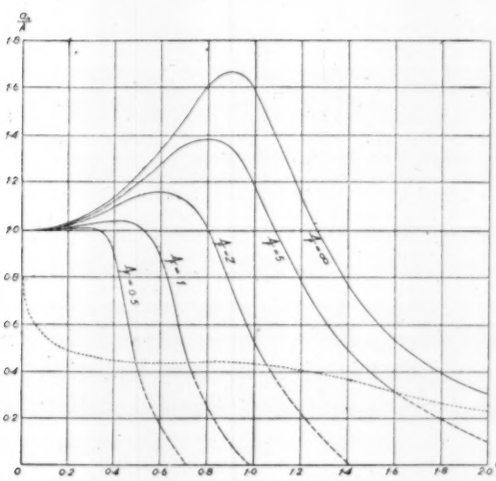

Fig. 2. $h=0.316$ (Damping ratio 2·85).

a_0: The maximum displacement on the record,

A: The maximum amplitude of earth movement multiplied by V,

u: Ratio of the period of forced oscillation to the natural period of seismograph,

ρ: Constant of the solid friction.

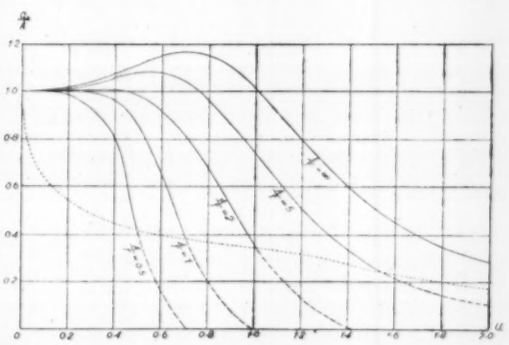

Fig. 3. $h=0.5$ (Damping ratio 6·13).

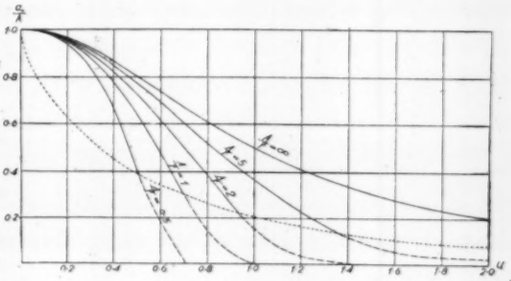

Fig. 4. $h=1.0$ (Critical damping)

it occurs only when the motion of index approaches the threshold of immovility; so that we will not discuss it further but will find only the limit within which the fiirst assumption can be applied. This condition is such that under which the index can be in motion just after $t=0$, and is given by consulting the the equation (1),

$$n^2\rho < a_0 n^2 + V x_m p^2 \cos\delta, \quad \ldots\ldots\ldots\ldots\ldots\ldots (16)$$

combining this with the equation (14),

$$\frac{a_0}{\rho} > u^2 + (u^2-1)S_A + 2huS_B \quad \ldots\ldots\ldots\ldots\ldots (17)$$

Moreover the condition that the index can never start at any moment can be easily given in the same manner.

$$n^2\rho \geqq V x_m p^2, \quad \ldots\ldots\ldots\ldots\ldots\ldots (18)$$

that is,

$$\frac{A}{\rho} \leqq u^2 \ldots\ldots\ldots\ldots\ldots\ldots (19)$$

5. A few numerical examples will be shown in the following. Fig. 2, 3 and 4 show the variation of dynamical magnification when h is 0·316, 0·5 and 1·0 respectively. It will be seen that when the amplitude of earth movement multiplied by V is very large compared with the frictional term ρ, that is, $\frac{A}{\rho}=\infty$,

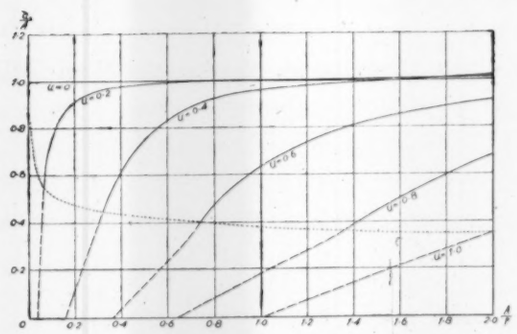

Fig. 5. $h=0{\cdot}316$ (Damping ratio 2·85)

the dynamical magnification is not affected by solid friction and its curve agrees with the ordinary curve of magnification well known in seismometry which tends to zero when the ratio of the period of forced oscillation to the natural period of seismograph, u, tends to infinity. Nevertheless if A is not large, as compared with ρ, the solid friction plays an important rôle and the magnifying power becomes zero beyond a certain value of u. And the smaller A is, the more is the influence of solid friction. In these figures the full lines mean the cases where the solid friction has always its full value and the broken lines mean the case where this assumption does not hold. Fig. 5, 6 and 7 show how the dynamical magnification is modified by the amplitude of earth movement. It is

noticed that the dynamical magnification without solid friction does not depend upon the amplitude of earth movement but when the solid friction exists the magnifying power of seismograph becomes a function of the amplitude. Fig. 8 shows the deviation of recorded curve from a sine curve. The curves are not symmetrical with respect to its maximum point, namely the motion of index attains its maximum quickly and leavesit slowly. If the amplitude is smaller than a certain limit a state of rest of the index continues for a certain time and then the motion begins, as is shown in the figure with broken line.

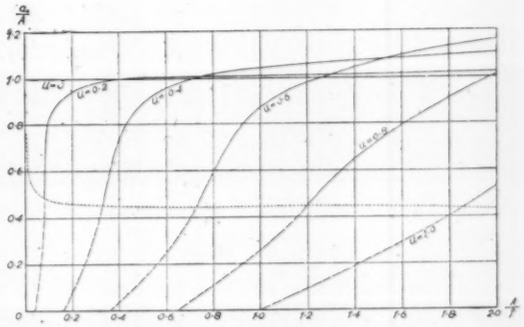

Fig. 6. $h=0.5$ (Damping ratio 6·13)

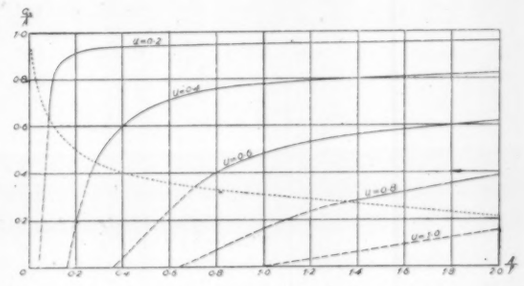

Fig. 7. $h=1.0$ (Critical damping)

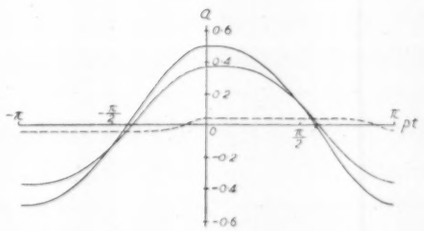

Fig. 8. Displacement of the writing index when $h=0.5$, $u=0.6$, and $\rho=1$.

6. It is necessary for seismograph with mechanical registration that it is constructed so as not to be affected by solid friction within a certain range. If we need that the deviation of reading on seismogram from the corrected value remains within a certain limit, it is not only necessary that the natural period of seismograph is sufficiently large compared with that of forced oscillation but also that the frictional term ρ is less than a certain value. Such a value of ρ can be found by the relation already described. If f denotes the value of solid frictin acting upon the index,[9] we can write the relation between f and ρ as follows:

9) M. Ishimoto obtained 0·38 dynes of this value by experiment for the index of his accelerometer. (M. Ishimoto, *Bull. Earthq. Res. Inst.*, **9** (1931), 322.) The present writer. obtained 0·45 dynes by the same method for the index of seismograph of ordinary type. (T. Hagiwara, *Disin*, **4** (1932), 206.)

As regards the value of friction upon pivots, see M. Ishimoto and others, *Bull. Earthq. Res. Inst.*, **10** (1932). 858.

$$\rho = f \cdot \frac{T_n^2}{4\pi^2} \cdot V^2 \cdot \frac{l^2}{r^2} \cdot \frac{1}{M}, \quad \cdots\cdots\cdots\cdots\cdots\cdots (20)$$

where V is dynamical magnification for infinitely rapid oscillation,

T_n: natural period of pendulum,

l: reduced length of pendulum,

r: radius of gyration of pendulum,

M: mass of bob.

This relation shows us how to determine the size of bob in designing a seismograph with mechanical registration.

In conclusion, the present writer wishes to express his best thanks to Professor M. Ishimoto, Professor T. Matuzawa and Dr. H. Kawasumi for their kind advices and criticisms in regard to the problems.

---

2. 固體摩擦の振動倍率に及ぼす影響

地震學教室　萩　原　尊　禮

機械的に地動を擴大し或は記錄せしめる地震計に於ては描針，擴大用槓杆を支へるピボットに働く固體摩擦の影響が問題となる．此の固體摩擦は一般には絕對値は常に一定で唯符號のみが描針の速度の方向に依つて異るものと考へられる．かゝる場合の固體摩擦の影響は近似的には既に知られて居るが，此處では近似的の方法に依らずに其の影響の計算を試みた．

計算の結果は（14）式に示す如く簡單な形に於て得られた．此の式に依り記象上の振幅に對して補正を施すことが出來る．此の場合，地震計の倍率は制振常數，地動と地震計との週期の比の他に，記錄された振幅と摩擦項との比の函數となる．振幅が摩擦項に比して充分大きい場合は固體摩擦の影響は省略出來るが，之と反對に振幅が小い時は其の影響は大である．

（15）式は與へられた振幅，週期を有する地動に對する地震計の倍率を與へる．或る地動に對する記象が補正を施すことなしに與へられた誤差以內にあるためには，地動と地震計との週期の比が充分大きいのみならず，固體摩擦の項も亦或る値以下であることを要する．

描針，ピボットに働く固體摩擦力の大さは既に實驗的に求められて居るから，以上の議論と合せて、或る地動を誤差何パーセント以下に記錄せしむるには地震計重錘の重量を少くとも幾何になすべきかを知ることが出來る．

---

3. *Tilt of the Earth's Crust observed at the Asama Volcano.*

By Ryûtarô TAKAHASI,

Earthquake Research Institute.

(Read Sept. 20, 1932.–Received Dec. 20, 1932.)

1. Mt. Asama, which is situated on the boundary of Gumma and Nagano Prefectures, about 100 km. north-west of Tokyo, is one of the most active volcanoes in Japan. From ancient times it has often repeated violent eruptions,[1] among which that of 1783 was the largest. In the case of this eruption, 1150 lives were lost and several villages were buried under mud-flows. The lava-flow which was issued from the crater by this eruption covered the greater part of the north slope of the mountain, and is called now Oni-no-osidasi.

The mountain is a composite volcano made of acidic lava and gravels and rises 2542 m. above the sea level. As classified by the character of its eruptions, it belongs to the Stromboli type. Its active period seems to come at the interval of several tens of years. The recent activity of the volcano commenced in September of 1929, and has continued since.

Several geophysical researches has been made at this volcano, among which the observations made by Prof. Omori[1] of the volcanic earthquakes and other phenomena are most remarkable. There has been made, however, no research, as far as the author is aware of, concerning the deformation of the earth's crust connected with the eruption of this volcano.

2. In recent years, levelling surveys have revealed in several cases the deformation of the earth's crust associated with the eruption of a volcano. As the examples of these cases, we can point out the eruptions of the Sakurazima Volcano, in 1914[2] the Usu Volcano in 1910[3] and the Komagatake Volcano, Hokkaido, in 1929[4].

These levelling surveys did not, however, tell us in what manner

1) *Bull. Imp. Earthq. Inv. Comm.*, **6** (1912-1914); **7** (1914-1919).
2) F OMORI, *Bull. Imp. Earthq. Inv. Comm.*, **8** (1914-1922).
3) F. OMORI, *Bull. Imp. Earthq. Inv. Comm.*, **5** (1911-1913), 1-38, 101-107.
4) Ch. TSUBOI, *Bull. Earthq. Res. Inst.*, **8** (1930), 298.

the deformation of the crust arround a volcano makes its development during the active period of the volcano. In connection with this question, a pair of clinographs was installed, in the case of the last eruption of the Komagatake Volcano in 1929, at the north slope of the mountain and the tilt of the earth's crust was observed for about 6 months. By this observation we could recognize the existence of certain correlations between the activity of the volcano and the tilt of the crust arround the volcano, though they were not very distinct owing to the facts that the eruption was of a single explosion having no subsequent remarkable event and that the observation was commenced after that main explosion.

In 1929, T. A. Jagger and R. H. Finch[5] reported about the remarkable correlation existing between the tilt of the ground observed at the Hawaiian Volcano Observatory and the height of the molten lava in the Halemaumau pit, Kilauea Volcano.

The present writer has long been considering that it is very promissing to execute a clinograph observation at Mt. Asama for the purpose of getting some informations regarding the problem described above and also, if possible, the mechanism of the eruption and the under-ground structure of the volcano. The idea has not been realized under certain circumstances until April of this year, when it siezed the first opportunity to go out in the day-light, and the observation was commenced in the summer of the same year. The results of the observation harmonize well with those obtained by Jagger at Kilauea, if we take into consideration the difference of the characters of the eruptions of the two volcanoes.

3. The present observation was commenced on June 3, 1932, with a pair of clinographs, at Komoro, a village which lie at the south-west foot of the Asama Volcano. The clinograph is essentially a horizontal pendulum made of fused quartz. The deflection of the pendulum is recorded photographically. The pendulums were installed in a masonry refrigerating cellar, situated at the north suburb of the village of Komoro, in such directions as to record respectively N–S and E–W components of tilt of the ground. The cellar is built on a natural bed of consolidated volcanic scolia and gravels ejected by some pre-historical eruptions. It belongs to the Zyunsuikawan Silk-worm Egg Company and is used in summer for the storage of silk-worm eggs. The sensibility of the instrument was so adjusted, at the beginning of the observation, that a

5) *Bull. Seis. Soc. Amer.*, 19 (1929), 38.

Fig. 1. Map showing the Asama Volcano and the vicinity.

deflection of 20 mm. is produced on the record against the tilt of the ground of 1 sec. of arc. The sensibility was examined since then many times by measuring the period of free oscillation of the pendulum. The time-marks on the records were introduced at 6h and 18h of each day. The air temperature and humidity in the cellar were kept prety constant during the period of the present observation.

The installation of the instrument was finished at 21h 30m of June 3, and the observation has been continued since. The attendance to and the manipulation of the instrument have been done by Mr. Oi of the Komoro Primary School.

4. Fortunately enough, on June 4, the next day of the installation of the instrument, a great explosion took place at 20h 29m, with a loud detonation sound. This explosion was so large that the ash-precipitation was experienced in abroad area arround the volcano. At Nagano, which is distant some 40 km. from the volcano, the quantity of the ash-precipitation was measured to be 50 cc./m^2. The detonation sound reached as far as

200 km. This explosion was followed then by smaller ones, which occurred at 4h 20ma nd 12h 30m of June 5. Since then many eruptions of various magnitude have occurred, which exceeded 70 in number at the end of August. The magnitude and the time of occurrence of each eruption was kindly reported by Mr. Utibori, the host of the Minenotyaya Cottage (see Fig. 1). Eruptions reported in the "Kisyô-yôran", issued from the Central Meteorological Observatory, were also taken into considerations. At Minenotyaya, which is distant only 5 km. from the crater, even a minute eruption, which cannot be recognized at distances, especially in rainy or cloudy weather, is observed, while the magnitude of the eruption seems to be judged more exactly by distant observations given in the Kisyô-yôran.

The eruptions occurred during the period of the present observation are listed in the following pages. The list includes eruptions and other volcanic events reported both by Mr. Utibori and by the Kisyô-yôran.

Date	Time of Occurrence h	m	Remark
June 4	11	30	Low detonation.
	20	25	Strong explosion; detonation sound being heard at Minenotyaya. Oiwake, Ueda, Sugadaira, etc. Detonation sounds like gun-shots were heard at 20h 34m at Gihu Observatory, which is distant so far as 200km. from the volcano. An earthquake was felt at Minenotyaya and Oiwake. Ashes fell at Koasama, Minenotyaya, Togemati, Nagakubo, etc. The quantity of ash-fall was 30 gr./m² at Nagakubo and 50 cc./m² at Nagano.
5	3	53	Explosion with rumblings. Windows vibrated slightly at Oiwake. Black smoke flowed towards north.
	5	40	Low detonation. Ashes fell at Osidasi.
	12	27	Rumblings and smoke emission.
7	14	00	Small eruption. Ashes fell at the north of Minenotyaya.
8	8	00	Small eruption. Ashes fell at Minenotyaya & Koasama.
9	20	20	Do.
10	2	—	Weak detonation.
	6	18	Rumblings were heard for 20 minutes.
12	7	30	Rumblings were heard till 12h. White smoke was emitted at times.
13	11	—	Detonation. Ashes fell at Osidasi.
14	17	09	Explosion. Ashes fell in all part of Kita-saku district and a part of Minami-saku and Tiisagata districts. Ashes fell for 8 minutes at Oiwake.
21	—	—	Rumblings.

(*to be continued.*)

(*continued.*)

Date		Time of Occurrence h	m	Remark
June	22	9	58	A rather conspicuous earthquake.
	24	14	57	Explosion. Weak earthquake was felt at Minenotyaya, Oiwake and Kutukake. Sands and stones as large as an cube-sugar fell near Wakasarityaya.
		19	42	Explosion. Weak earthquake was felt at Oiwake.
	25	12	—	Small eruption. Ashes fell at Sengataki and Kutukake.
		18	—	Do.
		22	45	Small eruption. At Oiwake windows vibrated.
	26	4	55	Smoke emission. Ash-fall at Minenotyaya.
	27	—	—	Rumblings heard from 3h till 5h 30m.
	28	9	02	Loud detonation and explosion. Weak earthquake was felt at Oiwake. Sound reached a considerable distance. Sands fell at Minenotyaya for 25 minutes.
		18	21	Detonation.
	29	15	—	Ashes fell a little at Minenotyaya, Kamahara and Wakasarityaya.
	30	14	—	Ashes fell at Osidasi.
July	1	5	25	Small eruption. Ash-fall at Wakasarityaya.
	2	19	—	Small eruption. Ash-fall at Minenotyaya. Rumblings were heard all the day.
	3	4	52	Loud detonation and explosion. At Kutukake detonation sound was heard like a thunder and vibrations were prety strong. At Togemati low explosion sound was heard and ashes fell for 5 minutes. At Minenotyaya the explosion sound was like a gun-shot and stones as large as 2 cm. dia. have fallen.
		5	03	Eruption.
		5	38	Small eruption.
		10	50	Small eruption. Smoke emission continued till 11h 30m.
		16	47	Do. Smoke emission continued till 17h 30m.
		20	25	Do.
	4	—	—	Small eruptions at about 4h, 6h and 11h 30m.
	5	—	—	Small eruptions at about 7h, 14h and 20h 30m.
	9	14	30	Small eruption.
		18	30	Do.
	10	4	37	Small eruption. At Minenotyaya, rumblings were heard and ashes fell for 2 hours.
		9	—	Small eruption. Ashes fell at Minenotyaya.
		11	20	Smoke emission. Ashes fell at the E base of the mountain.

(*to be continued.*)

(*continued.*)

Date	Time of Occurrence h	m	Remark
July 10	12	40	Do.
	13	40	Small eruption. Ashes fell for 25m. at Minenotyaya.
	16	—	Smoke emission for 30m.
	20	—	Much smoke emitted. Ashes fell at N of the mountain.
11	10	16	Small eruption.
	11	10	Do. Ashes fell at Minenotyaya.
	14	07	Do.
	19	20	Do.
	20	20	Do. Sands fell at Minenotyaya.
12	3	30	Eruption. Black smoke was driven towards ES. Ashes fell for 40m. at Minenotyaya.
	7	15	Smoke emission.
	13	50	Smoke emission with low detonation sound.
	15	20	Small eruption.
	18	55	Smoke emission. Ashes fell for 5m. at Minenotyaya.
13	15	20	Smoke emission for 10m.
	19	20	Small eruption.
14	12	30	Smoke emission for 5m.
15	11	10	Smoke emission.
	14	—	Low detonation.
	17	20	Small eruption.
16	8	—	Small eruption. Ashes fell a little at Minenotyaya.
	11	—	Do.
	15	—	Smoke emission.
17	—	—	3 small eruptions during 9h and 16h. Ashes fell a little at Minenotyaya.
18	3	36	Small eruption with rumblings.
	11	26	Rumblings. A large quantity of black smoke was emitted
19	6	15	Small eruption. Ashes fell much at Minenotyaya.
	8	—	Do.
	11	15	Do.
20	7	30	Small eruption with much smoke emitted.
	8	15	Smoke emission for about 1 hour.
21	0	—	No smoke.
	4	45	Smoke emission without rumblings.

(*to be continued.*)

(*continued.*)

Date	Time of Occurrence h	m	Remark
July 21	14	20	Smoke emission after 20 minutes' rumblings.
	17	—	Rumblings for about 40m.
	19	20	Rumblings.
22	17	—	Small eruption and rumblings.
	19	35	Do.
23	7	35	Loud detonation. Ash- clouds were driven towards NE.
	8	—	Small eruption and rumblings.
	12	20	Detonation.
	13	—	Small eruption with rumblings. Ashes fell at Kutukake.
	18	35	Small eruption with loud rumblings.
	19	08	Smoke emission.
24	9	50	Rumblings.
	11	30	Do.
	15	40	Small eruption. Much black smoke.
	17	41	Rumblings.
25	9	40	Rumblings and smoke emission.
26	7	—	Low rumblings.
29	5	10	Rumblings. A large quantity of black smoke was emitted.
	14	17	Small eruption.
	14	35	Rumblings. Smoke emission. Ashes fell for 5m. at Minenotyaya.
30	11	08	Small eruption. Much black smoke.
Aug. 4	5	—	Smoke emission. Ashes fell at Minenotyaya, Wakasarityaya and Koasama.
	10	50	Smoke emission without rumblings.
	11	45	Smoke emission. Ash-clouds were driven towards NE.
	17	—	Do.
6	6	—	Small eruption.
9	4	—	Smoke emmission.
	11	20	Do.
20	—	—	Smoke emission.
27	11	40	Smoke emission without rumbings.
Sept. 10	15	30	Small eruption with thunder-like detonation sounds. Ashes fell at Minenotyaya and Osidasi.
20			Detonation.
21	10	58	Explosion. The column of smoke was observed well at Nagano, and was estimated by a theodolite to be 4100m. high above the sea level.
	12	50	Small eruption.

In the Kisyô-yôran is given, besides these reports of eruptions of the volcano, the frequency of the volcanic micro-seisms observed at the Oiwake Observatory. It is listed as follows:

Number of volcanic micro-seisms observed at the Oiwake Observatory.

Month / Day	June	July	Aug.	Sept.	Month / Day	June	July	Aug.	Sept.
1	—	10	5	0	17	—	7	1	0
2	—	9	1	1	18	—	5	2	0
3	—	14	3	1	19	—	1	1	0
4	6	8	7	0	20	1	5	1	0
5	5	3	1	0					
6	3	0	1	1	21	—	5	0	2
7	3	0	0	2	22	—	3	0	5
8	1	1	1	0	23	—	21	0	8
9	1	3	0	1	24	13	16	0	5
10	3	12	0	0	25	35	6	0	5
					26	26	8	0	5
11	—	9	1	0	27	1	0	2	5
12	6	11	3	0	28	9	7	0	4
13	9	5	3	0	29	6	13	1	0
14	4	1	0	0	30	2	9	0	0
15	3	5	0	0					
16	—	12	0	0	31		3	3	

5. Fig. 2 is the reproduction of the tilt-records obtained by the clinographs during the period from June 3 to Sept. 10, 1932. In the figure are also shown, in parallel with these tilt-curves, the daily numbers of the volcanic micro-seisms observed at Oiwake, and the eruptions listed above. The thin vertical lines under dates show the noon of that day. The great explosions are indicated by large dots, while small eruptions, smoke emissions and detonations are all represented by small dots. Very minute volcanic events are omitted in the figure. The position of each dot represents the time of occurrence of the event, while the daily number of micro-seisms is assigned to the noon of each day. The letters E, W, S and N attached to the tilt-curves show respectively the directions towards which the ground tilt *down*. The deviation of E–W tilt-curve to the side of the letter E shows therefore that the ground tilted in the sense *east down and west up*.

As can be noticed in the figure, eruptions seem to occur in groups, and the largest one stands generally at the head of a group. There are cases in which the greatest eruption in a group is preceded by one eruption or two of smaller scale, but it never occur at the rear of a group. Series of small eruptions, such as appeared in the present

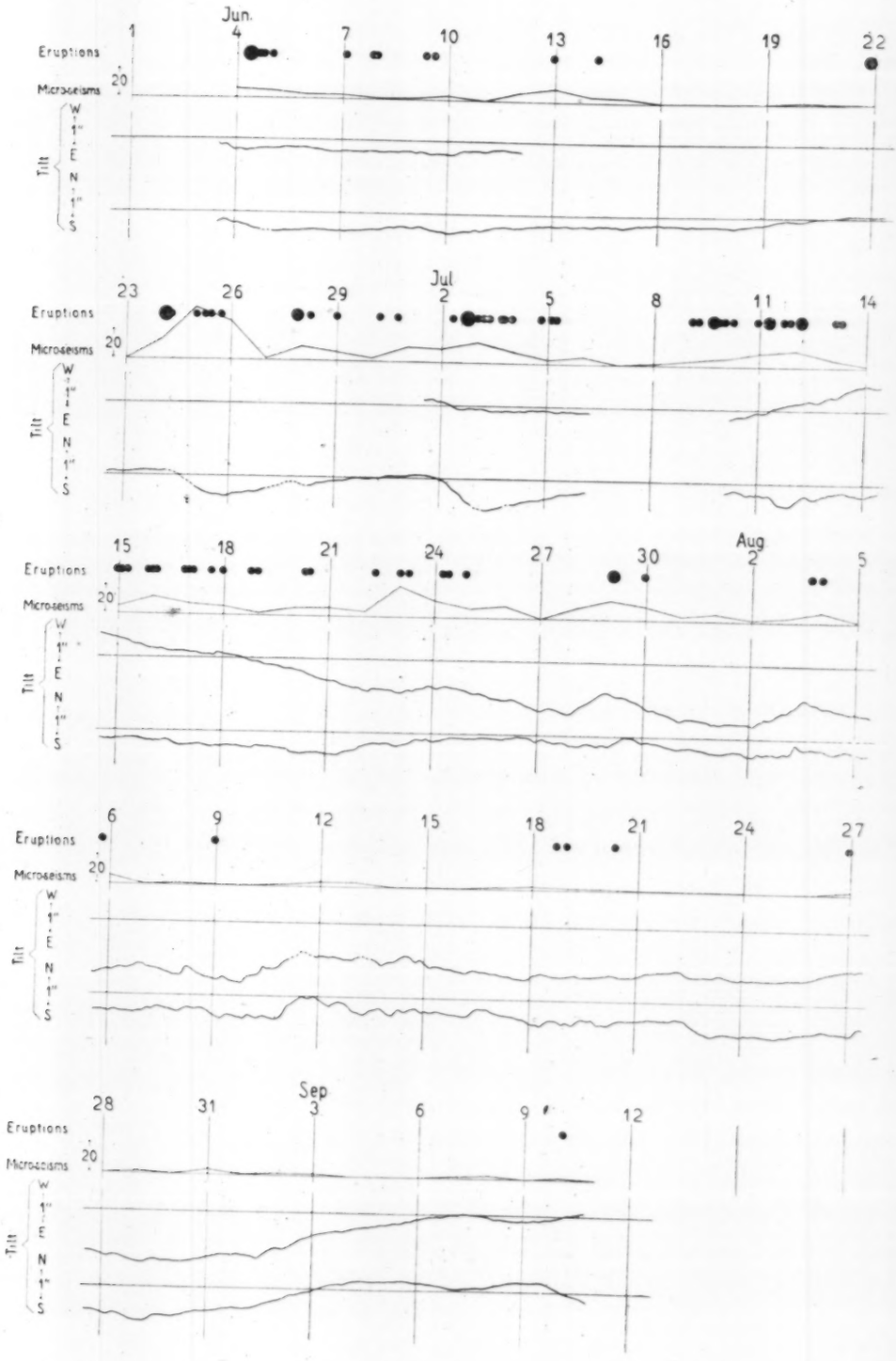

Fig. 2. Tilt-curves.

observation during the period from July 15 to July 25, seems to come to an end without resulting to any remarkable eruption.

These feature of eruptions may be understood by the speculation that the quantity of energy spent by the first eruption must be greater than those spent by the subsequent ones, because the volcano shaft is probably corked firmly at the time of the first eruption. When the corking of the shaft is not so firm, the eruptive energy will be dissipated by series of small eruptions. This speculation harmonizes well with the mechanism of the tilt of the earth's crust considered later.

The activity of such a volcano as Asama is very difficult to estimate. We may however take without much errors the frequency and magnitude of eruptions as a measure of the quantity. An alternative measure of the activity of a volcano will be the frequency and magnitude of seisms of which the origin is under the volcano.

Indeed, we can notice in Fig. 2 that the frequency of the volcanic micro-seisms is, generally speaking, in a considerable correlation with the frequency and magnitude of eruptions. In making this comparison however, volcanic earthquakes were all neglected, because they are very few in number compared with the micro-seisms and the negléction of them will have no effect upon the general feature of the matter. Small discrepancies in the parallelism of the two quantities have probably their origins in the difficulty of estimating the magnitude of an eruption.

In the recent number of the "Volcano Letter", A. E. Johnes and T. A. Jagger[6] have reported that the sismicity observed at the Hawaiian Volcano Observatory is related closely with the lava-inflow of the Halemaumau. It is interesting that there is a similarity also in this respect between the Asama and the Kilauea, notwithstanding the difference of types of the two volcanses.

Now we will proceed to study how the tilt of the earth's crust found by the present observation is related to the activity of the volcano. In the first place, we can find in Fig. 2 that the daily variation of tilt, which is mainly caused by the thermal stresses produced in the ground by solar radiation and amounts usually to 1″ or 2″, is very small at Komoro. This is likely due to the sandy soil of the place. We will find further that there are fluctuations of the tilt of which the period is about a week. This is, we think, probably due to the variation of the same period of the atmospheric pressure. Other weather conditions, such as rainfall, do

6) *Volcano Letter*, Feb. 4, 1932.

not seem to have any remarkable effect on the tilt observed.

We can see, referring to N–S tilt-curve, that the earth's crust began to tilt from its mean position on June 18, six days before the great explosion of June 24, making since then a steady, constantly increasing tilt until the day of occurrence of the explosion. Similar tilts will be found before the explosions of June 28, July 3 and July 29. The explosion of June 4 must also have had a similar tilt. These tilts are all directed towards NW.

This feature of tilt will likely mean the accumulation of the volcanic energy and the consequent increase of the pressure under the mountain, resulting in the deformation of the crust. It will probably be due to some local structure of the crust near the observation station that the tilt is not radial with respect to the mountain but is circumferential. An alternative explanation of the direction of tilt will be that the tumescence centre of the volcano is not coincident with the crater of the volcano but lies somewhat south of the mountain.

This tilt of the crust, which proceeds the occurrence of a group of eruptions, usually stops increasing at the same time with, or a little time before the first eruption of the group. Then the crust begins generally to tilt to the opposit sense, recovering to the original state with the subsequent eruptions. This will probably mean that the accumulated energy of the eruption was spent by the sequence of eruptions, and the crust returns to its original state because of the decreased pressure under it. The variation of the tilt of this type are to be seen by the groups of eruptions extending respectively from June 24 to June 26, from July 3 to July 5, etc.

When the dissipation of energy by series of eruptions balances with the accumulation of energy, there will be no tilt. If the accumulation velocity surmount the velocity of dissipation by eruptions, the crust will swell out notwithstanding the eruptions occurring. The feature of the tilt-curve extending from July 7 to July 21 will be regarded as an example of such a case.

When the accumulated energy is not sufficient to break the crater plug, there will occur no eruption, but some deformations will be produced arround the volcano. On the contrary, when the crater plug is not perfect, there will be no remarkable deformation of the earth's crust, though a sequence of small eruptions will be observed.

Thus the results of the present observation will be explained, without conflicts, by the hypothesis as follows. The increase of the pressure of

magma under the Asama Volcano by the magmaic differentiation, which appears afterwards as the a group of eruptions, causes the deformation of the crust and accordingly the deflection of the clinograph installed at the foot of the mountain, before the commencement of the group of eruptions.

In the case of the Kilauea Volcano, the under-ground pressure will, in the first approximation, be equal to the hydrostatic pressure of the column of the molten lava in the crater, but in the case of Mt. Asama individual feature of the tilt of the crust arround the volcano depends on the velocity of increase and decrease of the pressure under the volcano and also on the condition of the crater bottom of the volcano at the time under consideration.

Detailed elucidation of the phenomena depends largely on the execution of the observations similar with the present one at different places arround the volcano. For this purpose, we are now going to make a observation at Minenotyaya. With the accomplishment of that observation, we hope that we can give a forecast of the commencement of the active period of this volcano, even if we cannot know the magnitude of individual eruptions.

---

3. 淺間山麓に於ける地表傾斜變化の觀測

地震研究所 高 橋 龍 太 郎

火山の噴火に伴つて地殻の變形が生じる事は，有珠火山，櫻島火山，北海道駒ケ岳火山の噴火の場合に，水準測量に依つて確かめられた處である．然し乍ら，此の地殻の變形が火山活動の道程と時間的に如何なる關係を以て起るものであらうか，と言ふ疑問に對して吾人の知識は餘り豐富ではない．此の觀測は此の問題を明にする爲と，更に出來れば火山活動の機巧を覗ふ爲に企てられたものである．

觀測に用ひられた器械は熔融水晶製の石本式傾斜計である．觀測場所は淺間山の西南麓なる小諸町の郊外，純水館靈種會社の冷藏地下室である．觀測上の實際の仕事は小諸補習學校の大井一夫氏を煩はした．又噴火記事に就て內堀定市氏の報告に據るものが多い．著者は此處に上記靈種會社と大井氏內堀氏とに深謝の意を表する次第である．

觀測の結果は第二圖に於て見られる．同圖に於ては同時に，噴火回數と追分測候所觀測の火山性微動の回數を擧げてある．圖に於て E. W. N. S の文字で曲線が其の字の側に偏れた事に依つて，其字の表す方向へ地面が傾いた事を示す．

圖から見られる如く，(1) 噴火は群を爲して起り，概して群の先頭に大きな噴火が起る樣である．

(2) 火山性微動の回數は大體に於て噴火と並行してゐる樣に見える. (3) 噴火群の起る五六日前から地殻の傾斜變化が起る. 而して最初の噴火か又は其の少しく前に傾斜變化の方向は反對になり, 其の後に續く噴火と共に原狀に復する. 噴火前の傾斜の方向は北西であつて噴火時の傾斜の方向は南東になる. 此の樣の例は六月四日, 六月二十四日, 六月二十八日, 七月三日, 七月二十九日等に始まる噴火群の前後に見られる. (4) 噴火を爲しつゝ西北に傾き引續いて東南に傾く場合がある. 例へば七月九日以後の噴火群である. 此の樣の場合には餘り大きな噴火は起らぬ樣である.

此等の噴火と傾斜變化の關係は次の樣の考で說明出來る. 卽ち, 岩漿の分漿作用によつて岩漿内の壓力が次第に高くなつて來ると, 地殻が押上げられて地表の傾斜變化が起る. 而して噴火群と共に壓力の減少を來し, 從つて地殻は元に復する. 殆も餅を燒く時に吾人が屢〻經驗する現象の大規模なものであると考へられる. 但し傾斜の方向が, 山の方向, 又は其の反對方向に向はずして, 之と直角の方向へ向く事は恐らく觀測所の附近の局部的地殻構造によるものと考へられる.

且又噴火群中の個々の噴火の大小等は其の時々の活動勢力の蓄積と其の消失の速さ, 火口底の狀態等に因つて定まるものであらう.

4. *Measurement of a Land-creep in Wakayama Prefecture.*

By Fuyuhiko KISHINOUYE,

Seismological Institute.

(Read Sept. 20, 1932.—Received Dec. 20, 1932.)

Introduction.

An area of about forty thousand square metres in Syôbata, Higasi-Nogami, Wakayama Prefecture, was found creeping down towards the River Nogami, a tributary of the Kinokawa (River). The land-creep was already described elaborately by T. Iwanisi,[1] so here a brief information will be given.

The creeping area lie on diluvial terrace covered with soil, and at the southern part of it there stand houses along a road (Figs 1, 2, 3 and

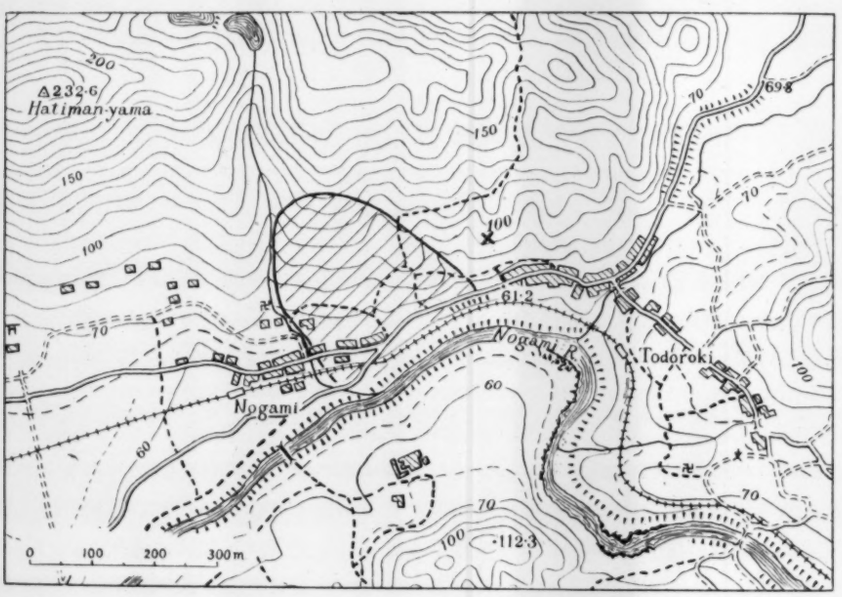

Fig. 1. Topographical map of the creeping area and its environment, (hatched area indicates deduced creeping area and cross the stating point of the closed traverse).

1) T. IWANISI, *Disin*, 2 (1930), 632, (in Japanese).

4). Outcrops of chlorite schist are seen without east and west sides of the district. In the creeping area the rocks under the soil are badly decomposed (Fig. 5), and the surface is cultivated mostly as mulberry-fields. The plane of the field gradually sinks and undulates, but no cracks were noticed except small fissures found under a floor of a house. Many houses in the creeping area inclined southward, and some stone walls swell out by the stress due to the deformation of the land. A well in the field was drained its water, and its section formally round deformed to oblong as shown in Fig. 6. Owing to the local subsidence a drain of the village along the road do not flow well, and the water stands at the middle of the drain in the area. So the drain is said to be repaired nearly every three years. The distance between the surface of the standing water of the drain and the plane of the road gradually changes, and it shows a result of a levelling carried out by Nature.

Measurement with a Theodolite of the Land-Creep.

The deformation of the land due to the land-creep was measured by comparison between results of the traverse surveys carried out in 1931 and 1932 with a theodolite and its attachments. The results of the comparison provisionally obtained are given below.

The Zeiss's Theodolite II. was used for the survey, because it is handy and can be used easilly by a few men. The instrument is supplied with vertical and horizontal circles which are divided into 0·5 grade throughout. The vertical circle is connected with an alidade bubble, sensitiveness of which is 30 sec. per 2 mm.

The writer decided his mind to survey the area by a method of closed traverse with the theodolite. Before the survey was carried out, fifteen surveying stations had been placed on the area early in April 1931 as shown in Fig. 7. The station No. 2 is the starting point of the traverse, and it was set in the surface of the schist which is thought as the base rock of the area and does not creep. The mark of these stations is a cross engraved on a round bolt head 2·2 cm. in diameter, and the bolt head is embedded in a concrete block. The block

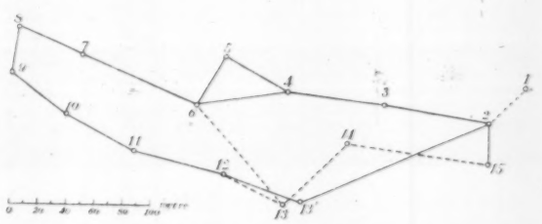

Fig. 7. Stations and routes of traverse (dotted lines surveyed only 1931).

was moulded in a shape of frustrum of triangular pyramid and buried in the ground. Or in other case, the bolt head is set in the rock and fastened with cement mortar.

The distances between stations were measured by the subtense method with the theodolite fitted with a tangential micrometer, and a horizontal distance staff.

Before the results of the survey are described, it is necessary to decide upon the standard of accurracy and the permissible errors which are justified by the local circumstances. The difference of micrometer readings of the staff points, say n_1-n_2, gives the horizontal distance between instrument and staff by following formula,

$$d=k\frac{L}{n_1-n_2},$$

where d is the distance, L the length of the staff in metre, and k a constant of the micrometer. For the instrument, the value of k is given as 20000. Then the equation of linear errors is found by

$$\frac{\Delta d}{d}=-\frac{\Delta n}{n_1-n_2}.$$

The staff 3 m. long was used in general. But the distance between station No. 2 and No. 15 was measured with another staff 1 m. long. Now putting 300 for the value of L in the above equation, the permissible error of the horizontal distance is calculated under following assumptions: $n_1-n_2=8400$ ($d=7138$ cm.) and $\Delta n=5$. Then

$$\Delta d=4{\cdot}25 \text{ cm.}$$

For this instrument, the value of $\Delta n/(n_1-n_2)$ is estimated to be less than 1/1000 by experiences, so the result has a error not exceeding 10 cm. An accuracy of such degree is sufficient for this study, for the displacement of the land is estimated as 10 cm. for a year by natives.

In the next, the precision of height will be discussed. The measurement of angles is more accurate in this case than that of lengths. Its closing difference was 1/100 grade at the first survey, in another expression 32.4 seconds of angle. At the second survey the measurement was done better, and angles closed just at the starting point. Errors of height measurement are calculated by the deviation of vertical angles multiplied by the distances between two stations. Then the permissible error would not exceed 1 cm., when the angular deviation is less than 1/100 grade and the distance assumed as 100 m.

M. Matuyama[2] measured land movements in the Kwansai District also with a theodolite. He put a Wild's Theodolite, which is more precise than the instrument used by the present writer, at two trigonometrical points set up by the Imperial Land Survey. Positions of signals erected on the land were determined at two or more times, and the displacements of signals were obtained by a graphical method. The accuracy of the survey is less than several milimetres for horizontal distances and 1–2 cm. for vertical. For other examples, land-creeps occurred in Niigata Prefecture were described by K. Nakamura.[3] According to his paper, the maximum displacement of the land from 1928 till 1930 amounted to 35 cm. But method and accuracy of the measurement are not stated in his paper. Then in regard to the accuracy, the measurement made by the writer would not be so worse as the above examples.

The positions of stations were determined with reference to several trigonometrical stations, and these positions and routes of the traverse are shown in Fig. 7. At the second survey made in July 1932, the position of the station No. 1 was not measured because the leaves of trees were so thick around the station that the signal of the station could not be sighted from the other stations. The stations Nos. 13 and 14 were removed out of the previous places, so omitted also at the second time. The former one was seen from the station No. 6 at the first survey, and the upper and the lower routes of the traverse were connected at there to check the result. Though the station mark No. 13 was put again near the old place as No. 13′ in Fig. 7, there are no stations on the two branches of the route which can be seen each other.

Comparison of First and Second Surveys.

The station No. 2 was put as the starting point of the traverse, and at the same time as the origin of rectangular coordinates which were determined referring to several triangular points. The signs of the coordinates are determined by two conventions:

(i) x-coordinates are considered as $\frac{+}{-}$ according as the point is $\frac{\text{east}}{\text{west}}$ of the origin.

2) M. Matsuyama, *Tikyû*, **17** (1932), 323, (in Japanese).

3) K. Nakamura, *Journ. Geol. Soc.*, Tokyo, **37** (1929), 411, and **38** (1930), 25, (in Japanese).

(ii) y-coordinates are considered as $\frac{+}{-}$ as according as the point is $\frac{\text{north}}{\text{south}}$ of the origin.

The horizontal distances between every stations were not changed within the allowable limit of errors of the subtence method. Then displacements of stations are to be found only with regards to changes of angles, for the accurracy of angles is greater than that of lengths in this case.

The distribution of the differences between the old and the new angles are systematic. It would seem that there have been no earth movements at the stations Nos. 2, 3 and 4, azimuths of which did not change. One of these stations, No. 2, is on the bed rock, so their positions would not be affected by the land-creep. Stations Nos. 8 and 9 which are also on the rock would not have change their positions.

Under the above-stated suppositions, and moreover assuming horizontal distances between two consecutive azimuth stations are not affected by the creep, displacements of the points Nos. 5, 6 and 7 are calculated. The calculated results are given in Table I.

Table I.

No. of station	Δx	Δy	Δz	Δr
	m	m	m	m
5	0·129	0·258	0·027	0·289
6	0·057	0 251	0·014	0·254
7	0·003	0·045	0·002	0·045

Δx, Δy and Δz represent three components of the displacements, and $\Delta r = \sqrt{\Delta x^2 + \Delta y^2}$.

Next, displacements of stations of lower traverse route, Nos. 10, 11 and 12 are obtained. But Nos. 13 and 14 which were removed from the old place are ommitted from the calculation. In this case, the positions of the stations Nos. 8 and 9 are assumed unchanged as the above. The station No. 2 is too far to be refered as a fixed point, so errors of the results will be greater of No. 11 than No. 10, and No. 12 than No. 11. The following table gives the results of the calculation. But the accuracy of the results is less than that of the results shown in Table I.

Table II.

No. of station	Δx	Δy	Δz	Δr
	m	m	m	m
10	0·017	0·018	0·009	0·025
11	0·017	0·022	0·000	0·028
12	0·045	0·138	0·010	0·145

The results in Tables I and II are shown graphically in Fig. 8. It is obviously seen that displaced stations went downward in nearly normal direction to contour lines. In other words, the creeping area moved down southward along the slope on which it lays. It is interesting that the topographical features of the area suggests that the contour lines there have been projected southward by the creeping.

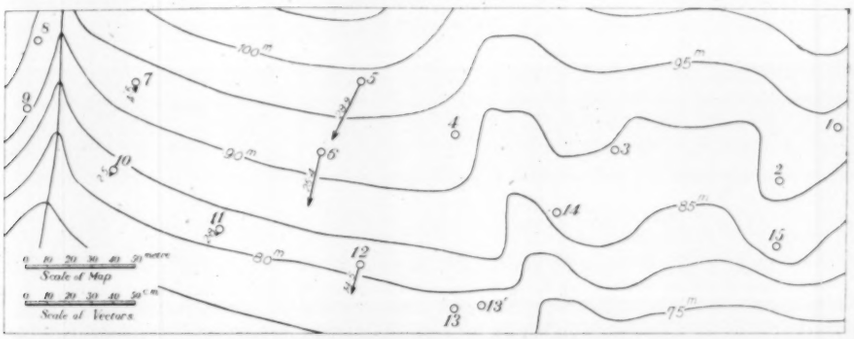

Fig. 8. Changes of positions of stations.

The land-creep was measured by another simple method in a place. Three crosses were marked on the schist across a small stream which runs between the stations Nos. 7 and 8 as shown in Figs. 1. and 8. These marks were put on a straight line in April 1931 (see Fig. 9); two marks, A and B in Fig. 9, are on a block of the rock, and the other, C, is beyond the stream on a different large block which consists eastern bank of the flow. The distance AB is about 91·6 cm., and BC about 51·3 cm. Relative displacement between two blocks was found in July 1932, that the mark C moved about 1·2 cm. northward relatively to the line AB.

Conclusion.

By the above results, the displacement of each station seems to indicate that unstable surface rock and soil creep down towards the

River Nogami. Or considering that the mark C displaced upward, a land block would go downward rotating clockwise around a vertical axis.

There are several land-creeps already known in the vicinity of the present place, and lately since the land-slide occurred in Nov. 1931 at Tôge, Osaka Prefecture, many creeping places[4),5)] were newly found. The distribution of these places is shown in Fig. 10.

Fig. 10. Circles indicate places of land-creep.

The direction of movement of all the land-creeps nearly coincides with that of the inclination of the land. So the gravity will be the main force which causes these creeps. The writer inspected some of these places and found that the rock which was thought lying under the creeping area was decomposed or even broken into fragments. Then it will not be unreasonable to conceive that surface soil and rock lying on broken fragments commence movement such as creeping or sliding by some minute change in the stable condition. But further discussions have to be given by future studies.

In conclusion, the writer expresses his best thanks to Dr. Imamura for his interest in this study, and also Messrs T. Iwanisi, H. Imamura and Z. Kawase for their kind help during the survey. Thanks are also due to the authorities of the Earthquake Research Institute for aids by which he was enabled to measure the land-creep.

4) T. IWANISI, *Disin*, 4 (1932), 163, (in Japanese).

5) S. Yehara reported some of these land-creeps at the meeting of the Geol. Soc. of Tokyo in November 1932. The creeping places seem to be on a tectonic line which was studied geologically by him.

Fig. 2. General view of the creeping area from south across the River Nogami. (Photo. July. 1932)

Fig. 3. The creeping area. (Photo. eastward from near the station No. 8. April, 1931.)

Fig. 4. Photo. eastward from the station No. 9.

Fig. 5. Decomposed chlorite schist.

Fig. 6. A dry well. (Diameter is about 1m., photo. downward.)

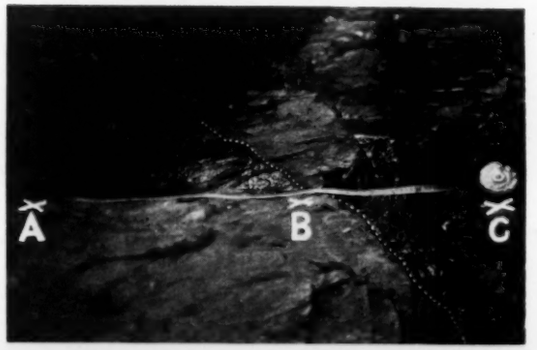

Fig. 7. Three marks curved in the schist. (Photo. by Mr. Iwanisi in 1932)

(震研彙報、第十一號、圖版、岸上)

4. 和歌山縣に於ける土地潛動の測定

地震學教室 岸 上 冬 彦

和歌山縣那賀郡東野上町大字小畑の土地潛動に就いては，既に岩西忠一氏によつて「地震」第二卷（昭和五年）に述べられてゐる．其處を昭和六年四月と昭和七年七月との二回測量して，得られた結果の比較から土地の變動を測つた．第一圖は其の潛動地域の大體の廣さと，其の附近の地形とを示したものである．

潛動地域及び其の附近に豫め十數個の測點を置き，「カール，ツアイス」會社製の經緯儀第二號型を用ひて，閉折線測量を實施した．其等の測點の位置及び測量線路は第七圖に示される．

二回の測量を比較した結果，測點第二，第三，第四，第八，第九，及び第十五は不動と推定され，其の他の測點の變動は第一表，第二表及び第八圖に示されてゐる．併し，第二回目の測量の際には測點第一は其の周圍は草木が繁つて見通しがよく出來なかつた爲，且重要な點ではないので省略し，第十三及び第十四は土地の人によつて取去られた爲に，其等の變動は求められなかつた．併し第十三のみは舊位置に近く，今後の爲に再び据えて置いた．

以上の測量の他に，西側にある谷川を越して，第九圖の如く岩石上に三箇の印 A, B 及び C をつけておいたものが，第二回目の時に見ると C が A, B に對し約 1·2 cm. 北方に移動した．

以上の結果から見ると，潛動地域は大體同高線に直角の方向に辷り落ちてゐる樣であるが，谷川の所では反對の方向に動いてゐるから或ひは一つの地塊が時計の針の動く方向に少し廻轉しながら辷り落ちてゐるのかも知れない．

和歌山縣下には他にも第十圖に示めされてゐる樣に十數箇所の潛動地域が知られてゐる．其等は皆土地の傾斜に沿つて下方に動いてゐる樣である．又此等の基盤をなす岩石が甚しく風化されてゐる樣に見える．若し以上の推測が當つてゐれば，此等の潛動は基盤の支持力が小さくなり，重力によつて辷り落ちると考へられる．併し正確なことは將來の研究によつて知られるであらう．

5. *On Time and Space Distribution of Earthquakes.*

By Seiti YAMAGUTI.

(Received Dec. 20, 1932.)

1. Introduction.

It was already remarked by the seismologists of our country, that the seismic activities in different districts seem to be connected by some statistical law of sequence, that is, the earthquakes are liable to occur in some particular regions immediately following an earthquake in a certain region.

The present investigation was made with the intention of testing this opinion statistically and also of studying the relation between the direction of the apparent "movement"[1] or "transfer" of epicentre and the barometric gradients as well as the other meteorological elements.

It was hoped also that we may obtain by this investigation some hint on the existence and location of the "weak lines" of the earth's crust in our country.

The investigation was made with regard to the earthquakes in the different parts of Japan as well as of the entire world.

The statistical frequencies of time intervals of the successive earthquakes were also investigated and thus the probable "periods" of occurrence were obtained.

2. Methods of Investigations.

1) Kwantô Districts.

From the Abridged Monthly Report of the Central Meteorological Observatory in Japan, the "felt" earthquakes, 2370 in number, were taken, which occurred in Kwantô Districts (Provinces of Iwaki, Suruga, Kai, and a southern part of Sinano included), during the period of 7 years, June, 1924—May, 1931. The epicentres[2] were plotted on a map

1) For convenience's sake, the epicentre is supposed to move from one spot to another to cause the successive earthquakes.

2) The position could only roughly be estimated as the name of the district is only known.

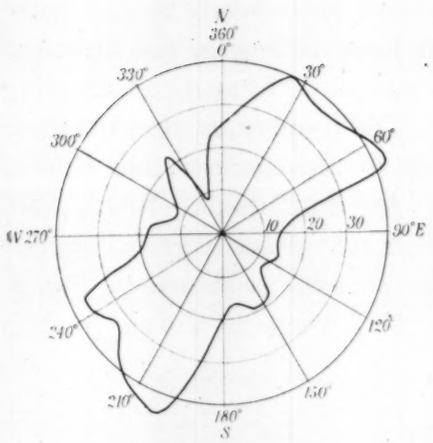

Fig. 1, *a*. Spring.

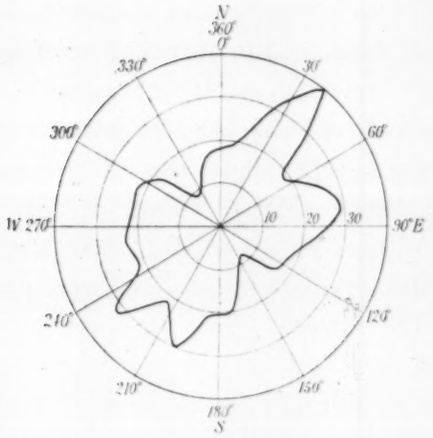

Fig. 1, *b*. Summer.

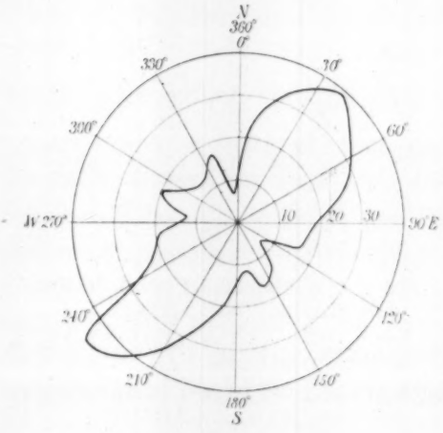

Fig. 1, *c*. Autumn.

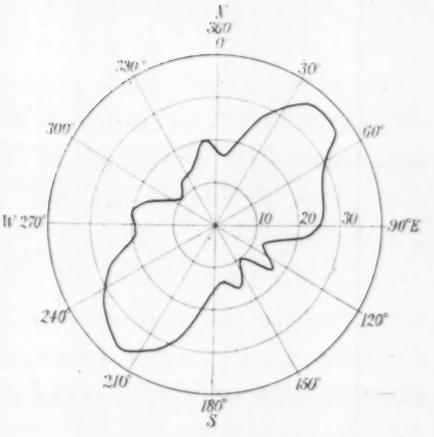

Fig. 1, *d*. Winter.

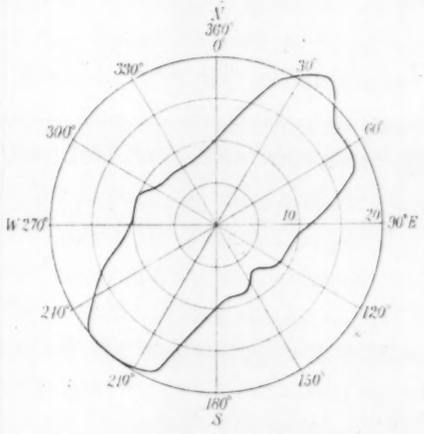

Fig. 1, *e*. Yearly Mean.

for each month and connected by a straight line successively in the order of time. The number, n, of these straight lines, falling in the direction within each sector of azimuth angle 15°, which is formed by dividing all directions into 24 parts, were counted. The number, n, thus obtained were separated into 4 groups, according to the seasons, i.e., Spring (March—May), Summer (June—Aug.), Autumn (Sept.—Nov.), and Winter (Dec.—Feb.), and they were plotted in vector diagrams against the azimuth angle, N-direction being taken as zero, as shown in Fig. 1. The yearly mean diagram for all seasons of 7 years is shown in Fig. 1, *e*.

For 120 "conspicuous" and "rather conspicuous" earthquakes, which occurred in the same districts, during the same period, the azimuthal distribution of the direction of epicentre "transfer" were investigated and plotted in the similar manner, as shown in Fig. 2. In this case, the positions of epicentres are more distinctly known than the former case.

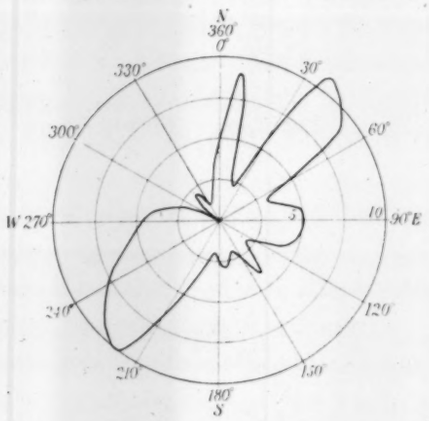

Fig. 2 "Conspicuous" and "rather conspicuous" earthquakes.

Vector diagrams were also drawn which show the characteristics of given districts in the mode of sequence of earthquakes, giving the azimuthal distributions of epicentres of the earthquakes which occurred immediately

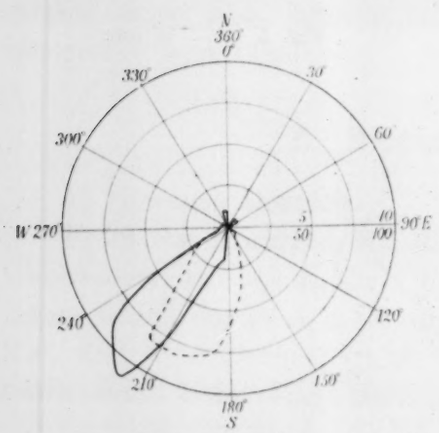

Fig. 3, *a*. Before and After an earthquake at Iwaki.
——"conspicuous" and "rather conspicuous" earthquake.
·····"felt" earthquakes.

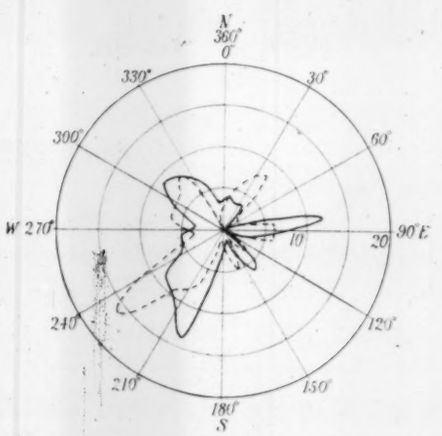

Fig. 3, *b*. "Felt" earthquakes. Kasumigaura.
—— Before
····· After

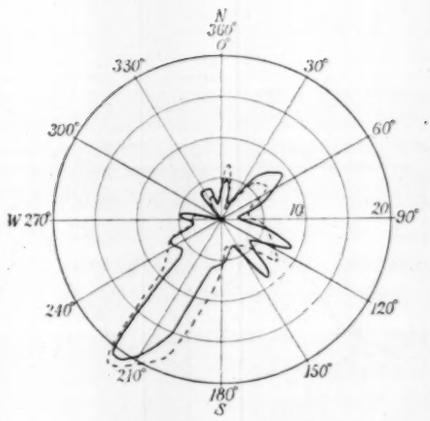

Fig. 3, *c*. "Felt" earthquakes.
Tukuba.
—— Before
------ After

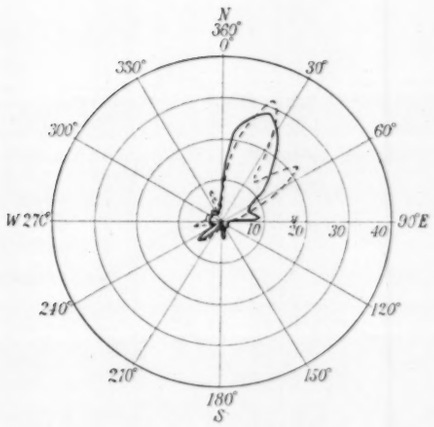

Fig. 3, *d*. "Felt" earthquakes.
Tôkyô.
——After
------ Before

before and after an earthquake in a definite locality, as shown in Fig. 3.

To get a hint of the physical meanings of transfers of epicentres in such directions as shown in the above figures, the number, n, were separated into 12 groups for 12 months, and compared with the directions of pressure gradients at Iwaki, using the results of investigation "On the Relation between the Frequencies of Earthquakes and the Pressure Gradients", by Prof. T. Terada.[3]

The vector diagram for n's were transformed into the corresponding xy-diagrams and arranged as in Fig. 4, *a*, taking the directions of the monthly mean pressure gradients at Iwaki as the respective origins of directions, the error of $\pm 7.^{\circ}5$ being admitted. The similar xy-diagrams are also constructed for the deviations of n from the yearly mean. The results are shown in Fig. 4, *b*, *c*, in which dotted lines on the left-hand quarter are the means of the four quadrants.

Before we may inquire into the physical meaning of the above result, it is necessary to make a calculation regarding the statistical probability of n for the case in which the earthquakes occur quite at random. For this purpose, the whole region were divided into 13 districts according to the usual classification made by the Central Meteorological Observatory, and the following calculation of probability was made.

Let N_K, N_L, ... be the number of earthquakes which occurred at

3) *Journ. Meteorolog. Soc.*, Japan, **28** (1909).

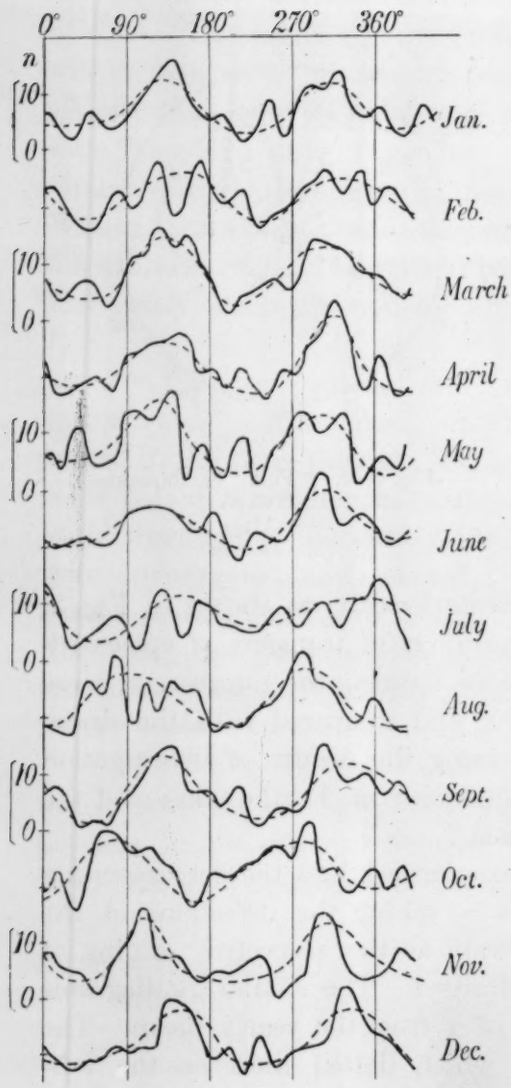

Fig. 4, *a*. *xy*-diagrams for n's, with the directions of the monthly mean presure gredients at Iwaki as the respective origins of directions.

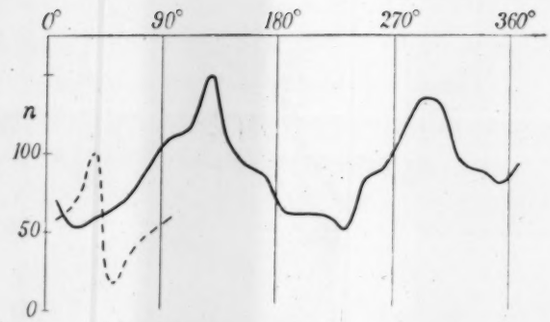

Fig. 4, *b*. Yearly Sum. Broken line shows the mean of the four quadrants.

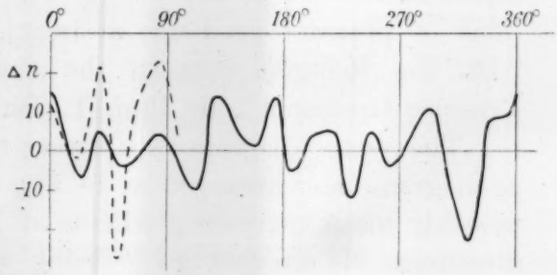

Fig. 4, *c*. Deviation from the yearly mean.

the districts, K, L, ...respectively during the epoch taken, then the probability, P_{KL}, that the earthquakes will occur at the district L, next to K, may be expressed by $P_{KL}=\frac{N_K N_L}{\Sigma\Sigma N_K N_L}$, and the expected number, N', to occur at L, next to K, will be given by $N'=P_{KL}\Sigma N$, where $\Sigma N=2370$. The value of the ratio, r, of the actual number of occurrences, N_0, to the calculated number, N', that is $r=\frac{N_0}{N'}$, were calculated as shown in Table I.

Table I. Kwantô District.

$r>1\cdot3$ and $r<0\cdot6$ are distinguished by different types respectively.

1. Iwaki,
2. Kasimanada,
3. Kasumigaura,
4. Tukuba,
5. Kinugawa,
6. Kuzyûkuri-Oki,
7. Bôsô Hantô,
8. Tôkyô,
9. Simotuke-Koduke,
10. Sagami Wan,
11. Sagami (land),
12. Suruga-Kai,
13. Idu Hantô.

After / Before	1	2	3	4	5	6	7	8	9	10	11	12	13
1	**2·1**	0·91	1·1	0·87	0·97	1·1	0·75	*0·56*	1·0	0·85	1·1	0·65	**1·3**
2	1·0	**1·3**	1·1	0·78	0·92	0·76	0·85	0·96	1·1	1·1	0·87	1·2	0·92
3	1·1	1·2	1·0	1·1	1·2	0·71	1·0	0·63	0·93	0·69	1·1	1·05	1·01
4	0·80	0·72	**1·8**	0·92	0·83	*0·28*	0·77	1·2	**1·7**	1·03	1·1	*0·59*	**1·4**
5	0·87	1·2	0·84	**1·5**	1·2	0·77	0·81	1·1	1·0	0·80	0·64	0·94	*0·59*
6	0·71	1·1	0·64	0·93	0·73	**3·2**	*0·42*	0·77	0·67	**1·6**	**1·3**	0·64	0·95
7	0·87	*0·55*	1·0	0·92	0·85	**1·3**	**2·4**	1·0	1·0	1·1	0·84	*0·43*	0·80
8	1·1	0·96	**1·5**	*0·50*	1·0	0·77	0·87	**1·6**	0·93	0·67	0·86	1·1	*0·50*
9	1·0	1·1	1·1	0·79	**1·4**	*0·47*	0 57	0·79	**2·0**	*0·52*	0·91	1·2	*0·37*
10	0·77	0·93	0·69	0·72	0·75	**1·4**	1·2	1·0	0·72	**4·0**	*0·18*	*0·56*	*0·43*
11	0·93	0·77	1·0	1·2	0·71	0·65	0·71	**1·4**	0·61	*0·53*	**2·4**	**2·6**	0·85
12	*0·56*	1·0	*0·35*	**1·8**	1·1	0·64	**1·4**	0·77	*0·48*	*0·56*	**2·3**	**2·1**	1·2
13	**1·3**	0·77	0·64	0·74	0·82	0·81	0·91	**1·3**	*0·37*	*0·43*	0·64	1·02	**4·4**

The particular pairs of districts which correspond to values of r greater than 1·3, and those less than 0·6, were respectively taken and shown on the maps of Fig. 5, *a*, *b*. The arrows show the order of sequence of earthquakes. Two arrows connecting a pair of districts in opposite senses show that between these two districts the either sense of transfer is probable in Fig. 5, *a*, and improbable in Fig. 5, *b*. A single arrow shows that the transfer in that sense only is so.

Similarly, such pairs of "conspicuous" and "rather conspicuous" earthquakes with $r>1\cdot5$ and $r<0\cdot45$, is shown in Fig. 5, *c*.

Taking the directions of the straight lines, connecting all the possible pairs of the centres of these 13 districts, the vector diagrams for the mean of r in each azimuth, were constructed as shown in Fig. 6.

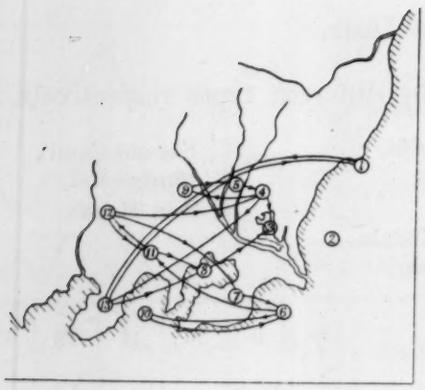

Fig. 5, *a*. Pairs of regions with $r>1{\cdot}3$

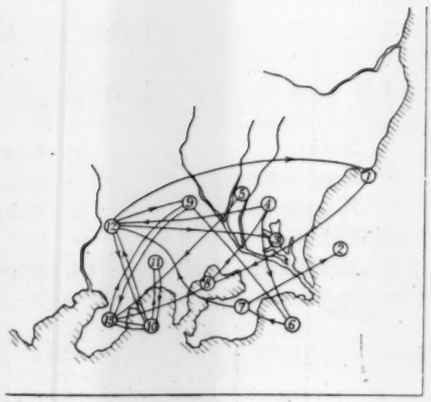

Fig. 5, *b*. Pairs of regions with $r<0{\cdot}6$

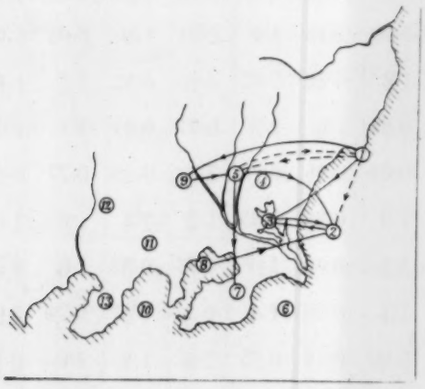

Fig. 5, *c*. "Conspicuous" and "rather conspicuous" earthquakes.
$\longrightarrow$ $r>1{\cdot}5$ $\dashrightarrow$ $r<0{\cdot}45$

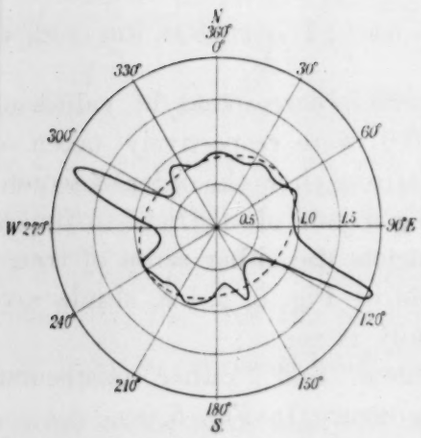

Fig. 6, *a*. Azimuthal mean of r's for all possible combinations.

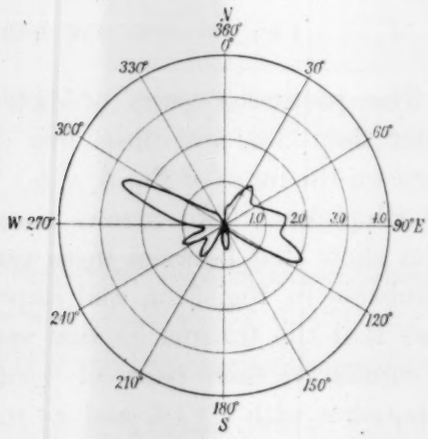

Fig. 6, *b*. Azimuthal means of r's taken for those combinations with $r>1{\cdot}3$ and $r<0{\cdot}6$, excluding the cases $1{\cdot}3>r>0{\cdot}6$.

2) Tôhoku and Hokkaidô.

The "felt" earthquakes, 1410 in number, which occurred during the same period as in the case of Kwantô District above investigated, were taken and similarly treated. In this case, however, the directions of transfer of epicentres were comparatively simple, and seemed to be conveniently separated into two kinds, one of which is N–S direction, and the other E–W direction approximately. For the first kind, we have divided the entire regions into 8 groups according to latitudes i.e., 37°–38°, 38°–39°, ... 43°–44°, and 44°–46°, and calculated the values of $r=\frac{N_0}{N'}$, for each pair of groups, which are shown in Table II.

Table II. Tôhoku and Hokkaidô

1. Near Iwaki (37°–38°*N*)
2. „ Kinkwazan (38–39)
3. „ Miyako (39–40)
4. „ Mabutigawa (40–41)
5. Near Mutu Oki (41–42°*N*)
6. „ Hokkaidô, S. part (42–43)
7. „ „ , mid. (43–44)
8. „ „ , N. (44–46)

Before \ After	1	2	3	4	5	6	7	8
1	**1·4**	**1·4**	0·84	0·86	0·70	0·76	1·0	0·78
2	1·1	1·02	1·1	*0*	0·80	1·0	1·1	1·03
3	0·92	0·65	**1·4**	**1·4**	0·66	0·79	1·15	**1·3**
4	*0·47*	*0*	**1·4**	**5·4**	0·97	**1·3**	*0·58*	*0*
5	0·87	1·2	*0·50*	0·65	**2·1**	0·89	1·04	0·79
6	0·95	0·80	0·97	*0·53*	0·93	**1·6**	0·78	1·16
7	0·84	1·17	1·1	0·77	1·1	0·84	1·2	*0·53*
8	**1·3**	*0*	0·87	**1·9**	**1·3**	1·0	*0·32*	**5·2**

For the second kind of epicentre transfer, we have counted the number, *J*, of the transfer of epicentres in E→W or W→E direction, remaining in nearly the same latitude, for every month of 7 years, and investigated, in which month the value of *J* is relatively great. On the other hand, the corresponding monthly barometric pressure gradients towards north and towards east, were calculated from the data for Sapporo, Isinomaki, Nemuro, and Niigata, respectively, and compared with *J*. No sensible correlation could be found between them. Next, the number of tracks of cyclones for every month traversing these regions

were taken from the Abridged Monthly Report of the Central Meteorological Observatory in Japan, and compared with J in the following manner.

The values of J and the number of tracks of cyclones were respectively plotted side by side against the same time axis. A certain tendency of parallelism is observed between two curves.[4]

Taking J and the number of tracks as ordinate and abscissa respectively, xy-diagram was plotted (Fig. 7, a). We have imagined that some better correlation may be revealed between J and number of cyclones, if we take J in the limitted region near Hokkaidô, with greater latitude than 42°, and a corresponding diagram was also drawn for this region alone (Fig. 7, b).

Taking, instead of J, the ratio, r', of J to the total number of earthquakes, N, for each month which occurred in the whole region, an xy-diagram was similarly drawn (Fig. 7, c). In these diagrams, curved lines are constructed by connecting the mean point of each y corresponding to each x, and the ellipse in the last diagram is drawn by inspection so as to contain all points properly.

For the last diagram, the similar method of analysis was applied as explained in the previous paper[5], and obtained the percentage values of $a=43$, $b=25$, $c=28$, $d=4$, showing a predominance of positive correlation.

We have also calculated the correlation coefficient, c, of r' with respect to the number of tracks of cyclones, applying the ordinary

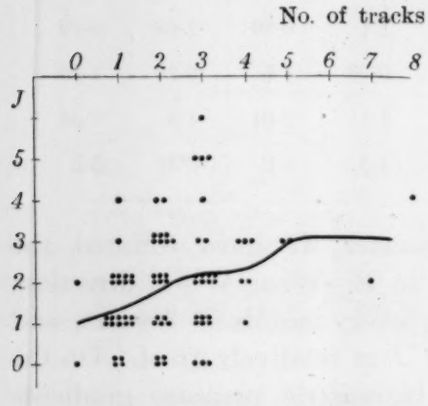

Fig. 7, a. Whole region (37°–46°N).

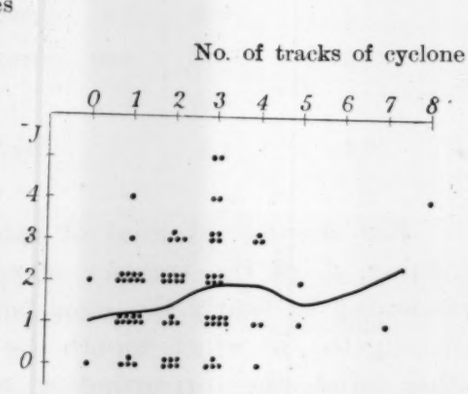

Fig. 7, b. Near Hokkaidô (>42°N).

4) Curves here omitted.

5) S. YAMAGUTI, *Bull. Earthq. Res. Inst.*, 10 (1932), 36.

formula, $c=\frac{\Sigma\xi_k\eta_k}{\sqrt{\Sigma\xi_k^2\Sigma\eta_k^2}}$, where $k=1,2,\ldots.$ 84, and obtained 0.47 for its value. The results may suggest the possible existence of such an effect of cyclone.

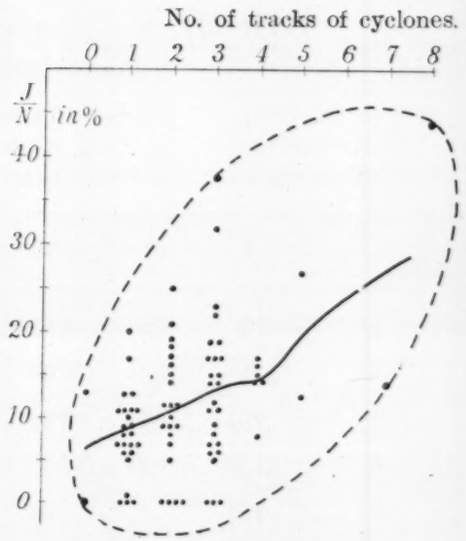

Fig. 7, *c*. Whole region.

3) All Parts in Japan.

a) The "conspicuous" and "rather conspicuous" earthquakes, 370 in number, which occurred in Japan, during the period of 7 years (June, 1924—May, 1931), were taken from the Abridged Monthly Report and investigated with regard to their mode of sequence from one group of latitude to another, in the similar manner as before. Corea was excluded for obvious reason.

Table III, *a*. "Conspicuous" and "rather conspicuous" earthquakes in Japan taken from Kisyô Yôran.

1. 22°–26°*N* 3. 32°–34°*N* 5. 35°–36°*N* 7. 37°–38°*N* 9. 40°–42°*N*
2. 26 –32 4. 34 –35 6. 36 –37 8. 38 –40 10. 42 –45

After / Before	1	2	3	4	5	6	7	8	9	10
1	**3·3**	0	0·91	0·53	0·81	0·98	*0*	0·59	0·57	**2·1**
2	0	0	0	**2·5**	0·62	*0·38*	**0**	**2·8**	**2·0**	**1·7**
3	**1·4**	1·1	1·2	0·87	0·91	1·0	1·0	1·0	**1·4**	0·29
4	1·05	1·25	0·87	**2·5**	0·77	0·94	*0·38*	1·1	0·83	1·03
5	1·1	0·62	*0·45*	1·02	**2·4**	*0·58*	1·2	*0·29*	**1·4**	*0·18*
6	0·78	0·95	1·2	*0·38*	0·68	**1·6**	**1·6**	*0·21*	*0·52*	**1·3**
7	0·80	**1·8**	1·0	1·15	**1·4**	**1·3**	0·86	**1·3**	*0·20*	0·77
8	*0*	**1·4**	1·0	*0*	1·2	0·85	**2·6**	**3·1**	*0·31*	*0·38*
9	*0·57*	**1·3**	**1·4**	**1·4**	*0·56*	*0·52*	*0·41*	*0·31*	**2·4**	**1·3**
10	1·1	0·83	1·2	0·69	*0·35*	1·02	**1·3**	**2·3**	*0·56*	**1·4**

b) The "destructive" earthquakes, 315 in number, which occured

Table III, b. "Destructive" earthquakes in Japan taken from Rikwa-Nenpyô.

1. Tyôsen.
2. Taiwan
3. Kyûsyû
4. Sikoku-Tyûgoku
5. Kinki
6. Nôbi-Hokuroku
7. Kwantô
8. Tôhoku (37°–40°N)
9. Mutu-Hokkaidô

Before \ After	1	2	3	4	5	6	7	8	9
1	2·9	*0·26*	0·61	0·42	0·84	*0·22*	1·1	0·88	*0·35*
2	0	2·9	0·95	2·7	0·68	1·1	0·91	*0·56*	1·1
3	0·91	1·4	3·3	1·5	0·79	0·83	*0·21*	0·67	1·2
4	*0·42*	1·33	1·5	2·2	*0·37*	2·4	*0·59*	0·45	1·8
5	0·99	*0*	1·05	*0*	2·6	0·99	0·79	0·77	*0·3*
6	*0·44*	1·8	0·83	0·59	0·59	2·5	0·95	1·2	*0*
7	0·67	0·73	0·83	2·1	0·79	*0·48*	1·4	1·1	1·2
8	1·05	1·1	0·67	*0*	0·77	0·73	0·99	1·7	1·5
9	*0·35*	1·1	0·62	0	0·3	1·4	1·4	1·1	2·9

in Japan during the period from 27 A.D. to 1931, were taken from Rikwa-Nenpyô (the Scientific chronological Table), and similarly treated as before. In this latter case, however, all regions were divided into 9 parts, those are, Tyôsen, Taiwan, Kyûsyû, Sikoku-Tyûgoku, Kinki, Nôbi-Hokuroku, Kwantô, Tôhoku, and Mutu-Hokkaidô.

The results for these two cases are shown in Table III, *a*, *b*.

Among such cases with $r<0{\cdot}6$, those, which have too small expected number, N′, are to be disregarded in discussions of the results.

4) All Parts of the World.

The Great Earthquakes, 420 in number, which occurred in different parts of the world, during the period of 31 years, 1900—1931, were taken from Rikwa-Nenpyô, and they were classified into 8 groups according to the geographical regions of occurrence: those are, the Coast of the Mediterranean Sea, Continent of Asia, Japan, the Philippines with neighbouring oceanic regions, Australia including the oceanic environments, North America, Central America, and South America, and similarly treated as before. The results are shown in Table 4, *a*, and in Fig. 8, *a*, *b*. In this case, the probability, P, that the earthquakes will occur at any three regions J, K, L, successively, was also calculated

by $P=\dfrac{N_J N_K N_L}{\sum_J \sum_K \sum_L N_J N_K N_L}$ and the expected number, $N'=P\Sigma N$, and the values of the ratio, $r=\dfrac{N_0}{N'}$, were calculated for about three hundred combinations. The particular combinations of 3 regions which correspond to $r>4$, $4>r>3$, and $3>r>2$, where $N_0>3$, were taken out as shown in following Table IV, *b*.

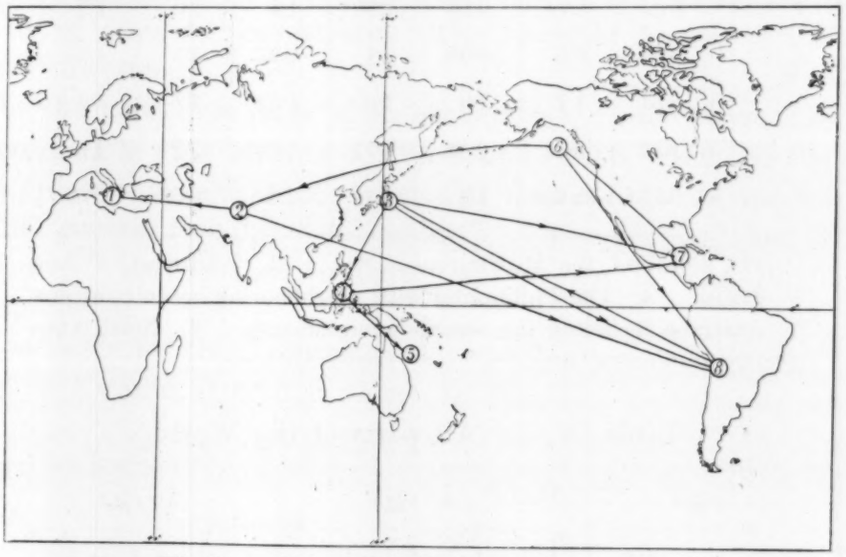

Fig 8, *a*. Pairs of earthguakes with $r>1{\cdot}25$.

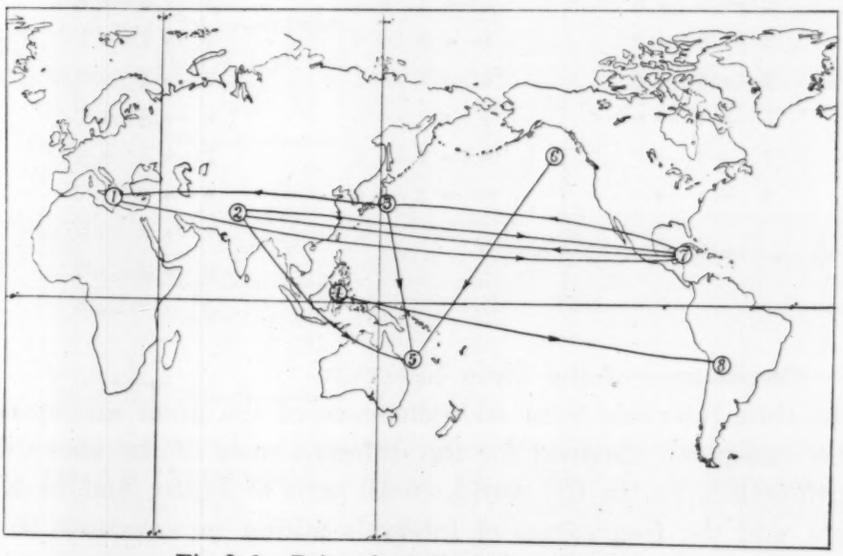

Fig 8, *b*. Pairs of earthquakes with $r<0{\cdot}6$.

Table IV, *a*. All Parts of the World.

After / Before	1	2	3	4	5	6	7	8
1	1·8	9·4	1·03	1·2	1·2	*0·37*	*0·16*	0·73
2	1·3	2·34	1·2	0·63	*0·53*	0·85	*0·37*	1·3
3	*0·59*	1·0	0·66	1·65	*0·53*	*0·33*	1·3	1·64
4	0·89	0·76	0·83	0·90	1·6	1·0	1·3	*0·49*
5	0·94	0·8	0·95	1·1	0·92	1·1	1·15	1·05
6	*0·37*	1·7	1·0	1·0	*0·54*	1·7	1·1	1·3
7	1·13	*0·55*	*0·58*	0·77	1·03	2·2	1·6	0·90
8	0·73	0·625	1·8	0·74	1·2	0·83	0·90	1·02

1. The Coast of the Mediterranean Sea. 2. Continent of Asia. 3. Japan. 4. The Philippines with neighbouring oceanic regions. 5. Australia including the oceanic environments. 6. North America. 7. Central America. 8. South America.

Table IV, *b*. All parts of the World.

$r \geqq 4$	$4 > r \geqq 3$	$3 > r \geqq 2$
2 → 1 → 2	1 → 3 → 4	1 → 4 → 4
2 → 2 → 2	2 → 8 → 5	1 → 5 → 7
2 → 2 → 8	3 → 4 → 1	3 → 4 → 8
3 → 8 → 2	4 → 6 → 4	4 → 1 → 1
8 → 3 → 8	4 → 7 → 1	5 → 5 → 5
5 → 4 → 6	5 → 4 → 5	5 → 8 → 7
7 → 7 → 7	5 → 2 → 2	7 → 3 → 4
8 → 1 → 1	8 → 5 → 8	4 → 3 → 7
		7 → 5 → 3
		8 → 3 → 4
		8 → 7 → 5

5) Frequencies of the Time Intervals.

The time intervals from an occurrence of the great earthquakes to the next one, were obtained for the different cases of the above data of the earthquakes, i.e. in the world, in all parts of Japan, and in Kwantô Districts, and the frequencies of intervals falling in successive 10 or 100 days, respectively, were counted and plotted as ordinates, the days of

the intervals being taken as abscissa. The general trend of these curves shows the random occurrence of the earthquakes. We have calculated the frequencies, f, for purely random occurrence, assuming, $f=ae^{-bt}$, and obtained the deviations of the actual frequencies from these theoretical values of f, which are shown in Fig. 9, *a*, *b*, for the Great Earthquakes in the World. In order to ensure that the periodicity of the deviation curve is not due to the apparent one proper to any accidental phenomena[6], we have also tried to take the half intervals, or the overlapping intervals of days for comparison. The essential feature of the curves remained the same.

For the particular pairs of the earthquakes, in the above three cases, corresponding to $r>1\cdot25$, $r>1\cdot4$, $r>1\cdot6$, and $r<0\cdot6$, which are the results in the previous investigation, the similar treatments were applied.

The curves for the "destructive", "conspicuous" and "rather conspicuous" earthquakes in Japan are shown in Fig. 10, 11, and 12, respectively.

The curve for the "conspicuous" and "rather conspicuous" earthquakes in Kwantô District is shown in Fig. 13.

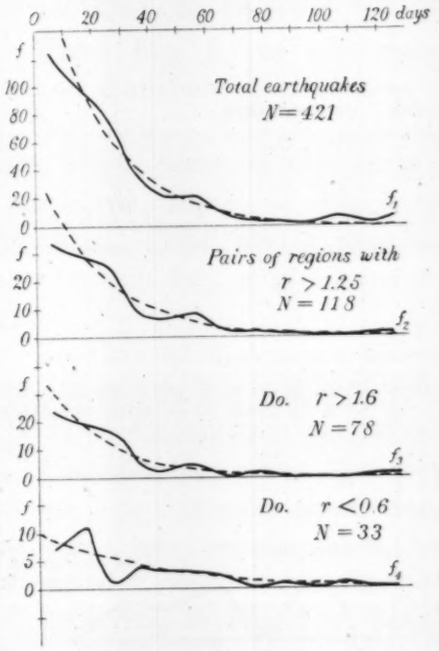

Fig. 9, *a*. In the world.
——actual curve.
·····theoretical curve.

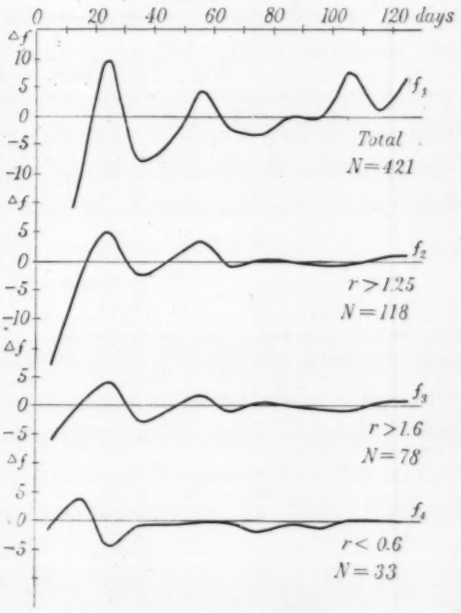

Fig. 9, *b*. In the world.
Deviation curves of frequency.

6) T. Terada, *Proc. Tôkyô Physico-Math. Soc.*, [2], 8 (1916).

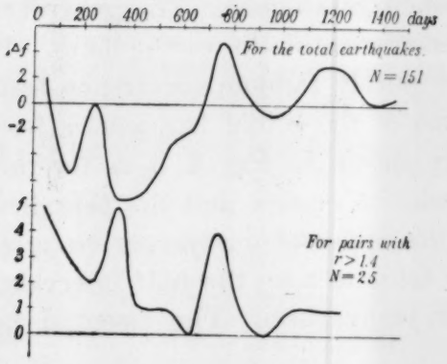

Fig. 10. Japan. "Destructive" earthquakes.

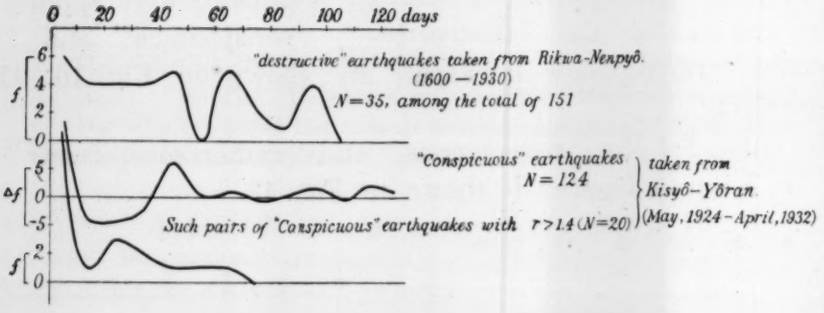

Fig. 11. Japan. "Conspicuous" earthquakes.

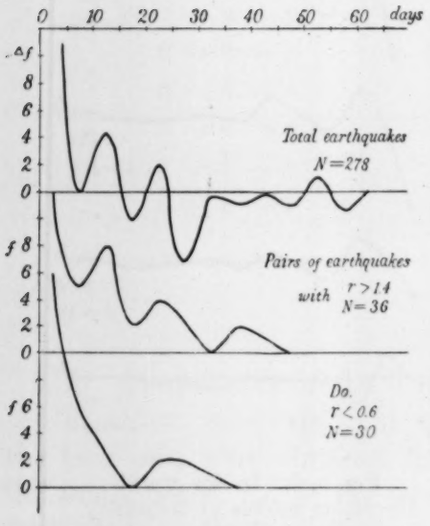

Fig. 12, *a*. Japan. "Rather conspicuous" earthquakes.

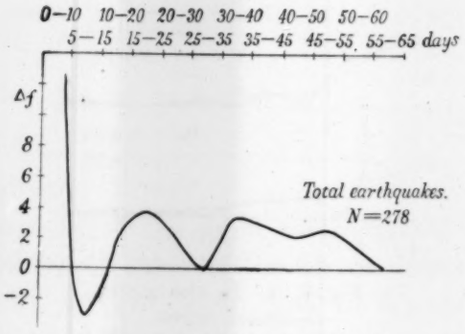

Fig. 12, *b*. Do. Overlapping intervals.

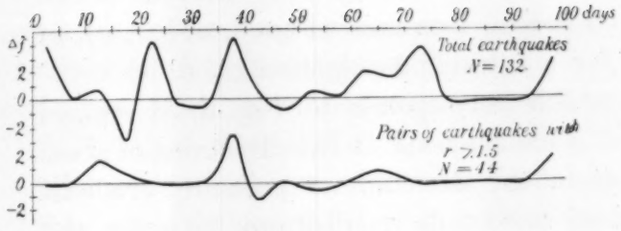

Fig 13. Kwantô.
"Conspicuous" and "rather conspicuous" earthquakes.

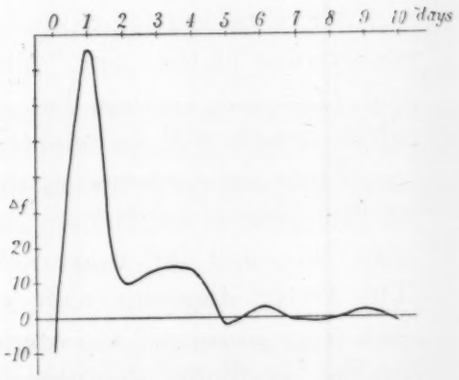

Fig. 14. "Felt" earthquakes in Kwantô Districts (May, 1925—April, 1928)
$N=573$

In the case of Kwantô Districts, the similar investigation was made for the "felt" earthquakes also, successive one day intervals being taken here, which result is shown in Fig. 14.

3. Results and Discussions.

1) Kwantô Districts.

From Fig. 1, we can recognize some seasonal variations in the mode of transfers of epicentres, which may probably be connected with the barometric pressure gradients. If we take the annual mean of 7 years, above seasonal variations entirely vanish, and the diagram forms a smoothed ellipse, of which the major axis runs from NE to SW directions. The vector diagram for winter resembles to this yearly mean, which fact might have some physical meanings to be still investigated.

Looking at the curves showing the deviation from the yearly mean, opposite trends are observed between the curves for spring and summer, as well as for autumn and winter.

The diagram (Fig. 2) for the "conspicuous" and "rather conspicuous" earthquakes shows somewhat different features compared with that for "felt" earthquakes, i. e. the protuberances in NE, SW and northward directions are sharply defined.

Referring to Fig. 3, *a*, before and after the earthquakes in the Sea off Iwaki, there is a large probability of finding the "felt" earthquakes in SSW-direction, and the "conspicuous" and "rather conspicuous" earthquakes, in SW-direction.

Many interesting features are observed regarding probabilities of occurrences of the next "felt" earthquakes in different azimuth before and after the earthquakes at different localities (Fig. 3, *a*, *b*, *c*, *d*), of which details will be reserved for a future investigation.

From the vector diagram which corresponds to Fig. 4, it seemed at first glance, as if there exist some maxima at the directions of about zero, 45°, and 90° measured from the direction of pressure gradient. The vector diagrams were transformed into xy-diagram to make this fact more apparent, the angle being taken in clockwise sense, as shown in Fig. 4. Form the mean of the four quadrants of the yearly sum curve, given by broken curve, we can see the distinct maximum somewhere near 45°, which may correspond to the direction of maximum shearing stress in the earth crust due to the pressure gradient (Fig. 4, *b*). The yearly sum curve for the deviations from eilipse (yearly mean) above cited, has shown maxima of curve at about 0°, 45°, and 90°. The maxima at 0°, and 90° may mean that a tangential or normal stress upon a preexisting fissure may call forth a succession of earthquakes along that fissure line. It is interesting to observe that the pressure gradient at Tôhoku has given the better results than that at Tôkyô. The comparison of pressure gradient with the "conspicuous" and "rather conspicuous" earthquakes is omitted here, the number of cases being too scanty for this purpose.

From Table I and Fig. 5, *a*, *b*, we may be able to remark as to the "felt" earthquakes, the followings:—

a) The earthquake is most probable to occur once more immediately in the same district when an earthquake occurs in a certain district.

b) The earthquakes are liable to occur at Idu next to Iwaki, and vice versa.

c) The following combinations of districts have large probability of epicentral transfer ($r>1\cdot7$):
Tukuba → Kasumigaura, Tukuba → Simotuke-Koduke-Nisimusasi, and Suruga-Kai-Minamisinano → Tukuba.

d) Two combinations of districts such as, Tyôsi-Kuzyûkuri-Oki and the Sagami Bay, as well as Sagami (land) and Suruga-Kai-Minamisinano, have large probability of epicentral transfer to and from each other.

e) After an earthquake in Tôkyô and the Tôkyô Bay, Kasumigaura has a large probability of occurrence of the next earthquake, and it is 3 times as large as that at Tukuba, which is situated very near to Kasumigaura, while on the contrary, after the earthquakes in Suruga-

Kai-Minamisinano, Tukuba has 5 times as large probability than Kasumigaura.

f) After an earthquake at Tukuba, the next one occurs very rarely off Kuzyûkuri ($r=0\cdot28$).

g) Such combinations as, Off Kuzûykuri→Bôsô Peninsula, Bôsô Peninsula → Suruga-Kai-Minamisinano, and Tukuba → Suruga-Kai-Minamisinano, habe very small probability of epicentral transfers, and they are only one third of those for the reverse directions.

h) Sagami Bay seems to be indifferent toward Sagami (land), Idu, and Suruga-Kai-Minamisinano as for the occurrence of "felt" earthquakes, as well as Idu towards Simotuke-Kôduke-Nisimusasi.

i) If we connect the pairs of districts with large probability of epicentral transfer in due order of succession, we may be able to draw the following two loops:—

Tukuba→Simotuke-Kôduke-Nisimusasi→Kinugawa→Tukuba.

Off Kuzyûkuri→Sagami (land)→Suruga-Kai-Minamisinano→Bôsô Peninsula→Off Kuzyûkuri.

j) Kasimanada earthquakes occur very frequently in succession with an earthquake in different districts both before and after the latter, except only that the earthquakes at Kasimanada very rarely occur next to Bôsô Peninsula.

As for the "conspicuous" and "rather conspicuous" earthquakes, (Fig. 5, *c*) the following tendencies are observed though the total number of earthquakes taken is only 126.

a) Next to a "conspicuous" and "rather conspicuous" earthquake at Iwaki, either Kasumigaura or Simotuke-Kôduke-Nisimusasi is very liable to have such an earthquake, while Kasimanada has little chance to have such one, which results are also to be seen in Fig. 3.

b) Kasimanada has large values of probability of occurrence of such an earthquake immediately after Tôkyô, Kasumigaura, or Kinugawa.

c) Iwaki and Kinugawa are indifferent toward each other, as for the occurrence of earthquakes.

On the diagram of the mean r (Fig. 6, *a*), we can draw an ellipse, major axis of which is inclined about 50° from north. Besides, the graph has conspicuous maxima in the directions WNW and ESE. On the other hand, the azimuthal mean of r's, such as $r>1\cdot3$ and $r<0\cdot6$, (Fig. 6, *b*), gives somewhat similar diagram as the former.

2) Tôhoku and Hokkaidô.

From Table II, we may be able to remark the followings :—

a) An earthquake in a certain district is liable to be followed by another in the same district.

b) After an earthquake in North Hokkaidô (>44°N), another is liable to occur near Iwaki, but such rarely occurs near Kinkwazan (38°–39°N), in spite of the neighbouring situation.

c) From North Hokkaidô to near Mabutigawa (40°–41°N), and from Mabutigawa to South Hokkaidô (42°–43°N), the transfer of epicentres frequently occurs, but it is seldom that the transfer occurs in the reversed directions.

d) The regions near Mabutigawa and near Miyako (39°–40°N) are closely connected with each other as regards the transfer of epicentres.

e) It is interesting to observe that the regions, North Hokkaidô and Central Hokkaidô (43°–44°N) are indifferent to each other as for the occurrence of earthquakes. The regions, near Mabutigawa and near Kinkwazan are also independent with each other.

3) All Parts in Japan.

From Table III, *a*, *b*, we can remark the followings :—

a) An earthquake is liable to be followed by another in the same district.

b) If we connect different district in chain, choosing the pairs with large r's>1·4, we obtain the following cycle or half-cycle for the "conspicuous" and "rather conspicuous" earthquakes and for the "destructive" earthquakes, respectively : Taiwan→Hokkaidô→Sanriku →Iwaki→Kwantô→Mutu→Sikoku-Kyûsyû→Taiwan.

Tôhoku→Hokkaidô→Kwantô→Sikoku-Tyûgoku→Nôbi-Hokuroku→ Taiwan→Sikoku-Tyûgoku.

Of course, this does not mean that the actual sequence of earthquakes occurs in this order, but that each successive pair of districts in this chain shows frequent connection in the temporal sequence of earthquakes.

c) Near Kinugawa and Iwaki are indifferent towards Mutu as for the occurrence of the "conspicuous" and "rather conspicuous" earthquakes, and also Taiwan and Nôbi-Hokuroku towards Tyôsen for the "destructive" earthquakes.

d) There is irreversibility of the directions of transfer of epicentres between Kwantô and Mutu for the "conspicuous" and "rather cons-

picuous" earthquakes, as well as Kwantô and Sikoku-Tyûgoku for the "destructive" earthquakes.

4) All Parts of the World.

From Table IV, and Fig. 8, *a*, *b*, we may be able to remark the followings:—

a) Among 8 regions, the Coast of the Mediterranean Sea and Continent of Asia, of which the boundary was assumed to be the line of longitude 50°, or Caspian Sea, as well as North America and Central America have large probability of occurrence of two earthquakes in succession in the same region while Japan has the least value of this probability ($r=0\cdot66$).
The rest of these regions have normal values of this probability.

b) From Continent of Asia, epicentres are liable to be transfered towards South America, but not to Central America. A similar relation holds for the cases, from Japan to the Philippines ($r=1\cdot65$), and to Australia ($r=0\cdot53$).

c) Epicentres are liable to be transfered in the direction such as to cross over the Pacific Ocean from Asiatic side to American side and also to travel about the Pacific Coast in counter-clockwise sense. Above all, Japan and South America seem to be intimately connected with each other as for the sequence of occurrence of earthquakes both before and after one another ($r=1\cdot64$ and $r=1\cdot80$), which may be considered to verify the result of the preceding paper[7] that an earthquake seems to be liable to induce another in the antipodal region.

d) It is of rare occurrence that the transfer of epicentre cross over the Atlantic Ocean.

e) For the transfer, Asia→South America, we have $r=1\cdot25$.

Investigations were also made as regards the probabilities that earthquakes occur in three regions in a definite sequence one after another. We can say yet nothing definite in this respect, as the data are still too scanty for this purpose.

5) Frequencies of the Time Intervals.

The frequency curve of the time intervals of the Great Earthquakes in the world seem to show a period of 27·5 days. The same period

7) S. Yamaguti, *loc. cit.*, 5).

is obtained whether we choose 5 days or 10 days for the division of the time axis of the curve. This period seems to correspond to the period of rotation of the sun, 27·3 days, relative to the earth. In Fig. 9, *a*, the theoretical frequency curves, for random distribution, $f=ae^{-bt}$, are calculated, and in Fig. 9, *b*, the deviation curves are drawn.

The intervals of successive two earthquakes were classified into different groups according to the combinations of the two epicentral regions. The value of r for each pair of regions was assigned. Next, those pairs were picked up for which $r>1{\cdot}25$, and the frequency curve as well as the deviation curve were constructed for these earthquakes only as shown in the curve f_2 in Fig. 9, *a*, and *b*. The number of the cases taken is given there by N. Similarly f_3, f_4, were obtained for $r>1{\cdot}6$, and $r<0{\cdot}6$ respectively.

It is interesting to observe that the curves for large values of $r>1{\cdot}25$ ($N=118$), are parallel to those for the total earthquakes (f_1, $N=421$) while on the contrary, the curves for small r ($r<0{\cdot}6$, $N=33$), show a different course compared with the former.

The "destructive" earthquakes in Japan, taken from Rikwa-Nenpyô for which $r>1{\cdot}4$, ($N=25$ among the total of 151), during the period of 330 years (1600–1930), show the period of 363 and 727 days, which correspond to one year. The curves for the total number of earthquakes show the opposite course in the interval from 150 to 650 days and the parallel course in the interval over 650 days, compared with the above case (Fig. 10).

"Conspicuous" earthquakes taken from Kisyô-Yôran, during the period of 8 years (May, 1924–April, 1932) show the periods of about 45, 65 and 95 days, which are also observed as the secondary periods in the case of "destructive" earthquakes taken from Rikwa-Nenpyô above cited, while the particular groups for $r>1{\cdot}4$ ($N=20$) of the former earthquakes, show a somewhat opposite course (Fig. 11).

"Rather conspicuous" earthquakes in Japan, taken from Kisyô-Yôran, which occurred during the same period as above, show the periods of about 20, 38 and 53 days, (Fig 12, *a*), which are obtained either we divide the time axis by 5 days or overlapping 10 days interval. The maximum at about 13 days which is seen in Fig. 12, *a*, vanishes when the overlapping intervals of the time axis are taken as shown in Fig. 12, *b*.

For the "conspicuous" and "rather conspicuous" earthquakes in Kwantô Districts (May, 1924–April, 1932), the periods of about 23 and 38 days are seen from the deviation curves for the successive intervals

of 5 days, as well as for the overlapping intervals of 10 days as shown in Fig. 13.

For the "felt" earthquakes in Kwantô Districts (May, 1924—April, 1932), the remarkable maximum of frequencies of occurrence takes place at 1 day (i. e. 12 hours-36 hours), and moreover, three maxima at about 3, 6 and 9 days (Fig. 14). The period of 9 days is also seen from the curve for the Great Earthquakes in the World, when we take 5 days for the division of the time axis.

In conclusion, I wish to express my best thanks to Prof. T. Terada under whose supervision the entire work has been carried out and who has given me many useful suggestions throughout the course of my investigation.

---

5. 地震の時間的及び空間的分布に就いて

山　口　生　知

或る場所に一つの地震が起ると，或る特定の場所に引續いて地震が起り易いと云ふ事が，日本の地震學者に依つて既に述べられて居る．

本研究は此の說を統計的に確むべく，又所謂震源移動の方向と，氣壓勾配との間の關係を，調査する目的で行はれた．

それから又，この研究に依つて我國に於ける地殼の斷層線の存在及び位置を，見出す手懸ともならんことを望んだ．

又この研究は日本の各地に於ける地震に就いてのみならず，全世界の地震に就いても同樣に調査を進めた．

相次いで起る地震の間の，時間的間隔の統計的頻度に就いても，同樣の研究を進めて，地震の起り得べき週期を求めて見た．

其結果は關東方面に於いては，東北より南西の方向に所謂震源の移動の起り易いこと，及び震源移動の方向と，氣壓勾配との間には密接なる關係の有ることを發見した．

卽ち磐城に於ける氣壓勾配の方向を基線として 0°, 45°, 及び 90° の方向に震源が最も移り易いことを知つた．

この 0° 及び 90° の方向は，切線應力及び垂直應力の方向に相當するので，豫め地殼の割目が存在するとすれば，此の割目の線に沿ふて地震の誘發を見るかも知れない．

又 45° の方向は剪斷應力の最大なる方向に相當するものと考へられる．

關東方面に於ける有感覺地震に就いて，一つの面白い事柄と思はれることは東京地方に地震が有

ると續いて霞ケ浦に地震の起る確率が非常に大きく，しかも霞ケ浦と接近して居る筑波に於いて地震の起ることに比較して，約三倍の値を持つて居ると云ふこと，及び之に反して駿河，甲斐地方に地震が有ると其の次には筑波に於いて起る可能性が大きく，霞ケ浦に於けるものゝ約五倍の値を持つて居ると云ふことである．

次に東北方面に於いて，震源が略々同一緯度内にて東西に移動することと，此の地方の區域に現はるゝ低氣壓の數との間には正の相關關係有ることを知り，其の相關係數として 0·47 と云ふ値を得た．

世界地震に就いては震源が亞細亞側より，亞米利加側に太平洋を，横斷する如き方向に移動する場合が多く，又太平洋岸を時計の針と反對の方向に移る場合が多い．

就中，日本と南米とは地震が互に相前後して起ることに關し密接な關係のあることを知り，「或る地點に起る地震は，地球上之と對蹠的位置にある地點の地震を誘導する」と云ふ前論文（本邦地震と世界各地地震の頻度間に存する統計的關係）の結果を一層明瞭に確めることが出來た．

尙世界地震に就いて，時間的分布を調べた結果 27·5 日と云ふ週期を得た．之は恐らく地球に對する太陽の自轉の週期 27·3 日に相當するものと考へられる．

日本に於ける破壞的地震に就いては 363 日及び 727 日と云ふ約一年及び其の倍數に相當する週期を得た．

又關東地方全部の有感覺地震に就いては一日（12 時間—36 時間）と云ふ著しい週期の存在することを知つた．（第十四圖參照）．

6. *Observations of Near Earthquakes on Mt. Tukuba with an Ishimoto Acceleration Seismograph.*

By Win INOUYE,

Earthquake Research Institute.

(Read Oct. 18, 1932.—Received Dec. 20, 1932.)

1. Instruments.

A pair of Ishimoto acceleration seismographs[1] was installed at our station on March 10, this year, and has been working ever since in the constant observation of near earthquakes.

The constants of the instruments are as follows.

Component	Own period	Weight of the heavy bob	Sensitivity
E-W	0·114 sec.	15·3 kg	1 mm—1·77 gal
N-S	0·114 sec.	15·3 kg	1 mm—1·69 gal

Sensitivity in the above table means a deflection of 1 mm on the record correspoding to the acceleration of the ground. But the sensitivity of the instrument depends upon the ratio of the oscillation period of the ground to the period of the instrument itself. If this ratio is somewhat large, (say >2), the sensitivity of the instrument is constant for all values of the oscillation period of the ground. This is the sensitivity that is shown in the above table.

An example of calibration of the instrument, or the curve representing the extent to which the sensitivity of the instrument depends on the periods of the forced oscillations, is shown in Fig. 1.

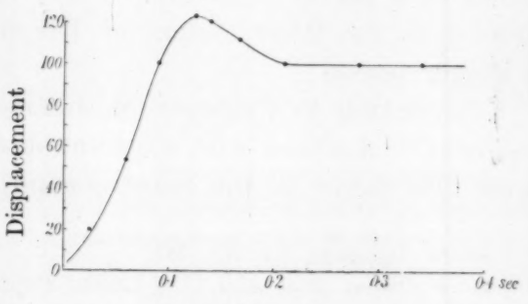

Fig. 1.

The sensitivity of the instrument moreover depens upon the damping of the instrument, so

1) M. ISHIMOTO, *Bull. Earthq. Res. Inst.*, 9 (1931), 316.

that the damper had constantly to be adjusted in order to modify the viscosity of the oil to keep the instrument under the same condition as shown in the figure.

To the auther's regrets, it was found in observing earthquakes with these acceleration seismographs that the periods of the ground motions, which consist in the main of acceleration, were generally shorter than the periods of the instruments themselves. The instrument is very sensitive to such short period vibrations, that is, readily affected by the period of the vibrations. For these reasons the instruments were frequently calibrated by a simple apparatus, designed to apply forces of varying frequency to the heavy bobs of both instruments by a rubber band stretched between the heavy bob and an eccentric point on a massive wheel which is controlled by hand. Every effort was made to keep the instruments under the same conditions throughout the period of investigation. Nevertheless, the results, particularly those concerning the magnitudes of the acceleration of the earthquakes obtained by these instruments, may contain some uncertainties. At any rate, it is very desirable to use instruments whose own periods are very much shorter than the periods of the seismic waves. We must bear in mind however that the sensitivity of an acceleration seismograph[2] is proportional to the square of its own period, so that the sensitivity diminishes rapidly as the period of the instrument becomes shorter.

2. The Periods of Earthquake Waves.

Authorities like the late Prof. F. Omori,[3] the late Prof. K. Suyehiro,[4] and Professor A. Imamura[5] agree that the dilluvial ground about Hongô, a part of the hilly district of Tôkyô, has a mode of free oscillation of a period of about 0·3 sec. They also showed that the alluvial ground in the lower section of Tôkyô has a mode of free oscillation of a longer period.

According to Professor M. Ishimoto,[6] the earthquake periods most frequently observed with acceleration seismographs at Hongô and Marunouti (the latter in the lower section) are 0·3 sec. and 0·6 sec. respecti-

2) M. ISHIMOTO, *loc. cit.*, 317.
3) F. OMORI, *Bull. E. I. C.*, **2** (1908), *Pub. E. I. C.*, **11** (1902), **13** (1903).
4) K. SUYEHIRO, *Bull. Earthq. Res. Inst.*, **7** (1929).
5) A. IMAMURA, *Bull. Earthq. Res. Inst.*, **7** (1929).
6) M. ISHIMOTO, *Bull. Earthq. Res. Inst.*, **10** (1932), 171.

vely. At Hongô, the period of acceleration of the ground motion is not constant throughout an earthquake, but lengthens as the earthquake continues, being about 0·2～0·3 sec. in the preliminary portion and about 0·3～0·4 sec. in the principal portion of an earthquake.[7] This suggests that the ground about Hongô is subject to free oscillations, somewhat resembling the longitudinal and transverse vibrations of a bar, during the preliminary and the principal portion of an earthquake. Moreover, it was observed by an ordinary seismometer that, at Hongô and Maruno-uti, the energetic portion of the movements of near earthquakes had the

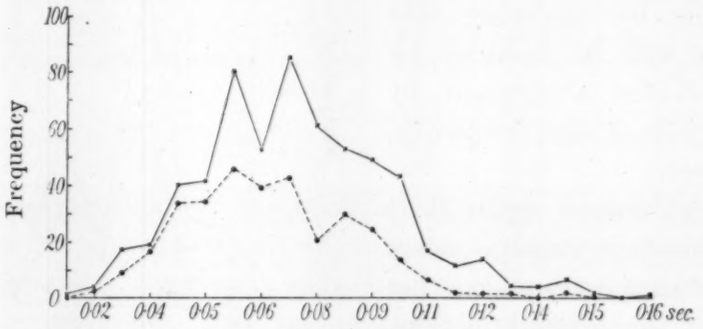

Fig. 2. The frequency distribution of the periods of waves in the earthquake of April 12, 1932.
● represent that of P-phase.
× represent that of S-phase.

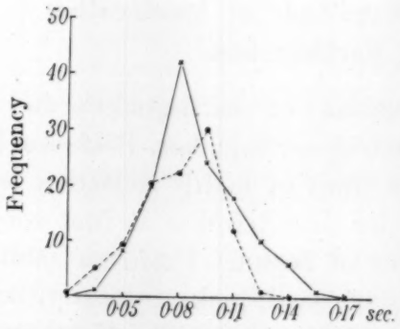

Fig. 3. The frequency distribution of the periods of waves in the earthquake of June 16, 1932.
● represent that of P-phase.
× represent that of S-phase.

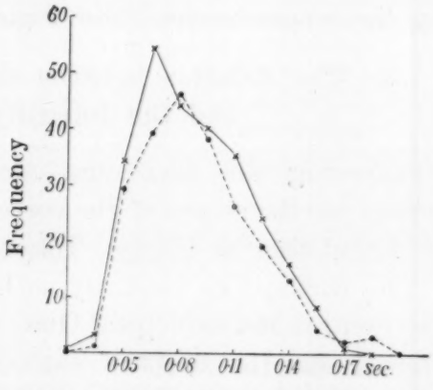

Fig. 4. The frequency distribution of the periods of waves in the earthquake of June 28, 1932.
● represent that of P-phase.
× represent that of S-phase.

7) M. Ishimoto, *Bull. Earthq. Res. Inst.*, **9** (1931), 480.

same period as that of the acceleration of those earthquakes.

Next, the frequency distributions of the periods of waves in some of the near earthquakes observed by acceleration seismographs at Mt. Tukuba are shown in Figs. 2, 3 and 4. As will be seen in these figures, the maximums in these frequency curves are at about 0·08 sec. in both the preliminary and principal portions of the earthquakes.

At Mt. Tukuba we heard earth-sounds[8] in most of the felt earthquakes and even in unfelt earthquakes of near origin, which is understandable by assuming that sound waves will be induced by refraction into the atmosphere by earthquake waves of high frequency, as above shown.

In this mountain again it is observed with ordinary seismometers in the case of near earthquakes that the period of the ground motions is about 0·16 sec., which is twice that of the acceleration of earthquakes. Waves with a period of 0·08 sec. are observed as ripples among the longer waves. See Fig. 5.

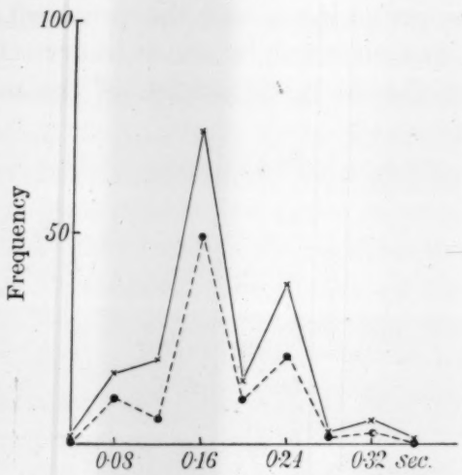

Fig. 5. The frequency distribution of the periods of waves in near earthquakes observed with an ordinary seismometer.
● represent that of P-phase.
× represent that of S-phase.

3. The Relation between the Magnitude of Acceleration and the Intensity of Earthquakes.

Comparing the maximum accelerations of earthquakes and the intensities to the senses of the corresponding earthquakes, Professor Ishimoto[9] found that at Hongô, Tôkyô, the limit of bodily sensation is 0·5 gal. The earthquake intensity scale under consideration is that adopted by the Central Meteorological Observatory of Japan. Professor Ishimoto also found that the limit of each scale of earthquake intensity, or acceleration is just 4 times that of the one that precedes it. He moreover found that Weber-Fechner's law of sensation, which is that the sensation increases in arithmetical progression as the stimulus increas s in algebraical progression, applies here.

8) F. OMORI, *Pub. E. I. C.*, **22** A (1908), 1.
9) M. ISHIMOTO, *Bull. Earthq. Res. Inst.*, **10** (1932), 614.

The relation between the magnitudes of maximum acceleration and the numbers in the intensity scale of near earthquakes at Mt. Tukuba is shown in Fig. 6. As will be seen in the figure, at Mt. Tukuba the shaking of the ground by an earthquake is noticed only when the

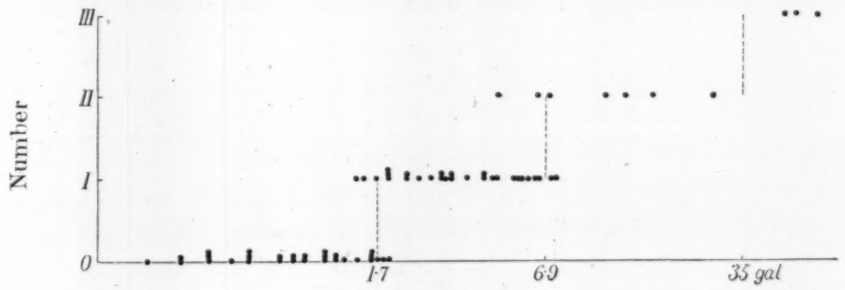

Fig. 6.

maximum acceleration of the motion is greater than 1·7 gal. We also notice that the magnitude of acceleration defining the number in the scale of intensities becomes nearly as much as four times that of the number that precedes it as the number advances.

For reference, the magnitudes of acceleration for each grade of the intensity scale at Mt. Tukuba and at Hongô, Tôkyô, are shown in the following table.

Intensity	Acceleration of Earthquakes	
	at Mt. Tukuba	at Hongô, Tôkyô
0	0~1·7 gal	0~ 0·5 gal
I	1·7~6·9	0·5~ 2·0
II	6·9~35	2·0~ 8·0
III	35~ —	8·0~32·0

Not long ago the late Professor Suyehiro[10] determined by experiment the minimum accelerations of oscillations of various period which are felt by the unaided senses.

The results obtained by him and also those obtained at Hongô and at Mt. Tukuba are plotted on the same figure, as shown in Fig. 7.

The late Professor Omori[11] obtained 1·7 gal as the mean of the

10) K. Suyehiro, *Proc. Imp. Acad.*, **5** (1929), 411.

11) F. Omori, *Pub. E. I. C.*, **11** (1902), 60.

lowest intensities felt of earthquakes, from seismometrical observations at several places in Tôkyô. With these data, the author studied the law governing the dependence of the limit of sensibility to earthquakes upon the periods of earthquake waves. The results are shown in Fig. 8.

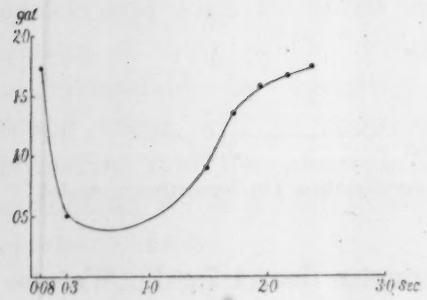

Fig. 7. Minimum accelerations of oscillations of various period which are felt by the unaided senses.

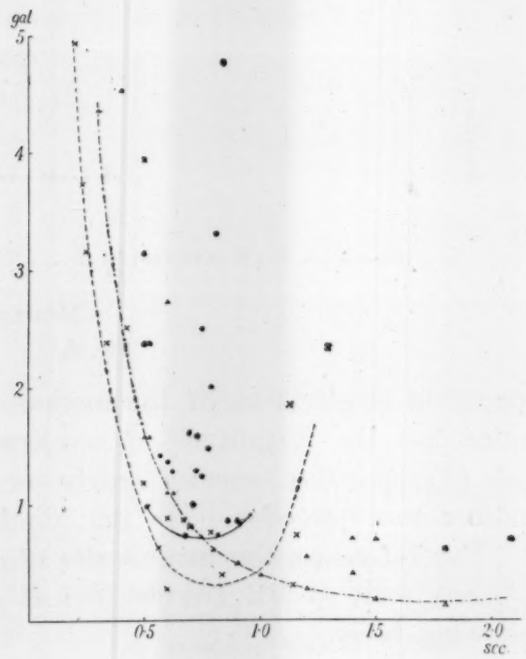

Fig. 8. × Hongô.
△ Central meteo. Obs.
● Hitotubasi.

As will be seen from these figures, the curve representing variations in the sensibilities to earthquakes according to the periods of the seismic waves, is the resonance curve of a pendulum with a period of slightly less than 1 sec., inverted.

4. Echoes or Internal Reflections of Seismic Waves.

From bodily sensation of earthquakes, it seems that the ground movements undergo somewhat periodic increase and decrease in their intensities several times.

As a matter of fact, in most of the records obtained by acceleration sesimographs at various places we can observe in several places the common phenomenon of repetitions of a periodic rise and fall of amplitudes of seismic waves, forming wave groups.

The mean periods of the wave groups for each of the two phases of earthquakes in three different localities are shown in the following table.

Locality	The mean period of the wave groups	
	in P-phase	in S-phase
Mt. Tukuba	0·80 sec.	0·97 sec.
Hongô, Tôkyô	2·8	3·1
Marunouti, Tôkyô	3·2	3·4

On the other hand, if we consider the frequency distributions of the periods of the wave groups at Mt. Tukuba, we shall find that the most frequent ones are 0·6 sec. in the P-phases and 1·0 sec. in the S-phases, so that the latter is 1·67 times larger than the former. See Fig. 9.

For earthquakes at the foot of Mt. Tukuba, the records obtained by acceleration seismographs are quite simple, consisting of a few wave groups in each phase, as will be seen in Figs. 16, 17, 18 and 21.

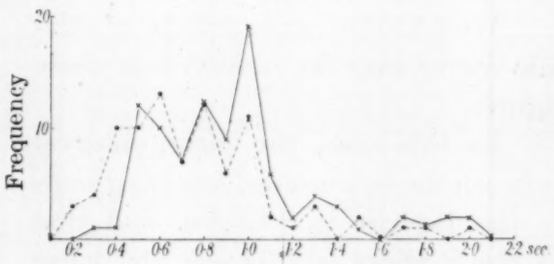

Fig. 9. The frequency distribution of the periods of the wave groups at Mt. Tukuba.
● represent that of P-phase.
× represent that of S-phase.

The durations of the main part of each of the two phases of earthquakes in the above cases are tabulated below.

Date of earthquake	Duration of the main part of the earthquake				The ratio T_2/T_1	
	in P-phase (T_1) (E-W),	(N-S)	in S-phase (T_2) (E-W),	(N-S)	(E-W),	(N-S)
April 9, 1932	1·38 sec	1·27 sec	2·43 sec	2·65 sec	1·76	2·08
April 21	0·69	0·64	0·95	1·06	1·38	1·66
May 20	1·22	——	2·02	——	1·66	——
June 22	——	0·90	——	1·54	——	1·70
June 23	0·54	——	0·85	——	1·58	——
June 28	0·95	0·95	1·59	1·59	1·67	1·67
July 1	0·74	0·85	1·27	1·27	1·72	1·49
July 5	0·85	1·06	1·38	1·70	1·62	1·60
Sept. 19	0·85		1·38	——	1·62	——
Sept. 24	1·17	0·85	2·22	1·59	1·90	1·87
Mean	$T_1 = 0·92$		$T_2 = 1·59$		$T_2/T_1 = 1·69$	

As will be seen in the table, the S-phase has a longer duration than the P-phase in the ratio 1·69.

We made a seismic wave analyser with a proper period of 0·09 sec. and a damping factor $v=a_1/a_2=2$, after the pattern of Suyehiro's seismic wave analysers, the instrument having been set up to record the NW-SE component of earthquakes. It is shown in Fig. 14.

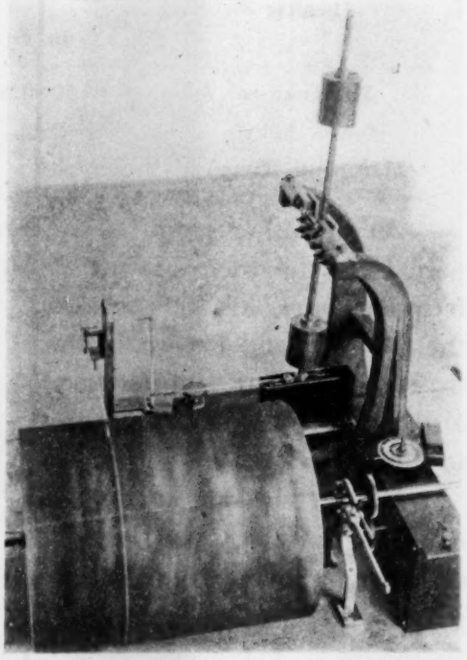

Fig. 14. A seismic wave analyser with a proper period of 0·09 sec.

Some examples of records obtained with this instrument are shown in Figs. 15, 17, 18, 19 and 20.

Well-defined wave groups of seismic waves may be observed in these figures.

In this case, the mean interval between the two successive wave groups in the P-phase is 0·82 sec. and that in the S-phase is 1·34 sec., the latter being longer than the former by as much as 1·72 in the mean. Moreover, in cases of near earthquakes at the foot of Mt. Tukuba, the mean duration of the main parts of the P-phases is 1·19 sec. (T_1) and that of the S-phases 2·01 sec. (T_2), and the mean ratio $T_2/T_1=1·69$.

As just stated, according to the results of observations made with acceleration seismographs and a seismic wave analyser at Mt. Tukuba, we know that an earthquake consists of many wave groups, the periods of these wave groups being different for the two phases of earthquake, those in the S-phase being longer than those in the P-phase by as smuch as nearly 1·69.

According to Professor K. Sezawa's[12] mathematical investigations, the period of the echoes of seismic waves at the boundaries of a layer of thickness H is expressed by the formula

$$T=2H/V,$$

where T is the period and V is the velocity of the seismic waves.

By writing the periods of wave groups in the P-phase and in the

12) K. SEZAWA, *Bull. Earthq. Res. Inst.*, **10** (1932), 1.

S-phase T_1 and T_2 respectively, they are expressed by the following formulae.

$$T_1=2H/V_1, \text{ and } T_2=2H/V_2,$$

where V_1 and V_2 are the velocities of the waves in the P-phase and in the S-phase. Consequently

$$T_2/T_1=V_1/V_2.$$

According to Professor Imamura, the velocities of seismic waves in the Kwantô district are as follows.

Layer	V_1	V_2	V_1/V_2
Upper Layer	5·0 km/sec	3·15 km/sec	1·59
Second Layer	6·1	3·70	1·65
Bottom Medium	7·5	4·45	1·69

As the ratio T_2/T_1 works out to 1·69 from our observations at Mt. Tukuba, it is highly probable that the wave groups of seismic waves are due to the echoes or multiple reflections at the boundaries of a layer in the earth's crust. The Poisson's ratio of this layer may be about 0·23.

As the mean period of the wave groups is about 0·7 sec. in the S-phase, and about 1·2 sec, in the S-phase, the thickness of the layer is about 2 km if we assume that the velocity of the dilatational waves in the layer is 5·0 km/sec.

According to observations made by the late Professor Suyehiro[13] with his seismic wave analysers at Hongô, Tôkyô, the analyser with a proper period of 0·3 sec. resonated many times with the wave groups of seismic waves. Since in this case, the magnifications of the instruments were small, they were only sensible to the S-phases in most of the earthquakes observed.

The frequency distribution of the intervals between the two successive wave groups in the records of earthquakes obtain ed by the 0·3 sec. analyser is shown in Fig. 10. The figure shows two frequency maxima

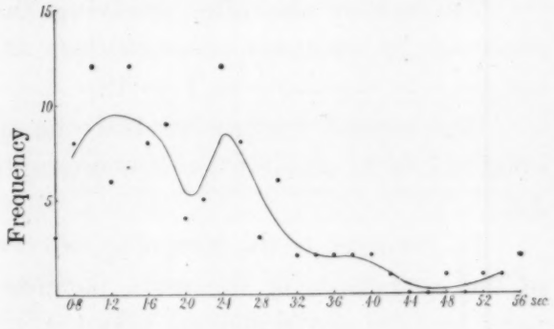

Fig. 10.

13) K. Suyehiro, *loc. cit.*

at 1·2 sec. and 2·4 sec.

It seems to the author that they are due to multiple reflections at the boundaries of two layers in the earth's crust, each having a thickness of several kms.

Moreover, in his paper on the seismic observations at Hongô with his acceleration seismograph Professor Ishimoto[14] noticed that solitary waves appeared repeatedly with a period of about five or six seconds, which he explained as multiple reflections at the boundaries of a surface layer.

It may be added that at Mt. Tukuba we heard earth-sounds when the earthquakes were near, especially at the P-phases. In the case of earthquakes at the foot of Mt. Tukuba, which earthquakes consisted of quite simple wave groups as will be seen in Figs. 17 and 18., we heard simple sounds like "boom," "boom, boom" (very short). On the other hand, in the case of an earthquake with many wave groups, as is shown in Fig. 15., we always notice rumbling noises like those of distant thunder.

5. The Scattering of Seismic Waves.

The late Professor F. Omori[15] studied the ratio of the magnitude of maximum amplitude of the principal portion to that of the preliminary tremor with respect to the focal distance of the earthquakes observed at Mt. Tukuba. Some of his data are plotted in Fig. 11. As will be seen in the figure, the S-phases were several times larger than the P-phases in their amplitudes, and the ratios increased as the focal distances decreased.

The author also after studying the same subject with earthquakes observed by ordinary seismometers at Mt. Tukuba, obtained identical results. It is shown in Fig. 12.

The author further studied the question of ratio, using the data obtained with acceleration seismographs. The result is shown in Fig. 13.

In contrast to the foregoing, we notice that, in the figure, the ratios of the magnitude of the main portions of earthquakes to their preliminary tremors are dispersed about a mean value of 3·5, independent of

14) M. ISHIMOTO, *loc. cit.*
15) F. OMORI, *loc. cit.*

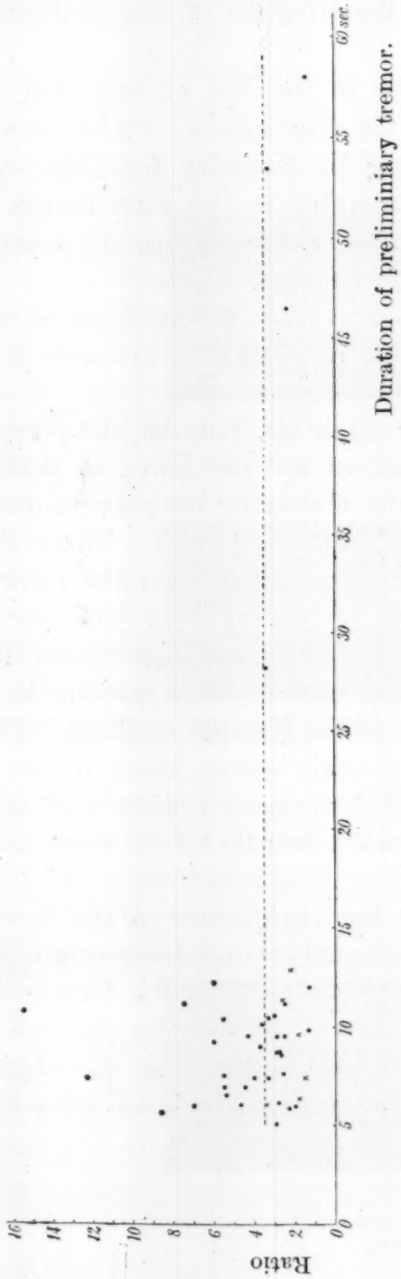

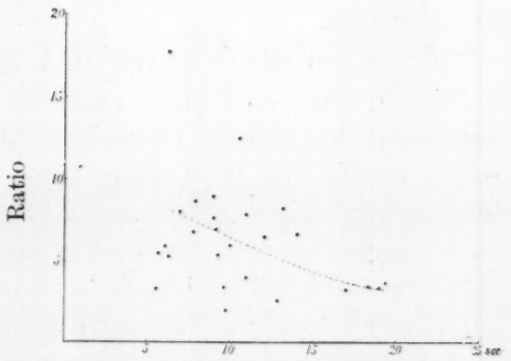

Fig. 11.

Fig. 13.

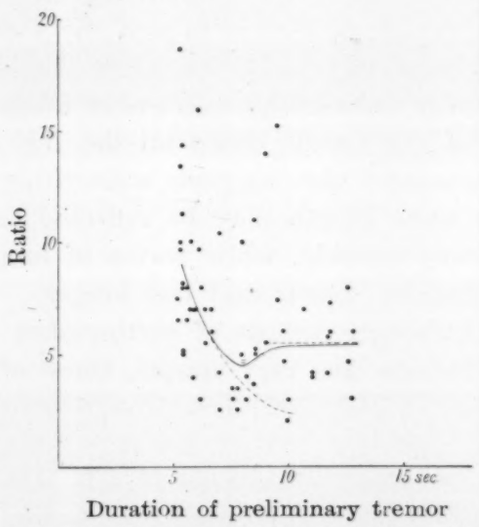

Fig. 12. The lower broken line represents the case of earthquakes of inland origin. The upper broken line represents mostly the case of earthquakes of oceanic origin.

the focal distance.

The ratio in question is quite complex, depending upon the mechanism of the earthquake origin, the azimuthal direction of the station with respect to the origin, the bending of the seismic rays in the earth's crust, the reflections and refractions at the discontinuous boundaries,

especially at the surface of the earth, and the direction of the oscillation of seimic waves.

Professor Ishimoto suggests that, just as in the case of scattering of solar rays by dust and other particles in the atmosphere, seismic waves are scattered by certain obstacles, differing in elasticity from the surrounding media and with dimensions comparable to the wave length of the earthquake waves, whether such obstacle be a cavity in the earth's crust, a magma pocket, hard rock masses, or crustal blocks.

The intensity of the scattered wave is inversely proportional to the fourth power of the wave length, so that its amplitude is inversely proportional to the square of the wave length.

As above stated, in earthquakes observed at Mt. Tukuba, the periods of the dilatational and the distortional waves are the same, so that if we confine out attention to the effect of the scattering the ratio in question is equal to 3, assuming that Poisson's ratio $\sigma=0{\cdot}25$. There are moreover characteristic features in the two different phases in the records of earthquakes, that is to say, the P-phases are fairly long with somewhat constant amplitudes, while the S-phases decay out logarithmically, especially in earthquakes about Tôkyô and under the Kastmanada (a part of the Pacific ocean on the *NE* side of the Kwantô district). This characteristic also suggests scatterings of seismic waves, since waves of short wave length may be reflected mostly from near objects and thus die away quickly, while waves of longer wave length return from near and distant objects and last longer.

Although records of earthquakes that have originated at the foot of Mt. Tukuba are very simple, those of earthquakes that have originated at Kasimanada and about Tôkyô are quite complex. In the former the ratios mentioned above are rather small as will be seen in the case of those marked × in Fig. 13. It seems to the author that the objects scattering the seismic wave may be densely or thinly distributed according to locality.

6. Conclusions.

a. The period of seismic waves most frequently observed with the acceleration seimograph at Mt. Tukuba is 0·08 sec.

b. The slightest acceleration of earthquakes which we can feel with the unaided senses at Mt. Tukuba is 1·7 gal. Our sensibility to earthquakes is in some respects like the sensitivity of a pendulum to external

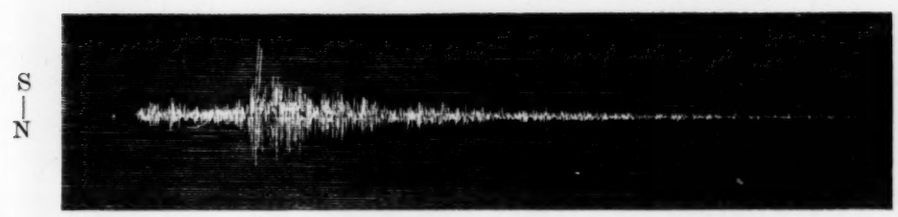

(1·2×the actual.)

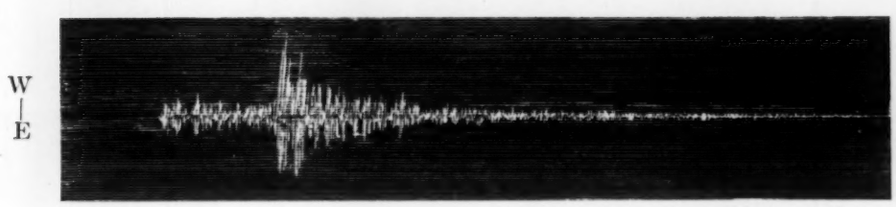

(1·2×the actual.) 1 min.=151 mm.
1 gal=0·71 mm.

(Ishimoto Acceleration Seismograph Diagrams.)

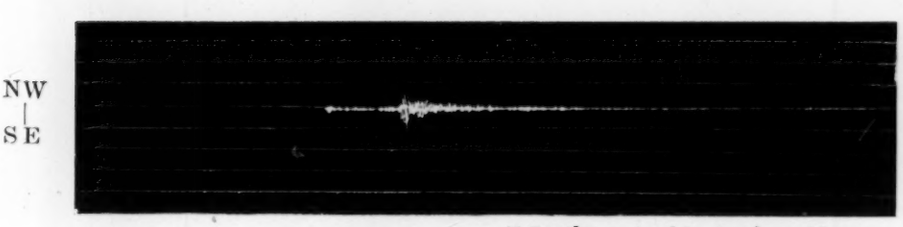

(1·7×the actual.) 1 min.=98 mm.

(Wave Analyser Diagram.)

Fig. 15. The Earthquake of June 16, 1932.

(震研彙報、第十一號、圖版、井上)

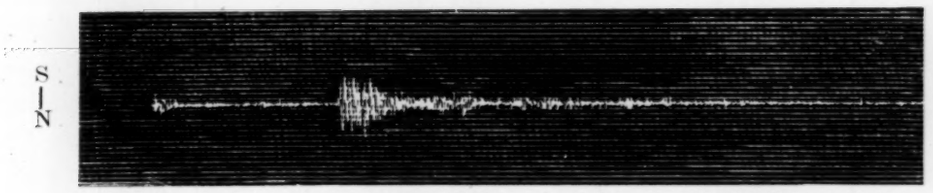

(1.9×the actual.)

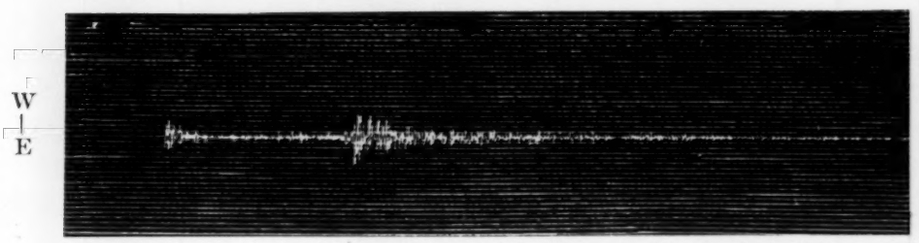

(1·9×the actual.) 1 min.=239 mm.
1 gal=1·12 mm

(Ishimoto Acceleration Seismograph Diagrams.)

(1·7×the actual.)

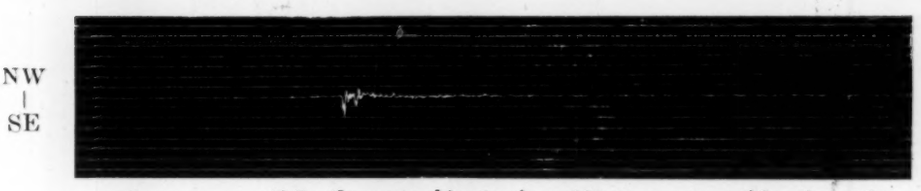

(1·7×the actual.) 1 min.=120 mm. magnification=50.

(Ordinary Seismograph Diagrams.)

Fig. 16. The Earthquake of June 22, 1932.

（震研彙報、第十一號、圖版、井上）

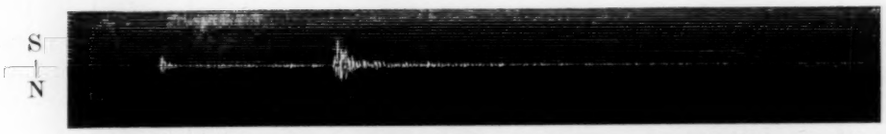

(1·08×the actual.)

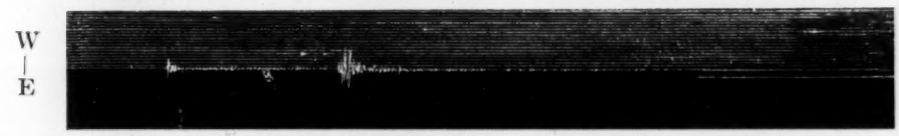

(1.08×the actual.) 1 min.=136 mm. 1 gal=6·04 mm.

(Ishimoto Acceleration Seismograph Diagrams.)

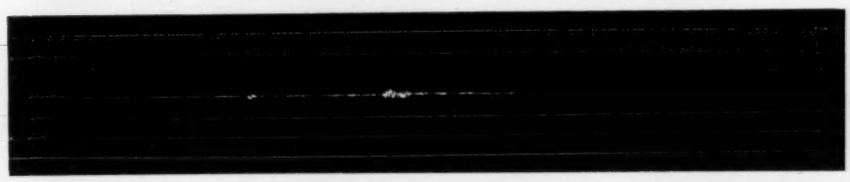

(Wave Analyser Diagram.) (1·6×the actual.)
1 min.=105 mm.

Fig. 17. The E rthquake of June 28, 1932.

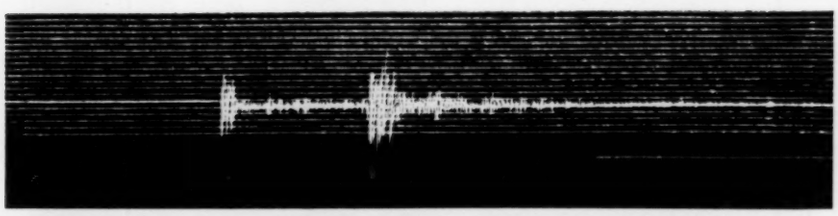

(2.35×the actual.)

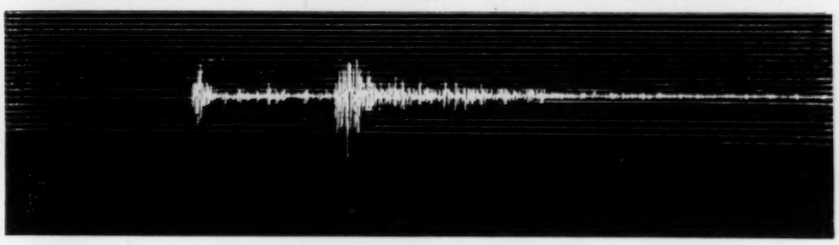

(2·35×the actual.) 1 min.=148 mm. 1 gal=1·38 mm.

(Ishimoto Acceleration Seismograph Diagrams.)

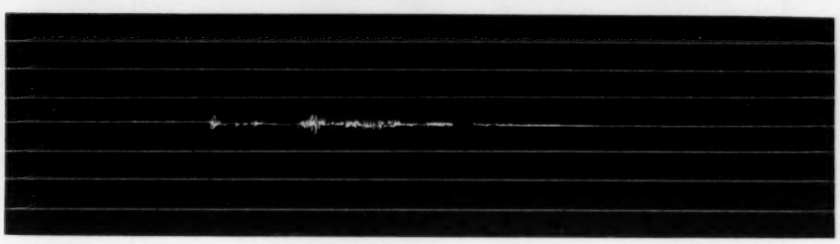

(Wave Analyser Diagram.) (2·3×the actual.)
1 min.=88 mm.

Fig. 18. The Earthquake of July 5, 1932.

（震研彙報、第十一號、圖版、井上）

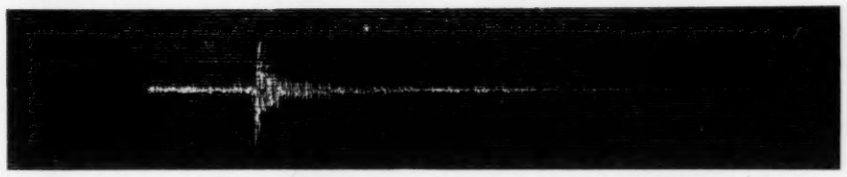

(1·2×the actual.)

(1·2×the actual) 1 min.=75 mm.
1 gal=0·71 mm.

(Ishimoto Acceleration Seismograph Diagrams.)

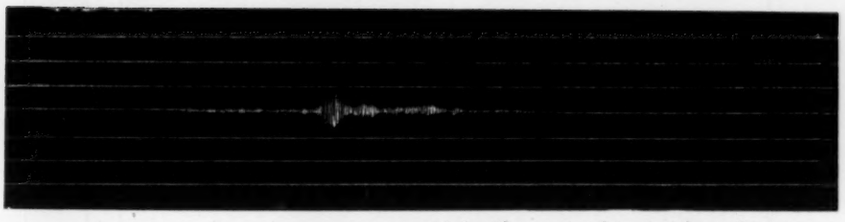

(1·9×the actual.) 1 min.=89 mm.

(Wave Analyser Diagram.)

Fig. 19. The Earthquake of Aug. 1, 1932.

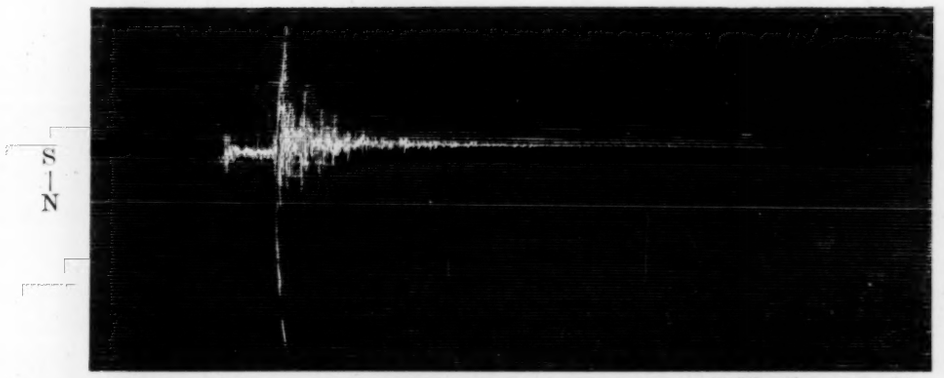

(1·08×the actual.)

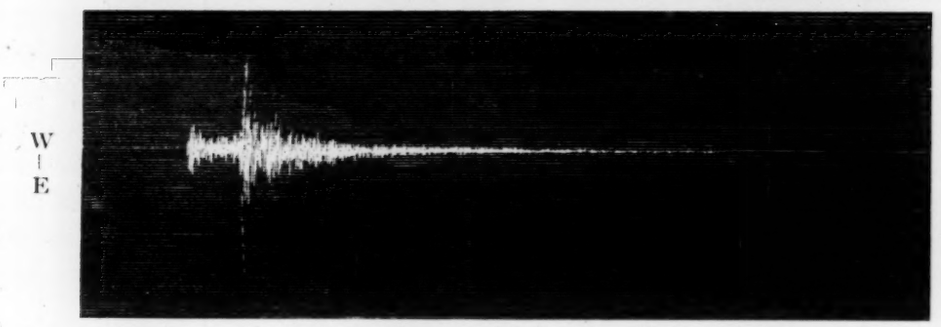

(1·08×the actual.) 1 min.=68 mm. 1 gal=0.64 mm.

(Ishimot› Acceleration Seismograph Diagrams.)

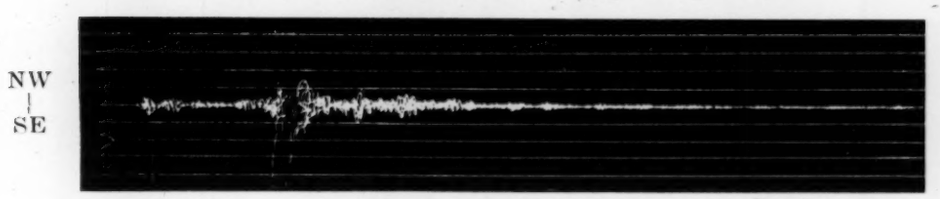

(Wave Analyser Diagram.) (1·4×the actual.)
1 min.=70 mm.

Fig. 20. The Earthquake of Aug. 7, 1932.

(1·2×the actual.)

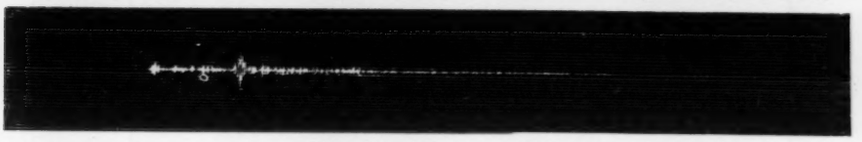

(1·2×the actual.) 1 min.=76 mm. 1 gal=0·71 mm.

(Ishimoto Acceleration Seismograph Diagrams.)

Fig. 21. The Earthquake of Sept. 19, 1932.

（震研彙報、第十一號、圖版、井上）

forces.

c. Earthquakes observed at Mt. Tukuba usually consist of many wave groups as the result of echoes or multiple reflections at the boundaries of layers in the earth's crust.

d. Some earthquake phenomena seem to be due to scattering of seismic waves by certain objects in the earth's crust or below it as already mentioned.

In conclusion the author desires to express his cordial thanks to Professor Ishimoto for his kind advice and encouragement and to Mr. Y. Inaba for his kind assistance in the course of these studies.

---

6. 筑波山に於ける加速度地震計に依る地震觀測報告

地震研究所　井　上　宇　胤

1. 筑波山に於ては加速度地震計に依つて觀測される地震波の最も優越せる週期は 0·08 秒である. 從つて筑波山地方に於て屢々經驗される鳴動の現象は此の種の地震波の大氣中への屈折に依つて生ずるものと考へられる.

2. 筑波山に於て人體に感じ得る地震波の最小加速度は 1·7 ガルである.

尙色々な異なつた週期の地震波に對する人體の感度は一秒に少し足りない固有週期を有する振子の外力に對する感度に類似する事を知つた.

3. 筑波山に於ては加速度地震計及び地震波共鳴器に依る地震記象に多數の波群が見られる。此等の波群は地殼內の層の境に於ける反響に依る事を知つた.

4. 地震波が地殼內の障害物に依つて散亂されて居ると考へられる場合のある事を示した.

---

7. *Explosive Activity of Volcano Kusatu-Siranê*[1] *in October, 1932.*

By Hiromichi TSUYA,

Earthquake Research Institute.

(Read Nov. 15, 1932.—Received Dec. 20, 1932.)

Introduction.

Tokyo newspapers of Oct. 2, reported the volcanic explosion of Siranésan, Province of Koduké,[2] at about 2^h p. m. on Oct. 1, 1932, and that, of the sulphur workers in the crater bowl called Yugama,[3] two were killed and seven injured by falling stones thrown out at the time of the explosion. This explosion marked the beginning of activities of this volcano in 1932, and, while nothing more as to further developments during the succeeding days was reported except the second explosion on Oct. 4, activities continued with rather increased intensity, particularly towards the end of that month. Thus, the third, forth, fifth, sixth, and seventh explosions occurred on Oct. 6, 8, 23, 25, and 27, respectively, of which the fifth, which the writer experienced on the summit of the volcano, appears to have been the worst of all. Of the sixth explosion, which occurred at midnight, Oct. 25, and of the seventh explosion, which occurred on Oct. 27, just after the writer's departure from the volcano, nothing definite is known.

In this paper the writer records his observations of the volcano, carried out during the four days from Oct. 21 to Oct. 24, 1932, and presents an account of the explosion of Oct. 23, of which he was an eye witness on the mountain viewing its various phenomena at close range. A short account of the past activities of the volcano will also be given. Of the structure of the volcano and its products only brief notes are given here, a detailed account of them being left for another occasion.

Morphology and Structure.

Volcano Siranésan in the Province of Koduké, or Kusatu-Siranê, as

1) 草津白根. 2) 上野國. 3) 湯釜.

it is frequently called to distinguish it from Nikko-Sirané,[4] lies in the northwest part of the province, near the northeastern boundary of the Province of Sinano,[5] about 25 km. north from the active volcano Asamayama,[6] (Fig. 1.) extending over 36°31′–39′ N and 138°31′–39′ E. The morphology and structure of this volcano have been investigated by R. Ohashi,[7] whose work has been freely drawn on in the account that follows.

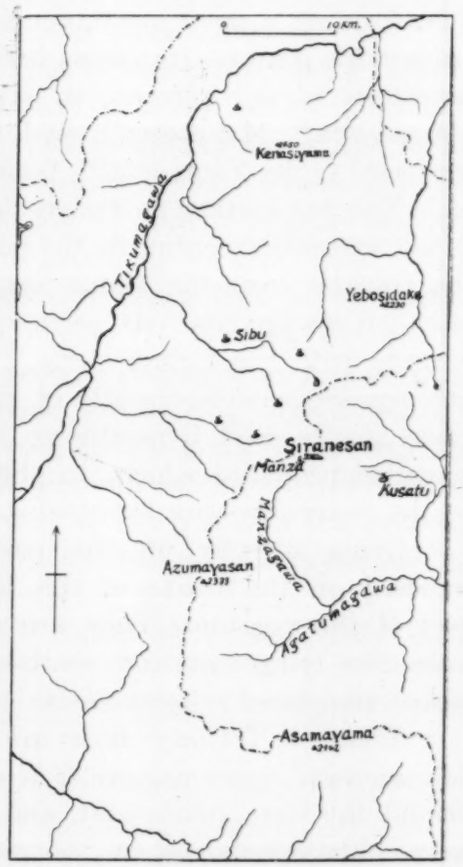

Fig. 1. Index map showing the position of the Kusatu-Sirané volcano.

Foundation. The immediate foundation on which the present volcano has been built up may be conjectured from the geology of the neighbouring districts. According to R. Ohashi, the districts adjoining the volcano are built up of various rocks, igneous as well as sedimentary, whose succession may be shown in the following scheme.

Younger Tertiary.....
Tuffs, mud-stone, clay, sand, gravel, and breccia.
Unconformity
Local lavas: A-lava (two-pyroxene-andesite) and Blava (two-pyroxene-andesite).
Unconformity
Older Tertiary .....Hypabyssal igneous body (quartz-bearing augite-hypersthene-porphyrite).

The porphyrite, which occupies extensive areas adjoining the west, northwest, and northeast of the volcano, constitutes the principal founda-

4) 日光白根 This is another volcano, 2578 m. above sea level, situated at the boundaries of the provinces of Koduké and Simotuké, (下野), over 70 km. northeast of the present volcano, and which has exploded four times during historic times, in 1625, 1649, 1872–73, and 1889.

5) 信濃. 6) 淺間山.

7) R. Ohashi, *Report Earthq. Invest. Com.*, **78** (1913), 1-47, (in Japanese).

tion, forming a great continuous mass within which various rock-facies[8] occur with gradual transition between any two facies. To the west and northwest of the volcano, it is exposed in the valleys of the rivers Manzagawa,[9] Matukawa,[10] and Kakumagawa,[11] extending far northwestward to the Yamanouti[12] hot-spring region in the Province of Sinano. The hot-springs in the region about volcano Kusatu-Sirané, with a few exceptions, occur in the porphyrite areas. At the western foot of the volcano, near the Manza spa, the writer collected specimens of the so-called porphyrite. It occurs as a partly decomposed massive rock covered with the Sirané ejecta. It is dark gray with a tinge of green, and consists microscopically of more or less altered phenocrysts (plagioclase, augite, and hypersthene) and a devitrified base, resembling the so-called propylite which, in the Idu region, is an important member of the lower Miocene formations.

Lying directly on the porphyrite mass, A-lava and B-lava are exposed on the banks of the River Kosame,[13] which bounds the east foot of the volcano. They are only local lavas fed from the ancient volcanoes lying east and south-east of volcano Sirané, and having no direct structural relation to it.

Younger Tertiary beds are exposed on the banks of the rivers Manzagawa, Agatumagawa,[14] Kosamegawa, and Nagasasagawa,[15] which bound the west, south, east, and northeast foot of the volcano respectively. These beds rest on the porphyrite masses, together with the last-mentioned local lavas, and are covered by the products (tuffs and breccia) of volcano Sirané. They have been subjected more or less to either tilting or slight folding that resulted from later disturbance, and show gentle dips generally no more than 10° to 20°, with various strikes. The materials constituting the younger Tertiary beds are largely volcanics of andesitic nature, supplied by local vents, but are partly detritus, among which porphyrite pebbles are frequently found.

As to the geological age of the foundation, Ohashi has been led to infer that the porphyrite mass is a hypabyssal intrusive in an older Tertiary, and that the last-mentioned beds are a shallow-sea deposit which took place at the close of the Tertiary; an inference however that

8) S. Shimizu mentions diorite exposed in the valleys of Matukawa and Kakumagawa, which, according to R. Ohashi, is nothing but a facies of the porphyrite. *cf.*, S. Shimidzu, *Report Earthq. Invest. Com.*, **8** (1896), 137–185, (in Japanese).

9) 萬座川. 10) 松川. 11) 角間川.

12) 山の内温泉. *cf.*, T. Yagi, *Jour. Geogr.*, **44** (1932), 126~132, (in Japanese).

13) 小雨川. 14) 吾妻川. 15) 長笹川.

is not supported by palaeontological or any other evidence.

The distributions of the above-mentioned members of the Tertiary terrane about volcano Siranê suggest that it is not at all improbable that they extend beneath the volcano. Their thicknesses at the bottom of the volcano and the tectonic lines with which they have been disturbed, if disturbance there has been, are unknown. But it may be said that at the bottom of the volcano exists a group of tectonic lines, mainly faults, which lie parallel with the volcanic chain that is made up of the volcanoes Asama, Siranê, Kenasi,[16] etc. It is evidently in this structural belt, in which are aligned several volcanoes in a N.-S. direction, that numerous craterlets of volcano Siranê are formed (see Fig. 3). The Siranê magma may have been forced upward through this structural belt, and its volcanic products ejected from the aligned openings that have spread down for the most part to the east and the southeast terranes, where the grounds composed of the basement complex are far lower in altitude than they are at the west of the volcano.

Volcano Siranê. This volcano consists of a main body called Moto-Siranésan[17] and a satellitic one called Siranésan, forming the southern extremity of a plateau-like volcanic field of an older and much greater centre (Kenasi volcano group) of volcanic activity of which little now remain. Thus, although from the south it appears isolated and stands out conspicuously as a truncated conical volcano (Fig. 2), its extension when viewed from other directions is a succession of elevations and depressions.

Fig. 2.—Oct. 19, 1932. Volcano Kusatu-Siranê as seen from the northeastern flank of Volcano Asama. Photo Tsuya.

The main body—Moto-Siranésan: Moto-Siranésan, which means older Siranésan, is a stratified volcano, built up of various lava-flows and fragmentary materials. Its height is 2176 m. above the sea, but it

16) 毛無山. *cf.*, S. Shimizu, *loc. cit.*
17) 本白根山.

is no more than 1300 m. above the adjoining terranes.

The flanks of the main body show various topographical features when viewed from different directions. On the eastern and southern sides, the outer slopes are relatively regular, but do not make a continuous curve. The inclination decreases uniformly toward the foot on those two sides, varying from 5° up to 30°, stepwise from the summit halfway down, until, on approaching the skirts of the mountain, they suddenly dwindle down to as little as 0°–3°. On these sides, the skirts of the main body are particularly well developed, whereas, on the west, where the steep upper slope of that body faces abruptly the Tertiary terrane (porphyrite and Tertiary sediment) on the banks of the River Manza, and on the north, where the satellitic body (Siranésan proper) and its nearest neighbour (Yokotéyama[18]) stand closely together, the skirts of the main body are not developed.

The main body has neither parasitic knobs, except the satellitic body, nor flank-openings on its flanks. But on its flanks there are two sulphur mines—one at Sessyogawara[19], a feeble solfatara or fumarole, on the east flank, and the other, Koménasi[20] sulphur mine, on the south flank, probable witnesses of volcanic activities in the remote past.

The summit of the main body shows a complicated morphological feature, presenting a succession of elevations and depressions owing to the numerous craterlets and conical hills packed close together. The craterlets and the conical hills however are not disposed in such a manner (cone-in-cone structure) as might be expected in a so-called somma-volcano, but are arranged roughly in two rows, each of which run in a N.-S. direction. According to Ohashi, there are six morphologically distinct craterlets, besides numerous explosion-craters, at present. The largest of these craterlets, the most southerly but one, is nearly oval, 400 m. by 250 m., dish-

Fig. 3. Map (1:50000) of the summit of Kusatu-Siranésan showing location of the craterlets. (After Ohashi).

18) 横手山. 19) 殺生河原. 20) 米無硫黄山.

shaped, with a narrow gap in its east rim. The rest, except the northernmost one which is a crescent-shaped hollow, are nearly circular. About 1 km. west of the northernmost craterlet is a truncated conical hill, with a crater (?) at its top. About 1 km. northeast of the last-mentioned conical hill is another one (2109·9 m. above the sea) with numerous explosion-pits on its northwest side near the southwest foot of the satellitic body (Siranésan proper). The activity of the craterlets at the summit of the main body, except one at the northeast bank of Yumiiké, an explosion-crater lake on the northwest side of the last-mentioned conical hill, has been long quiescent as far as historic records go.

The inner structure of the main body can be conjectured from the exposures on the valley-walls, which are developed radially on the flanks of the mountain, having reached a stage of development in which the mountain slopes are excavated to a depth as much as 300 m. But, although the development of the valleys is attributable principally to surface agencies (streams of meteoric water, snow-avalanches, etc.), numerous thick lava-flows, not all of which have extruded from a vent, have formed relatively deep intervales between any two adjoining lava-flows, with the result that meteoric water has flowed down the natural slopes of the intervales, further deepening the latter. The valley-walls thus formed not only make good natural profiles showing the order of succession of the volcanic products of the mountain, but also show the boundaries of any two adjoining superficial lava-flows that may occur.

According to Ohashi, the south side of the main body is built up of a lava called Koménasi lava; while its remaining part is younger in formation than that side, being built up of two successive lavas—the first (older) and the second (younger) types of the Sirané lavas—besides fragmentary material underlying them. The Koménasi lava is petrographically a gray augite-hypersthene-andesite, while the first and the second types of the Sirané lavas are a whitish quartz-augite-hypersthene-andesite and a dark olivine-augite-hypersthene-andesite respectively. He speaks of biotite as one of the subordinate components of these lavas, but made no attempt to unravel the sequence of eruptions of the numerous lava-flows, which he divided only roughly into the above-mentioned three kinds.

The writer has not yet studied in detail the structure of the main body. But, of the east flank from the top of the mountain half way down to the Kusatu spa, it may be said that its structure is represented in a complicated manner by numerous layers of lava-flows and fragmentary ejecta, disposed in the following succession:

Upper←	18. Explosion products	Olivine-two-pyroxene-andesite. / Two-pyroxene-andesite.
	17. F—lava	Olivine-two-pyroxene-andesite.
	16. Agglomerate	Two-pyroxene-andesite.
	15. E—lava	Two-pyroxene-andesite.
	14. Volcanic ashes, sands, and lapilli.	
	13. D—lava	Two-pyroxene-andesite.
	12. Mud-flow	Two-pyroxene-andesite. / Two-pyroxene-dacite.
	11. C—lava	Biotite-bearing-two-pyroxene-andesite.
	10. B—lava	Two-pyroxene-dacite.
	9. Agglomerate	Two-pyroxene-dacite.
	8. Volcanic ashes.	
	7. A—lava	Two-pyroxene-andesite.
	6. Pumice-lapilli.	
	5. Agglomerate	Two-pyroxene-dacite.
→Lower	4. Pumice-blocks.	
	3. Volcanic ashes.	
	2. Pumice-lapilli.	
	1. Pumiceous massive tuff and tuff-breccia.	

So far as the writer's observations go, the lava-flows are for the most part products of later eruptions of the main body, distributing from the top half way down, while the bulk of the fragmentary materials belong to the earlier eruptions that form the basal part of that body. The lava-flows are generally thick, sometimes attaining a hundred meters in thickness. Each of these thick lava-flows form flat-topped and steep-sided ridges, lava-coulee or Japanese *butai*[21], causing the stepped outline of the east flank of the mountain (Fig. 4).

As is usually the case with extrusive rocks of acid composition, the lavas of the main body are relatively glassy with fairly diversified appearance. They vary from white to black, phyric to aphyric, and dense to highly vesicular. Spherulitic structure, due to small spherulitic growths in the groundmasses, is seen in some of these lavas.

The fragmentary materials are of all grades, in size, from huge blocks to fine ash, and are stony, vitreous, or pumiceous, in appearance. Their deposits show some signs of stratification, often very finely laminated. They have yielded yet no organic remains, with the exception of small pieces of carbonized wood. Ohashi, referring to some volcanic material in the Tertiary beds which underlie the present volcano as the oldest ejecta of the same volcano, was led to believe that the

21) 舞臺.

earliest eruption of the volcano had occurred in shallow water at the end of the Tertiary. These statements have not however been proved by any evidences, petrological or stratigraphical, and are subjects of further study.

The satellitic body—Siranésan proper: Siranésan proper, which lies to the north of the main body, is a conical volcano composed of a few lava-flows and much fragmental material. Its height is 2162 m. above the sea, but less than 300 m. above its base.

The immediate base on which the cone has grown consists practically of products of the main body (Moto-Siranésan), except the Yokoté-yama volcanic body.[22] The terranes adjoining the south, the east, and the northeast, of the cone are lava-flows (biotite-bearing two-pyroxene-andesite, two-pyroxene-andesite, and two-pyroxene-dacite); while the districts immediately to the northwest and the west are of Yokoté lava

Fig. 5. The northeastern flank of the satellitic body, Siranésan proper, showing a lava-flow of two-pyroxene-andesite. Photo. Tomizawa.

Fig. 4. An ideal section of volcano Kusatu-Siranė showing succession of lavas and fragmentary material. T—tuff, tuff-breccia, pumice, etc.; l_1—two-pyroxene-dacite lava; l_2, l_3—two-pyroxene-andesite lavas; l_4—biotite-bearing two-pyroxene-andesite lava; l_5—olivine-two-pyroxene-andesite lava; L_1—two-pyroxene-andesite lava; L_2—olivine-two-pyroxene-andesite lava; Y—Yokoté lava?; P—porphyrite?

22) This forms the high rugged mountain, Yokotéyama (2304·9 m. above the sea), adjoining the north of Siranésan proper. According to Ohashi, this is an older member of volcano Siranė, consisting of a gray-colored augite-hypersthene-andesite (Yokoté lava) supplied by its own vent. But it has no direct structural relation to either Moto-Siranė-san or Siranésan proper; while the northern skirt of Siranésan proper lies on the south flank of Yokotéyama in a discordant relation. On these grounds, the writer has left this mountain out of the present discussion on volcano Siranė.

which, in turn, overlies the so-called porphyrite mass.

The development of the flanks of the cone is not uniform in all directions. The eastern flank is relatively well developed, with slopes whose inclinations are about 25° near the summit and 3–0° near the foot (Fig. 5). The northern and southern flanks (see Fig. 31) are equally developed, showing a slope as steep as 30°. But, in these directions, the skirts with gentle slopes are not so well developed as in the eastern direction. This is due to the existence of the Yokotéyama volcanic body on the north and a high lava-coulee of Moto-Siranê on the south, each of which has obstructed extensive development of the cone-skirts adjoining them. The western flank of the cone is abnormal, its steep upper slope facing abruptly on the upper course of the River Manza.

The satellitic cone is truncated at the top with an old crater-wall, whose northwest segment is clearly represented by an arciform crest line around it. The highest point (2162 m. above the sea) of the present

Fig. 6.—June, 1931. General view of the triple crater at the summit of Siranésan proper. Center, Yugama; upper left, Midugama; and lower, Karagama (*cf.* Fig. 34). Photo Tomizawa.

cone is the western crest of this old crater-wall. The southeastern segment of the old crater-wall cannot be traced at present. The crater, which, encircled with the old crater-wall, must have been about 1 km. in diameter, has been buried almost completely under the products of

later eruptions that took place in and around it. The morphologically quite young triple crater (Fig. 6), consisting of three crater-bowls—the central one called Yugama, the southwesterly one Karagama,[23] and the northeasterly one Midugama[24]—is a mute witness of these eruptions.

The Midugama, which contains cold water, is a nearly rectangular crater-bowl, the longer and the shorter sides of which are 250 m. from N. E. to S. W. and 200 m. from N. W. to S. E. respectively. The crater-bowl is surrounded by steep walls on all sides, except on the southwest, where there is a great V-shaped gap in the wall which serves as a passage to the adjoining crater-bowl (Yugama). The rim of the encircling wall is higher on the southeast than on the northwest, its highest point being 2102 m. above the sea on the east side. The bottom of the crater-bowl is about 80 m. deep from the highest point of the encircling rim, whereas it is only a few meters deep from the lowest point in the V-shaped gap in the southwest wall. The cold water occupies an oval pool measuring about 150 m. across from N. E. to S. W. and about 100 m. across from S. E. to N. W., covering the greater part of the bottom. Outside, near the northwest rim of this crater-bowl, is a small horseshoe-shaped explosion-crater.

The Karagama ("dried-up cauldron") is an oval crater-bowl, the major and minor axes of which are 200 m. from N. E. to S. W. and 100m. from N. W. to S. E. respectively. The northern wall of this bowl is an almost perpendicular cliff, whereas the southwestern wall is so gentle in slope as to be easily passable. A great V-shaped gap in the northeast wall of the bowl opens into the Yugama crater-bowl. The bottom of the Karagama crater-bowl is about 80m. deep from the highest point of the northern rim and about 30 m. from the southwestern rim. It is a flat ground, usually dry, but at the time of the writer's visit there was water in a small pool in the southeastern half of the bottom (Fig. 6).

The Yugama ("hot-water cauldron") lies between the above-mentioned two crater-bowls, into both of which it opens. It is an indented bowl, about 300 m. in diameter and surrounded by an almost perpendicular wall, except the V-shaped gaps in the wall on the southwest and northeast sides where it opens into the Karagama and the Midugama respectively. The rim of the rugged encircling wall is higher on the north than on the south. The bottom of the bowl is not level, its north-

23) 空釜. 24) 水釜.

eastern half being lower than the southwestern half. The former is occupied by a hot-water pool, about 150 m. in diameter, while upon the latter, which is dry ground, the sulphur miners have built sheds. The level-difference in these two parts of the bottom is about 10 m., the higher northeast margin of the dry ground forming steep scarp of this height fronting the adjoining hot-water pool (Fig. 7). The level of the hot-water pool is about 100m. below the highest point of the northern rim of the crater-bowl and about 20 m. below the lowest point in the V-shaped gap in the northeastern wall. The dry ground in the southwestern half of the Yugama is separated from the bottom of the Karagama by a low ridge in the V-shaped gap in the wall between them, the former being a few meters lower than the latter. Shiranê's activities in historic times, except that in 1902, were manifested exclusively in this crater-bowl, changing more or less the feature of its interior whenever it occurred, as will be described in the next chapter.

Fig. 7.—1921. Showing numerous layers, alternately accumulated sulphur and explosion products. Lower left, a portion of the hot-water pool in the northeastern half of the bottom of the Yugama crater-bowl; and upper middle, a portion of crest line of the northeast margin of the dry ground in the southwestern half of the bottom of that bowl, looking south.
Photo Tomizawa.

The inner structure of Siranésan proper may be conjectured from exposures on the encircling cliffs of the triple crater, as well as from those on the outer sides of the cone, where excavations in the rocky skin show frequent scars and slips. Structurally the mountain is a diminutive composite cone,[25] consisting of the somma represented by the older crater-wall and the one-sided cone with the triple crater at its top, whose northwest side is hemmed in by the old crater-wall.

The somma is a stratified cone built up of several layers of alternate accumulations of lava-flows (massive lava-flows and agglomerate lava-flows) and fragmentary materials (volcanic ash, sand, lapilli, and

25) Ohashi is of opinion that the mountain is a lava-dome with a summit-crater, about 1km. in diameter, and six explosion-craters within the host crater. This opinion however could not be verified so far as the writer's observations went.

blocks). The best exposures of the inner structure of this cone are found on both the northern flank and on the western flank near the crest of the arc-shaped older crater-wall. The materials composing this cone are petrographically quartz-bearing two-pyroxene-andesite and two-pyroxene-andesite. On the crest around the old crater-wall are to be found abundant explosion products, among which bread-crust bombs of olivine-two-pyroxene-andesite are frequently met with. These products were probably supplied through some vent or outlet represented by the triple crater.

The southeastern half of the mountain consists of lava-flows and fragmentary materials, probably ejected from the triple crater. The lava-flows are exposed on the surrounding walls of the crater, being overlain by numerous layers of fragmentary ejecta. The lava exposed on the southeast wall of the Karagama crater-bowl is petrographically an olivine-two-pyroxene-andesite, while the lava exposed on the southeast wall, below the highest point of the southeast rim of the Mizugama crater-bowl, is a two-pyroxene-andesite. The northern wall of the Yugama crater-bowl is a lava-cliff attaining a height of about 80 m. from its base near the northern shore of the hot-water pool up to near its upper rim. The lava exposed there, according to K. Nakajima,[26] is petrographically a two-pyroxene-andesite with the following chemical composition :

	Wt. %		Norm	Ratios
SiO_2	62·66	Q	41·20	$\frac{Sal}{Fem}=4{\cdot}57$
Al_2O_3	15·91	Or	2·23	
Fe_2O_3	5·91	Ab	1·57	$\frac{Q}{F}=1{\cdot}17$
FeO	2·11	An	31·43	
MgO	3·52	C	3·67	$\frac{Na_2O'+K_2O'}{CaO'}=0{\cdot}06$
CaO	6·70	Hy	8·93	
Na_2O	0·17	Mt	6·71	$\frac{K_2O'}{Na_2O'}=1{\cdot}33$
K_2O	0·36	Ap	0·62	
H_2O	1·32	Hm	1·28	
P_2O_5	0·31	Symbol (C. I. P. W.)		"II. 3. 5."3.
Total	99·97			

It is difficult to ascertain the distributions of these lavas on the outside of the crater-bowls, where the ground is thickly covered with

26) K. Nakajima, *Expl. Text, Geol. Map*, "Nagano" sheet (1:200000), (1888), 25, (in Japanese).

explosion products. These explosion products are mostly rock-fragments of various sizes, ranging from ash-grade to blocks of more than one meter in diameter, in which are not a few bread-crust bombs (olivine-two-pyroxene-andesite), similar petrographically to those just mentioned.

The bottom ground, except the water pools, of the triple crater are covered with explosion products. The southwestern half of the bottom of the Yugama crater-bowl is built up of numerous layers of alternately accumulated explosion-products and sulphur deposits (*yunohana*).[27] The sulphur deposit is being worked on a substantial scale (see Fig. 7).

Volcanic Activity in Historic Times.

The volcano has been active eight times during the last fifty years. The first activity in this period was the explosion that took place on Aug. 6, 1882. The last period of activity prior to this is supposed to have ended at least 120 years ago, as may be inferred from oral informations that during about seventy years before the explosion in 1882 the volcano was entirely quiescent without any trace of volcanic activity, but that previous to this dormant period it was issuing smokes from its summit. But nothing regarding this former active period has been recorded, the explosion of 1882 being the first ever mentioned in our chronology. A short account of the activities of the volcano in historic times will now be given.

1. The activity of 1882 A. D.[30] At about 2^h p. m. on Aug. 6, 1882, when an explosion of this volcano occurred, a strong detonation was heard at Yosigataira,[28] about 2km. distant northeast, but the mountain being concealed from view by heavy clouds, the explosion remained unsuspected until two days afterward, Aug. 8, when the mountain was seen to be emitting dark smoke.

As a result of this explosion, the Dokumidusawa[29]—a valley on the east flank of the mountain—into which flowed the mud-water expelled from the summit crater, inundated its banks in many places. Volcanic ashes fell in Sinano province northwest of the mountain.

This explosion took place in the floor of the Yugama crater-bowl and in eight other places near it, resulting in the formation of numerous

27) 湯花. 28) 芳ケ平. 29) 毒水澤.

30) E. NAUMANN, *Petermanns Mitteilungen, Ergänzungsband*, **23** (1893), 1~9; S. KANDA, *Tôyô Gakugei Zassi*, **37** (1920), 45~46, (in Japanese); F. OMORI, *Report Earthq. Invest. Com.*, **86** (1915), 80~82, (in Japanese).

hollows, from which vapors, hot water, mud, and stones were thrown out. These hollows were of varying sizes and depths, the largest being about 150 m. in diameter and about 90 m. in depth.

On Aug. 8, according to the then village master of Kusatu, who, on that day inspected the scene of the explosion, a succession of fairly strong vapor-clouds threw up before his eyes showers of rock-fragments to heights of at least 60 m. above the crater bottom. These fragments of varying sizes, the largest about 0·6 m. by 0·3 m., were projected northwestward to a distance of 2000 m. from the crater. At noon of the following day numerous openings, the largest of which was about 5·5 m. in diameter, were formed near the crater-rim on the southeast side, and from these openings hot water poured out for a week until Aug. 16.

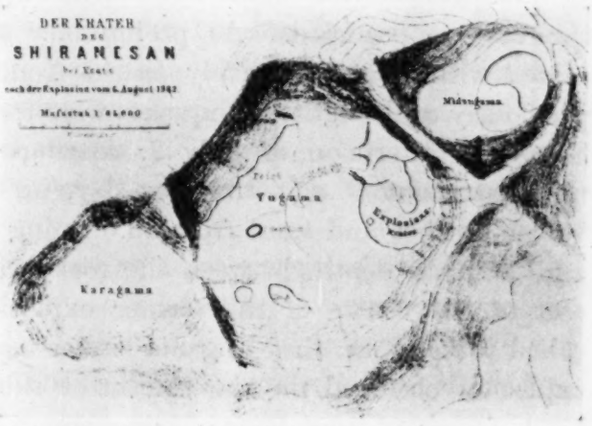

Fig. 8.—Sept. 5, 1882. (After Naumann).

Before this explosion, the ground in and around the Yugama crater-bowl had been covered with trees and bushes, with a pool of cold water at the centre of the bottom of the crater-bowl, but by the explosion the trees and bushes were completely ruined, and the position of the pool changed to another part near the base of the northern crater-wall, its old site becoming partly dry ground and partly a new pool of hot-water.

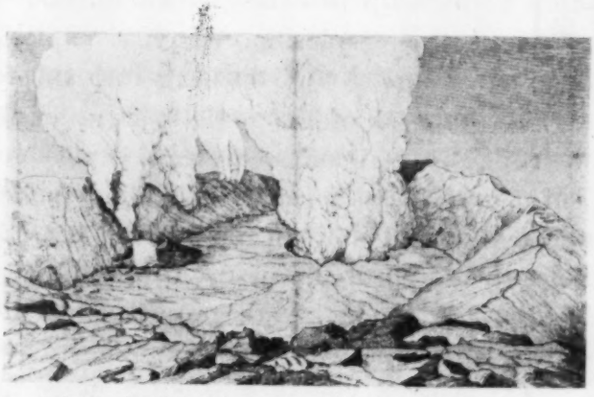

Fig. 9.—1882. The Yugama crater-bowl after the explosion on Aug. 6, 1882. (After Jingoro Yanazawa).

E. Naumann[31] visited this mountain on Sept. 5 and 7 of the same year, and made some geological observations. During his visit to the mountain, according to him, fairly strong emissions

31) *loc. cit.*

of dense vapor-clouds were taking place from several fissures on the northern wall of the Yugama crater-bowl, as well as from the horse-shoe-shaped explosion-crater and hot fountain (heisse sprudel) on the bottom of the crater-bowl (see Fig. 8). He observed that the horseshoe-shaped explosion-crater, which contained some milky white water, was very active, throwing out water to a height of about 4 m. above the water level at intervals of one minute or more with roaring sound.

When K. Nakajima[32] visited the mountain in 1888, he found that the explosion-crater in the Yugama crater-bowl was emitting white vapors from several places in its northern part.

2. Explosion of 1897.[33] On July 8, 1897, another explosion of the volcano occurred. As preliminary sign of this explosion, vapors mixed with sulphur actively issued from the Yugama since a month previously and slight earthquakes were frequently felt on the mountain. Since the afternoon of July 7, roarings were of frequent occurrence, until, at about 4^h a.m. the next day, an explosion took place, ejecting volcanic ashes and sand from an opening about 100 m. in circumference and 20 m. in depth, between the rocky ridges, and about 200 m. north-east of the centre of the former explosion crater (the hot-water pool called Oikê[34]) in the Yugama crater-bowl. An hour later, a second explosion occurred on the southwest side of the explosion crater and lasted for about three hours during which time hot water and mud were often thrown up to a height 150 m. above the level of the pool. As a result of this explosion, another explosion-crater was formed, about 80 m. in diameter and opening into the former pool.

On July 31 of the same year, an explosion took place about 5^h a.m., with slight earthquakes. Several explosion-holes, one of which measured 7 m. across, were formed in front of the lock-gate of the drainage tunnel at the southern shore of the pool (Oikê). About 40 m. eastward of these holes there appeared a fissure through which hot mud and blocks weighing nearly 150 kg. were projected northwestward over the crater-rim during the explosion.

On Aug. 2 violent rumblings were heard at 2^h a.m., followed by a period of paroxysmal activity with frequent ejections of rock-fragments that lasted until dawn. The next day, at about $2^h\,30^m$ p.m., an explosion

---

32) *loc. cit.*

33) *Jour. Geol. Soc.*, Tôkyô, 4 (1897), 437~438; *Jour. Geogr*, 9 (1897), 389~390, (in Japanese).

34) 大池

took place from an opening near the lock-gate with violent ejections of rock-fragments. One person was wounded. From then on till Aug. 16, rumblings and minor explosions were of frequent occurrence.

The next year (1898), according to K. Jimbo,[35] it was found that as a result of the last explosions, the level of the former pool (Oiké) had fallen about 5 m. When he visited the mountain on August 17, vapor-clouds were issuing from the northeast corner of the pool.

3. The explosion of 1900.[36] On Oct. 1900, feeble rumblings and explosions occurred at about 3^h a. m.

4. The explosion of 1902.[37] On July 15, 1902, an explosion occurred at about 4^h p. m. in a small conical mound on the northeastern shore of the Yumiike,[38] an explosion-crater lake on the saddle between Moto-Sirané and Sirané proper. Emissions of vapors and ejections of rock-fragments continued to the next evening. Four days later, on July 19, only a faint vapor-cloud was issuing.

On Aug. 20, occurred the second explosion which however was of moderate violence.

On Sept. 3, vapor-clouds were issuing from several openings within the explosion-crater at the top of the conical mound. Next day a violent explosion occurred, resulting in the formation of another explosion crater which was separated from the former one by only a narrow ridge.

On Sept. 17, an explosion occurred at about 1^h p. m., shooting up a column of black smoke to a height of several hundred meters above the top of the conical mound. Rumblings were then heard at Kusatu in the direction of the mountain. Volcanic ashes fell to the leeward within a distance of about 2 km., and accumulated to a depth of about 9 cm. not far from the crater. Although explosions continued intermittently throughout the following two days, the intensity gradually diminished. On Sept. 19, rumblings were heard at about 11^h a. m., with emission of smoke.

On Sept. 23, according to S. Kawasaki who was on the mountain that day, vapor began to issue violently from the top of the conical mound, and continued to issue with increasing intensity, until at about 11^h a. m. when it suddenly changed to black smoke densely charged

35) K. Jimbo, *Jour. Geol. Soc.*, Tôkyô, 5 (1898), 500~501, (in Japanese).

36) F. Omori, *loc. cit.*

37) S. Kawasaki, *Jour. Geol. Soc.*, Tôkyô, 9 (1902), 461~465, (in Japanese); *Jour. Geogr.*, 14 (1902), 647; 711.

38) 弓池

with volcanic ashes. For thirty minutes explosions were frequent, ejecting rock fragments to heights nearly 30 m. above the top of the mound. During this period rumblings were of continual occurrence. After that came a period of relative calm, but twenty minutes later emissions of black smoke and ejections of rock-fragments were repeated with rumblings, and in the afternoon, from 0^h15^m to 2^h, these phenomena occurred at intervals varying from 15 seconds to a minute. The same activity continued through the next day.

Fig. 10.—1902. The explosion crater of 1902. Lower, a portion of the Yumiiké; upper, the southwestern flank of Siranésan proper. Photo Tomizawa.

On Oct. 18, hot water was seen spouting from several places in the crater at the top of the conical mound near the Yumiiké.

All through the explosions of this year the Yugama crater-bowl remained quiet.

5. The explosion of 1905.[39] In Oct., 1905, another explosion of the volcano took place.

In 1910, according to R. Ohashi,[40] steam was issuing from the hot-water pool in the bottom of the Yugama crater, near the base of the inside northern wall. Water was also being projected.

In 1916, according to K. Aomi,[41] feeble fumaroles and fountains were observed at several places in the hot-water pool inside the Yugama crater. A very active fumaroles was noticed in the northwestern part of the pool. At that time the water in the pool was about 50°C.

6. The explosion of 1925.[42] On Jan. 22, 1925, an explosion took place on the inside northern wall of the Yugama crater, ejecting ash-laden clouds and rock-fragments with rumblings. On Jan. 25, it was found that a new explosion-pit, about 20 m. by 7 m., had opened near the upper rim of the inside northern wall of the crater. On that day, vapor-clouds were issuing from the new pit. About 35 m.

39) F. OMORI, *loc. cit.*

40) *loc. cit.*

41) K. AOMI, *Tôyô Gakugei Zassi*, **33** (1916), 828~832, (in Japanese).

42) *Kisyôyôran*, (1925), 26~27.

westward of this opening appeared a detatchment scar, 15 km^2. in area, on the inside crater-wall. The Yugama crater-bowl was, as before, emitting a feeble vapor-clouds from its floor. As a result of the explosion, the volcanic ashes, which fell on the southeast side of the mountain, accumulated to a depth of about 20 cm. for a distance of about 3 km.

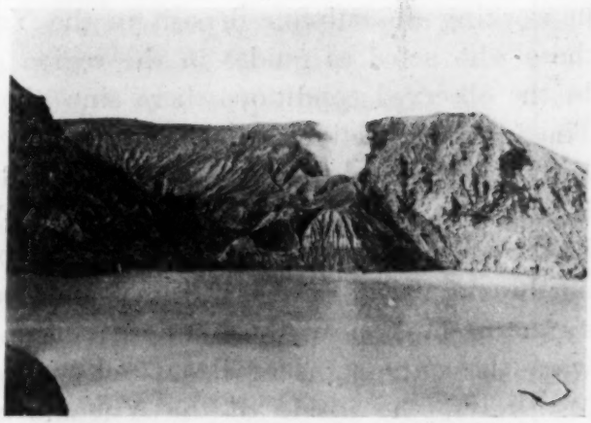

Fig. 11.—1925. The explosion crater of 1925, looking northeast. The crater is emitting only white vapors. In the foreground is the pool in the bottom of the Yugama crater-bowl. Photo Tomizawa.

7. The explosion of 1927.[43] On Dec. 31, 1927, an explosion occurred at about 11^h a. m. As a preliminary sign of this explosion, rumblings were heard twice during the preceding two days, viz., at 7^h a. m. on Dec. 29 and 9^h a. m. on Dec. 30. The explosion shot out enormous columns of vapor heavily charged with volcanic ashes from a fissure nearly 100 m. long at the base of inside northern wall of the Yugama crater, as well as from numerous other fissures on the southern flank adjoining the southern rim of the Yugama crater. At the same time, the inside northeast wall of the Yugama crater, which formerly had been a vertical cliff, caved in. As results of this explosion, the vent that opend in 1925 ceased activities, the water in the Yugama crater-bowl rose in temperature from 15° to 24°C., while its level sank about 14 m. On the southern flank near the south rim of the crater, a hot spring 80°C. began to gush out.

Since then fairly strong emissions of vapor-clouds continued during the following three months, but these gradually declined in intensity until, on June 26, 1928, when M. Kajima and K. Gomi visited the mountain, only gentle fumaroles, one of which was 64.5°C., was emitting white vapors from several places in the explosion-fissures of the preceding year.

The Explosions of Oct. 1932.

Sequence of events. The seasonal appearances of the crater region of Siranésan proper were well known to those who were engaged

43) M. Kajima and K. Gomi, *Kisyôsyûsi*, (1928), 400~408.

in working the sulphur deposit in the Yugama crater-bowl and also to those who acted as guides in the region. There is no record of changes in the observed conditions there since the last explosion (Dec. 31, 1927). The fumarolic activity, which at the time of Kajima's visit to the mountain was observed in several places, had been growing weaker, until, last year it became almost extinct (see Fig. 6). But gentle fumaroles had been observed before the outburst of Oct. 1, 1932, on the inside northeastern wall of the Yugama crater, as well as in a fissure on the southern flank near the southern rim of the crater. These fumaroles were the only signs of latent activity of the volcano during the last few years, the inside of the Yugama crater being very quiet. The explosive activities of 1932 began on Oct. 1, and repeated themselves several times during the succeeding days towards the end of that month. From accounts of eyewitnesses and of people living in the terranes about the mountain, the sequence of activities was as follows:

Oct. 1. Fine weather. Twenty nine miners were engaged working the sulphur deposit at the bottom of the Yugama crater. The first explosion came without warning at about 2^h5^m p. m.[44] No change was noticed either in the temperature or in the activity of the pre-existing fumaroles in and about the Yugama crater, neither were there any local earthquakes to attract particular attention. The miners, who were at work in the bottom of the Yugama crater, had no inkling of the danger until they were faced suddenly with the explosion. Two of them were instantly killed and seven seriously injured by stones that were thrown out by the first outbreak.

The first explosion occurred in the inside northeastern wall of the Yugama crater, as well as in the fissures on the outside of the southern rim of the crater, with ejection of old cone material ranging in size from ash-grade up to blocks about 100 cm. in diameter, besides vapors.

The explosion-clouds were clearly seen from Kusatu (Fig. 22). According to K. Yumoto, who witnessed the first explosion when it occurred, a small black mass of smoke was first seen to rise above the level of the mountain, and then to expanded outwardly, cauliflower-shape, against the surrounding air, and bent by the wind which was blowing from the southwest, without being projected into the upper region of the air. He dit not hear the first explosion, although it was

44) A seismogram set up at Minenotyaya (峯ノ茶屋) on the eastern flank of volcano Asama, 25 km. south of the volcano Sirané, recorded a minor volcanic tremor at 1^h50^m p.m. on Oct. 1.

heard in Kusatu. About fifteen minutes later, ashes began to fall in Kusatu and continued for about five minutes.

At the Manza spa, the explosion was clearly heard, like the noise caused by firing a heavy gun. There the rumblings were heard through out the day and into the evening hours but there was no fall of ash.

The first explosion was followed by a slighter one a few hours later.

After the explosions of Oct. 1, the mountain was relatively quiet, without issuing any noticeable amount of ash-laden cloud, until the afternoon of Oct. 4, when an explosion of the mountain occurred. During this period of relative quiescence a number of people visited the scene of the last explosions. Tomizawa, a Photographer of Kusatu, who visited the scene on Oct. 2, took the photographs that are shown in Fig. 25 and 29. He saw a tremendous volume of white vapors issuing with a hissing sound and heard rumblings from the crevices on the inside northeastern wall of the Yugama crater and also from the fissures on the outside of the southern rim of the crater.

Oct. 4. Rumblings of the mountain were heard frequently this day at Kusatu. An explosion took place at about 2^h 30^m p. m., and a moderate quantity of volcanic ashes was thrown out, while a vertical column of black smoke was seen from Kusatu (Fig. 23) to rise upward into the upper region of the air. But the explosion was not heard at Kusatu, nor did any ashes fall there.

During the next day rumblings of the mountain were frequently heard at Kusatu.

Oct. 6. On this day, at about 3^h a. m., there was an explosion with a detonation much stronger than was heard previously. Since it occurred at night nothing could be seen. From this day on the mountain was fairly quiet until the dawn of Oct. 23, when it seemed to have awaken from that tranquility into which it had elapsed during the preceding eighteen days. During this period of repose neither explosion nor ash-fall is said to have occurred,[45] and rumblings were seldom heard at Kusatu although a moderate quantity of vapors never ceased to issue from the mountain. The writer, observing from Asama-yama during the four days since Oct. 17, saw nothing but a column of vapor-cloud, bent by wind from the west, issuing constantly from the summit of the present volcano (see Fig. 2).

45) S. Kunitomi mentioned an explosion as having occurred at 6^h40^m a. m. on Oct. 8. *cf.*, *Kisyôyôran*, (1932), 998~1005.

In the afternoon of Oct. 20, when the writer arrived at Kusatu, the mountain was quiet, and nothing of its activity was noticed in Kusatu except the white vapors that rose slowly from its summit. The day after his arrival at Kusatu, a light rain was falling and the mountain shrouded so thickly in rain clouds, that he gave up the idea of gaining the summit of the mountain when he arrived at Yosigataira. At about 1^h30^m p. m. rumblings were heard at Yosigataira in the direction of the summit, but nothing of the summit could be seen. He visited the summit thrice, on Oct. 22, 23, and 24, and examined the present activity, besides making some geological observations. The conditions on the summit during these three days were as follows:

Oct. 22. was fine. Shortly after 5^h a. m. a loud noise was heard at Kusatsu in the direction of the mountain, of which it might have been an explosion. Two hours later, all that could be seen from Kusatsu was the usual vapor-cloud rising from the mountain. An ascent of the mountain was made this day by a short cut passing through Sainokawara[46] (a seat of a group of fumaroles, in Kusatu) and Sessyôgawara (a valley situated about 3·5 km. west of Kusatu, presenting a fumarolic activity). When he came near the Sessyôgawara rumblings and hissing noises became audible in the direction of the summit of the mountain. On approaching the summit the noises grew clearer and louder. When he arrived at the southern foot of the volcanic cone, Siranêsan proper, a distance of about 1 km. south from the summit triple crater, he saw vapors together with ash, sand, and stones being blown out from a number of vents in fissures on the southern flank of the cone (see Figs. 12, 13, 14, 15, and 28). The hissing noise was continual. The number of these vents then would be more than fifteen, although no accurate count could be made owing to the dense vapor-cloud which completely veiled the eastern half of the southern flank of the cone, where several vapor-columns were seen through rifts in the cloud. The most active vent was in a fissure situated a short distance below the top of the southern rim of the Yugama crater-bowl (see Fig. 12).

The inside of the Yugama crater-bowl was quiet with a glassy pool of hot (?) water in its bottom except in the southern inlet of the pool, where the water had become milk-white, evaporating misty vapors. There were two fumaroles on the inside wall of the crater—one situated

46) 西ノ河原.

at the base of the northern wall, emitting vapors plentifully but slowly from a cleft which was separated from the bottom of the Yugama crater-bowl by a narrow ridge (C_2 in Fig. 34), the other from a cleft that had been formed by explosions early in the month on the inside southeastern wall of the crater, extending from near the upper rim downward to the base of that wall. This latter fumarole was emitting volumes of white vapors with a continual hissing noise (Fig. 26). Besides these, there were a number of gentle fumaroles on the eastern half of the inside wall of the crater.

These activities of the mountain continued day and night.

Oct. 23 was also very fine. In the early morning the usual white vapors issuing from the summit of the mountain were seen from Kusatu, but the rumblings could not be heard. The writer ascended the mountain by the same route as that of the preceding day. At 10^h25^m a. m., when about 2 km. southeast of the summit, he saw a small mass of dark ash-cloud being injected into the white vapor-column which had been rising above the level of the mountain up to that time. The heavy charge of ashes clearly indicated an attack of a higher vapor pressure upon the crater-wall. But no noise other than rumblings was heard. From this time on, the emission of ash-laden cloud increased in violence. At about 11^h a. m., within distance of 1·5 km. from the scene of the explosion, he saw dense, dark whorles of ash-laden cloud shoot straight upward incessantly from the summit of the mountain. Simultaneously with these emissions, ejections of rock-fragments occurred frequently. Among these rock-fragments were blocks so large that their flights through the clear air on the weather side were readily seen at a distance of 1·5 km. A clinometer measurement at that distance showed that the maximum height of the column of the ash-laden cloud was about 1300 m. above the level of the mountain. The writer braved the light showers of ashes which he encountered at a distance of about 1 km. southeast from the summit in order to view the explosion at close range, but found it necessary to make a wide detour, owing to large blocks falling as far as almost to the foot of the cone itself.

At 11^h30^m a. m., when he stood watching the explosion from the shortest safe distance (about 750 m. south of the summit crater), the explosive activity at the summit crater (Yugama) culminated in paroxysmal conditions, with long, roaring explosions and emissions of dark clouds densely charged with solid materials. At the same time, the numerous vents in the fissures on the southern flank of the cone were

at the height of their activity, emitting dense whorls of ash-laden clouds (Figs. 17, 19, and 24). The explosions, which occurred at intervals of a few seconds at the summit crater, were often so powerful as to shoot upwards rock-fragments, non-incandescent, to heights at least 700 m. above the crater-rim, and send a tremendous column of heavily ash-laden cloud to heights of more than 1000 m. But no electrical phenomena could be discerned in these clouds. Heavy rumblings without any sensible air-concussion, and noises recalling rock-slides were of almost continual occurrence. Occasionally sharp staccato sounds like those of pistol shots in the open air were heard in rapid succession. Successive showers of rock-fragments upon the southwest flank of the cone, where the air was clear of the ash-laden cloud, raised a dust-cloud from the ground upon which they fell, forming a brilliant spectacle due to the continually changing directions of the particles composing it. Southwestward the rock-fragments reached as far as 500 m. from the summit crater whence they were ejected. They were of varying sizes, the largest appeared at that distances to be about 50 cm. in diameter. In falling upon the cone flank they rebounded to be broken into several fragments, or otherwise they sank deep into the ground upon which they fell.

Although the paroxysmal activity lasted throughout the entire afternoon, discharging vast quantities of solid material, the intensity of the forces gradually diminished, the greater projections of ejecta and the heavier rumblings being synchronous with the explosive maxima. After the explosive maxima, which lasted without any notable intensity variation for about one hour since 11^h30^m a. m., had passed, a visit to the southwestern rim of the Yugama crater-bowl showed that a new explosion-pit had been opened at the base of the inside southeastern wall of the bowl (C_3 in Fig. 34). This pit was the main one, so far as the writer could observe, that gave rise to the explosions of the day. By that time, the activity at this new pit was taking place in the form of a series of very sharp and sudden but moderate explosions in rapid succession, at intervals of $10–15^m$, emitting enormous whorls of ash-laden cloud. From time to time there were greater explosions with a roaring sound. They sent showers of rock-fragments to heights of 150–200 m. above the pit, and so nearly vertical that they invariably fell inside the crater-bowl (Figs. 18, 20, and 21). The bulk of the solid materials ejected by these explosions, except the ashes, fell into the pool in the bottom of the crater-bowl, raising splashes of mud-water, none of which

reached the writer as he stood watching the explosions at the highest point of the northwest rim of the crater-bowl. During these explosions, the ground upon which he stood vibrated continuously, but with a period and amplitude that could not be determined. In the central part of the pool in the bottom of the crater-bowl there appeared gentle fumaroles in two places, emitting white vapors, while numerous fumaroles on the inside wall of the bowl, except the one near the south shore of the pool which was more active than in the preceding day, did not show any notable change in activity.

The explosive conditions of the new pit continued all day and into the evening hours, while rumblings were heard in the night, 7^h p. m. at Manza.

Oct. 24. On visiting the summit again, the writer found, as a result of the explosions of the preceding day, some changes in the activity in and around the Yugama crater-bowl. The explosion pit, which the preceding day had been the centre of the paroxysmal activity, quieted down without emitting any vapors, while three new adjoining southerly pits, which, including the former one, lay side by side in the bottom of the large fissure in the southeastern wall of the crater-bowl, were fiercely throwing out spiral columns of ash-laden vapors with a roaring sound (Fig. 27) These sounds were recurrent, stopping suddenly for a few minutes at intervals of about fifteen minutes. The pool at the bottom of the crater-bowl was at the same level as that observed two days before, with two gentle fumaroles in its middle, while its southern shore became much indented with two circular inlets and a small pool, where white vapors were issuing, along with mud-waters spouting at intervals of a few seconds from a number of temporary vents of no fixed location (Fig. 27).

It was found this day that the number as well as the activity of the fumaroles on the southern flank of the cone had greatly diminished permitting a much better view of the fissures than formerly (Figs. 30, 31, and 32).

At 10^h30^m p. m., or a little later, the same day, the writer at Kusatu thought he could hear detonations in the direction of the mountain.

Oct. 25. At daybreak it was found that 1 mm. of volcanic ash had fallen in Kusatu during the preceding night.

During the remaining days of that month, ash-laden clouds were seen from Kusatu to rise continually from the summit[47]

47) According to Kunitomi, an explosion occurred at 1^h17^m a. m. on Oct. 26, and another one at 9^h3^m a. m. on Oct. 27. *loc. cit.*

In the early days of the succeeding month, according to Tomizawa of Kusatu, the volcano continued its activity as usual, throwing out a moderate quantity of ash-laden clouds which, arching eastward, dropped ashes in Kusatu and vicinity much as if snow had fallen.

Topographical Changes. During the paroxysmal phases of the recent activity, a certain quantity of solid materials that was projected accumulated on the ground in and about the Yugama crater-bowl. But the accumulation of the ejected materials has not made much morphological changes. The only noticeable topographical change was the fissuring, both inside and outside the Yugama crater-bowl, a direct result of the recent explosion. Fig. 34 is a sketch map showing the configuration of the Yugama crater and neighbourhood at the time the writer visited it.

Crater: The bottom of the Yugama crater-bowl, except its southeastern part near the base of the inside southeastern wall of the bowl, did not change either in its depth below the encircling rim or in its configuration. Its southwestern half was as dry as before, the recent ejecta having accumulated to a little less than a quater of a meter, while its northeastern half was a pool of hot (?) water whose level was about 10 m. below the southwestern dry ground. The south shore of this pool was somewhat altered in outline by the explosions of Oct. 23. On Oct. 22, there was an inlet about 10 m. in diameter on the south shore of the pool, and 20 m. northwest of this inlet was another smaller one. On Oct. 23 and 24, the south shore of the pool was indented by two circular inlets which had been formed during the explosions of Oct. 23 at the place where on the preceding day only one inlet was seen. West of these two inlets there was a small pond, about 7 m. in diameter.

The inside southern wall of the Yugama crater-bowl was scored with shallow vertical grooves. These grooves may have been formed by explosions that probably occurred in the last-mentioned inlets on the southern shore of the pool.

The inside southeastern wall of the Yugama crater-bowl was fissured deeply in nearly a north-and-south direction, whereas formerly it was an almost perpendicular cliff encircling the crater-bowl (see Fig. 6, p. 90). The fissure there appeared to extended the whole length from near the upper rim of the crater wall downward to the base near the shore of the pool, but separated from the pool by a narrow ridge. This fissure was probably formed by the explosions early on Oct. 1,

but in which, on Oct. 22 were found only fumaroles emitting white vapors (see Fig. 26). The centre of the explosive activity of Oct. 23 was located within this fissure, near the shore of the pool.

The inside northeast wall (C_1 in Fig. 34) of the Yugama crater-bowl, half way down on which the explosion of Oct. 1 occurred and where, on Oct. 2 occurred a continuous emission of vapor-clouds (see Fig. 25), was not much altered by the explosion of Oct. 23, remaining as before an almost perpendicular rocky cliff with a talus conoid at its base.

No change, except accumulation of solid ejecta, was noticed inside the Midugama and the Karagama crater-bowls.[48]

Fissures: Outside of the Yugama crater-bowl on the southeast were two noticeable fissures as indicated by new lines of fumaroles—one (F in Fig. 34) near the crest of the southeastern rim of the crater-bowl and the other ($f_1, f_2 \ldots$ in Fig. 34) half-way down on that side of the cone. The former, running in the S. W.-N. E. direction, is more than 50 m. long, and about 15 m. in its widest part, and separated by a thin wall of less than 15 m. in thickness at any point from the inside of the Yugama crater-bowl. The inside walls of the fissure form nearly perpendicular cliffs, with precipices overhanging the abyss in places (Fig. 12). A wire measurement of the fissure showed it to be over 30 m. deep, with mud and water at the bottom, although the bottom could not directly be seen owing to the thick vapors issuing violently from the fissure. To the southwest the fissure shallows stepwise, ending in the cone surface; while it extends northeastward toward the upper margin of the southeastern rim of the Yugama crater-bowl and appears to continue to the fissure on the inside southeastern wall of that bowl, although their actual connection at the surface could not be seen. The south wall of the fissure is opened by another branch fissure which extends southeastward

Fig. 12.—Oct. 22, 1932. The fissure (F in Fig. 34) near the crest of the Yugama crater-bowl, looking northeast from its southwestern end. Photo Tsuya.

48) According to Kunitomi, there was a fumarole in the bottom of the Karagama crater-bowl on Oct. 29 1932. *loc. cit.*

for a short distance and which seems to merge into the other lateral fissure.

The fissure half-way down on the southeast flank of the cone is more than 300 m. long, extending in a N. N. E.—S. S. W. direction with a zigzag course. It does not reach the surface at all points along its whole length, but, as indicated by a number of fumaroles, is represented at the surface by a long chain of minor clefts and hollows of various sizes. At the time of the first explosion on Oct. 1, vapor-clouds heavily charged with solid materials were violently projected from this fissure (Fig. 29), but later it gradually lessened in violence, until, on Oct. 22, vapor was seen only in a number of the fumaroles. The extraordinary length of the fissure was readily apparent, but only eye-measurements of its southern wing could be made owing to the presence of dense vapors which made it unsafe for the writer to trace the fissure further northward when he approached the seventh fumarole (f_7 in Fig. 34). The southern wing of the fissure consists of the following parts (see Fig. 34.):

f_1. A sigmoidal fissure, about 10 m. long, and a meter wide. Its bottom, except a place whence vapors were issuing, was about a meter deep. A fumarole within it was emitting white vapors charged with small rock-fragments, less than 3 cm. in diameter, from a cleft, about 10 cm. wide (Fig. 13). On the north, this fissure opens into an oval hollow, about 3 m. wide, 5 m. long, and 2 m. deep, which however had ceased to emit anything.

Fig. 13.—Oct. 22, 1932. The most southerly lying fumarole (f_1 in Fig. 34.), looking north. Photo Tsuya.

f_2. A lenticular opening, about 10 m. long, 4 m. wide, and more than 3 m. deep, surrounded by an almost perpendicular wall. Ash-laden vapors were issuing from the southern corner of its bottom. On the north of this opening was an oval hollow, about 3 m. long, 2 m. wide, and 2 m. deep, which however had ceased to emit anything.

f_3. A hunchback-shaped opening, about 3 m. wide, 10 m. long, and a meter deep. Vapors were issuing with ejection of rock-fragments of less than 5 cm. in diameter, from a round vent, about a meter in diameter, at the central part of its bottom

(Fig. 14). On the north of this opening was a lenticular one (f_4), about 10 m. long, 7 m. wide, and 2 m. deep, in which stood water in a small pool.

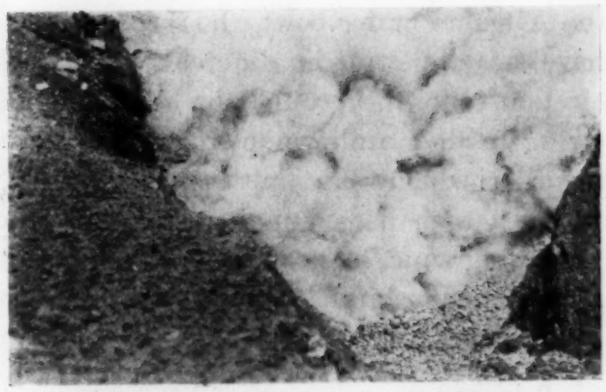

Fig. 14.—Oct. 22, 1932. f_3 fumarole looking north. Photo Tsuya.

f_5. A circular opening, about 10 m. across, and 6 m. deep. It is encircled by an almost perpendicular wall. Vapors were issuing from a circular vent, about a meter in diameter, at the northeast corner of its bottom (Fig. 15). A miniature mud-flow gushed out of this opening, extending southeastward for a distance of about 50 m.

f_6. An oval opening, 3 m. long, and 2 m. wide. Vapors were issuing from its unknown bottom.

f_7. A circular opening, about 5 m. across and a meter deep. Vapors were issuing from four holes at the centre of its bottom.

f_8. A circular dish-shaped hollow, about 2 m. across. Vapors were issuing from its bottom.

There were about six fumaroles north of the one last-mentioned. They were nearly in a line on the northern extension of the fissure represented by the above-mentioned seven openings (Fig. 32)

Fig. 15.—Oct. 22, 1932. f_5 fumarole looking east. Photo Tsuya.

Ejecta. *Solid ejecta.* Neither molten material nor incandescent blocks were thrown out by the recent explosions. The solid ejecta consist wholly of non-incandescent detritus, all coming under the title "accessory ejecta." They were projected from new explosion-craterlets within the Yugama crater-bowl as well as from the fissures on the outside, in many directions, not all of which ejecta, naturally, were the products of one and the same explosion. Since during the paroxysmal phases the centres of activity had shifted from place to place in and about

the Yugama crater-bowl, the products ejected from these centres must have accumulated in different areas, each according to the source of ejection. But they could not be distinguished the one from the other, owing to their uniform petrographic characters and to the thickness of the ashes which were emitted even during the relatively quiet period that followed each paroxysmal phase, and which under the influence of the prevailing wind had covered the greater part of the cone. Consequently any particular limit of distributions of solid ejecta, which might have furnished a clear picture of the explosion mechanism, was not to be found. Fig. 33 shows the distributions of the solid ejecta as observed on Oct. 22.

Stones from a few centimeter to more than 100 cm. in diameter were scattered in and around the Yugama crater-bowl, reaching an extreme distance of about 700 m. on the northwest and the southeast side of the cone. Their total quantity however may not be very large, as inferred from the density of the holes on the roofs of the cottages in the Yugama crater, which were riddled with the falling stones during the recent explosions.[49]

The large-sized ejecta are angular or subangular, but occasionally their corners are rounded off. They are generally dull gray, but often grayish white or yellow with a coating of salts. So far as microscopical observations go, they are olivine-two-pyroxene-andesite. Among the medium-sized ejecta, 10–5 cm. in diameter, were found quite a number of fragments of laminated ash-deposit, besides the olivine-two-pyroxene-andesite.

Volcanic ash and sand covered the country to the northeast side of the volcano, their deposits being the thickest in a zone running from the summit-crater northeast toward Yosigataira where it attained a thickness of about 3 cm. Toward the crater there is naturally an increase in the thickness of their deposits as well as in the size of the individual particles. Their accumulation upon the flanks of the cone, near the upper rim of the summit-crater, except the southwestern flank, attained a depth which in places was not less than a meter. They are light gray with a bluish tint, whereas in places where they are still damp with water condensed from the vapors with which they were ejected, they are dark gray. Petrographically they are nothing but finely divided

49) Kunitomi found on Oct. 29 that the cottages had been seriously damaged. It is probable therefore that not a few solid ejecta were projected to this direction by the explosions that followed the one of Oct. 23.

fragments of the old cone material.

On the southern flank of the cone were two small mud-flows one (Fig. 16) extending southeastward from fumarole f_5 in an area of about 5 m. in width and 50 m. in length, with a depth of about 20 cm., and the other, whose sourse could not be discovered, extending in a fan-shaped area to a distance of about 10 m. west of that fumarole. They are a mixture of rock-fragments of varying sizes, besides sulphur and other constituents of gaseous emanations. Their surface conformation is virtually that of a thin fluid, indicating that they must have possessed great fluidity through their large water content.

Fig. 16.—Oct. 22, 1932. A mud-flow on the southern flank of the mountain. Lower left, a portion of the f_5 fumarole. Photo Tsuya.

Fumaroles: All the fumaroles in and around the Yugama crater-bowl are of primary origin, having direct connection with explosive channels within the volcano, as inferred from the fact that they fluctuate in number, intensity, and location, according to the rise and fall in the activity of the main centres of the recent explosions.

The principal emanation from the fumaroles was steam, but some acid, among which sulphur dioxide and hydrogen sulphide were clearly detected, must have been present, as inferred from incrustations around the fumaroles. Qualitative analysis of the soluble matter from the volcanic ash showed fairly large amounts of Cl and SO_4 along with lesser amounts of Fe″, Ca, Al, Na, and Mg.

The temperature of a fumarole on the southern rim of the Yugama crater on Oct. 22, 1932, was as high as 98°C. (atm. temp. 11°C.).

Character of the Explosions of Oct., 1932.

The explosions of 1932 were of the same nature and of about the same intensity as previous explosions of the mountain, whose historic records provide us with a very clear picture of the character of the volcanic activities that have taken place on the mountain since 1882. They are just the type of volcanic activity that would be expected of a not very active,

long-dormant volcano, with characteristics as follows: (1) The solid materials ejected during the recent explosions were entirely old cone material. (2) There was no evidence of extremely high temperature on the mountain and in the ejecta. A new fumarole on the summit showed a temperature of 98°C.[51] (3) Steam was at all times the dominant gaseous emanation, both in the explosion clouds and in the outpourings from cracks, during as well as after the explosions. Mud-water gushed out during the explosions.

In short it may be said that the explosions of 1932 did not reach down to the zone of red heat, and that they were altogether of the so-called "steam-explosion," taking place near the earth's surface without the participation of fresh lava or more than insignificant quantities of the more active chemical constituents. The locations of the recent explosions are limited to a narrow zone which, passing through the inside northeastern wall of the Yugama crater-bowl, runs in a nearly N.-S. direction. The previous historic explosions of the volcano occurred for the most part in this zone. It is interesting to note in this connection that the arrangement of the craterlets on the main body—Moto-Siranê, and the general trend of volcanoes of this region is in this azimuth, all probably indicating structural weakness in this azimuth of the earth's crust of this region.

In the light of previous activities of this volcano during historic times, it may be said that the present activity of the volcano is not likely to be of long duration.

---

7. 昭和7年10月草津白根山の爆發

地震研究所 津 屋 弘 逵

昭和7年10月1日午後2時頃草津白根山が爆發し，2名の卽死者と7名の負傷者とを生じた．この爆發を最初として同月中に數回の爆發があり，その一は筆者が同山頂に居た同月23日に起つた．

本文では筆者がこの數回の爆發に就いて10月20日より25日までに同地に於て調査し得た結果を主として報告し，尙同火山の地質及び記錄に殘つてゐる爆發の概略を述べた．

---

50) It is noteworthy that measurements have revealed scarcely any changes in the temperatures of the hot springs in the Manza spa nor in the old fumaroles in the Sessyôgawara.

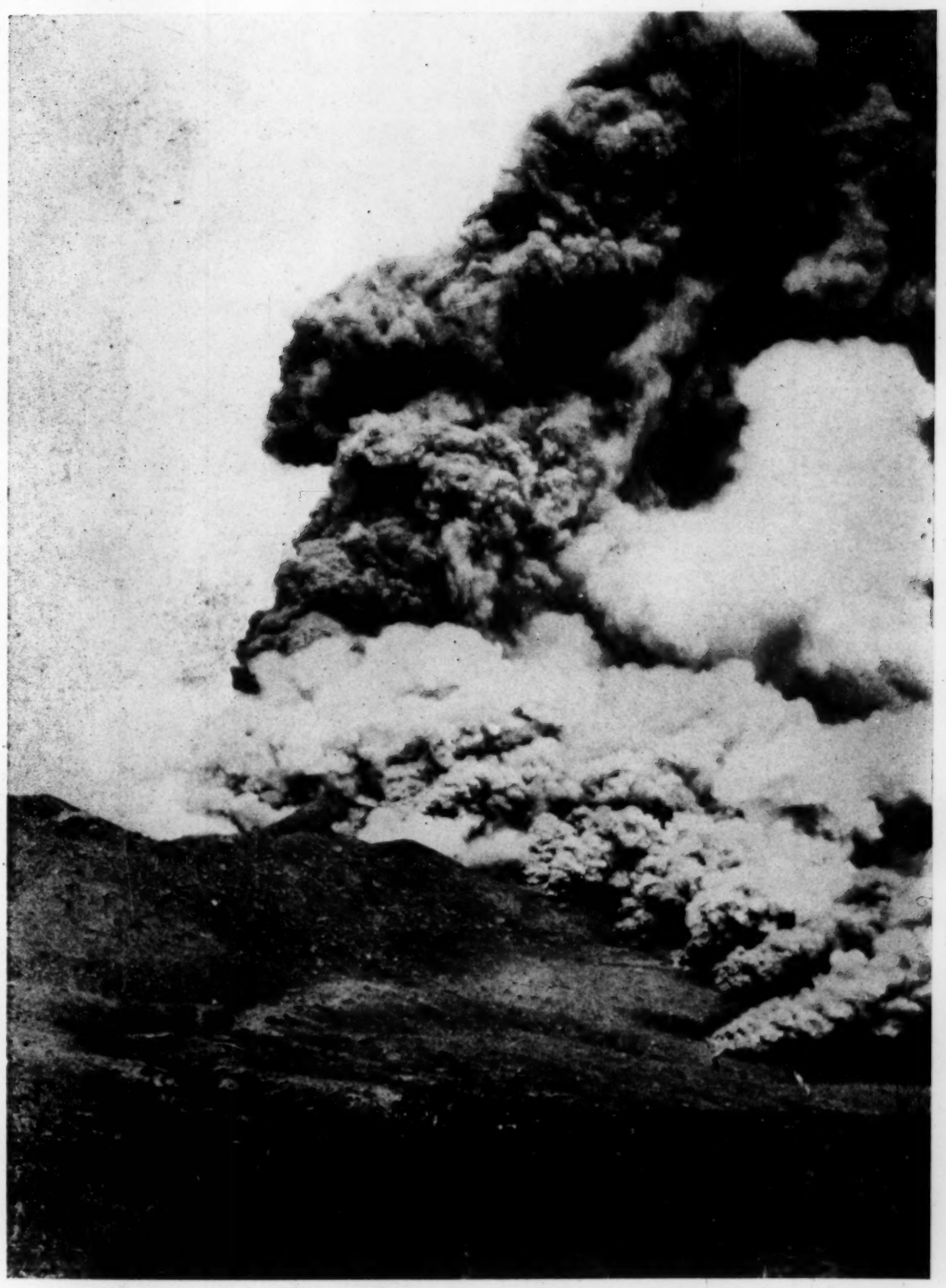

Fig. 17.—Oct. 23, 1932. The explosive culmination of Kusatu-Siranê at 11^h30^m a. m., taken near Yumiiké, 750 m. southwest by south of the summit crater (Yugama).
Photo Tsuya.

（震研彙報、第十一號、圖版、津屋）

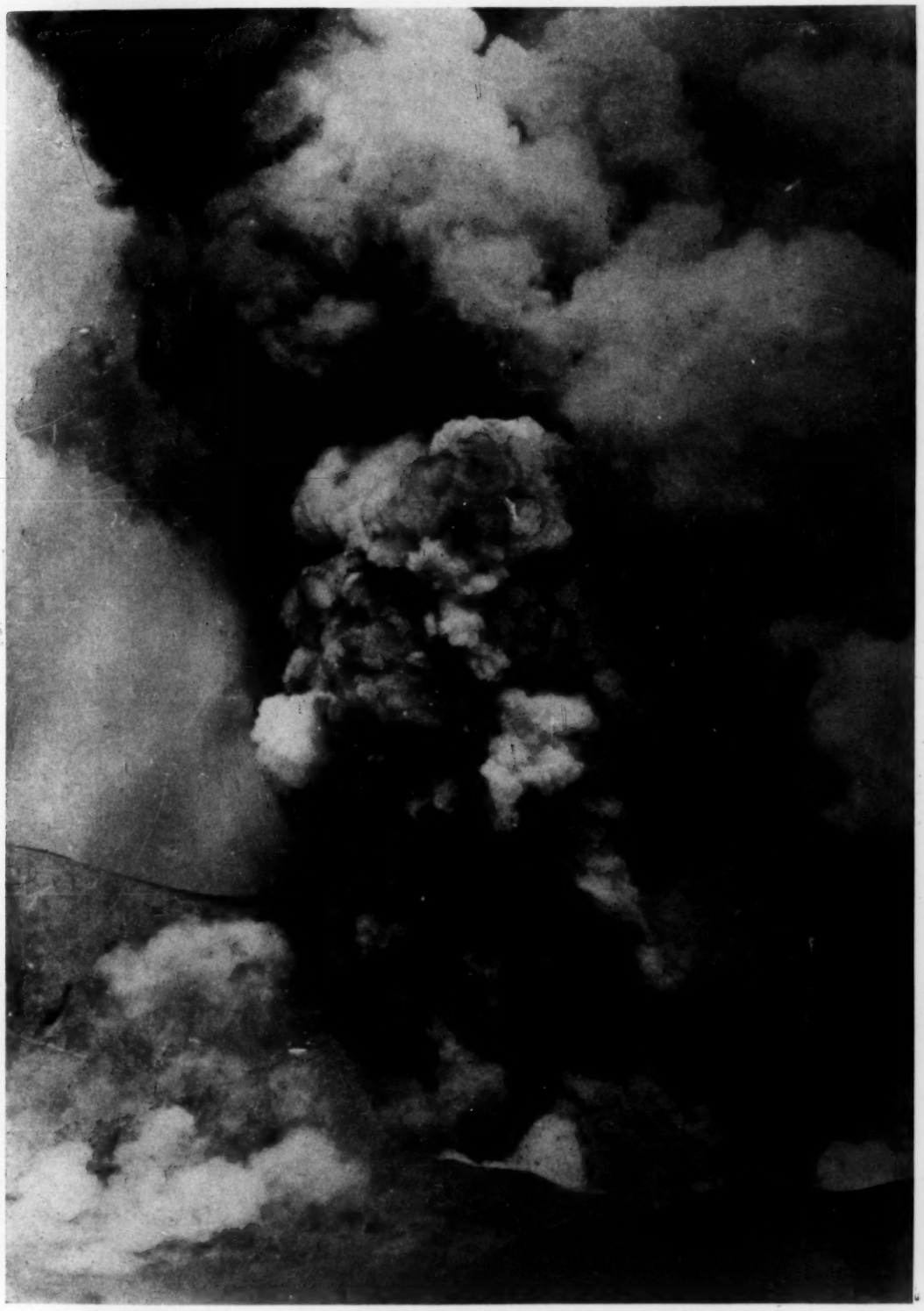

Fig. 18.—Oct. 23, 1932. An explosion of Kusatu-Siranê at 1^h30^m p. m. Looking northeast from the southwestern rim of the Yugama crater-bowl. Note the splashes (black spots above the pool, lower left in the figure) caused by falling stones. Photo Tsuya.

（震研彙報、第十一號、圖版、津屋）

（震研彙報、第十一號、圖版、津屋）

Fig. 19.—Oct. 23, 1932. Another view of the explosive culmination of Kusatu-Sirané at 11^h30^m a. m. (*cf.* Fig. 17).
Photo Tsuya.

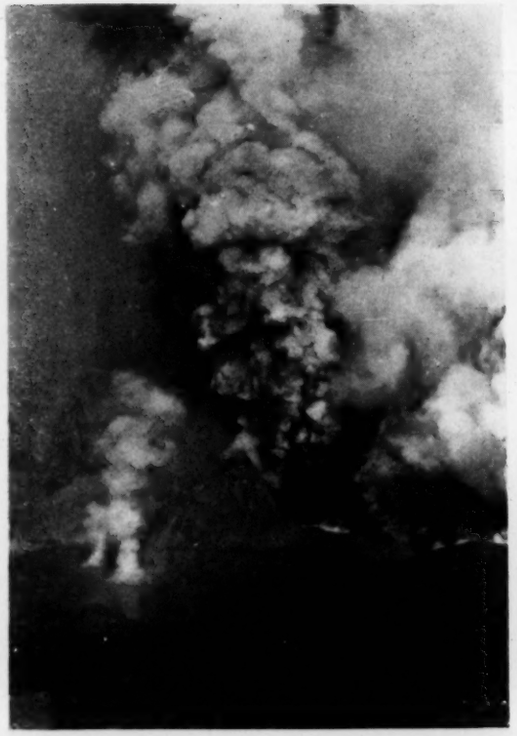

Fig. 20, and 21.—Oct. 23, 1932. Two different phases of the explosion of Kusatu-Sirané in the afternoon (*cf.* Fig. 18).
Photo Tsuya.

Fig. 22.—Oct. 1, 1932. The explosion of Kusatu-Sirané at 1^h50^m p. m., viewed from Kusatu. Photo Tomizawa.

Fig. 23.—Oct. 4, 1932. The explosion of Kusatu-Sirané at 2^h p. m, viewed from Kusatu. Photo Tomizawa.

（震研彙報、第十一號、圖版、津屋）

Fig. 24.—Oct. 23, 1932. The explosive culmination of Kusatu-Sirané at $11^{h}30^{m}$ a. m., viewed from Kusatu.
Photo Tomizawa.

Fig. 25.—Oct. 2, 1932. View of the northeastern inside wall of the Yugama crater-bowl at the summit of Kusatu-Sirané, where the explosion on Oct. 1, 1932, occurred.
Photo Tomizawa.

（震研彙報、第十一號、圖版、津屋）

Fig. 26.—Oct. 22, 1932. General view of the northeast inside wall of the Yugama crater-bowl at the summit of Kusatu-Siranê. Photo Tsuya.

Fig. 27.—Oct. 24, 1932. View of the southeastern side of the Yugama crater-bowl, where the explosion on Oct. 23, 1932, occurred (right half of Fig. 26). Photo Tomizawa.

（震研彙報、第十一號、圖版、津屋）

（震研彙報、第十一號、圖版、津屋）

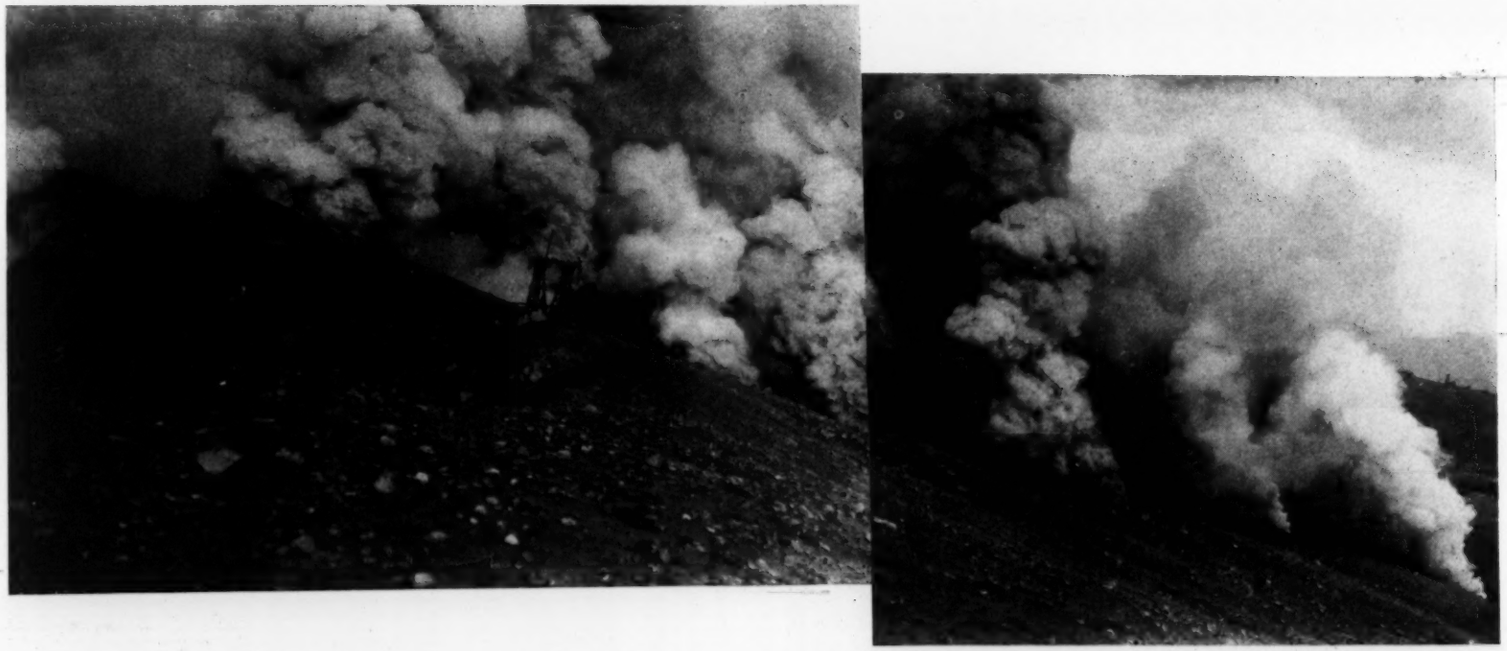

Fig. 28.—Oct. 22, 1932. A view of the southern flank near the summit of Kusatu-Siranê, showing a line of fumaroles on the fissure extending in N. N. E.-S. S. W. direction down the flank. Looking southeast from the southwestern rim of the Yugama crater-bowl. Photo Tsuya.

Fig. 29.—Oct. 2, 1932. View of the fissure extending in N N. E.-S. S. W. direction on the southern flank near the summit of Kusatu-Siranê after the explosion of Oct. 1, 1932. Photo Tomizawa.

Fig. 30.—Oct. 24, 1932. Ditto (*cf.* Fig. 19). Photo Tomizawa.

（震研彙報、第十一號、圖版、津屋）

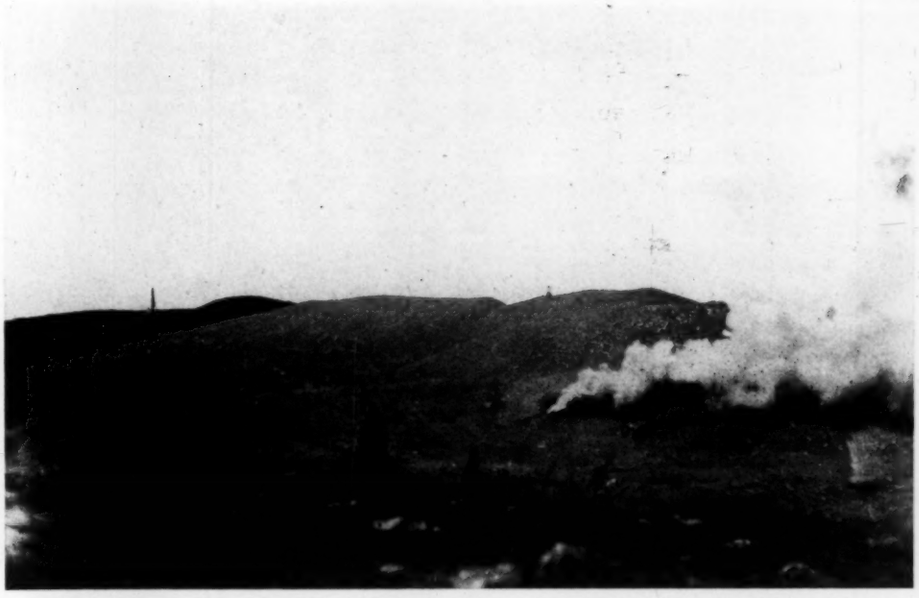

Fig. 31.—Oct. 24, 1932. View of the western half of the southern flank of Kusatu-Siranê proper after the explosion of Oct. 23, 1932. Photo Tsuya.

Fig. 32.—Oct. 24, 1932. View of the eastern half of the southern flank of Kusatu-Siranê proper after the explosion of Oct. 23, 1932.
Photo Tomizawa.

（震研彙報、第十一號、圖版、津屋）

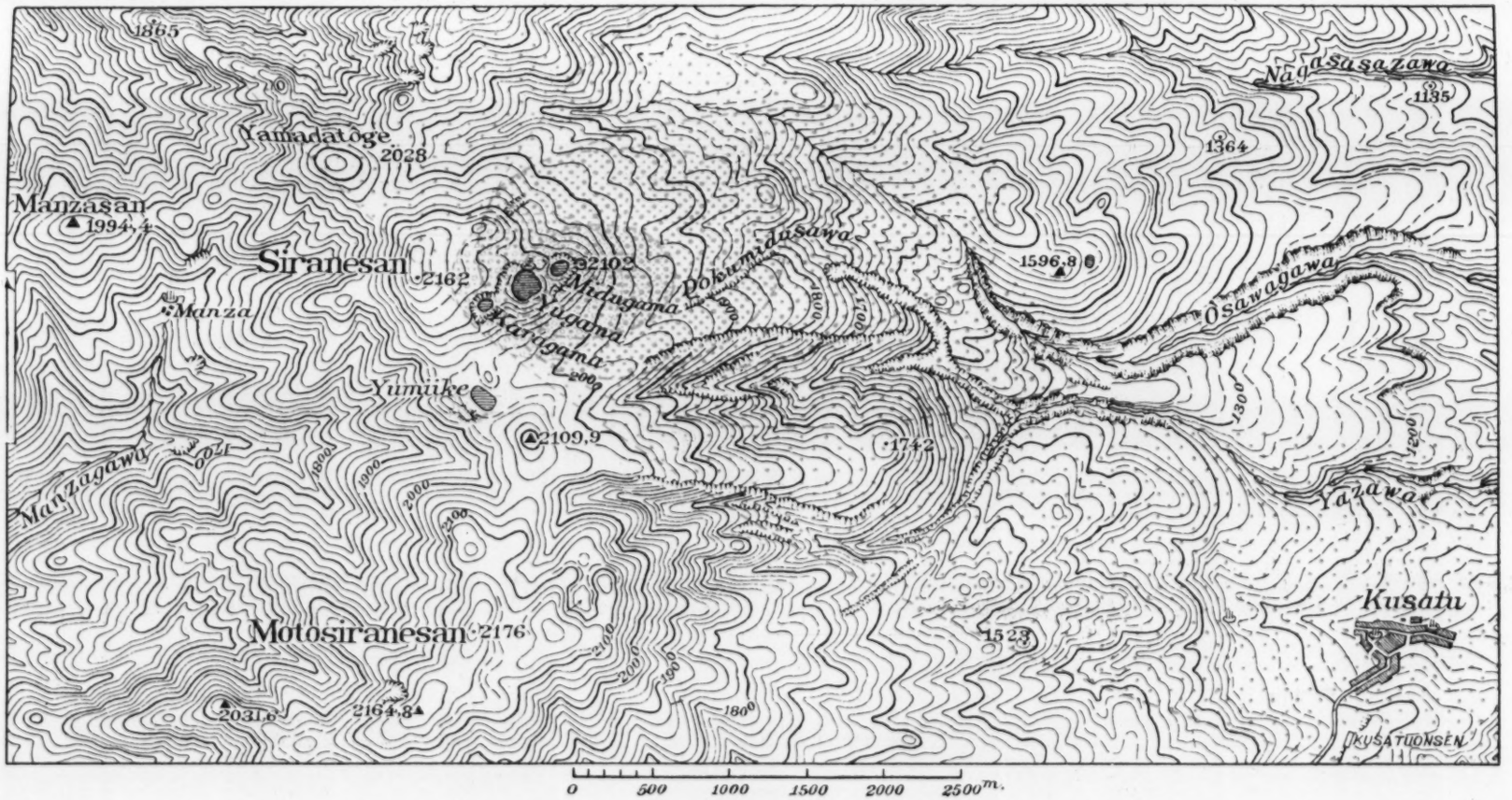

Fig, 33. Map of a portion of volcano Kusatu-Siranê showing distribution of the solid ejecta of Oct. 1-24, 1932.

（震研彙報、第十一號、圖版、津屋）

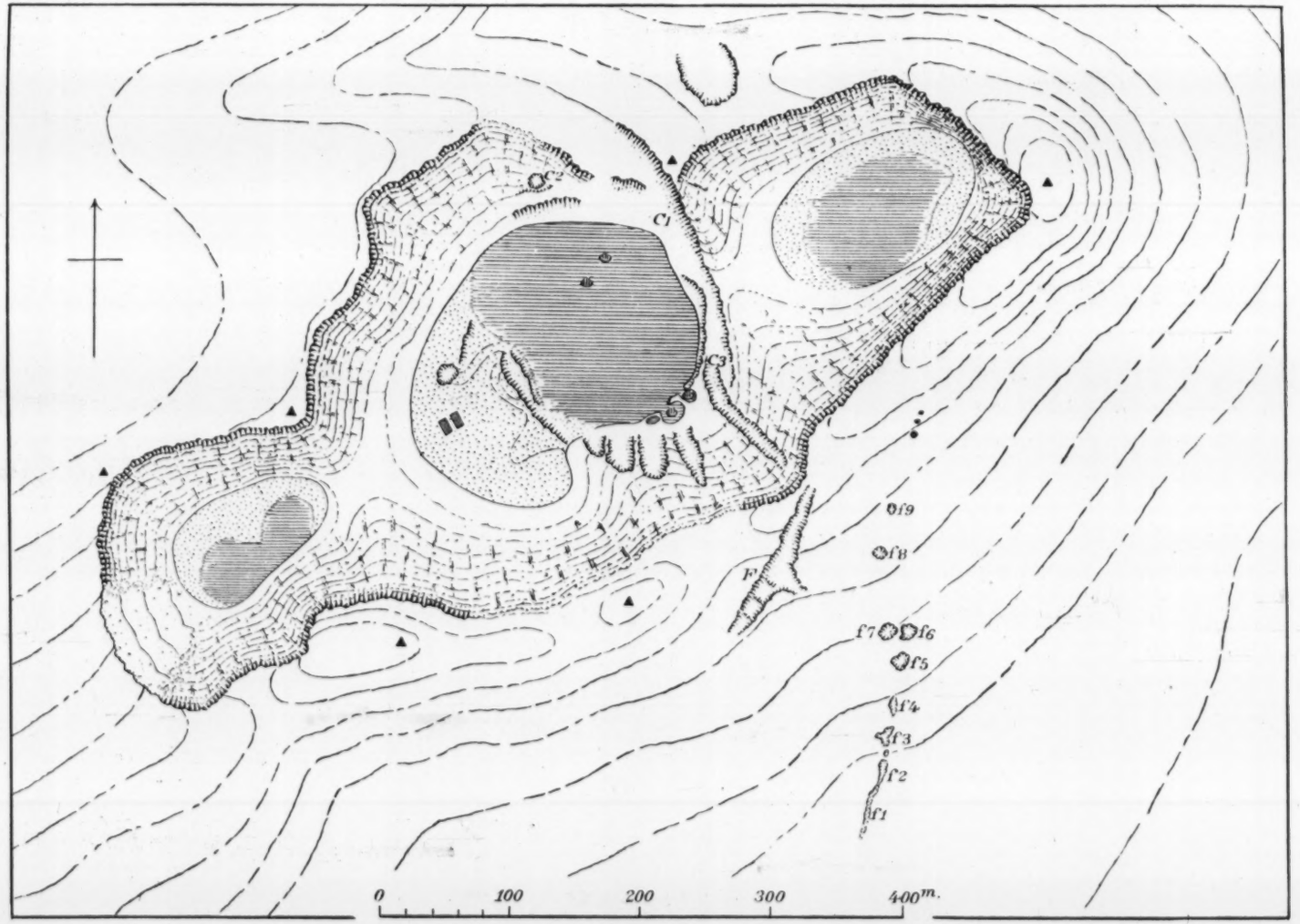

Fig. 34. Sketch map showing the state of the summit crater of volcano Kusatu-Siranê after the explosion of Oct. 23, 1923. See pp. 106~111.

（震研彙報、第十一號、圖版、津屋）

8. *Détermination de la limite perceptible des secousses*

par

Mishio ISHIMOTO et Minoru OOTUKA,

Institute de Recherches sur les Tremblements de terre.

(Lu le 20 Décembre 1932, reçu le 20 Décembre 1932)

1. Introduction.

Pour exprimer l'intensité sismique, on utilise une échelle dont le degré est défini suivant le produit de la conséquence des secousses. Les séismes appartenant au premier degré sont les secousses qui ne donnent aucune sensation aux hommes, tandis que les séismes appartenant aux autres degrés sont ressentis. Nous sommes certains qu'il y a un critérium distinct entre les deux degrés: c'est la limite perceptible des secousses. Nous voulons exécuter une expérience sur la sensibilité humaine aux secousses pour mettre en evidence ce critérium que l'on emploie comme définition dans l'échelle d'intensité sismique.

Certainement, comme un des auteurs[1] la déjà rapporté, il est possible de représenter l'intensité sismique avec l'accélération maxima des secousses. Il a ainsi proposé une échelle constituée par ce paramètre et obtenu 0,5 gal de l'accélération maxima pour la limite perceptible de secousses dont la période est 0,3 seconde. Naturellement, cette valeur d'accélération a été considéré comme correspondante au critérium.[2] Nous voulons déterminer ce critérium par une expérience, et voir s'il s'applique bien ou non.

En partant de cette idée, nous avons construit une plate-forme oscillante. Plusieurs expérience ont été déjà faites avec une plate-forme oscillante supportée par des roues ou des billes. Mais, l'existence du frottement solide dans ce système ne permet pas d'exécuter un mouvement doux de la plante-forme surtout dans le domaine des grandes périodes. Il nous semble donc qu'il est presque impossible de réaliser

1) M. ISHIMOTO, *Bull. Earthq. Res. Inst.*, 10 (1932), 614.

2) Il y a plusieurs valeurs de la limite perceptible déjà proposées. F. Omori a donné 1,7 gal; Cancani 0,25 gal dans son échelle d'intensité sismique; McAdie 1 gal; Suyehiro 0,89-1,73 gal correspondé 1,49-2,83 sec. de période. (Voir M. Ishimoto, loc. cit.)

les conditions du mouvement purement sinusoïdal. Pour calculer la valeur d'accélération maxima, on prend généralement l'amplitude et la période des secousses: cette façon de calculer est parfaitement juste tant que le mouvement reste purement sinusoïdal. Nous avons déjà indiqué qu'il y a un cas où les secousses de grande amplitude masquent les secousses de grande accélération: nous voulons éviter cette erreurs.

Nous sommes donc obligé de construire une plate-forme oscillante du système suspendu afin d'obtenir un mouvement parfaitement sinusoïdal. De plus, il est nécessaire de mesurer le mouvement de cette plate-forme directement par l'accélération pour connaître l'état d'oscillation en valeur d'accélération, sinon nous ne pouvons pas accepter avec confiance les résultats obtenus par l'expérience sur la détermination de la limite perceptible de secousses. C'est parce que comme on verra plus tard, la sensation de secousses depend simplement de la valeur d'accélération des secousses.

2. Construction d'une plate-forme oscillante.

Nous avons construit une plate-forme en bois dont la dimension est 200 cm × 93 cm. Elle est suspendue par quatre crochets au plafond au moyen de quatre cordons de chanvre. Ces cordons se croisent obliquement et l'oscillation de la plate-forme se limite à une direction: sa période propre d'oscillation a été measurée et est de 3 seconde environ.

Pour amortir la période propre d'oscillation nous avons mis un amortisseur à l'extrémité de la plate-forme; amortisseur dont le piston plonge dans un tube rempli d'huile épaisse. Nous avons employé comme la force motrice un moteur électrique de 1/2 cheval puissance.

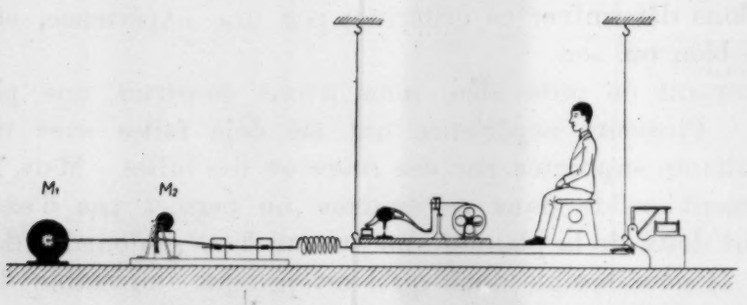

Fig. 1. Aspect général de la plate-forme oscillante.

Comme on l'a représenté dans la Fig. 1, il y a trois tiges qui servent à transmettre le mouvement périodique du moteur à la plate-forme.

Au moyen d'une vis attachée excentriquement à l'extrémité de l'arbre du moteur, la première tige fait le mouvent sinusoïdal. A la jonction de la première et la deuxième tiges, nous avons mis un système pouvant faire varier l'amplitude du mouvement.[2] La deuxième tige transporte directement son mouvement à une troisième tige constituant une coulisse. Le battement de cette coulisse provoque le mouvement de la plate-forme par l'intermédiare d'un ressort solénoïdal. Cet arrangement est tout à fait necéssaire pour avoir le mouvement sinusoïdal. Quand on examine simplement le déplacement de la plate-forme, tous les mouvements ressemblent à de mouvement parfaitement sinusoïdaux. Nous pouvons constater, cependant, que le mouvement n'est pas constitute par un seul mouvement sinusoïdal par l'emploi d'un appareil accélérométrique. On doit donc, absolument adopter le ressort pour avoir une plate-forme accompagnant une oscillation complètement sinusoïdale.

Quand la période de secousses reste assez petite, nous appliquous la fréquence de rotation du moteur directement à la plate-forme. Mais, nous mettons une paire de roues dentées entre le moteur et la première tige pour diminuer la fréquence d'oscillation dans le rapport de 1/4 surtout à l'égard des secousses de grande période.

En installant un sismographe accélérométrique sur la plate-forme, nous avons réussi à examiner toujours de la même façon le mouvement oscillatoire. L'étalonnage de ce sismographe a été fait avec beaucoup de soins surtout dans le domaine en question. En faisant incliner la plate-forme, nous avons constaté que la déviation de plume ξ est toujours proportionelle à l'inclinaison θ: on a la relation suivante :

$$\xi = kg\theta.$$

Nous avons obtenu une ligne droite comme la courbe d'étalonnage (Fig 2). Nous pouvons en tirer des conclusions assez précises sur la détermination de la valeur d'accélération.

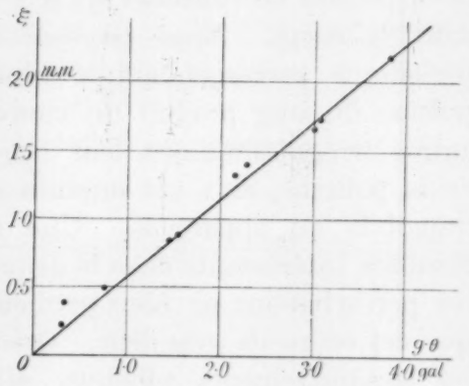

Fig. 2. Courbe d'etalonnage faisant le sismographe accélérométrique.

Nous avons exécuté un autre étalonnage : un fil élastique de caoutchouc dont une extrémité est attachée par un crochet à la masse du pendule, et dont l'autre extrémité du fil est animée d'un mouvement sinusoïdal d'amplitude constante et

3) Inventé par le regretté Directeur K. Suyehiro.

de différente périodes. Nous avons facilement obtenu une courbe d'étalonnage suivant le degré d'amortissement du pendule. En faisant régler le robinet attaché à l'amortisseur d'air, nous avons réussi à obtenir une courbe tout à fait horizontale dans la domaine de la période considérée. (Fig. 3) Le fonctionnement de cet appareil a été vérifié complétement avec ces deux types d'étalonnages et nous n'en n'avons dès lors plus exécuté au cours des autres expériences.

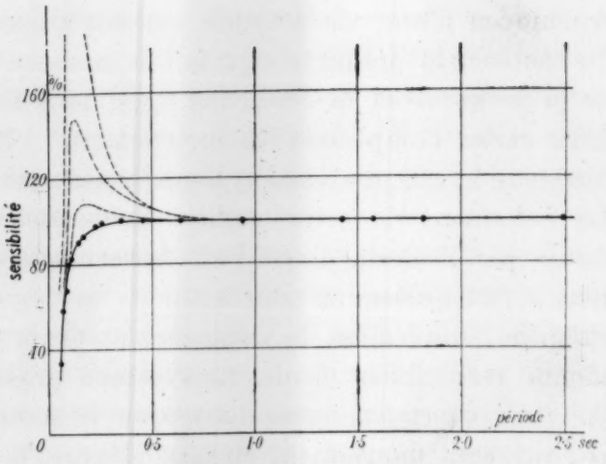

Fig. 3. Courbe d'étalonnage sous l'action de la force périodique.

3. Expériences.

Sur la plate-forme l'homme s'assied sur une chaise en bois tournée dans la direction des secousses. Bien qu'il soit aussi immobile que possible le sismographe enregistre toujours une courbe irrégulière. (Fig. 4) Cela nous permet de constater qu'il y a des mouvements ayant leur origine dans le corps. Nous pouvons distinguer parmi eux, le mouvement périodique correspondant à celui du coeur. Il nous semble que l'impulsion du sang produit un mouvement transmis à la plate-forme. Les autres irrégulalités ont leur origine dans les mouvements du ventre, de la poitrine, etc : ces organes remuent toujours quoique le corps soit immobile en apparence. Une étude de cette courbe, donnerait des résultats intéressants dans le domaine physiologique. Dans le cas présent ces perturbations ne nous permettent pas d'étudier l'accélération moindre que cet ordre de grandeur. Quoique ces perturbations apparaissent dans les enregistrements obtenus, elles sont assez petites comparées à la grandeur d'accélération en question et nous pouvons exécuter nos expériences dans les même conditions sans rien changer.

Pour exécuter l'expérience, un manipulateur maintiens la rotation du moteur toujours constante au moyen d'une disque sectionnée et d'une lampe de néon alimentée par le courant électrique de la ville. Conséquemment, la rotation de moteur reste constante autant que la fréquence

électrique demeure constante. On sait qu'il n'y a pas de variation supérieure à 1 p. 100.

Le manipulateur fait varier l'amplitude de la plate-forme au moyen d'un système que nous avons mis entre la première et la deuxième tiges. Quand il fait tourner une vis à l'aide d'un petit moteur (M_1), le rapport d'amplitude varie continuellement.

Après avoir donné la rotation au moteur M_1 pendant une certaine longueur de temps, le manipulateur coupe le circuit électrique et attend la réponse " ressenti " ou " non-ressenti " de l'homme sur la plate-forme. Quand la reponse est " non-ressenti," le manipulateur ferme un peu de temps le circuit électrique de M_2 afin d'augmenter l'amplitude de battement de la coulisse. On ferme, ensuite, le circuit électrique de M_1 et on continue le même procédé déjà décrit. On pourra, à la fin, avoir la réponse " ressenti " dans le domaine perceptible de secousses. A la suite, le manipulateur diminue l'amplitude progressivement jusqu'à une valeur où l'homme sur la plate-forme ne perçoit plus de secousses. Pendant cette manipulation, le sismographe inscri tous les mouvements de la plate-forme en valeur d'accélération. Nous pouvons, donc, déterminer tout de suite la valeur maxima d'accélération correspondant à la limite perceptible des secousses. Les valeurs de seuil pour les autres périodes sont aussi déterminees de la même façon.

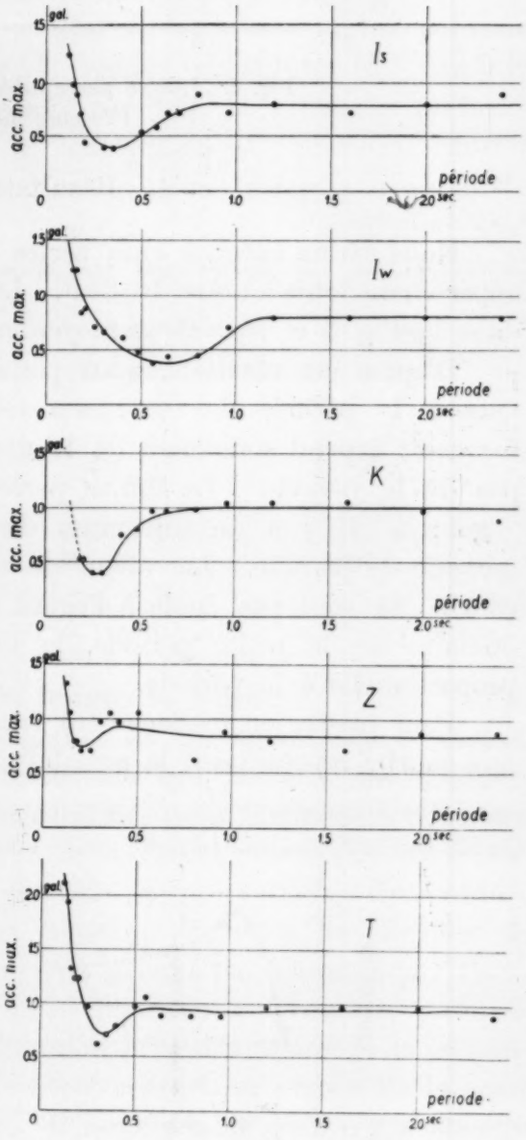

Fig. 5. Limite perceptible d'accélération maxima obtenue de chaque personne.

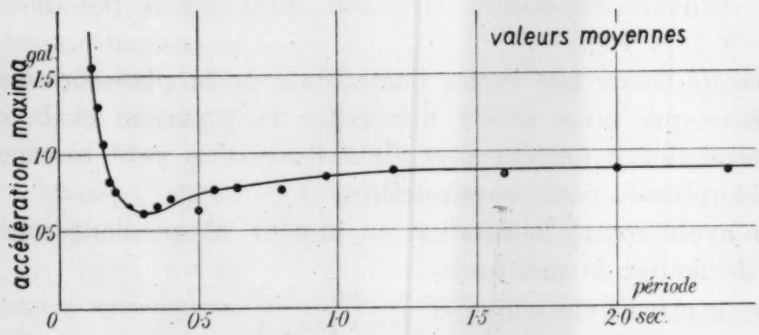

Fig. 6. Limite perceptible dáccélération maxima.
(Valeurs moyennes)

4. Résultate obtenus.

Nous avons exécuté cinq séries d'expériences avec cinq personnes appartenant touts à notre Institut. Les résultats obtenus sont représentés dans la Fig. 5 et les valeur moyennes des résultats dans la Fig. 6.

D'après ces résultats, nous pouvons tirer certaines conclusions. 1° Quand la période des secousses est assez grande, la perception de secousses depend seulement de la grandeur d'accélération et ne depend pas de la période. La limite perceptible d'accélération est voisine de gal: 2° Il y a un minimum dans la courbe aux environs de 0,5 seconde de période. La valeur du minimum ainsi que la forme de la courbe ne sont pas égale à l'egard de chaque personne: 3° Dans le domaine de la petite période, la limite de peception est inversement proportionelle à la période.

Pour mettre en évidence ces caractéristiques, il est mieu de tracer une courbe représentant la sensibilite humaine aux secousses en mainte-

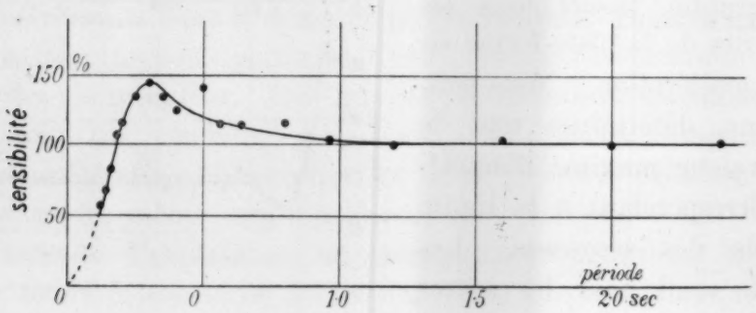

Fig. 7. Sensibilité humaine aux secousses tenant l'accélération maxima constante.

nant l'accélération constante : c'est la courbe dont l'ordonnée est représentée par la valeurs réciproque de l'accélération perceptible. (Fig. 7.) Nous rappelons que cette courbe ressemble beaucoup á celle qui représente l'amplitude d'un pendule sous l'action de secousses dont l'accélération maxima est constante. On verra dans la Fig 3 un bel exemple des courbes d'étalonnage du sismographe accélérométrique. La position maxima coïncide à peu près avec la période propre d'oscillation et la hauter maxima depend du degré d'amortissement du pendule.

D'après la caractérisque de la courbe de sensibilité, nous pouvons constater que l'homme assis sur la chaise constitute un pendule renversés, quoique ce pendule ne soit pas fait de substance parfaitement solide. L'homme-pendule a, naturellement, plusieurs modes d'oscillations. S'il agite son corps nous pouvons compter deux sortes de périodes propres d'oscillation. Ces deux modes d'oscillation sont montrés dans la Fig. 8 Le mode-a a une période de 0,7 sec. environ, tandis que le mode-b une période de 0,3 sec. environ. On pourra détecter ces deux modes d'oscillations qui prédominent dans les courbes représentées dans la Fig. 5. Il nous semble que chaque personne a différentes habitudes d'oscillation du corps sous l'action de secousses et ces différences produisent les différentes formes de courbe.

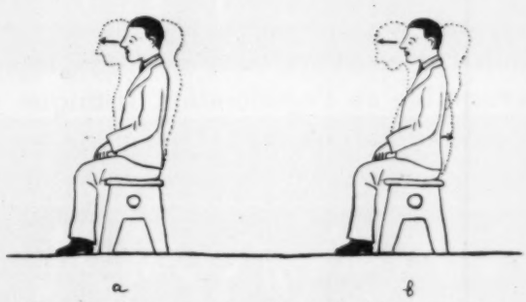

Fig. 8. Deux modes d'oscillation produits dans le corps humain.

Or, si nous considérons la fonction de perception des secousses, nous pouvons compter plusieurs sensations qui peuvent les détecter. Néanmoins, suivant la courbe de sensibilitié, nous inclinons à admettre une fonction ayant un rapport serré avec l'accélération des secousses. Mais, puis que l'homme est un pendule au point de vue dynamique, l'amplitude du corps ne reste plus constante à toutes les périodes de secousses. Nous disons, donc, que l'on perçoit les secousses par l'amplitude du corps. Si nous limitons notre discussion au problème statique, il s'agira d'une variation dans la direction perpendiculaire de la gravité. Cette variation produit un certaine effect sensuel au niveau de la peau ou des muscules ou du ventre, etc. Il nous semble qu'il n'y a aucune nécessité d'intoduire des organes associées avec les oreilles.

5. Remarques.

Nous sommes arrivés à expliquer la perception de secousses simplement avec l'amplitude du corps sous l'action de l'accélération. Nous ne voulons introduire aucune fonction mystérieuse dans la perception de ces secousses pas plus que dans le domaine de nos expériences.

Il y a en effet, une expérience que nous n'avons pas réalisée: c'est la même expérience avec des différentes conditions d'attitude. Il parait cependant possible de résoudre la question avec l'accélération appliquée et la période d'oscillation propre correspondant à chaque attitude.

Nous avons déjà obtenu 0,5 gal d'accélération pour la limite perceptible suivant les observations sismiques surtout pour les secousses dont la période est 0,3 seconde. Cette valeur s'accorde très bien avec la valeur obtenue après les expériences sur la plate-forme oscillante. Nous pouvons conclure, en effet, que l'on ressenti les séismes par la sensation d'accélération produite par les secousses.[4] Récemment, M. W. Inoué[5] a constanté avec le sismographe accélérométrique que la limite perceptible de l'accélération sismique est 1,7 gal à Tukuba: à Tukuba là période de secousses sismique se mesure toujours 0,08 sec. Ce fait s'accorde aussi très bien avec nos expériences. Quand la période diminue considérablement une grande valeur d'accélération est nécessaire pour que les secousses soient ressenties.

En fin, à l'égard du mémoire publié recémment par notre regretté Directeur K. Suyehiro, nous notons, qu'il a donné comparativement une grande valeur d'accélération pour la limite perceptible de secousses. Mais, son procédé d'expérience n'était pas le même que le notre: sur la plate-forme l'homme assied paterre sur un coussin. Cet arrangement nous posait susceptible de produire des résultats assez différents.

Pour terminer nous voulons exprimer nos vifs remerciment à tous ceux qui nous donné une partié de leurs temps pour aider à l'exécution de nos expériences.

---

4) Dans la maison la valeur d'accélérations era plus grande que celle inscrite par le sismographe accélérométrique. Mais, comme on n'attend pas toujours les seconsses, la limite perceptible d'accélération ne reste plus pareille ainsi que nous l'avons trouvé avec la plate forme oscillante. D'après ces deux modification nons avons obtenu 0,5 gal pour la limite parceptible d'accélération.

5) W. Inouye, *Bull. Earthq. Res. Inst.*, 11 (1933), 69.

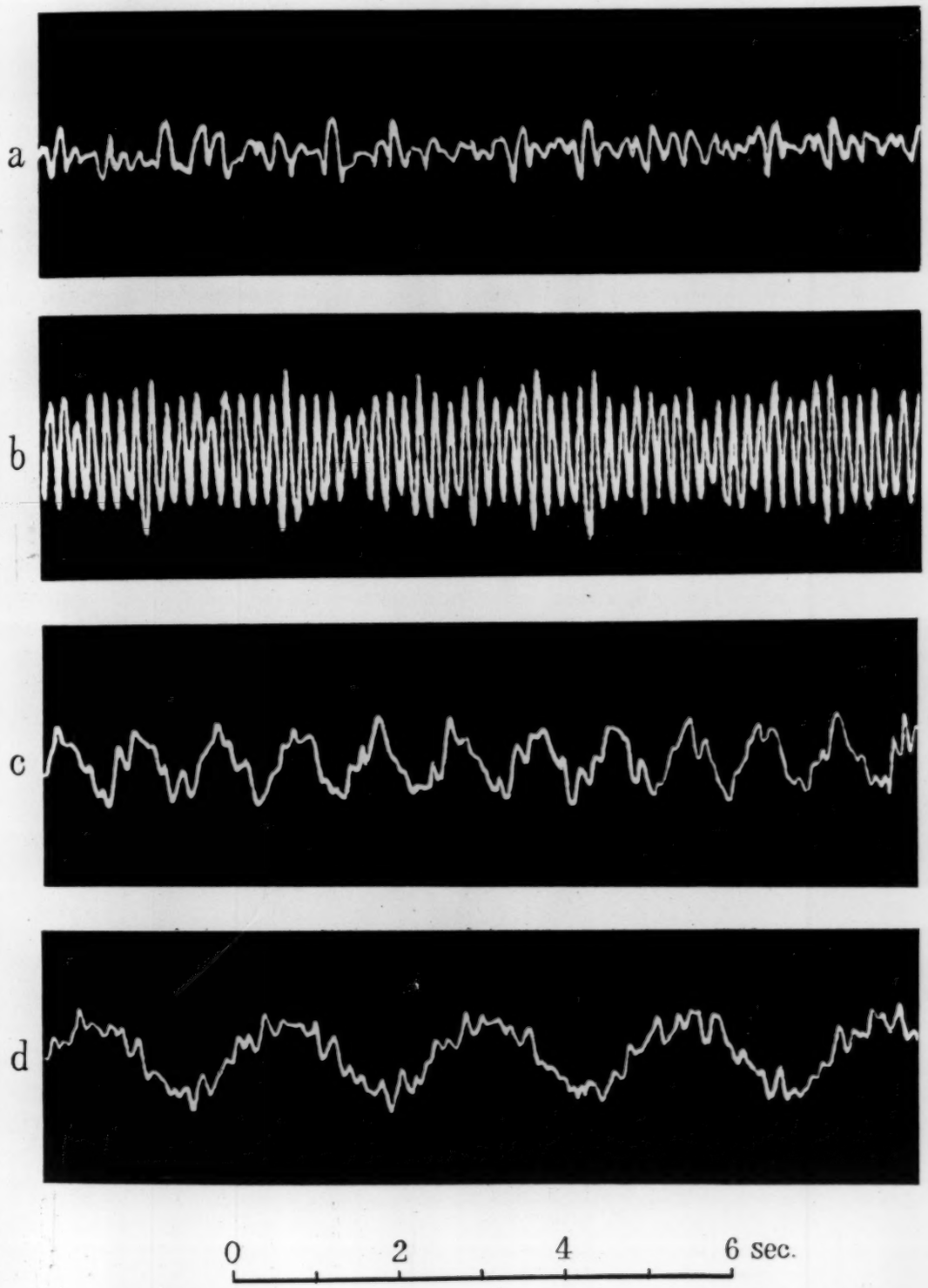

Fig. 4. Quelques exemples des enregistrements accélérométriques agrandis 10,8 fois.
a) état tranquil
b) secoué avec 0,18 s. de période
c) secoué avec 0,96 s. de période
d) secoué avec 2,4 s. de période
1 gal d'accélération correspond 6,95 mm. dans ces enregistrements.

（震研彙報、第十一號、圖版、石本、大塚）

8. 振動の知覺限界測定

地震研究所 { 石本巳四雄 / 大塚實 }

1. 震度階に規定せられたる所に從へば震動が人體に感覺を與へるや否やについて第一，第二階級の區別が生ずる．實際地震の階級が震動の最大加速度で表はされる事から見て，如何なる最大加速度を有する振動が人體に感覺を與へるかを實驗して見た．

2. 實驗に使用した振動臺は天井から吊し，$\frac{1}{2}$ 馬力の電動機によつて振動せしめた．但し電動機と振動臺との間には振幅を連續的に變化し得る裝置，及びバネが挿入されて振動臺に任意の正弦運動が與へられる樣に裝置してある．振動臺上に設置した加速度地震計は其の運動の加速度を常に記錄する．

3. 振動臺上に人が乘つて全く靜止して居ても加速度計は不規則な曲線を記錄する．然し之れを除去する事は出來ない．電動機の回轉は一定に保たれ次々に振動臺の振幅を增加する事によつて，被實驗者が有感覺の域に達する．其れより振幅を次々に減じて無感覺區域に達するが，何れの限界も加速度計記錄に徵して知覺限界を測定する事が出來る．

4. 五人の被實驗者に對して限界最大加速度が決定されたが，其の中一般通則と考へられるものは，1) 周期が大となれば知覺限界は周期に無關係で約 1·0 gal の最大加速度で與へられる．2) 0,5 秒附近に極小値がある．3) 周期が小となれば周期に逆比例して限界値が增加する．以上の事實を證明する爲めに最大加速度を一定にした知覺感度の曲線（限界加速度の逆數を y 軸にとりたるもの）を作つて見ると此れは一振子の附根が一定最大加速度の振動をなしたる時の振子の振幅と全く同一のものを示す．從つて人々の腰かけた姿勢は一つの逆振子であり，振動の感覺は全く上體に惹起される振幅の大いさによると云ふ事が出來る．卽ち振動知覺は皮膚或ひは筋肉感覺によつて起されると考へて差支へない樣である．

5. 地震觀測からは知覺限界として本鄕（卓越周期 0·3 秒）においては 0·5 gal．筑波（卓越周期 0·08 秒）において 1·7 gal と云ふ値が得られて居るが，此れは以上の實驗と殆ど一致する．又以上の實驗値と故末廣所長の得られた値との間に多少差異のある事は恐らく振動臺上における被實驗者の姿勢の異る結果であらうと思はれる．

9. 東京市及其附近と板橋町·富士見村間一等水準線檢測成果報告

昭和六年（一九三一）九月廿一日武藏北部地方に起りたる强震と連關する地殼變動を觀測する必要を生じ陸地測量部に委囑して東京より高崎·輕井澤·上諏訪を經て富士見に到る水準路の再觀測を遂行したり．其結果を別紙圖版に採錄す．此觀測に連關して同時に東京市內及其外廓を繞ぐる二つの環狀線路に就ても再測を行ひたるにより其結果をも同圖上に併記す．今回の再觀測は昭和七年（一九三二）四月より六月に亘りて行はれたるものにして，此れと比較して變動量を算出する爲に使用したる前回觀測は板橋高崎間に就ては大正十四年，高崎富士見間に就ては大正十五年に行はれたるものなり．なほ市內二條の環狀線に就ては昭和五年二，三月と昭和六年七月と及昭和七年五，六月の間に於ける變動を圖示せり．

今回觀測に要する費用の全額は帝國學士院より學術研究補助費として故末廣所長並に寺田現任所員兩名の申請により下付されたるものなり．玆に明記して深謝の意を表す．

9. *Relative Vertical Displacements of Bench Marks along Routes in Tôkyô and the Environs and from Itabasi to Huzimi.*

In connection with the strong earthquake which occurred in the northern part of the Province of Musasi, in the vicinity of Titibu, a revision of precise levelling along the route from Tôkyô to Huzimi, via Takasaki, Karuizawa and Kamisuwa, was carried out during the epoch April—June, 1932. The result was compared with the previous resúlts, 1925 for Itabasi—Takasaki and 1925 for Takasaki—Huzimi, and the relative vertical displacements thus obtained are shown in the annexed plate.

Besides, two closed loops of the levelling route, in the City of Tôkyô were also subjected to the revision and compared with the result obtained in Feb.—March, 1930. For a part of the latter route, the comparisons are also made for the epoch 1930 (Feb.—March)—1931 (July).

The present revison was carried out by means of the research fund granted from the Imperial Academy to Prof. Suyehiro, late Director, and Prof. Terada, the Member of the Institute. The best thanks of the above named and also of the present Director are due to Authorities of the Academy

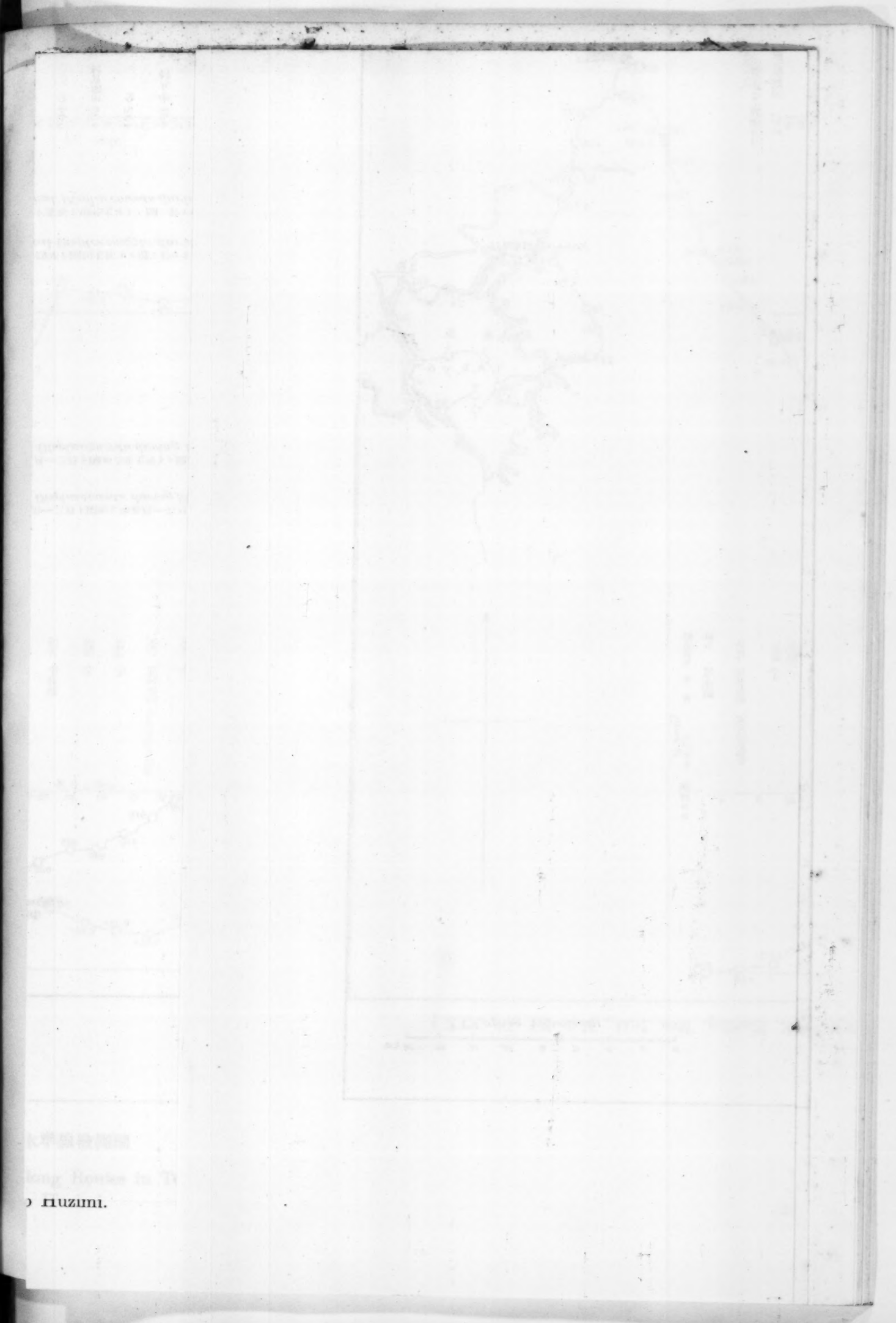

) Huzimi.

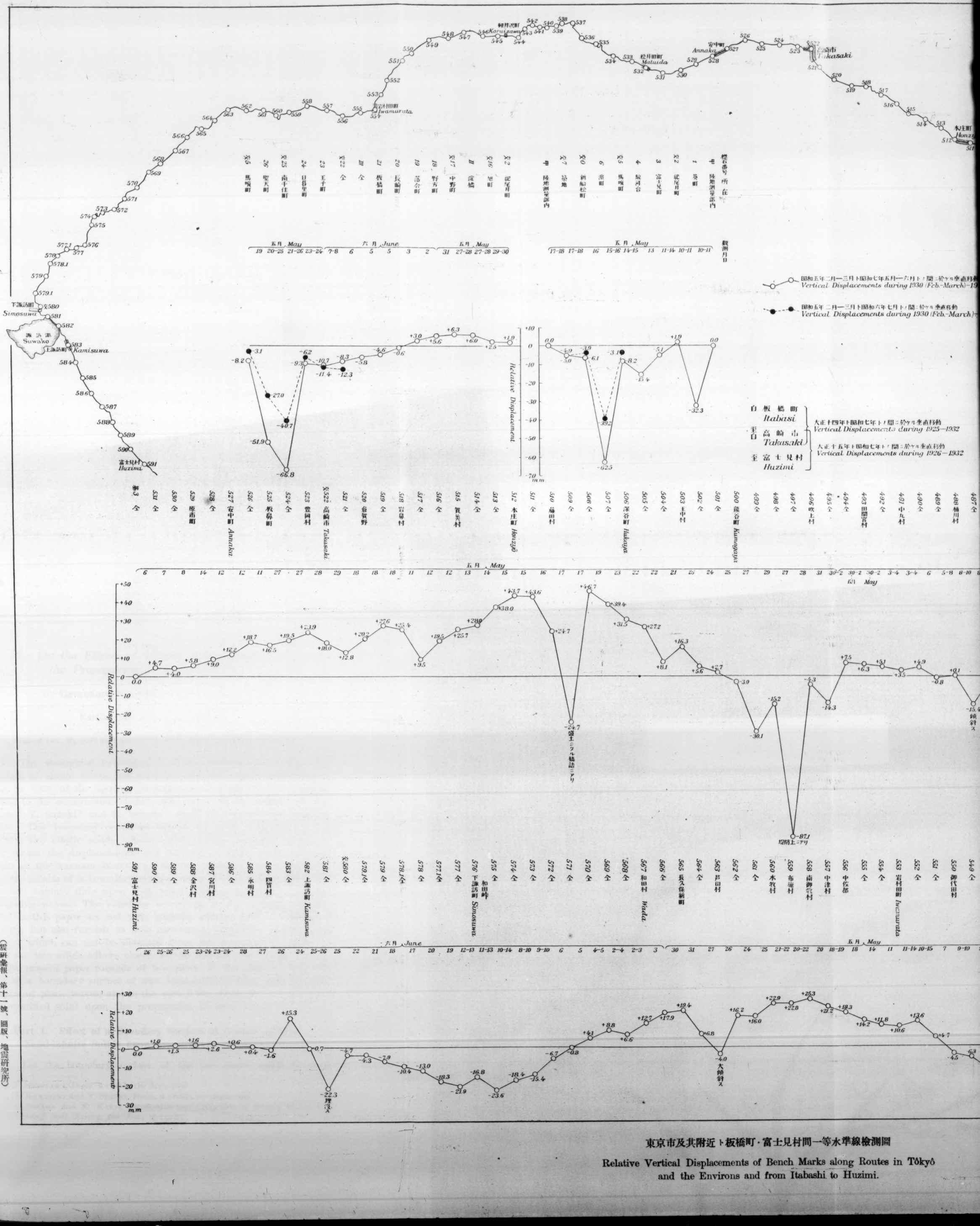

東京市及其附近ト板橋町・富士見村間一等水準線檢測圖

Relative Vertical Displacements of Bench Marks along Routes in Tôkyô and the Environs and from Itabashi to Huzimi.

昭和五年二月—三月ト昭和七年五月—六月ト ノ間ニ於ケル垂直移動
Vertical Displacements during 1930 (Feb.-March)—1932 (May—June).

昭和五年二月—三月ト昭和六年七月ト ノ間ニ於ケル垂直移動
Vertical Displacements during 1930 (Feb.-March)—1931 (July)

自 板橋町 *Itabasi*
至 高崎市 *Takasaki*
大正十四年ト昭和七年ト ノ間ニ於ケル垂直移動
Vertical Displacements during 1925—1932

自 高崎市 *Takasaki*
至 富士見村 *Huzimi*
大正十五年ト昭和七年ト ノ間ニ於ケル垂直移動
Vertical Displacements during 1926—1932

東京市及其附近ト板橋町・富士見村間一等水準線檢測圖

Relative Vertical Displacements of Bench Marks along Routes in Tôkyô and the Environs and from Itabashi to Huzimi.

10. *On the Effects of Discontinuity Surfaces upon the Propagation of Elastic Wave. (I)*

By Genrokuro NISHIMURA and Kiyoshi KANAI,

Earthquake Research Institute.

(Read Dec. 20, 1932 and March 20, 1933.—Received March 20, 1933.)

1. The theoretical investigation of the problem of reflection and refraction of elastic waves has come to the fore again, especially in Japan, in view of the marked development of seismometrical research relating to the construction of the earth's crust. T. Matuzawa,[1] H. Kawasumi,[2] T. Suzuki[2] and K. Sezawa[3] have all studied this problem of late. The boundary condition treated by these authorities is that in which two elastic solids adhere closely at the boundary surface, *i. e.*, in which the displacements and stresses of both solids are continuous at the common boundary. In the present paper, however, we study the effects of a boundary surface where the two elastic solids that come into contact slide upon each other without any friction on the propagating waves. The elasticity conditions at the boundary surface treated in this paper are not only perfectly correct from the theory of elasticity, but also furnish us with interesting properties of wave propagation which can not be obtained from the boundary condition in which the two solids adhere closely at the common boundary.

The present paper consists of two parts; in the first we study the effect of a boundary surface of two semi-infinite solids upon the propagation of plane waves, and in the second the effect of a surface layer of a stratified solid upon the propagation of these waves.

Part I. Effect of a Boundary Surface of Contact of Two Semi-infinite Solids upon the Propagation of Waves.

2. Let the boundary surface of the two elastic solids be $y=0$,

1) T. MATUZAWA, *Disin*, 4 (1932), (in Japanese).

2) H. KAWASUMI and T. SUZUKI, *Disin*, 4 (1932), (in Japanese).

3) K. SEZAWA and K. KANAI, "Reflection and Refraction of Seismic Waves in a Stratified Body," *Bull. Earthq. Res. Inst.*, 10 (1932).

and the axis x be on this contact surface. Again, let ρ and λ, μ be the density and Lame's elastic constants of the solid represented by I in Fig. 1, and ρ', λ', μ' be those of the solid II shown also in Fig. 1. We shall study the problems in the following two cases:

1. Incident Wave is Dilatational,
2. Incident Wave is Distortional.

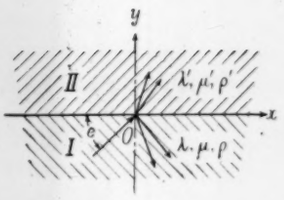

Fig. 1.

a) Incident Wave is Dilatational.

3. When the incident wave is dilatational and expressed by

$$\Delta = \mathfrak{A} e^{i(pt-fx-ry)}, \quad \ldots\ldots\ldots\ldots\ldots\ldots (1)$$

the $x-$, $y-$ components of displacement u_1, v_1 and the normal, tangential and shear components of stress $\widehat{xx}$, $\widehat{yy}$, $\widehat{xy}$ corresponding to this wave are respectively expressed by

$$\left.\begin{aligned} u_1 &= \frac{if}{h^2}\mathfrak{A} e^{i(pt-fx-ry)}, \\ v_1 &= \frac{ir}{h^2}\mathfrak{A} e^{i(pt-fx-ry)}, \end{aligned}\right\} \quad \ldots\ldots\ldots\ldots\ldots\ldots (2)$$

$$\left.\begin{aligned} \widehat{xx}_1 &= \mu\frac{(k^2-2h^2+2f^2)}{h^2}\mathfrak{A} e^{i(pt-fx-ry)}, \\ \widehat{yy}_1 &= \mu\frac{(k^2-2h^2+2r^2)}{h^2}\mathfrak{A} e^{i(pt-fx-ry)}, \\ \widehat{xy}_1 &= 2\mu\frac{fr}{h^2}\mathfrak{A} e^{i(pt-fx-ry)}, \end{aligned}\right\} \quad \ldots\ldots\ldots\ldots\ldots\ldots (3)$$

where

$$h^2 = \frac{\rho p^2}{\lambda+2\mu}, \quad k^2 = \frac{\rho p^2}{\mu}, \quad r^2+f^2 = h^2, \quad \ldots\ldots\ldots\ldots (4)$$

and $p = \dfrac{2\pi}{T_1}$, T_1 being the period of incident wave.

Let the wave length and velocity of the incident dilatational wave be L_1 and V_1 respectively. Then we have the following relations.

$$L_1 = V_1 T_1 = \frac{2\pi}{\sqrt{r^2+f^2}}. \quad \ldots\ldots\ldots\ldots\ldots\ldots (5)$$

Now we know the reflected waves of two kinds, one of which is dilatational and the other distortional, such that

$$\Delta' = A' e^{i(pt-fx+ry)}, \quad \ldots\ldots\ldots\ldots\ldots\ldots (6)$$

$$2\varpi' = B' e^{i(pt-fx+sy)}, \quad \ldots\ldots\ldots\ldots\ldots\ldots (7)$$

where A' and B' are arbitrary constants, and

$$s^2 = k^2 - f^2. \quad \ldots\ldots\ldots\ldots\ldots\ldots (8)$$

The $x-$, $y-$ components of displacement u_1', v_1' and the stress components $\widehat{xx_1}'$, $\widehat{yy_1}'$, $\widehat{xy_1}'$ corresponding to Δ' expressed by (6) are written in the following forms:

$$\left.\begin{aligned} u_1' &= \frac{if}{h^2} A' e^{i(pt-fx+ry)}, \\ v_1' &= -\frac{ir}{h^2} A' e^{i(pt-fx+ry)}, \end{aligned}\right\} \quad \ldots\ldots\ldots\ldots\ldots\ldots (9)$$

$$\left.\begin{aligned} \widehat{xx_1}' &= \mu \frac{(k^2-2h^2+2f^2)}{h^2} A' e^{i(pt-fx+ry)}, \\ \widehat{yy_1}' &= \mu \frac{(k^2-2h^2+2r^2)}{h^2} A' e^{i(pt-fx+ry)}, \\ \widehat{xy_1}' &= -\frac{2fr\mu}{h^2} A' e^{i(pt-fx+ry)}. \end{aligned}\right\} \quad \ldots\ldots\ldots\ldots\ldots\ldots (10)$$

The displacement u_2', v_2' and the stress components $\widehat{xx_2}'$, $\widehat{yy_2}'$, $\widehat{xy_2}'$ corresponding to $2\varpi'$ expressed by (7) are respectively expressed in the forms:

$$\left.\begin{aligned} u_2' &= \frac{is}{k^2} B' e^{i(pt-fx+sy)}, \\ v_2' &= \frac{if}{k^2} B' e^{i(pt-fx+sy)}, \end{aligned}\right\} \quad \ldots\ldots\ldots\ldots\ldots\ldots (11)$$

$$\left.\begin{aligned} \widehat{xx_2}' &= \frac{2sf\mu}{k^2} B' e^{i(pt-fx+sy)}, \\ \widehat{yy_2}' &= -\frac{2sf\mu}{k^2} B' e^{i(pt-fx+sy)}, \\ \widehat{xy_2}' &= \frac{(f^2+s^2)\mu}{k^2} B' e^{i(pt-fx+sy)}. \end{aligned}\right\} \quad \ldots\ldots\ldots\ldots\ldots\ldots (12)$$

The waves transmitted in the second medium also consist of two kinds such that

$$\Delta'' = A'' e^{i(pt-fx-r'y)}, \quad \ldots\ldots\ldots\ldots\ldots\ldots (13)$$

$$2\varpi'' = B'' e^{i(pt-fx-s'y)}, \quad \ldots\ldots\ldots\ldots\ldots\ldots (14)$$

where A'', B'' are arbitrary constants and

$$r'^2=h'^2-f^2, \quad s'^2=k'^2-f^2, \qquad \cdots\cdots\cdots\cdots(15)$$

$$h'^2=\frac{\rho' p^2}{\lambda'+2\mu'}, \quad k'^2=\frac{\rho' p^2}{\mu'}. \qquad \cdots\cdots\cdots\cdots(16)$$

The $x-$, $y-$ components of displacement u_1'', v_1'' and the stress components $\widehat{xx_1}''$, $\widehat{yy_1}''$, $\widehat{xy_1}''$ corresponding to Δ'' expressed by (13) are also of the forms:

$$\left.\begin{aligned} u_1''&=\frac{if}{h'^2}A''e^{i(pt-fx-r'y)},\\ v_1''&=\frac{ir'}{h'^2}A''e^{i(pt-fx-r'y)},\end{aligned}\right\} \qquad \cdots\cdots\cdots\cdots(17)$$

$$\left.\begin{aligned} \widehat{xy_1}''&=\mu'\frac{(k'^2-2h'^2+2f^2)}{h'^2}A''e^{i(pt-fx-r'y)},\\ \widehat{yy_1}''&=\mu'\frac{(k'^2-2h'^2+2r'^2)}{h'^2}A''e^{i(pt-fx-r'y)},\\ \widehat{xy_1}''&=\frac{2fr'\mu'}{h'^2}A''e^{i(pt-fx-r'y)}.\end{aligned}\right\} \qquad \cdots\cdots\cdots(18)$$

The displacement u_2'', v_2'' and the stress $\widehat{xx_2}''$, $\widehat{yy_2}''$ $\widehat{xy_2}''$ corresponding to $2\varpi''$ expressed by (14) are written by

$$\left.\begin{aligned} u_2''&=-\frac{is'}{k'^2}B''e^{i(pt-fx-s'y)},\\ v_2''&=\frac{if}{k'^2}B''e^{i(pt-fx-s'y)},\end{aligned}\right\} \qquad \cdots\cdots\cdots\cdots(19)$$

$$\left.\begin{aligned} \widehat{xx_2}''&=-\frac{2s'f\mu'}{k'^2}B''e^{i(pt-fx-s'y)},\\ \widehat{yy_2}''&=\frac{2s'f\mu'}{k'^2}B''e^{i(pt-fx-s'y)},\\ \widehat{xy_2}''&=\frac{(f^2-s'^2)\mu'}{k'^2}B''e^{i(pt-fx-s'y)}.\end{aligned}\right\} \qquad \cdots\cdots\cdots\cdots(20)$$

Now the boundary conditions which we have discussed in Section 1 are expressed in the following forms:

When $y=0$,

$$\left.\begin{aligned} &\widehat{yy_1}+\widehat{yy_1}'+\widehat{yy_2}'=\widehat{yy_1}''+\widehat{yy_2}'',\\ &v_1+v_1'+v_2'=v_1''+v_2'',\\ &\widehat{xy_1}+\widehat{xy_1}'+\widehat{xy_2}'=0,\\ &\widehat{xy_1}''+\widehat{xy_2}''=0.\end{aligned}\right\} \qquad \cdots\cdots\cdots\cdots(21)$$

The boundary conditions expressed by (21) gives us the following values of A', B', A'', B'' :

$$\left.\begin{aligned}
A' &= \mathfrak{A}\frac{\left[\frac{\mu'}{\mu}r(s^2+f^2)\{(s'^2-f^2)^2+4f^2s'r'\}-r'(f^2+s'^2)\{(s^2-f^2)^2-4f^2sr\}\right]}{\left[\frac{\mu'}{\mu}r(f^2+s^2)\{(s'^2-f^2)^2+4f^2s'r'\}+r'(f^2+s'^2)\{(s^2-f^2)^2+4f^2sr\}\right]},\\
B' &= \mathfrak{A}\frac{4frr'k^2(s'^2+f^2)(s^2-f^2)}{h^2\left[\frac{\mu'}{\mu}r(f^2+s^2)\{(s'^2-f^2)^2+4f^2s'r'\}+r'(f^2+s'^2)\{(s^2-f^2)^2+4f^2sr\}\right]},\\
A'' &= \mathfrak{A}\frac{2rh'^2(s'^2-f^2)(s^2-f^2)(s^2+f^2)}{h^2\left[\frac{\mu'}{\mu}r(f^2+s^2)\{(s'^2-f^2)^2+4f^2s'r'\}+r'(f^2+s'^2)\{(s^2-f^2)^2+4f^2sr\}\right]},\\
B'' &= \mathfrak{A}\frac{4frr'k'^2(s^2-f^2)(s^2+f^2)}{h^2\left[\frac{\mu'}{\mu}r(f^2+s^2)\{(s'^2-f^2)^2+4f^2s'r'\}+r'(f^2+s'^2)\{(s^2-f^2)^2+4f^2sr\}\right]}.
\end{aligned}\right\}(23)$$

Substituting these values for A', B', A'' and B'' in the expressions (9), (11), (17) and (19), we obtain the reflected and transmitted waves which are generated by the primary incident wave expressed by (1) as in the following expressions :

Reflected dilatational wave ;

$$\left.\begin{aligned}
u_1' &= \frac{if\mathfrak{A}}{h^2}\frac{\left[\frac{\mu'}{\mu}r(f^2+s^2)\{(s'^2-f^2)^2+4s'r'f^2\}\right.}{\left[\frac{\mu'}{\mu}r(s^2+f^2)\{(s'^2-f^2)^2+4s'r'f^2\}\right.}\\
&\qquad\left.\frac{-r'(s'^2+f^2)\{(s^2-f^2)^2-4rsf^2\}\right]}{\left.+r'(s'^2+f^2)\{(s^2-f^2)^2+4rsf^2\}\right]}e^{i(pt-fx+ry)},\\
v_1' &= -\frac{i\mathfrak{A}r}{h^2}\frac{\left[\frac{\mu'}{\mu}r(f^2+s^2)\{(s'^2-f^2)^2+4s'r'f^2\}\right.}{\left[\frac{\mu'}{\mu}r(s^2+f^2)\{(s'^2-f^2)^2+4s'r'f^2\}\right.}\\
&\qquad\left.\frac{-r'(s'^2+f^2)\{(s^2-f^2)^2-4rsf^2\}\right]}{\left.+r'(s'^2+f^2)\{(s^2-f^2)^2+4rsf^2\}\right]}e^{i(pt-fx+ry)}.
\end{aligned}\right\}\ldots.(24)$$

Reflected distortional wave ;

$$\left.\begin{aligned} u_2' &= \frac{i\mathfrak{A}}{h^2}\Bigg[\frac{\mu'}{\mu}r(s^2+f^2)\{(s'^2-f^2)^2+4s'^2r'f^2\} \\ &\qquad \frac{4sfrr'(s^2-f^2)}{+r'(s'^2+f^2)\{(s^2-f^2)^2+4rsf^2\}}\Bigg]e^{i(pt-fx+sy)}, \\ v_2' &= \frac{i\mathfrak{A}}{h^2}\Bigg[\frac{\mu'}{\mu}r(s^2+f^2)\{(s'^2-f^2)^2+4s'^2r'f^2\} \\ &\qquad \frac{4f^2rr'(s^2-f^2)}{+r'(s'^2+f^2)\{(s^2-f^2)^2+4rsf^2\}}\Bigg]e^{i(pt-fx+sy)}, \end{aligned}\right\} \quad \ldots(25)$$

Transmitted dilatational wave ;

$$\left.\begin{aligned} u_1'' &= \mathfrak{A}\frac{if}{h^2}\Bigg[\frac{\mu'}{\mu}r(s^2+f^2)\{(s'^2-f^2)^2+4s'^2r'f^2\} \\ &\qquad \frac{2r(s^2+f^2)(s^2-f^2)}{+r'(s'^2+f^2)\{(s^2-f^2)^2+4rsf^2\}}\Bigg]e^{i(pt-fx-r'y)}, \\ v_1'' &= \mathfrak{A}\frac{ir'}{h^2}\Bigg[\frac{\mu'}{\mu}r(s^2+f^2)\{(s'^2-f^2)^2+4s'^2r'f^2\} \\ &\qquad \frac{2r(s^2+f^2)(s^2-f^2)}{+r'(s'^2+f^2)\{(s^2-f^2)^2+4rsf^2\}}\Bigg]e^{i(pt-fx-r'y)}, \end{aligned}\right\} \quad \ldots(26)$$

Transmitted distortional wave ;

$$\left.\begin{aligned} v_2'' &= -\mathfrak{A}\frac{is'}{h^2}\Bigg[\frac{\mu'}{\mu}r(s^2+f^2)\{(s'^2-f^2)^2+4s'^2r'f^2\} \\ &\qquad \frac{4rr'f(s^2+f^2)}{+r'(s'^2+f^2)\{(s^2-f^2)^2+4rsf^2\}}\Bigg]e^{i(pt-fx-s'y)}, \\ u_2'' &= \mathfrak{A}\frac{if}{h^2}\Bigg[\frac{\mu'}{\mu}r(s^2+f^2)\{(s'^2-f^2)^2+4s'^2r'f^2\} \\ &\qquad \frac{4rr'f(s^2+f^2)}{+r'(s'^2+f^2)\{(s^2-f^2)^2+4rsf^2\}}\Bigg]e^{i(pt-fx-s'y)}. \end{aligned}\right\} \quad \ldots(27)$$

Let V_1 and V_2 be the velocities of dilatational and distortional waves in the medium I and V_1', V_2' be those of dilatational and distortional waves of the medium II respectively. And also let the emergency angle of incident dilatational wave expressed by (1) be e. Then the expressions (24), (25), (26) and (27) are written in the following forms:

$$\left.\begin{aligned} u_1' &= \frac{i\mathfrak{A}T_1V_1\cos e}{2\pi}\frac{\mathfrak{F}}{\Phi}e^{i(pt-fx+ry)}, \\ v_1' &= -\frac{i\mathfrak{A}T_1V_1\sin e}{2\pi}\frac{\mathfrak{F}}{\Phi}e^{i(pt-fx+ry)}, \end{aligned}\right\} \quad \cdots\cdots\cdots\cdots\cdots\cdots\cdots\cdots\cdots\cdots (24)'$$

$$\left.\begin{aligned} u_2' &= \frac{i\mathfrak{A}T_1V_1\cos e}{2\pi} \\ &\quad \times \frac{4\sin e\left(\frac{V_1}{V_2'}\right)^2\left\{\left(\frac{V_1}{V_1'}\right)^2-\cos^2 e\right\}^{\frac{1}{2}}\left\{\left(\frac{V_1}{V_2}\right)^2-2\cos^2 e\right\}\left\{\left(\frac{V_1}{V_2}\right)^2-\cos^2 e\right\}^{\frac{1}{2}}}{\Phi} \\ &\qquad \times e^{i(pt-fx+sy)}, \\ v_2' &= \frac{i\mathfrak{A}T_1V_1\cos^2 e}{2\pi} \\ &\quad \times \frac{4\sin e\left(\frac{V_1}{V_2'}\right)^2\left\{\left(\frac{V_1}{V_1'}\right)^2-\cos^2 e\right\}^{\frac{1}{2}}\left\{\left(\frac{V_1}{V_2}\right)^2-2\cos^2 e\right\}}{\Phi}e^{i(pt-fx+sy)}, \end{aligned}\right\} (25)'$$

$$\left.\begin{aligned} u_1'' &= \frac{i\mathfrak{A}T_1V_1\cos e}{2\pi} \\ &\quad \times \frac{2\sin e\left(\frac{V_1}{V_2}\right)^2\left\{\left(\frac{V_1}{V_2}\right)^2-2\cos^2 e\right\}\left\{\left(\frac{V_1}{V_2'}\right)^2-2\cos^2 e\right\}}{\Phi}e^{i(pt-fx-r'y)}, \\ v_1'' &= \frac{i\mathfrak{A}T_1V_1}{2\pi} \\ &\quad \times \frac{2\sin e\left(\frac{V_1}{V_2}\right)^2\left\{\left(\frac{V_1}{V_2}\right)^2-2\cos^2 e\right\}\left\{\left(\frac{V_1}{V_2'}\right)^2-2\cos^2 e\right\}\left\{\left(\frac{V_1}{V_1'}\right)^2-\cos^2 e\right\}^{\frac{1}{2}}}{\Phi} \\ &\qquad \times e^{i(pt-fx-r'y)}, \end{aligned}\right\} (26)'$$

$$\left.\begin{aligned} u_2'' &= -\frac{i\mathfrak{A}T_1V_1\cos e}{2\pi} \\ &\times \frac{4\sin e\left(\frac{V_1}{V_2}\right)^2\left\{\left(\frac{V_1}{V_2}\right)^2-2\cos^2 e\right\}\left\{\left(\frac{V_1}{V_1'}\right)^2-\cos^2 e\right\}^{\frac{1}{2}}\left\{\left(\frac{V_1}{V_2'}\right)^2-\cos^2 e\right\}^{\frac{1}{2}}}{\Phi} \\ &\times e^{i(pt-f\xi-s'y)}, \\ v_2'' &= \frac{i\mathfrak{A}T_1V_1\cos^2 e}{2\pi} \\ &\times \frac{4\sin e\left(\frac{V_1}{V_2}\right)^2\left\{\left(\frac{V_1}{V_2}\right)^2-2\cos^2 e\right\}\left\{\left(\frac{V_1}{V_1'}\right)^2-\cos^2 e\right\}^{\frac{1}{2}}}{\Phi} e^{i(pt-fx-s'y)}, \end{aligned}\right\} (27)'$$

where

$$\begin{aligned} \Phi = \frac{\mu'}{\mu}\sin e\left(\frac{V_1}{V_2}\right)^2\Bigg[&\left\{\left(\frac{V_1}{V_2'}\right)^2-2\cos^2 e\right\}^2 \\ &+4\cos^2 e\left\{\left(\frac{V_1}{V_2'}\right)^2-\cos^2 e\right\}^{\frac{1}{2}}\left\{\left(\frac{V_1}{V_1'}\right)^2-\cos^2 e\right\}^{\frac{1}{2}}\Bigg] \\ &+\left(\frac{V_1}{V_2'}\right)^2\left\{\left(\frac{V_1}{V_1'}\right)^2-\cos^2 e\right\}^{\frac{1}{2}}\Bigg[\left\{\left(\frac{V_1}{V_2}\right)^2-2\cos^2 e\right\}^2 \\ &+4\sin e\cos^2 e\left\{\left(\frac{V_1}{V_2}\right)^2-\cos^2 e\right\}^{\frac{1}{2}}\Bigg], \\ \Psi = \frac{\mu'}{\mu}\sin e\left(\frac{V_1}{V_2}\right)^2\Bigg[&\left\{\left(\frac{V_1}{V_2'}\right)^2-2\cos^2 e\right\}^2 \\ &+4\cos^2 e\left\{\left(\frac{V_1}{V_2'}\right)^2-\cos^2 e\right\}^{\frac{1}{2}}\left\{\left(\frac{V_1}{V_1'}\right)^2-\cos^2 e\right\}^{\frac{1}{2}}\Bigg] \\ &-\left(\frac{V_1}{V_2'}\right)^2\left\{\left(\frac{V_1}{V_1'}\right)^2-\cos^2 e\right\}^{\frac{1}{2}}\Bigg[\left\{\left(\frac{V_1}{V_2}\right)^2-2\cos^2 e\right\}^2 \\ &-4\sin e\cos^2 e\left\{\left(\frac{V_1}{V_2}\right)^2-\cos^2 e\right\}^{\frac{1}{2}}\Bigg]. \end{aligned}$$

When $\rho=\rho'$, Poisson's ratio of the medium I is $\frac{1}{4}$, and that of the medium II is also $\frac{1}{4}$, we obtain the following expressions of waves generated at the boundary surface by the incident dilatational wave :

$$u_1' = \frac{i\mathfrak{A}T_1V_1\cos e}{2\pi} \times \frac{\left[3\frac{\mu'}{\mu}\sin e\left\{\left(3\frac{\mu}{\mu'}-2\cos^2 e\right)^2+4\cos^2 e\left(3\frac{\mu}{\mu'}-\cos^2 e\right)^{\frac{1}{2}}\left(\frac{\mu}{\mu'}-\cos^2 e\right)^{\frac{1}{2}}\right\}\right.}{\left[3\frac{\mu'}{\mu}\sin e\left\{\left(3\frac{\mu}{\mu'}-2\cos^2 e\right)^2+4\cos^2 e\left(3\frac{\mu}{\mu'}-\cos^2 e\right)^{\frac{1}{2}}\left(\frac{\mu}{\mu'}-\cos^2 e\right)^{\frac{1}{2}}\right\}\right.} \times e^{i(pt-fx+ry)},$$

$$\left.-3\frac{\mu}{\mu'}\left(\frac{\mu}{\mu'}-\cos^2 e\right)^{\frac{1}{2}}\left\{(3-2\cos^2 e)^2-4\sin e\cos^2 e(3-\cos^2 e)^{\frac{1}{2}}\right\}\right]$$

$$\left.+3\frac{\mu}{\mu'}\left(\frac{\mu}{\mu'}-\cos^2 e\right)^{\frac{1}{2}}\left\{(3-2\cos^2 e)^2+4\sin e\cos^2 e(3-\cos^2 e)^{\frac{1}{2}}\right\}\right] \qquad (24)''$$

$$v_1' = -\frac{i\mathfrak{A}T_1V_1\sin e}{2\pi} \times \frac{\left[3\frac{\mu'}{\mu}\sin e\left\{\left(3\frac{\mu}{\mu'}-2\cos^2 e\right)^2+4\cos^2 e\left(3\frac{\mu}{\mu'}-\cos^2 e\right)^{\frac{1}{2}}\left(\frac{\mu}{\mu'}-\cos^2 e\right)^{\frac{1}{2}}\right\}\right.}{\left[3\frac{\mu'}{\mu}\sin e\left\{\left(3\frac{\mu}{\mu'}-2\cos^2 e\right)^2+4\cos^2 e\left(3\frac{\mu}{\mu'}-\cos^2 e\right)^{\frac{1}{2}}\left(\frac{\mu}{\mu'}-\cos^2 e\right)^{\frac{1}{2}}\right\}\right.} \times e^{i(pt-fx+ry)},$$

$$\left.-3\frac{\mu}{\mu'}\left(\frac{\mu}{\mu'}-\cos^2 e\right)^{\frac{1}{2}}\left\{(3-2\cos^2 e)^2-4\sin e\cos^2 e(3-\cos^2 e)^{\frac{1}{2}}\right\}\right]$$

$$\left.+3\frac{\mu}{\mu'}\left(\frac{\mu}{\mu'}-\cos^2 e\right)^{\frac{1}{2}}\left\{(3-2\cos^2 e)^2+4\sin e\cos^2 e(3-\cos^2 e)^{\frac{1}{2}}\right\}\right] \qquad (24)''$$

$$u_2' = \frac{i\mathfrak{A}T_1V_1}{2\pi} \times \frac{12\sin e\cos e\frac{\mu}{\mu'}\left(\frac{\mu}{\mu'}-\cos^2 e\right)^{\frac{1}{2}}(3-2\cos^2 e)(3-\cos^2 e)^{\frac{1}{2}}}{\left[3\frac{\mu'}{\mu}\sin e\left\{\left(3\frac{\mu}{\mu'}-2\cos^2 e\right)^2+4\cos^2 e\left(3\frac{\mu}{\mu'}-\cos^2 e\right)^{\frac{1}{2}}\left(\frac{\mu}{\mu'}-\cos^2 e\right)^{\frac{1}{2}}\right\}\right.} e^{i(pt-fx+sy)},$$

$$\left.+3\frac{\mu}{\mu'}\left(\frac{\mu}{\mu'}-\cos^2 e\right)^{\frac{1}{2}}\left\{(3-2\cos^2 e)^2+4\sin e\cos^2 e(3-\cos^2 e)^{\frac{1}{2}}\right\}\right] \qquad (25)''$$

$$
\left.
\begin{aligned}
v_2' &= \frac{i\mathfrak{A}T_1V_1}{2\pi} \\
&\times \frac{12\sin e\cos^2 e\left(\frac{\mu}{\mu'}-\cos^2 e\right)^{\frac{1}{2}}(3-2\cos^2 e)}{\left[3\frac{\mu'}{\mu}\sin e\left\{\left(3\frac{\mu}{\mu'}-2\cos^2 e\right)^2+4\cos^2 e\left(3\frac{\mu}{\mu'}-\cos^2 e\right)^{\frac{1}{2}}\left(\frac{\mu}{\mu'}-\cos^2 e\right)^{\frac{1}{2}}\right\}\right.} \\
&\qquad \frac{e^{i(\lambda t-fx+sy)}}{\left.+3\frac{\mu}{\mu'}\left(\frac{\mu}{\mu'}-\cos^2 e\right)^{\frac{1}{2}}\left\{(3-2\cos^2 e)^2+4\sin e\cos^2 e(3-\cos^2 e)^{\frac{1}{2}}\right\}\right]}, \\
u_1'' &= \frac{i\mathfrak{A}T_1V_1}{2\pi} \\
&\times \frac{6\sin e\cos e(3-2\cos^2 e)\left(3\frac{\mu}{\mu'}-2\cos^2 e\right)}{\left[3\frac{\mu'}{\mu}\sin e\left\{\left(3\frac{\mu}{\mu'}-2\cos^2 e\right)^2+4\cos^2 e\left(3\frac{\mu}{\mu'}-\cos^2 e\right)^{\frac{1}{2}}\left(\frac{\mu}{\mu'}-\cos^2 e\right)^{\frac{1}{2}}\right\}\right.} \\
&\qquad \frac{e^{i(pt-fx-r'y)}}{\left.+3\frac{\mu}{\mu'}\left(\frac{\mu}{\mu'}-\cos^2 e\right)^{\frac{1}{2}}\left\{(3-2\cos^2 e)^2+4\sin e\cos^2 e(3-\cos^2 e)^{\frac{1}{2}}\right\}\right]}, \\
v_1'' &= \frac{i\mathfrak{A}T_1V_1}{2\pi} \\
&\times \frac{6\sin e(3-2\cos^2 e)\left(3\frac{\mu}{\mu'}-2\cos^2 e\right)\left(\frac{\mu}{\mu'}-\cos^2 e\right)^{\frac{1}{2}}}{\left[3\frac{\mu'}{\mu}\sin e\left\{\left(3\frac{\mu}{\mu'}-2\cos^2 e\right)^2+4\cos^2 e\left(3\frac{\mu}{\mu'}-\cos^2 e\right)^{\frac{1}{2}}\left(\frac{\mu}{\mu'}-\cos^2 e\right)^{\frac{1}{2}}\right\}\right.} \\
&\qquad \frac{e^{i(pt-fx-r'y)}}{\left.+3\frac{\mu}{\mu'}\left(\frac{\mu}{\mu'}-\cos^2 e\right)^{\frac{1}{2}}\left\{(3-2\cos^2 e)^2+4\sin e\cos^2 e(3-\cos^2 e)^{\frac{1}{2}}\right\}\right]}, \\
u_2'' &= -\frac{i\mathfrak{A}T_1V_1}{2\pi} \\
&\times \frac{12\sin e\cos e(3-2\cos^2 e)\left(\frac{\mu}{\mu'}-\cos^2 e\right)^{\frac{1}{2}}\left(3\frac{\mu}{\mu'}-\cos^2 e\right)^{\frac{1}{2}}}{\left[3\frac{\mu'}{\mu}\sin e\left\{\left(3\frac{\mu}{\mu'}-2\cos^2 e\right)^2+4\cos^2 e\left(3\frac{\mu}{\mu'}-\cos^2 e\right)^{\frac{1}{2}}\left(\frac{\mu}{\mu'}-\cos^2 e\right)^{\frac{1}{2}}\right\}\right.}
\end{aligned}
\right\} \quad (26'')
$$

$$\left.\begin{aligned}
&\frac{e^{i(pt-fx-s'y)}}{+3\frac{\mu}{\mu'}\left(\frac{\mu}{\mu'}-\cos^2 e\right)^{\frac{1}{2}}\left\{(3-2\cos^2 e)^2+4\sin e\cos^2 e(3-\cos^2 e)^{\frac{1}{2}}\right\}}\Bigg],\\
v_2''=&\frac{i\mathfrak{A}T_1V_1}{2\pi}\\
&\times\frac{12\sin e\cos^2 e(3-2\cos^2 e)\left(\frac{\mu}{\mu'}-\cos^2 e\right)^{\frac{1}{2}}}{\left[3\frac{\mu'}{\mu}\sin e\left\{\left(3\frac{\mu}{\mu'}-2\cos^2 e\right)^2+4\cos^2 e\left(3\frac{\mu}{\mu'}-\cos^2 e\right)^{\frac{1}{2}}\left(\frac{\mu}{\mu'}-\cos^2 e\right)^{\frac{1}{2}}\right\}\right.}\\
&\left.\frac{e^{i(pt-fx-s'y)}}{+3\frac{\mu}{\mu'}\left(\frac{\mu}{\mu'}-\cos^2 e\right)^{\frac{1}{2}}\left\{(3-2\cos^2 e)^2+4\sin e\cos^2 e(3-\cos^2 e)^{\frac{1}{2}}\right\}}\Bigg].
\end{aligned}\right\}\quad(27)''$$

When $\frac{\mu'}{\mu}=1$, the expressions (24)″, (25)″, (26)″, (27)″ are expressed by

$$\left.\begin{aligned}
u_1'&=\frac{i\mathfrak{A}T_1V_1}{2\pi}\cdot\frac{4\sin e\cos^3 e(3-\cos^2 e)^{\frac{1}{2}}}{\{(3-2\cos^2 e)^2+4\cos^2 e\sin e(3-\cos^2 e)^{\frac{1}{2}}\}}e^{i\left(pt-fx+\frac{2\pi\sin e}{T_1V_1}y\right)},\\
v_1'&=-\frac{i\mathfrak{A}T_1V_1}{2\pi}\cdot\frac{4\sin^2 e\cos^2 e(3-\cos^2 e)^{\frac{1}{2}}}{\{(3-2\cos^2 e)^2+4\cos^2 e\sin e(3-\cos^2 e)^{\frac{1}{2}}\}}e^{i\left(pt-fx+\frac{2\pi\sin e}{T_1V_1}y\right)},
\end{aligned}\right\}\quad(28)$$

$$\left.\begin{aligned}
u_2'&=\frac{i\mathfrak{A}T_1V_1}{2\pi}\cdot\frac{2\sin e\cos e(3-2\cos^2 e)(3-\cos^2 e)^{\frac{1}{2}}}{\{(3-2\cos^2 e)^2+4\cos^2 e\sin e(3-\cos^2 e)^{\frac{1}{2}}\}}e^{i\left(pt-fx+\frac{2\sqrt{3}\pi\sin e}{T_1V_1}y\right)},\\
v_2'&=\frac{i\mathfrak{A}T_1V_1}{2\pi}\cdot\frac{2\sin e\cos^2 e(3-2\cos^2 e)}{\{(3-2\cos^2 e)^2+4\cos^2 e\sin e(3-\cos^2 e)^{\frac{1}{2}}\}}e^{i\left(pt-fx+\frac{2\sqrt{3}\pi\sin e}{T_1V_1}y\right)},
\end{aligned}\right\}\quad(29)$$

$$\left.\begin{aligned}
u_1''&=\frac{i\mathfrak{A}T_1V_1}{2\pi}\cdot\frac{\cos e(3-2\cos^2 e)^2}{\{(3-2\cos^2 e)^2+4\cos^2 e\sin e(3-\cos^2 e)^{\frac{1}{2}}\}}e^{i\left(pt-fx-\frac{2\pi\sin e}{T_1V_1}y\right)},\\
v_1''&=\frac{i\mathfrak{A}T_1V_1}{2\pi}\cdot\frac{\sin e(3-2\cos^2 e)^2}{\{(3-2\cos^2 e)^2+4\cos^2 e\sin e(3-\cos^2 e)^{\frac{1}{2}}\}}e^{i\left(pt-fx-\frac{2\pi\sin e}{T_1V_1}y\right)},
\end{aligned}\right\}\quad(30)$$

$$\left.\begin{aligned}
u_2''&=-\frac{i\mathfrak{A}T_1V_1}{2\pi}\cdot\frac{2\sin e\cos e(3-2\cos^2 e)(3-\cos^2 e)^{\frac{1}{2}}}{\{(3-2\cos^2 e)^2+4\cos^2 e\sin e(3-\cos^2 e)^{\frac{1}{2}}\}}e^{i\left(pt-fx-\frac{2\sqrt{3}\pi\sin e}{T_1V_1}y\right)},\\
v_2''&=\frac{i\mathfrak{A}T_1V_1}{2\pi}\cdot\frac{2\sin e\cos^2 e(3-2\cos^2 e)}{\{(3-2\cos^2 e)^2+4\cos^2 e\sin e(3-\cos^2 e)^{\frac{1}{2}}\}}e^{i\left(pt-fx-\frac{2\sqrt{3}\pi\sin e}{T_1V_1}y\right)}.
\end{aligned}\right\}\quad(31)$$

The maximum amplitudes of these waves[4] expressed by (28), (29), (30) and (31) are given in Table I and II in which the amplitudes of the incident waves are also given, and Fig. 2 and 3 show us graphically these amplitudes.

Table I.

Max. Amp. \ e	0°	10°	20°	30°	45°	60°	70°	80°	90°
u_1	1	0·9848	0·9397	0·8659	0·70711	0·5000	0·3421	0·1736	0
u_1'	0	0·4590	0·5250	0·4320	0·2518	0·0939	0·0325	0·00394	0
u_2'	0	0·2479	0·3525	0·4328	0·5065	0·4665	0·3585	0·1958	0
u_1''	1	0·5313	0·4353	0·4335	0·4535	0·4065	0·3115	0·1696	0
u_2''	0	−0·2479	−0·3525	−0·4328	−0·5065	−0·4665	−0·3585	−0·1958	0

Table II.

Max. Amp. \ e	0°	10°	20°	30°	45°	60°	70°	80°	90°
v_1	0	0·1736	0·3420	0·5000	0·7071	0·8660	0·9397	0·9848	1
v_1'	0	−0·0805	−0·1828	−0·2492	−0·2518	−0·1615	−0·08325	−0·0224	0
v_2'	0	0·1714	0·2275	0·2500	0·2265	0·1408	0·0724	0·0197	0
v_1''	0	0·0937	0·1587	0·2505	0·4535	0·7032	0·8562	0·9620	1
v_2''	0	0·1714	0·2275	0·2500	0·2265	0·1408	0·0724	0·0197	0

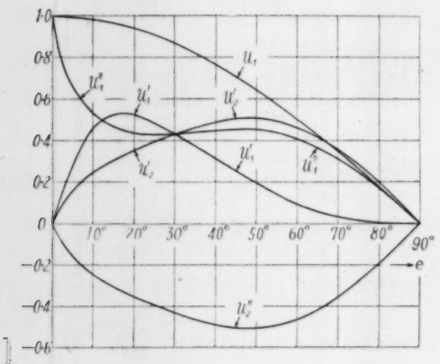

Fig. 2.

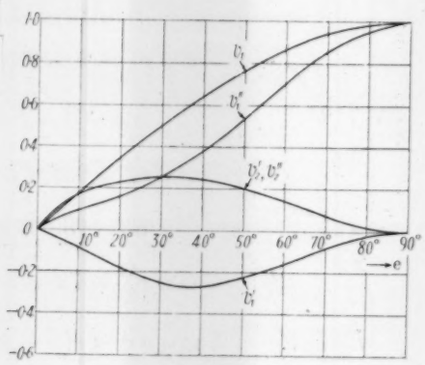

Fig. 3.

4) When the two solids adhere closely, these waves are never generated at the boundary surface.

These tables and figures show us many interesting facts, and some of them are summarised as follows:

1. When the incident wave is dilatational, reflected and transmitted waves are, in general, simultaneously generated at the contact surface, both of which consist of dilatational and distortional waves. When the two solids, however, adhere closely, these waves are never generated at the boundary.

2. When $e=0°$, the y-components of all generated waves vanish, and consequently there exist no reflected wave. And x-components of transmitted waves of dilatational type u_1'' of which the amplitude is equal to that of x-component of incident wave u_1 are generated at the contact surface of two solids.

3. When $e=90°$, x-components of all generated waves vanish, and wherefore there exist no reflected wave. And x-component of transmitted wave of dilatational type v_1'' of which the amplitude is equal to that of y-component of incident wave v_1 is generated at the contact surface of two solids.

b) Incident Wave is Distortional.

4. Putting the incident wave of distortional type, referring to Fig. 1,

$$2\varpi=\mathfrak{B}e^{i(pt-fx-sy)}, \qquad \cdots\cdots\cdots\cdots\cdots\cdots (32)$$

where $\mathfrak{B}$ is the amplitude of this wave, we obtain the corresponding $x-$, $y-$ components of displacement u_2, v_2 and the normal, tangential and shear components of stress $\widehat{xx_2}$, $\widehat{yy_2}$, $\widehat{xy_2}$ as in the following forms:

$$\left.\begin{aligned} u_2&=-\frac{is}{k^2}\mathfrak{B}e^{i(pt-fx-sy)},\\ v_2&=\frac{if}{k^2}\mathfrak{B}e^{i(pt-fx-sy)}, \end{aligned}\right\} \cdots\cdots\cdots\cdots\cdots\cdots (33)$$

$$\left.\begin{aligned} \widehat{xx_2}&=-\frac{2sf\mu}{k^2}\mathfrak{B}e^{i(pt-fx-sy)},\\ \widehat{yy_2}&=\frac{2sf\mu}{k^2}\mathfrak{B}e^{i(pt-fx-sy)},\\ \widehat{xy_2}&=\frac{(f^2-s^2)\mu}{k^2}\mathfrak{B}e^{i(pt-fx-sy)}, \end{aligned}\right\} \cdots\cdots\cdots\cdots\cdots\cdots (34)$$

where $p=\dfrac{2\pi}{T_2}$, T_2 being the period of incident wave expressed by (32).

Let the wave length and velocity of the incident wave be L_2 and V_2 respectively. Then we have

$$L_2 = V_2 T_2 = \frac{2\pi}{\sqrt{s^2+f^2}}. \qquad \cdots\cdots\cdots \quad (35)$$

By the general expressions of reflected waves expressed by (6) and (7) and those of transmitted waves expressed by (13) and (14), we obtain the boundary conditions which must be satisfied at the boundary surface $y=0$ as follows:

When $y=0$,

$$\left.\begin{aligned} &\widehat{yy_1}' + \widehat{yy_2}' - \widehat{yy_1}'' - \widehat{yy_2}'' = -\widehat{yy_2}, \\ &v_1' + v_2' - v_1'' - v_2'' = -v_2, \\ &\widehat{xy_1}' + \widehat{xy_2}' = -\widehat{xy_2}, \\ &\widehat{xy_1}'' + \widehat{xy_2}'' = 0. \end{aligned}\right\} \quad \cdots\cdots\cdots\cdots (36)$$

These conditions give us the following four equations to determine A', B', A'', B'':

$$\left.\begin{aligned} &\frac{2fr'}{h'^2}A'' + \frac{(f^2-s'^2)}{k'^2}B'' = 0, \\ &-\frac{2fr}{h^2}A' + \frac{(f^2-s^2)}{k^2}B' = -\frac{(f^2-s^2)}{k^2}\mathfrak{B}, \\ &-\frac{r}{h^2}A' + \frac{f}{k^2}B' - \frac{r'}{h'^2}A'' - \frac{f}{k'^2}B'' = -\frac{f}{k^2}\mathfrak{B}, \\ &\frac{\mu}{h^2}(s^2-f^2)A' - \frac{2\mu sf}{k^2}B' - \frac{\mu'}{h'^2}(s'^2-f^2)A'' - \frac{2\mu' s' f}{k'^2}B'' = -\frac{4sf\mu}{k^2}\mathfrak{B}. \end{aligned}\right\} \quad (37)$$

Solving these equations, we obtain

$$\left.\begin{aligned} A' &= \mathfrak{B}\frac{4sr'fh^2(f^2-s^2)(f^2+s'^2)}{k^2\left[r'(s'^2+f^2)\{(s^2-f^2)^2+4srf^2\}+\frac{\mu'}{\mu}r(s^2+f^2)\{(s'^2-f^2)^2+4s'r'f^2\}\right]}, \\ B' &= \mathfrak{B}\frac{\left[r'(s'^2+f^2)\{4srf^2-(s^2-f^2)^2\}-\frac{\mu'}{\mu}r(s^2+f^2)\{(s'^2-f^2)^2+4s'r'f^2\}\right]}{k^2\left[r'(s'^2+f^2)\{(s^2-f^2)^2+4srf^2\}+\frac{\mu'}{\mu}r(s^2+f^2)\{(s'^2-f^2)^2+4s'r'f^2\}\right]}, \\ A'' &= \mathfrak{B}\frac{4srfh'^2(s^2+f^2)(s'^2-f^2)}{k^2\left[r'(s'^2+f^2)\{(s^2-f^2)^2+4srf^2\}+\frac{\mu'}{\mu}r(s^2+f^2)\{(s'^2-f^2)^2+4s'r'f^2\}\right]}, \\ B'' &= \mathfrak{B}\frac{8srr'k'^2f^2(s^2+f^2)}{k^2\left[r'(s'^2+f^2)\{(s^2-f^2)^2+4srf^2\}+\frac{\mu'}{\mu}r(s^2+f^2)\{(s'^2-f^2)^2+4s'r'f^2\}\right]}. \end{aligned}\right\} \quad (38)$$

Substituting these values for A', B', A'', B'' in (9), (11), (17), (19), we obtain the displacements of reflected waves and those of transmitted waves which are due to the incident wave expressed by (32) as in the following forms:

Reflected distortional wave;

$$\left.\begin{aligned} u_1' &= \frac{if\mathfrak{B}}{h^2}\frac{4sr'fh^2(f^2-s^2)(f^2+s'^2)}{k^2\left[r'(s'^2+f^2)\{(s^2-f^2)^2+4srf^2\}+\frac{\mu'}{\mu}r(s^2+f^2)\{(s'^2-f^2)^2+4s'r'f^2\}\right]} \\ &\qquad \times e^{i(pt-fx+ry)}, \\ v_1' &= -\frac{ir\mathfrak{B}}{h^2}\frac{4sr'fh^2(f^2-s^2)(f^2+s'^2)}{k^2\left[r'(s'^2+f^2)\{(s^2-f^2)^2+4srf^2\}+\frac{\mu'}{\mu}r(s^2+f^2)\{(s'^2-f^2)^2+4s'r'f^2\}\right]} \\ &\qquad \times e^{i(pt-fx+ry)}, \end{aligned}\right\} \quad \ldots\ldots\ldots\ldots (39)$$

Reflected distortional wave;

$$\left.\begin{aligned} v_2' &= \frac{is\mathfrak{B}}{k^2}\frac{\left[r'(s'^2+f^2)\{4srf^2-(s^2-f^2)^2\}-\frac{\mu'}{\mu}r(s^2+f^2)\{(s'^2-f^2)^2+4s'r'f^2\}\right]}{k^2\left[r'(s'^2+f^2)\{(s^2-f^2)^2+4srf^2\}+\frac{\mu'}{\mu}r(s^2+f^2)\{(s'^2-f^2)^2+4s'r'f^2\}\right]} \\ &\qquad \times e^{i(pt-fx+sy)}, \\ v_2' &= \frac{if\mathfrak{B}}{k^2}\frac{\left[r'(s'^2+f^2)\{4srf^2-(s^2-f^2)^2\}-\frac{\mu'}{\mu}r(s^2+f^2)\{(s'^2-f^2)^2+4s'r'f^2\}\right]}{k^2\left[r'(s'^2+f^2)\{(s^2-f^2)^2+4srf^2\}+\frac{\mu'}{\mu}r(s^2+f^2)\{(s'^2-f^2)^2+4s'r'f^2\}\right]} \\ &\qquad \times e^{i(pt-fx+sy)}, \end{aligned}\right\} \quad \ldots\ldots\ldots\ldots (40)$$

Transmitted dilatational wave;

$$\left.\begin{aligned} u_1'' &= \frac{if\mathfrak{B}}{h'^2}\frac{4srfh'^2(s^2+f^2)(s'^2-f^2)}{k^2\left[r'(s'^2+f^2)\{(s^2-f^2)^2+4srf^2\}+\frac{\mu'}{\mu}r(s^2+f^2)\{(s'^2-f^2)^2+4s'r'f^2\}\right]} \\ &\qquad \times e^{i(pt-fx-r'y)}, \\ v_1'' &= \frac{ir'\mathfrak{B}}{h'^2}\frac{4srfh'^2(s^2+f^2)(s'^2-f^2)}{k^2\left[r'(s'^2+f^2)\{(s^2-f^2)^2+4srf^2\}+\frac{\mu'}{\mu}r(s^2+f^2)\{(s'^2-f^2)^2+4s'r'f^2\}\right]} \\ &\qquad \times e^{i(pt-fx-r'y)}, \end{aligned}\right\} \quad \ldots\ldots\ldots\ldots (41)$$

Transmitted distortional wave ;

$$\left.\begin{aligned} u_2'' &= -\frac{is'\mathfrak{B}}{k'^2}\frac{8srr'k'^2f^2(s^2+f^2)}{k^2\left[r'(s'^2+f^2)\{(s^2-f^2)^2+4srf^2\}+\frac{\mu'}{\mu}r(s^2+f^2)\{(s'^2-f^2)^2+4s'r'f^2\}\right]} \\ &\qquad \times e^{i(pt-fx-s'y)}, \\ v_2'' &= \frac{if\mathfrak{B}}{k'^2}\frac{8srr'k'^2f^2(s^2+f^2)}{k^2\left[r'(s'^2+f^2)\{(s^2-f^2)^2+4srf^2\}+\frac{\mu'}{\mu}r(s^2+f^2)\{(s'^2-f^2)^2+4s'r'f^2\}\right]} \\ &\qquad \times e^{i(pt-fx-s'y)}. \end{aligned}\right\} \quad \cdots\cdots\cdots\cdots\cdots\cdots (42)$$

Let the emergency angle of incident distortional wave expressed by (32) be e. Then (39), (40), (41) and (42) are transformed into the following forms :

$$\left.\begin{aligned} u_1' &= \frac{i\mathfrak{B}T_2V_2}{2\pi}\cdot\frac{4\cos^2 e\sin e\left(\frac{V_2}{V_2'}\right)^2(\cos^2 e-\sin^2 e)\left\{\left(\frac{V_2}{V_1'}\right)^2-\cos^2 e\right\}^{\frac{1}{2}}}{\Phi}e^{i(pt-fx+ry)}, \\ v_1' &= -\frac{i\mathfrak{B}T_2V_2}{2\pi} \\ &\quad \times\frac{4\cos e\sin e\left(\frac{V_2}{V_2'}\right)^2(\cos^2 e-\sin^2 e)\left\{\left(\frac{V_2}{V_1}\right)^2-\cos^2 e\right\}^{\frac{1}{2}}\left\{\left(\frac{V_2}{V_1'}\right)^2-\cos^2 e\right\}^{\frac{1}{2}}}{\Phi} \\ &\qquad \times e^{i(pt-fx+ry)}, \end{aligned}\right\} \quad (39)'$$

$$\left.\begin{aligned} u_2' &= \frac{i\mathfrak{B}T_2V_2}{2\pi}\cdot\frac{\Psi\sin e}{\Phi}e^{i(pt-fx+sy)}, \\ v_2' &= \frac{i\mathfrak{B}T_2V_2}{2\pi}\cdot\frac{\Psi\cos e}{\Phi}e^{i(pt-fx+sy)}, \end{aligned}\right\} \quad \cdots\cdots\cdots\cdots\cdots\cdots (40)'$$

$$\left.\begin{aligned} u_1'' &= \frac{i\mathfrak{B}T_2V_2}{2\pi}\cdot\frac{4\sin e\cos^2 e\left\{\left(\frac{V_2}{V_2'}\right)^2-2\cos^2 e\right\}\left\{\left(\frac{V_2}{V_1}\right)^2-\cos^2 e\right\}^{\frac{1}{2}}}{\Phi}e^{i(pt-fx-r'y)}, \\ v_1'' &= \frac{i\mathfrak{B}T_2V_2}{2\pi}\cdot\frac{4\sin e\cos e\left\{\left(\frac{V_2}{V_2'}\right)^2-2\cos^2 e\right\}\left\{\left(\frac{V_2}{V_1}\right)^2-\cos^2 e\right\}^{\frac{1}{2}}\left\{\left(\frac{V_1}{V_1'}\right)^2-\cos^2 e\right\}^{\frac{1}{2}}}{\Phi} \\ &\qquad \times e^{i(pt-fx-r'y)}, \end{aligned}\right\} \quad \cdots\cdots\cdots\cdots\cdots\cdots (41)'$$

$$\left.\begin{aligned} u_2'' &= -\frac{i\mathfrak{B}T_2V_2}{2\pi} \\ &\quad \times \frac{8\sin e\cos^2 e\left\{\left(\frac{V_2}{V_1}\right)^2-\cos^2 e\right\}^{\frac{1}{2}}\left\{\left(\frac{V_2}{V_1'}\right)^2-\cos^2 e\right\}^{\frac{1}{2}}\left\{\left(\frac{V_2}{V_2'}\right)^2-\cos^2 e\right\}^{\frac{1}{2}}}{\Phi} \\ &\qquad\qquad \times e^{i(pt-fx-s'y)}, \\ v_2'' &= \frac{i\mathfrak{B}T_2V_2}{2\pi}\frac{8\sin e\cos^3 e\left\{\left(\frac{V_2}{V_1}\right)^2-\cos^2 e\right\}^{\frac{1}{2}}\left\{\left(\frac{V_2}{V_1'}\right)^2-\cos^2 e\right\}^{\frac{1}{2}}}{\Phi}e^{i(pt-fx-s'y)}, \end{aligned}\right\} (42)'$$

where

$$\begin{aligned} \Phi &= \left\{\left(\frac{V_2}{V_1'}\right)^2-\cos^2 e\right\}^{\frac{1}{2}}\left(\frac{V_2}{V_2'}\right)^2\left[4\cos^2 e\sin e\left\{\left(\frac{V_2}{V_1}\right)^2-\cos^2 e\right\}^{\frac{1}{2}}+(\sin^2 e-\cos^2 e)^2\right] \\ &\quad +\frac{\mu'}{\mu}\left\{\left(\frac{V_2}{V_1}\right)^2-\cos^2 e\right\}^{\frac{1}{2}}\left[\left\{\left(\frac{V_2}{V_2'}\right)^2-2\cos^2 e\right\}^2\right. \\ &\quad \left.+4\cos^2 e\left\{\left(\frac{V_2}{V_2'}\right)^2-\cos^2 e\right\}^{\frac{1}{2}}\left\{\left(\frac{V_2}{V_1'}\right)^2-\cos^2 e\right\}^{\frac{1}{2}}\right], \\ \Psi &= \left\{\left(\frac{V_2}{V_1'}\right)^2-\cos^2 e\right\}^{\frac{1}{2}}\left(\frac{V_2}{V_2'}\right)^2\left[4\cos^2 e\sin e\left\{\left(\frac{V_2}{V_1}\right)^2-\cos^2 e\right\}^{\frac{1}{2}}-(\sin^2 e-\cos^2 e)^2\right] \\ &\quad -\frac{\mu'}{\mu}\left\{\left(\frac{V_2}{V_1}\right)^2-\cos^2 e\right\}^{\frac{1}{2}}\left[\left\{\left(\frac{V_2}{V_2'}\right)^2-2\cos^2 e\right\}^2\right. \\ &\quad \left.+4\cos^2 e\left\{\left(\frac{V_2}{V_2'}\right)^2-\cos^2 e\right\}^{\frac{1}{2}}\left\{\left(\frac{V_2}{V_1'}\right)^2-\cos^2 e\right\}^{\frac{1}{2}}\right]. \end{aligned}$$

When $\rho=\rho'$ and the respective Poisson's ratios of two media are $\frac{1}{4}$,

$$\left.\begin{aligned} u_1' &= \frac{i\mathfrak{B}T_2V_2}{2\pi}\frac{4\frac{\mu}{\mu'}\cos^2 e\sin e(\cos^2 e-\sin^2 e)\left(\frac{1}{3}\frac{\mu}{\mu'}-\cos^2 e\right)^{\frac{1}{2}}}{\left[\frac{\mu}{\mu'}\left(\frac{1}{3}\frac{\mu}{\mu'}-\cos^2 e\right)^{\frac{1}{2}}\left\{4\cos^2 e\sin e\left(\frac{1}{3}-\cos^2 e\right)^{\frac{1}{2}}+(\sin^2 e-\cos^2 e)^2\right\}\right.} \\ &\quad \left.\frac{e^{i(pt-fx+ry)}}{+\frac{\mu'}{\mu}\left(\frac{1}{3}-\cos^2 e\right)^{\frac{1}{2}}\left\{\left(\frac{\mu}{\mu'}-2\cos^2 e\right)^2+4\cos^2 e\left(\frac{\mu}{\mu'}-\cos^2 e\right)^{\frac{1}{2}}\left(\frac{1}{3}\frac{\mu}{\mu'}-\cos^2 e\right)^{\frac{1}{2}}\right\}\right]}, \end{aligned}\right|$$

$$v_1' = -\frac{i\mathfrak{B}T_2V_2}{2\pi}\left\{\frac{4\frac{\mu}{\mu'}\cos e\sin e(\cos^2 e-\sin^2 e)\left(\frac{1}{3}-\cos^2 e\right)^{\frac{1}{2}}\left(\frac{1}{3}\frac{\mu}{\mu'}-\cos^2 e\right)^{\frac{1}{2}}}{\left[\frac{\mu}{\mu'}\left(\frac{1}{3}\frac{\mu}{\mu'}-\cos^2 e\right)^{\frac{1}{2}}\left\{4\cos^2 e\sin e\left(\frac{1}{3}-\cos^2 e\right)^{\frac{1}{2}}+(\sin^2 e-\cos^2 e)^2\right\}\right.}\right.$$

$$\left.\left.+\frac{\mu'}{\mu}\left(\frac{1}{3}-\cos^2 e\right)^{\frac{1}{2}}\left\{\left(\frac{\mu}{\mu'}-2\cos^2 e\right)^2+4\cos^2 e\left(\frac{\mu}{\mu'}-\cos^2 e\right)^{\frac{1}{2}}\left(\frac{1}{3}\frac{\mu}{\mu'}-\cos^2 e\right)^{\frac{1}{2}}\right\}\right]\right\}e^{i(pt-fx+ry)},$$

.....(39)″

$$u_2' = \frac{i\mathfrak{B}T_2V_2}{2\pi}$$

$$\times\frac{\sin e\left[\frac{\mu}{\mu'}\left(\frac{1}{3}\frac{\mu}{\mu'}-\cos^2 e\right)^{\frac{1}{2}}\left\{4\cos^2 e\sin e\left(\frac{1}{3}-\cos^2 e\right)^{\frac{1}{2}}-(\sin^2 e-\cos^2 e)^2\right\}\right.}{\left[\frac{\mu}{\mu'}\left(\frac{1}{3}\frac{\mu}{\mu'}-\cos^2 e\right)^{\frac{1}{2}}\left\{4\cos^2 e\sin e\left(\frac{1}{3}-\cos^2 e\right)^{\frac{1}{2}}+(\sin^2 e-\cos^2 e)^2\right\}\right.}$$

$$\left.-\frac{\mu'}{\mu}\left(\frac{1}{3}-\cos^2 e\right)^{\frac{1}{2}}\left\{\left(\frac{\mu}{\mu'}-2\cos^2 e\right)^2+4\cos^2 e\left(\frac{\mu}{\mu'}-\cos^2 e\right)^{\frac{1}{2}}\left(\frac{1}{3}\frac{\mu}{\mu'}-\cos^2 e\right)^{\frac{1}{2}}\right\}\right]$$

$$\left.+\frac{\mu'}{\mu}\left(\frac{1}{3}-\cos^2 e\right)^{\frac{1}{2}}\left\{\left(\frac{\mu}{\mu'}-2\cos^2 e\right)^2+4\cos^2 e\left(\frac{\mu}{\mu'}-\cos^2 e\right)^{\frac{1}{2}}\left(\frac{1}{3}\frac{\mu}{\mu'}-\cos^2 e\right)^{\frac{1}{2}}\right\}\right]$$

$$\times e^{i(pt-fx+sy)},$$

$$v_2' = \frac{i\mathfrak{B}T_2V_2}{2\pi}$$

$$\times\frac{\cos e\left[\frac{\mu'}{\mu}\left(\frac{1}{3}\frac{\mu}{\mu'}-\cos^2 e\right)^{\frac{1}{2}}\left\{4\cos^2 e\sin e\left(\frac{1}{3}-\cos^2 e\right)^{\frac{1}{2}}-(\sin^2 e-\cos^2 e)^2\right\}\right.}{\left[\frac{\mu}{\mu'}\left(\frac{1}{3}\frac{\mu}{\mu'}-\cos^2 e\right)^{\frac{1}{2}}\left\{4\cos^2 e\sin e\left(\frac{1}{3}-\cos^2 e\right)^{\frac{1}{2}}+(\sin^2 e-\cos^2 e)^2\right\}\right.}$$

$$\left.-\frac{\mu'}{\mu}\left(\frac{1}{3}-\cos^2 e\right)^{\frac{1}{2}}\left\{\left(\frac{\mu}{\mu'}-2\cos^2 e\right)^2+4\cos^2 e\left(\frac{\mu}{\mu'}-\cos^2 e\right)^{\frac{1}{2}}\left(\frac{1}{3}\frac{\mu}{\mu'}-\cos^2 e\right)^{\frac{1}{2}}\right\}\right]$$

$$\left.+\frac{\mu'}{\mu}\left(\frac{1}{3}-\cos^2 e\right)^{\frac{1}{2}}\left\{\left(\frac{\mu}{\mu'}-2\cos^2 e\right)^2+4\cos^2 e\left(\frac{\mu}{\mu'}-\cos^2 e\right)^{\frac{1}{2}}\left(\frac{1}{3}\frac{\mu}{\mu'}-\cos^2 e\right)^{\frac{1}{2}}\right\}\right]$$

$$\times e^{i(pt-fx+sy)},$$

.....(40)″

$$u_1'' = \frac{i\mathfrak{B}T_2V_2}{2\pi} \left\{ \frac{4\sin e\cos^2 e\left(\frac{\mu}{\mu'}-2\cos^2 e\right)\left(\frac{1}{3}-\cos^2 e\right)^{\frac{1}{2}}}{\left[\frac{\mu}{\mu'}\left(\frac{1}{3}\frac{\mu}{\mu'}-\cos^2 e\right)^{\frac{1}{2}}\left\{4\cos^2 e\sin e\left(\frac{1}{3}-\cos^2 e\right)^{\frac{1}{2}}+(\sin^2 e-\cos^2 e)^2\right\}\right.} \right.$$

$$\left. \frac{e^{i(pt-fx-r'y)}}{\left.+\frac{\mu'}{\mu}\left(\frac{1}{3}-\cos^2 e\right)^{\frac{1}{2}}\left\{\left(\frac{\mu}{\mu'}-2\cos^2 e\right)^2+4\cos^2 e\left(\frac{\mu}{\mu'}-\cos^2 e\right)^{\frac{1}{2}}\left(\frac{1}{3}\frac{\mu}{\mu'}-\cos^2 e\right)^{\frac{1}{2}}\right\}\right]}, \right.$$

$$v_1'' = \frac{i\mathfrak{B}T_2V_2}{2\pi} \left\{ \frac{4\sin e\cos e\left(\frac{\mu}{\mu'}-2\cos^2 e\right)\left(\frac{1}{3}-\cos^2 e\right)^{\frac{1}{2}}\left(\frac{1}{3}\frac{\mu}{\mu'}-\cos^2 e\right)^{\frac{1}{2}}}{\left[\frac{\mu}{\mu'}\left(\frac{1}{3}\frac{\mu}{\mu'}-\cos^2 e\right)^{\frac{1}{2}}\left\{4\cos^2 e\sin e\left(\frac{1}{3}-\cos^2 e\right)^{\frac{1}{2}}+(\sin^2 e-\cos^2 e)^2\right\}\right.} \right.$$

$$\left. \frac{e^{i(pt-fx-r'y)}}{\left.+\frac{\mu'}{\mu}\left(\frac{1}{3}-\cos^2 e\right)^{\frac{1}{2}}\left\{\left(\frac{\mu}{\mu'}-2\cos^2 e\right)^2+4\cos^2 e\left(\frac{\mu}{\mu'}-\cos^2 e\right)^{\frac{1}{2}}\left(\frac{1}{3}\frac{\mu}{\mu'}-\cos^2 e\right)^{\frac{1}{2}}\right\}\right]}, \right.$$

.....(41)''

$$u_2'' = -\frac{i\mathfrak{B}T_2V_2}{2\pi} \left\{ \times \frac{8\sin e\cos^2 e\left(\frac{1}{3}-\cos^2 e\right)^{\frac{1}{2}}\left(\frac{1}{3}\frac{\mu}{\mu'}-\cos^2 e\right)^{\frac{1}{2}}\left(\frac{\mu}{\mu'}-\cos^2 e\right)^{\frac{1}{2}}}{\left[\frac{\mu}{\mu'}\left(\frac{1}{3}\frac{\mu}{\mu'}-\cos^2 e\right)^{\frac{1}{2}}\left\{4\cos^2 e\sin e\left(\frac{1}{3}-\cos^2 e\right)^{\frac{1}{2}}+(\sin^2 e-\cos^2 e)^2\right\}\right.} \right.$$

$$\left. \frac{e^{i(pt-fx-s'y)}}{\left.+\frac{\mu'}{\mu}\left(\frac{1}{3}-\cos^2 e\right)^{\frac{1}{2}}\left\{\left(\frac{\mu}{\mu'}-2\cos^2 e\right)^2+4\cos^2 e\left(\frac{\mu}{\mu'}-\cos^2 e\right)^{\frac{1}{2}}\left(\frac{1}{3}\frac{\mu}{\mu'}-\cos^2 e\right)^{\frac{1}{2}}\right\}\right]}, \right.$$

$$v_2'' = \frac{i\mathfrak{B}T_2V_2}{2\pi} \left\{ \frac{8\sin e\cos^3 e\left(\frac{1}{3}-\cos^2 e\right)^{\frac{1}{2}}\left(\frac{1}{3}\frac{\mu}{\mu'}-\cos^2 e\right)^{\frac{1}{2}}}{\left[\frac{\mu}{\mu'}\left(\frac{1}{3}\frac{\mu}{\mu'}-\cos^2 e\right)^{\frac{1}{2}}\left\{4\cos^2 e\sin e\left(\frac{1}{3}-\cos^2 e\right)^{\frac{1}{2}}+(\sin^2 e-\cos^2 e)^2\right\}\right.} \right.$$

$$\left. \frac{e^{i(pt-fx-s'y)}}{\left.+\frac{\mu'}{\mu}\left(\frac{1}{3}-\cos^2 e\right)^{\frac{1}{2}}\left\{\left(\frac{\mu}{\mu'}-2\cos^2 e\right)^2+4\cos^2 e\left(\frac{\mu}{\mu'}-\cos^2 e\right)^{\frac{1}{2}}\left(\frac{1}{3}\frac{\mu}{\mu'}-\cos^2 e\right)^{\frac{1}{2}}\right\}\right]}. \right.$$

.....(42)''

When $\frac{\mu'}{\mu}=1$, expressions (39)″, (40)″, (41)″, (42)″ are rewritten by

$$\left.\begin{aligned} u_1' &= -\frac{i\mathfrak{B}T_2V_2}{2\pi}\frac{2\cos^2 e\sin e(\sin^2 e-\cos^2 e)}{\left\{(\sin^2 e-\cos^2 e)^2+4\cos^2 e\sin e\left(\frac{1}{3}-\cos^2 e\right)^{\frac{1}{2}}\right\}}e^{i\left(pt-fx+\frac{2\pi\sin e}{\sqrt{3}T_2V_2}y\right)},\\ v_1' &= \frac{i\mathfrak{B}T_2V_2}{2\pi}\frac{2\cos e\sin e(\sin^2 e-\cos^2 e)\left(\frac{1}{3}-\cos^2 e\right)^{\frac{1}{2}}}{\left\{(\sin^2 e-\cos^2 e)^2+4\cos^2 e\sin e\left(\frac{1}{3}-\cos^2 e\right)^{\frac{1}{2}}\right\}}e^{i\left(pt-fx+\frac{2\pi\sin e}{\sqrt{3}T_2V_2}y\right)}, \end{aligned}\right\} \quad \cdots\cdots\cdots\cdots\cdots\cdots (43)$$

$$\left.\begin{aligned} u_2' &= -\frac{i\mathfrak{B}T_2V_2}{2\pi}\frac{\sin e(\sin^2 e-\cos^2 e)^2}{\left\{(\sin^2 e-\cos^2 e)^2+4\cos^2 e\sin e\left(\frac{1}{3}-\cos^2 e\right)^{\frac{1}{2}}\right\}}e^{i\left(pt-fx+\frac{2\pi\sin e}{T_2V_2}y\right)},\\ v_2' &= -\frac{i\mathfrak{B}T_2V_2}{2\pi}\frac{\cos e(\sin^2 e-\cos^2 e)^2}{\left\{(\sin^2 e-\cos^2 e)^2+4\cos^2 e\sin e\left(\frac{1}{3}-\cos^2 e\right)^{\frac{1}{2}}\right\}}e^{i\left(pt-fx+\frac{2\pi\sin e}{T_2V_2}y\right)}, \end{aligned}\right\} \quad \cdots\cdots\cdots\cdots\cdots\cdots (44)$$

$$\left.\begin{aligned} u_1'' &= \frac{i\mathfrak{B}T_2V_2}{2\pi}\frac{2\sin e\cos^2 e(\sin^2 e-\cos^2 e)}{\left\{(\sin^2 e-\cos^2 e)^2+4\cos^2 e\sin e\left(\frac{1}{3}-\cos^2 e\right)^{\frac{1}{2}}\right\}}e^{i\left(pt-fx-\frac{2\pi\sin e}{\sqrt{3}T_2V_2}y\right)},\\ v_1'' &= \frac{i\mathfrak{B}T_2V_2}{2\pi}\frac{2\sin e\cos e(\sin^2 e-\cos^2 e)\left(\frac{1}{3}-\cos^2 e\right)^{\frac{1}{2}}}{\left\{(\sin^2 e-\cos^2 e)^2+4\cos^2 e\sin e\left(\frac{1}{3}-\cos^2 e\right)^{\frac{1}{2}}\right\}}e^{i\left(pt-fx-\frac{2\pi\sin e}{\sqrt{3}T_2V_2}y\right)}, \end{aligned}\right\} \quad \cdots\cdots\cdots\cdots\cdots\cdots (45)$$

$$\left.\begin{aligned} u_2'' &= -\frac{i\mathfrak{B}T_2V_2}{2\pi}\frac{4\sin^2 e\cos^2 e\left(\frac{1}{3}-\cos^2 e\right)^{\frac{1}{2}}}{\left\{(\sin^2 e-\cos^2 e)^2+4\cos^2 e\sin e\left(\frac{1}{3}-\cos^2 e\right)^{\frac{1}{2}}\right\}}e^{i\left(pt-fx-\frac{2\pi\sin e}{T_2V_2}y\right)},\\ v_2'' &= \frac{i\mathfrak{B}T_2V_2}{2\pi}\frac{4\sin e\cos^3 e\left(\frac{1}{3}-\cos^2 e\right)^{\frac{1}{2}}}{\left\{(\sin^2 e-\cos^2 e)^2+4\cos^2 e\sin e\left(\frac{1}{3}-\cos^2 e\right)^{\frac{1}{2}}\right\}}e^{i\left(pt-fx-\frac{2\pi\sin e}{T_2V_2}y\right)}. \end{aligned}\right\} \quad \cdots\cdots\cdots\cdots\cdots\cdots (46)$$

When the emergency angle is smaller than 54°44′, the expressions (43), (44), (45), (46) should be replaced by the following formulae:

$$\left.\begin{aligned} u_1' &= -\frac{i\mathfrak{B}T_2V_2}{2\pi}\frac{2\cos^2 e\sin e(\sin^2 e-\cos^2 e)}{\left\{(\sin^2 e-\cos^2 e)^4+16\cos^4 e\sin^2 e\left(\cos^2 e-\frac{1}{3}\right)\right\}^{\frac{1}{2}}}\\ &\qquad\times e^{i\left(pt-fx+\frac{2\pi\sin e}{\sqrt{3}\,T_2V_2}y-\varphi\right)},\\ v_1' &= \frac{i\mathfrak{B}T_2V_2}{2\pi}\frac{2\cos e\sin e(\sin^2 e-\cos^2 e)\left(\cos^2 e-\frac{1}{3}\right)^{\frac{1}{2}}}{\left\{(\sin^2 e-\cos^2 e)^4+16\cos^4 e\sin^2 e\left(\cos^2 e-\frac{1}{3}\right)\right\}^{\frac{1}{2}}}\\ &\qquad\times e^{i\left(pt-fx+\frac{2\pi\sin e}{\sqrt{3}\,T_2V_2}y-\varphi+\frac{\pi}{2}\right)}, \end{aligned}\right\}\ldots(47)$$

$$\left.\begin{aligned} u_2' &= -\frac{i\mathfrak{B}T_2V_2}{2\pi}\frac{\sin e(\sin^2 e-\cos^2 e)^2}{\left\{(\sin^2 e-\cos^2 e)^4+16\cos^4 e\sin^2 e\left(\cos^2 e-\frac{1}{3}\right)\right\}^{\frac{1}{2}}}\\ &\qquad\times e^{i\left(pt-fx+\frac{2\pi\sin e}{T_2V_2}y-\varphi\right)},\\ v_2' &= -\frac{i\mathfrak{B}T_2V_2}{2\pi}\frac{\cos e(\sin^2 e-\cos^2 e)^2}{\left\{(\sin^2 e-\cos^2 e)^4+16\cos^4 e\sin^2 e\left(\cos^2 e-\frac{1}{3}\right)\right\}^{\frac{1}{2}}}\\ &\qquad\times e^{i\left(pt-fx+\frac{2\pi\sin e}{T_2V_2}y-\varphi\right)}, \end{aligned}\right\}\ldots(48)$$

$$\left.\begin{aligned} u_1'' &= \frac{i\mathfrak{B}T_2V_2}{2\pi}\frac{2\sin e\cos^2 e(\sin^2 e-\cos^2 e)}{\left\{(\sin^2 e-\cos^2 e)^4+16\cos^4 e\sin^2 e\left(\cos^2 e-\frac{1}{3}\right)\right\}^{\frac{1}{2}}}\\ &\qquad\times e^{i\left(pt-fx-\frac{2\pi\sin e}{\sqrt{3}\,T_2V_2}y-\varphi\right)},\\ v_1'' &= \frac{i\mathfrak{B}T_2V_2}{2\pi}\frac{2\sin e\cos e(\sin^2 e-\cos^2 e)\left(\cos^2 e-\frac{1}{3}\right)^{\frac{1}{2}}}{\left\{(\sin^2 e-\cos^2 e)^4+16\cos^4 e\sin^2 e\left(\cos^2 e-\frac{1}{3}\right)\right\}^{\frac{1}{2}}}\\ &\qquad\times e^{i\left(pt-fx-\frac{2\pi\sin e}{\sqrt{3}\,T_2V_2}y-\varphi+\frac{\pi}{2}\right)}, \end{aligned}\right\}\ldots(49)$$

$$\left.\begin{aligned} u_2'' &= -\frac{i\mathfrak{B}T_2V_2}{2\pi}\frac{4\sin^2 e\cos^2 e\left(\cos^2 e-\frac{1}{3}\right)^{\frac{1}{2}}}{\left\{(\sin^2 e-\cos^2 e)^4+16\cos^4 e\sin^2 e\left(\cos^2 e-\frac{1}{3}\right)\right\}^{\frac{1}{2}}} \\ &\qquad \times e^{i\left(pt-fx-\frac{2\pi\sin e}{T_2V_2}y-\varphi+\frac{\pi}{2}\right)}, \\ v_2'' &= \frac{i\mathfrak{B}T_2V_2}{2\pi}\frac{4\sin e\cos^3 e\left(\cos^2 e-\frac{1}{3}\right)^{\frac{1}{2}}}{\left\{(\sin^2 e-\cos^2 e)^4+16\cos^4 e\sin^2 e\left(\cos^2 e-\frac{1}{3}\right)\right\}^{\frac{1}{2}}} \\ &\qquad \times e^{i\left(pt-fx-\frac{2\pi\sin e}{T_2V_2}y-\varphi+\frac{\pi}{2}\right)}, \end{aligned}\right\} \quad \ldots(50)$$

where $$\varphi=\tan^{-1}\left\{\frac{4\sin e\cos^2 e\left(\cos^2 e-\frac{1}{3}\right)^{\frac{1}{2}}}{(\sin^2 e-\cos^2 e)^2}\right\}.$$

By the numerical calculations we obtain the following Table III, IV, in which the maximum amplitudes of the generated waves expressed by (43), (44), (45), (46), (47), (48), (49), (50), together with the amplitude of incident wave expressed by (33) are tabulated. (47), (48), (49), (50) shew us that when the emergency angle e is smaller than 54°44′, the

Table III.

Max. Amp. \ e	0°	10°	20°	30°	40°	45°	50°	52°30′	53°30′	54°
u_2	0	−0·1736	−0·3420	−0·5000	−0·6428	−0·7071	−0·7661	−0·7935	−0·8038	−0·8090
u_1'	0	0·3061	0·4315	0·375	0·1722	0	−0·3057	−0·645	−0·903	−1·106
u_2'	0	−0·1481	−0·1875	−0·125	−0·0255	0	−0·0643	−0·226	−0·374	−0·4435
u_1''	0	−0·3061	−0·4315	−0·375	−0·1722	0	0·3057	0·645	0·903	1·106
u_2''	0	−0·0902	−0·2865	−0·485	−0·643	−0·7071	−0·763	−0·76	−0·711	−0·637

Max. Amp. \ e	54°44′	55°	56°30′	57°30′	60°	65°	70°	80°	90°
u_2	−0·8165	−0·820	−0·8339	−0·8435	−0·866	−0·9064	−0·9397	−0·9848	−1
u_1'	−1·634	−0·997	−0·6115	−0·534	−0·433	−0·3115	−0·213	−0·0588	0
u_2'	−0·8165	−0·520	−0·392	−0·392	−0·433	−0·5605	−0·699	−0·919	−1
u_1''	1·634	0·997	0·6115	0·534	0·433	0·3115	0·213	0·0588	0
u_2''	0	−0·2993	−0·442	−0·4535	−0·433	−0·3455	−0·242	−0·0679	0

Table IV.

Max. Amp. \ e	0°	10°	20°	30°	40°	45°	50°	52°30′	53°30′	54°
v_2	1	0·9848	0·9397	0·8659	0·7661	0·7071	0·6428	0·6086	0·5949	0·5878
v_1'	0	−0·2480	−0·3405	−0·279	−0·1133	0	0·1345	0·204	0·217	0·2075
v_2'	−1	−0·8430	−0·515	−0·2165	−0·0304	0	−0·054	−0·173	−0·276	−0·3225
v_1''	0	−0·2480	−0·3405	−0·279	−0·1133	0	0·1345	0·204	0·217	0·2075
v_2''	0	0·5119	0·7875	0·840	0·766	0·7071	0·641	0·582	0·527	0·463

Max. Amp. \ e	54°44′	55°	56°30′	57°30′	60°	65°	70°	80°	90°
v_2	0·5773	0·574	0·552	0·5372	0·500	0·4224	0·3421	0·1736	0
v_1'	0	0·110	0·1875	0·2105	0·25	0·2905	0·2893	0·1867	0
v_2'	−0·5773	−0·364	−0·2595	−0·25	−0·25	−0·2615	−0·254	−0·1612	0
v_1''	0	0·110	0·1875	0·2105	0·25	0·2905	0·2893	0·1867	0
v_2''	0	0·210	0·2925	0·2885	0·25	0·1613	0·0883	0·0119	0

Table V.

e	0°	10°	20°	30°	40°	45°	50°	52°30′	54°44′	60°	70°	80°	90°
φ	0	0·546	0·992	1·318	1·531	1·570	1·487	1·282	0	0	0	0	0

waves generated by the incident distortional wave accumulate on the surface $y=0$, and have the phase differences which vary with the emergency angle e. The phase difference φ is also calculated and tabulated in Table V, and graphically shewn in Fig. 6.

From Fig. 4, 5 and 6 in which the values in Table III, IV, V are graphically shewn, we can see many remarkable facts, and some of them are summarised as follows:

1. When the incident wave is distortional, reflected and transmitted waves are, in general, simultaneously generated at the contact surface, both of which consist of dilatational and distortional waves. When the two solids, however, adhere closely, these waves are never generated at this boundary.

2. When $e=0°$, x-components of all generated waves vanish, and moreover there exist no transmitted wave. The amplitude of y-component of reflected wave (v_2'), in this case, is equal to that of incident wave v_2.

3. When $0°<e<54°44'$, all generated waves become to have the properties of surface waves of which the energies are accumulated on

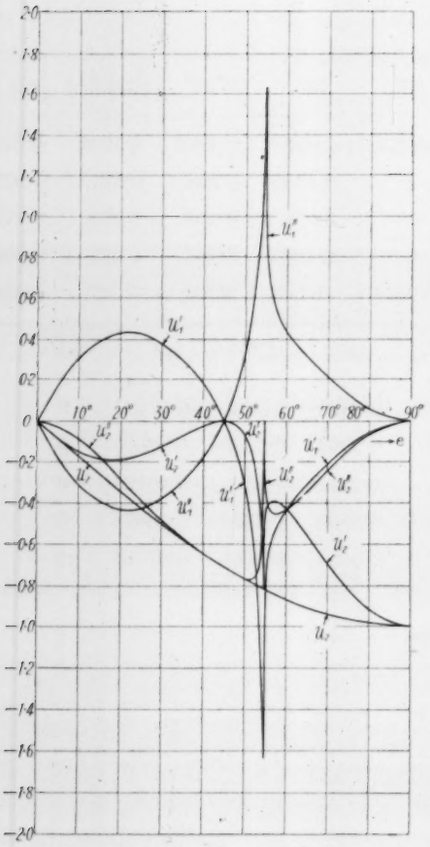

Fig. 4.

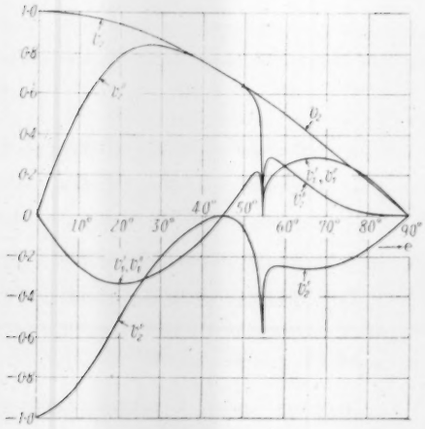

Fig. 5.

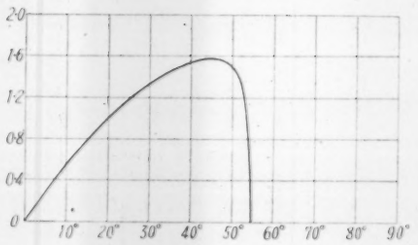

Fig. 6.

the contact surface mainly. In this case, the phase differences of which the magnitudes depend upon the magnitude of the emergency angle of the incident wave exist between these surface waves and the incident wave. (See (47), (48), (49), (50) and Fig. 6.)

4. When $e=45°$, the transmitted distortional wave (u_2'', v_2'') are only generated, and the other waves such as transmitted dilatational wave, and reflected dilatational and distortional ones vanish.

5. When $e \fallingdotseq 54°44'$, the amplitude of the x-component of reflected dilatational wave (u_1') and that of transmitted dilatational wave (u_1'') become very large, and that of the reflected distortional one (u_2') is also moderately large. In this case, however, there is no x-component of transmitted distortional wave (u_2''). And the amplitude of y-component of reflected dilatational wave (v_1'), and those of the transmitted dilatational (v_1'') and distortional waves (v_2'') are zero, and in the contrary the amplitude of y-component of reflected distortional wave

(v_2') is moderately large.

6. When $e=90°$, the y-components of the generated waves vanish and there exist no transmitted waves.

Part II. Initial Movement of the Free Surface of a Stratified Solid.

5. We intend to investigate the problems that when the transmitted waves generated by the waves, which are primarily incident obliquely to the bottom surface $x=0$ of a stratified layer residing on the surface of a semi-infinite elastic solid, are incident to the free surface $y=H$, what kinds of waves are generated at this free surface, and what movements should the free surface take at initial stage. It is not necessary in the present study, therefore, to consider the effect of multiple reflections of waves at $y=H$ and $y=0$. Of course, at the boundary surface the two elastic solids slide upon each other without any friction.

Before entering this investigation, we shall study the following two problems, as the preliminary calculation, relating to the reflections of the waves which are generated by a transmitted wave when it is incident to the free surface $y=H$.

a) Transmitted wave is dilatational.

b) Transmitted wave is distortional.

a) Transmitted Wave is Dilatational.

6. Let the transmitted wave, which is generated by a primary wave of any type when it is incident to the boundary surface, be a dilatational one which is expressed by

$$\Delta_U=A_U e^{i(pt-fx-r'y)}. \qquad \text{.....(51)}$$

Then the corresponding displacement u_{1U}, v_{1U} and the stress $\widehat{xx}_{1U}$, $\widehat{yy}_{1U}$, $\widehat{xy}_{1U}$ are expressed by

$$\left.\begin{aligned} u_{1U}&=\frac{if(\lambda'+2\mu')}{\rho' p^2}A_U e^{i(pt-fx-r'y)},\\ v_{1U}&=\frac{ir'(\lambda'+2\mu')}{\rho' p^2}A_U e^{i(pt-fx-r'y)},\end{aligned}\right\} \qquad \text{.....(52)}$$

$$\left.\begin{aligned} \widehat{xx}_{1U}&=\left\{\lambda'+\frac{2f^2\mu'(\lambda'+2\mu')}{\rho' p^2}\right\}A_U e^{i(pt-fx-r'y)},\\ \widehat{yy}_{1U}&=\left\{\lambda'+\frac{2r'^2\mu'(\lambda'+2\mu')}{\rho' p^2}\right\}A_U e^{i(pt-fx-r'y)},\end{aligned}\right\} \qquad \text{.....(53)}$$

$$\widehat{xy}_{1U}=\frac{2fr'\mu'(\lambda'+2\mu')}{\rho'p^2}A_U e^{i(pt-fx-r'y)},$$

where A_U is a constant determined by the boundary conditions at $y=0$, and is a certain function of the emergency angle, the velocity and the period of a primary wave incident to the plane $y=0$.

Now we know the reflected waves of two types such that

$$\Delta_U'=A_U' e^{i(pt-fx+r'y)}, \quad \ldots\ldots\ldots\ldots\ldots\ldots (54)$$

$$2\varpi_U'=B_U' e^{i(pt-fx+s'y)}, \quad \ldots\ldots\ldots\ldots\ldots\ldots (55)$$

where A_U', B_U' are arbitrary constants and

$$r'^2=h'^2-f^2, \quad s'^2=k'^2-f^2, \quad h'^2=\frac{\rho'p^2}{(\lambda'+2\mu')}, \quad k'^2=\frac{\rho'p^2}{\mu'}.$$

The displacement u_{1U}', v_{1U}' and the stress $\widehat{xx}_{1U}'$, $\widehat{yy}_{1U}'$, $\widehat{xy}_{1U}'$ corresponding to Δ_U' are written as follows:

$$\left.\begin{aligned} u_{1U}'&=\frac{if(\lambda'+2\mu')}{\rho'p^2}A_U' e^{i(pt-fx+r'y)},\\ v_{1U}'&=-\frac{ir'(\lambda'+2\mu')}{\rho'p^2}A_U' e^{i(pt-fx+r'y)},\end{aligned}\right\} \ldots\ldots\ldots\ldots (56)$$

$$\left.\begin{aligned} \widehat{xx}_{1U}'&=\left\{\lambda'+\frac{2f^2\mu'(\lambda'+2\mu')}{\rho'p^2}\right\}A_U' e^{i(pt-fx+r'y)},\\ \widehat{yy}_{1U}'&=\left\{\lambda'+\frac{2r'^2\mu'(\lambda'+2\mu')}{\rho'p^2}\right\}A_U' e^{i(pt-fx+r'y)},\\ \widehat{xy}_{1U}'&=-\frac{2fr'\mu'(\lambda'+2\mu')}{\rho'p^2}A_U' e^{i(pt-fx+r'y)}.\end{aligned}\right\} \ldots\ldots (57)$$

The displacement u_{2U}', v_{2U}' and the stress $\widehat{xx}_{2U}'$, $\widehat{yy}_{2U}'$, $\widehat{xy}_{2U}'$ corresponding to $2\varpi'_U$ expressed by (55) are expressed by

$$\left.\begin{aligned} u_{2U}'&=\frac{is'\mu'}{\rho'p^2}B_U' e^{i(pt-fx+s'y)},\\ v_{2U}'&=\frac{if\mu'}{\rho'p^2}B_U' e^{i(pt-fx+s'y)},\end{aligned}\right\} \ldots\ldots\ldots\ldots\ldots (58)$$

$$\left.\begin{aligned} \widehat{xx}_{2U}'&=\frac{2s'f\mu'^2}{\rho'p^2}B_U' e^{i(pt-fx+s'y)},\\ \widehat{yy}_{2U}'&=-\frac{2s'f\mu'^2}{\rho'p^2}B_U' e^{i(pt-fx+s'y)},\\ \widehat{xy}_{2U}'&=\frac{(f^2-s'^2)\mu'^2}{\rho'p^2}B_U' e^{i(pt-fx+s'y)}.\end{aligned}\right\} \ldots\ldots\ldots\ldots (59)$$

Using (54) and (55), we shall adjust A_U' and B_U' to make shear stress on the free surface $y=H$ due to the incident wave expressed by (51) be nil and to make a certain normal stress and tangential stress existent on this surface. The boundary conditions thus confined at $y=H$ are written as follows:

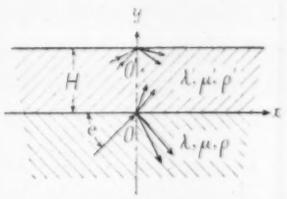

Fig. 7.

When $y=H$,

$$\left.\begin{aligned} \widehat{xy}_{1U}+\widehat{xy}_{1U}'+\widehat{xy}_{2U}'&=0,\\ \widehat{yy}_{1U}'+\widehat{yy}_{2U}'&=\widehat{yy}_{1U}. \end{aligned}\right\} \quad \cdots\cdots\cdots\cdots\cdots (60)$$

These conditions give us two equations to determine the values of A_U' and B_U' such that

$$\left.\begin{aligned} \frac{2fr'}{h'^2}A_U'e^{ir'H}-\frac{(f^2-s'^2)}{k'^2}B_U'e^{is'H}&=\frac{2fr'}{h'^2}A_Ue^{-ir'H},\\ \left(\frac{\lambda'}{\mu'}+\frac{2r'^2}{h'^2}\right)A_U'e^{ir'H}-\frac{2s'f}{k'^2}B_U'e^{is'H}&=\left(\frac{\lambda'}{\mu'}+\frac{2r'^2}{h'^2}\right)A_Ue^{-ir'H}. \end{aligned}\right\} \quad \cdots\cdots(61)$$

Solving these equations, we obtain

$$\left.\begin{aligned} A_U'&=A_Ue^{-2ir'H},\\ B_U'&=0. \end{aligned}\right\} \quad \cdots\cdots\cdots\cdots\cdots\cdots(62)$$

Substituting (62) in (56), (58), we get

$$\left.\begin{aligned} u_{1U}'&=\frac{if}{h'^2}A_Ue^{i(pt-fx+r'y-2r'H)},\\ v_{1U}'&=-\frac{ir'}{h'^2}A_Ue^{i(pt-fx+r'y-2r'H)}, \end{aligned}\right\} \quad \cdots\cdots\cdots\cdots(63)$$

$$\left.\begin{aligned} u_{2U}'&=0,\\ v_{2U}'&=0. \end{aligned}\right\} \quad \cdots\cdots\cdots\cdots\cdots\cdots\cdots\cdots\cdots\cdots(64)$$

To make shear stress at $y=H$ due to the incident wave (51) be nil, it is sufficient to use the reflected waves of dilatational type expressed by (63) only, and there is no necessity to take distortional wave (55) of reflected type. And the normal stress in the medium II due to (51) and (54) is expressed by

$$\widehat{yy}_U=\frac{\mu'}{h'^2}(k'^2-2h'^2+2r'^2)A_U\{e^{-ir'y}+e^{i(r'y-2r'H)}\}e^{i(pt-fx)}. \quad \cdots(65)$$

Next, to make the normal stress (65) at the plane $y=H$ be nil in order to make the surface $y=H$ be completely free from traction, we

use the following two waves which predominate on the surface $y=H$ such that

$$\Delta_U'' = A_U'' e^{r''(y-H)} e^{i(pt-fx)}, \quad \cdots\cdots\cdots\cdots (66)$$

$$2\varpi_U'' = B_U'' e^{s''(y-H)} e^{i(pt-fx)}, \quad \cdots\cdots\cdots\cdots (67)$$

where A_U'' and B_U'' are arbitrary constants and

$$r''^2 = f^2 - h'^2, \quad s''^2 = f^2 - k'^2. \quad \cdots\cdots\cdots\cdots (68)$$

The displacement u_{1U}'', v_{1U}'' and the stress $\widehat{xx}_{1U}''$, $\widehat{yy}_{1U}''$, $\widehat{xy}_{1U}''$ corresponding to (66), and the displacement u_{2U}'', v_{2U}'' and the stress $\widehat{xx}_{2U}''$, $\widehat{yy}_{2U}''$, $\widehat{xy}_{2U}''$ corresponding to (67) are easily obtained as follows:

$$\left.\begin{aligned} u_{1U}'' &= \frac{if}{h'^2} A_U'' e^{r''(y-H)+i(pt-fx)}, \\ v_{1U}'' &= -\frac{r''}{h'^2} A_U'' e^{r''(y-H)+i(pt-fx)}, \end{aligned}\right\} \quad \cdots\cdots\cdots\cdots (69)$$

$$\left.\begin{aligned} \widehat{xx}_{1U}'' &= \left(\lambda' + 2\mu' \frac{f^2}{h'^2}\right) A_U'' e^{r''(y-H)+i(pt-fx)}, \\ \widehat{yy}_{1U}'' &= \left(\lambda' - 2\mu' \frac{r''^2}{h'^2}\right) A_U'' e^{r''(y-H)+i(pt-fx)}, \\ \widehat{xy}_{1U}'' &= \frac{2i\mu' f r''}{h'^2} A_U'' e^{r''(y-H)+i(pt-fx)}, \end{aligned}\right\} \quad \cdots\cdots\cdots\cdots (70)$$

$$\left.\begin{aligned} u_{2U}'' &= \frac{s''}{k'^2} B_U'' e^{s''(y-H)+i(pt-fx)}, \\ v_{2U}'' &= \frac{if}{k'^2} B_U'' e^{s''(y-H)+i(pt-fx)}, \end{aligned}\right\} \quad \cdots\cdots\cdots\cdots (71)$$

$$\left.\begin{aligned} \widehat{xx}_{2U}'' &= -\frac{2i\mu' f s''}{k'^2} B_U'' e^{s''(y-H)+i(pt-fx)}, \\ \widehat{yy}_{2U}'' &= \frac{2i\mu' f s''}{k'^2} B_U'' e^{s''(y-H)+i(pt-fx)}, \\ \widehat{xy}_{2U}'' &= \frac{\mu'}{k'^2}(f^2 + s''^2) B_U'' e^{s''(y-H)+i(pt-fx)}. \end{aligned}\right\} \quad \cdots\cdots\cdots\cdots (72)$$

Making the shear stress on the surface $y=H$ due to (66) and (67) be nil, we obtained the following relations between A_U'' and B_U'' such that

$$B_U'' = -\frac{2if r'' k'^2}{h'^2(f^2 + s''^2)} A_U''. \quad \cdots\cdots\cdots\cdots (73)$$

Then (69) and (71) give us

$$\left.\begin{aligned} u_{1U}'' &= \frac{if}{h'^2} A_U'' e^{r''(y-H)+i(pt-fx)}, \\ v_{1U}'' &= -\frac{r''}{h'^2} A_U'' e^{r''(y-H)+i(pt-fx)}, \end{aligned}\right\} \quad \ldots\ldots\ldots\ldots\ldots\ldots (69)'$$

$$\left.\begin{aligned} u_{2U}'' &= -\frac{2ifr''s''}{h'^2(f^2+s''^2)} A_U'' e^{s''(y-H)+i(pt-fx)}, \\ v_{2U}'' &= \frac{2f^2r''}{h'^2(f^2+s''^2)} A_U'' e^{s''(y-H)+i(pt-fx)}. \end{aligned}\right\} \quad \ldots\ldots\ldots (71)'$$

The normal stress $\widehat{yy}_U''$ due to (69) and (71) are expressed by

$$\widehat{yy}_U'' = \frac{\mu'}{h'^2(f^2+s''^2)} \{(f^2+s''^2)(k'^2-2h'^2-2r''^2) e^{r''(y-H)} + 4f^2r''s'' e^{s''(y-H)}\} A_U'' e^{i(pt-fx)}. \quad \ldots\ldots (74)$$

Now, using these expressions (69)′, (71)′ and (74), we obtain the following conditions at the surface $y=H$ in order to satisfy completely the free surface conditions at $y=H$ when the waves expressed by (51) are incident to the surface $y=H$:

When $y=H$,

$$\widehat{yy}_{U_{y=H}} \text{expressed by (74)} + \widehat{yy}_{U_{y=H}} \text{expressed by (65)} = 0, \quad \ldots\ldots (75)$$

which gives us the following values of A_U'' after some reductions:

$$A_U'' = -\frac{2\left(\frac{k'^2}{f^2}-2\right)^2}{\left\{\left(\frac{k'^2}{f^2}-2\right)^2 - 4\frac{r''s''}{f^2}\right\}} A_U e^{-ir'H}. \quad \ldots\ldots\ldots\ldots (76)$$

Substituting from (76) in (69)′ and (71)′, we get

$$\left.\begin{aligned} u_{1U}'' &= -\frac{2if\left(\frac{k'^2}{f^2}-2\right)^2}{h'^2\left\{\left(\frac{k'^2}{f^2}-2\right)^2 - 4\frac{r''s''}{f^2}\right\}} A_U e^{r''(y-H)+i(pt-fx-r'H)}, \\ v_{1U}'' &= \frac{2r''\left(\frac{k'^2}{f^2}-2\right)^2}{h'^2\left\{\left(\frac{k'^2}{f^2}-2\right)^2 - 4\frac{r''s''}{f^2}\right\}} A_U e^{r''(y-H)+i(pt-fx-r'H)}, \end{aligned}\right\} \quad \ldots\ldots (77)$$

$$\left.\begin{aligned} u_{2U}'' &= -\frac{4ir''s''\left(\frac{k'^2}{f^2}-2\right)}{fh'^2\left\{\left(\frac{k'^2}{f^2}-2\right)^2-4\frac{r''s''}{f^2}\right\}}A_U e^{s''(y-H)+i(pt-fx-r'H)}, \\ v_{2U}'' &= \frac{4r''\left(\frac{k'^2}{f^2}-2\right)}{h'^2\left\{\left(\frac{k'^2}{f^2}-2\right)^2-4\frac{r''s''}{f^2}\right\}}A_U e^{s''(y-H)+i(pt-fx-r'H)}. \end{aligned}\right\} \quad \ldots\ldots(78)$$

For the convenience sake, we summarise the results obtained in this section as follows:

When the transmitted wave of dilatational type expressed by A_U'*51) is primarily incident to the free surface* $y=H$*, the following waves are reflected at the surface* $y=H$*:*

$$\left.\begin{aligned} u_{1U}' &= \frac{if}{h'^2}A_U e^{i(pt-fx+r'y-2r'H)}, \\ v_{1U}' &= -\frac{ir'}{h'^2}A_U e^{i(pt-fx+r'y-2r'H)}, \end{aligned}\right\} \text{dilatational type.} \quad \ldots\ldots(63)$$

$$\left.\begin{aligned} u_{1U}'' &= -\frac{2if\left(\frac{k'^2}{f^2}-2\right)^2}{h'^2\left\{\left(\frac{k'^2}{f^2}-2\right)^2-4\frac{r''s''}{f^2}\right\}}A_U e^{r''(y-H)+i(pt-fx-r'H)}, \\ v_{1U}'' &= \frac{2r''\left(\frac{k'^2}{f^2}-2\right)^2}{h'^2\left\{\left(\frac{k'^2}{f^2}-2\right)^2-4\frac{r''s''}{f^2}\right\}}A_U e^{r''(y-H)+i(pt-fx-r'H)}, \end{aligned}\right\} \text{dilatational type.} \quad (77)$$

$$\left.\begin{aligned} u_{2U}'' &= -\frac{4ir''s''\left(\frac{k'^2}{f^2}-2\right)}{fh'^2\left\{\left(\frac{k'^2}{f^2}-2\right)^2-\frac{4r''s''}{f^2}\right\}}A_U e^{s''(y-H)+i(pt-fx-r'H)}, \\ v_{2U}'' &= \frac{4r''\left(\frac{k'^2}{f^2}-2\right)}{h'^2\left\{\left(\frac{k'^2}{f^2}-2\right)^2-\frac{4r''s''}{f^2}\right\}}A_U e^{s''(y-H)+i(pt-fx-r'H)}. \end{aligned}\right\} \text{distortional type.} \quad (78)$$

b) Transmitted Wave is Distortional.

7. Let the transmitted wave, which is generated by a primary wave of any type when it is incident to the boundary surface $y=0$, be a distor-

tional one $2\varpi_U$ which is expressed by

$$2\varpi_U = B_U e^{i(pt-fx-s'y)}. \quad \ldots\ldots\ldots\ldots\ldots\ldots (79)$$

Then the displacement u_{2U}, v_{2U} and the stress $\widehat{xx}_{2U}$, $\widehat{yy}_{2U}$, $\widehat{xy}_{2U}$ corresponding to (79) are written by

$$\left.\begin{aligned} u_{2U} &= -\frac{is'}{k'^2} B_U e^{i(pt-fx-s'y)}, \\ v_{2U} &= \frac{if}{k'^2} B_U e^{i(pt-fx-s'y)}, \end{aligned}\right\} \quad \ldots\ldots\ldots\ldots\ldots\ldots (80)$$

$$\left.\begin{aligned} \widehat{xx}_{2U} &= -\frac{2s'f\mu'}{k'^2} B_U e^{i(pt-fx-s'y)}, \\ \widehat{yy}_{2U} &= \frac{2s'f\mu'}{k'^2} B_U e^{i(pt-fx-s'y)}, \\ \widehat{xy}_{2U} &= \frac{(f^2-s'^2)\mu'}{k'^2} B_U e^{i(pt-fx-s'y)}, \end{aligned}\right\} \quad \ldots\ldots\ldots\ldots\ldots\ldots (81)$$

where B_U is a constant to be determined by the boundary conditions of elasticity at $y=0$ and is a certain function of the emergency angle, the velocity and the period of the primary wave incident to the plane $y=0$.

Using the two waves (54), (55) of reflected type, we shall adjust A_U' and B_U' to make shear stress on the free surface $y=H$ due to the incident wave expressed by (79) be nil and to make a certain normal stress and the tangential stress only existent on this surface.

The boundary conditions at the surface $y=H$ thus confined are written as follows:

When $y=H$,

$$\left.\begin{aligned} \widehat{xy}_{2U} + \widehat{xy}_{1U'} + \widehat{xy}_{2U'} &= 0, \\ \widehat{yy}_{1U'} + \widehat{yy}_{2U'} &= \widehat{yy}_{2U}, \end{aligned}\right\} \quad \ldots\ldots\ldots\ldots\ldots\ldots (82)$$

where $\widehat{yy}_{1U'}$, $\widehat{xy}_{1U'}$ and $\widehat{yy}_{2U'}$, $\widehat{xy}_{2U'}$ are already shewn by (57) and (59).

These conditions give us the two equations to determine A_U' and B_U' such that

$$\left.\begin{aligned} \frac{2fr'}{h'^2} A_U' e^{ir'H} - \frac{(f^2-s'^2)}{k'^2} B_U' e^{is'H} &= \frac{(f^2-s'^2)}{k'^2} B_U e^{-is'H}, \\ \frac{1}{h'^2}(s'^2-f^2) A_U' e^{ir'H} - \frac{2s'f}{k'^2} B_U' e^{is'H} &= \frac{2s'f}{k'^2} B_U e^{-is'H}. \end{aligned}\right\} \quad \ldots (83)$$

Solving (83), we obtain

$$\left.\begin{aligned} A'_U &= 0, \\ B_U' &= -B_U e^{-2is'H}. \end{aligned}\right\} \quad \cdots\cdots\cdots\cdots\cdots\cdots (84)$$

Substituting from (84) in (56) and (58), we get

$$\left.\begin{aligned} u_{1U}' &= 0, \\ v_{1U}' &= 0, \end{aligned}\right\} \quad \cdots\cdots\cdots\cdots\cdots\cdots\cdots\cdots (85)$$

$$\left.\begin{aligned} u_{2U}' &= -\frac{is'}{k'^2} B_U e^{i(pt-fx+s'y-2s'H)}, \\ v_{2U}' &= -\frac{if}{k'^2} B_U e^{i(pt-fx+s'y-2s'H)}. \end{aligned}\right\} \quad \cdots\cdots\cdots\cdots\cdots\cdots (86)$$

To make shear stress at $y=H$ due to the incident wave (79) be nil, it is sufficient to use the reflected distortional wave (86) only, and there is no necessity to take the dilatational wave (85). The normal stress in the medium II due to (80) and (86) is expressed by

$$\widehat{yy}_U = \frac{2\mu' s' f}{k'^2} B_U \{e^{-is'y} + e^{i(s'y-2s'H)}\} e^{i(pt-fx)}. \quad \cdots\cdots\cdots (87)$$

Now we have obtained in the preceding section the two waves expressed by (69) and (71) which apparently predominate on the surface $y=H$ and make shear stress at $y=H$ be nil and the normal stress be equal to the one expressed by (74). Using these two waves, we obtain the following condition at the surface $y=H$ in order to satisfy completely the free surface conditions at $y=H$ when the wave expressed by (79) are incident to the surface $y=H$:

When $y=H$,

$$\widehat{yy}_U''{}_{y=H} \text{expressed by (74)} + \widehat{yy}_{U_{y=H}} \text{expressed by (87)} = 0. \quad \cdots\cdots (88)$$

By this condition we obtain the following values of A_U'' after some reductions:

$$A_U'' = -\frac{4s'h'^2\left(\frac{k'^2}{f^2}-2\right)}{fk'^2\left\{\left(\frac{k'^2}{f^2}-2\right)^2 - \frac{4s''r''}{f^2}\right\}} B_U e^{-is'H}. \quad \cdots\cdots\cdots (89)$$

Substituting from (89) in (69)′ and (71)′, we get

$$\left.\begin{aligned} u_{1U}'' &= -\frac{4is'\left(\frac{k'^2}{f^2}-2\right)}{k'^2\left\{\left(\frac{k'^2}{f^2}-2\right)^2 - \frac{4r''s''}{f^2}\right\}} B_U e^{r''(y-H)+i(pt-fx-s'H)}, \\ &\qquad\qquad \cdots\cdots (90) \end{aligned}\right.$$

$$\left.\begin{aligned} v_{1U}'' &= \frac{4r''s'\left(\frac{k'^2}{f^2}-2\right)}{fk'^2\left\{\left(\frac{k'^2}{f^2}-2\right)^2-\frac{4r''s''}{f^2}\right\}}B_U e^{r''(y-H)+i(pt-fx-s'H)}, \\ u_{2U}'' &= -\frac{8ir''s's''}{f^2k'^2\left\{\left(\frac{k'^2}{f^2}-2\right)^2-\frac{4r''s''}{f^2}\right\}}B_U e^{s''(y-H)+i(pt-fx-s'H)}, \\ v_{2U}'' &= \frac{8r''s'}{fk'^2\left\{\left(\frac{k'^2}{f^2}-2\right)^2-\frac{4r''s''}{f^2}\right\}}B_U e^{s''(y-H)+i(pt-fx-s'H)}. \end{aligned}\right\} \quad \ldots\ldots (91)$$

The results obtained in this section are summarised as follows:

When the transmitted distortional wave expressed by (79) *is primarily incident to the free surface* $y=H$, *the following waves are reflected at* $y=H$.

$$\left.\begin{aligned} u_{2U}' &= -\frac{is'}{k'^2}B_U e^{i(pt-fx+s'y-2s'H)}, \\ v_{2U}' &= = -\frac{if}{k'^2}B_U e^{i(pt-fx+s'y-2s'H)}, \end{aligned}\right\} \text{distortional type} \quad \ldots\ldots (86)$$

$$\left.\begin{aligned} u_{1U}'' &= -\frac{4is'\left(\frac{k'^2}{f^2}-2\right)}{k'^2\left\{\left(\frac{k'^2}{f^2}-2\right)^2-\frac{4r''s''}{f^2}\right\}}B_U e^{r''(y-H)+i(pt-fx-s'H)}, \\ v_{1U}'' &= \frac{4r''s'\left(\frac{k'^2}{f^2}-2\right)}{fk'^2\left\{\left(\frac{k'^2}{f^2}-2\right)^2-\frac{4r''s''}{f^2}\right\}}B_U e^{r''(y-H)+i(pt-fx-s'H)}, \end{aligned}\right\} \text{dilatational type} \quad \ldots (90)$$

$$\left.\begin{aligned} u_{2U}'' &= -\frac{8ir''s's''}{f^2k'^2\left\{\left(\frac{k'^2}{f^2}-2\right)^2-\frac{4r''s''}{f^2}\right\}}B_U e^{s''(y-H)+i(pt-fx-s'H)}, \\ v_{2U}'' &= \frac{8r''s'}{fk'^2\left\{\left(\frac{k'^2}{f^2}-2\right)^2-\frac{4r''s''}{f^2}\right\}}B_U e^{s''(y-H)+i(pt-fx-s'H)}. \end{aligned}\right\} \text{distortional type} \quad (91)$$

A. Initial Motion of the Free Surface of a Stratified Solid When a Dilatational Wave is Incident to the Lower Boundary.

8. Using the results obtained in Section 6 and 7 as the preliminary calculations, we shall study the problem of reflection of waves at the free

surface of the upper layer which resides on a semi-infinite solid. Of course, at the boundary surface the two elastic solids slide upon each other without any friction. (Fig. 7.)

Using the results of Section 3 of Part I, and those of Section 6 and 7, we obtain the following results after some reductions.

When the dilatational wave expressed by the following form is primarily incident to the boundary surface $y=0$;

$$\Delta=\mathfrak{A}e^{i(pt-fx-ry)}, \quad \cdots\cdots\cdots\cdots\cdots\cdots (92)$$

of which the displacements are

$$\left.\begin{aligned} u_1&=\frac{if}{h^2}\mathfrak{A}e^{i(pt-fx-ry)},\\ v_1&=\frac{ir}{h^2}\mathfrak{A}e^{i(pt-fx-ry)},\end{aligned}\right\} \quad \cdots\cdots\cdots\cdots\cdots\cdots (93)$$

the transmitted[5] waves are expressed by

$$\Delta''=\frac{2rh'^2k^2\left(\frac{k'^2}{f^2}-2\right)\left(\frac{k^2}{f^2}-2\right)}{h^2\left[\frac{\mu'}{\mu}rk^2\left\{\left(\frac{k'^2}{f^2}-2\right)^2+\frac{4r's'}{f^2}\right\}+r'k'^2\left\{\left(\frac{k^2}{f^2}-2\right)^2+\frac{4rs}{f^2}\right\}\right]}\mathfrak{A}e^{i(pt-fx-r'y)}, \quad \cdots (94)$$

$$2\varpi_z''=\frac{4rr'k'^2k^2\left(\frac{k^2}{f^2}-2\right)}{h^2f\left[\frac{\mu'}{\mu}rk^2\left\{\left(\frac{k'^2}{f^2}-2\right)^2+\frac{4r's'}{f^2}\right\}+r'k'^2\left\{\left(\frac{k^2}{f^2}-2\right)^2+\frac{4rs}{f^2}\right\}\right]}\mathfrak{A}e^{i(pt-fx-s'y)}. \quad (95)$$

The displacement corresponding to Δ'' expressed by (94) are written in the forms of

$$\left.\begin{aligned} u_{1U}&=\frac{2ifrk^2\left(\frac{k'^2}{f^2}-2\right)\left(\frac{k^2}{f^2}-2\right)}{h^2\left[\frac{\mu'}{\mu}rk^2\left\{\left(\frac{k'^2}{f^2}-2\right)^2+\frac{4r's'}{f^2}\right\}+r'k'^2\left\{\left(\frac{k^2}{f^2}-2\right)^2+\frac{4rs}{f^2}\right\}\right]}\mathfrak{A}e^{i(pt-fx-r'y)},\\ v_{1U}&=\frac{2irr'k^2\left(\frac{k'^2}{f^2}-2\right)\left(\frac{k^2}{f^2}-2\right)}{h^2\left[\frac{\mu'}{\mu}rk^2\left\{\left(\frac{k'^2}{f^2}-2\right)^2+\frac{4r's'}{f^2}\right\}+r'k'^2\left\{\left(\frac{k^2}{f^2}-2\right)^2+\frac{4rs}{f^2}\right\}\right]}\mathfrak{A}e^{i(pt-fx-r'y)}.\end{aligned}\right\} \quad (96)$$

Therefore we obtain the following waves reflected at $y=H$ when the wave (93) is incident to this plane:

5) We omit the expressions of reflected wave of which the details are discussed in Section 3 minutely.

$$\left.\begin{aligned} u_{1U}' &= \frac{2ifrk^2\left(\frac{k'^2}{f^2}-2\right)\left(\frac{k^2}{f^2}-2\right)}{h^2\left[\frac{\mu'}{\mu}rk^2\left\{\left(\frac{k'^2}{f^2}-2\right)^2+\frac{4r's'}{f^2}\right\}+r'k'^2\left\{\left(\frac{k^2}{f^2}-2\right)^2+\frac{4rs}{f^2}\right\}\right]}\mathfrak{A}e^{i(pt-fx+r'y-2r'H)}, \\ v_{1U}' &= -\frac{2irr'k^2\left(\frac{k'^2}{f^2}-2\right)\left(\frac{k^2}{f^2}-2\right)}{h^2\left[\frac{\mu'}{\mu}rk^2\left\{\left(\frac{k'^2}{f^2}-2\right)^2+\frac{4r's'}{f^2}\right\}+r'k'^2\left\{\left(\frac{k^2}{f^2}-2\right)^2+\frac{4rs}{f^2}\right\}\right]}\mathfrak{A}e^{i(pt-fx+r'y-2r'H)}, \end{aligned}\right\} \quad \ldots\ldots\ldots\ldots\ldots(97)$$

$$\left.\begin{aligned} u_{1U}'' &= -\frac{4ifrk^2\left(\frac{k'^2}{f^2}-2\right)^3\left(\frac{k^2}{f^2}-2\right)}{h^2\left\{\left(\frac{k'^2}{f^2}-2\right)^2-\frac{4r''s''}{f^2}\right\}\left[\frac{\mu'}{\mu}rk^2\left\{\left(\frac{k'^2}{f^2}-2\right)^2+\frac{4r's'}{f^2}\right\}+r'k'^2\left\{\left(\frac{k^2}{f^2}-2\right)^2+\frac{4rs}{f^2}\right\}\right]} \\ &\qquad \times\mathfrak{A}e^{r''(y-H)+i(pt-fx-r'H)}, \\ v_{1U}'' &= \frac{4rr''k^2\left(\frac{k'^2}{f^2}-2\right)^3\left(\frac{k^2}{f^2}-2\right)}{h^2\left\{\left(\frac{k'^2}{f^2}-2\right)^2-4\frac{r''s''}{f^2}\right\}\left[\frac{\mu'}{\mu}rk^2\left\{\left(\frac{k'^2}{f^2}-2\right)^2+\frac{4r's'}{f^2}\right\}+r'k'^2\left\{\left(\frac{k^2}{f^2}-2\right)^2+\frac{4rs}{f^2}\right\}\right]} \\ &\qquad \times\mathfrak{A}e^{r''(y-H)+i(pt-fx-r'H)}, \end{aligned}\right\} \quad \ldots\ldots\ldots\ldots\ldots(98)$$

$$\left.\begin{aligned} u_{2U}'' &= -\frac{8irr''s''k^2\left(\frac{k'^2}{f^2}-2\right)^2\left(\frac{k^2}{f^2}-2\right)}{fh^2\left\{\left(\frac{k'^2}{f^2}-2\right)^2-\frac{4r''s''}{f^2}\right\}\left[\frac{\mu'}{\mu}rk^2\left\{\left(\frac{k'^2}{f^2}-2\right)^2+\frac{4r's'}{f^2}\right\}+r'k'^2\left\{\left(\frac{k^2}{f^2}-2\right)^2+\frac{4rs}{f^2}\right\}\right]} \\ &\qquad \times\mathfrak{A}e^{s''(y-H)+i(pt-fx-r'H)}, \\ v_{2U}'' &= \frac{8rr''k^2\left(\frac{k'^2}{f^2}-2\right)^2\left(\frac{k^2}{f^2}-2\right)}{h^2\left\{\left(\frac{k'^2}{f^2}-2\right)^2-\frac{4r''s''}{f^2}\right\}\left[\frac{\mu'}{\mu}rk^2\left\{\left(\frac{k'^2}{f^2}-2\right)^2+\frac{4r's'}{f^2}\right\}+r'k'^2\left\{\left(\frac{k^2}{f^2}-2\right)^2+\frac{4rs}{f^2}\right\}\right]} \\ &\qquad \times\mathfrak{A}e^{s''(y-H)+i(pt-fx-r'H)}. \end{aligned}\right\} \quad \ldots\ldots\ldots\ldots\ldots(99)$$

The displacements corresponding to $2\varpi_z''$ expressed by (95) are written by

$$\left.\begin{aligned} u_{2U} &= -\frac{4irr's'k^2\left(\frac{k^2}{f^2}-2\right)}{h^2f\left[\frac{\mu'}{\mu}rk^2\left\{\left(\frac{k'^2}{f^2}-2\right)^2+\frac{4r's'}{f^2}\right\}+r'k'^2\left\{\left(\frac{k^2}{f^2}-2\right)^2+\frac{4rs}{f^2}\right\}\right]}\mathfrak{A}e^{i(pt-fx-s'y)},\\ v_{2U} &= \frac{4irr'k^2\left(\frac{k^2}{f^2}-2\right)}{h^2\left[\frac{\mu'}{\mu}rk^2\left\{\left(\frac{k'^2}{f^2}-2\right)^2+\frac{4r's'}{f^2}\right\}+r'k'^2\left\{\left(\frac{k^2}{f^2}-2\right)^2+\frac{4rs}{f^2}\right\}\right]}\mathfrak{A}e^{i(pt-fx-s'y)}, \end{aligned}\right\} \quad \cdots\cdots\cdots\cdots\cdots (100)$$

and therefore

$$\left.\begin{aligned} u_{2U}' &= -\frac{4irr's'k^2\left(\frac{k^2}{f^2}-2\right)}{h^2f\left[\frac{\mu'}{\mu}rk^2\left\{\left(\frac{k'^2}{f^2}-2\right)^2+\frac{4r's'}{f^2}\right\}+r'k'^2\left\{\left(\frac{k^2}{f^2}-2\right)^2+\frac{4rs}{f^2}\right\}\right]}\mathfrak{A}e^{i(pt-fx+s'y-2s'H)},\\ v_{2U}' &= -\frac{4irr'k^2\left(\frac{k^2}{f^2}-2\right)}{h^2\left[\frac{\mu'}{\mu}rk^2\left\{\left(\frac{k'^2}{f^2}-2\right)^2+\frac{4r's'}{f^2}\right\}+r'k'^2\left\{\left(\frac{k^2}{f^2}-2\right)^2+\frac{4rs}{f^2}\right\}\right]}\mathfrak{A}e^{i(pt-fx+s'y-2s'H)}, \end{aligned}\right\} \quad \cdots\cdots\cdots\cdots\cdots (101)$$

$$\left.\begin{aligned} u_{1U}'' &= -\frac{16irr's'k^2\left(\frac{k'^2}{f^2}-2\right)\left(\frac{k^2}{f^2}-2\right)}{h^2f\left\{\left(\frac{k'^2}{f^2}-2\right)^2-\frac{4r''s''}{f^2}\right\}\left[\frac{\mu'}{\mu}rk^2\left\{\left(\frac{k'^2}{f^2}-2\right)^2+\frac{4r's'}{f^2}\right\}+r'k'^2\left\{\left(\frac{k^2}{f^2}-2\right)^2+\frac{4rs}{f^2}\right\}\right]}\\ &\qquad\times\mathfrak{A}e^{r''(y-H)+i(pt-fx-s'H)},\\ v_{1U}'' &= \frac{16rr'r''s'k^2\left(\frac{k'^2}{f^2}-2\right)\left(\frac{k^2}{f^2}-2\right)}{h^2f^2\left\{\left(\frac{k'^2}{f^2}-2\right)^2-\frac{4r''s''}{f^2}\right\}\left[\frac{\mu'}{\mu}rk^2\left\{\left(\frac{k'^2}{f^2}-2\right)^2+\frac{4r's'}{f^2}\right\}+r'k'^2\left\{\left(\frac{k^2}{f^2}-2\right)^2+\frac{4rs}{f^2}\right\}\right]}\\ &\qquad\times\mathfrak{A}e^{r''(y-H)+i(pt-fx-s'H)}, \end{aligned}\right\} \quad \cdots\cdots\cdots\cdots\cdots (102)$$

$$u_{2U}'' = -\frac{32irr'r''s's''k^2\left(\frac{k^2}{f^2}-2\right)}{h^2f^3\left\{\left(\frac{k'^2}{f^2}-2\right)^2-\frac{4r''s''}{f^2}\right\}\left[\frac{\mu'}{\mu}rk^2\left\{\left(\frac{k'^2}{f^2}-2\right)^2+\frac{4r's'}{f^2}\right\}+r'k'^2\left\{\left(\frac{k^2}{f}-2\right)^2+\frac{4rs}{f^2}\right\}\right]}\times\mathfrak{A}e^{s''(y-H)+i(pt-fx-s'H)},$$

$$v_{2v}''=\frac{32rr'r''s'k^2\left(\frac{k^2}{f^2}-2\right)}{h^2f^2\left\{\left(\frac{k'^2}{f^2}-2\right)^2-\frac{4r''s''}{f^2}\right\}\left[\frac{\mu'}{\mu}rk^2\left\{\left(\frac{k'^2}{f^2}-2\right)^2+\frac{4r's'}{f^2}\right\}+r'k'^2\left\{\left(\frac{k^2}{f^2}-2\right)^2+\frac{4rs}{f^2}\right\}\right]}\times\mathfrak{R}e^{s''(y-H)+i(pt-fx-s'H)}.\qquad\text{.....(103)}$$

When the transmitted dilatational wave (94) is incident to the surface $y=H$ primarily, the waves such as dilatational and distortional ones expressed by (97), (98) and (99) are generated at and reflected at the free surface $y=H$. When the transmitted rotational wave expressed by (95) is incident to the free surface $y=H$ secondarily, the waves of distortional and dilatational types expressed by (101), (103) and (102) are generated at and reflected at the free surface $y=H$. In this case, there is no wave predominating on the free surface which is ordinarily generated at the free surface by the incidence of distortional wave.

When $\rho=\rho'$ and the Poisson's ratios of both touched solids are respectively $\frac{1}{4}$, the waves generated in the second medium due to the transmitted waves of (94) and (95) are expressed by the following formulae:

$$\left.\begin{aligned}u_{1v}&=\frac{2i\left[\frac{3\mu}{\mu'}\left\{\left(\frac{r}{f}\right)^2+1\right\}-2\right]\left\{3\left(\frac{r}{f}\right)^2+1\right\}}{f\left\{\left(\frac{r}{f}\right)^2+1\right\}\Phi}\mathfrak{R}e^{i(pt-fx-r'y)},\\ v_{1v}&=\frac{2i\left[\frac{\mu}{\mu'}\left\{\left(\frac{r}{f}\right)^2+1\right\}-1\right]^{\frac{1}{2}}\left[\frac{3\mu}{\mu'}\left\{\left(\frac{r}{f}\right)^2+1\right\}-2\right]\left\{3\left(\frac{r}{f}\right)^2+1\right\}}{f\left\{\left(\frac{r}{f}\right)^2+1\right\}\Phi}\mathfrak{R}e^{i(pt-fx-r'y)},\end{aligned}\right\}\qquad\text{.....(104)}$$

$$\left.\begin{aligned}u_{1v}'&=\frac{2i\left[\frac{3\mu}{\mu'}\left\{\left(\frac{r}{f}\right)^2+1\right\}-2\right]\left\{3\left(\frac{r}{f}\right)^2+1\right\}}{f\left\{\left(\frac{r}{f}\right)^2+1\right\}\Phi}\mathfrak{R}e^{i(pt-fx+r'y-2r'H)},\\ v_{1v}'&=-\frac{2i\left[\frac{\mu}{\mu'}\left\{\left(\frac{r}{f}\right)^2+1\right\}-1\right]^{\frac{1}{2}}\left[\frac{3\mu}{\mu'}\left\{\left(\frac{r}{f}\right)^2+1\right\}-2\right]\left\{3\left(\frac{r}{f}\right)^2+1\right\}}{f\left\{\left(\frac{r}{f}\right)^2+1\right\}\Phi}\\ &\qquad\times\mathfrak{R}e^{i(pt-fx+r'y-2r'H)},\end{aligned}\right\}\qquad(105)$$

$$v_{1v}''=\frac{16i\left[\frac{\mu}{\mu'}\left\{\left(\frac{r}{f}\right)^2+1\right\}-1\right]\left[\frac{3\mu}{\mu'}\left\{\left(\frac{r}{f}\right)^2+1\right\}-1\right]^{\frac{1}{2}}}{f\left\{\left(\frac{r}{f}\right)^2+1\right\}\left[\left\{\frac{3\mu}{\mu'}\left(\left(\frac{r}{f}\right)^2+1\right)-2\right\}^2\right.}$$

$$\left.\frac{\left\{3\left(\frac{r}{f}\right)^2+1\right\}\left[\frac{3\mu}{\mu'}\left\{\left(\frac{r}{f}\right)^2+1\right\}-2\right]}{+4\left\{\frac{\mu}{\mu'}\left(\left(\frac{r}{f}\right)^2+1\right)-1\right\}^{\frac{1}{2}}\left\{\frac{3\mu}{\mu'}\left(\left(\frac{r}{f}\right)^2+1\right)-1\right\}^{\frac{1}{2}}\right]\Phi}\mathfrak{Re}^{r''(y-H)+i(pt-fx-s'H)},\right\}$$

.....(111)

$$u_{2v}''=\frac{32i\left[\frac{\mu}{\mu'}\left\{\left(\frac{r}{f}\right)^2+1\right\}-1\right]}{f\left\{\left(\frac{r}{f}\right)^2+1\right\}\left[\left\{\frac{3\mu}{\mu'}\left(\left(\frac{r}{f}\right)^2+1\right)-2\right\}^2\right.}$$

$$\left.\frac{\left[\frac{3\mu}{\mu'}\left\{\left(\frac{r}{f}\right)^2+1\right\}-1\right]\left\{3\left(\frac{r}{f}\right)^2+1\right\}}{+4\left\{\frac{\mu}{\mu'}\left(\left(\frac{r}{f}\right)^2+1\right)-1\right\}^{\frac{1}{2}}\left\{\frac{3\mu}{\mu'}\left(\left(\frac{r}{f}\right)^2+1\right)-1\right\}^{\frac{1}{2}}\right]\Phi}\mathfrak{Re}^{s''(y-H)+i(pt-fx-s'H)},\right\}$$

$$v_{2v}''=\frac{32i\left[\frac{\mu}{\mu'}\left\{\left(\frac{r}{f}\right)^2+1\right\}-1\right]}{f\left\{\left(\frac{r}{f}\right)^2+1\right\}\left[\left\{\frac{3\mu}{\mu'}\left(\left(\frac{r}{f}\right)^2+1\right)-2\right\}^2\right.}$$

$$\left.\frac{\left[\frac{3\mu}{\mu'}\left\{\left(\frac{r}{f}\right)^2+1\right\}-1\right]^{\frac{1}{2}}\left\{3\left(\frac{r}{f}\right)^2+1\right\}}{+4\left\{\frac{\mu}{\mu'}\left(\left(\frac{r}{f}\right)^2+1\right)-1\right\}^{\frac{1}{2}}\left\{\frac{3\mu}{\mu'}\left(\left(\frac{r}{f}\right)^2+1\right)-1\right\}^{\frac{1}{2}}\right]\Phi}\mathfrak{Re}^{s''(y-H)+i(pt-fx-s'H)}.\right\}$$

.....(112)

When $\frac{\mu'}{\mu}=1$, expressions (104), (105), (106), (107) and (109), (110), (111), (112) are written by

$$u_{1v}=\frac{i\left\{3\left(\frac{r}{f}\right)^2+1\right\}^2}{f\left\{\left(\frac{r}{f}\right)^2+1\right\}\left[\left\{3\left(\frac{r}{f}\right)^2+1\right\}^2+4\left(\frac{r}{f}\right)\left\{3\left(\frac{r}{f}\right)^2+2\right\}^{\frac{1}{2}}\right]}\mathfrak{Re}^{i(pt-fx-ry)},\right\}$$

$$\left.\begin{aligned} v_{1U} &= \frac{i\left(\frac{r}{f}\right)\left\{3\left(\frac{r}{f}\right)^2+1\right\}^2}{f\left\{\left(\frac{r}{f}\right)^2+1\right\}\left[\left\{3\left(\frac{r}{f}\right)^2+1\right\}^2+4\left(\frac{r}{f}\right)\left\{3\left(\frac{r}{f}\right)^2+2\right\}^{\frac{1}{2}}\right]}\mathfrak{R}e^{i(pt-fx-ry)}, \\ u_{1U}' &= \frac{i\left\{3\left(\frac{r}{f}\right)^2+1\right\}^2}{f\left\{\left(\frac{r}{f}\right)^2+1\right\}\left[\left\{3\left(\frac{r}{f}\right)^2+1\right\}^2+4\left(\frac{r}{f}\right)\left\{3\left(\frac{r}{f}\right)^2+2\right\}^{\frac{1}{2}}\right]}\mathfrak{R}e^{i(pt-fx+ry-2rH)}, \\ v_{1U}' &= -\frac{i\left(\frac{r}{f}\right)\left\{3\left(\frac{r}{f}\right)^2+1\right\}^2}{f\left\{\left(\frac{r}{f}\right)^2+1\right\}\left[\left\{3\left(\frac{r}{f}\right)^2+1\right\}^2+4\left(\frac{r}{f}\right)\left\{3\left(\frac{r}{f}\right)^2+2\right\}^{\frac{1}{2}}\right]}\mathfrak{R}e^{i(pt-fx+ry-2rH)}, \end{aligned}\right\} \quad (113)$$

$$\left.\begin{aligned} u_{1U}'' &= -\frac{2i\left\{3\left(\frac{r}{f}\right)^2+1\right\}^4}{f\left\{\left(\frac{r}{f}\right)^2+1\right\}\left[\left\{3\left(\frac{r}{f}\right)^2+1\right\}^2+4\left(\frac{r}{f}\right)\left\{3\left(\frac{r}{f}\right)^2+2\right\}^{\frac{1}{2}}\right]^2}\mathfrak{R}e^{i(pt-fx+ry-2rH)}, \\ v_{1U}'' &= \frac{2i\left(\frac{r}{f}\right)\left\{3\left(\frac{r}{f}\right)^2+1\right\}^4}{f\left\{\left(\frac{r}{f}\right)^2+1\right\}\left[\left\{3\left(\frac{r}{f}\right)^2+1\right\}^2+4\left(\frac{r}{f}\right)\left\{3\left(\frac{r}{f}\right)^2+2\right\}^{\frac{1}{2}}\right]^2}\mathfrak{R}e^{i(pt-fx+ry-2rH)}, \end{aligned}\right\} \quad \ldots\ldots\ldots\ldots (114)$$

$$\left.\begin{aligned} u_{2U}'' &= \frac{4i\left(\frac{r}{f}\right)\left\{3\left(\frac{r}{f}\right)^2+2\right\}^{\frac{1}{2}}\left\{3\left(\frac{r}{f}\right)^2+1\right\}^3}{f\left\{\left(\frac{r}{f}\right)^2+1\right\}\left[\left\{3\left(\frac{r}{f}\right)^2+1\right\}^2+4\left(\frac{r}{f}\right)\left\{3\left(\frac{r}{f}\right)^2+2\right\}^{\frac{1}{2}}\right]^2}\mathfrak{R}e^{i(pt-fx+sy-rH-sH)}, \\ v_{2U}'' &= \frac{4i\left(\frac{r}{f}\right)\left\{3\left(\frac{r}{f}\right)^2+1\right\}^3}{f\left\{\left(\frac{r}{f}\right)^2+1\right\}\left[\left\{3\left(\frac{r}{f}\right)^2+1\right\}^2+4\left(\frac{r}{f}\right)\left\{3\left(\frac{r}{f}\right)^2+2\right\}^{\frac{1}{2}}\right]^2}\mathfrak{R}e^{i(pt-fx+sy-rH-sH)}, \end{aligned}\right\} \quad \ldots\ldots\ldots\ldots (115)$$

$$\ldots\ldots\ldots\ldots\ldots\ldots (116)$$

and

$$
\left.
\begin{aligned}
u_{1v}'' &= -\frac{4i\left[\frac{3\mu}{\mu'}\left\{\left(\frac{r}{f}\right)^2+1\right\}-2\right]^3}{f\left\{\left(\frac{r}{f}\right)^2+1\right\}\left[\left\{\frac{3\mu}{\mu'}\left(\left(\frac{r}{f}\right)^2+1\right)-2\right\}^2\right.} \\
&\quad \frac{\left\{3\left(\frac{r}{f}\right)^2+1\right\}}{\left.+4\left\{\frac{\mu}{\mu'}\left(\left(\frac{r}{f}\right)^2+1\right)-1\right\}^{\frac{1}{2}}\left\{\frac{3\mu}{\mu'}\left(\left(\frac{r}{f}\right)^2+1\right)-1\right\}^{\frac{1}{2}}\right]\Phi}\,\mathfrak{A}e^{r''(y-H)+i(pt-fx-r'H)}, \\
v_{1v}'' &= \frac{4i\left[\frac{\mu}{\mu'}\left\{\left(\frac{r}{f}\right)^2+1\right\}-1\right]^{\frac{1}{2}}}{f\left\{\left(\frac{r}{f}\right)^2+1\right\}\left[\left\{\frac{3\mu}{\mu'}\left(\left(\frac{r}{f}\right)^2+1\right)-2\right\}^2\right.} \\
&\quad \frac{\left[\frac{3\mu}{\mu'}\left\{\left(\frac{r}{f}\right)^2+1\right\}-2\right]^3\left\{3\left(\frac{r}{f}\right)^2+1\right\}}{\left.+4\left\{\frac{\mu}{\mu'}\left(\left(\frac{r}{f}\right)^2+1\right)-1\right\}^{\frac{1}{2}}\left\{\frac{3\mu}{\mu'}\left(\left(\frac{r}{f}\right)^2+1\right)-1\right\}^{\frac{1}{2}}\right]\Phi}\,\mathfrak{A}e^{r''(y-H)+i(pt-fx-r'H)},
\end{aligned}
\right\}
\qquad \cdots\cdots\cdots\cdots\cdots\cdots (106)
$$

$$
\left.
\begin{aligned}
u_{2v}'' &= \frac{8i\left[\frac{3\mu}{\mu'}\left\{\left(\frac{r}{f}\right)^2+1\right\}-1\right]^{\frac{1}{2}}\left[\frac{\mu}{\mu'}\left\{\left(\frac{r}{f}\right)^2+1\right\}-1\right]^{\frac{1}{2}}}{f\left\{\left(\frac{r}{f}\right)^2+1\right\}\left[\left\{\frac{3\mu}{\mu'}\left(\left(\frac{r}{f}\right)^2+1\right)-2\right\}^2\right.} \\
&\quad \frac{\left[\frac{3\mu}{\mu'}\left\{\left(\frac{r}{f}\right)^2+1\right\}-2\right]^2\left\{3\left(\frac{r}{f}\right)^2+1\right\}}{\left.+4\left\{\frac{\mu}{\mu'}\left(\left(\frac{r}{f}\right)^2+1\right)-1\right\}^{\frac{1}{2}}\left\{\frac{3\mu}{\mu'}\left(\left(\frac{r}{f}\right)^2+1\right)-1\right\}^{\frac{1}{2}}\right]\Phi}\,\mathfrak{A}e^{s''(y-H)+i(pt-fx-r'H)}, \\
v_{2v}'' &= \frac{8i\left[\frac{\mu}{\mu'}\left\{\left(\frac{r}{f}\right)^2+1\right\}-1\right]^{\frac{1}{2}}}{f\left\{\left(\frac{r}{f}\right)^2+1\right\}\left[\left\{\frac{3\mu}{\mu'}\left(\left(\frac{r}{f}\right)^2+1\right)-2\right\}^2\right.} \\
&\quad \frac{\left[\frac{3\mu}{\mu'}\left\{\left(\frac{r}{f}\right)^2+1\right\}-2\right]^2\left\{3\left(\frac{r}{f}\right)^2+1\right\}}{\left.+4\left\{\frac{\mu}{\mu'}\left(\left(\frac{r}{f}\right)^2+1\right)-1\right\}^{\frac{1}{2}}\left\{\frac{3\mu}{\mu'}\left(\left(\frac{r}{f}\right)^2+1\right)-1\right\}^{\frac{1}{2}}\right]\Phi}\,\mathfrak{A}e^{s''(y-H)+i(pt-fx-r'H)},
\end{aligned}
\right\}
\qquad \cdots\cdots\cdots\cdots\cdots\cdots (107)
$$

where

$$\Phi=\frac{\mu'}{\mu}\left[\left\{\frac{3\mu}{\mu'}\left(\left(\frac{r}{f}\right)^2+1\right)-2\right\}^2+4\left\{\frac{\mu}{\mu'}\left(\left(\frac{r}{f}\right)^2+1\right)-1\right\}^{\frac{1}{2}}\left\{\frac{3\mu}{\mu'}\left(\left(\frac{r}{f}\right)^2+1\right)-1\right\}^{\frac{1}{2}}\right]$$
$$+\frac{f}{r}\frac{\mu}{\mu'}\left\{\frac{\mu}{\mu'}\left(\left(\frac{r}{f}\right)^2+1\right)-1\right\}^{\frac{1}{2}}\left[\left\{3\left(\frac{r}{f}\right)^2+1\right\}^2+\frac{4r}{f}\left\{3\left(\frac{r}{f}\right)^2+2\right\}^{\frac{1}{2}}\right]. \quad (108)$$

And

$$\left.\begin{aligned} u_{2U}&=-\frac{4i\left[\frac{\mu}{\mu'}\left\{\left(\frac{r}{f}\right)^2+1\right\}-1\right]^{\frac{1}{2}}\left[\frac{3\mu}{\mu'}\left\{\left(\frac{r}{f}\right)^2+1\right\}-1\right]^{\frac{1}{2}}\left\{3\left(\frac{r}{f}\right)^2+1\right\}}{f\left\{\left(\frac{r}{f}\right)^2+1\right\}\Phi}\mathfrak{A}e^{i(pt-fx-s'y)},\\ v_{2U}&=\frac{4i\left[\frac{\mu}{\mu'}\left\{\left(\frac{r}{f}\right)^2+1\right\}-1\right]^{\frac{1}{2}}\left\{3\left(\frac{r}{f}\right)^2+1\right\}}{f\left\{\left(\frac{r}{f}\right)^2+1\right\}\Phi}\mathfrak{A}e^{i(pt-fx-s'y)},\end{aligned}\right\} \quad \ldots\ldots\ldots\ldots\ldots\ldots (109)$$

$$\left.\begin{aligned} u_{2U}'&=-\frac{4i\left[\frac{\mu}{\mu'}\left\{\left(\frac{r}{f}\right)^2+1\right\}-1\right]^{\frac{1}{2}}\left[\frac{3\mu}{\mu'}\left\{\left(\frac{r}{f}\right)^2+1\right\}-1\right]^{\frac{1}{2}}\left\{3\left(\frac{r}{f}\right)^2+1\right]}{f\left\{\left(\frac{r}{f}\right)^2+1\right\}\Phi}\\ &\qquad\qquad\times\mathfrak{A}e^{i(pt-fx+s'y-2s'H)},\\ v_{2U}'&=-\frac{4i\left[\frac{\mu}{\mu'}\left\{\left(\frac{r}{f}\right)^2+1\right\}-1\right]^{\frac{1}{2}}\left\{3\left(\frac{r}{f}\right)^2+1\right\}}{f\left\{\left(\frac{r}{f}\right)^2+1\right\}\Phi}\mathfrak{A}e^{i(pt-fx+s'y+2s'H)},\end{aligned}\right\} \quad (110)$$

$$\left.\begin{aligned} u_{1U}''=-\frac{16i\left[\frac{\mu}{\mu'}\left\{\left(\frac{r}{f}\right)^2+1\right\}-1\right]^{\frac{1}{2}}\left[\frac{3\mu}{\mu'}\left\{\left(\frac{r}{f}\right)^2+1\right\}-1\right]^{\frac{1}{2}}}{f\left\{\left(\frac{r}{f}\right)^2+1\right\}\left[\left\{\frac{3\mu}{\mu'}\left(\left(\frac{r}{f}\right)^2+1\right)-2\right\}^2\right.}\\ \left.\frac{\left\{3\left(\frac{r}{f}\right)^2+1\right\}\left[\frac{3\mu}{\mu'}\left\{\left(\frac{r}{f}\right)^2+1\right\}-2\right]}{+4\left\{\frac{\mu}{\mu'}\left(\left(\frac{r}{f}\right)^2+1\right)-1\right\}^{\frac{1}{2}}\left\{\frac{3\mu}{\mu'}\left(\left(\frac{r}{f}\right)^2+1\right)-1\right\}^{\frac{1}{2}}\right]\Phi}\mathfrak{A}e^{r''(y-H)+i(pt-fx-s'H)},\end{aligned}\right.$$

$$\left.\begin{aligned} u_{2U} &= -\frac{2i\left(\frac{r}{f}\right)\left\{3\left(\frac{r}{f}\right)^2+2\right\}^{\frac{1}{2}}\left\{3\left(\frac{r}{f}\right)^2+1\right\}}{f\left\{\left(\frac{r}{f}\right)^2+1\right\}\left[\left\{3\left(\frac{r}{f}\right)^2+1\right\}^2+4\left(\frac{r}{f}\right)\left\{3\left(\frac{r}{f}\right)^2+2\right\}^{\frac{1}{2}}\right]}\mathfrak{A}e^{i(pt-fx-sy)}, \\ v_{2U} &= \frac{2i\left(\frac{r}{f}\right)\left\{3\left(\frac{r}{f}\right)^2+1\right\}}{f\left\{\left(\frac{r}{f}\right)^2+1\right\}\left[\left\{3\left(\frac{r}{f}\right)^2+1\right\}^2+4\left(\frac{r}{f}\right)\left\{3\left(\frac{r}{f}\right)^2+2\right\}^{\frac{1}{2}}\right]}\mathfrak{A}e^{i(pt-fx-sy)}, \end{aligned}\right\} \quad (117)$$

$$\left.\begin{aligned} u_{2U}' &= -\frac{2i\left(\frac{r}{f}\right)\left\{3\left(\frac{r}{f}\right)^2+2\right\}^{\frac{1}{2}}\left\{3\left(\frac{r}{f}\right)^2+1\right\}}{f\left\{\left(\frac{r}{f}\right)^2+1\right\}\left[\left\{3\left(\frac{r}{f}\right)^2+1\right\}^2+4\left(\frac{r}{f}\right)\left\{3\left(\frac{r}{f}\right)^2+2\right\}^{\frac{1}{2}}\right]}\mathfrak{A}e^{i(pt-fx+sy-2sH)}, \\ v_{2U}' &= -\frac{2i\left(\frac{r}{f}\right)\left\{3\left(\frac{r}{f}\right)^2+1\right\}}{f\left\{\left(\frac{r}{f}\right)^2+1\right\}\left[\left\{3\left(\frac{r}{f}\right)^2+1\right\}^2+4\left(\frac{r}{f}\right)\left\{3\left(\frac{r}{f}\right)^2+2\right\}^{\frac{1}{2}}\right]}\mathfrak{A}e^{i(pt-fx+sy-2sH)}, \end{aligned}\right\} \quad \cdots\cdots\cdots\cdots (118)$$

$$\left.\begin{aligned} u_{1U}'' &= -\frac{8i\left(\frac{r}{f}\right)\left\{3\left(\frac{r}{f}\right)^2+2\right\}^{\frac{1}{2}}\left\{3\left(\frac{r}{f}\right)^2+1\right\}^2}{f\left\{\left(\frac{r}{f}\right)^2+1\right\}\left[\left\{3\left(\frac{r}{f}\right)^2+1\right\}^2+4\left(\frac{r}{f}\right)\left\{3\left(\frac{r}{f}\right)^2+2\right\}^{\frac{1}{2}}\right]^2}\mathfrak{A}e^{i(pt-fx+ry-rH-sH)}, \\ v_{1U}'' &= \frac{8i\left(\frac{r}{f}\right)^2\left\{3\left(\frac{r}{f}\right)^2+2\right\}^{\frac{1}{2}}\left\{3\left(\frac{r}{f}\right)^2+1\right\}^2}{f\left\{\left(\frac{r}{f}\right)^2+1\right\}\left[\left\{3\left(\frac{r}{f}\right)^2+1\right\}^2+4\left(\frac{r}{f}\right)\left\{3\left(\frac{r}{f}\right)^2+2\right\}^{\frac{1}{2}}\right]^2}\mathfrak{A}e^{i(pt-fx+ry-rH-sH)}, \end{aligned}\right\} \quad \cdots\cdots\cdots\cdots (119)$$

$$\left.\begin{aligned} u_{2U}'' &= -\frac{16i\left(\frac{r}{f}\right)^2\left\{3\left(\frac{r}{f}\right)^2+2\right\}\left\{3\left(\frac{r}{f}\right)^2+1\right\}}{f\left\{\left(\frac{r}{f}\right)^2+1\right\}\left[\left\{3\left(\frac{r}{f}\right)^2+1\right\}^2+4\left(\frac{r}{f}\right)\left\{3\left(\frac{r}{f}\right)^2+2\right\}^{\frac{1}{2}}\right]^2}\mathfrak{A}e^{i(pt-fx+sy-2sH)}, \\ v_{2U}'' &= \frac{16i\left(\frac{r}{f}\right)^2\left\{3\left(\frac{r}{f}\right)^2+2\right\}^{\frac{1}{2}}\left\{3\left(\frac{r}{f}\right)^2+1\right\}}{f\left\{\left(\frac{r}{f}\right)^2+1\right\}\left[\left\{3\left(\frac{r}{f}\right)^2+1\right\}^2+4\left(\frac{r}{f}\right)\left\{3\left(\frac{r}{f}\right)^2+2\right\}^{\frac{1}{2}}\right]^2}\mathfrak{A}e^{i(pt-fx+sy-2sH)}. \end{aligned}\right\} \quad (120)$$

Let the velocity, period and emergency angle of the primary dilatational wave which is incident to the boundary surface $y=0$ be V_1, T_1 and e respectively. Then the waves on the free surface $y=H$ are expressed by

$$\left.\begin{aligned} u_{1U} &= \frac{iT_1V_1\mathfrak{A}}{2\pi}\frac{\cos e(2\sin^2 e+1)^2}{\{(2\sin^2 e+1)^2+4\sin e\cos^2 e(\sin^2 e+2)^{\frac{1}{2}}\}}e^{i\left(pt-fx-\frac{2\pi H}{T_1V_1}\sin e\right)},\\ v_{1U} &= \frac{iT_1V_1\mathfrak{A}}{2\pi}\frac{\sin e(2\sin^2 e+1)^2}{\{(2\sin^2 e+1)^2+4\sin e\cos^2 e(\sin^2 e+2)^{\frac{1}{2}}\}}e^{i\left(pt-fx-\frac{2\pi H}{T_1V_1}\sin e\right)},\end{aligned}\right\}\quad(113)'$$

$$\left.\begin{aligned} u_{1U}' &= \frac{iT_1V_1\mathfrak{A}}{2\pi}\frac{\cos e(2\sin^2 e+1)^2}{\{(2\sin^2 e+1)^2+4\sin e\cos^2 e(\sin^2 e+2)^{\frac{1}{2}}\}}e^{i\left(pt-fx-\frac{2\pi H}{T_1V_1}\sin e\right)},\\ v_{1U}' &= -\frac{iT_1V_1\mathfrak{A}}{2\pi}\frac{\sin e(2\sin^2 e+1)^2}{\{(2\sin^2 e+1)^2+4\sin e\cos^2 e(\sin^2 e+2)^{\frac{1}{2}}\}}e^{i\left(pt-fx-\frac{2\pi H}{T_1V_1}\sin e\right)},\end{aligned}\right\}\quad(114)'$$

$$\left.\begin{aligned} u_{1U}'' &= -\frac{iT_1V_1\mathfrak{A}}{2\pi}\frac{2\cos e(2\sin^2 e+1)^4}{\{(2\sin^2 e+1)^2+4\sin e\cos^2 e(\sin^2 e+2)^{\frac{1}{2}}\}^2}e^{i\left(pt-fx-\frac{2\pi H}{T_1V_1}\sin e\right)},\\ v_{1U}'' &= \frac{iT_1V_1\mathfrak{A}}{2\pi}\frac{2\sin e(2\sin^2 e+1)^4}{\{(2\sin^2 e+1)^2+4\sin e\cos^2 e(\sin^2 e+2)^{\frac{1}{2}}\}^2}e^{i\left(pt-fx-\frac{2\pi H}{T_1V_1}\sin e\right)},\end{aligned}\right\}\quad(115)'$$

$$\left.\begin{aligned} u_{2U}'' &= \frac{iT_1V_1\mathfrak{A}}{2\pi}\frac{4\sin e\cos e(\sin^2 e+2)^{\frac{1}{2}}(2\sin^2 e+1)^3}{\{(2\sin^2 e+1)^2+4\sin e\cos^2 e(\sin^2 e+2)^{\frac{1}{2}}\}^2}e^{i\left(pt-fx-\frac{2\pi H}{T_1V_1}\sin e\right)},\\ v_{2U}'' &= \frac{iT_1V_1\mathfrak{A}}{2\pi}\frac{4\sin e\cos^2 e(2\sin^2 e+1)^3}{\{(2\sin^2 e+1)^2+4\sin e\cos^2 e(\sin^2 e+2)^{\frac{1}{2}}\}^2}e^{i\left(pt-fx-\frac{2\pi H}{T_1V_1}\sin e\right)},\end{aligned}\right\}\quad(116)'$$

and

$$\left.\begin{aligned} u_{2U} &= -\frac{iT_1V_1\mathfrak{A}}{2\pi}\frac{2\sin e\cos e(\sin^2 e+2)^{\frac{1}{2}}(2\sin^2 e+1)}{\{(2\sin^2 e+1)^2+4\sin e\cos^2 e(\sin^2 e+2)^{\frac{1}{2}}\}}e^{i\left(pt-fx-\frac{2\sqrt{3}\pi H}{T_1V_1}\sin e\right)},\\ v_{2U} &= \frac{iT_1V_1\mathfrak{A}}{2\pi}\frac{2\sin e\cos^2 e(2\sin^2 e+1)}{\{(2\sin^2 e+1)^2+4\sin e\cos^2 e(\sin^2 e+2)^{\frac{1}{2}}\}}e^{i\left(pt-fx-\frac{2\sqrt{3}\pi H}{T_1V_1}\sin e\right)},\end{aligned}\right\}$$

$$\cdots\cdots\cdots\cdots\cdots\cdots(117)'$$

$$\left.\begin{aligned} u_{2U}' &= -\frac{iT_1V_1\mathfrak{A}}{2\pi}\frac{2\sin e\cos e(\sin^2 e+2)^{\frac{1}{2}}(2\sin^2 e+1)}{\{(2\sin^2 e+1)^2+4\sin e\cos^2 e(\sin^2 e+2)^{\frac{1}{2}}\}}e^{i\left(pt-fx-\frac{2\sqrt{3}\pi H}{T_1V_1}\sin e\right)},\\ v_{2U}' &= -\frac{iT_1V_1\mathfrak{A}}{2\pi}\frac{2\sin e\cos^2 e(2\sin^2 e+1)}{\{(2\sin^2 e+1)^2+4\sin e\cos^2 e(\sin^2 e+2)^{\frac{1}{2}}\}}e^{i\left(pt-fx-\frac{2\sqrt{3}\pi H}{T_1V_1}\sin e\right)},\end{aligned}\right\}$$

$$\cdots\cdots\cdots\cdots\cdots\cdots(118)'$$

$$\left.\begin{aligned} u_{1U}'' &= -\frac{iT_1V_1\mathfrak{A}}{2\pi}\frac{8\sin e\cos^3 e(\sin^2 e+2)^{\frac{1}{2}}(2\sin^2 e+1)^2}{\{(2\sin^2 e+1)^2+4\sin e\cos^2 e(\sin^2 e+2)^{\frac{1}{2}}\}^2}e^{i\left(pt-fx-\frac{2\sqrt{3}\,\pi H}{T_1V_1}\sin e\right)},\\ v_{1U}'' &= \frac{iT_1V_1\mathfrak{A}}{2\pi}\frac{8\sin^2 e\cos^2 e(\sin^2 e+2)^{\frac{1}{2}}(2\sin^2 e+1)^2}{\{(2\sin^2 e+1)^2+4\sin e\cos^2 e(\sin^2 e+2)^{\frac{1}{2}}\}^2}e^{i\left(pt-fx-\frac{2\sqrt{3}\,\pi H}{T_1V_1}\sin e\right)}, \end{aligned}\right\} \quad \cdots\cdots\cdots\cdots\cdots\cdots (119)'$$

$$\left.\begin{aligned} u_{2U}'' &= \frac{iT_1V_1\mathfrak{A}}{2\pi}\frac{16\sin^2 e\cos^3 e(\sin^2 e+2)(2\sin^2 e+1)}{\{(2\sin^2 e+1)^2+4\sin e\cos^2 e(\sin^2 e+2)^{\frac{1}{2}}\}^2}e^{i\left(pt-fx-\frac{2\sqrt{3}\,\pi H}{T_1V_1}\sin e\right)},\\ v_{2U}'' &= \frac{iT_1V_1\mathfrak{A}}{2\pi}\frac{16\sin^2 e\cos^4 e(\sin^2 e+2)^{\frac{1}{2}}(2\sin^2 e+1)}{\{(2\sin^2 e+1)^2+4\sin e\cos^2 e(\sin^2 e+2)^{\frac{1}{2}}\}^2}e^{i\left(pt-fx-\frac{2\sqrt{3}\,\pi H}{T_1V_1}\sin e\right)}. \end{aligned}\right\} \quad (120)'$$

Table VI.

Max. Amp. \ e	0°	10°	20°	30°	45°	60°	70°	80°	90°
u_{1U}	1	0·5313	0·4353	0·4335	0·4535	0·4065	0·3115	0·1696	0
u_{1U}'	1	0·5313	0·4353	0·4335	0·4535	0·4065	0·3115	0·1696	0
u_{1U}''	−2	−0·5733	−0·4035	−0·4345	−0·5825	−0·6620	−0·5685	−0·3313	0
u_{2U}''	0	0·2675	0·3263	0·4340	0·6505	0·7595	0·6555	0·3826	0

Table VII.

Max. Amp. \ e	0°	10°	20°	30°	45°	60°	70°	80°	90°
v_{1U}	0	0·0937	0·1587	0·2505	0·4535	0·7032	0·8562	0·9620	1
v_{1U}'	0	−0·0937	−0·1587	−0·2505	−0·4535	−0·7032	−0·8562	−0·9620	−1
v_{1U}''	0	0·1008	0·1472	0·2510	0·5825	1·145	1·56	1·88	2
v_{2U}''	0	0·1849	0·2107	0·2505	0·2910	0·2290	0·1322	0·03854	0

Table VIII.

Max. Amp. \ e	0°	10°	20°	30°	45°	60°	70°	80°	90°
u_{2U}	0	−0·2479	−0·3525	−0·4328	−0·5065	−0·4665	−0·3585	−0·1958	0
u_{2U}'	0	−0·2479	−0·3525	−0·4328	−0·5065	−0·4665	−0·3585	−0·1958	0
u_{1U}''	0	−0·4893	−0·4680	−0·4330	−0·3255	−0·1520	−0·0554	−0·00784	0
u_{2U}''	0	0·2282	0·3780	0·4335	0·3635	0·1747	0·0640	0·00906	0

Table IX.

Max. Amp. \ e	0°	10°	20°	30°	45°	60°	70°	80°	90°
v_{2U}	0	0·1714	0·2275	0·2500	0·2265	0·1408	0·0724	0·0197	0
v_{-U}'	0	−0·1714	−0·2275	−0·2500	−0·2265	−0·1408	−0·0724	−0·0197	0
v_{1U}''	0	0·08626	0·1708	0·2505	0·3255	0·2633	0·1520	0·0445	0
v_{2U}''	0	0·1577	0·2445	0·2505	0·1630	0·0526	0·0129	0·00091	0

To see the properties of these waves expressed by (113)′, (114)′, (115)′, (116)′, (117)′, (118)′, (119′, (120)′ minutely, we obtain the following tables (Table VI, VII, VIII, IX) in which the maximum amplitudes of these waves corresponding to the magnitude of the emergency angle e are tabulated. The results in these tables are graphically shewn in Fig. 8, 9, 10, 11.

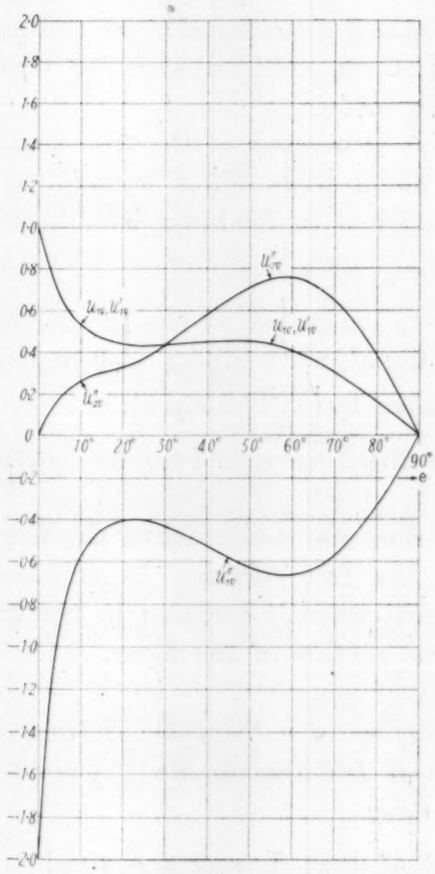

Fig. 8.

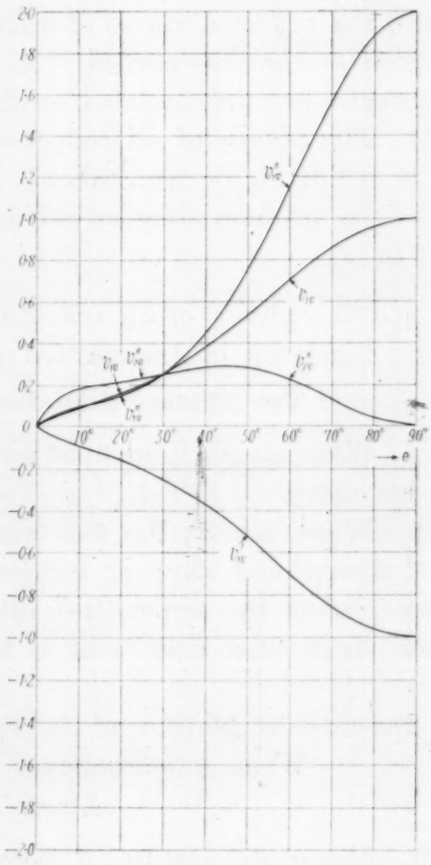

Fig. 9.

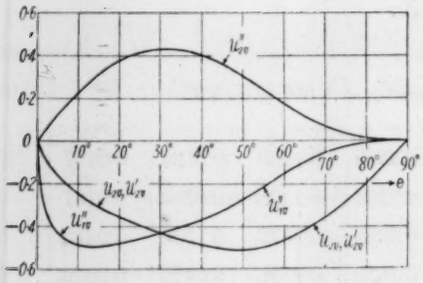

Fig. 10.

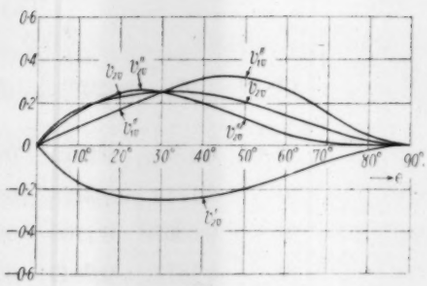

Fig. 11.

These tables and figures shew us many important properties of the waves, and some of them are summarised as follows:

1. When the transmitted dilatational wave is incident to the free surface, the reflected waves of dilatational and distortional types are only generated at the free surface.

And when the transmitted distortional wave is incident to the free surface, the reflected waves of dilatational and distortional types are only generated at the free surface. Moreover there exist no waves of which the energies are accumulated on the free surface.

2. The phases of all reflected waves generated at the free surface by the incidence of transmitted distortional wave differ equally from that of the primary dilatational wave incident to the lower boundary by $\left(\frac{2H\pi}{T_1V_1}\sin e\right)$.

And the phases of all reflected waves generated at the free surface by the incidence of transmitted dilatational wave differ also equally from that of the primary dilatational wave by $\left(\frac{2\sqrt{3}\pi H}{T_1V_1}\sin e\right)$.

3. When $e=0°$, there exist no transmitted wave, and the free surface does not move.

4. When $e=90°$, the free surface does not move when the transmitted distortional wave is incident to the free surface. In this case, however, when the transmitted dilatational wave is incident to the free surface, there exist movement of the free surface of the layer.

B. Initial Motion of the Free Surface of a Stratified Solid When a Distortional Wave is Incident to the Lower Boundary.

9. Using the results of Section 4 of Part I, and the results in Section 6 and 7, we obtain the following results after some reductions:

When the distortional wave expressed by the following form is incident to the boundary surface $y=0$,

$$2\varpi=\mathfrak{B}e^{i(pt-fx-sy)}, \quad \cdots\cdots\cdots\cdots\cdots\cdots(121)$$

of which the displacement are

$$\left.\begin{aligned} u_2&=-\frac{is}{k^2}\mathfrak{B}e^{i(pt-fx-sy)},\\ v_2&=\frac{if}{k^2}\mathfrak{B}e^{i(pt-fx-sy)}, \end{aligned}\right\} \cdots\cdots\cdots\cdots\cdots\cdots(122)$$

the transmitted[6] waves are expressed by

$$\Delta''=\frac{4rsh'^2\left(\frac{k'^2}{f^2}-2\right)}{f\left[r'k'^2\left\{\left(\frac{k^2}{f^2}-2\right)^2+\frac{4rs}{f^2}\right\}+\frac{\mu'}{\mu}rk^2\left\{\left(\frac{k'^2}{f^2}-2\right)^2+\frac{4r's'}{f^2}\right\}\right]}\mathfrak{B}e^{i(pt-fx-r'y)}, \quad \cdots(123)$$

$$2\varpi''=\frac{8vr's'k'^2}{f^2\left[r'k'^2\left\{\left(\frac{k^2}{f^2}-2\right)^2+\frac{4rs}{f^2}\right\}+\frac{\mu'}{\mu}rk^2\left\{\left(\frac{k'^2}{f^2}-2\right)^2+\frac{4r's'}{f^2}\right\}\right]}\mathfrak{B}e^{i(pt-fx-s'y)}. \quad \cdots(124)$$

The displacement corresponding to Δ'' expressed by (123) are written as follows;

$$\left.\begin{aligned} u_{1v}&=\frac{4irs\left(\frac{k'^2}{f^2}-2\right)}{\left[r'k'^2\left\{\left(\frac{k^2}{f^2}-2\right)^2+\frac{4rs}{f^2}\right\}+\frac{\mu'}{\mu}rk^2\left\{\left(\frac{k'^2}{f^2}-2\right)^2+\frac{4r's'}{f^2}\right\}\right]}\mathfrak{B}e^{i(pt-fx-r'y)},\\ v_{1v}&=\frac{4irr's\left(\frac{k'^2}{f^2}-2\right)}{f\left[r'k'^2\left\{\left(\frac{k^2}{f^2}-2\right)^2+\frac{4rs}{f^2}\right\}+\frac{\mu'}{\mu}rk^2\left\{\left(\frac{k'^2}{f^2}-2\right)^2+\frac{4r's'}{f^2}\right\}\right]}\mathfrak{B}e^{i(pt-fx-r'y)}. \end{aligned}\right\} (125)$$

Therefore we obtain the following waves reflected at $y=H$ when the wave expressed by (123) is incident to this surface;

$$u_{1v}'=\frac{4irs\left(\frac{k'^2}{f^2}-2\right)}{\left[r'k'^2\left\{\left(\frac{k^2}{f^2}-2\right)^2+\frac{4rs}{f^2}\right\}+\frac{\mu'}{\mu}rk^2\left\{\left(\frac{k'^2}{f^2}-2\right)^2+\frac{4r's'}{f^2}\right\}\right]}\mathfrak{B}e^{i(pt-fx+r'y-2r'H)},$$

6) The discussions of waves which are reflected at the boundary surface are already made in the preceding section.

$$v_{1U}' = -\frac{4irr's\left(\frac{k'^2}{f^2}-2\right)}{f\left[r'k'^2\left\{\left(\frac{k^2}{f^2}-2\right)^2+\frac{4rs}{f^2}\right\}+\frac{\mu'}{\mu}rk^2\left\{\left(\frac{k'^2}{f^2}-2\right)^2+\frac{4r's'}{f^2}\right\}\right]}\mathfrak{B}e^{i(pt-fx+r'y-2r'H)},$$

.....(126)

$$u_{1U}'' = -\frac{8irs\left(\frac{k'^2}{f^2}-2\right)^3\mathfrak{B}e^{r''(y-H)+i(pt-fx-r'H)}}{\left\{\left(\frac{k'^2}{f^2}-2\right)^2-\frac{4r''s''}{f^2}\right\}\left[r'k'^2\left\{\left(\frac{k^2}{f^2}-2\right)^2+\frac{4rs}{f^2}\right\}+\frac{\mu'}{\mu}rk^2\left\{\left(\frac{k'^2}{f^2}-2\right)^2+\frac{4r's'}{f^2}\right\}\right]},$$

$$v_{1U}'' = \frac{8rr''s\left(\frac{k'^2}{f^2}-2\right)^3\mathfrak{B}e^{r''(y-H)+i(pt-fx-r'H)}}{f\left\{\left(\frac{k'^2}{f^2}-2\right)^2-\frac{4r''s''}{f^2}\right\}\left[r'k'^2\left\{\left(\frac{k^2}{f^2}-2\right)^2+\frac{4rs}{f^2}\right\}+\frac{\mu'}{\mu}rk^2\left\{\left(\frac{k'^2}{f^2}-2\right)^2+\frac{4r's'}{f^2}\right\}\right]},$$

.....(127)

$$u_{2U}'' = -\frac{16irsr''s''\left(\frac{k'^2}{f^2}-2\right)^2\mathfrak{B}e^{s''(y-H)+i(pt-fx-r'H)}}{f^2\left\{\left(\frac{k'^2}{f^2}-2\right)^2-\frac{4r''s''}{f^2}\right\}\left[r'k'^2\left\{\left(\frac{k^2}{f^2}-2\right)^2+\frac{4rs}{f^2}\right\}+\frac{\mu'}{\mu}rk^2\left\{\left(\frac{k'^2}{f^2}-2\right)^2+\frac{4r's'}{f^2}\right\}\right]},$$

$$v_{2U}'' = \frac{16rr''s\left(\frac{k'^2}{f^2}-2\right)^2\mathfrak{B}e^{s''(y-H)+i(pt-fx-r'H)}}{f\left\{\left(\frac{k'^2}{f^2}-2\right)^2-\frac{4r''s''}{f^2}\right\}\left[r'k'^2\left\{\left(\frac{k^2}{f^2}-2\right)^2+\frac{4rs}{f^2}\right\}+\frac{\mu'}{\mu}rk^2\left\{\left(\frac{k'^2}{f^2}-2\right)^2+\frac{4r's'}{f^2}\right\}\right)}.$$

.....(128)

The displacement corresponding to $2\varpi''$ expressed by (124) are written by

$$u_{2U} = -\frac{8irr'ss'}{f^2\left[r'k'^2\left\{\left(\frac{k^2}{f^2}-2\right)^2+\frac{4rs}{f^2}\right\}+\frac{\mu'}{\mu}rk^2\left\{\left(\frac{k'^2}{f^2}-2\right)^2+\frac{4r's'}{f^2}\right\}\right]}\mathfrak{B}e^{i(pt-fx-s'y)},$$

$$v_{2U} = \frac{8irr's}{f\left[r'k'^2\left\{\left(\frac{k^2}{f^2}-2\right)^2+\frac{4rs}{f^2}\right\}+\frac{\mu'}{\mu}rk^2\left\{\left(\frac{k'^2}{f^2}-2\right)^2+\frac{4r's'}{f^2}\right\}\right]}\mathfrak{B}e^{i(pt-fx-s'y)}.$$

.....(129)

And therefore the waves, which are generated by the wave (129), on the surface $y=H$ are expressed by

$$\left.\begin{aligned} u_{2U}' &= -\frac{8irr's s'}{f^2\left[r'k'^2\left\{\left(\frac{k}{f^2}-2\right)^2+\frac{4rs}{f^2}\right\}+\frac{\mu'}{\mu}rk^2\left\{\left(\frac{k'^2}{f^2}-2\right)^2+\frac{4r's'}{f^2}\right\}\right]}\mathfrak{B}e^{i(pt-fx+s'y-2s'H)}, \\ v_{2U}' &= -\frac{8irr's}{f\left[r'k'^2\left\{\left(\frac{k^2}{f^2}-2\right)^2+\frac{4rs}{f^2}\right\}+\frac{\mu'}{\mu}rk^2\left\{\left(\frac{k'^2}{f^2}-2\right)^2+\frac{4r's'}{f^2}\right\}\right]}\mathfrak{B}e^{i(pt-fx+s'y-2s'H)}, \end{aligned}\right\} \quad \cdots\cdots\cdots\cdots\cdots\cdots (130)$$

$$\left.\begin{aligned} u_{1U}'' &= -\frac{32irr's s'\left(\frac{k'^2}{f^2}-2\right)\mathfrak{B}e^{r''(y-H)+i(pt-fx-s'H)}}{f^2\left\{\left(\frac{k'^2}{f^2}-2\right)^2-\frac{4r''s''}{f^2}\right\}\left[r'k'^2\left\{\left(\frac{k^2}{f^2}-2\right)^2+\frac{4rs}{f^2}\right\}+\frac{\mu'}{\mu}rk^2\left\{\left(\frac{k'^2}{f^2}-2\right)^2+\frac{4r's'}{f^2}\right\}\right]}, \\ v_{1U}'' &= \frac{32rr'r''ss'\left(\frac{k'^2}{f^2}-2\right)\mathfrak{B}e^{r''(y-H)+i(pt-fx-s'H)}}{f^3\left\{\left(\frac{k'^2}{f^2}-2\right)^2-\frac{4r''s''}{f^2}\right\}\left[r'k'^2\left\{\left(\frac{k^2}{f^2}-2\right)^2+\frac{4rs}{f^2}\right\}+\frac{\mu'}{\mu}rk^2\left\{\left(\frac{k'^2}{f^2}-2\right)^2+\frac{4r's'}{f^2}\right\}\right]}, \end{aligned}\right\} \quad \cdots\cdots\cdots\cdots\cdots (131)$$

$$\left.\begin{aligned} u_{2U}'' &= -\frac{64irr'r''ss's''\mathfrak{B}e^{s''(y-H)+i(pt-fx-s'H)}}{f^4\left\{\left(\frac{k'^2}{f^2}-2\right)^2-\frac{4r''s''}{f^2}\right\}\left[r'k'^2\left\{\left(\frac{k^2}{f^2}-2\right)^2+\frac{4rs}{f^2}\right\}+\frac{\mu'}{\mu}rk^2\left\{\left(\frac{k'^2}{f^2}-2\right)^2+\frac{4r's'}{f^2}\right\}\right]}, \\ v_{2U}'' &= \frac{64rr'r''ss'\mathfrak{B}e^{s''(y-H)+i(pt-fx-s'H)}}{f^3\left\{\left(\frac{k'^2}{f^2}-2\right)^2-\frac{4r''s''}{f^2}\right\}\left[r'k'^2\left\{\left(\frac{k^2}{f^2}-2\right)^2+\frac{4rs}{f^2}\right\}+\frac{\mu'}{\mu}rk^2\left\{\left(\frac{k'^2}{f^2}-2\right)^2+\frac{4r's'}{f^2}\right\}\right]}, \end{aligned}\right\} \quad \cdots\cdots\cdots\cdots\cdots (132)$$

When the transmitted dilatational wave expressed by (124) is incident to the free surface $y=H$ primarily, the waves of dilatational and distortional types expressed by (126), (127) and (128) are generated at the free surface $y=H$ and reflected at this plane. When the emergency angle of the distortional wave (121) which is incident to the boundary $y=0$ is smaller than a certain magnitude, these waves are predominated on the free surface and not reflected in the interior of the medium,

and there is the phase difference between these waves and the distortional wave which is incident to the boundary $y=0$.

When the transmitted distortional wave expressed by (129) is incident to the free surface $y=H$ secondarily, the waves of dilatational and distortional types expressed by (130), (131) and (132) are generated at the plane $y=H$ and reflected at this plane. In this case, also, these waves are predominated on the free surface, and have also the phase difference when the emergency angle of the primary incident distortional wave (121) is smaller than a certain magnitude.

When $\rho=\rho'$ and the Poisson's ratios of both media are equally $\frac{1}{4}$, the wave generated in the second medium due to the transmitted waves of (123) and (124) are expressed by the following formulae:

$$\left.\begin{aligned} u_{1V}&=\frac{4i\left(\frac{s}{f}\right)\left\{\frac{1}{3}\left(\frac{s}{f}\right)^2-\frac{2}{3}\right\}^{\frac{1}{2}}\left[\frac{\mu}{\mu'}\left\{\left(\frac{s}{f}\right)^2+1\right\}-2\right]}{f\Psi}\mathfrak{B}e^{i(pt-fx-r'y)},\\ v_{1V}&=\frac{4i\left(\frac{s}{f}\right)\left\{\frac{1}{3}\left(\frac{s}{f}\right)^2-\frac{2}{3}\right\}^{\frac{1}{2}}\left[\frac{\mu}{3\mu'}\left\{\left(\frac{s}{f}\right)^2+1\right\}-1\right]^{\frac{1}{2}}\left[\frac{\mu}{\mu'}\left\{\left(\frac{s}{f}\right)^2+1\right\}-2\right]}{f\Psi}\\ &\qquad\times\mathfrak{B}e^{i(pt-fx-r'y)},\end{aligned}\right\}\quad\cdots\cdots\cdots\cdots\cdots(133)$$

$$\left.\begin{aligned} u_{1V'}&=\frac{4i\left(\frac{s}{f}\right)\left\{\frac{1}{3}\left(\frac{s}{f}\right)^2-\frac{2}{3}\right\}^{\frac{1}{2}}\left[\frac{\mu}{\mu'}\left\{\left(\frac{s}{f}\right)^2+1\right\}-2\right]}{f\Psi}\mathfrak{B}e^{i(pt-fx+r'y-2r'H)},\\ v_{1V'}&=-\frac{4i\left(\frac{s}{f}\right)\left\{\frac{1}{3}\left(\frac{s}{f}\right)^2-\frac{2}{3}\right\}^{\frac{1}{2}}\left[\frac{1}{3}\frac{\mu}{\mu'}\left\{\left(\frac{s}{f}\right)^2+1\right\}-1\right]^{\frac{1}{2}}\left[\frac{\mu}{\mu'}\left\{\left(\frac{s}{f}\right)^2+1\right\}-2\right]}{f\Psi}\\ &\qquad\times\mathfrak{B}e^{i(pt-fx+r'y-2r'H)},\end{aligned}\right\}\quad\cdots\cdots\cdots\cdots(134)$$

$$\left.\begin{aligned} u_{1V''}=-\frac{8i\left(\frac{s}{f}\right)\left\{\frac{1}{3}\left(\frac{s}{f}\right)^2-\frac{2}{3}\right\}^{\frac{1}{2}}}{f\left[\left\{\frac{\mu}{\mu'}\left(\left(\frac{s}{f}\right)^2+1\right)-2\right\}^2\right.}\\ \frac{\left[\frac{\mu}{\mu'}\left\{\left(\frac{s}{f}\right)^2+1\right\}-2\right]^3}{\left.+4\left\{\frac{1}{3}\frac{\mu}{\mu'}\left(\left(\frac{s}{f}\right)^2+1\right)-1\right\}^2\left\{\frac{\mu}{\mu'}\left(\left(\frac{s}{f}\right)^2+1\right)-1\right\}^{\frac{1}{2}}\right]\Psi}\mathfrak{B}e^{r''(y-H)+i(pt-fx-r'H)},\end{aligned}\right\}$$

$$v_{1v}''=\frac{8i\left(\frac{s}{f}\right)\left\{\frac{1}{3}\left(\frac{s}{f}\right)^2-\frac{2}{3}\right\}^{\frac{1}{2}}\left[\frac{1}{3}\frac{\mu}{\mu'}\left\{\left(\frac{s}{f}\right)^2+1\right\}-1\right]^{\frac{1}{2}}}{f\left[\left\{\frac{\mu}{\mu'}\left(\left(\frac{s}{f}\right)^2+1\right)-2\right\}^2\right.}$$

$$\left.\frac{\left[\frac{\mu}{\mu'}\left\{\left(\frac{s}{f}\right)^2+1\right\}-2\right]^3}{+4\left\{\frac{1}{3}\frac{\mu}{\mu'}\left(\left(\frac{s}{f}\right)^2+1\right)-1\right\}^{\frac{1}{2}}\left\{\frac{\mu}{\mu'}\left(\left(\frac{s}{f}\right)^2+1\right)-1\right\}^{\frac{1}{2}}\right]\Psi}\mathfrak{B}e^{r''(y-H)+i(pt-fx-r'H)},\right\}$$

.....(135)

$$v_{2v}''=\frac{16i\left(\frac{s}{f}\right)\left\{\frac{1}{3}\left(\frac{s}{f}\right)^2-\frac{2}{3}\right\}^{\frac{1}{2}}\left[\frac{1}{3}\frac{\mu}{\mu'}\left\{\left(\frac{s}{f}\right)^2+1\right\}-1\right]^{\frac{1}{2}}}{f\left[\left\{\frac{\mu}{\mu'}\left(\left(\frac{s}{f}\right)^2+1\right)-2\right\}^2\right.}$$

$$\frac{\left[\frac{\mu}{\mu'}\left\{\left(\frac{s}{f}\right)^2+1\right\}-1\right]^{\frac{1}{2}}\left[\frac{\mu}{\mu'}\left\{\left(\frac{s}{f}\right)^2+1\right\}-2\right]^2}{+4\left\{\frac{1}{3}\frac{\mu}{\mu'}\left(\left(\frac{s}{f}\right)^2+1\right)-1\right\}^{\frac{1}{2}}\left\{\frac{\mu}{\mu'}\left(\left(\frac{s}{f}\right)^2+1\right)-1\right]^{\frac{1}{2}}\Psi}\mathfrak{B}e^{s''(y-H)+i(pt-fx-r'H)},$$

$$v_{2v}''=\frac{16i\left(\frac{s}{f}\right)\left\{\frac{1}{3}\left(\frac{s}{f}\right)^2-\frac{2}{3}\right\}^{\frac{1}{2}}\left[\frac{1}{3}\frac{\mu}{\mu'}\left\{\left(\frac{s}{f}\right)^2+1\right\}-1\right]^{\frac{1}{2}}}{f\left[\left\{\frac{\mu}{\mu'}\left(\left(\frac{s}{f}\right)^2+1\right)-2\right\}^2\right.}$$

$$\left.\frac{\left[\frac{\mu}{\mu'}\left\{\left(\frac{s}{f}\right)^2+1\right\}-2\right]^2}{+4\left\{\frac{1}{3}\frac{\mu}{\mu'}\left(\left(\frac{s}{f}\right)^2+1\right)-1\right\}^{\frac{1}{2}}\left\{\frac{\mu}{\mu'}\left(\left(\frac{s}{f}\right)^2+1\right)-1\right\}^{\frac{1}{2}}\right]\Psi}\mathfrak{B}e^{s''(y-H)+i(pt-fx-r'H)},\right\}$$

.....(136)

where

$$\Psi=\frac{\mu}{\mu'}\left\{\left(\frac{s}{f}\right)^2+1\right\}\left[\frac{1}{3}\frac{\mu}{\mu'}\left\{\left(\frac{s}{f}\right)^2+1\right\}-1\right]^{\frac{1}{2}}\left[\left\{\left(\frac{s}{f}\right)^2-1\right\}^2\right.$$

$$\left.+4\left(\frac{s}{f}\right)\left\{\frac{1}{3}\left(\frac{s}{f}\right)^2-\frac{2}{3}\right\}^{\frac{1}{2}}\right]$$

$$+\frac{\mu'}{\mu}\left\{\left(\frac{s}{f}\right)^2+1\right\}\left\{\frac{1}{3}\left(\frac{s}{f}\right)^2-\frac{2}{3}\right\}^{\frac{1}{2}}\left[\left\{\frac{\mu}{\mu'}\left(\left(\frac{s}{f}\right)^2+1\right)-2\right\}^2\right.$$

$$\left.+4\left\{\frac{1}{3}\frac{\mu}{\mu'}\left(\left(\frac{s}{f}\right)^2+1\right)-1\right\}^{\frac{1}{2}}\left\{\frac{\mu}{\mu'}\left(\left(\frac{s}{f}\right)^2+1\right)-1\right\}^{\frac{1}{2}}\right].\quad\ldots.(137)$$

And

$$\left.\begin{aligned} u_{2U}&=-\frac{8i\left(\frac{s}{f}\right)\left\{\frac{1}{3}\left(\frac{s}{f}\right)^2-\frac{2}{3}\right\}^{\frac{1}{2}}\left[\frac{1}{3}\frac{\mu}{\mu'}\left\{\left(\frac{s}{f}\right)^2+1\right\}-1\right]^{\frac{1}{2}}\left[\frac{\mu}{\mu'}\left\{\left(\frac{s}{f}\right)^2+1\right\}-1\right]^{\frac{1}{2}}}{f\Psi}\\ &\qquad\times\mathfrak{B}e^{i(pt-fx-s'y)},\\ v_{2U}&=\frac{8i\left(\frac{s}{f}\right)\left\{\frac{1}{3}\left(\frac{s}{f}\right)^2-\frac{2}{3}\right\}^{\frac{1}{2}}\left[\frac{1}{3}\frac{\mu}{\mu'}\left\{\left(\frac{s}{f}\right)^2+1\right\}-1\right]^{\frac{1}{2}}}{f\Psi}\mathfrak{B}e^{i(pt-fx-s'y)},\end{aligned}\right\}$$

.....(138)

$$\left.\begin{aligned} u_{2U'}&=-\frac{8i\left(\frac{s}{f}\right)\left\{\frac{1}{3}\left(\frac{s}{f}\right)^2-\frac{2}{3}\right\}^{\frac{1}{2}}\left[\frac{1}{3}\frac{\mu}{\mu'}\left\{\left(\frac{s}{f}\right)^2+1\right\}-1\right]^{\frac{1}{2}}\left[\frac{\mu}{\mu'}\left\{\left(\frac{s}{f}\right)^2+1\right\}-1\right]^{\frac{1}{2}}}{f\Psi}\\ &\qquad\times\mathfrak{B}e^{i(pt-fx+s'y-2s'H)},\\ v_{2U'}&=-\frac{8i\left(\frac{s}{f}\right)\left\{\frac{1}{3}\left(\frac{s}{f}\right)^2-\frac{2}{3}\right\}^{\frac{1}{2}}\left[\frac{1}{3}\frac{\mu}{\mu'}\left\{\left(\frac{s}{f}\right)^2+1\right\}-1\right]^{\frac{1}{2}}}{f\Psi}\mathfrak{B}e^{i(pt-fx+s'y-2s'H)},\end{aligned}\right\}$$

.....(139)

$$\left.\begin{aligned} u_{1U}''&=-\frac{32i\left(\frac{s}{f}\right)\left\{\frac{1}{3}\left(\frac{s}{f}\right)^2-\frac{2}{3}\right\}^{\frac{1}{2}}\left[\frac{1}{3}\frac{\mu}{\mu'}\left\{\left(\frac{s}{f}\right)^2+1\right\}-1\right]^{\frac{1}{2}}}{f\left[\left\{\frac{\mu}{\mu'}\left(\left(\frac{s}{f}\right)^2+1\right)-2\right\}^2\right.}\\ &\quad\frac{\left[\frac{\mu}{\mu'}\left\{\left(\frac{s}{f}\right)^2+1\right\}-1\right]^{\frac{1}{2}}\left[\frac{\mu}{\mu'}\left\{\left(\frac{s}{f}\right)^2+1\right\}-2\right]}{\left.+4\left\{\frac{1}{3}\frac{\mu}{\mu'}\left(\left(\frac{s}{f}\right)^2+1\right)-1\right\}^{\frac{1}{2}}\left\{\frac{\mu}{\mu'}\left(\left(\frac{s}{f}\right)^2+1\right)-1\right\}^{\frac{1}{2}}\right]\Psi}\mathfrak{B}e^{r'(y-H)+i(pt-fx-s'H)},\\ v_{1U}''&=\frac{32i\left(\frac{s}{f}\right)\left\{\frac{1}{3}\left(\frac{s}{f}\right)^2-\frac{2}{3}\right\}^{\frac{1}{2}}\left[\frac{1}{3}\frac{\mu}{\mu'}\left\{\left(\frac{s}{f}\right)^2+1\right\}-1\right]}{f\left[\left\{\frac{\mu}{\mu'}\left(\left(\frac{s}{f}\right)^2+1\right)-2\right\}^2\right.}\\ &\quad\frac{\left[\frac{\mu}{\mu'}\left\{\left(\frac{s}{f}\right)^2+1\right\}-1\right]^{\frac{1}{2}}\left[\frac{\mu}{\mu'}\left\{\left(\frac{s}{f}\right)^2+1\right\}-2\right]}{\left.+4\left\{\frac{1}{3}\frac{\mu}{\mu'}\left(\left(\frac{s}{f}\right)^2+1\right)-1\right\}^{\frac{1}{2}}\left\{\frac{\mu}{\mu'}\left(\left(\frac{s}{f}\right)^2+1\right)-1\right\}^{\frac{1}{2}}\right]\Psi}\mathfrak{B}e^{r''(y-H)+i(pt-fx-s'H)},\end{aligned}\right\}$$

.....(140)

$$u_{2U}''=\frac{64i\left(\frac{s}{f}\right)\left\{\frac{1}{3}\left(\frac{s}{f}\right)^2-\frac{2}{3}\right\}^{\frac{1}{2}}}{f\left[\left\{\frac{\mu}{\mu'}\left(\left(\frac{s}{f}\right)^2+1\right)-2\right\}^2\right.}$$

$$\left.\frac{\left[\frac{1}{3}\frac{\mu}{\mu'}\left\{\left(\frac{s}{f}\right)^2+1\right)-1\right]\left[\frac{\mu}{\mu'}\left\{\left(\frac{s}{f}\right)^2+1\right\}-1\right]}{+4\left\{\frac{1}{3}\frac{\mu}{\mu'}\left(\left(\frac{s}{f}\right)^2+1\right)-1\right\}^{\frac{1}{2}}\left\{\frac{\mu}{\mu'}\left(\left(\frac{s}{f}\right)^2+1\right)-1\right\}^{\frac{1}{2}}\right]\mathfrak{F}}\mathfrak{B}e^{s''(y-H)+i(pt-fx-s'H)},\right\}$$

$$v_{2U}''=\frac{64i\left(\frac{s}{f}\right)\left\{\frac{1}{3}\left(\frac{s}{f}\right)^2-\frac{2}{3}\right\}^{\frac{1}{2}}}{f\left[\left\{\frac{\mu}{\mu'}\left(\left(\frac{s}{f}\right)^2+1\right)-2\right\}^2\right.}$$

$$\left.\frac{\left[\frac{1}{3}\frac{\mu}{\mu'}\left\{\left(\frac{s}{f}\right)^2+1\right\}-1\right]\left[\frac{\mu}{\mu'}\left\{\left(\frac{s}{f}\right)^2+1\right\}-1\right]^{\frac{1}{2}}}{+4\left\{\frac{1}{3}\frac{\mu}{\mu'}\left(\left(\frac{s}{f}\right)^2+1\right)-1\right\}^{\frac{1}{2}}\left\{\frac{\mu}{\mu'}\left(\left(\frac{s}{f}\right)^2+1\right)-1\right\}^{\frac{1}{2}}\right]\mathfrak{F}}\mathfrak{B}e^{s''(y-H)+i(pt-fx-s'H)}.\right\}$$

.....(141)

When $\frac{\mu'}{\mu}=1$, the expressions (133), (134), (135), (136) and (138), (139), (140), (141) are expressed by

$$\left.\begin{aligned}u_{1U}&=\frac{2i\left(\frac{s}{f}\right)\left\{\left(\frac{s}{f}\right)^2-1\right\}}{f\left\{\left(\frac{s}{f}\right)^2+1\right\}\left[\left\{\left(\frac{s}{f}\right)^2-1\right\}^2+4\left(\frac{s}{f}\right)\left\{\frac{1}{3}\left(\frac{s}{f}\right)^2-\frac{2}{3}\right\}^{\frac{1}{2}}\right]}\mathfrak{B}e^{i(pt-fx-ry)},\\ v_{1U}&=\frac{2i\left(\frac{s}{f}\right)\left\{\frac{1}{3}\left(\frac{s}{f}\right)^2-\frac{2}{3}\right\}^{\frac{1}{2}}\left\{\left(\frac{s}{f}\right)^2-1\right\}}{f\left\{\left(\frac{s}{f}\right)^2+1\right\}\left[\left\{\left(\frac{s}{f}\right)^2-1\right\}^2+4\left(\frac{s}{f}\right)\left\{\frac{1}{3}\left(\frac{s}{f}\right)^2-\frac{2}{3}\right\}^{\frac{1}{2}}\right]}\mathfrak{B}e^{i(pt-fx-ry)},\end{aligned}\right\}(142)$$

$$u_{1U}'=\frac{2i\left(\frac{s}{f}\right)\left\{\left(\frac{s}{f}\right)^2-1\right\}}{f\left\{\left(\frac{s}{f}\right)^2+1\right\}\left[\left\{\left(\frac{s}{f}\right)^2-1\right\}^2+4\left(\frac{s}{f}\right)\left\{\frac{1}{3}\left(\frac{s}{f}\right)^2-\frac{2}{3}\right\}^{\frac{1}{2}}\right]}\mathfrak{B}e^{i(pt-fx+ry-2rH)},$$

$$v_{1U}' = \frac{2i\left(\frac{s}{f}\right)\left\{\frac{1}{3}\left(\frac{s}{f}\right)^2-\frac{2}{3}\right\}^{\frac{1}{2}}\left\{\left(\frac{s}{f}\right)^2-1\right\}}{f\left\{\left(\frac{s}{f}\right)^2+1\right\}\left[\left\{\left(\frac{s}{f}\right)^2-1\right\}^2+4\left(\frac{s}{f}\right)\left\{\frac{1}{3}\left(\frac{s}{f}\right)^2-\frac{2}{3}\right\}^{\frac{1}{2}}\right]}\mathfrak{B}e^{i(pt-fx+ry-2rH)},$$

.....(143)

$$u_{1U}'' = -\frac{4i\left(\frac{s}{f}\right)\left\{\left(\frac{s}{f}\right)^2-1\right\}^3}{f\left\{\left(\frac{s}{f}\right)^2+1\right\}\left[\left\{\left(\frac{s}{f}\right)^2-1\right\}^2+4\left(\frac{s}{f}\right)\left\{\frac{1}{3}\left(\frac{s}{f}\right)^2-\frac{2}{3}\right\}^{\frac{1}{2}}\right]^2}\mathfrak{B}e^{i(pt-fx+ry-2rH)},$$

$$v_{1U}'' = \frac{4i\left(\frac{s}{f}\right)\left\{\frac{1}{3}\left(\frac{s}{f}\right)^2-\frac{2}{3}\right\}^{\frac{1}{2}}\left\{\left(\frac{s}{f}\right)^2-1\right\}^3}{f\left\{\left(\frac{s}{f}\right)^2+1\right\}\left[\left\{\left(\frac{s}{f}\right)^2-1\right\}^2+4\left(\frac{s}{f}\right)\left\{\frac{1}{3}\left(\frac{s}{f}\right)^2-\frac{2}{3}\right\}^{\frac{1}{2}}\right]^2}\mathfrak{B}e^{i(pt-fx+ry-2rH)},$$

.....(144)

$$u_{2U}'' = \frac{8i\left(\frac{s}{f}\right)^2\left\{\frac{1}{3}\left(\frac{s}{f}\right)^2-\frac{2}{3}\right\}^{\frac{1}{2}}\left\{\left(\frac{s}{f}\right)^2-1\right\}^2}{f\left\{\left(\frac{s}{f}\right)^2+1\right\}\left[\left\{\left(\frac{s}{f}\right)^2-1\right\}^2+4\left(\frac{s}{f}\right)\left\{\frac{1}{3}\left(\frac{s}{f}\right)^2-\frac{2}{3}\right\}^{\frac{1}{2}}\right]^2}\mathfrak{B}e^{i(pt-fx+ry-rH-sH)},$$

$$v_{2U}'' = \frac{8i\left(\frac{s}{f}\right)\left\{\frac{1}{3}\left(\frac{s}{f}\right)^2-\frac{2}{3}\right\}^{\frac{1}{2}}\left\{\left(\frac{s}{f}\right)^2-1\right\}^2}{f\left\{\left(\frac{s}{f}\right)^2+1\right\}\left[\left\{\left(\frac{s}{f}\right)^2-1\right\}^2+4\left(\frac{s}{f}\right)\left\{\frac{1}{3}\left(\frac{s}{f}\right)^2-\frac{2}{3}\right\}^{\frac{1}{2}}\right]^2}\mathfrak{B}e^{i(pt-fx+ry-rH-sH)},$$

.....(145)

and

$$u_{2U} = -\frac{4i\left(\frac{s}{f}\right)^2\left\{\frac{1}{3}\left(\frac{s}{f}\right)^2-\frac{2}{3}\right\}^{\frac{1}{2}}}{f\left\{\left(\frac{s}{f}\right)^2+1\right\}\left[\left\{\left(\frac{s}{f}\right)^2-1\right\}^2+4\left(\frac{s}{f}\right)\left\{\frac{1}{3}\left(\frac{s}{f}\right)^2-\frac{2}{3}\right\}^{\frac{1}{2}}\right]}\mathfrak{B}e^{i(pt-fx-sy)},$$

$$v_{2U} = \frac{4i\left(\frac{s}{f}\right)\left\{\frac{1}{3}\left(\frac{s}{f}\right)^2-\frac{2}{3}\right\}^{\frac{1}{2}}}{f\left\{\left(\frac{s}{f}\right)^2+1\right\}\left[\left\{\left(\frac{s}{f}\right)^2-1\right\}^2+4\left(\frac{s}{f}\right)\left\{\frac{1}{3}\left(\frac{s}{f}\right)^2-\frac{2}{3}\right\}^{\frac{1}{2}}\right]}\mathfrak{B}e^{i(pt-fx-sy)},$$

.....(146)

$$\left.\begin{aligned} u_{2U}' &= -\frac{4i\left(\frac{s}{f}\right)^2\left\{\frac{1}{3}\left(\frac{s}{f}\right)^2-\frac{2}{3}\right\}^{\frac{1}{2}}}{f\left\{\left(\frac{s}{f}\right)^2+1\right\}\left[\left\{\left(\frac{s}{f}\right)^2-1\right\}^2+4\left(\frac{s}{f}\right)\left\{\frac{1}{3}\left(\frac{s}{f}\right)^2-\frac{2}{3}\right\}^{\frac{1}{2}}\right]}\mathfrak{B}e^{i(pt-fx+sy-2sH)}, \\ v_{2U}' &= -\frac{4i\left(\frac{s}{f}\right)\left\{\frac{1}{3}\left(\frac{s}{f}\right)^2-\frac{2}{3}\right\}^{\frac{1}{2}}}{f\left\{\left(\frac{s}{f}\right)^2+1\right\}\left[\left\{\left(\frac{s}{f}\right)^2-1\right\}^2+4\left(\frac{s}{f}\right)\left\{\frac{1}{3}\left(\frac{s}{f}\right)^2-\frac{2}{3}\right\}^{\frac{1}{2}}\right]}\mathfrak{B}e^{i(pt-fx+sy-2sH)}, \end{aligned}\right\}$$

.....(147)

$$\left.\begin{aligned} u_{1U}'' &= -\frac{16i\left(\frac{s}{f}\right)^2\left\{\left(\frac{s}{f}\right)^2-1\right\}\left\{\frac{1}{3}\left(\frac{s}{f}\right)^2-\frac{2}{3}\right\}^{\frac{1}{2}}}{f\left\{\left(\frac{s}{f}\right)^2+1\right\}\left[\left\{\left(\frac{s}{f}\right)^2-1\right\}^2+4\left(\frac{s}{f}\right)\left\{\frac{1}{3}\left(\frac{s}{f}\right)^2-\frac{2}{3}\right\}^{\frac{1}{2}}\right]^2}\mathfrak{B}e^{i(pt-fx+ry-rH-sH)}, \\ v_{1U}'' &= \frac{16i\left(\frac{s}{f}\right)^2\left\{\left(\frac{s}{f}\right)^2-1\right\}\left\{\frac{1}{3}\left(\frac{s}{f}\right)^2-\frac{2}{3}\right\}}{f\left\{\left(\frac{s}{f}\right)^2+1\right\}\left[\left\{\left(\frac{s}{f}\right)^2-1\right\}^2+4\left(\frac{s}{f}\right)\left\{\frac{1}{3}\left(\frac{s}{f}\right)^2-\frac{2}{3}\right\}^{\frac{1}{2}}\right]^2}\mathfrak{B}e^{i(pt-fx+ry-rH-sH)}, \end{aligned}\right\}$$

.....(148)

$$\left.\begin{aligned} u_{2U}'' &= \frac{32i\left(\frac{s}{f}\right)^3\left\{\frac{1}{3}\left(\frac{s}{f}\right)^2-\frac{2}{3}\right\}}{f\left\{\left(\frac{s}{f}\right)^2+1\right\}\left[\left\{\left(\frac{s}{f}\right)^2-1\right\}^2+4\left(\frac{s}{f}\right)\left\{\frac{1}{3}\left(\frac{s}{f}\right)^2-\frac{2}{3}\right\}^{\frac{1}{2}}\right]^2}\mathfrak{B}e^{i(pt-fx+sy-2sH)}, \\ v_{2U}'' &= \frac{32i\left(\frac{s}{f}\right)^2\left\{\frac{1}{3}\left(\frac{s}{f}\right)^2-\frac{2}{3}\right\}}{f\left\{\left(\frac{s}{f}\right)^2+1\right\}\left[\left\{\left(\frac{s}{f}\right)^2-1\right\}^2+4\left(\frac{s}{f}\right)\left\{\frac{1}{3}\left(\frac{s}{f}\right)^2-\frac{2}{3}\right\}^{\frac{1}{2}}\right]^2}\mathfrak{B}e^{i(pt-fx+sy-2sH)}. \end{aligned}\right\}$$

.....(149)

Let the velocity, period and emergency angle of the primary distortional wave (121) which is incident to the boundary surface $y=0$ be V_2, T_2 and e respectively. Then the waves on the free surface $y=H$ are expressed by

$$\left.\begin{aligned} u_{1U}&=\frac{iT_2V_2\mathfrak{B}}{2\pi}\frac{2\sin e\cos^2 e(\sin^2 e-\cos^2 e)}{\left\{(\sin^2 e-\cos^2 e)^2+4\sin e\cos^2 e\left(\frac{1}{3}-\cos^2 e\right)^{\frac{1}{2}}\right\}}e^{i\left(pt-fx-\frac{2\pi H}{\sqrt{3}\,T_2V_2}\sin e\right)},\\ v_{1U}&=\frac{iT_2V_2\mathfrak{B}}{2\pi}\frac{2\sin e\cos e\left(\frac{1}{3}-\cos^2 e\right)^{\frac{1}{2}}(\sin^2 e-\cos^2 e)}{\left\{(\sin^2 e-\cos^2 e)^2+4\sin e\cos^2 e\left(\frac{1}{3}-\cos^2 e\right)^{\frac{1}{2}}\right\}}e^{i\left(pt-fx-\frac{2\pi H}{\sqrt{3}\,T_2V_2}\sin e\right)},\end{aligned}\right\}$$

$$\cdots\cdots\cdots\cdots\cdots(142)'$$

$$\left.\begin{aligned} u_{1V}'&=\frac{iT_2V_2\mathfrak{B}}{2\pi}\frac{2\sin e\cos^2 e(\sin^2 e-\cos^2 e)}{\left\{(\sin^2 e-\cos^2 e)^2+4\sin e\cos^2 e\left(\frac{1}{3}-\cos^2 e\right)^{\frac{1}{2}}\right\}}e^{i\left(pt-fx-\frac{2\pi H}{\sqrt{3}\,T_2V_2}\sin e\right)},\\ v_{1V}'&=-\frac{iT_2V_2\mathfrak{B}}{2\pi}\frac{2\sin e\cos e\left(\frac{1}{3}-\cos^2 e\right)^{\frac{1}{2}}(\sin^2 e-\cos^2 e)}{\left\{(\sin^2 e-\cos^2 e)^2+4\sin e\cos^2 e\left(\frac{1}{3}-\cos^2 e\right)^{\frac{1}{2}}\right\}}e^{i\left(pt-fx-\frac{2\pi H}{\sqrt{3}\,T_2V_2}\sin e\right)},\end{aligned}\right\}$$

$$\cdots\cdots\cdots\cdots\cdots(143)'$$

$$\left.\begin{aligned} u_{1V}''&=-\frac{iT_2V_2\mathfrak{B}}{2\pi}\frac{4\sin e\cos^2 e(\sin^2 e-\cos^2 e)^3}{\left\{(\sin^2 e-\cos^2 e)^2+4\sin e\cos^2 e\left(\frac{1}{3}-\cos^2 e\right)^{\frac{1}{2}}\right\}^2}e^{i\left(pt-fx-\frac{2\pi H}{\sqrt{3}\,T_2V_2}\sin e\right)},\\ v_{1V}''&=\frac{iT_2V_2\mathfrak{B}}{2\pi}\frac{4\sin e\cos e\left(\frac{1}{3}-\cos^2 e\right)^{\frac{1}{2}}(\sin^2 e-\cos^2 e)^3}{\left\{(\sin^2 e-\cos^2 e)^2+4\sin e\cos^2 e\left(\frac{1}{3}-\cos^2 e\right)^{\frac{1}{2}}\right\}^2}e^{i\left(pt-fx-\frac{2\pi H}{\sqrt{3}\,T_2V_2}\sin e\right)},\end{aligned}\right\}$$

$$\cdots\cdots\cdots\cdots\cdots(144)'$$

$$\left.\begin{aligned} u_{2V}''&=\frac{iT_2V_2\mathfrak{B}}{2\pi}\frac{8\sin^2 e\cos^2 e\left(\frac{1}{3}-\cos^2 e\right)^{\frac{1}{2}}(\sin^2 e-\cos^2 e)^2}{\left\{(\sin^2 e-\cos^2 e)^2+4\sin e\cos^2 e\left(\frac{1}{3}-\cos^2 e\right)^{\frac{1}{2}}\right\}^2}e^{i\left(pt-fx-\frac{2\pi H}{\sqrt{3}\,T_2V_2}\sin e\right)},\\ v_{2V}''&=\frac{iT_2V_2\mathfrak{B}}{2\pi}\frac{8\sin^2 e\cos e\left(\frac{1}{3}-\cos^2 e\right)^{\frac{1}{2}}(\sin^2 e-\cos^2 e)^2}{\left\{(\sin^2 e-\cos^2 e)^2+4\sin e\cos^2 e\left(\frac{1}{3}-\cos^2 e\right)^{\frac{1}{2}}\right\}^2}e^{i\left(pt-fx-\frac{2\pi H}{\sqrt{3}\,T_2V_2}\sin e\right)},\end{aligned}\right\}$$

$$\cdots\cdots\cdots\cdots\cdots(145)'$$

and

$$\left.\begin{aligned} u_{2U} &= -\frac{iT_2V_2\mathfrak{B}}{2\pi}\frac{4\sin^2 e\cos^2 e\left(\frac{1}{3}-\cos^2 e\right)^{\frac{1}{2}}}{\left\{(\sin^2 e-\cos^2 e)^2+4\sin e\cos^2 e\left(\frac{1}{3}-\cos^2 e\right)^{\frac{1}{2}}\right\}}e^{i\left(pt-fx-\frac{2\pi H}{T_2V_2}\sin e\right)},\\ v_{2U} &= \frac{iT_2V_2\mathfrak{B}}{2\pi}\frac{4\sin e\cos^3 e\left(\frac{1}{3}-\cos^2 e\right)^{\frac{1}{2}}}{\left\{(\sin^2 e-\cos^2 e)^2+4\sin e\cos^2 e\left(\frac{1}{3}-\cos^2 e\right)^{\frac{1}{2}}\right\}}e^{i\left(pt-fx-\frac{2\pi H}{T_2V_2}\sin e\right)}, \end{aligned}\right\} \quad \ldots\ldots\ldots\ldots\ldots\ldots (146)'$$

$$\left.\begin{aligned} u_{2U}' &= -\frac{iT_2V_2\mathfrak{B}}{2\pi}\frac{4\sin^2 e\cos^2 e\left(\frac{1}{3}-\cos^2 e\right)^{\frac{1}{2}}}{\left\{(\sin^2 e-\cos^2 e)^2+4\sin e\cos^2 e\left(\frac{1}{3}-\cos^2 e\right)^{\frac{1}{2}}\right\}}e^{i\left(pt-fx-\frac{2\pi H}{T_2V_2}\sin e\right)},\\ v_{2U}' &= -\frac{iT_2V_2\mathfrak{B}}{2\pi}\frac{4\sin e\cos^3 e\left(\frac{1}{3}-\cos^2 e\right)^{\frac{1}{2}}}{\left\{(\sin^2 e-\cos^2 e)^2+4\sin e\cos^2 e\left(\frac{1}{3}-\cos^2 e\right)^{\frac{1}{2}}\right\}}e^{i\left(pt-fx-\frac{2\pi H}{T_2V_2}\sin e\right)}, \end{aligned}\right\} \quad \ldots\ldots\ldots\ldots\ldots\ldots (147)'$$

$$\left.\begin{aligned} u_{1U}'' &= -\frac{iT_2V_2\mathfrak{B}}{2\pi}\frac{16\sin^2 e\cos^4 e(\sin^2 e-\cos^2 e)\left(\frac{1}{3}-\cos^2 e\right)^{\frac{1}{2}}}{\left\{(\sin^2 e-\cos^2 e)^2+4\sin e\cos^2 e\left(\frac{1}{3}-\cos^2 e\right)^{\frac{1}{2}}\right\}^2}e^{i\left(pt-fx-\frac{2\pi H}{T_2V_2}\sin e\right)},\\ v_{1U}'' &= \frac{iT_2V_2\mathfrak{B}}{2\pi}\frac{16\sin^2 e\cos^3 e(\sin^2 e-\cos^2 e)\left(\frac{1}{3}-\cos^2 e\right)}{\left\{(\sin^2 e-\cos^2 e)^2+4\sin e\cos^2 e\left(\frac{1}{3}-\cos^2 e\right)^{\frac{1}{2}}\right\}^2}e^{i\left(pt-fx-\frac{2\pi H}{T_2V_2}\sin e\right)}, \end{aligned}\right\} \quad \ldots\ldots\ldots\ldots\ldots\ldots (148)'$$

$$u_{2U}'' = \frac{iT_2V_2\mathfrak{B}}{2\pi}\frac{32\sin^3 e\cos^4 e\left(\frac{1}{3}-\cos^2 e\right)}{\left\{(\sin^2 e-\cos^2 e)^2+4\sin e\cos^2 e\left(\frac{1}{3}-\cos^2 e\right)^{\frac{1}{2}}\right\}^2}e^{i\left(pt-fx-\frac{2\pi H}{T_2V_2}\sin e\right)},$$

$$v_{2U}''=\frac{iT_2V_2\mathfrak{B}}{2\pi}\frac{32\sin^2e\cos^5e\left(\frac{1}{3}-\cos^2e\right)}{\left\{(\sin^2e-\cos^2e)^2+4\sin e\cos^2e\left(\frac{1}{3}-\cos^2e\right)^{\frac{1}{2}}\right\}^2}e^{i\left(pt-fx-\frac{2\pi H}{T_2V_2}\sin e\right)}.$$

.....(149)′

When the emergency angle is smaller than 54°44′, the expressions (142)′, (143)′, (144)′, (145)′, (146)′, (147)′, (148)′ and (149)′ should be replaced by the following formulae:

$$\left.\begin{aligned}u_{1U}&=\frac{iT_2V_2\mathfrak{B}}{2\pi}\frac{2\sin e\cos^2e(\sin^2e-\cos^2e)}{\left\{(\sin^2e-\cos^2e)^4+16\sin^2e\cos^4e\left(\cos^2e-\frac{1}{3}\right)\right\}^{\frac{1}{2}}}\\&\qquad\times e^{i\left(pt-fx-\frac{2\pi}{\sqrt{3}\,T_2V_2}H\sin e-\varphi\right)},\\v_{1U}&=\frac{iT_2V_2\mathfrak{B}}{2\pi}\frac{2\sin e\cos e\left(\cos^2e-\frac{1}{3}\right)^{\frac{1}{2}}(\sin^2e-\cos^2e)}{\left\{(\sin^2e-\cos^2e)^4+16\sin^2e\cos^4e\left(\cos^2e-\frac{1}{3}\right)\right\}^{\frac{1}{2}}}\\&\qquad\times e^{i\left(pt-fx-\frac{2\pi}{\sqrt{3}\,T_2V_2}H\sin e-\varphi+\frac{\pi}{2}\right)},\end{aligned}\right\}\quad(142)''$$

$$\left.\begin{aligned}u_{1U}'&=\frac{iT_2V_2\mathfrak{B}}{2\pi}\frac{2\sin e\cos^2e(\sin^2e-\cos^2e)}{\left\{(\sin^2e-\cos^2e)^4+16\sin^2e\cos^4e\left(\cos^2e-\frac{1}{3}\right)\right\}^{\frac{1}{2}}}\\&\qquad\times e^{i\left(pt-fx-\frac{2\pi}{\sqrt{3}\,T_2V_2}H\sin e-\varphi\right)},\\v_{1U}'&=-\frac{iT_2V_2\mathfrak{B}}{2\pi}\frac{2\sin e\cos e\left(\cos^2e-\frac{1}{3}\right)^{\frac{1}{2}}(\sin^2e-\cos^2e)}{\left\{(\sin^2e-\cos^2e)^4+16\sin^2e\cos^4e\left(\cos^2e-\frac{1}{3}\right)\right\}^{\frac{1}{2}}}\\&\qquad\times e^{i\left(pt-fx-\frac{2\pi}{\sqrt{3}\,T_2V_2}H\sin e-\varphi+\frac{\pi}{2}\right)},\end{aligned}\right\}\quad(143)''$$

$$u_{1U}''=-\frac{iT_2V_2\mathfrak{B}}{2\pi}\frac{4\sin e\cos^2e(\sin^2e-\cos^2e)^3}{\left\{(\sin^2e-\cos^2e)^4+16\sin^2e\cos^4e\left(\cos^2e-\frac{1}{3}\right)\right\}}\times e^{i\left(pt-fx-\frac{2\pi}{\sqrt{3}\,T_2V_2}H\sin e-2\varphi\right)},$$

$$v_{1U}'' = \frac{iT_2V_2\mathfrak{B}}{2\pi} \frac{4\sin e\cos e\left(\cos^2 e-\frac{1}{3}\right)^{\frac{1}{2}}(\sin^2 e-\cos^2 e)^3}{\left\{(\sin^2 e-\cos^2 e)^4+16\sin^2 e\cos^4 e\left(\cos^2 e-\frac{1}{3}\right)\right\}^{\frac{1}{2}}} \times e^{i\left(pt-fx-\frac{2\pi}{\sqrt{3}\,T_2V_2}H\sin e-2\varphi+\frac{\pi}{2}\right)}, \quad (144)''$$

$$u_{2U}'' = \frac{iT_2V_2\mathfrak{B}}{2\pi} \frac{8\sin^2 e\cos^2 e\left(\cos^2 e-\frac{1}{3}\right)^{\frac{1}{2}}(\sin^2 e-\cos^2 e)^2}{\left\{(\sin^2 e-\cos^2 e)^4+16\sin^2 e\cos^4 e\left(\cos^2 e-\frac{1}{3}\right)\right\}^{\frac{1}{2}}} \times e^{i\left(pt-fx-\frac{2\pi}{\sqrt{3}\,T_2V_2}H\sin e-2\varphi+\frac{\pi}{2}\right)},$$

$$v_{2U}'' = \frac{iT_2V_2\mathfrak{B}}{2\pi} \frac{8\sin e\cos^3 e\left(\cos^2 e-\frac{1}{3}\right)^{\frac{1}{2}}(\sin^2 e-\cos^2 e)^2}{\left\{(\sin^2 e-\cos^2 e)^4+16\sin^2 e\cos^4 e\left(\cos^2 e-\frac{1}{3}\right)\right\}^{\frac{1}{2}}} \times e^{i\left(pt-fx-\frac{2\pi}{\sqrt{3}\,T_2V_2}H\sin e-2\varphi+\frac{\pi}{2}\right)}, \quad (145)''$$

and

$$u_{2U} = -\frac{iT_2V_2\mathfrak{B}}{2\pi} \frac{4\sin^2 e\cos^2 e\left(\cos^2 e-\frac{1}{3}\right)^{\frac{1}{2}}}{\left\{(\sin^2 e-\cos^2 e)^4+16\sin^2 e\cos^4 e\left(\cos^2 e-\frac{1}{3}\right)\right\}^{\frac{1}{2}}} \times e^{i\left(pt-fx-\frac{2\pi H}{T_2V_2}\sin e-\varphi+\frac{\pi}{2}\right)},$$

$$v_{2U} = \frac{iT_2V_2\mathfrak{B}}{2\pi} \frac{4\sin e\cos^3 e\left(\cos^2 e-\frac{1}{3}\right)^{\frac{1}{2}}}{\left\{(\sin^2 e-\cos^2 e)^4+16\sin^2 e\cos^4 e\left(\cos^2 e-\frac{1}{3}\right)\right\}^{\frac{1}{2}}} \times e^{i\left(pt-fx-\frac{2\pi H}{T_2V_2}\sin e-\varphi+\frac{\pi}{2}\right)}, \quad (146)''$$

$$u_{2U}' = -\frac{iT_2V_2\mathfrak{B}}{2\pi} \frac{4\sin^2 e\cos^2 e\left(\cos^2 e-\frac{1}{3}\right)^{\frac{1}{2}}}{\left\{(\sin^2 e-\cos^2 e)^4+16\sin^2 e\cos^4 e\left(\cos^2 e-\frac{1}{3}\right)\right\}^{\frac{1}{2}}} \times e^{i\left(pt-fx-\frac{2\pi H}{T_2V_2}\sin e-\varphi+\frac{\pi}{2}\right)}, \quad (147)''$$

$$v_{2U}' = -\frac{iT_2V_2\mathfrak{B}}{2\pi}\frac{4\sin e\cos^3 e\left(\cos^2 e-\frac{1}{3}\right)^{\frac{1}{2}}}{\left\{(\sin^2 e-\cos^2 e)^4+16\sin^2 e\cos^4 e\left(\cos^2 e-\frac{1}{3}\right)\right\}^{\frac{1}{2}}}\times e^{i\left(pt-fx-\frac{2\pi H}{T_2V_2}\sin e-\varphi+\frac{\pi}{2}\right)},$$

$$\left.\begin{aligned} u_{1U}'' &= -\frac{iT_2V_2\mathfrak{B}}{2\pi}\frac{16\sin^2 e\cos^4 e(\sin^2 e-\cos^2 e)\left(\cos^2 e-\frac{1}{3}\right)^{\frac{1}{2}}}{\left\{(\sin^2 e-\cos^2 e)^4+16\sin^2 e\cos^4 e\left(\cos^2 e-\frac{1}{3}\right)\right\}}\times e^{i\left(pt-fx-\frac{2\pi H}{T_2V_2}\sin e-2\varphi+\frac{\pi}{2}\right)},\\ v_{1U}'' &= -\frac{iT_2V_2\mathfrak{B}}{2\pi}\frac{16\sin^2 e\cos^3 e(\sin^2 e-\cos^2 e)\left(\cos^2 e-\frac{1}{3}\right)}{\left\{(\sin^2 e-\cos^2 e)^4+16\sin^2 e\cos^4 e\left(\cos^2 e-\frac{1}{3}\right)\right\}}\times e^{i\left(pt-fx-\frac{2\pi H}{T_2V_2}\sin e-2\varphi\right)}, \end{aligned}\right\}\quad(148)''$$

$$\left.\begin{aligned} u_{2U}'' &= -\frac{iT_2V_2\mathfrak{B}}{2\pi}\frac{32\sin^3 e\cos^4 e\left(\cos^2 e-\frac{1}{3}\right)}{\left\{(\sin^2 e-\cos^2 e)^4+16\sin^2 e\cos^4 e\left(\cos^2 e-\frac{1}{3}\right)\right\}}\times e^{i\left(pt-fx-\frac{2\pi H}{T_2V_2}\sin e-2\varphi\right)},\\ v_{2U}'' &= -\frac{iT_2V_2\mathfrak{B}}{2\pi}\frac{32\sin^2 e\cos^5 e\left(\cos^2 e-\frac{1}{3}\right)}{\left\{(\sin^2 e-\cos^2 e)^4+16\sin^2 e\cos^4 e\left(\cos^2 c-\frac{1}{3}\right)\right\}}\times e^{i\left(pt-fx-\frac{2\pi H}{T_2V_2}\sin e-2\varphi\right)}, \end{aligned}\right\}\quad(149)''$$

where $$\varphi=\tan^{-1}\left\{\frac{4\sin e\cos^2 e\left(\cos^2 e-\frac{1}{3}\right)^{\frac{1}{2}}}{(\sin^2 e-\cos^2 e)^2}\right\}.\qquad\ldots\ldots\ldots(150)$$

To see the natures of these waves closely, the maximum amplitudes of them corresponding to the magnitude of emergency angle e are given in Table X, XI, XII and XIII and also are shewn graphically in Fig. 12, 13, 14, 15.

We can see the following facts from these tables and figures:

1. When $0° < e < 54°44'$, the energy of the reflected waves of dilatational and distortional types which are generated by the incidence of the transmitted dilatational and distortional waves are accumulated on the free surface of the layer.

2. When $0° < e < 54°44'$, the phases of the waves generated by the incidence of the transmitted waves at the free surface are all different

Table X.

Max. Amp. \ e	0°	10°	20°	30°	40°	45°	50°	52°30′	53°30′
u_{1U}	0	−0·3061	−0·4315	−0·3750	−0·1722	0	0·3057	0·6450	0·9030
$u_{1U'}$	0	−0·3061	−0·4315	−0·3750	−0·1722	0	0·3057	0·6450	0·9030
$u_{1U''}$	0	0·5230	0·4730	0·1873	0·0137	0	−0·0515	−0·3665	−0·8400
$u_{2U''}$	0	0·1542	0·3140	0·2420	0·0511	0	0·1285	0·4350	0·6610

Max. Amp. \ e	54°	54°44′	56°30′	57°30′	60°	65°	70°	80°	90°
u_{1U}	1.106	1·634	0·6115	0·534	0·4330	0·3115	0·2130	0·0588	0
$u_{1U'}$	1.106	1·634	0·6115	0·534	0·4330	0·3115	0·2130	0·0588	0
$u_{1U''}$	−1·36	−3·275	−0·5760	−0·4963	−0·4330	−0·3850	−0·3165	−0·1094	0
$u_{2U''}$	0·7820	0	0·4155	0·4205	0·4330	0·4257	0·3605	0·1266	0

Table XI.

Max. Amp. \ e	0°	10°	20°	30°	40°	45°	50°	52°30′	53°30′
v_{1U}	0	−0·2480	−0·3405	−0·2790	−0·1133	0	0·1345	0·2040	0·2170
$v_{1U'}$	0	0·2480	0·3405	0·2790	0·1133	0	−0·1345	−0·2040	−0·2170
$v_{1U''}$	0	−0·4237	−0·3735	−0·1396	−0·0090	0	0·0226	0·1160	0·2015
$v_{2U''}$	0	0·8746	0·8615	0·4190	0·0610	0	0·1080	0·3330	0·4895

Max. Amp. \ e	54°	54°44′	56°30′	57°30′	60°	65°	70°	80°	90°
v_{1U}	0·2075	0	0·1875	0·2105	0·2500	0·2905	0·2893	0·1867	0
$v_{1U'}$	−0·2075	0	−0·1875	−0·2105	−0·2500	−0·2905	−0·2893	−0·1867	0
$v_{1U''}$	0·2550	0	0·1760	0·1960	0·2500	0·3580	0·4300	0·3470	0
$v_{2U''}$	0·5690	0	0·2750	0·2680	0·2500	0·1987	0·1315	0·0223	0

Table XII.

Max. Amp. \ e	0°	10°	20°	30°	40°	45°	50°	52°30′	53°30′
u_{2U}	0	−0·0902	−0·2865	−0·4850	−0·6430	−0·7071	−0·7630	−0·7600	−0·7110
u_{2U}'	0	−0·0902	−0·2865	−0·4850	−0·6430	−0·7071	−0·7630	−0·7600	−0·7110
u_{1U}''	0	0·3175	0·7210	0·7285	0·3450	0	−0·6100	−1·235	−1·6
u_{2U}''	0	−0·0937	−0·4785	−0·9380	−1·286	−1·4142	−1·517	−1·46	−1·26

Max. Amp. \ e	54°	54°44′	56°30′	57°30′	60°	65°	70°	80°	90°
u_{2U}	−0·6370	0	−0·4420	−0·4535	−0·4330	−0·3455	−0·2420	−0·0679	0
u_{2U}'	−0·6370	0	−0·4420	−0·4535	−0·4330	−0·3455	−0·2420	−0·0679	0
u_{1U}''	−1·752	0	−0·6480	−0·5730	−0·4330	−0·2300	−0·1102	−0·0081	0
u_{2U}''	−1·008	0	0·4690	0·4845	0·4330	0·2630	0·1260	0·00934	0

Table XIII.

Max. Amp. \ e	0°	10°	20°	30°	40°	45°	50°	52°30′	53°30′
v_{2U}	0	0·5119	0·7875	0·8400	0·7660	0·7071	0·6410	0·5820	0·5270
v_{2U}'	0	−0·5119	−0·7875	−0·8400	−0·7660	−0·7071	−0·6410	−0·5820	−0·5270
v_{1U}''	0	0·2575	0·5690	0·5423	0·2265	0	−0·2680	−0·3910	−0·3845
v_{2U}''	0	−0·5310	−1·313	−1·625	−1·532	−1·4142	−1·275	−1·12	−0·9315

Max. Amp. \ e	54°	54°44′	56°30′	57°30′	60°	65°	70°	80°	90°
v_{2U}	0·4630	0	0·2925	0·2885	0·2500	0·1613	0·0883	0·0119	0
v_{2U}'	−0·4630	0	−0·2925	−0·2885	−0·2500	−0·1613	−0·0883	−0·0119	0
v_{1U}''	−0·3280	0	0·1983	0·2260	0·2500	0·2145	0·1496	0·02165	0
v_{2U}''	−0·7325	0	0·3110	0·3085	0·2500	0·1226	0·0459	0·00165	0

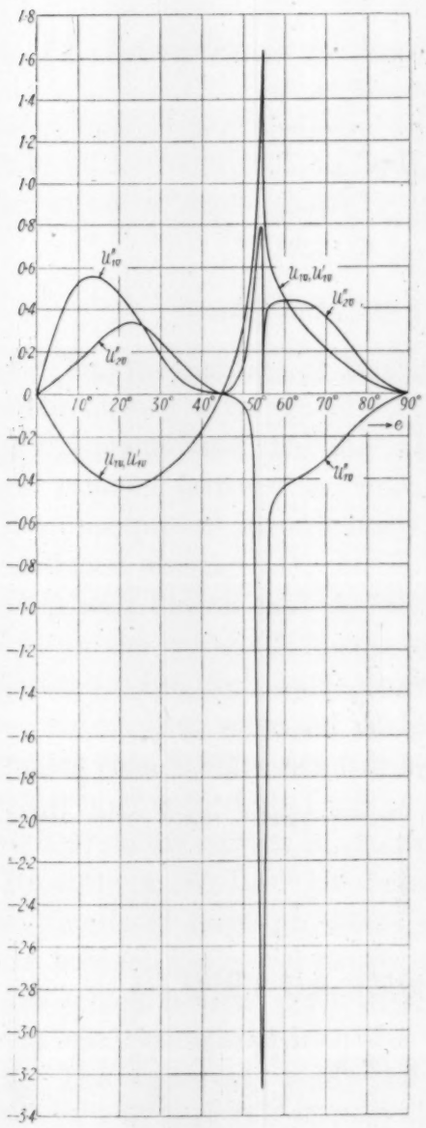

Fig. 12.

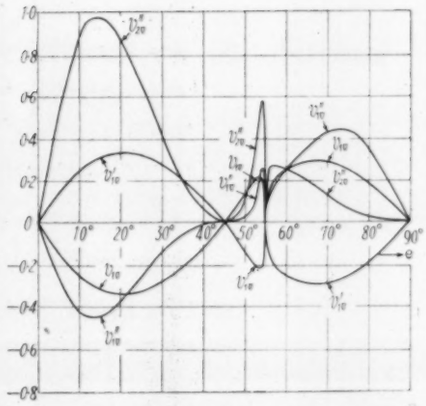

Fig. 13.

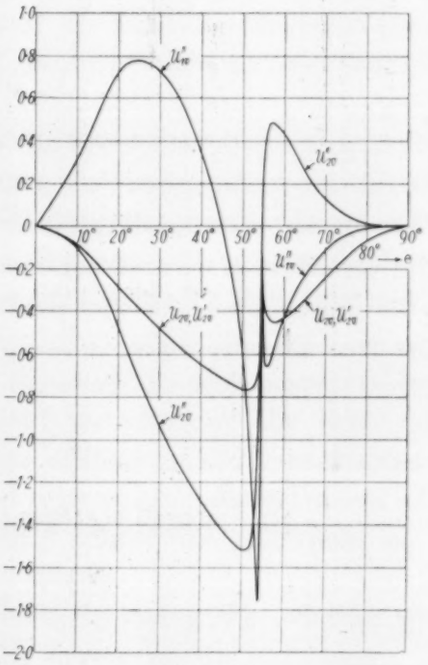

Fig. 14.

from the phase of the primary wave of distortional type incident to the lower boundary of the two solids, and the magnitudes of these differences vary with the magnitudes of e, V_2, T_2 and H.

3. When $e=0°$ and $e=90°$, there exist no transmitted waves in the upper layer, and therefore the free surface does not move.

4. When $e=45°$, no transmitted dilatational wave in the layer exists, and therefore the free surface does not move.

5. When $e=54°44'$, and the transmitted dilatational wave is incident to the free surface, the surface of the layer does only move horizontally

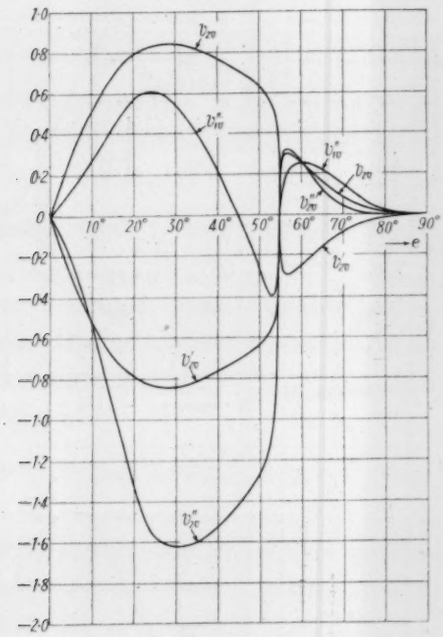

Fig. 15.

in the direction of x, and not move in the direction of y.

6. When $e=54°44'$ and the transmitted distortional wave is incident to the free surface, there is no wave in the upper layer and therefore the free surface does not move.

---

10. 不連續面が彈性波の傳播に及ぼす影響 (I)

地震研究所 西村源六郎 金井清

彈性體がその不連續面でお互に自由に辷り得るとし，全く摩擦の影響がないとした時，その附近ではどの様な彈性波が生ずるものであるかを先づ研究した．次に一つの表面層を有する半無限彈性體内を傳播する波が表面にあたつた時，表面にはどの様な波が起されるかを檢べた．(勿論表面層と半無限體との境では全く摩擦はなく自由に辷り得るものとした.)

計算の結果は可なり面白い彈性波生成に關する性質を示してゐるが，殊に二つの物質がその密度彈性係數が全く同じ時でも，その境で辷り得るとした時には，その境で色々彈性波理論上面白い生成波のある事を知つた．實際上地殼内部に不連續面があるとしても，その面で完全に兩物質が密着してゐるか如何かは分らない事であり或は多少の摩擦が存在してゐて辷り得るかも知れない故，この意味から云つても，その極端である全く摩擦がないとして彈性波の生成を研究するのも無益な事でなく又彈性理論上から云つても面白い事と思ひ，敢て本研究を始めてみた．

11. *Amplitude of Rayleigh Waves on the Surface of a Stratified Medium.*

By Takeo SUZUKI,

Seismological Institute.

(Read Feb. 21, 1933.—Received March 20, 1933.)

1. The propagation of Rayleigh-type waves on the stratified surface has been already investigated by J.I'A. Bromwich[1] and A.E.H. Love[2] under the assumption that the media are incompressible. However, the general relation between the thickness of the layer and the wave velocity has been completely investigated by K. Sezawa[3] without any assumption as mentioned above.

It is well known that the ratio of the horizontal displacement to the vertical on the surface is always constant and independent of the wave length for the Rayleigh waves propagated along the surface of semi-infinite elastic body. But, when the medium is covered with a superficial layer, the matter may become somewhat different. After K. Sezawa's method, the writer intends to study how the ratio of the horizontal displacement to the vertical on the surface is affected by the existence of a superficial layer.

Recently A. W. Lee[4] has investigated the effect of the layer upon the amplitude of Rayleigh waves on the surface in order to discuss the relation between geological structure and microseismic disturbances. But, the case which he has dealt with is that where the thickness of the layer is small compared with the wave length.

2. The writer will study the problem by using the solution given by Sezawa and here the method will be shown in the following. The origin of coordinates is taken on the lower boundary of the layer of thickness H and let the axis of y vertically upwards and the axis of x in the direction of propagation of the waves. Quantities in the upper layer shall be distinguished with (') from those in the lower. The equations of motion in the lower medium are expressed by

1) J.I'A. BROMWICH, *London Math. Soc. Proc.*, **30** (1898).

2) A.E.H. LOVE, *Some Problems of Geodynamics*, (Cambridge, 1926), 165.

3) K. SEZAWA, *Bull. Earthq. Res. Inst.*, **3** (1927), 1-18; *Handb. d. Geophys.*, **4** (1929), 92-94.

4) A.W. LEE, *M.N.R.A.Soc., Geophys. Suppl.*, **3** (1932), 83-105.

$$\left.\begin{aligned}\rho\frac{\partial^2\Delta}{\partial t^2}&=(\lambda+2\mu)\left(\frac{\partial^2\Delta}{\partial x^2}+\frac{\partial^2\Delta}{\partial y^2}\right),\\ \rho\frac{\partial^2\varpi}{\partial t^2}&=\mu\left(\frac{\partial^2\varpi}{\partial x^2}+\frac{\partial^2\varpi}{\partial y^2}\right),\end{aligned}\right\}\quad\cdots\cdots\cdots\cdots\cdots(1)$$

where

$$\Delta=\frac{\partial u}{\partial x}+\frac{\partial v}{\partial y},$$

$$2\varpi=\frac{\partial v}{\partial x}-\frac{\partial u}{\partial y}.$$

u, v=horizontal and vertical components of displacement respectively, ρ=density and λ, μ=Lamé's elastic constants.

The solutions of (1) can be written in the forms:—

$$\left.\begin{aligned}\Delta&=Ae^{ry+i(pt-fx)},\\ 2\varpi&=Be^{sy+i(pt-fx)},\end{aligned}\right\}\quad\cdots\cdots\cdots\cdots\cdots(2)$$

where

$$r^2=f^2-h^2,\qquad s^2=f^2-k^2,$$

$$h^2=\frac{\rho p^2}{\lambda+2\mu},\qquad k^2=\frac{\rho p^2}{\mu}.$$

$\frac{2\pi}{f}$=wave length, and $\frac{2\pi}{p}$=period of the motion.

Let u_1, v_1 the displacement answering to Δ in (2) and satisfying $\varpi=0$, then

$$\left.\begin{aligned}u_1&=\frac{if}{h^2}Ae^{ry+i(pt-fx)},\\ v_1&=-\frac{r}{h^2}Ae^{ry+i(pt-fx)}.\end{aligned}\right\}\quad\cdots\cdots\cdots\cdots\cdots(3)$$

Displacements (u_2, v_2) derived from 2ϖ in (2) and satisfying $\Delta=0$ are given by

$$\left.\begin{aligned}u_2&=\frac{s}{k^2}Be^{sy+i(pt-fx)},\\ v_2&=\frac{if}{k^2}Be^{sy+i(pt-fx)}.\end{aligned}\right\}\quad\cdots\cdots\cdots\cdots\cdots(4)$$

By using the similar notations, the equations of motion in the layer are expressed by

$$\left.\begin{aligned}\rho'\frac{\partial^2\Delta'}{\partial t^2}&=(\lambda'+2\mu')\left(\frac{\partial^2\Delta'}{\partial x^2}+\frac{\partial^2\Delta'}{\partial y^2}\right),\\ \rho'\frac{\partial^2\varpi'}{\partial t^2}&=\mu'\left(\frac{\partial^2\varpi'}{\partial x^2}+\frac{\partial^2\varpi'}{\partial y^2}\right),\end{aligned}\right\}\quad\ldots\ldots\ldots\ldots(5)$$

in which

$$\Delta'=\frac{\partial u'}{\partial x}+\frac{\partial v'}{\partial y},$$

$$2\varpi'=\frac{\partial v'}{\partial x}-\frac{\partial u'}{\partial y}.$$

The solutions of (5), especially in case of $f^2>k'^2$, are expressed by

$$\left.\begin{aligned}\Delta'&=(C\cosh r'y+D\sinh r'y)\,e^{i(pt-fx)},\\ 2\varpi'&=(E\cosh s'y+F\sinh s'y)\,e^{i(pt-fx)},\end{aligned}\right\}\quad\ldots\ldots\ldots\ldots(6)$$

where

$$r'^2=f^2-h'^2\gtrless 0,\qquad s'^2=f^2-k'^2\gtrless 0,$$

$$h'^2=\frac{\rho'p^2}{\lambda'+2\mu'},\qquad k'^2=\frac{\rho'p^2}{\mu'},$$

and A, B, C, D, E, F are arbitrary constants to be determined by the boundary conditions.

From (6) the following expressions will be obtained:—

$$\left.\begin{aligned}u_1'&=\frac{if}{h'^2}(C\cosh r'y+D\sinh r'y)\,e^{i(pt-fx)},\\ v_1'&=-\frac{r'}{h'^2}(C\sinh r'y+D\cosh r'y)e^{i(pt-fx)},\\ u_2'&=\frac{s'}{k'^2}(E\sinh s'y+F\cosh s'y)\,e^{i(pt-fx)},\\ v_2'&=\frac{if}{k'^2}(E\cosh s'y+F\sinh s'y)\,e^{i(pt-fx)}.\end{aligned}\right\}\quad\ldots\ldots\ldots(7)$$

The boundary conditions are expressed by
at $y=0$

$$\left.\begin{aligned}&u_1+u_2=u_1'+u_2',\\ &v_1+v_2=v_1'+v_2',\\ &\lambda\Delta+2\mu\frac{\partial}{\partial y}(v_1+v_2)=\lambda'\Delta'+2\mu'\frac{\partial}{\partial y}(v_1'+v_2'),\\ &\mu\left[\frac{\partial}{\partial y}(u_1+u_2)+\frac{\partial}{\partial x}(v_1+v_2)\right]=\mu'\left[\frac{\partial}{\partial y}(u_1'+u_2')+\frac{\partial}{\partial x}(v_1'+v_2')\right],\end{aligned}\right\}\quad(8)$$

at $y=H$

$$\left.\begin{aligned} &\lambda'\Delta'+2\mu'\frac{\partial}{\partial y}(v_1'+v_2')=0,\\ &\frac{\partial}{\partial y}(u_1'+u_2')+\frac{\partial}{\partial x}(v_1'+v_2')=0. \end{aligned}\right\} \quad \cdots\cdots\cdots\cdots(9)$$

On substitution of (3), (4), and (7), assuming that $\lambda=\mu$, $\lambda'=\mu'$ and $\rho=\rho'$, the conditions of (8) and (9) become

$$\left.\begin{aligned} &\frac{if}{h^2}A+\frac{s}{k^2}B=\frac{if}{h'^2}C+\frac{s'}{k'^2}F,\\ &-\frac{r}{h^2}A+\frac{if}{k^2}B=-\frac{r'}{h'^2}D+\frac{if}{k'^2}E,\\ &\frac{f^2-3r^2}{h^2}A+2\frac{ifs}{k^2}B=\frac{\mu'}{\mu}\left[\frac{f^2-3r'^2}{h'^2}C+\frac{2ifs'}{k'^2}F\right],\\ &\frac{2ifr}{h^2}A+\frac{s^2+f^2}{k^2}B=\frac{\mu'}{\mu}\left[\frac{2ifr'}{h'^2}D+\frac{f^2+s'^2}{k'^2}E\right]. \end{aligned}\right\} \quad \cdots\cdots(10)$$

$$\left.\begin{aligned} &(k'^2-2f^2)(C\cosh r'H+D\sinh r'H)+\frac{2ifs'}{3}(E\sinh s'H+F\cosh s'H)=0,\\ &\frac{2ifr'}{h'^2}(C\sinh r'H+D\cosh r'H)+\frac{s'^2+f^2}{k'^2}(E\cosh s'H+F\sinh s'H)=0. \end{aligned}\right\}$$

$$\cdots\cdots\cdots\cdots\cdots\cdots\cdots\cdots\cdots\cdots\cdots\cdots\cdots\cdots(11)$$

From (10)

$$\left.\begin{aligned} &\frac{\mu'}{\mu}C=PA+\frac{ifs}{3k^2}QB,\\ &\frac{s'}{f}\frac{\mu'}{\mu}F=3iRA+\frac{s}{f}SB,\\ &-\frac{\mu'}{\mu}E=\frac{3ifr}{k^2}QA-PB,\\ &\frac{r'}{f}\frac{\mu'}{\mu}D=\frac{r}{f}SA-i\frac{R}{3}B, \end{aligned}\right\} \quad \cdots\cdots\cdots\cdots(12)$$

where

$$P=1-\frac{2f^2}{k^2}\left(1-\frac{\mu'}{\mu}\right), \qquad Q=2\left(1-\frac{\mu'}{\mu}\right),$$

$$R=\frac{2f^2}{k^2}\left(1-\frac{\mu'}{\mu}\right), \qquad S=1+\frac{2f^2}{k^2}\left(1-\frac{\mu'}{\mu}\right).$$

Substituting (12), the first equation of (11) reduces to

$$\xi A + i\eta B = 0, \quad \ldots\ldots\ldots\ldots\ldots\ldots\ldots\ldots (13)$$

in which

$$\left.\begin{aligned} \xi &= \left(\frac{k'^2}{f^2} - 2\right)\left[P\cosh r'H + \frac{r}{r'} S \sinh r'H\right] \\ &\quad - 2\left[-\frac{s'r}{k^2} Q \sinh s'H + R\cosh s'H\right], \\ 3\eta &= \left(\frac{k'^2}{f^2} - 2\right)\left[\frac{fs}{k^2} Q\cosh r'H - \frac{f}{r'} R \sinh r'H\right] \\ &\quad + 2\left[\frac{s'}{f} P \sinh s'H + \frac{s}{f} S\cosh s'H\right]. \end{aligned}\right\} \quad (14)$$

The horizontal and the vertical component of the displacement on the surface is obtained by putting $y = H$ in (7), that is

$$\left.\begin{aligned} u_1' + u_2' &= \frac{s'}{k'^2 - 2f^2}\left(E\sinh s'H + F\cosh s'H\right) e^{i(pt - fx)}, \\ v_1' + v_2' &= -\frac{1}{2if}\left(E\cosh s'H + F\sinh s'H\right) e^{i(pt - fx)}. \end{aligned}\right\} \quad \ldots\ldots (15)$$

Accordingly the ratio of the horizontal displacement to the vertical on the surface is given by

$$\frac{u_1' + u_2'}{v_1' + v_2'} = i\frac{\sqrt{1 - \frac{k'^2}{f^2}}}{1 - \frac{k'^2}{2f^2}} \cdot \frac{\frac{E}{F}\tanh s'H + 1}{\frac{E}{F} + \tanh s'H}, \quad \ldots\ldots\ldots (16)$$

where

$$\frac{E}{F} = \frac{s'}{f} \cdot \frac{\frac{3fr}{k^2} Q - P\frac{\xi}{\eta}}{-3R - \frac{s}{f} S\frac{\xi}{\eta}}. \quad \ldots\ldots\ldots\ldots (17)$$

When $k'^2 > f^2 > h'^2$, the solutions subjected to the boundary conditions will be obtained if $\cos s'y$ and $\sin s'y$ are taken instead of $\cosh s'y$ and $\sinh s'y$; and when $h'^2 > f^2$, similarly $\cos r'y$ and $\sin r'y$ shall be taken instead of $\cosh r'y$ and $\sinh r'y$. For these cases the ratio is expressed by

$$\left.\begin{aligned} \frac{u_1' + u_2'}{v_1' + v_2'} &= i\frac{\sqrt{\frac{k'^2}{f^2} - 1}}{1 - \frac{k'^2}{2f^2}} \cdot \frac{-\frac{E}{F}\tan s'H + 1}{\frac{E}{F} + \tan s'H}, \end{aligned}\right\}$$

where

$$\left.\begin{aligned}\frac{E}{F}=\frac{s'}{f}\cdot\frac{\dfrac{3fr}{k^2}Q-P\dfrac{\xi}{\eta}}{-3R-\dfrac{s}{f}S\dfrac{\xi}{\eta}}.\end{aligned}\right\}\quad\ldots\ldots(18)$$

When $\frac{s'}{f}$ becomes zero, (16) and (18) reduce to the same expression.

Thus the value of $\frac{u}{v}$ on the surface is not always constant but a function of wave length.

3. Since the relation between the velocity of Rayleigh waves and $\frac{L}{H}$, L being the wave length, has been already completely investigated by K. Sezawa for the cases $\mu=2\mu'$, $\mu=3\mu'$, $\mu=4\mu'$, and $\mu=5\mu'$, the value of $\frac{u}{v}$ is easily obtained from the formulas expressed in (16) or (18) for each case. The results of numerical calculation are shown in Table I—IV and plotted in Fig. 1. In these tables the value of $\frac{p}{f}$ corresponding to $\frac{L}{H}$ is taken from the curves of dispersion given by K. Sezawa.

Table I. ($\mu=2\mu'$)

$\frac{L}{H}$	$\frac{p}{f}$	$\frac{u}{v}$
0	$0{\cdot}9194\sqrt{\frac{\mu'}{\rho}}$	0·6811
1·0	0·929	0·6657
1·5	0·953	0·6563
2·08	1·000	0·766
2·5	1·035	0·678
3·0	1.075	0·688
4·0	1·155	0·737
6·0	1·215	0·763
10·0	1·255	0·808
15·0	1·2714	0·8135
20·0	1·285	0 784
∞	1·301	0·684

Table II. ($\mu=3\mu'$)

$\frac{L}{H}$	$\frac{p}{f}$	$\frac{u}{v}$
0	$0{\cdot}9194\sqrt{\frac{\mu'}{\rho}}$	0·6811
1·0	0·930	0·665
1·5	0·956	0·659
1·854	1·000	0·731
2·5	1·076	0·678
3·0	1·1445	0·707
4·0	1·261	0·793
6·0	1·373	0·945
10·0	1·470	0·979
15·0	1·510	0·942
20·0	1·535	0·868
∞	1·593	0·682

Table III. ($\mu=4\mu'$)

$\frac{L}{H}$	$\frac{p}{f}$	$\frac{u}{v}$
0	$0{\cdot}9194\sqrt{\frac{\mu'}{\rho}}$	0·6811
1·0	0·930	0·667
1·5	0·956	0·6772
1·840	1·000	0·7166
2·5	1·120	0·6202
3·0	1·216	0·6202
4·0	1·365	0·744
4·48	1·414	0·8933
6·0	1·515	1·071
10·0	1·648	1·126
15·0	1·704	1·0301
18·0	1·726	0·9826
20·0	1·736	0·9588
∞	1·840	0·6830

Table IV. ($\mu=5\mu'$)

$\frac{L}{H}$	$\frac{p}{f}$	$\frac{u}{v}$
0	$0{\cdot}9194\sqrt{\frac{\mu'}{\rho}}$	0·6811
1·0	0·930	0·6682
1·5	0·956	0·6822
1·753	1·000	0·7152
2·5	1·146	0·5822
3·0	1·276	0·4851
3·66	1·414	0·511
4·00	1·465	0·6089
6·00	1·633	1·186
8·152	1·732	1·299
10·0	1·794	1·2533
15·0	1·891	1·0999
20·0	1·920	0·9943
∞	2·057	0·6866

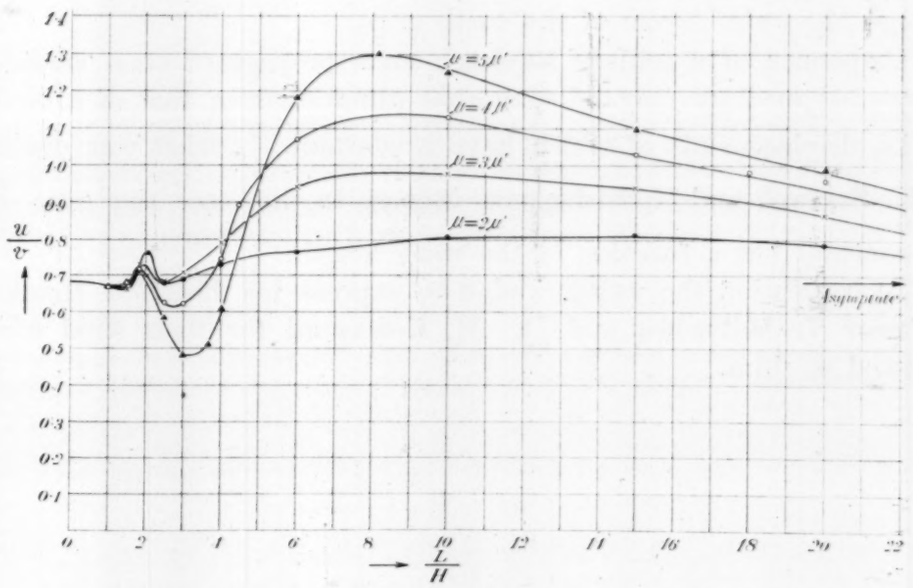

Fig. 1.

In the case where the wave length is very small compared with the thickness, $\frac{u}{v}$ approaches that of simple Rayleigh waves, that is 0·6811, as $\tanh s'H$ tends to unity in the expression of (16). When the wave length becomes very large compared with the thickness, again $\frac{u}{v}$ tends asymptotically to the value of simple Rayleigh waves. In the intermediate case where the wave length is comparable with the thickness, the velocity of propagation and the ratio of amplitude are much affected by the existence of a superficial layer.

According to the observations obtained hitherto, the ratio of the horizontal movement to the vertical of Rayleigh waves described in the seismographic records is in most cases larger than the theoretical value for simple Rayleigh waves. It may be remarked that this discrepancy may be to a certain degree explained under the plausible hypothesis of the stratified structure of the earth crust.

Next, it is still in question whether the microseismic movements with a period of a few seconds which are often observed at various places, consist mainly of progressive disturbances or of stationary vibrations proper to each locality[5]. Hence, at the present it may be safe to refrain from discussing the problems of microseisms as surface waves transmitted through the outer layers of the earth crust.

Dispersion of a solitary Rayleigh wave propagated on a surface of a stratified medium may be somewhat different from that of a kind of shocks, displacements of which have a constant $\frac{u}{v}$, what was discussed by K. Sezawa[6] and G. Nishimura, because in this case the ratio $\frac{u}{v}$ is not constant but a function of the wave length.

In conclusion the writer wishes to express his heartfelt thanks to Professor T. Matuzawa and Dr. H. Kawasumi for their kind advices bestowed on him.

5) For example, F. OMORI, *Bull. Imp. Earthq. Invest. Commit.*, **3** (1909). T. MATUZAWA, *Journ. Fac. Sci., Imp. Univ.*, Tôkyô, Sec. II, **2** (1927), 5.

6) K. SEZAWA and G. NISHIMURA, *Bull. Earthq. Res. Inst.*, **8** (1930), 330-335.

11. 表面層のある場合の表面に於けるレーリー波の振幅

地震學教室 鈴 木 武 夫

半無限彈性體に表面層がある場合に於けるレーリー波の傳播に就ては既にプロムウィッチ，ラブ等により論ぜられ最近には妹澤博士によりて詳しく研究せられた．筆者は妹澤博士によるレーリー波の分散の結果を用ひて表面に於ける變位の水平成分と鉛直成分との比を波長と層の厚さとの函數として計算した．この比は表面層が下層より軟い場合には波長が層の厚さに比して非常に短い場合に於ても又非常に長い場合に於ても共に普通のレーリー波の値に漸近的に近い値を示すが，波長と層の厚さとが同程度である場合には概して云へば普通のレーリー波のそれよりも大なる値となる．

12. *On Stresses in the Interior and in the Vicinity of a Spherical Inclusion in a Gravitating Semi-infinite Elastic Solid. (I)*

By Genrokuro NISHIMURA and Takeo TAKAYAMA,

Earthquake Research Institute.

(Read Dec., 20, 1932.—Received March 20, 1933.)

1. It is quite reasonable to suppose that the interior of the earth's crust consists of heterogeneous materials if the stress accumulation is a necessary condition for the occurrence of an earthquake, seeing that the stresses are accumulated mainly in the vicinity of common boundaries of contiguous materials having different physical properties. Thus it may be of some importance to study the effects of heterogeneous inclusions upon stress distribution in the interior of the crust of the earth. For this purpose, we shall investigate the stress distribution in the interior and in the neighbourhood of a spherical inclusion in a gravitating semi-infinite elastic solid, assuming that the state of the gravitating semi-infinite medium is one of plane strain[1], and that the elasticity and the density of the spherical inclusion differ from those of the surrounding medium. The study of stress distribution in the vicinity of a spherical cavity in a gravitating semi-infinite elastic solid, which is a special case of the present study, has already been carried out by us[2].

2. In the present study, we use the spherical coordinates (r, θ, ϕ) and the rectangular (x, y, z), the relations between them being

$$\left.\begin{aligned} x &= r\cos\theta\sin\phi, \\ y &= r\cos\theta\cos\phi, \\ z &= r\sin\theta. \end{aligned}\right\} \quad \cdots\cdots\cdots\cdots\cdots\cdots \quad (1)$$

Fig. 1 shows this relation. Let the origin o of the coordinates be at the centre of a spherical inclusion of radius a, and the distance from o to the upper horizontal surface of the solid be ξ. u, v, w indicate the

1) The problem of plane stress will be discussed on another occasion.

2) G. NISHIMURA and T. TAKAYAMA, "On the Effect of a Spherical Cavity on the Equilibrium of the Gravitating Semi-infinite Elastic Solid," *Bull. Earthq. Res. Inst.*, 10 (1932), 352–383.

components of displacement in the directions of radius r, colatitude θ, and azimuth ϕ respectively, and $\widehat{rr}$, $\widehat{\theta\theta}$, $\widehat{\phi\phi}$, the normal components of traction, $\widehat{r\theta}$, $\widehat{r\phi}$, $\widehat{\theta\phi}$ the shearing components of stress separately in regard to the spherical coordinates in the interior of the semi-infinite elastic solid of which the density is ρ and the gravity constant is g. Again, let u', v', w' be the components of displacement and $\widehat{rr}'$, $\widehat{\theta\theta}'$, $\widehat{\phi\phi}'$, $\widehat{r\theta}'$, $\widehat{\theta\phi}'$ the components of stress in the interior of the spherical inclusion of which the density is ρ'.

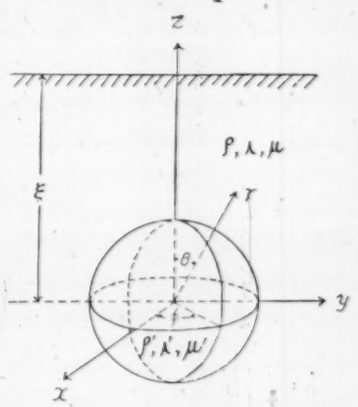

Fig. 1.

Now the top surface ($z=\xi$) of the solid is horizontal, and therefore there is no variation of azimuthal components of displacement and stress. Then the stress equations of the equilibrium of gravitating semi-infinite solid and that of gravitating spherical inclusion are respectively expressed by

$$\left.\begin{aligned}
&\frac{\partial\widehat{rr}}{\partial r}+\frac{1}{r}\frac{\partial\widehat{r\theta}}{\partial\theta}+\frac{1}{r}\left\{2\widehat{rr}-\widehat{\theta\theta}-\widehat{\phi\phi}+\widehat{r\theta}\cot\theta\right\}=\rho g\cos\theta,\\
&\frac{\partial\widehat{r\theta}}{\partial r}+\frac{1}{r}\frac{\partial\widehat{\theta\theta}}{\partial\theta}+\frac{1}{r}\left\{(\widehat{\theta\theta}-\widehat{\phi\phi})\cot\theta+3\widehat{r\theta}\right\}=-\rho g\sin\theta,
\end{aligned}\right\}\quad\ldots\ldots(2)$$

and

$$\left.\begin{aligned}
&\frac{\partial\widehat{rr}'}{\partial r}+\frac{1}{r}\frac{\partial\widehat{r\theta}'}{\partial\vartheta}+\frac{1}{r}\left\{2\widehat{rr}'-\widehat{\theta\theta}'-\widehat{\phi\phi}'+\widehat{r\theta}'\cot\theta\right\}=\rho' g\cos\theta,\\
&\frac{\partial\widehat{r\theta}'}{\partial r}+\frac{1}{r}\frac{\partial\widehat{\theta\theta}'}{\partial\theta}+\frac{1}{r}\left\{(\widehat{\theta\theta}'-\widehat{\phi\phi}')\cot\theta+3\widehat{r\theta}'\right\}=-\rho' g\sin\theta.
\end{aligned}\right\}\quad\ldots\ldots(3)$$

The components of stresses of the medium and the inclusion are respectively expressed in the following forms:

$$\left.\begin{aligned}
\widehat{rr}&=\frac{\lambda}{r^2\sin\theta}\left\{\frac{\partial}{\partial r}(r^2u\sin\theta)+\frac{\partial}{\partial\theta}(rv\sin\theta)\right\}+2\mu\frac{\partial u}{\partial r},\\
\widehat{\theta\theta}&=\frac{\lambda}{r^2\sin\theta}\left\{\frac{\partial}{\partial r}(r^2u\sin\theta)+\frac{\partial}{\partial\theta}(rv\sin\theta)\right\}+2\mu\left\{\frac{1}{r}\frac{\partial v}{\partial\theta}+\frac{u}{r}\right\},\\
\widehat{\phi\phi}&=\frac{\lambda}{r^2\sin\theta}\left\{\frac{\partial}{\partial r}(r^2u\sin\theta)+\frac{\partial}{\partial\theta}(rv\sin\theta)\right\}+2\mu\left\{\frac{v}{r}\cot\theta+\frac{u}{r}\right\},
\end{aligned}\right\}\quad(4)$$

$$\left.\begin{aligned}
\widehat{r\theta} &= \mu\left\{\frac{\partial v}{\partial r}-\frac{v}{r}+\frac{1}{r}\frac{\partial u}{\partial\theta}\right\},\\
\widehat{rr'} &= \frac{\lambda'}{r^2\sin\theta}\left\{\frac{\partial}{\partial r}(r^2u'\sin\theta)+\frac{\partial}{\partial\theta}(rv'\sin\theta)\right\}+2\mu'\frac{\partial u'}{\partial r},\\
\widehat{\theta\theta'} &= \frac{\lambda'}{r^2\sin\theta}\left\{\frac{\partial}{\partial r}(r^2u'\sin\theta)+\frac{\partial}{\partial\theta}(rv'\sin\theta)\right\}+2\mu'\left\{\frac{1}{r}\frac{\partial v'}{\partial\theta}+\frac{u'}{r}\right\},\\
\widehat{\phi\phi'} &= \frac{\lambda'}{r^2\sin\theta}\left\{\frac{\partial}{\partial r}(r^2u'\sin\theta)+\frac{\partial}{\partial\theta}(rv'\sin\theta)\right\}+2\mu'\left\{\frac{v}{r}\cot\theta+\frac{u'}{r}\right\},\\
\widehat{r\theta'} &= \mu'\left\{\frac{\partial v'}{\partial r}-\frac{v'}{r}+\frac{1}{r}\frac{\partial u'}{\partial\theta}\right\},
\end{aligned}\right\} \quad (5)$$

where λ, μ are Lame's elastic constants of the gravitating semiinfinite solid and λ', μ' are those of the spherical inclusion.

In equations (2) and (3), we substitute for the components of stresses the eqations (4) and (5) respectively; and we thus obtain the following equations of equlibrium of solid and inclusion:

$$\left.\begin{aligned}
(\lambda+2\mu)\frac{\partial\Delta}{\partial r}-\frac{2\mu}{r}\frac{\partial\varpi}{\partial\theta}-\frac{2\mu}{r}\varpi\cot\theta &= \rho g\cos\theta,\\
(\lambda+2\mu)\frac{1}{r}\frac{\partial\Delta}{\partial\theta}+2\mu\frac{\partial\varpi}{\partial r}+2\mu\frac{\varpi}{r} &= -\rho g\sin\theta,
\end{aligned}\right\} \quad \cdots\cdots \quad (6)$$

$$\left.\begin{aligned}
(\lambda'+2\mu)\frac{\partial\Delta'}{\partial r}-\frac{2\mu'}{r}\frac{\partial\varpi'}{\partial\theta}-\frac{2\mu'}{r}\varpi'\cot\theta &= \rho' g\cos\theta,\\
(\lambda'+2\mu')\frac{1}{r}\frac{\partial\Delta'}{\partial\theta}+2\mu'\frac{\partial\varpi'}{\partial r}+2\mu' &= -\rho' g\sin\theta,
\end{aligned}\right\} \quad \cdots\cdots \quad (7)$$

where

$$\left.\begin{aligned}
\Delta &= \frac{1}{r^2\sin\theta}\left\{\frac{\partial}{\partial r}(r^2u\sin\theta)+\frac{\partial}{\partial\theta}(rv\sin\theta)\right\},\\
2\varpi &= \frac{\partial v}{\partial r}+\frac{v}{r}-\frac{1}{r}\frac{\partial u}{\partial\theta},
\end{aligned}\right\} \quad \cdots\cdots \quad (8)$$

$$\left.\begin{aligned}
\Delta' &= \frac{1}{r^2\sin\theta}\left\{\frac{\partial}{\partial r}(r^2u'\sin\theta)+\frac{\partial}{\partial\theta}(rv'\sin\partial)\right\},\\
2\varpi' &= \frac{\partial v'}{\partial r}+\frac{v'}{r}-\frac{1}{r}\frac{\partial u'}{\partial\theta}.
\end{aligned}\right\} \quad \cdots\cdots \quad (9)$$

Among the particular solutions satisfying (6) and (7), we take the following solutions which are favourable to the present study:

$$\left.\begin{aligned} \Delta &= \frac{\rho g r}{(\lambda+2\mu)} P_1(\cos\theta), \\ 2\varpi &= 0, \end{aligned}\right\} \quad \ldots\ldots\ldots\ldots\ldots (10)$$

$$\left.\begin{aligned} \Delta' &= \frac{\rho' g r}{(\lambda'+2\mu')} P_1(\cos\theta), \\ 2\varpi' &= 0, \end{aligned}\right\} \quad \ldots\ldots\ldots\ldots\ldots (11)$$

where $P_1(x)$ is the zonal harmonics of the first order.

Next we must obtain the complementary solutions of (6) and (7) which are necessary to satisfy the boundary conditions of the solids. Now we obtain the following equations, using equations (6) and (7), after some reductions:

$$\frac{\partial^2\Delta}{\partial r^2}+\frac{2}{r}\frac{\partial\Delta}{\partial r}+\frac{1}{r^2}\frac{\partial^2\Delta}{\partial\theta^2}+\frac{\cot\theta}{r}\frac{\partial\Delta}{\partial\theta}=0, \quad \ldots\ldots\ldots\ldots (12)$$

$$\frac{\partial^2\Delta'}{\partial r^2}+\frac{2}{r}\frac{\partial\Delta'}{\partial r}+\frac{1}{r^2}\frac{\partial^2\Delta'}{\partial\theta^2}+\frac{\cot\theta}{r}\frac{\partial\Delta'}{\partial\theta}=0. \quad \ldots\ldots\ldots\ldots (13)$$

We obtain the following solutions of (12) and (13):

$$\Delta=\left\{A_0+\frac{A_0'}{r}\right\}P_0(\cos\theta)+\left\{A_1 r+\frac{A_1'}{r^2}\right\}P_1(\cos\theta)$$

$$+\left\{A_2 r^2+\frac{A_2'}{r^3}\right\}P_2(\cos\theta)+\left\{A_3 r^3+\frac{A_3'}{r^4}\right\}P_3(\cos\theta), \quad \ldots\ldots\ldots (14)$$

$$\Delta'=D_0P_0(\cos\theta)+D_1 r P_1(\cos\theta)+D_2 r^2 P_2(\cos\theta)+D_3 r^3 P_3(\cos\theta), \quad (15)$$

where A_0, A_0', A_1, A_1', A_2, A_2', A_3', A_3', D_0, D_1, D_2, D_3, are the arbitrary constants, and $P_0(\cos\theta)$, $P_2(\cos\theta)$, $P_3(\cos\theta)$ are the zonal harmonics of zero, second and third order.

Using (14) and (15) respectively, we obtain the following forms of 2ϖ and $2\varpi'$ which are particular solutions of (6) and (7):

$$2\varpi=-\frac{(\lambda+2\mu)}{\mu}\left\{\frac{A_1 r}{2}-\frac{A_1'}{r^2}\right\}\frac{\partial P_1(\cos\theta)}{\partial\theta}$$

$$-\frac{(\lambda+2\mu)}{\mu}\left\{\frac{A_2 r^2}{3}-\frac{A_2'}{2r^3}\right\}\frac{\partial P_2(\cos\theta)}{\partial\theta}$$

$$-\frac{(\lambda+2\mu)}{\mu}\left\{\frac{A_3 r^3}{4}-\frac{A_3'}{3r^3}\right\}\frac{\partial P_3(\cos\theta)}{\partial\theta}, \quad \ldots\ldots\ldots (16)$$

$$2\varpi'=-\frac{(\lambda'+2\mu')}{\mu'}\frac{D_1 r}{2}\frac{\partial P_1(\cos\theta)}{\partial\theta}$$

$$-\frac{(\lambda'+2\mu')}{\mu'}\frac{D_2r^2}{3}\frac{\partial P_2(\cos\theta)}{\partial\theta}$$
$$-\frac{(\lambda'+2\mu')}{\mu'}\frac{D_3r^2}{4}\frac{\partial P_3(\cos\theta)}{\partial\theta}. \quad \cdots\cdots\cdots(17)$$

Now we find the following two differential equations in relation to u, v, Δ and 2ϖ after some reductions from relations expressed by (8):

$$\frac{\partial^2(r^2u)}{\partial r^2}+\frac{1}{r^2\sin\theta}\frac{\partial}{\partial\theta}\left\{\sin\theta\frac{\partial(r^2u)}{\partial\theta}\right\}=\frac{\partial}{\partial r}(r^2\Delta)-\frac{2r}{\sin\theta}\frac{\partial}{\partial\theta}(\sin\theta\varpi), \quad \cdots(18)$$

$$\frac{\partial}{\partial r}\left\{\frac{r^2\partial(rv\sin\theta)}{\partial r}\right\}+\frac{1}{\sin\theta}\frac{\partial}{\partial\theta}\left\{\sin\theta\frac{\partial(rv\sin\theta)}{\partial\theta}\right\}+2\cot\theta\frac{\partial(r^2u)}{\partial r}$$
$$=\frac{r^2}{\sin\theta}\frac{\partial}{\partial\theta}(\sin^2\theta\Delta)+2\sin\theta\frac{\partial}{\partial r}(r^3\varpi), \quad \cdots\cdots\cdots(19)$$

and also we have the following equations in relation to u', v', Δ' and $2\varpi'$ from the relations expressed by (9):

$$\frac{\partial^2(r^2u')}{\partial r^2}+\frac{1}{r^2\sin\theta}\frac{\partial}{\partial\theta}\left\{\sin\theta\frac{\partial(r^2u')}{\partial\theta}\right\}=\frac{\partial}{\partial r}(r^2\Delta')-\frac{2r}{\sin\theta}\frac{\partial}{\partial\theta}(\sin\theta\varpi'), \quad (20)$$

$$\frac{\partial}{\partial r}\left\{\frac{r^2\partial(rv'\sin\theta)}{\partial r}\right\}+\frac{1}{\sin\theta}\frac{\partial}{\partial\theta}\left\{\sin\theta\frac{\partial(rv'\sin\theta)}{\partial\theta}\right\}+2\cot\theta\frac{\partial(r^2u')}{\partial r}$$
$$=\frac{r^2}{\sin\theta}\frac{\partial}{\partial\theta}(\sin^2\theta\Delta')+2\sin\theta\frac{\partial}{\partial r}(r^3\varpi'). \quad \cdots\cdots\cdots(21)$$

Substituting (10), (14) and (16) for the expressions of Δ and 2ϖ in the equation (18), we obtaion the following particular solutions of (18):

$$r^2u=\frac{3}{10}\frac{\rho gr^4}{(\lambda+2\mu)}P_1(\cos\theta)+\frac{1}{5}\frac{\rho gr^4}{(\lambda+2\mu)}P_3(\cos\theta)$$
$$+\left[\frac{1}{3}A_0r^3+\frac{(\lambda+3\mu)}{2\mu}A_0'r^2\right]P_0(\cos\theta)$$
$$+\left[\frac{(-\lambda+\mu)}{10\mu}r^4A_1-\frac{(\lambda+2\mu)}{\mu}A_1'r\right]P_1(\cos\theta)$$
$$-\left[\frac{\lambda}{7\mu}A_2r^5+\frac{(3\lambda+5\mu)}{6\mu}A_2'\right]P_2(\cos\theta)$$
$$-\left[\frac{(3\lambda+\mu)}{18\mu}A_3r^6+\frac{(2\lambda+3\mu)}{5\mu}\frac{A_3'}{r}\right]P_3(\cos\theta). \quad \cdots\cdots\cdots(22)$$

Next substituting (10), (14), (16) and (22) for the expression of Δ, 2ϖ and r^2u in equation (19), we obtain the particular solution of (19)

in the following forms:

$$rv\sin\theta=\frac{1}{10}\frac{\rho g r^3}{(\lambda+2\mu)}\sin\frac{\partial P_1(\cos\theta)}{\partial\theta}+\frac{1}{15}\frac{\rho g r^3}{(\lambda+2\mu)}\sin\theta\frac{\partial P_3(\cos\theta)}{\partial\theta}$$
$$-\left[\frac{(2\lambda+3\mu)}{10\mu}A_1 r^3+\frac{(\lambda+3\mu)}{2\mu}A_1'\right]\sin\theta\frac{\partial P_1(\cos\theta)}{\partial\theta}$$
$$-\left[\frac{(5\lambda+7\mu)}{42\mu}A_2 r^4+\frac{A_2'}{6r}\right]\sin\theta\frac{\partial P_2(\cos\theta)}{\partial\theta}$$
$$-\left[\frac{(3\lambda+4\mu)}{36\mu}A_3 r^5+\frac{(-\lambda+\mu)}{30\mu}\frac{A_3'}{r^2}\right]\sin\theta\frac{\partial P_3(\cos\theta)}{\partial\theta}. \quad (23)$$

Also substituting (11), (15) and (17) in the right-hand of the equation (20), we obtain the particular solutions $r^2 u'$ which are favourable for the spherical inclusion in the following forms:

$$r^2 u'=\frac{3}{10}\frac{\rho' g r^4}{(\lambda'+2\mu')}P_1(\cos\theta)+\frac{1}{5}\frac{\rho' g r^4}{(\lambda'+2\mu')}P_3(\cos\theta)$$
$$+\frac{1}{3}D_0 r^3 P_0(\cos\theta)+\frac{(-\lambda+\mu)}{10\mu}r^4 D_1 P_1(\cos\theta)$$
$$-\frac{\lambda}{7\mu}D_2 r^5 P_2(\cos\theta)-\frac{(3\lambda+\mu)}{18\mu}D_3 r^6 P_3(\cos\theta). \quad \ldots\ldots\ldots(24)$$

Using (11), (15), (17) and (24), we obtain the following particular solutions of $rv'\sin\theta$ from the equation (21):

$$rv'\sin\theta=\frac{1}{10}\frac{\rho' g r^3}{(\lambda'+2\mu')}\sin\theta\frac{\partial P_1(\cos\theta)}{\partial\theta}+\frac{1}{15}\frac{\rho' g r^3}{(\lambda'+2\mu')}\sin\theta\frac{\partial P_3(\cos\theta)}{\partial\theta}$$
$$-\frac{(2\lambda'+3\mu')}{10\mu'}D_1 r^3\sin\theta\frac{\partial P_1(\cos\theta)}{\partial\theta}$$
$$-\frac{(5\lambda'+7\mu')}{42\mu'}D_2 r^4\sin\theta\frac{\partial P_2(\cos\theta)}{\partial\theta}$$
$$-\frac{3\lambda'+4\mu'}{36\mu}P_3 r^5\sin\theta\frac{\partial P_3(\cos\theta)}{\partial\theta}. \quad \ldots\ldots\ldots\ldots\ldots\ldots(25)$$

The complementary solutions of (18) and (19) and (20), (21), are easily obtained in the following forms:

$$r^2 u=-C_0' P_0(\cos\theta)+\left[C_1 r^2-\frac{2}{r}C_1'\right]P_1(\cos\theta)$$
$$+\left[2r^3 C_2-\frac{3}{r^2}C_2'\right]P_2(\cos\theta)+\left[3r^4 C_3-\frac{3C_4'}{r^3}\right]P_3(\cos\theta), \quad \ldots.(26)$$

$$rv\sin\theta=\left[C_1r+\frac{C_1'}{r^2}\right]\sin\theta\frac{\partial P_1(\cos\theta)}{\partial\theta}+\left[C_2r^2+\frac{C_2'}{r^3}\right]\sin\theta\frac{\partial P_2(\cos\theta)}{\partial\theta}$$

and
$$+\left[C_3r^3+\frac{C_3'}{r^4}\right]\sin\theta\frac{\partial P_3(\cos\theta)}{\partial\theta}, \quad \ldots\ldots\ldots\ldots\ldots\ldots\ldots\ldots(27)$$

$$r^2u'=E_1r^2P_1(\cos\theta)+2E_2r^3P_2(\cos\theta)+3E_3r^4P_3(\cos\theta), \quad \ldots\ldots\ldots(28)$$

$$rv'\sin\theta=E_1r\sin\theta\frac{\partial P_1(\cos\theta)}{\partial\theta}+E_2r^2\sin\theta\frac{\partial P_2(\cos\theta)}{\partial\theta}$$

$$+E_3r^3\sin\theta\frac{\partial P_3(\cos\theta)}{\partial\theta}. \quad \ldots\ldots\ldots\ldots\ldots\ldots\ldots(29)$$

The general solutions of u, v and u', v' expressed by (22), (23), (26), (27) and (24), (25), (28), (29) satisfy, of course, the equations of equilibrium of elastic gravitating solid (6) and (7) respectively. Using these general expressions of displacements, we find the general expressions of components of stresses $\widehat{rr}$, $\widehat{\theta\theta}$, $\widehat{\phi\phi}$, $\widehat{r\theta}$ and $\widehat{rr'}$, $\widehat{\theta\theta'}$, $\widehat{\phi\phi'}$, $\widehat{r\theta'}$ as in the following forms by the relations of (4) and (5):

$r\geqq a$:—

$$\widehat{rr}=\left[\left(\lambda+\frac{2\mu}{3}\right)A_0+\frac{\lambda A_0'}{r}+\frac{4\mu}{r^3}C_0'\right]P_0(\cos\theta)$$

$$+\left[\frac{(5\lambda+6\mu)}{5(\lambda+2\mu)}\rho gr+\frac{(3\lambda+2\mu)}{5}A_1r+\frac{(3\lambda+4\mu)}{r^2}A_1'+\frac{12\mu}{r^4}C_1'\right]P_1(\cos\theta)$$

$$+\left[\frac{\lambda}{7}A_2r^2+\frac{(9\lambda+10\mu)}{3r^3}A_2'+4\mu C_2+\frac{24\mu}{r^5}C_2'\right]P_2(\cos\theta)$$

$$+\left[\frac{4\mu}{5(\lambda+2\mu)}\rho gr-\frac{(3\lambda+4\mu)}{9}A_3r^3\right.$$

$$\left.+\frac{(17\lambda+18\mu)}{5r^4}A_3'+12\mu C_3r+\frac{40\mu}{r_6}C_3'\right]P_3(\cos\theta), \quad \ldots(30)$$

$$\widehat{\theta\theta}=\left[\left(\lambda+\frac{2\mu}{3}\right)A_0+\frac{(2\lambda+3\mu)}{r}A_0'-\frac{2\mu}{r^3}C_0'\right]P_0(\cos\theta)$$

$$+\left[\frac{(5\lambda+3\mu)}{5(\lambda+2\mu)}\rho gr-\frac{(\lambda+4\mu)}{r^2}A_1'+\frac{(4\lambda+\mu)}{5}A_1r+\frac{2\mu}{r}C_1-\frac{4\mu}{r^4}C_1'\right]P_1(\cos\theta)$$

$$+\left[\frac{5}{7}\lambda A_2r^2-\frac{5\mu}{3r^3}A_2'+4\mu C_2-\frac{6\mu}{r^5}C_2'\right]P_2(\cos\theta)$$

$$+\left[\frac{2\mu}{5(\lambda+2\mu)}\rho gr+\frac{(6\lambda-\mu)}{9}A_3r^3+\frac{(\lambda-6\mu)}{5r^4}A_3'+6\mu C_3r-\frac{8\mu}{r^6}C_3'\right]P_3(\cos\theta)$$

$$+\left[\frac{\mu}{5(\lambda+2\mu)}\rho g r-\frac{(2\lambda+3\mu)}{5}A_1 r-\frac{(\lambda+3\mu)}{r^2}A_1'+\frac{2\mu}{r}C_1+\frac{2\mu}{r^4}C_1'\right]\frac{\partial^2 P_1(\cos\theta)}{\partial\theta^2}$$

$$+\left[-\frac{(5\lambda+7\mu)}{21}A_2 r^2-\frac{\mu}{3}\frac{A_2'}{r^2}+2\mu C_2+\frac{2\mu}{r^5}C_2'\right]\frac{\partial^2 P_2(\cos\theta)}{\partial\theta^2}$$

$$+\left[\frac{2\mu}{15(\lambda+2\mu)}\rho g r-\frac{(3\lambda+4\mu)}{18}A_3 r^3+\frac{(\lambda-\mu)}{15r^4}A_3'+2\mu C_3 r\right.$$

$$\left.+\frac{2\mu}{r^6}C_3'\right]\frac{\partial^2 P_3(\cos\theta)}{\partial\theta^2}, \quad \ldots\ldots(31)$$

$$\widehat{\phi\phi}=\left[\left(\lambda+\frac{2\mu}{3}\right)A_0+\frac{(2\lambda+3\mu)}{r}A_0'-\frac{2\mu}{r^3}C_0'\right]P_0(\cos\theta)$$

$$+\left[\frac{(5\lambda+3\mu)}{5(\lambda+2\mu)}\rho g r+\frac{(4\lambda+\mu)}{5}A_1 r-\frac{(\lambda+4\mu)}{r^2}A_1'+\frac{2\mu}{r}C_1-\frac{4\mu}{r^4}C_1'\right]P_1(\cos\theta)$$

$$+\left[\frac{5}{7}\lambda A_2 r^2-\frac{5\mu}{3r^2}A_2'+4\mu C_2-\frac{6\mu}{r^5}C_2'\right]P_2(\cos\theta)$$

$$+\left[\frac{2}{5}\frac{\mu\rho g r}{(\lambda+2\mu)}+\frac{(6\lambda-\mu)}{9}A_3 r^3+\frac{(\lambda-6\mu)}{5r^4}A_3'+6\mu C_3 r-\frac{8\mu}{r^6}C_3'\right]P_3(\cos\theta)$$

$$+\left[\frac{\mu\rho g r}{5(\lambda+2\mu)}-\frac{(2\lambda+3\mu)}{5}A_1 r-\frac{(\lambda+3\mu)}{r^2}A_1'+\frac{2\mu}{r}C_1+\frac{2\mu}{r^4}C_1'\right]\cot\theta\frac{\partial P_1(\cos\theta)}{\partial\theta}$$

$$+\left[-\frac{(5\lambda+7\mu)}{21}A_2 r^2-\frac{\mu}{3r^3}A_2'+2\mu C_2+\frac{2\mu}{r^5}C_2'\right]\cot\theta\frac{\partial P_2(\cos\theta)}{\partial\theta}$$

$$+\left[\frac{2}{15}\frac{\mu\rho g r}{(\lambda+2\mu)}-\frac{(3\lambda+4\mu)}{18}A_3 r^3+\frac{(\lambda-\mu)}{15r^4}A_3'+2\mu C_3 r\right.$$

$$\left.+\frac{2\mu}{r^6}C_3'\right]\cot\theta\frac{\partial P_3(\cos\theta)}{\partial\theta}, \quad \ldots\ldots(32)$$

$$\widehat{r\theta}=\left[\frac{2}{5}\frac{\mu\rho g r}{(\lambda+2\mu)}-\frac{(3\lambda+2\mu)}{10}A_1 r+\frac{\mu A_1'}{r^2}-\frac{6\mu}{r^4}C_1'\right]\frac{\partial P_1(\cos\theta)}{\partial\theta}$$

$$+\left[-\frac{(8\lambda+7\mu)}{21}A_2 r^2-\frac{8\mu}{r^5}C_2'-\frac{(3\lambda+2\mu)}{6r^3}A_2'+2C_2\mu\right]\frac{\partial P_2(\cos\theta)}{\partial\theta}$$

$$+\left[\frac{4}{15}\frac{\mu\rho g r}{(\lambda+2\mu)}-\frac{(15\lambda+14\mu)}{36}A_3 r^3-\frac{(8\lambda+7\mu)}{15}\frac{A_3'}{r^4}\right.$$

$$\left.+4\mu C_3 r-\frac{10\mu}{r^6}C_3'\right]\frac{\partial P_3(\cos\theta)}{\partial\theta}. \quad \ldots\ldots(33)$$

$r\leq a$:—

$$\widehat{rr'}=\left[\left(\lambda'+\frac{2\mu'}{3}\right)D_0 P_0(\cos\theta)+\left[\frac{5\lambda'+6\mu'}{5(\lambda'+2\mu')}\rho' g r+\frac{(3\lambda'+2\mu')}{5}D_1 r\right]P_1(\cos\theta)\right.$$

$$+\left[\frac{\lambda'}{7}D_2r^2+4\mu'E_2\right]P_2(\cos\theta)+\left[\frac{4\mu'}{5(\lambda'+2\mu')}\rho'gr-\frac{(3\lambda'+4\mu')}{9}D_3r^3+12\mu'E_3r\right]P_3(\cos\theta), \quad \ldots\ldots\ldots\ldots (34)$$

$$\widehat{\theta\theta'}=\left[\left(\lambda'+\frac{2\mu'}{3}\right)D_0\right]P_0(\cos\theta)+\left[\frac{5\lambda'+3\mu'}{5(\lambda'+2\mu')}\rho'gr+\frac{(4\lambda'+\mu')}{5}D_1r\right]P_1(\cos\theta)$$
$$+\left[\frac{5}{7}\lambda'D_2r^2+4\mu'C_2\right]P_2(\cos\theta)+\left[\frac{2\mu'}{5(\lambda'+2\mu')}\rho'gr+\frac{(6\lambda'+\mu')}{9}D_3r^3+6\mu'E_3r\right]P_3(\cos\theta)$$
$$+\left[\frac{\mu'}{5(\lambda'+2\mu')}\rho'gr-\frac{(2\lambda'+3\mu')}{5}D_1r\right]\frac{\partial^2P_1(\cos\theta)}{\partial\theta^2}+\left[-\frac{(5\lambda'+7\mu')}{21}P_2r^2+2\mu'E_2\right]\frac{\partial^2P_2(\cos\theta)}{\partial\theta^2}$$
$$+\left[\frac{2\mu'}{15(\lambda'+2\mu')}\rho'gr-\frac{(3\lambda'+4\mu')}{18}D_3r^3+2\mu'E^3r\right]\frac{\partial^2P_3(\cos\theta)}{\partial\theta^2}, \quad \ldots (35)$$

$$\widehat{\phi\phi'}=\left[\lambda'+\frac{2\mu'}{3}\right]D_0P_0(\cos\theta)+\left[\frac{5\lambda'+3\mu'}{5(\lambda'+2\mu')}\rho'gr+\frac{(4\lambda'+\mu')}{5}D_1r\right]P_1(\cos\theta)$$
$$+\left[\frac{5}{7}\lambda'D_2r^2+4\mu'E_2\right]P_2(\cos\theta)+\left[\frac{2}{5}\frac{\mu'\rho'gr}{(\lambda'+2\mu')}+\frac{(6\lambda'-\mu')}{9}D_3r^3+6\mu'E_3r\right]P_3(\cos\theta)$$
$$+\left[\frac{\mu'\rho'gr}{5(\lambda'+2\mu')}-\frac{(2\lambda'+3\mu')}{5}D_1r\right]\cot\theta\frac{\partial P_1(\cos\theta)}{\partial\theta}+\left[-\frac{(5\lambda'+7\mu')}{21}D_2r^2+2\mu'E^2\right]\cot\theta\frac{\partial P_2(\cos\theta)}{\partial\theta}$$
$$+\left[\frac{2}{15}\frac{\mu'\rho gr}{(\lambda'+2\mu')}-\frac{(3\lambda'+4\mu')}{18}D_3r^3+2\mu'E_3r\right]\cot\theta\frac{\partial P_3(\cos\theta)}{\partial\theta}, \quad \ldots (36)$$

$$\widehat{r\theta'}=\left[\frac{2}{5}\frac{\mu'\rho gr}{(\lambda'+2\mu')}-\frac{(3\lambda'+2\mu')}{10}D_1r\right]\frac{\partial P_1(\cos\theta)}{\partial\theta}$$
$$+\left[-\frac{(8\lambda'+7\mu')}{21}D_2r^2+2\mu'E_2\right]\frac{\partial P_2(\cos\theta)}{\partial\theta}$$
$$+\left[\frac{4}{15}\frac{\mu'\rho'gr}{(\lambda'+2\mu')}-\frac{(15\lambda'+14\mu')}{36}D_3r^3+4\mu'E_3r\right]\frac{\partial P_3(\cos\theta)}{\partial\theta}. \quad \ldots\ldots (37)$$

The general expressions of the components of stresses thus obtained

satisfy, of course, the equations of equilibrium of elastic bodies under gravitating field expressed by (2) and (3).

Using these general expressions of displacements and stresses, we shall study the problem of the effect of an internal spherical heterogeneous matter on the stress distributions in the interior of gravitating semi-infinite elastic solid.

Referring to Fig. 1, we obtain the following expressions of the components of displacement and stresses which are the solutions of the gravitating semi-infinite elastic solid having no heterogeneous matter in its interior:

$$u=-\frac{\rho g r}{3(\lambda+2\mu)}P_0(\cos\theta)+\left[\frac{\rho g\xi^2}{2(\lambda+2\mu)}+\frac{3}{10}\frac{\rho g r^2}{(\lambda+2\mu)}\right]P_1(\cos\theta)$$
$$-\frac{2}{3}\frac{\rho g\xi r}{(\lambda+2\mu)}P_2(\cos\theta)+\frac{1}{5}\frac{\rho g r^2}{(\lambda+2\mu)}P_3(\cos\theta) \quad \ldots\ldots\ldots\ldots\ldots (38)$$

$$v=\left[\frac{\rho g\xi^2}{2(\lambda+2\mu)}+\frac{1}{10}\frac{\rho g r^2}{(\lambda+2\mu)}\right]\frac{\partial P_1(\cos\theta)}{\partial\theta}$$
$$-\frac{\rho g\xi r}{3(\lambda+2\mu)}\frac{\partial P_2(\cos\theta)}{\partial\theta}+\frac{1}{15}\frac{\rho g r^2}{(\lambda+2\mu)}\frac{\partial P_3(\cos\theta)}{\partial\theta}, \quad \ldots\ldots\ldots\ldots\ldots (39)$$

$$\widehat{rr}=-\frac{(3\lambda+2\mu)}{3(\lambda+2\mu)}\rho g\xi P_0(\cos\theta)+\frac{(5\lambda+6\mu)\rho g r}{5(\lambda+2\mu)}P_1(\cos\theta)$$
$$-\frac{4}{3}\frac{\mu\rho g\xi}{(\lambda+2\mu)}P_2(\cos\theta)+\frac{4}{5}\frac{\mu\rho g r}{(\lambda+2\mu)}P_3(\cos\theta), \quad \ldots\ldots\ldots\ldots (40)$$

$$\widehat{\theta\theta}=-\frac{(3\lambda+2\mu)}{3(\lambda+2\mu)}\rho g\xi P_0(\cos\theta)+\frac{5\lambda+3\mu}{5(\lambda+2\mu)}\rho g r P_1(\cos\theta)$$
$$-\frac{4}{3}\frac{\mu\rho g\xi}{(\lambda+2\mu)}P_2(\cos\theta)+\frac{2}{5}\frac{\mu\rho g r}{(\lambda+2\mu)}P_3(\cos\theta)$$
$$+\frac{\mu\rho g r}{5(\lambda+2\mu)}\frac{\partial^2 P_1(\cos\theta)}{\partial\theta^2}-\frac{2}{3}\frac{\mu\rho g\xi}{(\lambda+2\mu)}\frac{\partial^2 P_2(\cos\theta)}{\partial\theta^2}$$
$$+\frac{2}{15}\frac{\mu\rho g r}{(\lambda+2\mu)}\frac{\partial^2 P_3(\cos\theta)}{\partial\theta^2}, \quad \ldots\ldots\ldots\ldots\ldots\ldots\ldots (41)$$

$$\widehat{\phi\phi}=-\frac{(3\lambda+2\mu)\rho g\xi}{3(\lambda+2\mu)}P_0(\cos\theta)+\frac{5\lambda+3\mu}{5(\lambda+2\mu)}\rho g r P_1(\cos\theta)$$
$$-\frac{4}{3}\frac{\mu\rho g\xi}{(\lambda+2\mu)}P_2(\cos\theta)+\frac{2}{5}\frac{\mu\rho g r}{(\lambda+2\mu)}P_3(\cos\theta)$$
$$+\frac{1}{5}\frac{\mu\rho g r}{(\lambda+2\mu)}\cot\theta\frac{\partial P_1(\cos\theta)}{\partial\theta}-\frac{2}{3}\frac{\mu\rho g\xi}{(\lambda+2\mu)}\cot\theta\frac{\partial P_2(\cos\theta)}{\partial\theta}$$

$$+\frac{2}{15}\frac{\mu\rho gr}{(\lambda+2\mu)}\cot\theta\frac{\partial P_3(\cos\theta)}{\partial\theta}, \quad \cdots\cdots\cdots\cdots\cdots\cdots\cdots\cdots(42)$$

$$\widehat{r\theta}=\frac{2}{5}\frac{\mu\rho gr}{(\lambda+2\mu)}\frac{\partial P_1(\cos\theta)}{\partial\theta}-\frac{2}{3}\frac{\mu\rho g\xi}{(\lambda+2\mu)}\frac{\partial P_2(\cos\theta)}{\partial\theta}$$
$$+\frac{4}{15}\frac{\mu\rho gr}{(\lambda+2\mu)}\frac{\partial P_3(\cos\theta)}{\partial\theta}. \quad \cdots\cdots\cdots\cdots\cdots\cdots\cdots\cdots(43)$$

These expressions satisfy, of course, the following conditions: the normal and the shearing components of stress vanish at the free surface $z=\xi$, and the stress at any point in the gravitating solid increases according to the increase of the position from the upper surface of the solid. And the state of the semi-infinite solid is one of plane strain.

Now the boundary conditions of the present problem are as follows:

1. The heterogeneous gravitating inclusion and the gravitating semi-infinite elastic medium are perfectly cemented at the contact surface and they are forbidden to slide upon each other on this contact surface.

2. The displacement and the stress at the whole spaces in the medium far from the spherical inclusion are equal to the ones expressed by (38), (39), (40), (41), (42) and (43) respectively.

These are denoted by

$$r=a\,; \quad u=u',\ v=v',\ \widehat{rr}=\widehat{rr}',\ \widehat{r\theta}=\widehat{r\theta}'. \quad \cdots\cdots\cdots\cdots(44)$$

$$\left.\begin{aligned} r\to\infty:\ & u=u \text{ expressed by (38)},\\ & v=v \quad ,, \quad ,, \text{ (39)},\\ & \widehat{rr}=\widehat{rr} \quad ,, \quad ,, \text{ (40)},\\ & \widehat{\theta\theta}=\widehat{\theta\theta} \quad ,, \quad ,, \text{ (41)},\\ & \widehat{\phi\phi}=\widehat{\phi\phi} \quad ,, \quad ,, \text{ (42)},\\ & \widehat{r\theta}=\widehat{r\theta} \quad ,, \quad ,, \text{ (43)}. \end{aligned}\right\} \cdots\cdots\cdots(45)$$

Using the expressions of displacements (22), (23), (24), (25), (26), (27), (28), (29) and those of stresses (30), (31), (32), (33), (34), (35), (36), (37), we find the following values of the arbitrary constants by the conditions expressed by (44) and (45):

$$\left.\begin{aligned} & A_0=-\frac{\rho g\xi}{(\lambda+2\mu)},\quad C_0'=\frac{\rho g\xi a^3(3\lambda+2\mu-3\lambda'-2\mu')}{3(\lambda+2\mu)(4\mu+3\lambda'+2\mu')},\\ & A_0'=0,\quad D_0'=0,\quad D_0=-\frac{3\rho g\xi}{(4\mu+3\lambda'+2\mu')}, \end{aligned}\right\} \quad (46)$$

$$
\left.\begin{aligned}
&A_1=0,\ C_1=\frac{\rho g\xi^2}{2(\lambda+2\mu)},\quad A_1'=\frac{ga^3(\rho'-\rho)}{3(\lambda+2\mu)},\\
&D_1=-\frac{2}{3}\,\frac{g\mu'\{\rho'(6\mu+5\lambda'+4\mu')-5\rho(\lambda'+2\mu')\}}{(\lambda'+2\mu')\{2\mu(\lambda'+4\mu')+\mu'(3\lambda'+2\mu')\}},\\
&C_1'=-\frac{\rho' ga^5\{6\mu'(\lambda+2\mu)-5\mu(\lambda'+2\mu')\}}{90\mu(\lambda+2\mu)(\lambda'+2\mu')}\\
&\qquad-\frac{\rho' ga^5\mu'(3\lambda'+2\mu')(6\mu+5\lambda'+4\mu')}{90\mu(\lambda'+2\mu)\{2\mu(\lambda'+4\mu')+\mu'(3\lambda'+2\mu')\}}\\
&\qquad+\frac{\rho ga^5}{90(\lambda+2\mu)}+\frac{5\rho ga^5\mu'(3\lambda'+2\mu')}{90\mu\{2\mu(\lambda'+4\mu')+\mu'(3\lambda'+2\mu')\}},\\
&E_1=\frac{\rho g\xi^2}{2(\lambda+2\mu)}+\frac{3}{10}\,\frac{\rho ga^2}{(\lambda+2\mu)}-\frac{3}{10}\,\frac{\rho' ga^2}{(\lambda'+2\mu')}-\frac{ga^2(\rho'-\rho)}{3\mu}\\
&\qquad+\frac{ga^2\mu'(-\lambda'+\mu')\{\rho'(6\mu+5\lambda'+4\mu')-5\rho(\lambda'+2\mu')\}}{15\mu'(\lambda'+2\mu')\{2\mu(\lambda'+4\mu')+\mu'(3\lambda'+2\mu')\}}\\
&\qquad+\frac{\rho' ga^2[\{2\mu(\lambda'+4\mu')+\mu'(3\lambda'+2\mu')\}\{6\mu'(\lambda+2\mu)-5\mu(\lambda'+2\mu')\}}{45\mu(\lambda+2\mu)(\lambda'+2\mu')}\\
&\qquad\qquad\frac{+\mu'(\lambda+2\mu)(3\lambda'+2\mu')(6\mu+5\lambda'+4\mu')]}{\{2\mu(\lambda'+4\mu')+\mu'(3\lambda'+2\mu')\}}\\
&\qquad-\frac{\rho ga^2[\{2\mu(\lambda'+4\mu')+\mu'(3\lambda'+2\mu')\}\{6\mu(\lambda'+2\mu')-5\mu(\lambda'+2\mu')\}}{(\lambda+2\mu)(\lambda'+2\mu')}\\
&\qquad\qquad\frac{+5\mu'(\lambda+2\mu)(\lambda'+2\mu')(3\lambda'+2\mu')]}{\{2\mu(\lambda'+4\mu')+\mu'(3\lambda'+2\mu')\}},
\end{aligned}\right\}
\qquad\ldots\ldots\ldots(47)
$$

$$
\left.\begin{aligned}
&A_2=0,\quad C_2=-\frac{\rho g\xi}{3(\lambda+2\mu)},\quad D_2=0,\\
&A_2'=\frac{20\rho ga^3\xi\mu(\mu-\mu')}{(\lambda+2\mu)\{3\lambda(3\mu+2\mu')+2\mu(7\mu+8\mu')\}},\\
&C_2'=\frac{2\rho ga^5\xi(\lambda+\mu)(\mu'-\mu)}{(\lambda+2\mu)\{3\lambda(3\mu+2\mu')+2\mu(7\mu+8\mu')\}},\\
&E_2=-\frac{5\rho g\xi\mu}{\{3\lambda(3\mu+2\mu')+2\mu(7\mu+8\mu')\}},
\end{aligned}\right\}
\qquad\ldots\ldots\ldots(48)
$$

$$
\left.\begin{aligned}
&A_3=0,\quad C_3=0,\quad D_3=0,\\
&A_3'=\frac{28\rho ga^5\mu(\mu'-\mu)}{(\lambda+2\mu)\{\lambda(16\mu'+19\mu)+2\mu(22\mu'+13\mu)\}},\\
&C_3'=-\frac{2\rho ga^7(\lambda+\mu)(\mu'-\mu)}{(\lambda+2\mu)\{\lambda(16\mu'+19\mu)+2\mu(22\mu'+13\mu)\}},\\
&E_3=\frac{7}{3}\,\frac{\rho g\mu}{\{\lambda(16\mu'+19\mu)+2\mu(22\mu'+13\mu)\}}-\frac{\rho' g}{15(\lambda'+2\mu')}.
\end{aligned}\right\}
\qquad\ldots\ldots\ldots(49)
$$

Substituting these values (46), (47), (48) and (49) in the expressions (22), (23), (24), (25), (26), (27), (28), (29) and (30), (31), (32), (33), (34), (45), (36), (37), we obtain the final results which are favourable to the present study in the following forms: (The expressions of the displacements u, v, u', v' are omitted here.)

$r \geq a$:—

$$\widehat{rr}=\rho g\xi\Bigg[\Bigg\{-\frac{(3\lambda+2\mu)}{3(\lambda+2\mu)}+\frac{4a^3\mu(3\lambda+2\mu-3\lambda'-2\mu')}{3r^3(\lambda+2\mu)(4\mu+3\lambda'+2\mu')}\Bigg\}P_0(\cos\theta)$$
$$-\frac{4\mu}{3(\lambda+2\mu)}P_2(\cos\theta)\Bigg]$$
$$+\rho g a\Bigg[\Bigg\{\frac{2a^4\mu}{15r^4(\lambda+2\mu)}+\frac{2a^4\mu\mu'(3\lambda'+2\mu')}{3r^4\{2\mu(\lambda'+4\mu')+\mu'(3\lambda'+2\mu')\}}\Bigg\}P_1(\cos\theta)$$
$$+\Bigg\{\frac{4r\mu}{25a(\lambda+2\mu)}+\frac{28a^4\mu(17\lambda+18\mu)(\mu'-\mu)}{5r^4(\lambda+2\mu)\{\lambda(16\mu'+19\mu)+2\mu(22\mu'+13\mu)\}}$$
$$-\frac{80a^6\mu(\lambda+\mu)(\mu'-\mu)}{r^6(\lambda+2\mu)\{\lambda(16\mu'+19\mu)+2\mu(22\mu'13\mu)\}}\Bigg\}P_3(\cos\theta)\Bigg]$$
$$+\rho' g a\Bigg[-\frac{2a^4\{6\mu'(\lambda+2\mu)-5\mu(\lambda'+2\mu')\}}{15r^4(\lambda+2\mu)(\lambda'+2\mu')}$$
$$-\frac{2a^4\mu'(3\lambda'+2\mu')(6\mu+5\lambda'+4\mu')}{15r^4(\lambda'+2\mu')\{2\mu(\lambda'+4\mu')+\mu'(3\lambda'+2\mu')\}}\Bigg]P_1(\cos\theta),$$

.....(50)

$$\widehat{\theta\theta}=\rho g\xi\Bigg[\Bigg\{-\frac{(3\lambda+2\mu)}{3(\lambda+2\mu)}-\frac{2a^3\mu(3\lambda+2\mu-3\lambda'-2\mu')}{3r^3(\lambda+2\mu)(4\mu+3\lambda'+2\mu')}\Bigg\}P_0(\cos\theta)$$
$$+\Bigg\{-\frac{100a^3\mu^2(\mu-\mu')}{3r^3(\lambda+2\mu)\{3\lambda(3\mu+2\mu')+2\mu(7\mu+8\mu')\}}$$
$$-\frac{4\mu}{3(\lambda+2\mu)}-\frac{12a^5\mu(\lambda+\mu)(\mu'-\mu)}{r^5(\lambda+2\mu)\{3\lambda(3\mu+2\mu')+2\mu(7\mu+8\mu')\}}\Bigg\}P_2(\cos\theta)$$
$$+\Bigg\{-\frac{20a^3\mu^2(\mu-\mu')}{3r^3(\lambda+2\mu)\{3\lambda(3\mu+2\mu')+2\mu(7\mu+8\mu')\}}$$
$$-\frac{2\mu}{3(\lambda+2\mu)}+\frac{4a^5\mu(\lambda+\mu)(\mu'-\mu)}{r^5(\lambda+2\mu)\{3\lambda(3\mu+2\mu')+2\mu(7\mu+8\mu')\}}\Bigg\}\frac{\partial^2P_2(\cos\theta)}{\partial\theta^2}\Bigg]$$
$$+\rho g a\Bigg[\Bigg\{\frac{r(5\lambda+3\mu)}{5a(\lambda+2\mu)}+\frac{a^2(\lambda+4\mu)}{3r^2(\lambda+2\mu)}-\frac{4a^4\mu}{90r^4(\lambda+2\mu)}$$
$$-\frac{2a^4\mu'(3\lambda'+2\mu')}{9r^4\{2\mu(\lambda'+4\mu')+\mu'(3\lambda'+2\mu')\}}\Bigg\}P_1(\cos\theta)$$

$$+\left\{\frac{2r\mu}{5a(\lambda+2\mu)}+\frac{28a^4\mu(\mu'-\mu)(\lambda-6\mu)}{5r^4(\lambda+2\mu)\{\lambda(16\mu'+19\mu)+2\mu(22\mu'+13\mu)\}}\right.$$
$$\left.+\frac{16a^6\mu(\lambda+\mu)(\mu'-\mu)}{r^6(\lambda+22\mu)\{\lambda(16\mu'+19\mu)+2\mu(22\mu'+13\mu)\}}\right\}P_3(\cos\theta)$$
$$+\left\{\frac{r\mu}{5a(\lambda+2\mu)}+\frac{a^2(\lambda+3\mu)}{3r^2(\lambda+2\mu)}+\frac{a^4\mu}{45r^4(\lambda+2\mu)}\right.$$
$$\left.+\frac{a^4\mu'(3\lambda'+2\mu')}{9r^4\{2\mu(\lambda'+4\mu')+\mu'(3\lambda'+2\mu')\}}\right\}\frac{\partial^2P_1(\cos\theta)}{\partial\theta^2}$$
$$+\left\{\frac{2r\mu}{15a(\lambda+2\mu)}+\frac{28a^4\mu(\lambda-\mu)(\mu'-\mu)}{15r^4(\lambda+2\mu)\{\lambda(16\mu'+19\mu)+2\mu(22\mu'+13\mu)\}}\right.$$
$$\left.\left.-\frac{4a^6\mu(\lambda+\mu)(\mu'-\mu)}{r^6(\lambda+2\mu)\{\lambda(16\mu'+19\mu)+2\mu(22\mu'+13\mu)\}}\right\}\frac{\partial^2P_3(\cos\theta)}{\partial\theta^2}\right]$$
$$+\rho' ga\left[\left\{-\frac{a^2(\lambda+4\mu)}{3r^2(\lambda+2\mu)}+\frac{4a^4\{6\mu'(\lambda+2\mu)-5\mu(\lambda'+2\mu')\}}{90r^4(\lambda+2\mu)(\lambda'+2\mu')}\right.\right.$$
$$\left.+\frac{2a^4\mu'(3\lambda'+2\mu')(6\mu+5\lambda'+4\mu')}{45r^4(\lambda'+2\mu')\{2\mu(\lambda'+4\mu')+\mu'(3\lambda'+2\mu')\}}\right\}P_1(\cos\theta)$$
$$+\left\{-\frac{a^2(\lambda+3\mu)}{3r^2(\lambda+2\mu)}-\frac{a^4\{6\mu'(\lambda+2\mu)-5\mu(\lambda'+2\mu')\}}{45r^4(\lambda+2\mu)(\lambda'+2\mu')}\right.$$
$$\left.\left.-\frac{2a^4\mu'(3\lambda'+2\mu')(6\mu+5\lambda'+4\mu')}{90r^4(\lambda'+2\mu')\{2\mu(\lambda'+4\mu')+\mu'(3\lambda'+2\mu')\}}\right\}\frac{\partial^2P_1(\cos\theta)}{\partial\theta^2}\right],$$
$$\ldots\ldots\ldots\ldots(51)$$

$$\widehat{\phi\phi}=\rho g\xi\left[\left\{-\frac{3\lambda+2\mu}{3(\lambda+2\mu)}-\frac{2a^3(3\lambda+2\mu-3\lambda'-2\mu')}{3r^3(\lambda+2\mu)(4\mu+3\lambda'+2\mu')}\right\}P_0(\cos\theta)\right.$$
$$+\left\{-\frac{100a^3\mu(\mu-\mu')}{3r^3(\lambda+2\mu)\{3\lambda(3\mu+2\mu')+2\mu(7\mu+8\mu')\}}\right.$$
$$\left.-\frac{4\mu}{3(\lambda+2\mu)}-\frac{12a^5\mu(\lambda+\mu)(\mu'-\mu)}{r^5(\lambda+2\mu)\{3\lambda(3\mu+2\mu')+2\mu(7\mu+8\mu')\}}\right\}P_2(\cos\theta)$$
$$+\left\{\frac{-20a^3\mu^2(\mu-\mu')}{3r^3(\lambda+2\mu)\{3\lambda(3\mu+2\mu')+2\mu(7\mu+8\mu')\}}-\frac{2\mu}{3(\lambda+2\mu)}\right.$$
$$\left.\left.+\frac{4a^5\mu(\lambda+\mu)(\mu'-\mu)}{r^5(\lambda+2\mu)\{3\lambda(3\mu+2\mu')+2\mu(7\mu+8\mu')\}}\right\}\cot\theta\frac{\partial P_2(\cos\theta)}{\partial\theta}\right]$$
$$+\rho ga\left[\left\{\frac{r(5\lambda+3\mu)}{5a(\lambda+2\mu)}+\frac{a^2(\lambda+4\mu)}{3r^2(\lambda+2\mu)}-\frac{2a^4\mu}{45r^4(\lambda+2\mu)}\right.\right.$$
$$\left.\left.-\frac{2a^4\mu'(3\lambda'+2\mu')}{9r^4\{2\mu(\mu'+4\mu')+\mu'(3\lambda'+2\mu')\}}\right\}P_1(\cos\theta)\right.$$

$$+\left\{\frac{2r\mu}{5a(\lambda+2\mu)}+\frac{28a^4\mu(\lambda-6\mu)(\mu'-\mu)}{5r^4(\lambda+2\mu)\{\lambda(16\mu'+19\mu)+2\mu)22\mu'+13\mu)}\right.$$
$$\left.+\frac{16a^6\mu(\lambda+\mu)(\mu'-\mu)}{r^6(\lambda+2\mu)\{\lambda(16\mu'+19\mu)+2\mu(22\mu'+13\mu)\}}\right\}P_3(\cos\theta)$$
$$+\left\{\frac{r\mu}{5a(\lambda+2\mu)}+\frac{a^2(\lambda+3\mu)}{3r^2(\lambda+2\mu)}+\frac{a^4\mu}{45r^4(\lambda+2\mu)}\right.$$
$$\left.+\frac{a^4\mu'(3\lambda'+2\mu')}{9r^4\{2\mu(\lambda'+4\mu')+\mu'(3\lambda'+2\mu')\}}\right\}\cot\theta\frac{\partial P_1(\cos\theta)}{\partial\theta}$$
$$+\left\{\frac{2r\mu}{15a(\lambda+2\mu)}+\frac{28a^4\mu(\lambda-\mu)(\mu'-\mu)}{15r^4(\lambda+2\mu)\{\lambda(16\mu'+19\mu)+2\mu(22\mu'+13\mu)\}}\right.$$
$$\left.-\frac{4a^6\mu(\lambda+\mu)(\mu'-\mu)}{r^6(\lambda+2\mu)\{\lambda(16\mu'+19\mu)+2\mu(22\mu'+13\mu)\}}\right\}\frac{\partial P_3(\cos\theta)}{\partial\theta}\Big]$$
$$+\rho' ga\Big[\Big\{-\frac{a^2(\lambda+4\mu)}{3r^2(\lambda+2\mu)}+\frac{2a^4\{6\mu'(\lambda+2\mu)-5\mu(\lambda'+2\mu')\}}{45r^4(\lambda+2\mu)(\lambda'+2\mu')}$$
$$+\frac{2a^4\mu'(3\lambda'+2\mu')(6\mu+5\lambda'+4\mu')}{45r^4(\lambda'+2\mu')\{2\mu(\lambda'+4\mu')+\mu'(3'\lambda+2\mu')\}}\Big\}P_1(\cos\theta)$$
$$+\Big\{-\frac{a^2(\lambda+3\mu)}{3r^2(\lambda+2\mu)}-\frac{a^4\{6\mu'(\lambda+2\mu)-5\mu(\lambda'+2\mu')\}}{45r^4(\lambda+2\mu)(r'+2\mu')}$$
$$-\frac{a^4\mu'(3\lambda'+2\mu')(6\mu+5\lambda'+4\mu')}{45r^4(\lambda'+2\mu')\{2\mu(\lambda'+4\mu')+\mu'(3\lambda'+2\mu')\}}\Big\}\cot\theta\frac{\partial P_1(\cos\theta)}{\partial\theta}\Big]$$
$$\cdots\cdots\cdots\cdots(52)$$

$$\widehat{r\theta}=\rho g\xi\Big[\Big\{-\frac{16a^5\mu(\lambda+\mu)(\mu'-\mu)}{r^5(\lambda+2\mu)\{3\lambda(3\mu+2\mu')+2\mu(7\mu+8\mu')\}}$$
$$-\frac{10a^3\mu(3\lambda+2\mu)(\mu-\mu')}{3r^3(\lambda+2\mu)\{3\lambda(3\mu+2\mu')+2\mu(7\mu+8\mu')\}}$$
$$-\frac{2\mu}{3(\lambda+2\mu)}\Big\}\frac{\partial P_2(\cos\theta)}{\partial\theta}\Big]$$
$$+\rho ga\Big[\Big\{\frac{2r\mu}{5a(\lambda+2\mu)}-\frac{a^2\mu}{3r(\lambda+2\mu)}-\frac{2\mu a^4}{30r^4(\lambda+2\mu)}$$
$$-\frac{a^4\mu'(3\lambda'+2\mu')}{3r^4\{2\mu(\lambda'+4\mu')+\mu'(3\lambda'+2\mu')\}}\Big\}\frac{\partial P_1(\cos\theta)}{\partial\theta}$$
$$+\Big\{\frac{4r\mu}{15a(\lambda+2\mu)}-\frac{28a^4\mu(8\lambda+7\mu)(\mu'-\mu)}{15r^4(\lambda+2\mu)\{\lambda(16\mu'+19\mu)+2\mu(22\mu'+13\mu)\}}$$
$$+\frac{20a^6\mu(\lambda+\mu)(\mu'-\mu)}{r^6(\lambda+2\mu)\{\lambda(16\mu'+19\mu)+2\mu(22\mu'+13\mu)\}}\Big\}\frac{\partial P_3(\cos\theta)}{\partial\theta}\Big]$$

$$+\rho' ga\left[\left\{\frac{a^2\mu}{3r^2(\lambda+2\mu)}+\frac{a^4\mu'(3\lambda'+2\mu')(6\mu+5\lambda'+4\mu')}{15r^4(\lambda'+2\mu')\{2\mu(\lambda'+4\mu')+\mu'(3\lambda'+2\mu')\}}\right.\right.$$
$$\left.\left.+\frac{a^4\{6\mu'(\lambda+2\mu)-5\mu(\lambda'+2\mu')\}}{15r^4(\lambda+2\mu)(\lambda'+2\mu')}\right\}\frac{\partial P_1(\cos\theta)}{\partial\theta}\right] \quad \ldots\ldots\ldots(53)$$

$r\leq a$:

$$\widehat{rr'}=\rho g\xi\left[-\frac{(3\lambda'+2\mu')}{(4\mu+3\lambda'+2\mu')}P_0(\cos\theta)-\frac{20\mu\mu'}{3\lambda(3\mu+2\mu')+2\mu(7\mu+8\mu')}P_2(\cos\theta)\right]$$
$$+\rho ga\left[\frac{2r(3\lambda'+2\mu')(\lambda'+2\mu')}{3a(\lambda'+2\mu')\{2\mu(\lambda'+4\mu')+\mu'(3\lambda'+2\mu')\}}P_1(\cos\theta)\right.$$
$$\left.+\frac{28r\mu\mu'}{a\{\lambda(16\mu'+19\mu)+2\mu(22\mu'+13\mu)\}}P_3(\cos\theta)\right]$$
$$+\rho' ga\left[\left\{\frac{r(5\lambda'+6\mu')}{5a(\lambda'+2\mu')}-\frac{2r(3\lambda'+2\mu')\mu'(6\mu+5\lambda'+4\mu')}{3a(\lambda'+2\mu')\{2\mu(\lambda'+4\mu')+\mu'(3\lambda'+2\mu')\}}\right\}P_1(\cos\theta)\right.$$
$$\left.-\frac{4r\mu'}{5(\lambda'+2\mu')}P_3(\cos\theta)\right],\ldots\ldots\ldots\ldots\ldots\ldots\ldots\ldots\ldots(54)$$

$$\widehat{\theta\theta'}=\rho g\xi\left[-\frac{3\lambda'+2\mu'}{4\mu+3\lambda'+2\mu'}P_0(\cos\theta)-\frac{4\mu'}{3(\lambda+2\mu)}P_2(\cos\theta)\right.$$
$$\left.-\frac{10\mu\mu'}{3\lambda(3\mu+2\mu')+2\mu(7\mu+8\mu')}\frac{\partial^2P_2(\cos\theta)}{\partial\theta^2}\right]$$
$$+\rho ga\left[\frac{2r\mu'(4\lambda'+\mu')(\lambda'+2\mu')}{3a(\lambda'+2\mu')\{2\mu(\lambda'+4\mu')+\mu'(3\lambda'+2\mu')\}}P_1(\cos\theta)\right.$$
$$+\frac{14r\mu}{a\{\lambda(16\mu'+19\mu)+2\mu(22\mu'+13\mu)\}}P_3(\cos\theta)$$
$$-\frac{2r(2\lambda'+3\mu')(\lambda'+2\mu')}{3a(\lambda'+2\mu')\{2\mu(\lambda'+4\mu')+\mu'(3\lambda'+2\mu')\}}\frac{\partial^2P_1(\cos\theta)}{\partial\theta^2}$$
$$\left.+\frac{14r\mu\mu'}{3a\{\lambda(16\mu'+19\mu)+2\mu(22\mu'+13\mu)}\frac{\partial^2P_3(\cos\theta)}{\partial\theta^2}\right]$$
$$+\rho' ga\left[\left\{\frac{r(5\lambda'+3\mu')}{5a(\lambda'+2\mu')}-\frac{2r\mu'(4\lambda'+\mu')(6\mu+5\lambda'+4\mu')}{15a(\lambda'+2\mu')\{2\mu(\lambda'+4\mu')+\mu'(3\lambda'+2\mu')\}}\right\}P_1(\cos\theta)\right.$$
$$+\left\{\frac{r\mu'}{5a(\lambda'+2\mu')}+\frac{2r\mu'(2\lambda'+3\mu')(6\mu+5\lambda'+4\mu')}{15a(\lambda'+2\mu')\{2\mu(\lambda'+4\mu')+\mu'(3\lambda'+2\mu')\}}\right\}$$
$$\left.\times\frac{\partial^2P_1(\cos\theta)}{\partial\theta^2}\right],$$
$$\ldots\ldots\ldots\ldots(55)$$

$$\widehat{\phi\phi'}=\rho g\xi\Big[-\frac{(3\lambda'+2\mu')}{4\mu+3\lambda'+2\mu'}P_0(\cos\theta)-\frac{20\mu\mu'}{3\lambda(3\mu+2\mu')+2\mu(7\mu+8\mu')}P_2(\cos\theta)$$
$$-\frac{10\mu\mu'}{3\lambda(3\mu+2\mu')+2\mu(7\mu+8\mu')}\cot\theta\frac{P_2(\cos\theta)}{\partial\theta}\Big]$$
$$+\rho ga\Big[\frac{2r\mu'(4\lambda'+\mu')(\lambda'+2\mu')}{3(\lambda'+2\mu')\{2\mu(\lambda'+4\mu')+\mu'(3\lambda'+2\mu')\}}P_1(\cos\theta)$$
$$+\frac{14r\mu\mu'}{\lambda(16\mu'+19\mu)+2\mu(22\mu'+13\mu)}P_3(\cos\theta)$$
$$+\frac{14r\mu\mu'}{3a\{\lambda(16\mu'+19\mu)+2\mu(22\mu'+13\mu)\}}\cot\theta\frac{\partial P_3(\cos\theta)}{\partial\theta}\Big]$$
$$+\rho' ga\Big[\Big\{\frac{r(5\lambda'+3\mu')}{5a(\lambda'+2\mu')}-\frac{2r\mu'(4\lambda'+\mu')(6\mu+5\lambda'+4\mu')}{15a(\lambda'+2\mu')\{2\mu(\lambda'+4\mu')+\mu'(3\lambda'+2\mu')\}}\Big\}P_1(\cos\theta)$$
$$+\Big\{\frac{2r\mu'}{5a(\lambda'+2\mu')}-\frac{2r\mu'}{5(\lambda'+2\mu')}\Big\}P_3(\cos\theta)$$
$$+\Big\{\frac{r\mu'}{5a(\lambda'+2\mu')}+\frac{2r\mu'(2\lambda'+3\mu')(6\mu+5\lambda'+4\mu')}{15a(\lambda'+2\mu')\{2\mu(\lambda'+4\mu')+\mu'(3\lambda'+2\mu')\}}\Big\}$$
$$\times\cot\theta\frac{\partial P_1(\cos\theta)}{\partial\theta}\Big],$$
$$\cdots\cdots\cdots(56)$$

$$\widehat{r\theta'}=\rho g\xi\Big[-\frac{10\mu\mu'}{3\lambda(3\mu+2\mu')+2\mu(7\mu+8\mu')}\frac{\partial P_2(\cos\theta)}{\partial\theta}\Big]$$
$$+\rho ga\Big[-\frac{r(3\lambda'+2\mu')(\lambda'+2\mu')}{3a(\lambda'+2\mu')\{2\mu(\lambda'+4\mu')+\mu'(3\lambda'+2\mu')\}}\frac{\partial P_1(\cos\theta)}{\partial\theta}$$
$$+\frac{7r\mu\mu'}{3a\{\lambda(16\mu'+19\mu)+2\mu(22\mu'+13\mu)\}}\frac{\partial P_3(\cos\theta)}{\partial\theta}\Big]$$
$$+\rho' ga\Big[\Big\{\frac{2}{5}\frac{r\mu'}{a(\lambda'+2\mu')}+\frac{r\mu'(3\lambda'+2\mu')(6\mu+5\lambda'+4\mu')}{15a(\lambda'+2\mu')\{2\mu(\lambda'+4\mu')+\mu'(3\lambda'+2\mu')\}}\Big\}$$
$$\times\frac{\partial P_1(\cos\theta)}{\partial\theta}\Big].$$
$$\cdots\cdots\cdots\cdots(57)$$

When $\lambda=\mu$, $\lambda'=\mu'$, namely the Poisson's ratio of the semi-infinite

solid and that of the heterogeneous inclusion are equally $\frac{1}{4}$, we obtain the expressions of the stress distributions in the solid and those in the inclusion as follows:

$r \geq a$:--

$$\widehat{rr} = \rho g \xi \Big[-\frac{2}{3} + \Big\{ \frac{20(\mu-\mu')}{9(4\mu+5\mu')} + \frac{95(\mu-\mu')}{9(23\mu+22\mu')} \Big\} \Big(\frac{a}{r}\Big)^3 + \frac{8(\mu'-\mu)}{23\mu+22\mu'} \Big(\frac{a}{r}\Big)^5$$
$$+ \Big\{ -\frac{1}{3} + \frac{95}{3} \frac{(\mu-\mu')}{(23\mu+2\mu')} \Big(\frac{a}{r}\Big)^3 + \frac{24(\mu'-\mu)}{(23\mu+22\mu')} \Big(\frac{a}{r}\Big)^5 \Big\} \cos 2\theta \Big]$$
$$+ \rho g a \Big[\Big\{ \frac{5}{6}\Big(\frac{r}{a}\Big) - \frac{7}{9}\Big(\frac{a}{r}\Big)^2 + \frac{4(\mu+8\mu')}{45(2\mu+\mu')} \Big(\frac{a}{r}\Big)^4$$
$$+ \frac{49(\mu'-\mu)}{30(4\mu'+3\mu)}\Big(\frac{a}{r}\Big)^4 - \frac{4(\mu'-\mu)}{3(4\mu'+3\mu)}\Big(\frac{a}{r}\Big)^6 \Big\} \cos\theta$$
$$+ \Big\{ \frac{1}{6}\Big(\frac{r}{a}\Big) + \frac{49(\mu'-\mu)}{18(4\mu'+3\mu)}\Big(\frac{a}{r}\Big)^4 - \frac{20(\mu'-\mu)}{9(4\mu'+3\mu)}\Big(\frac{a}{r}\Big)^6 \Big\} \cos 3\theta \Big]$$
$$+ \rho' g a \Big[\frac{7}{9}\Big(\frac{a}{r}\Big)^2 - \frac{4(4\mu+5\mu')}{45(2\mu+\mu')}\Big(\frac{a}{r}\Big)^4 \cos\theta \Big], \quad \ldots\ldots\ldots\ldots\ldots\ldots\ldots (58)$$

$$\widehat{\theta\theta} = \rho g \xi \Big[-\frac{2}{3} - \Big\{ \frac{10(\mu-\mu')}{9(4\mu+5\mu')} + \frac{25(\mu-\mu')}{9(23\mu+22\mu')} \Big\} \Big(\frac{a}{r}\Big)^3$$
$$- \frac{2(\mu'-\mu)}{(23\mu+22\mu')}\Big(\frac{a}{r}\Big)^5 + \Big\{ \frac{1}{3} - \frac{5(\mu-\mu')}{3(23\mu+22\mu')}\Big(\frac{a}{r}\Big)^3$$
$$- \frac{14(\mu'-\mu)}{(23\mu+22\mu')}\Big(\frac{a}{r}\Big)^5 \Big\} \cos 2\theta \Big]$$
$$+ \rho g a \Big[\Big\{ \frac{1}{2}\Big(\frac{r}{a}\Big) + \frac{1}{9}\Big(\frac{a}{r}\Big)^2 - \Big\{ \frac{6(\mu+8\mu')}{135(2\mu+\mu')} + \frac{7(\mu'-\mu)}{30(4\mu'+3\mu)} \Big\} \Big(\frac{a}{r}\Big)^4$$
$$+ \frac{(\mu'-\mu)}{3(4\mu'+3\mu)}\Big(\frac{a}{r}\Big)^6 \Big\} \cos\theta$$
$$+ \Big\{ -\frac{1}{6}\Big(\frac{r}{a}\Big) - \frac{7(\mu'-\mu)}{18(4\mu'+3\mu)}\Big(\frac{a}{r}\Big)^4 + \frac{13(\mu'-\mu)}{9(4\mu'+3\mu)}\Big(\frac{a}{r}\Big)^6 \Big\} \cos 3\theta \Big]$$
$$+ \rho' g a \Big[\Big\{ -\frac{1}{9}\Big(\frac{a}{r}\Big)^2 + \frac{6(4\mu+5\mu')}{135(2\mu+\mu')}\Big(\frac{a}{r}\Big)^4 \Big\} \cos\theta \Big], \quad \ldots\ldots\ldots\ldots\ldots\ldots (59)$$

$$\widehat{\phi\phi} = \rho g \xi \Big[-\frac{1}{3} + \Big\{ -\frac{10(\mu-\mu')}{9(4\mu+5\mu')} + \frac{5(\mu-\mu')}{9(23\mu+22\mu')} \Big\} \Big(\frac{a}{r}\Big)^3$$
$$- \frac{6(\mu'-\mu)}{(23\mu+22\mu')}\Big(\frac{a}{r}\Big)^5 + \Big\{ -\frac{5\mu(\mu-\mu')}{23\mu+22\mu'}\Big(\frac{a}{r}\Big)^3 - \frac{10(\mu'-\mu)}{23\mu+22\mu'}\Big(\frac{a}{r}\Big)^5 \Big\} \cos 2\theta \Big]$$

$$+\rho g a\left[\left\{\frac{1}{3}\left(\frac{r}{a}\right)+\frac{1}{9}\left(\frac{a}{r}\right)^2-\frac{7(\mu'-\mu)}{30(4\mu'+3\mu)}\left(\frac{a}{r}\right)^4-\frac{6(\mu+8\mu')}{135(2\mu+\mu')}\left(\frac{a}{r}\right)^4\right.\right.$$
$$\left.+\frac{\mu'-\mu}{4\mu'+3\mu}\left(\frac{a}{r}\right)^6\right\}\cos\theta$$
$$\left.+\left\{-\frac{7(\mu'-\mu)}{18(4\mu'+3\mu)}\left(\frac{a}{r}\right)^4+\frac{7(\mu'-\mu)}{9(4\mu'+3\mu)}\left(\frac{a}{r}\right)^6\right\}\cos 3\theta\right]$$
$$+\rho' g a\left[-\frac{1}{9}\left(\frac{a}{r}\right)^2+\frac{6(4\mu+5\mu')}{135(2\mu+\mu')}\left(\frac{a}{r}\right)^4\right]\cos\theta, \quad \ldots\ldots\ldots\ldots\ldots\ldots (60)$$

$$\widehat{r\theta}=\rho g\xi\left[\frac{1}{3}+\frac{25(\mu-\mu')}{3(23\mu+22\mu')}\left(\frac{a}{r}\right)^3+\frac{16(\mu'-\mu)}{(23\mu+22\mu')}\left(\frac{a}{r}\right)^5\right]\sin 2\theta$$
$$+\rho g a\left[\left\{-\frac{1}{6}\left(\frac{r}{a}\right)+\frac{1}{9}\left(\frac{a}{r}\right)^2+\frac{6(\mu+8\mu')}{135(2\mu+\mu')}\left(\frac{a}{r}\right)^4\right.\right.$$
$$\left.+\frac{7(\mu'-\mu)}{30(4\mu'+3\mu)}\left(\frac{a}{r}\right)^4-\frac{(\mu'-\mu)}{3(4\mu'+3\mu)}\left(\frac{a}{r}\right)^6\right\}\sin\theta$$
$$\left.+\left\{-\frac{1}{6}\left(\frac{r}{a}\right)+\frac{7(\mu'-\mu)}{6(4\mu'+3\mu)}\left(\frac{a}{r}\right)^4-\frac{5(\mu'-\mu)}{3(4\mu'+3\mu)}\left(\frac{a}{r}\right)^6\right\}\sin 3\theta\right]$$
$$+\rho' g a\left[-\frac{1}{9}\left(\frac{a}{r}\right)^2-\frac{6(4\mu+5\mu')}{135(2\mu+\mu')}\left(\frac{a}{r}\right)^4\right]\sin\theta. \quad \ldots\ldots\ldots\ldots\ldots\ldots (61)$$

$r\leqq a$:—

$$\widehat{rr'}=\rho g\xi\left[-\frac{5\mu'}{4\mu+5\mu'}-\frac{5\mu'}{23\mu+22\mu'}-\frac{15\mu'}{23\mu+22\mu'}\cos 2\theta\right]$$
$$+\rho g a\left[\left\{\frac{2\mu'}{3(2\mu+\mu')}\left(\frac{r}{a}\right)+\frac{7\mu'}{10(4\mu'+3\mu)}\left(\frac{r}{a}\right)\right\}\cos\theta\right.$$
$$\left.+\frac{7\mu'}{6(4\mu'+3\mu)}\left(\frac{r}{a}\right)\cos 3\theta\right]$$
$$+\rho' g a\left[\left\{\frac{11}{15}\left(\frac{r}{a}\right)-\frac{2(2\mu+3\mu')}{15(2\mu+\mu')}\left(\frac{r}{a}\right)\right\}\cos\theta\right], \quad \ldots\ldots\ldots\ldots\ldots\ldots (62)$$

$$\widehat{\theta\theta'}=\rho g\xi\left[-\frac{5\mu'}{4\mu+5\mu'}-\frac{5\mu'}{23\mu+22\mu'}+\frac{15\mu'}{23\mu+22\mu'}\cos 2\theta\right]$$
$$+\rho g a\left[\frac{4\mu'}{3(2\mu+\mu')}\left(\frac{r}{a}\right)+\frac{7\mu'}{30(4\mu'+3\mu)}\left(\frac{r}{a}\right)\right\}\cos\theta-\frac{7\mu'}{6(4\mu'+3\mu)}\left(\frac{r}{a}\right)\cos 3\theta\Big]$$
$$+\rho' g a\left[\frac{7}{15}\left(\frac{r}{a}\right)-\frac{4}{15}\frac{(2\mu+3\mu')}{(2\mu+\mu')}\left(\frac{r}{a}\right)\right]\cos\theta, \quad \ldots\ldots\ldots\ldots\ldots\ldots (63)$$

$$\widehat{\phi\phi'}=\rho g\xi\left[-\frac{5\mu'}{4\mu+5\mu'}+\frac{10\mu'}{23\mu+22\mu'}-\frac{15\mu'}{2(23\mu+22\mu')}\cos 2\theta\right]$$

$$+\rho ga\left[\frac{4\mu'}{3(2\mu+\mu')}\left(\frac{r}{a}\right)-\frac{14\mu'}{15(4\mu'+3\mu)}\left(\frac{r}{a}\right)\right]\cos\theta$$

$$+\rho' ga\left[\frac{7}{15}\left(\frac{r}{a}\right)-\frac{4(2\mu+3\mu')}{15(2\mu+\mu')}\left(\frac{r}{a}\right)\right]\cos\theta, \quad \ldots\ldots\ldots\ldots\ldots\ldots (64)$$

$$\widehat{r\theta}'=\rho g\xi\left[\frac{15\mu'}{23\mu+22\mu'}\sin 2\theta\right]$$

$$+\rho ga\left[\left\{\frac{\mu'}{3(2\mu+\mu')}\left(\frac{r}{a}\right)-\frac{7\mu'}{30(4\mu'+3\mu)}\left(\frac{r}{a}\right)\right\}\sin\theta\right.$$

$$\left.-\frac{7\mu'}{6(4\mu'+3\mu)}\left(\frac{r}{a}\right)\sin 3\theta\right]$$

$$+\rho' ga\left[-\frac{2}{15}\left(\frac{r}{a}\right)-\frac{2\mu+3\mu'}{15(2\mu+\mu')}\left(\frac{r}{a}\right)\right]\sin\theta. \quad \ldots\ldots\ldots\ldots\ldots\ldots (65)$$

To obtain these expressions (58), (59), (60), (61), (62), (63), (64) and (65), use has been made of the following formulae:

$$\left.\begin{aligned} &P_0(\cos\theta)=1,\ P_1(\cos\theta)=\cos\theta,\ P_2(\cos\theta)=\frac{1}{4}(1+3\cos 2\theta),\\ &P_3(\cos\theta)=\frac{1}{8}(3\cos\theta+5\cos 3\theta). \end{aligned}\right\} \quad \ldots\ldots (66)$$

To ascertain the distributions of stresses in the medium and those in the spherical inclusion, we take the following numerical examples. Putting $\frac{r}{a}=1$, we tabulated the magnitudes of the separate terms related to $\rho g\xi$, ρga and $\rho' ga$ in all stress components expressed by (58), (59), (60), (61), (62), (63), (64), (65) in the annexed tables when $\frac{\mu'}{\mu}=\frac{1}{5}$, 5, and ∞ (Table I, II, III, IV, V, VI, VII, VIII, IX, X, XI, XII, XIII, XIV, XV, XVI, XVII, XVIII), and the following figures (Fig. 2a, 2b, 2c, 3a, 3b, 3c, 4a, 4b, 4c, 5a, 5b, 5c, 6a, 6b, 6c, 7a, 7b, 7c) shew us these results. In these figures, the abscissa is the angle of colatitude θ from 0° to 180°, and the parameter of each curve is the magnitude of $\frac{\mu'}{\mu}$.

From these figures we can see many valuable facts, and some of them are summarised as follows:

1. The terms related to $\rho g\xi$ of the components of stresses $\widehat{rr}'_{r=a}$, $\widehat{\theta\theta}'_{r=a}$, $\widehat{\phi\phi}'_{r=a}$ of the heterogeneous spherical inclusion and those of the components of stresses $\widehat{rr}_{r=a}$, $\widehat{\theta\theta}_{r=a}$, $\widehat{\phi\phi}_{r=a}$ of the surrounding medium have

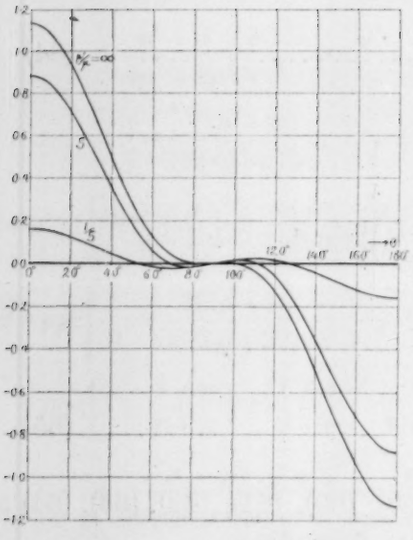

Fig. 2a. Magnitude of the term related to ρga of $\widehat{rr}_{r=a}$ $(=\widehat{rr'}_{r=a})$ when $\frac{\mu'}{\mu}=\frac{1}{5}$, 5 and ∞.

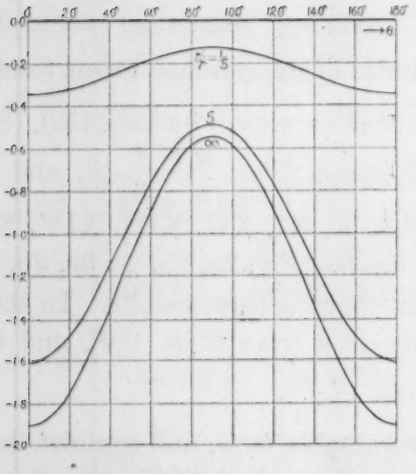

Fig. 2b. Magnitude of the term related to $\rho g\xi$ of $\widehat{rr}_{r=a}$ $(=\widehat{rr'}_{r=a})$ when $\frac{\mu'}{\mu}=\frac{1}{5}$, 5 and ∞.

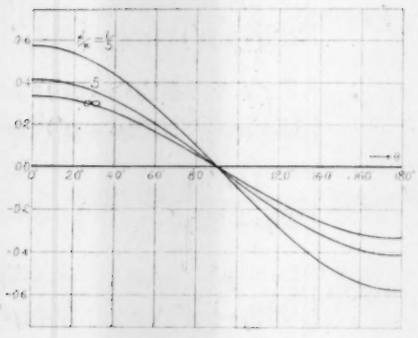

Fig. 2c. Magnitude of the term related to $\rho' ga$ of $\widehat{rr}_{r=a}$ $(=\widehat{rr'}_{r=a})$ when $\frac{\mu'}{\mu}=\frac{1}{5}$, 5 and ∞.

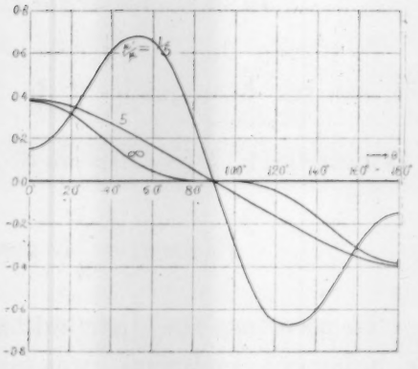

Fig. 3a. Magnitude of the term related to ρga of $\widehat{\theta\theta}_{r=a}$ when $\frac{\mu'}{\mu}=\frac{1}{5}, 5, \infty$.

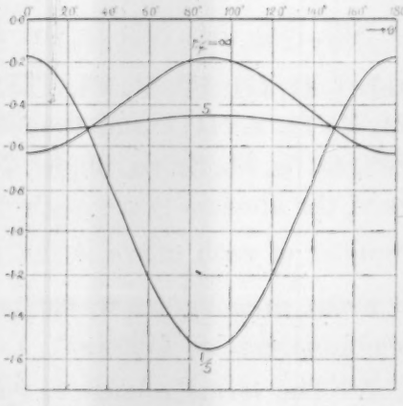

Fig. 3b. Magnitude of term related to $\rho g\xi$ of $\widehat{\theta\theta}_{r=a}$ when $\frac{\mu'}{\mu}=\frac{1}{5}$, 5 and ∞.

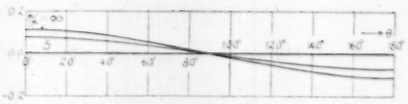

Fig. 3c. Magnitude of term related to $\rho' ga$ of $\widehat{\theta\theta}_{r=a}$ when $\frac{\mu'}{\mu}=\frac{1}{5}$, 5 and ∞.

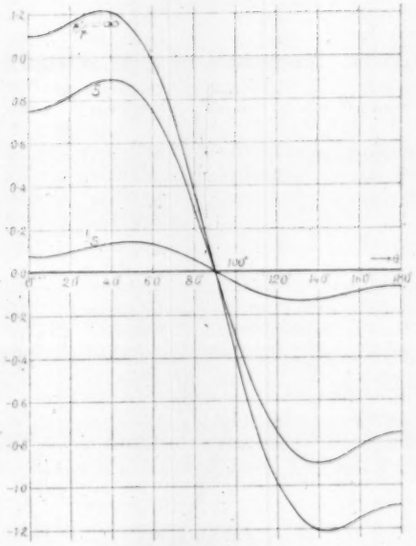

Fig. 4a. Magnitude of term related to ρga of $\widehat{\theta\theta'}_{r=a}$ when $\frac{\mu'}{\mu}=\frac{1}{5}$, 5 and ∞.

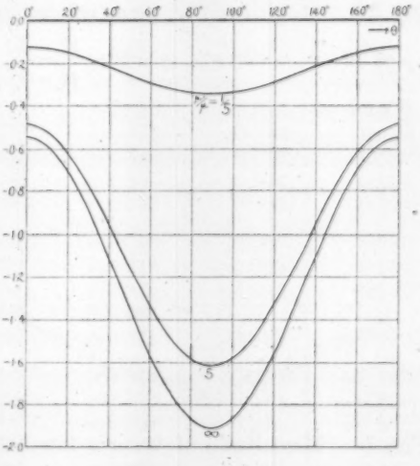

Fig. 4b. Magnitude of term related to $\rho g\xi$ of $\widehat{\theta\theta'}_{r=a}$ when $\frac{\mu'}{\mu}=\frac{1}{5}$, 5 and ∞.

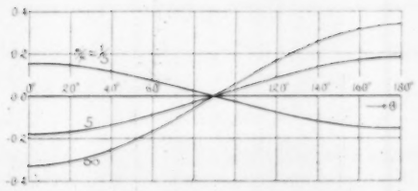

Fig. 4c. Magnitude of term related to $\rho' ga$ of $\widehat{\theta\theta'}_{r=a}$ when $\frac{\mu'}{\mu}=\frac{1}{5}$, 5 and ∞.

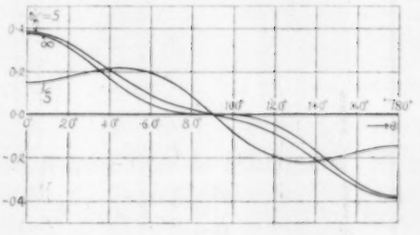

Fig. 5a. Magnitude of term related to ρga of $\widehat{\phi\phi}_{r=a}$ when $\frac{\mu'}{\mu}=\frac{1}{5}$, 5 and ∞.

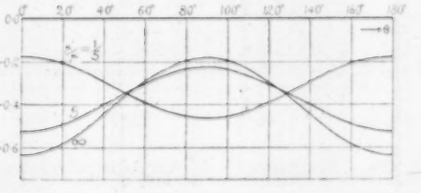

Fig. 5b. Magnitude of term related to $\rho g\xi$ of $\widehat{\phi\phi}_{r=a}$ when $\frac{\mu'}{\mu}=\frac{1}{5}$, 5 and ∞.

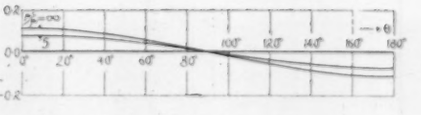

Fig. 5c. Magnitude of term related to $\rho' ga$ of $\widehat{\phi\phi}_{r=a}$ when $\frac{\mu'}{\mu}=\frac{1}{5}$, 5 and ∞.

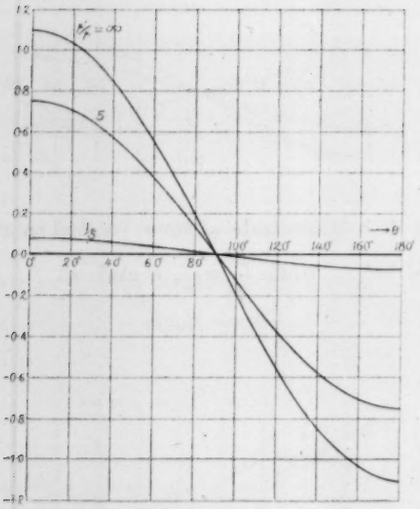

Fig. 6a. Magnitude of term related to ρga of $\widehat{\phi\phi'}_{r=a'}$ when $\frac{\mu'}{\mu}=\frac{1}{5}$, 5 and ∞.

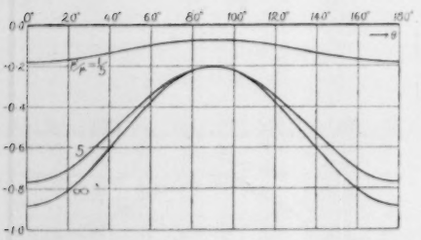

Fig. 6b. Magnitude of term related to $\rho g\xi$ of $\widehat{\phi\phi'}_{r=a}$ when $\frac{\mu'}{\mu}=\frac{1}{5}$, 5 and ∞.

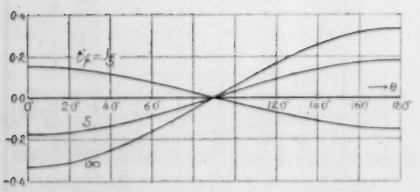

Fig. 6c. Magnitude of term related to $\rho' ga$ of $\widehat{\phi\phi'}_{r=a}$ when $\frac{\mu'}{\mu}=\frac{1}{5}$, 5 and ∞.

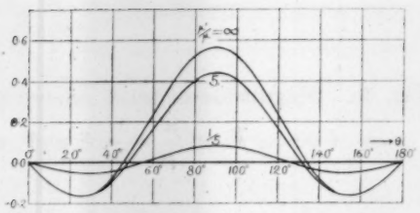

Fig. 7a. Magnitude of term related to ρga of $\widehat{r\theta}_{r=a}$ $(=\widehat{r\theta'}_{r=a})$ when $\frac{\mu'}{\mu}=\frac{1}{5}$, 5 and ∞.

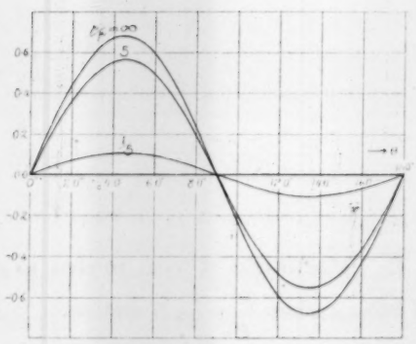

Fig. 7b. Magnitude of term related to $\rho g\xi$ of $\widehat{r\theta}_{r=a}$ $(=\widehat{r\theta'}_{r=a})$ when $\frac{\mu'}{\mu}=\frac{1}{5}$, 5 and ∞.

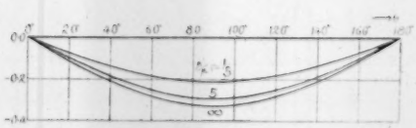

Fig. 7c. Magnitude of term related to $\rho' ga$ of $\widehat{r\theta}_{r=a}$ $(=\widehat{r\theta'}_{r=a})$ when $\frac{\mu'}{\mu}=\frac{1}{5}$, 5 and ∞.

Table I.

Magnitudes of separate terms related to $\rho g\xi$, ρga and $\rho' ga$ of $\widehat{rr}_{r=a}$ $(=\widehat{rr'}_{r=a})$ when $\frac{\mu'}{\mu}=\frac{1}{5}$.

θ	$\rho g\xi$	ρga	$\rho' ga$
0°	−0·347	0·160	0·576
10°	−0·340	0·150	0·567
20°	−0·321	0·123	0·541
30°	−0·292	0·085	0·498
45°	−0·236	0·025	0·407
60°	−0·180	−0·013	0·288
70°	−0·151	−0·020	0·196
80°	−0·132	−0·014	0·100
90°	−0·125	0	0
100°	−0·132	0·014	0·100
110°	−0·151	0·020	−0·196
120°	−0·180	0·013	−0·288
135°	−0·236	−0·025	−0·407
150°	−0·292	−0·085	−0·498
160°	−0·321	−0·123	−0·541
170°	−0·340	−0·150	−0·567
180°	−0·347	−0·160	−0·576

Table II.

Magnitudes of separate terms related to $\rho g\xi$, ρga and $\rho' ga$ of $\widehat{rr}_{r=a}$ $(\widehat{rr'}_{r=a})$ when $\frac{\mu'}{\mu}=5$.

	$\rho g\xi$	ρga	$\rho' ga$
0°	−1·613	0·882	0·412
10°	−1·579	0·838	0·406
20°	−1·482	0·717	0·387
30°	−1·331	0·544	0·357
45°	−1·050	0·264	0·291
60°	−0·769	0·060	0·206
70°	−0·618	−0·005	0·142
80°	−0·521	−0·018	0·072
90°	−0·487	0	0
100°	−0·521	0·018	−0·072
110°	−0·618	0·005	−0·142
120°	−0·769	−0·060	−0·206
135°	−1·050	−0·264	−0·291
150°	−1·331	−0·544	−0·357
160°	−1·482	−0·717	−0·387
170°	−1·579	−0·838	−0·406
180°	−1·613	−0·882	−0·412

Table III.

Magnitudes of separate terms related to $\rho g\xi$, ρga and $\rho' ga$ of $\widehat{rr}_{r=a}$ $(\widehat{rr'}_{r=a})$ when $\frac{\mu'}{\mu}=\infty$.

θ	$\rho g\xi$	ρga	$\rho' ga$
0°	−1·909	1·138	0·335
10°	−1·868	1·083	0·330
20°	−1·749	0·936	0·315
30°	−1·568	0·729	0·290
45°	−1·228	0·388	0·236
60°	−0·888	0·129	0·167
70°	−0·707	0·035	0·114
80°	−0·588	0	0·058
90°	−0·547	0	0
100°	−0·588	0	−0·058
110°	−0·707	−0·035	−0·114
120°	−0·888	−0·129	−0·167
135°	−1·228	−0·388	−0·236
150°	−1·568	−0·729	−0·290
160°	−1·749	−0·936	−0·315
170°	−1·863	−1·083	−0·330
180°	−1·909	−1·138	−0·335

Table IV.

Magnitudes of separate terms related to ρga, $\rho g\xi$ and $\rho' ga$ of $\widehat{\theta\theta}_{r=a}$ when $\frac{\mu'}{\mu}=\frac{1}{5}$.

θ	$\rho g\xi$	ρga	$\rho' ga$
0°	−0·174	0·149	−0·010
10°	−0·216	0·193	−0·010
20°	−0·337	0·312	−0·010
30°	−0·521	0·466	−0·009
45°	−0·867	0·655	−0·009
60°	−1·213	0·658	−0·007
70°	−1·397	0·521	−0·005
80°	−1·518	0·288	−0·003
90°	−1·560	0	−0·002
100°	−1·518	−0·288	0
110°	−1·397	−0·521	0·002
120°	−1·213	−0·658	0·003
135°	−0·867	−0·655	0·005
150°	−0·521	−0·466	0·007
160°	−0·337	−0·312	0·009
170°	−0·216	−0·193	0·010
180°	−0·174	−0·149	0·010

Table V.

Magnitudes of separate terms related to $\rho g\xi$, ρga and $\rho' ga$ of $\widehat{\theta\theta}_{r=a}$ when $\frac{\mu'}{\mu}=5$.

θ	$\rho g\xi$	ρga	$\rho' ga$
0°	-0·529	0·385	0·073
10°	−0·527	0·377	0·072
20°	−0·520	0·355	0·069
30°	−0·510	0·318	0·063
45°	−0·491	0·248	0·052
60°	−0·472	0·167	0·036
70°	−0·462	0·111	0·025
80°	−0·455	0·055	0·013
90°	−0·453	0	0
100°	−0·455	−0·055	−0·013
110°	−0·462	−0·111	−0·025
120°	−0·472	-0·167	−0·036
135°	−0·491	-0·248	−0·052
150°	−0·510	−0·318	−0·063
160°	−0·520	−0·355	−0·069
170°	−0·527	−0·377	−0·072
180°	-0·529	−0·385	−0·073

Table VI.

Magnitudes of separate terms related to $\rho g\xi$, ρga and $\rho' ga$ of $\widehat{\theta\theta}_{r=a}$ when $\frac{\mu'}{\mu}=\infty$.

θ	$\rho g\xi$	ρga	$\rho' ga$
0°	−0·637	0·378	0·111
10°	−0·623	0·361	0·109
20°	−0·584	0·313	0·104
30°	−0·523	0·243	0·096
45°	−0·410	0·130	0·079
60°	−0·297	0·043	0·056
70°	−0·236	0·012	0·038
80°	−0·197	0	0·019
90°	−0·183	0	0
100°	−0·197	0	−0·019
110°	−0·236	−0·012	−0·038
120°	−0·297	−0·043	−0·056
135°	−0·410	−0·130	−0·079
150°	−0·523	−0·243	−0·096
160°	−0·584	−0·313	−0·104
170°	−0·623	−0·361	−0·109
180°	−0·637	−0·378	−0·111

Table VII.

Magnitudes of separate terms related to $\rho g\xi$, ρga and $\rho' ga$ of $\widehat{\theta\theta'}_{r=a}$ when $\frac{\mu'}{\mu}=\frac{1}{5}$.

θ	$\rho g\xi$	ρga	$\rho' ga$
0°	−0·127	0·072	0·152
10°	−0·134	0·078	0·150
20°	−0·152	0·095	0·143
30°	−0·181	0·115	0·132
45°	−0·236	0·137	0·107
60°	−0·291	0·128	0·076
70°	−0·320	0·099	0·052
80°	−0·338	0·053	0·026
90°	−0·345	0	0
100°	−0·338	−0·053	−0·026
110°	−0·320	−0·099	−0·052
120°	−0·291	−0·128	−0·076
135°	−0·236	−0·137	−0·107
150°	−0·181	−0·115	−0·132
160°	−0·152	−0·095	−0·143
170°	−0·134	−0·078	−0·150
180°	−0·127	−0·072	−0·152

Table VIII.

Magnitudes of separate terms related to $\rho g\xi$, ρga and $\rho' ga$ of $\widehat{\theta\theta'}_{r=a}$ when $\frac{\mu'}{\mu}=5$.

θ	$\rho g\xi$	ρga	$\rho' ga$
0°	−0·488	0·751	−0·180
10°	−0·522	0·772	−0·177
20°	−0·619	0·819	−0·169
30°	−0·770	0·871	−0·156
45°	−1·051	0·890	−0·127
60°	−1·332	0·756	−0·090
70°	−1·483	0·563	−0·062
80°	−1·580	0·301	−0·031
90°	−1·614	0	0
100°	−1·580	−0·301	0·031
100°	−1·483	−0·563	0·062
120°	−1·332	−0·756	0·090
135°	−1·051	−0·890	0·127
150°	−0·770	−0·871	0·156
160°	−0·619	−0·819	0·169
170°	−0·522	−0·772	0·177
180°	−0·488	−0·751	0·180

Table IX.

Magnitudes of separate terms related to $\rho g\xi$, ρga and $\rho' ga$ of $\widehat{\theta\theta'}_{r=a}$ when $\frac{\mu'}{\mu}=\infty$.

θ	$\rho g\xi$	ρga	$\rho' ga$
0°	−0·544	1·098	−0·333
10°	−0·585	1·112	−0·328
20°	−0·704	1·159	−0·313
30°	−0·886	1·203	−0·288
45°	−1·227	1·186	−0·235
60°	−1·568	0·987	−0·166
70°	−1·750	0·733	−0·114
80°	−1·869	0·388	−0·058
90°	−1·910	0	0
100°	−1·869	−0·388	0·058
110°	−1·750	−0·733	0·114
120°	−1·568	−0·987	0·166
135°	−1·227	−1·186	0·235
150°	−0·886	−1·203	0·288
160°	−0·704	−1·159	0·313
170°	−0·585	−1·912	0·328
180°	−0·544	−1·098	0·333

Table X.

Magnitudes of separate terms related to $\rho g\xi$, ρga and $\rho' ga$ of $\widehat{\phi\phi}_{r=a}$ when $\frac{\mu'}{\mu}=\frac{1}{5}$.

θ	$\rho g\xi$	ρga	$\rho' ga$
0°	−0·173	0·149	−0·010
10°	−0·182	0·157	−0·010
20°	−0·207	0·176	−0·009
30°	−0·246	0·200	−0·009
45°	−0·319	0·221	−0·007
60°	−0·392	0·197	−0·005
70°	−0·431	0·150	−0·003
80°	−0·456	0·081	−0·002
90°	−0·465	0	0
100°	−0·456	−0·081	0·002
110°	−0·431	−0·150	0·003
120°	−0·392	−0·197	0·005
135°	−0·319	−0·221	0·007
150°	−0·246	−0·200	0·009
160°	−0·207	−0·176	0·009
170°	−0·182	−0·157	0·010
180°	−0·173	−0·149	0·010

Table XI.

Magnitudes of separate terms related to $\rho g\xi$, ρga and $\rho' ga$ of $\widehat{\phi\phi}_{r=a}$ when $\frac{\mu'}{\mu}=5$.

θ	$\rho g\xi$	ρga	$\rho' ga$
0°	−0·527	0·385	0·073
10°	−0·518	0·371	0·072
20°	−0·492	0·332	0·069
30°	−0·452	0·274	0·063
45°	−0·377	0·176	0·052
60°	−0·302	0·090	0·036
70°	−0·262	0·049	0·025
80°	−0·236	0·021	0·013
90°	−0·227	0	0
100°	−0·236	−0·021	−0·013
110°	−0·262	−0·049	−0·025
120°	−0·302	−0·090	−0·036
135°	−0·377	−0·176	−0·052
150°	−0·452	−0·274	−0·063
160°	−0·492	−0·332	−0·069
170°	−0·518	−0·371	−0·072
180°	−0·527	−0·385	−0·073

Table XII.

Magnitudes of separate terms related to $\rho g\xi$, ρga and $\rho' ga$ of $\widehat{\phi\phi}_{r=a}$ when $\frac{\mu'}{\mu}=\infty$.

θ	$\rho g\xi$	ρga	$\rho' ga$
0°	−0·636	0·378	0·111
10°	−0·622	0·361	0·109
20°	−0·583	0·313	0·104
30°	−0·522	0·243	0·096
45°	−0·409	0·130	0·079
60°	−0·296	0·043	0·056
70°	−0·235	0·012	0·038
80°	−0·196	0	0·019
90°	−0·182	0	0
100°	−0·196	0	−0·019
110°	−0·235	−0·012	−0·038
120°	−0·296	−0·043	−0·056
135°	−0·409	−0·130	−0·079
150°	−0·522	−0·243	−0·096
160°	−0·583	−0·313	−0·104
170°	−0·622	−0·361	−0·109
180°	−0·636	−0·378	−0·111

Table XIII.

Magnitudes of separate terms related to $\rho g\xi$, ρga and $\rho' ga$ of $\widehat{\phi\phi'}_{r=a}$ when $\frac{\mu'}{\mu}=\frac{1}{5}$.

θ	$\rho g\xi$	ρga	$\rho' ga$
0°	−0·182	0·072	0·152
10°	−0·179	0·071	0·150
20°	−0·169	0·068	0·143
30°	−0·155	0·062	0·132
45°	−0·127	0·051	0·107
60°	−0·099	0·036	0·076
70°	−0·085	0·025	0·052
80°	−0·075	0·013	0·026
90°	−0·072	0	0
100°	−0·075	−0·013	−0·026
110°	−0·085	−0·025	−0·052
120°	−0·099	−0·036	−0·076
135°	−0·127	−0·051	−0·107
150°	−0·155	−0·062	−0·132
160°	−0·169	−0·068	−0·143
170°	−0·179	−0·071	−0·150
180°	−0·182	−0·072	−0·152

Table XIV.

Magnitudes of separate terms related to $\rho g\xi$, ρga and $\rho' ga$ of $\widehat{\phi\phi}_{r=a}$ when $\frac{\mu'}{\mu}=5$.

θ	$\rho g\xi$	ρga	$\rho' ga$
0°	−0·769	0·750	−0·180
10°	−0·752	0·739	−0·177
20°	−0·703	0·705	−0·169
30°	−0·628	0·649	−0·156
45°	−0·487	0·530	−0·127
60°	−0·346	0·375	−0·090
70°	−0·271	0·256	−0·062
80°	−0·222	0·130	−0·031
90°	−0·205	0	0
100°	−0·222	−0·130	0·031
110°	−0·271	−0·256	0·062
120°	−0·346	−0·375	0·090
135°	−0·487	−0·530	0·127
150°	−0·628	−0·649	0·156
160°	−0·703	−0·705	0·169
170°	−0·752	−0·739	0·177
180°	−0·769	−0·750	0·180

Table XV.

Magnitudes of separate terms related to $\rho g\xi$, ρga and $\rho' ga$ of $\widehat{\phi\phi'}_{r=a}$ when $\frac{\mu'}{\mu}=\infty$.

θ	$\rho g\xi$	ρga	$\rho' ga$
0°	−0·887	1·10	−0·333
10°	−0·866	1·083	−0·328
20°	−0·807	1·033	−0·313
30°	−0·716	6·954	−0·288
45°	−0·546	0·778	−0·235
60°	−0·376	0·550	−0·166
70°	−0·285	0·376	−0·114
80°	−0·226	0·191	−0·058
90°	−0·205	0	0
100°	−0·226	−0·191	0·058
110°	−0·285	−0·376	0·114
120°	−0·376	−0·550	0·166
135°	−0·546	−0·778	0·235
150°	−0·716	−0·954	0·288
160°	−0·807	−0·033	0·313
170°	−0·866	−1·083	0·328
180°	−0·887	−1·10	0·333

Table XVI.

Magnitudes of separate terms related to $\rho g\xi$, ρga and $\rho' ga$ $\widehat{r\theta}_{r=a}$ $(=\widehat{r\theta'}_{r=a})$ when $\frac{\mu'}{\mu}=\frac{1}{5}$.

θ	$\rho g\xi$	ρga	$\rho' ga$
0°	0	0	0
10°	0·037	−0·028	−0·037
20°	0·070	−0·048	−0·073
30°	0·094	−0·053	−0·106
45°	0·109	−0·032	−0·150
60°	0·094	0·015	−0·184
70°	0·070	0·047	−0·199
80°	0·037	0·071	−0·209
90°	0	0·079	−0·212
100°	−0·037	0·071	−0·209
110°	−0·070	0·047	−0·199
120°	−0·098	0·015	−0·184
135°	−0·109	−0·032	−0·150
150°	−0·098	−0·053	−0·106
160°	−0·070	−0·048	−0·703
170°	−0·037	−0·028	−0·037
180°	0	0	0

Table XVII.

Magnitudes of separate terms related to $\rho g\xi$, ρga and $\rho' ga$ of $\widehat{r\theta}_{r=a}$ $(=\widehat{r\theta'}_{r=a})$ when $\frac{\mu'}{\mu}=\frac{1}{5}$.

θ	$\rho g\xi$	ρga	$\rho' ga$
0°	0	0	0
10°	0·193	−0·094	−0·051
20°	0·362	−0·156	−0·101
30°	0·490	−0·160	−0·147
45°	0·564	−0·047	−0·208
60°	0·490	0·162	−0·255
70°	0·362	0·303	−0·277
80°	0·193	0·404	−0·290
90°	0	0·441	−0·295
100°	−0·193	0·404	−0·290
110°	−0·362	0·303	−0·277
120°	−0·490	0·162	−0·255
135°	−0·564	−0·047	−0·208
150°	−0·490	−0·160	−0·147
160°	−0·362	−1·156	−0·101
170°	−0·193	−0·094	−0·051
180°	0	0	0

Table XVIII.

Magnitudes of separate terms related to $\rho g\xi$, ρga and $\rho' ga$ of $\widehat{r\theta}_{r=a}$ $(\widehat{r\theta'}_{r=a})$ when $\frac{\mu'}{\mu}=\infty$.

θ	$\rho g\xi$	ρga	$\rho' ga$
0°	0	0	0
10°	0·233	−0·098	−0·058
20°	0·438	−0·159	−0·114
30°	0·590	−0·155	−0·167
45°	0·682	−0·012	−0·236
60°	0·590	0·237	−0·278
70°	0·438	0·404	−0·313
80°	0·233	0·523	−0·328
90°	0	0·564	−0·333
100°	−0·233	0·523	−0·328
110°	−0·438	0·404	−0·313
120°	−0·590	0·237	−0·268
135°	−0·682	−0·012	−3·236
150°	−0·590	−0·155	−0·167
160°	−0·438	−0·159	−0·114
170°	−0·233	−0·098	−0·058
180°	0	0	0

symmetrical distributions with respect to the plane $\theta=90°$. The terms related to $\rho g\xi$ of the shear stresses $\widehat{r\theta}_{r=a}$, $\widehat{r\theta'}_{r=a}$ have, however, unsymmetrical distributions with respect to this plane.

2. The terms related to ρga of the components of stresses $\widehat{rr}_{r=a}$, $\widehat{\theta\theta}_{r=a}$, $\widehat{\phi\phi}_{r=a}$, and $\widehat{rr'}_{r=a}$, $\widehat{\theta\theta'}_{r=a}$, $\widehat{\phi\phi'}_{r=a}$ have unsymmetrical distributions with respect to the plane $\theta=90°$ and those related to ρga of $\widehat{r\theta}_{r=a}$, $\widehat{r\theta'}_{r=a}$ have symmetrical ones with respect to this plane.

3. The terms concerning $\rho' ga$ of $\widehat{rr}$, $\widehat{\theta\theta}$, $\widehat{\phi\phi}$, $\widehat{rr'}$, $\widehat{\theta\theta'}$, $\widehat{\phi\phi'}$ are also unsymmetry with respect to the plane $\theta=90°$, and those related to of $\widehat{r\theta}$ and $\widehat{r\theta'}$ have symmetrical ones with respect to the plane $\theta=90°$.

4. When the depth ξ of the centre of spherical inclusion is deep, the stress distributions are mainly affected by the terms related to $\rho g\xi$ and the terms connected with ρga and $\rho' ga$ have no much effect upon the stress distributions. When ρ' is very large, however, the terms related to $\rho' ga$ have some effects upon them.

5. When the depth is moderately shallow, the respective terms related to ρga and $\rho' ga$, which are unbalancing force due to the body force, have some effects upon the stress distributions.

6. When the spherical inclusion is more rigid than the surrounding solid, the magnitudes of the respective terms with respect to $\rho g\xi$ and ρga of $\widehat{rr}_{r=a}$, $\widehat{rr'}_{r=a}$, $\widehat{r\theta}_{r=a}$, $\widehat{r\theta'}_{r=a}$ are large, and those of the terms related to $\rho' ga$ of $\widehat{r\theta}_{r=a}$ and $\widehat{r\theta'}_{r=a}$ are also large. The magnitudes of the terms related to $\rho' ga$ of $\widehat{rr}_{r=a}$ and $\widehat{rr'}_{r=a}$, however, are small in this case.

7. When the spherical inclusion is more rigid than the surrounding medium, the magnitudes of the respective terms related to $\rho g\xi$, ρga and $\rho' ga$ of $\widehat{\theta\theta}_{r=a}$ are generally small, and those of the terms related to $\rho g\xi$, ρga and $\rho' ga$ of $\widehat{\theta\theta'}_{r=a}$, $\widehat{\phi\phi'}_{r=a}$, on the contrary, are generally large. The terms related to $\rho g\xi$ and ρga, $\rho' ga$ of the component of stress $\widehat{\phi\phi}_{r=a}$ have special distributions differ from those of all other components of stress when the magnitude of $\frac{\mu'}{\mu}$ is large.

To see the properties of stress distributions along radial directions from the center of spherical inclusion, we obtained the following figures by the usage of the expressions (66), (67), (68), (69), (70), (71), (72), and (73). (Fig. 8a, 8b, 8c, 9a, 9b, 9c, 10a, 10b, 10c, 11a, 11b, 11c.)

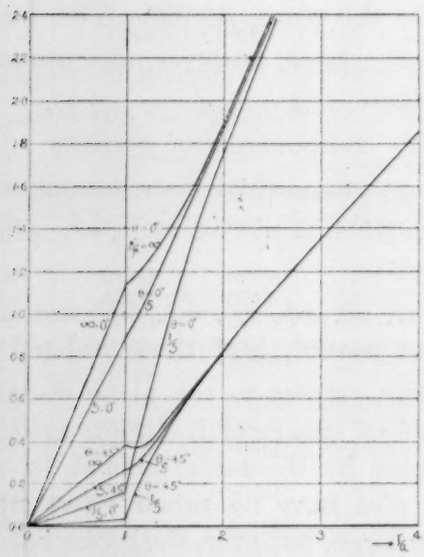

Fig. 8a. Magnitudes of respective terms related to ρga of $\widehat{rr}_{\substack{\theta=0^\circ \\ \theta=45^\circ}}$ and $\widehat{rr'}_{\substack{\theta=0^\circ \\ \theta=45^\circ}}$ when $\frac{\mu'}{\mu}=\frac{1}{5}$, 5 and ∞.

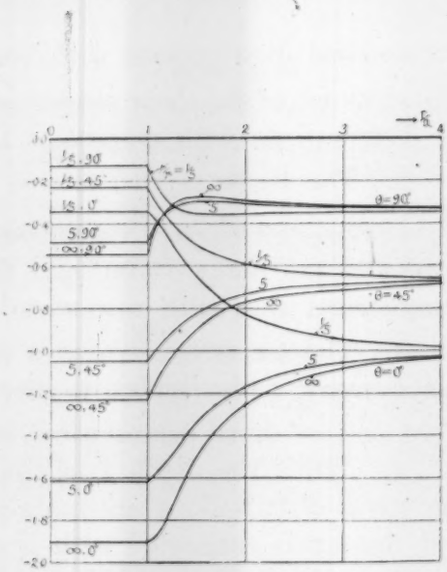

Fig. 8b. Magnitudes of respective terms related to $\rho g\xi$ of $\widehat{rr}_{\substack{\theta=0^\circ \\ \theta=40^\circ \\ \theta=90^\circ}}$ and $\widehat{rr'}_{\substack{\theta=0^\circ \\ \theta=45^\circ \\ \theta=90^\circ}}$ when $\frac{\mu}{\mu}=\frac{1}{5}$, 5 and ∞.

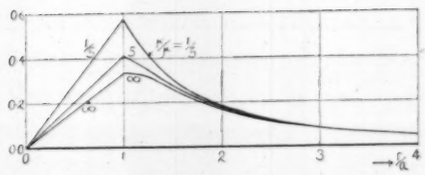

Fig. 8c. Magnitudes of respective terms related to $\rho' ga$ of $\widehat{rr}_{\theta=0^\circ}$ and $\widehat{rr}'_{\theta=0^\circ}$ when $\frac{\mu'}{\mu}=\frac{1}{5}$, 5 and ∞.

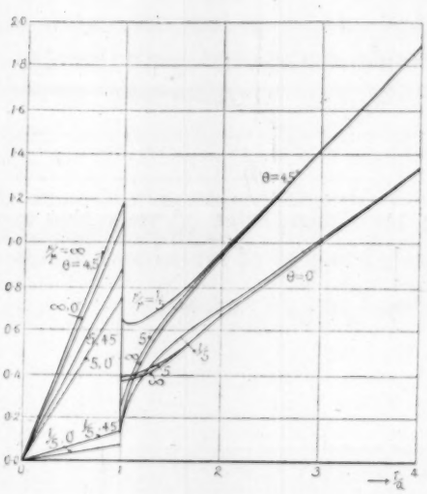

Fig. 9a. Magnitudes of respective terms related to ρga of $\widehat{\theta\theta}_{\substack{\theta=0^\circ \\ \theta=45^\circ}}$ and $\widehat{\theta\theta}'_{\substack{\theta=0^\circ \\ \theta=45^\circ}}$ when $\frac{\mu'}{\mu}=\frac{1}{5}$, 5 and ∞.

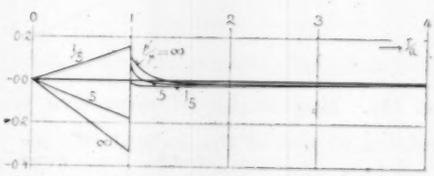

Fig. 9c. Magnitudes of respective terms related to $\rho' ga$ of $\widehat{\theta\theta}_{\theta=0^\circ}$ and $\widehat{\theta\theta}'_{\theta=0^\circ}$ when $\frac{\mu'}{\mu}=\frac{1}{5}$, 5 and ∞.

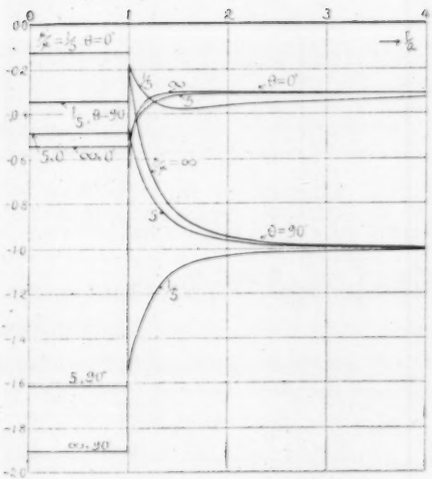

Fig. 9b. Magnitudes of respective terms related to $\rho g\xi$ of $\widehat{\theta\theta}_{\substack{\theta=0^\circ \\ \theta=90^\circ}}$ and $\widehat{\theta\theta}'_{\substack{\theta=0^\circ \\ \theta=90^\circ}}$ when $\frac{\mu'}{\mu}=\frac{1}{5}$, 5 and ∞.

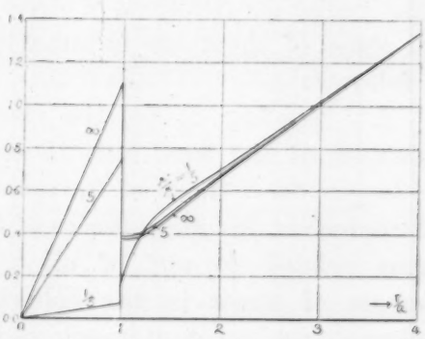

Fig. 10a. Magnitudes of respective terms related to ρga of $\widehat{\phi\phi}_{\theta=0^\circ}$ and $\widehat{\phi\phi}'_{\theta=0^\circ}$ when $\frac{\mu'}{\mu}=\frac{1}{5}$, 5 and ∞.

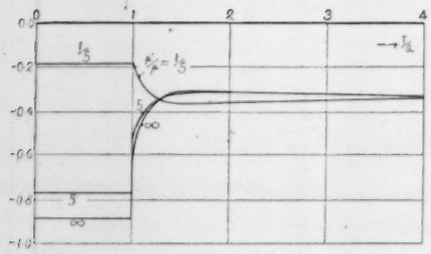

Fig. 10b. Magnitudes of respective terms related to $\rho g\xi$ of $\widehat{\phi\phi}_{\theta=0^\circ}$ and $\widehat{\phi\phi'}_{\theta=0^\circ}$ when $\frac{\mu'}{\mu}=\frac{1}{5}$, 5 and ∞.

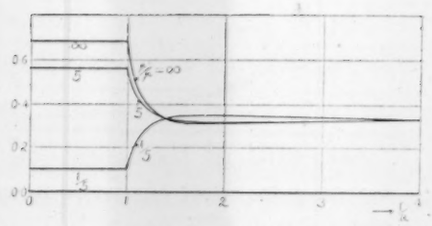

Fig. 11b. Magnitudes of respective terms related to $\rho g\xi$ of $\widehat{r\theta}_{\theta=45^\circ}$ and $\widehat{r\theta'}_{\theta=45^\circ}$ when $\frac{\mu'}{\mu}=\frac{1}{2}$, 5 and ∞.

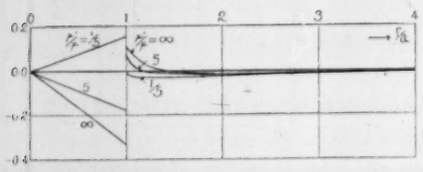

Fig. 10c. Magnitudes of respective terms related to $\rho' ga$ of $\widehat{\phi\phi}_{\theta=0^\circ}$ and $\widehat{\phi\phi'}_{\theta=0^\circ}$ when $\frac{\mu'}{\mu}=\frac{1}{5}$, 5 and ∞.

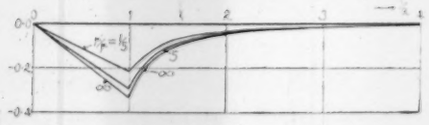

Fig. 11c. Magnitudes of respective terms related to $\rho' ga$ of $\widehat{r\theta}_{\theta=90^\circ}$ and $\widehat{r\theta'}_{\theta=90^\circ}$ when $\frac{\mu'}{\mu}=\frac{1}{5}$, 5 and ∞.

From the figures we can see many interesting facts with respect to the radial distributions of stresses, and some of them are summarised as follows:

1. Whether or not the elastic constants of the semi-infinite solid are larger than those of the spherical inclusion, the magnitudes of the terms related to $\rho g\xi$ of all components of stress in the spherical inclusion are constant along radial directions but not along colatitudinal directions. And the magnitudes of the terms related to ρga and $\rho' ga$ of the respective components of stresses of the heterogeneous inclusion increase linearly along radial directions.

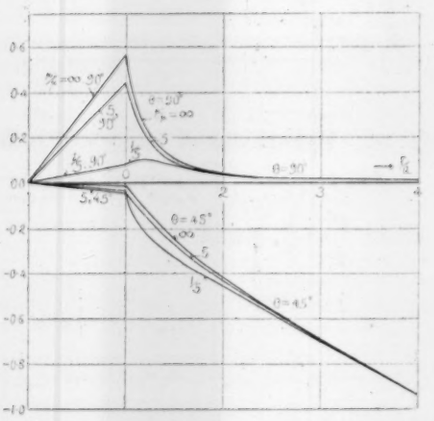

Fig. 11a. Magnitudes of respective terms related to ρga of $\widehat{r\theta}_{\substack{\theta=45^\circ \\ \theta=90^\circ}}$ and $\widehat{r\theta'}_{\substack{\theta=45^\circ \\ \theta=90^\circ}}$ when $\frac{\mu'}{\mu}=\frac{1}{5}$, 5 and ∞.

2. When the spherical inclusion is more rigid than the surrounding solid, the stresses are mainly accumulated in the spherical inclusion, and the stress components of the surrounding medium in the neighbourhood of the boundary surface are generally more or less released. In the reversed case, when the surrounding medium is more rigid than the included, the stresses are mainly accumulated in the former, especially in the neighbourhood of the boundary surface.

3. The region where the stress distributions in the semi-infinite solid affected by the presence of a spherical inclusion is limited in the boundary region of that spherical inclusion and the effective radius upon the distributions of stresses in the boundary medium is approximately four times the radius of the spherical inclusion.

Concluding this paper some remarkes are written as follows:[3]

The mathematical results obtained in this paper are not applicable to the case where $\frac{\mu'}{\mu}=0$ and the spherical inclusion has no rigidity. In this case the problem should be formally solved anew by the following boundary conditions.

$$r=a: \quad \left.\begin{aligned} &\widehat{rr}=\widehat{rr'},\\ &r\theta=\widehat{r\theta'}=0,\\ &u=u'. \end{aligned}\right\} \quad \ldots\ldots\ldots\ldots\ldots\ldots\ldots\ldots(67)$$

$$r\to\infty: \quad \left.\begin{aligned} &\widehat{rr}=\widehat{rr} \text{ expressed by (40),}\\ &\widehat{\theta\theta}=\widehat{\theta\theta} \quad \text{,,} \quad \text{,, (41),}\\ &\widehat{\phi\phi}=\widehat{\phi\phi} \quad \text{,,} \quad \text{,, (42),}\\ &\widehat{r\theta}=\widehat{r\theta} \quad \text{,,} \quad \text{,, (43),} \end{aligned}\right\} \quad \ldots\ldots\ldots\ldots(68)$$

---

3) The present writers must express their thanks to Dr. C. Tsuboi for his discussions on this point at the 70th coll. meeting of the institute, Dec. 20, 1932.

12. 重力の働ける半無限彈性體内に存在する球状塡充物附近の應力 (I)

地震研究所 { 西村源六郎
高山威雄

重力の作用してゐる半無限彈性體内に，それと密度，彈性常數の異つた球狀な物質が塡充してゐる場合，この物質の内外に於ける應力釣合を論じた．目的は地殻内部に異物質のある場合その附近で地殻内部の釣合がどの様にたもたれてゐるかを知り，地震發生の原因が應力釣合の破れる事にあるとすれば，どの様な關係でやぶれるものであるかを知る爲めに必要な第一の階段として試みたものである．解き方は半無限彈性體は plane strain に保たれてゐるとしてやり，異物質との硬さの異ひによる應力分布の趣を圖によつて詳しく示した．

13. *On Stresses in the Interior and in the Vicinity of a Horizontal Cylindrical Inclusion of Circular Section in a Gravitating Semi-infinite Elastic Solid. (I)*

By Genrokuro NISHIMURA and Takeo TAKAYAMA,

Earthquake Research Institute.

(Read Oct. 18, 1932.—Received March 20, 1933.)

1. For the same object of investigation stated in the previous paper,[1] we shall study the stress distribution in the interior and in the vicinity of a horizontal cylindrical matter of circular section included in a gravitating semi-infinite elastic solid. The investigation of the stress distribution around a horizontal circular hole in a semi-infinite gravitating solid has already been carried out by Professor N. Yamaguti[2] who solved the problem by the usage of stress function. The problem of a cylindrical matter of heterogeneity included in a semi-infinite gravitating solid has not yet been solved.

In the present study, as in the previous paper,[3] the state of the gravitating semi-infinite elastic solid is also one of *plane strain*.

2. Cylindrical coordinates (r, θ, z) are used. The axis z is coincident with the axis Oz of the cylindrical inclusion of which the radius is a, and the centre O is at the point $(x=-\xi,\ y=0)$ as shewn in Fig. 1. The azimuthal angle θ is taken counterclockwise from the axis ox which is taken to be vertically upward positive, and the axis oy is taken to be horizontal. The plane $x=\xi$ is the horizontal surface of the semi-infinite gravitating elastic solid of which the density and the gravity constant are respectively ρ and g. Let the density of the cylindrical inclusion be ρ', and also the gravity constant be g.

---

1) G. NISHIMURA and T. TAKAYAMA, "On Stresses in the Interior and in the Vicinity of a Spherical Inclusion in a Gravitating Semi-infinite Elastic Solid," *Bull. Earthq. Res. Intst.* **11** (1933).

2) N. YAMAGUTI," On the stresses Around a Horizontal Circular Hole in a Gravitating Solid," *Jour. Civil Engg.* Tokyo **15** (1929), 291.

3) G. NISHIMURA and T. TAKAYAMA, *loc. cit.*

4) The problem treated as plane stress was read in the Meeting of this Institute, Feb. 21, 1933, but is not yet pressed. N. Yamaguti also treated the problem as *plane strain* problem.

Now the top surface ($x=\xi$) of the solid is horizontal, and therefore there is no variation of the axial components of displacement and stress. Then the stress equations of equilibrium of the gravitating semi-infinite solid and the equilibrium of the gravitating cylindrical matter included in the solid are respectively expressed by the following equations:

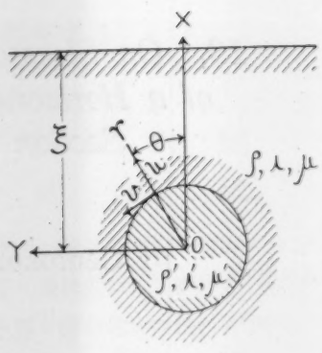

Fig. 1.

$$\left.\begin{aligned}&\frac{\partial \widehat{rr}}{\partial r}+\frac{1}{r}\frac{\partial \widehat{r\theta}}{\partial \theta}+\frac{\widehat{rr}-\widehat{\theta\theta}}{r}=\rho g\cos\theta,\\&\frac{\partial \widehat{r\theta}}{\partial r}+\frac{1}{r}\frac{\partial \widehat{\theta\theta}}{\partial \theta}+2\frac{\widehat{r\theta}}{r}=-\rho g\sin\theta,\end{aligned}\right\}\quad\cdots\cdots\cdots\cdots(1)$$

$$\left.\begin{aligned}&\frac{\partial \widehat{rr'}}{\partial r}+\frac{1}{r}\frac{\partial \widehat{r\theta'}}{\partial \theta}+\frac{\widehat{rr'}-\widehat{\theta\theta'}}{r}=\rho' g\cos\theta,\\&\frac{\partial \widehat{r\theta'}}{\partial r}+\frac{1}{r}\frac{\partial \widehat{\theta\theta'}}{\partial \theta}+2\frac{\widehat{r\theta'}}{r}=-\rho' g\sin\theta.\end{aligned}\right\}\quad\cdots\cdots\cdots\cdots(2)$$

The normal components of stress $\widehat{rr}$, $\widehat{\theta\theta}$, $\widehat{zz}$ and the shearing components of stress $\widehat{r\theta}$ of the gravitating semi-infinite solid are expressed by the radial and tangential components of displacement u, v in the following forms:

$$\left.\begin{aligned}&\widehat{rr}=\lambda\left\{\frac{1}{r}\frac{\partial(ru)}{\partial r}+\frac{1}{r}\frac{\partial v}{\partial\theta}\right\}+2\mu\frac{\partial u}{\partial r},\\&\widehat{\theta\theta}=\lambda\left\{\frac{1}{r}\frac{\partial(ru)}{\partial r}+\frac{1}{r}\frac{\partial v}{\partial\theta}\right\}+2\mu\left\{\frac{1}{r}\frac{\partial v}{\partial\theta}+\frac{u}{r}\right\},\\&\widehat{zz}=\lambda\left\{\frac{1}{r}\frac{\partial(ru)}{\partial r}+\frac{1}{r}\frac{\partial v}{\partial\theta}\right\},\\&\widehat{r\theta}=\mu\left\{\frac{\partial v}{\partial r}-\frac{v}{r}+\frac{1}{r}\frac{\partial u}{\partial\theta}\right\},\end{aligned}\right\}\quad\cdots\cdots\cdots(3)$$

where λ and μ are the Lame's elastic constants of the solid.

The normal components of stress $\widehat{rr'}$, $\widehat{\theta\theta'}$ and the shearing components of stress $\widehat{r\theta'}$ of the cylindrical matter of which the Lame's elastic constants are λ', μ' have the following expressions with respect to the radial and tangential components of displacements u', v' as follows:

$$\left.\begin{aligned}
\widehat{rr'} &= \lambda'\left\{\frac{1}{r}\frac{\partial(ru')}{\partial r}+\frac{1}{r}\frac{\partial v'}{\partial\theta}\right\}+2\mu'\frac{\partial u'}{\partial r'},\\
\widehat{\theta\theta'} &= \lambda'\left\{\frac{1}{r}\frac{\partial(ru')}{\partial r}+\frac{1}{r}\frac{\partial v'}{\partial\theta}\right\}+2\mu'\left\{\frac{1}{r}\frac{\partial v'}{\partial\theta}+\frac{u'}{r}\right\},\\
\widehat{zz'} &= \lambda'\left\{\frac{1}{r}\frac{\partial(ru')}{\partial r}+\frac{1}{r}\frac{\partial v'}{\partial\theta}\right\}.\\
\widehat{r\theta'} &= \mu'\left\{\frac{\partial v'}{\partial r}-\frac{v'}{r}+\frac{1}{r}\frac{\partial u'}{\partial\theta}\right\},
\end{aligned}\right\} \quad \ldots\ldots\ldots(4)$$

Eliminating $\widehat{rr}$, $\widehat{\theta\theta}$, $\widehat{r\theta}$ and $\widehat{rr'}$, $\widehat{\theta\theta'}$, $\widehat{r\theta'}$ from the equations (1) and (2) separately by the usage of (3) and (4), we obtain the following equations of equilibrium of the solid and the cylindrical matter included in the medium :

$$\left.\begin{aligned}
(\lambda+2\mu)\frac{\partial\Delta}{\partial r}-\frac{2\mu}{r}\frac{\partial\varpi}{\partial\theta} &= \rho g\cos\theta,\\
(\lambda+2\mu)\frac{1}{r}\frac{\partial\Delta}{\partial\theta}+2\mu\frac{\partial\varpi}{\partial r} &= -\rho g\sin\theta,
\end{aligned}\right\} \quad \ldots\ldots\ldots\ldots(5)$$

$$\left.\begin{aligned}
(\lambda'+2\mu')\frac{\partial\Delta'}{\partial r}-\frac{2\mu'}{r}\frac{\partial\varpi'}{\partial\theta} &= \rho' g\cos\theta,\\
(\lambda'+2\mu')\frac{1}{r}\frac{\partial\Delta'}{\partial\theta}+2\mu'\frac{\partial\varpi'}{\partial r} &= -\rho' g\sin\theta,
\end{aligned}\right\} \quad \ldots\ldots\ldots\ldots(6)$$

where

$$\left.\begin{aligned}
\Delta &= \frac{\partial u}{\partial r}+\frac{u}{r}+\frac{1}{r}\frac{\partial v}{\partial\partial},\\
2\varpi &= \frac{\partial v}{\partial r}+\frac{v}{r}-\frac{1}{r}\frac{\partial u}{\partial\theta},
\end{aligned}\right\} \quad \ldots\ldots\ldots\ldots\ldots\ldots(7)$$

$$\left.\begin{aligned}
\Delta' &= \frac{\partial u'}{\partial r}+\frac{u'}{r}+\frac{1}{r}\frac{\partial v'}{\partial\theta},\\
2\varpi' &= \frac{\partial v'}{\partial r}+\frac{v'}{r}-\frac{1}{r}\frac{\partial u'}{\partial\theta}.
\end{aligned}\right\} \quad \ldots\ldots\ldots\ldots\ldots\ldots(8)$$

Among the particular solutions satisfying (5) and (6) respectively, we take the following solutions which are useful for the present study :

$$\left.\begin{aligned}
\Delta &= 0,\\
2\varpi &= -\frac{\rho g}{\mu}r\sin\theta,
\end{aligned}\right\} \quad \ldots\ldots\ldots\ldots\ldots\ldots(9)$$

and

$$\left.\begin{aligned} \Delta' &= \frac{\rho' g r}{(\lambda'+2\mu')}\cos\theta, \\ 2\varpi' &= 0. \end{aligned}\right\} \quad \cdots\cdots\cdots\cdots\cdots\cdots (10)$$

Now the equations (5) and (6) give us the following equations:

$$\frac{\partial^2 \Delta}{\partial r^2}+\frac{1}{r}\frac{\partial \Delta}{\partial r}+\frac{1}{r^2}\frac{\partial^2 \Delta}{\partial \theta^2}=0, \quad \cdots\cdots\cdots\cdots (11)$$

$$\frac{\partial^2 \Delta'}{\partial r^2}+\frac{1}{r}\frac{\partial \Delta'}{\partial r}+\frac{1}{r^2}\frac{\partial^2 \Delta'}{\partial \theta^2}=0. \quad \cdots\cdots\cdots\cdots (12)$$

The respective solutions of (11) and (12) are expressed by

$$\Delta = B_0+\left\{B_1 r+\frac{C_1}{r}\right\}\cos\theta+\left\{B_2 r^2+\frac{C_2}{r^2}\right\}\cos 2\theta + \left\{B_3 r^3+\frac{C_3}{r^3}\right\}\cos 3\theta \quad \cdots\cdots\cdots\cdots\cdots\cdots (13)$$

$$\Delta' = D_0+D_1 r\cos\theta+D_2 r^2\cos 2\theta+D_3 r^3\cos 3\theta, \quad \cdots\cdots (14)$$

where B_0, B_1, B_2, B_3, C_1, C_2, C_3, D_0, D_1, D_2, D_3 are arbitrary constants to be determined by elasticity conditions.

Using (13) and (14) respectively, we obtain the following forms of 2ϖ and $2\varpi'$ which are particular solutions of (5) and (6):

$$2\varpi = \left\{\frac{(\lambda+2\mu)}{\mu}B_1 r+\frac{(\lambda+2\mu)}{\mu}\frac{C_1}{r}\right\}\sin\theta + \left\{\frac{(\lambda+2\mu)}{\mu}B_2 r^2+\frac{(\lambda+2\mu)}{\mu}\frac{C_2}{r^2}\right\}\sin 2\theta + \left\{\frac{(\lambda+2\mu)}{\mu}B_3 r^3+\frac{(\lambda+2\mu)}{\mu}\frac{C_3}{r^3}\right\}\sin 3\theta, \quad \cdots\cdots\cdots (15)$$

$$2\varpi' = \frac{(\lambda'+2\mu')}{\mu'}D_1 r\sin\theta+\frac{(\lambda'+2\mu')}{\mu}D_2 r^2\sin 2\theta + \frac{(\lambda'+2\mu')}{\mu'}D_3 r^3\sin 3\theta. \quad \cdots\cdots\cdots\cdots\cdots (16)$$

After some reductions we obtain the following equations in relation to u, v and Δ, 2ϖ from the relations expressed by (7):

$$\frac{\partial^2(ru)}{\partial r^2}+\frac{1}{r}\frac{\partial(ru)}{\partial r}+\frac{1}{r^2}\frac{\partial^2(ru)}{\partial\theta^2}=\frac{1}{r}\frac{\partial(r^2\Delta)}{\partial r}-2\frac{\partial\varpi}{\partial\theta}, \quad \cdots\cdots (17)$$

$$\frac{\partial^2(rv)}{\partial r^2}+\frac{1}{r}\frac{\partial(rv)}{\partial r}+\frac{1}{r^2}\frac{\partial^2(rv)}{\partial\theta^2}=\frac{\partial\Delta}{\partial\vartheta}+\frac{2}{r}\frac{\partial(r\varpi)}{\partial r}. \quad \cdots\cdots (18)$$

And also we have the following equations in relation to u', v', Δ' and $2\varpi'$ from the equations (8):

$$\frac{\partial^2(ru')}{\partial r^2}+\frac{1}{r}\frac{\partial(ru')}{\partial r}+\frac{1}{r^2}\frac{\partial^2(ru')}{\partial\theta^2}=\frac{1}{r}\frac{\partial(r^2\Delta')}{\partial r}-2\frac{\partial\varpi'}{\partial\theta}, \quad \ldots\ldots(19)$$

$$\frac{\partial^2(rv')}{\partial r^2}+\frac{1}{r}\frac{\partial(rv')}{\partial r}+\frac{1}{r^2}\frac{\partial^2(rv')}{\partial\theta^2}=\frac{\partial\Delta'}{\partial\theta}+\frac{2}{r}\frac{\partial(r\varpi')}{\partial r}. \quad \ldots\ldots(20)$$

Substituting (9), (13), (15) for the expressions of Δ and 2ϖ in the equations (17), (18), we obtain the particular solutions of (17) and (18) as follows:

$$\left.\begin{aligned} u=&\frac{1}{2}B_0r''+\left[B_1''+\frac{\rho g}{8\mu}r^2+\frac{(-\lambda+\mu)}{8\mu}B_1r^2+\left\{\frac{1}{2}+\frac{(\lambda+3\mu)}{2\mu}ln\frac{r}{a}\right\}\right]\cos\theta\\ &-\left\{\frac{\lambda}{6\mu}B_2r^3+\frac{(\lambda+2\mu)}{2\mu}\frac{C_2}{r}\right\}\cos 2\theta-\left\{\frac{(3\lambda+\mu)}{16\mu}B_3r^4+\frac{(3\lambda+5\mu)}{8\mu}\frac{C_3}{r^2}\right\}\cos 3\theta,\\ v=&\left[-\frac{3}{8}\frac{\rho g}{\mu}r^2+\frac{(3\lambda+5\mu)}{8\mu}B_1r^2-\left\{\frac{(\lambda+3\mu)}{2\mu}ln\frac{r}{a}+\frac{(\lambda+2\mu)}{2\mu}\right\}F_1-B_1''\right]\sin\theta\\ &+\left[\frac{(2\lambda+3\mu)}{6\mu}B_2r^3+\frac{1}{2}\frac{C_2}{r}\right]\sin 2\theta+\left[\frac{(5\lambda+7\mu)}{16\mu}B_3r^4-\frac{(\lambda-\mu)}{8\mu}\frac{C_3}{r^2}\right]\sin 3\theta, \end{aligned}\right\} \quad \ldots\ldots(21)$$

and we obtain the following expressions of u and v as the complementary solutions of (17), (18):

$$\left.\begin{aligned} u=&\frac{B_0''}{r}+\frac{C_1''}{r^2}\cos\theta+\left\{B_2''r+\frac{C_2''}{r^3}\right\}\cos 2\theta+\left\{B_3''r^2+\frac{C_3''}{r^4}\right\}\cos 3\theta,\\ v=&\frac{C_1''}{r^2}\sin\theta-\left\{B_2''r-\frac{C_2''}{r^3}\right\}\sin 2\theta-\left\{B_3''r^2-\frac{C_3''}{r^4}\right\}\sin 3\theta. \end{aligned}\right\} \quad (22)$$

Substituting (10), (14), (16) for the expressions of Δ' and $2\varpi'$ in the equations (19) and (20), we obtain the particular solutions u' and v' which are favourable for the cylindrical inclusion as follows:

$$\left.\begin{aligned} u'=&\frac{1}{2}D_1r+\left[\frac{3\rho' g}{8(\lambda'+2\mu')}r^2+\frac{(-\lambda'+\mu')}{8\mu'}D_1r^2+D_1''\right]\cos\theta\\ &-\frac{\lambda'}{6\mu'}D_2r^3\cos 2\theta-\frac{(3\lambda'+\mu')}{16\mu'}D_3r^4\cos 3\theta,\\ v'=&\left[-\frac{\rho' g}{8(\lambda'+2\mu')}r^2+\frac{(3\lambda'+5\mu')}{8\mu'}D_1r^2-D_1''\right]\sin\theta\\ &+\frac{(2\lambda'+3\mu')}{6\mu'}D_2r^3\sin 2\theta+\frac{(5\lambda'+7\mu')}{16\mu'}D_3r^4\sin 4\theta, \end{aligned}\right\} \quad (23)$$

while the complementary solutions of (19) and (20) are expressed by

$$\left.\begin{aligned} u' &= D''r\cos 2\theta + D_3''r^2\cos 3\theta, \\ v' &= -D_2''r\sin 2\theta + D_3''r^2\sin 3\theta. \end{aligned}\right\} \quad \cdots\cdots\cdots\cdots (24)$$

The general expressions of the components of displacement thus obtained (21), (22) and (23), (24) satisfy, of course, the equations of equilibrium of the solids (5) and (6) respectively. Using these general expressions we get the general expressions of the components of stresses $\widehat{rr}$, $\widehat{\theta\theta}$, $\widehat{r\theta}$, $\widehat{zz}$ and $\widehat{rr'}$, $\widehat{\theta\theta'}$, $\widehat{r\theta'}$, $\widehat{zz'}$ as in the following forms by the relations of (3) and (4) separately.

$$\left.\begin{aligned}
\widehat{rr} &= (\lambda+\mu)B_0 - 2\mu\frac{B_0''}{r^2} + \left[\frac{1}{2}\rho g r + \frac{(\lambda+\mu)}{2}B_1 r - \frac{4\mu}{r^3}C_1'' + \frac{(2\lambda+3\mu)}{r}F_1\right]\cos\theta \\
&\quad + \left[2\mu B_2'' + \frac{2(\lambda+\mu)}{r^2}C_2 - \frac{6\mu}{r^4}C_2''\right]\cos 2\theta \\
&\quad + \left[-\frac{(\lambda+\mu)}{2}B_3 r^3 + 4\mu B_3''r + \frac{5(\lambda+\mu)}{2}\frac{C_3}{r^3} - \frac{8\mu}{r^5}C_3''\right]\cos 3\theta, \\
\widehat{\theta\theta} &= (\lambda+\mu)B_0 + 2\mu\frac{B_0''}{r^2} + \left[-\frac{\rho g}{2}r + \frac{3(\lambda+\mu)}{2}B_1 r + \frac{4\mu}{r^3}C_1'' - \frac{\mu}{r}F_1\right]\cos\theta \\
&\quad + \left[2(\lambda+\mu)B_2 r^2 - 2\mu B_2'' + \frac{6\mu}{r^4}C_2''\right]\cos 2\theta \\
&\quad + \left[\frac{5}{2}(\lambda+\mu)B_3 r^3 - 4\mu B_3''r - \frac{(\lambda+\mu)}{2}\frac{C_3}{r^3} + \frac{8\mu}{r^5}C_3''\right]\cos 3\theta, \\
\widehat{zz} &= \lambda B_0 + \left[\lambda B_1 r + \frac{\lambda}{r}F_1\right]\cos\theta + \left[\lambda B_2 r^2 + \frac{\lambda}{r^2}C_2\right]\cos 2\theta \\
&\quad + \left[\lambda B_3 r^3 + \frac{\lambda}{r^3}C_3\right]\cos 3\theta, \\
\widehat{r\theta} &= \left[-\frac{\rho g r}{2} + \frac{(\lambda+\mu)}{2}B_1 r - \frac{4\mu}{r^3}C_1'' - \frac{\mu}{r}F_1\right]\sin\theta \\
&\quad + \left[(\lambda+\mu)B_2 r^2 - 2\mu B_2'' + (\lambda+\mu)\frac{C_2}{r^2} - \frac{6\mu}{r^4}C_2''\right]\sin 2\theta \\
&\quad + \left[\frac{3(\lambda+\mu)}{2}B_3 r^3 - 4\mu B_3''r + \frac{3}{2}\frac{(\lambda+\mu)}{r^3}C_3 - \frac{8\mu}{r^5}C_3''\right]\sin 3\theta.
\end{aligned}\right\} \quad \cdots\cdots\cdots\cdots (25)$$

$$\left.\begin{aligned}
\widehat{rr'} &= (\lambda'+\mu')D_0 + \left[\frac{(2\lambda'+3\mu')}{2(\lambda'+2\mu')}\rho' g r + \frac{(\lambda'+\mu')}{2}D_1 r\right]\cos\theta \\
&\quad + 2\mu' D_2''\cos 2\theta + \left[4\mu' D_3''r - \frac{(\lambda'+\mu')}{2}D_3 r^3\right]\cos 3\theta,
\end{aligned}\right.$$

$$\left.\begin{aligned}
\widehat{\theta\theta'} &= (\lambda'+\mu')D_0 + \left[\frac{(2\lambda'+\mu')}{2(\lambda'+2\mu')}\rho' g r + \frac{3}{2}(\lambda'+\mu')D_1 r\right]\cos\theta \\
&\quad + [2(\lambda'+\mu')r^2 D_2 - 2\mu' D_2'']\cos 2\theta \\
&\quad + \left[\frac{5}{2}(\lambda'+\mu')D_3 r^3 - 4\mu' D_3'' r\right]\cos 3\theta, \\
\widehat{zz'} &= \lambda' D_0 + \left[\frac{\lambda'}{(\lambda'+2\mu')}\rho' g r + \lambda' D_1 r\right]\cos\theta \\
&\quad + [\lambda' r^2 D_2]\cos 2\theta + \lambda' r^3 D_3 \cos 3\theta, \\
\widehat{r\theta'} &= \left[-\frac{\mu'}{2(\lambda'+2\mu')}\rho' g r + \frac{(\lambda'+\mu')}{2} D_1 r\right]\sin\theta \\
&\quad + [(\lambda'+\mu')D_2 r^2 - 2\mu' D_2'']\sin 2\theta \\
&\quad + \left[\frac{3(\lambda'+\mu')}{2} D_3 r^3 - 4\mu' D_3'' r\right]\sin 3\theta.
\end{aligned}\right\} \quad \ldots(26)$$

These stress expressions satisfy, of course, the stress equations of the gravitating elastic solids expressed by (1) and (2).

Using these general expressions of displacements and stresses we shall study the stresses in the vicinity of a horizontal cylindrical inclusion in the semi-infinite solid.

Referring to Fig. 1, we have the following expressions of the components of stresses which are the solutions of the gravitating semi-infinite elastic solid having no heterogeneous inclusion in its interior :

$$\left.\begin{aligned}
\widehat{rr} &= -\rho g\xi\frac{(\lambda+\mu)}{(\lambda+2\mu)} + \rho g r\frac{(2\lambda+3\mu)}{2(\lambda+2\mu)}\cos\theta \\
&\quad - \rho g\xi\frac{\mu}{(\lambda+2\mu)}\cos 2\theta + \rho g r\frac{\mu}{2(\lambda+2\mu)}\cos 3\theta, \\
\widehat{\theta\theta} &= -\rho g\xi\frac{(\lambda+\mu)}{(\lambda+2\mu)} + \rho g r\frac{(2\lambda+\mu)}{2(\lambda+2\mu)}\cos\theta \\
&\quad + \rho g\xi\frac{\mu}{(\lambda+2\mu)}\cos 2\theta - \rho g r\frac{\mu}{2(\lambda+2\mu)}\cos 3\theta, \\
\widehat{r\theta} &= -\frac{\mu}{2(\lambda+2\mu)}\rho g r\sin\theta + \rho g\xi\frac{\mu}{(\lambda+2\mu)}\sin 2\theta \\
&\quad - \rho g r\frac{\mu}{2(\lambda+2\mu)}\sin 3\theta.
\end{aligned}\right\} \quad \ldots\ (27)$$

These expressions are obtained by the following conditions: The normal and the shearing components of stress vanish at the horizontal surface $x=\xi$, and the stress at any point in the gravitating solid increases linearly according with the increase of the position form the upper surface of the solid. And the semi-infinite solid is in plane strain.

Now the boundary conditions of the present study are as follows:

$$\left.\begin{aligned} r=a\,; \quad & u=u', \quad v=v', \\ & \widehat{rr}=\widehat{rr}', \ \widehat{r\theta}=\widehat{r\theta}', \end{aligned}\right\} \quad \cdots\cdots\cdots\cdots\cdots\cdots (28)$$

$$\left.\begin{aligned} r\to\infty\,; \quad & \widehat{rr}=\widehat{rr} \text{ expressed by (27)}, \\ & \widehat{\theta\theta}=\widehat{\theta\theta} \text{ expressed by (27)}, \\ & \widehat{r\theta}=\widehat{r\theta} \text{ expressed by (27)}. \end{aligned}\right\} \quad \cdots\cdots\cdots (29)$$

Condition (28) indicates us that the heterogeneous inclusion and the outer medium are perfectly cemented at the contact surface and they are forbidden to slide upn each other on this contact surface. And the condition expressed by (29) shews that the stress distribution at the whole spaces in the medium far from the inclusion are equal to the ones expressed by (27).

By the expressions of (21), (22), (23), (24), (25), (26) to satisfy (28), (29), we find the following values of the arbitrary constants:

$$\left.\begin{aligned} B_0 &= -\frac{\rho g\xi}{(\lambda+2\mu)}, \quad D_0 = -\frac{\rho g\xi}{(\mu+\lambda'+\mu')}, \\ B_0'' &= \frac{\rho g\xi a^2}{2}\frac{(\lambda'+\mu'-\lambda-\mu)}{(\lambda+2\mu)(\mu+\lambda'+\mu')}, \end{aligned}\right\} \quad \cdots\cdots (30)$$

$$\left.\begin{aligned} B_1 &= \frac{\rho g}{(\lambda+2\mu)}, \quad F_1 = \frac{(\rho'-\rho)ga^2}{2(\lambda+2\mu)}, \\ D_1 &= \frac{\rho g\mu'}{\{\mu(\lambda'+3\mu')+\mu'(\lambda'+\mu')\}} - \frac{\rho' g\mu'(\mu+\lambda'+\mu')}{(\lambda'+2\mu')\{\mu(\lambda'+3\mu')+\mu'(\lambda'+\mu')\}}, \\ C_1 &= -\frac{\rho g a^4\mu'(\lambda'+\mu')}{8\mu\{\mu(\lambda'+3\mu')+\mu'(\lambda'+\mu')\}} \\ &\quad -\frac{\rho' g a^4}{8\mu(\lambda'+2\mu')}\left[\frac{\{(\lambda+2\mu)(2\lambda'+3\mu')+(2\lambda+3\mu)(\lambda'+2\mu')\}}{(\lambda+2\mu)}\right. \\ &\qquad \left. -\frac{\mu'(\lambda'+\mu')(\mu+\lambda'+\mu')}{\{\mu(\lambda'+3\mu')+\mu'(\lambda'+\mu')\}}\right], \end{aligned}\right\}$$

$$\cdots\cdots\cdots\cdots (31)$$

$$\left.\begin{aligned} &B_2=0, \quad B_2''=-\frac{\rho g\xi}{2(\lambda+2\mu)}, \\ &C_2=\frac{\rho g\xi a^2}{(\lambda+2\mu)}\frac{\vartheta_{C_2}}{\vartheta_2}, \quad C_2''=\frac{\rho g\xi a^4}{(\lambda+2\mu)}\frac{\vartheta_{C_2''}}{\vartheta_2}, \\ &D_2''=\frac{\rho g\xi}{(\lambda+2\mu)}\frac{\vartheta_{D_2''}}{\vartheta_2}, \quad D_2=\frac{\rho g\xi}{a^2}\frac{\vartheta_{D_2}}{\vartheta_2}, \end{aligned}\right\} \quad \ldots\ldots\ldots(32)$$

$$\left.\begin{aligned} &B_3=0, \quad B_3''=\frac{\rho g}{8(\lambda+2\mu)}, \\ &C_3=\frac{\rho g a^4}{2(\lambda+2\mu)}\frac{\vartheta_{C_3}}{\vartheta_3}, \quad C_3=-\frac{\rho g a^6}{2(\lambda+2\mu)}\frac{\vartheta_{C_3''}}{\vartheta_3}, \\ &D_3=\frac{\rho g}{2(\lambda+2\mu)a^2}\frac{\vartheta_{D_3}}{\vartheta_3}, \quad D_3''=-\frac{\rho g}{2(\lambda+2\mu)}\frac{\vartheta_{D_3''}}{\vartheta_3}, \end{aligned}\right\} \quad \ldots.(33)$$

where ϑ_2, ϑ_{C_2}, $\vartheta_{C_2''}$, ϑ_{D_2}, $\vartheta_{D_2''}$ and ϑ_3, ϑ_{C_3}, $\vartheta_{C_3''}$, ϑ_{D_3}, $\vartheta_{D_3''}$ are expressed by the following determinants:

$$\left.\begin{aligned} \vartheta_2&=\begin{vmatrix} 2(\lambda+\mu), & -6\mu, & -2\mu', & 0 \\ -(\lambda+\mu), & 6\mu, & -2\mu', & (\lambda'+\mu') \\ -\frac{(\lambda+2\mu)}{2\mu}, & 1, & -1, & \frac{\lambda'}{6\mu'} \\ -\frac{1}{2}, & -1, & -1, & \frac{(2\lambda'+3\mu')}{6\mu'} \end{vmatrix}, \\ \vartheta_{C_2}&=\begin{vmatrix} \mu, & -6\mu, & -2\mu' & 0 \\ \mu, & 6\mu, & -2\mu', & (\lambda'+\mu') \\ \frac{1}{2}, & 1, & -1, & \frac{\lambda'}{6\mu'} \\ \frac{1}{2}, & -1, & -1, & \frac{(2\lambda'+3\mu')}{6\mu'} \end{vmatrix}, \\ \vartheta_{C_2''}&=\begin{vmatrix} 2(\lambda+\mu), & \mu, & -2\mu', & 0 \\ -(\lambda+\mu), & \mu, & -2\mu', & (\lambda'+\mu') \\ -\frac{(\lambda+2\mu)}{2\mu}, & \frac{1}{2}, & -1, & \frac{\lambda'}{6\mu'} \\ -\frac{1}{2} & \frac{1}{2}, & -1, & \frac{(2\lambda'+3\mu')}{6\mu'} \end{vmatrix}, \end{aligned}\right\} \quad \ldots.(34)$$

$$\left.\begin{aligned}
\vartheta_{D_2} &= \begin{vmatrix} 2(\lambda+\mu), & -6\mu, & -2\mu', & \mu \\ -(\lambda+\mu), & 6\mu, & -2\mu', & \mu \\ -\frac{(\lambda+2\mu)}{2\mu} & 1, & -1, & \frac{1}{2} \\ -\frac{1}{2}, & -1, & -1, & \frac{1}{2} \end{vmatrix}, \\
\vartheta_{D_2''} &= \begin{vmatrix} 2(\lambda+\mu), & -6\mu, & \mu, & 0 \\ -(\lambda+\mu), & 6\mu, & \mu, & (\lambda'+\mu') \\ -\frac{(\lambda+2\mu)}{2\mu}, & 1, & \frac{1}{2}, & \frac{\lambda'}{6\mu'} \\ -\frac{1}{2} & -1, & \frac{1}{2}, & \frac{(2\lambda'+3\mu')}{6\mu'} \end{vmatrix}.
\end{aligned}\right\}$$

$$\left.\begin{aligned}
\vartheta_{3} &= \begin{vmatrix} \frac{5}{2}(\lambda+\mu), & -8\mu, & \frac{(\lambda'+\mu')}{2}, & -4\mu' \\ -\frac{3}{2}(\lambda+\mu), & 8\mu, & \frac{3}{2}(\lambda'+\mu'), & -4\mu, \\ -\frac{(3\lambda+5\mu)}{8\mu} & 1, & \frac{(3\lambda'+\mu')}{16\mu'}, & -1 \\ \frac{(\lambda-\mu)}{8\mu}, & -1, & \frac{(5\lambda'+7\mu')}{16\mu'}, & -1 \end{vmatrix}, \\
\vartheta_{C_3} &= \begin{vmatrix} \mu, & -8\mu, & \frac{(\lambda'+\mu')}{2}, & -4\mu' \\ \mu, & 8\mu, & \frac{3}{2}(\lambda'+\mu'), & -4'\mu \\ \frac{1}{4}, & 1, & \frac{(3\lambda'+\mu')}{16\mu'} & -1 \\ \frac{1}{4}, & -1, & \frac{(3\lambda'+7\mu')}{16\mu'}, & -1 \end{vmatrix}, \\
\vartheta_{C_3''} &= \begin{vmatrix} \frac{5}{2}(\lambda+\mu), & \mu, & \frac{(\lambda'+\mu')}{2}, & -4\mu' \\ -\frac{3}{2}(\lambda+\mu), & \mu, & \frac{3}{2}(\lambda'+\mu'), & -4\mu' \\ -\frac{(3\lambda+5\mu)}{8\mu}, & \frac{1}{4}, & \frac{(3\lambda'+\mu')}{16\mu'}, & -1 \\ \frac{(\lambda-\mu)}{8\mu}, & \frac{1}{4}, & \frac{(5\lambda'+7\mu')}{16\mu'}, & -1 \end{vmatrix},
\end{aligned}\right\} \quad \ldots(35)$$

$$\left.\begin{aligned}
\vartheta_{D_3} &= \begin{vmatrix} \frac{5}{2}(\lambda+\mu), & -8\mu, & \mu, & -4\mu' \\ -\frac{3}{2}(\lambda+\mu), & 8\mu, & \mu, & -4\mu' \\ -\frac{(3\lambda+5\mu)}{8\mu}, & 1, & \frac{1}{4}, & -1 \\ \frac{(\lambda-\mu)}{8\mu}, & -1, & \frac{1}{4}, & -1 \end{vmatrix}, \\
\vartheta_{D_{3''}} &= \begin{vmatrix} \frac{5}{2}(\lambda+\mu), & -8\mu, & \frac{(\lambda'+\mu')}{2}, & \mu \\ -\frac{3}{2}(\lambda+\mu), & 8\mu, & \frac{3}{2}(\lambda'+\mu'), & \mu \\ -\frac{(3\lambda+5\mu)}{8\mu}, & 1, & \frac{(3'\lambda+\mu')}{16\mu'} & \frac{1}{4} \\ \frac{(\lambda-\mu)}{8\mu} & -1, & \frac{(5\lambda'+7\mu')}{16\mu'}, & \frac{1}{4} \end{vmatrix},
\end{aligned}\right\}$$

Substituting these values (30), (31), (32), (33) in the expressions (25), (26), we obtain the final results of the stresses in the medium and those in the inclusion.

$r \geq a$:

$$\begin{aligned}
\widehat{rr} = &-\rho g\xi\frac{(\lambda+\mu)}{(\lambda+2\mu)} - \frac{2\mu}{r^2}\times\frac{a^2\rho g\xi}{2}\frac{(\lambda'+\mu'-\lambda-\mu)}{(\lambda+2\mu)(\mu+\lambda'+\mu')} + \frac{(2\lambda+3\mu)}{2(\lambda+2\mu)}\rho g r\cos\theta \\
&+\frac{(2\lambda+3\mu)}{2(\lambda+2\mu)}\frac{(\rho' g a-\rho g a)a}{r}\cos\theta + \frac{\mu'(\lambda'+\mu')\rho g a^4\cos\theta}{2\{\mu(\lambda'+3\mu')+\mu'(\lambda'+\mu')\}r^3} \\
&+\frac{\rho' g a^4}{2(\lambda'+2\mu')r^3}\Big[\frac{\{(\lambda+2\mu)(2\lambda'+3\mu')-(2\lambda+3\mu)(\lambda'+2\mu')\}}{(\lambda+2\mu)} \\
&\qquad -\frac{\mu'(\lambda'+\mu')(\mu+\lambda'+\mu')}{\{\mu(\lambda'+3\mu')+\mu'(\lambda'+\mu')\}}\Big]\cos\theta \\
&+\frac{\rho g\xi}{(\lambda+2\mu)}\Big[-\mu+\frac{2(\lambda+\mu)\vartheta_{C_2}}{\vartheta_2}\Big(\frac{a}{r}\Big)^2-\frac{6\mu\vartheta_{C_{2''}}}{\vartheta_2}\Big(\frac{a}{r}\Big)^4\Big]\cos 2\theta \\
&+\frac{\rho g r}{(\lambda+2\mu)}\Big[\frac{\mu}{2}-\frac{5}{4}\frac{(\lambda+\mu)\vartheta_{C_3}}{\vartheta_3}\Big(\frac{a}{r}\Big)^4+\frac{4\mu\vartheta_{C_{3''}}}{\vartheta^3}\Big(\frac{a}{r}\Big)^6\Big]\cos 3\theta, \ldots . \quad (36) \\
\widehat{\theta\theta} = &\frac{\rho g\xi}{(\lambda+2\mu)}\Big[-(\lambda+\mu)+\frac{\mu(\lambda'+\mu'-\lambda-\mu)}{(\mu+\lambda'+\mu')}\Big(\frac{a}{r}\Big)^2\Big]+\frac{(2\lambda+\mu)}{2(\lambda+2\mu)}\rho g r\cos\theta
\end{aligned}$$

$$-\frac{\mu(\rho'-\rho)ga^2}{2(\lambda+2\mu)r}\cos\theta-\frac{\rho ga\mu'(\lambda'+\mu')}{2\{\mu(\lambda'+3\mu')+\mu'(\lambda'+\mu')\}}\left(\frac{a}{r}\right)^3\cos\theta$$
$$-\frac{\rho' ga^4}{2(\lambda'+2\mu')r^3}\left[\frac{\{(\lambda+2\mu)(2\lambda'+3\mu')-(2\lambda+3\mu)(\lambda'+2\mu')\}}{(\lambda+2\mu)}\right.$$
$$\left.-\frac{\mu'(\lambda'+\mu')(\mu+\lambda'+\mu')}{\{\mu(\lambda'+3\mu')+\mu'(\lambda'+\mu')\}}\right]\cos\theta$$
$$+\frac{\rho g\xi}{(\lambda+2\mu)}\left[\mu+\frac{6\mu\vartheta_{C_2''}}{\vartheta_2}\left(\frac{a}{r}\right)^4\right]\cos 2\theta$$
$$+\frac{\rho gr}{(\lambda+2\mu)}\left[-\frac{\mu}{2}+\frac{(\lambda+\mu)\vartheta_{C_2}}{4\vartheta_3}\left(\frac{a}{r}\right)^4-\frac{4\mu\vartheta_{C_3''}}{\vartheta}\left(\frac{a}{r}\right)^6\right]\cos 3\theta, \quad ..(37)$$

$$\widehat{zz}=\frac{\lambda}{2(\lambda+\mu)}\{\widehat{rr}+\widehat{\theta\theta}\}, \quad .....(38)$$

$$\widehat{r\theta}=-\frac{\mu\rho gr}{2(\lambda+2\mu)}\sin\theta+\frac{\mu(\rho-\rho')ga^2}{2(\lambda+2\mu)r}\sin\theta+\frac{\rho ga^4\mu'(\lambda'+\mu')}{2\{\mu(\lambda'+3\mu')+\mu'(\lambda'+\mu')\}r^3}\sin\theta$$
$$+\frac{\rho' ga^4}{2(\lambda'+2\mu')r^3}\left[\frac{\{(\lambda+2\mu)(2\lambda'+3\mu')-(2\lambda+3\mu)(\lambda'+2\mu')\}}{(\lambda+2\mu)}\right.$$
$$\left.-\frac{\mu'(\lambda'+\mu')(\mu+\lambda'+\mu')}{\{\mu(\lambda'+3\mu')+\mu'(\lambda'+\mu')\}}\right]\sin\theta$$
$$+\frac{\rho g\xi}{(\lambda+9\mu)}\left[\mu+\frac{(\lambda+\mu)\vartheta_{C_2}}{\vartheta_2}\left(\frac{a}{r}\right)^2-\frac{6\mu\vartheta_{C_2''}}{\vartheta}\left(\frac{a}{r}\right)^4\right]\sin 2\theta$$
$$+\frac{\rho gr}{(\lambda+2\mu)}\left[-\frac{\mu}{2}-\frac{3(\lambda+\mu)\vartheta_C}{4\vartheta_3}\left(\frac{a}{r}\right)^4+\frac{4\mu\vartheta_{C_3''}}{\vartheta_3}\left(\frac{a}{r}\right)^6\right]\sin 3\theta, \quad ..(39)$$

$r\geq a$:

$$\widehat{rr'}=-\frac{(\lambda'+\mu')}{(\mu+\lambda'+\mu')}\rho g\xi+\frac{2(\lambda'+3\mu')}{2(\lambda'+9\mu')}\theta' gr\cos\theta$$
$$+\frac{(\lambda'+\mu')}{2}\left[\frac{\rho g\mu r}{\{\mu(\lambda'+3\mu')+\mu'(\lambda'+\mu')\}}\right.$$
$$\left.-\frac{\rho' gr\mu'(\mu+\lambda'+\mu')}{(\lambda'+2\mu')\{\mu(\lambda'+3\mu')+\mu'(\lambda'+\mu')\}}\right]\cos\theta$$
$$+\frac{2\mu'\rho g\xi\vartheta_{D_2''}}{(\lambda+2\mu)\vartheta_2}\cos 2\theta$$
$$+\frac{\rho ga}{(\lambda+2\mu)}\left[\frac{(\lambda'+'\mu)\vartheta_{D_3}}{4\vartheta_3}\left(\frac{r}{a}\right)^3-\frac{2\mu'\vartheta_{D_3''}}{\vartheta_3}\left(\frac{r}{a}\right)\right]\cos 3\theta, \quad .....(40)$$

$$\widehat{\theta\theta'}=-\frac{(\lambda'+\mu')}{(\mu+\lambda'+\mu')}\rho g\xi+\frac{(2\lambda'+\mu')}{2(\lambda'+2\mu')}\rho' gr\cos\theta$$

$$+\frac{3}{2}(\lambda'+\mu')\Bigg[\frac{\rho g\mu' r}{\{\mu(\lambda'+3\mu')+\mu'(\lambda'+\mu')\}} - \frac{\rho' g r\mu'(\mu+\lambda'+\mu')}{(\lambda'+2\mu')\{\mu(\lambda'+3\mu')+\mu'(\lambda'+\mu')\}}\Bigg]\cos\theta$$

$$+\frac{\rho g\xi}{(\lambda+2\mu)}\Bigg[-\frac{2\mu'\vartheta_{D_2''}}{\vartheta_2}+\frac{2(\lambda'+\mu')\vartheta_{D_2}}{\vartheta_2}\left(\frac{r}{a}\right)^2\Bigg]\cos 2\theta$$

$$+\frac{\rho g r}{(\lambda+2\mu)}\Bigg[-\frac{5(\lambda'+\mu')\vartheta_{D_3}}{4\vartheta_3}\left(\frac{r}{a}\right)^3+\frac{2\mu'\vartheta_{D_3''}}{\vartheta_3}\left(\frac{r}{a}\right)\Bigg]\cos\theta \quad \ldots\ldots (41)$$

$$\widehat{zz'}=\frac{\lambda'}{2(\lambda'+\mu')}\{\widehat{rr'}+\widehat{\theta\theta'}\}, \quad \ldots\ldots (42)$$

$$\widehat{r\theta'}=-\frac{\mu'\rho' g r\sin\theta}{2(\lambda'+2\mu')}+\frac{(\lambda'+\mu')}{2}\Bigg[\frac{\rho g\mu' r}{\{\mu(\lambda'+3\mu')+\mu'(\lambda'+\mu')\}} - \frac{\rho' g r\mu'(\lambda'+\mu'+\mu)}{(\lambda'+2\mu')\{\mu(\lambda'+3\mu')+\mu'(\lambda'+\mu')\}}\Bigg]\sin\theta$$

$$+\frac{\rho g\xi}{(\lambda+2\mu)}\Bigg[-\frac{2\mu'\vartheta_{D_2''}}{\vartheta_2}+\frac{(\lambda'+\mu')\vartheta_{D_2}}{\vartheta_2}\left(\frac{r}{a}\right)^2\Bigg]\sin 2\theta$$

$$+\frac{\rho g r}{(\lambda+2\mu)}\Bigg[\frac{2\mu'\vartheta_{D_3''}}{\vartheta_3}-\frac{3(\lambda'+\mu')\vartheta_{D_3}}{\vartheta_3}\left(\frac{r}{a}\right)^3\Bigg]\sin 3\theta. \quad \ldots\ldots (43)$$

When $\lambda=\mu$, $\lambda'=\mu'$ (Poisson's ratio of the semi-infinite solid and that of the heterogeneous inclusion are equally $\frac{1}{4}$), we obtain the expressions of the stress distributions in the solid and that in the inclusion as in the following forms:

$r\geqq a$:

$$\widehat{rr}=\rho g\xi\Bigg[\frac{2}{3}\left\{-1+\frac{(\mu-\mu')}{(\mu+2\mu')}\left(\frac{a}{r}\right)^2\right\} + \left\{-\frac{1}{3}+\frac{4(\mu-\mu')}{3(\mu+2\mu')}\left(\frac{a}{r}\right)^2-\frac{(\mu-\mu')}{(\mu+2\mu')}\left(\frac{a}{r}\right)^4\right\}\cos 2\theta\Bigg]$$

$$+\rho g a\Bigg[\left\{\frac{5}{6}\left(\frac{r}{a}\right)-\frac{5}{6}\left(\frac{a}{r}\right)+\frac{\mu'}{2(2\mu+\mu')}\left(\frac{a}{r}\right)^3\right\}\cos\theta + \left\{\frac{1}{6}\left(\frac{r}{a}\right)-\frac{5(\mu-\mu')}{6(\mu+2\mu')}\left(\frac{a}{r}\right)^3+\frac{2(\mu-\mu')}{3(\mu+2\mu')}\left(\frac{a}{r}\right)^5\right\}\cos 3\theta\Bigg]$$

$$+\rho' g a\Bigg[\frac{5}{6}\left(\frac{a}{r}\right)-\frac{1}{6}\frac{(\mu+2\mu')}{(2\mu+\mu')}\left(\frac{a}{r}\right)^3\Bigg]\cos\theta, \quad \ldots\ldots (44)$$

$$\widehat{\theta\theta}=\rho g\xi\left[\frac{2}{3}\left\{-1-\frac{(\mu-\mu')}{(\mu+2\mu')}\left(\frac{a}{r}\right)^2\right\}+\left\{\frac{1}{3}+\frac{(\mu-\mu')}{(\mu+2\mu')}\left(\frac{a}{r}\right)^4\right\}\cos 2\theta\right]$$
$$+\rho ga\left[\left\{\frac{1}{2}\left(\frac{r}{a}\right)+\frac{1}{6}\left(\frac{a}{r}\right)-\frac{\mu'}{2(2\mu+\mu')}\left(\frac{a}{r}\right)^3\right\}\cos\theta\right.$$
$$\left.+\left\{-\frac{1}{6}\left(\frac{r}{a}\right)+\frac{(\mu-\mu')}{6(\mu+2\mu')}\left(\frac{a}{r}\right)^3-\frac{2(\mu-\mu')}{3(\mu+2\mu')}\left(\frac{a}{r}\right)^5\right\}\cos 3\theta\right]$$
$$+\rho' ga\left[-\frac{1}{6}\left(\frac{a}{r}\right)+\frac{1}{6}\frac{(\mu+2\mu')}{(2\mu+\mu')}\left(\frac{a}{r}\right)^3\right]\cos\theta, \quad \cdots\cdots\cdots\cdots (45)$$

$$\widehat{zz}=\rho g\xi\left[-\frac{1}{3}+\frac{(\mu-\mu')}{3(\mu+2\mu')}\left(\frac{a}{r}\right)^2\cos 2\theta\right]$$
$$+\rho ga\left[\left\{\frac{1}{3}\left(\frac{r}{a}\right)-\frac{1}{6}\left(\frac{a}{r}\right)\right\}\cos\theta-\frac{1}{6}\frac{(\mu-'\mu)}{(\mu+2\mu')}\left(\frac{a}{r}\right)^3\cos 3\theta\right]$$
$$+\rho' ga\left[\frac{1}{6}\left(\frac{a}{r}\right)\right]\cos\theta, \quad \cdots\cdots\cdots\cdots (46)$$

$$\widehat{r\theta}=\rho g\xi\left[\frac{1}{3}+\frac{2(\mu-\mu')}{3(\mu+2\mu')}\left(\frac{a}{r}\right)^2-\frac{(\mu-\mu')}{(\mu+2\mu')}\left(\frac{a}{r}\right)^4\right]\sin 2\theta$$
$$+\rho ga\left[\left\{-\frac{1}{6}\left(\frac{r}{a}\right)+\frac{1}{6}\left(\frac{a}{r}\right)+\frac{\mu'}{2(2\mu+\mu')}\left(\frac{a}{r}\right)^3\right\}\sin\theta\right.$$
$$\left.-\left\{\frac{1}{6}\left(\frac{r}{a}\right)+\frac{(\mu-\mu')}{2(\mu+2\mu')}\left(\frac{a}{r}\right)^3-\frac{2(\mu-\mu')}{3(\mu+2\mu')}\left(\frac{a}{r}\right)^5\right\}\sin 3\theta\right]$$
$$+\rho' ga\left[-\frac{1}{6}\left(\frac{a}{r}\right)-\frac{1}{6}\frac{(\mu+9\mu')}{(2\mu+\mu')}\left(\frac{a}{r}\right)^3\right]\sin\theta \quad \cdots\cdots\cdots\cdots (47)$$

$r\geq a$:

$$\widehat{rr'}=\rho g\xi\left[-\frac{2\mu'}{(\mu+2\mu')}-\frac{\mu'}{(\mu+2'\mu)}\cos 2\theta\right]$$
$$+\rho ga\left[\frac{\mu'}{2(2\mu+\mu')}\left(\frac{r}{a}\right)\cos\theta+\frac{\mu'}{2(\mu+2\mu')}\left(\frac{r}{a}\right)\cos 3\theta\right]$$
$$+\rho' ga\left[\frac{5}{6}\left(\frac{r}{a}\right)-\frac{1}{6}\frac{(\mu+2\mu')}{(2\mu+\mu')}\left(\frac{r}{a}\right)\right]\cos\theta, \quad \cdots\cdots\cdots\cdots (48)$$

$$\widehat{\theta\theta'}=\rho g\xi\left[-\frac{2\mu'}{(\mu+2\mu')}+\frac{\mu'}{(\mu+2\mu')}\cos 2\theta\right]$$
$$+\rho ga\left[\frac{3\mu'}{2(2\mu+\mu')}\left(\frac{r}{a}\right)\cos\theta-\frac{\mu'}{2(\mu+2\mu')}\left(\frac{r}{a}\right)\cos 3\theta\right]$$
$$+\rho' ga\left[\frac{1}{2}\left(\frac{r}{a}\right)-\frac{1}{2}\frac{(\mu+2\mu')}{(2\mu+\mu')}\left(\frac{r}{a}\right)\right]\cos\theta, \quad \cdots\cdots\cdots\cdots (49)$$

$$\widehat{zz'}=\rho g\xi\left[-\frac{\mu'}{(\mu+2\mu')}\right]$$
$$+\rho ga\left[\frac{\mu'}{2(2\mu+\mu')}\left(\frac{r}{a}\right)\cos\theta\right]$$
$$+\rho' ga\left[\frac{1}{4}\left(\frac{r}{a}\right)-\frac{1}{6}\frac{(\mu+'2\mu)}{(2\mu+\mu')}\left(\frac{r}{a}\right)\right]\cos\theta, \quad \ldots\ldots\ldots\ldots\ldots\ldots(50)$$

$$\widehat{r\theta'}=\rho g\xi\left[\frac{\mu'}{(\mu+2\mu')}\right]\sin 2\theta$$
$$+\rho ga\left[\frac{\mu'}{2(2\mu+\mu')}\left(\frac{r}{a}\right)\sin\theta-\frac{\mu'}{2\mu(+2\mu')}\left(\frac{r}{a}\right)\sin 3\theta\right]$$
$$+\rho' ga\left[-\frac{1}{6}\left(\frac{r}{a}\right)-\frac{(\mu+2\mu')}{2(2\mu+\mu')}\left(\frac{r}{a}\right)\right]\sin\theta, \quad \ldots\ldots\ldots\ldots\ldots\ldots(51)$$

We shall investigate closely the stress distributions on the boundary surface $r=a$ by the numerical calculations. Putting $r=a$, we calculate the magnitudes of the separate terms related to $\rho g\xi$, ρga and $\rho' ga$ in all stress components expressed by (44), (45), (46), (47), (48), (49), (50), (51) in the annexed tables when $\frac{\mu'}{\mu}=\frac{1}{5}$, $\frac{\mu'}{\mu}=1$, $\frac{\mu'}{\mu}=5$ and $\frac{\mu'}{\mu}=\infty$. (Table I, II, III, IV, V, VI, VII, VIII, IX, X, XI, XII, XIII, XIV, XV, XVI.) And the following figures (Fig. 2a, 2b, 2c, 3a, 3b, 3c, 4a, 4b, 4c, 5a, 5b, 5c.) shew us these results. In these figures, abscissa is the angle θ, and the parameter of each curve is the magnitude of $\frac{\mu'}{\mu}$.

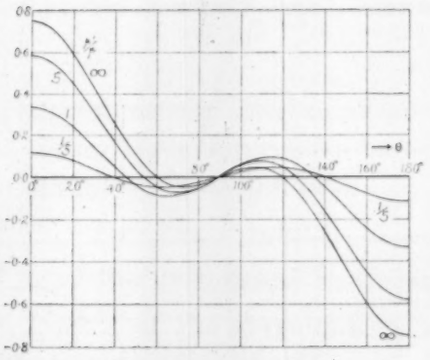

Fig. 2a. Magnitude of term related to ρga of $\widehat{rr}_{r=a}$ $(=\widehat{rr'}_{r=a})$ when $\frac{\mu'}{\mu}=\frac{1}{5}$, 1, 5 and ∞.

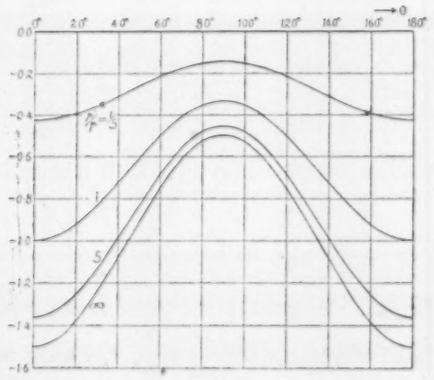

Fig. 2b. Magnitude of term related to $\rho g\xi$ of $\widehat{rr'}_{r=a}$ $(=\widehat{rr'}_{r=a})$ when $\frac{\mu'}{\mu}=\frac{1}{5}$, 1, 5 and ∞.

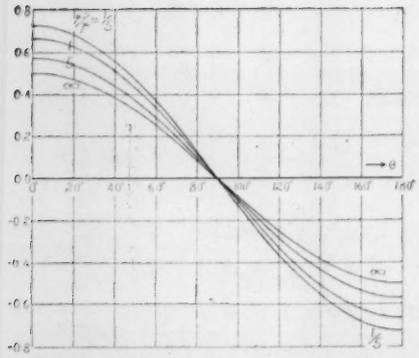

Fig. 2c. Magnitude of term related to $\rho' ga$ of $\widehat{rr}_{r=a}$ $(=\widehat{rr'}_{r=a})$ when $\frac{\mu'}{\mu}=\frac{1}{5}$, 1, 5 and ∞.

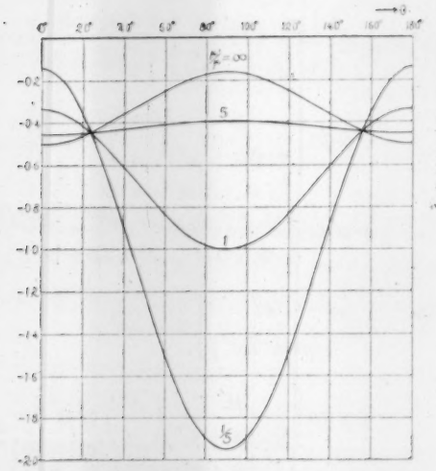

Fig. 3b. Magnitude of term related to $\rho g\xi$ of $\widehat{\theta\theta}_{r=a}$ when $\frac{\mu'}{\mu}=\frac{1}{5}$, 1, 5 and ∞.

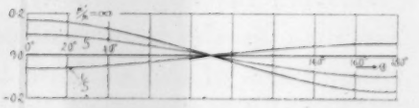

Fig. 3c. Magnitude of term related to $\rho' ga$ of $\widehat{\theta\theta}_{r=a}$ when $\frac{\mu'}{\mu}=\frac{1}{5}$, 1, 5 and ∞.

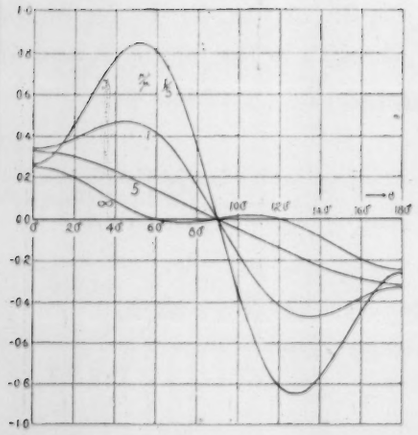

Fig. 3a. Magnitude of term related to ρga of $\widehat{\theta\theta}_{r=a}$ when $\frac{\mu'}{\mu}=\frac{1}{5}$, 1, 5 and ∞.

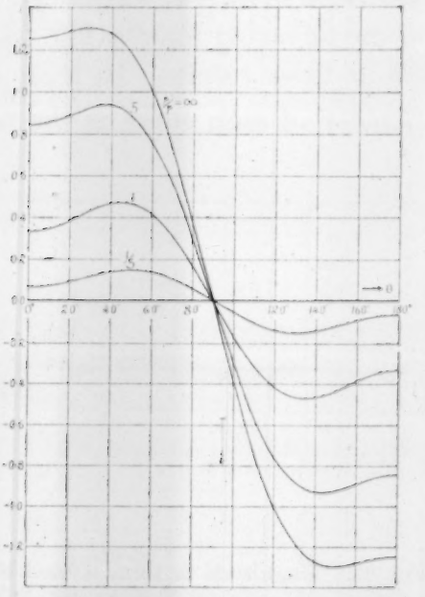

Fig. 4a. Magnitude of term related to ρga of $\widehat{\theta\theta'}_{r=a}$ when $\frac{\mu'}{\mu}=\frac{1}{5}$, 1, 5 and ∞.

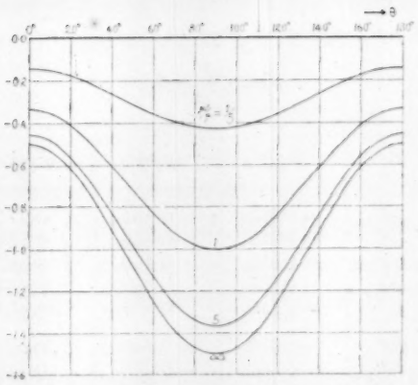

Fig. 4b. Magnitude of term related to $\rho g\xi$ of $\widehat{\theta\theta'}_{r=a}$ when $\frac{\mu'}{\mu}=\frac{1}{5}$, 1, 5 and ∞.

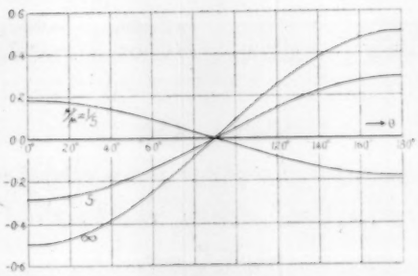

Fig. 4c. Magnitude of term related to $\rho' ga$ of $\widehat{\theta\theta'}_{r=a}$ when $\frac{\mu'}{\mu}=\frac{1}{5}$, 1, 5 and ∞.

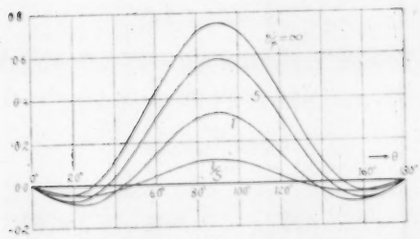

Fig. 5a. Magnitude of term related to ρga of $\widehat{r\theta}_{r=a}$ $(=\widehat{r\theta'}_{r=a})$ when $\frac{\mu'}{\mu}=\frac{1}{5}$, 1, 5 and ∞.

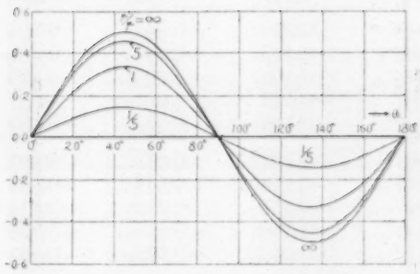

Fig. 5b. Magnitude of term related to $\rho g\xi$ of $\widehat{r\theta}_{r=a}$ $(=\widehat{r\theta'}_{r=a})$ when $\frac{\mu'}{\mu}=\frac{1}{5}$, 1, 5 and ∞.

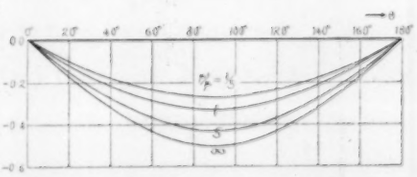

Fig. 5c. Magnitude of term related to $\rho' ga$ of $\widehat{r\theta}_{r=a}$ $(=\widehat{r\theta'}_{r=a})$ when $\frac{\mu'}{\mu}=\frac{1}{5}$, 1, 5 and ∞.

From these figures we can see interesting facts and some of them are summarised as follows:

1. The terms related to $\rho g\xi$ of the components of stresses $\widehat{rr'}_{r=a}$, $\widehat{\theta\theta'}_{r=a}$ of the cylindrical inclusion and those of the components of stresses $\widehat{rr}_{r=a}$, $\widehat{\theta\theta}_{r=a}$ of the surrounding medium have symmetrical distributions with respect to the plane $\theta=90°$. The terms related to $\rho g\xi$ of the components of shear stresses $\widehat{r\theta}_{r=a}$ $\widehat{r\theta'}_{r=a}$ have, however, unsymmetrical distributions with respect to this plane.

2. The terms related to ρga of the components of stresses $\widehat{rr}_{r=a}$,

Table I.

Magnitudes of separate terms related to $\rho g\xi$, ρga and $\rho' ga$ of $\widehat{rr}_{r=a}$ $(=\widehat{rr'}_{r=a})$ when $\frac{\mu'}{\mu}=\frac{1}{5}$.

θ	$\rho g\xi$	ρga	$\rho' ga$
1°	−0·429	0·116	0·727
10°	−0·420	0·107	0·717
20°	−0·395	0·079	0·684
30°	−0·358	0·039	0·630
45°	−0·286	−0·019	0·514
60°	−0·214	−0·048	0·364
70°	−0·177	−0·046	0·298
80°	−0·152	−0·028	0·126
90°	−0·143	0	0
100°	−0·152	0·028	−0·126
110°	−0·177	0·046	−0·293
120°	−0·214	0·048	−0·364
135°	−0·286	0·019	−0·514
150°	−0·358	−0·039	−0·630
160°	−0·395	−0·079	−0·684
170°	−0·420	−0·107	−0·717
180°	−0·429	−0·116	−0·727

Table II.

Magnitudes of separate terms related to $\rho g\xi$, ρga and $\rho' ga$ of $\widehat{rr}_{r=a}$ $(=\widehat{rr'}_{r=a})$ when $\frac{\mu'}{\mu}=1$.

θ	$\rho g\xi$	ρga	$\rho' ga$
0°	−1·00	0·334	0·667
10°	−0·981	0·308	0·657
20°	−0·923	0·240	0·627
30°	−0·834	0·144	0·577
45°	−0·667	0	0·472
60°	−0·500	−0·084	0·333
70°	−0·411	−0·087	0·228
80°	−0·353	−0·054	0·116
90°	−0·334	0	0
100°	−0·353	0·054	−0·116
110°	−0·411	0·087	−0·228
120°	−0·500	0·084	−0·333
135°	−0·667	0	−0·472
150°	−0·834	−0·144	−0·577
160°	−0·923	−0·240	−0·627
170°	−0·981	−0·308	−0·657
180°	−1·00	−0·334	−0·667

Table III.

Magnitudes of separate terms related to to ρga, $\rho g\xi$ and $\rho' ga$ of $\widehat{rr}_{r=a}$ $(=\widehat{rr'}_{r=a})$ when $\frac{\mu'}{\mu}=5$.

θ	$\rho g\xi$	ρga	$\rho' ga$
0°	−1·365	0·584	0·571
10°	−1·337	0·549	0·563
20°	−1·258	0·450	0·537
30°	−1·137	0·309	0·494
45°	−1·910	0·091	0·403
60°	−0·683	−0·049	0·286
70°	−0·562	−0·075	0·195
80°	−0·483	−0·052	0·100
90°	−0·455	0	0
100°	−0·483	0·052	−0·100
110°	−0·562	0·075	−0·195
120°	−0·683	0·049	−0·286
135°	−0·910	−0·091	−0·403
150°	−1·137	−0·309	−0·494
160°	−1·258	−0·450	−0·537
170°	−13·37	−0·549	−0·563
180°	−13·65	−0·584	−0·571

Table IV.

Magnitudes of separate terms related to ρga, $\rho g\xi$ and $\rho' ga$ of $\widehat{rr}_{r=a}$ $(=\widehat{rr'}_{r=a})$ when $\frac{\mu'}{\mu}=\infty$.

θ	$\rho g\xi$	ρga	$\rho' ga$
0°	−1·500	0·750	0·500
10°	−1·470	0·708	0·492
20°	−1·383	0·595	0·470
30°	−1·250	0·433	0·433
45°	−1·000	0·176	0·353
60°	−0·750	0	0·250
70°	−0·617	−0·045	0·171
80°	−0·530	−0·038	0·087
90°	−0·500	0	0
100°	−0·530	0·038	−0·087
110°	−0·617	0·045	−0·171
120°	−0·750	0	−0·250
135°	−1·000	−0·176	−0·353
150°	−1·250	−0·433	−0·433
160°	−1·383	−0·595	−0·470
170°	−1·470	−0·708	−0·492
180°	−1·500	−0·750	−0·500

Table V.

Magnitudes of separate terms related to ρga, $\rho' ga$ and $\rho g\xi$ of $\widehat{\theta\theta}_{r=a}$ when $\frac{\mu'}{\mu}=\frac{1}{5}$.

θ	$\rho g\xi$	ρga	$\rho' ga$
0°	−0·14	0·26	−0·06
10°	−0·20	0·310	−0·059
20°	−0·35	0·444	−0·056
30°	−0·59	0·618	−0·052
45°	−1·05	0·824	−0·042
60°	−1·50	0·809	−0·030
70°	−1·74	0·636	−0·021
80°	−1·90	0·350	−0·010
90°	−1·95	0	0
100°	−1·90	−0·350	0.010
110°	−1·74	−0·636	0.021
120°	−1·50	−0·809	0.030
135°	−1·05	−0·824	0.042
150°	−0·59	−0·618	0.052
160°	−0·35	−0·444	0.056
170°	−0·20	−0·310	0.059
180°	−0·14	−0·260	0.06

Table VI.

Magnitudes of separate terms related to $\rho g\xi$, ρga and $\rho' ga$ of $\widehat{\theta\theta}_{r=a}$ when $\frac{\mu'}{\mu}=1$.

θ	$\rho g\xi$	ρga	$\rho' ga$
0°	−0·334	0·333	0
10°	−0·353	0·348	0
20°	−0·411	0·387	0
30°	−0·550	0·433	0
45°	−0·667	0·471	0
60°	−0·834	0·417	0
70°	−0·923	0·315	0
80°	−0·981	0·170	0
90°	−1·000	0	0
100°	−0·981	−0·170	0
110°	−0·923	−0·315	0
120°	−0·834	−0·417	0
135°	−0·667	−0·471	0
150°	−0·500	−0·433	0
160°	−0·411	−0·387	0
170°	−0·353	−0·348	0
180°	−0·334	−0·333	0

Table VII.

Magnitudes of separate terms related to ρga, $\rho' ga$ and $\rho g\xi$ of $\widehat{\theta\theta}_{r=a}$ when $\frac{\mu'}{\mu}=5$.

θ	$\rho g\xi$	ρga	$\rho' ga$
0°	−0·454	0·325	0·095
10°	−0·452	0·318	0·094
20°	−0·447	0·299	0·090
30°	−0·439	0·268	0·082
45°	−0·424	0·208	0·067
60°	−0·409	0·140	0·048
70°	−0·401	0·093	0·033
80°	−0·396	0·046	0·017
90°	−0·394	0	0
100°	−0·396	−0·046	−0·017
110°	−0·401	−0·093	−0·033
120°	−0·409	−0·140	−0·048
135°	−0·424	−0·208	−0·067
150°	−0·439	−0·268	−0·082
160°	−0·447	−0·299	−0·090
170°	−0·452	−0·318	−0·094
180°	−0·454	−0·325	−0·095

Table VIII.

Magnitudes of separate terms related to ρga, $\rho g\xi$ and $\rho' ga$ of $\widehat{\theta\theta}_{r=a}$ when $\frac{\mu'}{\mu}=\infty$.

θ	$\rho g\xi$	ρga	$\rho' ga$
0°	−0·50	0·250	0·167
10°	−0·49	0·237	0·165
20°	−0·46	0·198	0·157
30°	−0·42	0·144	0·145
45°	−0·33	0·059	0·118
60°	−0·25	0	0·083
70°	−0·21	−0·015	0·057
80°	−0·18	−0·013	0·029
90°	−0·17	0	0
100°	−0·18	0·013	−0·029
110°	−0·21	0·015	−0·057
120°	−0·25	0	−0·083
135°	−0·33	−0·059	−0·118
150°	−0·42	−0·144	−0·145
160°	−0·46	−0·198	−0·157
170°	−0·49	−0·237	−0·165
180°	−0·50	−0·250	−0·167

Table IX.

Magnitudes of separate terms related to $\rho g\xi$, ρga and $\rho' ga$ of $\widehat{\theta\theta'}_{r=a}$ when $\frac{\mu'}{\mu}=\frac{1}{5}$.

θ	$\rho g\xi$	ρga	$\rho' ga$
0°	−0·14	0·065	0·182
10°	−0·15	0·072	0·179
20°	−0·18	0·092	0·171
30°	−0·21	0·118	0·157
45°	−0·29	0·147	0·128
60°	−0·36	0·140	0·091
70°	−0·40	0·109	0·062
80°	−0·42	0·060	0·032
90°	−0·43	0	0
100°	−0·42	−0·060	−0·032
110°	−0·40	−0·109	−0·062
120°	−0·36	−0·140	−0·091
135°	−0·29	−0·147	−0·128
150°	−0·21	−0·118	−0·157
160°	−0·18	−0·092	−0·171
170°	−0·15	−0·072	−0·179
180°	−0·14	−0·065	−0·182

Table X.

Magnitudes of separate terms related to $\rho g\xi$, ρga and $\rho' ga$ of $\widehat{\theta\theta'}_{r=a}$ when $\frac{\mu'}{\mu}=1$.

θ	$\rho g\xi$	ρga	$\rho' ga$
0°	−0·334	0·333	0
10°	−0·353	0·348	0
20°	−0·411	0·387	0
30°	−0·500	0·433	0
45°	−0·667	0·471	0
60°	−0·834	0·417	0
70°	−0·923	0·315	0
80°	−0·981	0·170	0
90°	−1·000	0	0
100°	−0·981	−0·170	0
110°	−0·923	−0·315	0
120°	−0·834	−0·417	0
135°	−0·667	−0·471	0
150°	−0·500	−0·433	0
160°	−0·411	−0·387	0
170°	−0·353	−0·348	0
180°	−0·334	−0·333	0

Table XI.

Magnitudes of separate terms related to $\rho g\xi$, ρga and $\rho' ga$ of $\widehat{\theta\theta'}_{r=a}$ when $\frac{\mu'}{\mu}=5$.

θ	$\rho g\xi$	ρga	$\rho' ga$
0°	−0·455	0.845	−0·286
10°	−0·483	0·858	−0·281
20°	−0·562	0·892	−0·269
30°	−0·683	0·928	−0·247
45°	−0·910	0·918	−0·202
60°	−1·137	0·763	−0·143
70°	−1·258	0·563	−0·098
80°	−1·337	0·300	−0·050
90°	−1·365	0	0
100°	−1·337	−0·300	0·050
110°	−1·258	−0·563	0·098
120°	−1·137	−0·763	0·143
135°	−0·910	−0·918	0·202
150°	−0·683	−0·928	0·247
160°	−0·562	−0·892	0·269
170°	−0·483	−0·858	0·281
180°	−0·455	−0·845	0·286

Table XII.

Magnitudes of separate terms related to $\rho g\xi$, ρga and $\rho' ga$ of $\widehat{\theta\theta'}_{r=a}$ when $\frac{\mu'}{\mu}=\infty$.

θ	$\rho g\xi$	ρga	$\rho' ga$
0°	−0·50	1·250	−0·50
10°	−0·53	1·261	−0·493
20°	−0·62	1·285	−0·470
30°	−0·75	1·30	−0·433
45°	−0·00	1·237	−0·353
60°	−1·25	1·00	−0·25
70°	−1·38	0·730	−0·171
80°	−1·47	0·386	−0·087
90°	−1·50	0	0
100°	−1·47	−0·386	0·087
110°	−1·38	−0·730	0·171
120°	−1·25	−1·00	0·25
135°	−1·00	−1·237	0·353
150°	−0·75	−1·30	0·433
160°	−0·62	−1·285	0·470
170°	−0·53	−1·261	0·493
180°	−0·50	−1·250	0·50

Table XIII.

Magnitudes of separate terms related to $\rho g\xi$, ρga and $\rho' ga$ of $\widehat{r\theta}_{r=a}$ $(=\widehat{r\theta'}_{r=a})$ when $\frac{\mu'}{\mu}=\frac{1}{5}$.

θ	$\rho g\xi$	ρga	$\rho' ga$
0°	0	0	0
10°	0·049	−0·028	−0·047
20°	0·092	−0·046	−0·093
30°	0·124	−0·048	−0·156
45°	0·143	−0·018	−0·193
60°	0·124	0·039	−0·236
70°	0·092	0·079	−0·256
80°	0·049	0·107	−0·269
90°	0	0·117	−0·273
100°	−0·049	0·107	−0·269
110°	−0·092	0·079	−0·256
120°	−0·124	0·039	−0·236
135°	−0·143	−0·018	−0·193
150°	−0·124	−0·048	−0·156
160°	−0·092	−0·046	−0·093
170°	−0·049	−0·023	−0·047
180°	0	0	0

Table XIV.

Magnitudes of separate terms related to $\rho g\xi$, ρga and $\rho' ga$ of $\widehat{r\theta}_{r=a}$ $(=\widehat{r\theta'}_{r=a})$ when $\frac{\mu'}{\mu}=1$.

θ	$\rho g\xi$	ρga	$\rho' ga$
0°	0	0	0
10°	0·114	−0·054	−0·058
20°	0·214	−0·087	−0·114
30°	0·289	−0·084	−0·167
45°	0·333	0	−0·236
60°	0·289	0·144	−0·289
70°	0·214	0·240	−0·314
80°	0·114	0·308	−0·328
90°	0	0·334	−0·333
100°	−0·114	0·308	−0·328
110°	−0·214	0·240	−0·314
120°	−0·289	0·144	−0·289
135°	−0·333	0	−0·236
150°	−0·289	−0·084	−0·167
160°	−0·214	−0·087	−0·114
170°	−0·114	−0·054	−0·058
180°	0	0	0

Table XV.

Magnitudes of separate terms related to ρga, $\rho' ga$ and $\rho g\xi$ of $\widehat{r\theta}_{r=a}$ $(=\widehat{r\theta'}_{r=a})$ when $\frac{\mu'}{\mu}=5$.

θ	$\rho g\xi$	ρga	$\rho' ga$
0°	0	0	0
10°	0·156	−0·051	−0·075
20°	0·292	−0·075	−0·146
30°	0·394	−0·048	−0·214
45°	0·455	0·091	−0·303
60°	0·394	0·309	−0·371
70°	0·292	0·449	−0·403
80°	0·156	0·549	−0·422
90°	0	0·584	−0·428
100°	−0·156	0·549	−0·422
110°	−0·292	0·449	−0·403
120°	−0·394	0·309	−0·371
135°	−0·455	0·091	−0·303
150°	−0·394	−0·048	−0·214
160°	−0·292	−0·075	−0·146
170°	−0·156	−0·051	−0·075
180°	0	0	0

Table XVI.

Magnitudes of separate terms related to $\rho g\xi$, ρga and $\rho' ga$ of $\widehat{r\theta}_{r=a}$ $(=\widehat{r\theta'}_{r=a})$ when $\frac{\mu'}{\mu}=\infty$.

θ	$\rho g\xi$	ρga	$\rho' ga$
0°	0	0	0
10°	0·171	−0·038	−0·087
20°	0·321	−0·046	−0·171
30°	0·433	0	−0·250
45°	0·500	0·176	−0·353
60°	0·433	0·433	−0·433
70°	0·321	0·595	−0·470
80°	0·171	0·709	−0·492
90°	0	0·750	−0·500
100°	−0·171	0·709	−0·492
110°	−0·321	0·595	−0·470
120°	−0·433	0·433	−0·433
135°	−0·500	0·176	−0·353
150°	−0·433	0	−0·250
160°	−0·321	−0·046	−0·171
170°	−0·171	−0·038	−0·087
180°	0	0	0

$\widehat{\theta\theta}_{r=a}$, $\widehat{rr'}_{r=a}$, $\widehat{\theta\theta'}_{r=a}$ have unsymmetrical distributions with respect to the plane of $\theta=90°$, and those related to ρga of $\widehat{r\theta}_{r=a}$, $\widehat{r\theta'}_{r=a}$ have symmetrical distributions with respect to this plane.

3. The terms related to $\rho' ga$ of $\widehat{rr}_{r=a}$, $\widehat{\theta\theta}_{r=a}$, $\widehat{rr'}_{r=a}$, $\widehat{\theta\theta'}_{r=a}$ are also unsymmetrical with respect to the plane $\theta=90°$. The terms concerning $\rho' ga$ of $\widehat{r\theta}_{r=a}$, $\widehat{r\theta'}_{r=a}$ have, however, symmetrical distributions with respect to the plane of $\theta=90°$.

4. When the depth ξ of the center of cylindrical inclusion is deep, the respective distributions of stresses in the inclusion and in the medium are mainly affected by the terms related to $\rho g\xi$ and the terms related to ρga and $\rho' ga$ have no much effects upon the stress distributions. When ρ' is very large, however, the terms related to $\rho' ga$ have some effects upon them.

5. When the depth ξ is moderately shallow, the respective terms related to ρga and $\rho' ga$, which are the unbalancing forces due to body force, have some effects upon the stress distributions.

6. When the cylindrical inclusion is more rigid than the surrounding medium, the magnitudes of the respective terms related to ρga and $\rho g\xi$ of $\widehat{rr}_{r=a}$, $\widehat{r\theta}_{r=a}$, $\widehat{rr'}_{r=a}$, $\widehat{r\theta'}_{r=a}$ are large, and those of the terms related to $\rho' ga$ of $\widehat{r\theta}_{r=a}$ and $\widehat{r\theta'}_{r=a}$ are also large. The magnitudes of the terms related to $\rho' ga$ of $\widehat{rr}_{r=a}$ and $\widehat{rr'}_{r=a}$, however, are small in this case.

7. When the cylindrical inclusion is more rigid than the surrounding medium, the magnitudes of the respective terms related to $\rho g\xi$ and ρga of $\widehat{\theta\theta}_{r=a}$ are generally small, and those of the terms related to $\widehat{\theta\theta'}_{r=a}$, on the contrary, are generally large. The terms related to $\rho' ga$ of the components of stresses $\widehat{\theta\theta}_{r=a}$ and $\widehat{\theta\theta'}_{r=a}$ have special distributions which differ from those of all other components of stresses when the magnitude of $\frac{\mu'}{\mu}$ is large.

To see the properties of distributions of stresses along a radial direction we obtained the annexed figures by numerical calculations of the expressions (44), (45), (46), (47), (48), (49), (50), (51). (Fig. 6a, 6b, 6c, 7a, 7b, 7c, 8a, 8b, 8c). These figures shew us the following facts.

1. Whether or not the elastic constants of the semi-infinite solid are larger than those of the cylindrical inclusion, the magnitudes of the terms related to $\rho g\xi$ of all components of stresses in the cylindrical inclusion are constant along a radial direction but not along azimuthal

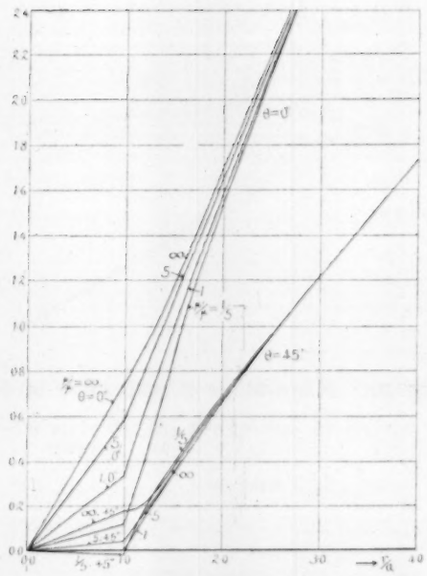

Fig. 6a. Magnitudes of respective terms related to ρga of $\widehat{rr}_{\substack{\theta=0^\circ \\ \theta=45^\circ}}$, $\widehat{rr'}_{\substack{\theta=0^\circ \\ \theta=45^\circ}}$ wnen $\frac{\mu'}{\mu}=\frac{1}{5}$, 1, 5 and ∞.

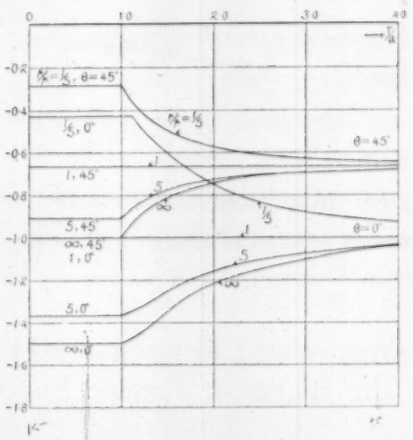

Fig. 6b. Magnitudes of respective terms related to $\rho g\xi$ of $\widehat{rr}_{\substack{\theta=0^\circ \\ \theta=45^\circ}}$, $\widehat{rr'}_{\substack{\theta=0^\circ \\ \theta=45^\circ}}$ when $\frac{\mu'}{\mu}=\frac{1}{5}$, 1, 5 and ∞.

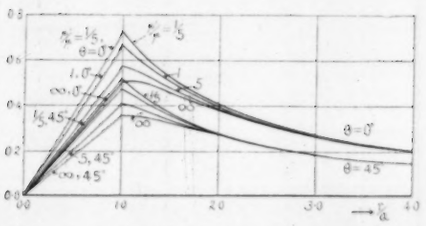

Fig. 6c. Magnitudes of respective terms related to $\rho' ga$ of $\widehat{rr}_{\substack{\theta=0^\circ \\ \theta=45^\circ}}$, $\widehat{rr'}_{\substack{\theta=0^\circ \\ \theta=45^\circ}}$ when $\frac{\mu'}{\mu}=\frac{1}{5}$, 1, 5 and ∞.

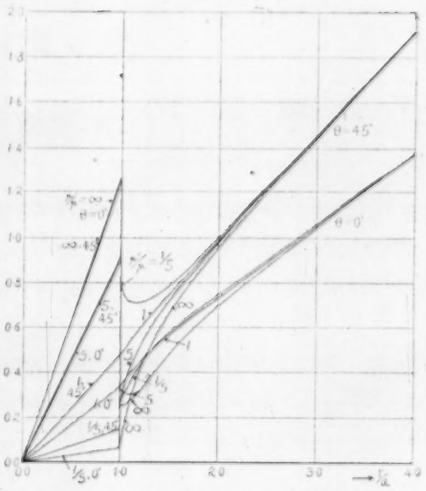

Fig. 7a. Magnitudes of respective terms related to ρga of $\widehat{\theta\theta}_{\substack{\theta=0^\circ \\ \theta=45^\circ}}$, $\widehat{\theta\theta'}_{\substack{\theta=0^\circ \\ \theta=45^\circ}}$ when $\frac{\mu'}{\mu}=\frac{1}{5}$, 1, 5 and ∞.

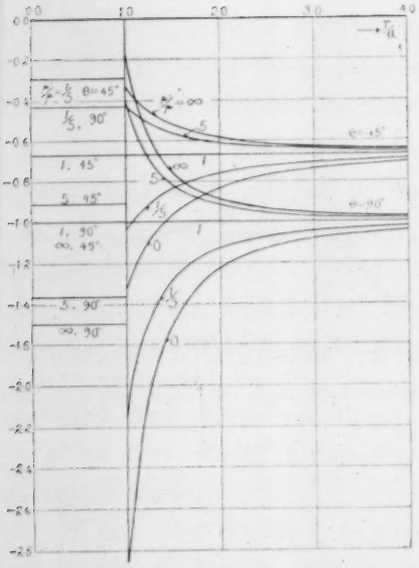

Fig. 7b. Magnitudes of respective terms related to $\rho g\xi$ of $\widehat{\theta\theta}_{\theta=45^\circ}$, $\widehat{\theta\theta'}_{\theta=45^\circ}$ when $\theta=90^\circ$ $\theta=90^\circ$ $\frac{\mu'}{\mu}=\frac{1}{5}$, 1, 5 and ∞.

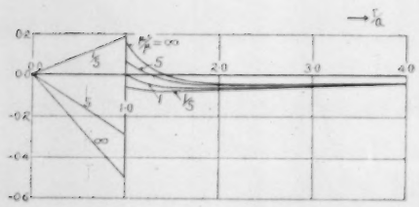

Fig. 7c. Magnitudes of respective terms related to $\rho' ga$ of $\widehat{\theta\theta}_{\theta=0^\circ}$, $\widehat{\theta\theta'}_{\theta=0^\circ}$ when $\frac{\mu'}{\mu}=\frac{1}{5}$, 1, 5 and ∞.

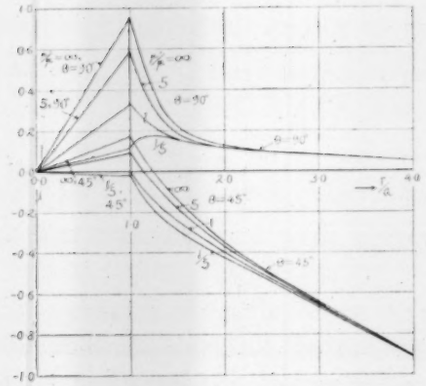

Fig. 8a. Magnitudes of respective terms related to ρga of $\widehat{r\theta}_{\theta=45^\circ}$, $\widehat{r\theta'}_{\theta=45^\circ}$ when $\theta=90^\circ$ $\theta=90^\circ$ $\frac{\mu'}{\mu}=\frac{1}{5}$, 1, 5 and ∞.

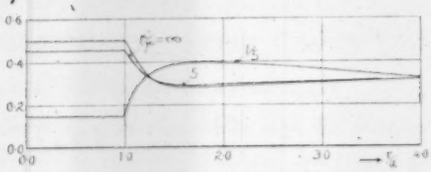

Fig. 8b. Magnitudes of respective terms related to $\rho g\xi$ of $\widehat{r\theta}_{\theta=45^\circ}$ and $\widehat{r\theta'}_{\theta=45^\circ}$ when $\frac{\mu'}{\mu}=\frac{1}{5}$, 5 and ∞.

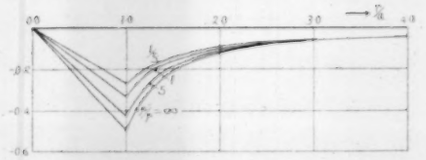

Fig. 8c. Magnitudes of respective terms related to $\rho' ga$ of $\widehat{r\theta}_{\theta=90^\circ}$ and $\widehat{r\theta'}_{\theta=90^\circ}$ when $\frac{\mu'}{\mu}=\frac{1}{5}$, 1, 5 and ∞.

direction. And the magnitudes of the terms related to ρga and $\rho' ga$ of the respective components of stresses of the inclusion increase linearly along radial direction.

2. The region where the stress distributions in the semi-infinite solid affected by the presence of a cylindrical inclusion is limited in the boundary region of that inclusion and the effective radius upon the distributions of stresses in the boundary medium is approximately four times the radius of the cylindrical inclusion.

The mathematical results obtained in this paper are not applicable to the case where $\frac{\mu'}{\mu}=0$ and the cylindrical inclusion has no rigidity. In this case the problem should be formally solved anew by the following boundary conditions

$$
\begin{aligned}
r=a: \quad & \left.\begin{aligned} u&=u', \\ \widehat{rr}&=\widehat{rr}', \\ \widehat{r\theta}&=0, \\ \widehat{r\theta}'&=0. \end{aligned}\right\} \\
r=\infty: \quad & \widehat{rr}=\widehat{rr} \text{ expressed by (27)}, \\
& \widehat{\theta\theta}=\widehat{\theta\theta} \text{ expressed by (27)}, \\
& \widehat{r\theta}=\widehat{r\theta} \text{ expressed by (27)}.
\end{aligned}
$$

13. 重力の働ける半無限彈性體内に存在する圓形塡充物附近の應力 (I)

地震研究所 西村源六郎 高山威雄

重力の作用してゐる半無限彈性體内にそれと密度及び彈性常數の異つた圓形な異物質が塡充してゐる場合，この物質の内外に於ける應力釣合を論じた．目的は地殻内部に異物質のある場合，それが地殻の釣合に如何なる影響を與へるかを知る爲めに行つた計算である．直ちに役立つとは思はないが，幾分でも定量的に參考になる所があれば幸である．

計算は，半無限彈性體は plane strain の狀態に置れてあるとしてやり，異物質との硬さの關係を色々にとつて應力の分布狀態を圖示してある．

14. *La déformation de la croûte terrestre et la production des ondes sismique au foyer*

par Mishio ISHIMOTO,

Institut de Recherches sur les Tremblements de terre.

(Lu le 17 janvier 1933, reçu le 20 mars 1933)

1. Introduction.

L'année dernière nous avons publié un mémoire[1] sur le mécanisme de la production des ondes sismiques au foyer : nous avons constaté tout d'abord que deux sortes d'ondes, onde poussante et onde tirante, sont séparées par une courbe de section conique. Pour expliquer cette façon de distribution, nous avons introduit au foyer une source quadruple. Bien que cette hypothèse explique le rayonnement des ondes sismiques du foyer au moyen de l'analyse mathématique, nous sommes obligés d'attribuer une certain dimension au foyer considéré étant la source énergique des ondes sismiques. Supposons donc un foyer sismique ayant une certaine dimension dans la croûte. Il corresponde à un réservoir contenant une haute pression hydrostatique qui augmente progressivement. Quand la pression intérieure atteindra la limite de la pression extérieure, il se produira une destruction violente du réservoir. Le mouvement initial de cette destruction déterminera certainement la propagation sphérique des ondes de type $P_2(\cos\theta)$. D'un autre côté, nous pouvons supposer des projections de matière en dehors de ce réservoir ce qui produira ainsi un train d'ondes élastiques. Si cette projection est assez violente, il y aura une certaine déformation à la surface terrestre ayant une figure définie par la direction des jets de matière. Nous nous proposons donc d'exécuter une revision des produits topographique résultant surtout des grands tremblements de terre et correspondant à la distribution des mouvements initiaux des secousses sismiques.

Quand on étudie la déformation de la croûte produite par un séisme, on prête attention sourtout à l'apparition des dislocations. Il nous semble que l'on est toujours content de découvrir au moins une trace de faille dans la région épicentrale. Mais l'apparition des failles n'est pas le seul phénomène important dans la déformation générale de la croûte. On

1) M. ISHIMOTO, *Bull. Earthq. Res. Inst.*, 10 (1932), 449.

peut constater en outre un exhaussement du terrain qui se produit souvent, surtout au bord de la mer. Evidemment ce qu'on peut observer à l'oeil nu sur le terrain, ce sont des changements dont le gradient de déformation demeure assez grand : on voit donc généralement le phénomène de bordure. Mais quand on veut savoir le fait réel des changements topographiques, on doit consulter les résultats obtenus au moyen des mesures géodésiques : la triangulation et le nivellement de précision.

Les changements topographiques produits par les deux tremblements de terre de Kantô en 1923, et de Tango en 1927, ont été mis au clair par les deux sortes de mesures géodésiques. D'autre côté nous avons les données sur la distribution régionale des mouvements initiaux des secousses correspondant à chaque séisme. Nous voulons découvrir le rapport, s'il y en a, entre la déformation de la croûte, et les mouvements initiaux des secousses. Cette comparaison nous permettra de faire progresser notre discussion sur le mécanisme de la production des ondes sismiques ainsi que sur la force motrice capable de donner une déformation permanente à la croûte.

Nous étudions, tout d'abord, la distribution des mouvements initiaux suivant l'hypothèse de la source quadruple au foyer dont le pôle est dirigé vers une direction convenable.

S'il y a une certain correspondance entre les deux phénomènes, l'action de la production des ondes sismiques deviendra un mouvement important pour décider la façon de déformation de la croûte.

Nous avons déjà écrit que la propagation sphérique des ondes longitudinales rayonnant du foyer sera représentée par la formule suivante, spécialement dans un milieu assez éloigné du foyer :

$$\phi = \left[P_2(\cos\theta) - \frac{1}{4} P_0(\cos\theta) \right] \frac{e^{ik(vt-r)}}{r}$$

où l'angle de cône demeure 45°. Nous allons maintenant considérer spécialement deux cas ; a) son pôle (direction de l'axe de cône) a une direction horizontale, b) son pôle a une direction faisant un angle de 20° avec la verticale. Nous pouvons facilement calculer l'amplitude du mouvement de chaque position à la surface suivant une formule[2]. La

2) $h \dfrac{2(h^2+\rho r\cos\theta)^2-(h^2+r^2)(h^2+\rho^2)}{(h^2+r^2)(h^2+\rho^2)^2}$ .....pour la composante verticale.

$\rho \dfrac{2(h^2+\rho r\cos\theta)^2-(h^2+r^2)(h^2+\rho^2)}{(h^2+r^2)(h^2+\rho^2)^2}$ .....pour la composante horizontale.

où θ et r : deux paramètres, h: profondeur du foyer et ρ: distance entre le point percé du pôle à la surfaee et l'épicentre.

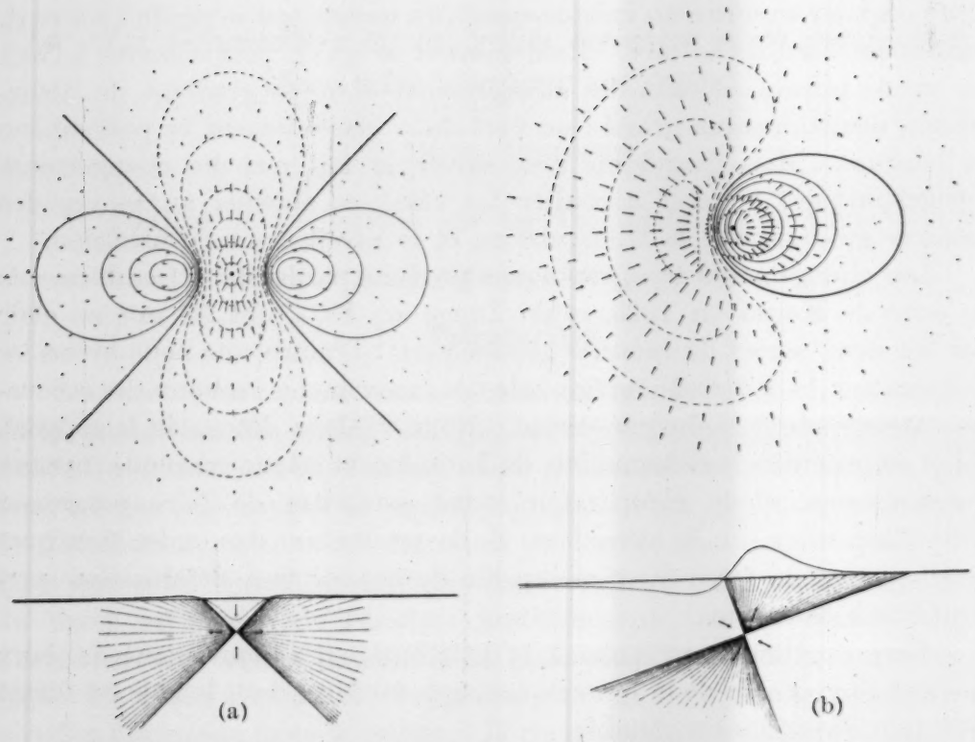

Fig. 1. Déplacement de chaque point à la surface terrestre causé par une source quadruple dane la croûte : a) le pôle dirige dans la direction horizontale, b) le pôle dirige dans 20° avec la direction verticale.

Fig. 1 représente la distribution régionale des déplacements calculés dont la courbe nodale est représentée par une hyperbole pour a), par une ellipse pour b). La région intérieure de la courbe est toujours occupée par les ondes poussantes : c'est-à-dire que la composante verticale se dirige vers le haut et que la composante horizontale se dirige dans un sens opposé à l'épicentre.

En supposant quelque déplacement de matière au foyer pour produire une telle distribution des ondes, on trouvera un certain effet de ce mouvement comme la déformation permanente de la croûte surtout aux environs de l'épicentre. La déformation de la croûte ressemblera plutôt au mouvement initial de chaque point représenté dans la Fig. 1.

Partant de cette idée, nous nous sommes mis à comparer la distribution régionale des mouvements initiaux des secousses avec les changements topographiques produits spécialement dans les environs de l'épicentre.

2. Comparaison de la distribution des mouvements initiaux des secousses sismiques avec la déformation permanente de la croûte.

a) *Le tremblement de terre de Kantô en 1923.*

L'épicentre de ce tremblement de terre a été déterminé par plusieurs personnes. Il nous semble que la conclusion de S. Kunitomi[3] est la meilleure, du fait qu'il a consulté tous les enregistrements sismographiques obtenus dans toutes les régions du Japon. A l'égard de la distribution des mouvements initiaux, il y a aussi plusieurs hypothèses possibles d'après l'adoptation des différents mécanismes de la production des ondes. Probablement, il n'y a plus de changement sur le fait de la distribution des deux sortes d'ondes, tandis qu'il y aura lieu de modifier le choix de la forme de courbe nodale. Cette différence depend, d'une part, de la conséquence de la considération sur le mécanisme de la production des ondes sismiques, d'autre part de l'adoption de la réflection des ondes sur une surface discontinue supposée existant dans la croûte terrestre. Quant à nous, cependant, nous mettons une source quadruple au foyer. Nous traçons, en effet, une ellipse pour expliquer le mécanisme de la production des ondes sismiques: l'autre fois,[4] nous avons adopté une ellipse ayant une forme très voisine de la parabole quoiqu'il y ait un certain nombre de disconvenances.

D'un autre côté nous pouvons considérer sur un séisme du 27 juillet 1929 dont la position épicentrale se trouve tout près de celle du tremblement de terre de 1923. En 1929, comme les conditions de l'installation sismographique de chaque station étaient améliorées comparativement, nous pouvons savoir le fait réel sur la distribution des mouvement initiax des secousses sismqiues. Nous espérons réussir enfin à connaître le mécanisme du séisme de 1923 avec l'étude sur le séisme de 1929.

Lors que nous avons publié le mémoire précédant, nous n'avons pu trouver aucune étude sur ce séisme. Dans la suite cependant, grâce à H. Kawasumi, ayant su qu'il y avait une étude de K. Hayata,[5] nous avons constaté que son étude n'était pas complètement identique à celle rapportée dans Kisyôyôran. Suivant cette étude, il y a un domaine d'ondes poussantes autour de l'épicentre et une zone d'ondes tirantes en dehors

3) S. Kunitomi, *Geophys. Mag.*, **3** (1931), 149.
4) M. Ishimoto, *loc. cit.*
5) K. Hayata, *Kensin Zihô*, **4** (1930), 17.

de ce domaine. Pour mettre ce fait en évidence nous traçons une série de lignes nodales pour séparer les différentes ondes (Fig. 2). Naturellement, nous supposons l'existence d'une source quadruple au foyer et nous supposons que l'écorce terrestre est un milieu hétérogène. Le trajectoire du rayon sismique montre sa convéxité vers en bas et des ondes poussantes rayonnant obliquement dans le sein de l'écorce apparaissent à la surface dehors de la zone des ondes tirantes. En considérant ces faits, nous traçons deux courbes pour représenter la node. Cette fois-ci, l'axe de cône se dirige vers la verticale avec un peu de déviation à l'Est. La profondeur hypocentrale se trouve à peu près 40 km.

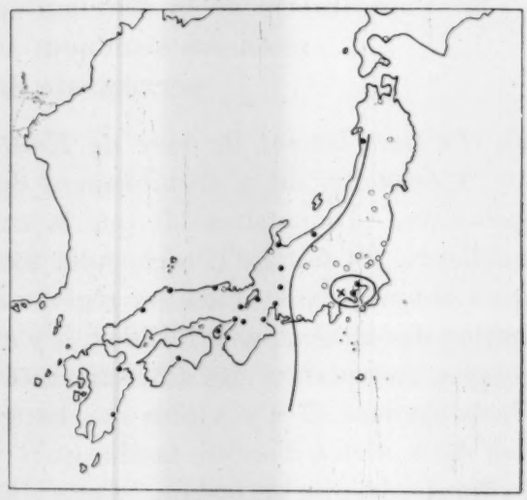

Fig. 2. Distribution des mouvements initiaux des secouses sismiques pour le séisme du 27 juillet 1929. • onde poussante ○ onde tirante, × épicentre.

Cette distribution des deux sortes d'ondes nous suggère un trace des courbes nodales pour le séisme de 1923 quoiqu'il n'y eut aucune station existée correspondant à la région tirante (Fig. 3). La profondeur hypocentrale se trouve à peu près 30 km, moins grande que l'autre. Comme on voit dans la Fig. 3, presque toutes les deux sortes d'ondes sont partagées par ces courbes et l'axe du cône se dirige aussi vers la verticale avec un peu de déviation à l'Est. Les aspects généraux des mouvements initiaux à la surface terrestre correspondront au modèle-b dans la Fig. 1.

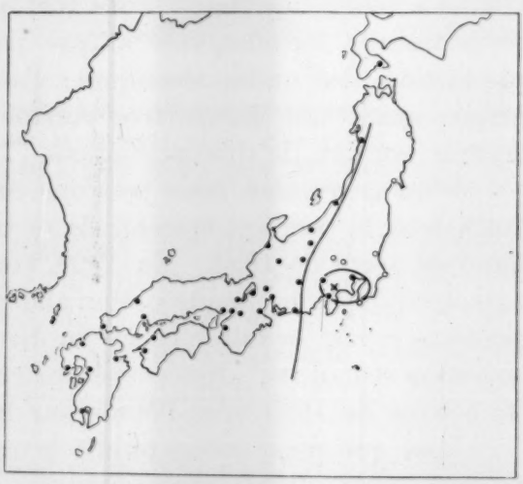

Fig. 3. Distribution des mouvements initiaux des secousses sismique pour le séisme de Kantô (le 1er Sept. 1923) • onde poussante ○ onde tirante, × épicentre.

Les changements topographiques qui ont accompagné le tremblement de terre de Kantô ont été déterminés au moyen des mesures géo-

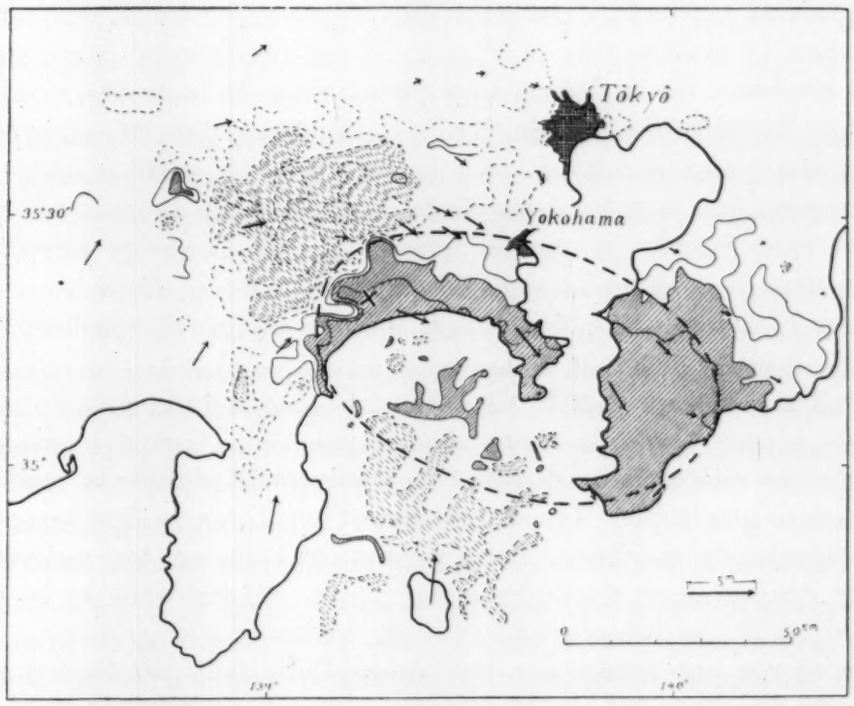

Fig. 4. Déformation de la croûte terrestre causée par le séisme de Kantô. (D'après les cartes publiées par Rikuti-Sokuryôbu)

désiques par Rikuti-Sokuryôbu.[6] (Bureau Militaire pour le Levé de terrain) (Fig. 4) Il y a un exhaussement de terrain dans les régions de la côte du golfe de Sagami ainsi que de la moitié sud de la péninsule de Bôsô. La dépression du terrain a été constaté aux régions placées sur le côté Nord-Ouest voisines de la région exhaussée où nous trouvons l'épicentre.

A l'égard du déplacement horizontal du terrain, les résultats dependent entièrement du choix des points supposés fixes. Il y a deux sortes de données d'après deux différentes conditions. De plus, K. Mutô[7] a introduit certaines corrections sur les valeurs de déplacements. Il a supposé qu'il y a certaines erreurs dans le résultat des mesures de la base ainsi que dans la direction de deux points de triangulation supposées fixes. Dans la Fig. 4 nous avons pris un des données originaux.

Comparant ces déplacements de la composante horizontale à ceux de

6) Rituki-Sokuryôbu. *Travaux de la Section de Géodésie, Tome 7.*
7) K. Mutô, *Bull. Earthq. Res. Inst.*, 10 (1932), 384.

la composante verticale, nous pouvons trouver une relation serrée représentée dans le modèle-b de la Fig. 1. Nous conclurons, donc, que les aspects généraux de la déformation permanente de la croûte, produite à l'occasion du tremblement de terre, sont définis par les mouvements initiaux des ondes sismiques. En constatant cette relation entre eux, nous croyons que le mécanisme de la production des ondes sismiques est toujours assez simple et que la déformation de la croûte terrestre est réalisée dans le sens de l'action initiale provoquée au foyer.

Pour comprendre ces faits, nous sommes obligés de constater, d'une part, la propriété plastique de la croûte terrestre qui conserve la déformation produite, d'autre part le déplacement brusque du magma au sein de la croûte, connu comme le phénomène d'intrusion. Quand le magma se déplace dans une certaine direction ce mouvement signife la production d'une source quadruple. Conséquemment l'hypothèse de l'existence d'une source quadruple au foyer, nous permet d'expliquer les mouvements initiaux des secousses sismiques ainsi que la déformation de la croûte terrestre.

Or, il y a une étude[8] sur l'existence d'une faille au fond du golfe de Sagami d'après le fait que le déplacement horizontal du terrain deviend plus grand quand on approche de cette faille supposée. Il y a encore cependant une autre étude[9] qui montre que l'existence d'une faille n'est pas juste quand on revise minitieusement sur les déplacements horizontaux surtout auprès de la faille supposée. Suivant notre opinion, la constation de la faille n'est pas possible seulement avec la composante horizontale, nous allons voir le fait produit dans la direction verticale. A l'égard des déplacements verticaux du fond du golfe de Sagami, on a les résultats publiés par le Bureau hydrographique naval.[10] Nous distinguons certainement la dépression du fond dans la partie extérieure de la courbe nodale et l'exhaussement du fond à son intérieur. Ces changements s'accordent avec notre hypothèse quoique les valeurs quantitatives des changements ne soient pas pareilles avec celles obtenus sur le terrain. Au fond de la mer, la matière composante ne reste plus égale a celle qui existe sur le terrain : on y constate souvent l'apparition d'un volcan, la dépression brusque du fond, etc. D'après ces phénomènes, nous inclinons à croire à l'apparition d'un grand changement du found même à l'occasion d'un sévère tremblement de terre. Il sera probable

8) A. Imamura et H. Kisinoué, *Bull. Earthq. Res. Inst.*, 5 (1928), 35.

9) S. Hudiwara, *Kisyô-Syûsi*, 10 (1932), 713.

10) T. Utida, *Report Imp. Earthq. Inv. Com.*, No 100, B (1929), 61.

que la production d'une faille sera réalisée en correspondance avec la position de la courbe nodale.

b) *Le tremblement de terre de Tazima en 1925.*

Plusieurs[11] personnes ont essayé de déterminer la position épicentrale de ce séisme. D'après l'habitude de poser l'épicentre sur une faille, tous ont choisi l'embouchure du fleuve Maruyama comme sa position : parce qu'il y a eu des dommages catastrophiques au long de ce fleuve. Suivant notre considération, cependant, il n'y a aucune raison de fixer l'épicentre sur cette position même d'après les enregistrements sismographiques obtenus à chacune des stations qui se trouvent autour de la région troublée. Les dommages catastrophiques survenus le bassin de fleuve sont dus au phénomène que les ondes stationaires se ont produites secondairement à cet endroit et que leur accélération, aussi bien que leur période a été sensiblement grande.

Il nous semble, cependant, que l'épicentre était situé près de Takenomura au fond de la mer. Nous le pensons parce que d'une part, un exhaussement de terrain a été observé dans cette région et que d'autre part le Prof. Nakamura[12] rapporte qu'on a entendu, auprès de Takeno, sur la mer, des bruits sismiques au moment du tremblement de terre dans la direction N-O : probablement cette direction coïncide avec celle de l'épicentre.

A l'égard de la distribution régionale des mouvements initiaux des secousses de ce séisme, il y a plusieurs études. Nous citerons ici les données de Dr. K. Wadati et K. Suda[13]. Pour mettre cette distribution en evidence, K. Suda se base sur l'effet de reflection produit sur la surface discontinue dans la croûte. Nous adoptions, cependant, une source quadruple au foyer et nous con-

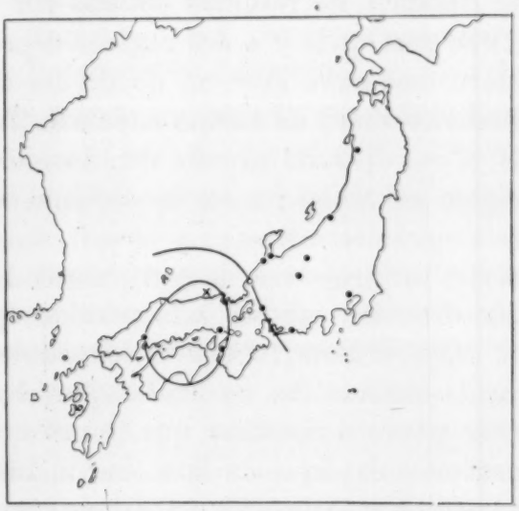

Fig. 5. Distribution des mouvements initiaux des secousses sismiques pour le séisme de Tazima. (le 23 mai 1925) • onde poussante, ○ onde tirante, × épicentre.

11) K. Suda, *Umi to Sora*, 5 (1925), 127. A. Imamura, *Reports. Imp. Erthq. Inv. Com*, 101 (1927), 1.

12) Saem. Nakamura, *Saito Hôonkai*, 1 (1925), 22.

13) K. Wadati, *Kisyô-syûsi*, [2], 3 (1925), 1 ; Suda, *loc. cit.*

sidérons le rayon sismique comme traversant un milieu hétérogène. Avec cette idée, nous pouvons expliquer la distribution régionale de deux sortes d'ondes comme nous l'avons fait dans le cas du tremblement de terre de Kantô de 1923. Les ondes rayonnées obliquement dans le sein de la croûte apparaissent à la surface suivant la loi de refraction. Cette fois-ci la profondeur du foyer était un peu plus grande que l'autre.

On a observé une dislocation du terrain auprès de Taï: à laquelle on a donné le nom de la faille de Taï. Mais, en tout cas, ce changement topographique n'a pas une grande importance: car nous ne trouvons pas aucune influence dans les résultats obtenus au moyen des mesures géodésiques.

Les mesures des changements topographiques produits par ce tremblement de terre n'ont pas été exécutées tout de suite. Après le tremblement de terre de Tango de 1927, la maille de la triangulation a été étendue jusqu'à la région de Tazima et on a pu ainsi assurer qu'une certaine déformation de la croûte avait été produite par ce tremblement de terre. Naturellement, il y a des influences de deux séismes prédominant surtout aux endroits situés entre les deux positions épicentrales.

D'après les résultats obtenus par la triangulation, nous constatons, d'une part qu'il y a des régions dépressionées surtout dans le bassin de Maruyama-gawa avec un maximum de 36 cm; d'autre part qu'il y a de l'exhaussement de terrain auprès de Takeno, avec un maximum de 34 cm. Il n'y a pas de grands déplacements horizontaux de terrain dans la région exhaussée: mais ils deviennent grands aux points qui s'éloignent de l'épicentre, comme on le voit, dans la Fig. 5. Le sens des déplacements se dirige vers le Sud: c'est-à-dire que le terrain a été déplacé dans une direction opposée à la position épicentrale.

Quand nous faisons la comparaison entre la distribution des mouvements initiaux des secousses et les changements topographiques produits, nous pouvons constater que le mécanisme de ce tremblement de terre peut être expliqué de la même manière que celui du tremblement de terre de Kantô de 1923. L'axe de cône se dirige dans le sens vertical avec un peu de déviation vers le Sud. Dans la région épicentrale, le déplacement vertical prédomine remarquablement, tandis que dans les régions lointaines le déplacement horizontal devient remarquable au lieu du déplacement vertical. Ces faits nous suggèrent l'existence d'une source quadruple au foyer comme nous l'avons déjà noté pour le tremblement de terre de Kantô. En tout cas, il y a ce fait notable que la caractéristique de la déformation de la croûte est produite par le même procédé

que la production des ondes initiales.

c) *Le tremblement de terre de Tango en 1927.*

Le tremblement de terre de Tango de 1927 a causé des dommages catastrophiques aux villes situées surtout auprès de la région épicentrale. D'après S. Kunitomi[14] l'épicentre de ce séisme a été déterminé au large d'Amino. Parmi les nombreuses répliques apparues partout dans la région catastrophée, on peut en distinguer quelques unes apparaîssant toujours au Nord de la faille de Yamada (à Mié-mura) pendant assez longtempe après le premier grand séisme.

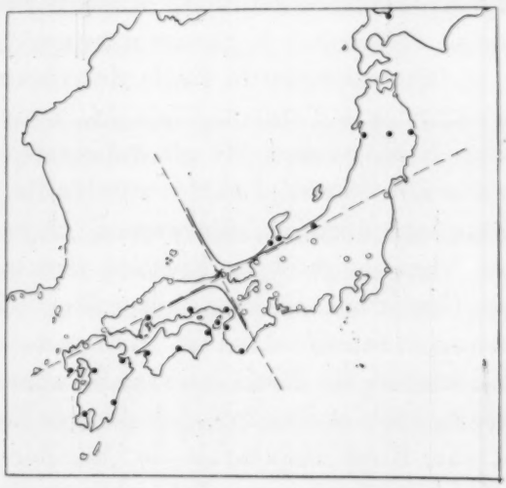

Fig. 6. Distribution des mouvements initiaux des secousses sismiques pour le séisme de Tango. (le 7 mai 1927) • onde poussante, ○ onde tirante, × épicentre.

La distribution régionale des mouvements initiaux des secousses a été étudiée aussi par S. Kunitomi avec les enregistrements sismographiques obtenus toutes les stations au Japon. D'après sa conclusion, les deux sortes d'ondes se distribuent dans les quadrants dont une des deux lignes partageantes coïncide avec la direction de la faille de Gômura ; il conclut donc que le déplacement relatif de la croûte terrestre au long de cette faille sera la cause de la production des ondes sismiques. Certainement, quand on remarque seulement la distribution des mouvements initiaux de la composante horizontale, elle coïncide parfaitement bien avec les déplacements horizontaux produits dans la région épicentrale. Nous remarquons, cependant, en même temps l'existence d'un déplacement vertical du terrain qui prédomine quelquefois plus que le déplacement horizontal. Pour expliquer les phénomènes sismiques, en effet, on doit tenir compte de ces deux éléments de la déformation de la croûte ; autrement la conclusion n'aura pas beaucoup de valeur, parce qu'elle s'appuiera seulement sur une des deux composantes.

Les changements topographiques constatés à l'oeil nu sont d'une part l'exhaussement du terrain sur la côte de la mer du Japon, d'autre part

14) S. Kunitomi, *Geophys. Mag.*, 2 (1930), 65.

l'apparition d'une série de failles. Sur la côte, nous avons constaté 0,8 m d'exhaussment de terrain rapporté au niveau moyen de la mer : sur la plage on trouve sur les roches l'attachement des huîtres ainsi que des herbes marines comme index de l'ancien niveau moyen de la mer. Le Prof. Saem. Nakamura[15] a étudi la distribution régionale de l'exhaussement au long de la côte et a trouvé le maximum auprès de la Hamadumé.

On considère la faille de Gômura comme la faille principale. Elle commence à l'embouchure de la rivière d'Asamo et court dans la direction S-E, quoiqu'elle ait été suivie sous une forme d'échelon. Le terrain situé sur le côté Est de cette faille a glissé relativement vers le Nord avec une certaine, dépression, Il y a une autre faille produite auprès de Yamada dont la direction demeure perpendiculaire à celle de la faille de Gômura. A l'égard de cette faille nous n'avons vu que le déplacement relatif dans la composante verticale. Ce que nous observons au moyen de l'oeil nu est l'exhaussement relatif du terrain au niveau de la mer et l'endroit où le gradiant de changement est assez grand. Donc, il est impossible de discuter la déformation veritable du terrain. Nous sommes, en effet, obligés de consulter les résultats obtenus au

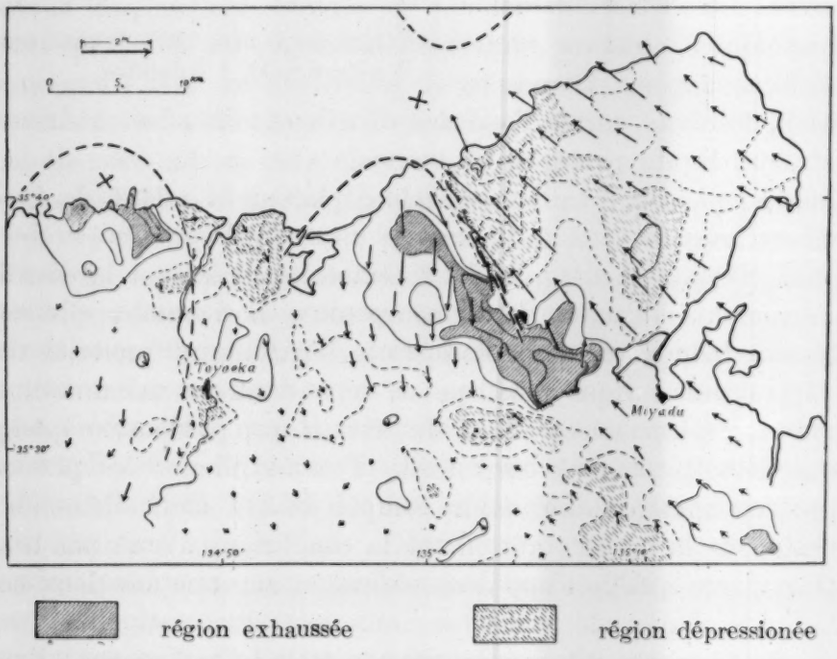

région exhaussée région dépressionée

Fig. 7. Déformation de la croûte terrestre causée par le séisme de Tango (le 7 mai 1927) (d'après les cartes publiées par Rikuti-Sokuryôbu)

15) Saem. Nakamura, *Saitô Hôonkai Hôkoku*, No. 5.

moyen des mesures géodésiques.

La déformation de la croûte qui a accompagné ce séisme a été déterminée au moyen de la trianglation ainsi que du nivellement de précision. Leurs résultats ont été déjà publié de Rikuti-sokuryôbu. Nous pouvons constater tout de suite les aspects généraux de déformation représentée par une série de cartes: nous avons fait la Fig 5 d'après ces deux cartes.

Certainement, ce que nous avons observé à l'oeil nu coïncide parfaitement avec les résultats représentés dans la Fig. 5. Nous pouvons déterminer de plus la limite de l'extension de la déformation. Sans entrer dans aucune discussion sur les détails, nous voulons examiner la déformation produite. L'exhaussement du terrain devient maximum sur le côté nord de la faille de Yamada: mais cette déformation n'est pas le résultat simple du grand séisme, car nous y avons constate l'apparition des nombreuses répliques même assez longtemps après le grand séisme. L'exhaussement de cette région a été probablement achevé à la suite d'un certain cours du temps.

Etant partagée par la faille de Gomura, la portion d'Est de la croûte a été déplacée dans la direction épicentrale avec la dépression du terrain, tandis que la portion d'Oust a été déplacée dans la direction opposée à l'épicentre avec l'exhaussement du terrain. Ces faits coïncident très bien avec notre hypothèse posant une source quadruple au foyer. Quand on limite la discussion seulement à la composante horizontale, le mouvement du terrain au long de la faille coïncide naturellement avec la distribution des mouvements initiaux des secousses. On suppose que la production d'une faille accompagne le rayonnement des ondes sismiques, et on ne fait pas beaucoup d'attention au déplacement vertical du terrain. Quand on considère en même temps la composante verticale, on est amené à changer l'explication sur la production des ondes sismiques. Nous proposons donc que la force motrice au foyer qui produit des ondes sismiques et puis la déformation de la croûte soit considérée comme présentant les caractéristiques d'une source quadruple.

Nous avon déjà écrit que la production des ondes sismiques est due au mouvements magmatique dans le sein de la croûte.[16] Quand la pression de la vapour dans le magma augmente au delà de la limite de la pression extérieure, il y a certainement un phénomène d'explosion produisant une déformation de la croûte: naturellement l'explosion se

16) M. Ishimoto, *loc. cit.*

manifestera sur la partie inférieure de la croûte. Puisque la faille est la zone inférieure de la croûte, le mouvement relatif de la croûte y apparaîtra quand le foyer reste peu profond. Il y a deux cas : le magma se déplace dans la direction verticale ou dans la direction horizontale. Nous voyons d'une part l'apparition d'une faille quand le déplacement du magma se dirige horizontalement, d'autre part l'exhaussement du terrain à la région épicentrale quand le déplacement du magma se dirige verticalement. Nous avons déjà cité des exemples correspondant aux deux cas. L'apparition de la faille n'est plus une règle de déformation relativement à un grand tremblement de terre.

Quand on considère que l'origine des secousses sismiques est dues au mouvement relatif de deux portions de la croûte, les ondes transversales deviennent plus importantes que les ondes longitudinales. A notre avis le déplacement magmatique détermine des ondes longitudinales comme produits directs et des ondes transversales comme les produits secondaires. Le Prof. K. Sezawa[17] a déjà montré théoriquement que les ondes longitudinales accompagnent toujours les ondes transversales dans le cas de la propagation sphérique des ondes dans un milieu solide.

En tout cas, ce que nous avons constaté sur la déformation de la croûte est toujours explique avec l'hypothèse d'une source quadruple au foyer. Quelquefois, l'axe du cône se dirige dans la direction verticale, quelquefois il se dirige dans la direction horizontale. Nous voulons maintenant appliquer notre hypothèse à toutes les déformations produites par les tremblements de terre pour voir si elle s'y adapte bien ou non.

d) *Le tremblement de terre de Nobi en 1891.*

Lors de ce tremblement de terre l'organization des stations sismologiques était médiocre et cela ne nous permet pas d'étudier la distribution régionale des mouvements initiaux des secousses. La déformation de la croûte produite par ce séisme a été assez remarquable. Pour savoir les aspects généraux des changements topographiques, nous citerons ici la description de F. Omori :[18]

> La faille produite court généralement dans la direction de NO à SE. Partant de Kinbara vers SE, c'est sur le côté NE que se fait la dépression ; tandis que à Midutori, (dans la vallée de Néo) c'est sur le côté SO que se fait la dépression. Même à l'extrémité de la faille, à Noziri, dans la province d'Etizen, le côté

17) K. SEZAWA, *Bull. Earthq. Res. Inst.*, 2 (1927), 13.

18) F. OMORI, "*Disin-gaku Kôwa*", 337.

SO a une dépression : la dépression maxima a été mesurée de 18 pouces à Mizutori. Partant de Kinbura vers le Nord, on remarque surtout le déplacement horizontal dont le côté SO a glissé relativement au côté NE dans la direction SE. On a mesuré 18 pouces de déplacement maximum à Nakamura.

Les savants qui ont constaté grande dislocation de la croûte terrestre, ont considéré tout de suite que la production des ondes sismiques a été provoquée la rupture de la matière qui compose la croûte terrestre. Autrement dit, ils ont considéré les changements topographiques comme les résultats de la rupture du terrain à la suite de l'accumulation de l'effort.

Pour savoir la déformation exacte du terrain, le nivellement de précision a été rexécuté dans cette région. D'après les résultats obtenus, nous pouvons constater un exhaussement de terrain sur le côté SO de la faille et une dépression de terrain sur le côté NE de la faille : l'exhaussement a été plus grand que la dépression. Dans le mémoire publié par M. Sugiyama,[19] ingénieur de Rikuti-sokuryôbu, on trouve une carte représentant la distribution du déplacement vertical du terrain surtout dans le domaine catastrophé. Malheureusement, il n'a pas étendu ses observations jusqu'à Midutori à cause du manque de données. Rikuti-sokuryôbu[20] aussi a exécuté en 1913 la triangulation dans le domaine catastrophé et a publié le déplacement horizontal du terrain ; mais le choix des points supposés fixes n'est pas convenable et les résultats obtenus n'ont pas grande valeur pour faire progresser nos discussions.

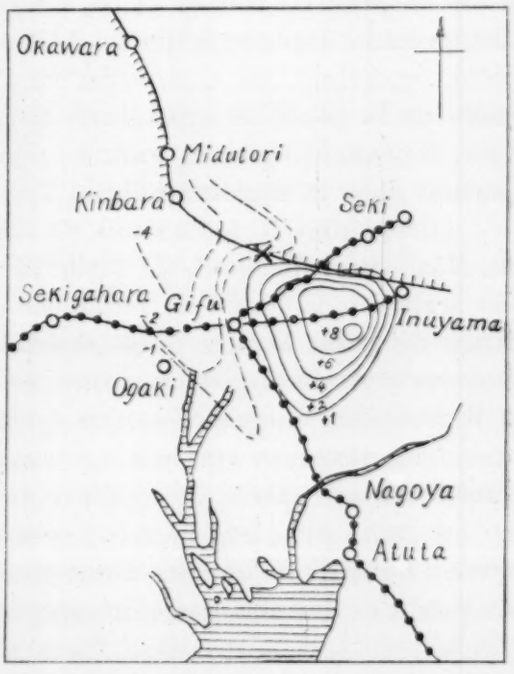

Fig. 8. Déformation de la croûte terrestre causée par le séisme de Nôbi (le 28 oct. 1891) (d'après la carte de M. Sugiyama)

D'après la carte de Sugiyama ainsi que d'après les descriptions faites

19) M. Sugiyama, *C. R. Séances, 14e Conf. gén. Ass. Géodésique Int.*, I (Berlin, 1894), 138.

20) Rikuti-Sokuryôbu, *Annual Report of Military Land Survey* (1882-1921).

par Omori, nous pouvons fixer l'épicentre sur la faille entre Kinbara et Takatomi. La déformation de la croûte est ainsi expliquée avec une source quadruple au foyer, dont la direction de l'axe est presque horizontale. Ainsi nous trouvons le côté dépressioné tantôt à EN, tantôt à OS de la faille. On verra la production du même type de faille à l'occasion du grand tremblement de terre d'Idu en 1930.

En tout cas, les changements topographiques produits sont expliqués entièrement avec une source quadruple. Cette fois-ci l'épicentre se place à la région dépressionée et la faille apparaît à la place où l'éffort a été son maximum. Au cas du tremblement de terre de Tango, l'épicentre a été au fond de la mer et on n'a observé que la moitié de l'aspect des changements topographiques. A l'occasion du tremblement de terre de Nôbi, cependant, on a pu observer l'aspect entier de la déformation à cause de la possition épicentrale qui était sur le terrain. Nous regrettons, cependant, que les mesures géodésiques n'aient pas été appliquées partout dans la région troublée.

Considérons le mécanisme de l'apparition de la faille dans la vallée de Néo. Probablement, au foyer la pression hydrostatique du magma est arrivée à la limite de résistance de la pression extérieure. En profitant du point le plus faible endroit de la croûte, c'est-à-dire la faille, une certaine portion de la croûte se sont déplacées pour livrer passage à l'écoulement magmatique. Jusqu'aujourd'hui on a supposé qu'il y a une force poussant agir sur un certain domaine de la croûte afin que provoquer la rupture de matière.

A notre avis, cependant, il y a simplement la pression hydrostatique au foyer d'une certaine dimension. Cette sorte de pression est capable de produire des changements topographiques soit dans la direction verticale, soit dans la direction horizontale.

f) *Eruption volcanique de Sakura-zima en 1914.*

Le volcan de Sakura-zima a fait l'éruption en 1914. Les secousses sismiques produites ont apporté des dommages aux maisons en bois situées dans la ville de Kagosima, à 10 km de distance du cratère du volcan. A cette époque-là, l'organisation de l'observation sismique n'était pas comparable à celle d'aujourd'hui, et il est difficil d'observer la distribution des mouvements initiaux des secousses. On a pu constater cependant, à Kagosima que l'onde poussante a été tracée par le séisme principal et qu'une de deux sortes d'ondes a été tracée par chaque réplique.

La triangulation a été exécutée dans le golfe de Kagosima[21] ainsi

21) F. Omori, *Bull. Imp. Earthq. Inv. Com.*, 8 (1920), 322.

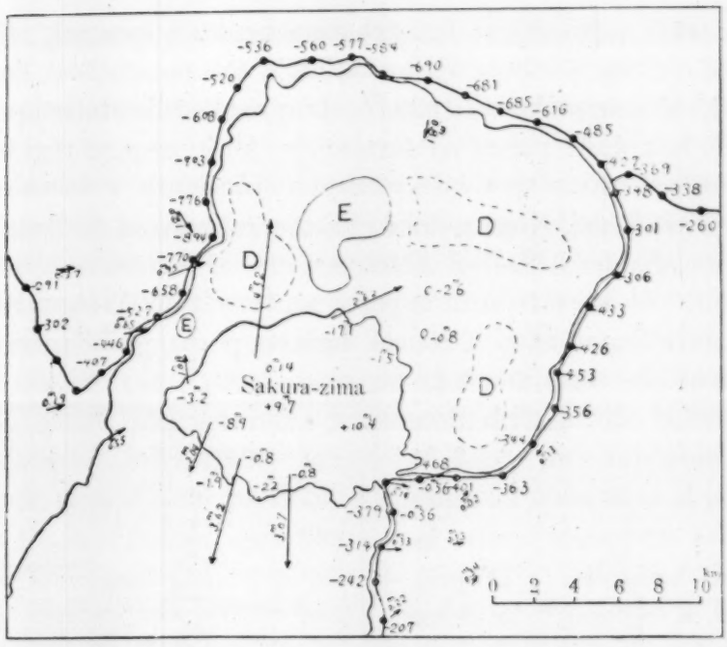

Fig. 9. Déformation de la croûte terrestre causée par l'éruption de Sakura-zima de 1914 (d'après F. Omori.)

que le nivellement de précision autour du golfe. D'après ces mesures, on peut constater qu'au sommet du volcan, plusieurs mètres d'exhaussement, et au pied une dépression de même ordre. Quant au déplacement horizontal, les points dans l'île se sont déplacés vers la direction opposée au cratère. Sur la plage du golfe, cependant, le terrain a été dépressionée de plusieurs centaines de centimètres et déplacé horizontalement vers le volcan. Le nivellement de précision étendu à Miyazaki nous prouve qu'il y a une région dépressionée même à 50 km de distance.

La déformation de la croûte résultant de l'éruption volcanique est expliquée par le mouvement du magma. Nous pouvons poser une source quadruple juste au desous du volcan : naturellement, l'axe du cône se dirige dans le sens vertical. Il y a au sommet un exhaussement avec un déplacement horizontal vers l'extérieur tandis qu'il y a au pied une dépression avec un déplacement horizontal vers le cratère. Ce type de déformation de la croûte nous permet de concevoir le mécanisme du grand tremblement de terre, quoiqu'il n'y ait pas en d'échappement magmatique.

Certainement une éruption volcanique est accompagnée toujours d'un mouvement magmatique dont la direction est définie dans le sens vertical. Donc, les aspects généraux d'un volcan réalisent un type, ce qu'on

appelle la forme volcanique : un exhaussement au sommet, une dépression au pied. Cette sorte de déformation a été constatée à l'occasion de l'éruption de Komagataké en 1929.[22] D'après l'étude statistique du Prof. T. Terada,[23] le volcan prend sa forme avec toujours une région dépressionée à son pied. Nous pouvons compter plusieurs volcans ayant des lacs à leur pied : Huzi, Komagataké et Sakurazima sont de bons exemples.

g) *Foule de séismes à Itô en 1930.*

Une foule de séismes sont apparus aux environs d'Itô en 1930. Cette apparition de séismes nous a fourni beaucoup de problèmes sismométriques ainsi qu'une certaine image sur le modèle de distribution du foyer sismique en foule.[24] Parmis eux, le séisme du 22 mars a produit les secousses ayant la plus grand intensité. D'après l'étude de S. Kunitomi,[25] les deux sortes d'ondes des mouvements initiaux se distribuent dans les quadrants. Les résultats obtenus[26] par les sismographes installés temporairement autour de la région épicentrale nous montrent aussi que les deux sortes d'ondes ont même distribution.

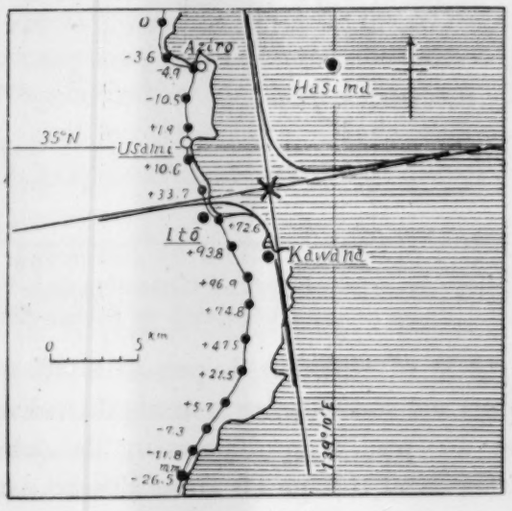

Fig. 10. Déformation de la croûte terrestre causée par la foule de séismes apparus aux environs d'Itô en 1930.

Pour constater la déformation de la croûte le nivellement de précision a été exécuté au long de la côte orientale d'Idu.[27] Suivant les résultats obtenus, nous sommes certains de l'exhaussement du terrain auprès de Kawana et la dépression auprès d'Aziro. Cette déformation du terrain est expliquée avec la distribution régionale des mouvements initiaux des secousses. Ce fait est suffisant pour permettre de supposer une source quadruple au foyer.

h) *Le tremblement de terre d'Idu en 1930.*

---

22) C. TUBOI, *Bull. Earthq. Res. Inst.*, 8 (1930), 298.
23) T. TERADA, *ibid.*, 7 (1929), 207.
24) N. NASU, *ibid.*, 2 (1931), 22.
25) S. KUNITOMI, "*Iwanami-Kôza*", sur physique et chimie, section physique 8.
26) d'après les enregistrements obtenus par N. Nasu.
27) *Bull. Earthq. Res. Inst.*, 8 (1930), 375.

Ce tremblement de terre s'est produit le 26 Nov. 1930. Son l'épicentre s'est trouvé auprès d'Ukihasi. Suivant l'étude de K. Honda[28] les deux sortes d'ondes aux mouvements initiaux des secousses ont été distribué dans les quadrants. En considérant le fait qu'une des ses lignes nodales coïncide avec la faille produite, il a conclu, que plupart des ondes sismiques ont été rayonnées par le mouvement glissant de deux portions de la croûte terrestre à la surface de la faille.[29]

Certainement, d'une part nous pouvons observer à la surface terrestre une dislocation distincte en reliant les trois bassions (Tasiro, Tanna et Ukihasi): d'autre part, nous avons pu observer cette dislocation même dans le tunnel de Tanna creusé justement au desous du bassin de Tanna. La composante horizontale du délplacement relatif a été mesurée 2, 40 m. dans le tunnel, tandis qu'elle était comparativement plus petite à la surface terrestre. La surface glissante de la faille à permis constater qu'elle était constituée par le plan poli de la roche recouvert par de l'eau. Autrement dit, le mouvement relatif des deux portions de la croûte a été produit en profitant de la position où le glissement était le plus facilement réalisé.

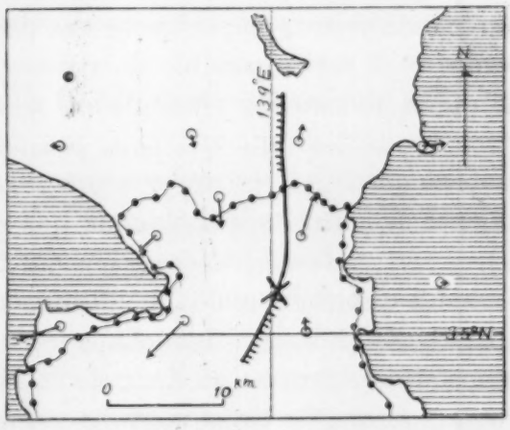

Fig. 11. Déformation de la croûte terrestre causée par le séisme d'Idu (le 26 nov. 1930).

Donc, il est bien difficile de croire que toutes les énergies des ondes élastiques ont été rayonnées en suivant le glissement sur l'ancienne faille. Nous considérons en tout cas que la plus grande partie de l'énergie sismique a été royonnée d'un foyer situé dans le sein de la croûte, probablement plus profondement que la faille.

Quand nous examinons le mouvement relatif du terrain au long de cette faille, nous trouvons que dans sa portion Nord, le côté E de la faille se trouve plus haut que le côté 0, tandis que dans sa portion Sud, la hauteur relative devient contraire. A l'égard du déplacement holizontale, la portion E de la faille a glissé vers le Nord relativement à la portion 0. Cette sorte d'apparition d'une faille a été observée à l'occasion du tremblement de terre de Nôbi en 1891.

28) K. Honda, *Kïsyô-syûsi*, 9 (1931), 293.

29) K. Honda, . *loc. cit.*

La triangulation de second ordre a été exécuté dans cette région[30] et ses résultats nous montrent le même sens de déplacement horizontaux au long de la faille. Le nivellement de précision a été exécuté d'une part au long de la route autour de la côte d'Idu, d'autre part au long de la route d'Atami à Misima. Suivant ces mesures, nous constatons un exhaussement du terrain auprès d'Atami et une dépression traversée par la faille.

D'après ces faits, nous pouvons aussi supposer une source quadruple au foyer comme nous l'avons fait pour les autres tremblements de terre. Comme l'épicentre du séisme d'Idu a été sur le terrain, nous avons eu la chance d'observer la faille tournante avec le glissement horizontal : identique à celle du tremblement de terre du Nôbi.

Maintenant, nous n'avons que des résultats de triangulation de second ordre et il est impossible de pousser notre discussion dans les détails. Si nous avions les résultats de triangulation de troisième ordre, nous trouverons des faits qui nous permettraient de constater l'existence d'une source quadruple au foyer comme nous l'avons fait pour les tremblements de terre de Kantô ainsi que pour celui de Tango.

i) *Le tremblement de terre de Titibu en 1931.*

La distribution des mouvements initiaux des secousses a été étudiée par S. Kunitomi.[31] Les changements de la hauteur des repères ont été constatés seulement au long de la route allant de Tôkyô à Takasaki et puis à Suwa.[32] Nous pouvons relever un certain exhaussement et une certaine dépression du terrain corespandant à la distribution des mouvements initiaux des secousses.

3. Conclusion.

Nous avons constaté que la distribution régionale des mouvements initiaux des secousses sismiques explique très bien la déformation de la croûte produite surtout dans la région épicentrale. Jusqu'aujourd'hui la plupart de discussions sur la déformation de la croûte ont été faites en prêtant attention sur le déplacement horizontal du terrain. Naturellement, on considère que les déplacements horizontaux du terrain jeuent un rôle plus important que les déplacements verticaux dans le phénomène sismique.

30) *Bull. Earthq. Res. Inst.*, 10 (1932), 261.
31) S. Kunitomi, *Kensin-Zihô*, 5 (1932), 223.
32) T. Terada et N. Miyabe, *Proc. Imp. Acad.*, 8 (1932), 413.

Il nous semble qu'on a cherché à résoudre ce problème en supposant seulement une force horizontale existant *à priori* dans la croûte terrestre. Naturellement, il est nécessaire de supposer une force pour expliquer le mouvement d'un objet. Mais, il ne faut pas limiter la force à la direction horizontale. Pourquoi, se borne-t-on à noter la force horizontale? Parce qu'il y a une idée pré-existante en sa faveur. On considère cette force comme suffisante pour donner le glissement horizontale à la faille, quoique l'origine de la force soit inconnue : mais il y a plusieurs moyens pour réaliser une telle déformation. Nous savons qu'il y a une force qui provoque le plissement des couches dans la croûte et qui détermine les chaînes de montagnes à la surface de la terre. Il n'est pas certain, cependant, que ce mouvement de la croûte ait été réalisé par une force d'origine purement horizontale : nous disons qu'il sera mieux expliqué l'influence de l'action plutonique.

Quand on limite son attention à la déformation locale de la croûte, telle qu'on la constate à l'occasion des tremblements de terre, l'action d'une force de grande échelle ne donnera pas beaucoup d'influence directes. Nous considérons d'ailleurs l'action plutonique plutôt dans le domaine local sur la zone volcanique du monde. Le magma produit une grand pression au cours de son refroidissement.[33] L'action ultime de pression sera suffisante pour produire des ondes sismiques ainsi qu'une déformation brusque à la surface de la croûte. Nous savons que l'écoulement du magma dans la croûte arrive seuvent assez violemment pour qu'on le compare avec l'explosion volcanique.[34]

Nous proposons donc une source quadruple au foyer pour expliquer le mécanisme de la production des ondes sismiques ainsi que la déformation de la croûte. Naturellement, la croûte conserve d'une part une propriété élastique permettant passage des ondes sismiques, d'autre part une propriété plastique adomettant les déformations permanentes. Il nous semble, de plus, que la portion superficielle de la croûte est assez fragile sous l'action brusque des forces : nous pouvons constater un ensemble de blocs dans la déformation produite par le grand tremblement de terre.

---

33) G. W. Morey, *Journ. Wash. Acad. Sci.*, **12** (1922), 219.
34) J. Barrell, Prof. Paper, **57** (1907), 157.

14. 地殻變動と震源における地震波發生

地震研究所 石本巳四雄

1) 著者は昨年震源における地震波發生機巧に關して一論文を提出したが，其れは地震初動分布の狀況から察して四重源の存在を想定したものである．波動の傳播を對象として，之れを力學的に考へるならば，震源を一點と考へて差支へないであらうが，波動勢力を問題として物理的に之れを考へる場合においては，震源に相當大なる容積の存在を必要とし，波動成生と同時に物質移動を考へる事が至當である．四重源の假說からすれば，物質移動は正に岩漿移動として考へられ，地震に伴ふ地形變動は以上の機巧によつて起され得る筈である．從つて地形變動と初動方向分布との間には密接の關係が存在しなくてはならない．

2) 1923年の關東地震における初動方向分布は極が殆ど上方に向つた四重源を地殻内に想像する事によつて說明されると同時に，地形變動も震源における同一力が生ぜしめたと考へる事が出來る．卽ち初動分布より推定し得る節線は楕圓形であり，此の楕圓内は隆起すると同時に震央より遠ざかる水平方向に移動し，楕圓外は陷沒すると同時に震央に向つて水平移動が行はれて居る．

但馬地震においても同樣四重源を假定して初動方向分布と地形變動とが說明出來る．

丹後地震においては以上の二地震と異り，肉眼により斷層の出現が確められたが，此の場合の初動方向分布は四重源の極が水平方向にある事を示し，剪斷力の最も大なる所は斷層の出現場所と一致する．水平移動が震央に向ふ區域は沈降を，又水平移動が震央から遠ざかる所は隆起を示して居る．之れは四重源存在を確めるものとなる．

1891年濃尾地震に伴つて生じた地變の中斷層として認められるものは蝶番型であつた事から，此れは極方向が水平である四重源を想像してよく說明が出來る．なほ震央が陸上にあつた爲め震央においては陷沒を呈した事も判斷し得る．

1914年櫻島噴火に伴つた地形變動は全く極の上方に向つた四重源を火山下に想像する事によつて說明出來る．此の場合岩漿運動が上方に向つたと云ふ事實と結びつけて考へるならば地震原因が岩漿流動であると云ふ事を充分推定し得るであらう．

1930年伊東附近に發生した小地震においても水準測量によつて得られた地形變動と一地震の初動方向分との關係は全く同樣である．

1930年伊豆地震に伴つて生じた斷層も蝶番型であつた事，又其の水平移動の卓越した區域に震央が決定される事から見て同じく地變は岩漿壓力增進によつて地殻の最も弱い個所において相互移動が行はれた結果生じたと見られる．

3) 卽ち大地震によつて生ぜられた地形變動は全く初動方向分布と密接の關係を持し，四重源の存在を以て說明出來るのである．從來の水平力を地殻内に假定したものに對し，著者は震源に岩漿の靜水壓力を假定して此れが外力を超過する場合，最も移動せしめ易き地殻の一部分を移動して地形變動を出現せしめるが一方に此等運動に伴ふ衝動は地震波を放射せしめるものと考へる．

15. *Notes on the Mechanical Strength of the Earth's Crust.*

By Chûji TSUBOI,

Earthquake Research Institute.

(Read April 2, 1933, before the Physico-Mathematical Society of Japan.—
Received March 20, 1933.)

In my earlier papers[1], the horizontal strain components, namely dilatation, rotation, and shear of the deformation caused on the earth's surface in the Tango and Idu earthquake districts were calculated by using for data the horizontal displacements of a number of triangulation points in the respective districts. The deformations of the earth's surface in these districts were brought about in connection respectively with the Tango earthquake of 1927 and the Idu earthquake of 1930, both of which were destructive and associated with the appearance of remarkable earthquake faults. It was found by these calculations that the strain components on the earth's surface are generally of the order of 10^{-5} in magnitude, and that it is only in zones of earthquake faults that they exceed 10×10^{-5}. It might be of some interest to give a tentative explanation of this fact as it seems to have an important bearing on the mechanical behavior of the material of which the earth's crust is composed.

The calculations of these strain components were based upon the distribution of contour lines of equal eastward and nothward displacements, which were drawn as if they were continuous throughout the districts to be studied. This of course is far from reality, since there were actually discontinuities across the earthquake faults. The strains calculated in this way are therefore only what *would be* produced on the surface of a hypothetical elastic material if a number of points on it were subjected to horizontal displacements equalling those of the corresponding points on the actual surface of the earth's crust. Strictly speaking, therefore, the statement just made means that the zones in which the strain is greater than 10×10^{-5} on the hypothetical elastic medium correspond in position to the zones of the earthquake fault on the earth's actual surface. It

1) C. TSUBOI, *Bull. Earthq. Res. Inst.*, 8 (1930), 153; 10 (1932), 411; 10 (1932), 435; *Jap. Journ. Astr. Geophys.*, 10 (1933), 93.

is thus obvious that a strain of magnitude 10×10^{-5} is the utmost that the actual material of the earth's crust could withstand without resulting in fissures or discontinuities—in other words, its ultimate strain.

As to the ultimate strain of natural rocks, so far as I know, there is scarecely any data extant based on direct measurements. We can however estimate their orders of magnitude by dividing the ultimate strength of the rocks by their elastic moduli.

In one of the professional papers published by the Department of Finance[2] are tabulated the ultimate strengths of various rocks from a number of localities of Japan. The values given therein differ widely even for rocks listed under the same nomenclature. To give only one instance, the ultimate shearing strength of "granite" ranges from 10×10^{7} to 20×10^{7} c.g.s. for 40 specimens, the mean being $13{\cdot}9\times10^{7}$.

H. Nagaoka[3] and S. Kusakabe[4] have measured the modulus of rigidity of various kinds of rocks. In their results too there is considerable diversity of values, ranging in the case of "granite" for instance, from $4{\cdot}43\times10^{11}$ to $18{\cdot}43\times10^{11}$ c.g.s. The mean here is $9{\cdot}04\times10^{11}$.

As both the ultimate shearing strength and the modulus of rigidity of "granite" were obtained for different specimens from different localities, to obtain its ultimate strain by dividing the former by the latter is, needless to say, illogical. Yet in view of the order of magnitude of the strain concerned, the objection may tentatively be overruled. We then have,

$$\text{Ultimate shearing strain of "granite"} = \frac{\text{ultimate shearing strength}}{\text{modulus of rigidity}} = \frac{13{\cdot}9\times10^{7}}{9{\cdot}04\times10^{11}} = 15{\cdot}4\times10^{-5}.$$

This calculation was made on the assumption that Hooke's law is valid up to the breaking point of the rock specimen, which is far from reality, as both H. Nagaoka and S. Kusakabe have emphasised. But here again, in view of the order of magnitude of the ultimte strain concerned, the assumption is not likely to seriously affect our results.

Now if we may be allowed to assume 10×10^{-5}—20×10^{-5} c.g.s. to be the ultimate shearing strain of rocks, this is in close agreement with

2) I am indebted to Prof. S. Fujiwhara for his courtesy in allowing my perusal of the report.

3) H. NAGAOKA, *Pub. Imp. Earthq. Inv. Comm.*, 4 (1900), 47.

4) S. KUSAKABE, *ibid.*, 14 (1903), 1.

the value obtained by the analyses of the deformation of the earth's crust.

In order to obtain further information in this matter, it will be necessary to make direct measurements of the ultimate strain of different kinds of rocks. According to the preliminary experiments that I have made with a few specimens of "basalt," the ultimate strain found direct showed a mean of 8×10^{-5}.

Summarising the foregoing, the value of the earth strain 10×10^{-5} found in zones of earthquake faults may be interpreted as representing the ultimate strain of rocks composing the earth's crust in these zones. A somewhat similar discussion has been published by T. Terada[5] in connection with the tilting deformation of the earth's crust. The present note is merely an extension of his arguments.

---

15. 地殻の強さに就いて

地震研究所　坪井忠二

曩に丹後地方及び伊豆地方に於ける三角點の水平移動から地表に於ける變形の大きさを計算した際に，その大きさは大體 10^{-5} の程度のものであるが，所謂斷層の出來た近所では之が 10×10^{-5} 以上である事を注意しておいた．卽ち之は地殻を構成して居る物質の變形の極限であると考へられる．

實驗室内で岩石の試片に就いて直接之を測つたものが見當らないので，假りに岩石の强度をその彈性率で割つて求めて見ると，花崗岩の歪力 (shear) に對する極限の變形として $15{\cdot}4\times10^{-5}$ と云ふ數字が得られた．又若干の玄武岩の試片に就いて直接測つて見ると 8×10^{-5} と云ふ値が得られた．

卽 10×10^{-5} を以て岩石の變形の極限として差支へないものの樣である．勿論以上の如き計算を用ひるとしても，岩石の强度と彈性率とは同一の試片で求められて居るのではないし，又フックの法則も成立しない所の問題であるから頗る大膽に見當をつけたに過ぎないが，オーダーに關する限り大した誤はないかと思ふ．

---

5) T. Terada, *Proc. Imp. Acad.*, 8 (1932), 288.

16. The Crust Deformations in the District between Okitu and Kusimoto, along the Pacific Coast of the Main Island of Japan.

By Naomi MIYABE,

Earthquake Research Institute.

(Read Jan. 17, 1933.—Received March 20, 1933.)

Introduction.

The recent revision of precise levelling along the route from Okitu to Kusimoto revealed a considerable crust deformations. Thus, as the result[1] of this recent revision the vertical displacements of the bench-marks on the said route along the Pacific coast were measured which are regarded to have occurred since the previous survey. No destructive earthquake was experienced during this time interval in the most part of the district in question. The dates of the previous levelling surveys for the different sections of this route are not the same. They are given in Table I.

Table I. Dates of earlier surveys in different sections of the levelling route.

Section	Earlier Survey
From Okitu to Okazaki.	June—October, 1900.
〃 Okazaki to Nagoya.*	January—May, 1895.
〃 Nagoya to Issinden.**	February—May, 1895.
〃 Issinden to Sana.	April—August, 1889.
〃 Sana to Owase.	November, 1895—March, 1896.
〃 Owase to Kusimoto.	May—November, 1899.

* B.M. 174·2 (Junction point) is situated at Atuta, Nagoya.
** Issinden is close to Tu.
As for the levelling route from Atuta to Matuzaka via Issinden, a revision of precise levelling was carried out also in August-November, 1929.

1) A preliminary report of the result of this recent revision of the precise levelling is published in Proceedings of the Imperial Academy. T. Terada, *Proc. Imp. Acad.*, 8 (1932), 411.

The results of the recent revisions, i.e., the vertical displacements of the bench-marks on the route from Okitu to Kusimoto, are discussed in the following pages, with regard to the deformations of the earth's crust in the district thus revealed, in connection with allied geological and geographical evidences.

The earth's crust in the district under consideration had not been much disturbed by a destructive earthquake, as noted above, but for a part of the route near Nagoya, where it was presumably much disturbed by an acute crust movements associated with the Nôbi Earthquake of 1891. Hence, the crust deformations in the most parts of the district examined may be regarded as due mainly to the chronic movements, but for the district near Nagoya, where the after effect of local disturbances due to the destructive earthquake is still evident in the crust deformation due to the later time intervals from which the Nôbi earthquake is excluded. These specific effects of the destructive earthquake of 1891 may be better discussed by using the results of several post-seismic revisions of the precise levellings carried out in the district where the earth's crust is considered to have been disturbed conspicuously by this earthquake. The general mode of the crust deformations in the entire district under consideration, however, may not be much affected by these local disturbances.

The Results of the Recent Revision of the Precise Levelling.

The vertical displacements of the bench-marks on the levelling route from Okitu to Kusimoto obtained as the result of 1931 revision are shown in Fig. 1,[2] for which the horizontal scale was contracted considerably in order that the general mode of the crust deformation may easily be seen[3]. The map of the district under consideration with the location of the levelling route is shown in Fig. 2.

The vertical displacements, shown in Fig. 1, may be regarded as indicating those which had occurred during the time interval of some 30 years or more, though the previous surveys of precise levellings have not been carried out at the same time in different sections of the route.

---

2) The vertical displacements of the bench-marks are reproduced from the Report in *Bull. Earthq. Res. Inst.*, 10 (1932), 490.

3) As for the general mode of the crust deformation in the district, discussions are given by Mr. C. Tsuboi. *Jap. Journ. Astr. Geophys.*, 10 (1933), 93.

According to difference in the modes of crust deformations due to these 30 years, the district along the levelling route under consideration may conveniently be divided into four different parts. The first part is

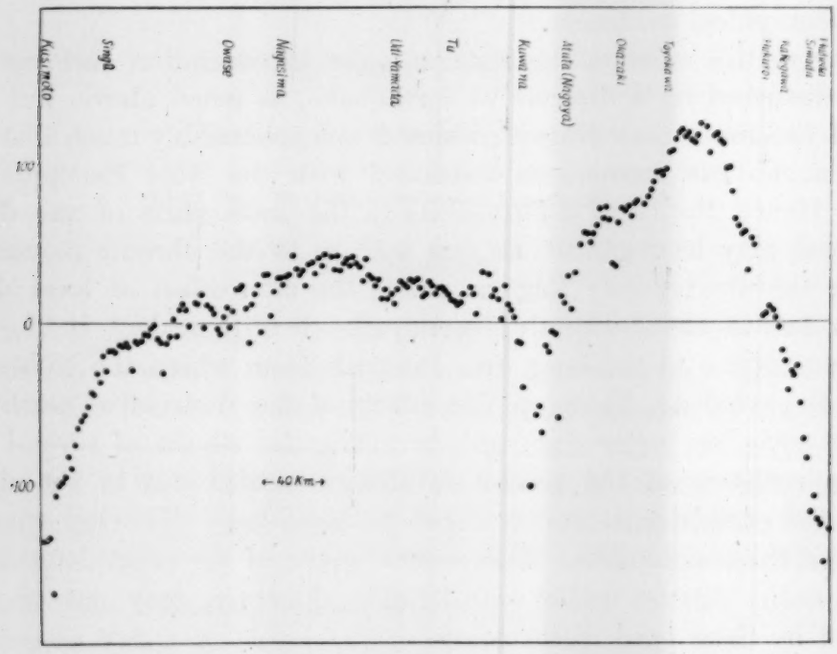

Fig. 1. The vertical displacements of the bench-marks on the route from Hudieda, near Siduoka, to Kusimoto.

the district corresponding to the section of the levelling route from Okitu to Toyokawa, in which the deformation of the earth's crust seems, at a glance on Fig. 1, to consist of a simple tilting towards the east. The horizontal dimensions of this part of the district is some 100 km. and the difference in vertical displacements between the bench-marks of the both ends amounts to about 27 cm. Hence, the tilting of the earth's crust in this part, along the levelling route, is $2{\cdot}7 \times 10^{-6}$, or $0{\cdot}5''$.

The second part is the district around Ise-wan (the Bay of Ise), in which the general mode of crust deformation is downwarping, having the synclinal axis extended from N to S approximately coincident with the axis of the trough of Ise-wan.

The third part is the district from Udiyamada to Singû. The southern part of the levelling route in this district is situated along the coast of Kumano-nada. As to the general mode of the crust deformation in this district, we notice, as the curve of Fig. 1 shows, a south-

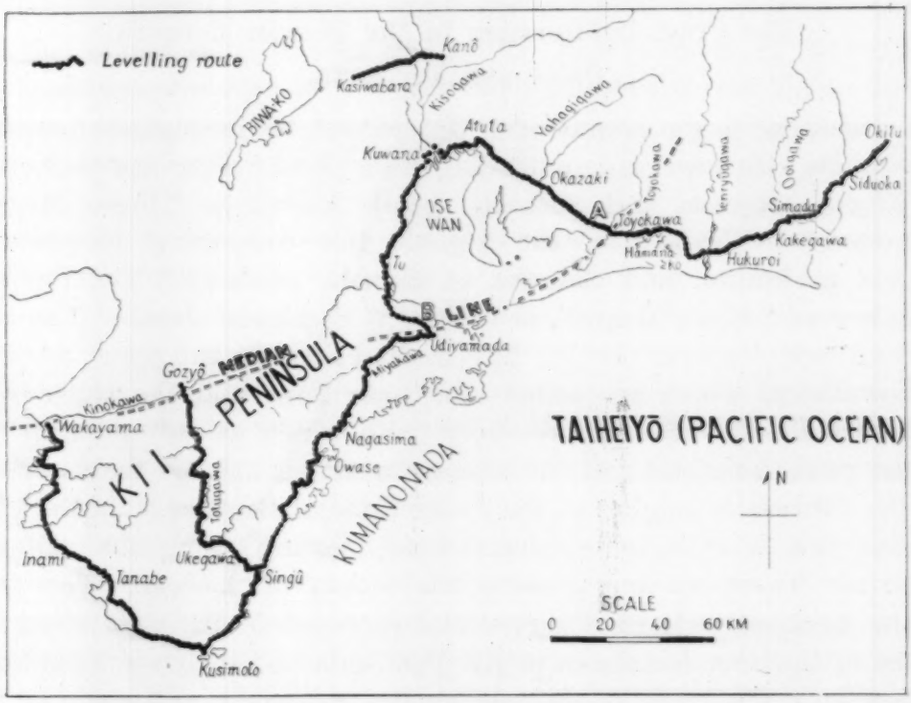

Fig. 2. The location of the levelling Routes.

or southwest-ward tilting with the amount of some $0{\cdot}4\times10^{-6}$ in radians accompanied by fluctuations.

In the district between Singû and Kusimoto, i.e., the fourth part, the general trend of the levelling route may be regarded as a straight continuation of the third part, whereas the amount of tilting of the earth's crust is discontinuously changed in comparison with the third part, i.e., tilting in this district, along the trend of the levelling route, amounts to $2{\cdot}5\times10^{-6}$ in radians, or six times the tilting in the district of the third part, both of the amounts of tiltings being due to the time interval of these 30 years.

The details of the present investigation on the crust deformations are described below under three separate chapters, i.e., the districts between Okitu and Toyokawa, the first part, between Toyokawa and Udiyamada via Atuta and Kuwana, the second part, and between Udiyamada and Kusimoto, the third and fourth part.

The Crust Deformation in the District Between Okitu and Toyokawa.

According to the results of investigations by geologists, there is a remarkable structural zone extending from N to S over the prefectures of Niigata, Nagano and Siduoka usually known as "Fossa Magna." The district to the west of the tectonic line connecting Itoigawa, in Niigata prefecture, and Siduoka, in Siduoka prefecture, i.e., the west boundary of "Fossa Magna", is known as Southwest Japan. The land of Southwest Japan is divided by a median line into two zones, northern and southern, which are called the Inner Zone and the Outer Zone respectively. The crust deformations, with which we are going to deal in the present chapter and the chapter next but one, are those occurred in the districts belonging to the Outer Zone of Southwest Japan. The median line is extended southwest-ward, passing along the valley of the river Toyokawa and crossing the mouth of Ise-wan. The trend of the median line is then curved and extended to the west along the valley of the river Kinokawa in Kii Peninsula and the river Yosinogawa in Sikoku. The trend of the median line intersects, as shown in Fig. 2, the levelling route under consideration at Point A, very near Toyokawa, to the north of Toyohasi, and at Point B, near Udiyamada. At these points, the signs of the general gradients of the vertical displacements are changed. The district to the east of Point A corresponds to Part I, for which the general mode of the vertical crust deformation is an eastward tilting along the route with an amount of some 0.5″, as already referred to in the preceding chapter.

The first precise levelling was carried out in 1885 along the route from Okitu to Okazaki, and the survey was revised in 1900. The vertical displacements of the bench-marks on this route, which are shown in Fig. 1, are those measured recently due to the time interval 1900–1931. The vertical displacements due to the time interval 1885–1900 are shown in Fig. 3. The data were kindly placed at our disposal by Messrs. K. Mutô and Y. Kawabata of the Military Land Survey[4], to whom the present writer's cordial thanks are due.

As may be seen in Fig. 3, the vertical crust deformation during 1885–1900, in the district between Okitu and Simada, the district to

4) The data are published in this volume of the Bulletin. K. MUTÔ and Y. KAWABATA, *Bull. Earthq. Res. Inst.*, 11 (1933), 315.

the east of the river Ooigawa is approximately in positive correlation with that of the same district due to the time interval of 1900–1931. The negative correlation of the vertical displacements due to the different time intervals in the district between the river Ooigawa and Toyokawa is shown by the diagram of Fig. 4.

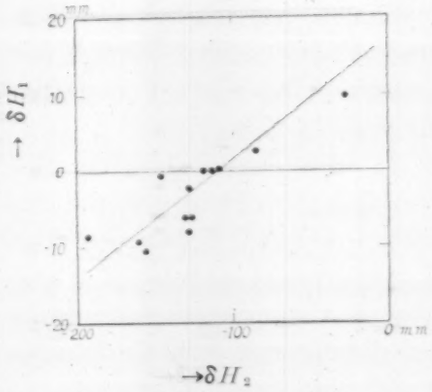

Fig. 3. The Relation between δH_1 and δH_2 of the bench-marks on the route from Siduoka to Simada.

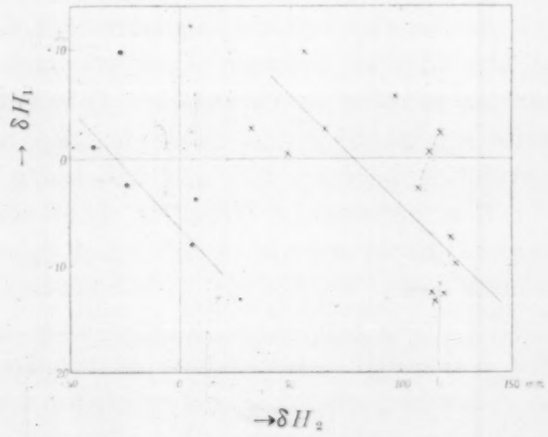

Fig. 4. The relation between δH_1 and δH_2, of the bench-marks on the rout from Kanaya to Hukuroi (•) and these from Hukuroi to Toyokawa (×).

The relation between δH_1, the vertical displacements during 1885–1900, and δH_2, those during 1900–1931, in the district between Siduoka and Simada, may be expressed approximately by

$$\delta H_2^{(\text{mm.})} = -110{\cdot}0^{(\text{mm.})} + (90/14)\delta H_1^{(\text{mm.})}.$$

It may be remarked that the coefficient to δH_1 in the above expression $90/14 = 6{\cdot}4$ is much different from $31/16 = 1{\cdot}9$, the ratio of the time intervals to which the vertical displacements, δH_1 and δH_2, are respectively due. The district has not experienced any destructive earthquakes which was accompanied by a conspicuous deformation of the earth's crust, as remarked above. Hence, the fact, that the coefficient in the above expression is much greater than the ratio of the time intervals to which the vertical displacements δH_1, and δH_2, are due, may lead us to a conclusion that the rate of deformation of the earth's crust during 1900-1931 is three times as great as those during 1885–1900, i.e., the rate has been sensibly accelerated in the recent epoch.

In the district adjoining to the west of that mentioned above, i.e., the district between Kanaya and Hukuroi, the correlation between δH_1

and δH_2 seems to be negative, as shown in the diagram of Fig. 4. It may also be noticed, in Fig. 4, that the rates of the vertical displacements due to the different time intervals are, in this district, much different from that which may be expected from the time intervals, besides the difference in senses of the gradients of the vertical displacements.

As for the vertical displacements δH_1 and δH_2 of the bench-marks in the district between Hukuroi and Toyokawa, we cannot notice a definite relation in its details. It may, however, be noticed, though not quite remarkable, that there is also a general tendency of negative correlation between δH_1 and δH_2 along this part of the route.

The apparently irregular fluctuations in the curve showing the vertical displacements of the bench-marks in this district are found, in several cases, significant in connection with the local features of the district from geological, geographical and geophysical points of view. For a detailed investigation of the features of the crust deformations in different parts of this district, the vertical displacements of the bench-marks are reproduced in Fig. 5.

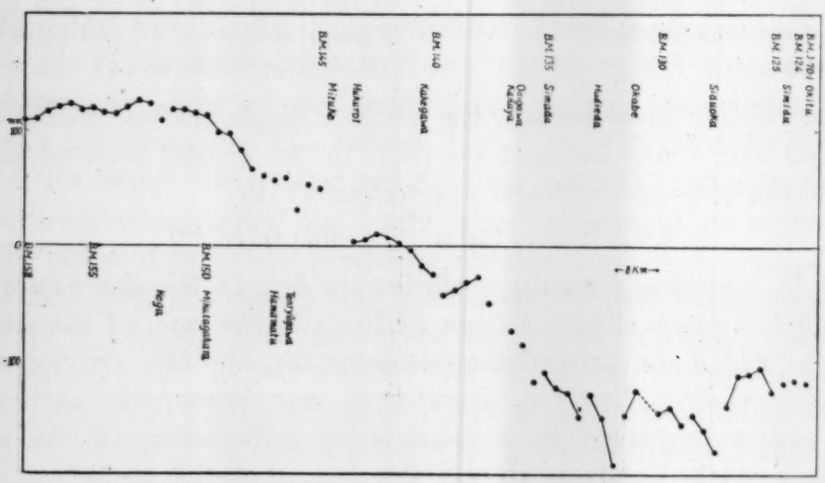

Fig. 5. Vertical displacements of the bench-marks along the route from Okitu to Toyokawa.

The details of the features of the crust deformations are described as follows:

a) There are five bench-marks, B.M.'s 125, 125·1, 126, 126·1 and 127, situated on the route passing through the region to the north of

Kunô-san (Mt. Kuno). The geographical distribution of these bench-marks is shown in Fig. 6, and their heights are shown in Fig. 7. As shown in Fig. 5, the vertical displacements of these bench-marks may

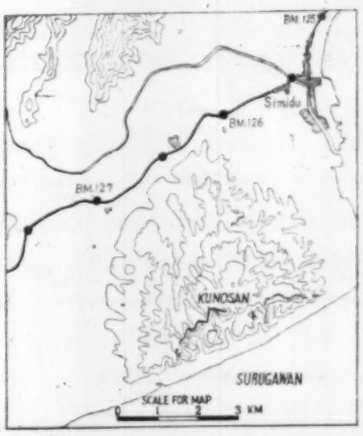

Fig. 6. Bench marks and topographical features in the neighbourhood of Kunôsan.

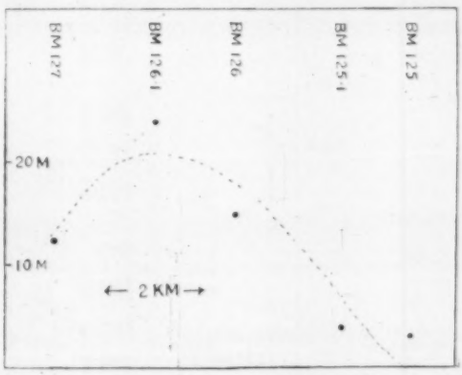

Fig. 7. Profile of the earth's surface along the route situated to the north of Kunôsan.

suggest us that the earth's crust in this region has been subjected to an upwarping crust movement. Moreover, the curve of the vertical displacements of the bench-marks, representing the upwarping crust movement in this region is, in some measure, similar to the curve showing the profile of the region along the route represented by the heights of the same bench-marks. The fact may suggest that the present crust deformation in this region is a continuation of the past one which had produced the present feature in topography of this region.

On the other hand, however, a slightly curved trend of the levelling route in this region may result in an apparent warping deformation, when the earth's crust including Kunô-san was tilted to N or NW. The actual crust deformation may include a resultant effect of these two factors.

b) In the region between Siduoka and Simada, the bench-marks may be classified into several groups with respect to their vertical displacements. These groups of the bench-marks are given in the following Table (Table II), and topographical features in the regions, in which the bench-marks under consideration are distributed, are shown in Fig. 8.

As may be seen in Fig. 8 and Table II, we notice different features in topography corresponding to each group of the bench-marks. B.M.'s 127.1, 128 and 128.1, belonging to Group A_2 are distributed in an alluvial plain in which the city of Siduoka is situated.

Table II. Groups, vertical displacements and heights of the bench-marks situated on the route from Siduoka to Simada.

Group	Locality	B.M.	δH	δH	H.
			mm.	mm.	m.
A_2	Siduoka	127·1	−179·4	−163·1	17·05
		128	−160·8		21·49
		128·1	−149·0		17·77
A_3	Utunoya-tôge (Pass.)	129	−156·3	−143·9	12·74
		129·1	−141·4		26·09
		130	−145·9		45·76
		130·1	——		——
		131	−127·5		35·64
	Okabe	131·1	−148·6		18·08
A_4	Hudieda	132	−191·9	−157·3	11·22
		132·1	−150·4		15·12
		133	−129·7		24·66
A_5		133·1	−149·5	−127·9	22·78
		134	−127·9		30·76
		134·1	−124·0		39·00
		135	−110·0		48·34
	Simada	135·1	−118·8		58·40

N.B. The vertical displacements of the bench-marks are due to the time interval 1900–1931.

B.M.'s 129, 129·1, 130, 130·1, 131 and 131·1, the bench-marks belonging to Group A_3, are distributed on the route crossing a mountain range through the pass of Utunoya-tôge. The crust movement in this region is similar to that of the region to the north of Kunô-san. The earth's crust in this region is upwarped, approximately parallel to the topographical feature along the levelling route, which is represented by the heights of the bench-marks under consideration. The route is, on the other hand, arcuated convex to NW, which may produce an apparent mode of crust deformation as above described, when the earth's crust in this region was as a whole tilted to SE.

Between the mountain range of this region, extending southeast-

ward to the coast of Suruga-wan (the Bay of Suruga), and the river Ooigawa, there is an alluvial plain of considerable extent. The bench-marks belonging to Group A_4 and A_5, B.M.'s 132, 132.1, 133 and 133.1, 134, 134.1, 135, are distributed on the levelling route passing the NW margin of this alluvial plain. Corresponding to the regions occupied by the bench-marks belonging to Groups A_4 and A_5 respectively, we may notice two distinct blocks in the topographical features of the mountain mass close to NW margin of this alluvial plain. The present slope of the earth's surface, represented by the curve giving the heights of the bench-marks is parallel to the curve showing the gradients of the vertical displacements of the bench-marks measured.

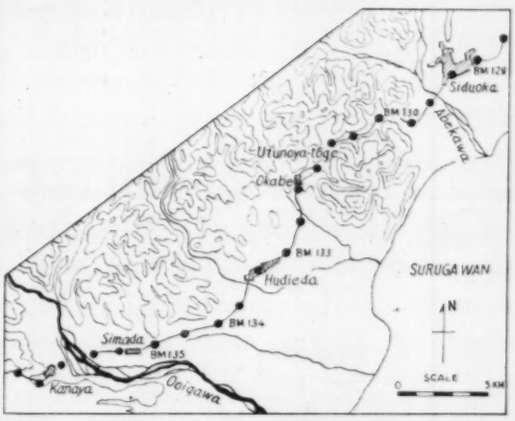

Fig. 8. The topographical features along the route from Siduoka to Simada (to the east of the river Ooigawa).

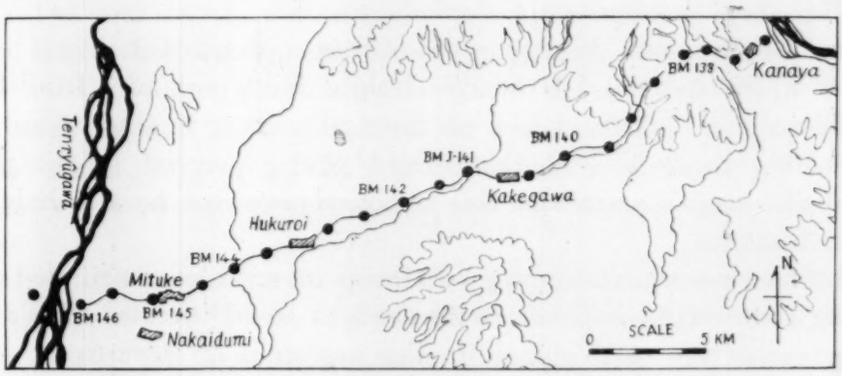

Fig. 9. The topographical features along the route between the river Tenryûgawa and the river Ooigawa.

c) In the region between the river Ooigawa and the river Tenryûgawa, we notice two groups of the bench-marks. The vertical displacements measured and the present heights of these bench-marks are given in Table III. The topographical map of the regions is shown in Fig. 9.

Table III. Groups, vertical displacements and heights of the bench-marks situated on the route from B.M. 138 to B.M. 143·1 (from Kanaya to Hukuroi).

Group	Locality	B.M.	δH	$\overline{\delta H}$	H
			mm.	mm.	m.
	(Kanaya)	138	−27·2		157·51
		138·1	−31·5		72·16
A_6		139	−39·2	−35·3	50·72
		139·1	−43·3		40·66
		140	−24·2		34·29
	Kakegawa	140·1	−16·9		27·07
		141	− 3·4		22·02
		141·1	2·3		19·02
A_7		142	7·2	− 2·0	16·70
		142·1	9·5		12·78
		143	5·4		10·26
	Hukuroi	143·1	4·0		7·94

N.B.: The vertical displacements of the bench-marks are due to the time interval 1900–1931.

The bench-marks belonging to Group A_6 are distributed on the route of which the trend is nearly straight being extended from SW to NE. The mode of deformation of the earth's crust in this region along the levelling route is a southwestward tilting parallel to the present slope of the earth's surface in this region represented by the heights of the bench-marks.

The bench-marks belonging to Group A_7 are also distributed on the levelling route of an approximately straight trend directed E-W. The deformation of the earth's crust in this region is an upwarping, which is not parallel to the profile of the surface of the earth represented by the present heights of the bench-marks, contrary to several other cases already referred to. As the trend of the route is straight, the configuration of the levelling route cannot explain the present mode of distribution of vertical displacements. On the other hand, however, as the results of investigations by geologists[5], it was concluded that the earth's crust in this region was subjected to an upwarping movement in the

5) Z. MAKIYAMA, *Tikyû*, 9 (1928), 23–35, 100–118. (in Japanese).

later period of the Tertiary Formation. This crust movement in the Tertiary period is approximately coincident with the crust deformation in recent epoch, discovered by means of the present geodetic method.

The crust deformation in the neighbourhood of the Ooi-gawa seems to be complicated. The vertical displacements of the bench-marks, i.e., of B.M.'s 135.1, 136.1, 137 and 137.1, appear to show that the earth's crust in this region was displaced as a single block, if the data of the vertical displacement of B.M. 137, which is wanting, were also in accord with the tilting of the earth's crust represented by the vertical displacements of the other bench-marks. The topographical features in this region, however, is not in good accord with the mode of the crust deformation described above. Moreover, in the west part of the region near Kanaya, the phenomena of creeping or sliding of land mass occurred for several times[6], producing cracks in the wall of the railway tunnel of Kanaya. These facts may appear rather unfavourable for regarding the region under consideration as a single crust block.

A similar case is met with in the region in the neighbourhood of the river Tenryûgawa. The conspicuous depression of B.M. 146, situated on the east embankment of the river Tenryûgawa relative to the adjoining bench-marks, the wanting data of the vertical displacements for B.M.'s 144 and 144·1, and complicated topographical features in this region render it difficult to determine a definite mode of the crust deformation. The irregularities in the crust deformations in this region may partly be due to the fact that the bench-marks are situated in the alluvial plain, except for B.M.'s 144.1 and 145, which are situated on a part of the levelling route crossing the mountain range to the east of Mituke.

Lastly, it may be remarked that the general mode of the crust deformation in the district to the east of the Tenryûgawa, i.e., the district between the Tenryûgawa and Siduoka, may be regarded as a simple tilting. The amount and the direction of the tilting of the land may be determined by the amounts of general tilting in two branches of the levelling route and their directions. The two branches are a part of the route from the Tenryûgawa to Hudieda and that from Hudieda to Siduoka. The trends of the routes in these two parts are nearly straight. The amounts of general tiltings may be estimated

6) K. Jimbo, *Sinsai-Yobô-Tyôsakwai Hôkoku* (*Bull. Imp. Earthq. Invest. Comm.*), No. 38.

from the data of δH's for each of the groups of the bench-marks, given in Table II and III. The estimated amounts of general tiltings and the directions of these two parts of the levelling route are shown in Table IV.

Table IV. Directions and amounts of tilting of the earth's crust in two different sections of the route.

Section	Amount	Direction
The Tenryûgawa-Hudieda	$5{\cdot}5\times10^{-6}$	N 68° E
Hudieda-Siduoka	0·0	N 37° E

The amount of the general tilting of the earth's crust in the region, thus determined, is $6{\cdot}5\times10^{-6}$ in the direction of E 37° S.

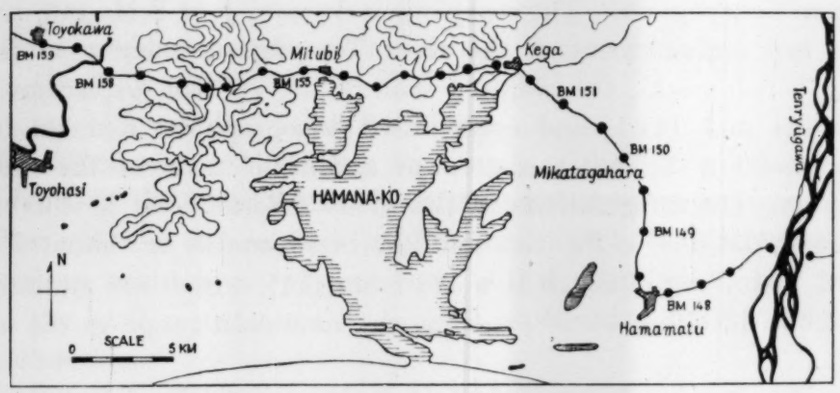

Fig. 10. The topographical features in the neighbourhood of Hamana-ko (Lake).

d) In the region to the west of the Tenryûgawa, the trend of the levelling route is directed N-S in the region from Hamamatu to Kega, crossing the high land of Mikatagahara. The trend of the levelling route is again directed E-W, in the region to the west of Kega, along the northern coast of Hamana-ko (lake). The topographical features in this district are shown in Fig. 10. In this district, the vertical displacements of the bench-marks are approximately proportional to the heights of the bench-marks, as shown in Table V.

Table V. Groups, vertical displacements and heights of the bench-marks situated on the route from Hamamatu to Toyokawa.

Group.	Locality	B. M.	δH	H
			mm	m
	Hamamatu	148	65·8	4·00
		148·1	82·9	30·43
		149	97·5	38·05
A_8		149·1	98·9	43·96
		150	113·0	51·18
		150·1	115·2	52·76
		151	118·0	50·72
		151·1	117·7	12·09
	Kega	152	108·9	7·25
		152·1	122·5	32·79
		153	124·9	78·82
A_9		153·1	119·4	38·85
		154	114·3	6·65
	Mikahi	154·1	115·3	12·37
		155	119·0	13·67
		155·1	117·1	21·64
		156	122·6	131·66
		156·1	120·5	193·58
		157	115·8	61·97
A_{10}		157·1	109·8	36·20
		158	108·5	13·20
		158·1	97·8	6·33
	Toyokawa	159	93·4	12·72

N. B. The vertical displacements of the bench-marks are due to the time interval 1900–1931.

Among these different parts of the route, the earth's crust of the region from Hamamatu to Kega may be regarded to have been tilted south-or southwestward, while, that of the region to the west of Kega has been deformed into a form similar to that which is represented by the present profile of the route. The boundary of these two regions are coincident with a valley extending SW-NE, which was pointed out by

Mr. T. Okayama,[7] as the boundary of Blocks A_2 and B_5, in his investigation on land blocks from topographical or geomorphological point of view.

Between B. M.'s 156 and 156·1, there is a fault traced by Mr. K. Ishii.[8] This may form a boundary between the regions in which the bench-marks belonging to Groups A_9 and A_{10} are distributed respectively. If, however, this fault were disregarded, the regions occupied by the bench-marks belonging to Groups A_9 and A_{10} may be bound up together and regarded as one block. The crust deformation in the this region is then regarded as an upwarping which is similar in form with the profile of the topographical features along the levelling route. If, on the contrary, the geological fault was active and significant as a boundary of the crust blocks, the regions occupied by the bench-marks belonging to Groups A_9 and A_{10} respectively may be separated as different crust blocks and the latter regions may be regarded as tilted westward parallel to the profile of the route.

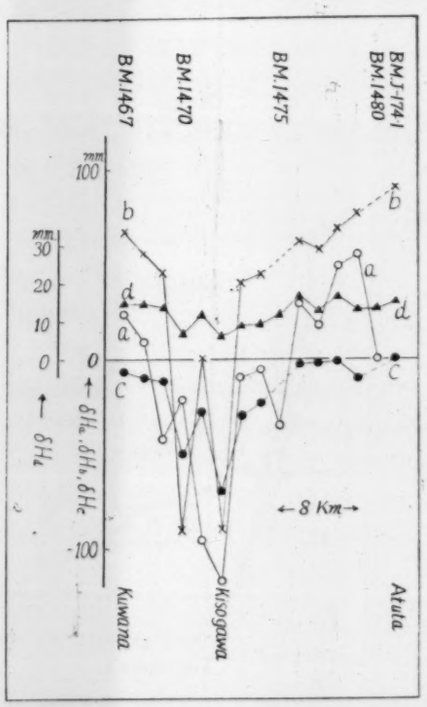

Fig. 11. The vertical displacements of the bench-marks, between Atuta and Kuwana, due to different time intervals.

The crust Deformation in the District around Ise-Wan.

To investigate the general mode of the crust deformation in the district around Ise-wan (the Bay of Ise), it is convenient first to investigate the local crust deformation in the region between Atuta and Kuwana. In this region, the levelling surveys were revised several times after the Nôbi Earthquake of 1891. The vertical displacements of the bench-marks distributed in this region due to the time intervals 1885–1895,[9] 1895–1918, 1918–1929 and 1929–1931 are shown respectively by the curves a, b, c and d in Fig. 11. In these curves, we notice the remarkable depression of the

7) T. OKAYAMA, *Tirigaku-Hyôron*, **6** (1930), 479.

8) K. ISHII, Geological Map, "Toyohashi" Sheet, Scale 1/75000.

9) The data of the vertical displacements due to the earlier epochs are kindly placed by Mr. K. Mutô, of the Military Land Survey.

bench-marks situated near the mouth of the river Kisogawa, except for the curve corresponding to the time interval 1929–1931. It may be remarked that, in each of these series of the data of the vertical displacements, the reference bench-mark is not the same of which the vertical displacement during the corresponding time interval is assumed to be zero. Hence, the absolute amounts of the vertical displacements may want a later correction, but the relative dispalcements which are only significant as due to the local crust deformations are here correctly represented.

In comparing the curves *a*, *b* and *c* in Fig. 11, we notice that the bench-marks situated near the mouth of the river Kisogawa, B. M. 1470 and B. M. 1472, were depressed remarkably during the time interval including the destructive Nôbi earthquake and the post-seismic period of a certain duration. A closer inspection of the curve *d*, we also notice that the form of this curve is similar to that of *a*, *b* or *c*. This may show that the earth's crust in the neighbourhood of B. M.'s 1470 and 1472 has been deformed in the same sense in these some fourty years, including the disturbance due to the acute crust deformation associated with the destructive Nôbi earthquake of 1891.

On the other hand, the vertical displacements of the bench-marks on the route from Kanô to Kasiwabara were also measured for several times since the year 1885. The trend of this levelling route is parallel to that of the route from Atuta to Kuwana and located several tens of kilometers to the north of it, as shown in Fig. 2. In Fig. 12 the vertical displacements of the bench-marks situated between Kanô and Kasiwabara due to the time intervals 1885-1896, 1896-1899, 1899-1917 and 1917-1928, are shown by

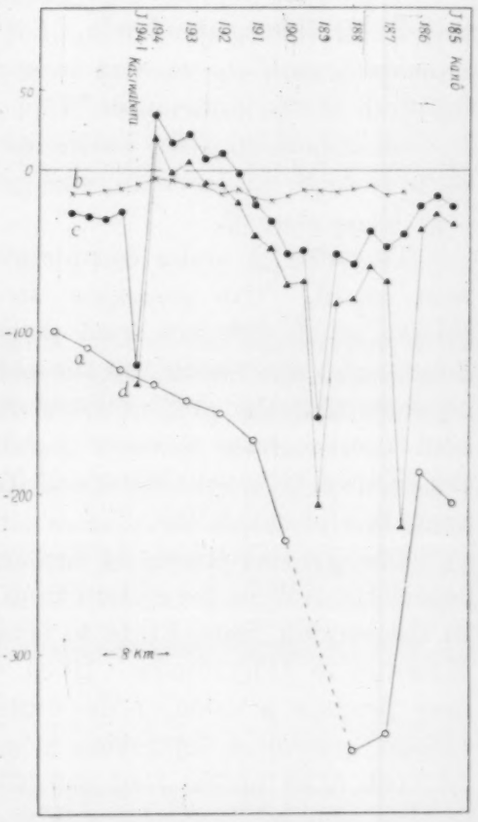

Fig. 12. The vertical displacements of the bench-marks, between Kanô and Kasiwabara, due to different time intervals.

the curves a, b, c, and d.[10] It may be noticed that the curves are similar in form, though the scales for each of the curves are different, except for the curve b, representing the vertical displacements due to the time interval 1896-1899. B. M. 189 shows the maximum depression in each epoch and the region to the west of this bench-mark is tilted to the east whereas to the east of the bench-mark has a tendency of westward tilting throughout the whole period of times. B. M. 1941, situated very near Kasiwabara was remarkably depressed during 1899-1917 and 1917-1928. B. M. 1861 was depressed conspicuously during 1917-1928. B. M. 189, the bench-mark of the maximum depression in all period of times, is situated to the north of the region of depression in the neighbourhood of B. M. 1470 on the southern levelling route.

A zone of depression, including B. M.'s 1470 and 1472 in the south and B. M. 189 in the north, if it really existed may be approximately coincident with the central zone of the area disturbed most severely at the time of the destructive Nôbi earthquake of 1891.

On considering the existence of this zone of depression extending from N to S, in Ise-Wan, the general mode of the crust deformation may be explained.

The district under consideration belongs to the Inner Zone of Southwest Japan. The geological structures in the district may be considered much different from those of the district belonging to the Outer Zone, as it was shown by the gelogists. Hence, it may be allowed to consider that the present crust deformation in this district is more or less different from those of the district belonging to Outer Zone, i. e., the district between Okitu and Toyokawa and the district between Udiyamada and Kûsimoto.

The general trends of the levelling route in this district are i) directed SE-NW in the section from Point A, Toyokawa, to Atuta, ii) E-W in the section from Atuta to Kuwana, and iii) N-S in the section from Kuwana to Udiyamada. Such a configuration of the levelling route may produce a mode of the crust deformation shown in Fig. 1, if there existed a zone of depression as mentioned above, and the earth's crust on both sides of the zone are tilted as a whole towards the central line of this zone of depression. The trend of the levelling route on the east side of the zone of depression, or Ise-wan obliquely intersects the axial

10) The data of the vertical displacements of these bench-marks are reproduced from Prof. Imamura's paper. A. IMAMURA, *Publication of Imp. Earthq. Invest. Comm.*, No. 25 (1930).

line of the zone of depression, while the levelling route on the west side of the bay is approximately parallel to the trend of the axial line of depression. Hence, the amount of tilting of the earth's crust along the former levelling route is considerable, while that of the earth's crust along the latter levelling route is approximately zero, as far as the minor fluctuations are disregarded.

It may also be pointed out as a noteworthy fact that the bench-marks situated very near the river Yahagigawa are depressed remarkably in comparison with the adjoining bench-marks. The depression of B. M. 166, situated close to the Yahagigawa is noticed in the result of the revision of the survey of precise levelling carried out in 1899, which is shown in Fig. 13.

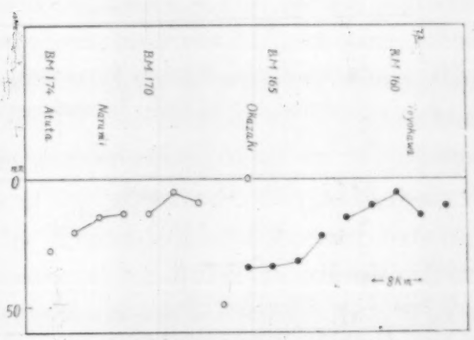

Fig. 13. The vertical displacements of the bench-marks along the route Toyokawa-Okazaki-Atuta, due to the earlier epoch.

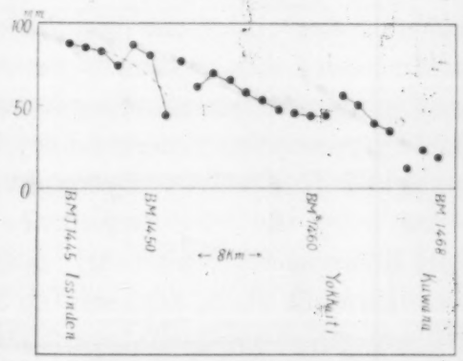

Fig. 14. The vertical displacements of the bench-marks on the route from Kuwana to Issinden, due to the earlier epoch.

As already referred to in the preceding chapter, we have the data of vertical displacements for earlier epochs of the bench-marks situated in the district under consideration. The sections of the levelling route and the time intervals to which the vertical displacements of the earlier epochs are due, are :

1.	Toyokawa-Okazaki	1885–1900	displacements shown in Fig. 13
2.	Okazaki-Atuta	1885–1895	,, ,, ,, ,, 13
3.	Kuwana-Tu (Issinden)	1888–1895	,, ,, ,, ,, 14

As for the sections 1 and 2 the correlations between δH_1 and δH_2 are positive as shown in Fig. 15, in which δH_1 denotes the vertical displacements of the bench-marks due to the time interval of 1885–

11) As for the vertical displacements of the bench-marks on the route from Atuta to Kuwana due to various time intervals, we have already referred to them in the above.

1900 for the district 1 and those due to the time interval of 1885–1895 for the district 2, while δH_2 denote the vertical displacements of the same bench-marks due to the time interval of 1900–1931 for the district 1 and those due to the time interval of 1895–1931 for the district 2.

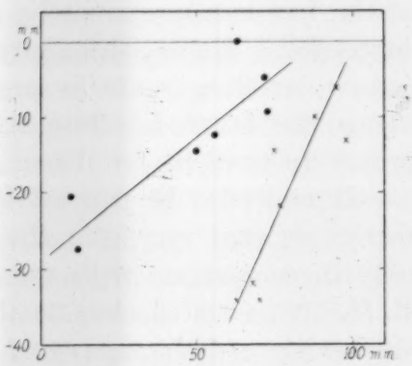

Fig. 15. The relation between δH_1 and δH_2 of the bench-marks, situated in the districts Toyokawa —Okazaki (×) and Okazaki—Atuta (•).

It may be remarked that the rates of variations of the gradients of the vertical displacement of the bench-marks are approximately the same in different time intervals or a little less in the recent epochs than in the earlier in the district between Toyokawa and Atuta, as may be understood by comparing the inclinations of straight lines representing the relations between δH_1 and δH_2 with the ratios of the time intervals to which δH_1 and δH_2 are due. The inclinations of these straight lines, representing approximate linear relations between δH_1 and δH_2 in Fig. 15, are $40/34=1{\cdot}2$ for the district between Toyokawa and Okazaki and $90/32=2{\cdot}8$ for the district between Okazaki and Atuta, while the ratios of the time intervals, to which δH_1 and δH_2 are due, are $31/16=62/32=1{\cdot}9$ for the former district and $36/10=108/10=3{\cdot}6$ for the latter district.

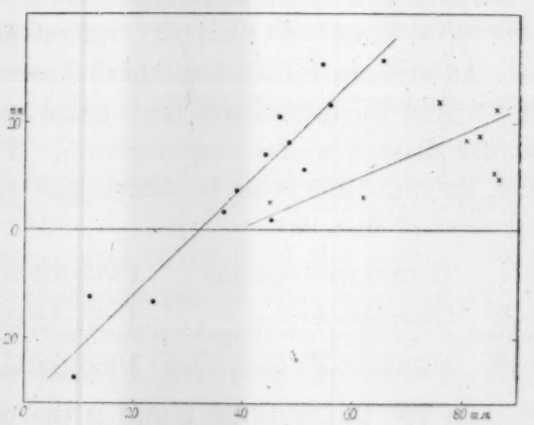

Fig. 16. The relation between δH_1 and δH_2 of the bench-marks situated in the district Kuwana-Issinden.

As for the vertical displacements of the bench-marks on the route from Kuwana to Tu, a correlation diagram is given in Fig. 16, taking δH_2, the vertical displacements due to the time interval of 1895–1931, in abscissae, and δH_1, the vertical displacements due to the time interval of 1888–1895, in ordinates. The diagram shows that the correlation is approximately

positive for the group of the bench-marks, B. M.'s 1468–1455. As for the other bench-marks, the correlation is also positive, but the slope of the straight line representing an approximate linear relation between δH_1 and δH_2 is a little gentler than that referred to above.

It may be remarked that the line representing the approximate linear relation between δH_1 rnd δH_2 of the bench-marks, B. M.'s 1468–1455, is inclined by some 45° to the horizontal line, the scale for δH_1 and δH_2 being the same. As the time interval to which δH_1 are due is about one fifth of that for δH_2, the rates of gradients of the vertical displacements is greater in the earlier epoch than in the recent epoch. The mode of the variation in rates of the gradients is reversed in comparison with those of the earth's crust in the district between Okitu and Hukuroi. The straight line representing the approximate linear relation between δH_1 and δH_2 of the bench-marks, B. M.'s 1455-1445 is gentler than 45°, which shows that the variation in the rates of gradients of the vertical displacements is, in this region, much more greater in earlier epoch than in recent epoch, in comparison with the case in the northern region, which was referred to above.

The detail of the crust deformation in the district between Toyokawa and Udiyamada are described as follows, the crust deformations in the districts on the east and west sides of Ise-Wan being treated separately :

a) The vertical displacements of the bench-marks on the route from Toyokawa to Atuta are plotted again in Fig. 17, and the topographical feature of the district between Toyokawa and Atuta is shown in Fig. 18. The route may be divided into several parts, as before, according to the modes of the crust deformation. These parts of the levelling route, or the groups of the bench-marks, are given in Table VI.

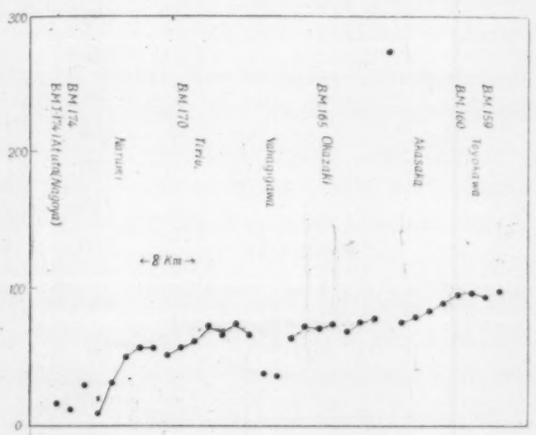

Fig. 17. The vertical displacements of the bench marks, between Toyokawa—Atuta, due to the time interval 1900–1931.

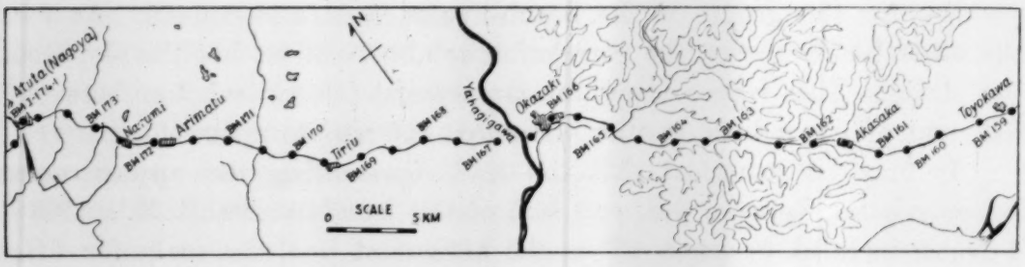

Fig. 18. The topographical features along the route from Toyokawa to Atuta.

Table VI. Groups, vertical displacements and heights of the bench-marks situated on the route from Toyokawa to Atuta.

Group	Locality	B. M.	δH mm	H m
	Toyokawa	159	93·4	12·72
		159·1	95·8	14·66
		160	95·0	12·74
B_1		160·1	88·7	23·96
		161	83·3	29·05
	Akasaka	161·1	79·1	46·35
		162	75·0	67·83
		162·1	274·2 *	105·31
		163	77·0	94·22
		163·1	74·6	78·39
		164	68·1	56·50
B_2		164·1	73·5	43·85
		165	70·3	29·32
		165·1	71·7	25·73
	Okazaki	166	62·9	24.50
	The Yahagigawa (river)	166·1	35·9	17·47
		167	37·5	14·52
		167·1	65·8	20·90
		168	73·4	21.49
		168·1	66·5	17·05

(to be continued.)

Table VI. (continued.)

Group	Locality	B. M.	δH	H
			mm	m
B_2	Tiriu	169	72·0	16·22
		169·1	61·5	11·74
		170	56·4	4·92
		170·1	50·6	5·86
		171	56·3	20·56
		171·1	56·9	26·34
B_4	Arimatu	172	49·7	8·97
	Narumi	172·1	30·7	3·60
		173	* 8·8	3·62
		173·1	29·1	13·57
		174	11·9	1·15
	Atuta	J-174·1	16·1	5·71

N. B. The vertical displacements of the bench-marks from B. M. 159 to B. M. 166 are due to the time interval 1900–1931, and those from B. M. 166–J-174·1 are due to the time interval 1895–1931. The vertical displacement marked by asterisks may be due to the local disturbance at the point where the bench-mark in question is situated.

One of the characteristics in the modes of the crust deformations in this district is regional upwarpings superposed on a general northwestward tilting. A typical example of the crust deformation of this sort is that of the region between Toyokawa and Akasaka, i. e., between B. M.'s 159 and 162. A similar mode of the crust deformation is shown in this region between B. M.'s 169–172, where the vertical displacements of the bench-marks are nearly proportional to their topographical heights.

B. M. 162·1 was upheaved abnormally, but nothing particular, either artificial or natural, is recorded which might have caused this abnormal upheaval.

The region in which the bench-marks belonging to Group B_2 are distributed may be subdivided into two regions as Groups B_2' and B_2''. This division, however, has no counterpart in the topographical features along this section of the levelling route. There is indeed a fault line, which may divided up the regions, but the trend of this fault line is nearly parallel to that of the levelling route. Hence, within the limit of accuracy in determining the trend of the fault line in the map, we

cannot find a point where the trend of the fault line intersects that of the levelling route which might be the boundary of the two regions mentioned above.

b) The vertical displacements of the bench-marks situated on the west side of Ise-wan are reproduced in Fig. 19. The trend of the

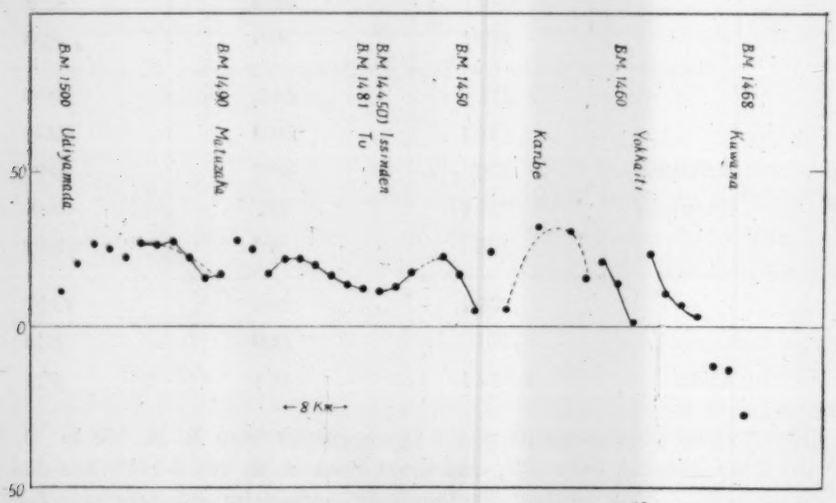

Fig. 19. The vertical displacements of the bench-marks along the route from Kuwana to Udiyamada; the result of 1931 revision.

levelling route in this district is directed approximately N-S, being not much deviated from a straight line, as shown in the map of Fig. 20.

From the curve of Fig. 19, we notice several crust blocks either tilted to the north or upwarped. Among them, the crust deformation in the region occupied by the groups of B. M.'s 1465–1462, and 1461–1459 are in a negative and that of B. M.'s 1451–1445 is approximately in positive correlation with the topographical features represented by the heights of the bench-marks. As for the region between B. M.'s 1458 and 1454, the mode of the crust deformation cannot be determined, for the lack of the data of the vertical displacements of B. M.'s 1456 and 1454. If, however, the vertical displacements were approximately proportional to the heights of the bench-marks, as we have noticed in several other cases, the crust deformation is an upwarping in this region.

The correlation between the vertical displacements and heights of the bench-marks may be seen in the numerical figures given in Table VII.

As may be seen in the table above, the correlations between the

vertical displace ments and the heights of the bench-marks belonging to Groups B_5 and B_6 are negative and that of Group B_7 are positive. But no correlation, neither positive nor negative, existed for the relation between the heights and the vertical displacements of the bench-marks, belonging to Groups B_8, B_9 and B_{10}, which are distributed in the alluvial plain. In this alluvial plain, the crust deformations, shown by the vertical displacements of the bench-marks, seem to be a general upwarping. Among them, the crust deformation in the regions occupied by the bench-marks belonging to Groups B_9 and B_{10} are similar with that which we have noticed in the crust deformation in the region belonging to Group B_1.

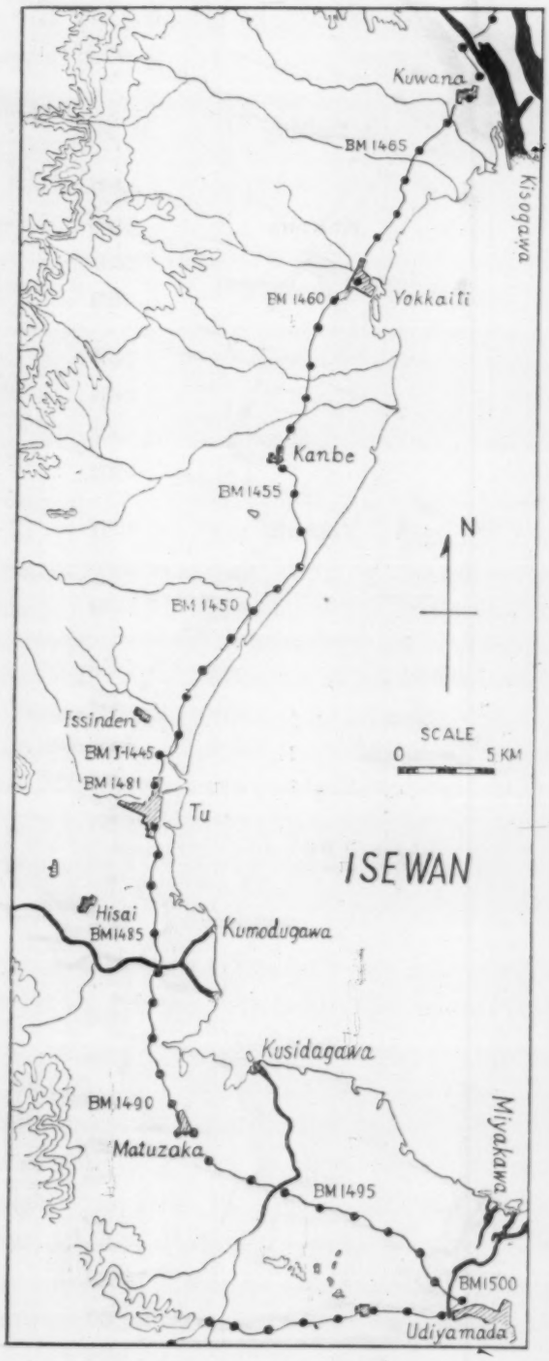

Fig. 20. The topographical features alo ng the route from Kuwana to Udiyamada.

The Crust Deformation in Kii Peninsula.

In Kii peninsula, the precise levelling has been already revised in 1927 along the route from Kusimoto to Osaka via Tanabe, Yuasa and Wakayama and then in 1931 along the route from Singû to Gozyô via Ukegawa, the route passing through the central part of the peninsula, from S to N. By using these data, Prof.

Table VII, Groups, vertical displacements and heights of the bench-marks situated on the route from Kuwana to Udiyamada.

Group	Locality	B. M.	δH	H
			mm.	m.
		1469	−40·1	6·03
	Kuwana	1468	−27·4	2·66
		1467	−13·3	1·66
		1466	−12·3	6·90
		1465	2·3	6·76
B_5		1464	7·3	4·73
		1463	11·1	1·51
		1462	23·2	3·44
	Yokkaiti	1461	1·7	4·48
P_6		1460	14·1	2·90
		1459	21·0	2·73
		1458	16·3	6·42
		1457	30·7	8·93
		1456	—	10·27
B_7	Kanbe	1455	31·5	9·52
		1454	—	7·74
		1453	5·9	11·64
		1452	23·8	3·06
		1451	5·1	1·83
		1450	17·0	1·66
		1449	22·4	2·53
B_8		1448	—	3·53
		1447	17·7	2·67
		1446	12·9	2·35
	Issinden	J-1445	11·6	1·29
B_9	Tu	1481	12·9	3·88
		1482	13·9	2·28
		1483	17·2	2·67

(to be continued.)

Table VII. (continued.)

Group.	Locality	B. M.	δH	H
			mm.	m.
B_9		1484	20·0	2·02
		1485	21·7	2·99
		1486	21·6	7·34
		1487	17·4	3·01
		1488	24·9	2·52
		1489	27.6	3·43
	Matuzaka	1490	17·0	8·33
		1491	16·2	7·87
		1492	22·2	5·33
B_{10}		1493	26·8	11·15
		1494	26·2	11·11
		1495	26·5	14·27
		1496	22·6	8·92
		1497	25·0	10·30
		1498	26·2	10·15
		1499	20·6	10·46
	Udiyamada	1500	11·9	5·13

N. B. The vertical displacements of the bench-marks from 1469 to J-1445 are due to he time interval 1895-1931, and those from J-1445 to 1500 are due to the time interval 1889-1931.

Imamura[12] discussed the crust deformations, particularly the movements of the crust blocks in this district in association with the occurrenec of the earthquakes.

Disregarding the irregular minor fluctuations in the vertical displacements, shown in Fig. 1 of the present paper and also in the figures in Prof. Imamura's paper, and considering the general aspect of displacement which may be considered as due to the movements of the crust blocks, the crust deformation in Kii Peninsula may be regarded to consist of two different modes. One of them is a southward tilting near the southern end of the peninsula, which we have pointed out in

12) A. Imamura, *Jap. Journ. Astr. Geophys.*, 1 (1929), 31.
Disin, 1 (1924), 321; 4 (1932), 474, (in Japanese).

the preceding paper.[13] The tilting of the earth's crust in this part of the peninsula was determined by smoothing the displacement curve along the routes from Inami to Kusimoto and from Kusimoto to Singû. It may be added that the general tilting of the earth's crust along the route from Singû to Ukegawa, a part of the levelling route from Singû to Gozyô, also well agree with the tilting near the end of the peninsula.

In the map showing the distribution of the coastal terraces and the topography of the sea bottom in the neighbourhood of the promontary of Kii Peninsula, which is given in Prof. T. Tsujimura and Mr. S. Kawada's paper,[14] it may be noticed that the earth's crust near the southern end of the peninsula may be regarded as a single or an united crust block which seems to have been tilted to SW in geological past.

Another mode of the crust deformation is an upwarping movement of the earth's crust in the district adjoining to the north of the above mentioned part of the peninsula forming its southern end.

The upwarping movement of the earth's crust in this district may be shown by combining the results of the levellings carried out recently. The dates of the revisions of the precise levellings are not the same for different sections of the levelling route in the peninsula. Hence, the time intervals to which the vertical displacements measured of the bench-marks on different sections of the routes are due, are not exactly but approximately coincident. Therefore, the vertical displacements on different routes are compared on the assumption that the vertical displacement of the bench-mark situated at Kusimoto, B. M. 3, is the same for the two slightly different periods of time, i. e., 1889–1929 and 1889–1931. In Fig. 21, Curves I and II show the vertical displacements of the bench-marks on the route from Kusimoto Wakayama and those on the route from Singû to Gozyô, reproduced from Prof. Imamura's paper. Curve III shows the vertical displacements on the route from Udiyamada to Kusimoto. It may be noticed, in Fig. 22, that the earth's crust in the region along the route corresponding to Curve II, i. e., the central part of the peninsula, has been upheaved more conspicuously that those in the regions corresponding to Curves I and III, i. e., the eastern and western sides of the peninsula, as we have referred to above.

The upwarping movement of the earth's crust in this district which had occurred in the recent epoch, may be, in some measure, coincident with the crust movement in the recent geological period which was

13) T. TERADA and N. MIYABE, *Proc. Imp. Acad.*, 8 (1932), 288.

14) T. TSUJIMURA and S. KAWADA, *Tirigaku-Hyôron*, 6 (1930), 1754, (in Japanese).

shown by the geologists.[15]

Regarding the detail of the vertical crust deformation in this dis-

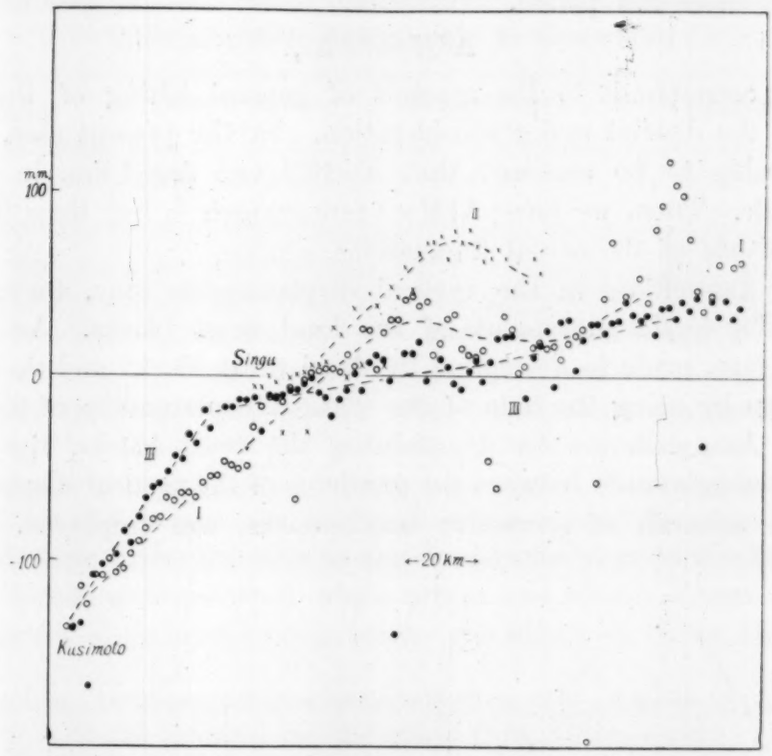

Fig. 21. The vertical displacements of the bench-marks situated in Kii Peninsula due to these 30 years.

I: along the route, Kusimoto—Wakayama.
II: „ Singû—Gozyô.
III: „ Kusimoto—Udiyamada.

trict, it may be noticed that the curve representing the vertical displacements on the route Udiyamada to Kusimoto, is superposed by irregular fluctuations. The amplitudes of the fluctuations in several place exceed several tens of milimetres. On the other hand, the form of the levelling route is also irregular and fluctuating from the general straight trend directed NE-SW. Hence, the fluctuations in the vertical displacements may be considered as partly due to the fluctuations in the form of the levelling route. For the purpose of a rough estimation, take the extreme case in which the general trend of the route is perpendicular to the direction of general tilting of the crust. If two successive bench-marks be situated on opposite sides of the straight line representing the trend

15) Y. Ôtuka, *Bull. Earthq. Res. Inst.*, 9 (1931), 240.

of the route and the sum of the distances of these two points from the straight line be Δs, we have, for the difference of the vertical displacements of these two points,

$$\Delta\delta H = a \times \Delta s,$$

where a corresponds to the amount of general tilting of the earth's crust in the district under consideration. In the present case, it may be probable to be assumed that $a = 10^{-6}$ and $\Delta s = 1$ km. in order of magnitude. Then, we have $\Delta\delta H = 1$ mm., which is less than the order of magnitude of the actual fluctuations.

The fluctuations in the vertical displacements may, therefore, be largely due to the movements of the local crust blocks. An attempt is, therefore, made to determine the local crust blocks and their modes of tiltings by using the data of the vertical displacements of the bench-marks. As a criterion for determining the crust blocks, the already established relation[16] between the gradients of the vertical displacements and the azimuth of successive bench-marks, was employed. Several

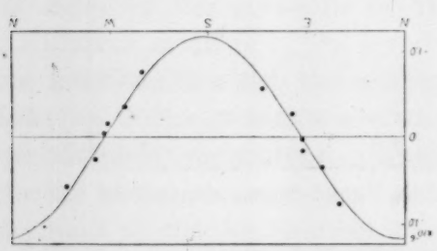

Fig. 22. a. The sine curve used for determining the tilting of Block V.

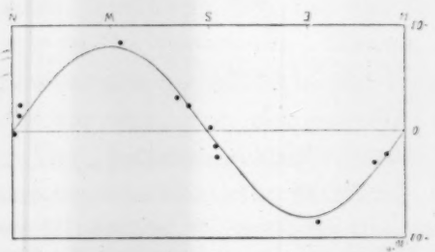

Fig. 22 b. The sine curve used for determining tilting of Block VII.

curves, used for determining the crust blocks are shown in Figs. 22 a and b. Thus, the crust blocks and their modes of tilting are determined and they are given in Table VIII.

The crust blocks thus determined seem to be significant also with respect to the local features of the topography.

Even in several regions, where the levelling route is straight and therefore the crust blocks cannot be completely determined by the usual geometrical method, it may be noticed that approximately corresponding to some discontinuity in the vertical displacements, there are also discontinuities in the local features of the topography. If we were allowed

16) N. MIYABE, *Proc. Imp. Acad.*, **7** (1931), 150.
Bull. Earthq. Res. Inst., **9** (1931), 257.

Table VIII. Crust Blocks in Kii Peninsula, determined by using the data of the vertical displacements of bench-marks on the route from Udiyamada to Kusimoto.

Block	Bench-marks situated	Magnitude of Tilting	Azimuth
I	BM's 1503–1506	$4{\cdot}8\times10^{-6}$	E-75°-S
II	„ 4749–4752	$1{\cdot}4_4$ „	E-49°-S
III	„ 4753–4756	$2{\cdot}9$ „	E-2°-S
IV	„ 4759–4762	$0{\cdot}8_8$ „	E-46°-S
V	„ 4771–4774	$2{\cdot}0_4$ „	E-7°-S
VI	„ 4784–4787	$2{\cdot}3_6$ „	E-85°-N
VII	„ 4795–4798	$2{\cdot}3$ „	W-84°-S
VIII	„ 4809–4810 4966–4967	$0{\cdot}1_6$ „	E-1°-S
IX	„ 4979–4982	$1{\cdot}9_6$ „	E-68°-S.

to regard these discontinuities as the boundaries of crust blocks, several of these blocks are upwarped while others are tilted. These divisions of the earth's crust or the crust blocks are shown in Table IX.

Table IX. Groups, vertical displacements and heights of bench-marks situated on the route from Udiyamada to Kusimoto.

Group.	Locality	B. M.	δH	H
			mm.	m.
	Udiyamada	1500	11·9	5·13
		1501	17·5	8·10
		1502	14·8	15·34
Block I		1503	21·6	19·67
		1504	15·0	22·64
		1505	26·6	41·47
		1506	22·7	42·30
C_1		1507	28·5	48·51
		1508	30·3	38·83
		1509	40·4	53·30
		J-1510	26·2	34·40

(to be continued.)

Table IX. (continued.)

Group.	Locality	B. M.	δH	H
			mm.	m.
		4736	35·3	44·38
C_2		4737	37·8	75·57
		4738	41·8	56·74
		4739	35·6	68·33
		4740	40·3	71·91
C_3		4741	36·7	93·60
		4742	33·4	82·82
		4743	42·0	77·72
		4744	33·6	97·95
		4745	42·3	101·32
		4746	* −37·1	106·36
		4747	43.1	115·81
		4748	36·2	127·17
		4749	41·1	124·73
Block II		4750	31·2	138·50
		4751	38·2	145·18
		4752	36·8	157·38
		4753	22·4	169·40
Block III		4754	33·2	182·14
		4755	29·6	202·92
		4756	34·3	242·35
		4757	44·6	147·96
		4758	30·0	22·42
		4759	29·1	1·98
Block IV	Nagasima	4760	24·3	3·21
		4761	28·4	2·44
		4762	28·4	49·72
		4763	19·3	47·23
		4764	3·5 *	64·66

(to be continued.)

Table IX. (continued.)

Group.	Locality	B. M.	δH	H
			mm.	m.
		4765	30·1	36·83
		4766	29·8	22·50
		4767	* − 5·7	148·22
		4768	24·1	37·63
C_4		4769	17·7	11·04
		4770	11·1	8·93
		4771	−13·1	5·89
Block V		4772	8·0	2·44
		4773	22·5	45·28
		4774	20·5	86·96
	Owase	4775	20·3	43·19
C_5		4776	7·8	34·19
		4777	−2·6	3·20
		4778	9·9	6·41
C_6		4779	2·6	37·13
		4780	− 7·3	81·45
		4781	− 4·7	203·55
C_7		4782	5·3	390·65
		4783	8·5	560·02
		4784	10·8	676·53
Block VI		4785	− 8·5	807·82
		4786	17·8	703·32
		4787	12·0	601·09
		4788	12·2	497·10
		4789	* 140·4	405·38
		4790	− 2·5	364·58
		4791	8·1	340·20
C_8		4792	11·5	320·45
		4793	7·0	301·90

(to be continued.)

Table IX. (continued.)

Group.	Locality	B. M.	δH	H
		4794	mm. − 8·7	m. 331·94
Block VII	Kinomoto	4795	1·6	388·12
		4796	− 8·1	310·33
		4797	−13·4	156·03
		4798	−32·0	7·34
		4799	−12·2	11·40
		4800	−10·3	12·04
C_9		4801	− 1·5	12·77
		4802	− 3·3	11·17
		4803	− 7·6	7·10
C_{10}		4804	− 6·9	17·93
		4805	−10·9	4·00
		4806	−12·2	11·57
		4807	−11·2	7·62
		4808	−30·0	6·17
Block VIII	Singû	4809	−15·1	6·91
		J 4810	−12·6	9·82
		4966	−13·6	5·42
		4967	−13·5	33·58
	Miwasaki	4968	−17·1	8·10
		4969	−16·9	9·57
		4970	—	7·22
		4971	−29·6	40·53
		4992	−19·6	14·58
		4973	−36·9	3·82
C_{11}		4974	−31·7	69·76
		4975	−45·1	1·64
		4976	−44·1	10·92
		4977	−52·0	3·19

(to be continued.)

Table IX. (continued.)

Group.	Locality	B. M.	δH	H
		4978	mm. −58·2	m. 3·26
Block IX		4979	−61·5	2·90
		4980	−65·6	5·60
		4981	−75·9	12·04
		4982	−91·2	2·35
C_{12}	Koza	4983	−84·6	5·78
		4984	−97·2	7·25
		4985	−100·4	5·69
		4986	−102·4	7·51
	Kusimoto	4987	−108·8	5·58
		4988	* −169·4	2·79
		4989	−133·9	3·16
		9221	−136·2	2·73
		3	−136·1	3·33

N. B. The vertical displacements of the bench-marks from 1500 to J-1510 are due to the time interval 1889–1931, those from J-1510 to 4775 are due to the time interval 1895–1931, and those from 4775 to 3 are due to the time interval 1899–1931. The vertical displacements marked by asterisks may be due to the local disturbances at the points where the bench-marks in question are situated.

The locations of the crust blocks, including the divisions of the earth's crust mentioned above, are shown in Fig. 23. In this figure, the crust blocks determined by the usual geometrical method are shown with arrows indicating the directions and magnitudes of their tiltings.

As for the crust deformations in this district, it may be remarked that the amounts of tilting of local crust blocks are of the same order of magnitudes while they are tilted in various directions. The order of magnitude of tilting of these local crust blocks is 1–5 $\times 10^{-6}$, those situated near the southern end of the peninsula and the district to the north of it being included. On the other hand, the general tilting of the earth's near the southern end of the peninsula and that of the district adjoining to the north of the former are evidently different, as already referred to. Moreover, the general tilting in the northern district is smaller in order of magnitude than those of smaller crust

blocks situated there. It may, therefore, be pointed out that the tilting of the local crust blocks does not always represent the general tilting of the earth's crust in the district including these crust blocks. The case is similar with that which has already been shown in the crust deformation in Bôsô Peninsula.[17]

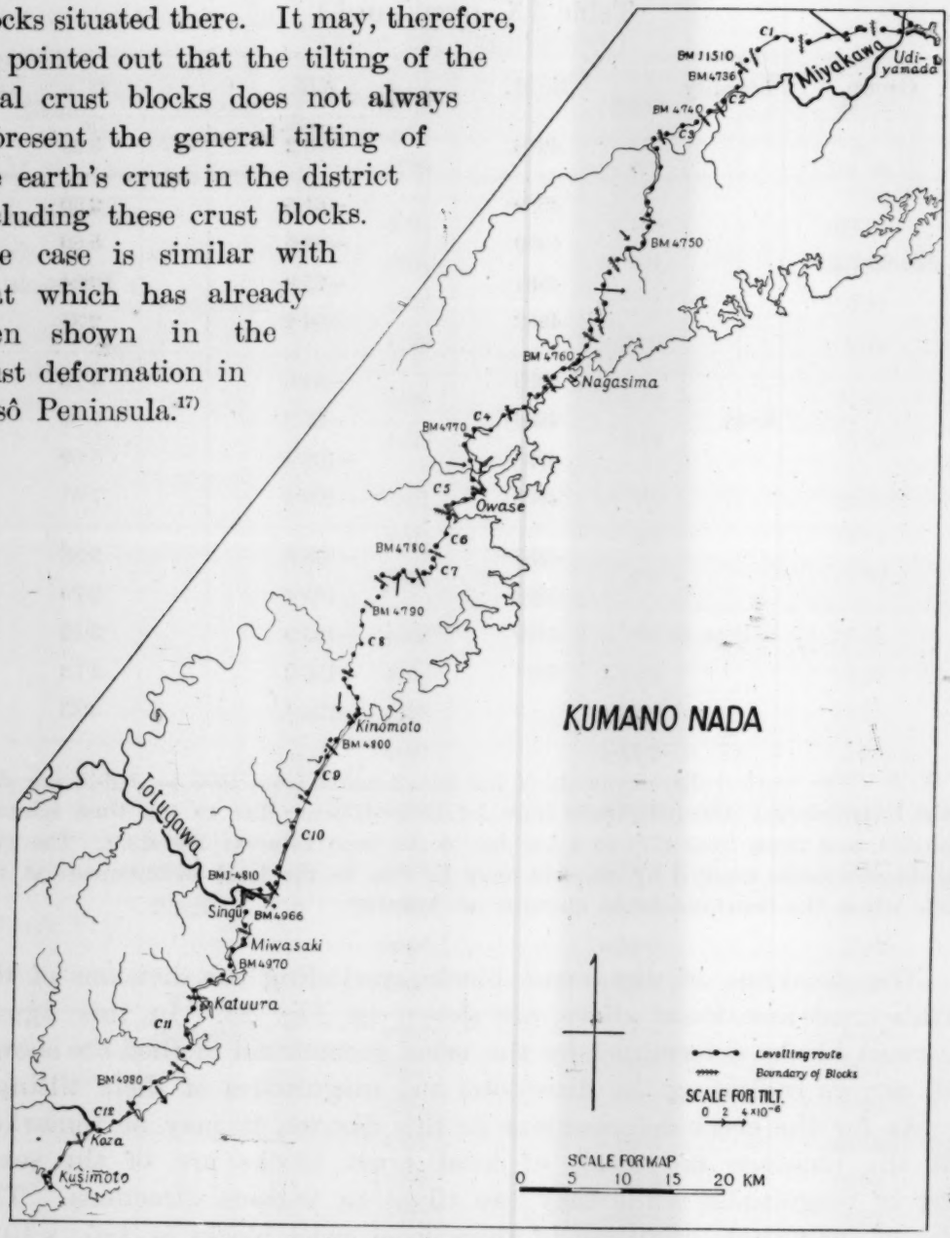

Fig. 23. Levelling-route and blocks in the eastern coast of Kii Peninsula.

17) N. MIYABE, *Bull. Earthq. Res. Inst.*, 9 (1931), 407.

Summary.

The results of the present investigation may be summarized as follows:

1) The district between Okitu and Kusimoto, along the Pacific coast, may be divided into three or four districts with regard to the difference in the modes of crust deformations. The first, third and fourth parts of the district belong to the Outer Zone and the second part belongs to the Inner Zone of Southwest Japan, according to the division which has been established by the geologists on the basis of the geological evidences.

2) Taking these parts separately, general modes of the crust deformations and also the local ones, such as due to the movements of the local crust blocks are investigated. The results in detail are described in respective chapters. It may be remarked that the general mode of the crust deformation in Kii Peninsula is in accord with the results of geological and geomorphological investigations and that in most cases, the discontinuities in local crust deformation or the boundaries of the crust blocks are also significant with regard to topographical features and geological evidences.

3) In the districts between Okitu and Okazaki, Okazaki and Atuta and Atuta and Tu, the vertical displacements of the bench-marks recently measured are compared with those of the earlier epoch. The correlatians between the vertical displacements of recent and earlier data are generally positive, disregarding the negative correlations in smaller regions.

It may be remarked however, that, in the district between Okitu to Simada, the rate of variation of the gradient of the vertical displacement was several times as great in the recent epoch, compared with the rate in the early epoch.

4) As for the crust deformation in Kii Peninsula, it was pointed out that the modes of local crust deformation are not always coincident with the mode of the general crust deformation.

Before concluding, it must be stated with acknowledgements and gratitude that the entire cost of the recent revision of the precise levelling, along the route under consideration, was defrayed by the grant from Harada Sekizenkwai.

In conclusion, the present writer wishes to express his sincere thanks

to Professor Torahiko Terada for his kind advices and guidance. Cordial thanks are also due to Mr. K. Mutô of the Miltary Land Survey for his kindness in placing valuable data at the writer's disposal.

---

16. 興津串本間に於ける地殻の變動.

地震研究所 宮 部 直 巳

昭和 6 年 (1931 年) に靜岡縣下の興津から紀伊半島の南端串本に至る水準線の改測が行はれ, この間にある水準點の 30–40 年間の垂直變動量が知られた. 本文はその結果に基いて, この地域の地殻の變動を調べたものである.

水準點の垂直變動の示す所を見るに, 豐川以東に於ける地殻は大體東に傾斜し, 宇治山田以西に於いては南又は西南に傾斜してゐる模樣であつて, この兩區域は地質學上の西南日本外帶に屬してゐる. 又, 豐川から宇治山田に至る伊勢灣周圍の地域は, 東側では西に傾斜し西側では殆ど傾斜してゐない樣に見える. 是等の三つの區域について二三の著明な事實を指摘すれば, 次のやうなものがある.

i) 興津—豐川.

a) 天龍川以東の地域は大體東 37 度南へ約 1·3″ 傾斜してゐる.

b) 1885–1900 の間の垂直變動と 1900–1931 の間のそれとを比較すると後の期間の方が變動の割合が大になつてゐる.

ii) 豐川—宇治山田.

a) 熱田—桑名の間には濃美地震後數回の測量が行はれてゐて, その各期間に起つた垂直變動を示す曲線は何れもその形が似てゐる.

殊に木曾川河口にある水準點の沈下が何れも著明である. そこで, もし, この點を通つて南北に亙る沈降地帶がありとすれば, 伊勢灣の兩岸の地域はこの地帶の沈降運動に伴つて夫々東岸は西に西岸は東に傾いたものの如くに思はれる.

b) 豐川—熱田間, 桑名—一身田間の變動を, 以前の變動に較べれば, 大體に於いて, 同一の向きに變動を繼續しつゝあるかの如き樣子を示しその變動の割合はあまり變らないか或は寧ろ小さくなつてゐる.

iii) 宇治山田—串本.

a) 宇治山田—新宮と新宮—串本とは垂直變動を示す曲線の上でかなり明瞭な區別が認められるが, その中, 宇治山田—新宮間の變動は, 緩なる西南又は南への傾斜を示し, 先に今村博士の發表された, 紀伊半島西岸並に中部に於ける水準測量の結果と併せて, 紀伊半島の中部以北では, 全體として, 地殻が南北線を背斜軸とする warping をなしつゝあるかの如く見える.

b) 新宮以南の地域は, 嘗ても指摘されたやうに大體南へ傾斜してゐる.

以上の外, 各地域を通じて, 地塊を認めることが出來る. 是等の地塊は必ずしも單一な傾斜を示さず曲隆的な變形を示してゐるものもある樣に思はれる. 又地形や地質の上から認めらる地塊と, 測量によつて見出された上記の地塊とが略〻一致してゐるやうな場所も尠なからず存在する.

尙, 上述の水準測量は, 原田積善會から提供された資金により, 陸地測量部に委囑して遂行されたものであつて, 同會に對して筆者も亦篤く御禮を申上げたいと思ふ.

17. 濃尾震災地及び其他の地方に於ける檢測水準測量の調査

陸地測量部　武藤勝彦
　　川畑幸夫

陸地測量部の古い水準線の檢測結果中には未だ發表されてゐないものも二三あり，又發表されたものでも檢測水準線の兩端點の値を舊値に一致させる爲め局部的平均計算を施したものが多い．併し，變動を問題とする場合には，かゝる平均計算を施さない方が寧ろ妥當ではないかと思はれるので，古い檢測を有する水準線につき，各水準點間に於いて觀測された比高の差より直接に變動量を求めて見た．

各檢測出發點の標高の正確な變化は知る事が出來ないので，出發點に變化がなかつたものと假定し，出發點から $(n-1)$ 番目の水準點と n 番目の水準點との間の比高の差を δ_n とすれば，n 番目の水準點の出發點に對する變動量は

$$\Delta H_n=\sum_1^n \delta_n$$

で求められる．この様な意味での水準點の變動量を，第一圖にその地理的分布を示してある所の次の各水準線(第一表)について求め，それを第二圖乃至第十一圖に示した．

第　一　表

番號	區間	期間	摘要
1	高輪——興津	明治16,7年——明治 29 年	未發表
2	代々幡——甲府——興津	明治 17 年——明治 28 年 明治 28 年——明治 36 年	〃
3	興津——岡崎	明治 18 年——明治 33 年	局部平均
4	岡崎——加納	明治 18 年——明治27, 8年	〃
5	加納——日吉	明治 22 年——明治 27 年 明治 28 年IV月——同年 V月	〃
6	加納——下原	明治 23 年——明治27, 8年	〃
7	熱田——津	明治 21 年——明治 28 年	〃
8	大津——加納	明治 18 年——明治 29 年 明治 29 年——明治 32 年	〃
9	大阪——大津	明治 18 年——明治 29 年 明治 29 年——明治 32 年	〃
10	丹後喜多村——山城川勝村	明治 20 年——明治 25 年	未發表

第二表乃至第十一表には是等の新觀測から舊觀測を引いた變動量が數字的に與へられてある．

以上の様な次第であるから，圖に表はされてゐる變動は，正しく言へば單に各水準線に沿うて生じた傾斜を示してゐるに過ぎない．

本比較に於ける新舊兩水準測量に使用せる器材はカール・バンベルヒ製一等水準儀並に一等標尺であつて，測定の方法は新舊とも同一である．

尙，加納——下原間の明治 27, 8 年に於ける測量に際しては，この水準線を往復施行されたので，その間の變動をも併せて示した．斯の如き短期間內に檢測された變動量は，その量も小さく，觀測誤差と見られる場合も無いことはあるまいが，叙上の區域が濃美大震の變動を受けた直後の觀測でもあり，變動を示す曲線の形からも，この

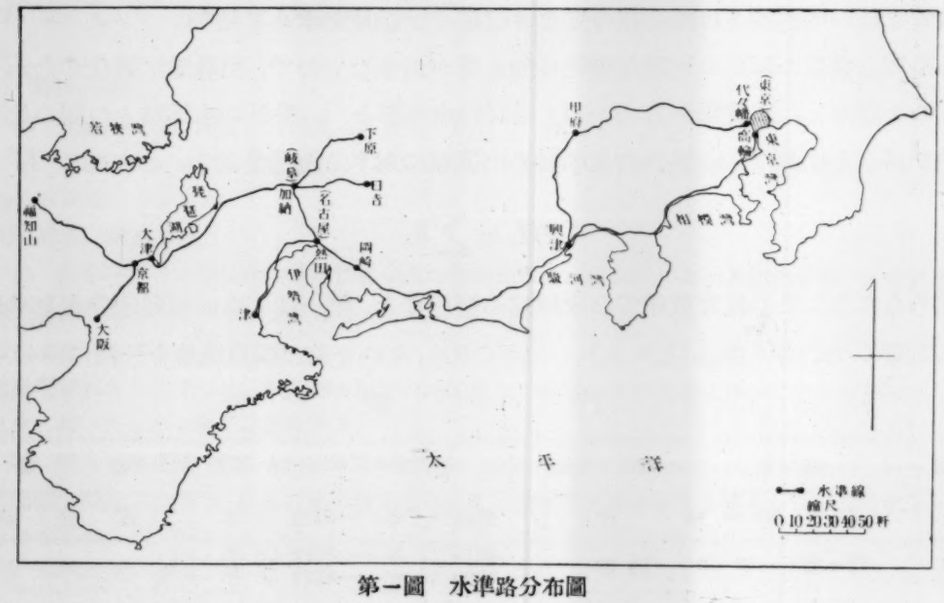

第一圖 水準路分布圖

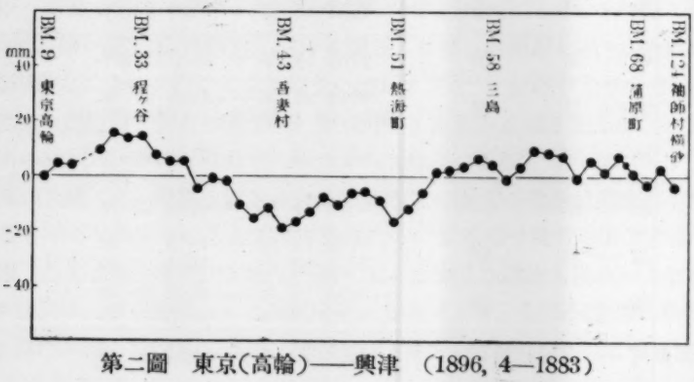

第二圖 東京(高輪)——興津 (1896, 4—1883)

往復測量の期間内に相當の變動があつたと考へてもよいのではないかと思はれる.

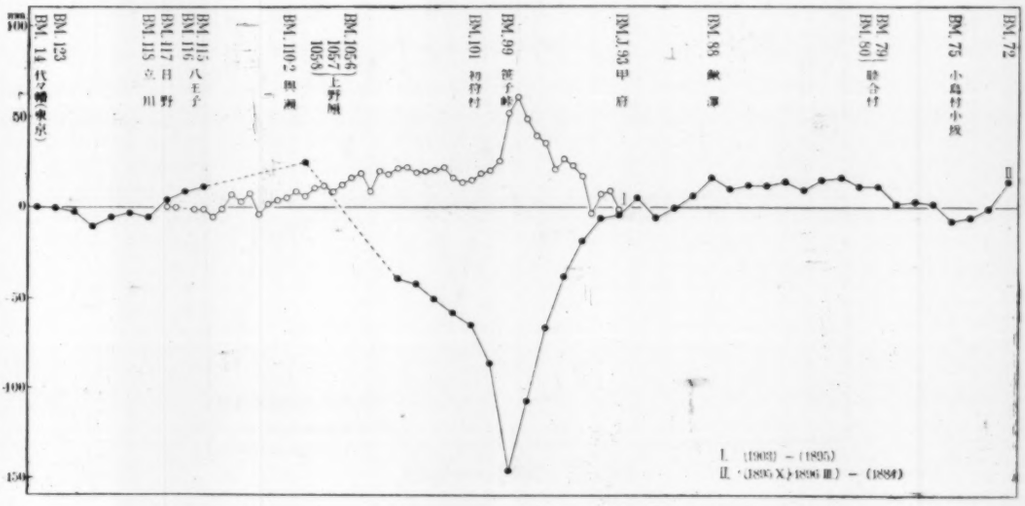

第三圖 代々幡(東京)——小島村但沼(與津附近)

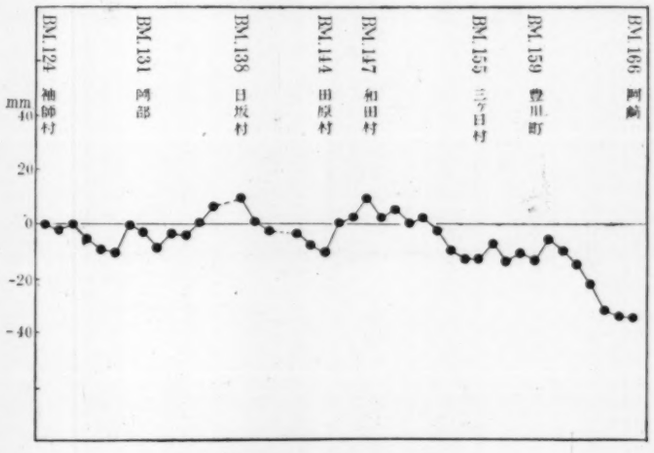

第四圖 與津——岡崎
(1900—1885)

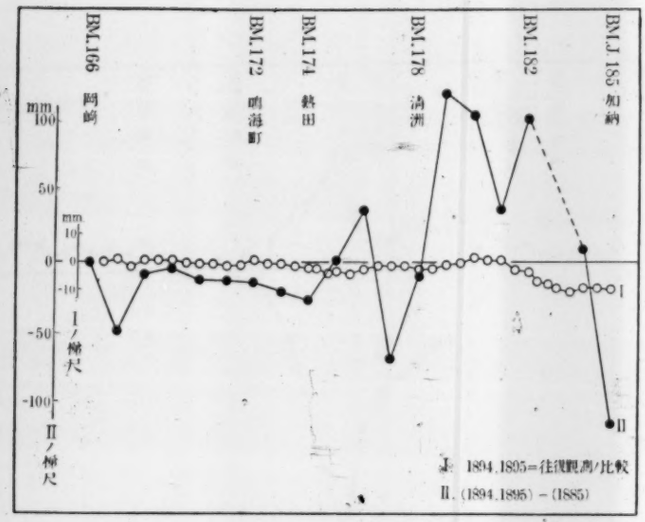

第五圖 岡崎——加納

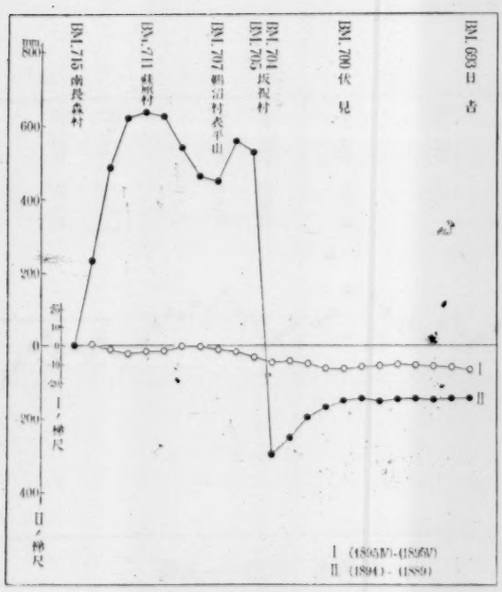

第六圖 加納——日吉

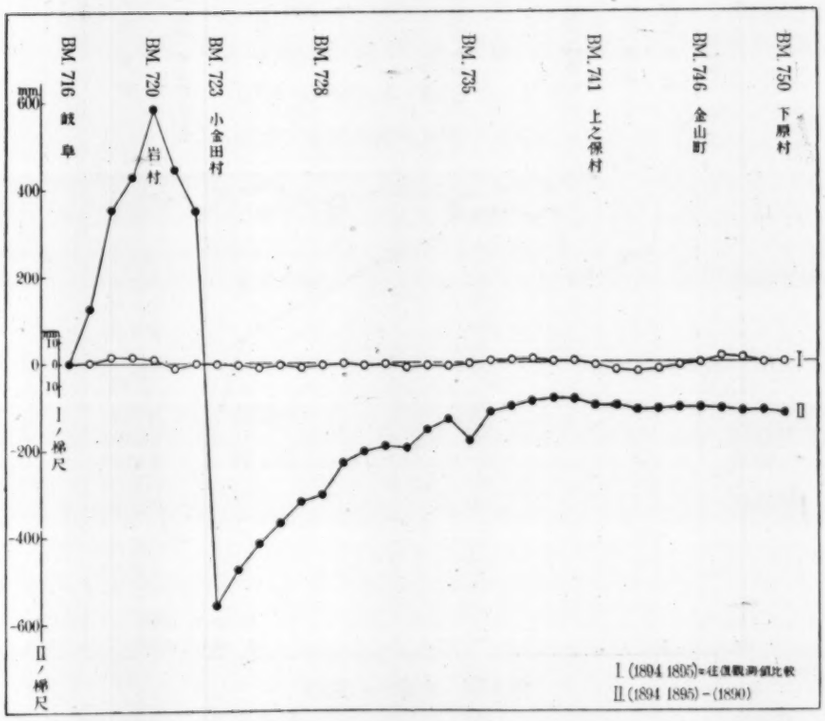

第七圖　岐阜(加納)——下原

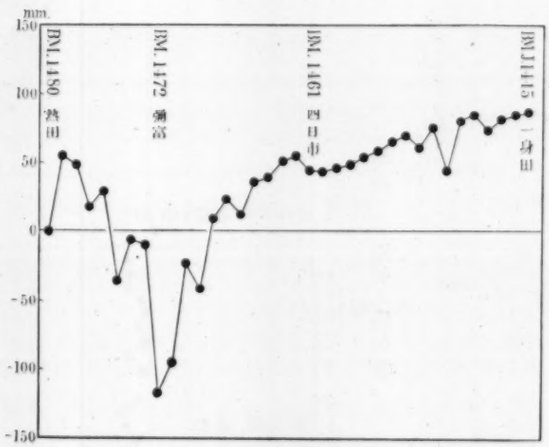

第八圖　熱田(名古屋)——一身田(津)
(1895—1888)

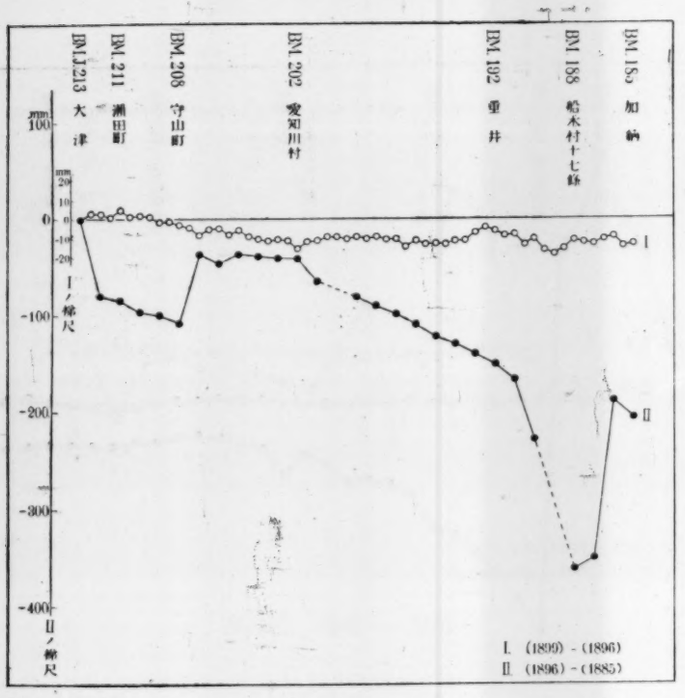

第九圖 大津——加納

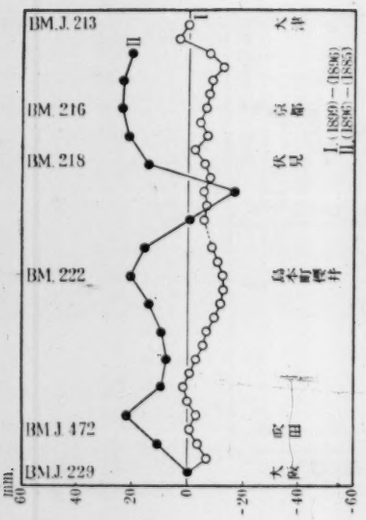

第十圖 大阪——大津

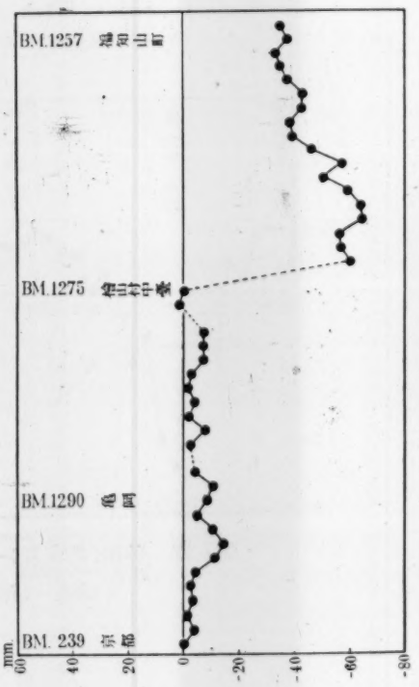

第十一圖 丹後與謝郡喜多村(福知山附近)——山城，葛野郡川勝寺村(京都附近)
(1892—1887)

第 二 表

自 高 輪 至 興 津

(明治 29 年)——(明治 16, 17年)

注意 水準點間の距離は 4 km.

B. M.	δH	位 置	B. M.	δH	位 置
	mm.			mm.	
9	0·0	東京高輪	51	−16·7	熱海町伊豆山
27	+ 4·2		52	−11·9	
28	+ 4·0		53	− 5·9	
29			54	+ 1·2	
30	+ 9·6		55	+ 2·2	
31	+15·4	神奈川	56	+ 3·4	
32	+13·7		57	+ 6·7	函南村平井
33	+14·3	程ヶ谷	58	+ 4·1	三島
34	+ 7·3		59	− 0·9	
35	+ 5·3		J. 60	+ 3·2	揚原村
36	+ 5·2		61	+ 9·2	
37	− 4·5		62	+ 8·4	
38	− 0·9		63	+ 7·7	
39	− 1·9		64	− 0·8	
40	−10·3		65	+ 5·9	
41	−15·1		66	+ 1·7	
42	−11·8		67	+ 7·1	
43	−19·0	吾妻村	68	+ 1·1	蒲原村
44	−16·7		69	− 2·9	
45	−13·0		70	+ 2·9	
46	− 7·6	早川村	124	− 3·5	袖師村横砂 (興津西方 2 km.)
47	−10·1				
48	− 6·2				
49	− 5·1	岩村			
50	− 8·8				

第 二 表 續 き

B. M.	δH	位 置	B. M.	δH	位 置
	mm.			mm.	
90	− 0·8		80	+10·4	
89	+ 5·7		79	+10·8	
88 (鰍澤)	+15·8		78	+ 1·1	睦合村
87	+ 9·5		77	+ 2·3	
86	+11·9		76	+ 1·0	
85	+11·9		75	− 8·7	小島村小坂
84	+13·3		74	− 6·3	
83	+ 9·0		73	− 1·1	
82	+14·5		72	+13·3	小島村但沼
81	+15·7				(興津北方 5 km.)

第 三 表

自代々幡14號至興津70號

B. M.	(明治 28. X—29. III)—(明治 17 年) δH	(明治 30)—(明治 28) δH	B. M.	δH	δH
14（代々幡）	0·0		105·4		+18·3
			105·3		+ 8·3
123	− 0·2		105·2		+19·9
			105·1		+18·0
122	− 2·8		105	−39·8	+21·1
					+21·7
121	−10·1		104	−42·6	+18·5
					+19·4
120	− 5·8		103	−50·9	+20·0
					+21·4
119	− 3·4		102	−58·8	+15·3
					+13·1
118（立川）	− 5·9		101（初狩村）	−65·2	+14·3
					+18·2
117（日野）	+ 3·9	± 0·0	100	−86·6	+19·8
		− 0·1			+25·2
116	+ 8·1	改	99（笹子峠）	−146·3	+51·6
（八王寺）		− 1·7	〃 驛口		+60·3
115	+11·0	− 1·7	98	−107·9	+48·3
110·10		− 5·4			+39·5
110·9		− 1·1	97	−66·9	+35·1
110·8		+ 6·3			+20·1
110·7		+ 2·3	96	−38·3	+26·7
110·6		+ 7·0			+22·7
110·5		− 4·4	95	−18·5	+16·9
110·4		+ 1·2	石和町		− 3·1
110·3		+ 3·5	94	− 6·6	+ 6·8
110·2（興瀬）		+ 4·9			+ 8·5
110·1		+ 8·0	J. 93（甲府）	− 4·1	− 1·5
110·	+24·9	+ 5·6			
105·9		+10·0	92	+ 4·8	
105·8		+11·2			
105·7 上野原		+ 8·0	91	− 6·6	
105·6		+11·8			
105·5		+16·0			

第 四 表

自 興 津 至 岡 崎

(明治 33 年)——(明治 18 年)

注意 水準點間の距離は 4 km.

B. M.	δH	位 置	B. M.	δH	位 置
	mm.			mm.	
124	0·0	袖師村	146	+ 2·8	
125	− 2·3	(興津西方 2 km.)	147	+ 9·8	和田村
126	− 0·1		148	+ 2·7	
127	− 5·2		149	+ 5·8	
128	− 9·1		150	+ 0·6	
129	−10·5		151	+ 2·4	
130	− 0·6		152	− 2·7	
131	− 3·1	岡部	153	− 9·8	
132	− 8·6		154	−12·5	
133	− 3·2	藤枝	155	−12·7	三ヶ日町
134	− 4·2		156	− 7·3	
135	+ 0·4		157	−13·3	
136	+ 6·5		158	−10·6	
137	改埋		159	−13·1	豐川町
138	+ 9·8	日坂村	160	− 5·3	
139	+ 1·1		161	− 9·8	
140	− 2·4		162	−14·4	
141	改		163	−21·8	
142	− 3·8		164	−31·8	
143	− 8·0		165	−33·9	
144	−10·7	田原村	166	−34·2	岡崎
145	+ 0·5				

第 五 表

自 岡 崎 至 加 納

B. M.	明治 27, 8 年に往復檢測の比較 δH	(明治27, 8年) (明治 18 年) δH	位 置	B. M.	δH	δH	位 置
166		0.0	岡崎	176	−2·5	+37·1	
	0·0				−1·3		
167	+0·8	−48.5	矢作町	177	−1·5	−68·4	西枇杷町
	−1·6				−1·7		
168	+0·2	− 9.2		178	−2·3	−10·1	清洲
	+0·4				−2·6		
169	+0·4	− 4.7	知立	179	−1·2	+120·6	
	−0·2				−0·7		
170	−0·7	−12.8		180	+1·3	+105·1	
	−0·5				+0·7		
171	−1·6	−13.1		181	+0·7	+37·1	
	−1·2				−2·8		
172	+0·6	−14.5	鳴海町	182	−3·5	+102·7	木曾川町
	−0·4			182.1	−7·0		
173	−0·7	−20.5		182.2	−8·0		
	−1·6			183	−9·3		
174	−2·0	−27.4	熱田		−10·7		
174.1	−2·4			184	−9·3	+ 8·7	
174.2	−4·0				−9·4		
175	−3·7	+ 0.7		J 185	−10·0	−117·1	加納
	−4·1		名古屋				

第 六 表

自 加 納 至 日 吉

B. M.	(明 27 年)—(明 22 年) δH	(明 28 年 IV)—(明 28 年 V) δH	B. M.	δH	δH
715 南長森村	0·0	0·0	703	−254·7	− 8·6
714	+230·9	+0·4	702	−195·9	− 9·9
713	+483·2	−2·6	701	−169·2	−12·3
712	+619·8	−4·6	700 伏見	−149·2	−12·4
711 蘇原村	+635·3	−3·4	699	−143·4	−11·2
710	+624·5	−3·2	698	−151·5	−11·0
709	+538·0	−0·8	697	−144·9	−10·6
708 鵜沼村	+462·5	−1·0	696	−141·0	−10·8
707 表平山	+449·5	−2·4	665	−146·5	−11·2
706	+559·5	−3·6	994	−141·9	−11·9
705 坂祝村	+526·9	−6·3	693 日吉	−143·2	−13·0
704	−298·3	−9·0			

第 七 表

自 岐 阜 至 下 原

B M.	(明 28 年)—(明 23 年) δH	明 27, 8 年に往復觀測値の比較 δH	B. M.	δH	δH
716 岐阜	0·0	0·0	734	−131·3	−1·9
717	+122·8	0·0	735 富之保村	−179·0	−0·8
718	+352·0	+2·5	736	−109·0	+0·1
719	+425·6	+2·3	737	−102·0	+0·6
720 岩村	+585·9	+1·3	738	− 90·1	+1·0
721	+442·9	−2·4	739	− 85·7	+0·0
722	+350·9	−0·5	740 上之保村	− 85·9	+0·0
723 小金田村	−556·5	−0·9	741 峠向	− 95·4	−1·4
724	−474·5	−1·1	742	− 97·1	−3·8
725	−415·2	−2·6	743	−110·0	−4·2
726	−365·4	−1·0	744	−105·9	−3·3
727	−318·4	−2·7	245	−104·3	−2·0
728	−302·3	−1·6	746 金山町	−105·5	−0·9
729	−227·6	−0·6	747	−106·8	+2·0
730	−202·2	−1·2	748	−112·3	+1·3
731	−187·6	−0·9	749	−412·4	−0·3
732	−192·8	−2·2	750 下原村	−118·9	−0·1
733	−153·5	−1·7			

第 八 表

自 熱田 至 津 (明治 28 年)——(明治 21 年)

B. M.	δH	位 置	B. M.	δH	位 置
1480	± 0·0	熱田	1462	+55·6	
1479	+54·8		1461	+45·1	四日市
1478	+48·7		1460	+44·0	
1477	+17·5		1459	+46·4	
1476	+29·7		1458	+48·2	
1475	−35·4	蟹江	1457	+54·2	
1474	− 6·3		1456	+58·5	
1473	−10·0		1455	+65·3	
1472	−117·4	彌富	1454	+69·9	
1471	−95·8		1453	+61·8	
1470	−22·1		1452	+75·5	
1469	−41·7		1451	+44·8	
1468	+ 9·2	桑名	1450	+80·3	
1467	+23·6		1449	+85·9	
1466	+12·0		1448	+73·6	
1465	+36·3		1447	+82·7	
1464	+38·9		1446	+85·4	
1463	+51·1		J 1445	+86·8	一身田

第 九 表

自 大津 至 加納

B M.	(明 32 年)—(明 29 年) δH	(明 29 年)—(明 18 年) δH	B. M.	δH	δH
J. 213 大津	0·0	0·0	198	− 9·7	− 90·1
212.1	+ 3·0			−11·0	
212	+ 3·0	−80·0	197	−10·6	−100·0
	+ 1·0			−14·8	
211	+ 4·9	−85·0	196	−11·8	− 11·0
	+ 1·3			−13·7	
210	+ 1·9	−96·9	195	−13·0	−123·3
	+ 1·1			−13·6	
209	− 1·6	−100·0	194	−11·8	−131·3
	− 1·4			−11·3	
208 守山町	− 3·0	−108·6	193	− 7·7	−141·6
	− 4·7			− 4·7	
207	− 8·3	−36·6	192 (垂井)	− 6·3	−150·3
	− 5·6			− 8·8	
206	− 5·6	−46·0	191	− 9·3	−167·7
	− 8·4			−13·8	
205	− 6·0	−37·5	190	−10·9	−229·7
	− 9·2			−16·4	
204	−10·3	−39·2	189	−18·5	改埋
	−11·4			−15·3	
203	−11·0	−40·6	188 (船木村七條)	−11·5	− 362·0
	−11·7			−12·3	
202(愛知川村)	−15·9	−40·8	187	−13·3	−350·4
	−12·0			−11·0	
201	−11·2	−64·8	186	− 9·2	−188·4
	− 9·3			−14·9	
200	− 9·5	改埋	185 加納	−13·3	−206·8
	−10·7				
199	− 9·8	−80·9			
	−10·2				

第 十 表

自 大 阪 至 大 津

B. M.	(明治32年)−(明治29年) δH	(明治29年)−(明治18年) δH	位 置	B. M.	δH	δH	位 置
J. 229	0·0	0·0	大阪	220	− 5·4	− 0·9	
228.1	− 6·4				− 6·6		
228	− 3·2	+16·6		219	− 5·9	−16·6	
J. 472	− 0·6		吹田		− 7·9		
227	− 2·6	+21·8		218	− 5·9	−14·0	伏見
	+ 0·2				− 2·5		
226	+ 1·4	+ 9·2		217	− 6·7	+21·2	
	− 0·8		茨木		− 4·3		
225	− 2·9	+ 7·4		216	− 6·5	+23·4	京都
	− 5·5				− 7·3		
224	− 6·9	+ 9·3		215	− 8·1	+23·6	
	− 9·5				−12·7		
223	−11·5	+14·0		214	− 7·6	+20·2	
	−12·2				+ 3·6		
222	−12·3	+20·8	島本町櫻井	J. 213	0·0		大津
	−10·2						
221	− 8·5	+15·5					

第 十 一 表

自丹後與謝郡喜多村至山城國葛野郡川勝寺村

(明治 25 年)—(明治 20 年)

B. M.	δH	位 置	B. M.	δH	位 置
239	0·0	京都	1277	改埋	
1299	− 3·7		1276	+ 1·9	
1298	− 1·1		1275	± 0·0	檜山村中臺
1297	− 3·1		1274	改埋	
1296	− 2·7		1273	−60·8	檜山村井尻
1295	− 4·1		1272	−56·9	
1294	−11·1		1271	−56·3	
1293	−14·4	篠	1270	−64·9	
1292	−10·8		1269	−64·3	
1291	− 5·0		1268	−59·7	
1290	− 8·5	龜岡	1267	−50·4	
1289	−10·5		1266	−57·2	
1288	− 4·2		1265	−46·4	
1287	改埋		1264	−39·6	
1286	− 2·4		1263	−38·4	
1285	− 7·9		1262	−42·9	
1284	− 1·9		1261	−43·1	
1283	− 4·3		1260	−37·3	
1282	− 1·8		1259	−35·0	
1281	− 2·9		1258	−33·6	
1280	− 7·5		1257	−37·4	福知山町
1279	− 7·0		1256	−35·1	福知山西北2 km. 下川口
1278	− 7·1				

17. *Vertical Displacements of Bench Marks in the Nôbi and other Districts.*

By Katsuhiko Mutô and Yukio Kawabata,

The Imperial Japanese Military Land Survey.

While the results of some of the relevellings of this region made by the Imperial Japanese Military Land Survey are not yet published, in those that have been published adjustments were made so that the values of the two ends of the routes shall coincide. But since in studying relative vertical changes of bench marks it is preferable to take the observed instead of the adjusted values, we have compared the observations that were made on the following routes:—

No.	Routes		Period	Remarks
1	From Takanawa	to Okitu	1883, 84~1896	Not published
2	„ Yoyohata	„ Okitu	1884~1895 1995~1903	„
3	„ Okitu	„ Okazaki	1885~1900	Adjusted
4*	„ Okazaki	„ Kanô	1885~1894, 95	„
5*	„ Kanô	„ Hiyosi	1889~1894 1895, IV „ , V	„
6*	„ Kanô	„ Simobara	1890~1894, 95	„
7*	„ Atuta	„ Tu	1888~1895	„
8*	„ Ootu	„ Kanô	1885~1896 1896~1899	„
9*	„ Oosaka	„ Ootu	1885~1896 1896~1899	„
10	„ Tango Kitamura	„ Yamasiro Kawakatumura	1887~1892	Not published

* As those routes traverse the region devastated by the great Nôbi earthquake, the results of the relevellings were published after making the adjustments in the manner above mentioned.

Figs. 2-11 show the relative displacement thus obtained, assuming that the initial

bench marks of these routes had not been displaced, since the absolute vertical changes of the bench marks could not be determined. Strictly speaking, these figures merely show the tiltings that occurred on these levelling routes during the period between the two observations.

Carl Bamberg's precise levels were used in these levellings.

18. *Fluggeschwindigkeit einiger vulkanischen Bomben.*

von Takeo MATUZAWA.

(Vorgelegt 21. Feb. 1933.—Eingegangen 20. März 1933.)

1. Einleitung.

Vulkanische Auswürflinge liefern uns manchmal sehr wichtige zahlenmäßige Daten über die betreffende Vulkantätigkeit. Mehrere Autoren[1] hatten bisher gelegentlich manche Fälle der Bombenflüge diskutiert. C. G. Knott, C. M. Smith, und G. Wagener hatten auf den Luftwiderstand von Projektil achtgegeben, aber einigermaßen qualitativ. Andere Autoren hatten diese Wirkung für die erste Annäherung vernachlässigt. Aber die Wirkung des Luftwiderstandes auf Projektil beträgt manchmal bedeutend groß, besonders wenn Auswürflinge klein sind, so daß man sie nicht als Kleinigkeit vernachlässigen kann; es sei denn daß der Endzustand von Auswürflinge ungenau bekannt ist. Im vorliegenden ist hauptsächlich der Luftwiderstand berücksichtigt.

2. Allgemeines über Luftwiderstand.

Nach dem experimentellen Untersuchung von Reynolds wissen wir daß der Luftwiderstand eines Körpers proportional ist dem Quadrat der relativen Geschwindingkeit der Luft, der Luftdichte und dem senkrecht zur Bewegungsrichtung genommenen Maximalquerschnitt und zwar der Proportionalitätsfaktor von der geometrischen Form des Körpers und von der Reynoldsschen Zahl abhängt.

Formen von vulkanischen Bomben sind natürlich-mannigfaltig, aber im folgenden will ich die Berechnung auf die kugelförmigen Körper beschränken.

Für kleine Reynoldszahlen (etwa $R=Vd/\nu<1$) gilt das Gesetz von Stokes

1) E. ODLUM, *Transactions of the Seismological Society of Japan*, **13** (1890), 21-40.
S. SEKIYA and Y. KIKUCHI, *ibid.*, **13** (1890), 139-222.
C. G. KNOTT and C. M. SMITH, *ibid.*, **13** (1890), 223-254.
G. WAGENER, *ibid.*, **13** (1890), 254-257.
F. OMORI, *Seismological Journal of Japan*, **19** (1894), 1-22.
F. OMORI, *Bull. Imp. Earthq. Invest. Commit.*, **7** (1914), 11-26.
T. NOMITU and M. NAMBA, *Mem. Coll. Sci., Kyôto Imp. Univ.*, [A] **15** (1932), 215-233.
T. FUKUTOMI, *Disin* (Erdbeben), **1** (1929), 852-862.

$$W=3\pi\mu d V,$$

wo, μ : Viskosität der Luft, ρ: Dichte der Luft, $\nu=\frac{\mu}{\rho}$, d: Durchmesser der Kugel, V: relative Geschwindigkeit des Körpers ist.

Wenn die Reynoldssche Zahl zunimmt, geht der Luftwiderstand zum Newtonschen Gesetz über, nämlich

$$W=K\rho d^2V^2,$$

wo, K von $R=Vd/\nu$ abhängt.

Für K gibt es bisher eine Menge Untersuchungen, z. B. Wieselsberger,[2] H. S. Allen,[3] L. Schiller[4] u. a., G. A. Shakespear,[5] F. S. Schmidt,[6] G. Cooke,[7] R. G. Lunnon,[8] Z. Aka[9] u. a. u. s. w.

Aus diesen Untersuchungen kann man wie folgt zusammenfassen; für etwa $1{\cdot}0<R<10^2$, nimmt $\log K$ ungefähr geradlinig für $\log R$ ab, für $10^3<R<1{\cdot}24\times10^5$ ist K praktisch konstant und beträgt etwa 0·12, dann nimmt K plötzlich ab und nimmt den Wert etwa 0·08. Im folgenden wird dieser Wert angenommen, obgleich K für ungeheur großen Wert von R unbekannt sei.

3. Bewegungsgleichungen einer Kugel in der Atmosphäre.

Als Koordinaten sind die x-Achse horizontal auf dem Meeresniveau und die y-Achse vertikal nach oben genommen.

In der Atmosphäre herrscht das Barometergesetz, nämlich

$$dp=-\rho g dy,$$

und die Zustandsgleichung der Gase ist $p=R\rho T$, wo R die Gaskonstante für ein Gramm Luft ist. In der Troposphäre nimmt die Lufttemperatur gewöhnlich ungefähr geradlinig ab, also

$$T=T_0-\beta y.$$

Nach Substitution ergibt sich

$$R(T_0-\beta y)d\rho=-\rho(g-R\rho\beta)dy=-\rho g dy.$$

$R\rho\beta$ kann gegen g vernachlässigt werden, weil $R\rho\beta=0{\cdot}000189$ g. wenn

2) K. WIESELSBERGER, *Z. F. M.*, (1914), 140.
3) H. S. ALLEN, *Phil. Mag.*, [V] **50** (1900), 323-338; 519-536.
4) L. SCHILLER u. A. DÖGE, *Phys. Zeits.*, **13** (1912), 234-240.
5) G. A. SHAKESPEAR, *Phil. Mag.*, **28** (1914), 728-734.
6) F. S. SCHMIDT, *Ann. d. Phys.*, **61** (1920), 633.
7) G. COOKE, *Phil. Mag.*, **39** (1920), 350-352.
8) R. G. LUNNON, *Phil. Mag.*, **47** (1924), 173-182.
9) Z. AKA, M. TAIMA und S. SIMIDU, *Journ. Aeron. Res. Inst., Tôkyô Imp. Univ.*, **49** (1928), 240-243.

$\beta = 0{\cdot}005\,°\text{C/m.}$, wie gewöhnlich der Fall ist. Wenn man für $y=0$, $\rho=\rho_0$, $p=p_0$ setzt,

$$\rho=\rho_0\left(1-\frac{\beta}{T_0}y\right)^{A-1},$$

wo $A=\dfrac{\rho_0 T_0}{p_0\beta}g$.

Wenn der Temperaturdradient vernachlässigt werden kann, was manchmal der Fall ist, kann man durch Grenzübergang direkt finden

$$\rho=\rho_0 e^{-\frac{\rho_0}{p_0}gy},$$

weil $$\lim_{\beta\to 0}\left(1-\frac{\beta}{T_0}y\right)^{\frac{\rho_0 T_0}{p_0\beta}g}=e^{-\frac{\rho_0}{p_0}gy}.$$

Dieser Ausdruck ist nichts anders als die Barometerformel. Die Bewegungsgleichungen für eine Kugel mit Durchmesser d und Dichte ρ' lauten also

$$\ddot{x}+\lambda\left(1-\frac{\beta}{T_0}y\right)^{A}\dot{x}^2=0, \quad \ldots\ldots\ldots\ldots\ldots\ldots (1)$$

$$\ddot{y}+\delta\lambda\left(1-\frac{\beta}{T_0}y\right)^{A}\dot{y}^2+g=0, \quad \ldots\ldots\ldots\ldots\ldots\ldots (2)$$

wo $\delta=+1$ für $\dot{y}\geqq 0$, $\delta=-1$ für $\dot{y}\leqq 0$, und $\lambda=\dfrac{6}{\pi}\dfrac{K}{d}\dfrac{\rho_0}{\rho'}$.

In gewöhnlichen Fällen könne man ruhig das Stokesgebiet außer acht lassen, denn in der Atmosphäre beschränkt sich die Geschwindigkeit für kleine Reynoldszahl nur auf ganz kleines Bereich, insofern es Auswürflinge mit Durchmesser über mehreren Zentimetern betrifft, z. B. für eine Kugel mit $d=40\,\text{cm.}$ in der Atmosphäre 0°C ($\nu=0{\cdot}1325$)

$$R=302\,v, \qquad v, \text{ in cm/sek.}$$

Noch eine Bemerkung über die Luftdichte bei der Explosion soll hinzugefügt werden. In der Explosionswolke sind eine Menge Aschen vermengt, und die Dichte muß erheblich größer sein als in der freien Atmosphäre. Aber die Bombe läuft der durch Aschen vermengten Luft vor, abgesehen von der kleinen Strecke in der Nähe vom Krater. Darum kann dieser Umstand außer acht gelassen werden.

4. Integration der Gleichungen.

Zuerst muß man die Gleichung für die Vertikalbewegung lösen und dann kommt die Lösung für die Horizontalbewegung. Die einmalige Integration lautet wie folgt,

$$e^{-\frac{2\beta\lambda T_0}{\beta(1+A)}\left(1-\frac{\beta}{T_0}y\right)^{1+A}}\dot{y}^2+2g\int_0^y e^{-\frac{2\beta\lambda T_0}{\beta(1+A)}\left(1-\frac{\beta}{T_0}y\right)^{1+A}}dy=C, \quad \ldots\ldots(3)$$

wo C eine Integrationskonstant ist.

Weitere Integration ist theoretisch nicht schwer, aber praktisch nicht bequem. Es sei viel zweckmäßiger mechnisch zu integrieren in einzelnem Fall. In dieser Weise kann man $\left(1-\frac{\beta}{T_0}y\right)^A$ als Funktion von Zeit t finden, und dann die x-Gleichung finden, nämlich

$$\dot{x}=\frac{{}_0V_x}{1+\lambda_0 V_x\int_0^t\left(1-\frac{\beta}{T_0}y\right)^A dt}, \quad \ldots\ldots(4)$$

$$x={}_0V_x\int_0^t\frac{dt}{1+\lambda_0 V_x\int_0^t\left(1-\frac{\beta}{T_0}y\right)^A dt}, \quad \ldots\ldots(5)$$

wo ${}_0V_x$ die x Komponente der Anfangsgeschwindigkeit ist.

Durch Grenzübergang $\beta\to 0$ ergibt sich für den Fall ohne Temperaturgradient,

$$e^{-\frac{2\beta\lambda}{\alpha}e^{-\alpha y}}\dot{y}^2+2g\int_0^y e^{-\frac{2\beta\lambda}{\alpha}e^{-\alpha y}}dy=C, \quad \ldots\ldots(3')$$

$$\dot{x}=\frac{{}_0V_x}{1+\lambda_0 V_x\int_0^t e^{-\alpha y}dt}, \quad \ldots\ldots(4')$$

$$x={}_0V_x\int_0^t\frac{dt}{1+\lambda_0 V_x\int_0^t e^{-\alpha y}dt}, \quad \ldots\ldots(5')$$

wo $\alpha=\frac{\rho_0}{p_0}g$, C eine Integrationskonstant ist.

5. Ausbruch des Asamayama vom 18. September 1929.

T. Fukutomi[10] hatte die vertikale Geschwindigkeit der Bomben im Endzustand geschätzt durch Untersuchungen von mehreren durch Bombeneinschlag erzeugten kegelförmigen Höhlen in der Nähe von Yunotaira ungefähr 2070 m. weit horizontal und 430 m. unten vom Krater. Die Kraterhöhe ist 2430 m. ü. d. M. Nach ihm war die Vertikalkomponente der Endgeschwindigkeit 216 m/Sek. Obgleich er bei der Schätzung sehr weite Extrapolation gemacht hatte, hier werde ich diesen Wert als

10) T. FUKUTOMI, *loc. cit.*, 1)

richtig annehmen um die große Wirkung des Luftwiderstandes klar zu machen. Der Durchmesser der von ihm untersuchten Bomben reiht sich 20~80 cm. Als Mittelwert ist $d=40$ cm. angenommen.

Am 18. Sept. 1929 gegen 1 a. m. im Zentraljapan herrschten im Durchschnitt $p_0=765$ mm. und $T_0=283°\mathrm{K}$, also $\rho_0=0{\cdot}001256$. Der Temperaturdradient in der Nähe vom Vulkan war leider nicht genau bekannt. Das war immer der Fall bei den in dieser Arbeit geschilderten Beispielen. Darum will ich den gewöhnlichen Wert $\beta=0{\cdot}005°\mathrm{C/m}$. annehmen.

Also,

$$\frac{\beta}{T_0}=0{\cdot}00001765,$$

$$A=6{\cdot}83,$$

$$\lambda=1{\cdot}920\times10^{-4}\,\mathrm{m}^{-1}.$$

Nun ist die Endvertikalgeschwindigkeit $-\dot{y}_{1900}=216$ m/Sek. gegeben, wo das Präfix $(-)$ die nach unten gerichtete Geschwindigkeit bedeutet und das Suffix die Höhe gibt, wo die Geschwindigkeit beobachtet wurde.

Aus Gleichung (3) ergibt sich allgemein

$$-\dot{y}_y^2=e^{-\frac{2\lambda T_0}{\beta(1+A)}\left(1-\frac{\beta}{T_0}y\right)^{1+A}}\left\{e^{\frac{2\lambda T_0}{\beta(1+A)}\left(1-\frac{\beta}{T_0}h\right)^{1+A}}-\dot{y}_h^2-2g\int_h^y e^{\frac{2\lambda T_0}{\beta(1+A)}\left(1-\frac{\beta}{T_0}y\right)^{1+A}}dy\right\},\quad(3'')$$

wenn $-\dot{y}_h^2$ gegeben ist.

Die Scheitelhöhe H der Flugbahn wird gegeben aus der Gleichung

$$-\dot{y}_h^2=2ge^{-\frac{2\lambda T_0}{\beta(1+A)}\left(1-\frac{\beta}{T_0}h\right)^{1+A}}\int_h^H e^{\frac{2\lambda T_0}{\beta(1+A)}\left(1-\frac{\beta}{T_0}y\right)^{1+A}}dy.\quad\ldots\ldots\ldots(3''')$$

Wenn einmal H bestimmt wird, dann ist $-\dot{y}_y$ bequemer gegeben durch Gleichung (3''') (statt h soll y eingesetzt werden) als durch (3''),

$$-\dot{y}_y^2=2ge^{-\frac{2\lambda T_0}{\beta(1+A)}\left(1-\frac{\beta}{T_0}y\right)^{1+A}}\int_y^H e^{\frac{2\lambda T_0}{\beta(1+A)}\left(1-\frac{\beta}{T_0}y\right)^{1+A}}dy.$$

In ähnlicher Weise ergibt sich für die nach oben gerichtete Geschwindigkeit $+\dot{y}_y$,

$$+\dot{y}_y^2=2ge^{\frac{2\lambda T_0}{\beta(1+A)}\left(1-\frac{\beta}{T_0}y\right)^{1+A}}\int_y^H e^{-\frac{2\lambda T_0}{\beta(1+A)}\left(1-\frac{\beta}{T_0}y\right)^{1+A}}dy.$$

Für kleine Strecke (Δ) vom Scheitelpunkt kann man bequemer die folgenden Annäherungsformeln benutzen

$$\pm\dot{y}_\Delta=\sqrt{2g\Delta}\left\{1\pm\frac{1}{2}\lambda\Delta\left(1-\frac{\beta}{T_0}H\right)^A\right\},\quad\ldots\ldots\ldots(6)$$

$$\pm t_\Delta = \sqrt{\frac{2\Delta}{g}}\left(1 \mp \frac{1}{6}\lambda\Delta\left(1-\frac{\beta}{T_0}H\right)^4\right), \quad \ldots\ldots\ldots\ldots(7)$$

wo t die Zeit, die nötig ist die Strecke Δ zurückzulegen, bedeutet. Durch mechanische Integration kann man natürlich nicht t_Δ genau bekommen, weil $1/\pm\dot{y}_H$ unendlich wird.

Die Rechenergebnisse sind in der folgenden Tabelle zusammengestellt. (Tabelle I.)

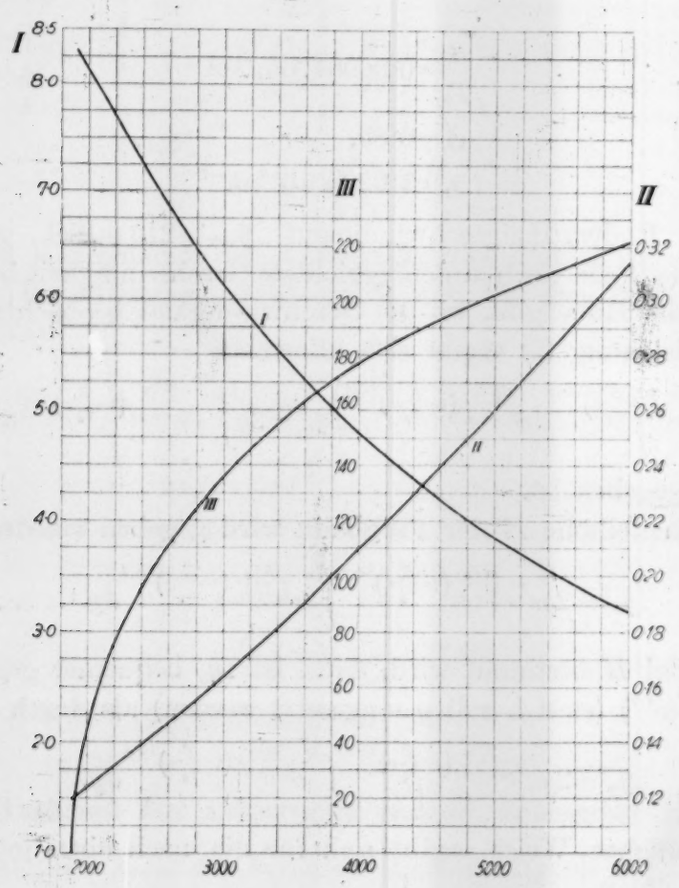

Fig. 1. I: $e^{+\frac{2\lambda T_0}{\beta(1+A)}\left(1-\frac{\beta}{T_0}\right)^{1+A}}$, II: $e^{-\frac{2\lambda T_0}{\beta(1+A)}\left(1-\frac{\beta}{T_0}y\right)^{1+A}}$, III: $-\dot{y}_{y\to 1900}$

Kurve III in Fig. 1 gibt $-\dot{y}_{y\to 1900}$. Die Scheitelhöhe H wird graphisch so bestimmt daß $-\dot{y}_{H\to 1900}=216$. Sie ergibt sich zu 5690 m.

Kurve I und II in Fig. 2 zeigt respektiv $1/_+\dot{y}_y$, $1/_-\dot{y}_y$. Dann wird die Flugzeit $_\pm t$ graphisch integriert mit Hilfe der Annäherung (6) und (7) in der Nähe vom Scheitelpunkt. (Kurve III und IV in Fig. 2.)

Tabelle I.

$$\text{I}: \; e^{+\frac{2\lambda T_0}{\beta(1+A)}\left(1-\frac{\beta}{T_0}y\right)^{1+A}} \qquad \text{II}: \; e^{-\frac{2\lambda T_0}{\beta(1+A)}\left(1-\frac{\beta}{T_0}y\right)^{1+A}}$$

y	$\left(1-\frac{\beta}{T_0}y\right)^A$	I	II	$\int_{1900}^{y} \text{I}\,dy$	$-\dot{y}_{y\to 1900}$	$-\dot{y}_y$	$\int_{y}^{5690} \text{II}\,dy$	$+\dot{y}_y$	$+t$	$-t$
1900	0·7923	8·373	0·1194	00·0	00·0	216				30·19
2000	0·7823	8 125	0·1231	824·9	43·8	215·2				29·73
2430							698·2	313·8	0·00	
2500	0·7348	7·043	0·1420	4617·0	103·8	207 0	688·4	308·0	0 22	27·36
3000	0 6894	6·123	0·1633	7908·0	136·0	196·8	612·1	271·0	1·95	24·88
3500	9·6468	5·403	0·1851	10790	158·8	182·9	525·0	236·0	3·93	22·24
4000	0·6065	4·778	0·2093	13335	177·2	165·5	426·4	199·7	6·24	19·36
4500	0·5683	4 276	0·2339	15598	190·8	142·2	315·6	162·5	9·03	16·09
5000	0·5319	3·846	0·2600	17529	202·5	112·5	192·1	120·3	12·51	12·07
5500	0·4977	3·487	0·2868	19262	212·5	60·5	55·4	61·5	18·16	6·25
5690	0·4855				216·0	00·0	00·0	00 0	24·36	0·00
6000	0 4656	3·180	0·3144	21029	221·8					

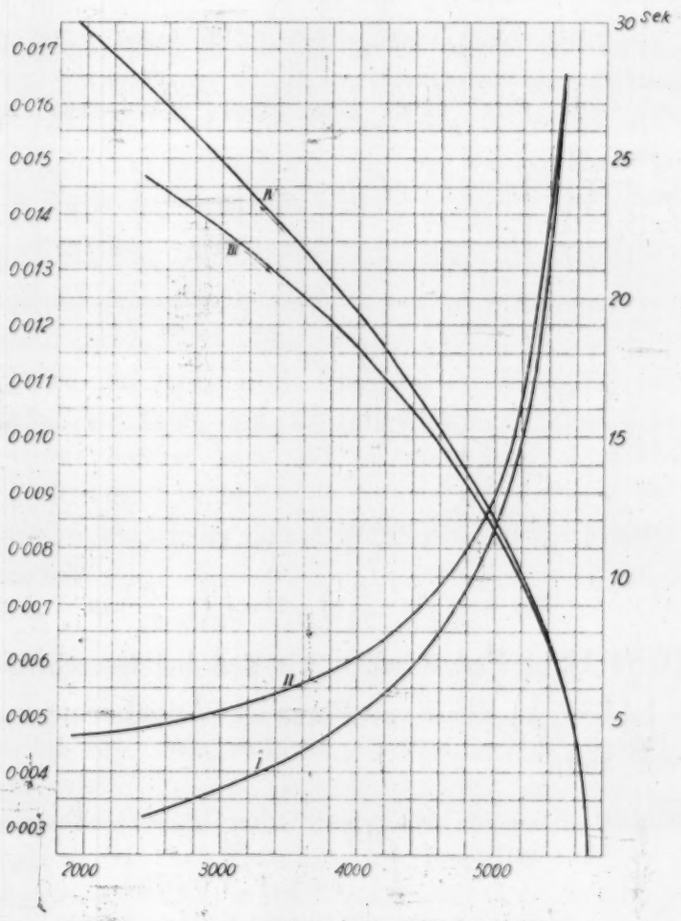

Fig. 2. I: $1/+\dot{y}_y$. II: $1/-\dot{y}_y$. III: $+t$. IV: $-t$.

Die senkrechte Komponente der Anfangsgeschwindigkeit ergibt sich zu 313·8 m/Sek.

So ist die vertikale Bewegung gelöst. Um die horizontale Bewegung zu lösen muß man $\left(1-\frac{\beta}{T_0}y\right)^{\Lambda}$ als Funktion von t zuordnen. (Tabelle II).

Tabelle II.

t	0·00	0·22	1·95	3·93	6·24	9·03	12·57	18·16	24·36
$\left(1-\frac{\beta}{T_0}y\right)^{\Lambda}$	0·7415	0·7348	0·6894	0·6468	0·6065	0·5683	0·5319	0·4977	0·4855
$\int_0^t\left(1-\frac{\beta}{T_0}y\right)^{\Lambda}dt$	0·00	0·1624	1·394	2·717	4·166	5·805	7·752	10·630	13·68
t	30·61	36·43	40·45	43·72	46·60	49·24	51·72	54·09	54·55
$\left(1-\frac{\beta}{T_0}y\right)^{\Lambda}$	0·4977	0·5319	0·5683	0·6065	0·6468	0·6894	0·7348	0·7823	0·7923
$\int_0^t\left(1-\frac{\beta}{T_0}y\right)^{\Lambda}dt$	16·75	19·74	21·96	23·88	25·68	27·44	29·20	30·99	31·35

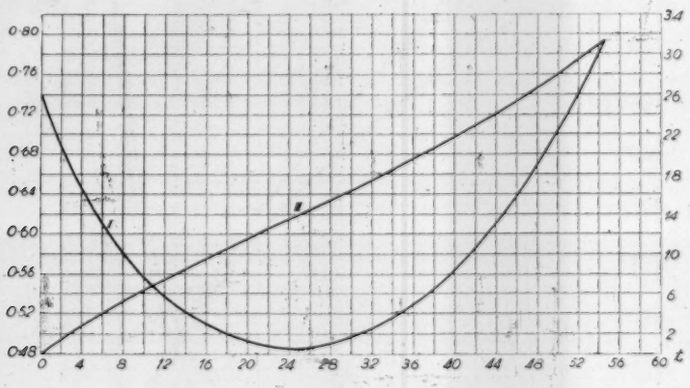

Fig. 3. I: $\left(1-\frac{\beta}{T_0}y\right)^{\Lambda}$. II: $\int_0^t\left(1-\frac{\beta}{T_0}\right)^{\Lambda}dt$.

Aus Kurve II in Fig. 3 sehen wir daß bei Berechnung von Gleichung (5) $\int_0^t\left(1-\frac{\beta}{T_0}y\right)^{\Lambda}dt$ in genügender Annäherung durch $0{\cdot}573\,t$ ersetzt werden kann.

Nun aus

$$2070={}_0V_x\int_0^{54{\cdot}57}\frac{dt}{1+\lambda_0 V_x\times 0{\cdot}573\,t}$$

bekommt man $${}_0V_x=42{\cdot}5\text{ m/Sek.}$$

Also die Horizontalgeschwindigkeit im Endzustand ist

$$_eV_x = 33{\cdot}9 \text{ m/Sek.}$$

Die Rechenergebnisse sind so zusammengefasst wie folgt,

$$_0V_x = 42{\cdot}5 \text{ m/Sek.},$$

$$_+\dot{y}_{2430} = 313{\cdot}8 \text{ m/Sek.},$$

$$H = 5690 \text{ m. also } 3270 \text{ m. vom Krater.}$$

Diese Höhe stimmt mit der Beobachtung der Wolkenhöhe beim Ausbruch überein. T. Fukutomi berechnete ohne Berücksichtigung des Luftwiderstandes $_+\dot{y}_{2430} = 195$ m/sek. und $H = 4300$ m. Wir sehen also daß man bei Berechnung des Anfangszustandes die Wirkung des Luftwiderstandes nicht Vernachlässigen kann.

6. Ausbruch des Asamayama vom 22. Okt. 1911.[11]

F. Omori untersuchte genau die Endzustande der Auswürflinge. Nach ihm ereignete sich dieser Ausbruch um $3^h\ 46^m\ 04^s$ a. m. am 22. Okt. 1911. Im Zentraljapan herrschte damals der atmosphärische Druck ungefähr zu 763 mm. und die Temperatur ungefähr zu 12°C. Die Windgeschwindigkeit erreichte höchstens nur wenige Meter per Sekunde.

In diesem Falle ergeben sich also

$$\rho_0 = 0{\cdot}001248, \qquad T_0 = 285°\text{K}, \qquad p_0 = 763 \text{ mm. Hg.}$$

$$\frac{\beta}{T_0} = 0{\cdot}00001755, \qquad A = 6{\cdot}86, \qquad \lambda = 7{\cdot}34 \times 10^{-5}.$$

Der Durchmesser der von ihm betrachteten Bomben war ungefähr $d = 3{\cdot}5 \approx 100$ cm. Er fand den Einfallswinkel 63° mit dem Horizont. Der Einfallspunkt befand sich 2000 m. weit vom Krater und 490 m. darunter, also 1910 m. ü. d. M.

Damit können wir wieder den Anfangszustand der Bombe berechnen. Erstens haben wir

$$\tan 63° = {}_eV_y / {}_eV_x = 1{\cdot}963,$$

wo $_eV_y$: Vertikalkomponente der Endgeschwindigkeit, $_eV_x$: Horizontalkomponente der Endgeschwindigkeit bedeutet. Zweitens ist gegeben $x = 2000$ m. in Gl. (5). Wir müssen $_eV_y$ bzw. $_eV_x$, $_0V_y$ und $_0V_x$ so finden daß $x = 2000$ m. wird.

Für Berechnung bilde man zuerst die folgende Tabelle (Tabelle III) wie vorher.

11) F. Omori, *Bull. Imp. Earthq. Invest. Commit.*, **7** (1914), 17.

Tabelle III.

$$\text{I}: \; e^{\frac{2\lambda T_0}{\beta(1+A)}\left(1-\frac{\beta}{T_0}y\right)^{1+A}}, \qquad \text{II}: \; e^{-\frac{2\lambda T_0}{\beta(1+A)}\left(1-\frac{\beta}{T_0}y\right)^{1+A}}.$$

y	$\left(1-\frac{\beta}{T_0}y\right)^A$	I	II	$\int_{1910}^{y} \text{I}\, dy$	$-\dot{y}_{y\to 1910}$
1910	0·795	2·259	0·4426	000	00·0
2400	0·745	2·138	0·4677	1077·2	96·6
3000	0·690	2.008	0·4981	2321·0	141·7
3500	0·6475	1·912	0·5231	3301·0	169·0
4000	0·607	1·826	0·5477	4235.0	191.5

Kurve III in Fig, 4 gibt $-\dot{y}_{y\to 1910}$.

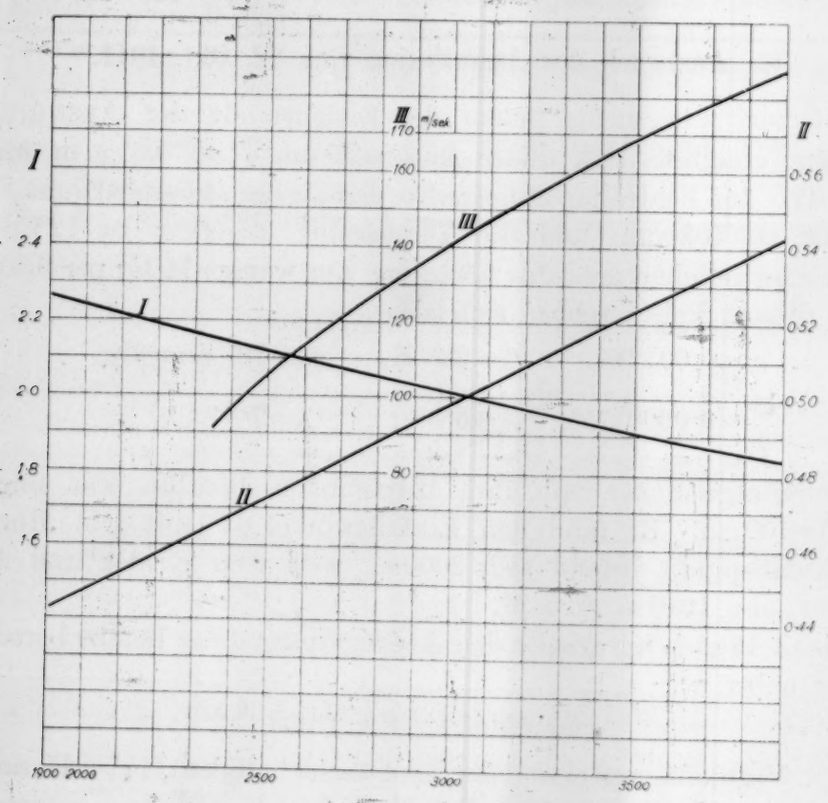

Fig. 4. $\text{I}: \; e^{\frac{2\lambda T_0}{\beta(1+A)}\left(1-\frac{\beta}{T_0}y\right)^{1+A}}$, $\text{II}: \; e^{-\frac{2\lambda T_0}{\beta(1+A)}\left(1-\frac{\beta}{T_0}y\right)^{1+A}}$, $\text{III}: \; -\dot{y}_{y\to 1910}$.

Durch sukzessive Annäherung kann man ${}_eV_y$ u. s. w. finden. Für ${}_eV_y = -\dot{y}_{1910} = 140{\cdot}5$ m/Sek. bzw. ${}_0V_x = 71{\cdot}5$ m/Sek. bekommt man $H = 2985$ m. und ${}_0V_y = +\dot{y}_{2400} = 110{\cdot}3$ m/Sek. Man erhält wieder $\left(1-\frac{\beta}{T_0}y\right)^A$ als

Funktion von t. (Tabelle IV).

Tabelle IV.

t	000	4·57	10·7	16·85	25·3
$\left(1-\frac{\beta}{T_0}y\right)^4$	0·745		0·692		0·795
y	2400	2800	2985	2800	1910

Kurve II in Fig. 5 zeigt diese Funktion.

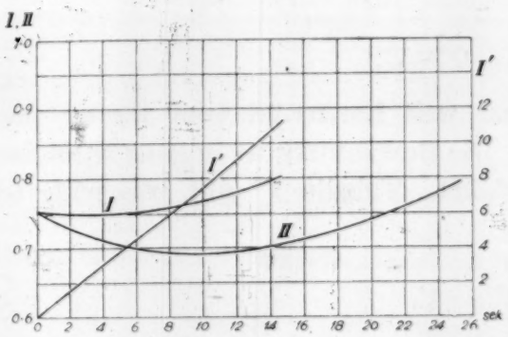

Fig. 5.

I: $\left(1-\frac{\beta}{T_0}y\right)^4$, I': $\int_0^t\left(1-\frac{\beta}{T_0}y\right)^4 dt$.

Ausbruch des Asama vom 12. Aug. 1913.

II: $\left(1-\frac{\beta}{T_0}y\right)^4$

Ausbruch des Asama vom 22. Okt. 1911.

Durch Einsetzen von ${}_eV_x=71{\cdot}5$ m/Sek. bekommt man ${}_0V_x=79{\cdot}1$ m/Sek. Dann aus Gl. (5) ergibt sich $x=1995$ m., was genügend genau ist.

Die Zusammenfassung gibt also

${}_0V_x=79{\cdot}1$ m/Sek., ${}_0V_y=110{\cdot}3$ m/Sek., ${}_eV_y=140{\cdot}5$ m/Sek.,
${}_eV_x=71{\cdot}5$ m/Sek., und $H=2985$ m. ü. d. M.

Die Flugzeit ist $\tau=25{\cdot}3$ Sek. Die zusammengesetzte Anfangsgeschwindigkeit ist ${}_0V=135{\cdot}7$ m/Sek. Nach F. Omori ergibt sich ohne Berücksichtigung des Luftwiderstandes ${}_0V=134$ m/Sek. und $\tau=26$ Sek. In diesem Falle ist die Abweichung nicht so groß, weil λ ziemlich kleiner ist als im vorigen Falle. Das kommt natürlich von der Größe der Bombe. Man sehe also, daß für die Bomben von solcher Größe die Wirkung des Luftwiderstandes praktisch vernachlässigt werden kann, wenn die Flugstrecke nicht ungewöhnlich weit ist.

7. Ausbruch des Asamayama vom 12. Aug. 1913.

Dieser Ausbruch wurde auch von F. Omori[12] eingehend untersucht. Nach ihm ereignete sich dieser Ausbruch um $7^h\ 45^m\ 08^s$ am 12. Aug. 1913. Einfallswinkel der Auswürflinge war 44°. Der Durchmesser betrug ungefähr 15 cm. Die Windgeschwindigkeit war kleiner als 4 m/Sek. Der atmosphärische Druck und die Temperatur in Zentraljapan waren respektiv etwa 753 mm. Hg und 25°C.

Also

$$\rho_0=0{\cdot}001173, \qquad \lambda=4{\cdot}78\times10^{-4}$$

$$A=6{\cdot}84, \qquad \frac{\beta}{T_0}=0{\cdot}00001678,$$

$$\tan 44^\circ={}_eV_y/{}_eV_x=0{\cdot}9657.$$

Der Einfallspunkt war 2080 m. weit horizontal vom Krater und 500 m. darunter (1900 m. ü. d. M.) Die Berechnung ist in ganz ähnlicher Weise wie in Abschnitt (5) ausgeführt. Tabelle V gibt, was nötig ist für diese Berechnung.

Tabelle V.

$$\text{I}: \quad e^{+\frac{2\lambda T_0}{\beta(1+A)}\left(1-\frac{\beta}{T_0}y\right)^{1+A}}, \qquad \text{II}: \quad e^{-\frac{2\lambda T_0}{\beta(1+A)}\left(1-\frac{\beta}{T_0}y\right)^{1+A}}.$$

y	$\left(1-\frac{\beta}{T_0}y\right)^A$	I	II	$\int_{1900}^{y}\text{I}\,dy$	$-\dot{y}_{y\to1900}$
1900	0·8011	281·5	0·003553	000	00 0
2000	0·7916	262·4	0·003810	27195	43·4
2200	0·7732	225·9	0·004427	76025	72·7
2400	0·7548	194·4	0·005144	118060	90·7
2460	0·7496				
2500	0·7462	181·3	0·005517	136850	97·7

Kurve III in Fig. 6 zeigt $-\dot{y}_{y\to1900}$.

Für $-\dot{y}_{y\to1900}={}_eV_y=95{\cdot}0$ m/Sek. bzw. ${}_eV_x=98{\cdot}3$ m/Sek. erhält man $H=2460$ m. und ${}_0V_y=+\dot{y}_{2400}=34{\cdot}8$ m/Sek. $\left(1-\frac{\beta}{T_0}y\right)^A$ als Funktion von t ist gegeben in der folgenden Tabelle. (Tabelle VI.)

12) F. OMORI, *Bull. Imp. Earthq. Invest. Comm.*, **7** (1914), 14–15.

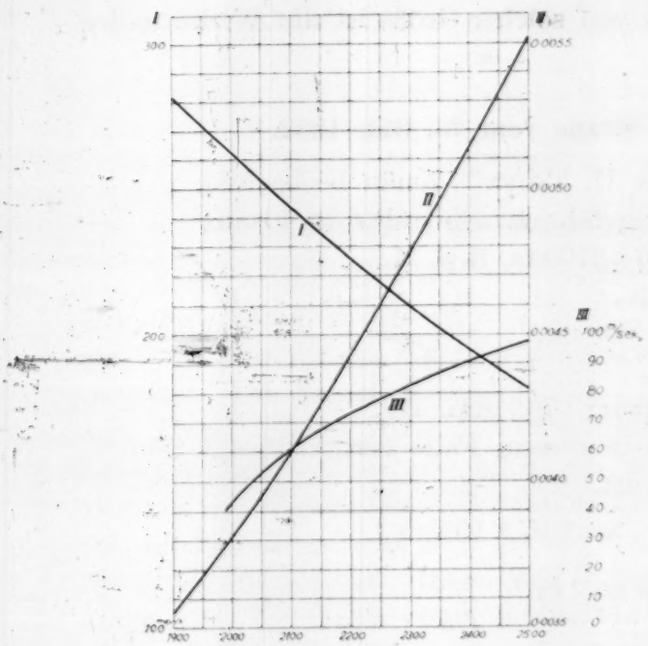

$$\text{I}: \quad e^{\frac{2\lambda T_0}{\beta(1+A)}\left(1-\frac{\beta}{T_0}y\right)^{1+A}},$$

$$\text{II}: \quad e^{-\frac{2\lambda T_0}{\beta(1+A)}\left(1-\frac{\beta}{T_0}y\right)^{1+A}},$$

$$\text{III}: \quad -\dot{y}/y \to 1910.$$

Fig. 6.

Tabelle VI.

t	000	3·47	7·00	11·04	13·58	14·68
$\left(1-\frac{\beta}{T_0}y\right)^A$	0·7548	0·7496	0·7548	0·7732	0·7916	0·8011
y	2400	2460	2400	2200	2000	1900
$\int_0^t\left(1-\frac{\beta}{T_0}y\right)^A dt$	000	2·618	5·276	8·362	10·35	11·23

Kurve I und I′ in Fig. 5 machen diese Rechenergebnisse anschaulich.

In ähnlicher Weise wie im Abschnitt (6) ergibt sich

$$_0V_x = 208 \text{ m/Sek.},$$

$$x \fallingdotseq 208\int_0^{14\cdot68} \frac{dt}{1+4\cdot78\times10^{-4}\times0\cdot766\,t\times208} = 2050 \text{ m},$$

womit man zufrieden sein kann.

Die Anfangsgeschwindigkeit ergibt sich zu $_0V = 211$ m/Sek. Ohne Berücksichtigung des Luftwiderstandes ist $_0V = 131$ m/Sek., bzw.

${}_0V_x=118{\cdot}2$ m/Sek. Für Bomben von solcher Größe ist die Wirkung der Luft sehr bedeutend.

8. Ausbruch des Sirane vom 23. Okt. 1932.

Dieser Ausbruch wurde von H. Tsuya[13] genau beobachtet.
Die Größe der Bomben: ungefähr armvoll also $d \fallingdotseq 40$ cm.,
die Scheitelhöhe: $H=2800\sim3100$ m. ü. d. M.
die Kraterhöhe: $h=2100$ m.,
die Reichweite: höchstens 500 m.,
die Lufttemperatur: 11°C.,
der Luftdruck in Zentraljapan: 768 mm. Hg.

Der Temperatureffekt kann in diesem Falle vernachlässigt werden, weil die Flugstrecke nicht weit ist.

$$\rho_0=0{\cdot}00126, \qquad \lambda=1{\cdot}97\times10^{-4}\,\mathrm{m}^{-1},$$

$$\alpha=\frac{\rho_0}{p_0}g=1{\cdot}25\times10^{-4}\,\mathrm{m}^{-1}.$$

Da in diesem Falle die Scheitelhöhe gegeben ist, ist die Berechnung von ${}_0V_y$ nicht schwer.

Aus Gleichung (3') ergeben sich

$${}_+\dot{y}_y^2={}_0V_y^2=2ge^{\frac{2\lambda}{\alpha}e^{+\alpha y}}\int_y^H e^{-\frac{2\lambda}{\alpha}e^{-\alpha y}}dy,$$

und

$$x={}_0V_x\int_0^t\frac{dt}{1+\lambda\,{}_0V_x\int_0^t e^{-\alpha y}dt}.$$

${}_0V_y=126$ m/Sek. für $H=2800$ m.,
${}_0V_y=154$ m/Sek. für $H=3100$ m.

Die Flugzeit für $H=2800$ m. ist angeordnet wie folgt (Tabelle VII.)

Tabelle VII.

t	000	3·9	7·2	11·7	16·25	19·65	23·9
y	2100	2500	2700	2800	2700	2500	2100

13) H. TSUYA, *Bull. Earthq. Inst. Res.*, **11** (1933), 82-112.

Also

$$_0V_x \approx \frac{e^{0.731\,\lambda x}-1}{0.731\,\lambda t} = 21.7 \text{ m/Sek.},$$

$$_0V = 128 \text{ m/Sek.}$$

9. Ausbruch des Bandaisan vom 15. Juli 1888.

Dieser Ausbruch wurde von mehreren Autoren[14] beschrieben und diskutiert. Nach S. Sekiya und Y. Kikuchi begann die erste Explosion um $7^h\ 45^m$ an diesem Tage, dann folgten 15~20 Explosionen hintereinander. Die Explosionswolkensäule erreichte die Höhe 1280 m. über dem Krater, dessen Höhe ü. d. M. ungefähr 1200 m. ist. Die damaligen meteorologischen Zustände habe ich nicht wissen können wegen des Mangels der Materialien. Darum will ich hier annehmen 755 mm. Hg für den Luftdruck und 20°C als die Lufttemperatur für $y=0$ m. in der Nähe von Bandaisan. Diese sind ungefähr die Mittelwerte in dieser Jahreszeit. Die Größe einer Bombe, die sie beschrieben, war etwa 50 cm.

Also

$$\lambda = 1.464 \times 10^{-4}\ \text{m}^{-1}.$$

$$A = 6.84$$

Die Berechnung wird in ähnlicher Weise im Abschnitt (8) ausgeführt. Die Rechenergebnisse sind in Tabelle VIII gegeben.

Tabelle VIII.

$$\text{I}: \quad e^{\frac{2\lambda T_0}{\beta(1+A)}\left(1-\frac{\beta}{T_0}y\right)^{1+A}}, \qquad \text{II}: \quad e^{-\frac{2\lambda T_0}{\beta(1+A)}\left(1-\frac{\beta}{T_0}y\right)^{1+A}}.$$

y	$\left(1-\frac{\beta}{T_0}y\right)^A$	I	II	$\int_y^{2480} \text{I}\,dy$	$\int_y^{2480} \text{II}\,dy$	$+\dot{y}$	$-\dot{y}$	$+t$	$-t$
1200	0·9795	6·599	0·1515	735·4	227·9	171·5	147·7	000	16·47
1500	0·9744	6·110	0·1636	5447	180·7	147·0	132·1	1·90	14·31
2000	0·9659	5·425	0·1843	2563	93·67	99·8	96·2	5·96	9·99
2200	0·9625	5·165	0·1936	1404	55·88	75·2	73·0	8·26	7·61
2400						39·8	39·5	11·79	4·04
2480	0·9577	4·865	0·2056	000	000	000	000	15·81	000

14) E. Odlum, *Trans. Seism. Soc.*, Japan., **13** (1890), 21–40.
S. Sekiya und Y. Kikuchi, *ebenda.*, **13** (1890), 139–222.
C. G. Knott and C. M. Smith, *ebenda.*, **13** (1890), 223–257.

In diesem Falle kann man I und II über y stückweise integrieren bequemer als graphisch, weil die Krümmungen dieser Kurven verhältnismäßig klein sind. Kurve I und II in Fig. 7 zeigen $1/_{-}\dot{y}_y$ und $1/_{+}\dot{y}$, woraus man die Flugzeit mechanisch integrieren kann.

In der Nähe vom Scheitelpunkt benutzt man natürlich die Näherungsformeln.

Die Anfangsvertikalgeschwindigkeit $_{+}\dot{y}_{1200}$ ergibt sich zu 171·5 m/Sek.

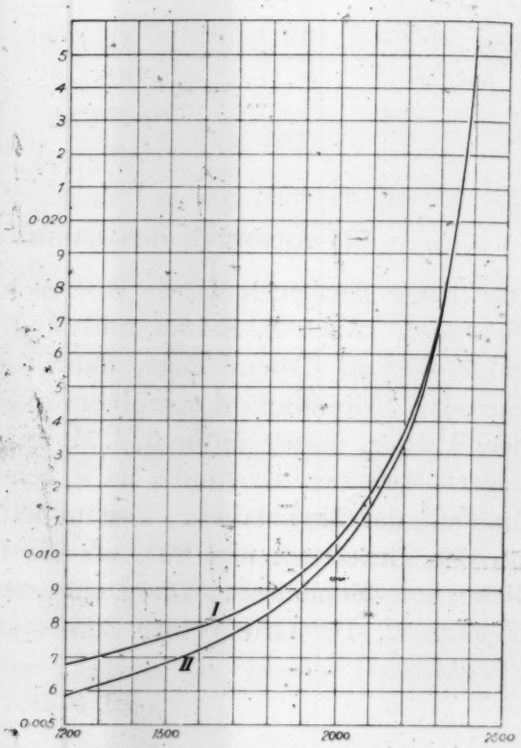

Fig. 7. I: $\frac{1}{-\dot{y}_y}$, II: $\frac{1}{+\dot{y}_y}$.

10. Ausbruch des Azumasan vom 4. Juni 1893.

Dieser Ausbruch wurde von F. Omori[15] beschrieben. Nach ihm war die Maximalreichweite der Bomben ungefähr $1\frac{1}{2}$ km. Die Bombengröße war 15 cm. ca. Die Kraterhöhe ist 1600 m. ü. d. M. Als meteorologischen Elementen für diese Jahreszeit nehme ich an $p=760$ mm. und $T_0=15°C$.

Daraus ergeben sich

$$\rho_0=0{\cdot}001226, \qquad \lambda=5{\cdot}00\times10^{-4},$$

$$A=6{\cdot}83, \qquad \frac{\beta}{T_0}=0{\cdot}00001735.$$

In diesem Falle ist die Maximalreichweite gegeben. Es ist nicht einfach, daraus die Anfangsgeschwindigkeit zu berechnen, weil die Maximalreichweite nicht nur von dem Anfangswinkel sondern auch von der Anfangsgeschwindigkeit abhängt. Die Tabelle (Tabelle IX), die zur Berechnung nötig ist, ist gegeben wie folgt.

Kurve III und Kurve IV in Fig. 8 geben respektiv $_{+}\dot{y}_{1600\to y}$ und $_{-}\dot{y}_{y\to 1600}$.

15) F. OMORI, *Seism. Journ.*, Japan, 19 (1894), 1-22.

Tabelle IX.

$$\text{I}: e^{\frac{2\lambda T_0}{\beta(1+A)}\left(1-\frac{\beta}{T_0}y\right)^{1+A}}, \qquad \text{II}: e^{-\frac{2\lambda T_0}{\beta(1+A)}\left(1-\frac{\beta}{T_0}y\right)^{1+A}}$$

y	$\left(1-\frac{\beta}{T_0}y\right)^A$	I	II	$\int_{1600}^{y} \text{I}\,dy$	$\int_{1600}^{y} \text{II}\,dy$	$-\dot{y}_{y\to 1600}$	$+\dot{y}_{1600\to y}$
1600	0·8252	366·8	0·002725	000	000	000	000
1700	0·8151	337·0	0·002960	35290	0·2843	43·4	45·2
1800	0·8059	312·2	0·003203	67740	0·5924	60·2	65·2
1900	0·7953	287·4	0·003480	97710	0·9266	72·3	81·6
2000	0·7856	265·6	0·003765	125360	1·2888	81·8	96·2
2100	0·7759	245·4	0·004075	150910	1·6808	89·7	110·0
2200	0·9619	227·5	0·004390	174560	2·1040	96·6	122·9
2400	0·9584	195·4	0·005117	216850	3·0547	107·5	148·0

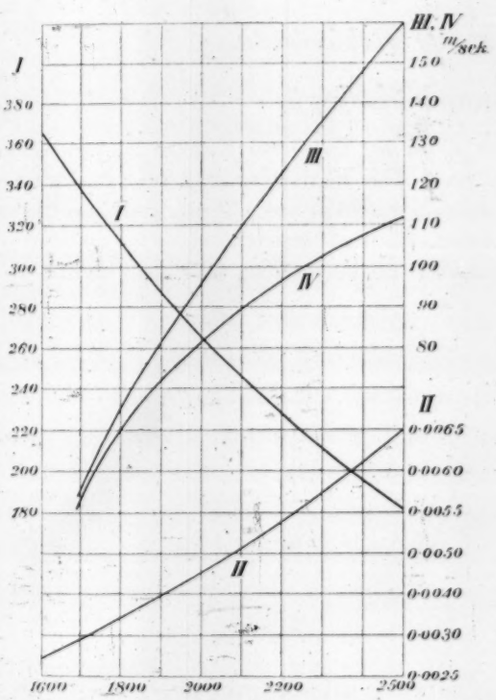

$$\text{I}: e^{\frac{2\lambda T_0}{\beta(1+A)}\left(1-\frac{\beta}{T_0}y\right)^{1+A}},$$

$$\text{II}: e^{-\frac{2\lambda T_0}{\beta(1+A)}\left(1-\frac{\beta}{T_0}y\right)^{1+A}},$$

III: $+\dot{y}_{1600\to y}$, IV: $-\dot{y}_{y\to 1600}$

Fig. 8.

Nach umständlichen Berechnungen ergibt sich das folgende Ergebnis. (Tabelle X)

Tabelle X.

Anfangsgeschwindigkeit = 148·5 m/Sek.

θ; Anfangswinkel mit dem Horizont.

x; Reichweite in m.

H; Scheitelhöhe in m.

τ; Flugzeit in Sek.

θ	x	H	τ
43°	1518	2035	9·99
44°	1529	2050	10·11
45°	1510	2065	10·12

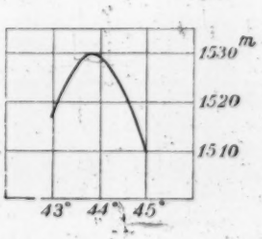

Fig. 9.

$\theta - x$ Kurve ist in Fig. 9 eingetragen. Daraus kann man sehen, daß in diesem Falle die Maximalreichweite dem Anfangswinkel 43°·8 entspricht. Als die erste Annäherung könne man die Anfangsgeschwindigkeit 148·5 m/Sek. annehmen.

11. Zusammenfassung.

Die obigen Rechenergebnisse lehren uns, daß in gewöhnlichem Falle vulkanischer Ausbrüche die Wirkung des Luftwiderstandes auf den Bombenflug bedeutend groß ist, wenn die betreffende Bombe klein ist, genauer zu sagen, wenn deren Durchmesser etwa unter 50 cm. ist. Dagegen wenn der Durchmesser etwa ein Meter übertrifft, kann man in gewöhnlichen Fällen der Explosionen die Luftwirkung vernachlässigen.

---

18. Aru Kwazandan no Hikôsokudo.

Nukigaki (Zusammenfassung.)

Kwazandan wo Tama no Katati to site Kûki no Teikô wo Kangae ni irete sono Hikôsokudo wo sirabeta. Tyokkei 1 m. gurai no Ookisa ni nareba hutû no Hunkwa no Baai niwa madu Kûki no Teikô wa Kangaenakumo sasitukae nai. 50 cm. gurai no Tama dewa 2 km. mo tobuto daibu Eikyô ga arawareru.

Nippon no Kwazan no Rei dewa tobidasu Toki no Hayasa wa ôkii Baai de 200-210 m/Sek. gurai no mono de aru.

19. *Gasdruck bei einigen vulkanischen Ausbrüchen in Japan.*

von Takeo MATUZAWA.

(Vorgelegt 21. Feb. 1933.—Eingegangen 20. März 1933.)

Vulkanische Explosionen können nur durch die adiabatische Ausdehnung vulkanischer Gase erzeugt werden. Die Gase trennen sich vom Magma ab. Dabei handelt es sich allgemein um einen sehr komplizierten Fall der Phasenregel mit mehrfachen Bestandteilen.

Die Temperatur des Magmas in der Nähe von der Erdoberfläche ist allgemein ziemlich genau bekannt. Dagegen ist der Innendruck der Gase, die bei solcher Temperatur mit dem betreffenden Magma im Gleichgewicht stehen, nicht genau bekannt. Dieser Druck spielt natürlich sehr wichtige Rolle in der mechanischen Wirkung bei vielen vulkanischen Erscheinungen, besonders in der Nähe von der Erdoberfläche.

Die Anfangsgeschwindigkeit der Auswürflinge bei vulkanischen Explosionen hängt hauptsächlich von dem Gasdruck ab. Umgekehrt wenn man diese Geschwindigkeit wissen kann, kann man sie unter geeigneten Annahmen berechnen.

Vor dem Moment einer Explosion wird das Bodenteilchen, das den obersten Teil des betreffenden Schlotes verstopft hat, praktisch als locker angesehen, nämlich der elastische Widerstand des Krustenteils kann praktisch vernachlässigt werden. In gewöhnlichen Fällen werden die Vertikalstrecke im Krater, die die Masse zurückgelegt hat bis sie ganz frei vom Gasdruck ist, und die Druckänderung durch die Verschiebung der Masse im Schlot vernachlässigt. Dann lautet eben so wie in der Hydrodynamik der Energiesatz

$$p=\frac{1}{2}\rho v^2,$$

wo p der Druckunterschied zwischen dem Innenraum und dem Aussenraum, ρ die Dichte der Masse und v die Geschwindigkeit des Auswürflings bedeutet.

T. Fukutomi[1] wandte eine andere Formel $p=\rho v^2$ an auf die Schätzung von p, was mir aber ungeeignet scheint.

1) T. FUKUTOMI, *Disin* (Erdbeben), 1 (1929), 852-862.

Am anderen Orte berechnete ich[2] die Anfangsgeschwindigkeit einiger Bomben. Daraus kann man den Druck p schätzen. Die Rechenergebnisse werden wie folgt tabellarisch zugeordnet, abgesehen vom Fall des Asamayama vom 18. Sept. 1929, weil die außerordentliche Extrapolation bei der Schätzung der Endgeschwindigkeit der Bomben zu einiger Vorsicht mahnt.

Tabell I.

h bedeutet die Höhe der Magmasäule, die dem Druck p entspricht.
Bei allen Fällen ist $\rho = 2{\cdot}5$ angenommen.

	Ausbruch des Asama vom 22. Okt. 1911	Ausbruch des Asama vom 12. Aug. 1913.	Ausbruch des Sirane vom 23. Okt. 1932	Ausbruch des Bandaisan vom 15. Juli 1888	Ausbruch des Azumasan vom 4. Juni
v m/sek.	135·8	210·8	154	171·5	148·6
p at.	227	548	293	363	272
h m.	938	2270	1210	1500	1125

Zum Vergleich will ich auf die Resultate von F. von Wolff Bezug nehemen, wer auf die Schätzung des Druckes eine ganz andere Tatsache, nämlich die adiabatische Ausdehnung der vulkanischen Gase anwandte.

Tabelle II.

Ausbruch	Gasdruck at.	Ausbruch	Gasdruck at.
Krakatau 1883	425·0	Cotopaxi 1877	134·0
Katmai 1912	195·5	Santorin 1925	123·4
Santa Maria, San Salvador	444·7	Stromboli 1923	1·67
Vesuv 1906	266·0	Kilauea	3·367
Mt. Pelé 1902	123·0	La Galera. Columbien 1925	444·7
Lassen Peak 1914	69·4		

2) T. MATUZAWA, *dieses Bull.*, 329–346.
3) F. von WOLFF, „Handbuch der Geophys," Berlin Geb. Bornträger (1930), 228–229.

Wir sehen also auch in diesen Rechenergebnissen, daß der maximale Wert des Gasdruckes vor vulkanischen Explosionen ungefähr rund 450 at. ist. Hier liegt die Vermutung nahe, daß dieser Wert des Gasdruckes 450–500 at. der Innendruck der Gase sei, die mit Magma, dessen Temperatur etwa 1200° C ist, in der Nähe von der Erdoberfläche im Gleichgewicht stehen.

Bei den von Dana erwähnten halbvulkanischen Explosionen, die durch den Zutritt größerer Wassermassen zu dem noch heißen Schlot eines schwach tätigen Vulkans ausgelöst werden, soll das Problem etwas anders sein. Der kritische Zustand des Wassers lautet wie folgt:

Die kritische Temperatur = 374° C,
der „ Druck = 217·7 at.,
die „ Dichte = 0·4.

Die Ausbrüche des Sirane, des Bandaisan oder des Azumasan standen wahrscheinlich im Zusammenhang mit diesem kritischen Druck des Wassers. Wenn Wasserdampf im kritischen Zustand erhitzt wird ohne Volumenänderung bis zur Temperatur 1200° C, dann wird der Druck bis 495 at. erhöht, der ungefähr dem oben erwähnten Maximalwert entspricht, was bemerkenswert sei, obgleich die Rolle des Wassers bei Explosionen sehr bestritten ist.

Der Druck 548 at. entspricht einer Magmasäule von 2270 m. (Tabelle I). Die Magmatemperatur ändert sich natürlich mit der Tiefe, und dementsprechend auch der Innendruck der Gase. Aber er bleibt wahrscheinlich in derselben Größenordnung innerhalb mehererer Kilometer unter der Erdoberfläche. Also liegt eine Vermutung nahe, daß die Gase, die mechanisch nach außen durchbrechen können, höchstens innerhalb ca. 2·5 km. unter der Erdoberfläche entstammen können.

---

19. Hunkwa no Toki no Gas no Aturyoku.

Nukigaki.

Kwazandan no Tobidasu Hayasa kara sono Toki no Gas no Aturyoku wo kaisan site mita. Ookii Baai de 450–500 Kiatu gurai to naru. Korewa Wolff ga Gas no Dannetu-Bôtyô wo tukatte dasita mono to nite iru. Suizyôki tono Kwankei mo ronzite aru.

20. *Earthquakes of the Kwantô District.*

By Takao KODAIRA,

Earthquake Research Institute.

(Read Dec. 20, 1932.—Received March 20, 1933.)

Introduction.

Since the violent earthquake of September 1, 1923, which shook the southern part of the Kwantô district, the science of Seismology has made considerable progress in Japan. To enable better observations several new stations, equipped with improved or newly designed seismographs, have been established by the Earthquake Research Institute of the Tôkyô Imperial University. With the increased and more accurate data thus made available, many new studies in fields hitherto unexplored or insufficiently investigated have been prosecuted.

This paper is merely an attempt to examine these newly acquired data. It discusses the general characteristics of earthquakes that trouble the Kwantô region, their activities, and the distribution of the seismic foci during the period between 1924 and 1931.

Variation of the Yearly Seismic Frequency.

Although in the north-eastern part of Japan, the sea floor of the Pacific off the Hokkaidô, the Tôhoku, and the Kwantô districts shows marked activity, the first two are relatively quiet, so far as the land is concerned. As to the Kwantô, over 500 shocks are recorded a year, which number, in 1931, the year of the severe Titibu earthquake of September 21, rose to 1481. The yearly frequency of sensible Kwantô earthquakes since 1924 is shown in the following table.

Table I.

Year	1924	1925	1926	1927	1928	1929	1930	1931
Frequency	504	247	187	176	221	168	213	360

The yearly diminution in the frequency of sensible shocks since 1924 indicates the waning influence of the great 1923 earthquake.

The yearly frequency of sensible shocks in Tôkyô, the center of the

Kwantô district, may be seen from the following table.

Table II.

Year	1914	1915	1916	1917	1918	1919	1920	1921	1922
Frequency	19	49	24	34	25	24	12	12	57
Year	1923	1924	1925	1926	1927	1928	1929	1930	1931
Frequency	—	128	77	58	72	81	50	92	82

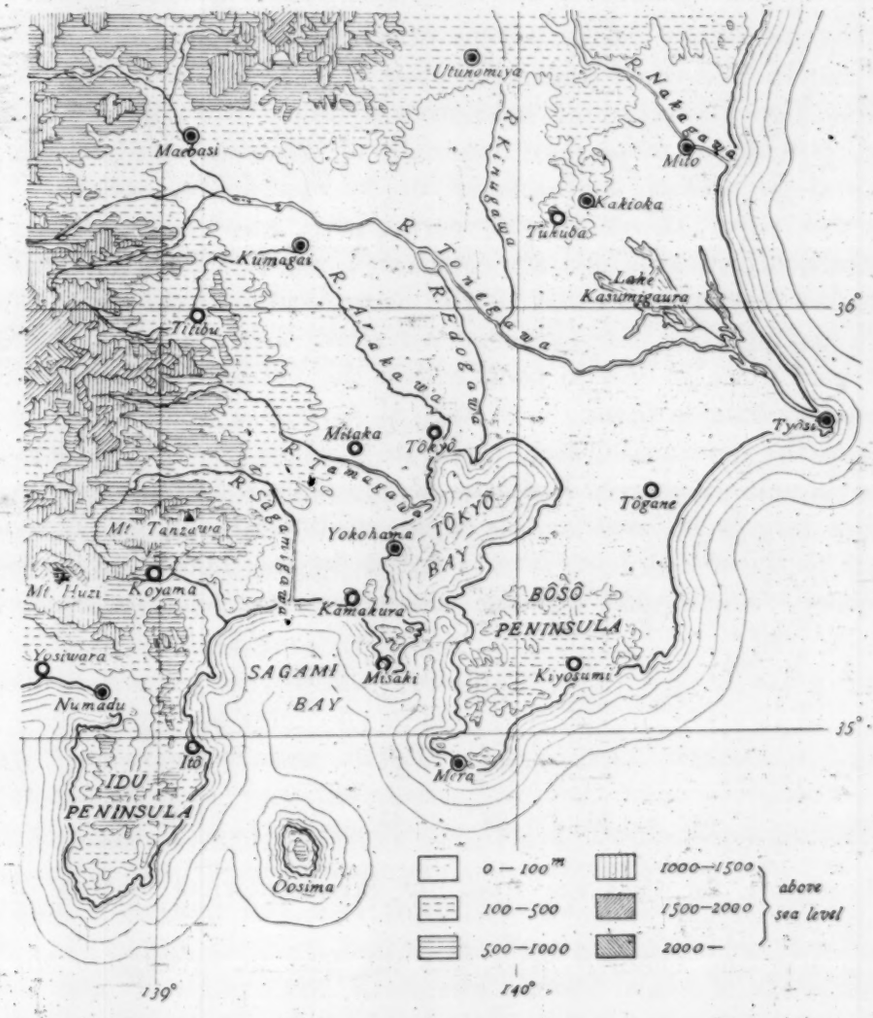

Fig. 1. Geographical features of the Kwantô District.
○ Seismological Station. ◉ Local Meteorological Observatory.

This table gives an idea of the great difference in seismic activities before 1923 and after, and shows how strong has been the influence of that severe earthquake of 1923 on the seismicity of the district in question during the years that followed.

Epicentral Distribution.

An ideal method of studying the seismic activity of any particular region would be to find the epicentres of all earthquakes that occur there, both sensible and insensible. But, in practise these determinations cannot accurately be made with the present network of stations and their equipments for observation, because only one or two stations could record the insensible shocks. Some of the stations may miss even the fainter shocks that come under the class of perceptible shocks. Under these conditions, determining epicentres is largely a matter of approximating, so that not more than one-tenth of the number of seismic foci determined for sensible earthquakes can be regarded as accurate.

In this paper, therefore, only earthquakes whose origins have been seismometrically determined are considered, all small earthquakes and earthquakes that have occurred in the margins of our network or outside of them having been disregarded. We shall then find that the earthquakes tend more or less to pack within the net and are scarse in the margins and outside them.

As to the determined foci, those deduced by stations belonging to the Earthquake Research Institute of the Tôkyô Imperial University will most largely be used in this paper, while references will frequently be made to those that have been deduced by the Local Meteorological Observatory. Earthquake number whose foci have been determined.

Table III.

Year	1924	1925	1926	1927	1928	1929	1930	1931
Frequency	33	25	40	43	51	28	30	57

The datum for 1931 are from the Seismometrical Report of this Institute.

The late Dr. Omori,[1] who was the first to investigate the dis-

1) F. OMORI, *Seismological Notes of the Imperial Earthquake Investigation Committee*, No. 2 (1922).

tribution of earthquake origins in this district, in examining the sensible earthquakes of Tôkyô during the period between 1914 and 1921, noticed that the earthquakes there originated chiefly from three regions, (1) the Bôsô peninsula; (2) the drainage of the rivers Tonegawa and Kinugawa; (3) the Tanzawa mountainland and the Sagami Bay and vicinity. According to Mr. Yasuda,[2] the immediate after-shocks of the earthquake of September 1, 1923, occurred almost in the same regions as found by Omori.

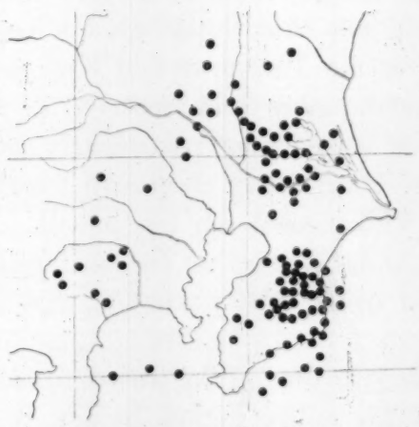

Fig. 2. Distribution of the epicentres in the period 1914–1921. (after Omori)

Fig. 3. Distribution of the epicentres in Sept., 1923. (after Yasuda)

During September frequency was greatest in the Bôsô peninsula, with Sagami Bay and vicinity ranking next in order, although the individual shocks were severer in Sagami Bay, where the main shock had occurred. The Tonegawa-Kinugawa regions, which were the very active in the preceding period were now relatively quiet.

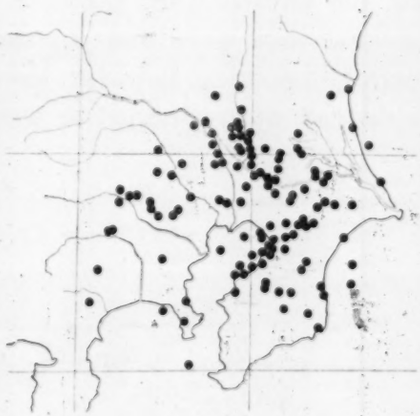

Fig. 4. Distribution of the epicentres in the period Oct.-Dec., 1923. (after Yasuda)

In October, November and December of the same year the distribution greately changed. A few shocks originated in the Tanzawa mountainland and in Sagami Bay, and fairly severe ones in the southern half of the Bôsô peninsula, but the drainage valleys—the Tonegawa and Kinugawa regions began to show activity,

2) 保田柱二 震災豫防調査會報告 第百號 (甲) (1924).

while Musasi plain and the northern part of Tôkyô Bay and vicinity, which had hitherto been very quiet, rapidly became active. The wane of energy in the Bôsô peninsula, from south to north, had however been noticed already in September.

The late Dr. Omori, in his investigations, largely used the observed results for Tôkyô with reference to those for Mito and Tyôsi, and determined the epicentres by means of the duration of the preliminary tremors and the direction of the initial motion, without paying much attention to the focal depth. The result was that, although his determinations of the origin of earthquakes of the Tonegawa and Kinugawa region were fairly correct, those for earthquakes that occurred to the south of this region are supposed to show large errors, particularly those of Tôkyô Bay, where, as will be shown later, fairly deep-seated earthquakes are known to occur. Working with present day equipments and improved methods of observation it is doubtful whether the earthquakes set down by Omori as having originated in the Bôsô peninsula, had not actually originated in Tôkyô Bay.

The epicentral distribution for each year during the period between 1924–1931 are shown in Fig. 5 and for the entire period in Fig. 6, in which the depths are also given.

We can see from this that the regions of seismic activity were not fixed, but shifted from place to place every year, with the result that sometimes they were seen in the same localities as in 1925 and 1928. Generally speaking however the earthquakes throughout the period in this district were confined to the lowlands, rarely occurring in the high

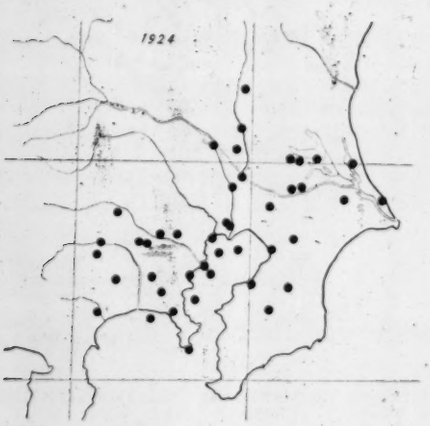

Fig. 5 a.

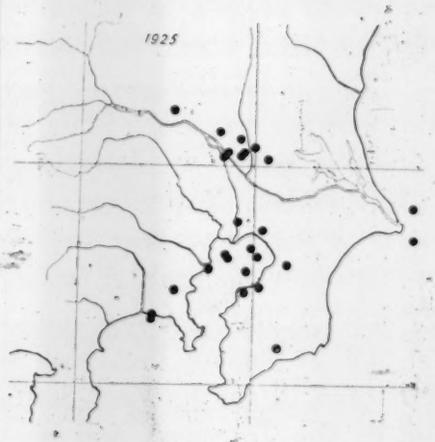

Fig. 5 b.

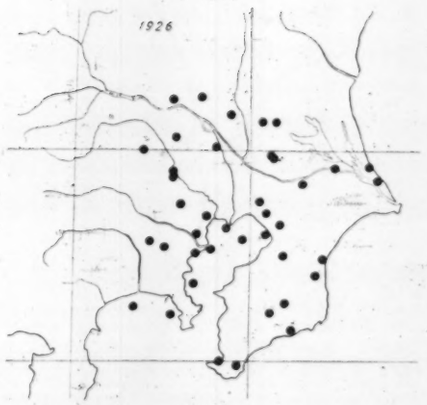

Fig. 5 c.

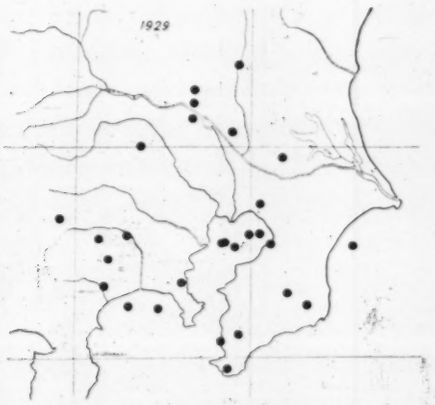

Fig. 5 f.

Fig. 5 d.

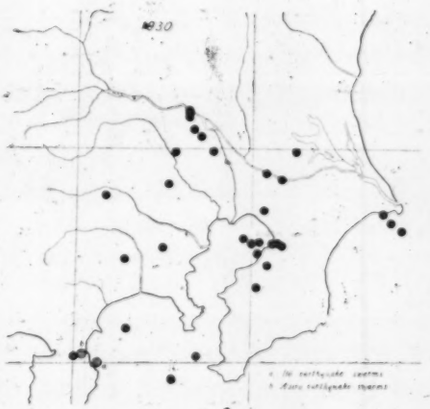

Fig. 5 g.

Fig. 5 e.

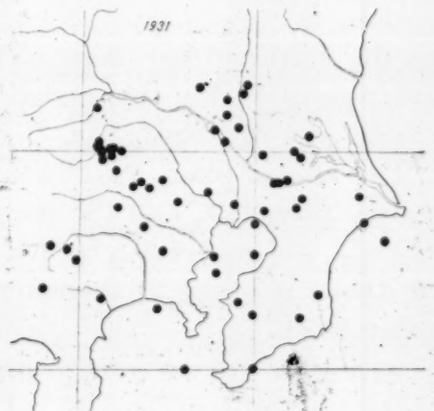

Fig. 5 h.

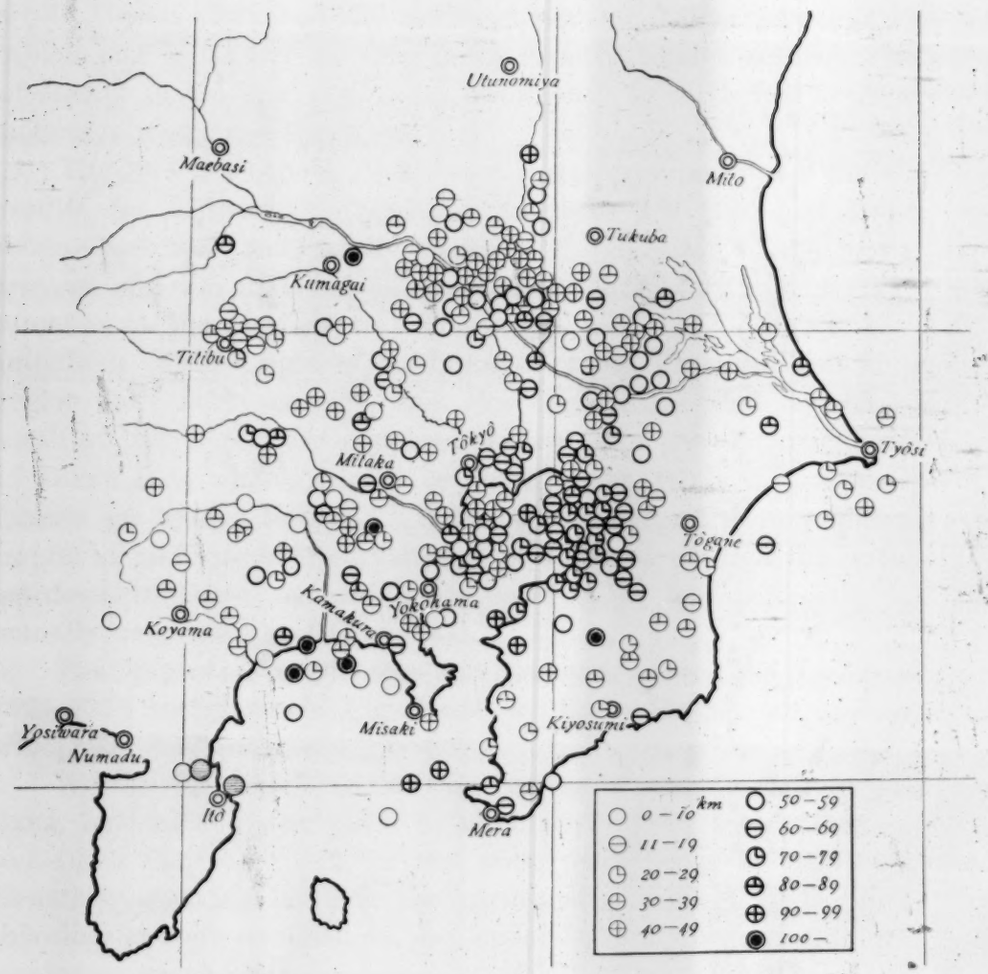

Fig. 6. Distribution of the epicentres in the period 1924–1931.

mountainous regions, especially in the Kwantô and Mikuni ranges, which form the northern and western boundaries of this district. The most active regions during this period were the Tonegawa-Kinugawa and the northern part of Tôkyô Bay.

The Musasi plain, the Tama upland, the Tanzawa mountainland, the Bôsô peninsula, and the neighbourhood of lake Kasumigaura were uniformly and moderately active. The comparatively dense distribution near Titibu is owing to the severe earthquake of September 21, 1931 and its after-shock.

In Fig. 6 will be noticed two quiet regions in the lowlands, south of Mito and north of Tôgane, where no epicentres appear. In the latter region, as a matter of fact, no earthquake of any consequence occurred

during this period, whereas in the former, small shocks often originated in the neighbourhood of Kakioka and Hinuma, although the one of June 1, 1930, near Mito, is seen to have been severe, however, owing to the difficulty of accurately determing their origins on account of their small magnitude and marginal position, these earthquakes are not considered in these discussions.

Depth Distribution of the Seismic Origins.

As an aid in the quest for the cause of earthquakes in any region, a study of the vertical distribution of seismic origins is of the utmost importance. Studies made of such distributions in the case of the Tango earthquake[3] and in those of the Itô earthquake swarms[4] by Mr. Nasu have given remarkable results.

We shall now try to get the depths from which the earthquakes of this district originated. The next Table gives the frequency according to depths of origin of 318 earthquakes whose foci were determined.

Table IV.

Depth	0–10 km.	11–19	20–29	30–39	40–49	50–59	60–69	70–79	80–89	90–99	100–
Frequency	16	14	35	49	69	43	42	26	10	6	6

It will be seen that the number of shocks gradually increase with depth of foci, attaining maximum at 40–49 km., where it is 69, whence it deminishes with depth.

Fig. 6 shows that the focal depths of earthquakes of a certain region keep on the whole to the same order of depth. To illustrate, those originating in Tôkyô Bay generally do so at depths greater than 50 km., while most of those in the Tonegawa-Kinugawa region come from depths of the order of 40 km. For earthquakes that have originated in the Tanzawa mountainland, Sagami Bay, and the Bôsô peninsula, the depths are much under 30 km.

Generally speaking the origins are deepest for earthquakes that originate under the northern part of Tôkyô Bay, getting shallower as they originate from the margin of this district, while the very deep earthquakes, over 100 km., originate under the mouth of the river

3) 那須信治 地震研究所彙報 6 (1928), 7 (1928).

4) N. Nasu, F. Kishinouye and T. Kodaira, *Bull. Earthq. Res. Inst.*, 9 (1931).

Sagamigawa.

Next, in order to ascertain the focal distribution in detail, we have tried the method of stereometrical projection, first applied by Mr. Nasu to the investigation of after-shocks of the Tango earthquake. We shall assume two hypothetical vertical planes, extending N. W. to S. E. and N. E. to S. W. in this district, and project on these planes all the earthquake foci. The result is shown in Fig. 7.

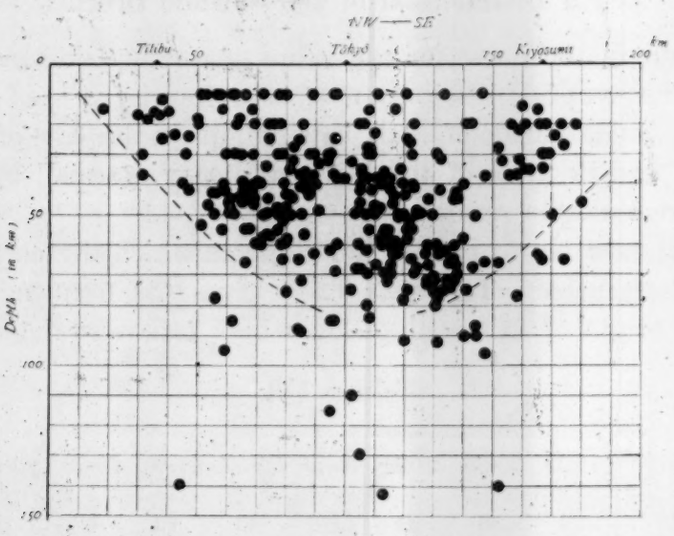

Fig. 7. a. Seismic foci projected on a vertical plane extending N. W. to S. E.

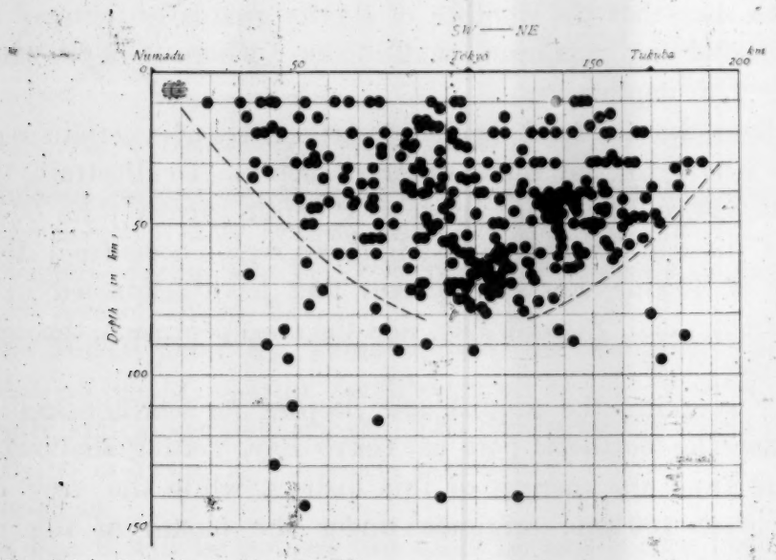

Fig. 7 b. Seismic foci projected on a vertical plane extending S. W. to N. E.

We see from these two projections that, excepting those that ori-

ginated at very great depths, the majority of earthquakes felt in this district originated from a region having the shape of a shallow bowl, whose bottom would be about 70 km. beneath the northern part of Tôkyô Bay, with the slope of the bowl inclined about 45° to the earth's surface. The diameter of the surface of this bowl, from brim to brim, would be over 200 km.

It has been pointed out by Mr. C. Tsuboi, that earthquakes frequently originate from regions having remarkable gravity variation, and the Kwantô region is well known for gravity anomalies. The Tonegawa-Kinugawa region, one of the most seismically active in the Kwantô has also one of the steepest gravity gradient in this locality.

On the other hand, the northern part of Tôkyô Bay, another active region, corresponds to the only place in this district that shows a negative gravity anomaly, notwithstanding that its surroundings show a positive anomaly.

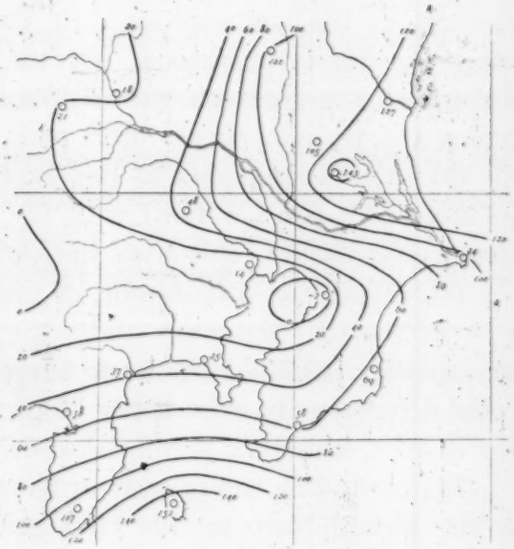

Fig. 8. Distribution of the Gravity Anormalies in the Kwantô District (unit : 10^{-3} cm/sec^2)

The inference from this is that the structure of the earth below 70 km. from the floor of the northern part of Tôkyô Bay differs markedly from that of the regions surrounding it, and that this lack of homogeneity in the structure below the earth's crust interferes with the stability of the upper layers, resulting in numerous fissures in the upper crust with consequent earthquakes along these fissures.

Studies of the focal distribution of the Itô and Aziro earthquake swarms lead us to suppose that these earthquakes give rise to volcanic activities that are not apparent at the earth's surface. The two regions just mentioned lie on the Huzi volcanic belt, which, as shown in Fig. 7 b. corresponds to the vicinity of the intersection of the earth's surface and some of the fissures above mentioned. It may therefore be supposed that these earthquake of the Idu district caused active movements of magma along some of those fissures in the earth's crust.

Summary.

(1). Seismic activity in the Kwantô district before and after the great earthquake of September 1, 1923, shows a marked difference, the influence of the great disturbance continuing to the present day.

(2) The earthquakes in this district have a tendency to originate far more in the lowlands than in the mountainous regions, the latter being very rarely disturbed. Of the former, the Tonegawa-Kinugawa region and the northern part of Tôkyô Bay showed the greatest activity during the period between 1924 and 1931.

(3) The earthquakes of this district originate in a region having the form of a shallow bowl with the northern part of Tôkyô Bay as its bottom and its top level with the earth's surface.

(4) From the distribution of gravity anomaly in this district it is believed that the structure under the northern part of Tôkyô Bay lacks homogeneity, which leads us to suppose that the numerous fissures due to the heterogeneity exist below 70 km., extending into the upper crust of this district, and that earthquakes originate along these fresh fissures.

In conclusion, the present writer wishes to express his sincere thanks to Mr. Nobuji Nasu for his kind guidance. He is also much indebted to Mr. Chuji Yasuda for his kindness in placing the valuable data at the writer's disposal.

---

20. 關東地方の地震

地震研究所 小平孝雄

大正 12 年の關東大地震以來，關東地方に於ける地震觀測の設備は次第に整備し，且つ一方に於ては地震波傳播に關する研究も漸く進歩して來た爲に，此の區域内に發生する地震の震原位置は大震當時に比べると遙かに正確に決定することが出來る樣になつた．

筆者は關東大地震以後の關東地方に於ける地震活動の狀態を詳にする目的を以て，大正 13 年より昭和 6 年に至る 8 ケ年間の當地方に發生した主なる地震に就いて其の震原分布の狀態を調査し，併せて二三の事項に關して考察を試みた．

大正 12 年の關東大地震を境として當地方の地震活動の狀態は著しい相違を示して居る．東京に於ける有感地震の回數を見ても，地震前 9 年間の平均 28 回に對して大正 13 年以後の 8 年間には平均 80 回に上り，明かに同大地震が其後の當地方の地震活動に大きな影響を及ぼして居ることを知る．

鹿島灘，房總半島沖等の太平洋底を除き，當地方内に發生した地震の震央分布の狀態を見るに，概して云へば山岳地方に粗で，低地に密なる傾向がある．殊に隣接地方との境をなす關東山脈，三國

山脈内に於ては非常に數が少ない．最も活潑なる活動を示して居るものは利根川，鬼怒川流域地方と東京灣の北半であつて，丹澤山地，相模灣，多摩丘陵，武藏野，房總半島及び霞浦地方も多少の活動力を示し，屢々地震の發生を見て居る．

震原の深さに關して云へば，當地方の地震は極く地表近くの淺所より 140 km. 位の深所にまで發生して居る．最も多いのは 40 km. 臺である．特別に深所に發生した地震を除けば，一般に東京灣北部に發生する地震が最も深い震原を有し，其れより四方に遠ざかるに連れて次第に發生する地震の震原の深さは淺くなる傾きがある．大體東京灣北部の地表下 70 km. 附近の場所を底とし，地表に對して約 45° 位の傾きを有する緣を持つ一つの椀形の部分内に大部分の地震は發生して居るのを見る．

重力殘餘分布圖によつて見ると，東京灣北部の地震の最も頻發する地方は當地方唯一の負の偏差を有する地方である．この事實は此の區域下の地殼内の構造狀態が周圍の地方とは可成り相違して居ることを暗示して居る．恐らく此の構造の異常に原因して幾つもの裂罅が此處を中心として關東地方の地殼内に生じ，これ等の裂罅に沿ふて關東地方の地震は發生するのではないかと想像される．

21. *Kasokudo-disinkei no Seisaku oyobi Kenkyû.*

TAMARU-Takurô.*

Mokuzi.

Yôryô.
Riron oyobi Sekkei.
Zentai no Sekkei oyobi Ryô no kikagakutekina Kwankei.
Undô no Hôteisiki.
Kasokudo no Domori, Hyô oyobi Kyokusen wo soeru.
Omori no Sekkei.
Omori wo sasaeru Bane no Sekkei.
Teko S_1 S_2 oyobi sonohokano Bubun no Sekkei.
Ondo no Eikyô.
Sisin no Hazi no Masatu.
Hokano Seibun wo sirusu Bubun no Eikyô.
Dimen-keisya no Eikyô.
Ziko-sindô no Eikyô.
Hito no kanzinai Disin wo kirokusuru Kikai.
Genzai Sekkei no Kikai, Hiyô, Ryakudu wo soeru.

Yôryô.

1. Koremadeno Disinkei niwa Dimen no Undô no Hen'i wo kirokusuru mono to Sokudo wo kirokusuru mono to aru. Korerano Kikai wa rikigakutekini syuyôna Bubun ni oitewa dôyôna mono de, yôsurunii Disin no saini Dimen no Undô ni narubeku tomonawarenai yôna Omor, wo sôtisi, sore ni taisite Dimen no Hen'i matawa Sokudo wo kirokusuru mono de aru.

Kokoni tukurô to suru Kasokudo-disinkei wa, sorera to mattaku kotonaru Sayô ni motoduite, tyokusetuni Dimen no Undô no Kasokudo wo kirokusuru mono de aru.

---

* Kono Ronbun wa Tamaru Hakusi ga katute watakusi ni kasi-ataerareta mono de aru ga, Konniti dewa Hakusi no Sigoto tosite nokosareta mono no hitotu to natta sidai de aru. Hakusi wa Taisyô 6 nen ni Nippon Sûgaku-Buturi Gakkwai ni oite, mata Syôwa 2 nen ni Teikoku Gakusiin ni oite dôyôno Ronbun wo yomareta no de aru. Zensya wa insatusarenaide owari, Kôsya wa Teikoku Gakusiin Kizi [3 (1927), 35] to site kantanna Hôkoku ni todomatte iru. Sitagatte kono Ronbun wa Hakusi no kono Hômen no Kenkyû tosite mottomo kuwasiku kakarete iru mono tosite Neuti ga aru to omou. Hakusi no Kenkyû wo eikyûni tutaetai to omou Hitobito no Kibô kara Ooyake to sareru sidai de aru. Genbun wa Kwanzimaziri de kakareta mono de aru ga nisanno Katagata no Gotyûi ni yori Tauti Hakusi ni onegai site Rôma zi-gaki to nasita mono de aru. (Ishimoto-M.)

2. Ittai, Disin ni okeru Dimen no Undô ni tuitewa, Hen'i yorimo musiro Kasokudo no hô ga syuzyuno Ten de kaette yôyôna Kwankei ga aru yôni omowareru (tatoeba Tatemono no Tagui ga Disin no tameni ukeru Muri wa Kasokudo no Ookisa ni sitagau mono de aru) noni, Hen'i matawa Sokudo no Kiroku kara Kasokudo wo keisansuru koto wa seimituni okonawarenikui kara, tyokusetuni Kasokudo wo kirokusuru Disinkei ga tukurare uru naraba kiwamete yûyôna mono de arô to omowareru.

Sin'anno Disinkei wa kono Imi de omosiroi dake de naku sekkei-oyobi zituyôzyônimo, koremadeno Disinkei ni kurabete, (a) Higasi-nisi, Minami-kita, Ue-sita sanbôno Undô wo tada hitotuno Omori wo tukatte, sikamo mattaku dôyôna Sôti wo tukatte kakase uru koto, (b) koremadeno Disinkei ga huantei ni tikai Sôti de aru ni hansite kiwamete anteina Sôti de aru koto, (c) koremadeno Disinkei ni kurabete Ziko-sindô no Samatage wa sukunaku, Ondo-henkwa kara syôzuru Konnan wo sukuu nimo tayasui yôni yosôsareru koto nado, Omomuki no tigau Ten ga sukunaku nai node, katagata Seisaku wo kokoromi kenkyûsuru Neuti ga aru mono to sinzuru.

3. Nao, sin'anno Disinkei niwa, betuno Hômen ni oite atarasii Kuhû wo site aru. Sore wa, koremadeno Kikai dewa Oodisin no tokini Sisin ga amari ôkina Sindô wo nasi ôkuwa Kirokugami no sotoni hadure-satte zyûbunno Yô wo sinai koto wo manukareru tameni, tokubetuna Sôti wo môkete Sisin no Undô-kuiki wo itteino Kagiri inaini tomeru yôni sita koto de aru.

Riron oyobi Sekkei.

4. Kokoni kokoromiyô to omou Kasokudo-disinkei no Mokuteki taru Kasokudo wo kirokusaseru koto no konponno Kangae wa, sôtôni ôkina Situryô wo motu Omori ni Dimen to onazi Undô wo saseru yôni sôtisi, Omori to sore wo sasaeru Bubun to no aidani okonawareru Tikara wo kirokusaseru ni aru. Kono Tikara wa, Omori wo site Dimen to onazi Undô wo saseru ni hituyôna Tikara de aru kara, tadatini Dimen-undô no Kasokudo ni hireisuru no de aru.

Tanni kono Tikara wo kirokusuru dakeno Mokuteki naraba, Omori wo sasaeru no ni Ue-sita, Higasi-nisi, Minami-kita, subete no Hôkô ni oite tuyoi Bane wo tukai, kono Bane no kiwamete tiisai Undô wo hi-zyôni ôkiku site kirokusasereba yoi. Bane ga tuyoi kara, Omori no Undô wa Dimen no Undô to onazi to mirareru (Sa wa sûhyakubunno iti ni suginai yôni tukuru koto ga dekiru), mata Bane no Henkei wa, kore to

Omori to no aidani hataraku Tikara no Henkwa ni hireisuru kara, konoyôni site eru Kiroku wa Kasokudo wo simesu koto ni naru.

5. Kokoni sekkeisite aru Kikai dewa, 3 ni nobeta Mokuteki ga aru node, Omori wo sasaeru no ni tanni tuyoi Bane wo tukau koto ni sezu, Dai 1 Du oyobi Dai 2 Du ni simesu yôna Sikake ni yotte, Omori ni sayôsuru Tikara (sunawati Omori ni Dimen to onazi Undô wo saseru ni hituyôna Tikara) ga ôkiku naru ni sitagatte, Sisin no Kanzi ga sidaini nibuku natte, kono Tikara ga dokomademo ôkiku nareba, Sisin no Muki ga itteino Iti ni tikaduku yôni site aru.

6. Ima kono Kikai no uti, suiheina hitotuno Hôkô no Disindô no Kasokudo wo kirokusuru Bubun dake ni tuite Sikake no Ryakudu wo kakagete rironzyôno Keisan wo suru.

Zentai no Sekkei oyobi Ryô no kikagakutekina Kwankei.

7. Miginono Du(Dai 1 Du) wa Suihei-hôkô no Kasokudo sirusu Bubun no Heimendu wo wo simesu.

O wa Omori, kore no Omosa wo sasaeru Sôt iwa Du ni simesite nai ga, Sayû-hôkô no Undô wo samatagenai yôni site aru.

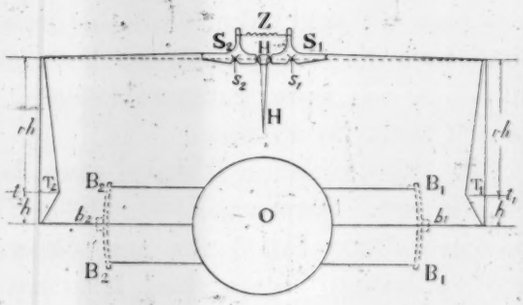

Dai 1 Du.

$B_1 B_1$, $B_2 B_2$ wa Bane, $b_1 b_2$ de koteisite aru.

$T_1 T_2$, wa Teko, $t_1 t_2$ de sasaete aru. Kore to o to no aida wa tawamiyasui Obi de tunaide aru.

$S_1 S_2$ wa sanbôhidino Teko, $s_1 s_2$ ni Siten ga aru. Ippô wa $T_1 T_2$ ni tunagari, ippô wa Zenmaibane Z de tagaini renrakusi, nokoru ippô wa Sisin $H H$ no Entyû-bubun wo hasande, onore no Undô de kono Entyû wo mawasi, sitagatte Hari no Hazi wo ugokasu yôni sôtisite aru.

Zentai no Sôti ga Migi-hidari taisyôni tukutte atte, Turiai no Iti ni oite $T_1 T_2$ no $S_1 S_2$ ni renrakusuru Hazi wo musubu Tyokusen no ueni Siten $s_1 s_2$ no aru yôni, sikamo $S_1 S_2$ no $T_1 T_2$ ni renrakusuru Ten wa kono Tyokusen wo sukosi hadurete iru yôni site aru.

Dimen no Hen'i wo migino hô ni ξ to si, Dimen ni taisite Turiai no Iti kara Omori no ututta Hen'i wo onaziku migino hô ni x to suru.

Teko $T_1 T_2$ no Hidi no Nagasa wo Dai 1 Du ni simesita yôni h, rh to suru.

Teko $S_1 S_2$ ni kwansuru Ryô wo sitano Du (Dai 2 Du) ni sirusu yôni toru.

$x=0$ ni taisite $\theta_1=\theta_2=\theta_0$ to si, x, θ_1, θ_2, Hari no Kwaiten no Kaku θ, Hari no Hazi no Hure X nado no Kwankei wo siraberu.

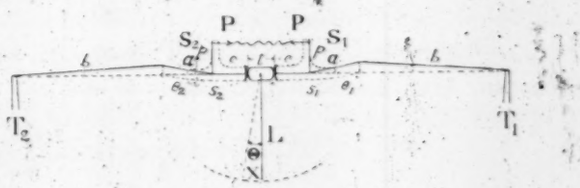

Dai 2 Du.

Omori no Hen'i x ni taisite, $T_1 T_2$ no $S_1 S_2$ ni turanaru Hazi no Hen'i wa rx de, kore wa kiwamete tiisai Ryô de aru. Mata θ_1, θ_2 mo tuneni hanahada tiisai yue,

$$\left(a\cos\theta_0+b\cos\frac{a\theta_0}{b}\right)-\left(a\cos\theta_1+b\cos\frac{a\theta_1}{b}\right)=rx,$$

$$\left(a\cos\theta_2+b\cos\frac{a\theta_2}{b}\right)-\left(a\cos\theta_0+b\cos\frac{a\theta_0}{b}\right)=rx$$

wa tugino yôni naru

$$a\frac{\theta_1^2-\theta_0^2}{2}+\frac{b}{2}\frac{a^2}{b^2}(\theta_1^2-\theta_0^2)=rx,$$

sunawati $\theta_1^2-\theta_0^2=\frac{2r}{a'}x$: Tadasi $a'=a\left(1+\frac{a}{b}\right)$.

Dôyôni $\theta_2^2-\theta_0^2=-\frac{2r}{a'}x$.

Sitagatte $\theta_1^2+\theta_2^2=2\theta_0^2$, $\theta_1^2-\theta_2^2=\frac{4r}{a'}x$.

Mata $X=L\Theta=L\frac{c(\theta_1-\theta_0+\theta_0-\theta_2)}{t}=\frac{Lc}{t}(\theta_1-\theta_2)$,

$\theta_1-\theta_2=\theta$ to kakeba, $\theta_1+\theta_2=\sqrt{4\theta_0^2-\theta^2}$.

Sitagatte $\theta_1=\frac{1}{2}(\sqrt{4\theta_0^2-\theta^2}+\theta)$, $\theta_2=\frac{1}{2}(\sqrt{4\theta_0^2-\theta^2}-\theta)$, $x=\frac{a'}{4r}\theta\sqrt{4\theta_0^2-\theta^2}$;

$$\theta=\theta\frac{t}{c}=X\frac{t}{Lc}.$$

Benri no tameni $\theta=2\theta_0\sin\varphi$

to site Hozyo-no-Kaku φ wo tukaeba,

$$\theta=2\theta_0\frac{c}{t}\sin\varphi, \qquad X=2L\theta_0\frac{c}{t}\sin\varphi,$$

$$\theta_1=\sqrt{2}\theta_0\sin\left(\frac{\pi}{4}+\varphi\right), \qquad \theta_2=\sqrt{2}\theta_0\sin\left(\frac{\pi}{4}-\varphi\right),$$

$$x=\frac{a'}{r}\theta_0^2\sin\varphi\cos\varphi=\frac{a'}{2r}\theta_0^2\sin 2\varphi.$$

Omori ni hoka kara Tikara ga sayôsuru ni yotte syôzuru kyokutanno Atai wa $\theta_2=0$, matawa $\theta_1=0$ no Baai de, tugino tôri,—

$$\theta=\pm\sqrt{2}\theta_0,\ \varphi=\pm\frac{\pi}{4},\ x=\pm\frac{a'\theta_0^2}{2r},\ \Theta=\sqrt{2}\theta_0\frac{c}{t},\ X=\sqrt{2}\theta_0\frac{cL}{t}.$$

Genzaino Sekkei dewa kono kyokutanno x wa 0·00373 cm. ni naru. Kore ni yottemo Omori ga Dimen to issyoni ugokasarete iru to mite yoi koto ga sireru.

[Tyûi: $\theta_1\theta_2$ ga θ_0 wo hedataru koto ga ôku naruto, dôzini okoru ryôhô no Henkwaryô ga hitosiku naku nari, sono kekkwa Sisin no Ziku no Iti ga sukosi sotono hô ni uturu wake de aru ga, kore no tameni Sisin to S_1S_2 to no aidano Renraku (usui Hagane-ita wo tukau) ni Sasitukae wo syôzuru Teido niwa naranai to omowareru.]

Undô no Hôteisiki.

8. Omori no Situryô wo m, Teko $T_1(T_2)$, $S_1(S_2)$, Sisin H no Kwansei-moment wo sorezore M, M', M'' to sureba, Undô-seiryoku T wa

$$T=\frac{m}{2}(\dot{\xi}+\dot{x})^2+2\cdot\frac{M}{2}\left(\frac{\dot{x}}{h}\right)^2+\frac{M'}{2}(\dot{\theta}_1^2+\dot{\theta}_2^2)+\frac{M''}{2}\dot{\theta}^2$$

$$=\frac{m}{2}(\dot{\xi}+\dot{x})^2+\frac{M}{h^2}\dot{x}^2+\left(M'+2M''\frac{c^2}{t^2}\cos^2\varphi\right)\theta_0^2\left(\frac{d\varphi}{dx}\right)^2\dot{x}^2.$$

Tugini Iti-seiryoku V wo kangaeru ni,

Bane B_1B_1, B_2B_2 no x ni taisuru Tikara no Keisû wo onoonono Hazi ni tuki K,

Zenmaibane Z no Tyôryoku wo P,

Teko S_1S_2 wo sasaete iru Bane no θ ni taisuru Nôritu no Keisû wo k

to sureba,

$$V=4\cdot\frac{1}{2}Kx^2+Pp(\overline{\theta_0-\theta_2}-\overline{\theta_1-\theta_0})+\frac{1}{2}k(\overline{\theta_1-\theta_0}^2+\overline{\theta_2-\theta_0}^2)$$

$$=2Kx^2+2(Pp\theta_0+k\theta_0^2)(1-\cos\varphi),$$

Sitagatte Undô no Hôteisiki wa tugino yôni naru.

$$\left\{m+\frac{2M}{h^2}+2\left(M'+2M''\frac{c^2}{t^2}\cos^2\varphi\right)\theta_0^2\left(\frac{d\varphi}{dx}\right)^2\right\}\ddot{x}+\frac{d}{dx}\left[\left(M'\right.\right.$$

$$\left.\left.+2M''\frac{c^2}{t^2}\cos^2\varphi\right)\left(\frac{d\varphi}{dx}\right)^2\right]\theta_0^2\dot{x}^2+4Kx+2(Pp\theta_0+k\theta_0^2)\sin\varphi\frac{d\varphi}{dx}=-m\ddot{\xi}.$$

Kasokudo-disinkei dewa, Ziko-sindô no Syûkî wo tiisaku site, $\ddot{\xi}$ no Atai ga ôku kawaranai utini Ziko-sindô ga sûkwai okonawarete sono heikinno Iti sunawati genzaino ξ ni taisite turiau Iti ga simesareru yôni suru no de aru.

Kasokudo no Domori.

9. Turiau Iti wa

$$4Kx+2(Pp\theta_0+k\theta_0^2)\sin\varphi\frac{d\varphi}{dx}=-m\ddot{\xi}$$

de ataerareru. Soreyueni

$$-\ddot{\xi}=\frac{4K}{m}\frac{a'}{2r}\theta_0^2\sin 2\varphi+\frac{2r(Pp+k\theta_0)}{ma'\theta_0}\frac{\sin\varphi}{\cos 2\varphi},$$

Ima $$\alpha=\frac{4Ka'}{mr}\theta_0^2,\ \beta=\frac{2r(Pp+k\theta_0)}{ma'\theta_0},\ \beta=\mu\alpha$$

to okeba

$$-\ddot{\xi}=\alpha\frac{\sin 2\varphi}{2}+\beta\frac{\sin\varphi}{\cos 2\varphi}=\alpha\left(\frac{\sin 2\varphi}{2}+\mu\frac{\sin\varphi}{\cos 2\varphi}\right).$$

$\ddot{\xi}=0$ wa $\varphi=0$ ni atari, $\ddot{\xi}=\infty$ wa $\varphi=\frac{\pi}{4}$ ni ataru. Sisin no Hazi no Hure no tiisai Sa de arawasareru Kasokudo no Sa nó Wariai wa

$$\frac{\partial(-\ddot{\xi})}{\partial X}=\alpha\left\{\cos 2\varphi+\mu\left(\frac{\cos\varphi}{\cos 2\varphi}+\frac{2\sin\varphi\sin 2\varphi}{\cos^2 2\varphi}\right)\right\}\frac{t^2}{2Lc\theta_0\cos\varphi}.$$

Kono Wariai ga $\varphi=0$ kara $\varphi=\frac{\pi}{4}$ made sidaini masu yôni toru ga yoi. Sore niwa tugino Siki wo itumo (+) ni suru koto ga hituyô de aru.

$$\frac{\partial^2(-\ddot{\xi})}{\partial X^2}=\frac{\alpha t^2}{4c^2L^2\theta_0^2}\frac{\sin\varphi}{\cos\varphi}(2+\sec^2\varphi)$$
$$\times\left[-1+4\mu\left(\frac{1+\cos^2\varphi}{1+2\cos^2\varphi}\cdot\frac{\cos\varphi}{\cos^2 2\varphi}+\frac{1+4\sin^2\varphi\cos^2\varphi}{1+2\cos^2\varphi}\cdot\frac{\cos\varphi}{\cos^3 2\varphi}\right)\right].$$

Kono Siki wa $\varphi=0$ no tokini (+) naraba tuneni (+) de aru. Sore niwa.

$$\mu>\frac{1}{4}.$$

Genzaino Sekkei dewa, sitani simesu hokano Dyôken kara $\mu=0{\cdot}35$ ni totte aru. Mata α no Atai wa $89{\cdot}0\,\frac{\text{cm}}{\text{sec}^2}$ ni natte iru. Kore de kan-

dyôsuruto, tugino Hyô (Dai 1 Hyô) oyobi Kyokusen (Dai 3 Du) ni simesu yôna Kasokudo no Domori wo eru.

Dai 1 Hyô.

φ	X(cm)	$-\ddot{\xi}\left(\frac{\text{cm}}{\text{sec}^2}\right)$	φ	X(cm)	$-\ddot{\xi}\left(\frac{\text{cm}}{\text{sec}^2}\right)$
0	0	0	35	4·06	93·9
5	0·62	10·5	40	4·55	159·0
10	1·23	21·0	42	4·73	243·1
15	1·83	31·6	43	4·82	348·4
20	2·42	42·6	44	4·91	660·0
25	2·99	54·6	45	5·00	∞
30	3·54	69·7			

Tokuni Hure no tiisai Kuiki dewa, X no 1 mm ga Kasokudo no 17 $\frac{\text{mm}}{\text{sec}^2}$ ni atatte iru.

Mata Disin no Undô ga Sinpuku A cm, Syûki T_D byô no Tansindô da to kateisureba, Saidaikasokudo wa $4\pi^2\frac{A}{T_D^2}$ de, kore wa, tuyoku nai Disin dewa $X=\frac{1}{17}4\pi^2\times\frac{1}{T_D^2}A$ cm ni arawareru. Soreyue kono Disinkei ga Hen'i wo arawasu Bairitu wa $\frac{4\pi^2}{17}\frac{1}{T_D^2}$ ni naru. $T_D=0{\cdot}5$ no Baai niwa oyoso 9·5-bai, $T_D=1$ no Baai niwa oyoso 2·3-bai ni naru. Mata konotoki Omori no Dimen ni taisite ugoku Kyori wa X no $\frac{1}{947}$ de, $T_D=0{\cdot}5$ no tokini Dimen no Undô no $\frac{1}{100}$, $T_D=1$ no tokini oyoso $\frac{1}{250}$ de aru. Kore demo Omori ga Dimen to Undô wo tomonisite iru to mite ôkina Ayamari no nai koto ga sireru.

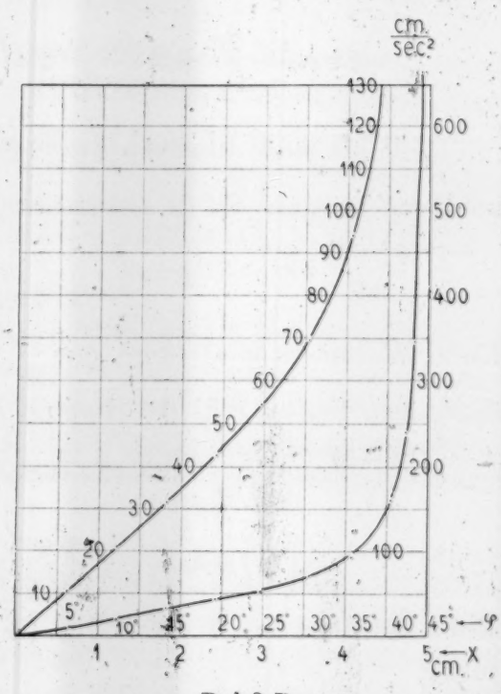

Dai 3 Du.

Omori no Sekkei.

10. Omori no Situryô no Saisyôgen wa, hanahada tiisai Kasokuko wo kaku koto wo Mokuteki to suru no de nakereba, Ziko-sindô no Syûki to Kasokudo-domori no Wariai to kara kimaru. Ziko-sindô no Syûki wa φ no tiisai tokini ôkiku, φ ga yaya ôkiku nareba itizirusiku tiisaku naru kara, φ no tiisai Baai ni tyûisureba tariru.

φ no tiisai Baai no Syûki T wa

$$\left\{m+\frac{2M}{h^2}+2\left(M'+2M''\frac{c^2}{t^2}\right)\theta_0^2\frac{r^2}{a'^2\theta_0^4}\right\}\ddot{x}$$
$$+\left\{4K+2(Pp\theta_0+k\theta_0^2)\frac{r^2}{a'^2\theta_0^4}\right\}x=0$$

kara, $\mu=\frac{\beta}{\alpha}=\frac{(Pp+k\theta_0)r^2}{2a'^2\theta_0^3K}$ wo tukatte tugino Siki de ataerareru,

$$T^2=\pi^2\frac{m+\frac{2M}{h^2}+2\left(M'+2M''\frac{c^2}{t^2}\right)\frac{r^2}{a'^2\theta_0^2}}{K(1+\mu)}.$$

Ima kono T oyobi tiisai φ ni taisuru

$$\frac{-\ddot{\xi}}{X}=\frac{\alpha+\beta}{\frac{Lc}{t}2\theta_0}=\frac{4Ka'\theta_0t(1+\mu)}{2mrLc}=q$$

ga ataete aru to site, m oyobi $K(1+\mu)$ wo sirô to suruto,

$$m=\frac{\frac{2M}{h^2}+2M'\frac{r^2}{a'^2\theta_0^2}+4M''\frac{c^2r^2}{t^2a'^2\theta_0^2}}{\frac{T^2}{2\pi^2}Lq\frac{cr}{ta'\theta_0}-1}.$$

$$K(1+\mu)=\frac{mrLcq}{2a'\theta_0t}.$$

to naru. Ima tiisai φ ni taisuru $\frac{X}{x}$ wo "Kwakudairitu" N_0 to sureba,

$$N_0=\frac{X}{x}=\frac{2Lrc}{a't\theta_0},\quad \text{sitagatte}\quad \frac{rc}{ta'\theta_0}=\frac{N_0}{2L}$$

Kore wa ôkina Kazu de nakereba naranai. Mata Sisin niwa, Kyokusen wo kakaseru tugô kara Mizikasa ni Kagiri ga atte, taitei $L=15$ cm gurai yorimo mizikakuwa dekinai (mottomo, hizyôni tiisai Undô dake wo Mokuteki to suru Baai wa, sô to kagiranai). Sitagatte sore no M'' wa Tiisasa ni Kagiri ga aru. Kore no kekkwa, m no Siki no Bunsi no uti

de, saigono Kô $4M''\frac{c^2r^2}{t^2a'^2\theta_0^2}$ ga mottomo ôkina Atai wo moti, nakano Kô $2M'\frac{r^2}{a'^2\theta_0^2}$ wa sore ni kurabereba tiisai ga, nao suterareru hodo dewa nai. Sikasi daiitino Kô $\frac{2M}{h^2}$ wa itizirusiku tiisai kara, kore wo sasioite kangaete sasitukae-nai. Yotte

$$m=\frac{\frac{1}{L^2}\left(M''+\frac{t^2}{2c^2}M'\right)N_0^2}{\frac{T^2q}{4\pi^2}N_0-1}$$

to tori, $LM''Tq\frac{t^2}{c^2}M'$ wo itteino mono to site, m wo saisyôni suru N_0 wo motomereba,

$$\frac{T^2q}{4\pi^2}\frac{1}{N_0}-\frac{1}{N_0^2}=\max.$$

no Keisan kara

$$\frac{T^2q}{4\pi^2}N_0=2$$

wo eru. Yueni

$$N_0=\frac{2Lrc}{a't\theta_0}=\frac{8\pi^2}{T^2q},$$

$$m=\frac{1}{L^2}\left(M''+\frac{t^2}{2c^2}M'\right)N_0^2=\frac{1}{L^2}\left(\frac{8\pi^2}{T^2q}\right)^2\left(M''+\frac{t^2}{2c^2}M'\right).$$

Mata

$$K(1+\mu)=\frac{mqN_0}{4}=\frac{2\pi^2m}{T^2}.$$

Genzaino Sekkei dewa,

$$T=0\cdot07\ \text{sec},\quad q=\frac{1\cdot7}{0\cdot1}\ \frac{1}{\text{sec}^2}$$

to totte,

$$N_0=947.$$

Mata Sisin wo, Atusa 0·15 mm, Haba Moto de 8 mm Sue de 0 no Aruminyûmu-ita de tukuru mono to mite $M''=9\cdot12\ \text{gr.cm.}^2$ t, c wa atoni aru Kandyô ni yotte $t=0\cdot6$ cm, $c=2$ cm, M' wa gaisan 23 to totte keisansuruto,

$$m=40\ \text{kgr},$$

$$K(1+\mu)=16\cdot1\times10^7\ C.G.S.$$

to naru.

Omori wo sasaeru Bane no Sekkei.

11. Zyôgedô to Suiheidô ni taisite mattaku dôyôna Sôti wo tukurô to suruto, Omori no Omomi wo sasaeru ni Dansei-bô wo tukai, sore ga

ueni dasita to onazi K no Atai wo motu yôni sureba yoi. Sosite kono Bô wa mg no Tikara wo uketemo zyûbunni Dansei-no-Sakai no utini aru koto ga hituyô de aru.

Bô no Tawami wo tukau Bane de areba, Danmen ga ataete aru tokini, Bô no naka deno saidaino Tawami no itteino Atai ni taisite Tikara no Sayô-ten no Hen'i ga narubeku ôkii yôna Katati wo tukau ga yoi. Kono Imi de, Dai 4 Du no Katati no Sôti wo tukau koto ni suru. Konoyôna Bô wo nihon suiheini, tagaini suityokuni sôtisuru kara, onoonono Ten ni $\frac{1}{4}mg$ dutu kakaru mono to suru.

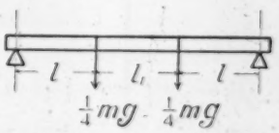

Dai 4 Du.

Bô no Haba wo b, Atusa wo t, $l\,l_1$ wo Du no yôni toruto, Omori no kakaru Ten no sagaru Taka wa, Dansei-keisû wo ε to site,

$$x=\frac{\frac{1}{4}mg}{\varepsilon\frac{bt^3}{12}}\left(\frac{l}{3}+\frac{l_1}{2}\right)l^2=\frac{mg}{\varepsilon bt^3}\left(l+\frac{3}{2}l_1\right)l^2.$$

Ima Bô no Dansei-no-Sakai ni okeru Nobi wo λ, Tyôryoku wo $H=\lambda\varepsilon$ to sureba, Bô no Tyûô-bubun no Sitadura no Nobi wo

$$\frac{3}{2}\frac{mgl}{\varepsilon bt^2}=\frac{1}{f}\lambda$$

to si, f wo 1 yorimo ôkiku, sikamo narubeku ôkina Kazu ni subeki de aru. Kore wo

$$\frac{bt^2}{l}=\frac{3}{2}f\frac{mg}{H} \qquad \text{.....(I)}$$

to kaku.

Mata kono Sôti ni tuite, onoonono Tikara no Sayô-ten ni taisuru K wa

$$K=\frac{\frac{1}{4}mg}{x}=\frac{1}{4}\frac{\varepsilon bt^3}{\left(l+\frac{3}{2}l_1\right)l^2}.$$

Sitagatte maeno Setu no Owari ni eta K no Kwankeisiki wa tugino Siki wo ataeru,

$$\frac{l^2\left(l+\frac{3}{2}l_1\right)}{bt^3}=\frac{\varepsilon}{4K}=\frac{\varepsilon T^2(1+\mu)}{8\pi^2 m} \qquad \text{.....(II)}$$

(I), (II), hutatuno Siki to maeni dasita μ no Dyôken ni kanau yôni, katu f wo narubeku ôkiku suru yôni Bô wo sekkeisureba yoi.

Genzaino Sekkei dewa, $H=20\frac{\text{kgr}}{\text{mm}^2}$ to tori, mata $\varepsilon=2{\cdot}1\times10^{12}$, $T=0{\cdot}07$ sec, $m=40$ kgr to totta node, tugino yôni eranda,

$$l=13{\cdot}5,\quad l_1=9{\cdot}2,\quad b=3{\cdot}3,\quad t=0{\cdot}7\text{ cm}.$$

Kore de keisansuruto,

$$f=4{\cdot}0,\quad \mu=0{\cdot}35;$$

mata

$$K=11{\cdot}93\times10^7;$$

Omori no kakaru Ten no sagatte iru Taka wa 0·82 mm ni naru.

12. Suihei-hôkô de Omori wo sasaeru Bane wa, Omori no Omomi hodo ôkina Tikara de hatte oku hituyô ga nai kara, Dai 1 Du ni Tensen de simesita yôna Katati ni tukutte zyûbun de aru. Sosite, Zyôge-hôkô no Bane to dôituno K wo motaseru. Soreyue, b' t' l' wo mae to dôyôna Ryô to site,

$$\frac{\varepsilon b't'^3}{4l'^3}=K,$$

$$\frac{b't'^2}{l'}=6f\frac{F}{H},$$

to suru. Tadasi F wa Bane no kaku Hazi wo hatte iru Tikara.

Genzaino Sekkei dewa tugino yôni eranda,

$$l'=7,\quad t'=0{\cdot}4,\quad b'=1{\cdot}22\text{ cm}.$$

$F=2$ kgr to sureba, $f=4{\cdot}65$ to naru. Kono F no tameni Bane no Hazi no hikiyoserarete iru Taka wa 0·16 mm ni naru.

Teko S_1 S_2 oyobi sonohokano Bubun no Sekkei.

13. Sisin no Hazi no Hure no Saidaigen (Ko no Nagasa) wo D to sureba,

$$\sqrt{2}\frac{c}{t}\theta_0=\frac{D}{L},$$

mata Kwakudairitu no Kwankei kara,

$$\frac{2Lrc}{a't\theta_0}=N_b.$$

Korera hutatuno Dyôken ni kanau yôni a, b, $\left(a'=a+\frac{a^2}{b}\right)$, θ_0, r, c, t wo tekigini kimeru. Mata μ no Atai kara Pp mo kimaru.

Genzaino Sekkei dewa,

$$N_0=947,\quad D=5,\quad L=15$$

wo kiteino mono to site, tugino Atai wo erabu koto ni sita,

$$a=4\cdot25,\quad b=9\cdot0,\quad (\text{sitagatte } a'=6\cdot26),$$

$$a\theta_0=0\cdot3,\quad c=2,\quad t=0\cdot6,\quad r=4\cdot18.$$

$(Pp+k\theta_0)\frac{r^2}{2a'^2\theta_0^3}=\mu K$ de, $k\theta_0$ wo tiisai mono to kateisite Pp wo kandyôsuruto, $Pp=65900$ dyne×cm.

$p=1\cdot5$ cm to suruto, $P=44\cdot8$ gr no Omosa ni naru.

14. S_1S_2 no Teko wo sasaeru Bane wa, Disin ni okoru saidaino Kasokudo α_1 ni saisite, Omori ni sono Undô wo saseru ni taeru koto ga hituyô de aru. Kore niwa 45° ni katamuita Bane wo nihon kôsasite tukau koto ni suru. Soredè, ipponno Bane wa

$$\frac{1}{\sqrt{2}}\frac{1}{r}m\alpha_1$$

no Tikara ni taeru koto ga hituyô de aru.

α_1 wo g to tori, r ni ueno Atai (4·18) wo toreba ipponno Bane wa 7 kgr no Omori wo sasaeru koto ga hituyô de, tatoeba Haba 7 mm, Atusa 0·05 mm no Hagane-himo wo tukau to site yoi. Kono Hagane-himo wo, tawamu Bubun no Nagas ga $\sqrt{2}$ mm dake aru yôni sôtisureba $k\theta_0$ wa 7800 gurai ni natte Pp ni taisite oyoso 9-bunno iti gurai ni ataru.

Hokano Renrakuyô oyobi Sasae no Bane mo doyô de,

S_1T_1 no aidano mono, S_2T_2 no aidano mono wa $\frac{1}{x}m\alpha_1$ ni,

Omori to T_1T_2 to no aidano mono wa $m\alpha_1$ ni,

$T_1\cdot T_2$ no Sasae no Bane wa $\left(1+\frac{1}{r}\right)m\alpha_1$ ni,

taeru koto ga hituyô de aru.

$S_1S_2T_1T_2$ nado no Teko no Sasae ga onoono itten de nakute Bane ni natte iru tameni Siten ga yokoni ugoku koto no Eikyô wo kandyôsite miru ni, sore wo midikaku sae tukuru naraba Eikyô ga nai mono to mite yoi.

Ondo no Eikyô.

15. Ondo-henkwa no tameni onoonono Bubun no Bôtyô ya Danseiritu no Henkwa ga okoru ga, kono Kikai de sono Eikyô wo tokuni eibinni kanzuru no wa,

(1) Omori no Omosa wo sasaeru Bane no Danseiritu no Henkwa to,

(2) OT_1 no aida, OT_2 no aida, T_1S_1 no aida, T_2S_2 no aidano Renrakusen no Bôtyô

de aru.

Omori no turiau Iti ga Bane no Danseiritu no Henkwa no tameni sagaru Ryô wa, Danseiritu no Henkwa no Ritu wo γ to sureba, itido no Nobori ni tuki

$$\frac{mg}{4K}\times\gamma$$

de aru. Kore wo oginau niwa Bane no Sasae ni Sintyû wo tukau. Kono Sasae no Takasa wo z to sureba,—Sintyû to Tetu to no Bôtyôkeisû wo sorezore $\alpha_S\,\alpha_T$ to site,

$$z(\alpha_S-\alpha_T)=\frac{mg}{4K}\times\gamma$$

no Kwankei kara

$$z=\frac{mg}{4K}\frac{\gamma}{\alpha_S-\alpha_T}$$

ni toreba yoi. Nao Bane to Omori to wo tunagu Sen no Bôtyôritu to Tetu-imono no Bôtyôritu to no Sa no Eikyô mo, z wo kagensuru koto ni yotte oginawareru.

Genzaino Sekkei dewa, $\frac{mg}{4K}=0{\cdot}82$ mm, $\gamma=\frac{1}{10000}$, $\alpha_S-\alpha_T=\frac{0{\cdot}7}{100000}$ to totte $z=1{\cdot}17$ cm ni tukureba yoi. Nao Bôtyôritu no Eikyô wo sukuu tameni, Sintyû no Takasa wo 3 cm gurai madeni nasi uru yôni sekkei-suru ga yoi to omowareru.

16. Omori to T to S to wo renrakusuru Sen (Hagane-himo) to Imono to ni Bôtyô no Sa ga aruto, $\theta_1\,\theta_2$ ni hikakutekini ôkina Eikyô wo syôzuru. Sôti wo Migi-hidari taisyôni tukutte aru kekkwa, Sisin no Reiten niwa Eikyô ga nai ga, θ_0 niwa Eikyô wo syôzuru.

Renrakusen no zentaino Nagasa wo s to sureba, itido no Sa ni tuki θ_0 no Kawari wa,—hutatu no Bôtyôritu wo $\alpha_1\,\alpha_2$ to site,

$$\frac{a'}{2r}\delta(\theta_0^2)=\frac{a'}{r}\theta_0\delta\theta_0=s(\alpha_1-\alpha_2).$$

Sitagatte

$$\frac{\delta(\text{saidaino }X)}{\text{saidaino }X}=\frac{\delta\theta_0}{\theta_0}=\frac{rs(\alpha_1-\alpha_2)}{a'\theta_0^2}.$$

Genzaino Sekkei ni taisite, $s=20$, $\alpha_1-\alpha_2=\frac{1}{1000000}$ to kateisureba, Ondo no Sa 30-do ni yotte oyoso $\frac{1}{12}$ hodono Henkwa ni naru. Kono Henkwa wa warini ôkii keredomo, Kikai ga Disinkei no Yô wo nasu ueniwa sahodono Sasitukae wo syôzuru koto wa nakarô to omowareru.

Mosi Sôti ga taisyôni tukutte nakute, s no Atai ga Ryôgawa de tigau tokiniwa, Turiai no Iti ga Ondo ni yotte kawari, toriatukaizyô Tugô ga warui de arô to omowareru.

Sisin no Hazi no Masatu.

17. Sisin no Hazi no Masaturyoku wo R dyne to sureba, Omori ni sayôsuru Tikara no N_0R dyne madewa Sisin wo ugokasu ni tarinai. Kono Tikara wa Kasokudo ni oite,

$$\frac{N_0R}{m} \quad \frac{\text{cm}}{\text{sec}^2}$$

ni ataru.

Osoi Disindô no hizyôni tiisai Kasokudo wo sirusaseru niwa, N_0 wo ôkiku suru (T wo ôkiku suru koto ga Tugô ga warui Baai) koto ga hituyô de aru noni, ueno Ryô wo kaette hanahada tiisaku suru koto wo yôsuru kara, kono Mondai wa yôinaranai Konnan wo syôzuru. Konoyôna Baai ni kokoromite yûkô ka to omowareru hitotuno Hôhô wa, Omori ni Onsa wo kuttukete oki, Denryû wo tukatte tuneni sore wo sindôsasete oku. Sô sureba, Sisin no Hazi wa tuneni aru tiisai Haba wo yûsuru Kyokusen wo egaki, Haba no Tyûô-no-Sen wa Masatu no Eikyô wo ukenai Hari no Iti wo simesu wake ni naru. Tadasi kono An no Yosiasi wa zittini kokoromite minakereba tasikaniwa ienai.

Genni sekkeisite iru Kikai dewa, ueni sirusita Kasokudo wa hanahada tiisakute nanno Konnan womo syôzinai.

Hokano Seibun wo sirusu Bubun no Eikyô.

18. Omori ga arû Hôkô (x-Hôkô) ni sukosi uturuto, ueni simesita Tikara (K ni yoru mono, P ni yoru mono, k ni yoru mono) no hokani, hokano Hôkô ni Omori wo sasaete iru Tikara ga x-Hôkô ni Seibun wo syôzite, KP nado to dôyôna Sayô wo syôzuru. Kono Sayô wa, Suiheidô ni taisuru Dyûryoku no Bunryoku ni oite itiban ôkiku arawareru.

Omori wo turu Sen no tawami-yasui Bubun no Nagasa wo L_1 to si, x to suityokuna Suihei-hôkô ni Omori to Bane to wo tunagu Sen ni kwansuru dôyôna Nagasa wo L_2 to si, Kiroku-bubun ni renrakusite iru Sen ni kwansuru dôyôna Nagasa wo L_3 to sureba, korerano Sen wo tôsite Omori ni sayôsuru x-Hôkô no Tikara wa

$$-\left(mg\frac{x}{L_1}+4F\frac{x}{L_2}+\frac{4Ppr}{a'}\frac{x}{L_3}\right)$$

de aru. Kore wo, maeni dasita, φ no tiisai Baai no Tikara

$$4Kx+2(Pp+k\theta_0)\frac{r^2}{a'^2\theta_0^2}x=4K(1+\mu)x$$

ni kuraberuto, $4K(1+\mu)=mqN_0$ no Kwankei ga aru kara,

$$\frac{\frac{mg}{L_1}+\frac{4F}{L_2}+\frac{4Ppr}{a'L_3}}{mqN_0}$$

no Hi ni naru. Kono naka de omona Kô wa

$$\frac{g}{L_1qN_0}$$

de, genzaino Sekkei dewa $\frac{1}{160}$ guraino mono de aru.

Dimen-keisya no Eikyô.

19. Dimen no Keisya wa Kikai no Kiroku no ue de, suiheino Disin to dôyôna Eikyô wo syôzuru koto wa, koremadeno Disinkei nimo aru ga, Kasokudo-disinkei nimo sore ga aru.

Dimen no Keisya no Kaku ga ε de aru to sureba, Kikai wa εg dakeno Suihei-kasokudo wo kirokusuru.

Ima kokoromini, onazi ε no Keisya ga atta Baai no Turiai no Iti ni tuite, ueno Eikyô wo Suihei-sinsi ni taisuru Eikyô ni kurabete miru.

Suihei-sinsi no Diku no Entyokusen ni taisuru Katamuki wo i, Omori no Dyûsin ga Diku kara hedatatte iru Kyori wo D to sureba, Suihei-sinsi wa ε no Keisya wo

$$\frac{\varepsilon}{\sin i}D$$

dakeno Dimen no Hen'i to dôyôni kirokusuru. Suihei-sinsi no Zikosindô no Syûki wo T_H to sureba,

$$\frac{D}{\sin i}=\frac{gT_H^2}{4\pi^2}$$

no Kwankei ga aru kara,

$$\frac{\varepsilon D}{\sin i}=\frac{\varepsilon gT_H^2}{4\pi^2}$$

Ima 2-syuruino Disinkei ga onazi Teido no Disin wo kirokusuru yôni tukutte aru mono to site kuraberu ni, sono Disin no Syûki wo T_D, Sinpuku wo A to sureba, Suihei-sinsi wa A, Kasokudo-disinkei wa $\frac{4\pi^2}{T_D^2}A$ wo onazi Teido ni kirokusuru wake de aru. Korera ni, ueno Keisya no Eikyô wo kuraberuto,

Suihei-sinsi de $\frac{\varepsilon gT_H^2}{4\pi^2A}$ bai,

Kasokudo-disinkei de $\dfrac{\varepsilon g}{\dfrac{4\pi^2}{T_D^2}A} = \dfrac{\varepsilon g T_D^2}{4\pi^2 A}$ bai

de aru. Hutatu no Hi wo toreba, Kasokudo-disinkei ni arawareru Eikyô wa Suihei-sinsi no sore ni kurabete

$$T_D^2 : T_H^2$$

ni naru. T_H wa tûzyô T_D ni kurabete hanahada ôkiku tukutte aru kara, Kasokudo-disinkei dewa, Suihei-sinsi yoriwa Dimen-keisya no Eikyô wo ukeru koto ga yohodo tiisai to ieru.

Tadasi, Keisya no Henkwa wa Suihei-sinsi dewa tadatini Sisin ni arawarenakute, Kasokudo-disinkei dewa tadatini arawareru to iu Sa ga aru. Mata, Suihei-sinsi dewa kotonaru i ya D wo yûsuru Kikai wo tukaeba, Dimen no Hen'i to Keisya to wo wakeru koto ga dekiru kamo sirenai ga, Kasokudo-disinkei dewa, sore no seisituzyô kara akiraka de aru tôri, Keisya to Suihei-kasokudo to wa donna Kikai nimo mattaku dôtôna Sayô wo teisuru mono de aru.

Kono Ten wa Kasokudo-disinkei no Tansyo de aru ka to omowareru keredomo, Disin no saini Dimen ni koteisite iru Buttai, tatoeba Tatemono nado ga yahari Keisya to Suihei-kasokudo to kara mattaku dôtôna Sayô wo ukeru koto wo kangaereba, kaette kono Seisitu no tameni Tugô ga yoi Ten mo aru ka to omowareru. Tonikaku Kono Kikai no Sido ga Kwako ni kwankei-naku Maisyunzi ni genzaisurù arù Ryô wo simesite iru koto wa Kiroku wo Mokuteki to suru Kikai tosite musiro yoi Seisitu to iubeki de aru.

Genzai sekkeisite iru Kikai dewa, Hito no kanzuru Disin wo Mokuteki to site iru kara Keisya wa mattaku mondaigwai da to itte yoi. Sore ni kakawarazu, ueni nobeta Koto wa Kasokudo-disinkei no Seisitu tosite itizirusii Koto de aru kara, tati-itte ronzita no-de aru.

Ziko-sindô no Eikyô.

20. Gwanrai, Toki ni taisuru Kasokudo no Henkwa wa, Hen'i ya Sokudo no sore no yôni yôyôna Imi wo motanai kara, Kasokudo-disinkei dewa, komakai Ziko-sindô ga mazitte itemo Sasitukae ga nai rasiku omowareru. Sikasi, Ziko-sindô no Syûki ga Disindô no Syûki ni kurabete hanahada tiisaku nai yôna Baai niwa, Ziko-sindô wo nibumeru Sôti ga hituyôni naru de arô.

Genzai sekkeisite iru Kikai dewa, Sisin no Diku no sitani, konoyôna Nibume-sôti wo toritukeru koto mo guwaiyoku dekiru. Kore no Hituyô no Arunasi wa syôraino Kenkyû ni yotte sadameru.

Hito no kanzinai Disindô wo kirokusuru Kikai.

21. Syûki ga sû-byô ni wataru yôna yowai Disin no Kasokudo wo kirokusuru ni, ueni dasita Siki ni sitagatte, Syûki wo onazi Teido ni tukurô to suruto, sûhyaku-ton matawa sûsen-ton no Omori ga hituyôni naru. Sorehodo ôkiku nai Omori de tukurô to suru niwa,

(1) Kôgakuteki-Kiroku no Hôhô wo toru ga hitotuno Hôhô de aru. Kore wa M'' wo tiisaku site, sitagatte m wo tiisaku si, mata Masatu no Eikyô wo manugareru Rieki ga aru. Kore niwa, daitaino Katati wo genzai sekkei no mono to dôyôni tukutte guwaiyoku dekiru. Mata

(2) Ziko-sindô no Syûki wo ôkiku si, dôzini Nibume no Sôti wo soe Masatu no Eikyô wo manugareru Kuhû wo suru no mo hitotuno Hôhô de aru.

Korera wa syôraino Kenkyû ni matubeki mono de aru.

Genzai sekkei no Kikai.

22. Genzai sekkeisite iru Kikai wa tugini soeru Ryakudu (Dai 5 Du oyobi Dai 6 Du) ni aru yôna Katati wo nasite iru. Sore no Yôbu no Ryô wa ueni tokorodokoro ni kakageta tôri de, Tetu-imono wa Maeusiro, Migi-hidari onoono 42 cm, Takasa 41 cm, Tyûô ni aru Omori no

Heimendu 12-bunno 1.

Itiban ueno Bubun wo syôryakusite simesu. Mata Imono wa Hasira dake wo simesu.

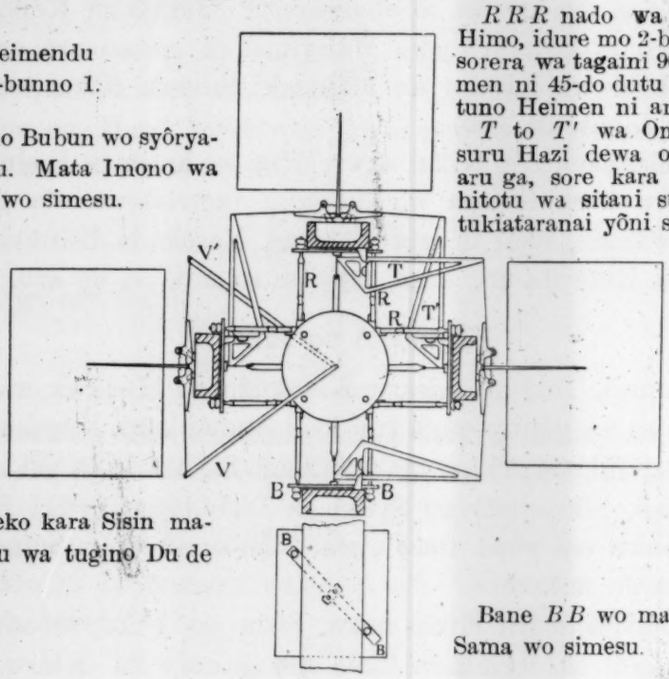

RRR nado wa usui haganeno Himo, idure mo 2-bubun kara natte, sorera wa tagaini 90-do, Du no Heimen ni 45-do dutu katamuita hutatuno Heimen ni aru.

T to T' wa Omori ni renrakusuru Hazi dewa onazi Takasa ni aru ga, sore kara hitotu wa ueni, hitotu wa sitani sukosi katamuite tukiataranai yôni site aru.

$V\,V'$ no Teko kara Sisin madeno Renraku wa tugino Du de sireru.

Bane BB wo mae kara mita Sama wo simesu.

Dai 5 Du.

Kikai no ueno Bubun wo ue kara mita Du

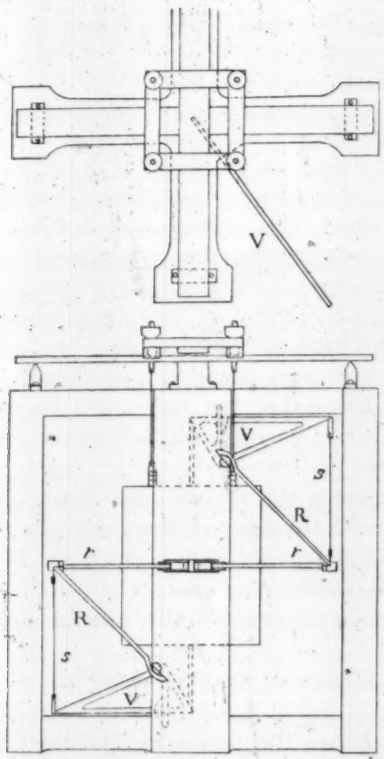

Zyôgedô wo sirusu Bubun wo simesu tameni maeno Du no hidarino hô kara mita Du.

Omori no Zyôgedô wa *V* ni yotte *s*-sen no Zyôgedô wo syôzi, mata Teko *R* ni yotte *r* no Suiheidô wo syôzi, sore ga hakano Seibun to dôyôni kirokusareru.

s-sen to *r*-sen to no Renraku wo simesu Du

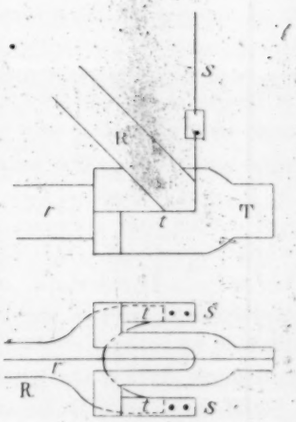

(Sita kara mita Du)

s-sen no Sitahazi to R-bô no Hazi to wa hutamatuni nari, R niwa *s* to suiheina Hagane-himo *t* to ga kuttuki, kono *t*-kire no Hidarihazi wo torituketa *T* ni *r* no Himo ga tukete aru.

Dai 6 Du

Omosa 40 kgr, migino hô to maeno hô ni Suiheidô wo sirusu Sisin, hidarino hô ni Zyôgedô wo sirusu Sisin ga atte, onoono betubetuno Taiko no ueni hudan Kiroku wa suru. Taiko no Kwaiten wa, maihun 9 cm gurai ni nasi, ittyûya no Kiroku wo onoonono Seibun ni itimaino Kami ni kakaseru.

23. Kono Kikai wo tukuri katu sore no Hatarakiburi wo kensasuru tameniwa, Huzoku-kikai (Taiko, Tokeizikake nado) wo awasete oyoso 500 En no Hiyô wo yôsuru Mikomi de aru.

21. *The Construction and Study of an Acceleration Seismograph.*

By Takuro TAMARU.

1. *The Object of the present Seismograph.* It has been too difficult for the hitherto built seismograph to calculate the acceleration minutely from its record of displacement or velocity of the earth's movement. So I think it will be very usefull to construct a seismograph capable of recording acceleration directly. The hitherto one, besides, has been nearly unstable in arrangement, incapable of recording the three dimentional movement by a single mass, full of obstruction on the proper oscillation, deflection of the index outside of the limit of the recording paper as the result of too great amplitude of oscillations and so on. The new seismograph will save all these defects.

2. *The General Structure.* It is composed of the main frame, the pendulum, and three sets of drums and indexes. The cast iron frame has the width and length of 42 cm., the height of 41 cm. The single mass of pendulum, which finds itself in the centre of frame has 40 kg. In the right, and in the front, we find two indexes which register the horizontal movement, and in the left, one which records the vertical movement. Each index touches on its respective drum, which rotates with the speed of 9 cm. per min., and draws the diagram during the whole day on a sheet of paper in each component. It will be costed about 500 Yen with its accessories (drums, clockworks, etc.).

3. *The General Characteristics.* The special arrangements and the general characteristics derived therefrom are the followings:

(i) Recording of Acceleration. It is our fundamental idea attaining the aimed record of acceleration, to arrange a pendulum with fairly great mass so as to move similarly as the earth, and to record the force between the pendulum and the frame sustaining it. This force, which is necessary to make the pendulum move samely with the earth, has a direct proportion to the acceleration of the earth's movement. If we aim only to record this force, we may well use strong springs in every direction—upwards and down wards, east and west, north and south. The deformation of the spring is therefore in proportion to the kinematic changes of the motion of the pendulum. The record thus obtined shows the acceleration. We will not, however, simply use a strong spring in holding the pendulum, for the sake of the fifth characteristics.

(ii) It can register the three dimentional movement using a single pendulum being connected with the same arrangement for each component.

(iii) It has a very stable equilibrium while the hitherto one has been nearly unstable.

(iv) Less influence of proper oscillation and thermal changes. It seems for an acceleration seismograph to have minute proper oscillations mixed within. It is, however, necessary to lessen the proper oscillation, when the period of the proper oscillation is not so small compared to that of the earth's shocks. This apparatus will have a special arrangement under the holder of the index, to absorb the proper oscillation. To lessen the thermal influence which may be given to the spring, the brass holding of the spring, the wire connecting the spring and the pendulum, the cast iron frame etc., we can make a preparatory calculation of the expansion coefficient of their material, and consequently neglect the thermal deformation of the apparatus as a seismograph.

(v) In order to get rid of the deflection of the index outside of the recording paper as the result of too great shocks, it has a special arrangement to restrict the index mo-

ton within a certain limit. In other words, we do not simply use strong springs in holding the pendulum, but the degre of deflection of the index is made to lessen according as the force increases, (the force necessary for making it movable samely with the earth) and when this force increases more and more, the index approches near to a certain position asymptotically in a cetain direction.

(vi) To lessen the effect of the friction at the end of the index when we register very small acceleration of a slow earth movement, we may efficiently attempt to join a tuning fork with the pendulum, which is constantly vibrated by electric current. Thus the end of the index always draws a curve having a certain width, and the middle line of the width will show the position of the index free from the frictional effects. The validity of this plan, however, depends on experiment.

(vii) The acceleration seismograph sufferr less influence of the earth's tilting than the horizontal pendulum. Besides, the tilting appears enormously in the index in the latter, while it appears directly in the former. The tilting and the horizontal acceleration make entirely same action in the nature of the acceleration seismograph. But this is not the defect of this apparatus. Considering that in case of earthquake the body fixed on the earth (e.g., a building) also suffers the same action from tilting and horizontal acceleration. We may, therefore, neglect the tilting motion of the present apparatus as to be applied to every thing.

To make a record of feeble earthquakes having the period of several seconds we will need a pendulum of the weight several hundred or several thousand kgs. Else, we may either take a method of optical recording, or make the period of proper oscillation great, therewith connecting an arrangement which lessens the influence of friction. All these I hope for the future study.

22. *On Silica Minerals Occurring in the Groundmass of Common Japanese Volcanic Rocks.*

By Hisashi KUNO,

Geological Institute.

(Received March 20, 1933.)

I. Introduction.

In the course of my microscopical examination of thin sections of the basic volcanic rocks from north Idu district, central Japan, my attention was attracted to the occurrence of very low-refracting and low-double-refracting clear minerals as essential primary constituents of the groundmass. They are undoubtedly crystalline and distinct from interstitial glass. A microchemical test proved that they are not zeolite. From their optical properties and other characters in thin section the minerals were identified to be tridymite and cristobalite. The presence of cristobalite was further affirmed by taking an X-ray powder photograph of the rock and comparing it with that of the artificial cristobalite prepared in the electric furnace.

A brief preliminary note on the occurrence of these minerals has already been given.[1] Here it is intended to give a more detailed account on their modes of occurrence, their optical properties and the methods by which they have been identified.

The occurrence of tridymite in cavities of volcanic rocks is very common in Japan, while the occurrence of the same mineral in the groundmass is less common. Some earlier writers spoke of "tridymite and cryptocrystalline acid mesostasis as occurring in groundmass, but not of cristobalite.[2] However, according to my own observation of the north Idu rocks, cristobalite occurs as commonly as tridymite in the

1) S. TSUBOI and H. KUNO, *Bull. Volcanol. Soc.*, Japan, 1 (1932), 34. *Jour. Geol. Soc.*, Tokyo, 39 (1932), 297.

2) B. KOTÔ, *Quart. Jour. Geol. Soc.*, 40 (1884), 441.
J. HARADA, *Jour. Geol. Soc.*, Tokyo, 31 (1924), 357.
S. YAMADA, *Jour. Geol. Soc.*, Tokyo, 36 (1929), 434.
T. NEMOTO, *Jour. Jap. Ass. Min. Petro. Econ. Geol.*, 4 (1930), 27.
T. TOMIDA, "Geology of the Lake Towada," *Tennen-Kinenbutu Chôsa Hôkoku*, 4 (1930), 22.

groudmass; and it is possible that some "tridymite etc." of the earlier writers are in reality cristobalite.

In the Idu district, tridymite and cristobalite occur almost universally in the lavas of every age from Miocene to Recent and of every composition from liparitic to basaltic, regardless the presence or absence of olivine as phenocryst, or its amount.

Recently, B. Yoshiki described the cristobalite in the groundmass of the andesites from Sambe volcano, southwest Japan, and of the volcanic rocks from some other districts, as well as of some Tertiary basalts near Sendai, northeast Japan.[3] Thus, it is probable that these minerals are not so rare as has been generally supposed, but that they are rather common as essential constituents of the Japanese volcanic rocks.[4]

In some instances there occurs interstitial quartz in the groundmass of the similar rocks. Its mode of occurrence deserves special attention.

It has long been known as one of the characteristics of the Japanese volcanic rocks, that a considerable amount of excess silica appears in the norms calculated from their chemical analyses. The presence of silica minerals in these rocks may well account for the normative quartz, the modal equivalent of which has hitherto been uncertain. The quantitative comparison of normative and modal silica, will be made in the succeeding paper.

The following description is based on the observation of the basic and intermediate lavas (the so-called "pyroxene andesite" of the bandaite or miharaite type) exclusively of the north Idu district, the constituent minerals of which are plagioclase, augite, hypersthene and olivine as phenocryst, and plagioclase, pyroxene (usually pigeonite), magnetite, silica minerals and glass in the groundmass.

My special thanks are due to Professor Dr. S. Tsuboi who has given me valuable suggestions in every occasion concerning the probable existence of some silicious minerals in the Japanese volcanic rocks, and has afforded me every facility throughout this study. Thanks are also due to Professor Dr. S. Nishikawa who granted the use of the X-ray apparatus belonging to his laboratory in the Institute of Physical and Chemical Research, Tokyo, and to Mr. I. Kazumoto who has kindly undertaken the X-ray experiment for me.

3) B. Yoshiki, *Jour. Jap. Ass. Min. Petro. Econ. Geol.*, 8 (1932), 18 and 61.
4) C. N. Fenner, *Amer. Jour. Sci.*, 36 (1913), 345.

II. Microscopical Features and Optical Properties.

(1) *Quartz.*

In the volcanic rocks of Idu the quartz is not common. Its occurrence is limited only in less basic rocks (with or without olivine) of rather high crystallinity. Tridymite or cristobalite may be present occasionally with quartz. Quartz occurs either filling the interstitial spaces or forming mosaic aggregates of subhedral grains between plagioclase laths, usually in association with more acid interstitial feldspar, from which it can hardly be discriminated without the aid of conoscope. (Fig. 1.)

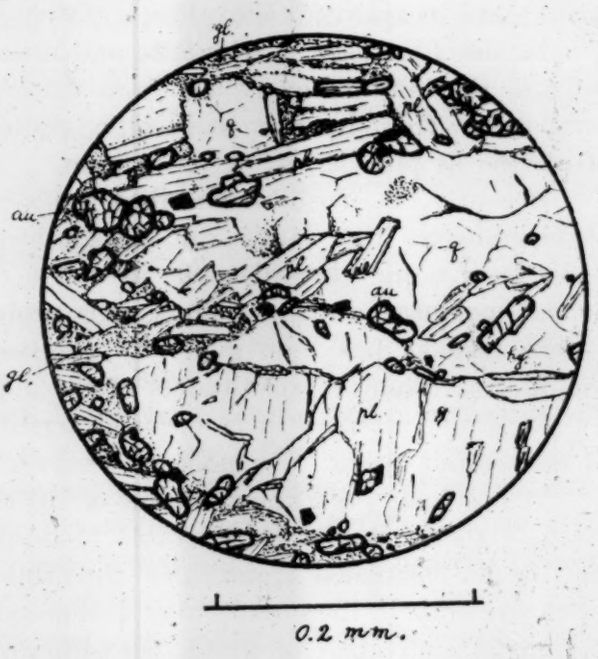

Fig. 1. The groundmass of olivine-augite-hypersthene andesite from Usami, Idu, (31041526).

au.....augite hy.....hypersthene
pl.....plagioclase q.....quartz
gl.....glass

(2) *Tridymite and Cristobalite.*

General Remarks.—The two minerals appear alike in thin section, and both fill the interstices between the groundmass-minerals, usually with a small quantity of glass. They are colourless, clear, and almost free from inclusions. In refraction they are lower than the ordinary interstitial glass which is pale brown and dotted with fine dusts. (Fig. 2.) They show cleavages and cracks and weak but distinct double-refraction, with definite extinction and twinning phenomena. With these characters the minerals can be distinguished from the glass which is completely isotropic and with no trace of cracks. In some rare instances, the glass is replaced by a cryptocrystalline mesostasis, consisting of fibrous or granophyric aggregate of acid feldspar and quartz (?), turbid throughout, and higher in refraction than the silica minerals.

Microchemical Test.—In order to show that the mineral, identified optically as cristobalite, is not zeolite, with which it may be sometimes confused, the result of a microchemical staining test undertaken by K.

Shibata of the Geological Institute will be cited.

A rock section containg the mineral in question was kept in dilute hydrochloric acid (about 16% HCl) for 20 minutes, i. e. long enough for zeolite (even for chabazite, the most resistant zeolite) to be completely gelatinized, and then in NH_4OH fume for 5 minutes to make the product on the surface of the rock section alkaline. Lastly, the aniline green solution was applied for staining for 15 minutes. After these operations it was found that only the calcic part of the plagioclase in the rock was sensibly stained, while the mineral in question remained quite unattacked.

Tridymite.—The tridymite occurs most commonly in the rocks of intermediate basicity, though not rare in the basic ones.

Good crystals are comparatively rare, and are found in highly crystalline rocks or in coarse-grained parts present in patches through the finer-grained groundmass. They have euhedral or subhedral platy form, showing in cross section an elongated outline up to 0·2 mm. in length. In most instances tridymite occurs filling interstitices between other minerals. Occasionally it developes in microscopical cavities in skeletal form due to the interpenetration of thin plates.

It shows straight extinction and negative elongation, and has distinct basal cleavage, but is free from cracks. The most characteristic is the twinning, like that in cordierite, consisting of wedge-shaped sectors with negative elongation, and showing in cross section indistinctly striations like the albite-twinning lamellae (Fig. 5.). It is very low in double-refraction, often almost isotropic.

The mean refractive index determined by the immersion method and the optic axial angle measured by means of the conoscope and the universal-stage are shown in the following table. Those of tridymites from several localities as well as those of artificial one are also given for comparison.

groundmass tridymite, oliv.-two-pyrox andesite, (31072302), Atami, Idu.	N_D=1·480	(+) 2V small nearly uniaxial
groundmass tridymite, oliv.-two-pyrox. andesite, (31073110), Atami, Idu.	N_D=1·478	(+) 2V small nearly uniaxial
groundmass tridymite, oliv.-two-pyrox. andesite, (31042804), Aziro, Idu.	N_D=1·479	(+) 2V small nearly uniaxial
cavity tridymite (2 mm.), oliv.-two-pyrox. andesite, (31042804), Aziro, Idu.	N_D=1·472	(+) 2V=64°
cavity tridymite, andesites from Gôroyama, Sinano	N_D=1·476	(+) 2V about 36°
Siduoka, Suruga.	N_D=1·476	not determined

artificial tridymite, by C. N. Fenner.[5] $\begin{cases}\alpha = \beta = 1{\cdot}469 \\ \gamma = 1{\cdot}473\end{cases}$ (+) $2V = 35{\cdot}5°$

natural tridymite, by E. Mallard.[6] $\frac{\beta+\gamma}{2} = 1{\cdot}477$ (+) $2V = 43°$

It must be noted that the tridymite crystals occurring in the groundmass are all alike in refractive index, being slightly higher than those of other occurrences. This relation reveals itself even within a single rock (31042804). It is likely then that the mineral is variable in properties according to the conditions under which it has been formed.

Cristobalite. — Cristobalite is found either in aggregates of extremely fine grains of random orientation or in well-developed crystals with an appearance like roofing-tiles, sometimes filling the interstitial irregular spaces between other minerals, and sometimes in round patches (up to 0·2 mm. across), through the intergranular groundmass. (Fig. 2, 6 and 7.)

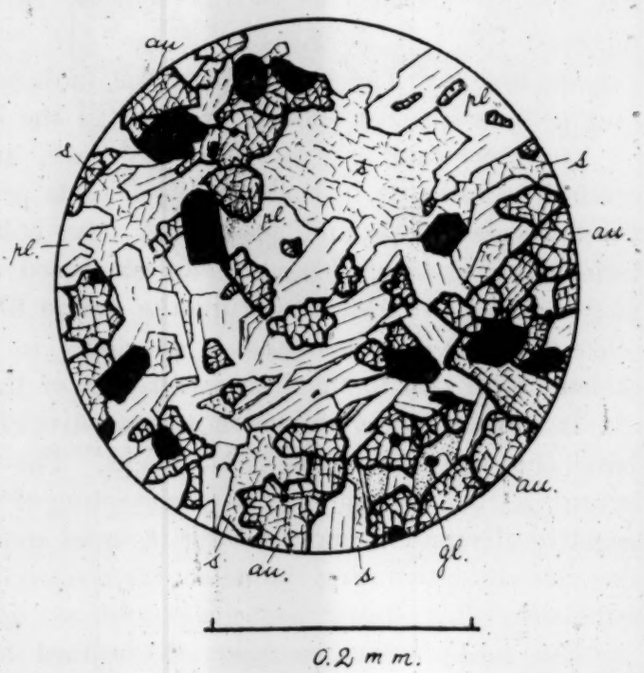

Fig. 2. The groundmass of augite-bearing olivine basalt from Usami, Idu, (31041812), showing well-developed cristobalite.

au.... pigeonite pl.... plagioclase
gl.... glass s.... cristobalite

The well-developed crystal has two sets of cleavage intersecting at right angle. (Fig. 4 and 7.) Between crossed nicols it shows uniformly a diagonal extinction, as if it had the same orientation throughout the whole parts of the crystal. But when examined by inserting gypsum plate it is found that the crystal is polysynthetically twinned, consisting of numerous small rectangular parts, each of which is bounded by planes parallel to the cleavage-planes. These parts are of two sets in orientation, X' in one set being parallel to Z' in the other. (Fig. 3, 4 and 8.)

5) C. N. FENNER, *op. cit.*, 352.

6) E. MALLARD, *Bull. Soc. Min.*, 13 (1890), 161.

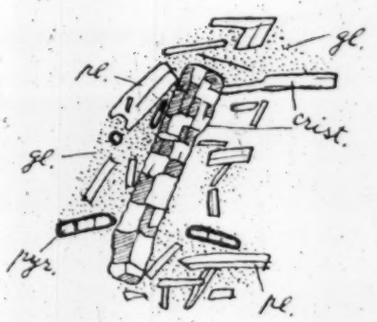

Fig. 3. Cristobalite replacing tridymite (0·3 mm. in length), andesite from Hutagoyama, Hakone, (33012001)

pl.....plagioclase
gl.....glass
pyr.....pyroxene
crist.....cristobalite

The two sets of orientation are shown by hatching.

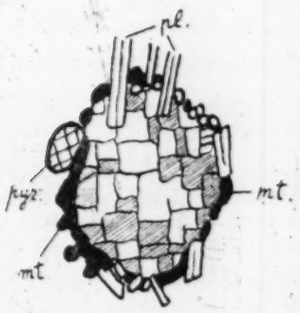

Fig. 4. Rounded patch of cristobalite (0·1 mm. across), basaltic bandaite from Habu, Ôsima, (33012002), showing the polysynthetic twinning and the rim of magnetite grains.

pl.....plagioclase
pyr.....pyroxene
mt.....magnetite

The two sets of orientation are shown by hatching.

In the Hutagoyama lava, Hakone volcano, (olivine-two-pyroxene andesite (33012001)), cristobalite crystals are euhedral with hexagonal platy outline. They are found either embedded in the glass base (Fig. 3.) or attached on the walls of microscopic cavities. In the latter occurrence, the interpenetration of thin plates is a characteristic feature, which suggests that the cristobalite in this rock represents paramorphic replacement after tridymite. The tridymite appears to be of earlier formation than the glass in which it is embedded, as is indicated by its being euhedral.

In basaltic bandaite from Habu, Ôsima, numerous rounded patches of well-crystallised cristobalite are found in compact intergranular groundmass. These rounded patches are not infrequently surrounded by rims of small magnetite grains. (Fig. 4.)

The optical data of cristobalites from several localities are given in the follwing table. It is to be noted that all the cristobalite crystals as far examined, though various in their modes of occurrence, are alike in optical properties.

groundmass cristobalite, olivine-bearing basaltic bandaite, (33012002), Habu, Ôsima.[7]	$N_D = 1{\cdot}486$	(−) nearly uniaxial sometimes biaxial

7) It belongs to the somma lava, a representative specimen of which has 9·6% normative quartz. S. Tsuboi, *Jour. Coll. Sci., Tokyo Imp. Univ.*, **43** Art. 6, (1920), 71.

groundmass cristobalite, oliv.-two-pyrox. andesite, (33012001), Hutagoyama, Hakone.	$\alpha=1{\cdot}485$ $\gamma=1{\cdot}488$	(−) nearly uniaxial
groundmass cristobalite, basaltic rocks from north Idu.		
(31041812)	$N_D=1{\cdot}485$	
(31050201)	$N_D=1{\cdot}485$	2V not determined
(51227)	$N_D=1{\cdot}487$	
groundmass cristobalite, biot.-hornbl. dacite and andesite from Sambe and allied volcanoes, southwest Japan. by B. Yoshiki.[8]	$N_D=1{\cdot}484$-$1{\cdot}487$	2V not determined
groundmass cristobalite, basalts from Sendai, northeast Japan. by B. Yoshiki.[8]	$N_D=1{\cdot}485$-$1{\cdot}486$	2V not determined
cristobalite in silica blick. by B. Yoshiki[8]	$n_1=1{\cdot}488$ $n_2=1{\cdot}485$	(−) nearly uniaxial
artificial cristobalite. by C. N. Fenner.[9]	$\gamma=1{\cdot}487$ $\alpha=1{\cdot}484$	(−)

Any detailed discussion concerning the origin of tridymite and cristobalite is out of the scope of the present paper. But it may be suggested from what have been observed under the microscope, that the minerals in the rocks examined are of primary crystallisation belonging to the stage earlier than that of the formation of the glass base. Moreover, it appears that the groundmass-tridymite and the cavity-tridymite were formed perhaps under conditions somewhat different from each other, of which, however, little is known at present.

III. X-ray Powder Photograph of Cristobalite.

For further affirmation of the presence of cristobalite in some Japanese volcanic rocks, an X-ray photograph of the powdered rock containing cristobalite from Usami was taken, and this was compared with that of artificial cristobalite. Artificial cristobalite was prepared by heating pure silica glass[10] at 1400°C in an electric furnace for 6 hours.[11]

The cristobalite thus obtained has the optical properties as tabulated below. For comparison the refractive indices and the dispersion of natural cristobalite and silica glass are also given in parallel columns.

8) B. YOSHIKI, *op. cit.*, 25.

9) C. N. FENNER, *op. cit.*, 354-356.

10) The silica glass was obtained through the kindness of Dr. M. Ishimoto of the Earthquake Research Institute, Tokyo Imperial University, to whom my thanks are due.

11) R. B. SOSMAN, "The Properties of Silica," (1927), 97.

monochromatic light	C-line	D-line	F-line	dispersion F-C
natural cristobalite, (33012001), Hutagoyama, Hakone.	$\gamma = 1.486$	1.483	1.494	0.008
natural cristobalite, (31041812), Usami, Idu.	N (mean) = 1.484	1.485	1.493	0.009
artificial cristobalite.	N (mean) = 1.484	1.485	1.489	0.005
silica glass	N = 1.4568	1.4589	1.4642	0.0074

The basalt from Usami, north Idu, (31041812),[12] contains plagioclase, monoclinic pyroxenes (mostly pigeonite), magnetite, silica mineral, glass, and olivine, in the order of abundance (Fig. 2.). By the gravitational and magnetic means the greater part of the ferromagnesian constituents were removed and the residual part, which is made up chiefly of plagioclase (anorthite to labradorite) and subordinately of silica mineral and glass, was subjected to examination.

The X-ray powder photograph was kindly taken by Mr. I. Kazumoto of the laboratory of Dr. S. Nishikawa in the Institute of Physical and Chemical Research, Tokyo. The result is shown in Fig. 9, on which

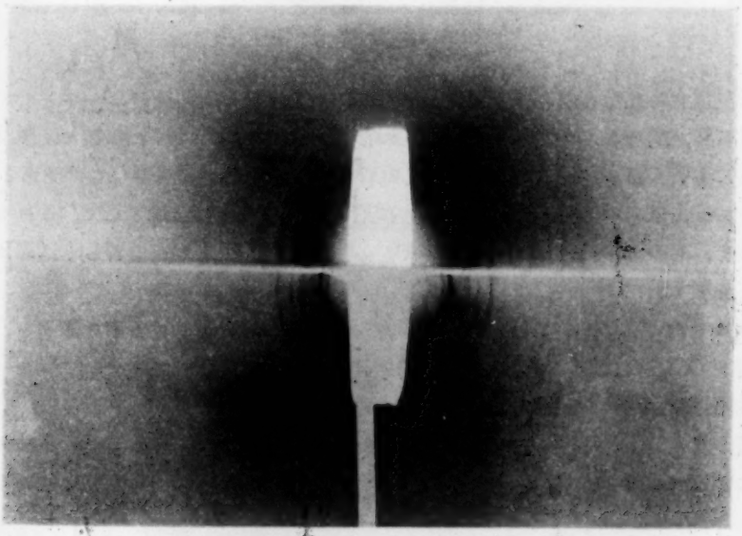

Fig. 9. X-ray powder photograph of the basalt from Usami, (31041812), (upper half), and the artificial cristobalite (lower half).
Exposure about 40 hours.
Taken with molybdenum anticathode.
Radius of the film semi-circle 4.5 cm.

12) The microchemical test was applied on this rock and it was proved that the "silica mineral" is not zeolite. The calculation of norm from the analysis revealed 6.12% excess silica.

the diffraction patterns for the powdered rock and for the artificial cristobalite can be compared.

The lines of the diffraction pattern for the powdered rock coinside mostly in position with those for plagiolase, the powder photograph of which has been separately taken for comparison, but some of them differ in intensity. Especially, the innermost two lines (α and β) on the photograph for the rock (Fig. 9) are too strong to be accounted for as due to plagioclase alone. No lines for augite, magnetite, olivine, quartz nor tridymite in their X-ray powder photographs coinside in position with the above two lines. Cristobalite, however, gives lines which are quite in agreement in position with those under consideration, as may be seen in the photograph of Fig. 9,—an evidence that cristobalite is present in our rook.

---

22. 本邦火山岩の石基に産する珪酸鑛物に就いて

地質學教室 久野 久

筆者は北伊豆地方の基性火山岩の顯微鏡的研究中，その石基の主要成分の一つとして極めて普通に珪酸鑛物（石英，鱗珪石，クリストバル石）の存在する事を認めた．これ等の珪酸鑛物は本邦他地方の火山岩にも廣く存在するらしく，本邦火山岩の造岩鑛物として重要なものである．

この論文にては，筆者の北伊豆地方火山岩の觀察により得た材料を基として，これらの鑛物の産出狀態を記載し，その光學的諸性質を擧げ，それと他の地方に産するもの若しくば産出狀態を異にするものとを比較した．

さらにクリストバル石に就いては，微化學的方法により沸石にあらざる事を證明し，又人工のクリストバル石と X 線粉末寫眞を比較して一層確實にした．

これらの珪酸鑛物は明に岩漿より晶出した初生鑛物である．

本邦火山岩の化學的特徵の一つであるノルムに於ける多量の過剩珪酸はモードに於けるこれらの珪酸鑛物の存在によつて容易に說明のつくものであるが，その定量的の關係に就いては直ぐ次の論文に述べる．

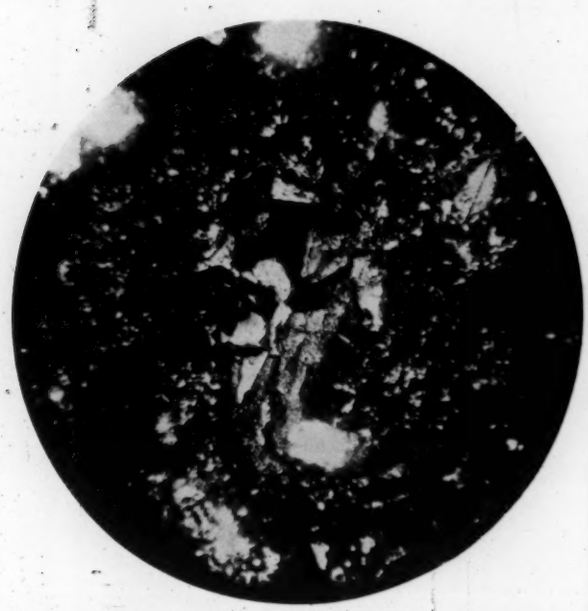

Fig. 5. The groundmass of oliv.-two-pyrox. andesite from Atami, Idu, (31073110), showing the wedge-shaped twinning of tridymite in the center of the photograph. +nicols ×167

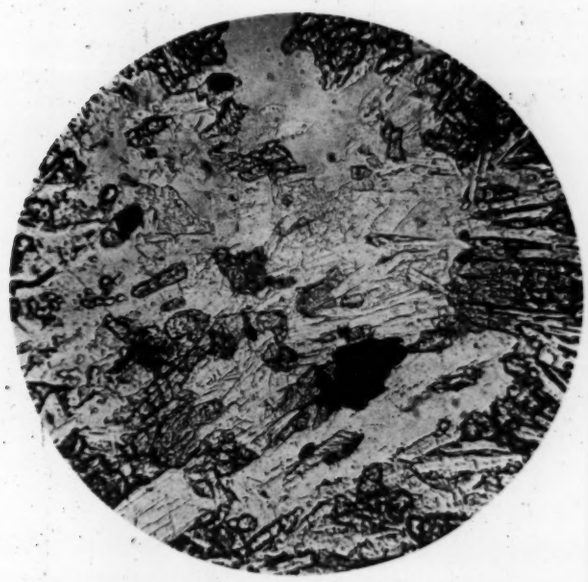

Fig. 6. The groundmass of augite-bearing oliv. basalt from Usami, Idu. (31041510). ×167

（震研彙報、第十一號、圖版、久野）

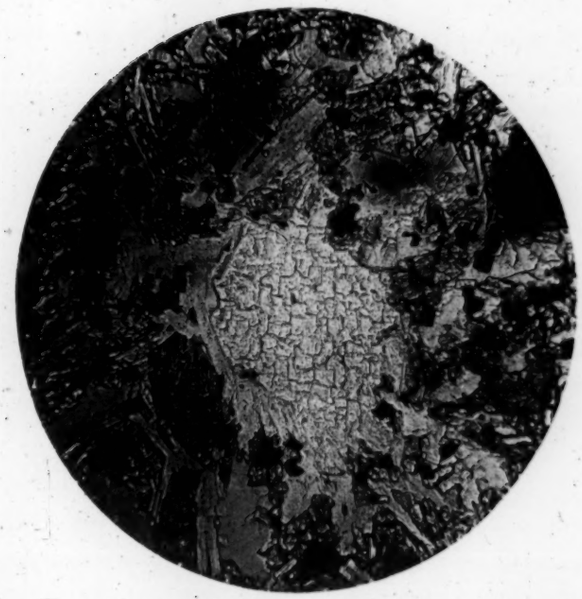

Fig. 7. The groundmass of oliv. basaltic bandaite from Habu, Ôsima, (33012002), showing a rounded patch of well-crystallised cristobalite. ×167

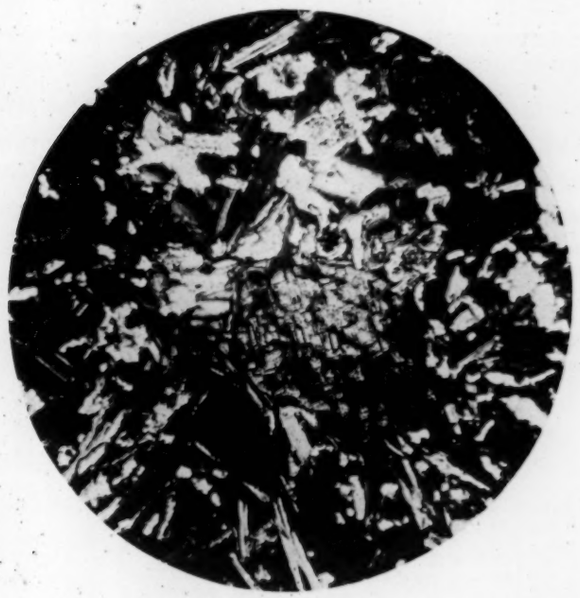

Fig. 8. Same as Fig. 7. +nicols

（震研彙報、第十一號、圖版、久野）

23. *Preliminary Note on Basalt from Aziro, Idu.*

By Hisashi KUNO,

Geological Institute.

(Read Dec. 20, 1932.—Received March 20, 1933.)

I. Introduction.

This paper forms a part of the report of my geological and petrological study of the volcanic district of north Idu, conducted under the auspice of the Earthquake Research Institute of the Imperial University of Tokyo. Here we are only concerned with a rock from Aziro. Special attention is directed to the occurrence of interstitial cristobalite in this rock, the composition of groundmass pyroxene and the contrast between the bulk composition of the rock and the composition of its groundmass.

My thanks are due to Professor Dr. Seitarô Tsuboi who has given me valuable suggestions and encouragements throughout the study.

II. Petrography.

The rock specimen (51227) now in question was collected by Dr. Seitarô Tsuboi on the main road from Aziro to Itô, at the spot immediately south of Aziro, or 7 km. south of Atami. It constitutes one of the numerous thin lava flows associated with bedded alternation of volcanic ash, scoriae, lapilli and bombs, probably of the upper Tertiary or the lowermost Quaternary age, to which I have given the name "Aziro beds."

The series of lavas of Aziro beds were microscopically examined and two petrological types have been distinguished: olivine-augite-anorthite basalt and olivine-augite-hypersthene-bytownite basalt. The rock under consideration belongs to the latter type.

Megascopically the rock is gray, slightly vesicular, and carries phenocrysts of abundant whitish plagioclase and subordinate yellowish olivine, dark greenish augite and dark brownish hypersthene, each crystal being usually 1 mm. and sometimes up to 2 mm. in diameter.

Under the microscope, there are phenocrysts of plagioclase, olivine, augite and hypersthene, scattered through a fine-grained compact groundmass consisting of plagioclase, pigeonite, magnetite, pale brown glass

and cristobalite. There is no sign of alteration. (Figs. 2 and 3.)

Phenocrysts :—

(a) Plagioclases are of two types, A and B. Plagioclase A is euhedral, short prismatic, broadly twinned according to Carlsbad and albite laws and is distinguished from plagioclase B by its larger size, generally 2 mm. in length and by having insensibly zoned calcic core surrounded by a strongly zoned thin sodic shell.

The most calcic part of the core has $n_1 = 1{\cdot}5798$,[1] corresponding to $Ab_1\ An_{99}$, while the average composition of the core as determined by observing n_1 of a great number of cleavage-flakes corresponds to $Ab_7\ An_{93}$. The most sodic part of the marginal shell has $\beta \fallingdotseq 1{\cdot}575$, corresponding to $Ab_{15}\ An_{85}$, as determined in thin section.[2] Consequently the bulk composition of the crystal is estimated as $Ab_8\ An_{92}$.

(b) Plagioclase B does not differ from A in any respects except of its smaller size, less than 1 mm. and of its marked zonal structure which is especially strong toward margin.

The most calcic part has $\beta \fallingdotseq 1{\cdot}580$ corresponding to $Ab_6\ An_{94}$ and the most sodic part of the margin $\beta \fallingdotseq 1{\cdot}568$ $Ab_{29}\ An_{71}$, as determined in thin section as before. The minimum value of n_1 on the cleavage-flakes including all kinds of plagioclase phenocrysts is determined as 1·5659, corresponding to $Ab_{29}\ An_{71}$ which coincides fairly well with the most sodic composition of the plagioclase B. Consequently its bulk composition is estimated as $Ab_{18}\ An_{82}$.

Both of the plagioclase phenocrysts are poor in inclusions except opaque glassy substance often elongated in rectangular form parallel to the elongation of the crystals and infrequent augite grains.

The plagioclase *B* may have been formed in a later generation than plagioclase A, probably under a condition where more rapid cooling prevailed.

(c) Olivine is most prominent among the porphyritic ferromagnesian minerals, forming slightly rounded crystal up to 1 mm. in diameter and surrounded by a thin rim of minute pyroxene grains of the groundmass. Frequently it is much resorbed and replaced by a thick aggregate of granular pyroxene.

---

1) By n_1 of plagioclase is meant the lower refractive index on (010) or (001) cleavage-flake, determined by Tsuboi's dispersion method. S. TSUBOI, *Miner. Mag.*, **20** (1923), 108.

2) The actual method is as follows: a thin section of the rock was put in benzol for a day to wash away the balsam, then pasted upon a slide glass and examined by the ordinary immersion method.

The refractive index was measured on five crystals taken from the hand specimen :[3]

(1) $\alpha=1{\cdot}675$–$1{\cdot}679$ (2) $\alpha=1{\cdot}690$ (3) $\alpha=1{\cdot}690$ (4) $\alpha=1{\cdot}690$
(5) $\alpha=1{\cdot}689$

Composition range : $Fo_{80}\ Fa_{20}$—$Fo_{72}\ Fa_{28}$ (in mol. %)[4]

The average composition is estimated as $Fo_{75}\ Fa_{25}$. The olivine is colorless and almost free from inclusions. Only in one case, however, a prismatic hypersthene has been found included in olivine.

The pyroxene aggregate around olivine may deserve special mention. It forms either a simple rim with rounded outline, or when the resorption of olivine is more advanced, a coarser aggregate containing vermicular rods of iron ore which are radially disposed from the core of the aggregate but not reaching to its margin.

These pyroxenes are of monoclinic variety as far as observed, showing multiple twinning on (100) and resembling in size and habit to pigeonite occurring as microphenocryst, to be refered to later ; while the optical examination reveals that only some of them are truely identical with the microphenocrystic pigeonite, and others with the porphyritic augite.

The measurements were made on two crystals in a single aggregate :

(1) $2V=51°$ (by the conoscope, assuming $\beta=1{\cdot}700$) $2V=51°$ (by the universal-stage), optical plane parallel to (010), optically positive.
(2) $2V=0°$ optically positive.

The measurements on the crystals of another aggregate gave also the same results as above.

(d) Augite is euhedral, short prismatic up to 2 mm. in length, twinned on (100) and free from inclusions except sporadic rounded olivine. It is slightly greenish without sensible pleochroism.

The refractive indices were measured on three crystals taken from the hand specimen :

(1) $n_1=1{\cdot}695$–$1{\cdot}696$ on (110) (2) $n_1=1{\cdot}693$–$1{\cdot}698$ on (110)
(3) $n_1=1{\cdot}693$–$1{\cdot}695$ on (110)

A slight zonal structure is discernible by the difference of extinction angle : $Z\wedge c$ on $(010)=42°$ in the margin,

3) The refractive indices of mafic minerals were determined by the ordinary immersion method, measuring α on (001) cleavage-flake for olivine and smaller refractive index n_1 on (110) cleavage-flake for pyroxenes.

4) The composition is estimated by Winchell's diagram ; Winchell, *Optical Mineralogy*, Part II (1927), 168.

$Z \wedge c$ on (010)=43° in the core.

The optic axial angle was measured on three crystals in the sections:

(1) 2V=51° (by the conoscope, assuming β=1·699) 2V=49° (by the universal-stage)

(2) 2V=49° (by the universal-stage in a crystal with an inclusion of olivine)

(3) 2V=48° (by the universal-stage)

Optically positive, optic plane parallel to (010), the dispersion of optic axial angle insensible.

The values of the optic axial angle coincide with those for the augite found in the aggregate around olivine as well as with those for the augite pseudomorph after hypersthene, to be refered to later.

From the average values of the optical constants (β=1·699 as estimated from n_1, 2V=50°) we have the approximate composition according to Barth's diagram[5]: $Wo_{35}En_{47}Fs_{18}$[6] (in mol. %)

(e) Hypersthene forms a prismatic euhedral crystal up to 1·5 mm. in length and is free from any inclusions, but is surrounded by a thin rim of minute monoclinic pyroxene of the groundmass. It is slightly pleochroic: Z=pale greenish, Y=pale brownish.

The refractive index was measured on three crystals taken from the hand specimen:

(1) n_1=1·687–1·691 on (110)

(2) n_1=1·688–1·692 on (110)

(3) n_1=1·689–1·694 on (110) (grouped phenocryst of hypersthene and augite)

Composition range: $En_{81}Fs_{19}$—$En_{77}Fs_{23}$[7] (in mol. %) Consequently the average composition is $En_{79}Fs_{21}$.

The optic axial angle as measured by the universal-stage in a crystal enclosed in olivine is as follows:

2V=80° optically negative, optic plane parallel to c-axis.

---

5) T. F. W. BARTH, *Amer. Jour. Sci.*, **21** (1931), 385. I have plotted several analysed augites from Japan containing sesquioxides and TiO_2 on his diagram and found that they have always slightly higher refractive indices than those expected in the diagram. Such a fact has been already noted by Winchell (*op. cit.*, p. 188) and it was taken in consideration in the present case for the estimation of the composition.

6) Fs is used here for the molecule $FeSiO_3$, according to the Washington's recent proposal of its use for the normative mineral. H. S. WASHINGTON, *Tsch. Miner. Petro. Mitt.*, **43** (1932), 63.

7) The composition was estimated by Tomida's diagram, though recalculated here in molecular percentage. T. TOMIDA, *Jour. Geol. Soc. Tokyo*, **31** (1924), 375.

Composition: $En_{78}Fs_{22}$, according to Winchell's diagram[8]

In a section there is found a closely packed aggregate of twinned augite, with an outline of a prismatic crystal and resembling in many respects to that forming the rim around olivine. It may be a pseudomorph of augite after hypersthene. This augite has $2V=49°$ (by the universal-stage) and is identical with the isolated porphyritic augite.

Groundmass:—

The groundmass is fine, compact and intergranular or intersertal in texture. The plagioclase crystals sometimes assume an indistinct fluidal arrangement, between which granules of pigeonite and magnetite occur. Minute interstices are filled with glass and cristobalite. Microphenocryst of pigeonite is a conspicuous feature of the groundmass.

(f) Plagioclase is euhedral, lath-shaped or short prismatic up to 0·1 mm. in length. The twinning and zonal structure are very common. It shows a range of refractive index from $\beta=1·568$ to $\beta=1·562$, corresponding to $Ab_{30}An_{70}$—$Ab_{42}An_{58}$, with the average composition estimated as $Ab_{37}An_{63}$.

(g) Pigeonite is of two types. Pigeonite A represents the microphenocryst with euhedral prismatic habit up to 0·2 mm. in length (Figs. 2 and 3.). Multiple twinning on (100) is common. It shows a weak pleochroism: Z=pale green X=Y=slightly brownish green. It is fairly uniaxial and positive in every crystal. $Z \wedge c=40°$–$43°$ on (010)

It represents the early formed crystal in the effusive stage.

(h) Pigeonite B is very fine and granular or prismatic, occurring between plagioclase laths, and is too minute for precise determination, but the conoscopic examination shows that it has at least a small optic axial angle.

(i) Magnetite occurs as minute octahedral grain, commonly in association with pigeonite.

(j) Glass fills the interstices between other crystals and is pale brownish in color with the mean refractive index $N=1·503$, that is, slightly higher than that of the average rhyolite obsidian and pointing to a dacitic or trachytic composition.

(k) Cristobalite also fills the interstices and sometimes occurs as minute rounded patch about 0·1 mm. in diameter. It is clear and free from inclusion and easily distinguished from the glass by the presence of cleavages and characteristic twinning.

8) Winchell, *op. cit.*, 177.

The rock may be called as hypersthene-bearing augite-olivine-bytownite basalt.

III. Chemical Composition.

The result of chemical analysis of the rock by Mr. Senzaburo Tanaka of the Earthquake Research Institute of the Tokyo Imperial University is cited below. It is given in Table I, with the norm calculated from it.

Table I.

Chemical composition and norm of the basalt from Aziro, Idu.
Hypersthene-bearing augite-olivine-bytownite basalt.
S. Tanaka analyst.

SiO_2	51·10	Q	6·48		
Al_2O_3	18·90	Or	1·67		
Fe_2O_3	3·56	Ab	17·82		
FeO	6·52	An	41·14		
MgO	5·03				
CaO	10·80	Di	9·49	Wo	4·87[9]
				En	2·90
				Fs	1·72
Na_2O	2·14				
K_2O	0·32	Hy	15·64	En	9·70
				Fs	5·94
H_2O+	0·50				
H_2O-	0·28	Mt	5·34		
TiO_2	0·83	Il	1·52		
P_2O_5	0·13	Ap	0·34		
MnO	0·13				
Total	100·24				

It must be noted that a considerable amount of excess silica is found in the norm in spite of a calcic composition of feldspar, and that the amount of normative feldspar exceeds that of mafic minerals. The rock has all the chemical and mineralogical characteristics of the common volcanic rocks of Japan, generally called pyroxene-andesite.[10]

IV. Volumetry and Calculation of Mode.

The volume percentages of the constituent minerals were measured by means of the Leitz's "Integrationstisch," counting their liniar proportions in thin sections. The weight percentages, obtained by assuming proper specific gravities for these minerals, are shown in Table II.

9) The change of the calculation of norm after Barth and Washington.
T. F. W. BARTH, *Tsch. Miner. Petro. Mitt.*, **42** (1931), 1.
H. S. WASHINGTON, *op. cit.*

10) S. TSUBOI and H. KUNO, *Bull. Volcanological Soc. Japan*, **1** (1932), 20.

Table II.

The volume and weight percentages of the constituent minerals.

minerals		composition	volume %	sp. gr.	weight %
phenocryst	plagio. A.	An_{92}	9·2	2·7	8·3
	plagio. B.	An_{82}	8·9	2·7	17·1
	olivine	Fa_{27}(mol.)	1·9	3·6	2·3
	augite	$Wo_{35}En_{47}Fs_{18}$ (mol.)	0·7	3·3	0·8
	hypersthene	Fs_{21} (mol.)	0·1	3·4	0·1
groundmass	plagioclase	An_{63}	28·0	2·7	25·4
	pigeonite A and B.[11]	unknown	19·7	3·4	22·5
	iron ore	$Fe_3O_4+TiFeO_3$	7·4	5·0	12·4
	glass	unknown	7·4	2·4	6·0
	cristobalite	SiO_2	6·7	2·3	5·2
			100·0		100·1

In calculating the mode, the analysis was recalculated as water-free, and then the molecules necessary to form those minerals of known composition to the amount given in the last column of Table II were first subtracted and the rest of them alloted to pigeonite and glass with the assumption that all available alumina left form the feldspar molecules in the glass and that the glass contained no ferromagnesian components. The results are shown in Table III.

Table III.

The calculated composition of the modes.

the bulk composition recalculated as water-free		the calculated modes			
		phenocryst	wt. %	groundmass	wt. %
SiO_2	51·38	plagio. A An_{92}	8·30	plagio. An_{63}	25·44
Al_2O_3	19·00	plagio. B An_{82}	17·11	pigeonite Wo_{21}(mol.) En_{53} Fs_{26}	21·53
Fe_2O_3	3·58	olivine Fa_{27}	2·32		
FeO	6·56	augite Wo_{35} En_{47} Fs_{18}	0·80	iron ore	6·86
MgO	5·06			glass An_{27} (mol.) Ab_{57} Or_{16} SiO_2	10·30
CaO	10·86	hypersth. Fs_{21}	0·10		
Na_2O	2·15				1·79
K_2O	0·32			cristobalite	5·20
TiO_2	0·83			apatite	0·34
P_2O_5	0·13				100·09
MnO	0·13				
Total	100·00				

11) Two kinds of pigeonite were counted together.

V. Interpretation of the Result.

The observed amount of the iron ore is about twice as much as the calculated one, even though all the available Fe_2O_3 and TiO_2 were alloted to it. This must be due to that the iron ore occurs as minute grains usually attached to pigeonite and is apt to be overestimated in volumetry. On the other hand the observed amount of the glass is too small. When it fills the minute intersitces between the pigeonite, it can scarcely be discriminated from the latter, and consequently it may be counted together with pigeonite.

The composition of the groundmass pyroxenes:—

It is possible to abtain a theoretical value of refractive index for the calculated composition of the glass after the method employed by C. E. Tilley.[12] The composition of the glass (feldspar+silica) is shown in Table IV, together with the norm and the specific refractivities of the normative constituents.

Table IV.

The calculated composition of the glass.

	wt. %	norm		sp. refr.
SiO_2	66·6	Q	15·00	0·2074
Al_2O_3	20·6	Or	13·34	0·2056
CaO	4·9	Ab	47·16	0·2053
Na_2O	5·6	An	24·46	0·2132
K_2O	2·3			
	100·0			

The interstitial glass under consideration has N=1·503, corresponding to the specific gravity d=2·40-2·43.[13] It is calculated according to Tilley, that N=1·498 if d=2·40 and N=1·504 if d=2·43, that is, a close agreement with the observed one. It is therefore probable that the anorthite molecule in the calculated composition of the glass does not enter into the natural pigeonite to any great extent.

Now that the calculated composition of the glass was found to be fairly correct, the composition of the groundmass pyroxene is considered to be equally so. It is plotted upon the triangular diagram showing the relation between composition and optical properties according to

12) C. E. TILLEY, *Miner. Mag.*, 19 (1922), 291.

13) C. E. TILLEY, *op. cit.*, 282.
W. O. GEORGE, *Jour. Geol.*, 32 (1924), 367.

Barth,[14] together with those of the porphyritic minerals; augite, hypersthene and olivine (olivine regarded as metasilicate). (Fig. 1)

The uniaxial pigeonite occurring in the groundmass as microphenocryst, of which I have already described, must have the composition lying upon the line 2V=O in the diagram. It is understood that pigeonite poorer in lime crystallised as an early mineral from a melt approximately with the calculated composition of the groundmass pyroxene, i. e. somewhat higher in lime, under the condition of the effusive stage, that is, the condition B according to S. Tsuboi.[15]

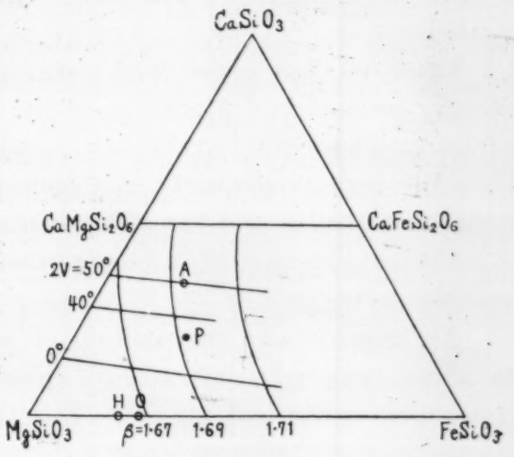

Fig. 1.
H....hypersthene
O....olivine
A....augite
P....pigeonite

The crystallisation of pyroxene under the condition B is comparable to that in the investigated system: diopside-forsterite-silica.[16] In this system, a certain liquid whose composition is represented by a point in the lower part of the pyroxene field will become, if quenching occurs, a crystalline aggregate of cristobalite and a monoclinic pyroxene with a certain composition of the diopside-clinoenstatite solid solution. But on the other hand, when the same liquid is slowly cooled, the first mineral to crystallise will be a monoclinic pyroxene with a composition somewhat higher in clinoenstatite molecule than that of the pyroxene formed by quenching.[17]

On the normative quartz:—

It has long been recognised as one of the characteristics of the common Japanese effusive rocks, that a notable amount of excess silica appears in their norms in spite of the calcic nature of the feldspar. In

14) T. F. W. Barth, *Amer. Jour. Sci.*, **21** (1931), 385.
15) S. Tsuboi, *Jap. Jour. Geol. Geogr.*, **10** (1932), 78.
16) N. L. Bowen, *Amer. Jour. Sci.*, **38** (1914), 245.
17) The similar type of the crystallisation of pyroxene as noted here was emphasized by A. Holmes and H. F. Harwood in the Whin Sill magma type. A. Holmes and H. F. Harwood, *Miner. Mag.*, **21** (1928), 506.
18) J. P. Iddings, *Igneous Rocks*, **2** (1913), 111.

emphasizing this characteristics some petrologists have given special names for them, viz., bandaite by J. P. Iddings[18] and miharaite by S. Tsuboi.[19]

Recently, Professor S. Tsuboi and I noted on the common occurrence of silica minerals (cristobalite, tridymite and quartz) in the groundmass of basic effusive rocks and remarked that this may explain the presence of normative quartz.[20] The rock now under consideration is a typical example.

There is 6·48 percent of normative quartz, while the cristobalite actually present is 5·2 percent of the rock. In addition there is a low-refracting glass, which probably contains a considerable amount of silica. Thus the normative quartz may correspond in amount to the sum of the modal cristobalite and the silica contained in the glass.

The comparison of the bulk analysis with the composition of the groundmass:—

An approximate composition of the groundmass was calculated from its actual mineral composition: plagioclase An_{32}, pigeonite, iron ore, glass, cristobalite and apatite. The result is shown in Table V.

Table V.

The calculated composition of the groundmass.

	wt. %	norm.			
SiO_2	53·4	Q	9·84		
Al_2O_3	14·4	Or	2·22		
Fe_2O_3	5·1	Ab	20·44		
FeO	8·4	An	27·24		
MgO	5·7			Wo	6·73
CaO	8·9	Di	13·14	En	3·50
Na_2O	2·4			Fs	2·51
K_2O	0·4			En	10·40
		Hy	17·26	Fs	6·86
TiO_2	1·1	Mt	7·42		
P_2O_5	0·2	Il	2·13		
Total	100·0	Ap	0·34		

It shows a marked contrast with the bulk analysis given in Table I. A smaller content of alumina and a greater content of iron oxides are especially striking, which may be attributed to the presence of calcic

19) S. TSUBOI, *Jour. Coll. Sci. Imp. Univ. Tokyo*, **43** (1920), 87.

20) S. TSUBOI and H. KUNO, *op. cit.*, 34.
See also my preceeding paper in this bulletin.

plagioclase and magnesia-rich ferromagnesian minerals as phenocrysts included in the bulk analysis. We have here a very similar relation as found between *the Non-Porphyritic Central Magma-Type* and *the Porphyritic Central-Magma-Type* in the Mull rocks,[21] the bulk composition of the latter type was reasonably explained by N. L. Bowen as a possible effect of crystal sorting in the course of its formation.[22]

It must be noted too that the composition of the groundmass representing a possible magmatic liquid has some resemblances to that of the plateau-basalt described by H. S. Washington.[23] The difference is only in the amounts of SiO_2 and of the normative quartz and the degree of oxidation of iron. The siliceous nature of the Japanese effusive rocks seems to be inherent, even in the basic varieties.

Then it may be understood that the Japanese basic effusive rocks are very similar or closely related to the well-known plateau-basalt. The bulk compositions of the Japanese rocks may be however, often controlled by the accumulation of calcic plagioclase crystals in the magma.

---

23. 伊豆網代産玄武岩に就いて（豫報）

地質學教室　久野　久

この論文は筆者が行ひつゝある北伊豆地方火山岩の地質學的並に岩石學的研究の結果の一部の報告である.

伊豆網代附近を構成する古い火山體の一部に熔岩流をなして産する紫蘇輝石普通輝石橄欖石亞灰長石玄武岩の顯微鏡的觀察，特にその構成鑛物の光學的研究の結果を記載し，これらの構成鑛物の推定成分並にその量比の測定値とを，この岩石の化學分析の結果より計算したる鑛物成分と比較した.

この結果より，石基輝石の結晶作用を論じ，又この岩石の化學分析結果に現はれたるノルム石英はその石基中に存在するクリストバル石並にガラスに負ふものなる事を明にし，最後にこの岩石の石基のみの化學成分を計算し，これとその總化學成分との關係に就いて注意した.

---

21) "Tertiary and Post-Tertiary Geology of Mull, etc.," *Memoir of Geol. Surv. Scotland*, (1924), 16 and 23.

22) N. L. Bowen, "The Evolution of the Igneous Rocks," (1929), 134.

23) H. S. Washington, *Bull. Geol. Soc. Amer.*, **33** (1922), 705.

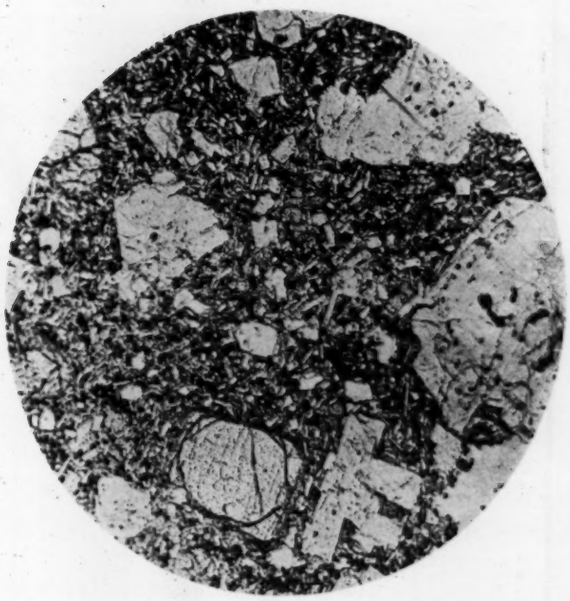

Fig. 2. Hypersthene-bearing augite-olivine-bytownite basalt from Aziro, Idu, (51227), showing phenocrysts of plagioclase and olivine (lower part), and microphenocryst of uniaxial pigeonite (slightly above the center). ×51

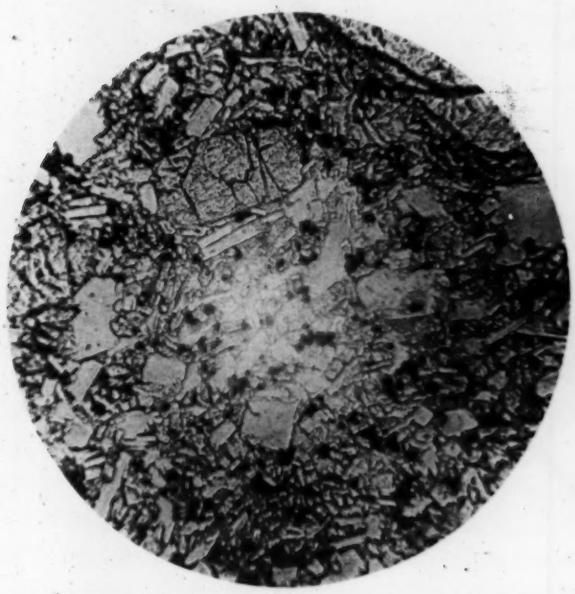

Fig. 3. Ditto, showing the groundmass and the prismatic microphenocryst of uniaxial pigeonite (upper part). ×167

（震研彙報、第十一號、圖版、久野）

24. Study on the Propagation of Seismic Waves. (The second paper)

Amplitude of Seismic Waves with the Structure of the Earth's Crust and Mechanisms of their Origin.[1]

By Hirosi KAWASUMI,

Seismological Institute.

(Read Mar. 15, June 21, Oct. 18, 1932; and Mar. 2, 1933.—
Received June 20, 1933.)

Introduction.

The foretelling the earthquake occurrence, which is one of the greatest aim of seismolgical investigation in the "Land of Earthquake" Japan, can not be realized without the exact knowledge of the chronological and inter-regional relations of the activity of earthquake generating forces. The late Prof. F. Omori[2] was the first to discuss the mechanism of earthquake occurrence from the results of seismometrical observations. In case of the earthquake of Feb. 6, 1907, a very peculiar seismograms showing no preliminary tremors were obtained at Osaka and its vicinity, while ordinary seismograms having distinct P and S phases were obtained at other places of Japan. Prof. Omori had to consider the mecanism of occurrence of the earthquake to explain these conspicuous phenomena. Since then he paid attention to the directions of the initial motions of the earthquakes accompanying the Asamayama explosions.[3] But Prof. T. Shida[4] was the first who could find the way actually to the purpose

1) Already published in Japanese in the *Disin* or the *Journ. Seismol. Soc. Japan*, September and November of 1932 and May of 1933.

2) F. OMORI, *Bull. Earthq. Invest. Commit.*, **1** (1907), 145–154.

3) F. OMORI, *ibid.*, **6** (1912), 11; **7** (1914), 1; and *Publ. Earthq. Invest. Commit.*, **21** (1905).

4) T. SHIDA, "Disingaku no Saikin" (Modern Topics in Seismology), (in Japanese). The manuscript of the lecture delivered at the Kamigamo Seismological Observatory on July 19, 1921. On page 31 we find the following passage. "Since about ten years I have been aware of the fact that we can judge from the records of an earthquake motion at neibouring stations whether the earthquake began with sudden cracking or depression at hypocentre, and we are able to know the direction of the crack as well in the former case. And I have now obtained considerable results. etc."

See also

Torahiko TERADA and Takeo MATUZAWA, A Historical Sketch of the Developement of Seismology in Japan. (1926).

M. HASEGAWA, *Beitr. z. Geophys.*, **27** (1930), 102–125.

M. MATUYAMA, Bankin no Disingaku—i. e., Modern Seismology, (in Japanese), (1925).

in the seismometrical investigations. He found very good examples, for which he had been seeking since several years, in the Tenryûgawa Earthquake of May 18, 1917 and the Awazi Earthquake of Nov. 26, 1916, and he delivered the results at the meetings of the Physico-mathematical Society of Japan and the Earthquake Investigation Committee in 1917 and 1918. In the former earthquake the distribution of dilatation and compression (or 'pull' and 'push' according to Prof. Shida) of the initial motion were divided into quadrants by two nodal lines crossing at right angles at the epicentre. In the latter earthquake the "pulls" (or dilatations) were confined within a circle near the epicentre. And Prof. Shida explained the former as "crack earthquake" and the latter as "depression earthquake." Since then ardent interrest of Japanese seismologists centred upon this interesting problem. From investigations of several earthquakes[5] Prof. S. T. Nakamura found intimate relation between the positions of nodal lines of initial motions of an earthquake and geological techtonic line near the epicentral region, and explained the mechanism of the earthquake which had been called the crack earthquake by Prof. Shida as sliding along one of the nodal planes. The "fault earthquake" theory thus introduced found its supporters among the members of the Central Meteorological Observatory and was applied to almost all earthquakes up to the close of the year 1931, when Mr. K. Tanahasi[6] found an example which could not be explained by this category. It was the deep-seated Central Japan Earthquake of June 2, 1931, in which we cannot find nodal planes consequential to the fault earthquake theory. But we find nodal lines resembling hyperbola, from which we can only conclude the existence of nodal cone surface. The theory for this model is due to Prof. M. Matuyama. Prof. M. Ishimoto[7] greatly interested upon this example and found another example of this type in the Ise-bay Earthquake of June 3, 1929. In case of shallow earthquake in which two dimensional relation can only be observed at the earth's surface near the epicentre we cannot find any differrence from the mere quadrant distributions of "pull and push" between the two mechanisms of the Prof. Matuyama's

5) The Omati earthquake of 1918 (*Journ. Met. Soc., Japan*, **37** (1918), 390-401.); the Miyosi earthquake of 1919 (*ibid.*, **38** (1919), 395-404); the Simabara earthquake of 1922 (*ibid.*, [ii], **1** (1923), 1-13), etc.

6) K. TANAHASI, *Umi to Sora*, **11** (1931), 277-288.

7) M. ISHIMOTO, Lecture delivered at the colloquium of the seismological Institute on Jan. 20, 1932.

M. ISHIMOTO, *Proc. Imp. Acad.*, **8** (1932), 36-39.

model and that of the fault earthquake theory. (We shall for convenience call in the following the former as Model A and the latter Model B.) But in case of deep-seated earthquake the spherical waves are observed as they are and the difference of the mechanisms are revealed at a glance. From the above consideration Prof. Ishimoto adovacated strongly the necessity of considering the problems in three dimensions. And in March of 1932 he reexamined the problems from this point of view and could explain almost all earthquakes by the model A, and he thought this as the evidence of his 'magma intrusion theory' or 'plutonic earthquake theory' of earthquake occurrence.[8] And this gave a new question of the validity between this hypothesis and the former 'fault earthquake theory.'

On the other hand Mr. H. Honda[9] studied in June of 1931 the magnitudes of initial motions of the North Idu and Ito Earthquakes quantitatively, and explained the result by Dr. H. Nakano's theoretical investigation[10] in homogenious isotropic semi-infinite solid. But the present writer[11] advocated in the next month the necessity of considering the effect of heterogeneity of the crust showing that the result of Mr. Honda could be enumerated by the method of K. Zoeppritz, E. Wiechert and Dr. H. Jeffreys. Since that time the writer has been intending the quantitative study of seismic waves, as he has stated in his first paper with the same title. He was encouraged by Mr. Tanahasi's result and Prof. Ishimoto's opinion and studied the amplitudes of seismic waves quantitatively taking the structure of the earth's crust into consideration for the purpose of verifying the mechanisms of earthquake occurrence. And a part of the result will be contributed here.

Before entering the main subject historical review of the former investigations, practical and theoretical, will be given for the indication of the way of future study.

Chapter I. Historical review of the former Investigations.

i) *Theoretical sides.*

In early part of last century Cauchy and Poisson determined the

8) M. Ishimoto, lectured on the meeting of the Earthquake Research Institute on Mar. 15, 1932. *Bull. Earthq. Res. Inst.*, 10 (1932), 449-471.

9) H. Honda, *Geophys. Mag.*, 4 (1931), 185-213.

10) H. Nakano, *Geophys. Mag.*, 2 (1930), 189-348.

11) H. Kawasumi, On the initial motion of earthquake, read at the meeting of the Earthquake Research Institute on July 7, 1931.

equations of motion in elastic solid. Poisson[12] used it to investigate the propagation of waves through an isotropic solid and found two types of waves which, at great distance from the source of disturbance, are practically "longitudinal" and "transverse." Cauchy[13] applied his equations to the questions of propagation of light in crystalline as well as in isotropic medium. Thus the theory of elastic waves drew attentions of many authrities on account of its applicability to the theory of light. Green[14] investigated the reflexion and refraction of an elastic waves, and waves in an crystalline medium. In 1849 Stokes solved most fundamental problems of elastic waves in his "Dynamical Theory of Diffraction.[15]" He found that the Poisson's two waves are waves of irrotational dilatation and equivoluminal distortion, the latter involving the rotation of elements of the medium. The Poisson's formula,[16] expressing the displacement at any time in terms of initial distribution of displacement and velocity in a medium in which only one kind of wave can exist was extended by him to the problems in elastic medium in which two kind of waves are possible. From the application of this formula Stokes obtained a solution of elastic waves due to a force opperative at a limmited portion in the medium. In 1871 Lord Rayleigh[17] obtained the solution of waves due to a force opperative at a point in a simpler fashion than that of Stokes in his investigation of the "Light from the Sky." Lord Kelvin[18] showed in 1884 that the solution of wave equation satisfies the original equation after it has subjected to multiple differentiation with respect to coordinates x, y and z. The well-known Rayleigh[19] wave was find in 1885. In 1904 H. Lamb[20] showed an elegant procedure in the investigation of "the Propagation of Tremors over the Surface of an Elastic Solid" which were followed by many later investigators, and A. E. H. Love[21] treated general problem of waves in isotropic

12) S. D. POISSON, *Paris Mèm. de l'Acad.*, **8** (1829).

13) A. L. CAUCHY, *Exercices de Mathematique*, (1830).

14) George GREEN, *Phil. Trans., Cambridge*, **7** (1939), or Math. Papers (1871), 245.

15) G. G. STOKES, *Phil. Trans., Cambridge*, **9** (1849) and *Math. and Phys. Papers*, **2**, 243-328.

16) S. D. POISSON, *Mèm. de l'Institute* **3**, (1820), 121.
Lord RAYLEIGH, "Theory of Sound," § 273 and Note to § 273.

17) Lord RAYLEIGH, *Phil. Mag.*, **61** (1871), 107, 274 and 447, or Scientific Papers, **1**, 87-103.

18) Lord KELVIN, Bartimore Lecture I 884, and *Phil. Mag.*, [v], **47** (1899), 480-493; **48** (1899), 227-236.

19) Lord RAYLEIGH, *Proc. Math. Soc., London*, **17** (1885), or Scientific Papers, **2**, 441.

20) H. LAMB, *Phil. Trans. Roy. Soc., London*, A **203** (1904), 1.

21) A. E. H. LOVE, *Proc. Math. Soc., London*, [ii], **1** (1904), 291-344.

medium in which he made corrections to the formula obtained by Stokes. Kirchhoff's formula is also extended to the waves in elastic solid. The waves due to body forces were solved by the application of Lord Kelvin's procedure in the solution of the corresponding statical problem. The effect of various nuclei of strain were also considered by the superpositon of the waves due to a force opperative at a point.

Few investigations have since appeared except the discovery of the Love wave[22] untill Prof. Shida discovered in actual earthquake of the fact already stated which had also been expected by G. W. Walker[23] on Stokes' dynamical theory of diffraction. New epoch was then made in Japan. In 1922 Prof. S. T. Nakamura[24] explained the mechanisms of earthquake occurrence by the analogy of the field due to a system of electric charges. He could explain sufficiently the direction of initial motion by this analogy, but the magnitudes were not explained. He should have to follow Lord Kelvin and use a wave function of the form $\frac{1}{r}e^{i(pt-hr)}$ instead of $\frac{1}{r}$. The paper of Dr. Nakano[25] on this problem published in 1923 was unfortunately burnt to ashes by the disastrous fire which ruined the City of Tokyo. In 1925 Mr. K. Suda[26] showed various models by the combination of Rayleigh's solution for a force at a point. But the mathematical solution for each of them were not given. In the treaties of Prof. Matuyama[27] on seismolgy published in the same year we find a few models obtained by the method of Lord Kelvin by the superposition of $\frac{1}{r}e^{i(pt-hr)}$. Prof. T. Matuzawa[28] calculated in the next year actually the models considered by Love in Cartesian coordinates.

All the investigations stated above belong to the so called "method of singularities[29]" and the model of Mr. M. Hasegawa[30] which appeared in 1930 also belong to this category. The "method of series[31]" which Stokes already used in other branch of science were introduced by

22) A. E. H. Love, "Some Problems of Geodynamics," (1911), 160-165.

23) G. W. Walker, "Modern Seismology," (1913), 64.

24) Saem. Nakamura, *Journ. Met. Soc. Japan*, **41** (1922), e. 1.

25) H. Nakano, *Seismol. Bull. Centr. Met. Obs. Japan*, **1** (1923), No. 3.

26) K. Suda, *Umi to Sora*, **5** (1925), 36-39; 46-51; 64-69; 80-88; and *ibid.*, **6** (1926), 24-31; 50-60.

27) M. Matuyama, *loc. cit.*, 4).

28) T. Matuzawa, *Jap. Journ. Astro. Geophs.*, **4** (1926), 1-33.

29) A. E. H. Love, Mathematical Theory of Elasticity, 4th Ed., 15.

30) M. Hasegawa, *loc. cit.*, 4).

31) *loc. cit.*, 29).

Prof. K. Sezawa and Dr. Nakano into studies of the waves in and on elastic solid. The problems treated by these authorities cover so wide a range that cannot the condenced in this narrow space that I will state here only the results concerning spherical waves.

In 1927 Prof. Sezawa obtained a waves expressed in zonal harmonics and discussed the distribution of energy among the dilatational and distortional waves,[32] and this solution was applied to the solution of the Rayleigh waves over a spherical surface.[33] The waves from an elliptical or ellipsoidal origin[34] were obtained to show the effect of the dimension of origin may be negligible at a distance from the origin. Applications of these waves were made to the scattering[35] of elastic waves by the obstacles of various forms. The waves in visco-elastic solid body[36] were also discussed but the solution of spherical waves in this medium was left behind. Prof. K. Sezawa investigated in 1928 the reflection of spherical waves[37] from an internal point of a sphere, and in the next 1929 he obtained most general spherical standing waves in course of the studies of Rayleigh-[38] and Love[39]-waves having azimuthal distributions. He also obtained waves in definite integrals answering to internal multiplet[40] and sheet[41] of internal sources in course of studies of genrations of Rayleigh waves. In July 1931 Prof. K. Sezawa[42] made an analysis of general spherical diverging waves but it was not published. But in February of last year he obtained general spherical waves in visco-elastic medium.[43] In the same month the present writer[44] obtained some spherical waves in a simpler formal fashion and applied them to the present investigation. Mr. Y. Kodaira[45] also read a paper in the next month on the same spherical waves at the meeting of Meteorological

32) K. SEZAWA, *Bull. Earthq. Res. Inst.*, 2 (1927), 13-20.
33) K. SEZAWA, *ibid.*, 2 (1927), 21-28.
34) K. SEZAWA, *do.*, 2 (1927), 29-48.
35) K. SEZAWA, *do.*, 3 (1927), 19-41.
36) K. SEZAWA, *do.*, 3 (1927), 43-53.
37) K. SEZAWA, *do.*, 4 (1928), 123-130.
38) K. SEZAWA, *do.*, 6 (1929), 1-18.
39) K. SEZAWA, *do.*, 7 (1929), 41-64.
40) K. SEZAWA, and G. NISIMURA, *do.*, 7 (1929), 41-64.
41) K. SEZAWA, *do.*, 7 (1929), 417-435.
42) K. SEZAWA, lectured at the Meeting of the Earthq. Res. Inst. on July 7, 1931.
43) K. SEZAWA, *Bull. Earthq. Res. Inst.*, 10 (1932), 299-334.
44) H. KAWASUMI, Mechanisms of Earthquake Occurrence and Abnormal Felt. Area, read at the colloquium of the Seismological Institute on Feb. 17, 1932.
45) Y. KODAIRA, *Journ. Met. Soc. Japan*, [ii], 10 (1932), 236-251.

Society of Japan.

I must also add here the investigation of Mr. R. Yosiyama[46] who is making investigations of waves in heterogeneous sphere and have already obtained some remarkable results.

ii) *Practical side.*

It was from the Ewing's observation[47] of the earthquake near Tokyo of Mar. 8, 1881 that the two waves in elastic body were distinctly registered. Ewing's tentative explanation of these two waves as normal (longitudinal) and transverse waves were confirmed by the experimental study of J. Milne[48] and T. Gray. But owing to the uncertainty of our knowledge of the nature of the material of the earth's crust several other tentative explanations were proposed by C. G. Knott[49] and S. Kusakabe.[50] And it was quite recent that the first part of preliminary and principal portion of near earthquake were believed to be longitudinal and transverse waves, being hindered also by the deficiency of our knowledge of surface waves. The direction of first motion of an earthquake, which had been used for the determination of the direction of epicentre and hypocentre, were investigated statistically by Mr. M. Kawazoe[51] and recently by Mr. F. Kishinouye.[52] Quite recently Mr. S. I. Kunitomi[53] studied systematically the deviation of this direction from that of epicentre.

But as to the fact found theoretically in 1849 by Stokes that the magnitude and sense of motion—away from (compression) and toward (dilatation) the origin—vary with the direction from the origin, the former once noticed by Prof. Omori in 1907[54] was again dismissed and the latter was left unnoticed untill in 1917 Prof. T. Shida,[55] who had been aware of the possibility contemporaneously with or earlier than the notion of G. W. Walker in his "Moder Seismology," made a new epoch

46) R. Yosiyama, *Bull. Earthq. Res. Inst.*, **11** (1933), 1-12.

47) J. A. Ewing, *Trans. Seismol. Soc. Japan*, **3** (1881), 121-128.

48) J. Milne and T. Gray, *Phil. Trans.*, (1882), 863-883.
J. Milne, *Trans. Seismol. Soc. Japan*, **8** (1885), 1-82.
J. Milne, "The Earthquake and other Earth movements," (1886), 57-66.

49) C. G. Knott, *Trans. Seismol. Soc. Japan*, **12** (1888), 115.

50) S. Kusakabe, *Publ. Imp. Earthq. Invest. Commit.*, **14** (1903), esp. 52.

51) M. Kawazoe, *Journ. Met. Soc. Japan*, **37** (1918), 53-57.

52) F. Kishinouye, *Journ. Seismol. Soc. Japan*, **4** (1932), 18-35.

53) S. J. Kunitomi, lectured at the meeting of Meterological Society of Japan on Feb. 19, 1932.

54) *loc. cit.*, 2).

55) *loc. cit.*, 4).

in seismometrical investigation finding actually the mechanism of occurrence of the Tenryû-gawa earthquake from the systematic observation of "pull" and "push" of initial motion of P-wave. The examination of the geographical distribution of the directions of initial motion, for the purpose of inducing the mechanism of earthquake occurrence, then became the centre of unceasing interest of many seismologists. Prof. S. T. Nakamura and his colleagues succeeded the method and applied it to the Ômati earthquake[56] of 1918; the Miyosi earthquake[57] of 1919; the earthquake[58] of May 21, 1920 originated in the western part of the Inland Sea of Japan; the great Kan-sou earthquake[59] of 1921; the strong earthquake[60] near Tokyo of April 6th, 1922; the earthquake[61] of June 18th, 1922 in the southern coast of Sima province; a small destructive earthquake[62] near the lake Imbanuma of Dec. 8, 1922; and the Simabara[63] and the great Kwanto earthquakes of 1923. It was revealed by these investigations the existence of other types of "pull-push" distribution than those which had been found by Prof. T. Shida. Some earthquakes showed the "pull-push" distribution devided by a straight line, and the other showed curved nodal lines intersecting each other. Prof. S. T. Nakamura[65] explained them by the specical situation and direction of of multiplets opperative at hypocentre at some depth from the earth's surface. (He only considered the quadruple source of type B.)

Mr. K. Suda[66] made studies not only the Simabara earthquake but also of theoretical problems[67] already mensioned and applied them to the earthquakes originating at various parts in Japan and showed the distribution of the direction of the earthquake generating forces in this country. Prof. Matuzawa[68] illustrated the results of his theoretical calculation by actual examples. The discovery of existence of the

56) S. T. NAKAMURA, *loc. cit.*, 5).
57) *do.*
58) S. AOKI, *Journ. Met. Soc. Japan*, **39** (1920), 192-194.
59) T. USIYAMA, *Journ. Met. Soc. Japan*, **40** (1921), 135-138.
60) S. T. NAKAMURA, *ibid.*, **41** (1922), 139-156.
61) T. USIYAMA, *ibid.*, **41** (1922), 222-229.
62) T. USIYAMA, *ibid.*, **41** (1922), 4-13.
63) S. T. NAKAMURA, *ibid.*, [ii], **1** (1922), 1-12.
64) S. T. NAKAMURA, *Rep. Earthq. Inv. Comit.*, **100** (1825) *A*, 67-140.
65) S. T. NAKAMURA, *Journ. Met. Soc. Japan*, **41** (1922), e. 1.
66) K. SUDA, *Umi to Sora*, **3** (1923), 14.
67) *loc. cit.*, 26).
68) T. MATUZAWA, *loc. cit.*, 28).

Mohorovičić's layer in Japan was made by Dr. K. Wadati[69] from the study of the Tazima earthquake, in which a circle, deviding pull and push and called by him an inflexion circle, appeared at a epicentral distance where normal P-wave arrives at the same time with individual $\bar{P}$-wave. The effect of this superficial crustal layer on the distribution of initial motions was taken into consideration by Mr. S. I. Kunitomi to the studies of the Tazima, Tango,[70] Middle Etigo,[71] the Great Kwanto,[72] Ito, North Idu,[73] and Saitama[74] earthquakes, and all these earthquakes were explained by the model B, in which two nodal planes intersect at right angles at the hypocentre. He called these earthquakes "fault earthquakes" and he considered that the earthquake motions are caused by the actual motion of the mass near the hypocentre, and he thought that the amplitude of the seismic P-wave is largest in the direction of the fault, which he termed as a "fault plane" and vanishes at the perpendiculer direction which he called a "nodal plane."

But we have had no example in which the fault and nodal planes are distinguished, and also no theoretical support to such hypothesis. This type of mechanism (model B) was applied by Messrs. Sagisaka,[75] Satô, Isikawa,[76] Hayata,[77] and Oka[78] of the Central Meteorological Observatory to almost all the earthquakes. Moreover Mr. Sagisaka[79] renoticed the relation between the regional distribution of seismogram-types and the mechanism of earthquake occurrence once found by Prof. Omori. Mesrrs. Taguti[80] and Tanahasi[81] also considered the same mechnism in the study of the earthquakes of Kii Province. Mr. K. Fukutomi[82] studied statistically the earthquakes originated in the Kwantô plane, and explained the "pull-push" distributions by one nodal straight

69) K. Wadati, *Geophys. Mag.*, 1 (1927), 89-86.
70) S. I. Kunitomi, *Geophys. Mag.*, 2 (1929), 65-89.
71) S. I. Kunitomi, *Journ. Met. Soc. Japan*, [ii], 3 (1928), 59-85.
72) S. I. Kunitomi, *Geophys. Mag.*, 3 (1930), 149-164.
73) S. I. Kunitomi, *ibid.*, 4 (1931), 73-102,
74) S. I. Kunitomi, read at the meating of the Met. Soc. of Japan, and Earthquake Research Institute, not yet published.
75) K. Sagisaka and H. Sato, *Journ. Met. Soc. Japan*, [ii], 4 (1926), 301-307
76) T. Isikawa, *ibid.*, [ii], 10 (1932), 152-216.
77) K. Hayata, *ibid.*, [ii], 7 (1929), 303-310.
78) Y. Oka, *Geophys. Mag.*, 6 (1932), 213-221.
79) K. Sagisaka, *Geophys. Mag.*, 3 (1930), 165-176.
80) K. Taguti, *Umi to Sora*, 4 (1924), 199-203.
81) K. Tanahasi, *Umi to Sora*, 9 (1929), 197-202; 10 (1930), 13-18 and 213-222.
82) K. Hukutomi, *Journ. Seismol. Soc. Japan*, 3 (1931), 592-616.

line or two nodal lines crossing at right angles which support also mechanism of model B, and found some favourable relations with the secondary causes of the earthquake occurence as the gradient of atmospheric and tidal pressures.[83] I must also add here Mr. Honda's investigation in which quantitative elucidation of Dr. Nakano's theory is made from the study of the North Idu and Ito earthquakes.

Thus it has been considered that almost all the earthquakes can be explained by the mechanism of model B, when Mr. Tanahasi discovered an example of the earthquake which cannot be explained by the mechanism of model B and is well explainable by that of model A. Mr. Tanahasi also discussed the mechanism of occurrence of the S-wave by the theory of Prof. Matuyama, but he mistook it a little and overlooked a conspicuous phenomenon, on which I will return later. Of the following investigations of Prof. Ishimoto and others are stated in the introduction.

Reviewing again the notions of authorities on this problem, we see that J. A. Ewing was the first to identify the preliminary tremor and the principal portion of the earthquake and the Poisson's two waves, longitudinal and transverse, but several questions were raised on this point so long as our knowledge on the nature of the materials consisting the earth's crust were limited, and it was quite recent that the Ewings opinion was generally accepted. The variation of relative magnitudes of these waves with bearings from the hypocentre theoretically expected by Stokes was found by Prof. Omori in 1906, and the corresponding variation of sense of vibration was discovered by Prof. Shida in 1917. Since that time the "pull-push" distribution was solely noticed, and the progress of our knowledge on the crustal structures introduced new features in this field, but the relation of the relative magnitude of P- and S-waves with the mechanism of their origin theoretically studied by Mr. K. Suda and Prof. Matuzawa was renoticed to be seen as seismogram-types by Mr. Sagisaka. But owing to the lack of our exact knowledge on the crustal structure and the reliability of seismographs prevented us to touch on the quantitative examination of the theoretical relations on the amplitudes of seismic waves. But recent rapid reformation of the net of seismic observations in Japan enabled Mr. Honda to enter into

83) Recently after this paper has been written Mr. Fukutomi reexamined these earthquakes and showed that the "pull-push" distributions are better explained by the mechanism of the model A.

84) H. HONDA, *loc. cit.*, 9).

this field in 1931. But all these studies above mensioned are the studies of waves in an isotropic homogeneous solid and their applications, and the effect of the structure of the crust was not taken into consideration. But the present writer noticed that the quantitative study can not be made without taking the actual structure into consideration, and the result of his study in these lines will be communicated in the followings. New epoch is still promissed with the accomplishment of the theory of waves in heterogeneous medium now being commenced by Mr. R. Yosiyama.

Chapter II. General Solution of Spherical Waves Propagated in an Isotropic Elastic Medium.

The solution was already obtained by Prof. K. Sezawa,[85] but I obtained in a different and easier way as his solution had not yet been published.[86]

Equation of motion in an isotropic medium

$$\rho\frac{\partial^2\boldsymbol{\sigma}}{\partial t^2}=(\lambda+2\mu)\ \text{grad div}\ \boldsymbol{\sigma}-\mu\ \text{rot rot}\ \boldsymbol{\sigma}, \quad \ldots\ldots(1)$$

(in which σ is displacement and ρ, λ and μ are dencity and Lamê's constants respectively) is satisfied by

$$\boldsymbol{\sigma}_1=\text{grad}\ \phi e^{ipt}, \quad \ldots\ldots(2)$$

$$\boldsymbol{\sigma}_2=\{\text{grad div}\ \boldsymbol{\psi}+k^2\boldsymbol{\psi}\}e^{ipt}, \quad \ldots\ldots(3)$$

provided the scalar and vector potentials ϕ and $\boldsymbol{\psi}$, is a solution of the wave equation

$$(\nabla^2+h^2)\phi=0\,, \quad \ldots\ldots (4)$$

$$(\nabla^2+k^2)\boldsymbol{\psi}=0, \quad \ldots\ldots (5)$$

in which

$$h^2=\frac{\rho p^2}{\lambda+2\mu}, \quad k^2=\frac{\rho p^2}{\mu}. \quad \ldots\ldots(6)$$

From these we have evidently

$$\boldsymbol{\sigma}_2=\text{rot rot}\ \boldsymbol{\psi}e^{ipt}. \quad \ldots\ldots(3')$$

---

85) K. Sezawa, On the Amplitudes and Periods of the P- and S-phases in the Earthquake Motion, Read on July 7, 1931, unpublished.

86) H. Kawasumi, The Mechnisms of Earthquake Occurrence and Abnormal Felt Area. Read at the Colloquium of Seismological Institute on Feb. 17, 1932. K. Sezawa's paper was published in June 1932.

$$\left.\begin{aligned}
&\operatorname{div}\boldsymbol{\sigma}_1 = -h^2\phi e^{ipt},\\
&\operatorname{div}\boldsymbol{\sigma}_2 = \operatorname{div}(\operatorname{rot}\operatorname{rot}\boldsymbol{\psi})e^{ipt} = 0,\\
&\operatorname{rot}\boldsymbol{\sigma}_1 = \operatorname{rotgrad}\phi e^{ipt} = 0,\\
&\operatorname{rot}\boldsymbol{\sigma}_2 = \operatorname{rot}(\operatorname{rot}\operatorname{rot}\boldsymbol{\psi})e^{ipt} = k^2\operatorname{rot}\boldsymbol{\psi}e^{ipt}.
\end{aligned}\right\} \quad \cdots\cdots\cdots (7)$$

Thus $\boldsymbol{\sigma}_1$ is irrotational and $\boldsymbol{\sigma}_2$ is equivoluminal.

General solutions of (4) and (5) in polar coordinates are, as are well known,

$$\phi = \sum_{n=0}^{\infty} \frac{A_n}{\sqrt{r}} C_{n+\frac{1}{2}}(hr) S_n, \quad \cdots\cdots\cdots (8)$$

$$= \sum_{n=0}^{\infty} \frac{\boldsymbol{B}_n}{\sqrt{r}} C_{n+\frac{1}{2}}(kr) S_n, \quad \cdots\cdots\cdots (9)$$

where C_n and S_n are cylindrical function and surface harmonics of order n. As we are now concerned to the diverging waves only, we have only take Hankel's cylindrical function of second kind $H_n^{(2)}$ for C_n and $P_n^m(\cos\theta)\begin{Bmatrix}\sin m\varphi\\ \cos m\varphi\end{Bmatrix}$ for S_n. Thus relevant solutions of (8) and (9) are

$$\phi = \sum_{n=0}^{\infty}\sum_{m=0}^{n} A_{nm} \frac{H^{(2)}_{n+\frac{1}{2}}(hr)}{\sqrt{r}} P_n^m(\cos\theta)\sin(m\varphi+\varepsilon), \quad \cdots\cdots (10)$$

$$\boldsymbol{\psi} = \sum_{n=0}^{\infty}\sum_{m=0}^{n} \boldsymbol{B}_{nm} \frac{H^{(2)}_{n+\frac{1}{2}}(kr)}{\sqrt{r}} P_n^m(\cos\theta)\sin(m\varphi+\varepsilon), \quad \cdots\cdots (11)$$

respectively. Displacements $\boldsymbol{\sigma}_1$ and $\boldsymbol{\sigma}_2$ can be culculated mechnically by the formula (2) and (3). We shall denote the components of displacement in the directions r, θ and φ by u, v and w respectively. A term in the series gives

$$\left.\begin{aligned}
u_1 &= \frac{\partial\phi}{\partial r}e^{ipt} = A_{nm}\frac{d}{dr}\left\{\frac{H^{(2)}_{n+\frac{1}{2}}(hr)}{\sqrt{r}}\right\} P_n^m(\cos\theta)\sin(m\varphi+\varepsilon)e^{ipt},\\
v_1 &= \frac{1}{r}\frac{\partial\phi}{\partial\theta}e^{ipt} = A_{nm}\frac{H^{(2)}_{n+\frac{1}{2}}(hr)}{r^{\frac{3}{2}}}\frac{dP_n^m(\cos\theta)}{d\theta}\sin(m\varphi+\varepsilon)e^{ipt},\\
w_1 &= \frac{1}{r\sin\theta}\frac{\partial\phi}{\partial\varphi}e^{ipt} = mA_{nm}\frac{H^{(2)}_{n+\frac{1}{2}}(hr)}{r^{\frac{3}{2}}}\frac{P_n^m(\cos\theta)}{\sin\theta}\cos(m\varphi+\varepsilon)e^{ipt}.
\end{aligned}\right\} \quad (12)$$

$$\left.\begin{aligned}
u_2 &= \left[\left\{\frac{n(n+1)}{r^{\frac{5}{2}}}H^{(2)}_{n+\frac{1}{2}}(kr) - \frac{2}{r^{\frac{3}{2}}}\frac{dH^{(2)}_{n+\frac{1}{2}}(kr)}{dr}\right\}B_r P^m_n(\cos\theta)\sin(m\varphi+\varepsilon)\right.\\
&\quad + \frac{d}{dr}\left(\frac{H^{(2)}_{n+\frac{1}{2}}(kr)}{r^{\frac{3}{2}}}\right)\left\{B_\theta \frac{dP^m_n(\cos\theta)}{d\theta}\sin(m\varphi+\varepsilon)\right.\\
&\quad \left.\left. - B_\varphi \frac{mP^m_n(\cos\theta)}{\sin\theta}\cos(m\varphi+\varepsilon)\right\}\right]e^{ipt},\\
v_2 &= \left\{\frac{1}{r}\frac{\partial}{\partial\theta}(\operatorname{div}\boldsymbol{\psi}) + k^2 B_\theta \frac{H^{(2)}_{n+\frac{1}{2}}(kr)}{\sqrt{r}}P^m_n(\cos\theta)\sin(m\varphi+\varepsilon)\right\}e^{ipt},\\
w_2 &= \left\{\frac{1}{r\sin\theta}\frac{\partial}{\partial\varphi}(\operatorname{div}\boldsymbol{\psi}) + k^2 B_\varphi \frac{1}{\sqrt{r}}H^{(2)}_{n+\frac{1}{2}}(kr)P^m_n(\cos\theta)\sin(m\varphi+\varepsilon)\right\}e^{ipt}.
\end{aligned}\right\} \quad (13)$$

In which $\boldsymbol{B}$ is assumed generally to be in the direction (θ_0, φ_0) and

$$\begin{aligned}
\operatorname{div}\boldsymbol{\psi} &= B_r\frac{d}{dr}\left\{\frac{H^{(2)}_{n+\frac{1}{2}}(kr)}{\sqrt{r}}\right\}P^m_n(\cos\theta)\sin(m\varphi+\varepsilon)\\
&\quad + \frac{H^{(2)}_{n+\frac{1}{2}}(kr)}{r^{\frac{3}{2}}}\left[\frac{d\{B_\theta P^m_n(\cos\theta)\}}{d\theta}\sin(m\varphi+\varepsilon)\right.\\
&\quad \left. - \frac{P^m_n(\cos\theta)}{\sin\theta}\frac{d\{B_\varphi\sin(m\varphi+\varepsilon)\}}{d\varphi}\right]. \qquad \cdots\cdots\cdots\cdots (14)
\end{aligned}$$

$$\left.\begin{aligned}
&B_x = B\sin\theta_0\cos\varphi_0, \quad B_y = B\sin\theta_0\sin\varphi_0, \quad B_z = B\cos\theta_0,\\
&B_r = B_x\sin\theta\cos\varphi + B_y\sin\theta\sin\varphi + B_z\cos\theta,\\
&B_\theta = B_x\cos\theta\cos\varphi + B_y\cos\theta\sin\varphi - B_z\sin\theta,\\
&B_\varphi = -B_x\sin\varphi + B_y\cos\varphi.
\end{aligned}\right\} \quad \cdots (15)$$

It is worthy of notice that the components v_1, w_1 of $\boldsymbol{\sigma}_1$, transverse to the direction of propagation, is of higher order with respect to $\frac{1}{r}$ than u_1, and conversely the radial component of $\boldsymbol{\sigma}_2$ is of higher order with respect to $\frac{1}{r}$ than the other components, and they approach the usual idea of longitudinal and transverse waves as they recede further from the origin.

The transverse wave above considered is that of first kind named by Prof. K. Sezawa.[87] He also found another type of transverse wave

87) K. Sezawa, *loc. cit.*, 43).

and called it transverse wave of the second kind. It is purely distortional wave and has no radial component of displacement.

$$\left.\begin{aligned} u_3&=0,\\ v_3&=\frac{m}{n(n+1)}D\frac{H^{(2)}_{n+\frac{1}{2}}(kr)}{\sqrt{r}}\frac{P_n^m(\cos\theta)}{\sin\theta}\cos(m\varphi+\varepsilon)e^{ipt},\\ w_3&=\frac{-1}{n(n+1)}D\frac{1}{\sqrt{r}}H^{(2)}_{n+\frac{1}{2}}(kr)\frac{dP_n^m(\cos\theta)}{d\theta}\sin(m\varphi+\varepsilon)e^{ipt}. \end{aligned}\right\}\quad\ldots\ldots(16)$$

Any condition near the origin for the displacement or the traction is fulfilled by suitable combination of these three kinds of waves.

Now I will pick out some simple examples from the above solutions and correlate it with the solutions already obtained by the application of the Stokes' formula, and reveal the relation with the models of the mechanisms of earthquake occurrence.

i) $n=0$.

$$\left.\begin{aligned} u_1&=A_0\frac{d}{dr}\left\{\frac{1}{\sqrt{r}}H^{(2)}_{\frac{1}{2}}(hr)\right\}e^{ipt}=-hA_0\frac{H^{(2)}_{1+\frac{1}{2}}(hr)}{\sqrt{r}}e^{ipt},\\ v_1&=w_1=0. \end{aligned}\right\}\quad\ldots\ldots\ldots\ldots(17)$$

This is the simple source, and corresponds to the compression or dilatation centre of A. E. H. Love.[88] The forces which give rise to this wave are, as Love already has shown, three pairs of doublets without moment perpendicular to each other. The transverse waves are not generated by these forces. This type of mechanism is considered as that of the volcanic eruption or explosion experiment. But, as Prof. Omori[89] observed in the earthquakes near the Mt. Asama, not only "push" or compression but also "pull" or dilatation, and in addition to this, transverse waves were clearly observed. So we cannot conclude that the volcanic earthquake is confined to that given rise by dilatational centre.

ii) $n=1$.

a) $m=0$,

$$\left.\begin{aligned} u_1&=A_1\frac{d}{dr}\left\{\frac{H^{(2)}_{1+\frac{1}{2}}(hr)}{\sqrt{r}}\right\}\cos\theta\, e^{ipt}=A_1\sqrt{\frac{2h}{\pi}}\sqrt{1+\left(\frac{2}{(hr)^2}\right)^2}\frac{e^{i(pt-hr+\delta_u)}}{r}\cos\theta,\\ v_1&=-A_1\frac{1}{r^{\frac{3}{2}}}H^{(2)}_{1+\frac{1}{2}}(hr)\sin\theta\, e^{ipt}=-A_1\sqrt{\frac{2h}{\pi}}\sqrt{1+\frac{1}{(hr)^2}}\frac{e^{i(pt-hr-\delta_v)}}{r^2}\sin\theta, \end{aligned}\right\}$$

88) A. E. H. LOVE, *loc. cit.*, 21) and 29).

89) F. OMORI, *loc. cit.*, 3).

$$w_1=0, \quad \tan\delta_u=\frac{h^2r^2-2}{2hr}, \quad \tan\delta_v=\frac{-1}{hr}. \Bigg\} \quad \cdots\cdots\cdots\cdots\cdots\cdots(18)$$

The force which give rise to the above wave is, as well known since the time of Stokes, a siglet in the direction of $\theta=0$.

$$F=A_1 4(\lambda+2\mu)\sqrt{4\pi h}\, e^{i\left(pt+\frac{\pi}{2}\right)}. \quad \cdots\cdots\cdots\cdots (19)$$

And the transverse wave due to this force is obtained by the transformation of the solutions, for example, obtained by Prof. Matuzawa[90] from Cartesian to polar coordinates.

$$\left.\begin{aligned} u_2&=A_1\left(\frac{k}{h}\right)^{\frac{3}{2}}\frac{2}{r^{\frac{3}{2}}}H^{(2)}_{1+\frac{1}{2}}(kr)P_1(\cos\theta)e^{ipt},\\ v_2&=A_1\left(\frac{k}{h}\right)^{\frac{3}{2}}\frac{1}{r}\frac{d}{dr}\left\{\sqrt{r}H^{(2)}_{1+\frac{1}{2}}(kr)\right\}\frac{dP_1(\cos\theta)}{d\theta}e^{ipt},\\ w_2&=0, \end{aligned}\right\} \quad \cdots\cdots(20)$$

which is identical with that obtained by (13) substituting

$$\psi=B_z\frac{H^{(2)}_{\frac{1}{2}}(kr)}{\sqrt{r}},$$

where $$B_z=A_1\frac{k^{\frac{1}{2}}}{h^{\frac{3}{2}}}.$$

It is also to be remarked that the longitudinal wave (18) is equivalent to a pair of simple sourse situated at $(r=0)$ and $(r=\delta z,\ \theta=0)$ with different sign and of the same strength $\frac{A_1}{h\delta z}$, that is a doublet

$$\phi=-\frac{A_1}{h}\frac{d}{dz}\left\{\frac{H^{(2)}_{\frac{1}{2}}(hr)}{\sqrt{r}}\right\} \quad \cdots\cdots\cdots\cdots\cdots\cdots(21)$$

and transverse wave (20) is the transverse wave of the first kind obtained by Prof. Sezawa. These waves were already shown by Lord Kelvin[91] to be generated by the vibration of a rigid sphere in the direction of $\theta=0$. Professors T. Shida and M. Matuyama considered them as the model of "depression earthquake or Abstürzbeben," though the existence

90) T. Matuzawa, *loc. cit.*, 28).
91) Lord Kelvin, *loc. cit.*, 18).

of this type of earthquake was suspected by Prof. S. T. Nakamura[92] and Prof. M. Ishimoto from the impossibility of vacant spaces under such high pressure within the earth and conservation of momentum.

b) $m=1$.

There will be no need to say that the waves generated by the force in the direction of $x\left(\theta=\frac{\pi}{2},\ \varphi=0\right)\left\{\text{or } y\left(\theta=\varphi=\frac{\pi}{2}\right)\right\}$ are

$$\left.\begin{aligned} &\phi=A_1\frac{H^{(2)}_{1+\frac{1}{2}}(hr)}{\sqrt{r}}\sin\theta\cos\varphi, \quad \left\{\phi=A_1\frac{H^{(2)}_{1+\frac{1}{2}}(hr)}{\sqrt{r}}\sin\theta\sin\varphi,\right\} \\ &\boldsymbol{\psi}=\boldsymbol{B}_x\frac{H^{(2)}_{\frac{1}{2}}(kr)}{\sqrt{r}}. \quad \left\{\boldsymbol{\psi}=\boldsymbol{B}_y\frac{H^{(2)}_{\frac{1}{2}}(kr)}{\sqrt{r}}.\right\} \end{aligned}\right\} \quad (22)$$

iii) $n=2$.

a) $m=0$,

$$\left.\begin{aligned} &\phi=A_{20}\frac{H^{(2)}_{2+\frac{1}{2}}(hr)}{\sqrt{r}}P_2(\cos\theta), \\ &u_1=A_{20}\left\{\frac{h}{\sqrt{r}}H^{(2)}_{1+\frac{1}{2}}(hr)-\frac{3}{r^{\frac{3}{2}}}H^{(2)}_{2+\frac{1}{2}}(hr)\right\}P_2(\cos\theta)e^{ipt} \\ &\qquad\approx A_{20}\sqrt{\frac{2h}{\pi}}\frac{e^{i(pt-hr)}}{r}\left(-1+\frac{4i}{hr}\right)P_2(\cos\theta), \\ &v_1=A_{20}\frac{H^{(2)}_{2+\frac{1}{2}}(hr)}{r^{\frac{3}{2}}}\frac{dP_2(\cos\theta)}{d\theta}e^{ipt}\approx iA_{20}\sqrt{\frac{2}{\pi h}}\frac{e^{i(pt-hr)}}{r^2}3\sin\theta\cos\theta. \end{aligned}\right\}$$

$$w_1=0 \qquad \ldots\ldots\ldots\ldots\ldots\ldots (23)$$

This is composed of a quadruple source and a simple source

$$\phi=\frac{A_{20}}{2}\left[\frac{3}{h^2}\frac{d^2}{dz^2}\left\{\frac{H^{(2)}_{\frac{1}{2}}(hr)}{\sqrt{r}}\right\}+\frac{H^{(2)}_{\frac{1}{2}}(hr)}{\sqrt{r}}\right] \qquad \ldots\ldots\ldots (24)$$

as Lord Rayleigh has already remarked. On the other hand double source is generated by a single force, so we can perceive that the waves here concerned is generated by doublet force and single source at the origin. Really as we have supposed the waves generated by a doublet without moment are[93]

92) S. T. NAKAMURA, *loc. cit.*, 24).

93) Prof. MATUZAWA has already obtained the solution in Cartesian Coordinates, with errors in the transverse wave. *loc. cit.*, 28).

$$
\left.\begin{aligned}
u_1&=\frac{-2iZ}{3\cdot4\pi(\lambda+2\mu)}\sqrt{\frac{\pi h}{2}}\frac{d}{dr}\left\{\frac{1}{2}\frac{H^{(2)}_{\frac{1}{2}}(hr)}{\sqrt{r}}-\frac{H^{(2)}_{2+\frac{1}{2}}(hr)}{\sqrt{r}}P_2(\cos\theta)\right\}e^{ipt}\\
&\approx\frac{-ihZ\,e^{i(pt-hr)}}{4\pi(\lambda+2\mu)r}\left\{\cos^2\theta+i\frac{1}{hr}(4\cos^2\theta-1)\right\},\\
v_1&=\frac{-2iZ}{3\cdot4\pi(\lambda+2\mu)}\sqrt{\frac{\pi h}{2}}\frac{H^{(2)}_{2+\frac{1}{2}}(hr)}{r^{\frac{3}{2}}}\frac{dP_2(\cos\theta)}{d\theta}e^{ipt}\\
&\approx\frac{-iZ}{4\pi(\lambda+2\mu)}\frac{e^{i(pt-hr)}}{r^2}\sin2\theta,\\
w_1&=0,\\
u_2&=\frac{2iZ}{4\pi\mu}\sqrt{\frac{\pi k}{2}}\frac{H^{(2)}_{2+\frac{1}{2}}(kr)}{r^{\frac{3}{2}}}P_2(\cos\theta)e^{ipt}\approx\frac{-2Z}{4\pi\mu}\frac{e^{i(pt-kr)}}{r^2}P_2(\cos\theta),\\
v_2&=\frac{iZ}{3\cdot4\pi\mu}\sqrt{\frac{\pi k}{2}}\frac{1}{r}\frac{d}{dr}\left\{\sqrt{r}H^{(2)}_{2+\frac{1}{2}}(kr)\right\}\sin\theta\cos\theta e^{ipt}\\
&\approx\frac{iZk}{4\pi\mu}\frac{e^{i(pt-kr)}}{r}\cos\theta\sin\theta\left(1-i\frac{3}{kr}\right),\\
w_2&=0.
\end{aligned}\right\}\quad(25)
$$

The transverse wave of (25) is equivalent to that given by

$$\Psi=B_z\frac{H^{(2)}_{1+\frac{1}{2}}(kr)}{\sqrt{r}}\cos\theta,\quad\cdots\cdots\cdots\cdots(26)$$

where $$B_z=\frac{iZ}{4\mu\sqrt{2\pi k}},$$

or Prof. Sezawa's transverse wave of the first kind when $n=2$, $m=0$.

The nodal surface of P-wave in (25) is a plane $\theta=\frac{\pi}{2}$, but in this case no difference in the "pull" or "push" of initial motion is observed on both sides of the nodal plane.

If we superpose to (25) simple source of suitable strength, we obtain nodal cone whose axis coincides with the pole $\theta=0$. The wave given by (23) is an example. The model of Proffessors Matuyama and Ishimoto, in which the generating line of the nodal cone meet with the axis at an angle $\frac{\pi}{4}$, is obtained by superposing

$$\phi_0=-\frac{3}{4}\mathfrak{A}\frac{H^{(2)}_{\frac{1}{2}}(kr)}{\sqrt{r}},\quad\left(\mathfrak{A}=\frac{-2iZ}{3\cdot4\pi(\lambda+2\mu)}\sqrt{\frac{\pi h}{2}}\right)$$

to (25).

From these reasoning, we can see that the intensity of simple source to be superposed is arbitrary so that we can obtain nodal cones of any vertical angle. However simple source does not accompany with transverse waves, and consequently the transverse wave accompanying with such mechanism, which give rise to longitudinal wave, having nodal cone, is therefore the same as that in (25). The relative magnitude of P- and S-waves is a function of θ as well as r, but the ratio of the maximum amplitudes at $r=$const. of the S- and P-waves due to doublet without moment is

$$\frac{1}{2}\left(\frac{k}{h}\right)^3=\frac{1}{2}\left(\frac{a}{b}\right)^3,$$

where a and b are the velocities of longitudinal and transverse waves respectively, that is the maximum amplitudes are inversely proportional to the cube of the velocities. This ratio becomes the larger when the vertical angle of the nodal cone becomes the smaller.

b) $m=1$.

$$\phi=A_{21}\frac{H^{(2)}_{2+\frac{1}{2}}(hr)}{\sqrt{r}}\frac{3}{2}\sin 2\theta\begin{Bmatrix}\cos\varphi\\ \sin\varphi\end{Bmatrix}.$$

These correspond to the similar case as c), the direction of doublet being in $x\left(\theta=\frac{\pi}{2},\ \varphi=0\right)$ or $y\left(\theta=\varphi=\frac{\pi}{2}\right)$ direction.

c) $m=2$.

$$\phi=A_{22}\frac{H^{(2)}_{2+\frac{1}{2}}(hr)}{\sqrt{r}}3\sin^2\theta\begin{Bmatrix}\sin 2\varphi\\ \cos 2\varphi\end{Bmatrix} \quad \ldots\ldots\ldots\ldots\ldots (27)$$

correspond to a quadruple source

$$\frac{\partial^2}{\partial x\partial y}\left\{\frac{3}{2}\frac{A_{22}}{h^2}\frac{H^{(2)}_{\frac{1}{2}}(hr)}{\sqrt{r}}\right\}, \quad \ldots\ldots\ldots\ldots\ldots (28)$$

and is hitherto been called the model B. This is equivalent to a longitudinal wave due to a doublet force with moment in the direction of x, studied already by Prof. Matuzawa.[94] The waves due to a doublet

$$F_x=\frac{X}{\delta y}e^{ipt} \quad \ldots\ldots\ldots\ldots\ldots\ldots\ldots (29)$$

94) T. MATUZAWA, *loc. cit.*, 28). In his solution we find small unimportant mistake in the higher order of $\frac{1}{r}$.

in polar coordinates are

$$\left.\begin{aligned}
u_1&=\frac{iX\sqrt{\frac{1}{2}\pi h}}{4\pi(\lambda+2\mu)}\frac{d}{dr}\left\{\frac{H^{(2)}_{2+\frac{1}{2}}(hr)}{\sqrt{r}}\right\}\frac{1}{2}\sin^2\theta\sin 2\varphi e^{ipt},\\
v_1&=\frac{iX\sqrt{\frac{1}{2}\pi h}}{4\pi(\lambda+2\mu)}\frac{H^{(2)}_{2+\frac{1}{2}}(hr)}{r^{\frac{3}{2}}}\sin\theta\cos\theta\sin 2\varphi e^{ipt},\\
w_1&=\frac{iX\sqrt{\frac{1}{2}\pi h}}{4\pi(\lambda+2\mu)}\frac{H^{(2)}_{2+\frac{1}{2}}(hr)}{r^{\frac{3}{2}}}\sin\theta\cos 2\varphi e^{ipt},\\
u_2&=\frac{iX\sqrt{\frac{1}{2}\pi k}}{4\pi\mu}\frac{H^{(2)}_{2+\frac{1}{2}}(kr)}{r^{\frac{3}{2}}}\frac{3}{2}\sin^2\theta\sin 2\varphi\, e^{ipt},\\
v_2&=\frac{iX\sqrt{\frac{1}{2}\pi k}}{4\pi\mu}\frac{1}{r}\frac{d}{dr}\left\{\sqrt{r}H^{(2)}_{2+\frac{1}{2}}(kr)\right\}\frac{1}{2}\sin\theta\cos\theta\sin 2\varphi e^{ipt},\\
w_2&=\frac{-iX\sqrt{\frac{1}{2}\pi k}}{4\pi\mu}\left\{\frac{kH^{(2)}_{1+\frac{1}{2}}(kr)}{\sqrt{r}}\sin^2\varphi+\frac{1}{r^{\frac{3}{2}}}H^{(2)}_{2+\frac{1}{2}}(kr)\cos 2\varphi\right\}\sin\theta e^{ipt}.
\end{aligned}\right\}$$

.....(30)

d) If we superpose to (30) another doublet with moment in the direction of $y\left(\theta=\varphi=\frac{\pi}{2}\right)$ with different sign and of the same strength, which is obtained by substituting $\varphi+\frac{\pi}{2}$ for φ of (30) and changing signs, then the components u_1, v_1, w_1, u_2, and v_2 become doubled and

$$w_2=\frac{iA\sqrt{\frac{1}{2}\pi k}}{4\pi\mu}\frac{1}{r}\frac{d}{dr}\left\{\sqrt{r}H^{(2)}_{2+\frac{1}{2}}(kr)\right\}\sin\theta\cos 2\varphi\, e^{ipt} \quad (31)$$

(where $A\equiv X=Y$). And this is a mechanism of model B.

The transverse wave (u_2, v_2, w_2) in this case is derivable from

$$\psi=B_x\frac{H^{(2)}_{1+\frac{1}{2}}(kr)}{\sqrt{r}}\sin\theta\sin\varphi, \quad \left(B_x=\frac{iA\sqrt{\frac{1}{2}\pi k}}{4\pi\mu}\right) \quad \ldots.(32)$$

and corresponds to the Prof. Sezawa's transverse wave of the first kind.

And if we put $\varphi+\frac{\pi}{4}$ for φ in the solutions above obtained we have exactly the same solution obtained by Mr. M. Hasegawa by the combination of two pairs of doublet without moment perpendicular to each other.

Thus we see that the model of Prof. Matuzawa corresponds to a kind of fault earthquake and that of Prof. Hasegawa corresponds to a kind of crack earthquake or Spaltungsbeben. This difference has not hitherto been noticed and sometimes confused.[95] It will be an interesting task of future investigation to distinguish these two mechanisms by observing the azimuthal component of the transverse wave w_2 given by (30) or (31).

iv)

a) If we superpose the two pairs of doublets with moment considered in iii), c) without changing the sign we have, as A. E. H. Love has already pointed out, a rotational centre round z-axis ($\theta=0$). Then the components u_1, v_1, w_1, u_2 and v_2 vanishes and only

$$w_2=-\frac{ikA}{4\pi\mu}\sqrt{\frac{1}{2}\pi k}\frac{H^{(2)}_{1+\frac{1}{2}}(kr)}{\sqrt{r}}\sin\theta\, e^{ipt} \quad \ldots\ldots\ldots (33)$$

remains. This is the simplest transverse wave of the second kind.

b) The distortional centre round z-axis is that obtained by differentiating the solution of the rotational centre (33) with respect to z,

$$w_3=-\frac{ik^2A}{4\pi\mu}\sqrt{\frac{1}{2}\pi k}\frac{H^{(2)}_{2+\frac{1}{2}}(kr)}{\sqrt{r}}\sin\theta\cos\theta \quad \ldots\ldots\ldots (34)$$

and this also is the transverse wave of the second kind. Thus it will be observed that longitudinal wave cannot be generated by the force which give rise to transverse waves of the second kind.

In what has been stated, the mechanisms which have hitherto been considered (being obtained by the method of singularities) are correlated with the general solutions obtained by the method of series. The remark will be unnecessary that any other case can be obtained by suitable combination of the general solutions given in (12), (13) and (16). But it is to be remarked that the solution of longitudinal wave (12) is identical with that of Prof. Sezawa and the solution of transverse wave (u_2, v_2, w_2) in (13) is not identical with those of the transverse wave of

95) M. HASEGAWA. *loc. cit.*, 4).
H. HONDA, *loc. cit.*, 9).

the second kind obtained by Prof. Sezawa except when $n=0$ and 1, but they are a combination of a few of the solutions of Prof. Sezawa, and it is worthy of note that general feature at a great distance which is given by the second term of (13) is conspicuously simple.

Another word to be added is about the word "force operative at a point." It is not indeed a force operative at a mathematical point. The definition of Prof. Love[96] is

$$X=\rho\int\int\int X'dx'dy'dz'=\rho V\bar{X} \quad \ldots\ldots\ldots\ldots(35)$$

provided the ρ and V are density and volume where the force is in operation, and $\bar{X}$ is mean force per unit mass in the volume V. Thus we may have a clue to the magnitude of hypocentral region from the observation of earthquake waves and some consideration on the relation of the mechnisms and the forces.

Chapter III. The crustal structure and the amplitude of Seismic bodily waves.

The elastic waves discussed in Chapter II is those in an isotropic homogeneous elastic body. But the material from which the earth consists is neither homogeneous nor perfect elastic, but they may have solid viscosity which causes the waves to decay. The influence of viscosity to the seismic waves seems comparatively small, but the reflexon and refraction is so much affected by the incidence angle that the effect of heterogeneity within the crust cannot be neglected. But the theory of elastic waves in such medium has only been began to be studied by Mr. R. Yosiyama and no rigorous theoretical culculation cannot be effected taking the actual structure of the crust into consideration. The effect on the amplitude of the curving of seismic rays due to continual variation of velocity was considered by Dr. H. Jeffreys.[97] He approximated the continual variation by the small discontinuous variation and the effect of the reflexion and refraction was culculated to show that the effect is negligible.

The variation of amplitude due to the divergence of wave front was first estimated by K. Zöppritz[98] from the consideration of surface density

96) A. E. H. Love, *loc. cit.*, 37), p. 184.

97) H. Jeffreys, *M. N. R. A. S. Geophys. Suppl.*, **1** (1926), 321-334.

98) K. Zöppritz, *Nachr. d. kgl. Ges. d. Wiss. zu Göttingen, Math.-phys. Klasse*, (1912), 123-143.

and conservation of energy. The defect of Zöppritz's method was supplemented after his death by E. Wiechert,[99] and the method was applied by L. Geiger and Prof. B. Gutenberg[100] in the investigation of structure of earth's interior. Dr. H. Jeffreys[101] also attacked the same problem, and the present writer[102] also could explain the variation of the amplitude found by Mr. H. Honda from the North Idu earthquake by the same method.

From the theory of spherical waves in homogeneous isotropic medium follows the amplitude of bodily wave is inversely proportional to hypocentral distance, which is identical with the law that follows from the energy density method. In the heterogeneous medium we should have closer approximation if we use the distance (s) along the curved path along which the wave propagated than the radial distance from the hypocentre.

Taking, for example, longitudinal wave ($n=2$, $m=0$) we can make use of

$$u_1 \approx A\sqrt{\frac{2h}{\pi}}\frac{1}{s}\cos(pt-hs)P_2(\cos\theta) \quad \ldots\ldots\ldots\ldots (36)$$

in place of $$u_1 \approx A\sqrt{\frac{2h}{\pi}}\frac{1}{r}\cos(pt-hr)P_2(\cos\theta).$$

Further approximation will be obtained by taking the variation of h along the path into consideration. By the relations

$$\int_0^s h\,ds = \int_0^s \frac{p}{a}\,ds = pt_P$$

(in which a is velocity of longitudinal wave and t_P is travel-time of P-wave), we have

$$u_1 \approx A\sqrt{\frac{2h}{\pi}}\frac{1}{\bar{a}\int_0^s \frac{ds}{a}}\cos\left(pt-\int_0^s h\,ds\right)P_2(\cos\theta)$$

$$= A\sqrt{\frac{2h}{\pi}}\frac{1}{\bar{a}t_P}\cos p(t-t_P)P_2(\cos\theta)$$

$$= A\sqrt{\frac{2p}{\pi a^3}}\left(\frac{a}{\bar{a}}\right)\frac{1}{t_P}\cos p(t-t_P)P_2(\cos\theta), \quad \ldots\ldots\ldots (37)$$

99) E. WIECHERT, *ibid.* foot note on page 127.

100) L. GEIGER u. B. GUTENBERG, *do.*, 144-206.

101) H. JEFFREYS, *M. N. R. A. S. Geophys. Suppl.*, 1 (1926), 334-348.

102) H. KAWASUMI, On the initial motion of earthquake motion. Read at the meetng of Earthquake Research Institute on July 7, 1931. See appendix.

from which we can perceive that the amplitude is nearly proportional to $a^{-\frac{3}{2}}$. Considering the constancy of the velocity on the earth's surface, we see that the amplitude on the earth's surface is inversely proportional to the travel-time. Now I will compare this method and the method already mensioned in which energy density is used. The variation of amplitude due to the divergence of wave front will be sufficiently given by the consideration of case in which energy is uniformly sent out in all directions.

Let us suppose that the energy emitted per unit solid angle is I. Then the energy within a range of angle de_h at the hypocentre is $2\pi I \cos e_h de_h$, and this energy is sent to a zone within the epicentral distance θ and $\theta+d\theta$, the area of which on the earth's surface is $2\pi R^2 \sin\theta d\theta$, where R is the radius of the earth. The angle between the wave front and the surface is $\frac{1}{2}\pi - e_0$, (where e_0 is angle of emergence at the earth's surface) so that unit surface corresponds to an area $\sin e_0$ of the wave front. Hence the enrgy per unit area of the wave front is

$$\frac{I}{R^2}\frac{\cos e_h de_h}{\sin\theta \sin e_0 d\theta} = -\frac{I}{R^2}\frac{d(\sin e_h)}{\sin e_0 d(\cos\theta)} \quad \ldots\ldots \quad (38)$$

Considering that the amplitude ($\mathfrak{A}$) of the incident wave at the surface is proportional to the energy density on the wave front, we have

$$\mathfrak{A} \propto \sqrt{\frac{-d(\sin e_h)}{\sin e_0 d(\cos\theta)}} \equiv U. \quad \ldots\ldots\ldots\ldots\ldots (39)$$

The writer already obtained the velocity of the seismic wave within the earth, and culculated time distance curve and the constants of seismic ray

$$K = \frac{r}{v}\sin i = \frac{r}{v}\cos e. \quad \ldots\ldots\ldots\ldots\ldots (40)$$

We can therefore easily culculate U by (39) and (40), but for simplicities sake $\frac{d\sin e_h}{d(\cos\theta)}$ is obtained graphically for the case of hypocentral depth of 250 km. The results are compared in Table 1 with those culculated by the "inverse travel-time formula."

We are naturally led to the notion that the distribution of amplitude given by spherical harmonics at the hypocentre is preserved along the seismic ray, and this is proved by the recent theoretical investigation of the waves in heterogeneous medium by Mr. R. Yosiyama.[103]

103) R. Yosiyama, *loc. cit.*, 46).

Table 1. Comparison of the variations of amplitude of seismic waves with epicentral distance (θ) culculated by the energy dencity formula (39) and inverse travel time formula.

θ	2°16′·6	3°20′·6	4°22′·8	5°24′·0	6°24′·4	7°24′·5	8°24′·4	9°24′·0
$\frac{1}{U}$	0·0687	0·0773	0·0953	0·1123	0·1421	0·1595	0·1786	0·1916
t_P	48·0	57·9	72·1	84·9	97·7	110·5	123·3	135·9
$\left(\frac{1}{U}\middle/t_P\right)\times 10^2$	1·43	1·30	1·32	1·32	1·45	1·45	1·45	1·41

We have hitherto considered the effect of divergence of wave front only, but if there is finite discontinuity in the nature of the medium in which the wave is propagated, the reflextion and refraction take place breaking usually into four kinds of waves. The reflexion and refraction of spherical waves at spherical discontinuity surface is not only too complicated to rigorous calculation, but it becomes of no use if the heterogeneity is not taken into consideration.

Thus the case of reflexion and refraction of plane wave at plane surface has been used practically. This effect at the discontinuities at crustal layers has been calculated by Mr. T. Suzuki and the writer.[104] Thus the amplitude of incident wave is diminished to

$$\frac{1}{\bar{a}t_P}\Pi\left(\frac{\mathfrak{A}'}{\mathfrak{A}}\right), \quad \cdots\cdots\cdots\cdots\cdots\cdots (41)$$

where the symbol $\Pi\left(\frac{\mathfrak{A}'}{\mathfrak{A}}\right)$ denotes the product of the ratio of the amplitude ($\mathfrak{A}'$) of refracted wave to that of incident wave ($\mathfrak{A}$) at every discontinuity the wave has traversed.

Thus the motion of a particle on the surface modified by the reflexion at the surface is, taking the former example,

$$u_{1H}=-A\sqrt{\frac{2h_0}{\pi}}\frac{1}{\bar{a}t_P}\Pi\left(\frac{\mathfrak{A}'}{\mathfrak{A}}\right)\left(\frac{u}{\mathfrak{A}}\right)_0 P_2(\cos\theta)\cos p(t-t_P), \quad \cdots (42)$$

$$u_{1z}=-A\sqrt{\frac{2h_0}{\pi}}\frac{1}{\bar{a}t_P}\Pi\left(\frac{\mathfrak{A}'}{\mathfrak{A}}\right)\left(\frac{w}{\mathfrak{A}}\right)_0 P_2(\cos\theta)\cos p(t-t_P), \quad (42)$$

where the factors $\left(\frac{u}{\mathfrak{A}}\right)_0$ and $\left(\frac{w}{\mathfrak{A}}\right)_0$ is the ratios of horizontal and veritcal (the surface being assumed horizontal) components to the amplitude of

104) H. KAWASUMI and T. SUZUKI, *Disin (Journ. Seismol. Soc. Japan)*, **4** (1932), 277-307, (in Japanese).

incident wave in case of surface reflexion.

In the next chapters the applications are made what has been stated to some actual earthquakes to reveal the mechanism of their occurrences.

Chapter IV. Amplitude of Seismic waves and the mechanism of occurrence of the deep-seated Central Japan earthquake of June 2nd 1931.

This earthquake was studied by Mr. K. Tanahasi[105] and is a conspicuous example which cannot be explained by any other mechanism than the model A. Mr. Tanahasi explained the distribution of pull and push of initial motion of P- and S-wave by means of the theory of Prof. M. Matuyama.[106] So long as the writer is aware of, Mr. Tanahasi is the first to discuss the direction of initial motion of S-wave, but he has a little misinterpreted the theory of Prof. Matuyama, and overlooked the existence of transverse wave of second kind which appear independently of the P-wave. The writer will here state the result of his quantitative study on the magnitude of the waves to reveal the mechanism of occurrence of the earthquake which has qualitatively been discussed by Mr. Tanahasi.

The depth of this earthquake is given in Kisyô Yôran as 250 km. and the result of Mr. Tanahasi is 240 km. The travel-time curve given by Mr. Tanahasi nearly coinsides with the author's calculated curve for the hypocentral depth of 253·3 km. I will therefore adopt the last value for the depth of this earthquake.

Let us first tabulate in Table II the observations of Mr. Tanahasi supplemented from those given in Kisyô Yôran.

From the distribution of the initial motions of P-wave writen on a map (Fig. 1) we see two nodal curves resembling hyperbola as were already found by Mr. Tanahasi. Thus we percieve the amplitude of P-wave is proportional to zonal harmonics. The shortest distance between these curves is along a line passing through the epicentre and in the azimuth of which lies the polar axis ($\theta=0$). The intersections of this straight line with the nodal lines are $\theta=0.^\circ5$ and $\theta=2.^\circ7$ where θ is epicentral distance. Since we know[107] hypocentral depth and constants of seismic ray K as a function of θ, we are able to know the inclination of seismic ray from the zenith at the hypocentre by the formula

105) K. Tanahasi, *loc. cit.*, 6).

106) M. Matuyama, *loc. cit.*, 4).

107) H. Kawasumi, *Bull. Earthq. Res. Inst.*, 10 (1932). 94-129. Table IX.

Table II. Observed magnitude of initial motions of P- and S-waves of the deep-seated Central-Japan earthquake of June 2, 1931. (Mainly due to Mr. Tanahasi.)

Station	P-wave (μ)			S-wave (μ)		
	E	N	Z	E	N	Z
Nagoya	13	54	− 87	560	−345	?
Gihu	35	40	−178	363	−250	47
Hikone	22	25	−190	413	−524	−102
Nagano	− 5	18	+117	318	698	−163
Numadu	−27	40	− 60	−925	263	43
Mishima	−26	17	− 74	−720	418	−218
Wazima	− 1	1	+ 4	680	−478	−116
Kumagaya	1	− 1	24	−142	433	98
Kyôto	64	34	− 69	152	−335	− 31
Wakayama	12	16	—	51	−216	—
Kakioka	18	4	—	− 33	264	—
Ôsaka	6	7	−129	−175	−565	− 8
Tokyo	Time mark			−173	240	indistinct
Yakohama	− 5	9	—	−152	216	—
Toyooka	57	21	−149	75	−217	− 27
Tukubasan	1	8	+ 5	− 82	247	100
Kôbe	70	18	− 77	−106	−273	+ 23
Sumoto	10	8	− 15	112	−224	− 76
Sionomisaki	− 5	−11	+ 18	160	−199	− 24
Tyôsi	−32	+ 5	− 22	98	149	− 20
Hatidyôzima	10	00	+ 6	−101	+	6
Sendai	39	49	87	−178	257	122
Sakai	58	20	—			
Kôti	− 2	− 2	4	122	− 67	27
Hamada	16	3	—	8	− 73	—
Akita	36	47	155	indistinct		
Marioka	79 to NE 14 to NW		—	61 to NE 90 to NW		—
Simidu	Time mark			43	− 46	—
Miyasaki	− 7	− 9	13	43	− 32	− 15
Kumamoto	− 1	− 2	4	Time mark		
Nagasaki	− 1	+ 1	2	7	− 13	?
Taikyû	+13	+ 1	—	00?	− 36	—
Zinsen	10	− 4	5			
Matumoto	−10	−10				
Kôhu	−10	+20				
Miyadu	+72	+38				
Hukusima	+42	+34	+ 65			
Yamagata	+70	+60				
Tu	+15	+55				
Aomori	+70	+42				
Kusiro	+ 8	+12				
Niihama	+18	+ 6				

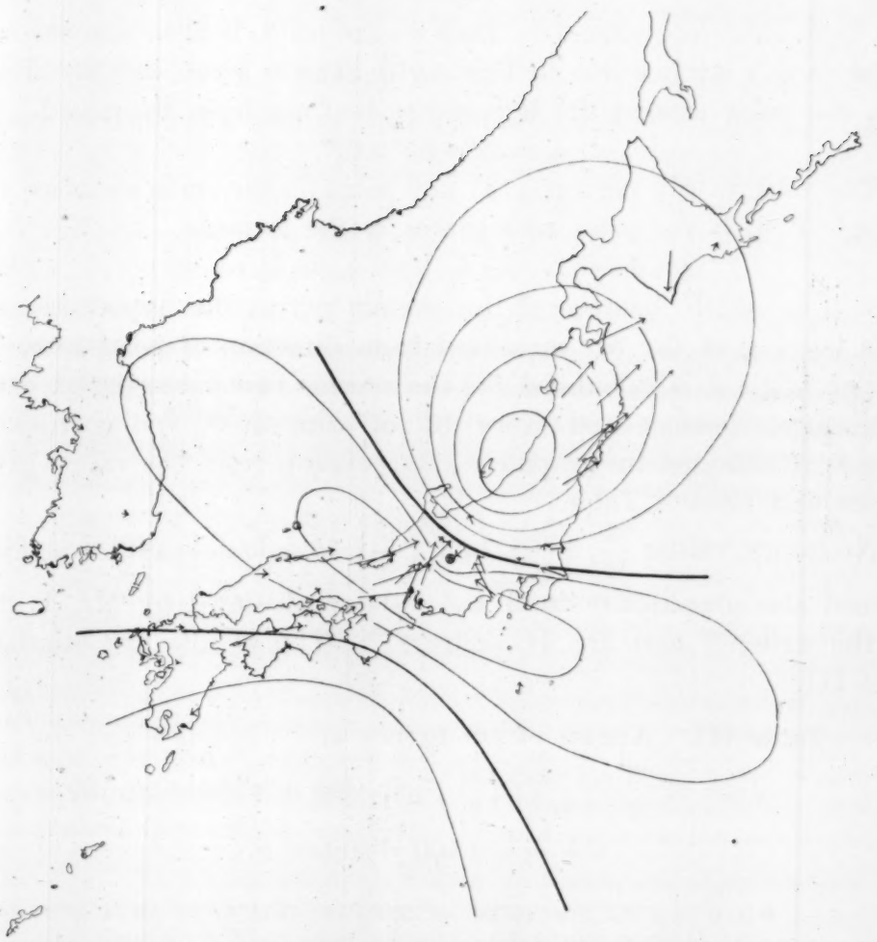

Fig. 1. The distribution of initial motions actually observed (arrows) of P-wave due to the deep-seated earthquake of June 2, 1931, and iso-amplitude lines calculated for the mechanism

$$\phi = A\frac{H^{(2)}_{2+\frac{1}{2}}(hr)}{\sqrt{r}}P_2(\cos\theta)$$

$$i_h = \sin^{-1}\frac{v_h}{r_h}K \quad \ldots\ldots\ldots\ldots\ldots\ldots (44)$$

as a function of θ (Table III), where the entities with suffix h are the values at the hypocentre.

Plotting these values on a section paper we obtain $i_h = f(\theta)$ curve from which we obtain $i_h = 12°$ and $58°$ for $\theta = 0°.5$ and $2°.7$ respectively. Thus the generating lines of the nodal cone in the plane passing the polar axis intersect at the hypocentre at an angle $12° + 58° = 70°$. The coincidence of this angle with that of $P_2(\cos\theta)$ may be considered as something

more than mere coincidence. Thus we are led to believe that the motion on the earth's surface due to this earthquake is given by (23) and (25). If so, the polar axis at the hypocentre inclines from the zenith

$$i_{h0}=12°+55°=67°.$$

The seismic ray emerging at any point on the earth's surface makes an angle θ with the polar axis given by the formula

$$\cos\theta=\cos i_h\cos i_{h0}+\sin i_h\sin i_{h0}\cos\Phi \quad \ldots\ldots\ldots(45)$$

where i_h is zenith distance of the seismic ray at the hypocentre and Φ is the bearing of the ray measured from direction of polar axis.

The angle θ is calculated for the seismic rays emerging at every 1° of epicentral distance and every 15° of azimuth Φ, and corresponding $P_2(\cos\theta)$ is obtained by graphical interpolation from the values given in Jahnke und Emde's Table.

Necessary values $\frac{\mathfrak{A}'}{\mathfrak{A}}$, $\left(\frac{u}{\mathfrak{A}}\right)_0$ and $\left(\frac{w}{\mathfrak{A}}\right)_0$ to calculate (42) and (43) are obtained also graphically from the values calculated by Mr. T. Suzuki and the writer[108] and Dr. H. Jeffreys.[109] The results are tabulated in Table III.

Table III. Angles of emergence and incidence and the values of $\frac{\mathfrak{A}'}{\mathfrak{A}}$, $\left(\frac{u}{\mathfrak{A}}\right)_0$, $\left(\frac{w}{\mathfrak{A}}\right)_0$ etc. for a seismic ray at the epicentral distance θ.

θ	0°	1°·9′7	2°16·′6	3°20·′6	4°22·′8	5°24·′0	6°24·′4	7°24·′5	8°24· 4	9°24·′0	10°23·′6
i_h	0	30°32′	51°39′	65°03′	74°11′	80°58′	86°13′	91°29′	94°55′	98°25′	101°34′
e_{50}	90°	64°05′	47°35′	38°45′	34°09′	31°51′	30°53′	30°42′	31°01	31°42′	32°35′
e_{20}	90°	69°01′	56°27′	50°16′	47°18′	55°53′	45°18′	45°12′	45°23′	45°47′	46°19′
e_0	90°	72°59′	63°09′	58°29′	56°21′	55°20′	54°55′	54°51′	54°59′	55°15′	55°39′
$\left(\frac{\mathfrak{A}'}{\mathfrak{A}}\right)_{50}$	1·143	1·119	1·067	1·022	·987	·965	·954	·952	·955	·963	·972
$\left(\frac{\mathfrak{A}'}{\mathfrak{A}}\right)_{20}$	1·143	1·123	1·100	1·078	1·066	1·059	1·056	1·055	1·057	1·059	1·061
$\left(\frac{u}{\mathfrak{A}}\right)_0$	0	·668	1·022	1·173	1 235	1·266	1·276	1·277	1·275	1·268	1·256
$\left(\frac{w}{u'}\right)_0$	∞	2·84	1·68	1·42	1·31	1·27	1·25	1·25	1·25	1·26	1·28
t_P	34·6	38·5	48·0	5·79	72·1	84·9	97·7	110·5	123·3	135·9	148·5
$\frac{1}{t_P}\Pi\left(\frac{\mathfrak{A}'}{\mathfrak{A}}\right)\left(\frac{u}{\mathfrak{A}}\right)_0$	0	0·02180	·02499	·02165	·01802	·01524	·01316	·01161	·01044	·00952	·00872

108) The assumption of crustal structure is almost the same as in the first paper (*Bull. Earthq. Res. Inst.*, 10 (1932) 94-129). The surfaces of discontinuity are assumed at the depth of 20 km. and 50 km. from the surface. The ratio of the velocities on both sides of the discontinuity is asumed to be $1:\sqrt{1\cdot5}$ and the ratio of the dencity is 0·9 : 1.

109) H. JEFFREYS, *loc. cit.* 97).

Using these values the motion on the earth's surface given by (42) and (43) are calculated except the constant factor $\left(-A\sqrt{\frac{2h_0}{\pi}}\frac{1}{\bar{a}}\right)$, and tabulated in Table IV and is shown on Fig. 1 and 2.

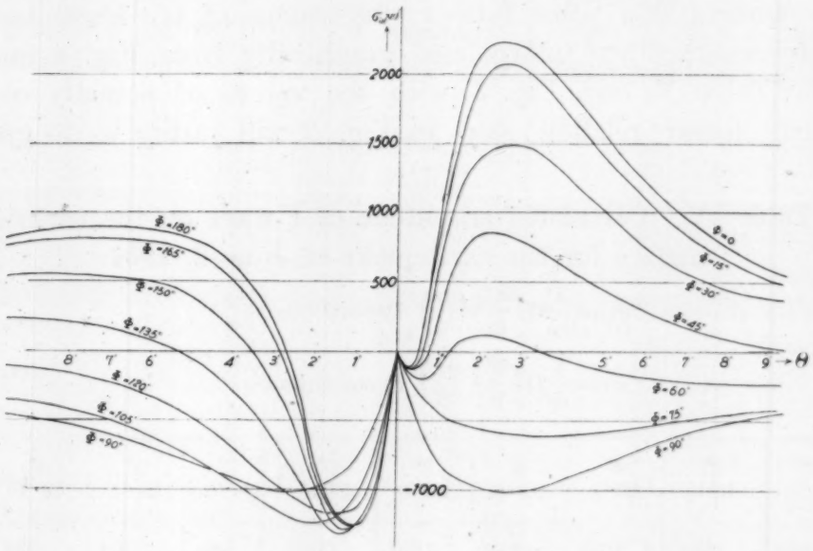

Fig. 2. Variation of Amplitude of P-wave, for the earthquake of June 2, 1931, with epicentral distance for respective azimuths.

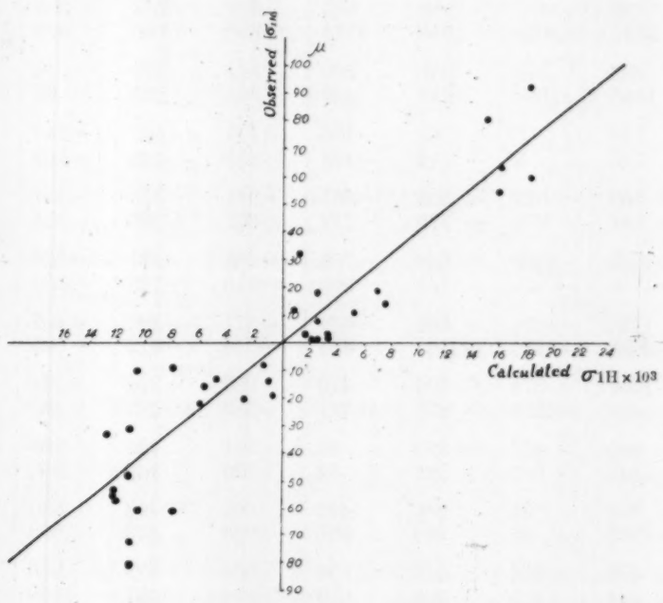

Fig. 3. Comparison of the observed magnitude of the initial motion of P-wave due to the earthquake of June 2, 1931, with that of calculated.

It is clearly observed from Fig. 3 that the distribution of pull and push divided by nodal lines calculated without exception and loci of equal amplitude are in good accord with the magnitude of the initial motions actually observed.

To confirm this point further, the values of u_{1H} for θ and Φ of every observatories are interpolated graphically from Fig. 4 and compared in Table V and Fig. 3 with the values of actually observed. The fairly linear relation seen in Fig. 3 will justify us to grant the

Table IV. Calculated amplitude of P-wave on the earth's surface for the earthquake of June 2, 1931.

$$\left.\begin{aligned}\sigma_{1H}&=\frac{1}{t_P}\Pi\left(\frac{\mathfrak{A}'}{\mathfrak{A}}\right)\left(\frac{u}{\mathfrak{A}}\right)_0 P_2(\cos\theta)\text{(above)}\\ \sigma_{1Z}&=\frac{1}{t_P}\Pi\left(\frac{\mathfrak{A}'}{\mathfrak{A}}\right)\left(\frac{w}{\mathfrak{A}}\right)_0 P_2(\cos\theta)\text{(below)}\end{aligned}\right\}\times 10^5$$

Φ \ θ	1° 9·'7	2° 16·'6	4° 20·'6	4° 22·'8	5° 24·'0	6° 24·'4	7° 24·'5	8° 24·'4	9° 24·'0	10° 23·'6
0°	1005	2234	2139	1759	1392	1101	924	702	563	452
	2854	3753	3037	2304	1768	1376	1155	878	709	579
15°	918	2061	1955	1598	1255	87	767	615	491	385
	2607	3462	2776	2093	1594	1234	959	769	619	493
30°	709	1752	1457	1159	885	672	551	383	288	209
	2014	2641	2069	1518	1124	840	689	479	363	268
45°	364	862	749	550	369	341	178	70	15	− 28
	1034	1465	1064	721	469	301	223	88	19	− 36
60°	− 28	115	2	− 88	−156	−193	−197	−246	−250	−262
	− 80	193	3	− 115	−198	−241	−246	−308	−315	−335
75°	− 405	− 560	− 619	− 595	−561	−521	−475	−457	−430	−405
	−1150	− 941	− 879	− 779	−712	−651	−539	−571	−542	−518
90°	− 717	−1030	−1000	− 869	−756	−655	−581	−520	−472	−427
	−2036	−1730	−1420	−1138	−960	−918	−726	−650	−595	−547
105°	− 942	−1240	−1074	− 860	−694	−571	−490	−407	−354	−310
	−2675	−2083	−1525	−1127	−881	−714	−613	−509	−446	−397
120°	− 978	−1097	− 872	− 593	−410	− 287	−228	−144	−102	70
	−2778	−1843	−1238	− 777	−521	−359	−285	− 180	−129	90
135°	−1081	− 980	− 487	− 173	11	111	135	206	244	232
	−3070	−1646	− 692	− 227	14	139	169	258	307	297
150°	−1075	− 700	− 61	240	442	509	498	550	545	529
	−3053	−1176	− 87	314	561	636	623	688	687	677
165°	−1046	− 477	264	613	764	808	825	906	776	745
	−2971	− 801	375	803	970	1010	1031	1133	987	951
180°	−1033	− 392	385	735	878	916	864	898	860	821
	−2934	− 659	547	963	1115	1145	1080	1118	1084	1051

Table V. Comparison of the observed magnitude of the initial motion of P-wave due to the earthquake of June 2, 1931 with that of calculated.

Station	Epicentral distance (θ)	Azimuth Φ	Horizontal Amplitude of P-wave (observed) $\sqrt{E^2+N^2}$	$\sigma_{1H} \times 10^4$
	°		μ	
Nagoya	0·97	−164	−55	−123
Gihu	0·88	−153	−53	−121
Hikone	1·31	−243	−33	−128
Nagano	0·89	6	19	70
Numadu	1·30	103	−48	−112
Misima	1·33	102	−31	−111
Wazima	1·62	− 45	+67	75
Kumagaya	1·48	57	(∠R) 1	24
Kyôto	1·80	−144	−73	−111
Wakayama	2·69	−155	−20	− 28
Kakioka	2·20	57	+18	25
Ôsaka	2·18	−149	− 9	− 80
Tôkyô	1·78	73	—	− 47
Yokohama	1·71	81	−10	− 73
Toyooka	2·36	−123	- 61	−105
Tukubasan	2·14	57	+ 8	25
Kôbe	2·40	−145	−72	− 67
Sumoto	2·78	−148	−13	− 48
Sionomisaki	2·92	−172	+12	+ 7
Tyôsi	2·63	70	−32	− 12
Hatidyôzima	2·43	122	−10	−107
Sendai	3·57	24	+63	161
Sakai	3·64	- 119	−61	− 80
Kôti	4·16	−149	+ 3	+ 17
Hamada	4·70	−117	−16	− 57
Akita	4·16	4	+59	183
Morioka	4·79	13	+80	150
Simidu	5·03	−153	—	+ 47
Miyazaki	6·63	−151	+11	+ 53
Kumamoto	6·61	−142	+ 2	33
Nagasaki	7·28	−138	(∠R) 1	+ 22
Taikyû	7·47	−113	−13	− 48
Zinsen	8·90	—	−11	− 45
Matûmoto	0.43	14	−14	− 10
Kôbu	0·81	84	−22	− 55
Miyadu	2·07	−125	−81	−111
Hukusima	2·97	27	+54	160
Yamagata	3·24	19	+92	182
Tu	1·55	166	- 57	−120
Aomori	5·60	3	+	133
Kusiro	8·90	12	+14	51
Niihama	4·11	−143	−	− 7

assumption above used, because the observed values are nothing but the amplitude measured on the seismograms divided by the mechanical

magnification of seismographs without taking any consideration of the effect of free vibrations due to the start from rest and that of friction more or less impeding seismographs.

If the observation becomes more acculate the deviation from the linear relation with the theoretical value will indicate some effect of geological structure near the observing station beside the deffect of calculation due to the difference of the law of variation of amplitude with hypocentral distance and damping due to viscosity etc. It will be interesting task of future study to know these factors through systematic and statistical observations.

From Fig. 3 we obtain the factor

$$1^{\mu}=\left(A\sqrt{\frac{2h_0}{\pi}}\frac{1}{\bar{a}}\right)2\cdot5\times10^{-4},$$

$$\text{or}\quad A=\frac{p}{2\cdot5}\sqrt{\frac{\pi}{2h_0^3}}\left(\frac{\bar{a}}{a_0}\right)\ \text{C. G. S.},$$

where

$$\bar{a}=\frac{1}{R-r_h}\int_{r_h}^{R}a\,dr,\qquad \left(\begin{array}{l}R:\text{ radius of the earth,}\\ r_h:\text{ distance of hypocentre from the centre}\\ \quad\text{of the earth.}\end{array}\right)$$

which comes out nearly 1·5 times of a_0 for the velocity obtained in the writer's first paper. And

$$A=\frac{3}{5}p\sqrt{\frac{\pi}{2h_0^3}}\ \text{C. G. S.}\qquad\qquad(46)$$

Now that we know the coefficient of the scalar displacement potential, all the quantities concerning the longitudinal wave are determined, if we know the period of the wave.

There may be a numher of mechanisms to give rise P-wave

$$\phi=A\frac{H^{(2)}_{2+\frac{1}{2}}(hr)}{\sqrt{r}}P_2(\cos\theta),$$

by suitable conditions of displacement and stress near the origin, but the transverse wave are determined corresponding to each mechanism. For instance Prof. Sezawa obtained waves due to pressure distribution given by $P_2(\cos\theta)e^{ipt}$, on a sphere of radius a, and the ratio R of maximum amplitudes of P- and S-waves becomes 0·24 for $ha=1$ when $\lambda=\mu$. Thus we can percieve the mechanism of occurrence of the earthquake if we know the ratio R. Fortunately we have observations of initial motions of transverse waves obtained by Mr. K. Tanahasi. So

I will determine the constants of spherical transverse waves.

The transverse waves accompanying the longitudinal wave (23) is

$$\psi = B_z \frac{H^{(2)}_{+\frac{1}{2}}(kr)}{\sqrt{r}} \cos\theta$$

irrespectively when the P-wave is generated by the pressure distributions as given by Prof. Sezawa or by the doublets without moment in combination with a simple source.

Then by the relation

$$\mathrm{rot}\,\psi = (\mathrm{rot}\,\psi)_\varphi = kB_z \frac{H^{(2)}_{2+\frac{1}{2}}(kr)}{\sqrt{r}} \sin\theta\cos\theta,$$

and (3′) we have

$$\left.\begin{aligned} u_2 &= 2kB_z \frac{H^{(2)}_{2+\frac{1}{2}}(kr)}{r^{\frac{3}{2}}} P_2(\cos\theta)\, e^{ipt}, \\ v_2 &= -kB_z \frac{1}{r}\frac{d}{dr}\left\{\sqrt{r} H^{(2)}_{2+\frac{1}{2}}(kr)\right\} \sin\theta\cos\theta\, e^{ipt}, \\ w_2 &= 0, \end{aligned}\right\} \quad \ldots\ldots (47)$$

and as we are now concerned with a deep-seated earthquake we have only to consider displacement in the direction of θ,

$$v_2 \approx B_z \sqrt{\frac{2}{\pi}}\, k^{\frac{3}{2}} \frac{e^{i(pt-kr)}}{r} \sin\theta\cos\theta. \quad \ldots\ldots\ldots (48)$$

Now I will draw the vector of initial motions of S-waves on the geographical map. (Fig. 4). Mr. Tanahasi drew a diagram representing the vector of amplitude of S-wave on the earth's surface from Prof. Matuyama's theory which is exactly the same with (47). In his drawing we see a large component (w) of displacement in the direction of φ near the epicentre.

Though, as we have seen, there is no w component in (47), we see conspicuously large w component in the actual observation, shown in Fig. 6 near the nodal line of v_2 i. e. near the equator $\theta = \frac{\pi}{2}$. If we pay special attention to the component in the direction of φ (that is parallel to the loci of θ=const. shown in the Fig. 6) we notice that the motion is of different sign on both sides of the equator and they gradually diminish as we recede from the equator and at last change their signs. On the other hand v_2 component, which is perpendicular to the direction

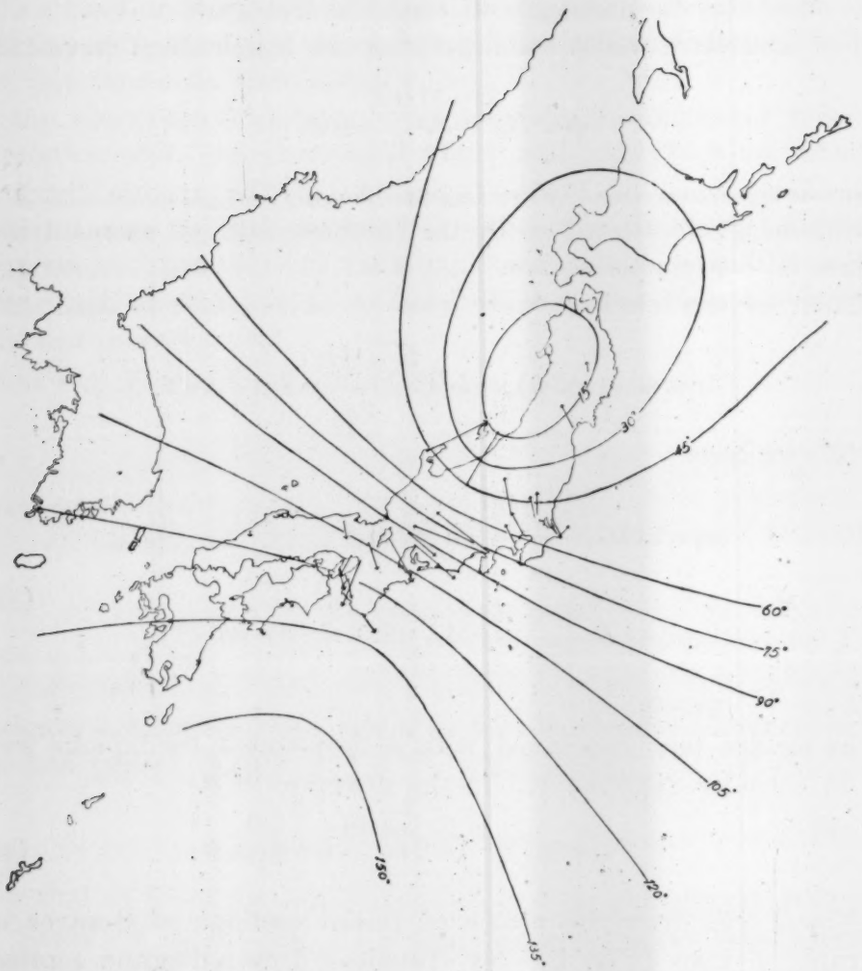

Fig. 4. The distribution of horizontal component of initial motions actually observed of the S-wave due to the earthquake of June 2, 1931 and the loci of constant θ.

of θ=const., is evanescent near the equator and the pole, and is maximum in the intermediate zone.

Thus it is to be considered the w component is due to the transverse wave of the second kind, and it is very interesting to think that the mechanism of occurrence of this wave is independent of the P-wave, and the existence of this makes an interesting contrast to that of simple source which is independent of the transverse waves. We must therefore be careful to pay attention to the existence of these waves in the consideration of the mechanism of earthquake occurrence.

Performing the similar calculation as the case of P-wave I will reveal the mechanisms by which this eanerthquake is generated. It is necessary to calculate separately the effects of reflexion and refraction for each component in the incident plane (σ_i) or perpendicular to it σ_Φ.

Considering a unit sphere near the hypocentre (Fig. 5) and by the cosine formula (12) and

$$\frac{\sin\beta}{\sin i_{h0}}=\frac{\sin\Phi}{\sin\theta}=\frac{\sin(\pi-\varphi)}{\sin i_h}, \quad \ldots(49)$$

we have

$$\left.\begin{aligned}\sigma_i&=v\cos\beta-w\sin\beta,\\ \sigma_\Phi&=v\sin\beta+w\cos\beta,\end{aligned}\right\} \quad \ldots(50)$$

or

$$\left.\begin{aligned}u&=\sigma_i\cos\beta+\sigma_\Phi\sin\beta,\\ w&=-\sigma_i\sin\beta+\sigma_\Phi\cos\beta.\end{aligned}\right\} \quad \ldots(51)$$

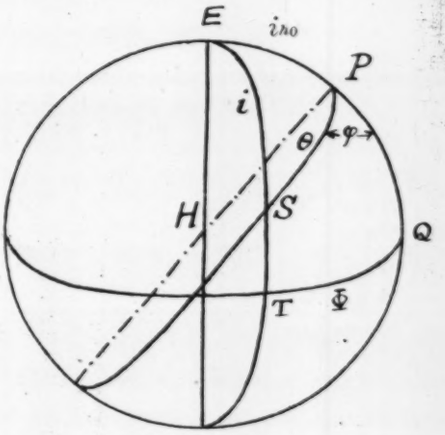

Fig. 5.

H: hypocentre;
HE: vertical line through H;
HP: polar axis; HS: seismic ray;
$ES=i$; $EP=i_{h0}$
$\angle QPS=\varphi$; $QT=\Phi$; $\angle ESP=\beta$.

And we can calculate the motion on earth's surface by

$$\left.\begin{aligned}v_{2iH}&=B_z\sqrt{\frac{2}{\pi}}(k_0)^{\frac{3}{2}}\frac{1}{\bar{a}t_P}e^{ip(t-t_s)}\sin\theta\cos\theta\,\Pi\left(\frac{\mathfrak{B}'}{\mathfrak{B}}\right)\left(\frac{u}{\mathfrak{B}}\right)_0\cos\beta,\\ v_{2iZ}&=B_z\sqrt{\frac{2}{\pi}}(k_0)^{\frac{3}{2}}\frac{1}{\bar{a}t_P}e^{ip(t-t_s)}\sin\theta\cos\theta\,\Pi\left(\frac{\mathfrak{B}'}{\mathfrak{B}}\right)\left(\frac{w}{\mathfrak{B}}\right)_0\cos\beta,\\ v_{2\Phi}&=B_z\sqrt{\frac{2}{\pi}}(k_0)^{\frac{3}{2}}\frac{1}{\bar{a}t_P}e^{ip(t-t_s)}\sin\theta\cos\theta\,\Pi\left(\frac{c'}{c}\right)2\sin\beta.\end{aligned}\right\} \quad \ldots(52)$$

The result of calculation is shown in Table VI, VII, and Fig. 6 and 7.

It is to be observed that the displacement due to the transverse wave (v_2) is nearly perpendicular to the loci of equal-θ and has very small w-component compared with those observed shown in Fig. 4. Thus it is necessary to separate out v_2-component and w_3-component from the actual observations. For this purpose we must first decompose the horizontal displacement vector actually observed into two components, the one in the radial direction (σ_{iH}) and the other perpendicular to the former (σ_Φ). If we divide σ_{iH} and σ_Φ by $\frac{1}{t_P}\Pi\left(\frac{\mathfrak{B}'}{\mathfrak{B}}\right)\left(\frac{u}{\mathfrak{B}}\right)_0$ and $\frac{1}{t_P}\Pi\left(\frac{c'}{c}\right)\cdot 2$ respectively we have the amplitudes σ_i' and σ_Φ' which are free from the

effects due to difference of hypocentral distance and the reflexion and refraction.

Table VI. $\frac{\mathfrak{B}'}{\mathfrak{B}}$, $\frac{c'}{c}$, $\left(\frac{u}{\mathfrak{B}}\right)_0$, $\left(\frac{w}{\mathfrak{B}}\right)$, etc. for a seismic ray of transverse wave emerging at epicentral distance θ.

θ	0°	1° 9·′7	2° 16·′6	3° 20·′6	4° 22·′8	5° 24·′0	6° 24·′4	7° 24·′5	8° 24·′4
$\left(\frac{\mathfrak{B}'}{\mathfrak{B}}\right)_{50}$	1·143	1·112	1·065	1·012	0·973	0·950	0·940	0·937	0·941
$\left(\frac{C'}{C}\right)_{50}$	1·143	1·140	1·082	1·038	1·006	0·988	0·977	0·977	0·980
$\left(\frac{\mathfrak{B}'}{\mathfrak{B}}\right)_{20}$	1·143	1·115	1·087	1·070	1·065	1·060	1·058	1·058	1·058
$\left(\frac{C'}{C}\right)_{20}$	1·143	1·139	1·116	1·093	1·080	1·075	1·072	1·071	1·073
$\left(\frac{u}{\mathfrak{B}}\right)_0$	2	1·86	1·725	1·775	2·03	2·511	3·23	3·43	3·11
$\left(\frac{w}{\mathfrak{B}}\right)_0$	0	0·65	0·944	1·006	0·950	0·811	0·600	0·370	0·70
$\frac{1}{t}\Pi\left(\frac{\mathfrak{B}'}{\mathfrak{B}}\right)\left(\frac{w}{\mathfrak{B}}\right)_0$	0·07512	0·05989	0·04160	0·03302	0·02918	0·02979	0·03289	0·03077	0·02509
$\frac{1}{t}\Pi\left(\frac{\mathfrak{B}'}{\mathfrak{B}}\right)\left(\frac{w}{\mathfrak{B}}\right)_0$	0	0·02093	0·02276	0·01872	0·01365	0·00962	0·00611	0·00331	0·00564
$\frac{1}{t}\Pi\left(\frac{C'}{C}\right)2$	0·07512	0·06726	0·05030	0·03801	0·03014	0·02502	0·02144	0·01894	0·01704

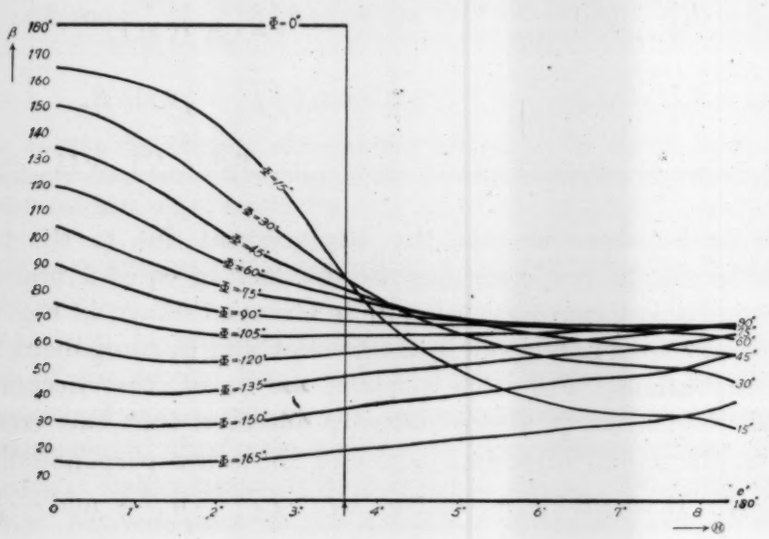

Fig. 6. $\beta-\theta$.

Table VII. Calculated amplitude of S-wave on the earth's surface for the earthquake of June 2, 1931.

$$\left.\begin{aligned} v_{2H} &= \frac{1}{t}\Pi\left(\frac{\mathfrak{B}'}{\mathfrak{B}}\right)\left(\frac{u}{\mathfrak{B}}\right)_0 \cos\theta \sin\theta \cos\beta \ldots\ldots \text{(above, } H\text{)} \\ v_{2Z} &= \frac{1}{t}\Pi\left(\frac{\mathfrak{B}'}{\mathfrak{B}}\right)\left(\frac{w}{\mathfrak{B}}\right)_0 \cos\theta \sin\theta \cos\beta \ldots\ldots \text{(middle, } Z\text{)} \\ v_{2\Phi} &= \frac{1}{t}\Pi\left(\frac{C'}{C}\right) 2\cos\theta \sin\theta \sin\beta \ldots\ldots\ldots \text{(below, } \Phi\text{)} \end{aligned}\right\} \times 10^5$$

Φ \ θ		1° 9·'7	2° 16·'6	3° 20·'6	4° 22·'8	5° 24·'0	6° 24·'4	7° 24·'5	8° 24·'4
0°	(H)	+2862	+1063	+ 36	− 362	− 698	−1022	−1055	−1038
	(Z)	−1000	− 581	− 21	+ 169	+ 225	+ 190	+ 113	+ 233
	(Φ)	0	0	0	0	0	0	0	0
15°	(H)	+2679	+ 965	− 7	− 375	− 689	− 995	−1021	− 996
	(Z)	− 936	− 528	− 4	+ 175	+ 223	+ 185	+ 110	+ 234
	(Φ)	1263	1126	879	691	560	466	405	346
30°	(H)	+2168	+ 680	− 6	− 404	− 659	− 911	− 922	− 873
	(Z)	− 758	− 372	− 3	+ 189	+ 213	+ 169	+ 99	+ 196
	(Φ)	2295	2008	1553	1212	977	810	703	597
45°	(H)	+1447	+ 306	− 199	− 424	− 598	− 781	− 807	− 687
	(Z)	− 506	− 168	+ 113	+ 198	+ 193	+ 145	+ 87	+ 154
	(Φ)	2921	2465	1868	1438	1147	942	814	682
60°	(H)	+ 676	− 54	− 308	− 401	− 482	− 574	− 549	− 457
	(Z)	− 236	+ 30	+ 175	+ 189	+ 156	+ 107	+ 59	+ 103
	(Φ)	3058	2419	1764	1320	1029	829	708	577
75°	(H)	+ 7	− 283	− 319	− 305	− 308	− 324	− 293	− 210
	(Z)	− 2	+ 155	+ 181	+ 143	+ 99	+ 60	+ 32	+ 47
	(Φ)	2736	1920	1287	900	660	502	417	309
90°	(H)	− 400	− 309	− 193	− 117	− 71	− 33	− 11	+ 33
	(Z)	+ 140	+ 169	+ 109	+ 55	+ 23	+ 6	+ 1	− 7
	(Φ)	2084	1123	577	296	141	51	16	− 53
105°	(H)	− 521	− 105	+ 77	+ 158	+ 219	+ 283	+ 279	+ 251
	(Z)	+ 182	+ 57	− 46	− 74	− 71	− 53	− 30	− 56
	(Φ)	1289	249	− 173	− 329	− 387	− 404	− 386	− 410
120°	(H)	− 366	+ 292	+ 457	+ 492	+ 540	+ 599	+ 559	+ 432
	(Z)	+ 128	− 160	− 259	− 230	− 117	− 111	− 60	− 97
	(Φ)	551	− 475	− 765	− 808	− 784	− 741	− 680	− 668
135°	(H)	− 27	+ 792	+ 883	+ 823	+ 845	+ 888	+ 801	+ 571
	(Z)	+ 9	− 433	− 501	− 385	− 273	− 165	− 86	− 128
	(Φ)	− 26	− 877	−1052	−1020	− 947	− 870	− 791	− 756
150°	(H)	+ 350	+1275	+1272	+1142	+1103	+1120	+ 992	+ 667
	(Z)	− 122	− 698	− 671	− 534	− 357	− 208	− 107	− 150
	(Φ)	− 212	− 886	− 976	− 933	− 836	− 759	− 687	− 649
165°	(H)	+ 665	+1623	+1545	+1351	+1279	+1271	+1114	+ 722
	(Z)	− 232	− 888	− 876	− 632	− 413	− 236	− 120	− 162
	(Φ)	− 184	− 545	− 581	− 538	− 487	− 440	− 397	− 373
180°	(H)	+ 778	+1750	+1642	+1388	+1339	+1323	+1156	+ 740
	(Z)	− 272	− 958	− 931	− 649	− 433	− 246	− 124	− 166
	(Φ)	.0	0	0	0	0	0	0	0

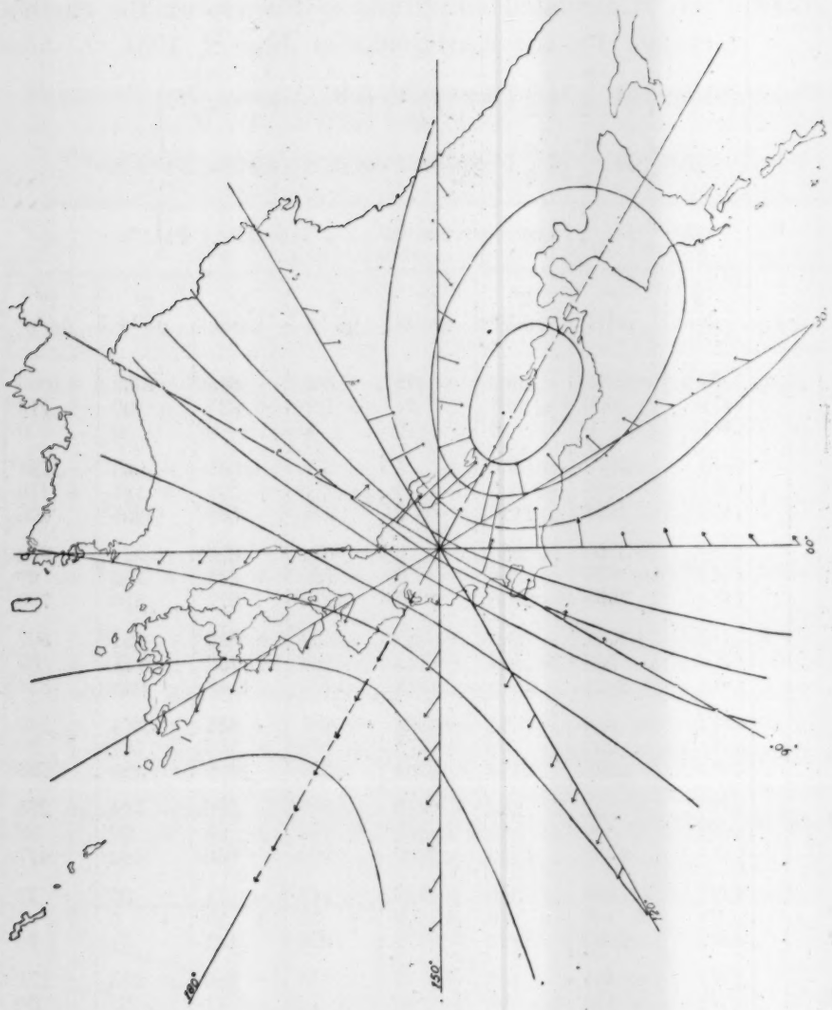

Fig. 7. Calculated amplitude of horizontal component of S-wave (σ_2) on the earth's surface for the earthquake of June 2, 1931.

Then we can calculate the components in the directions of θ and φ by means of the angle β shown in Fig. 6. Denote the values thus obtained with $[v_2]_1$, and $[w_3]_1$. Then $[v_2]_1$ (or $[w_3]_1$) is displacement due to a term inversely proportional to hypocentral distance in v_2 (or w_3) on a sphere at a distance of a second journey of longitudinal wave from the origin; and is proportional to the actual value on the sphere $(v_2)_1$ (or $(w_3)_1$). The results of graphical calculations with the aid of above mensioned values are given in Table VIII.

Now let us first discuss the component v_2 which accompany with

Table VIII. Reduction of observed amplitudes (σ_{iH}, $\sigma_{i\Phi}$) of S-wave of the earthquake of June 2, 1931, to those ($[v_2]_1$, $[w_3]_1$) on a sphere which is a second journey of P-wave from the hypocentre.

Station	σ_{iH}	σ_Φ	σ'_i	σ'_Φ	β	$[v_2]_1$	$[w_2]_1$	θ	$\sin\theta$
	μ	μ	mm	mm	°	mm	mm	°	
Nagano	764	− 67	11·74	− 0·95	172	−11·76	−0·69	44	996
Wazima	347	742	6·70	12·32	−110	−13·87	−1·92	44	996
Misima	−835	85	−14·75	1·31	68	− 4·31	14·07	76	470
Numadu	−910	366	−15·87	5·15	67	− 1·44	16·69	77	438
Kumagaya	− 60	−453	− 1·11	− 7·25	102	− 6·86	2·59	52	970
Hikone	− 93	−667	− 1·63	−10·22	− 34	4·37	−9·39	95	−174
Gihu	−252	−348	− 3·87	− 4·93	− 25	− 1·41	−6·11	91	−208
Kyôto	40	−361	0·82	− 6·31	− 36	− 4·37	−4·62	103	−438
Nagoya	− 87	−654	− 1·36	− 9·37	− 16	1·27	−9·38	92	−068
Ôsaka	414	−267	9·63	− 5·17	− 30	10·92	0·34	110	−643
Sumoto	36	−243	0·97	− 5·53	− 34	3·89	−4·04	118	−829
Sionomisaki	86	−236	2·39	− 5·56	− 8	3·14	−5·17	124	−927
Kôbe	292	− 52	7·25	− 1·07	− 35	6 55	3·28	112	−695
Toyooka	− 38	−226	− 0·93	− 4·58	− 50	2·90	−3·64	100	−342
Wakayama	103	−196	2·73	− 4·34	− 27	4·40	−2·63	119	−848
Kôti	− 60	−125	− 2·03	− 3·97	− 38	0·84	−4·38	129	−978
Hamada	− 13	− 74	− 0·34	− 2·60	− 60	2·08	−1·59	108	−588
Simidu	− 5	− 63	− 0·17	− 0·33	− 37	1·27	−1·99	136	−999
Miyazaki	− 15	− 51	− 0·46	− 2·45	− 45	1·41	−2·05	142	−970
Nagasaki	0	− 15	0	− 0·48	− 56	0·35	−0·27	134	−999
Taikyû	− 1	− 36	− 0·03	− 1·91	− 65	1·72	−0·84	112	−695
Tyôsi	90	−152	2·35	− 3·32	80	− 2·86	−2·89	62	829
Yokohama	−199	−168	− 3·97	− 2·80	81	− 3·39	3·48	67	719
Tôkyô	−199	−214	− 4·09	− 3·72	86	− 4·00	3·79	62	829
Tukuba	− 40	−257	− 0·92	− 4·92	92	− 4·88	1·17	50	985
Kakioka	14	−267	− 0·33	− 5·19	92	− 5·19	−0·15	51	978
Sendai	36	−312	1·14	− 8·67	85	− 8·44	−1·89	23	719
Morioka	73	− 80	2·54	− 2·09	46	− 0·26	−3·28	16	530

the P-wave. As $[v_2]_1$ is only dependent on $\sin\theta\cos\theta=\frac{1}{2}\sin 2\theta$, the comparison are made $[v_2]_1$ and $\sin 2\theta$ in Fig. 8. It is to be noticed that the correlation is not so good as in the case of P-wave, as will be justified from the difficulty of obseration of S-wave owing to the superposition of the longitudinal wave, but it is remarkable that the sign is in good harmony with only one exception. The ratio of $(v_2)_1$ to $[v_2]_1$ is obtained

$$\frac{(v_2)_1}{[v_2]_1}=\left(\frac{a_0}{a_1}\right)^{\frac{5}{2}}\left(\frac{\bar{a}}{a_0}\right)=0\cdot42$$

from the ratio of (48) and (52) and the assumption $(\bar{a})_1=a_h=a_1$ between hypocentre and the sphere ($t_P=1$ sec).

Now let us examine the ratio of the maximum amplitudes at the same hypocentral distance of the P- and S-waves due to the wave generated by doublet force without moment and a simple source. Comparing (23), (25) and (44) we have

$$A=\frac{2iZ}{3\cdot 4\pi\rho a^2}\sqrt{\frac{\pi h}{2}}=p\frac{3}{5}\sqrt{\frac{\pi}{2h_0^3}},$$

$$B_z=\frac{iZ}{4\pi\rho b^2}\sqrt{\frac{\pi}{2k}},$$

$$\frac{B_z}{A}=\frac{3}{2}\left(\frac{a}{b}\right)^{\frac{3}{2}}\frac{a}{p}=3\cdot 42\frac{a}{p},$$

$$\therefore\quad B_z=3\cdot 42\frac{a_h}{p}\frac{3}{5}p\sqrt{\frac{\pi}{2h_0^3}},\qquad\ldots.(53)$$

$$\therefore\quad (v_2)_1=0\cdot 48\sin 2\theta \text{ cm. and}$$

$$[v_2]_1=\frac{(v_2)_1}{0\cdot 42}=\frac{0\cdot 48}{0\cdot 42}\sin 2\theta$$

$$=1\cdot 14\sin 2\theta \text{ cm.}\quad..(54)$$

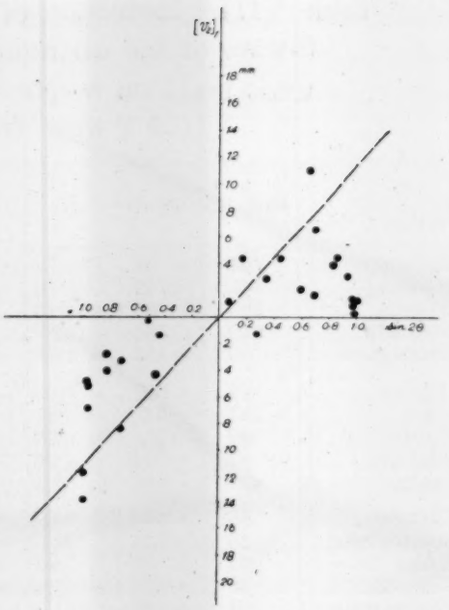

Fig. 8. Comparison of reduced amplitude $[v_2]_1$ from the observed value of the S-wave due to the earthquake of June 2, 1931 with those calculated.

from (46) corresponding to the magnitude of the observed P-wave if the transverse wave v_2 is generated by double force without moment.

This relation is represented by a straight line in Fig. 8. It may therefore be sufficient to conclude a part of S-wave and the P-wave of this earthquake were generated by a doublet without moment in combination with a simple source of strength

$$\phi=\frac{A}{2}\frac{H_{\frac{1}{2}}^{(2)}(hr)}{\sqrt{r}}\quad..(55)$$

Let us now consider the remaining component $[w_3]_1$. The variation of $[w_3]_1$ with θ is shown in Fig. 9. The

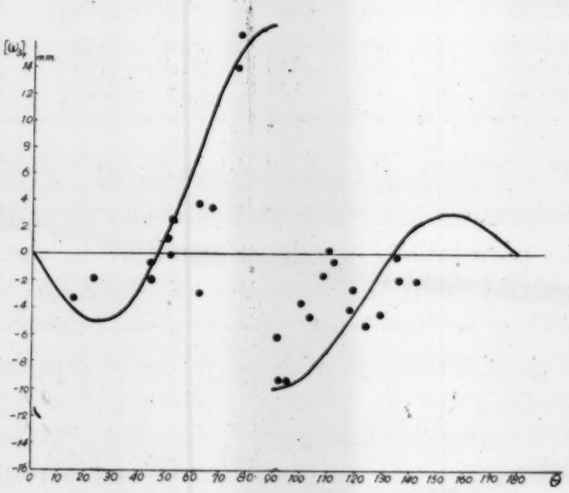

Fig. 9. The relation with θ of the reduced amplitude $[w_3]_1$ of the S-wave due to the earthquake of June 2, 1931.

spherical wave having w-component of transverse wave only is Prof. Sezawa's second kind of transverse wave. And the solutions depending only on θ are those in which

$$\left.\begin{aligned} &m=0,\\ &u_3=v_3=0,\\ &w_3=\frac{1}{n(n+1)}D\frac{H^{(2)}_{n+\frac{1}{2}}(kr)}{\sqrt{r}}\frac{dP_n(\cos\theta)}{d\theta}e^{ipt}. \end{aligned}\right\} \quad \cdots\cdots\cdots(56)$$

On the other hand it is clearly observed that the sign of $[w_3]_1$ is clearly opposite on both sides of $\theta=\frac{\pi}{2}$, and the solution having such nature is those of even n. But it is necessary to superpose the solutions whose $n=2$, 4 and 6. But for such large values of n as 6 the function $H^{(2)}_{n+\frac{1}{2}}(kr)$ becomes very large at short distance from origin, $(R\{H^{(2)}_{6+\frac{1}{2}}(1)\}=8632)$ and it is impossible to consider that the material at such point withstands failure. It will be more easily understood if the displacement is discontinuous at the equatorial plane $\left(\theta=\frac{\pi}{2}\right)$, because we can obtain amplitude shown by the curves in Fig. 9 by the superposition of the waves of $n=1$ and 3, cutting at the equator and changing the signs on both sides of the equator. This consideration is based on the supposition of the existence of a crack at the equatorial plane, and it harmonizes with the fact that the P- and S-waves observed in this earthquake are that generated by the mechanism called "crack earthquake" by Prof. M. Matuyama, and that the cracks expected in the former mechanism which generates w_3-wave is at the same place with the latter. Then it is easily understood the difference

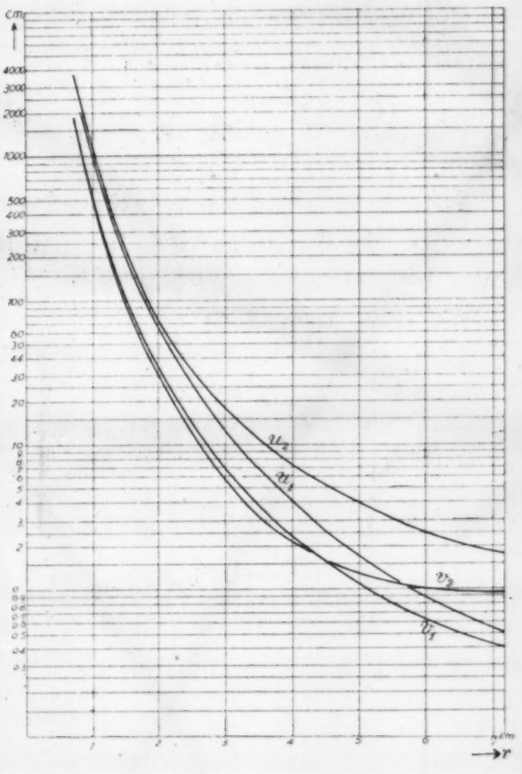

Fig. 10. Variation of maximum amplitudes of longitudinal and transverse waves with hypocentral distance.

of amplitude on both sides of $\theta=\frac{\pi}{2}$, the side of larger amplitude may easily considered to be the side mainly moved. But such wave is only possible when the crack is extending up to the earth's surface, and if it had not actually existed, it must have been impossible to come to exist at once by such an earthquake, and the wave should have been more or less modified when they were propagated to a distance. And the full interpretation is a matter of future when the theoretical investigation will have been completed. It is interesting, however, to remember that the origin of this eathquake is near the "ithmus" or the "rift vally" of the main island of Japan and the equatorial plane is nearly coincident with the line connecting the Wakasa-bay, the Lake Biwa and the Ise-bay, and, moreover, the side in which w_3 is of larger amplitude is the upper side of the equatorial plane which may be considered as the crack plane. It is interesting, if it be a mere chance, that the circumstances of the occurrence of this earthquake is the same with the orogenic movement in the geological ages. And if it is not event of mere chance, it is the more interesting to know that such orogenic force is acting at such a depth as 250 km. from the earth's surface.

Thus it is a matter of mere speculation at present, so I will give here only the formulae of spherical wave which give the displacement shown by the curves in Fig. 9.

We have from (56)

$n=1$.

$$w_3=\frac{1}{2}D_1\frac{H^{(2)}_{1+\frac{1}{2}}(kr)}{\sqrt{r}}\frac{dP_1(\cos\theta)}{d\theta}e^{ipt}\approx\frac{-D_1}{1}\sqrt{\frac{2}{\pi k}}\frac{e^{i(pt-kr)}}{r}\sin\theta. \quad (57)$$

$m=3$.

$$w_3=\frac{1}{12}D_3\frac{H^{(2)}_{3+\frac{1}{2}}(kr)}{\sqrt{r}}\frac{dP_3(\cos\theta)}{d\theta}\approx\frac{D_3}{12}\sqrt{\frac{2}{\pi k}}\frac{e^{i(pt-kr)}}{r}\frac{dP_3(\cos\theta)}{d\theta}, \quad (58)$$

and if we put

$$-3D_1=D_3, \quad \ldots\ldots\ldots\ldots\ldots\ldots (59)$$

and superpose these two solutions we have node at about $\theta=47°$. Thus we have by similar consideration as before,

$$(w_{3+n})_0=D_1\sqrt{\frac{2}{\pi k}}\sin\theta\left(1-\frac{15}{8}\sin^2\theta\right)\frac{1}{\bar{a}t_P}\Pi\left(\frac{\mathfrak{B}'}{\mathfrak{B}}\right)\left(\frac{u}{\mathfrak{B}}\right)_0\sin\beta,$$

$$(w_3)_1 = D_1\sqrt{\frac{2}{\pi k}}\sin\theta\left(1-\frac{15}{8}\sin^2\theta\right)\frac{1}{a_1},$$

$$\frac{(w_3)_1}{(w_{3H})_0} = \left(\frac{a_0}{a_1}\right)^{\frac{1}{2}}\left(\frac{\bar{a}}{a_0}\right)\frac{t_P}{\Pi\left(\frac{\mathfrak{B}'}{\mathfrak{B}}\right)\left(\frac{u}{\mathfrak{B}}\right)\sin\beta} = 1{\cdot}16\,\frac{t_P}{\Pi\left(\frac{\mathfrak{B}'}{\mathfrak{B}}\right)\left(\frac{u}{\mathfrak{B}}\right)_0\sin\beta}.$$

So we have $(w_3)_1$ by multiplying 1·16 into $[w_3]_1$ of Table VIII, and from Fig. 9,

$$\left.\begin{aligned} D_1 = \sqrt{\frac{2}{\pi k_1}}\frac{1}{a_1} &= 1{\cdot}16\text{ cm.}, \quad \text{for} \quad 0<\theta<\frac{\pi}{2}, \\ \text{or} \qquad &= 0{\cdot}66\text{ cm.}, \quad \text{for} \quad \frac{\pi}{2}<\theta<\pi. \end{aligned}\right\} \qquad \ldots\ldots\ldots (60)$$

Thus we have all the mathematical expressions for the bodily waves of the earthquake of June 2, 1931. And from these expressions we can know all the phenomena so far as the seismic waves are concerned, provided we know the properties of material consisting the earth and the period of the seismic waves. As to the former the velocities of the seismic waves in the region here concerned has been estimated by the writer in his first paper and we have to know the density only. The density within the earth has been estimated by several authorities[110] from geochemical and geophysical point of view. As to the period of the seismic waves I could determine to be about 2·7 seconds in both P- and S-waves from the seismograms obtained at Kobe which are reproduced in Mr. K. Tanahasi's paper. We have thus

$$a_0 = 5\text{ km./sec.},$$
$$a_h = 8{\cdot}35\text{ km./sec.},$$
$$a/b = \sqrt{3},$$
$$T = \frac{2\pi}{p} = 2{\cdot}7\text{ sec.},$$

$\rho = 3{\cdot}6$ approximately at the depth of 250 km. from the surface, and we have

$$Ah^{\frac{5}{2}} = 0{\cdot}81\text{ cm.}, \quad Bk^{\frac{3}{2}} = 5{\cdot}47\text{ cm.}$$

from (46).

Let us now examine the displacement, stress and energy near the hypocentre where we have no need of taking the effect of heterogeneity into consideration.

110) See for example B. Gutenberg, "Aufbau der Erde", (1925), 45.

We have already seen sufficient evidence to believe, at least, the u_1 and v_2 components of displacements of this earthquake were generated by simple source (55) and a doublet without moment

$$F\delta z = -iA4\pi\rho a^2\sqrt{\frac{2}{\pi h}}e^{ipt} = -iB_z 4\pi\rho b^2\sqrt{\frac{2k}{\pi}}e^{ipt} = 1{\cdot}23\times10^{25}e^{i\left(pt+\frac{\pi}{2}\right)} \quad \ldots(61)$$

And the corresponding mathematical expressions of these waves are

$$\left.\begin{aligned} u_1 &= 0{\cdot}81\frac{d}{d(hr)}\left(\frac{H^{(2)}_{2+\frac{1}{2}}(hr)}{\sqrt{r}}\right)P_2(\cos\theta)e^{ipt} \text{ cm.},\\ v_1 &= -1{\cdot}22\frac{H^{(2)}_{2+\frac{1}{2}}(hr)}{(hr)^{\frac{3}{2}}}\sin 2\theta e^{ipt} \text{ cm.},\\ u_2 &= +21{\cdot}90\frac{H^{(2)}_{2+\frac{1}{2}}(kr)}{(kr)^{\frac{3}{2}}}P_2(\cos\theta)e^{ipt} \text{ cm.},\\ v_2 &= -5{\cdot}47\frac{1}{kr}\frac{d}{d(kr)}\left\{\sqrt{kr}H^{(2)}_{2+\frac{1}{2}}(kr)\right\}\sin 2\theta e^{ipt} \text{ cm.},\\ w_1 &= w_2 = 0. \end{aligned}\right\} \quad \ldots(62)$$

The numerical values of these expressions at $r=0{\cdot}5/h=1{\cdot}8$ km. and $r=1/h=3{\cdot}6$ km. are tabulated in Table IX. It is to be remarked that the longitudinal and transverse waves are nearly opposite in phase, and the latter is not particularly larger than the former as at large distances from the hypocentre. These circumstances are clearly visualized from

Table IX. Amplitudes of longitudinal (u_1, v_1) and transverse (u_2, v_2) waves in cm. at the hypocentral distances (I) $r=0{\cdot}5/h=1{\cdot}8$ km. and (II) $r=1/h=3{\cdot}6$ km.

θ (degree)	u_1		v_1		u_2		v_2	
	(I)	(II)	(I)	(II)	(I)	(II)	(I)	(II)
0	86·2	6·10	0	0	−106·8	−5·97	0	0
10	82·3	5·82	+16·7	+1·20	−101·9	−5·70	−15·6	−0·99
20	71·1	5·03	+31·4	+2·26	− 88·0	−4·92	−29·4	−1·87
30	53·9	3·81	+42·3	+3·04	− 66·7	−3·73	−39·6	−2·52
40	32·8	2·32	+48·0	+3·46	− 40.6	−2·29	−45·0	−2·86
50	10·3	0·73	+48·0	+3·46	− 12·8	−0·72	−45·0	−2·86
60	−10·8	−0·76	+42·3	+3·04	+ 13·3	+0·75	−39·6	−2·52
70	−28·0	−1·98	+31·4	+2·26	+ 34·6	+1·94	−29·4	−1·87
80	−39·2	−2·77	+16·7	+1·20	+ 48·6	+2·72	−15·6	−0·99
90	−43·1	−3·05	+ 0	0	+ 53·4	+2·99	0	0

the variation of the maximum amplitudes with hypocentral distance which are shown in Table X and Fig. 10. It also shows so rapid an increase of amplitude as we approach the hypocentre that we can not extrapolate the amplitude at short epicentral distance by the simple law as inverse hypocentral distance. It is also seen from the diagram that the maximum amplitude of the wave reaches as large as 1 metre at about 2 km. from the hypocentre. It seems improbable that at such place the formula of elasticity is applicable, so we shall examine in the following whether the stress calculated from the theory of elasticity do not exceed the ultimate strength of the material.

Table X. Variation of maximum amplitudes of longitudinal and transverse waves with hypocentral distances.

P-wave	hr	0·2	0·4	0·6	0·8	1·0	1·2	1·4	1·6	1·8	2·0
	r (km.)	0·72	1·44	2·15	2·87	3·60	4·20	5·02	5·75	6·46	7·18
	u_1 (cm.)	3643	292	45·7	14·7	6·1	3·0	1·7	1·0	0·7	0·5
	v_1 (cm.)	1822	116	23·8	7·9	3·5	1·8	1·1	0·7	0·5	0·4
S-wave	kr	0·12	0·23	0·35	0·46	0·58	0·69	0·81	0·92	1·04	1·15
	r (km.)	0·41	0·83	1·24	1·66	2·07	2·48	2·90	3·31	3·73	4·14
	u_2 (cm.)	32981	2105	431	144	63·1	33·1	19·7	12·9	9.0	6·6
	v_2 (cm.)	19366	1022	201	62·9	25·4	12·0	7·0	3·8	2·6	2·0

The stress in an isotropic homogeneous medium in polar coordinates are given by the formulae

$$\left.\begin{aligned}
\widehat{rr} &= \lambda\Delta + 2\mu\frac{\partial u}{\partial r},\\
\widehat{\theta\theta} &= \lambda\Delta + 2\mu\left(\frac{1}{r}\frac{\partial v}{\partial\theta} + \frac{u}{r}\right),\\
\widehat{\varphi\varphi} &= \lambda\Delta + 2\mu\left(\frac{1}{r\sin\theta}\frac{\partial w}{\partial\varphi} + \frac{v}{r}\cot\theta + \frac{u}{r}\right),\\
\widehat{r\theta} &= \mu\left(\frac{\partial v}{\partial r} - \frac{v}{r} + \frac{1}{r}\frac{\partial u}{\partial\theta}\right),\\
\widehat{r\varphi} &= \mu\left(\frac{1}{r\sin\theta}\frac{\partial u}{\partial\varphi} + \frac{\partial w}{\partial r} - \frac{w}{r}\right),\\
\widehat{\varphi\theta} &= \mu\left\{\frac{1}{r}\left(\frac{\partial w}{\partial\theta} - w\cot\theta\right) + \frac{1}{r\sin\theta}\frac{\partial v}{\partial\varphi}\right\},
\end{aligned}\right\} \quad \ldots\ldots(63)$$

where

$$\Delta=\frac{1}{r^2\sin\theta}\left\{\frac{\partial}{\partial r}(r^2u\sin\theta)+\frac{\partial}{\partial\theta}(rv\sin\theta)+\frac{\partial}{\partial\varphi}(rw)\right\}. \quad \ldots\ldots(64)$$

And corresponding to (62),

$$\left.\begin{aligned}
\widehat{rr}&=\left[-\lambda h^2A\frac{H^{(2)}_{2+\frac{1}{2}}(hr)}{\sqrt{r}}+2\mu\left\{A\frac{d^2}{dr^2}\left(\frac{H^{(2)}_{2+\frac{1}{2}}(hr)}{\sqrt{r}}\right)\right.\right.\\
&\qquad\left.\left.+2kB_z\frac{d}{dr}\left(\frac{H^{(2)}_{2+\frac{1}{2}}(kr)}{r^{\frac{3}{2}}}\right)\right\}\right]P_2(\cos\theta)\,e^{ipt},\\
\widehat{\theta\theta}&=-\left\{\left[A\left\{\lambda h^2\frac{H^{(2)}_{2+\frac{1}{2}}(hr)}{\sqrt{r}}+2\mu\frac{1}{r}\frac{d}{dr}\left(\frac{H^{(2)}_{2+\frac{1}{2}}(hr)}{\sqrt{r}}\right)\right\}\right.\right.\\
&\qquad\left.-4\mu kB_z\frac{H^{(2)}_{2+\frac{1}{2}}(kr)}{r^{\frac{5}{2}}}\right]P_2(\cos\theta)\\
&\qquad\left.+2\mu\left[3A\frac{1}{r^{\frac{5}{2}}}H^{(2)}_{2+\frac{1}{2}}(hr)+kB_z\frac{1}{r^2}\frac{d}{dr}\left(\sqrt{r}H^{(2)}_{2+\frac{1}{2}}(kr)\right)\right]\cos 2\theta\right\}e^{ipt},\\
\widehat{\varphi\varphi}&=-\left[\lambda h^2A\frac{H^{(2)}_{2+\frac{1}{2}}(hr)}{\sqrt{r}}P_2(\cos\theta)\right.\\
&\qquad\left.+2\mu\left\{3A\frac{H^{(2)}_{2+\frac{1}{2}}(hr)}{r^{\frac{5}{2}}}+kB_z\frac{1}{r^2}\frac{d}{dr}\left(\sqrt{r}H^{(2)}_{2+\frac{1}{2}}(kr)\right)\right\}\cos^2\theta\right]e^{ipt},\\
\widehat{r\theta}&=\mu\left[6A\left\{\frac{4H^{(2)}_{2+\frac{1}{2}}(hr)}{r^{\frac{5}{2}}}-\frac{hH^{(2)}_{1+\frac{1}{2}}(hr)}{r^{\frac{3}{2}}}\right.\right.\\
&\qquad\left.\left.-kB_z\left\{16\frac{H^{(2)}_{2+\frac{1}{2}}(kr)}{r^{\frac{5}{2}}}-\frac{k^2H^{(2)}_{2+\frac{1}{2}}(kr)}{\sqrt{r}}-2k\frac{H^{(2)}_{1+\frac{1}{2}}(kr)}{r^{\frac{3}{2}}}\right\}\right]\sin\theta\cos\theta\,e^{ipt},\\
\widehat{r\varphi}&=\widehat{\varphi\theta}=0.
\end{aligned}\right\} \quad \ldots\ldots(65)$$

And from the constants already mensioned $\mu=8{\cdot}4\times10^{11}$ dyne/cm. and

$$\mu Ah^{\frac{5}{2}}=1{\cdot}90\times10^{6}\text{ dyne/cm.},$$

$$\mu B_zk^{\frac{7}{2}}=44{\cdot}4\times10^{6}\text{ dyne/cm.},$$

the numerical calculation was made and tabulated in table XI.

Table XI. The stresses in 10^6 dyne/cm^2. at hypocentral distances (I) $r=0{\cdot}5/h=1{\cdot}8$ km. and (II) $r=1/h=3{\cdot}6$ km.

(I) $r=1{\cdot}8$ km.	rr	$(0{\cdot}17+i1758{\cdot}5)P_2(\cos\theta)$	$(7{\cdot}89-i3716{\cdot}93)P_2(\cos\theta)$	$(8{\cdot}06-i1958{\cdot}4)P_2(\cos\theta)$
	$r\theta$	$(-0{\cdot}60+i3565{\cdot}8)\sin\theta\cos\theta$	$(-12{\cdot}33-i3668{\cdot}97)\sin\theta\cos\theta$	$(-12{\cdot}93-i103{\cdot}2)\sin\theta\cos\theta$
	$\theta\theta$	$(0{\cdot}37+i846{\cdot}7)P_2(\cos\theta)$	$(+8{\cdot}98+i999{\cdot}8)P_2(\cos\theta)$	$(9{\cdot}35+i153{\cdot}0)P_2(\cos\theta)$
		$(-0{\cdot}59+i991{\cdot}8)\cos 2\theta$	$(-12{\cdot}92+i857{\cdot}1)\cos 2\theta$	$(-13{\cdot}51-i54{\cdot}64)\cos 2\theta$
	$\varphi\varphi$	$(-0{\cdot}10-i152{\cdot}0)P_2(\cos\theta)$	$(-12{\cdot}92+i857{\cdot}1)\cos^2\theta$	$(-0{\cdot}10-i152{\cdot}0)P_2(\cos\theta)$
		$(-0{\cdot}59-i911{\cdot}8)\cos^2\theta)$		$+(-13{\cdot}51-i54{\cdot}64)\cos^2\theta$
(II) $r=3{\cdot}6$ km.	rr	$(0{\cdot}149+i106{\cdot}39)P_2(\cos\theta)$	$(4{\cdot}170-i144{\cdot}36)P_2(\cos\theta)$	$(4{\cdot}319-i37{\cdot}97)P_2(\cos\theta)$
	$r\theta$	$(0{\cdot}42+i118{\cdot}60)\sin\theta\cos\theta$	$(-7{\cdot}396-i130{\cdot}40)\sin\theta\cos\theta$	$(-6{\cdot}914-i11{\cdot}80)\sin\theta\cos\theta$
	$\theta\theta$	$(0{\cdot}255-i32{\cdot}17)P_2(\cos\theta)$	$(+7{\cdot}584+i46{\cdot}62)P_2(\cos\theta)$	$(7{\cdot}839+i14{\cdot}45)P_2(\cos\theta)$
		$(-0{\cdot}564-i32{\cdot}79)\cos 2\theta$	$(9{\cdot}667+25{\cdot}50)\cos 2\theta$	$(-102{\cdot}31-i7{\cdot}29)\cos 2\theta$
	$\varphi\varphi$	$(-0{\cdot}094-i5{\cdot}465)P_2(\cos\theta)$	$(-9.667+i25{\cdot}50)\cos^2\theta$	$(-0{\cdot}094-i5{\cdot}465)P_2(\cos\theta)$
		$(-0{\cdot}564-i32{\cdot}79)\cos^2\theta$		$(-102{\cdot}31-i7{\cdot}29)\cos^2\theta$

All the components of stress at $r=1{\cdot}8$ km. are the order of 10^9 dyne/cm.^{2}, and they are of the order 10^7–10^8 dyne/cm.^{2} at $r=3{\cdot}6$ km. Let us then consider the strength of material, We have seen the rigidity is nearly the same with that of steel. The region we are now considering is within the so-called sima and ultimate tensile strength of the material must be smaller than that of steel ($5-9\times10^9$ dyne/cm^2.) and will be larger than that of granite ($3-5\times10^7$ dyne/cm^2.). Even though we assume the ultimate strength as large as 10^9 dyne/cm^2. as Dr. H. Jeffreys[111] has already adopted, the stress at 1·8 km. outstrips this limit. We cannot therefore discuss what happened at the shorter distance from the data of observations of the elastic waves at larger distances. The magnitude of the hypocentral region in this sence may not be smaller than the sphere $r=2$ km. I have hitherto used the word hypocentre, which should of course mean the centre of the hypocentral region.

The energy stored up near the hypocentral region is consumed in the crustal deformation and a part of the energy is transmitted as the seismic waves. We can at present discuss the latter only. The energy flux across a surface due to periodic wave

$$F=\int(uX_s+vY_s+wZ_s)dS$$

changes its sign periodically, so we will here examine only the energy

111) H. Jeffreys, *M. N. R. A. S. Geophys. Suppl.*, 1 (1927), 483-494.

transmited in one period through a spherical surface $r=$const.

$$E=\int_0^T dt\int_0^{2\pi} d\varphi\int_0^U (\widehat{urr}+\widehat{vr\theta}+\widehat{wr\varphi})\,r^2\sin\theta d\theta. \quad \ldots\ldots (66)$$

We must however remember the stress, $\widehat{rr}$, $\widehat{r\theta}$ and $\widehat{r\varphi}$ is the force which the external portion of the sphere excert on the internal portion of the sphere, and E is consequently the energy which flow into the sphere in one period. Taking real values of u, v, $\widehat{rr}$ and $\widehat{r\theta}$ we have at $r=1/h=3{\cdot}6$ km.

$$u=u_1+u_2=(1{\cdot}694\cos pt-3{\cdot}861\sin pt)P_2(\cos\theta) \text{ cm.},$$
$$v=v_1+v_2=(-1{\cdot}091\cos pt+0{\cdot}788\sin pt)2\sin\theta\cos\theta \text{ cm.},$$
$$\widehat{rr}=(4{\cdot}319\cos pt+37{\cdot}97\sin pt)P_2(\cos\theta)\times 10^6 \text{ dyne/cm}^2.,$$
$$\widehat{r\theta}=(-6{\cdot}914\cos pt+11{\cdot}80\sin pt)\sin\theta\cos\theta\times 10^6 \text{ dyne/cm}^2.,$$

and

$$\mathrm{E}=-7{\cdot}23\times 10^{19} \text{ erg.} \quad \ldots\ldots\ldots\ldots\ldots\ldots (67)$$

At great distance from the hypocentre E becomes independent of r and can be calculated seperately for P- and S-waves.[112]

$$\mathrm{E}=-0{\cdot}3\times 10^{19} \text{ erg for P-wave},$$
$$\mathrm{E}=-6{\cdot}9\times 10^{19} \text{ erg for S-wave}.$$

And the total energy is nearly equal to that emitted through the spherical surface $r=3{\cdot}6$ km. In the deep-seated earthquakes it is usual that the wave motions are damped after a few vibrations, so that the total energy emitted as seismic waves from the hypocentral region is the order of 10^{20} or 10^{21} erg.

As we have already seen the strength of doublet force was about $1{\cdot}23\times 10^{25}$ dyne/cm., let us now examine the strength of simple sourse given by (58).

$$\phi=\frac{0{\cdot}81}{2h}\frac{H_{\frac{1}{2}}^{(2)}(hr)}{\sqrt{hr}}e^{ipt}=2{\cdot}91\times 10^5\frac{H_{\frac{1}{2}}^{(2)}(hr)}{\sqrt{hr}}e^{ipt} \text{ (cm.)}^2 \ldots\ldots (68)$$

And the pressure due to this at $r=1/h=3{\cdot}6$ km. is

$$\widehat{rr}=-i\,(1{\cdot}00+i\,2{\cdot}96)\,e^{ipt}\times 10^6 \text{ dyne/cm.}^2, \quad \ldots\ldots (69)$$

whose maximum absolute value is $3{\cdot}12\times 10^6$ dyne/cm^2 which is equal to about 3 atmosperic pressure on the other hand the pressure prevailing at a depfh of 250 km. from the surface is

112) The result is identical with the formula obtained in other way due to B. Galizin (*Eomtes Rendus*, **160** (1915), 810–813) and H. Jeffreys *M. N. R. A. S. Geophys. Suppl.*, **1** (1922), 22–31).

$3\times10^3\times250\times10^5$ dyne/cm^2.$=$7,500 atmospheric pressure,

(by taking simply the density 3 and the acceleration of gravity as 10^3), which is 2,000 times as large as the pressure due to the simple source.

Though still remains the transverse wave of the second kind, I will omit the discussion because it still being subjected to some umbiguities.

But I will state another word on the surface waves. Rayleigh-wave due to multiple sourse within a semi-infinite isotropic homogeneous solid has been solved by Prof. K. Sezawa[113] and G. Nishimura. If we assume for the moment that the earth is homogeneous and isotropic semi-infinite body, then the solution for simple source $\frac{e^{i(pt-hr)}}{r}$ is

$$\left.\begin{aligned} u&=\frac{4ie^{ipt}\pi\beta_1k^2\kappa^2e^{-\alpha_1\xi}}{h^2F'(\kappa)}\frac{\partial H_0^{(2)}(\kappa\Delta)}{\partial(\kappa\Delta)}=i7\cdot60\,e^{-\alpha_1\xi}H_1^{(2)}(\kappa\Delta)e^{ipt},\\ w&=-\frac{2ie^{ipt}\pi k^2(2\kappa^2-k^2)\kappa}{h^2F'(\kappa)}e^{-\alpha_1\xi}H_0^{(2)}(\kappa\Delta)=i11\cdot15e^{-\alpha_1\xi}H_0^{(2)}(\kappa\Delta)\,e^{ipt},\end{aligned}\right\}\quad(70)$$

which become at $\kappa\Delta=1$

$$\left.\begin{aligned} &[u]=8\cdot5e^{-\alpha_1\xi},\quad [w]=6\cdot8e^{-\alpha_1\xi},\\ &e^{-\alpha_1\xi}=1\cdot85\times10^{-48},\end{aligned}\right\}\quad\ldots.(80)$$

in which $\kappa=\frac{p}{v_R}$, $v_R=$velocity of Rayleigh wave, $\Delta=$epicentral distance and $\xi=$is hypocentral depth which is taken to be 250 km. The amplitude (u_l) of the direct longitudinal wave incident at the surface is incomparablly larger than that of Rayleigh-wave.

$$u_l=\frac{\partial}{\partial r}\left(\frac{e^{i(pt-hr)}}{r}\right)\approx\frac{-ih}{r}e^{i(pt-hr)}=1\cdot11\times10^{-23}e^{i\left(pt-hr-\frac{\pi}{2}\right)}.\quad..(81)$$

Thus, though Prof. Sezawa neglected the effect of direct and reflected bodily waves, we see here the necessity of taking these into consideration. The statement is also varid in case of waves due to quadruple source. On the other hand Rayleigh-wave as well as Love-wave due to transverse wave diminishes its amplitude with hypocentral depth with the factor $e^{-\beta_1\xi}$ and the factor for this earthquake is $e^{-\beta_1\xi}=2\cdot51\times10^{-22}$. And though this is conspicuously larger than that due to longitudinal wave, the amplitudes of the surface waves are still smaller than those due to direct bodily waves.

The above relation was the reason for the wide spread knowledge that the surface waves do not occure in case of deep-seated earthquake.

113) K. Sezawa and G. Nishimura, *loc. cit.*, 40).

And from the above values the absence of surface waves in case of deep-seated earthquake seems to be absolute. And indeed Prof. Sezawa[114] could satisfy the boundary conditions in the reflexion of elastic waves from an internal point of an isotropic homogeneous sphere without taking the surface waves into consideration.

(End of Chapter IV), (to be continued).

---

24. 地震波の傳播（第二報）
發震機巧，地殻構造と地震波の振幅に就て

地震學教室 河角廣

地震發生の機巧を審かにして其の發震力の地方的並びに時代的活動の有様を明かにし地震を豫知するは地震國日本に於ける地震研究の最大目的であるが，地震の計測から始めて發震機巧を推定したのは大森博士である．博士は地震記象型の特異性に注意せられたのであつたが，志田博士は地震初動の「押し」，「引き」の地理的分布から裂罅地震及び陥落地震等の區別をせられたが，中村左衞門太郎博士は前者を斷層（地辷）地震と解釋せられた．（此の型の地震の初動の「押し」「引き」分布は直交二平面によつて四つの部分に分けられる．此れを B 型と呼んでおく．）其の後殆ど凡ての地震が此の型で解釋出來る様に考へられて來たが，棚橋嘉一氏は昭和六年六月二日の日本中部の深發地震が所謂斷層地震説にて説明出來ず，志田博士の裂罅地震説に對する松山博士の型（即節圓錘によつて「押し」「引き」が分たれるもの．此れを A 型と呼ぶ）でよく説明される事を見出された．石本博士は此れに特に興味を持れた幾多の地震が此の A 型で説明出來る事から岩漿貫入説を出された．筆者は兼々地震動の大きさの定量的研究を企て居たので此處に此の問題を定量的に調査し發震機巧をも確めて見た．其の調査の一部を此處に報告する．

先づ第一章に從來の彈性波としての理論的諸研究及び實際的の地震の諸調査の歷史的概括を説べ，第二章に彈性球面波の一般解を簡單に求め，此れと從來の諸發震機巧に對する解との關係を調査し，第三章には實際に地球が一様な彈性體でない爲の影響を考へ，第四章には此等の諸理論を實際に應用して昭和六年六月二日の日本中部の深發地震を調査し，此の地震が地下約 250 粁の深にある震原に於て約 N 10° E の方向に 67° 傾いた方向に働く 1.23×10^{25} dyne/cm の强さの二重力及び震原距離約 3·6 粁に於て約 3 氣壓の靜水壓を與へるに相等する震原によつて起された波動と二重力に直角な面の兩側に於て二重力の方向のまはりに起されたと見へる違つた向きの回轉によつて起されたと見られる横波とよりなる事を確め，其等波動による震原近くの變位及び歪力を計算し，震原距離 1·8 粁に於て振幅約 2 米に達し歪力は約 10^9 dyne/cm^2 のものとなり恐らく物質强度の限界を越すと思はれる．卽此の約 3 粁以内の現象は地震波の觀測からは推知出來ないのではないかと思はれる．此の意味から其處を震原域と呼んだ．尙此の二重力及び單源によつて運ばれる勢力

114) K. SEZAWA, *loc. cit.*, 37).

は平均毎秒約 $2{\cdot}7\times10^{19}$ erg. である. 從つて此の地震の際に波動として運ばれた全勢力は 10^{20}～10^{21} erg. であつた事が推知出來た. 尙此等の波による表面波の問題も考へて見たが此れは理論的には到底觀測出來ない程の小さいものである事が知られ, 或は此の樣な深發地震では絕對的に表面波は起らないものかも知れない. (續く)

25. *On Stresses in the Interior and in the Vicinity of a Horizontal Cylindrical Inclusion of Circular Section in a Gravitating Semi-infinite Elastic Solid. (II)*

By Genrokuro NISHIMURA, Takeo TAKAYAMA and Kiyoshi KANAI,

Earthquake Research Institute.

(Read Jan. 17, 1933.—Received June 20, 1933.)

For the same object of investigation as stated in an earlier paper,[1] we shall solve the problem of a cylindrical heterogeneous matter included in a gravitating semi-infinite elastic solid in a state of plane stress, and study the difference in stress distribution of two cases, the state of the semi-infinite medium of one being a plane strain and the other plane stress.

In the present study we take the following expressions[2] of Δ, 2ϖ, Δ' and $2\varpi'$ as particular solutions of the equilibrium equations of the gravitating semi-infinite solid and the cylindrical inclusion:

$$\left.\begin{aligned} \Delta &= 0, \\ 2\varpi &= -\frac{\rho g r}{\mu}\sin\theta, \end{aligned}\right\} \quad \cdots\cdots\cdots\cdots\cdots\cdots (1)$$

$$\left.\begin{aligned} \Delta' &= \frac{\rho' g r}{2(\lambda'+\mu')}\cos\theta, \\ 2\varpi' &= \frac{\lambda'}{2\mu'}\frac{\rho' g r}{(\lambda'+\mu')}\sin\theta, \end{aligned}\right\} \quad \cdots\cdots\cdots\cdots\cdots (2)$$

which differ from the expressions used in problems relating to plane

1) G. NISHIMURA and T. TAKAYAMA, "On Stresses in the Interior and in the Vicinity of a Spherical Inclusion in a gravitating Semi-infinite Elastic Solid," *Bull. Earthq. Res. Inst.*, **11** (1933).

G. NISHIMURA and T. TAKAYAMA," On Stresses in the Interior and in the Vicinity of a Horizontal Cylindrical Inclusion of Circular Section in a Gravitating Semi-infinite Elastic Solid," *Bull. Earthq. Res. Inst.*, **11** (1933).

2) The notations of all physical quantities used in this paper have the same meanings as those in the previous paper.

strain.[3]

The respective displacements u, v and u', v' corresponding to (1) and (2) are obtained by the method used in the preceding papers. They are expressed by

$$\left.\begin{aligned} u &= \frac{\rho g}{8\mu} r^2 \cos\theta, \\ v &= -\frac{3\rho g}{8\mu} r^2 \sin\theta, \end{aligned}\right\} \quad \cdots\cdots\cdots\cdots\cdots\cdots\cdots\cdots (3)$$

$$\left.\begin{aligned} u' &= \frac{(\lambda' + 3\mu')}{16\mu'(\lambda' + \mu')} \rho' g r^2 \cos\theta, \\ v' &= -\frac{(3\lambda' + \mu')}{16\mu'(\lambda' + \mu')} \rho' g r^2 \sin\theta. \end{aligned}\right\} \quad \cdots\cdots\cdots\cdots\cdots (4)$$

The stresses corresponding to (1), (2) and (3), (4), respectively, are given by

$$\widehat{rr} = \frac{1}{2}\rho g r \cos\theta, \quad \widehat{\theta\theta} = -\frac{1}{2}\rho g r \cos\theta, \quad \widehat{r\theta} = -\frac{1}{2}\rho g r \sin\theta, \quad \cdots (5)$$

$$\widehat{rr'} = \frac{3}{4}\rho' g r \cos\theta, \quad \widehat{\theta\theta'} = \frac{1}{4}\rho' g r \cos\theta, \quad \widehat{r\theta'} = -\frac{1}{4}\rho' g r \sin\theta. \quad (6)$$

As complementary solutions of $\Delta, 2\varpi$ and $\Delta', 2\varpi'$ of the equilibrium equations of two solids, we use the same expressions which were used in the preceding paper,[4] so that the displacement expressions u, v, u', v' and the stress expressions $\widehat{rr}, \widehat{\theta\theta}, \widehat{zz}, \widehat{r\theta}, \widehat{rr'}, \widehat{\theta\theta'}, \widehat{zz'}, \widehat{r\theta'}$ corresponding to these dilatations and rotations are the same as those of the previous paper.

Now the stress components of a gravitating semi-infinite elastic solid, the state of which is one of plane stress, having no heterogeneous inclusion in its interior are expressed by

$$\left.\begin{aligned} \widehat{rr} &= -\frac{1}{2}\rho g\xi + \frac{3}{4}\rho g r\cos\theta - \frac{1}{2}\rho g\xi\cos 2\theta + \frac{1}{4}\rho g r\cos 3\theta, \\ \widehat{\theta\theta} &= -\frac{1}{2}\rho g\xi + \frac{1}{4}\rho g r\cos\theta + \frac{1}{2}\rho g\xi\cos 2\theta - \frac{1}{4}\rho g r\cos 3\theta, \\ \widehat{r\theta} &= -\frac{1}{4}\rho g r\sin\theta + \frac{1}{2}\rho g\xi\sin 2\theta - \frac{1}{4}\rho g r\sin 3\theta. \end{aligned}\right\} \quad \cdots (7)$$

3) In the plane strain problem we took the following expressions as particular solutions of the equilibrium equations:

$$\Delta = 0, \quad 2\varpi = -\frac{\rho g}{\mu} r\sin\theta, \quad \Delta' = \frac{\rho' g r}{(\lambda' + 2\mu')}\cos\theta, \quad 2\varpi' = 0.$$

4) G. Nishimura and T. Takayama, *loc. cit.*

These expressions are obtained by the following conditions: The normal and the shearing components of stress vanish at the horizontal surface $x=\xi$, and the stress at any point in the solid increases linearly with increase in its position from the upper surface of the solid. This semi-infinite solid is in a state of plane stress. Expressions (7) differ from those in the case of a plane strain problem.

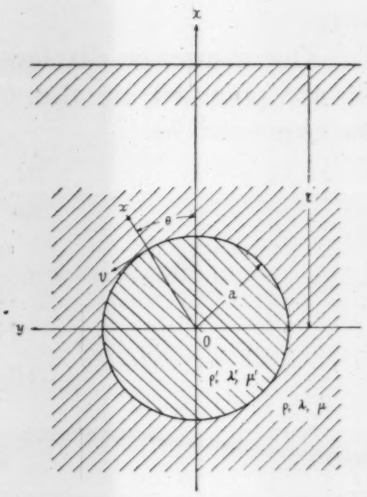

Fig. 1.

Now the boundary conditions of the present study are as follows: the heterogeneous inclusion and the outer medium are perfectly cemented at the contact surface, so that they cannot slide upon each other at the boundary. In all the spaces in the medium distant from the inclusion the stress distributions are equal to those expressed by (7).

Adjusting the arbitrary constants of the general expressions of displacement and stress to satisfy these conditions, we obtain the final results of the stresses in the gravitating semi-infinite medium and in the inclusion.

$$\widehat{rr}=-\frac{\rho g\xi}{2}-\frac{\mu(\lambda'+\mu'-\lambda-\mu)}{2(\lambda+\mu)(\lambda'+\mu'+\mu)}\left(\frac{a}{r}\right)^2\rho g\xi$$

$$+\left[\frac{3}{4}\rho gr+\frac{(\rho' ga-\rho ga)(2\lambda+3\mu)}{2(\lambda+2\mu)}\left(\frac{a}{r}\right)\right.$$

$$-\frac{[\lambda\{\mu(\lambda'+3\mu')+\mu'(\lambda'+\mu')\}+(\lambda+2\mu)\{\mu'(\lambda'+\mu')+\mu(-\lambda'+\mu')\}]\rho' ga^4}{4(\lambda+2\mu)\{\mu(\lambda'+3\mu')+\mu'(\lambda'+\mu')\}}\frac{}{r^3}$$

$$\left.+\frac{[\lambda(\lambda+\mu)\{\mu(\lambda'+3\mu')+\mu'(\lambda'+\mu')\}+2\mu\mu'(\lambda'+\mu')(\lambda+2\mu)]}{4(\lambda+\mu)(\lambda+2\mu)\{\mu(\lambda'+3\mu')+\mu'(\lambda'+\mu')\}}\frac{\rho ga^4}{r^3}\right]\cos\theta$$

$$+\frac{\rho g\xi}{2\mu}\left[-\mu+\frac{2(\lambda+\mu)\vartheta_{C_2}}{\vartheta_2}\left(\frac{a}{r}\right)^2-\frac{6\mu\vartheta_{C_2''}}{\vartheta_2}\left(\frac{a}{r}\right)^4\right]\cos 2\theta$$

$$+\frac{\rho gr}{2\mu}\left[\frac{\mu}{2}-\frac{5}{4}\frac{(\lambda+\mu)\vartheta_{C_3}}{\vartheta_3}\left(\frac{a}{r}\right)^4+\frac{4\mu\vartheta_{C_3''}}{\vartheta_3}\left(\frac{a}{r}\right)^6\right]\cos 3\theta, \quad \cdots\cdots\cdots(8)$$

$$\widehat{\theta\theta}=-\frac{\rho g\xi}{2}+\frac{\mu(\lambda'+\mu'-\lambda-\mu)}{2(\lambda+\mu)(\lambda'+\mu'+\mu)}\rho g\xi\left(\frac{a}{r}\right)^2$$

$$+\left[\frac{1}{4}\rho g r-\frac{\mu(\rho' g a-\rho g a)}{2(\lambda+2\mu)}\left(\frac{a}{r}\right)\right.$$
$$+\frac{[\lambda\{\mu(\lambda'+3\mu')+\mu'(\lambda'+\mu')\}+(\lambda+2\mu)\{\mu'(\lambda'+\mu')+\mu(-\lambda'+\mu')\}]}{4(\lambda+2\mu)\{\mu(\lambda'+3\mu')+\mu'(\lambda'+\mu')\}}\rho' g a\left(\frac{a}{r}\right)^3$$
$$\left.-\frac{[\lambda(\lambda+\mu)\{\mu(\lambda'+3\mu')+\mu'(\lambda'+\mu')\}+2\mu\mu'(\lambda'+\mu')(\lambda+2\mu)]}{4(\lambda+\mu)(\lambda+2\mu)\{\mu(\lambda'+3\mu')+\mu'(\lambda+\mu')\}}\rho g a\left(\frac{a}{r}\right)^3\right]\cos\theta$$
$$+\frac{\rho g\xi}{2\mu}\left[\mu+\frac{6\mu\vartheta_{C_2''}}{\vartheta_2}\left(\frac{a}{r}\right)^4\right]\cos 2\theta$$
$$+\frac{\rho g r}{2\mu}\left[-\frac{\mu}{2}+\frac{(\lambda+\mu)\vartheta_{C_3}}{\vartheta_3}\left(\frac{a}{r}\right)^4-\frac{4\mu\vartheta_{C_3''}}{\vartheta_3}\left(\frac{a}{r}\right)^6\right]\cos 3\theta, \quad \ldots\ldots\ldots\ldots\ldots (9)$$

$$\widehat{r\theta}=\left[\frac{1}{4}\rho g r+\frac{\mu(\rho' g a-\rho g a)}{2(\lambda+2\mu)}\left(\frac{a}{r}\right)\right.$$
$$+\frac{[\lambda\{\mu(\lambda'+3\mu')+\mu'(\lambda'+\mu')\}+(\lambda+2\mu)\{\mu'(\lambda'+\mu')+\mu(-\lambda'+\mu')\}]}{4(\lambda+2\mu)\{\mu(\lambda'+3\mu')+\mu'(\lambda'+\mu')\}}\rho' g a\left(\frac{a}{r}\right)^3$$
$$\left.-\frac{[\lambda(\lambda+\mu)\{\mu(\lambda'+3\mu')+\mu'(\lambda'+\mu')\}+2\mu\mu'(\lambda'+\mu')(\lambda+2\mu)]}{4(\lambda+\mu)(\lambda+2\mu)\{\mu(\lambda'+3\mu')+\mu'(\lambda'+\mu')\}}\rho g a\left(\frac{a}{r}\right)^3\right]$$
$$\times(-\sin\theta)$$
$$+\frac{\rho g\xi}{2\mu}\left[\mu+\frac{(\lambda+\mu)\vartheta_{C_2}}{\vartheta_2}\left(\frac{a}{r}\right)^2-\frac{6\mu\vartheta_{C_2''}}{\vartheta_2}\left(\frac{a}{r}\right)^4\right]\sin 2\theta$$
$$+\frac{\rho g\xi}{2\mu}\left[-\frac{\mu}{2}-\frac{3(\lambda+\mu)\vartheta_{C_3}}{\vartheta_3}\left(\frac{a}{r}\right)^4+\frac{4\mu\vartheta_{C_3''}}{\vartheta_3}\left(\frac{a}{r}\right)^6\right]\sin 3\theta, \quad \ldots\ldots\ldots (10)$$

$$\widehat{rr'}=-\frac{(\lambda+2\mu)(\lambda'+\mu')}{2(\lambda+\mu)(\mu+\lambda'+\mu')}\rho g\xi$$
$$+\left[\frac{3}{4}\rho' g r-\frac{\{\mu'(\lambda'+\mu')+\mu(-\lambda'+\mu')\}}{4\{\mu(\lambda'+3\mu')+\mu'(\lambda'+\mu')\}}\rho' g r\right.$$
$$\left.+\frac{\mu\mu'(\lambda'+\mu')\rho g r}{2(\lambda+\mu)\{\mu(\lambda'+3\mu')+\mu'(\lambda'+\mu')\}}\right]\cos\theta$$
$$+\frac{\mu'\rho g\xi}{\mu}\frac{\vartheta_{D_2''}}{\vartheta_2}\cos 2\theta$$
$$+\frac{\rho g a}{2\mu}\left[\frac{(\lambda'+\mu')}{4}\frac{\vartheta_{D_3}}{\vartheta_3}\left(\frac{r}{a}\right)^3-\frac{2\mu'\vartheta_{D_3''}}{\vartheta_3}\left(\frac{r}{a}\right)\right]\cos 3\theta, \quad \ldots\ldots\ldots (11)$$

$$\widehat{\theta\theta'}=-\frac{(\lambda+2\mu)(\lambda'+\mu')}{2(\lambda+\mu)(\mu+\lambda'+\mu')}\rho g\xi$$
$$+\left[\frac{1}{4}\rho' g r-\frac{3\{\mu'(\lambda'+\mu')+\mu(-\lambda'+\mu')\}\rho' g r}{4\{\mu(\lambda'+3\mu')+\mu'(\lambda'+\mu')\}}\right.$$

$$+\frac{3\mu\mu'(\lambda'+\mu')\rho g r}{2(\lambda+\mu)\{\mu(\lambda'+3\mu')+\mu'(\lambda'+\mu')\}}\Big]\cos\theta$$

$$+\frac{\rho g\xi}{2\mu}\Big[-\frac{2\mu'\vartheta_{D_2''}}{\vartheta_2}+\frac{2(\lambda'+\mu')\vartheta_{D2}}{\vartheta_2}\Big(\frac{r}{a}\Big)^2\Big]\cos 2\theta$$

$$+\frac{\rho g r}{2\mu}\Big[-\frac{5(\lambda'+\mu')}{4}\frac{\vartheta_{D_3}}{\vartheta_3}\Big(\frac{r}{a_3}\Big)^3+\frac{2\mu'\vartheta_{D_3''}}{\vartheta_3}\Big(\frac{r}{a}\Big)\Big]\cos 3\theta, \quad \ldots\ldots\ldots(12)$$

$$\widehat{r\theta'}=\Big[\frac{1}{4}\rho' g r+\frac{\{\mu'(\lambda'+\mu')+\mu(-\lambda'+\mu')\}\rho' g r}{4\{\mu(\lambda'+3\mu')+\mu'(\lambda'+\mu')\}}$$

$$-\frac{\mu\mu'(\lambda'+\mu')\rho g r}{2(\lambda+\mu)\{\mu(\lambda'+3\mu')+\mu'(\lambda'+\mu')\}}\Big](-\sin\theta)$$

$$+\frac{\rho g\xi}{2\mu}\Big[-\frac{2\mu'\vartheta_{D_2''}}{\vartheta_2}+\frac{(\lambda'+\mu')\vartheta_{D_2}}{\vartheta_2}\Big(\frac{r}{a}\Big)^2\Big]\sin 2\theta$$

$$+\frac{\rho g r}{2\mu}\Big[\frac{2\mu'\vartheta_{D_3''}}{\vartheta_3}-\frac{3(\lambda'+\mu')\vartheta_{D_3}}{\vartheta_3}\Big(\frac{r}{a}\Big)^3\Big]\sin 3\theta, \quad \ldots\ldots\ldots\ldots(13)$$

where $\vartheta_2, \vartheta_{C_2}, \vartheta_{C_2''}, \vartheta_{D_2}, \vartheta_{D_2''}$ and $\vartheta_3, \vartheta_{C_3}, \vartheta_{C_3''}, \vartheta_{D_3}, \vartheta_{D_3''}$ are expressed by the following determinants:

$$\left.\begin{aligned}
\vartheta_2&=\begin{vmatrix} 2(\lambda+\mu), & -6\mu, & -2\mu' & 0 \\ -(\lambda+\mu), & 6\mu, & -2\mu' & (\lambda'+\mu') \\ -\dfrac{(\lambda+2\mu)}{2\mu}, & 1, & -1, & \dfrac{\lambda'}{6\mu'} \\ -\dfrac{1}{2}, & -1, & -1, & \dfrac{(2\lambda'+3\mu')}{6\mu'} \end{vmatrix},\\
\vartheta_{C_2}&=\begin{vmatrix} \mu, & -6\mu, & -2\mu' & 0 \\ \mu, & 6\mu, & -2\mu', & (\lambda'+\mu') \\ \dfrac{1}{2}, & 1, & -1, & \dfrac{\lambda'}{6\mu'} \\ \dfrac{1}{2}, & -1, & -1, & \dfrac{(2\lambda'+3\mu)}{6\mu'} \end{vmatrix},\\
\vartheta_{C_2''}&=\begin{vmatrix} 2(\lambda+\mu), & \mu, & -2\mu', & 0 \\ -(\lambda+\mu), & \mu, & -2\mu', & (\lambda'+\mu') \\ -\dfrac{(\lambda+2\mu)}{2\mu}, & \dfrac{1}{2}, & -1, & \dfrac{\lambda'}{6\mu'} \\ -\dfrac{1}{2}, & \dfrac{1}{2}, & -1, & \dfrac{(2\lambda'+3\mu')}{6\mu'} \end{vmatrix},
\end{aligned}\right\} \quad \ldots\ldots(14)$$

$$\left.\begin{aligned}
\vartheta_{D_2} &= \begin{vmatrix} 2(\lambda+\mu), & -6\mu, & -2\mu', & \mu \\ -(\lambda+\mu), & 6\mu, & -2\mu', & \mu \\ -\frac{(\lambda+2\mu)}{2\mu}, & 1, & -1, & \frac{1}{2} \\ -\frac{1}{2}, & -1, & -1, & \frac{1}{2} \end{vmatrix}, \\
\vartheta_{D_2''} &= \begin{vmatrix} 2(\lambda+\mu), & -6\mu, & \mu, & 0 \\ -(\lambda+\mu), & 6\mu, & \mu, & (\lambda'+\mu') \\ -\frac{(\lambda+2\mu)}{2\mu}, & 1, & \frac{1}{2}, & \frac{\lambda'}{6\mu'} \\ -\frac{1}{2}, & -1, & \frac{1}{2}, & \frac{(2\lambda'+3\mu')}{6\mu'} \end{vmatrix}.
\end{aligned}\right\}$$

$$\left.\begin{aligned}
\vartheta_3 &= \begin{vmatrix} \frac{5}{2}(\lambda+\mu), & -8\mu, & \frac{(\lambda'+\mu')}{2}, & -4\mu' \\ -\frac{3}{2}(\lambda+\mu), & 8\mu, & \frac{3}{2}(\lambda'+\mu'), & -4\mu' \\ -\frac{(3\lambda+5\mu)}{8\mu}, & 1, & \frac{(3\lambda'+\mu')}{16\mu'}, & -1 \\ \frac{(\lambda-\mu)}{8\mu}, & -1, & \frac{(5\lambda'+7\mu')}{16\mu'}, & -1 \end{vmatrix}, \\
\vartheta_{C_3} &= \begin{vmatrix} \mu, & -8\mu, & \frac{(\lambda'+\mu')}{2}, & -4\mu' \\ \mu, & 8\mu, & \frac{3}{2}(\lambda'+\mu'), & -4\mu' \\ \frac{1}{4}, & 1, & \frac{(3\lambda'+\mu')}{16\mu'}, & -1 \\ \frac{1}{4}, & -1, & \frac{(3\lambda'+7\mu')}{16\mu'}, & -1 \end{vmatrix}, \\
\vartheta_{C_3''} &= \begin{vmatrix} \frac{5}{2}(\lambda+\mu), & \mu, & \frac{(\lambda'+\mu')}{2}, & -4\mu' \\ -\frac{3}{2}(\lambda+\mu), & \mu, & \frac{3}{2}(\lambda'+\mu'), & -4\mu' \\ -\frac{(3\lambda+5\mu)}{8\mu}, & \frac{1}{4}, & \frac{(3\lambda'+\mu')}{16\mu'}, & -1 \\ \frac{(\lambda-\mu)}{8\mu}, & \frac{1}{4}, & \frac{(5\lambda'+7\mu')}{16\mu'}, & -1 \end{vmatrix},
\end{aligned}\right\} \quad \ldots\ldots(15)$$

$$\vartheta_{D_3}=\begin{vmatrix} \frac{5}{2}(\lambda+\mu), & -8\mu, & \mu, & -4\mu' \\ -\frac{3}{2}(\lambda+\mu), & 8\mu, & \mu, & -4\mu' \\ -\frac{(3\lambda+5\mu)}{8\mu}, & 1, & \frac{1}{4}, & -1 \\ \frac{(\lambda-\mu)}{8\mu}, & -1, & \frac{1}{4}, & -1 \end{vmatrix},$$

$$\vartheta_{D_3''}=\begin{vmatrix} \frac{5}{2}(\lambda+\mu), & -8\mu, & \frac{(\lambda'+\mu')}{2}, & \mu \\ -\frac{3}{2}(\lambda+\mu), & 8\mu, & \frac{3}{2}(\lambda'+\mu'), & \mu \\ -\frac{(3\lambda+5\mu)}{8\mu}, & 1; & \frac{(3\lambda'+\mu')}{16\mu'}, & \frac{1}{4} \\ \frac{(\lambda-\mu)}{8\mu}, & -1, & \frac{(5\lambda'+7\mu')}{16\mu'}, & \frac{1}{4} \end{vmatrix}.$$

The foregoing results bring to light many interesting facts, some of which we have summarised as follows:

1. The stress distributions in the medium and in the inclusion vary, in general, with variation of radial distance from the center of inclusion and with variation of azimuthal direction. The magnitudes of all stresses at all points in and around the inclusion vary with the magnitudes of both densities ρ, ρ', the elastic constants of both solids, the distance ξ between the free surface of the semi-infinite solid and the center of inclusion, and with the radius a of the cylindrical inclusion.

2. All components of stresses in the interior of both the gravitating semi-infinite solid and the gravitating inclusion are expressed by three terms related to $\rho g\xi$, ρga, and $\rho' ga$ respectively.

3. The respective magnitudes related to the terms $\rho g\xi$ of $\widehat{rr}$, $\widehat{\theta\theta}$, and $\widehat{r\theta}$ become constant along the radial direction when the position in the medium is far from the inclusion.

4. The respective magnitudes related to the terms ρga of $\widehat{rr}$, $\widehat{\theta\theta}$, and $\widehat{r\theta}$ tend to increase linearly along the radial direction when the positions in the medium are far from the inclusion.

5. The respective magnitudes related to the term $\rho' ga$ of $\widehat{rr}$, $\widehat{\theta\theta}$ and $\widehat{r\theta}$ tend to decrease and finally vanish along the radial directions,

becoming inversely proportional to the radial distance from the center of the inclusion when the positions are far from the inclusion.

6. The magnitudes of the terms related to $\rho g\xi$ of all components of stress $\widehat{rr'}$, $\widehat{\theta\theta'}$ and $\widehat{r\theta'}$ in the cylindrical inclusion, although constant along the radial direction, are not so along the azimuthal direction.

7. The magnitudes of the terms related to ρga and $\rho' ga$ of the respective components of stresses increase linearly along the radial direction but not along the azimuthal direction.

8. The stress distributions in the medium, especially around the inclusion, are much affected by the presence of inclusion, and the effect of inclusion upon the stress distributions in the medium, especially in the vicinity of the inclusion, decrease also when the distance between the position in the medium and the center of the inclusion become large.

9. The magnitudes of all terms related to $\rho g\xi$, ρga and $\rho' ga$ of stresses in the inclusion vary with variation in magnitude of the elastic constants of both solids.

10. The distribution of stresses and the magnitudes of stresses all differ according as to whether the state of the medium is one of plane stress or whether the solids are in plane strain.

To find the general properties above mentioned we shall study more closely the stress distributions in and around the inclusion.

When the Poisson ratio of each of the solids are $\frac{1}{4}$, the stress distributions in and around the inclusion are expressed by

$$\begin{aligned}
\widehat{rr} = \rho g\xi\Big[& -\frac{1}{2} - \frac{(\mu'-\mu)}{2(\mu+2\mu')}\Big(\frac{a}{r}\Big)^2 \\
& + \Big\{-\frac{1}{2} + \frac{2(\mu-\mu')}{(\mu+2\mu')}\Big(\frac{a}{r}\Big)^2 - \frac{3(\mu-\mu')}{2(\mu+2\mu')}\Big(\frac{a}{r}\Big)^4\Big\}\cos 2\theta\Big] \\
& + \rho ga\Big[\Big\{\frac{3}{4}\Big(\frac{r}{a}\Big) - \frac{5}{6}\Big(\frac{a}{r}\Big) + \frac{(\mu+2\mu')}{6(2\mu+\mu')}\Big(\frac{a}{r}\Big)^3\Big\}\cos\theta \\
& + \Big\{\frac{1}{4}\Big(\frac{r}{a}\Big) + \frac{5(\mu'-\mu)}{4(\mu+2\mu')}\Big(\frac{a}{r}\Big)^3 + \frac{(\mu-\mu')}{(\mu+2\mu')}\Big(\frac{a}{r}\Big)^5\Big\}\cos 3\theta\Big] \\
& + \rho' ga\Big[\frac{5}{6}\Big(\frac{a}{r}\Big) - \frac{(\mu+2\mu')}{6(2\mu+\mu')}\Big(\frac{a}{r}\Big)^3\Big]\cos\theta, \quad \ldots\ldots\ldots\ldots\ldots\ldots (16)
\end{aligned}$$

$$\widehat{\theta\theta} = \rho g\xi\Big[-\frac{1}{2} - \frac{(\mu-\mu')}{2(\mu+2\mu')}\Big(\frac{a}{r}\Big)^2 + \Big\{\frac{1}{2} + \frac{3(\mu-\mu')}{2(\mu+2\mu')}\Big(\frac{a}{r}\Big)^4\Big\}\cos 2\theta\Big]$$

$$+\rho ga\left[\left\{\frac{1}{4}\left(\frac{r}{a}\right)+\frac{1}{6}\left(\frac{a}{r}\right)-\frac{(\mu+2\mu')}{6(2\mu+\mu')}\left(\frac{a}{r}\right)^3\right\}\cos\theta\right.$$

$$\left.+\left\{-\frac{1}{4}\left(\frac{r}{a}\right)+\frac{(\mu-\mu')}{4(\mu+2\mu')}\left(\frac{a}{r}\right)^3-\frac{(\mu-\mu')}{(\mu+2\mu')}\left(\frac{a}{r}\right)^5\right\}\cos 3\theta\right]$$

$$+\rho' ga\left[-\frac{1}{6}\left(\frac{a}{r}\right)+\frac{(\mu+2\mu')}{6(2\mu+\mu')}\left(\frac{a}{r}\right)^3\right]\cos\theta, \quad \cdots\cdots\cdots\cdots\cdots\cdots(17)$$

$$\widehat{r\theta}=\rho g\xi\left[\frac{1}{2}+\frac{(\mu-\mu')}{(\mu+2\mu')}\left(\frac{a}{r}\right)^2-\frac{3(\mu-\mu')}{2(\mu+2\mu')}\left(\frac{a}{r}\right)^4\right]\sin 2\theta$$

$$+\rho ga\left[\left\{-\frac{1}{4}\left(\frac{r}{a}\right)+\frac{1}{6}\left(\frac{a}{r}\right)+\frac{(\mu+2\mu')}{6(2\mu+\mu')}\left(\frac{a}{r}\right)^3\right\}\sin\theta\right.$$

$$\left.+\left\{-\frac{1}{4}\left(\frac{r}{a}\right)-\frac{3(\mu-\mu')}{4(\mu+2\mu')}\left(\frac{a}{r}\right)^3+\frac{(\mu-\mu')}{(\mu+2\mu')}\left(\frac{a}{r}\right)^5\right\}\sin 3\theta\right]$$

$$+\rho' ga\left[-\frac{1}{6}\left(\frac{a}{r}\right)-\frac{(\mu+2\mu')}{6(2\mu+\mu')}\left(\frac{a}{r}\right)^3\right]\sin 3\theta, \quad \cdots\cdots\cdots\cdots\cdots(18)$$

$$\widehat{rr'}=\rho g\xi\left[-\frac{3\mu'}{2(\mu+2\mu')}-\frac{3\mu'}{2(\mu+2\mu')}\cos 2\theta\right]$$

$$+\rho ga\left[\frac{\mu'}{4(2\mu+\mu')}\frac{r}{a}\cos\theta+\frac{3\mu'}{4(\mu+2\mu')}\frac{r}{a}\cos 3\theta\right]$$

$$+\rho' ga\left[\frac{3}{4}\frac{r}{a}-\frac{\mu'}{4(2\mu+\mu')}\frac{r}{a}\right]\cos\theta, \quad \cdots\cdots\cdots\cdots\cdots\cdots(19)$$

$$\widehat{\theta\theta'}=\rho g\xi\left[-\frac{3\mu'}{2(\mu+2\mu')}+\frac{3\mu'}{2(\mu+2\mu')}\cos 2\theta\right]$$

$$+\rho ga\left[\frac{3\mu'}{4(2\mu+\mu')}\frac{r}{a}\cos\theta-\frac{3\mu'}{4(\mu+2\mu')}\frac{r}{a}\cos 3\theta\right]$$

$$+\rho' ga\left[\frac{1}{4}\frac{r}{a}-\frac{3\mu'}{4(2\mu+\mu')}\frac{r}{a}\right]\cos\theta, \quad \cdots\cdots\cdots\cdots\cdots\cdots(20)$$

$$\widehat{r\theta'}=\rho g\xi\left[\frac{3}{2}\frac{\mu'}{(\mu+2\mu')}\sin 2\theta\right]$$

$$+\rho ga\left[\frac{\mu'}{4(2\mu+\mu')}\frac{r}{a}\sin\theta-\frac{3\mu'}{4(\mu+2\mu')}\frac{r}{a}\sin 3\theta\right]$$

$$+\rho' ga\left[-\frac{1}{4}\frac{r}{a}-\frac{\mu'}{4(2\mu+\mu')}\frac{r}{a}\right]\sin\theta, \quad \cdots\cdots\cdots\cdots\cdots\cdots(21)$$

A few examples in which different values of $\frac{\mu'}{\mu}\left(\text{or } \frac{\lambda'}{\lambda}\right)$ are given

are shown below:

$\frac{\mu'}{\mu}=\frac{1}{5}$, $\lambda=\mu$, $\lambda'=\mu'$:—

$$\widehat{rr}=\rho g\xi\left[\left\{-\frac{1}{2}+\frac{2}{7}\left(\frac{a}{r}\right)^2\right\}+\left\{-\frac{1}{2}+\frac{8}{7}\left(\frac{a}{r}\right)^2-\frac{6}{7}\left(\frac{a}{r}\right)^4\right\}\cos 2\theta\right]$$
$$+\rho ga\left[\left\{\frac{3}{4}\left(\frac{r}{a}\right)-\frac{5}{6}\left(\frac{a}{r}\right)+\frac{7}{66}\left(\frac{a}{r}\right)^3\right\}\cos\theta\right.$$
$$\left.+\left\{\frac{1}{4}\left(\frac{r}{a}\right)-\frac{5}{7}\left(\frac{a}{r}\right)^3+\frac{4}{7}\left(\frac{a}{r}\right)^5\right\}\cos 3\theta\right]$$
$$+\rho' ga\left[\frac{5}{6}\left(\frac{a}{r}\right)-\frac{7}{66}\left(\frac{a}{r}\right)^3\right]\cos\theta, \quad \ldots\ldots\ldots\ldots\ldots\ldots\ldots\ldots(22)$$

$$\widehat{\theta\theta}=\rho g\xi\left[-\left\{\frac{1}{2}+\frac{2}{7}\left(\frac{a}{r}\right)^2\right\}+\left\{\frac{1}{2}+\frac{6}{7}\left(\frac{a}{r}\right)^4\right\}\cos 2\theta\right]$$
$$+\rho ga\left[\left\{\frac{1}{4}\left(\frac{r}{a}\right)+\frac{1}{6}\left(\frac{a}{r}\right)-\frac{7}{66}\left(\frac{a}{r}\right)^3\right\}\cos\theta\right.$$
$$\left.+\left\{-\frac{1}{4}\left(\frac{r}{a}\right)+\frac{1}{7}\left(\frac{a}{r}\right)^3-\frac{4}{7}\left(\frac{a}{r}\right)^5\right\}\cos 3\theta\right]$$
$$+\rho' ga\left[-\frac{1}{6}\left(\frac{a}{r}\right)+\frac{7}{66}\left(\frac{a}{r}\right)^3\right]\cos\theta, \quad \ldots\ldots\ldots\ldots\ldots\ldots\ldots\ldots(23)$$

$$\widehat{r\theta}=\rho g\xi\left[\frac{1}{2}+\frac{4}{7}\left(\frac{a}{r}\right)^2-\frac{6}{7}\left(\frac{a}{r}\right)^4\right]\sin 2\theta$$
$$+\rho ga\left[\left\{-\frac{1}{4}\left(\frac{r}{a}\right)+\frac{1}{6}\left(\frac{a}{r}\right)+\frac{7}{66}\left(\frac{a}{r}\right)^3\right\}\sin\theta\right.$$
$$\left.+\left\{-\frac{1}{4}\left(\frac{r}{a}\right)-\frac{3}{7}\left(\frac{a}{r}\right)^3+\frac{4}{7}\left(\frac{a}{r}\right)^5\right\}\sin 3\theta\right]$$
$$+\rho' ga\left[-\frac{1}{6}\left(\frac{a}{r}\right)-\frac{7}{66}\left(\frac{a}{r}\right)^3\right]\sin\theta, \quad \ldots\ldots\ldots\ldots\ldots\ldots\ldots\ldots(24)$$

$$\widehat{rr'}=\rho g\xi\left[-\frac{3}{14}-\frac{3}{14}\cos 2\theta\right]$$
$$+\rho ga\left[\frac{1}{44}\left(\frac{r}{a}\right)\cos\theta+\frac{3}{28}\left(\frac{r}{a}\right)\cos 3\theta\right]$$
$$+\rho' ga\left[\frac{3}{4}\left(\frac{r}{a}\right)-\frac{1}{44}\left(\frac{r}{a}\right)\right]\cos\theta, \quad \ldots\ldots\ldots\ldots\ldots\ldots\ldots\ldots(25)$$

$$\widehat{\theta\theta'}=\rho g\xi\left[-\frac{3}{14}+\frac{3}{14}\cos 2\theta\right]+\rho ga\left[\frac{3}{44}\left(\frac{r}{a}\right)\cos\theta-\frac{3}{28}\left(\frac{r}{a}\right)\cos 3\theta\right]$$
$$+\rho' ga\left[\frac{1}{4}\left(\frac{r}{a}\right)-\frac{3}{44}\left(\frac{r}{a}\right)\right]\cos\theta, \quad \ldots\ldots\ldots\ldots\ldots\ldots\ldots\ldots(26)$$

$$\widehat{r\theta'}=\rho g\xi\left[\frac{3}{14}\sin 2\theta\right]+\rho ga\left[\frac{1}{44}\left(\frac{r}{a}\right)\sin\theta-\frac{3}{28}\left(\frac{r}{a}\right)\sin 3\theta\right]$$
$$+\rho' ga\left[-\frac{1}{4}\left(\frac{r}{a}\right)-\frac{1}{44}\left(\frac{r}{a}\right)\right]\sin\theta, \quad \ldots\ldots\ldots\ldots\ldots\ldots\ldots\ldots(27)$$

$\frac{\mu'}{\mu}=1$, $\lambda=\mu$, $\lambda'=\mu'$:—

$$\widehat{rr}=\rho g\xi\left[-\frac{1}{2}-\frac{1}{2}\cos 2\theta\right]$$
$$+\rho ga\left[\left\{\frac{3}{4}\left(\frac{r}{a}\right)-\frac{5}{6}\left(\frac{a}{r}\right)+\frac{1}{6}\left(\frac{a}{r}\right)^3\right\}\cos\theta+\frac{1}{4}\left(\frac{r}{a}\right)\cos 3\theta\right]$$
$$+\rho' ga\left[\frac{5}{6}\left(\frac{a}{r}\right)-\frac{1}{6}\left(\frac{a}{r}\right)^3\right]\cos\theta, \quad \ldots\ldots\ldots\ldots\ldots\ldots\ldots\ldots(28)$$

$$\widehat{\theta\theta}=\rho g\xi\left[-\frac{1}{2}+\frac{1}{2}\cos 2\theta\right]$$
$$+\rho ga\left[\left\{\frac{1}{4}\left(\frac{r}{a}\right)+\frac{1}{6}\left(\frac{a}{r}\right)-\frac{1}{6}\left(\frac{a}{r}\right)^3\right\}\cos\theta-\frac{1}{4}\left(\frac{r}{a}\right)\cos 3\theta\right]$$
$$+\rho' ga\left[-\frac{1}{6}\left(\frac{a}{r}\right)+\frac{1}{6}\left(\frac{a}{r}\right)^3\right]\cos\theta, \quad \ldots\ldots\ldots\ldots\ldots\ldots\ldots\ldots(29)$$

$$\widehat{r\theta}=\rho g\xi\frac{1}{2}\sin 2\theta$$
$$+\rho ga\left[\left\{-\frac{1}{4}\left(\frac{r}{a}\right)+\frac{1}{6}\left(\frac{a}{r}\right)+\frac{1}{6}\left(\frac{a}{r}\right)^3\right\}\sin\theta-\frac{1}{4}\left(\frac{r}{a}\right)\sin 3\theta\right]$$
$$+\rho' ga\left[-\frac{1}{6}\left(\frac{a}{r}\right)-\frac{1}{6}\left(\frac{a}{r}\right)^3\right]\sin\theta, \quad \ldots\ldots\ldots\ldots\ldots\ldots\ldots\ldots(30)$$

$$\widehat{rr'}=\rho g\xi\left[-\frac{1}{2}-\frac{1}{2}\cos 2\theta\right]$$
$$+\rho ga\left[\frac{1}{12}\left(\frac{r}{a}\right)\cos\theta+\frac{1}{4}\left(\frac{r}{a}\right)\cos 3\theta\right]$$
$$+\rho' ga\left[\frac{3}{4}\left(\frac{r}{a}\right)-\frac{1}{12}\left(\frac{r}{a}\right)\right]\cos\theta, \quad \ldots\ldots\ldots\ldots\ldots\ldots\ldots\ldots(31)$$

$$\widehat{\theta\theta'}=\rho g\xi\left[-\frac{1}{2}+\frac{1}{2}\cos 2\theta\right]+\rho ga\left[\frac{1}{4}\left(\frac{r}{a}\right)\cos\theta-\frac{1}{4}\left(\frac{r}{a}\right)\cos 3\theta\right]$$
$$+\rho' ga\left[-\frac{1}{6}\left(\frac{a}{r}\right)+\frac{1}{6}\left(\frac{a}{r}\right)^3\right]\cos\theta, \quad \ldots\ldots\ldots\ldots\ldots\ldots\ldots (32)$$

$$\widehat{r\theta'}=\rho g\xi\left[\frac{1}{2}\right]\sin 2\theta+\rho ga\left[\frac{1}{12}\left(\frac{r}{a}\right)\sin\theta-\frac{1}{4}\left(\frac{r}{a}\right)\sin 3\theta\right]$$
$$+\rho' ga\left[-\frac{1}{4}\left(\frac{r}{a}\right)-\frac{1}{12}\left(\frac{r}{a}\right)\right]\sin\theta, \quad \ldots\ldots\ldots\ldots\ldots\ldots\ldots (33)$$

$\frac{\mu'}{\mu}=5$, $\lambda=\mu$, $\lambda'=\mu'$:—

$$\widehat{rr}=\rho g\xi\left[-\left\{\frac{1}{2}+\frac{2}{11}\left(\frac{a}{r}\right)^2\right\}+\left\{-\frac{1}{2}-\frac{8}{11}\left(\frac{a}{r}\right)^2+\frac{6}{11}\left(\frac{a}{r}\right)^4\right\}\cos 2\theta\right]$$
$$+\rho ga\left[\left\{\frac{3}{4}\left(\frac{r}{a}\right)-\frac{5}{6}\left(\frac{a}{r}\right)+\frac{11}{42}\left(\frac{a}{r}\right)^3\right\}\cos\theta\right.$$
$$\left.+\left\{\frac{1}{4}\left(\frac{r}{a}\right)+\frac{5}{11}\left(\frac{a}{r}\right)^3-\frac{4}{11}\left(\frac{a}{r}\right)^2\right\}\cos 3\theta\right]$$
$$+\rho' ga\left[\frac{5}{6}\left(\frac{a}{r}\right)-\frac{11}{42}\left(\frac{a}{r}\right)^3\right]\cos\theta, \quad \ldots\ldots\ldots\ldots\ldots\ldots\ldots (34)$$

$$\widehat{\theta\theta}=\rho g\xi\left[\left\{-\frac{1}{2}+\frac{2}{11}\left(\frac{a}{r}\right)^2\right\}+\left\{\frac{1}{2}-\frac{6}{11}\left(\frac{a}{r}\right)^4\right\}\cos 2\theta\right]$$
$$+\rho ga\left[\left\{\frac{1}{4}\left(\frac{r}{a}\right)+\frac{1}{6}\left(\frac{a}{r}\right)-\frac{11}{42}\left(\frac{a}{r}\right)^3\right\}\cos\theta\right.$$
$$\left.+\left\{-\frac{1}{4}\left(\frac{r}{a}\right)-\frac{1}{11}\left(\frac{a}{r}\right)^3+\frac{4}{11}\left(\frac{a}{r}\right)^5\right\}\cos 3\theta\right]$$
$$+\rho' ga\left[-\frac{1}{6}\left(\frac{a}{r}\right)+\frac{11}{42}\left(\frac{a}{r}\right)^3\right]\cos\theta, \quad \ldots\ldots\ldots\ldots\ldots\ldots\ldots (35)$$

$$\widehat{r\theta}=\rho g\xi\left[\frac{1}{2}-\frac{4}{11}\left(\frac{a}{r}\right)^2+\frac{6}{11}\left(\frac{a}{r}\right)^4\right]\sin 2\theta$$
$$+\rho ga\left[\left\{-\frac{1}{4}\left(\frac{r}{a}\right)+\frac{1}{6}\left(\frac{a}{r}\right)+\frac{11}{42}\left(\frac{a}{r}\right)^3\right\}\sin\theta\right.$$
$$\left.+\left\{-\frac{1}{4}\left(\frac{r}{a}\right)+\frac{3}{11}\left(\frac{a}{r}\right)^3-\frac{4}{11}\left(\frac{a}{r}\right)^5\right\}\sin 3\theta\right]$$
$$+\rho' ga\left[-\frac{1}{6}\left(\frac{a}{r}\right)-\frac{11}{42}\left(\frac{a}{r}\right)^3\right]\sin\theta, \quad \ldots\ldots\ldots\ldots\ldots\ldots\ldots (36)$$

$$\widehat{rr'}=\rho g\xi\left[-\frac{15}{22}-\frac{15}{22}\cos 2\theta\right]+\rho ga\left[\frac{5}{28}\left(\frac{r}{a}\right)\cos\theta+\frac{15}{44}\left(\frac{r}{a}\right)\cos 3\theta\right]$$
$$+\rho' ga\left[\frac{3}{4}\left(\frac{r}{a}\right)-\frac{5}{28}\left(\frac{r}{a}\right)\right]\cos\theta, \quad \cdots\cdots\cdots\cdots\cdots (37)$$

$$\widehat{\theta\theta'}=\rho g\xi\left[-\frac{15}{22}+\frac{15}{22}\cos 2\theta\right]+\rho ga\left[\frac{15}{28}\left(\frac{r}{a}\right)\cos\theta-\frac{15}{44}\left(\frac{r}{a}\right)\cos 3\theta\right]$$
$$+\rho' ga\left[-\frac{1}{6}\left(\frac{a}{r}\right)+\frac{11}{42}\left(\frac{a}{r}\right)^3\right]\cos\theta, \quad \cdots\cdots\cdots\cdots\cdots (38)$$

$$\widehat{r\theta'}=\rho g\xi\left[\frac{15}{22}\right]\sin 2\theta+\rho ga\left[\frac{5}{28}\left(\frac{r}{a}\right)\sin\theta-\frac{15}{44}\left(\frac{r}{a}\right)\sin 3\theta\right]$$
$$+\rho' ga\left[-\frac{1}{4}\left(\frac{r}{a}\right)-\frac{5}{28}\left(\frac{r}{a}\right)\right]\sin\theta, \quad \cdots\cdots\cdots\cdots\cdots (39)$$

$\frac{\mu'}{\mu}=\infty$, $\lambda=\mu$, $\lambda'=\mu'$:

$$\widehat{rr}=\rho g\xi\left[-\left\{\frac{1}{2}+\frac{1}{4}\left(\frac{a}{r}\right)^2\right\}+\left\{-\frac{1}{2}-\left(\frac{a}{r}\right)^2+\frac{3}{4}\left(\frac{a}{r}\right)^4\right\}\cos 2\theta\right]$$
$$+\rho ga\left[\left\{\frac{3}{4}\left(\frac{r}{a}\right)-\frac{5}{6}\left(\frac{a}{r}\right)+\frac{1}{3}\left(\frac{a}{r}\right)^3\right\}\cos\theta\right.$$
$$\left.+\left\{\frac{1}{4}\left(\frac{r}{a}\right)+\frac{5}{8}\left(\frac{a}{r}\right)^3-\frac{1}{2}\left(\frac{a}{r}\right)^5\right\}\cos 3\theta\right]$$
$$+\rho' ga\left[\frac{5}{6}\left(\frac{a}{r}\right)-\frac{1}{3}\left(\frac{a}{r}\right)^3\right]\cos\theta, \quad \cdots\cdots\cdots\cdots\cdots (40)$$

$$\widehat{\theta\theta}=\rho g\xi\left[-\frac{1}{2}+\frac{1}{4}\left(\frac{a}{r}\right)^2+\left\{\frac{1}{2}-\frac{3}{4}\left(\frac{a}{r}\right)^4\right\}\cos 2\theta\right]$$
$$+\rho ga\left[\left\{\frac{1}{4}\left(\frac{r}{a}\right)+\frac{1}{6}\left(\frac{a}{r}\right)-\frac{1}{3}\left(\frac{a}{r}\right)^3\right\}\cos\theta\right.$$
$$\left.+\left\{-\frac{1}{4}\left(\frac{r}{a}\right)-\frac{1}{8}\left(\frac{a}{r}\right)^3+\frac{1}{2}\left(\frac{a}{r}\right)^5\right\}\cos 3\theta\right]$$
$$+\rho' ga\left[-\frac{1}{6}\left(\frac{a}{r}\right)+\frac{1}{3}\left(\frac{a}{r}\right)^3\right]\cos\theta, \quad \cdots\cdots\cdots\cdots\cdots (41)$$

$$\widehat{r\theta}=\rho g\xi\left[\frac{1}{2}-\frac{1}{2}\left(\frac{a}{r}\right)^2+\frac{3}{4}\left(\frac{a}{r}\right)^4\right]\sin 2\theta$$
$$+\rho ga\left[\left\{-\frac{1}{4}\left(\frac{r}{a}\right)+\frac{1}{6}\left(\frac{a}{r}\right)+\frac{1}{3}\left(\frac{a}{r}\right)^3\right\}\sin\theta\right.$$
$$\left.+\left\{-\frac{1}{4}\left(\frac{r}{a}\right)+\frac{3}{8}\left(\frac{a}{r}\right)^3-\frac{1}{2}\left(\frac{a}{r}\right)^5\right\}\sin 3\theta\right]$$

$$+\rho' ga\left[-\frac{1}{6}\left(\frac{a}{r}\right)-\frac{1}{3}\left(\frac{a}{r}\right)^3\right]\sin\theta, \quad \ldots\ldots\ldots\ldots\ldots\ldots\ldots\ldots (42)$$

$$\widehat{rr'}=\rho g\xi\left[-\frac{3}{4}-\frac{3}{4}\cos 2\theta\right]+\rho ga\left[\frac{1}{4}\left(\frac{r}{a}\right)\cos\theta+\frac{3}{8}\left(\frac{r}{a}\right)\cos 3\theta\right]$$

$$+\rho' ga\left[\frac{3}{4}\left(\frac{r}{a}\right)-\frac{1}{4}\left(\frac{r}{a}\right)\right]\cos\theta, \quad \ldots\ldots\ldots\ldots\ldots\ldots\ldots\ldots (43)$$

$$\widehat{\theta\theta'}=\rho g\xi\left[-\frac{3}{4}+\frac{3}{4}\cos 2\theta\right]+\rho ga\left[\frac{3}{4}\left(\frac{r}{a}\right)\cos\theta-\frac{3}{8}\left(\frac{r}{a}\right)\cos 3\theta\right]$$

$$+\rho' ga\left[\frac{1}{4}\left(\frac{r}{a}\right)-\frac{3}{4}\left(\frac{r}{a}\right)\right]\cos\theta, \quad \ldots\ldots\ldots\ldots\ldots\ldots\ldots\ldots (44)$$

$$\widehat{r\theta'}=\rho g\xi\left[\frac{3}{4}\sin 2\theta\right]+\rho ga\left[\frac{1}{4}\left(\frac{r}{a}\right)\sin\theta-\frac{3}{8}\left(\frac{r}{a}\right)\sin 3\theta\right]$$

$$+\rho' ga\left[-\frac{1}{4}\left(\frac{r}{a}\right)-\frac{1}{4}\left(\frac{r}{a}\right)\right]\sin\theta. \quad \ldots\ldots\ldots\ldots\ldots\ldots\ldots\ldots (45)$$

These results are numerically calculated and tabulated in the annexed tables and shewn in the annexed figures. These figures shew the properties of stress distributions in and around the inclusion already discussed.

When the cylindrical inclusion is more rigid than the surrounding medium, the magnitudes of the respective terms with respect to ρga and $\rho g\xi$ of $\widehat{rr}_{r=a}$, $\widehat{r\theta}_{r=a}$, $\widehat{rr'}_{r=a}$, $\widehat{r\theta'}_{r=a}$ are large, as are those of the terms related to $\rho' ga$ of $\widehat{r\theta}_{r=a}$ and $\widehat{r\theta'}_{r=a}$. The magnitudes of the terms related to $\rho' ga$ of $\widehat{rr}_{r=a}$ and $\widehat{rr'}_{r=a}$, however, are small in this case.

When the cylindrical inclusion is more rigid than the surrounding medium, the magnitudes of the respective terms related to $\rho g\xi$ and ρga of $\widehat{\theta\theta}_{r=a}$ are generally small, while those of the terms related to $\widehat{\theta\theta'}_{r=a}$, on the contrary, are generally large. The terms related to $\rho' ga$ of the components of stresses $\widehat{\theta\theta}_{r=a}$ and $\widehat{\theta\theta'}_{r=a}$ have special distributions, different from those of all other stress components, when the magnitude of $\frac{\mu'}{\mu}$ is large.

When the Poisson's ratio of each of the two solids are $\frac{1}{4}$, the effective radius of the existence of inclusion upon the stress distributions in the medium is about 2 times the radius of the inclusion. The rigidity ratio $\frac{\mu'}{\mu}$ has little effect upon this effective radius.

Even when $\frac{\mu'}{\mu}=\infty$, the magnitudes of all terms related to ρga, $\rho g\xi$ and $\rho' ga$ of stresses in the inclusion are finite.

For the differences in magnitude of stresses in and around the inclusion for the case when the medium is in plane stress and when it is in plane strain, the following table shews the magnitudes of stresses at special points in the two cases when $\lambda=\mu$, $\lambda'=\mu'$ and $\frac{\mu'}{\mu}=\frac{1}{5}$ and ∞.

Table I.

(Ordinary figures = plane stress
Figures in italics = plane strain)

$\frac{\mu'}{\mu}$	Stress components	$\frac{r}{a}$	θ	ρga	$\rho g\xi$	$\rho' ga$
$\frac{1}{5}$	$\widehat{rr}$	1	0°	0·130 *0·116*	−0·428 *−0·428*	0·727 *0·727*
	$\widehat{\theta\theta}$	1	60°	0·833 *0·809*		
		1	90°		−2·143 *−1·95*	
		1	0°			−0·06 *−0·06*
	$\widehat{r\theta}$	1	90°	0·130 *0·117*		
		1	45°		0·214 *0·143*	
		1	90°			−0·273 *−0·273*
	$\widehat{rr'}$	1	0°	0·130 *0·116*	−0·428 *−0·428*	0·727 *0·727*
	$\widehat{\theta\theta'}$	1	60°	0·141 *0·141*		
		1	90°		−0·428 *−0·428*	
		1	0°			0·1818 *0·1818*
	$\widehat{r\theta'}$	1	90°	0·130 *0·117*		
		1	45°		0·214 *0·143*	
		1	90°			−0·273 *−0·273*

(to be continued.)

Table I. (*continued*).

$\frac{\mu'}{\mu}$	Stress compononts	$\frac{r}{a}$	θ	ρga	$\rho g\xi$	$\rho' ga$
	$\widehat{rr}$	1	0°	0·625 *0·750*	−1·500 *−1·500*	0·500 *0·500*
	$\widehat{\theta\theta}$	1	0°	0·209 *0·250*		
		1	90°		0 *−0·17*	
∞		1	0°			0·167 *0·167*
	$\widehat{r\theta}$	1	90°	0·625 *0·750*		
		1	45°		0·750 *0·500*	
		1	90°			−0·500 *−0·500*
	$\widehat{rr'}$	1	0°	0·625 *0·750*	−1·500 *−1·500*	0·50 *0·50*
	$\widehat{\theta\theta'}$	1	45°	0·795 *1·237*		
		1	90°		−1·50 *−1·50*	
∞		1	0°			−0·50 *−0·50*
	$\widehat{r\theta'}$	1	90°	0·625 *0·750*		
		1	45°		0·750 *0·500*	
		1	90°			−0·500 *−0·500*

This table shews that the magnitudes related to ρga and $\rho g\xi$ of all stress components in and around the inclusion are generally different in the two cases, but the magnitude related to $\rho' ga$ of all stress components is exactly the same in both cases.

When the state of the medium is one of plane stress, the stress distribution in the medium far from the inclusion are not affected by the elasticity constants of the medium, but in the case of plane strain they are affected by the elasticity constants of the medium.

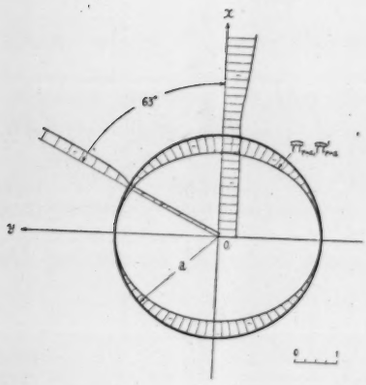

Fig. 2a. Distribution of the terms related to $\rho g\xi$ of $\widehat{rr}$ and $\widehat{rr'}$ when $\frac{\mu'}{\mu}=\frac{1}{5}$.

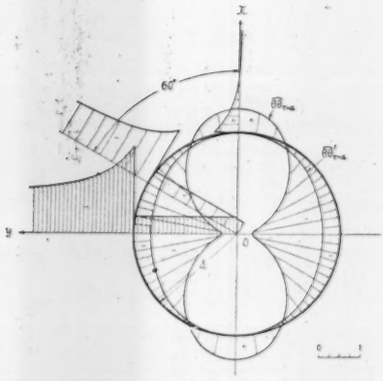

Fig. 3a. Distribution of the terms related to $\rho g\xi$ of $\widehat{\theta\theta}$ and $\widehat{\theta\theta'}$ when $\frac{\mu'}{\mu}=\frac{1}{5}$.

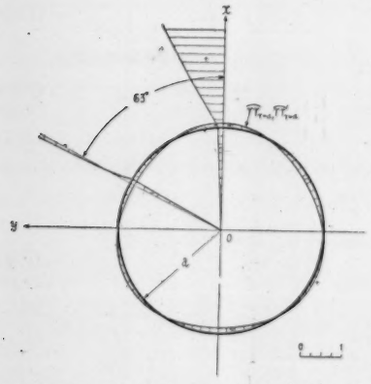

Fig. 2b. Distribution of the terms related to ρga of $\widehat{rr}$ and $\widehat{rr'}$ when $\frac{\mu'}{\mu}=\frac{1}{5}$.

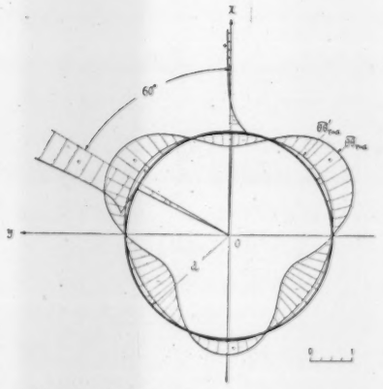

Fig. 3b. Distribution of the terms related to ρga of $\widehat{\theta\theta}$ and $\widehat{\theta\theta'}$ when $\frac{\mu'}{\mu}=\frac{1}{5}$.

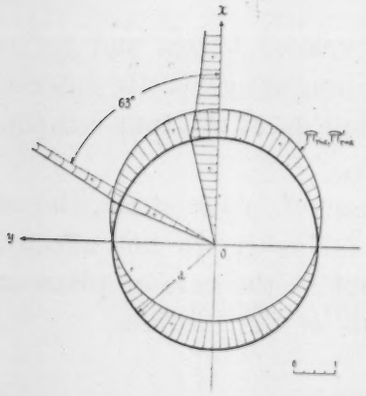

Fig. 2c. Distribution of the terms related to $\rho' ga$ of $\widehat{rr}$ and $\widehat{rr'}$ when $\frac{\mu'}{\mu}=\frac{1}{5}$.

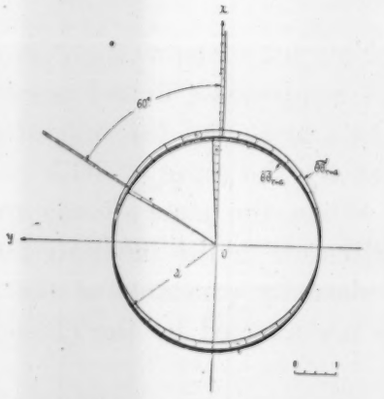

Fig. 3c. Distribution of the terms related to $\rho' ga$ of $\widehat{\theta\theta}$ and $\widehat{\theta\theta'}$ when $\frac{\mu'}{\mu}=\frac{1}{5}$.

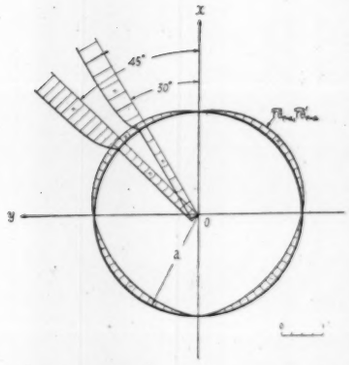

Fig. 4a. Distribution of the terms related to $\rho g \xi$ of $\widehat{r\theta}$ and $\widehat{r\theta'}$ when $\frac{\mu'}{\mu} = \frac{1}{5}$.

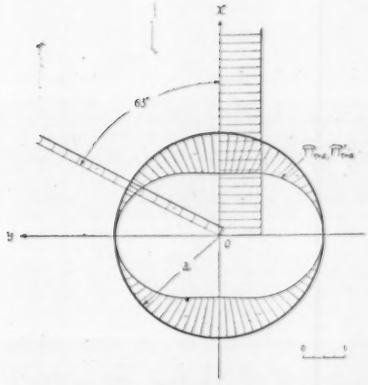

Fig. 5a. Distribution of the terms related to $\rho g \xi$ of $\widehat{rr}$ and $\widehat{rr'}$ when $\frac{\mu'}{\mu} = 1$.

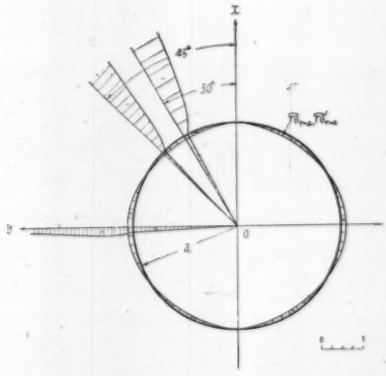

Fig. 4b. Distribution of the terms related to $\rho q a$ of $\widehat{r\theta}$ and $\widehat{r\theta'}$ when $\frac{\mu'}{\mu} = \frac{1}{5}$.

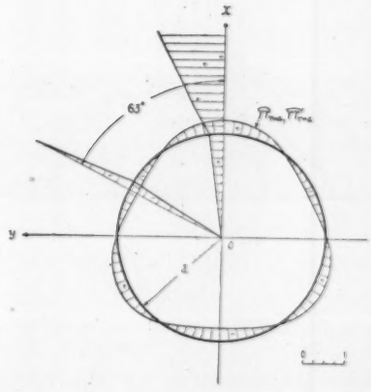

Fig. 5b. Distribution of the terms related to $\rho g a$ of $\widehat{rr}$ and $\widehat{rr'}$ when $\frac{\mu'}{\mu} = 1$.

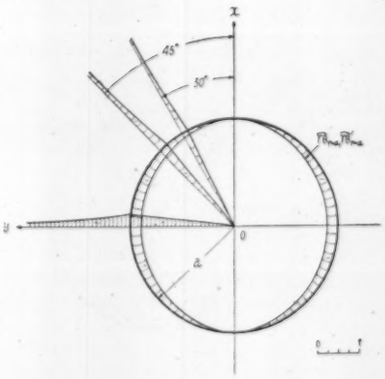

Fig. 4c. Distribution of the terms related to $\rho' g a$ of $\widehat{r\theta}$ and $\widehat{r\theta'}$ when $\frac{\mu'}{\mu} = \frac{1}{5}$.

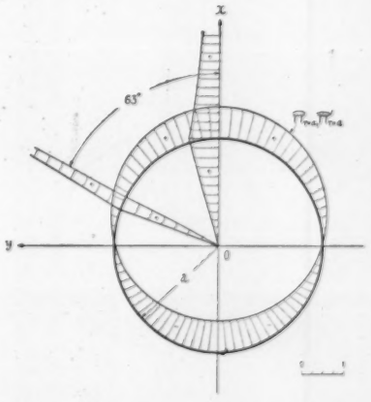

Fig. 5c. Distribution of the terms related to $\rho' g a$ of $\widehat{rr}$ and $\widehat{rr'}$ when $\frac{\mu'}{\mu} = 1$.

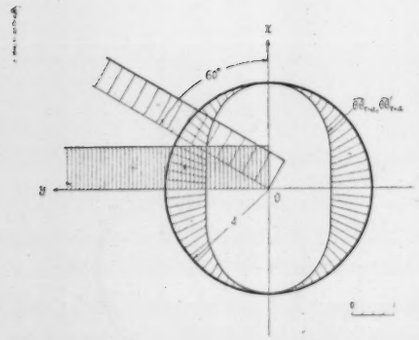

Fig. 6a. Distribution of the terms related to $\rho g\xi$ of $\widehat{\theta\theta}$ and $\widehat{\theta\theta'}$ when $\frac{\mu'}{\mu}=1$.

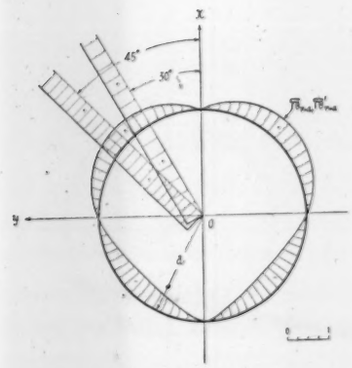

Fig. 7a. Distribution of the terms related to $\rho g\xi$ of $\widehat{r\theta}$ and $\widehat{r\theta'}$ when $\frac{\mu'}{\mu}=1$.

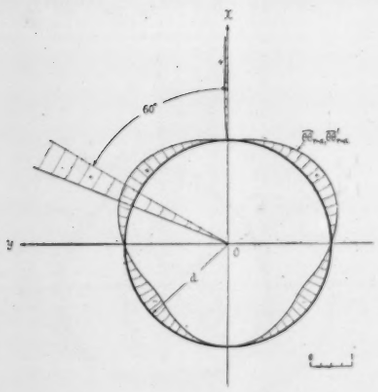

Fig. 6b. Distribution of the terms related to ρga of $\widehat{\theta\theta}$ and $\widehat{\theta\theta'}$ when $\frac{\mu'}{\mu}=1$.

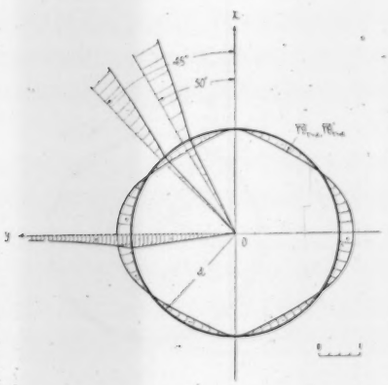

Fig. 7b. Distribution of the terms related to ρga of $\widehat{r\theta}$ and $\widehat{r\theta'}$ when $\frac{\mu'}{\mu}=1$.

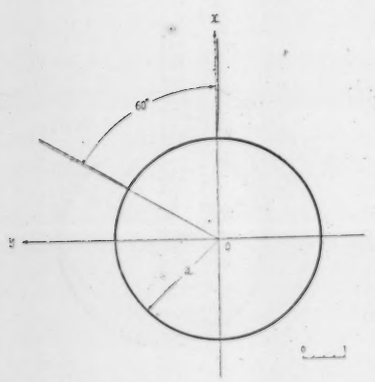

Fig. 6c. Distribution of the terms related to $\rho' ga$ of $\widehat{\theta\theta}$ and $\widehat{\theta\theta'}$ when $\frac{\mu'}{\mu}=1$.

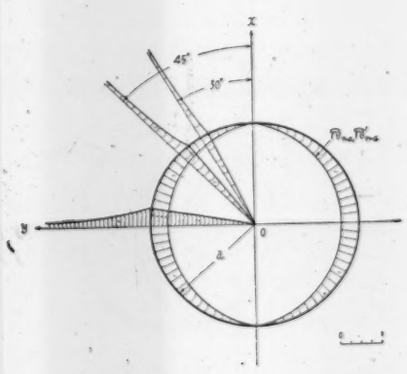

Fig. 7c. Distribution of the terms related to $\rho' ga$ of $\widehat{r\theta}$ and $\widehat{r\theta'}$ when $\frac{\mu'}{\mu}=1$.

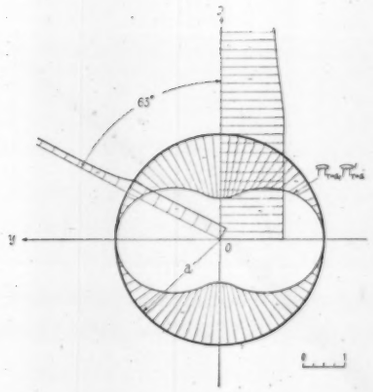

Fig. 8a. Distribution of the terms related to $\rho g\xi$ of $\widehat{rr}$ and $\widehat{rr'}$ when $\frac{\mu'}{\mu}=5$.

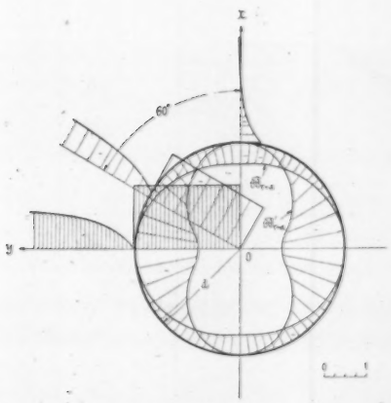

Fig. 9a. Distribution of the terms related to $\rho g\xi$ of $\widehat{\theta\theta}$ and $\widehat{\theta\theta'}$ when $\frac{\mu'}{\mu}=5$.

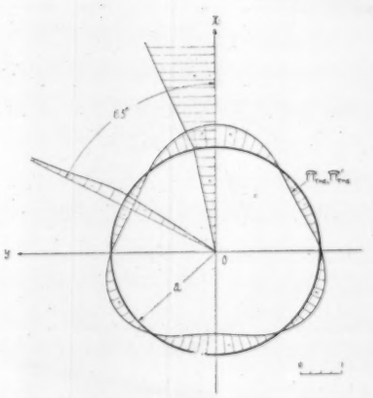

Fig. 8b. Distribution of the terms related to ρga of $\widehat{rr}$ and $\widehat{rr'}$ when $\frac{\mu'}{\mu}=5$.

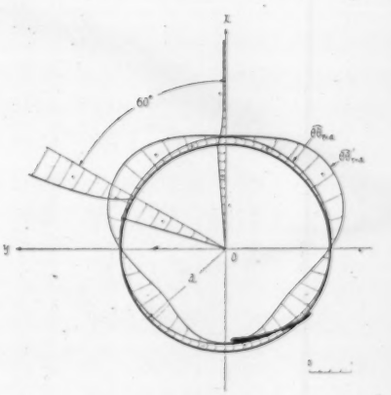

Fig. 9b. Distribution of the terms related to ρga of $\widehat{\theta\theta}$ and $\widehat{\theta\theta'}$ when $\frac{\mu'}{\mu}=5$.

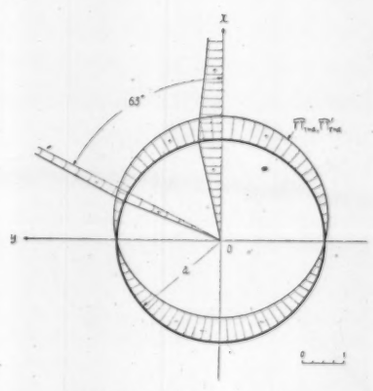

Fig. 8c. Distribution of the terms related to $\rho' ga$ of $\widehat{rr}$ and $\widehat{rr'}$ when $\frac{\mu'}{\mu}=5$.

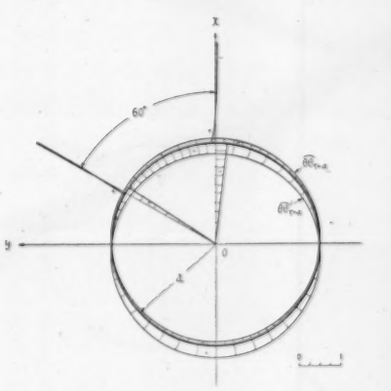

Fig. 9c. Distribution of the terms related to $\rho' ga$ of $\widehat{\theta\theta}$ and $\widehat{\theta\theta'}$ when $\frac{\mu'}{\mu}=5$.

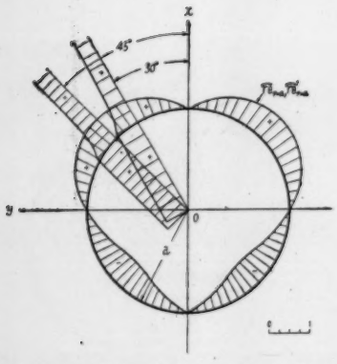

Fig. 10a. Distribution of the terms related to $\rho g\xi$ of $\widehat{r\theta}$ and $\widehat{r\theta'}$ when $\frac{\mu'}{\mu}=5$.

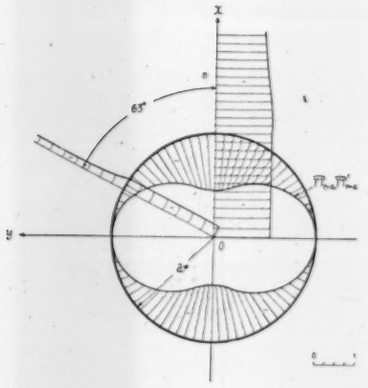

Fig. 11a. Distribution of the terms related to $\rho g\xi$ of $\widehat{rr}$ and $\widehat{rr'}$ when $\frac{\mu'}{\mu}=\infty$.

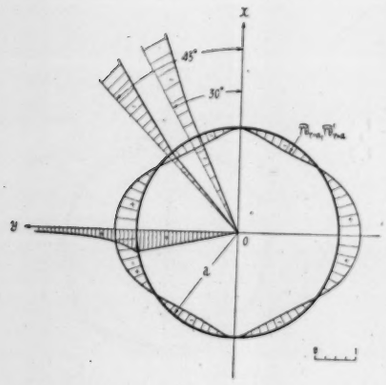

Fig. 10b. Distribution of the terms related to ρga of $\widehat{r\theta}$ and $\widehat{r\theta'}$ when $\frac{\mu'}{\mu}=5$

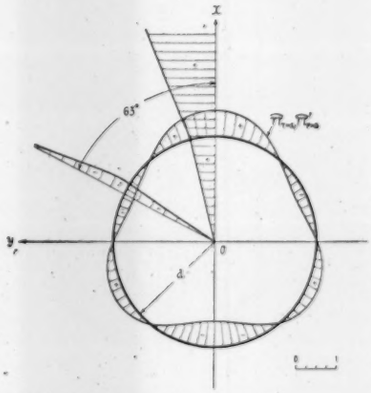

Fig. 11b. Distribution of the terms related to ρga of $\widehat{rr}$ and $\widehat{rr'}$ when $\frac{\mu'}{\mu}=\infty$.

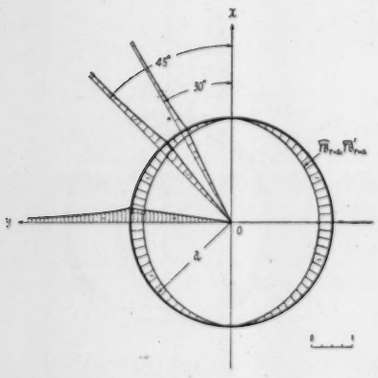

Fig. 10c. Distribution of the terms related to $\rho' ga$ of $\widehat{r\theta}$ and $\widehat{r\theta'}$ when $\frac{\mu'}{\mu}=5$.

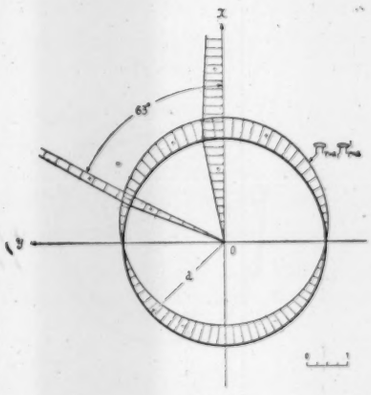

Fig. 11c. Distribution of the terms related to $\rho' ga$ of $\widehat{rr}$ and $\widehat{rr'}$ when $\frac{\mu'}{\mu}=\infty$.

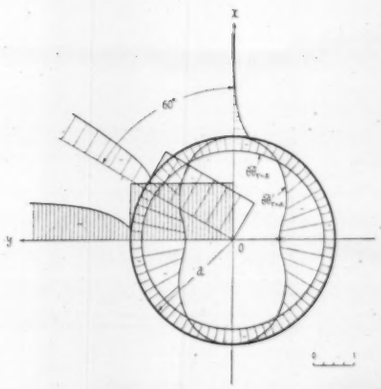

Fig. 12a. Distribution of the terms related to $\rho g\xi$ of $\widehat{\theta\theta}$ and $\widehat{\theta\theta'}$ when $\frac{\mu'}{\mu}=\infty$.

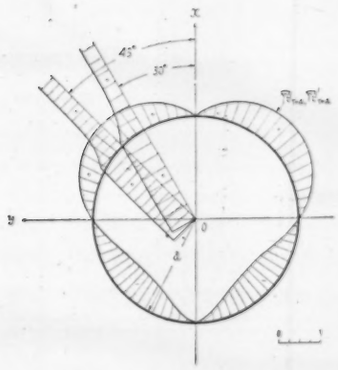

Fig. 13a. Distribution of the terms related to $\rho g\xi$ of $\widehat{r\theta}$ and $\widehat{r\theta'}$ when $\frac{\mu'}{\mu}=\infty$.

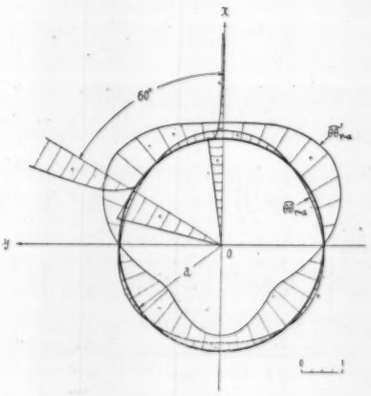

Fig. 12b. Distribution of the terms related to ρga of $\widehat{\theta\theta}$ and $\widehat{\theta\theta'}$ when $\frac{\mu'}{\mu}=\infty$.

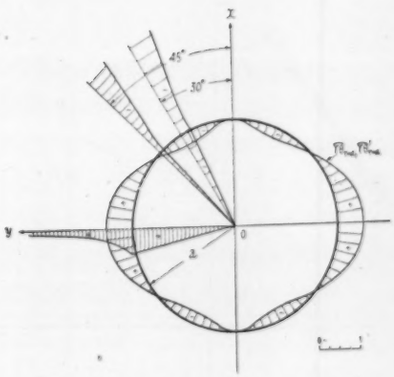

Fig. 13b. Distribution of the terms related to ρga of $\widehat{r\theta}$ and $\widehat{r\theta'}$ when $\frac{\mu'}{\mu}=\infty$.

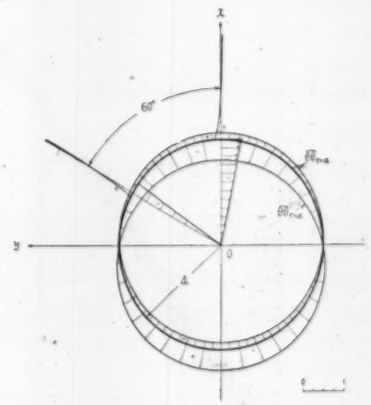

Fig. 12c. Distribution of the terms related to $\rho' ga$ of $\widehat{\theta\theta}$ and $\widehat{\theta\theta'}$ when $\frac{\mu'}{\mu}=\infty$.

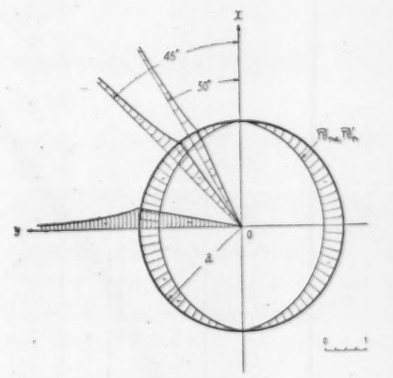

Fig. 13c. Distribution of the terms related to $\rho' ga$ of $\widehat{r\theta}$ and $\widehat{r\theta'}$ when $\frac{\mu'}{\mu}=\infty$.

Table IIa.

Magnitudes of the respective terms related to $\rho g\xi$, ρga and $\rho' ga$ of $rr_{r=a}$ $(=rr'_{r=a})$ when $\frac{\mu'}{\mu}=\frac{1}{5}$.

θ	0°	10°	20°	30°	45°	60°	70°	80°	90°
$\rho g\xi$	−0·428	−0·415	−0·378	−0·321	−0·214	−0·107	−0·050	−0·013	0
ρga	0·130	0·115	0·075	0·020	−0·060	−0·096	−0·085	−0·050	0
$\rho' ga$	0·727	0·716	0·683	0·630	0·514	0·363	0·248	0·126	0

θ	100°	110°	120°	135°	150°	160°	170°	180°
$\rho g\xi$	−0·013	−0·050	−0·107	−0·214	−0·321	−0·378	−0·415	−0·428
ρga	0·050	0·085	0·096	0·060	−0·020	−0·075	−0·115	−0·130
$\rho' ga$	−0·126	−0·248	−0·363	−0·514	0·630	−0·683	−0·716	−0·727

Table IIb.

Magnitudes of the respective terms related to $\rho q\xi$, ρga and $\rho' ga$ of $\widehat{\theta\theta}_{r=a}$ when $\frac{\mu'}{\mu}=\frac{1}{5}$.

θ	0°	10°	20°	30°	45°	60°	70°	80°	90°
$\rho g\xi$	0·5713	0·4893	0·2543	−0·1077	−0·7857	−1·4637	−1·8260	−2·0607	−2·1427
ρga	−0·368	−0·281	−0·047	0·269	0·700	0·833	0·693	0·393	0
$\rho' ga$	−0·0600	−0·0590	−0·0563	−0·0520	−0·0423	−0·030	−0·0205	−0·0104	0

θ	100°	110°	120°	135°	150°	160°	170°	180°
$\rho g\xi$	−2·0607	−1·8260	−1·4637	−0·7857	−0·1077	0·2543	0·4893	0·5713
ρga	−0·393	−0·693	−0·833	−0·700	−0·269	0·047	0·281	0·368
$\rho' ga$	0·0104	0·0205	0·0300	0·0423	0·0520	0·0563	0·0590	0·0600

Table IIc.

Magnitudes of the respective terms related to $\rho g\xi$, ρga and $\rho' ga$ of $\widehat{\theta\theta'}_{r=a}$ when $\frac{\mu'}{\mu}=\frac{1}{5}$.

θ	0°	10°	20°	30°	45°	60°	70°	80°	90°
$\rho g\xi$	0	−0·013	−0·050	−0·107	−0·214	−0·321	−0·378	−0·415	−0·428
ρga	−0·0390	−0·0254	0·0106	0·0591	0·1238	0·1411	0·1159	0·0653	0
$\rho' ga$	0·1818	0·1790	0·1710	0·1570	0·1280	0·0906	0·0620	0·0316	0

θ	100°	110°	120°	135°	150°	160°	170°	180°
$\rho q\xi$	−0·415	−0·378	−0·321	−0·214	−0·107	−0·050	−0·013	0
ρga	−0·0653	−0·1159	−0·1411	−0·1238	−0·0591	−0·0106	0·0254	0·0390
$\rho' ga$	−0·0316	−0·0620	−0·0906	−0·1280	−0·1570	−0·1710	−0·1790	−0·1818

Table IId.

Magnitudes of the respective terms related to $\rho g\xi$, ρga and $\rho' ga$ of $\widehat{r\theta}_{r=a}$ $(=\widehat{r\theta'}_{r=a})$ when $\frac{\mu'}{\mu}=\frac{1}{5}$.

θ	0°	10°	20°	30°	45°	60°	70°	80°	90°
$\rho g\xi$	0	0·073	0·138	0·186	0·214	0·186	0·138	0·073	0
ρga	0	−0·050	−0·085	−0·096	−0·060	0·020	0·075	0·115	0·130
$\rho' ga$	0	−0·047	−0·093	−0·136	−0·193	−0·236	−0·256	−0·268	−0·273

θ	100°	110°	120°	135°	150°	160°	170°	180°
$\rho g\xi$	−0·073	−0·138	−0·186	−0·214	−0·186	−0·138	−0·073	0
ρga	0·115	0·075	0·020	−0·060	−0·096	−0·085	−0·050	0
$\rho' ga$	−0·268	−0·256	−0·236	−0·193	−0·136	−0·093	−0·047	0

Table IIIa.

Magnitudes of the respective terms related to $\rho g\xi$, ρga and $\rho' ga$ of $\widehat{rr}_{r=a}$ $(=\widehat{rr'}_{r=a})$ when $\frac{\mu'}{\mu}=1$.

θ	0°	10°	20°	30°	45°	60°	70°	80°	90°
$\rho g\xi$	−1·000	−0·970	−0·883	−0·750	−0·500	−0·250	−0·117	−0·030	0
ρga	0·333	0·298	0·203	0·072	−0·118	−0·208	−0·188	−0·110	0
$\rho' ga$	0·667	0·656	0·627	0·578	0·472	0·333	0·228	0·116	0

θ	100°	110°	120°	135°	150°	160°	170°	180°
$\rho g\xi$	−0·030	−0·117	−0·250	−0·500	−0·750	−0·883	−0·970	−1·000
ρga	0·110	0·188	0·208	0·118	−0·072	−0·203	−0·298	−0·333
$\rho' ga$	−0·116	−0·228	−0·333	−0·472	−0·578	−0·427	−0·656	−0·667

Table IIIb.

Magnitudes of the respective terms related to $\rho g\xi$, ρga and $\rho' ga$ of $\widehat{\theta\theta}_{r=a}$ $(\widehat{\theta\theta'}_{r=a})$ when $\frac{\mu'}{\mu}=1$.

θ	0°	10°	20°	30°	45°	60°	70°	80°	90°
$\rho g\xi$	0	−0·030	−0·117	−0·250	−0·500	−0·750	−0·883	−0·970	−1·00
ρga	0	0·030	0·110	0·217	0·354	0·400	0·302	0·169	0
$\rho' ga$	0	0	0	0	0	0	0	0	0

θ	100°	110°	120°	135°	150°	160°	170°	180°
$\rho g\xi$	−0·970	−0·883	−0·750	−0·500	−0·250	−0·117	−0·030	0
ρga	−0·169	−0·320	−0·400	−0·354	−0·217	−0·110	−0·030	0
$\rho' ga$	0	0	0	0	0	0	0	0

Table IIIc.

Magnitudes of the respective terms related to $\rho g\xi$, ρga and $\rho' ga$ of $\widehat{r\theta}_{r=a}$ $(=\widehat{r\theta'}_{r=a})$ when $\frac{\mu'}{\mu}=1$.

θ	0°	10°	20°	30°	45°	60°	70°	80°	90°
$\rho g\xi$	0	0·171	0·321	0·433	0·500	0·433	0·321	0·171	0
ρga	0	−0·110	−0·189	−0·208	−0·117	0·072	0·203	0·299	0·333
$\rho' ga$	0	−0·058	−0·114	−0·167	−0·236	−0·288	−0·313	−0·328	−0·333

θ	100°	110°	120°	135°	150°	160°	170°	180°
$\rho g\xi$	−0·171	−0·321	−0·433	−0·500	−0·433	−0·321	−0·171	0
ρga	0·299	0·203	0·072	−0·117	−0·208	−0·189	−0·110	0
$\rho' ga$	−0·328	−0·313	−0·288	−0·236	−0·167	−0·114	−0·058	0

Table IVa.

Magnitudes of the respective terms related to $\rho g\xi$, ρga and $\rho' ga$ of $\widehat{rr}_{r=a}$ $(=\widehat{rr'}_{r=a})$ when $\frac{\mu'}{\mu}=5$.

θ	0°	10°	20°	30°	45°	60°	70°	80°	90°
$\rho g\xi$	−1·364	−1·324	−1·205	−1·024	−0·683	−0·342	−0·161	−0·042	0
ρga	0·519	0·471	0·338	0·155	−0·115	−0·252	−0·234	−0·139	0
$\rho' ga$	0·572	0·563	0·537	0·495	0·404	0·286	0·195	0·099	0

θ	100°	110°	120°	135°	150°	160°	170°	180°
$\rho g\xi$	−0·042	−0·161	−0·342	−0·683	−1·024	−1·205	−1·324	−1·366
ρga	0·139	0·234	0·252	0·115	−0·155	−0·338	−0·471	−0·519
$\rho' ga$	−0·099	−0·195	−0·286	−0·404	−0·495	−0·537	−0·563	−0·572

Table IVb.

Magnitudes of the respective terms related to $\rho g\xi$, ρga and $\rho' ga$ of $\widehat{\theta\theta}_{r=a}$ when $\frac{\mu'}{\mu}=5$.

θ	0°	10°	20°	30°	45°	60°	70°	80°	90°
$\rho g\xi$	−0·363	−0·361	−0·352	−0·341	−0·318	−0·295	−0·284	−0·275	−0·273
ρga	0·178	0·172	0·156	0·134	0·083	0·054	0·033	0·016	0
$\rho' ga$	0·095	0·094	0·090	0·083	0·067	0·048	0·033	0·016	0

θ	100°	110°	120°	135°	150°	160°	170°	180°
$\rho g\xi$	−0·275	−0·284	−0·295	−0·318	−0·341	−0·352	−0·361	−0·363
ρga	−0·016	−0·033	−0·054	−0·083	−0·134	−0·0156	−0·172	−0·178
$\rho' ga$	−0·016	−0·033	−0·048	−0·067	−0·083	−0·090	−0·094	−0·095

Table IVc.

Magnitudes of the respective terms related to $\rho g\xi$, ρga and $\rho' ga$ of $\widehat{\theta\theta'}_{r=a}$ when $\frac{\mu'}{\mu}=5$.

θ	0°	10°	20°	30°	45°	60°	70°	80°	90°
$\rho g\xi$	0	−0·041	−0·159	−0·341	−0·682	−1·023	−1·205	−1·323	−1·364
ρga	0·195	0·233	0·334	0·465	0·620	0·609	0·478	0·263	0
$\rho' ga$	−0·286	−0·282	−0·268	−0·248	−0·202	−0·143	−0·098	−0·050	0

θ	100°	110°	120°	135°	150°	160°	170°	180°
$\rho g\xi$	−1·323	−1·205	−1·023	−0·682	−0·341	−0·159	−0·041	0
ρga	−0·263	−0·478	−0·609	−0·620	−0·465	−0·334	−0·233	−0·195
$\rho' ga$	0·050	0·098	0·143	0·202	0·248	0·268	0·282	0·286

Table IVd.

Magnitudes of the respective terms related to $\rho g\xi$, ρga and $\rho' ga$ of $\widehat{r\theta}_{r=a}$ $(=\widehat{r\theta'}_{r=a})$ when $\frac{\mu'}{\mu}=5$.

θ	0°	10°	20°	30°	45°	60°	70°	80°	90°
$\rho g\xi$	0	0·233	0·438	0·591	0·682	0·591	0·438	0·233	0
ρga	0	−0·139	−0·234	−0·252	−0·115	0·155	0·338	0·471	0·519
$\rho' ga$	0	−0·075	−0·146	−0·214	−0·303	−0·372	−0·403	−0·422	−0·429

θ	100°	110°	120°	135°	150°	160°	170°	180°
$\rho g\xi$	−0·233	−0·438	−0·591	−0·682	−0·591	−0·438	−0·233	0
ρga	0·471	0·338	0·155	−0·115	−0·252	−0·234	−0·139	0
$\rho' ga$	−0·422	−0·403	−0·372	−0·303	−0·214	−0·146	−0·075	0

Table Va.

Magnitudes of the respective terms related to $\rho g\xi$, ρga and $\rho' ga$ of $\widehat{rr}_{r=a}$ $(=\widehat{rr'}_{r=a})$ when $\frac{\mu'}{\mu}=\infty$.

θ	0°	10°	20°	30°	45°	60°	70°	80°	90°
$\rho g\xi$	−1·500	−1·455	−1·325	−1·125	−0·750	−0·375	−0·175	−0·045	0
ρga	0·625	0·571	0·422	0·216	−0·088	−0·250	−0·239	−0·143	0
$\rho' ga$	0·500	0·492	0·470	0·433	0·353	0·250	0·171	0·087	0

θ	100°	110°	120°	135°	150°	160°	170°	180°
$\rho g\xi$	−0·045	−0·175	−0·375	−0·750	−1·125	−1·325	−1·455	−1·500
ρga	0·143	0·239	0·250	0·088	−0·216	−0·422	−0·571	−0·425
$\rho' ga$	−0·087	−0·171	−0·250	−0·353	−0·433	−0·470	−0·492	−0·500

Table Vb.

Magnitudes of the respective terms related to $\rho g\xi$, ρga and $\rho' ga$ of $\widehat{\theta\theta}_{r=a}$ when $\frac{\mu'}{\mu}=\infty$.

θ	0°	10°	20°	30°	45°	60°	70°	80°	90°
$\rho g\xi$	−0·5000	−0·4850	−0·4410	−0·3750	−0·2500	−0·1250	−0·0585	−0·0150	0
ρga	0·2085	0·1905	0·1410	0·0723	−0·0294	−0·0833	−0·0797	−0·0480	0
$\rho' ga$	0·1670	0·1645	0·1570	0·1445	0·1180	0·0834	0·0571	0·0290	0

θ	100°	110°	120°	135°	150°	160°	170°	180°
$\rho g\xi$	−0·0150	−0·0585	−0·1250	−0·2500	−0·3750	−0·4410	−0·4850	−0·5000
ρga	0·0480	0·0797	0·0833	0·0294	−0·0723	−0·1410	−0·1905	−0·2085
$\rho' ga$	−0·0290	−0·0571	−0·0834	−0·1180	−0·1445	−0·1570	−0·1645	−0·1670

Table Vc.

Magnitudes of the respective terms related to $\rho g\xi$, ρga and $\rho' ga$ of $\widehat{\theta\theta'}_{r=a}$ when $\frac{\mu'}{\mu}=\infty$.

θ	0°	10°	20°	30°	45°	60°	70°	80°	90°
$\rho g\xi$	0	−0·045	−0·175	−0·375	−0·750	−1·125	−1·325	−1·455	−1·500
ρga	0·375	0·414	0·518	0·650	0·795	0·750	0·575	0·3175	0
$\rho' ga$	−0·50	−0·493	−0·470	−0·433	−0·353	−0·250	−0·171	−0·087	0

θ	100°	110°	120°	135°	150°	160°	170°	180°
$\rho g\xi$	−1·455	−1·325	−1·125	−0·750	−0·375	−0·175	−0·045	0
ρga	−0·3175	−0·575	−0·750	−0·795	−0·650	−0·518	−0·414	−0·375
$\rho' ga$	0·087	0·171	0·250	0·353	0·433	0·470	0·493	0·500

Table Vd.

Magnitudes of the respective terms related to $\rho g\xi$, ρga and $\rho' ga$ of $\widehat{r\theta}_{r=a}$ $(=\widehat{r\theta'}_{r=a})$ when $\frac{\mu'}{\mu}=\infty$.

θ	0°	10°	20°	30°	45°	60°	70°	80°	90°
$\rho g\xi$	0	0·256	0·482	0·650	0·750	0·650	0·482	0·256	0
ρga	0	0·143	−0·239	−0·250	−0·088	0·216	0·422	0·571	0·625
$\rho' ga$	0	−0·087	−0·171	−0·250	−0·353	−0·433	−0·470	−0·492	−0·500

θ	100°	110°	120°	135°	150°	160°	170°	180°
$\rho g\xi$	−0·256	−0·482	−0·650	−0·750	−0·650	−0·482	−0·256	0
ρga	0·571	0·422	0·216	−0·088	−0·250	−0·239	−0·143	0
$\rho' ga$	−0·492	−0·470	−0·433	−0·353	−0·250	−0·171	−0·087	0

Table VIa.

Magnitudes of the respective terms of $\rho g\xi$, ρga and $\rho' ga$ of $\widehat{rr}_{\substack{\theta=0^\circ\\ \theta=63^\circ}}$ and $\widehat{rr'}_{\substack{\theta=0^\circ\\ \theta=63^\circ}}$ when $\frac{\mu'}{\mu}=\frac{1}{5}$.

	$\frac{r}{a}$	$\widehat{rr}$			$\widehat{rr'}$						
		0	0·5	1·0	1·0	1·1	1·2	1·5	2·0	3·0	4·0
$\theta=0^\circ$	$\rho g\xi$	−0·428	−0·428	−0·428	−0·428	−0·409	−0·422	−0·535	−0·696	−0·852	−0·914
	ρga	0	0·065	0·130	0·130	0·242	0·384	0·840	1·525	2·702	3·783
	$\rho' ga$	0	0·363	0·727	0·727	0·677	0·633	0·524	0·404	0·274	0·207
$\theta=63^\circ$	$\rho g\xi$	−0·0883	−0·0883	−0·0883	−0·0883	−0·1791	−0·2311	−0·2781	−0·2711	−0·2427	−0·2282
	ρga	0	−0·0476	−0·0955	−0·0955	−0·0251	−0·0052	0·0378	0·0743	0·1806	0·2906
	$\rho' ga$	0	0·1651	0·3302	0·3302	0·3083	0·2883	0·2377	0·1832	0·1242	0·0939

Table VIb.

Magnitudes of the respective terms of $\rho g\xi$, ρga and $\rho' ga$ of $\widehat{\theta\theta}_{\substack{\theta=0^\circ\\ \theta=60^\circ\\ \theta=90^\circ}}$ and $\widehat{\theta\theta'}_{\substack{\theta=0^\circ\\ \theta=60^\circ\\ \theta=90^\circ}}$ when $\frac{\mu'}{\mu}=\frac{1}{5}$.

	$\frac{r}{a}$	$\widehat{\theta\theta}$			$\widehat{\theta\theta'}$						
		0	0·5	1·0	1·0	1·1	1·2	1·5	2·0	3·0	4·0
$\theta=0^\circ$	$\rho g\xi$	0	0	0	0·5720	0·3517	0·2165	0·0423	0·0178	0·0211	0·0145
	ρga	0	−0·0195	−0·0390	−0·3682	−0·1764	−0·0703	0·0468	0·0700	0·0544	0·0417
	$\rho' ga$	0	0·0909	0·1818	−0·0606	−0·0717	−0·0778	−0·0796	−0·0700	−0·0515	−0·0400
$\theta=60^\circ$	$\rho g\xi$	−0·3220	−0·3220	−0·3220	−1·4642	−1·2798	−1·1561	−0·9610	−0·8482	−0·7870	−0·7696
	ρga	0	0·0706	0·1412	0·8342	0·6964	0·6365	0·6351	0·7850	1·1478	1·5183
	$\rho' ga$	0	0·0455	0·0909	−0·0303	−0·0358	−0·0388	−0·0399	−0·0350	−0·0257	−0·0200
$\theta=90^\circ$	$\rho g\xi$	−0·4280	−0·4280	−0·4280	−2·1430	−1·8233	−1·6135	−1·2957	−1·1250	−1·0423	−1·0213
	ρga	0	0	0	0	0	0	0	0	0	0
	$\rho' ga$	0	0	0	0	0	0	0	0	0	0

Table VIc.

Magnitudes of the respective terms of $\rho g\xi$, ρga and $\rho' ga$ of $\widehat{r\theta}_{\substack{\theta=30^\circ\\ \theta=45^\circ\\ \theta=90^\circ}}$ and $\widehat{r\theta'}_{\substack{\theta=30^\circ\\ \theta=45^\circ\\ \theta=90^\circ}}$ when $\frac{\mu'}{\mu}=\frac{1}{5}$.

	$\frac{r}{a}$	$\widehat{r\theta}$			$\widehat{r\theta'}$						
		0	0·5	1·0	1·0	1·1	1·2	1·5	2·0	3·0	4·0
$\theta=30^\circ$	$\rho g\xi$	0·1855	0·1855	0·1855	0·1855	0·3325	0·4177	0·5067	0·5103	0·4789	0·4611
	ρga	0	−0·0478	−0·0957	−0·0957	−0·2635	−0·3675	−0·5431	−0·7374	−1·1088	−1·4845
	$\rho' ga$	0	−0·0683	−0·1365	−0·1365	−0·1156	−0·1002	−0·0712	−0·0483	−0·0297	−0·0216
$\theta=45^\circ$	$\rho g\xi$	0·2140	0·214	0·2140	0·2140	0·3841	0·4820	0·5844	0·5892	0·5528	0·5324
	ρga	0	−0·0299	−0·0597	−0·0597	−0·2025	−0·2950	−0·4660	−0·6640	−1·0270	−1·3900
	$\rho' ga$	0	−0·0965	−0·1930	−0·1930	−0·1636	−0·1415	−0·1007	−0·0682	−0.0420	−0·0306
$\theta=90^\circ$	$\rho g\xi$	0	0	0	0	0	0	0	0	0	0
	ρga	0	0·0649	0·1297	0·1297	0·1984	0·2184	0·1944	0·1323	0·0728	0·0494
	$\rho' ga$	0	−0·1363	−0·2725	−0·2725	−0·2311	−0·2005	−0·1424	−0·0966	−0·0593	−0·0434

Table VIIa.

Magnitudes of the respective terms of $\rho g\xi$, ρga and $\rho' ga$ of $\widehat{rr}_{\substack{\theta=0^\circ\\ \theta=63^\circ}}$ and $\widehat{rr'}_{\substack{\theta=0^\circ\\ \theta=63^\circ}}$ when $\frac{\mu'}{\mu}=1$.

	$\frac{r}{a}$	$\widehat{rr}$			$\widehat{rr'}$						
		0	0·5	1·0	1·0	1·1	1·2	1·5	2·0	3·0	4·0
$\theta=0^\circ$	$\rho g\xi$	−1	−1	−1	−1	−1	−1	−1	−1	−1	−1
	ρga	0	0·1667	0.3333	0·3333	0·4684	0·6006	0·9944	1·6043	2·7292	3·7941
	$\rho' ga$	0	0·3333	0·6667	0·6667	0·6316	0·5994	0·5056	0·3957	0·2708	0·2059
$\theta=63^\circ$	$\rho g\xi$	−0·2061	−0·2061	−0·2061	−0·2061	−0·2061	−0·2061	−0·2061	−0·2061	−0·2061	−0·2061
	ρga	0	−0·1046	−0·2091	−0·2091	−0·1841	−0·1599	−0·0891	0·0073	0·1578	0·2806
	$\rho' ga$	0	0·1513	0·3027	0·3027	0·2870	0·2721	0·2296	0·1797	0·1232	0·0934

Table VIIb.

Magnitudes of the respective terms of $\rho g\xi$, ρga and $\rho' ga$ of $\widehat{\theta\theta}_{\substack{\theta=0^\circ \\ \theta=60^\circ \\ \theta=90^\circ}}$ and $\widehat{\theta\theta'}_{\substack{\theta=0^\circ \\ \theta=60^\circ \\ \theta=90^\circ}}$ when $\frac{\mu'}{\mu}=1$.

	$\frac{r}{a}$	$\widehat{\theta\theta}$			$\widehat{\theta\theta'}$						
		0	0·5	1·0	1·0	1·1	1·2	1·5	2·0	3·0	4·0
$\theta=0^\circ$	$\rho g\xi$	0	0	0	0	0	0	0	0	0	0
	ρga	0	0	0	0	0·0261	0·0424	0·0617	0·0624	0·0492	0·0391
	$\rho' ga$	0	0	0	0	−0·0261	−0·0424	−0·0617	−0·0624	−0·0492	−0·0391
$\theta=60^\circ$	$\rho g\xi$	−0·75	−0·75	−0·75	−0·75	−0·75	−0·75	−0·75	−0·75	−0·75	−0·75
	ρga	0	0·1875	0·3750	0·3750	0·4256	0·4711	0·5934	0·7813	1·1496	1·5195
	$\rho' ga$	0	0	0	0	−0·0130	−0·0211	−0·0309	−0·0313	−0·0246	−0·0195
$\theta=90^\circ$	$\rho g\xi$	−1	−1	−1	−1	−1	−1	−1	−1	−1	−1
	ρga	0	0	0	0	0	0	0	0	0	0
	$\rho' ga$	0	0	0	0	0	0	0	0	0	0

Table VIIc.

Magnitudes of the respective terms of $\rho g\xi$, ρga and $\rho' ga$ of $\widehat{r\theta}_{\substack{\theta=30^\circ \\ \theta=45^\circ \\ \theta=90^\circ}}$ and $\widehat{r\theta'}_{\substack{\theta=30^\circ \\ \theta=45^\circ \\ \theta=90^\circ}}$ when $\frac{\mu'}{\mu}=1$.

	$\frac{r}{a}$	$\widehat{r\theta}$			$\widehat{r\theta'}$						
		0	0·5	1·0	1·0	1·1	1·2	1·5	2·0	3·0	4·0
$\theta=30^\circ$	$\rho g\xi$	0·433	0·433	0·433	0·433	0·433	0·433	0·433	0·433	0·433	0·433
	ρga	0	−0·1042	−0·2083	−0·2083	−0·2742	−0·3323	−0·4824	−0·6979	−1·0942	−1·4779
	$\rho' ga$	0	−0·0834	−0·1667	−0·1668	−0·1383	−0·1177	−0·0801	−0·0521	−0·0308	−0·0221
$\theta=45^\circ$	$\rho g\xi$	0·5	0·5	0·5	0·5	0·5	0·5	0·5	0·5	0·5	0·5
	ρga	0	−0·0589	−0·1178	−0·1178	−0·1935	−0·2575	−0·4165	−0·6330	−1·0180	−1·3850
	$\rho' ga$	0	−0·1178	−0·2357	−0·2357	−0·1960	−0·1668	−0·1133	−0·0737	−0·0436	−0·0314
$\theta=90^\circ$	$\rho g\xi$	0	0	0	0	0	0	0	0	0	0
	ρga	0	0·1667	0·3333	0·3333	0·2767	0·2356	0·1603	0·1042	0·0616	0·0443
	$\rho' ga$	0	−0·1667	−0·3333	−0·3333	−0·2767	−0·2356	−0·1603	−0·1042	−0·0616	−0·0443

Table VIIIa.

Magnitudes of the respective terms of $\rho g\xi$, ρga and $\rho' ga$ of $\widehat{rr}_{\substack{\theta=0^\circ \\ \theta=63^\circ}}$ and $\widehat{rr'}_{\substack{\theta=0^\circ \\ \theta=63^\circ}}$ when $\frac{\mu'}{\mu}=5$.

	$\frac{r}{a}$	$\widehat{rr}$			$\widehat{rr'}$						
		0	0·5	1·0	1·0	1·1	1·2	1·5	2·0	3·0	4·0
$\theta=0^\circ$	$\rho g\xi$	−1·3636	−1·3636	−1·3636	−1·3636	−1·3760	−1·3670	−1·2955	−1·1929	−1·0941	−1·0547
	ρga	0	0·2597	0·5195	0·5195	0·6560	0·7729	1·1092	1·6617	2·7480	3·8023
	$\rho' ga$	0	0·2857	0·5714	0·5714	0·5600	0·5440	0·4774	0·3838	0·2673	0·2044
$\theta=63^\circ$	$\rho g\xi$	−0·2811	−0·2811	−0·2811	−0·2811	−0·2231	−0·1931	−0·1605	−0·1648	−0·1828	−0·1920
	ρga	0	−0·1278	−0·2557	−0·2557	−0·2656	−0·2498	−0·1620	−0·0322	0·1443	0·2746
	$\rho' ga$	0	0·1297	0·2594	0·2594	0·2551	0·2472	0·2168	0·1743	0·1216	0·0928

Table VIIIb.

Magnitudes of the respective terms of $\rho g\xi$, ρga and $\rho' ga$ of $\widehat{\theta\theta}_{\substack{\theta=0^\circ \\ \theta=60^\circ \\ \theta=90^\circ}}$ and $\widehat{\theta\theta'}_{\substack{\theta=0^\circ \\ \theta=60^\circ \\ \theta=90^\circ}}$ when $\frac{\mu'}{\mu}=5$.

	$\frac{r}{a}$	$\widehat{\theta\theta}$			$\widehat{\theta\theta'}$						
		0	0·5	1·0	1·0	1·1	1·2	1·5	2·0	3·0	4·0
$\theta=0^\circ$	$\rho g\xi$	0	0	0	−0·3635	−0·2239	−0·1380	−0·0268	0·0114	0·0135	0·0093
	ρga	0	0·0974	0·1948	0·1774	0·1118	0·0811	0·0543	0·0506	0·0438	0·0366
	$\rho' ga$	0	−0·1429	−0·2857	0·0954	0·0456	0·0129	−0·0334	−0·0505	−0·0457	−0·0376
$\theta=60^\circ$	$\rho g\xi$	−1·0227	−1·0227	−1·0227	−0·2952	−0·4129	−0·4915	−0·6155	−0·6874	−0·7265	−0·7376
	ρga	0	0·3044	0·6088	0·0549	0·2319	0·3492	0·5584	0·7753	1·1497	1·5199
	$\rho' ga$	0	−0·0714	−0·1428	0·0477	0·0228	0·0065	−0·0167	−0·0253	−0·0228	−0·0188
$\theta=90^\circ$	$\rho g\xi$	−1·3636	−1·3636	−1·3636	−0·2725	−0·4759	−0·6094	−0·8118	−0·9204	−0·9731	0·9865
	ρga	0	0	0	0	0	0	0	0	0	0
	$\rho' ga$	0	0	0	0	0	0	0	0	0	0

Table VIIIc.

Magnitudes of the respective terms of $\rho g\xi$, ρga and $\rho' ga$ of $\widehat{r\theta}_{\substack{\theta=30^\circ\\ \theta=45^\circ\\ \theta=90^\circ}}$ and $\widehat{r\theta'}_{\substack{\theta=30^\circ\\ \theta=45^\circ\\ \theta=90^\circ}}$ when $\frac{\mu'}{\mu}=5$.

	$\frac{r}{a}$	$\widehat{r\theta}$			$\widehat{r\theta'}$						
		0	0·5	1·0	1·0	1·1	1·2	1·5	2·0	3·0	4·0
$\theta=30^\circ$	$\rho g\xi$	0·5905	0·5905	0·5905	0·5905	0·4960	0·4440	0·3860	0·3840	0·4040	0·4150
	ρga	0	−0·1258	−0·2516	−0·2516	−0·2593	−0·2936	−0·4352	−0·6693	−1·0839	−1·4733
	$\rho' ga$	0	−0·1070	−0·2143	−0·2143	−0·1742	−0·1455	−0·0944	−0·0580	−0·0326	−0·0229
$\theta=45^\circ$	$\rho g\xi$	0·6820	0·6820	0·6820	0·6820	0·5738	0·5117	0·4461	0·4431	0·4664	0·4794
	ρga	0	−0·0575	−0·1150	−0·1150	−0·1575	−0·2110	−0·3740	−0·6800	−1·0100	−1·3800
	$\rho' ga$	0	−0·1515	−0·3030	−0·3030	−0·2460	−0·2060	−0·1340	−0·0820	−0·0461	−0·0325
$\theta=90^\circ$	$\rho g\xi$	0	0	0	0	0	0	0	0	0	0
	ρga	0	0·2599	0·5197	0·5197	0·3697	0·2800	0·1557	0·0934	0·0565	0·0419
	$\rho' ga$	0	−0·2143	−0·4286	−0·4286	−0·3434	−0·2910	−0·1888	−0·1160	−0·0652	−0·0458

Table IXa.

Magnitudes of the respective terms of $\rho g\xi$, ρga and $\rho' ga$ of $\widehat{rr}_{\substack{\theta=0^\circ\\ \theta=63^\circ}}$ and $\widehat{rr'}_{\substack{\theta=0^\circ\\ \theta=63^\circ}}$ when $\frac{\mu'}{\mu}=\infty$.

	$\frac{r}{a}$	$\widehat{rr}$			$\widehat{rr'}$						
		0	0·5	1·0	1·0	1·1	1·2	1·5	2·0	3·0	4·0
$\theta=0^\circ$	$\rho g\xi$	−1·5000	−1·5000	−1.5000	−1·5000	−1·5195	−1·5060	−1·4062	−1·2656	−1·1295	−1·0753
	ρga	0	0·3125	0·6250	0·6250	0·7520	0·8570	1·1632	1·6878	2·7563	3·8060
	$\rho' ga$	0	0·25	0·5	0·5	0·5063	0·5027	0·4563	0·3748	0·2647	0·2033
$\theta=63^\circ$	$\rho g\xi$	−0·3092	−0·3092	−0·3092	−0.3092	−0·2286	−0·1843	−0·1429	−0·1492	−0·1740	−0·1867
	ρga	0	−0·1284	−0·2569	−0·2569	−0·2831	−0·2738	−0·1845	−0·0449	0·1398	0·2726
	$\rho' ga$	0	0·1135	0·2270	0·2270	0·2306	0·2285	0·2072	0·1703	0·1204	0·0923

Table IXb.

Magnitudes of the respective terms of $\rho g\xi$, ρga and $\rho' ga$ of $\widehat{\theta\theta}_{\substack{\theta=0^\circ \\ \theta=60^\circ \\ \theta=90^\circ}}$ and $\widehat{\theta\theta'}_{\substack{\theta=0^\circ \\ \theta=60^\circ \\ \theta=90^\circ}}$ when $\frac{\mu'}{\mu}=\infty$.

	$\frac{r}{a}$	$\widehat{\theta\theta}$			$\widehat{\theta\theta'}$						
		0	0·5	1·0	1·0	1·1	1·2	1·5	2·0	3·0	4·0
$\theta=0^\circ$	$\rho g\xi$	0	0	0	−0·5000	−0·3065	−0·1892	−0·0368	0·0156	0·0185	0·0127
	ρga	0	0·1875	0·3750	0·2090	0·1176	0·0755	0·0410	0·0416	0·0405	0·0350
	$\rho' ga$	0	−0·2500	−0·5000	0·1666	0·0993	0·0542	−0·0123	−0·0416	−0·0431	0·0365
$\theta=60^\circ$	$\rho g\xi$	−1·1250	−1·1250	−1·1250	−0·1250	−0·2870	−0·3947	−0·5651	−0·6641	−0·7176	−0·7329
	ρga	0	0·3750	0·7500	−0·0833	0·1459	0·2933	0·5399	0·7708	1·1491	1·5197
	$\rho' ga$	0	−0·1250	−0·2500	0·0834	0·0496	0·0271	−0·0063	−0·0208	−0·0215	−0·0182
$\theta=90^\circ$	$\rho g\xi$	−1·5000	−1·5000	−1·5000	0	−0·2805	−0·4632	−0·7412	−0·8906	−0·9630	−0·9814
	ρga	0	0	0	0	0	0	0	0	0	0
	$\rho' ga$	0	0	0	0	0	0	0	0	0	0

Table IXc.

Magnitudes of the respective terms of $\rho g\xi$, ρga and $\rho' ga$ of $\widehat{r\theta}_{\substack{\theta=30^\circ \\ \theta=45^\circ \\ \theta=90^\circ}}$ and $\widehat{r\theta'}_{\substack{\theta=30^\circ \\ \theta=45^\circ \\ \theta=90^\circ}}$ when $\frac{\mu'}{\mu}=\infty$.

	$\frac{r}{a}$	$\widehat{r\theta}$			$\widehat{r\theta'}$						
		0	0·5	1·0	1·0	1·1	1·2	1·5	2·0	3·0	4·0
$\theta=30^\circ$	$\rho g\xi$	0·6495	0·6495	0·6495	0·6495	0·5195	0·4460	0·3690	0·3650	0·3930	0·4080
	ρga	0	−0·1250	−0·2500	−0·2500	−0·2408	−0·2686	−0·4125	−0·6563	−1·0794	−1·4712
	$\rho' ga$	0	−0·1250	−0·2500	−0·2500	−0·2010	−0·1661	−0·1049	−0·0625	−0·0339	−0·0235
$\theta=45^\circ$	$\rho g\xi$	0·7500	0·7500	0·7500	0·7500	0·6000	0·5155	0·4258	0·4219	0·4537	0·4717
	ρga	0	−0·0442	−0·0884	−0·0884	−0·1258	−0·1788	−0·3500	−0·5985	−1·0050	−1·3800
	$\rho' ga$	0	−0·1768	−0·3535	−0·3535	−0·2850	−0·2350	−0·1483	−0·0885	−0·0480	−0·0332
$\theta=90^\circ$	$\rho g\xi$	0	0	0	0	0	0	0	0	0	0
	ρga	0	0·3125	0·6250	0·6250	0·4311	0·3170	0·1645	0·0938	0·0559	0·0415
	$\rho' ga$	0	−0·2500	−0·5000	−0·5000	−0·4021	−0·3324	−0·2097	−0·1250	−0·0677	−0·0469

25. 重力の働ける半無限彈性體内に存在する圓形塡充物附近の應力 (II)

地震研究所 西村源六郎 高山威雄 金井清

前論文と全く同じ目的で塡充物内外の應力釣合を論じてあるが，重力の作用してゐる半無限彈性體は前論文と異ひ plane stress の狀態に保たれてゐると考へて計算を運んでみた．Plane strain 問題として取扱つた時の結果と詳しく定性定量的の比較をする爲めに數値計算を行ひその量を表と圖に示めした．

26. *Vertical Crustal Displacement in the Seismic Region of Itô, on the East Coast af the Idu Peninsula.*

By Chûji TSUBOI,

Earthquake Research Institute.

(Read May 16, 1933.—Received June 20, 1933.)

The town of Itô and neighbourhood on the east coast of the Idu peninsula were visited in 1930 by an unusually large number of small earthquakes, the sensible ones of which were reported to have been more than 4321 in number.[1] In order to ascertain whether the earth's crust of this seismic region was deformed or not in connection with these seismic activities, precise levels were run three times in 1930 in the region along the route shown in Fig. 1. These surveys showed that the earth's crust here upheaved in the form of an inverted V since the earlier surveys were made in 1923–1924. At the end of 1930 the largest upheaval amounted to as much as 220 mm., or more, with no sign of abatement. These crustal deformations were already discussed in the writer's earlier papers.[2]

It being now two years since the last survey of 1930, urgent need was felt for running a line of levels once more over the same ground in order to measure the amount of vertical crustal displacement that must have occurred in the interval. Thanks to the gene-

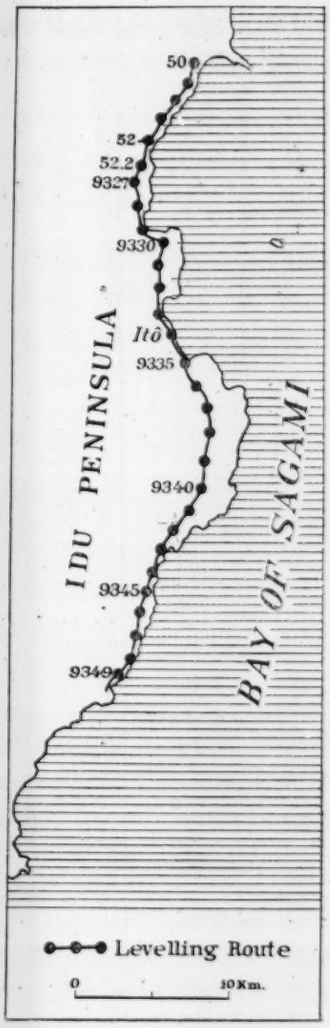

Fig. 1. Levelling Route over the Itô Seismic Region.

1) N. NASU, F. KISHINOUYE and T. KODAIRA, *Bull. Earthq. Res. Inst.*, 9 (1931), 22.

2) C. TSUBOI, *Bull. Earthq. Res. Inst.*, 9 (1931), 151; 10 (1932), 570; *Proc. Imp. Acad.*, 7 (1931), 153; *Jap. J. Astr. Geophys.*, 10 (1933), 93.

rous grant given the writer by the Hattori Hôkô-kwai Foundation, he was enabled to arrange with the Military Land Survey for the work of levelling. The survey, which was begun on Dec. 25, 1932, was finished on March 16, 1933. The changes of height of the bench marks since the earlier survey are given in Table I, together with those during the former intervals.

Table I. Changes of Height of Bench Marks in the Itô Seismic Region.

I....1923-1924.
II....March 15—April 14, 1930.
III....Nov. 9—Dec. 3, 1930.
IV....Dec. 19, 1930—Jan. 3, 1931.
V....Dec. 25, 1932—March 16, 1933.

B.M.	II—I	III—II	IV—III	IV—I	V—IV	B.M.	II—I	III—II	IV—III	IV—I	V—IV
	mm										
50				− 4·3	− 6·3	9336	+93·8	+118·1	+ 6·8		+127·2
50.1				+ 6·3	− 6·7	9337	+96·9	+122·1	+ 4·3		+116·3
51				+15·4	− 9·5	9338	+74·8	+ 88·1	− 2·5		+105·8
51.1				+22·5	− 15·4	9339	+47·5	+ 56·1	− 0·7		+ 93·4
52				+23·1	− 17·1	9340	+21·5	+ 31·8	− 4·5		+ 77·5
52.2				+ 3·7	− 13·8	9341	+ 5·7	+ 6·0	− 8·0		+ 63·9
9327				−11·0	− 13·4	9342	− 7·3	− 11·5	− 8·0		+ 50·6
9328	± 0·0	± 0·0	± 0·0	± 0·0	± 0·0	9343	−11·8	− 17·8	−10·1		+ 39·4
9329	− 3·6	+ 6·3	−21·6		+ 19·6	9344	− 26·5	− 21·4	−14·5		+ 33·7
9330	− 4·9	+ 5·6	+ 9·1		+ 27·2	9345				−38·8	+ 22·6
9331	−10·5	+ 21·5	+17·4		+ 61·6	9346				−44·3	+ 19·4
9332	+ 1·7	+ 35·6	+26·9		+ 96·7	9347				−52·1	+ 17·2
9333	+10·6	+ 59·4	+27·2		+123·4	9348				−51·8	+ 11·2
9334	+33·9	+ 81·0	+25·0		+137·0	9349				−52·2	+ 10·3
9335	+72·6	+102·3	+13·6		+135·8						

The values in Table I are graphically shown in Fig. 2. It will be seen from the figure that although the seismicity in the Itô region, in the two years that have elapsed since the last survey of 1930, has been quite inactive compared with that in 1930, the crustal deformation still goes on as before. It should be noted therefore that in the present case there is no apparent connection between the seismic activity and the rate of crustal deformation.

Seeing that we have now the results of four series of precise level-

ling, all executed in the course of three years, it is possible by simple interpolation to find the approximate height of any bench mark in the region at any time during the interval. In making this calculation, however, the following considerations should be borne in mind.

First of all, it must be emphasised that what we are measuring by means of precise levelling is the difference in the heights of two consecutive bench marks and not their individual heights. Consequently the levelling is nothing but an aid to determine the form of the curve of a land profile by integrating the differential equation

$$\frac{dh}{dx}=f(x) \quad \ldots(1)$$

into the form

$$h=\int_0^x f(x)\,dx,$$

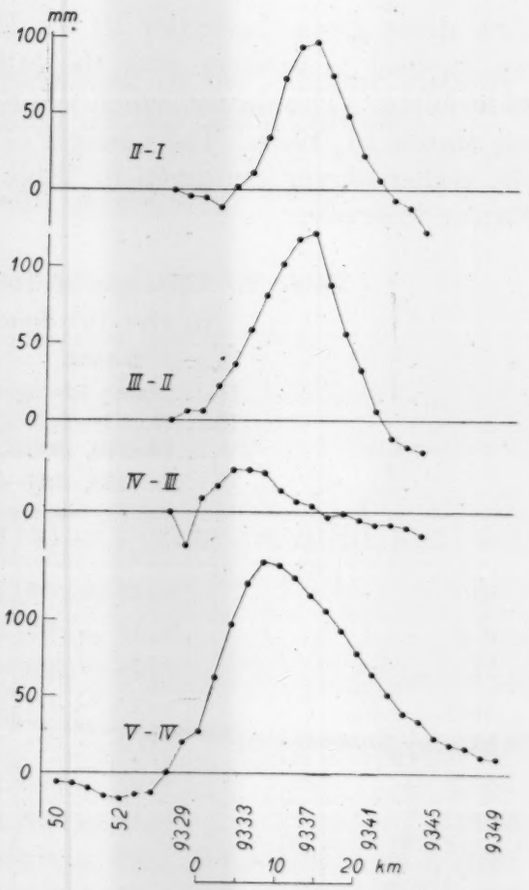

Fig 2. Changes of height of bench marks in the Itô seismic region.

where h is the relative height of a bench mark at $x=x$ with respect to the height of the reference bench mark at $x=0$. If $\frac{dh}{dx}$ is independent of time t as is generally assumed, the above method of integration is quite rigid. Strictly speaking however it is a function of t and instead of the differential equation (1), we should have

$$\frac{\partial h}{\partial x}=F(x,t). \quad \ldots\ldots\ldots\ldots\ldots\ldots\ldots\ldots(2)$$

It is not possible to integrate this equation from $x=0$ to $x=x$ unless it is known how t is involved in $F(x,t)$, but this is beyond the scope of a levelling survey. What is observed as the curve of land profile by the ordinary method is, therefore, in some cases only an apparent one which may be sensibly different from the true profile at a parti-

cular time.

By the following examples, it will be seen how, in some cases, false results are obtained if we neglect the change of $\frac{\partial h}{\partial x}$ with time. Suppose first that a straight line of length S is levelled, one end of which is fixed and the other is uniformly upheaving according to the relation

$$y=at. \quad \ldots\ldots\ldots\ldots\ldots\ldots\ldots\ldots (3)$$

If T is the time required for the levelling to cover the whole length of S, we have

$$\frac{x}{S}=\frac{t}{T}.$$

The differential equation of the profile to be determined is therefore

$$\frac{dh}{dx}=\frac{at}{S}=\frac{aT}{S^2}x,$$

and integrating this equation with respect to x, we have

$$h=\frac{1}{2}\frac{aT}{S^2}x^2. \quad \ldots\ldots\ldots\ldots\ldots\ldots\ldots\ldots (4)$$

The line S will appear, therefore, as if it were parabolic instead of straight. At $t=T$, $x=S$, we have according to (4)

$$y=\frac{1}{2}aT,$$

but the true y, according to (3), is $y=aT$, which is twice as large as the apparent y.

Suppose next that a line in levelled, one end of which is fixed and the other is subjected to a motion

$$y=\sin\frac{\pi}{T}t. \quad \ldots\ldots\ldots\ldots\ldots\ldots\ldots\ldots (5)$$

Then we have as before

$$\frac{dh}{dx}=\frac{1}{S}\sin\frac{\pi}{S}x,$$

and integrating this equation with respect to x, we have

$$h=\frac{1}{\pi}\left(1-\cos\frac{\pi}{S}x\right). \quad \ldots\ldots\ldots\ldots\ldots\ldots\ldots\ldots (6)$$

The line will appear as if it were of the form shown in Fig. 3 instead

of straight. At $t=T$, $x=S$, we have according to (6)

$$y=\frac{2}{\pi}$$

but the true y is 0 according to (5).

For the purpose of investigating the vertical crustal displacement, we calculate the difference of two series of old and new levellings along the same route. Our next problem then is to examine how the difference is affected if we neglect the change of $\frac{\partial h}{\partial x}$ with time during each of the surveys. Suppose a straight line is levelled, one end of which is fixed and the other is subjected to a motion

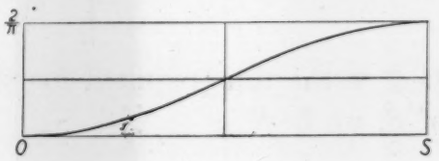

Fig. 3.

$$y=at$$

during the first levelling, and then to

$$y=a(T-t)$$

during the second, which is supposed to have begun the moment the first was finished. Then, for the former survey, integrating the equation

$$\frac{dh}{dx}=\frac{aT}{S^2}x,$$

we have $$h=\frac{1}{2}\frac{aT}{S^2}x^2,$$

while for the latter, integrating the equation

$$\frac{dh}{dx}=\frac{a(T-t)}{S}=\frac{aT}{S}-\frac{aT}{S^2}x,$$

we have $$h=\frac{aT}{S}x-\frac{1}{2}\frac{aT}{S^2}x^2.$$

The difference of these two curves is

$$\Delta h=\frac{aT}{S}x-\frac{aT}{S^2}x^2,$$

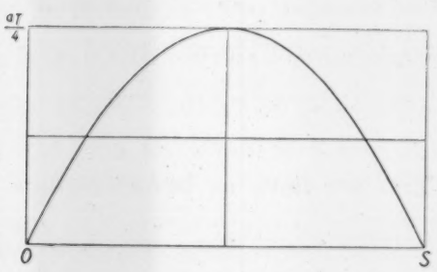

Fig. 4.

the form of which is shown in Fig. 4. Although the true crustal displacement is merely an alternate tilting, the apparent one is an upheaval with the form of an inverted U with its maximum $\frac{aT}{4}$.

Suppose in the second example, a line is levelled, one end of which is fixed and the other is subject to a motion

$$y=\sin\frac{\pi}{T}t$$

during the former survey and to a motion

$$y=-\sin\frac{\pi}{T}t$$

during the latter. Then, for the former survey, integrating the equation

$$\frac{dh}{dx}=\frac{1}{S}\sin\frac{\pi}{T}x,$$

we have

$$h=\frac{1}{\pi}\left(1-\cos\frac{\pi}{S}x\right),$$

while for the latter, integrating the equation

$$\frac{dh}{dx}=-\frac{1}{S}\sin\frac{\pi}{S}x,$$

we have

$$h=-\frac{1}{\pi}\left(1-\cos\frac{\pi}{S}x\right).$$

The difference of these two curves is

$$\Delta h=-\frac{2}{\pi}\left(1-\cos\frac{\pi}{S}x\right),$$

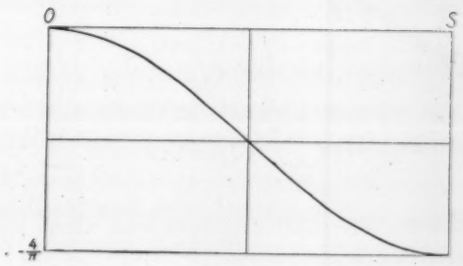

Fig. 5.

the form of which is shown is Fig. 5.

As is apparent in the preceding examples, we are in some cases led to false result if we do not take the change of $\frac{\partial h}{\partial x}$ with time into consideration. For the purpose of eliminating these effects, the following procedure is necessary.

Suppose we are making a levelling survey along a route on which lie bench marks $b_1, b_2, \ldots . b_n$, and we find by the survey that the height difference of b_p and b_{p+1} at $t_{p,p+1}$ is $h_{p.\,p+1}(t_{p,p+1})$. From these data alone, we cannot obtain the value of $h_{1,p}(T)$ because $t_{1,2}, t_{2,3} \ldots t_{n-1,n}$ are all different. By expanding $h_{p,p+1}(t)$ into Taylor's series, we have,

$$h_{1,2}(t)=h_{1,2}(t_{1,2})+(t-t_{1,2})\frac{dh_{1,2}(t_{1,2})}{dt}+\ldots$$

. . . . . .

$$h_{p,p+1}(t)=h_{p,p+1}(t_{p,p+1})+(t-t_{p,p+1})\frac{dh_{p,p+1}(t_{p,p+1})}{dt}+\cdots\cdots$$

$$\cdots\cdots\cdots\cdots\cdots\cdots\cdots\cdots$$

Therefore, we have

$$h_{1,n}(t)=\sum_{p=1}^{n-1}h_{p,p+1}(t_{p,p+1})+\sum_{p=1}^{n-1}(t-t_{p,p+1})\frac{dh_{p,p+1}(t_{p,p+1})}{dt}+\cdots\cdots$$

If by another series of levelling, we find $h_{1,2}(t'_{1,2})$, $h_{2,3}(t'_{2,3}),\ldots\ldots h_{n-1,n}(t'_{n-1,n})$, then in the first approximation, we have

$$h_{1,2}(t)=h_{1,2}(t_{1,2})+\frac{t-t_{1,2}}{t'_{1,2}-t_{1,2}}\{h_{1,2}(t'_{1,2})-h_{1,2}(t_{1,2})\}$$

$$\cdots\cdots\cdots\cdots\cdots\cdots\cdots\cdots$$

$$h_{p,p+1}(t)=h_{p,p+1}(t_{p,p+1})+\frac{t-t_{p,p+1}}{t'_{p,p+1}-t_{p,p+1}}\{h_{p,p+1}(t'_{p,p+1})-h_{p,p+1}(t_{p,p+1})\}$$

$$\cdots\cdots\cdots\cdots\cdots\cdots\cdots\cdots$$

Therefore we have,

$$h_{1,n}(t)=\sum_{p=1}^{n-1}h_{p,p+1}(t_{p,p+1})+\sum_{p=1}^{n-1}\frac{t-t_{p,p+1}}{t'_{p,p+1}-t_{p,p+1}}\{h_{p,p+1}(t'_{p,p+1})-h_{p,p+1}(t_{p,p+1})\}.$$

These are the expressions that give the heights of the bench marks at any particular time. The effect of the second term, which is generally assumed negligible, becomes sensible if $(t-t_{p,p+1})$ is comparable in length with $(t'_{p,p+1}-t_{p,p+1})$, and if $h_{p,p+1}(t_{p,p+1})$ and $h_{p,p+1}(t'_{p,p+1})$ are different to some extent.

This is found to be the case with the levelling over the Itô region. The second levelling in 1930 was begun on Nov. 9 and finished on Dec. 3, while the third was begun on Dec. 19 and finished on Jan. 15 of the year following. The interval between the two surveys is only 16 days—shorter than the time required for the surveys themselves. In calculating the successive heights of the bench marks in the region, therefore, the necessary reductions should be made for the effect of the second term in the above expressions.

From the values given in Table I, we know that the changes of height difference of two consecutive bench marks between two consecutive levellings were as follows;

Table II. Changes of Height Differences of Consecutive Bench Marks in the Itô Seismic Region.

B. M.	II—I	III—II	IV—III	V—IV
9328				
	mm			
9329	− 3·6	+ 6.3	−21·6	+19·6
9330	− 1·3	− 0·7	+30·7	+ 7·6
9331	− 5·6	+15·9	+ 8·3	+34·4
9332	+12·2	+14·1	+ 9·5	+35·1
9333	+ 8·9	+23·8	+ 0·3	+26·7
9334	+23·3	+21·6	− 2·2	+13.6
9335	+38·7	+21.3	−11·4	− 1·2
9336	+21·2	+15·8	− 6·8	− 8·6
9337	+ 3·1	+ 4·0	− 2·5	−10·9
9338	−22·1	−14·0	− 6·8	−10·5
9339	−27·3	−32·0	+ 1·8	−12·4
9340	−26·0	−24·3	− 3·8	−15·9
9341	−15·8	−25·8	− 3·5	−13·6
9342	−13·0	−17·5	0	−13·3
9343	− 4·5	− 6·3	− 2·1	−11·2
9344	−14·7	− 3·6	− 4·4	− 5·7

The successive height differences of two consecutive bench marks are therefore as follows;

Table III. Successive Height Differences of Consecutive Bench Makrs in the Itô Seismic Region.

B. M.	II—I	III—I	IV—I	V—I
9328				
	mm			
9329	− 3·6 (93)	+ 2·7 (314)	−18·9 (354)	+ 0·7 (1116)
9330	− 1·3 (93)	− 2·0 (315)	+28.7 (354)	+36·3 (1120)
9331	− 5·6 (81)	+10·3 (318)	+18·6 (357)	+53·0 (1120)
9332	+12·2 (76)	+26·3 (318)	+35·8 (357)	+70·9 (1120)
9333	+ 8·9 (76)	+32·7 (322)	+33·0 (361)	+59·7 (1115)
9334	+23·3 (78)	+44·9 (322)	+42·7 (361)	+56·3 (1115)
9335	+38·7 (82)	+60·0 (322)	+48·6 (361)	+47·4 (1114)
9336	+21·2 (83)	+37·0 (325)	+30·2 (365)	+21·6 (1113)
9337	+ 3·1 (83)	+ 7·1 (325)	+ 4·6 (364)	− 6·3 (1112)
9338	−22·1 (86)	−36·1 (326)	−42·9 (365)	−53·4 (1111)
9339	−27·3 (88)	−59·3 (330)	−57·5 (374)	−69·9 (1110)
9340	−26·0 (89)	−50·3 (330)	−54·1 (374)	−70·0 (1109)
9341	−15.8 (97)	−41·6 (331)	−45·1 (375)	−58·7 (1090)
9342	−13·0 (97)	−30·5 (335)	−30·5 (374)	−43·8 (1094)
9343	− 4·5 (100)	−10·8 (335)	−12·9 (374)	−24·1 (1093)
9344	−14·7 (104)	−18 3 (335)	−22·7 (376)	−28·4 (1097)

The numbers in brackets are the number of days that elapsed since Jan. 1, 1930 to the day on which the survey was made.

From these values we can, by linear interpolation, find the height differences of two consecutive bench marks at any particular time, and by summing them up into $\sum_{p=1}^{p} h_{p-1,p}(T)$, we obtain $h_{1,p}(T)$, which is the relative height of the bench mark b_p at time T with respect to the referred bench mark. In Table IV are given the relative heights of the bench marks on specified days with respect to the reference bench mark B. M. 9328. The successive land profiles which were obtained in this manner are shown in Fig. 6.

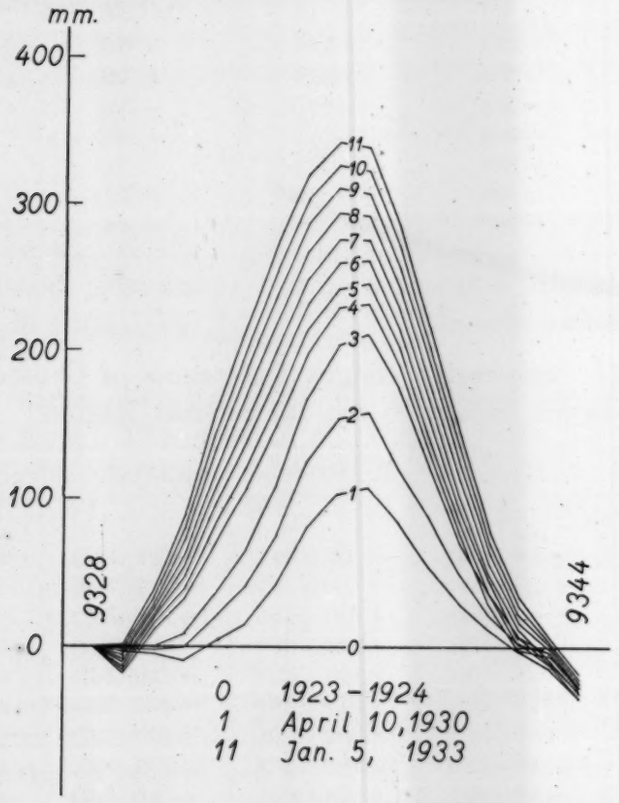

Fig. 6. Successive Heights of Bench Marks in the Itô Seismic Region at Every 100 Days Beginning with April 10, 1930.

The mean vertical velocities of the bench marks can be obtained from their successive heights given in Table IV and are given in Table V.

If the velocities are set down in parallel columns, arranged side

Table IV. Heights of Bench Marks in the Itô Seismic Region as Referred to B. M. 9328.

B.M.	100	200	300	350	400	500	600	700	800	900	1000	1100
	mm											
9328	0	0	0	0	0	0	0	0	0	0	0	0
9329	− 3·4	− 0·6	+ 2·2	− 16·6	− 17·7	− 15·1	− 12·5	− 9·9	− 7·4	− 4·8	− 2·3	+ 0·3
9330	− 4·8	− 2·3	+ 0·2	+ 8·9	+ 11·4	+ 15·0	+ 18·6	+ 22·3	+ 25·7	+ 29·3	+ 32·8	+ 36·4
9331	− 9·2	+ 0·1	+ 9·3	+ 22·6	+ 31·9	+ 40·0	+ 48·1	+ 56·3	+ 64·2	+ 72·3	+ 80·4	+ 88·5
9332	+ 4·3	+ 19·5	+ 34·5	+ 59·9	+ 69·7	+ 82·4	+ 95·1	+106·8	+120·3	+133·1	+145·8	+158·5
9333	+ 15·5	+ 40·4	+ 65·0	+ 92·8	+106·1	+120·3	+136·6	+151·8	+168·9	+185·2	+201·4	+215·6
9334	+ 40·8	+ 75·0	+108·8	+136·4	+149·5	+165·5	+183·6	+200·6	+219·5	+237·6	+255·6	+273·6
9335	+ 81·1	+124·6	+167·7	+188·5	+198·0	+213·9	+231·9	+248·8	+267·5	+285·5	+303·3	+321·1
9336	+103·3	+153·4	+203·0	+221·3	+227·8	+242·6	+259·4	+275·2	+292·7	+309·6	+326·2	+343·1
9337	+106·7	+158·4	+209·7	+226·8	+231·9	+245·2	+260·6	+274·9	+291·0	+306·4	+321·6	+336·8
9338	+ 83·8	+129·7	+175·2	+186·6	+188·5	+200·5	+214·5	+227·5	+242·2	+256·2	+270·1	+284·0
9339	+ 54·8	+ 87·6	+119·9	+128·1	+130·5	+140·9	+153·2	+164·5	+177·6	+189·6	+202·1	+214·3
9340	+ 28·5	+ 50·4	+ 72·6	+ 76·1	+ 75·9	+ 84·2	+ 94·3	+103·4	+114·3	+124·5	+134·5	+144·5
9341	+ 12·3	+ 23·3	+ 34·4	+ 33·0	+ 30·0	+ 35·1	+ 41·9	+ 47·7	+ 55·3	+ 62·2	+ 68·8	+ 75·4
9342	− 1·0	+ 2·8	+ 6·6	+ 2·5	− 1·0	+ 2·3	+ 7·3	+ 11·2	+ 17·0	+ 22·0	+ 26·8	+ 31·6
9343	− 5·5	− 4·4	− 3·3	− 9·1	− 14·3	− 12·5	− 9·0	− 6·6	− 2·4	+ 1·1	+ 4·4	+ 7·7
9344	− 20·1	− 20·6	− 21·1	− 29·0	− 37·2	− 36·2	− 33·4	− 31·8	− 28·4	− 25·6	− 23·2	− 20·8

Table V. Mean Daily Vertical Velocities of Bench Marks in the Itô Seismic Region in 0·001 mm.

B. M.	100	250	325	350	375	450	
9328	0	0	0	0	0	0	
9329	28	28	−376	−199	− 22	26	
9330	25	25	+174	112	+ 50	36	
9331	93	92	266	226	186	81	
9332	152	150	508	352	196	127	
9333	249	246	556	411	266	142	
9334	342	338	552	407	262	160	
9335	435	431	416	303	190	159	
9336	501	496	366	248	130	148	
9337	517	513	342	222	102	133	
9338	459	455	228	133	38	120	
9339	328	323	164	106	48	104	
9340	219	222	70	33	− 4	83	
9341	110	112	− 30	− 45	− 60	51	
9342	38	38	− 82	− 76	− 70	33	
9343	11	11	−116	−110	−104	18	
9344	− 5	− 5	−158	−161	−164	10	

uniform afterwards.

by side in the order of time, and the same values in the different columns are joined by contour lines, we get a system of curves as shown in Fig. 7. From this figure, it is apparent that the point of largest

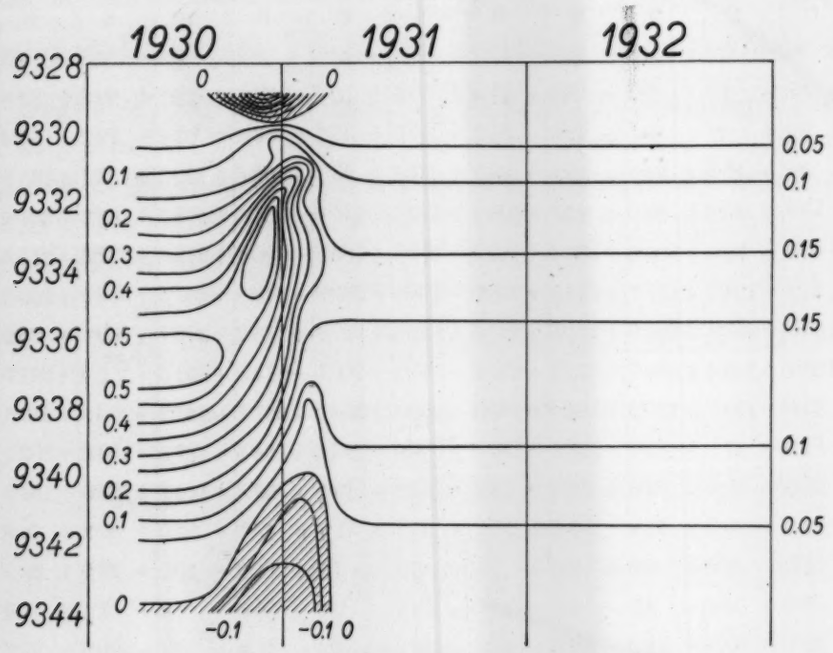

Fig. 7. Daily Vertical Velocities of Bench Marks in the Itô Seismic Region in mm.

upheaval velocity has not remained always in the same place, but has migrated northward with a monthly velocity of 1 km. until the occurrence of the North Idu destructive earthquake of Nov. 26, 1930. After that, the point suddenly moved down southward to a new position where it remained up to the time of the last survey. After the Idu earthquake, the upheaval velocity reduced to one-half of the former values. These facts may be regarded as evidences that the equilibrium of the earth's crust at a certain place is sensibly affected even by an earthquake whose epicentre may be situated some distance away from it.

The writer wishes to express his sincere thanks to Professor Torahiko Terada for his interest in this study and for his kindness in recommending the writer to the Hattori Hôkô-kwai for the grant. He wishes also to express his gratitude to the council of the Hattori Hôkô-kwai for the generous aid by means of which the survey was made possible.

26. 伊豆伊東地方に於ける地殻の垂直移動

地震研究所　坪　井　忠　二

昭和五年の伊東地震群に關する研究の一つとして，同地方に水準測量が三回行はれたが，其の結果に就いては前論文に於いて二三論じておいた。昭和七年の十二月二十五日から翌八年三月十六日にかけて更に新測量が行はれたので，此の論文は其の結果について若干の考察を行つたものである。昭和六年七年を通じて伊東地方の地震は殆んど終熄してゐたのであるが，地殻の變動は尙相當盛んで二年間に最大 137mm. の隆起をなした。玆に於いて地震活動と地殻變動の速さとが一見無關係の樣に見えるのは注意すべき事である。次に此の樣に變動の盛んな地方では，測量をしてゐる間に起つてゐる變動をも考慮に入れなければ正しい垂直移動の値が得られない事を指摘し，伊東の例に就いて之を應用して，百日毎の地表の形を算出した。更に其の結果から平均の一日の垂直速度を求めた。速度の最大な點は一定でなく，昭和五年中は伊東附近から始つて徐々に北上して行つたが伊豆地震後に突然南下した。

最後に此の測量は服部報公會の補助金によるものなる事を記して，深甚の謝意を表する。

27. *Distribution of Earthquakes in Japan.*

By S. YAMAGUTI.

(Read Dec. 20, 1932.—Received June 20, 1933.)

Introduction.

The present investigation may be regarded as a continuation of the report given in a previous paper,[1] dealing with the distribution of the "conspicuous and rather conspicuous" earthquakes, especially with reference to those experienced before and after the "deep" earthquakes in Japan.

The investigation was made with the intention of studying the geographical relation between the epicentres of the "conspicuous and rather conspicuous" earthquakes and the "deep" earthquakes, if such may exist, and to get a hint on the mechanism of occurrence of the "deep" earthquakes.

It was also aimed to find out the relation between these earthquakes and the cyclones which passed over the so-called "deep earthquake region."

We were obliged to take only the short period of investigation after 1926, as the data for the "deep" earthquakes are scanty before that epoch.

Those data for the earthquakes as well as the cyclones were taken from the Abridged Monthly Report of the Central Meteorological Observatory in Japan.

Method of Investigation and Results.

1. *Frequencies of Distances.*

The distances from the epicentres of "deep" earthquakes to the epicentres of the "conspicuous and rather conspicuous" earthquakes, which occurred immediately before and after the "deep" earthquakes, during the period of 6 years and half, Jan., 1926—June, 1932, were measured, and the frequencies of cases falling in successive 100 kilometres, were counted and plotted as ordinates, kilometres of the distances being taken as abscissa, as shown in Fig. 1, *a*. The similar frequency

1) S. YAMAGUTI, *Bull. Earthq. Res. Inst.*, 11 (1933), 46-68.

curve for the distances connecting the epicentres of two successive earthquakes taken, in the order of time of occurrences, for all the "conspicuous and rather conspicuous" earthquakes, which occurred during the same period, was drawn, as shown in Fig. 1, *b*, for the comparison with the above curve.

From these two curves, we can see at first glance that, before and after the "deep" earthquakes, the "conspicuous and rather conspicuous" earthquakes very rarely occur near the epicentres of the former, and their maxima of frequency exist at about 600, 950 and 1550 kilometres distant from the epicentres of the "deep" earthquakes, while on the contrary, the "conspicuous and rather conspicuous" earthquakes themselves, frequently occur at short distances one after another.

Next, to inquire after the meaning of this result more closely, the distances from the centre of gravity, G, (Lat.= 33°N, Long.=138·°4 E), of the epicentres of all the "deep" earthquakes which occurred in the region between the sea off Idu and Kumanonada, to the epicentres of the "conspicuous and rather conspicuous" earthquakes in all Japan, excluding

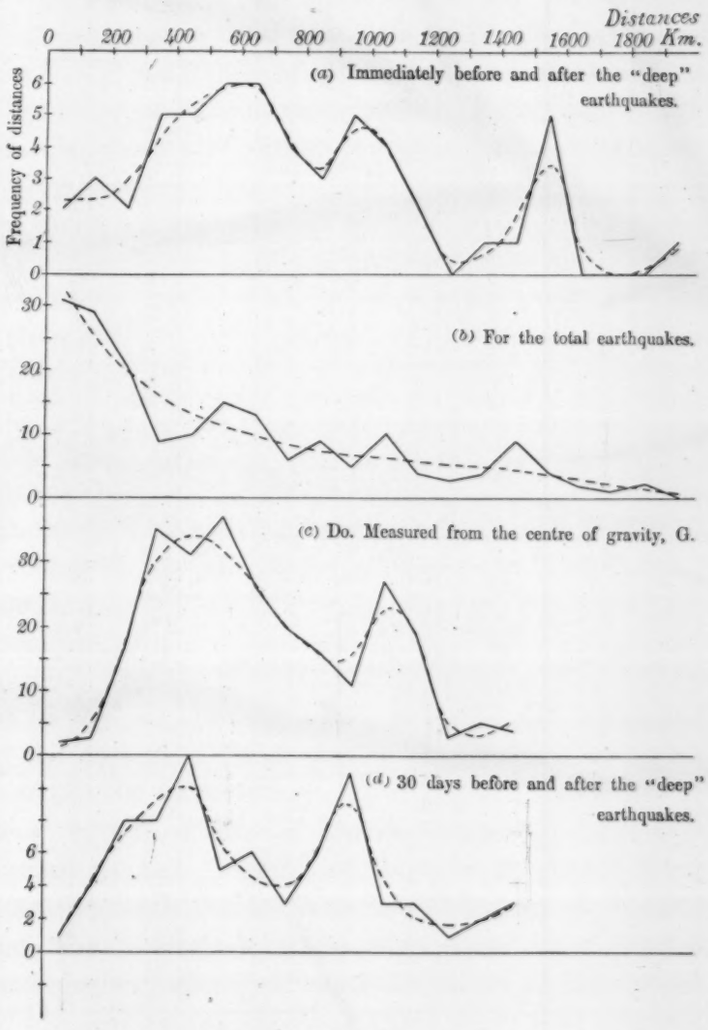
Distances
0 200 400 600 800 1000 1200 1400 1600 1800 Km.
Frequency of distances
(a) Immediately before and after the "deep" earthquakes.
(b) For the total earthquakes.
(c) Do. Measured from the centre of gravity, G.
(d) 30 days before and after the "deep" earthquakes.

Fig. 1. Frequency and distance curve for the "conspicuous and rather conspicuous" earthquakes.

Formosa, during the same period above cited, were taken, and similar *distance-frequency* curve was drawn as shown in Fig. 1, *c*. This curve shows the similar character as the preceding curve (Fig. 1, *a*), except that the maximum at 1550 *km*. has disappeared, as the origin, from which the distances are to be measured was defined at the middle part of Japan.

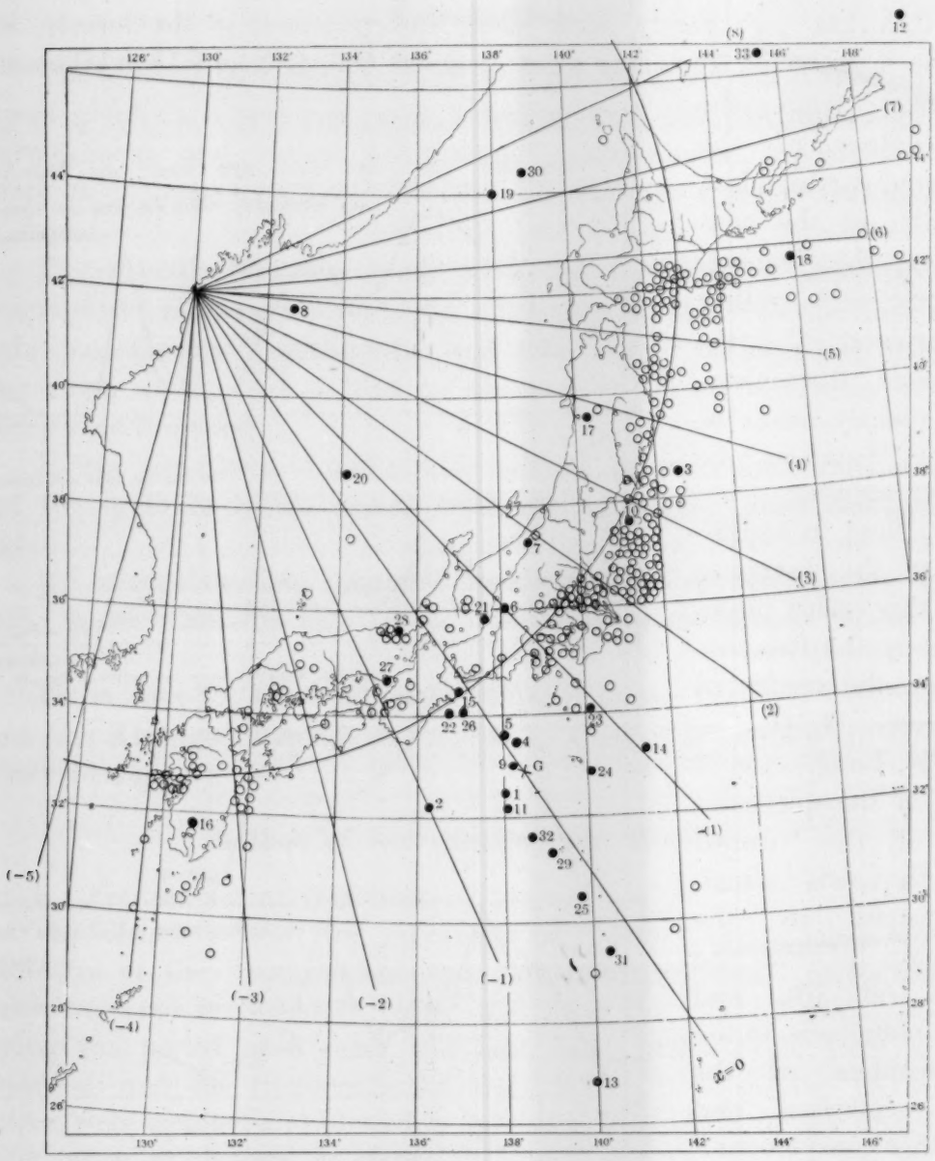

Fig. 2. ●: "deep" earthquakes;
○: conspicuous or rather conspicuous earthquakes.

A similar characteristic curve may be drawn with reference to the earthquakes which occurred within 30 days before and after the "deep" earthquakes, as shown in Fig. 1, *d*.

Next, we have drawn a circle with a radius of 1050 *km.*, and with a point in the coast of N. Corea (Lat.=42°N, Long.=130°E) as centre, of which the circumference touches the coast of Sanriku and the promontory Murotozaki in Tosa. The circular arc was divided into equal sectors by radii vector subtending an angle of 10°, $x=-5, -4, \ldots -1, 1, 2, \ldots 8$, where the prime vector $x=0$ passes through the centre of gravity, G, as shown in Fig. 2, in which, the epicentres of the "conspicuous or rather conspicuous" earthquakes and the "deep" earthquakes are marked by ○ and ●, respectively, the numbers affixed to the epicentres of the latter class, showing the order of time of occurrence. Referring to this map, the number of "conspicuous and rather conspicuous" earthquakes, and also that of "deep" earthquakes falling in each sector were respectively counted, and plotted against the sector number, x, as shown in Fig. 3, *a*, *b*, respectively.

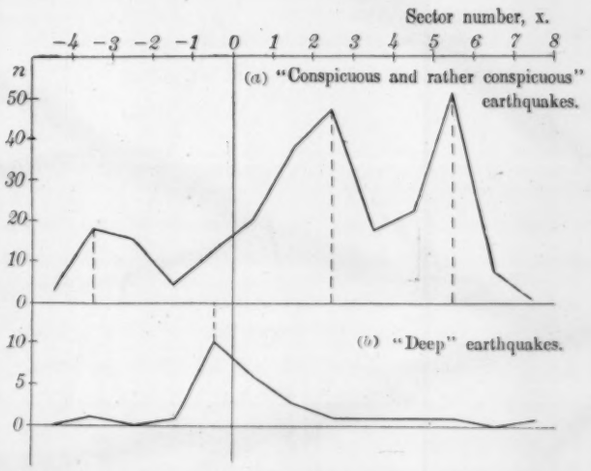

Fig. 3. Number of earthquakes in various regions.

From these curves, we remark that, near the point of maximum frequency of the "deep" earthquakes, very few "conspicuous and rather conspicuous" earthquakes occur, and that three conspicuous maxima of frequencies of the latter are found in the regions at −30°, 30°, and 60° measured from the maximum of the former. These results essentially agree with the preceding results as may be expected.

With regard to these results, Prof. T. Terada suggested, that if a spherical part of the crust at the "deep" earthquake epicentre lying several hundred kilometres beneath the earth surface, happens to expand or yield by some cause, the maximum stress may occur in a conical surface with semivertical angle of about 45° and the vertex at the centre of sphere, and the fracture may propagate along these directions towards the earth surface. Therefore, the "conspicuous and rather conspicuous" earthquakes of shallow origin rarely occur near the epicentral region of

the "deep" earthquakes, but frequently occur in the regions about 500 *km.* apart, which distance is comparable to the depth of the "deep" earthquakes.

To investigate the character of radial (i. e. in the direction normal to the arc of Japan) distribution of the "deep" earthquakes, the radial distances, y, ($+y$, directed outward, or towards Pacific Ocean side) were measured from the circumference of the circle above described (Fig. 2), and plotted against the time axis, as shown in Fig. 4, in which the times of occurrences of the "destructive" carthquakes and the great volcanic eruptions were marked on the curve, and on the time axis, by | and ○ respectively. The result seems to show some alternate radial "transfer" of epicentres of the "deep" earthquakes with the period of 3·5 years, as far as can be judged from the present scanty materials.

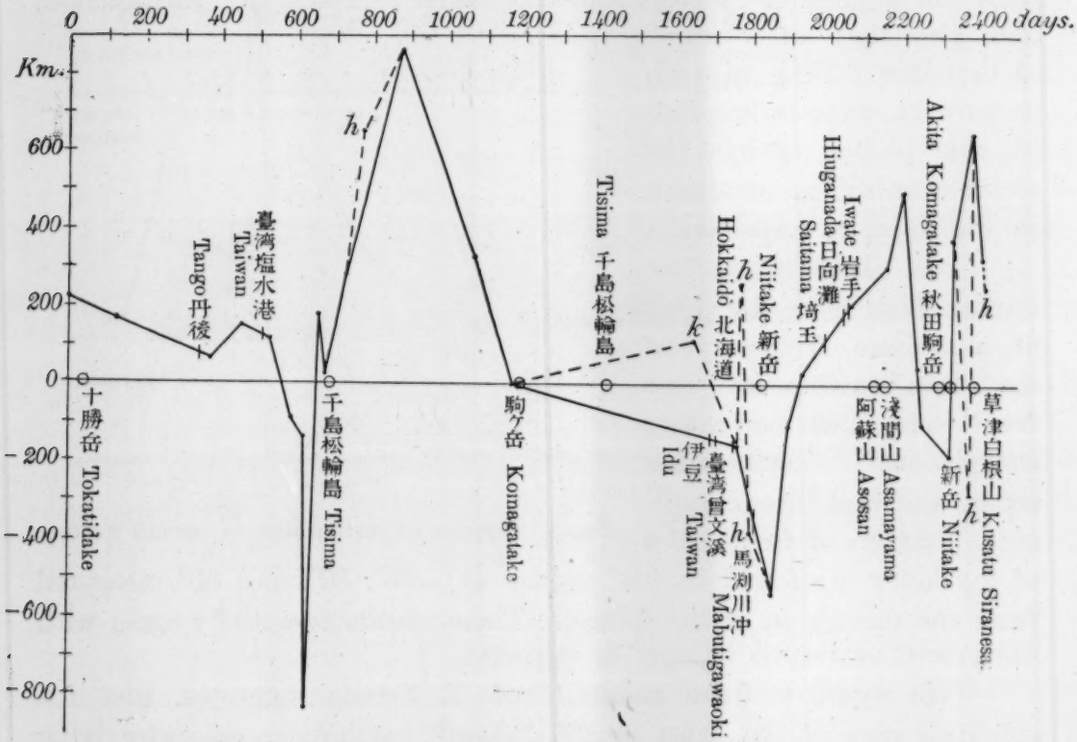

Fig. 4. Time and radial (normal to the arc of Japan) distance diagram for "deep" earthquakes. Dotted line is obtained, if we include the earthquakes in Hokkaidô and Kyûsyû.

h: near Hokkaidô, k: near Kyûsyû.

| "destructive" earthquakes.

○ great volcanic eruption.

2. *Relation between Earthquakes and Cyclones.*

The number, n, (a) of the "deep" earthquakes above cited, for successive 3 months, was counted and plotted against the time axis, those which occurred near Hokkaidô being omitted, as shown in Fig. 5, a. Similarly, (b) for the "conspicuous and rather conspicuous" earthquakes, which occurred in the region from Kyûsyû to the sea off Sanriku ($x=-4\ldots.+4$), and (c) also for those which occurred in the maximum-frequency-regions only, i. e., near Kyûsyû and near the sea off Iwaki, as well as (e) for the "felt" earthquakes, which occurred in the region from Wakayama to Idu ($x=-1\ldots.+1$), the curves for n were drawn

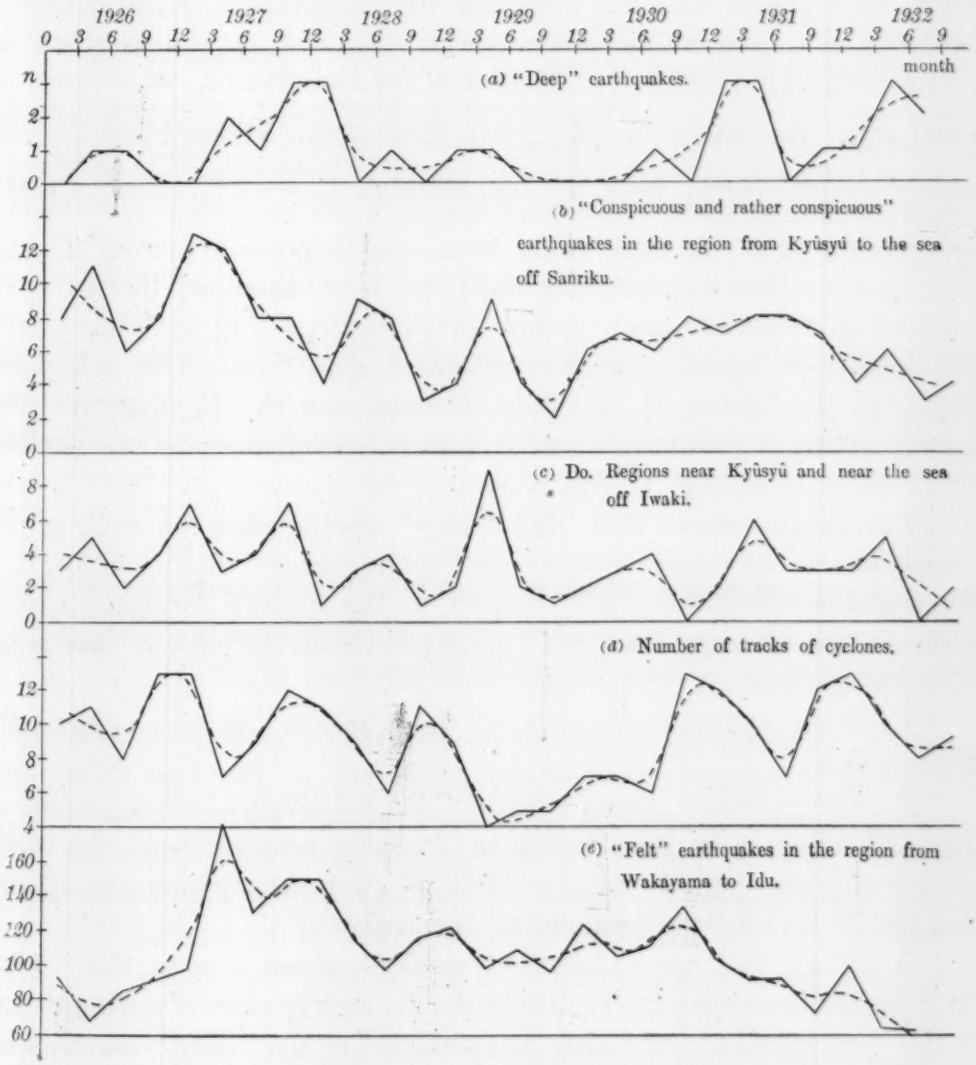

Fig. 5. Number of earthquakes and the tracks of cyclones for three months.

as shown in Fig. 5, b, c, and e, respectively. On the other hand, (d) the number of tracks of cyclones, which passed across the line $x=0$, between the limitted length of $y=\pm 1000\,km.$, for successive 3 months, were counted, and similarly plotted as shown in Fig. 5, d.

Looking at these curves, there seems to exist some fluctuations of a long period superposed upon an annual period.

Comparing the curves for the "deep" as well as the "conspicuous and rather conspicuous" earthquakes, with that for the cyclone, we may recognize some parallelism between the fluctuations of the longer period, and a nearly opposite course between those of annual period in general. Thus, we assumed that the curve for the earthquakes, E, to consist of two parts, i. e., one of the longer period, E_l, and the other of annual period, E_a, and $E=E_l+E_a$. Similarly, for the cyclons, we denoted by $C=C_l+C_a$. Assuming $C_l=kE_l$, and $C_a=-kE_a$, where $k=\frac{\sum|\Delta C|}{\sum|\Delta E|}$, we have $C_l=\frac{1}{2}(C+kE)$. Now, if the relation, $C_a=-kE_a$, holds exactly, C_l- curve, thus obtained, must be a smooth periodic curve. Though it is by no means so smooth actually, we have smoothed this curve by connecting successive mean points. The readings of C_l were taken from this smoothed curve, and the values of $C_a=C-C_l$, were calculated. Similarly, the values of E_a were obtained, and C_a-E_a diagrams were drawn, taking 4 combinations of respective earthquakes and the cyclone, above cited, as shown in Fig. 6, a, b, c, d.

The results show that the "deep" earthquakes as well as the "conspicuous and rather conspicuous" earthquakes of the two kinds, have the negative correlations with respect to the cyclone for some extent, while on the contrary, the "felt" earthquakes has the positive correlation with the cyclone.

As to the physical meaning of these results, we may suggest the followings :—

a) The excessive stress, stored in the relatively shallow portion of the earth crust, may be released by frequent occurrence of the earthquakes of such a degree as the "felt" earthquakes, which are affected directly by the cyclone frequenting the region.

b) When the release of the excessive stress due to the "felt" earthquakes is comparatively little, then the earthquakes of such a degree as the "conspicuous and rather conspicuous" or the "deep" earthquakes will occur.

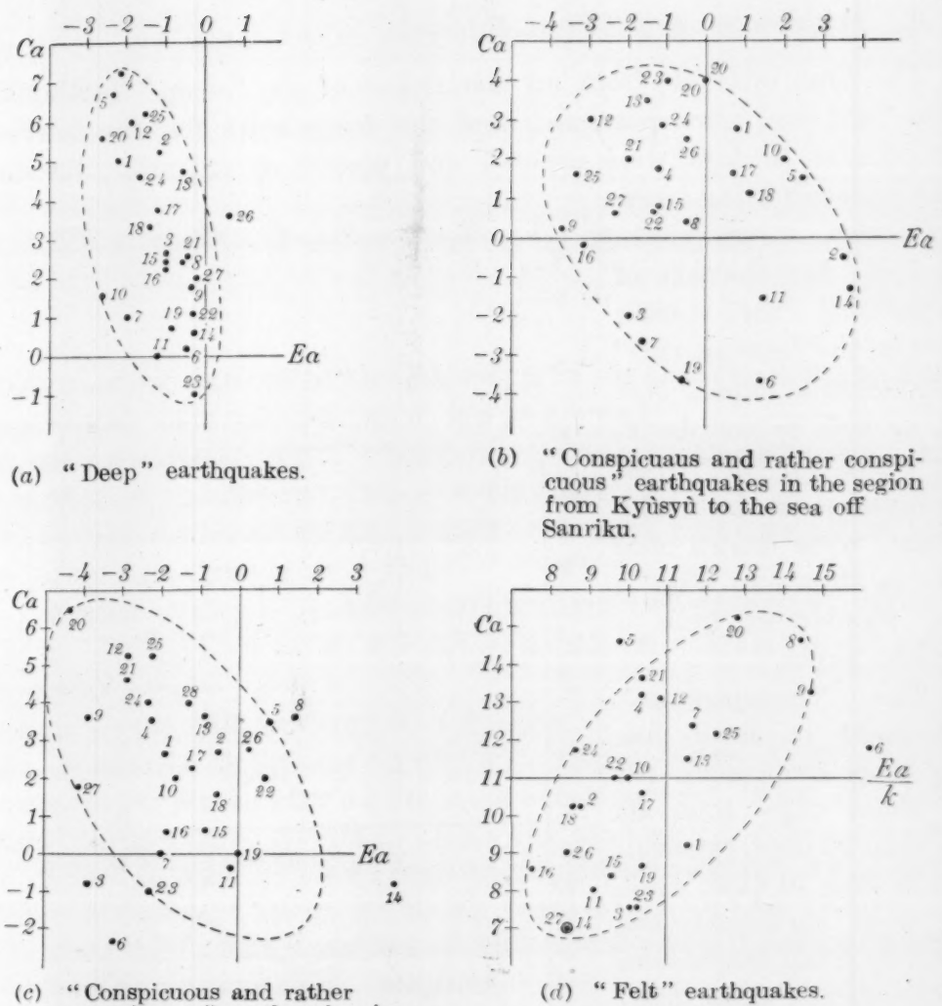

(*a*) "Deep" earthquakes.

(*b*) "Conspicuaus and rather conspicuous" earthquakes in the segion from Kyùsyù to the sea off Sanriku.

(*c*) "Conspicuous and rather conspicuous" earthquakes in maximum-frequency-regions only.

(*d*) "Felt" earthquakes.

Fig. 6. Earthquakes and cyclones curves.

In the case of those "conspicuous and rather conspicuous" earthquakes which occurred in the maximum-frequency-regions only, apart from the "deep" earthquake region by some 500 *km.*, the relation is not so clear as in the other cases, the cyclonic effect being probobly effaced by other causes such as the characteristic "habit" of those districts with regard to the occurrence of earthquakes; nevertheless, we have a small negative correlation coefficient of $-0{\cdot}23$, applying the ordinary formula for calculation.

3. *Frequencies of the Time Intervals.*

The time intervals from an occurrence of the "deep" earthquake to the next one, were examined, and the frequencies for the intervals of successive 10 days, were counted and plotted as ordinates, the days of the intervals being taken as abscissa, as shown in Fig. 7, *b*. For the sake of comparison, the similar curve for the "conspicuous" earthquakes in Japan, N=124, as well as the deviation curve for the Great Earthquakes in the world, N=421, were drawn once more as shown in Fig. 7, *a*, *c*, reproduced from a previous paper.[2]

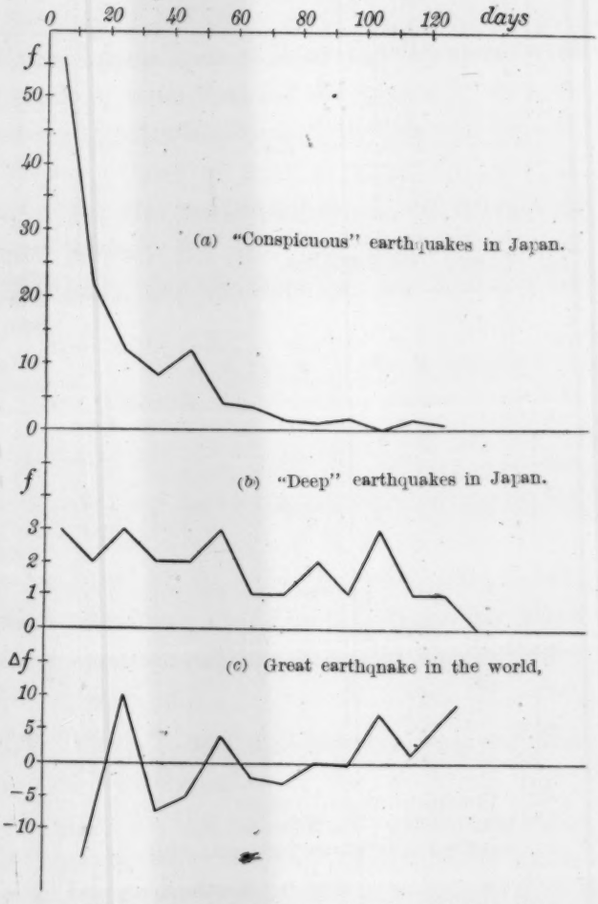

Fig. 7. Frequencies of the time intervals.

The "conspicuous" earthquake in Japan has very large frequencies for the short time intervals less than 20 days, especially, less than 10 days, while the "deep" earthquake has relatively small frequencies for the shorter time intervals compared with the case of purely accidental distribution.

The "deep" earthquake seems to show the periods of about 27·5, 55, and 105 days, which nearly correspond to the period of rotation of the sun, 27·3 days, relative to the earth, in fair coincidence with those for the Great Earthquakes in the world.

In conclusion, I wish to express my best thanks to Prof. T. Terada under whose supervision the entire work has been carried out and who

2) *loc. cit.*, 1).

has given me many useful suggestions throughout the course of my investigation.

---

27. 日本に於ける地震の分布

山口生知

本研究は，前論文「地震の時間的及び空間的分布に就て」の續きとして特に日本に於ける深層地震前後の顯著及び稍顯著地震の分布に就いて，調査したものである．

卽ち顯著及び稍顯著地震の震源と，深層地震の震源との間に存する地理的關係を研究し，延いては，深層地震の起り方の機巧に關して何か一つの手掛りを得んと試みた．

又之等の地震と所謂深層地震帶を通過した低氣壓との間の關係を見出さん事をも望んだ．之等の結果として吾々は次の事柄を知つた．

(1) 深層地震の前後に於いては，顯著及び稍顯著地震は深層地震の震源附近に於いて起ることは極めて稀にして，此處より約 500 粁，及び 1000 粁，等の地點に於いて最も起り易いことを知つた．(第一圖參照)

此結果に關し寺田寅彥博士は次の如き考へを暗示された．

卽ち「地球の表面より數百粁の深さの處に深層地震の震源たるべき地殼の或る球狀の部分が何等かの原因に依つて，膨脹或は收縮するならば，この球の中心に頂點を持ち，半頂角 45° なる圓錐面上に於いて最大應力が起り，其の破壞は，これ等の方向に沿ふて地表に向つて傳はるものと考へられる．それ故に淺い震源を有する顯著及び稍顯著地震は，深層地震の震源附近に起ること稀にして深層地震の深さと同程度なる約 500 粁を隔つる地方に屢々起ることゝなるものであらう」．と

(2) 深層地震並びに顯著及び稍顯著地震は低氣壓と負の相關々係を有し，有感地震と低氣壓とは正の相關々係あることが認められる．(第六圖參照)

此の物理學的意義に關しては，吾々は次のように考へることが出來るかと思ふ．

卽ち地殼の比較的淺い場所に蓄積された餘分の應力は，直接低氣壓の影響を受けて，屢々誘發されるところの有感地震程度の地震に依つて，濟し崩し的に解放される．

而してこの蓄積された餘分の應力の解放が比較的少ないような時に，顯著及び稍顯著地震，或は深層地震が起るものと考へられる．

(3) 時間的分布に就いて言はれることは，日本に於ける顯著地震は 20 日以內特に 10 日以內と云ふような短い時間的間隔內に於いて，非常に多く起り易いのに反し，深層地震は，純然たる偶發的分布の場合と比較すれば，短い間隔內に於いて起る度數が割合に少ないと言ふことである．

又深層地震は太陽の自轉の週期 27·3 日に相當する 27·5 日，55 日，及び 105 日と云ふ週期を持つてゐる．而して之等の週期が世界地震の週期とよく一致して居ると云ふことは，面白いことゝ思ふ．(第七圖參照)

---

28. *Some Statistical Problems concerning Initial Earthquake Motion. (The First Report.)*

By Takaharu FUKUTOMI,

Mitsui Institute of Marine Biology.

(Read Feb. 21, 1933.—Received June 20, 1933.)

1. Geographical Distribution of Initial Vertical Motion of Earthquakes observed at a Particular Station.

The presence of similarity of "Push" or "Pull" of initial motion due to earthquakes occurring at nearly the same place in the Kwantô district and observed at a particular station, has already been pointed out by the writer[1] and Mr. F. Kishinouye.[2] As the Seismometrical Data for recent and older years were gained, and also there happened the necessity to reconsider the mechanism of earthquake occurrence, the writer came again to discuss this problem.

For this purpose, the writer selected earthquakes with distinct initial motion among those which were felt at Tôkyô with unaided sense and which occurred within, say, a circle of a radius of about 160 km., Tôkyô at its centre, during about 18 years from 1914 up to 1931. As for the epicentres, the writer adopted the results obtained by Mr. Ch. Yasuda to whom the writer is greatly indepted. The writer has selected the records of the vertical motion seismographs, on the ground of the facts[3] that the initial motion of the earthquakes originating in the Kwantô district are more pronounced in vertical component than in horizontal, and that the direction of the initial motion indicated by horizontal component was not always coincident with that of epicentre. The writer classified the earthquakes above selected into two categories according to the direction of the initial motion indicated at a particular station. According as the direction of the initial motion of an earthquake is upward or downward, he will indicate the epicentre of the earthquake with mark ○ or with • respectively on the map as shown in Fig. 1. Table I and Fig. 1 (a), (b) are the results of Tôkyô observation. As

1) T. FUKUTOMI, *Disin*, **3** (1931), 592.
2) F. KISHINOUYE, *Disin*, **4** (1932), 18.
3) T. MATUZAWA, *Jap. Journ. Astr. Geophys.*, **4** (1926), 1-33.

the epicentres of earthquakes occurred during the ten years from 1914 to 1923 are considered to have a certain amount of error of position owning to wants of materials, they were shown in Fig. 1 (b) distingui-

Table I (a). Earthquakes of 1914–1923.

No.	Time of Occurrence at Hôngô				Direction of Initial Motion	No.	Time of Occurrence at Hôngô				Direction of Initial Motion
		h	m	s				h	m	s	
1	1914, Oct. 8th	10	38	28	upward	46	1918, July 26th	5	50	41	downward
2	„ Oct. 12th	2	28	54	„	47	„ July 30th	3	0	41	„
3	„ Dec. 20th	0	47	19	„	48	„ Oct. 4th	11	56	32	„
4	1915, Mar. 5th	15	11	49	downward	49	„ Oct. 15th	12	30	2	upward
5	„ Apr. 6th	3	31	49	upward	50	„ Oct. 17th	8	58	33	„
6	„ Apr. 25th	2	10	7	downward	51	„ Oct. 23rd	20	41	47	„
7	„ May 19th	5	45	27	„	52	1919, Jan. 24th	12	26	7	downward
8	„ May 27th	15	13	22	„	53	„ Feb. 12th	11	27	47	„
9	„ June 20th	1	0	55	„	54	„ Mar. 4th	21	4	6	„
10	„ June 25th	1	18	39	upward	55	„ Apr. 7th	10	28	36	upward
11	„ June 27th	22	16	0	downward	56	„ May 20th	9	45	22	„
12	„ Oct. 3rd	6	29	24	„	57	„ Aug. 4th	3	9	21	„
13	„ Oct. 7th	19	13	39	„	58	„ Aug. 4th	5	27	57	downward
14	„ Oct. 26th	22	55	2	upward	59	„ Aug. 4th	5	53	40	upward
15	„ Dec. 29th	9	36	26	„	60	„ Aug. 15th	11	6	42	downward
16	1916, Jan. 14th	11	57	31	„	61	„ Dec. 20th	9	28	41	upward
17	„ Aug. 21st	23	32	50	downward	62	1920, July 2nd	4	57	49	„
18	„ Aug. 28th	0	40	49	„	63	„ Nov. 9th	2	38	20	„
19	„ Oct. 8th	2	8	51	„	64	„ Dec. 3rd	8	40	27	„
20	„ Feb. 22th	18	11	49	„	65	„ Dec. 5th	4	45	40	downward
21	„ Nov. 3rd	15	4	5	„	66	„ Dec. 20th	5	11	27	upward
22	„ Nov. 6th	4	14	9	upward	67	1921, Feb. 14th	12	0	37	downward
23	„ Dec. 8th	20	10	53	downward	68	„ Apr. 18th	1	33	57	„
24	1917, Jan. 21st	2	39	1	upward	69	„ July 26th	7	45	48	upward
25	„ Jan. 23rd	0	29	9	downward	70	„ Oct. 2nd	23	58	20	downward
26	„ Jan. 27th	2	26	3	„	71	„ Nov. 29th	13	16	1	upward
27	„ Jan. 29th	12	25	18	„	72	„ Nov. 20th	17	4	45	downward
28	„ May 8th	21	48	45	„	73	„ Dec. 8th	21	31	41	upward
29	„ June 10th	7	41	23	„	74	1922, Apr. 26th	—	—	—	downward
30	„ June 29th	1	28	45	upward	75	„ May 9th	12	28	57	upward
31	„ July 29th	9	18	15	„	76	„ June 26th	3	41	23	„
32	„ Aug. 10th	3	24	26	downward	77	„ Nov. 9th	5	16	31	downward
33	„ Sept. 4th	11	41	20	upward	78	„ Dec. 27th	18	31	9	upward
34	„ Oct. 5th	11	22	57	„	79	„ Oct. 6th	1	48	38	„
35	„ Oct. 17th	3	3	42	downward	80	1923, Jan. 26th	21	35	45	„
36	„ Oct. 22nd	23	48	50	upward	81	„ Jan. 27th	14	4	17	downward
37	„ Nov. 6th	2	40	10	downward	82	„ Feb. 6th	6	27	49	„
38	„ Dec. 7th	22	12	44	upward	83	„ Feb. 12th	3	26	41	„
39	1918, Apr. 18th	11	35	32	downward	84	„ May 31st	14	56	14	„
40	„ Apr. 19th	7	22	37	upward	85	„ June 2nd	2	25	16	upward
41	„ Apr. 30th	21	46	51	downward	86	„ June 13th	1	49	47	downward
42	„ May 7th	15	28	59	„						
43	„ May 31st	13	56	50	upward						
44	„ June 24th	11	25	21	„						
45	„ June 26th	22	46	18	„						

Table I (b). Earthquake of 1923–1931.

No.	Time of Occurrence at Hôngô	Direction of Initial Motion				
		Hôngô (Tôkyô)	Kamakura	Tyôsi	Kakioka	Kumagai
	h m s					
1	1923, Sept. 1st 12 40 20	downward				
2	„ Sept. 1st 12 48 03	upward				
3	„ Sept. 1st 13 58 32	„				
4	„ Sept. 1st 14 22 49	downward				
5	„ Sept. 1st 16 38 21	upward				
6	„ Sept. 2nd 11 46 55	„				
7	„ Sept. 2nd 14 10 21	downward				
8	„ Sept. 2nd 18 27 04	„				
9	„ Sept. 2nd 18 49 02	„				
10	„ Sept. 2nd 23 16 46	„				
11	„ Sept. 26th 17 24 03	upward				
12	„ Oct. 5th 22 05 46	„				
13	„ Oct. 17th 3 4 05	„				
14	„ Nov. 1st 1 37 17	„				
15	„ Nov. 5th 5 45 15	„				
16	„ Nov. 22th 1 32 41	„				
17	„ Nov. 22th 2 0 26	„				
18	„ Dec. 11th 19 7 56	downward				
19	1924, Jan. 15th 5 50 24	upward				
20	„ Jan. 21st 0 33 59	„				
21	„ Mar. 5th 12 7 24	„				
22	„ Apr. 1st 4 5 58	„				
23	„ Apr. 20th 1 13 20	„				
24	„ May 14th 17 06 —	„				
25	„ May 21st 10 32 02	downward				
26	„ May 25th 12 10 5	„				
27	„ May 31st 21 2 48	upward				
28	„ May 31st 21 4 7	„				
29	„ June 1st 0 26 49	„				
30	„ June 23rd 7 32 2	„				
31	„ June 24th 3 30 31	downward				
32	„ July 4th 6 30 —	„				
33	„ July 14th 2 19 41	„				
34	„ Aug. 6th 23 22 49	„		upward		
35	„ Aug. 9th 20 45 58	upward				
36	„ Aug. 15th 3 3 10	downward		downward		
37	„ Aug. 17th 10 46 —	upward		upward		
38	„ Aug. 20th 4 29 —	„		downward		
39	„ Aug. 25th 23 31 16	downward				
40	„ Sept. 4th 15 24 13	„		upward		
41	„ Sept. 14th 19 40 —	upward		downward		
42	„ Sept. 18th 10 9 0	„		„		
43	„ Sept. 25th 3 41 —	„		upward		
44	„ Sept. 27th 13 22 26	downward				
45	„ Oct. 3rd 1 31 —	upward				
46	„ Oct. 5th 22 21 —	downward		downward		
47	„ Oct. 5th 22 46 —	„				
48	„ Oct. 8th 23 1 —	upward				
49	„ Oct. 13th 19 6 —	„				
50	„ Oct. 23rd 21 47 —	downward		upward		

(*to be continued.*)

Table I (b). (*continued.*)

No.	Time of Occurrence at Hôngô	Direction of Initial Motion				
		Hôngô (Tôkyô)	Kamakura	Tyôsi	Kakioka	Kumagai
	h m s					
51	1924, Oct. 25th 1 55 1	downward				
52	„ Dec. 29th 21 44 —	„				
53	1925, Jan. 2nd 4 30 55	„				
54	„ Jan. 9th 5 52 7	„		upw rd		
55	„ Jan. 9th 16 1 38	„				
56	„ Jan. 22nd 19 17 58	„		„		
57	„ Jan. 24th 17 26 57	upward		„		
58	„ Feb. 3rd 10 53 56	downward		„		
59	„ Feb. 6th 4 59 13	upward				
60	„ Feb. 13th 16 13 13	„		upward		
61	„ Feb. 14th 9 42 22	„		„		
62	„ Mar. 31st 10 6 47	„		„		
63	„ Apr. 18th 17 5 28	„				
64	„ June 3rd 1 29 8	„				
65	„ June 12th 8 2 35	„				
66	„ July 12th 11 41 5	downward				
67	„ Nov. 6th 3 42 58	upward				
68	„ Nov. 7th 0 13 35	„		upward		
69	„ Dec. 17th 12 39 13	„				
70	1926, Jan. 10th 18 3 —	downward		upward		
71	„ Jan. 15th 22 45 28	upward	upward			
72	„ Jan. 21st 15 7 22	„				
73	„ Jan. 28th 1 36 0	„		downward		
74	„ Feb. 13th 23 58 34	„				
75	„ Feb. 22th 10 20 —	downward				
76	„ Feb. 28th 5 34 5	upward				
77	„ Apr. 18th 15 54 —	downward	upward	upward		
78	„ Apr. 27th 23 17 —	„	„	„		
79	„ May 1st 2 35 —	upward	downward			
80	„ May 19th 1 59 —	„				
81	„ May 20th 20 48 —	„				
82	„ June 22nd 16 13 —	„				
83	„ July 11th 8 1 —	downward	downward	downward		
84	„ July 30th 0 41 —	upward	„			
85	„ Aug. 3rd 18 26 —	downward	„	downward		
86	„ Dec. 13th 7 1 —	„	„	upward		
87	1927, Jan. 2nd 0 20 —	„				
88	„ Jan. 9th 18 18 —	upward				
89	„ Jan. 12th 6 50 —	„				
90	„ Feb. 11th 23 27 13	downward	upward			
91	„ Feb. 25th 18 5 —	„	downward	downward		downward
92	„ May 20th 4 18 —	upward	upward			
93	„ May 26th 17 51 10	„	„			
94	„ May 31st 16 40 8	downward				
95	„ July 9th 6 11 36	„				downward
96	„ July 24th 5 26 44	upward	downward	upward		„
97	„ July 30th 23 18 51	downward	„			„
98	„ Aug. 7th 10 40 23	upward	upward			
99	„ Aug. 12th 5 53 4	downward				
100	„ Aug. 19th 21 43 41	„				upward

(*to be continued.*)

Table I (b). (*continued.*)

No.	Time of Occurrence at Hôngô	Direction of Initial Motion				
		Hôngô (Tôkyô)	Kamakura	Tyôsi	Kakioka	Kumagai
	h m s					
101	1927, Aug. 21st 7 14 27	downward				
102	„ Sept. 5th 9 33 15	„			downward	downward
103	„ Sept. 7th 19 33 36	upward			upward	„
104	„ Sept. 13th 13 56 13	downward		upward		
105	„ Sept. 18th 7 22 10	„				
106	„ Sept. 18th 18 19 52	upward				
107	„ Oct. 11th 10 13 20	downward		upward	downward	downward
108	„ Oct. 12th 2 58 53	upward				
109	„ Oct. 14th 19 7 24	downward				
110	„ Oct. 25th 15 2 29	„	upward			
111	„ Nov. 6th 15 35 2	„				
112	„ Nov. 7th 7 38 11	upward			downward	downward
113	„ Nov. 18th 5 22 18	downward	downward			
114	„ Nov. 30th 7 47 0	upward				
115	„ Dec. 31st 14 51 6	„	upward	upward		upward
116	1928, Jan. 1st 16 17 —	„	downward		upward	downward
117	„ Jan. 3rd 16 31 —	downward	„			
118	„ Jan. 8th 19 6 —	„		upward		
119	„ Jan. 16th 13 8 —	upward		„		
120	„ Feb. 3rd 7 34 —	„				
121	„ Feb. 12th 6 10 —	„	downward	upward	upward	downward
122	„ Feb. 19th 0 — —	„				
123	„ Mar. 1st 1 31 —	downward				
124	„ Mar. 2nd 6 28 —	upward				
125	„ Mar. 23rd 10 21 —	downward			upward	upward
126	„ Apr. 6th 19 33 —	upward				
127	„ Apr. 8th 17 57 —	„				
128	„ Apr. 13th 1 36 —	„		upward	upward	
129	„ Apr. 16th 12 50 —	„				
130	„ Apr. 20th 5 47 —	„				
131	„ May 19th 18 32 —	downward	downward	downward	downward	downward
132	„ May 21st 1 28 —	„	„	upward	upward	„
133	„ May 21st 2 32 —	„		„		
134	„ May 21st 2 58 —	„		„		
135	„ May 21st 4 23 —	„		„		
136	„ May 29th 6 9 —	upward			upward	downward
137	„ May 24th — — —	downward				
138	„ May 30th 12 35 —	„				
139	„ May 31st — — —	„		upward		
140	„ June 2nd 7 54 —	„				
141	„ June 3rd — — —	„				
142	„ June 11th 18 6 —	upward				
143	„ June 26th 7 54 —	downward				
144	„ July 5th 7 53 —	upward				
145	„ July 5th 16 52 —	downward	upward			
146	„ July 10th 9 16 —	upward				
147	„ July 15th 17 7 —	downward	downward			
148	„ July 15th 20 32 —	„				
149	„ Aug. 14th 17 25 —	„		upward		
150	„ Aug. 27th 3 11 —	„		„	downward	downward

(*to be continued.*)

Table I (b). (*continued.*)

No.	Time of Occurrence at Hôngô	Direction of Initial Motion				
		Hôngô (Tôkyô)	Kamakura	Tyôsi	Kakioka	Kumagai
	h m s					
151	1928, Oct. 5th 15 58 —	upward	downward	upward		
152	„ Oct. 7th 22 53 —	„				
153	„ Oct. 15th 15 38 —	„				
154	„ Dec. 13th 12 44 —	„				
155	„ Dec. 14th 5 6 —	„	upward	downward	downward	downward
156	„ Dec. 21st 10 40 —	downward	downward			
157	1929, Jan. 9th 3 7 38	„				downward
158	„ Jan. 21st 11 22 16	„				upward
159	„ Feb. 4th 4 8 33	„				
160	„ Feb. 5th 9 16 32	upward				
161	„ Apr. 14th 21 14 39	„				
162	„ Apr. 16th 9 53 22	downward	downward	downward	downward	downward
163	„ Apr. 18th 3 34 —	„			„	„
164	„ Apr. 23rd 23 16 —	upward	downward		upward	„
165	„ June 8th 11 54 52	„				
166	„ June 8th 18 24 26	„				
167	„ June 14th — — —	downward				
168	„ June 18th 3 34 33	„				
169	„ June 27th 1 49 34	upward				
170	„ July 17th 19 49 33	„	downward	upward		
171	„ July 27th 7 48 26	„	upward	downward	downward	downward
172	„ July 29th 2 33 —	„				
173	„ Sept. 3rd 0 39 —	„				
174	„ Sept. 27th 0 17 —	downward	upward			
175	„ Sept. 30th 4 41 40	upward	upward ?			
176	„ Oct. 20th 1 31 40	„				
177	„ Oct. 31st 22 3 29	downward				
178	„ Nov. 20th 1 31 43	„	downward			
179	„ Nov. 26th 22 9 9	upward	upward			
180	„ Dec. 6th 13 15 52	„	downward			
181	1930, Feb. 3rd 6 1 5	upward				
182	„ Mar. 2nd 2 42 47	downward				
183	„ Apr. 21st 8 36 31	„				
184	„ May 1st 9 58 12	„	downward	upward	downward	downward
185	„ May 1st 10 16 5	„				
186	„ May 1st 13 20 44	„			downward	downward
187	„ May 5th 1 56 33	upward	downward			
188	„ May 16th 4 39 19	downward		downward		
189	„ May 21st 7 11 33	„	upward			
190	„ May 22nd 2 37 24	upward	„			
191	„ May 29th 4 32 11	downward				
192	„ May 24th 1 38 38	„			upward	upward
193	„ June 1st 2 58 43	upward		upward	downward	downward
194	„ Feb. 21st 8 37 15	„	upward			
„	„ Mar. 4th 3 50 53	„	„			
„	„ Mar. 4th 5 11 17	„	„			
„	„ Mar. 9th 4 39 53	„	„			
„	„ Mar. 9th 19 54 49	„	„			
„	„ Mar. 14th 21 5 30	„	„			
„	„ Mar. 21st 23 4 24	„	„			

(*to be continued.*)

Table I (b). (*continued.*)

No.	Time of Occurrence at Hôngô	Direction of Initial Motion				
		Hôngô (Tôkyô)	Kamakura	Tyôsi	Kakioka	Kumagai
	h m s					
194	1930, Mar. 22nd 17 50 52	upward	upward			
„	„ Mar. 26th 14 22 59	„	„			
„	„ Mar. 27th 1 41 47	„	„			
„	„ Mar. 30th 0 6 37	„	„			
„	„ Apr. 1st 23 4 44	„	„			
195	„ June 23rd 15 14 13	downward				
196	„ June 29th 9 25 21	upward				
197	„ July 5th 1 33 55	downward		downward		
198	„ Aug. 17th 18 28 45	upward	downward		upward	upward
199	„ Aug. 20th 2 41 52	downward		downward		
200	„ Sept. 30th 13 55 27	„		upward		
201	„ Oct. 5th 21 4 25	„				
202	„ Oct. 12th 17 58 8	„		upward		
203	„ Oct. 25th 7 22 4	upward				
204	„ Nov. 26th 4 3 6	„	upward	upward	upward	upward
205	„ Dec. 15th 14 22 24	downward		„		
206	„ Dec. 30th 5 57 10	„				
207	1931, Jan. 30th 10 40 30	upward	upward			
208	„ Mar. 10th 3 41 2	downward	downward			
209	„ Mar. 27th 5 25 36	„				
210	„ Apr. 4th 9 16 42	„				
211	„ May 4th 23 48 29	upward	upward ?			
212	„ May 25th 19 27 57	„				
213	„ June 9th 14 8 9	downward				downward
214	„ June 11th 15 16 20	upward				„
215	„ June 14th 7 45 43	downward				
216	„ June 17th 21 9 50	„				upward
217	„ June 17th 22 53 13	„				
218	„ June 23rd 15 15 26	„				
219	„ June 30th 1 8 56	„				
220	„ July 8th 5 46 25	„				
221	„ July 10th 22 10 42	„				downward
222	„ July 26th 10 41 20	„		upward		
223	„ July 28th 11 6 42	upward				
224	„ July 31st 4 46 21	downward				
225	„ Aug. 18th 14 40 42	„		downward		
226	„ Aug. 27th 8 49 33	„				
227	„ Sept. 7th 5 35 5	upward				
228	„ Sept. 9th 4 9 31	„		upward		
229	„ Sept. 16th 21 43 23	downward		downward		
230	„ Sept. 21st 11 20 10	upward		„		
231	„ Sept. 21st 15 21 37	„				
232	„ Sept. 21st 15 49 13	„				
233	„ Sept. 23rd 21 46 19	„				
234	„ Sept. 24th 1 22 41	„				
235	„ Sept. 24th 21 11 26	„				
236	„ Sept. 26th 12 37 43	„				
237	„ Sept. 28th 4 50 41	„		upward		
238	„ Sept. 28th 13 54 28	„				
239	„ Oct. 3rd 2 36 55	„		upward		

(*to be continued.*)

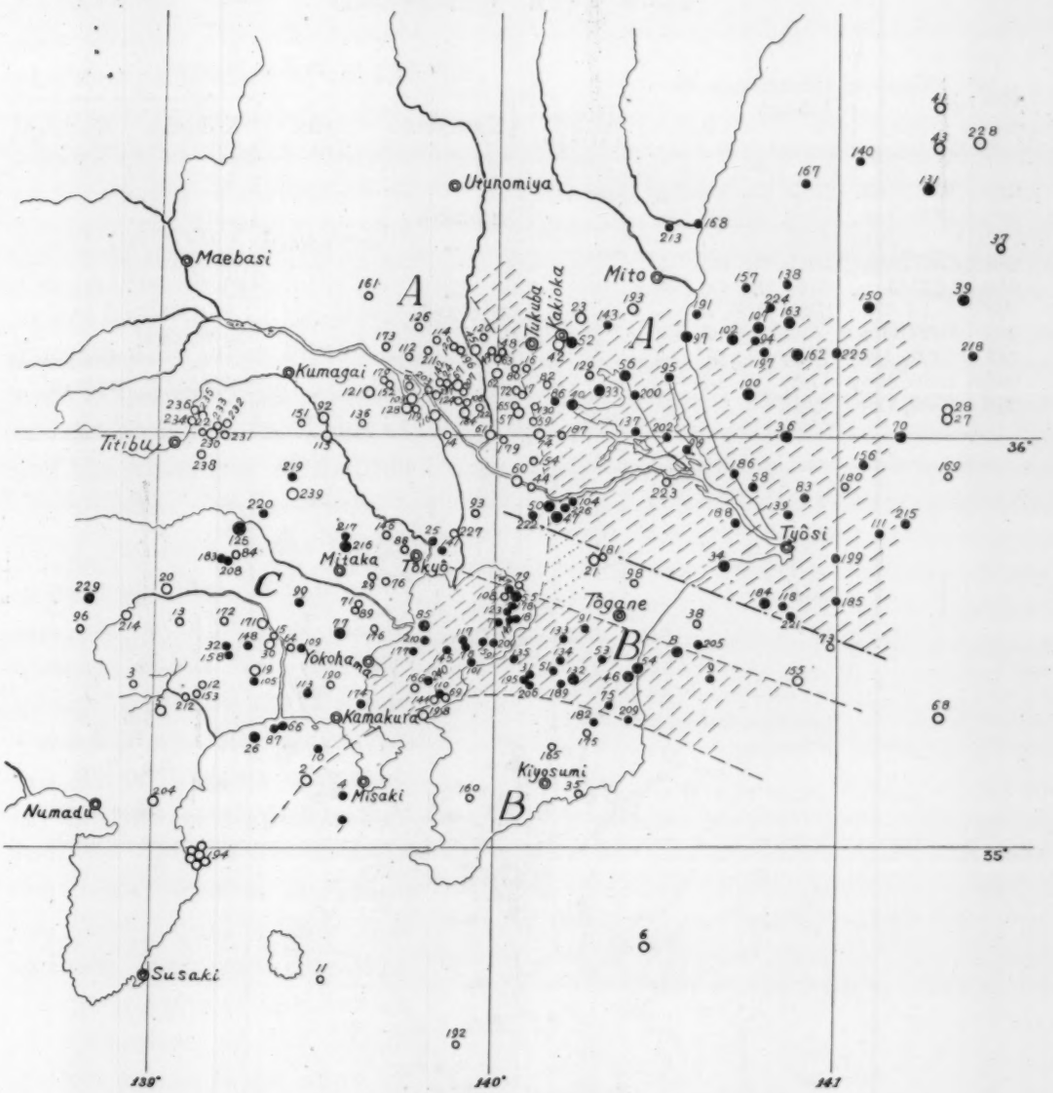

Fig. 1 (a). Distribution of initial motions of earthquakes observed at Hôngô (Tôkyô) from Sept. 1923 up to 1931.

Epicentres of earthquakes which began at Hongô with {upward ○ / downward ●} initial motions. Numerals against the circles correspond to the index number of the earthquakes in Table I. Large circles show the epicentres of larger earthquake.

Table I (b). (*continued.*)

No.	Time of Occurrence at Hôngô	Direction of Initial Motion				
		Hôngô (Tôkyô)	Kamakura	Tyôsi	Kakioka	Kumagai
	h m s					
240	1931, Oct. 13th 21 14 6	downward				
241	1926, Jan. 13th 6 59 —		upward			
242	„ June 27th 7 39 —		„	downward		
243	1927, Mar. 16th 16 46 —		„			
244	1929, Jan. 31st 21 56 —		„			
245	„ Mar. 20th 22 8 —		upward ?			
246	1926, Oct. 3rd 4 3 —				downward	
247	1929, Aug. 16th 22 21 —				„	downward
248	1930, May 17th 6 14 —				upward	upward
249	1932, Dec. 2nd					

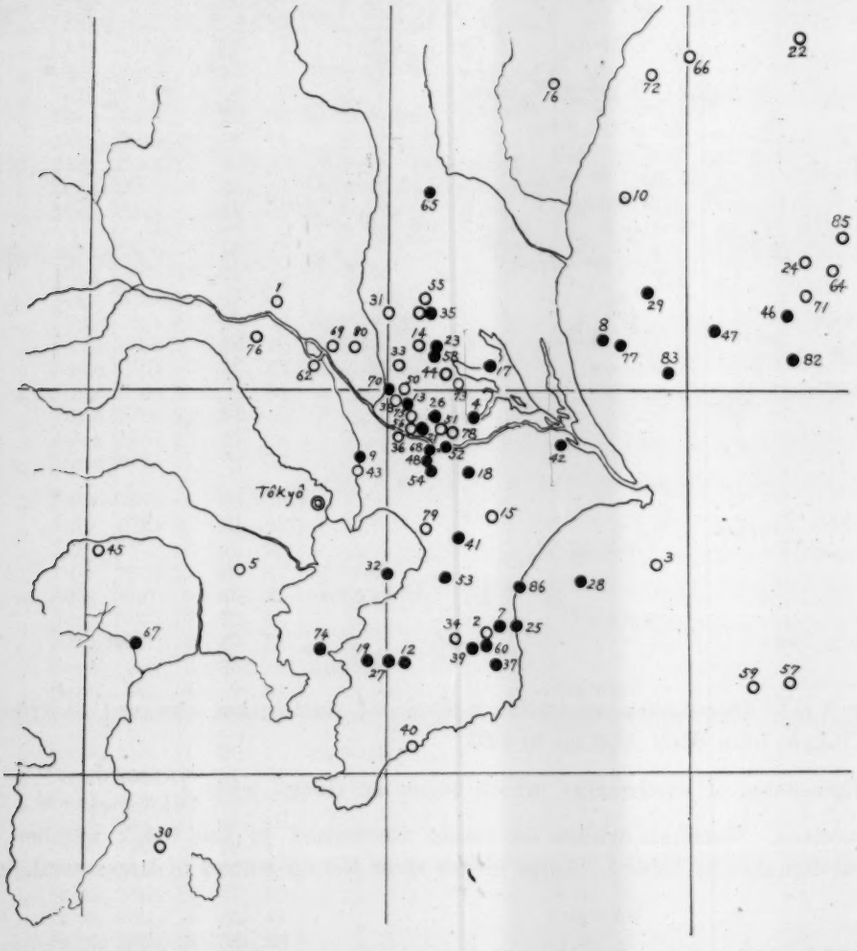

Fig. 1 (b). Distribution of initial motions of earthquakes observed at Hôngô (Tôkyô) from 1914 up to Aug. 1923.

Epicentres of earthquakes which began at Hongô with { upward ○ / downward ● } initial motions.

shing from those occurred after that. The discussion of the distribution of initial motion may be chiefly made regarding to Fig. 1 (a), because similar distribution is found between Fig. 1 (a) and Fig. 1 (b), though it is more or less indistinct in the latter. Figures and large circles in Fig. 1 indicate the number of earthquakes in Table I and the epicentres of distinct earthquakes respectively. Total numbers of the earthquakes adopted here are 337 and the numbers of earthquakes which fall into the groups with the mark ○ and • are 176 and 161 respectively. Thus it seems apparently that the earthquakes that indicate upward direction in the initial motion at Tôkyô are nearly equal to those that indicate downward direction. The geographical distribution of epicentres of the earthquakes seems to be more or less systematic, that is, the epicentres specified with the same sort of mark swarm together into rather definite local groups. Thus, the earthquakes originating in the drainage basin of the River Kinu and Ogai, the southern part of the Bôsô Peninsula, far off the coast of Kasima,

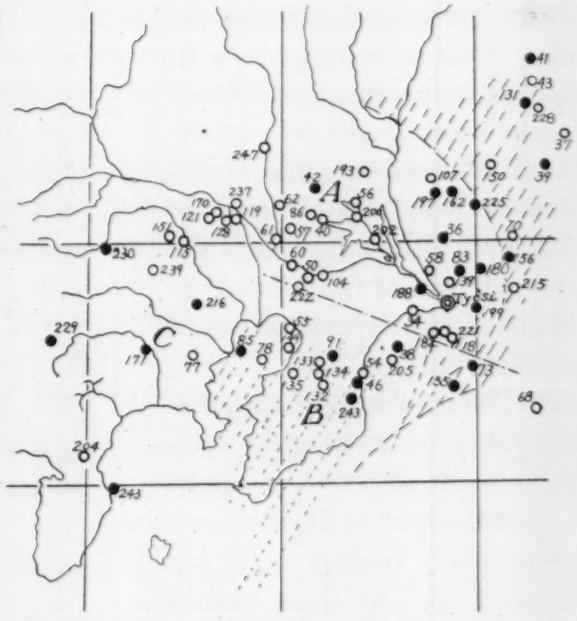

Fig. 1 (c). Distribution of initial motion observed at Tyôsi.
○ upward motion,
• downward motion.

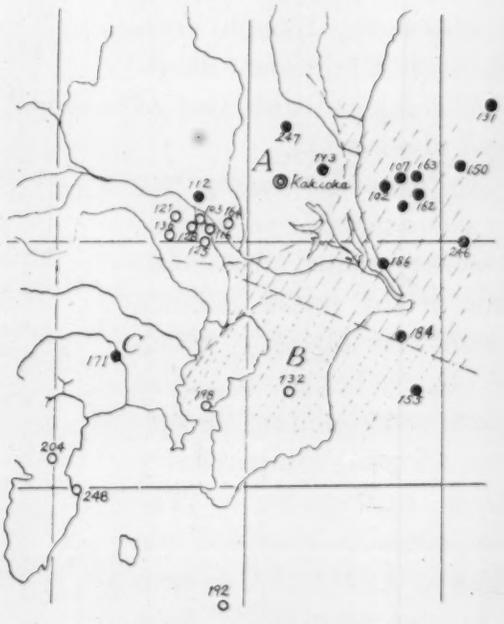

Fig. 1 (d). Distribution of initial motion observed at Kakioka.
○ upward motion,
• downward motion.

Titibu mountain land and the Idu Peninsula bigin with upward movement at Tôkyô, while those generated in the locality containing the Kasumigaura and the littoral of Kasima, Tôkyô Bay and the central part of the Bôsô Peninsula bigin with downward movement.

The results of observation of other seismological stations such as Tyôsi, Kakioka and Kumagai etc. are shown respectively in Fig. 1 (c), (d), (e) and (f). In these results of observation, the geographical distribution of the epicentres specified with the same mark seems to be more or less systematic, though each of them shows different distribution compared with that of Tôkyô observation.

To give the reason for the above-mentioned results, the writer studied the distribution of the initial motions of some earthquakes which were observed at seismological stations sourrounding the epicentre, adopting comparatively distinct earthquakes. The earthquakes are classified into 3 classes, A, B and C according to the position of their epicentres as shown in Fig. 1.

(A) The earthquakes originating in region A (Tone,

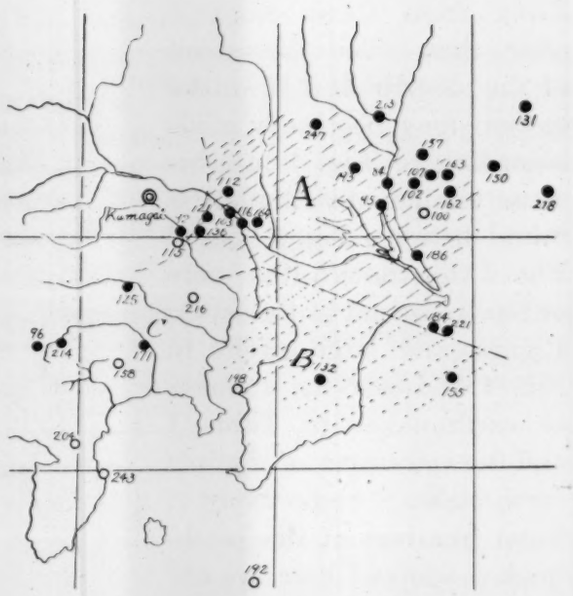

Fig. 1 (e). Distribution of initial motion observed at Kumagai.
○ upward motion,
• downward motion.

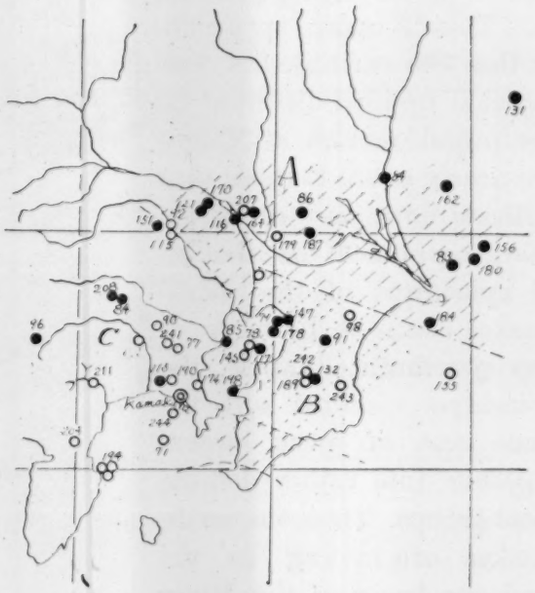

Fig. 1 (f). Distribution of initial motion observed at Kamakura.
○ upward motion,
• downward motion.

Kasima).

Most earthquakes originating in region A show upward or downward motion according as the observatory is situated inside or outside of the nodal ellipse in which the epicentre is included. Fig. 2 (a), (b), (c) indicate the typical examples which occurred in the drainage basin of the River Kinu on Jan. 1, 1928,[4] on Feb. 12, 1928 and off the coast of Tyôsi on May 1, 1930. Some examples of this type were earthquakes of Dec. 13, 1926 (86), May 20, 1927 (92), Sept. 5, 1927 (102), Sept. 7, 1927 (103), Jan. 1, 1928 (116), Feb. 12, 1928 (121), May 19, 1928 (131), Aug. 27, 1928 (150), Oct. 5, 1928 (151), April 16, 1929 (162), April 18, 1929 (163), April 23, 1929 (164), July 17, 1929 (170), May 1, 1930 (184), June 9, 1931 (213), June 9, 1931 (221). The mean dimension of the nodal ellipses is

$a=100$ km., $b=65$ km. (mean co-ordinates of epicentres
$x=-60\sim80$ km., $y=0$ km. relative to the ellipse.)

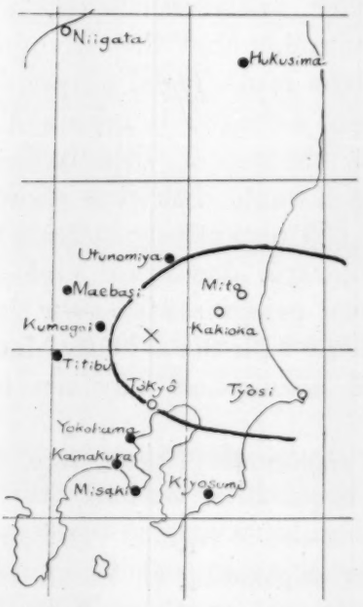

Fig. 2 (a). Distribution of initial motion of the earthq. occurred on Jan. 1, 1928.
× epicentre,
○ upward motion,
● downward motion.

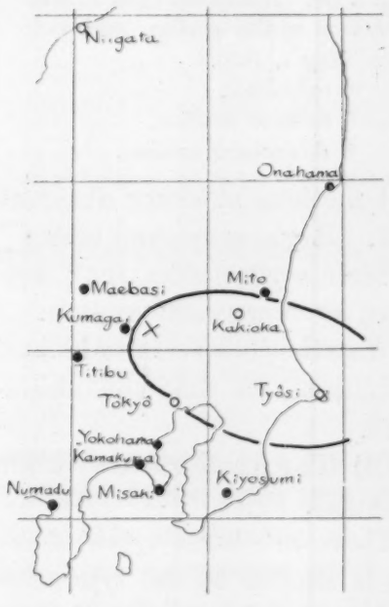

Fig. 2 (b). Distribution of initial motion of the earthq. occurred on Feb. 12, 1928.
× epicentre,
○ upward motion,
● downward motion.

4) M. Ishimoto, *Bull. Earthq. Res. Inst.*, 10 (1932), 449.

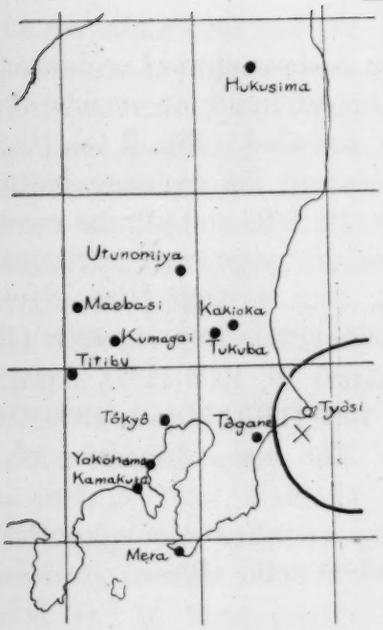

Fig. 2 (c). Distribution of initial motion of the earthq. occurred on May 1, 1930.
× epicentre,
○ upward motion,
● downward motion.

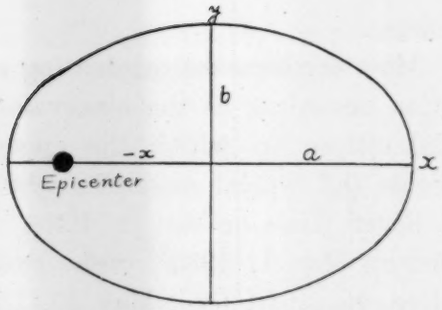

Fig. 3. The nodal ellipse.

h (focal depth) = about 40 km.
Azmuth of the x axis = nearly N 70°W

The above-mentioned results seem to suggest that earthquakes originating in particular region of the Kwantô district have similar mechanism of occurrence. To ascertain this further, the writer has constructed, under the assumption that the earthquakes having the mean nodal ellipse above mentioned occurred in region A, the map of theoretical distribution of initial motions at every observatory in the Kwantô district as shown in Fig. 1. Regions marked with ▭, ▩ and ▩ respectively indicate those in which earthquakes may begin with upward, downward and either upward or downward motion. Now, we can recognized that the theoretical distributions seem to be in fair agreement with the actually observed distributions, so that the above-mentioned assumption may not be so absurd.

(B) The earthquakes originating in region B (Tôkyô Bay, Bôsô Peninsula).

There are three types of earthquakes in the B region. The first of them is similar to the type of earthquakes originating in the A region as shown in the earthquake occurred in the central part of the Bôsô Peninsula on May 21, 1928[5] (Fig. 4). The earthquakes of this type are frequent in the western and the central part of the region and have nearly equal focal depth of about 60 km. The second type of them begins with upward or downward motion according as the observatory

5) M. ISHIMOTO, *loc. cit.*

is inside or outside of the nodal hyperbola which have an asymptote of. about N 70°W as shown for the earthquake occurred off the coast of Kuzyûkuri on Dec. 14, 1928 (Fig. 5). The earthquakes of this type are

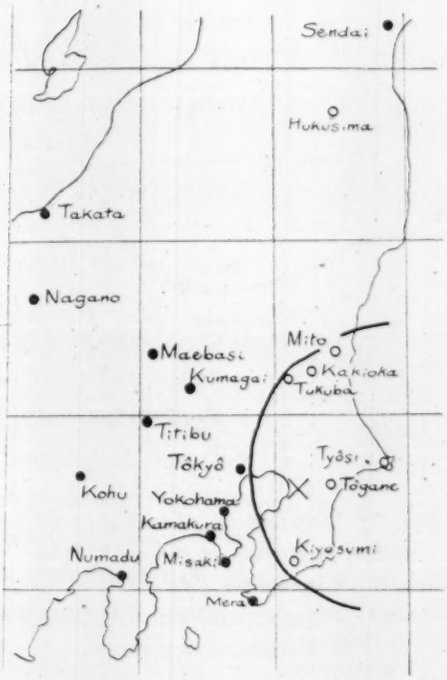

Fig. 4. Distribution of initial motion of earthquake occurred on May 21, 1928.
× epicentre,
○ upward initial motion,
● downward initial motion.

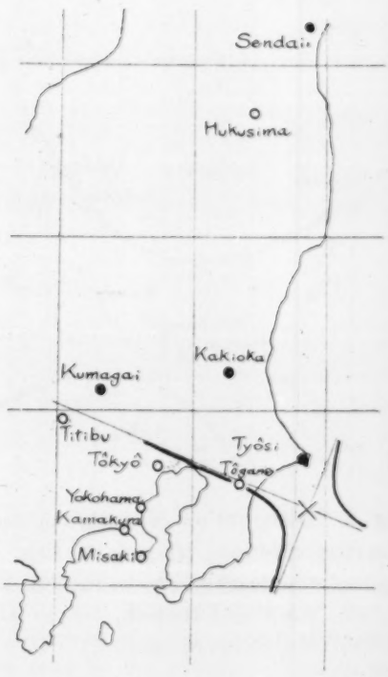

Fig. 5 Distribution of initial motion of earthq. occurred on Dec. 14, 1928.
× epicentre,
○ upward motion,
● downward motion.

frequent in the north-eastern and the eastern parts of the region and have very shallow focal depth of nearly 20 km. The third type bigins with upward or downward motion according as the observatory is within or without of the nodal hyperbola which have asymptotes of N 32°E and N 60°W as shown for the earthquakes of off the coast of Haneda on Aug. 3, 1926[6] and that of the Uraga channel on Aug. 17, 1930 (Fig. 6 & 7). The earthquakes of this type are frequent in the central and south-western parts of the Bôsô Peninsula and have nearly equal focal depth of 70–100 km.

6) M. Ishimoto, *loc. cit.*

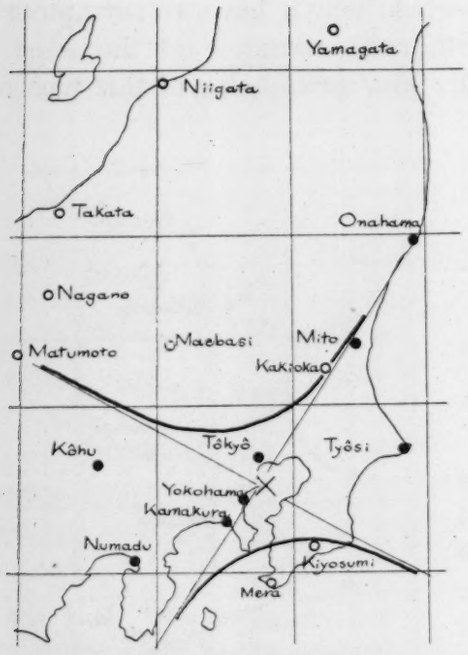

Fig. 6. Distribution of initial motion of earthq. occurred on Aug. 3, 1926.
× epicentre,
○ upward motion,
● downward motion,

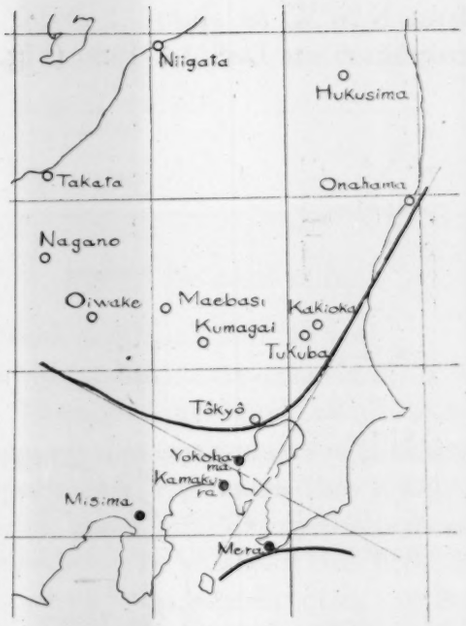

Fig. 7. Distribution of initial motion of earthq. occurred on Aug. 17, 1930.
× epicentre,
○ upward motion,
● downward motion.

The writer again constructed under the assumption that the earthquakes having one of the three nodal curves above mentioned occured in particular parts of the B region, the map of theoretical distribution of initial motions at every observatory in the Kwantô district as shown in Fig. 1. We can again recognize that the theoretical distributions seem to be in fair agreement with the actually observed distributions in the B region.

In the region except A and B, the distribution is not so systematic, especially in the Sagami region. Though it is not very obvious for the want of materials, it may be said that earthquakes occurred in this region have very shallow focal depth of less than 20 km. and show the nodal hyperbola of initial earthquake motion direction of asymptotes of which are not so constant. This may be attributable to the complicated structure of the surface layer of the earth.

The nodal curves of the earthquakes originating in any one of the three regions above quoted are shown in Fig. 8 with the mark -○- as the nodal ellipse and)×(as the nodal hyperbola. It may be interesting that

we can draw a line distinctly separating the regions where earthquakes with nodal ellipse only occur from those where earthquakes with hyperbola take place exclusively.

The writer studied above the initial motion of earthquakes originating in the Kwantô district and came to the conclusion that the earthquakes originating in the two regions A and B have respectively the constant mechanisms of occurrence of earthquake.

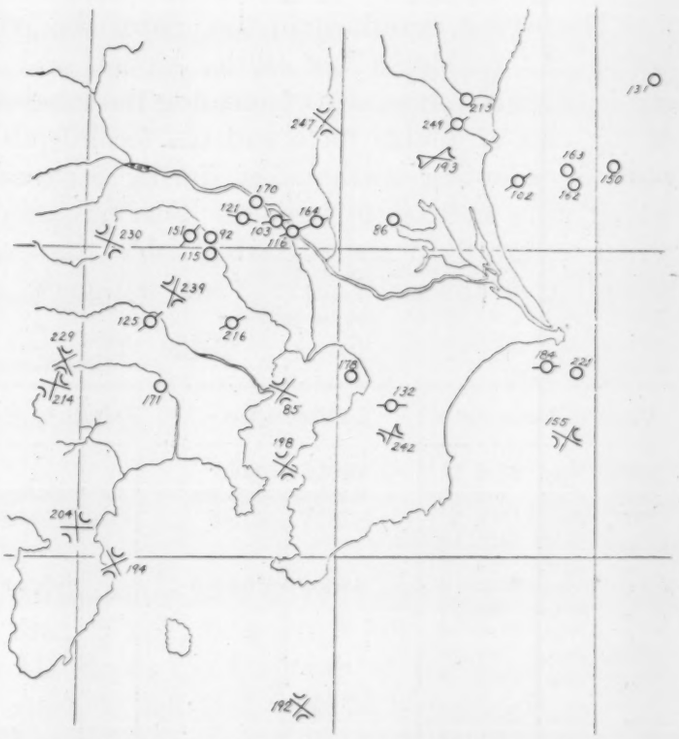

Fig. 8. Distribution of epicentres of nodal ellipse (-○-) and nodal hyperbola (›‹) in the Kwantô district. Bar or crossed bar indicate direction of majer axis or asymptotes respectively. Figures refer to the number of earthquake in table I.

2. On the Relation between Mechanism and Focal Depth of Earthquakes.

Dr. T. Shida[7] investigated the distribution of displacements by two forces of equal magnitude and opposite direction acting on a line at the hypocentre, and indicated actual examples of the mechanism of earthquake occurrence. Since then, Dr. M. Ishimoto[8] ascertained that most of the earthquakes occurred in Japan may be explained as those of this mechanism. In the earthquakes of this mechanism, "pull-push" distribution of initial motion on the earth-surface has nodal curves of second degree, namely ellipse or hyperbola in general, and parabola in special cases according to the inclination of the axis of double force to the earth-surface.

7) T. Shida, Read before the meeting of Imp. Earthq. Inv. Comm. (1917).
8) M. Ishimoto, *loc. cit.*

The writer examined in this paper the relation between the nodal curves of "pull-push" of initial motion and the focal depths of the earthquakes as a first step of examing the relation between the inclination of the axis of double force and the focal depth of earthquake. For the purpose, adopting earthquakes during 8 years from 1925 up to 1932 which were sufficiently large for determination of the nodal curve, the writer assigned in the following table the mark E or H respectively according as the nodal curve of an earthquake was ellipse or hyperbola.

Table II.

Time of Occurrence	Epicentre	Depth of Focus in Km	Form of Nodal Curve
1925, May 23rd 11h	Kinki district	33	Hyperbola
1926, Aug. 3rd 18	Kwantô district	about 70	„
1927, Jan. 15th 23	Kinki district	about 450	„
„ Mar. 7th 18	„	15	„
„ Apr. 1st 6	„	18	„
„ May 20th 4	Kwantô district	about 60	Ellipse
„ Sept. 7th 19	„	0~5	„
„ Dec. 31st 14	„	140	„
1928, Jan. 1st 16	„	35	„
„ Feb. 12th 6	„	40	„
„ Mar. 23rd 10	„	32	„
„ May 19th 18	„	40~25	„
„ May 21st 1	„	about 60	„
„ Aug. 27th 3	„	within 50 (not so shallow)	„
„ Oct. 5th 15	„	about 60	„
„ Dec. 14th 5	„	about 20	Hyperbola
1929, Apr. 16th 9	„	50~25	Ellipse
„ Apr. 18th 3	„	„	„
„ Apr. 23rd 23	„	about 30	„
„ June 3rd 6	Tyûbu district	360	„
„ July 4th 5	Kinki district	28	Hyperbola
„ July 27th 7	Kwantô district	23	Ellipse
„ Aug. 16th 22	„	about 100	Hyperbola
„ Nov. 20th 1	„	10	Ellipse
1930, Feb. 21st 8	„	within 20	Hyperbola
„ Feb. 22nd 20	„	„	„
„ Mar. 4th 3	„	„	„
„ Mar. 22th 17	„	„	„
„ May 1st 13	„	about 30	Ellipse
„ May 17th 6	„	within 20	Hyperbola
„ May 24th 1	„	80	„
„ June 1st 2	„	about 50	„
„ Aug. 17th 18	„	about 50	„
„ Sept. 29th 13	Kyûsyû district	300	„
„ Oct. 17th 6	Tyûbu district	within 20	„
„ Oct. 17th 6	„	„	„
„ Nov. 26th 4	„	within 10	„
„ Dec. 20th 23	Tyûgoku district	within 25	„
„ Dec 20th 23	„	„	„
„ Dec. 21th 21	„	„	„

(to be continued.)

Table II. (*continued.*)

Time of Occurrence	Epicentre	Depth of Focus in Km	Form of Nodal Curve
1931, Feb. 20th 14h	Northern part of the Japan Sea	about 400	Hyperbola
„ June 2nd 11	Tyûbu district	250	„
„ June 9th 14	Kwantô district	70	Ellipse
„ June 11th 15	Tyûbu district	10	Hyperbola
„ May 12th 3	Ôu district	within 50	Ellipse
„ May 26th 18	„	within 40	„
„ June 17th 21	Kwantô district	45	„
„ June 23rd 15	„	within 50	„
„ July 10th 22	„	30	„
„ Aug. 10th 23	Tyûbu district	3	Hyperbola
„ Sept. 16th 21	„	20	„
„ Sept. 21st 11	Kwantô district	about 20	„
„ Oct. 3rd 2	„	24	„
1932, June 22nd 9	„	40	„
„ Nov. 18th 5	Kyûsyû district	very deep	„
„ Dec. 2nd 2	Kwantô district	40	Ellipse

Now, classifying the earthquakes into three classes according to the focal depth, namely less than 25 km., between 25 km. and 50 km., and more than 50 km., Table III shows the frequency of earthquakes which fall into the group with mark E and that with H respectively.

Table III.

Locality / Focal depth in Km.	Kwantô district	Tyûbu, Kinki, Tyûgoku districts	Other district	Total		Calculated % $\alpha=45°$ (55°)
				Obs.	Reduced %	
0~25	E 3	E 0	E 0	E 3	13·6	29 (18)
	H 8	H 11	H 0	H 19	86·4	71 (82)
25~50	E 13	E 0	E 2	E 15	79·0	29 (18)
	H· 2	H 2	H 0	H 4	21·0	71 (82)
More than 50	E 5	E 1	E 0	E 6	40·0	29 (18)
	H 4	H 2	H 3	H 9	60·0	71 (82)
Total	E 21	E 1	E 2	E 24	42·9	29 (18)
	H 14	H 15	H 3	H 32	57·1	71 (82)

If the direction of the axis of double force is equally probable in all directions, the ratio of expectation of earthquakes with nodal ellipse to that of earthquakes with hyperbola may be

$$\frac{N_E}{N_H}=\frac{1-\sin\alpha}{\sin\alpha}=\begin{cases}\alpha=45^\circ \ldots \dfrac{0\cdot29}{0\cdot71}\\ \alpha=55^\circ \ldots \dfrac{0\cdot18}{0\cdot82}\end{cases}$$

where α is the angle between the axis of double force and the generating line of the nodal cone as shown in Fig. 9 and its numerical value is considered to be 45° or 55°.

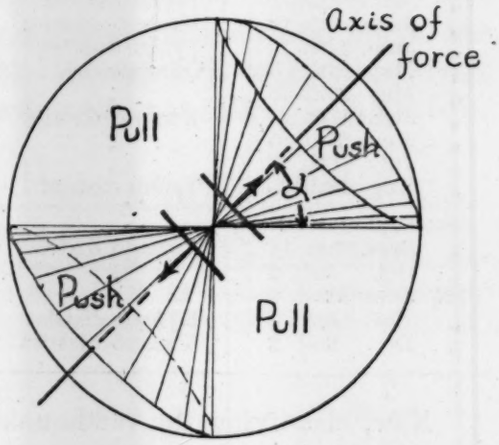

Fig. 9. Mechanism of earthquake.

Now, comparing the observed value with the calculated one, we can recognize that the earthquakes of nodal hyperbola are frequent in the uppermost layer and those of nodal ellipse also frequent in the middle layer, and observed ratio of N_E and N_H is nearly equal to the calculated value in the lowermost layer. It may be a natural consequence that earthquakes of nodal hyperbola are frequent in the uppermost layer, and the ratio of observed N_E to N_H is nearly equal to the calculated value in the lower layer, when it is taken into consideration that the normal stress is equal to zero in the earth's surface and the effect of the surface on elastic conditions may become smaller in the deeper layer. But, it may be an interesting fact, for the conjecture of the structure of middle layer that earthquakes of nodal ellipse are frequent in that layer.

In conclusion, the writer expresses his cordial thanks to Professor Akitune Imamura and Professor Takeo Matuzawa for their kind advices and the revision of this paper and to Mr. Ch. Yasuda for his kind information of the positions of epicentres.

28. 地震初動に關した二三の統計的問題

三井海洋生物學研究所　福　富　孝　治

1. 關東地方の色々な場所に起つた地震の初動の押し引きを或る定まつた觀測所例へば東京本郷で見ると，その押し，引きの分布に規則正しさがある事は既に指摘した所であつたが，其後並に其前の材料に就いても調査したし，又其說明として用ひた地震發生機構に就いても考へ改める必要を生じたので此處に再び此問題を考究した．其結果，是等の押し，引きの分布の規則正しさはその場所場所に起る地震の發生機構が相等しいと云ふ結論に達した．

2. 曾つて志田博士は地震の發生機構として震原に於て一軸上に大きさ相等しく方向相反する二力が外向きに働く場合の問題を解かれ，かゝる發生機構をもつ地震の存在を實證せられた．其後石本博士は我國に起る殆んど全部の地震が此機構で說明せられる事を研究された．此の機構の地震ではこの軸の方向が地表面と如何なる角をなすかに依つて初動の押し，引きの節線が橢圓，双曲線特別な場合として抛物線となる．筆者はこの軸の地表面となす角と地震の震原の深さとの關係を吟味する第一段として最近我國に起つた顯著な地震に就いて初動の押し，引きの節線が橢圓又は双曲線であるかに依つて地震原の深さと如何なる關係があるかを吟味した．其結果は深さ0～35粁では双曲線をなすもの多く，25～50粁では橢圓をなすものが多くあつた．又關東地方に於ては橢圓の節線を持つ地震の起る場所と双曲線の節線を持つ地震の起る場所とが區分せられる事にも注意した．

29. *The Geomorphology and Geology of Northern Idu Peninsula, the Earthquake Fissures of Nov. 26, 1930, and the Pre- and Post-Seismic Crust Deformations.*

By Yanosuke ÔTUKA,

Earthquake Research Institute.

(Received June 20, 1933.)

Contents.

Introduction.
Geology and geomorphology of Northern Idu Peninsula.
I. Region of the Kanogawa Alluvial plain.
1) Ukisimagahara.
2) Misima fan.
3) Hirai terrace.
4) Hatake terrace.
5) Kasiwanokubo terrace.
II. The western slope of Mt. Hakone.
III. The Tanakayama forest.
IV. The Simotanna slope.
V. The Tanna fault zone.
1) The Tasiro basin.
2) The Tanna basin.
3) The Atami pass fault.
4) The Ainohara fault.
5) The Karuizawa step fault.
6) Ukihasi and Tawarano.
7) The Yamabusi fault.
8) The Yasuno fault.
9) The Oono valley.
10) River pattern on both side of the Tanna fault zone.
VI. The Simoômi province.
VII. Tha Darumayama slope.
VIII. The Wasidu mountainland.
Brief summaries of the Post Tertiary geologic history of Northern Idu.
The grouud disturbances of Nov. 26, 1930.
I. The Kanogawa Alluvial plain.
II. The southwestern slope of Mt. Hakone.
III. The Tanakayama forest.
IV. The Simotanna province.
V. The Tanna fault zone.
a. Tasiro basin.

b. Karuizawa and Tanna basin.
c. The Ikenoyama pass.
d. Ukihasi basin.
e. Tawarano basin.
f. The Oono fault.

VI. The Simoômi province.
VII. The Darumayama province.
VIII. The Wasidu province.

Summary of ground disturbances of Nov. 26, 1930.

Pre- and Post-seismic crust deformation, ground disturbances associated with the earthquake of Nov. 1930, and the geomorphology of these regions.

Introduction.

Since the severe Northern Idu seismic disturbance of Nov. 26, 1930, the writer has been engaged chiefly in the geological survey of the disturbed region, in studying the earthquake fissures of Nov. 26, 1930, and the pre- and post-seismic crust deformations from the viewpoints of geomorphology, to the ground disturbances, and to the pre- and post-seismic crust deformations. Studies on somewhat similar lines have also been made, geologically, by Ihara and Ishii, and Tayama and Niino,[1] and geomorphologically by Prof. Tsujimura and Okayama.[2]

The megatectonical position of Northern Idu was dealt with by the writer in brief in an earlier paper,[3] namely, that northern Idu is a geotectonic unit, situated in the southern part of the "Fossa Magna," a weak transversal geotectonic zone in the central part of the main Japanese island formed during the Neogene, and by which the Kwanto mountain-land and Northeast Japan are

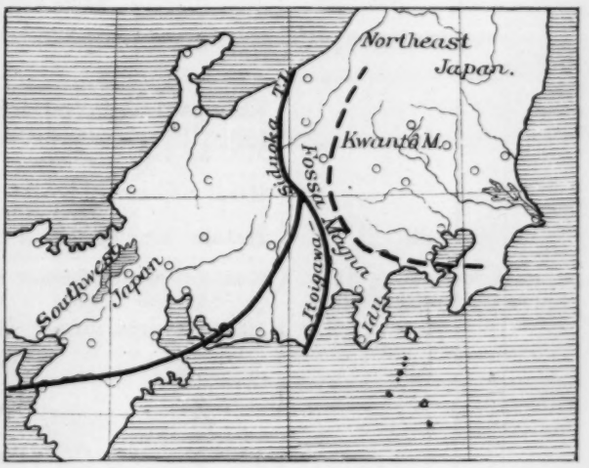

Fig. 1. The central part of Japan.

1) K. Ihara and K. Ishii, *Imp. Geol. Survey Japan*, Rep., 112 (1932).
R. Tayama, *Report of Saitô Hôonkwai*, 11 (1931).
R. Tayama and H. Niino, *Report of Saitô Hôonkwa* , 13 (1931).
2) T. Tsujimura and T. Okayama, *Jour. Geol. Soc., Tokyo*, 38 (1931).
T. Tsujimura, Collection of papers in Ootuka Tirigakukwai, 1 (1932).
3) Y. Ôtuka, *Bull. Earthq. Res. Inst.*, 11 (1932).

Table I.

Stratigraphic sequence of Idu[4] Peninsula according to Tayama and Niino, (1931).		
Quaternary.	Alluvium.	Recent deposits.
		PL-Terrace gravel beds.
	Upper Diluviu, Diluvium.	Loam.
		M- Terrace beds.
		T- Terrace beds.
	Lower Diluvium.	Atami group.
		Zyo group.
Tertiary.	Simoda series.	Matuzaki group.
		Sirahama group.
		Tateiwa group.
		Aoiti group.
	Yugasima series.	Yugasima group.

Table II.

Stratigraphic sequence of north Idu Peninsula according to Ishii and Ihara,[5] (1932).	
Alluvial deposits.	
Diluvium.	Terrace deposits.
	Talus and boulder deposits.
	Kasiwatoge beds.
	Ajiro beds.
	Zyo beds.
Tertiary.	

Table III.

Stratigraphic sequence proposed by the present writer.		
a.	Kanogawa Alluvial deposits.	
	Misima fan.	
du.	Hirai terrace deposits.	
	Hatake terrace deposits.	
	Kasiwanokubo terrace deposits.	
dlm.	Darumayama volc. deposits	Hakone volc. deposits.
		Yugahara volc. deposits.
		Tanakayama volc. deposits.
dll.	Zyo beds.	Simotanna beds.
		(Hata beds of Kuno).
Idu old Neogene Tertiary.		

4) R. TAYAMA and H. NIINO, *op. cit.*, (1931).

5) K. IHARA and K. ISHII, *op. cit.*, (1932).

seperated from the Outer and Inner zone of Southwest Japan (Fig. 1). For convenience, the writer has divided Northern Idu into the following eight geologic provinces.

1. The Kano-gawa Alluvial plain.
2. The western slope of Mt. Hakone.
3. The Tanakayama forest.
4. The Simotanna province.
5. The Tanna fault zone.
6. The Simoômi slope.
7. The Darumayama slope.
8. The Wasidu mountainland.

The post-Tertiary geology and geomorphology of the geologic provinces above listed follow.

The stratigraphy of Idu Peninsula was studied by R. Tayama and

Table IV.

Stratigraphic sequence proposed by H. Kuno.

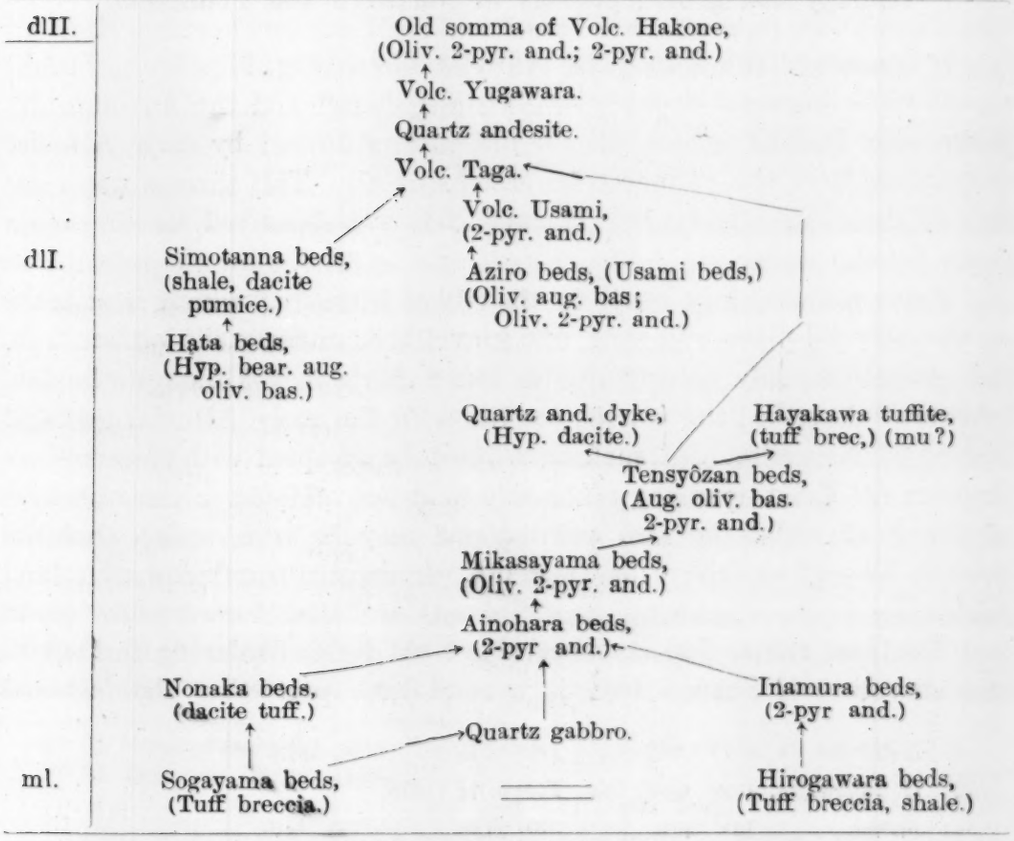

H. Niino and by Ishii and Ihara before the occurrence of the Idu earthquake, the preliminary reports of the former two having appeared in the Report of Saitô Hôonkwai and those of the latter two in the "Journal of Geography in Japan, or Imp. Geol. Surv. Japan, Report."

The following tables show the succession of the strata as deduced by the above authors (Tab. I, II.) The present writer's conclusion regarding the stratigraphy as based on his field observation differs but little from the above tables. But in the division of the older formations, the writer reserves comments as the field surveyed by him was not wide enough. In this paper therefore the writer treats these old formations as one under the name of "the Idu old Neogene." The stratigraphic division of the last-named writers is given in Table II, which shows some advances in the division of igneous rocks as compared with that of the first-named. The stratigraphic succession used by the writer is shown in table III in descending order. Recently the following stratigraphic sequence was proposed by H. Kuno (Table IV.)

Geology and geomorphology of Northern Idu Peninsula.

I. Region of the Kanogawa Alluvial Plain (Fig. 2).

1) The lagoonal deposits of Ukisimagahara[6] and the fluviatile deposits near Daiba,[7] which fill the old valleys formed by early Alluvial erosion are here the youngest formations of all. The chronologic relation of these deposits to the Misima[8] fan was described in an earlier paper by the writer.

From well-sinkings made in the city of Numadu,[9] which is situated on the Alluvial plain, silt, sand, and gravel beds underlie the surface soils, the gravels usually occupying the lower horizon. Although the late Ishiwara[10] described the marine condition in the early Alluvial geologic history of Numadu, his conclusions must be accepted with reserve since they are not based upon any conclusive evidence. However the upheaval of the land which he also pointed out may be true, seeing that the present Kanogawa (river) has a depth of about 10m. below the land surface.

The low ridge, 5m. or more above sea level, bordering the northeast shoreline of Suruga bay, is a sand-dune protecting the lagoonal

6) 浮島ヶ原. 7) 大場. 8) 三島. 9). 沼津.

10) H. ISHIWARA, *Jour. Geol. Soc., Tokyo*, **17** (1898).

11) 川西村. 12) 守山. 13) 北條. 14) 塚山.

deposits of Ukisimagahara from the sea. AIIu* in Fig. 2 shows the lowland of Ukishimagahara and AIIs the sand-dune. AIId* in Fig. 2, representing the Alluvial plain near Daiba previously discussed by the writer, is almost contemporaneous with the Ukisimagahara (AIIu and AIIs).

The loose brown sand beds exposed on the shore of the Kano in Kawanisi-mura[11] correspond to all (d.) The isolated mountain, Moriyama,[12] near Hôzyo,[13] a small hill in Tukayama,[14] consist of Neogene rocks. They are relic peaks of basal Neogene rocks, which the deposits of aII could not completely cover owing to the relatively great height of the former, which was increased during early Alluvial epoch.

The Alluvial beds of the Tanna and Tasiro basins will be described in a later chapter.

2) AI. Misima fan. As already described in an earlier paper of the writer the Misima fan is a fan-spread skirt of Mt. Huzi. On the river wall and floor of the Kise and Sakai, dissecting the fan, may be seen exposed the lava of Huzi. The lava is similar to that cropping out on the surface of the fan near the Ri-o, hostelyn. This means that the early ejecta of volcano Huzi had flowed down through the "Susoaidani" (meaning valley between the foot of two mountains) between Mount Hakone and Mount Asitaka, which were already in existence, and spread out to form the beautiful fan shaped topography near Misima, after which the basal lava of Huzi overflowed the surface of the fan. This overflow may antedate the formation of the present Huzi volcanic cone and may be comtemporaneous with or later than the dissection of the western slope of Mount Hakone, for the materials composing the Misima fan are deposited in the dissected valleys of Mt. Hakone. Although there is no palaeontological evidence, the age of the Misima fan may be lowest Alluvium.

According to Prof. Hirabayashi[15] and the late Ishiwara,[16] the lava exposed on the Misima fan is the basal part of the Huzi lava flows, which is composed of Olivine basalt. The distribution of the lava flow on the Misima fan is shown as "al" in Fig. 2. Similar lava is exposed in the valley from Yosida[17] to Ootuki[18] and Saruhasi,[19] all of which are situated on the northeastern foot of Mt. Huzi, and on the southern foot nr. Oomiya.[20]

15) T. Hirabayashi, *Rep. Imp. Earthq. Invest. Comit.*, **16** (1896), (in Japanese).
16) H. Ishiwara, *op. cit.*, (1898).
17) 吉田. 18) 大月. 19) 猿橋. 20) 大宮.
* In Fig. 2, AIIu and AIId are erroneously represented by symbol AII.

Other deposits contemporaneous with the Misima fan are found developed in some of the tributal valleys in this province, but their ages have not yet been definitely determined.

3) Hirai terrace. duIIh. The Hirai terrace, thus called by the present writer, is about 50m. above sea level, and situated east of Daiba. The small village of Hirai,[21] from which the name is derived, is on the eastern corner of the terrace, which slopes down gently toward the Kanogawa Alluvial plain, being only about 20m. above sea-level at Nitta. The materials forming the terrace are horizontally stratified beds of dark reddish brown volcanic ash and yellow pumice, all pointing to the subaqueous origin of these beds. Fig. 3 is a geologic sketch map of this terrace. The western and northern limits of this terrace are bounded by the Raikogawa(river),[22] a tributary of the Kano, by which the Tasiro basin is drained. The south part of the terrace is dissected by the Kakizawa river and its tributaries. The low ridge of the Simotanna province, between the rivers Kakizawa[23] and Raiko, orientated in a S. N. direction, borders the eastern limit of the terrace. On the south-east part of Kasiya,[24] the bordering ridge diminishes in height, being covered by pumiceous materials that compose the Hirai terrace, while the high peaks of the ridge project like isolated hills above the surface of Hirai terrace.

4) Hatake terrace duIIt. Similar terraces are scattered about the east corner of the Kanogawa Alluvial plain from the Hatake[25] Hot springs to Nakoya.[26] They are about 30–40 metres high above sea-level and are long narrow ridges projecting into the Alluvial plain and lying between the lower courses of the valleys that drain the Tanakayama forest to be described later. But the beds composing these terraces are roughly stratified, the size of the pumice being larger than that of Hirai, whose pumiceous beds are underlain by these irregularly stratified pumiceous beds as may be seen on a cutting wall between Hatake and Daiba, in loc. A in Fig. 3. Fig. 4 is a sketch of this wall. The Hirai beds may therefore be younger than that of the Hatake terrace, but their heights are so nearly alike that the surface of these terraces appear as though they were formed during the same geologic age.

Rock terrace of the same height as the Hirai terrace is developed near Nirayama,[27] which consists of Miocene andesite. Near Narutaki,[28] Naka,[29] and Dai,[30] terraces develop in the same way, rising to heights

21) 平井. 22) 來光. 23) 柿澤. 24) 柏屋. 25) 畑毛.
26) 奈古谷. 27) 韮山. 28) 鳴瀧. 29) 中. 30). 臺.

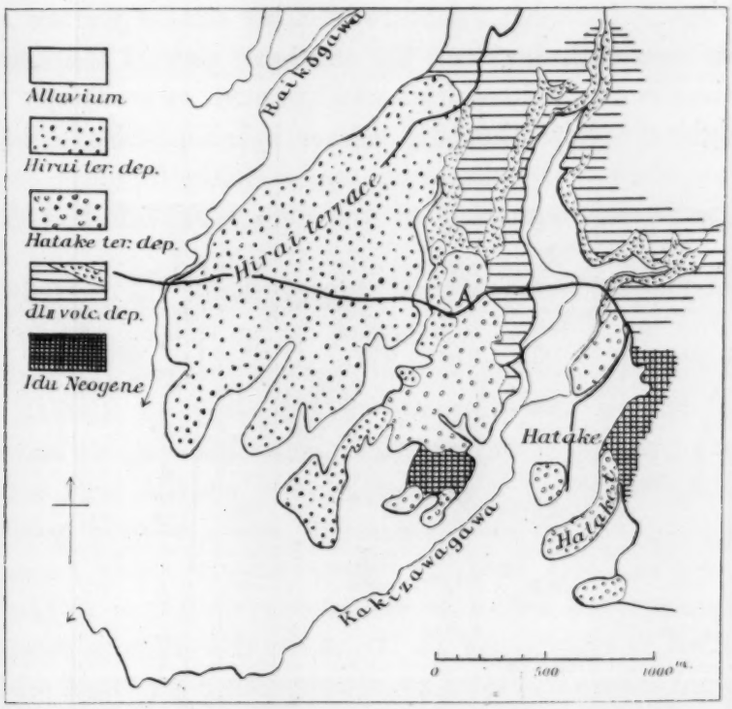

Fig. 3. Geologic sketch map of region near Hatake. (gawa=river).

of 30-35 metres above sea-level.

A similar terrace about 30m. high may also be seen at Ema-mura,[31] on the west side of the Kano. The low hill, about 30-35m. high, on the way from Hora[32] to the southern limit of Uzyo,[33] on the west part (back) of the Nagaoka hot springs is another terrace. The pumice bed composing this terrace crops out on the cutting wall in Uzyo along the highway from Nagaoka to Mito. These pumiceous materials closely resemble those forming the terrace in Hatake. Ishii and Ihara regard these two pumiceous beds in widely seperated localities to be of the same age.

Fig. 4. The exposure of the south wall of excavation on the highway between Hatake and Daiba. (Loc A in Fig. 3.)

A. Andesite and breccia bearing pumiceous sand and gravel. } Hatake t. d.
B. Pumiceous sand and gravel. }
C. Yellow pumiceous bed. } Hirai t. d.
D. Brown volcanic ash. }

31) 江間村. 32) 洞. 33) 有城. 34) 長岡. 35) 三津.

At Bessyo,[36] in Kawanisi-mura, another similar terrace is observed. The terrace near Mihuku,[37] on the southern part of the Kanogawa Alluvial plain, is about 40m. high. Exposures near Takyo[38] along the Simoda highway show that the terrace is composed also of pumiceous

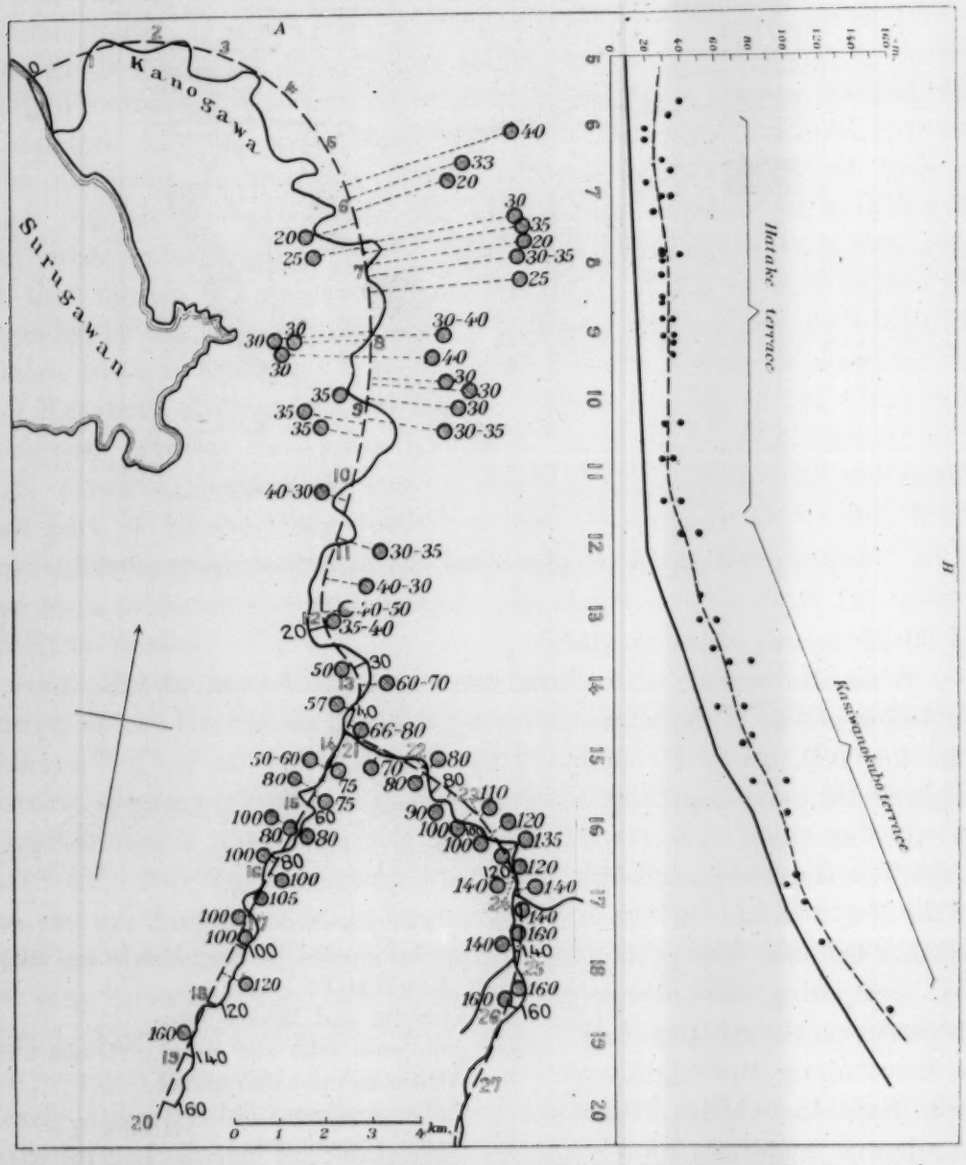

Fig. 16. A. Map shows the areal distribution of Hirai, Hatake and Kasiwanokubo terrace. (Numerals in orlinally type show the heights of terrace. Numerals gothic type show the heights of river floor).
B. Numerals show the vertical distribution of these terraces along the Kanogawa. Full line shows the heights of river floor.

36) 別所. 37) 三福. 38) 田京.

beds. From its height and material it may safely be considered a similar terrace to the Hatake terrace. Of the two terraces of unequal height near the town of Oohito,[39] the heigher has the same height as that of Mihuku, while the lower one gradually transits its height to the Kanogawa Alluvial plain, which diminishes in width in this district. The age of the lower one may be contemporaneous with that of Misima fan.

To summarise, all the foregoing terraces have heights from about 30 to 40m., chiefly consisting of pumiceous material or volcanic ash, excepting, however, the rock terraces near Nirayama, which has little or no gravel. It will be noticed that generally the size of the pumice grows larger as we go northward. The pumice composing the slope of Mount Hakone near Misima closely resembles petrographically that of the terrace near Hatake. The writer therefore believes that the above terrrce has some close relation to the slope of Mt. Hakone. Judging from their heights and their constituent materials the terraces then may be contemporaneous with each other. If so, the terraces of Hatake on the east side of the Kano are contemporaneous with that on the opposites side of the river; and it may be inferred that the pumiceous materials flowed down and filled in the old Kano valley from the north, probably from Mount Hakone, and was denuded to a topographic plain (at the level of the Hatake terrace). The topographic plain of the terrace was then re-excavated by the Kano and left as scattered terraces on both sides of the Kano. The Hirai terrace was no doubt formed in the Hatake terrace during the early stage of this erosion.

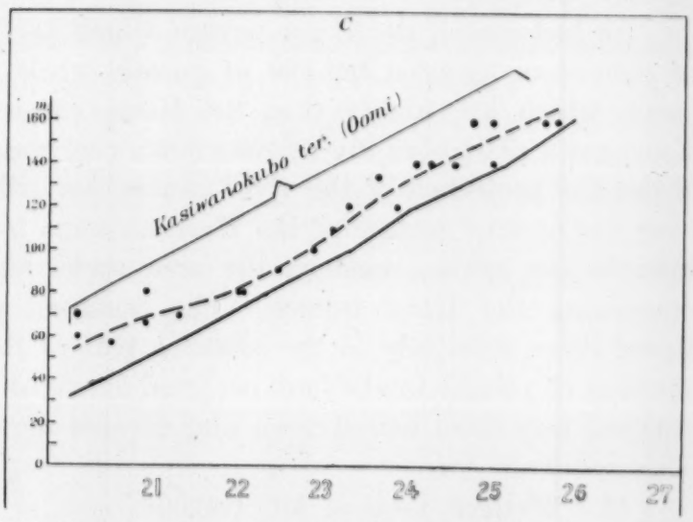

Fig. 16. C. Fig. shows the vertical distribution of the Kasiwanokubo terrace along the Oomi-gawa.

5) The Kasiwanokubo terrace. The Kasiwanokubo terrace is well preserved on the upper course of the Kano, about 80–135m. above

39) 大仁.

sea-level. Near Kumokane[40] and Yugasima[41] on the Kano, they begin to get high, reaching 135m. near Hatuma[42] on the Oomi river. These terraces are composed of gravel beds or Tertiary bed rock. Many river terraces along the tributaries of the Kano and the Oomi may belong to these terraces.

Because of the unevenness and steep inclination of the terrace surface, it is not expected that these terraces could be accurately correlated with each other by referring to their heights, without any other precise data. But these terraces have roughly been traced from Kasiwanokubo to Hatuma along the river Oomi and up to Yugasima along the Kano. Fig. 16 shows the distribution of these terraces.

The chronologic relation between the age of formation of the Kasiwanokubo terrace and the Hatake terrace is not yet definitely known. Measuring their relative heights from the present river floor, they are about 20m. and 30m. respectively (excepting the lower terrace near Oohito). But the relative heights tell nothing of the chronologic relationship between these two terraces. Their chronologic relation must therefore be considered with respect to their absolute heights and their geologic structures.

As just stated, the Hirai terrace which is 30–40m. high, consists of pumiceous material but not of gravels, while the Kasiwanokubo terraces, which are higher than the Hirai, consist of gravels. And the Kano-gawa plain abruptly narrows down near the town of Oohito. Fig. 16 shows the projection of the river course, its tributaries having flowed over the ancient surface of the Kasiwanokubo terrace, which developed towards the north, namely, the area under the pumiceous material composing the Hirai terrace. The northern part of Kasiwanokubo flexed down relatively to the southern part of the town of Oohito. The ejection of pumice might have occurred during this period. The pumice, further, may have flowed down and covered the downwarped area of the Kasiwanokubo terrace.

II. Western slope of Mt. Hakone.

Fig. 5 shows the summit level of Northern Idu Peninsula drawn by Okayama's method in 500m. mesh. On the north side of the line joining Hirai and Tasiro, the contour lines of the summit-level curve very gradually, running toward the northwest, and suggesting the conical slope of a volcano, but on the south side they trend in a meridional direction, sharply, and turning south of the line. The

40) 雲金. 41) 湯ヶ島. 42) 八幡.

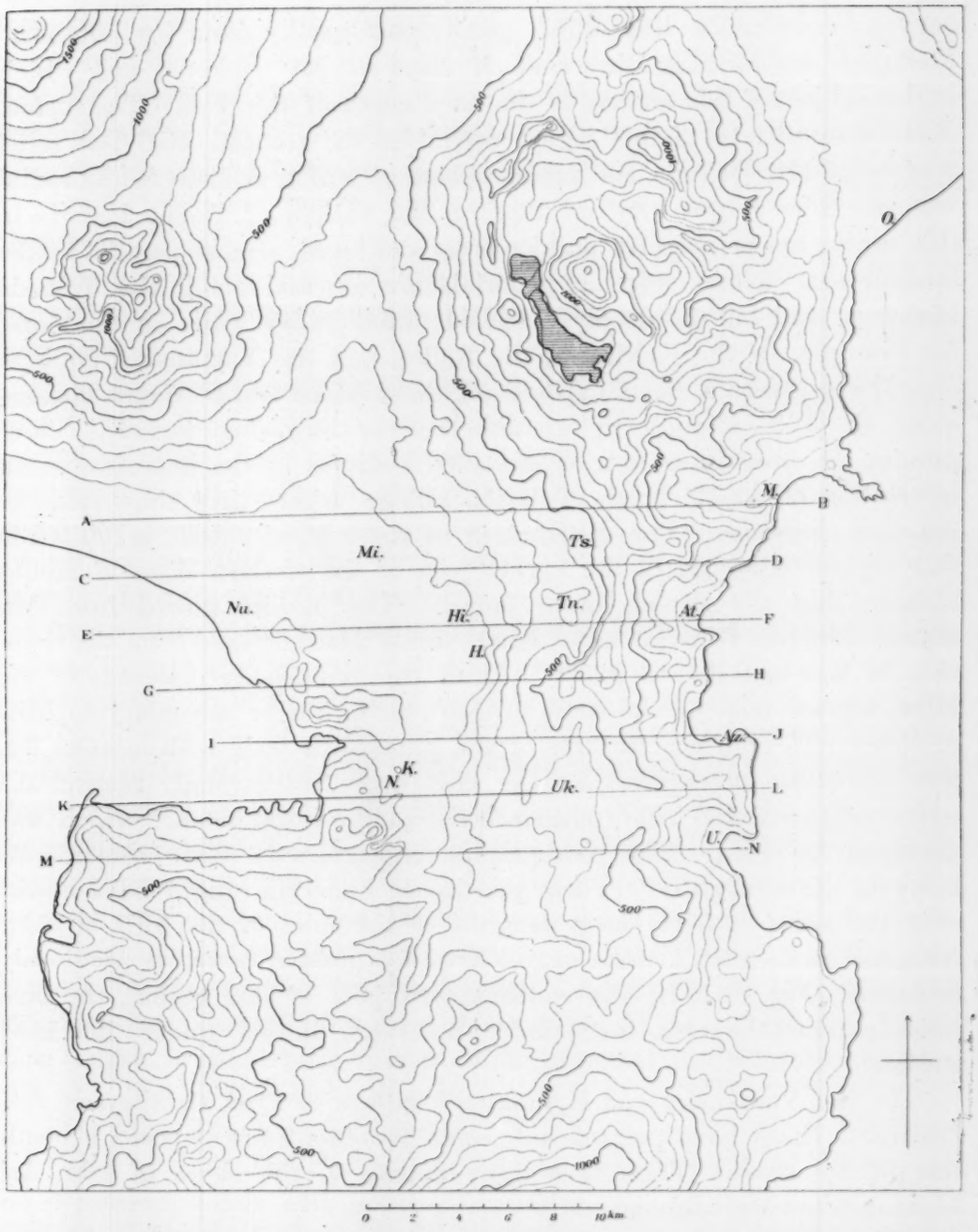

Fig. 5. Summit-level of Northern Idu. (Contour line is referred to the highest points in the 500m. nets. Line AB, CD, EF, GH, IJ, KL, MN show the position of profile which are shown in Fig. 8.)

At. Atami.	K. Kona.	Nu. Numadu.	U. Usami.
Az. Aziro.	M. Monkawa.	O. Odawara.	Uk. Ukihasi.
H. Hatake.	Mi. Misima.	Tn. Tanna.	
Hi. Hirai.	N. Nagaoka.	Ts. Tasiro.	

northern side of the line differs geomorphologically from the southern. The province forming the western slope of Mt. Hakone, and which is the subject of this section, is the area north of this line. The surface of the summit level of this region resembles the reconstructed low relief surface of Mt. Hakone, the present slope of which is dissected by radial valleys. The ridges between these radial valleys of Mount Hakone in this region are principally pumice flows and lavas, almost parallel to the landsurface. These volcanic materials are exposed along the Tôkaidô highway, and on the deeply dissected radial valley walls on the slope, for example, in the Kakizawa, the Raiko, and the Yamanaka[43] valleys.

The pumiceous flows exposed on the western foot of Mount Hakone along the Tôkaidô highway resemble those of the Hatake terrace. These pumice are sometimes seen as stratified beds, as in the exposure on an excavation at Ako,[44] north of Daiba village, where they show more or less flow structure. The distribution of these pumice beds is limited to this region, although in the higher part of the western slope of Mount Hakone they are scarcely to be found. The pumice flowed from Mt. Hakone during Diluvial times in the same manner as during the eruption of Komagatake in 1930.[45] And the pumiceous materials of the Hirai terrace may be the same eruptive materials or secondary deposits of them. The surface features of the pumiceous beds with more or less flow structure as exposed on the cliff near Ako strongly remind the writer of the Takao beds (pumice beds) in the Ooiso block,[46] which was surveyed by him. The petrographic characters of their constituents however differ slightly. These pumiceous materials might have flowed over the relief at fairly large heights, as the sides of the hills of older Neogene rocks near Hatake are covered by pumice flows, as previously described (Fig. 3). In the southwestern part of this region, the lava flows exposed beneath the pumice flows are buried under the land surface.

In the Yamanaka and Ryûtakuzi[47] valleys, as Prof. Hirabayashi and Ishii and Ihara have pointed out, some lava flows are exposed beneath the pumice flows. These lava flows extend to the shore of lake Asi (Asinoko) on Mt. Hakone.

The following geologic history may then be inferred of this region

43) 山中. 44) 赤王.
45) H. Tsuya, *Bull. Earthq. Res. Inst.*, 8 (1930).
46) Y. Otuka, *Jonr. Geol. Soc., Tokyo*, 36 (1929).
47) 龍澤寺.

from the evidences above enumerated. First some lava and ash poured down over the southwest slope of Mt. Hakone in a southwest direction. But the extent of these lava flows is limited on the south by a line roughly joining Yanai[48] (a small village northwest of Tasiro) and Hatake. The pumice ejected from Mt. Hakone deposited over this surface.

Small patches of pumice are seen as far the Simotanna region and elsewhere.

The pumiceous material that crops out between Karuizawa[49] and Tanna[50] was distributed probably during this period in the middle or late Diluvial.

The form of the southwest slope shown by the summit level may accord with the original accumulated surface of these pumice beds. During or after their accumulation followed river erosion, deepening the valleys on the slope of Mount Hakone. The pumiceous material which was removed from its original position to the lowlands through the valleys, resettled in the lower levels. Part of the material removed probably formed the Hatake terrace.

The rivers, by continually dissecting the southwest slope of Mount Hakone, would also resettle the pumiceous material. The age of dissection of the Hirai and Hatake terraces may be contemporaneous with this age. The lower courses of these rivers are buried under recent fluviatile materials (deposits aI and aII), and volcanic material from Mount Huzi (e. g., lava of the Misima fan). The Huzi lava flow consequently postdates the dissection of Mount Hakone. Though no fault topographies are observed in this region, its southwest boundary, namely, the line joining Yanai and Hatake, may be a tectonic line as Prof. T. Tsujimura and Okayama[51] conjectured. A brief reference to this line is made in the writer's previous paper. According to H. Kuno, the boundary line between the lava flow of Mt. Hakone and Mt. Yugawara (whose original form is now almost dissected out) roughly coincides with this line in its northeast part.

III. The Tanakayama[52] forest.

Other striking features noticed on the summit-level in fig. 5 are the depressed reliefs and peculiar arrangements of the contour lines near the village of Tanna. These features are characteristic of the region south of the line joining Yanai and Hatake. In the Tanna

48) 柳井. 49). 軽井澤. 50). 丹那.

51) T. Tsujimura and T. Okayama, *op. cit.*, (1931).

52) 田中山.

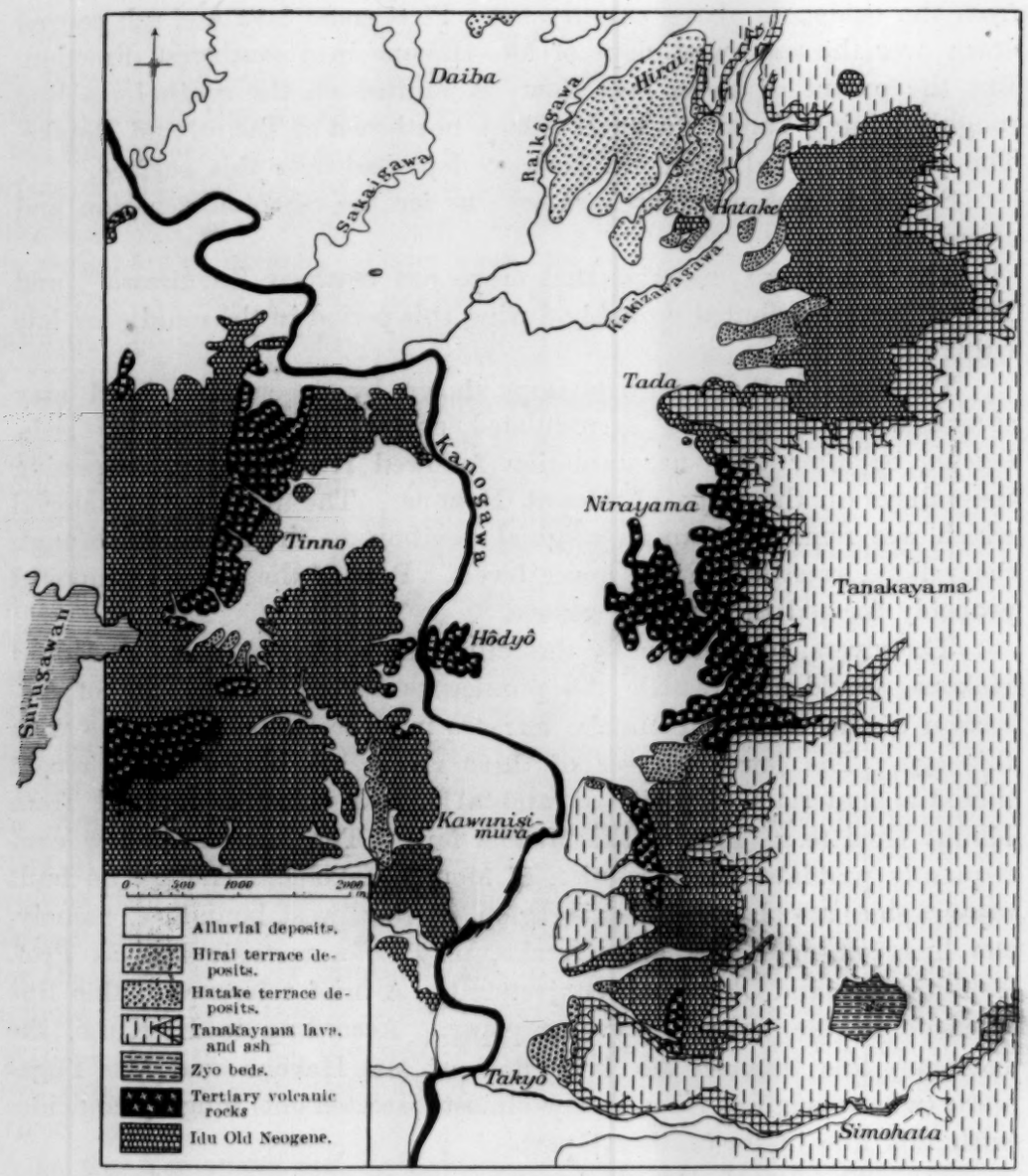

Fig. 6. Geologic map of the western part of Tanakayama forest.

basin, the 300m. contour line in the summit level is a closed curve The 400, 500, and 600m. contour lines south of this closed one are constricted and show a saddle shaped surface. Valleys vertically opposite the saddle trend meridionally. The closed or constricted contour lines are due to the depressed zone of the Tanna fault zone which will be described later, the zone in which severe ground disturbances occurred

at the time of the Northern Idu earthquake. The area between the Tanna fault zone and the Kano-gawa Alluvial plain is divided into the Simotanna region on the north and the Tanakayama forest on the south by the Kakizawa valley, which runs from the southern corner of the Tanna basin to Hatake village in an E. W. direction. The geomorphologic and geologic characters of one side of the boundary of the Kakizawa valley differ from those on the other. The Tanakayama forest, which is the southern part of the boundary is higher than the opposite part, and has a more simple geologic structure. But as is generally the case, a rigid boundary line can not be drawn between them. It may be called the "boundary zone" or the "transitional zone." The surface of the Tanakayama forest is a low relief surface, and consists of almost horizontal lava flows or pumiceous materials extruded from the early Diluvial volcano Taga. The bedding planes of these volcanic materials are roughly parallel to the surface of the summit-level, while the surface of the summit-level of the Tanakayama forest suggests the fragmental conic surface of a volcano. The surface of the Tanakayama forest may then be the remnant of a slightly dissected volcanic slope. On the eastern limit of this forest, the low relief surface is bounded abruptly by a steep meridional scarp facing the east, which is the western fault scarp of the Tanna fault zone. It therefore follows that the peculiar arrangement of the contour line in the summit-level already mentioned, namely, the depressed topography along the Tanna fault zone, could only have been formed after the surface of the Tanakayama forest was formed. The western limit of this forest, like the eastern, is bounded by a steep slope facing the lowland of the Kano-gawa Alluvial plain. Exposures of the lava flows that have built up the Tanakayama forest may be seen on this steep westerly slope resting upon old Neogene rocks at a height of about 250–300m. above sea-level. They may be seen also on the valley walls of the Hukazawa and Kakizawa, which deeply cut the forest region.

In the village of Takyo, the lava flows down from the Tanakayama forest to the level of the Kano-gawa Alluvial plain through the lower part of erosion reliefs of Neogene rocks. At Tada[53] also the lava flows down to the lower level. Dl in Fig. 2 of the Tanakayama region shows this low relief surface covered with these lava flows and volcanic ash, while the "steep relief" of Fig. 2 shows the steep erosion surface of

53) 多田.

the old Neogene rocks without any covering material.

The 363 m. triangulation point situated 2 km. North of Simohata[54] (Fig. 6), an isolated hill projecting above the low relief surface of the Tanakayama forest, consists of volcanic sandstone that may be seen cropping out on the valley floor near Simohata, and with which the Tanakayama lava flows are underlain. Owing to old surface inequalities in the volcanic sandstone, the lava and volcanic material could not completely cover it. The underlying sandstone will be described later.

The Hukazawa river deeply excavates the Tanakayama forest, on the valley wall of which the Tanakayama lavas show beautiful columnar joints. But the Neogene rocks that crop out on the eastern limit of this region are not exposed in this valley. Fig. 18 shows the columnar joints of the lava flows near Takyo. It seems that the buried relief of the Neogene rocks in the east part of this region has been reduced in height through tectonic movement or some other cause.

Near Simohata, on the Hukazawa velley under the Tanakayama lava flow, may be observed bluish-grey, muddy sandstone containning some fragments of fossil plants, the same sandstone that forms the 363 m. point above mentioned. The Tanakayama lava on the valley wall of Hukazawa, which crops out along the upper course disappears beneoth the land surface near Yasuno, while thick agglomerate and micaceous or ashy beds develop above its lava, which beds we shall call the "Zyo" beds in this paper. The area between the Hukazawa and the Oono-Doodoko[55] valleys, which limits the southern part of this region, is covered also by lava flows and other material, the upper part of which consists of volcanic ash and lava and the lower of conglomerate and pumice beds. The lower pa. is the Zyo beds of Tayama.

Summarising the foregoing, the geologic history of the Tanakayama forest may be inferred as follows:

During or after the deposition of the Zyo beds, subaerial erosion sculptured the land surface to a relatively great height. The Tanakayama lava and volcanic flows then covered the sculptured reliefs from east to west. Some Tanakayama lava sheets flowed down, as in Takyo and Tada, through the lower part of the highly ragged reliefs towards the ancient Kano-gawa valley. During or after the deposition of these flows, the Tanna fault line became active and the topographic, that is, the visible Tanna fault zone was formed. The rivers of the forest dis-

54) 下畑. 55) 大野一堂處.

sected the land surface, resulting in the Hukazawa, Kakizawa, and other valleys.

IV. The Simotanna slope.

The geologic province of the Simotanna slope, situated at somewhat lower level north of the Tanakayama forest, has already deen studied by Professor Hirabayashi and T. Watanabe.[56] Recently the complicated underground geologic structure of this province was brought partly to light by the tunnelling work proceeding on the Atami railway line. Professor Tsuya will shortly publish a paper on this complicated geologic structure.

According to him, and to his drawn geologic section along the tunnel wall, the Tanna tunnel consists of Olivine bearing andesite lava and agglomerate in the upper horizon, and alternations of sand, mud, and gravel containning dacitic pumice in the middle horizon. The latter beds, which contain some plant remains (e. g., *Fagus crenata*), are folded, flexed, and thrusted over the younger olivine bearing andesite flows from west to east, forming a low-angled thrust plain (Fig. 7).

This alternative formation may be almost contemporaneous with the beds exposed on the floor of the Hukazawa valley near Simohata, described above, or with the Zyo beds of Tayama.

According to Prof. Tsuya, the petrographic characters of the pumice contained in the alternative formation of Simotanna, which is considered almost identical to the beds exposed on the tunnel wall, perfectly agree with that contained in the writer's Tutizawa beds[57] on the Ooiso block. The Tutizawa beds, according to the author's stratigraphic study, may be lower Pleistocene, judging from their stratigraphic positions and their fossils.

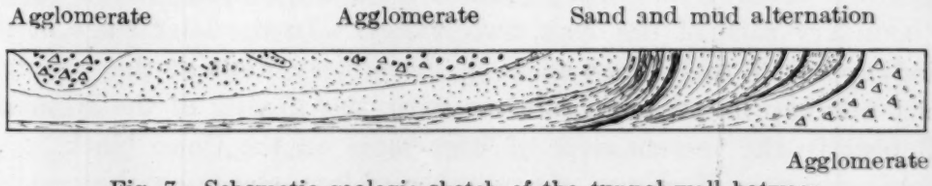

Fig. 7. Schematic geologic sketch of the tunnel wall between stations 6950 ft. and 7350 ft. from the western mouth.

From these considerations, the Tutizawa beds in the Ooiso block, the alternative formations of Simotanna, the beds exposed on the walls of Tanna tunnel, and the Zyo beds of Tayama may all be contempor-

56) T. Hirabayashi and T. Watanabe, "Geological report near Tanna Basin," *Atami Construction Office, Government Railways Japan*, (1924).

57) Y. Otuka, *op. cit.*, (1926).

aneous with one another. They seem to be interesting examples of the post-Pliocene palaeogeography of these regions.

Below the alternative beds of the tunnel wall, the agglomeratic beds, the Simotanna sand, mud, and gravel alternations, and the basic lava flows rest unconformably either upon Neogene tuffite beds or upon agglomeratic beds. In these tuffite beds are contained *Amussiopecten* aff. *praesigne* (Yokoyama), and *Venericardia panda* Yokoyama, which seem to indicate middle Neogene age.

These Neogene rocks crop out in small patches along the valley wall of the Kakizawa, 200m. West of Simotanna and 2000m. North of Hatake-Yuduka, forming sometimes a projecting hill on the low relief land surface of young formation. Although the general height of the land surface of the Simotanna province is somewhat lower than the Tanakayama forest, the former is more dissected than the latter. And some faults, which may be inferred from certain topographic characters, run in a N-S direction in the province near Simotanna and Binnosawa. On the western margin of this forest the underlying basal Neogene rocks are less exposed than that in the Tanakayama forest, as shown in Fig. 6.

The Tanakayama forest and the Simotanna province were dissected by river erosion during late Tertiary, followed by early Pleistocene volcanic activities. During this period the dl_I formation deposited on the rugged land surface of Neogene rocks. After the deposition, the younger lava flows covered the erosion surface of the dl_I formation. During or after the extrusion of the olivine bearing andesite flow, the Simotanna province suffered overthrusts from west to east and other crustal movements, and was seperated from the Tanakayama forest by the boundary zone of the Kakizawa valley. In the later stage of this period appeared the Tanna fault in the eastern limit of this province. This fault may be contemporaneous with the flexing of the Ninomiya shell beds in the eastern slope of Soga-yama on the Ooiso block.

According to H. Kuno, the number of lava sheets on the east side of the Tanna fault zone is larger than that on the west. This difference in the number of lava sheets seems to indicate that it was in times past the wall of a caldera, the east side of the Tanna fault zone having lowered gradually with accumulations of the lava sheet.

As already explained, the Tanakayama lava on the west side of the fault zone flowed from east to west, while some of the lava flowed down to lower levels through the lower part of the ancient reliefs.

After that the Tanna fault resumed activities by which movements the topographic (visible) nuclear fault began to form.

But the northern spread of this topographic character of the Tanna fault zone seems to be obscured by accumulation of new volcanic material from Mt. Hakone; or it may be traversed by the inferred fault line connecting Yanai and Hatake, cutting the northern extension of the Tanna fault. But the writer is unable to say anything definite in these respects. Some writers recognize the northern extension of the Tanna fault as connecting the depressed topography extending from the Hakone pass to the saddle-shaped topography between Mt. Kintoki[58] and Myôzin[59] through lake Asi. But the topographic character of this depressed zone is quite different from that of the Tanna fault zone. The topographic characters of the Tanna fault zone show the narrow graben or ramp[60] form, but that of Hakone merely broadly depressed reliefs. The writer however, while not denying the existence of a fault structure under the lowered reliefs of Mt. Hakone, finds himself unable to recognize what is mentioned above as a fault topography.

V. The Tanna fault zone (Fig. 2).

As already stated, the eastern limit of the Simotanna and the Tanakayama forest is bounded by the steep straight slope to the long narrow depressed land which extends from the north, the Tasiro basin to the south, the Ukihasi basin through the Karuizawa and Tanna basin. This long narrow depressed zone is called the Tanna fault zone in the present paper. The depressed land has the form of an arc with large curvature, convexing to the east. From its form and tectonic characters, the Tanna fault zone reminds one of a kettle fault or a thrust fault topography. On the south part of the Ukihasi basin, this fault zone continues along the Oono valley.

The ridges to the east of this zone form the main divide of the Idu peninsula. This divide extends from Mt. Hakone to Amagi through Mt. Hikane, the Atami pass, and (Mount) Kuro-dake. The summit-level shows the distribution of the height on both side of the depressed Tanna fault zone. The east side is higher than the opposite side. But as stated above, the Tanakayama slope on the west side of it is believed to be the accumulated surface of volcanic materials and lava ejected from a crater that was at one time situated on the east side of the depressed zone. The crest or the slope of the east side should therefore

58) 金時. 59) 明神.
60) B. Willis, *Bull. Geol. Soc. Am.*, **39** (1923).

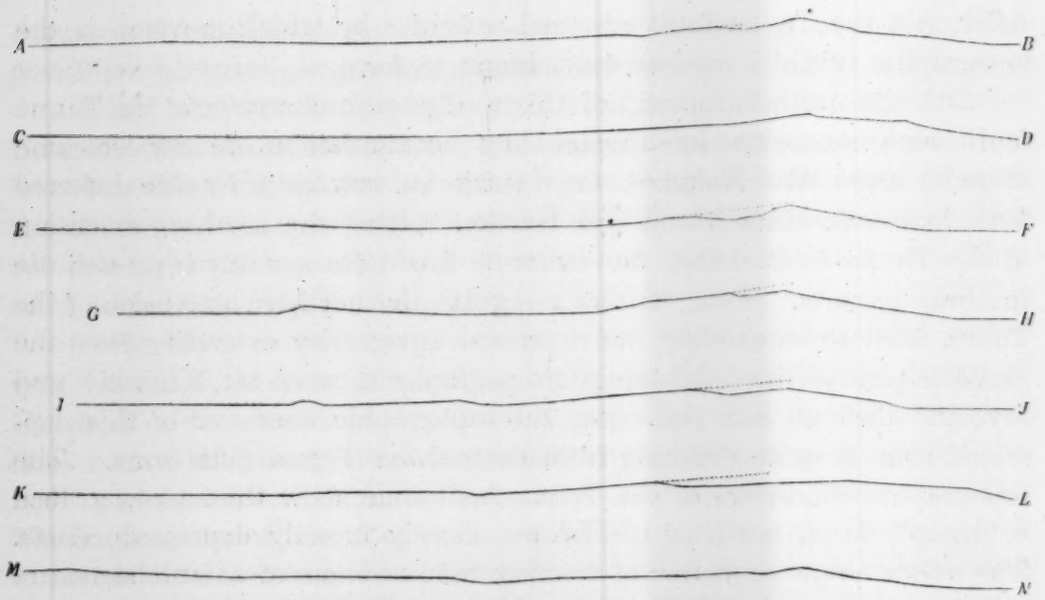

Fig. 8. Profiles of the summit-level (Lines AB, CD, EF, GH, IJ, KL, MN in Fig. 5).

be in the same plane as the surface plain of the Tanakayama forest. The land surface of the east slope of the Ukihasi basin roughly accords with the slope of the bedding plane of the lava flows. Fig. 8 gives profiles of the summit-level intersected in the direction at right angles to the general trend of the depressed fault zone. The larger parts of the straight lines touch the profile lines of the western slope as shown in Fig. 8. But by imagining that these straight lines of the eastern slope were prolonged, then the heights are larger than those of the west, which suggests that the west side of the fault zone had upheaved relatively to the east side, and in which case, if both sides of the fault zone were a continuous plane, the west part should have upheaved relatively to the east. Indeed, according to Prof. Tsuya and Kuno, the lavas forming the eastern slope are parallel to the surface of the summit-level of the east slope, in which case the lava on the eastern slope has not the same slope as the western, so that the eastward convexing curvature of the Tanna fault zone does not suggest a kettle fault.

1) Tasiro basin. Fig. 12 shows the topography of the Tasiro basin and its northern part. The form of the Tasiro basin is an obtuse angled triangle, with the long side parallel to the general trend of the Tanna fault zone on the west.

The west side of the basin is the steepest of all. This steep wall

develops from the northeastern corner of the basin and continues through Karuizawa village to the Tanna Primary School, at the northern corner of the Tanna basin. The crest line of this west wall is very even. The Simotanna low relief surface above mentioned is the western side of this line. The windgap like topography west of the 343m. triangulation point in Karuizawa, through which the Atami highway passes and then turns north along the foot of the steep slope, is a good example. A tributary of the Raiko, which drains the Tasiro basin, deepens the steep slope and forms narrow valleys. These facts show that the Simotanna slope and the river systems on its slope had existed before the western steep slope of the Tasiro basin came into existence. That steep slope was formed so quickly that the rivers flowing on both sides of the Tanna fault zone could not deepen their valleys fast enough to follow the upheaval of the steep wall. It is the belief of the author that the steep slope limiting the west side of the Tanna fault zone in these parts is the fault scarp that rises relatively to the basin area, as supposed by the late Prof. Yamasaki.[61]

The Tasiro, the Karuizawa, and the Tanna basins have been formed by local sedimentation of the rivers Raiko and Kakizawa which were dammed up by the quick formation of the steep western fault scarp, from which it follows that the deposits in these basins are quite recent accumulations. The disastrous results of the earthquake in these basins may be understood partly from the fact that these younger materials are loose and not so compact from its having only been recently dammed and also from its tectonic character, as has been shown by borings made in the Tanna basin by the railway authorities.

Normally the beheaded part of the valley, through which passes the Atami highway, should drain the Karuizawa basin and its eastern part, but the dissection of the Kakizawa along the Tanna fault zone, which erodes so easily, was so quick that the upper course of the former was captured by the Kakizawa. The ground disturbances of the 1930 earthquake mostly occurred at the foot of the fault scarps. The outflow of the Tasiro basin was blocked by a fault, resulting in the formation of a small lake at the time of that earthquake.

The steep fault-scarp topography which disappears north of the Tasiro basin is replaced by other kinds of fault topography. Fig. 12 shows this fault topography, which terminates at a point on the north,

61) N. Yamasaki, *Jour. Geol. Soc., Tokyo*, 26 (1919).

602m. above sea level, on which the Yanai and Hatake tectonic line meet the Tanna fault zone. The north-south ridge of 602m., which is one kilometer long, obstructs the streams on the east slope from flowing west, so that the streams turn their courses towards the west and conflux with other streams flowing on the eastern slope around the southern end of the ridge. The eastern slope of this ridge is steep, while topographies similar to it may be seen arranged linearly in accord with the general trend of the Tanna fault, so that if the volcanic slope were generally smooth, these ridges would have been formed by fault activities.

Although in the earthquake of 1930, the earthquake rents or fissures were limited to the northern part of this region, on the western side of the ridge occurred the great landslide of Kobutano and Magano. Consequently the topography in the northern extension of the Tanna fault shows relatively simple but very interesting characters. The only explanation of the fault topography the author can offer is the upheaval of the east side of the fault zone relatively to the opposite side.

2) The Tanna basin, which is subpentagonal in plan, is situated 2km. south of the Tasiro basin. Its west side is not like that of Tasiro. Its east and west sides are more or less steep, while its south and north sides are relatively low. The steep side of the fault scarp west of the Tasiro basin turns westward along the Kakizawa at the Tanna Naga[62] and is cut by the Kakizawa valley. This steep slope does not continue to Okkosi,[63] Sinyama,[64] on the south side of the basin. The flexed boundary zone between the Tanakayama forest and the Simotanna province has affected the trend of the fault scarp. Or it may be considered that they were deformed by the erosive action of the Kakizawa river which denuded parts of the fault scarps and broadened its fluviatile plain. The earthquake fissures of 1930 occurred along the westerly foot of the isolated hill in the central part of the Tanna basin. This isolated hill is about 10m. or so in height, and consists chiefly of coarse-grained pumiceous sand stone beds dipping steeply toward the west. The fault that is inferred from the topographic characters does not however accord strictly with that of the earthquake fissures. In the tunnel under this basin, many parallel, vertical, or steeply inclined faults whose directions are almost meridional cut the Diluvial agglomeratic rocks. One of these parallel faults almost completely blocked the

62) 名賀. 63) 乙越. 64) 新山.

western drain drift of the tunnel.[65]

The writer looked down into the Tanna basin to observe the topographic character of the fault zone from the Ikenoyama pass, situated south of the Tanna basin about 320m. above sea-level and continuous with the floor of the Karuizawa village, which is situated between the Tanna and Tasiro basin about 3m. above the Tanna basin. He believes that the terrace may be an old river floor of the Kakizawa. It was however difficult to verify it geologically as the region consists mostly of Quaternary agglomerates, it being impossible to observe the terrace deposits in a state of good preservation.

As above stated, although the western topography of the Tanna basin is a relatively simple fault topography, the eastern side of the fault zone is somewhat complicated. The following briefly describes the topographic characters of the east side-wall.

3) The Atami pass fault. The narrow indented saddle, through which the Atami highway passes, runs in a N. 45° W. trend, its northwest extension skirting the Atami highway for 1km., ending at the northern corner of the Tasiro basin, connecting the numerous Kernbut-like topographies. Its southern prolongation extends through Nisiyama in Atami to the northern limit of Atami town, connecting the saddle like topographies which are linearly arranged. These characters may be regarded as fault topography, which according to H. Kuno, may be confirmed geologically at the Atami pass and near Atami town. At the Atami pass, the same lava sheets on both sides of the fault line are dislocated.

4) The Ainohara[66] fault. The linear valley running from Wada[67] in Atami to Ainohara suggests a fault topography. This linear negative topography is traced to the northern part of the Tasiro village across the Atami highway and the north saddle of the 672·2m. point, which lies southwest of Atami pass. This fault has been verified geologically also by H. Kuno as the Ainohara fault.[68] In the earthquake of 1930, the wall of the Atami tunnel was displaced and cracked. These two fault lines above mentioned do not continue westward across the Tanna fault zone.

These faults, arranged obliquely to the general trend of the fault zone, were verified geologically and topographically. Some faults parallel to these two are also observed in this province.

65) R. Takahasi, *Bull. Earthq. Res. Inst.*, 9 (1931), 435–475.

66) 相原. 67) 和田.

68) Y. Ôtuka and H. Kuno, *Bull. Earthq. Res. Inst.*, 10 (1932), 472–475

5) Of the parallel are shaped fault topographies east of Karuizawa, one runs from the 250m. point east of Tasiro to Takizawa[69] of the Tanna basin, while the other is situated parallel to the east one. If the surface of these ridges bounded by these fault topographies are the fragments of a contemporaneous topographic plain, this feature should be considered as a step fault topography with the downthrow side on the west. The Tanna fault zone may be a new variant of the graben or Willis' "ramp," bounded by a reversed fault on the west and by a normal stepped fault on the east.

The southern part of the east side-wall of the Tanna basin is more or less steep, but there the step-fault topography is not clearly observable. The isolated hill in the Tanna basin mentioned above may be the top of a block thrown down step fashion by the faults.

6) In previous paragraphs it was stated that the arc-shaped trough-like zone, running from Okkosi to Ukihasi[70] and Tawarano[71] across the Ikenoyama[72] pass along the Hukazawa valley, is a fault topography. The gentle slope of the Tanakayama forest is abruptly limited by this zone, having a surface inclined steeply to the floor of this trough as in the case of the western wall of the Tasiro basin. But it differs from the west wall of Tasiro in the existence of an isolated hill clinging to the steep surface. The isolated hill north of Ukihasi, especially, may be regarded as a "kernbut" and "kernkol" topography. The earthquake faults of 1930 appeared on the "Kernbut" part as shown in Fig. 37. The southern part of the west side of the Tanna fault zone generally has high steep walls, while the eastern slope inclines very gently westward. The parallel step fault topographies as seen in the Tanna basin disappear in this slope.

7) The Yamabusi[73] fault. Near the Yamabusi pass is observed a faults system lying N. 60° W. In the northeast part of it, other fault topography suggesting a kettle fault are developed as shown in Fig. 2. The NE side of this fault is depressed relatively to the opposite side.

8) The Yasuno[74] fault. The northern valley of Yasuno, 1500m. north of Tawarano, suggests a hinge fault topography, its west wall being steep, while its east side is gentle. The difference in height of the two sides is fairly large—about 100m. or so—decreasing as one goes northward. The writer has illustrated the topographic fault in Fig. 2.

---

69) 瀧澤. 70) 浮橋. 71) 田原野. 72) 池ノ山. 73) 山伏.
74) 安野.

No geological evidences were obtained.

9) Southern extension of the Tanna fault. As to this question, topographic evidences of the extension are obtained along the Oono valley. It is not correct that the southern extensions are topographically observed between Warabo-Hiekawa[75] as generally stated, but as will be explained later, geological evidences may exist in the valley of the Hiekawa.

But ground disturbances occurred in the earthquake of 1930, and the many geologic faults that cut the Zyô beds in Oono valley seem to support the idea that the Ono valley is a fault valley.

10) Distribution of the river pattern on both side of the Tanna fault. Fig. 9 shows the distribution of river pattern on both side of the Tanna fault. As shown in Fig. 9, the valleys on the west side of the Tanna fault correspond roughly with those on the opposite side, as if they had been continuous valleys at one time before the activity of the Tanna fault zone.

But it must be noticed that the pattern of the western valleys must have been displaced north along the Tanna fault zone about 4km. or so in order to correspond accurately with the eastern. That is to say, the corresponding eastern valleys are situated always relatively north to those on the west. The streams on the east slope turn their courses southward along the Tanna fault zone, and then readjust themselves westward to the western valleys.

The earthquake faults of 1930, dislocated the western block horizontally, southward, about 3m. or so relatively to the eastern along the Tanna fault zone. The characteristic topographies of the river pattern above mentioned may therefore have been formed by repeated horizantal dislocation.

Consequently the Tanna fault zone is a young topographic fault zone consisting of some distributed minor parallel faults. The west side of it is generally thrust on the east side with steep fault planes. But careful observations show that the lowland of the fault zone is the depressed zone bounded on the west side by reverse fault planes, and on the east side by normal fault planes.

The river pattern on both side of the Tanna fault zone suggest that the horizontal dislocations were repeated during faulting, and had shifted the west side of the fault zone to the north relativelly to the

75) 原保－冷川.

east side in the same sense as those in the earthquake faults of 1930.

VI. The Simoômi province.

The southeast side of the valley which drains the Tawarano basin is a geologic and topographic province. As seen in the summit-level, this province gently slopes southwestward. The finely stratified volcanic sands cover but thinly, but they dip so steeply that the writer doubted if the crustal disturbances had occurred after the deposition of the ashes. But this steeply dipping stratification may be the usual condition of the volcanic sand as is seen easily in a volcanic region.

The gentle relief shown by the summit-level is dissected into narrow spurs by streams flowing southwest and confluxing with the Kano. On the walls and floors of the valleys the lava flows are exposed beneath the volcanic ashes, while in places mud and conglomerate alternately appear under these lava flows.

These alternative beds which are typically developed near Zyo, Simoômi-mura, were called Zyo beds by Tayama and Niino.[73] In the type locality, the Zyo beds are alternations of mud, sand, and pumice.

The Zyo beds consist of brown sand at the lowest horizon, followed by thinly altered pumice or tuff bearing beds and more or less hard, grey mud beds containning some fossil shells and foraminifera. Northern exposures of this mud bed contain some fossil leafs, e. g., *Fagus crenata*, etc. The species of fossil mollusca and foraminifera from the Yokoyama fossil zone in the lower part of the Zyo beds are *Limopsis tokaiensis* Yokoyama and *Glycymeris pilsbry* (Yokoyama), and many other species now living in the open seas. Table 5 shows these fossil mollusca and foraminifera. The faunal characters of these beds differ little from the living fauna of Suruga bay. The writer believes these beds to belong to the uppermost Pliocene or lowest Pleistocene, most probably to his dII. (Fig. 10).

According to Prof. Tsuya, the fossil bearing Zyo beds may be related to the mud alternations of Simotanna, the former occupying a slightly lower horizon. The petrographic characters of the pumice indicate that the Simotanna beds are contemporaneous with the Tutizawa beds of the Ooiso block, and that the horizon is slightly higher than the Ninomiya bed of the Ooiso block which is overlain by the Tutizawa beds, while the Ninomiya beds may be upper Pliocene in view of its palaeontological character and sedimentation cycle.[74] The stratigraphic correlation schemed

73) R. TAYAMA and H. NIINO, *op. cit.*, (1931).
74) OTUKA, *Geogr. Rev.*, Japan, 8 (1932).

Table V.

List of fossil foraminifera and mollusca collected from Zyo beds which crop out Yokoyama, near Zyo.

Foraminifera

Baggina zyoensis Otuka M. S.
Bolivina robusta Brady.
Bolivinita quadrilatera (Schwager).
Bulimina sp. (*aculeata* var.?) no. 2.
Cassidulina orientale Cushman.
Cassidulina subglobosa var.
Cibicides lobatulus (Walker et Jacob),
Cibicides lobatulus var.
Cibicides sp. 4.
Cibicides wuellerstorfi Schwager.
Elphidium crispum (Linné.)
Eponides praecincta Karrer.
Eponides sp.
Frondicularia sp.
Globigerina bulloides d'Orbigny.
Globigerina dubia Egger.
Globigerina inflata d'Orbigny.
Globorotalia tumida (H. B. Brady.)
Globorotalia aff. *oblonga* (Williamson).
Globorotalia truncatulinoides (d'Orbigny).
Guttulina sp. no. 1.
Gyroidina soldanii d'Orbigny.
Lagena strumosa Reuss.
Lagena sp. no. 1.
Lenticulina sp. no. 6.
Lenticulina sp. no. 7.
Lenticulina? sp.
Lenticulina sp.
Loxostomum karreiana (H. B. Brady).
"*Nodosaria.?*" sp.
Nodosaria (*Dentalina*) *consobrina emaciata* (Reuss).
Nodosaria sp. no. 1.
Nodosaria (*Glandulina*) *rotundata* (Reuss).
Nodosaria scalaris (Batsch).
Nonion boueana d'Orbigny.
Nonion sp.
Nonionella sp.
Orbulina universa d'Orbigny.
Pattellina aff. *corrugata* Williamson.
Patellina opercularis d'Orbigny.
Pseudopolymorphina sp.
Pyrgo vespertilio Schlumberger.
Pyrgo denticulata? (H. B. Brady).
Pyrgo sp. 4.
Pyrgo aff. *elongata* (d'Orbigny).
Quingeloculina sp. 4.
Quinqueloculina disparilis d'Orbigny.
Quinqueloculina sp. 10.
Quinqueloculina sp.
Quinqueloculina sp.
Rectobolivina bifrons (H. B. Brady).
Rotalia sp.
Robulus sp.
Sigmoidella sp. nov.
Spiroloculina grata Terquem var.
Spiroloculina sp. no. 1.
Textularia conica d'Orbigny.
Textularia aff. *sagittula* Defrance.
Triloculina tricarinata (d'Orbigny).
Triloculina trigonula (Lamarck).
Uvigerina pygmae d'Orbigny.

Mollusca

Cylichna sibaensis Yokoyama.
Erato callosa Adams.
Fusinus nipponicus? Smith.
"*Pleurotoma*" *braynsi* (Yokoyama).
Inquisitor sp.
Lora yokoyamai Onoyama
Bela sp.
Natica sp.
Typhis arcuatus Hinds.
Leptothyra rubra Dunker.
Dentalium totomiensis Makiyama.
Patellina sp.
Haliotis?. sp.
Yoldia ninomiyaensis Otuka M. S.
Glycymeris pilsbry (Yokoyama).
Limopsis tokaiensis Yokoyama.
Limopsis adamsiana Yokoyama.
Lima quantoana Yokoyama.
Lima subauriculata (Montagu).
Pecten laqueatus Gould.
Chlamys sp. (irregularis?)
Anomia sp.

Tellina sp.	*Lucina acutilineata* Conrad
Venericardia ferruginosa A. Adams et Reeve.	*Volsella* sp.(Fragmental).
Myadora fluctuosa Gould.	*Brachiopoda* sp. (fragmental).

by Prof. Tsuya has been confirmed palaeontologically. The continuation of the Zyo beds are exposed on the dissected valley floor of the Simotanna slope.

The Zyo beds are flexed, faulted, and reversely faulted, and in places intruded by andesite dykes. The muddy sand of the Zyo beds exposed near Simotanna and Simohata are covered with Tanakayama lava as already stated. But the only fossil remains obtained here were fragments of fossil plants. From this geologic structure of the Zyo beds, it may be concluded that the southern extension of the Tanna fault zone once extended southward.

The Zyo beds exposed near Oono, which is an alternation of sand and conglomerate, is overlain by lava flows, and unconformably underlain by the Simosiraiwa beds of Tayama of the Older Neogene. In these

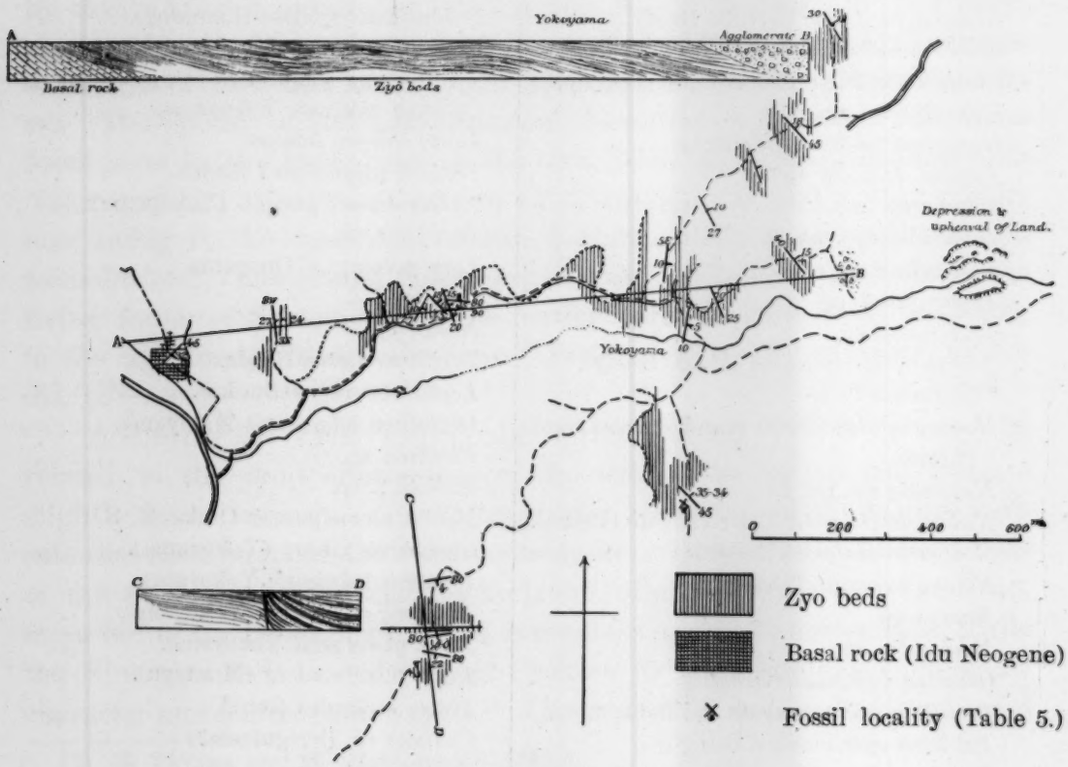

Fig. 10. Geologic route map near Zyô.

Oono valleys, the Zyo beds are severely disturbed by faulting parallel to the general trend of the Oono valley, suggesting that early Pleistocene tectonic movements occurred in this Oono valley. These exposures are seen on the northwest valley wall near Oono. Fig. 11 is a sketch of these faults exposed at Oono.

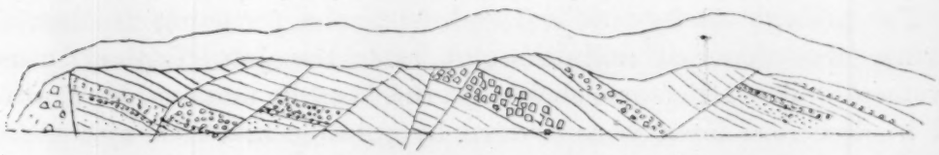

Fig. 11. The faults exposed on the cutting near Oono

The Zyo beds are exposed in the upstreams of the Tosikawa[75] valley in the same way as in the Oono valley. The beds here consist of pumiceous muddy sand and conglomerate, dragged and flexed at the southeast limit of the exposures as a result of faulting.

The sand and gravel alternation of the upper courses of the Kamisiraiwa[76] may belong also to the Zyo beds, covered by the Sukumo[77] lava. The alternation is horizontally in the large exposures of the eastern valley of Kamisiraiwa, but flexed upward in the southern limit of the exposure. The underlying Neogene rock exposed at the mouth of the Simosiraiwa valley contains many foraminifera. Hanzawa[78] has reported from these beds *Lepidocyclina* (*Amphilepidina*) *nipponica* Hanzawa, *Lepidocyclina* (*Amphilepidina*) *angulosa* Provale, etc.

VII. The Darumayama[79] province.

As the writer has not yet fully surveyed this province, only a few observed facts will be treated here. Darumayama, which is a Diluvial volcano like Taga, erupted on the southern part of the Wasidu[80] mountainland. Although the volcano lacks its western half, its broad skirts extend to the bay of Mito and Suruga and to the Kanogawa valley. Recent river erosion has dissected these skirts, sculpturing many radial valleys. These slopes consist of thick two-pyroxene andesite agglomerates covering Neogene agglomerate. This stratigraphic relation may be seen near Bentenzima, Omusu village, on the shore of Mito bay. Some lenticular conglometrate and sand beds exposed between the Darumayama volcanic materials and Neogene agglomerate is considered by Tayama to be the same as the Zyo beds. But in the writer's opinion they may be younger

75) 年川. 76). 上白岩. 77) 巣雲. 79) 達摩山. 80). 鷲頭.

78) S. Hanzawa, *Sci. Rep. Tohoku Imp. Univ.*, Sendai, Geplogy, 13 (1932).

than the Zyo beds, judging from its constituent materials and stratification.

The northeastern part of the Darumayama slope is divided by the high Hottanzyo-yama in the Wasidu mountainland into two slopes, the northern (Mito bay) and eastern (the Kanogawa valley). The eastern slope is well observed on the upper course of the Syuzenzi valley.

The geologic history as deduced from the foregoing is that this province was denuded and dissected after the late Tertiary crustal movement. The reliefs as shown in the Wasidu mountainland, which will be described later, were covered by volcanic materials ejected from the Darumayama. But the reliefs near Mt. Hottanzyo and Wasidu are often so high and steep that the materials did not cover these provinces. the activity of the Darumayama was then followed by the dissection of the volcanic slope and many radial valleys were sculptured, e. g. Kioi, Osumi, Syuzenzi valley, etc.

The submarine topography of Suruga bay (Fig. 2 and 17), which shows the drowned valleys extending from the mouth of the numerous land valleys to the sea, suggests that this area subsided after the formation of these radial valleys. These radial valleys therefore were formed in pre-Alluvial time or before the formation of Misima fan, which fills a similar valley in the Hakone slope.

VIII. The Wasidu mountainland.

As shown in Fig. 2, the west side of the Kanogawa Alluvial plain is a steep relief region, the Wasidu mountainland, which is higher than the regions referred to so far, the difference of height in an area of nearly 4 sq. km. being about 350m.

This mountainland consists of Neogene pyroclastic sedimentary rocks and igneous rocks, all lower Pliocene or lower Miocene. Fig. 6 is a geologic sketch map of this province. In the province treated thus far the old erosion surface of Neogene rock is covered thickly by younger volcanic detritus and sediments, while in this mountainland no covering strata are seen. Whether the Wasidu mountainland was covered once by young formations, and they have been removed by recent erosions, or whether from the beginning of the Diluvium young formations have not covered this mountainland, there is no young formation there now. The structural relation of the young formations to the old erosion surface of the Neogene rock observed in the other provinces previously dealt with, suggests that the latter case is more probable than the former, seeing that the high peaks of Hottanzyoyama

(or Katuragisan), which consist of Neogene rock (see Fig. 2), rises above the projected slope of Darumayama. It can therefore only be concluded that the old erosion surface of the fairly high old Neogene rocks were in existence in these provinces before the volcanic detritus of the Darumayama had accumulated. The stratigraphic relation of the Tanakayama lava flows to the Neogene bed rocks suggests that the mountainland of Neogene rocks were in existence at the time of the pre-Tanakayama lava. The Wasidu mountainland may therefore be a ruined topography of late Tertiary land surface, deformed by recent erosive action.

As above stated, no young formations exist in this province, where the writer failed to find any landslides or other ground disturbances caused by earthqnakes on account of the unconsolidated nature of the materials.

Brief summary of the post-Neogene geologic history of Northern Idu.

From the foregoing geologic and geomorphologic studies of these provinces, the following geologic history is inferred:

I. The formation of the erosion reliefs of the Neogene rocks.

The stratigraphic relation of the Neogene rock to the young lava flows and igneous materials in these provinces is the clear unconformity as seen in the western limit of the Tanakayama forest or the northerly limit of the Darumayama slope. Moreover the boundary surface of the unconformity has very irregular reliefs in the large relative heights, while the boundary plane between the Simotanna (plant) beds (Zyo beds) and the overhanging young volcanic rocks is not so irregular as that between the Neogene and the young volcanic rock. From these evidences, it is inferred that during late Neogene, the land surface of these provinces were dissected into fairly great relative heights.

II. Transgression of the waters that formed the marine and lacustrine Zyo beds.

As above stated, the distribution of the marine Zyo bed is limited to near the village of Zyo, Simoômi province. Although volcanic materials from Amagi volcano cover this marine deposit on its eastern limit of distribution, no marine deposits are seen in its western part, their places having been taken by young lava flows and old Neogene rocks. Consequently the sea, which deposited the marine Zyo beds, invaded this province, probably from the southeast, where it is covered by volcanic materials from Amagi. During the same age the fossil plant bearing sedimentary rocks below the Tanakayama lava, together

with that of Simotanna, were deposited in the depressed meridional zone. This depressed zone is cut diagonally by the topographic fault of Oono during post-Tanakayama lava. Since the Neogene the volcanoes maintained their activities. The period of Prof. H. Tsuya's[81] dacite tuff activity may correspond to the same period.

It is probable that at this stage, neither the Wasidu mountainland the west half of the Tanakayama forest and the Simotanna province, nor the Darumayama province were covered with any young formations.

According to Prof. Tsuya, complicated overthrust structures were formed in the Simotanna province. Old Simotanna sand and mud alternation beds thrust from the west over young lava flows. But the land surface of the complicated structures had been denuded, leaving no visible evidences on the land surface.

III. Extrusion of the lava flows forming a gentle surface.

In the Tanakayama forest, which is the south part of the complicated region, the Tanakayama lava-flows from Taga volcano cover these complicated structures with unconformity, so that the overthrust structure of Simotanna antedates the Tanakayama lava flow. The flexed structure of the Zyo beds may be traced also to this period. After the flexing and overthrusting, the Tanakayama lava overflowed this province. By this time the ancient lowland of the Kanogawa had already formed at the same place as that of the recent Kanogawa alluvial plain, while the south ends of the Tanakayama lava that extends to the lowland through the lower part of the mountain ridge also existed during this period.

IV. The formation of the Tanna fault zone.

After the extrusion of the Tanakayama and the Yugawara lavas, the Tanna fault zone began to make its appearance. The west part of the fault zone overhangs the depressed blocks and is shifted repeatedly toward the south compared with the east side. At this period were formed the diagonal fault of Atami pass and other faults. The imaginary tectonic line joining Yanai and Hatake was probably formed during this stage, when the southwestern slope of Mount Hakone, north of the line, was lowered slightly to the southern side. The Hakone volcanic materials then accumulated on the lower northeast side. The surfaces of the Kasiwanokubo and the Hatake terraces were formed at this stage. The flexual movement that divided the Kasiwanokubo from the

81) H. TSUYA, *Bull. Earthq. Res. Inst.*, 9 (1931).

Hatake probably occurred in the early stage of this period, followed successively by late Diluvial dissections, the formation of the Misima fan and the accumulation of the Alluvial deposits. More recently the land near Numadu upheaves. 10 m. or so.

The Ground Disturbances of Nov. 26, 1930:

The ground disturbances of Nov. 26, 1930, will now be described in the order of the eight geologic provinces that were affected.

I. The Kano-gawa Alluvial plain. As the ground disturbances of the Kano-gawa Alluvial plain have been described by the writer in a previous paper, their description will be omitted here, except of one example which occurrad on the Hirai terrace. At Hirai, Kannami-mura, a small village along the Atami highway, which suffered heavily from the earthquake, small parallel earthquake cracks running N. S. were noticed; an example of the fact that the boundaries between two beds having differerent physical properties are liable to suffer from severe ground disturbances. Here, the village of Hirai is situated on the geologic boundary of the Hirai terrace and the Simotanna slope.

II. The Southwestern slope of Mount Hakone.

The ground disturbances in this province occurred in its eastern part. The Tôkaidô highway, repaired just before the seismic disturbances, was shaken so severely that the piled up loose soil of the new highway broke off and slipped down along the steep slopes. Parallel meridional fissures were observed near the Yamanakasinden,[82] while on the southern slope of the village of Yamanakasinden a heavy land slide occurred, completely burying seven persons. Near the top of The Hakone pass many earthquake fissure formed on the volcanic cinder slope. Buts these fissures being merely manifestations of some underground tectonic activity, require no special mention. The Hakone station of the Central Meteorological Observatory was damaged and the anemograph tower tilted.

The present writer believes these earthquake fissures were formed by the action of gravity, the loosely accumulated ashy volcanic materials sliding down on account of the violent earthquake vibrations—materials materials that were poised in a state of unstable equilibrium on the upper part of the steep slope formed by recent river erosion.

II. The Tanakayama forest.

Ground disturbances in this province are rare, only some minor

82) 山中新田.

depressions, landslides, and earthquake fissures having been observed. According to Ihara and Ishii,[83] a depression occurred on a gentle slope about 1km. west of Yasuno. The ground, which consisted of volcanic ash and gravels was depressed for about 5 to 7m. and surrounded by a horseshoe-shaped scarp of about 110m. length. On the 278m. ridge about 1500m. east of Nirayama, some earthquake rents were observed by the writer (Fig. 19). They caused a horizontal displacement of 20cm. N.60°W. in a path a metre wide. The southwest side of all the rents were depressed 5cm.

In the eastern limit of this forest many earthquake fissures were formed. Their distribution is shown in Fig. 12 and 13. The west side of these fissures however was depressed relatively to the opposite side. Fig. 20, 21, 22 also show the distribution of these fissures.

IV. The Simotanna province.

On the Atami highway, about 400m. west of Binnosawa village, an earthquake rent ran across the highway in direction almost N.30°W. The vertical displacement was about 30cm., relative to the west side block. The horizontal displacement is very small. Near Simotanna village, the many earthquake fissures formed are of no special interest.

Seismic disturbances in the Atami tunnel, joining Atami and Ootake[83], have been reported by the government Railways. According to this report, written by Prof. R. Takahasi[84]; "faults and fissures appeared in the tunnel. At a point between bench marks Nos. 3 and 4 on the west side of the tunnel, a vertical dislocation of about 40cm. was measured. The most remarkable fault in the tunnel appeared near the heading of the third south drain-drift on the west side. The displacement, which was nearly in a horizontal direction, was as much as 270cm., so that the drain tunnel was completely closed by a fresh slickenside....."

V. The Tanna fault zone.

The ground disturbances on the Tanna fault zone are very interesting both geologically and geomorphologically. The present writer, for convenience, divides the Tanna fault zone into subregions.

a. Tasiro basin (Fig. 12).

In the Tasiro basin, situated on the northern limit of the Tanna fault zone, earthquake faults run N.-S. at the foot of the steep west slope (Fig. 29, 33, 34). Fig. 34 shows the torii (which was partly broken

83) K. IHARA and K. ISHII, *op. cit.*, (1932).
84) R. TAKAHASI, *op. cit.*, (1931).

by the earthquake) displaced toward the right (north) about 1.5m. relative to the stone steps on the west slope by the earthquake fault which runs between the torii and the stone steps at the same foot. It is visible in a field on the southwest corner of the basin, forming small parallel fissures arranged *en echélon*, and crosses the head of the valley which drains the basin. At the mouth of the basin, the ground surface was depressed and the water dammed (Fig. 28). The displacement of the fault is about 1m. horizontally and 30–60cm. vertically. The west side of this rent was depressed.

The northern extension of this rent goes N. 20° W. from the mouth of the basin to a point 500m. southwest of point 604.5m. and creeps up the west scarp. The earthquake rents appear discontinuously, *en echélon*, gradually decreasing in number as they go northward (Fig. 25, 26). In the kernkol and kernbut topography on the northern end of the Tanna fault zone referred to in previous sections, minor earthquake fissures with small diaplacements run N. 20° W. But on the western slope of the kern-kol, landslide (Fig. 23) occurred on a large scale, and mole-track and ploughshared like ground disturbances (Fig. 24, 27, 30) were formed above the land slide. The distribution of the ground disturbances is shown in Fig. 12.

b. Karuizawa and Tanna (Fig. 12.)

The earthquake fault runs from Tasiro basin through the western portion of the village of Karuizawa to Tanna basin, along the foot of the steep west scarp of the Tanna fault zone. The earthquake fault cuts the weathered agglomerate materials on the west wall of the Atami highway, west of Karuizawa village. The displacement of the fault here amounts to 60cm. vertically and 1m. horizontally, shifting the west side block of the earthquake fault southward and downward. North of Karuizawa, the earthquake fault runs through the base of the reservoir and has shifted a fence about 1m. or so horizontally (Fig. 31). Its displacement is in the same sense as the one previously mentioned.

The fault extends half way up the spur of point 405m. and then descends to the Tanna basin plain across the river Kakizawa at Naga.

In the Tanna basin, the earthquake fault leaves the western scarp and runs N. 10° W. from the western limit of Naga village to Okkosi, through the western foot of the hill (Kawaguti no Mori).

The small road that joins Tanna Nisikata and Takizawa and crossed by an earthquake fault running N. 20° W., has been displaced 1–0·7m. horizontally (Fig. 32). The fault here is continued by short

earthquake fissures running N. 45° W. and arranged *en échelon*.

In the rice field, west of Kawaguti no Mori,[85] the faults are continued. The western block here was shifted 1m. horizontally, southward relatively to the eastern block.

Near Okkosi, the earthquake fault shows the largest displacement of all, amounting to 2–2·6m. horizontally in the same sense as previously mentioned. The distribution of the earthquake fault in the Tanna basin is shown in Fig. 12.

c. Ikenoyama pass (Fig. 13).

The Ikenoyama pass between Tanna basin and the Ukihasi basin was disturbed by an earthquake fault in such a way as to make it appear that the west side of the pass had shifted 1m. southward relatively to the opposite side, along the topographic fault line. An earthquake fault runs N. 20° E. in the northern valley of the pass and another one N.10°W. in the southern part.

The earthquake fissures running E.-W., resulting from the earthquake fault, traverse a road joining Ukihasi and Ikenoyama near the north margin of the pond at Ikenoyama.

On the northern slope of the Ikenoyama pass, a meridional earthquake fault is cut abruptly by the earthquake fissures running E.-W. These fissures were observed on the southeastern slope of the Tanna basin. It seems that these fissures are intimately related to the boundary zone of the Tanakayama forest and the Simotanna province already mentioned.

On the kernbut topography of the steep east slope of the Tanakayama, appeared a group of small parallel earthquake faults (Fig. 36, 37). The west side of each fissure had shifted southward about 30cm. It may therefore be said that this fault topography was traced by means of this earthquake. Fig. 37 shows the group of small parallel earthquakes faults just mentioned.

d. Ukihasi basin (Fig. 13).

According to Ishii and Ihara, the ground disturbances of the Idu earthquake may be grouped into the Ukihasi east earthquake fault, the Ukihashi central earthquake fault, and the Ukihasi west earthquake fault.

The Ukihasi east earthquake fault (not observed by the writer) displaced the road that connects Yamabusi and Ukihasi, horizontally in the same sense as in the Tanna fault zone.

The Ukihasi central earthquake fault is the southern prolongation

85) 川口の森.

of the Tanna earthquake fault. It traversed the western part of the Ukihasi basin, cutting through the low ridge between this basin and the Tawarano basin.

The eastern block here subsided about 1m., in opposite sense to that in the northern part of this fault zone. The horizontal displacements here are about 1-2m. in the same sense as those already mentioned (Fig. 38).

The houses and rice fields on this fault line were severely damaged.

The Ukihasi west earthquake fault, referred to by Ihara and Ishii, may be the same earthquake fissure that appeared on the kernkol topography on the steep slope of Tanakayama forest. According to these writers the south part of this earthquake fault reappeared in the west part of the Ukihasi basin and shifted the west side block southward 1.5m.

e. The Tawarano basin. (Fig. 13).

The Tanna earthquake fault extends to this basin, but disappears in the southern corner of it, where another diagonal fault appears with direction N. 70° W. Fig. 40. shows a displaced rice-field dyke cut by the diagonal earthquake fault.

f. The Oono fault.

The earthquake fault in the Oono valley extends from Oono to Kadono across the Oomi valley. Appearing first in the sunken topography in the hills back of Oono village, it gradually descends to the valley floor of Oono. The horizontal and vertical displacement here is small. But the northwest side of the fault has shifted southwestwards relatively to the southeast side.

Near Doodoko, Oono-mura, an earthquake fault which runs N. 45° E. has shifted nearly 1m. horizontally and depressed the northwest block 60cm.

On the back surface of the ridge, southeast of Doodoko, a group of earthquake fissures appeared parallel to the Oono valley, shifting the west side of the slope 0·6m. southward. This earthquake fault runs across the Oono valley and appears on the Oomi valley near Kadono.

Across the saddle-like part of the spur between the Oomi valley and the Oono valley, the earthquake fault runs N. 10° E. See Fig. 14. These displacements are in the same sense as those last mentioned. The horizontal displacements here are about 1m. N., on the east side of the fault. The Itô-Syuzenzi higaway was displaced in the same sense as that in the Oono valley. This earthquake fault which extends from the Tanna

earthquake fault line disappears in the hill back of Kadono.

VI. The Simoômi province.

As the writer could not make a thorough survey of this province, only a short description is here made.

a. The Himenoyu[86] earthquake fault appears discontinuously from Warabo to Kumokane valley through Himenoyu valley, the displacements of the fissure at the top of this valley being 0·3m. horizontally, while on the south side of Himenoyu earthquake fault is shifted to northwestward.

b. Depression and upheaval of the ground at Zyo.

On the southern part of the spur, in Zyo-mura, 230–250m. above sea-level and 200m east from Yokoyama, an elliptical area with its longer axis about 180m. and its shorter axis about 80m., sank about 10–20m., while a long narrow hill about 150m. long and 15m. wide was upheaved about 5m. above the land surface. Fig. 10 is a sketch map of these areas. Houses on the upheaved area were so little affected that the furnitures and utensils retained their positions with not even the spilling over of liquids, facts indicating that the landslide occurred very slowly.

These areas consist of volcanic ash like the Kwantô loam, with Zyo beds and Sukumo lava exposed around them, as shown in Fig. 10. Between the upheaval land and the depressed grounds a stream is deepening its floor. From these facts the present writer concludes that these upheavals and depressions of the land may have been caused by a sort of landslide which moved slowly by gravity, whereas the upheaved and depressed parts were set in motion by the vibrations of the earthquake, and in slipping down broke into a number of small blocks.

c. Kaziyama,[87] Simokano-mura. The surface soil at the head of a small valley between Sano and Kaziyama, or the western slope of Okuno-yama (406m.), slipped down through this valley. Portions of the moving soil were thrown across the Kano-gawa to Sano on the opposite side of the river.

VII. The Darumayama province.

VIII. The Wasidu mountainland.

In these two provinces, the effect of the ground disturbances of Nov. 26, 1930, was so slight that it does not call for any mention.

The bank of the reservoir at the Syuzenzi hot springs was broken by the earthquake shock, resulting in the dammed water inundating

86) 姫ノ湯. 87) 梶山.

he lower part of the spa. In a quarry at Enoura, Enoura bay, northeast of Suruga bay, some boulders were shaken down by the earthquake.

Summary of the ground disturbances of Nov. 26, 1930.

From the foregoing observations, the ground disturbances in these provinces may be divided into the following four groups:

1) Slipping of fissured land surface due to gravity and set in motion by the earthquake.

2) Landslides.

3) Fissures formed by the shearing stress of the earth's crustal distortion.

4) Ground disturbances occurring along old tectonic lines.

1) The first type of earthquake fissure is observed in all these provinces. It occurred on the surface of loose material, such as on the slopes of volcanic ash, Alluvial plains, and soils piled on the road.

But the slopes of volcanoes in these provinces being dissected deeply by river erosion, volcanic materials accumulated on high cliffs are situated in unstable equilibrium, subject to the action of gravity. Violent earthquake shocks shake down these loosely held material, resulting in many fissures on the land surface caused by the slipping, examples of which may easily be seen in the western slope of Mount Hakone, the Tanakayama forest, Simoômi, and Darumayama. Most of these land surface are covered densely with grass and bushes. It seems that the slipping was effectually prevented by the vegetation.

2) The second type of landslide is an extreme form of the first type. Here gravity exceeds the resistence of the accumulated soil and vegetation, thus limiting these landslides to steep slopes where gravity easily exceeds the resistance and causes the landslide. Examples are the steep southwest slope of Yamanaka-sinden, Kobutano and Magano, Oono, Kaziyama, and Zyo. The landslides of Zyo however move much slower than the others.

3) The third type is to be seen in the Alluvial plain, as the writer has referred to in connection with the Kano-gawa Alluvial plain.

4) The fourth type of ground disturbance, which is the most important, occurred along the old tectonic line. The Tanna earthquake fault occurred in the fault zone which was established geologically.

These displacements were in the same sense as the foregoing, as inferred by the arrangements of river pattern.

These southward shiftings of all the western blocks is the outstanding

feature with the earthquake fissures and faults that took place Nov. 26, 1930.

As stated by the writer in an earlier paper, the Idu peninsula is situated on the southern part of the Fossa Magna, which dates to the Neogene. According to Professor H. Yabe,[88] Southwest Japan is cut off by the Itoigawa-Siduoka line, which is the west side of the Fossa Magna.

According to the writer's geologic study of the southwestern part of the Fossa Magna, it is inferred that many thrust faults occurred during post-Tertiary, and that the western blocks of those faults moved southward, relatively.

It may then be said that the displacements of tectonic lines in this megatectonic zone are repetitions of similar shiftings that have been taking place since the late Tertiary. In view of the foregoing, the Idu peninsula probably suffered always from megatectonic shearing stresses as above stated. Incidentally the North Idu earthquake of Nov. 26, 1930, stimulated local release of this stress, the region having been relieved of this stress by the horizontal shifting along the old fault plane.

Ground disturbances and crust deformations, pre- and post-seismic disturbances associated with the earthquake of Nov. 1930, and the geomorphology of these regions.

Soon after the Idu earthquake of 1930, precise levellings and triangulations were repeated by the Military Land Survey. The results of these measurements have been treated by Prof. C. Tsuboi[89] in this bulletin.

According to him, there is a block boundary between bench marks Nos. 54 and 56. The displacement that occurred between bench marks Nos 54 and 55·1, is about 360·6 mm., the two last-named bench marks being in the Tanna fault zone. The earthquake fault, as previously described, crosses the levelling route between bench marks Nos. 54 and 55·1. The bench marks in the Tanna fault zone are much depressed relatively to other bench marks.

According to the same investigator, post- seismic displacements of bench marks between Nos. 57, 56·1, 56, and 55·1 show tilting of the block towards N. 50°E. This tilting is not inconsistent with conditions relating to the ground disturbances of the Tanna fault zone.

88) Y. Otuka, *Bull Earthq. Res. Inst.*, 9 (1931), 340, foot note.

89) C. Tsuboi, *Bull. Earthq. Res. Inst.*, 9 (1931), 271-290.

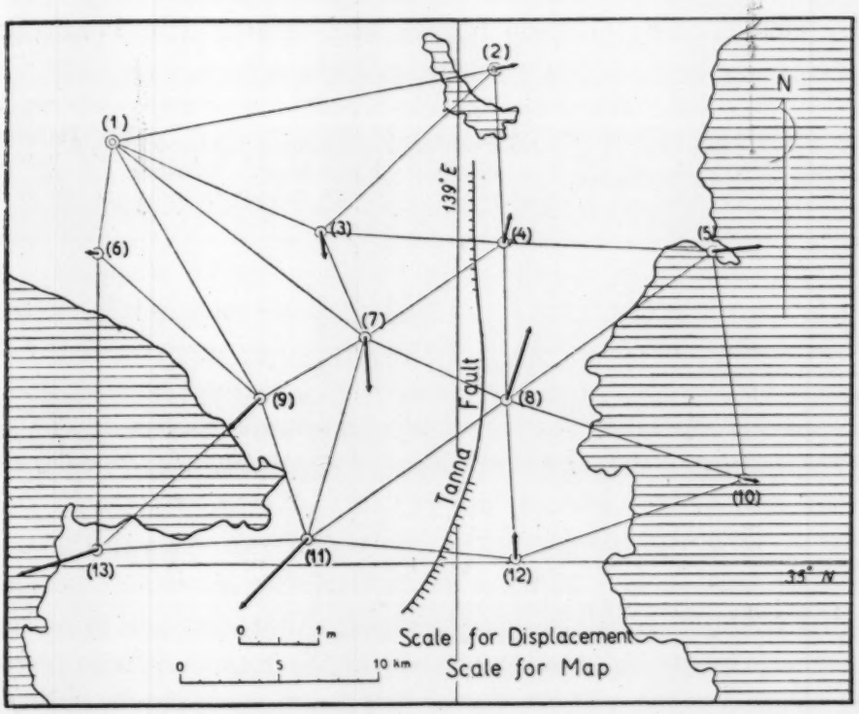

Fig. 15. Map showing the displacement of triangulation point in Northern Idu (after C. Tsuboi).

The movements of triangulation points indicate the distortion of Northern Idu. The displacements of the earthquake faults may be explained by shear action due to the distortion (Fig. 15). These horizontal displacements of triangulation points are in the same sense as that of the earthquake faults and the geomorphologic faults (Fig. 2).

Concluding remarks.

As stated in the foregoing, the geologic structure of Northern Idu, the pre- and post-seismic crust deformations as revealed by surveys, and the ground disturbances associated with the Idu earthquake of Nov. 30, 1930, are all closely connected with one another. The conclusions from this study may be stated as follows:

The post-Tertiary geologic history of Idu peninsula as shown in table VI.

Volcanic activities in this region were most marked during the post Tertiary. The topographic Tanna fault zone came into existence after the Tanakayama lava. The Tanna fault zone is graben or a ramp, the western limit of which is the reversed fault, the eastern limit of which may be normal. The river patterns on both sides of the fault zone

Table VI. Post-Tertiary geologic history of Northern Idu Peninsula. (1933).

	I. Kanogawa Alluvial Plain.	II. Western Slope of Mt. Hakone	III. Tanaka-yama Forest.	IV. Simotanna Slope.	V. Tanna Fault Zone.	VI. Simoôm Province.	VII. Daruma-yama Slope.	VIII. Wasidu Mountain-land.
aII.	Upheaval of land (10).	Dissection of radial valleys.	Stage of dissection.	Stage of dissection.	Accumulation of basin deposits.	Stage of dissection.	Formation of drowned valley (Mito bay.).	Formation of drowned valley.
	Accumulation of fluviatile deposits.							
	Subsidence of land.							
aI.	Formation of Misima fan and eruption of Mt. Huzi.							
	Stage of dissection.						Stage of dissection.	Stage of dissection.
du.	Hirai terrace, Hatake terrace deposits (pumiceous beds). Kasiwanokubo terr. dep.				Pumiceous dep. in fault zone.	Kasiwano-kubo terrace.		
	Stage of denudation.							
dIII	Formation of imaginary Hatake-Yanai tectonic line.		Activity of Kakizawa flexed zone.		Formation of topographic Tanna fault.	Amagi and Sukumo lava flows.	Darumayama lava	Stage of dissection.
	Stage of dissection.		Tanakayama lava (Taga volcano.)					
			Stage of denudation.					
dII			Overthrusting.				Stage of dissection.	
			Zyo beds nr Simohata.	Simotanna beds.	Deposition of Zyo beds.			
			Formation of meridional depressed zone.					
m.-p.	Late Tertiary dissection.							
	Idu Old Neogene Rock.							

suggest that the west side had shifted to the south, relatively.

2. The ground disturbances of the earthquake are divided into 4 groups.

a. Slipping of fissured land surfaces due to gravity and set in motion by the earthquake shock. Example—the south western slope of Mt. Hakone.

b. Fissures formed by the shearing stress of the earth's crust distortion. Example—the Kanogawa Alluvial plain.

c. Ground disturbances occurring along old tectonic lines. Example—The Tanna fault zone.

d. Landslides. Examples—Kaziyama, Yamanaka-sinden, Zyo, etc.

The ground disturbances seem to have been caused by gravity slipping, set in motion by the violent shocks. Even the earthquake fault itself may be the phenomenon by which the long accumulated megatectonic shearing stresses were released by violent earthquake shocks. The sense of the horizontal displacements of the earthquake faults agree in direction with that of the fault zone as inferred topographically. But the vertical displacements of the bench marks do not agree in sense with those inferred geologically, but do so with that of the earthquake fault.

A noteworthy fact is that the many faults in these provinces that were recognized by geological means alone failed to show any visible displacements at the time of the earthquake of 1930, whereas those recognized through geomorphologic features were active during that earthquake. All the earthquake faults recorded in Japan belong in the latter class of geologic faults.

From the foregoing considerations, the fundamental problem concerning the ground disturbances of the earthquake is to determine what is the prime agency that causes these disturbances; in what particular manner does the megatectonic agency affect the earth's crust in Japan; and what kind of tectonic line of weakness is easily affected by the earthquake shocks. To answer these questions it would be necessary to study the geologic and geomorphologic structures of the earthquake region of Japan as well as the megatectonic condition of the Japanese islands during post-Tertiary age.

29. 北伊豆の地形及び地質構造と昭和五年十一月二十六日伊豆地震の際にその地域に生じた地變及び地殻變形との關係

地震研究所 大塚彌之助

最初に北伊豆地方の鮮新世以後の地史を考究した．この地方は鮮新世末頃一度海進を受けた．之に前後してこの地方は洪積世と同樣に著しい火山活動の時代であつた．多賀火山，湯河原火山等がそれらから噴出物を出してこの地方の海成堆積物を被ふやうになつたのはこの後である．

丹那斷層はこの火山噴出物に被はれる以前に上記の海進時代の地層を複雜化してゐるやうであるが，現在地形的に明なものができたのは多賀火山の熔岩流出の後である．丹那斷層の性質は一種の地溝で，平行な斷層線の集合のやうに見え，西側は逆斷層，東側は正斷層の形式のやうに見える．この斷層線の兩側の河流の平面型は斷層の兩側で喰違つてゐて，一見西側が南へ移動してゐるやうに見える．斷層線の北限は箱根山地方では不明瞭になつてゐる．之は箱根火山の新しい噴出物で被はれたためか，又は山中新田から畑毛の方へ續く斷層線で切られてゐるためかである．

洪積世末期の開析作用はこれらの地方を開析して，冲積世の堆積物は之等の開析谷を埋めてゐる．

鷲頭山地はこれらの新しい火山物質に被はれない古い岩石からなる地方である．

伊豆地震の地變は主としてこの新しい火山物質に被はれてゐる地方に見られる．之等の地方では最近の開析作用で深められた谷に向つて重力に基く地辷りを起してゐるものも少くない．

地變の他の一つは斷層線に沿うてゐるもので，その移動の意味が地形地質から推定されるものと一致するのは面白い．

最後に水準點，三角點の改測の結果と比較し，地震地變と密接な關係にあることがよく認められた．

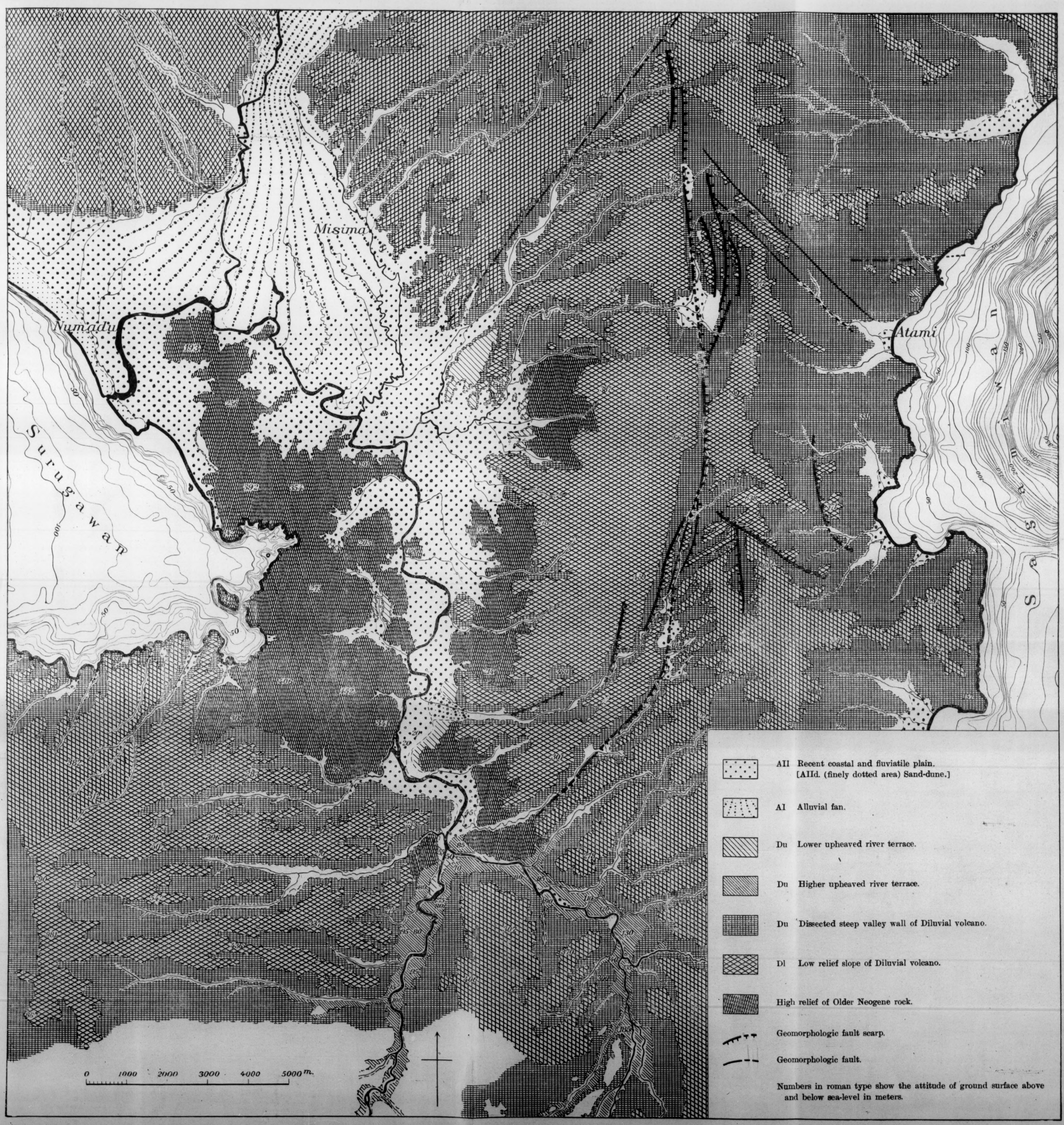
Misuna
Numadu
Atami
Suruga wan
Sea
0 1000 2000 3000 4000 5000 m.
AII Recent coastal and fluviatile plain.
[AIId. (finely dotted area) Sand-dune.]
AI Alluvial fan.
Du Lower upheaved river terrace.
Du Higher upheaved river terrace.
Du Dissected steep valley wall of Diluvial volcano.
Dl Low relief slope of Diluvial volcano.
High relief of Older Neogene rock.
Geomorphologic fault scarp.
Geomorphologic fault.
Numbers in roman type show the attitude of ground surface above and below sea-level in meters.

Fig. 2. Geomorphologic Map of Northern Idu

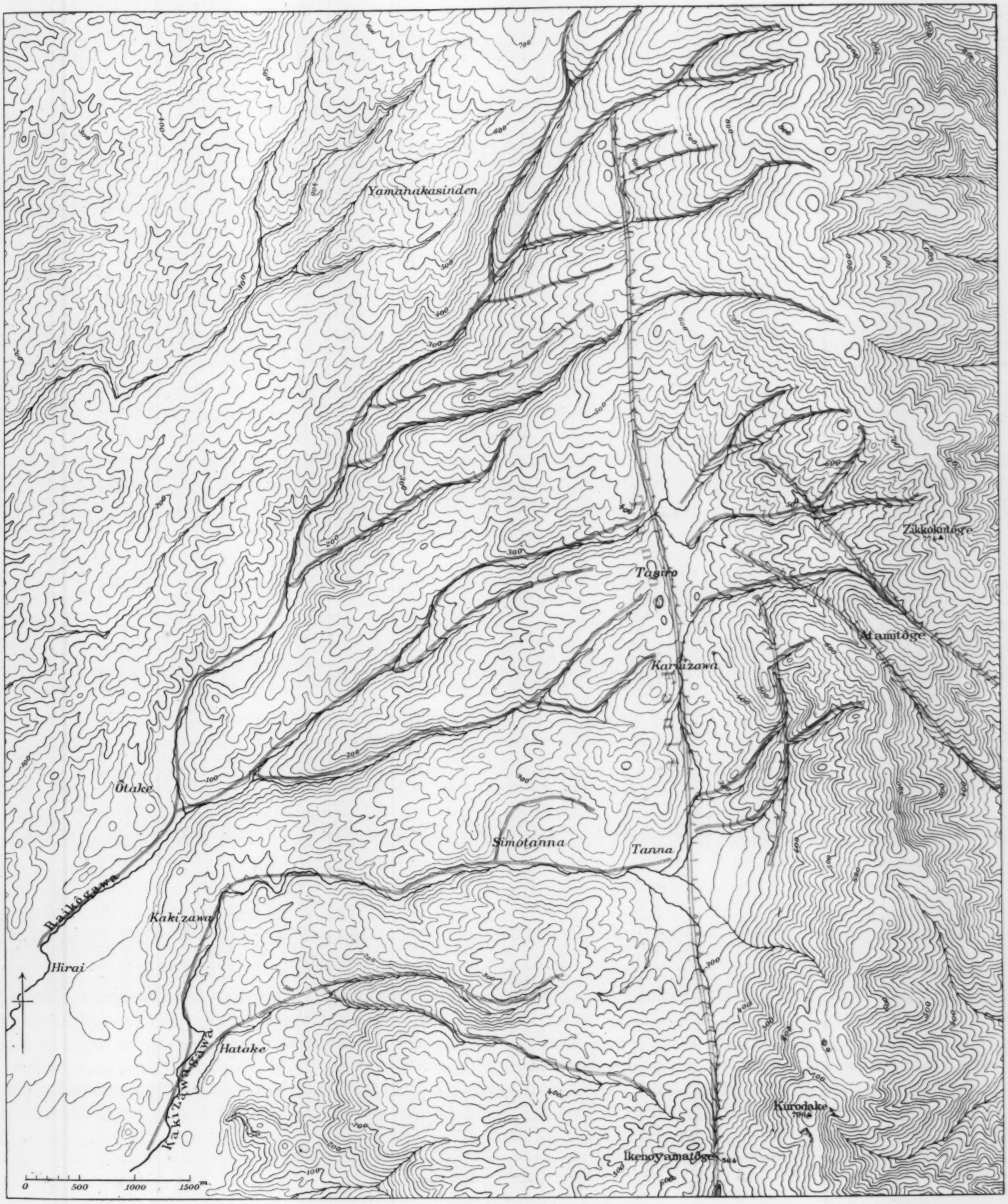

（震研彙報、第十一號、圖版、大塚）

Fig. 9. Map showing the river system near Tanna fault zone.

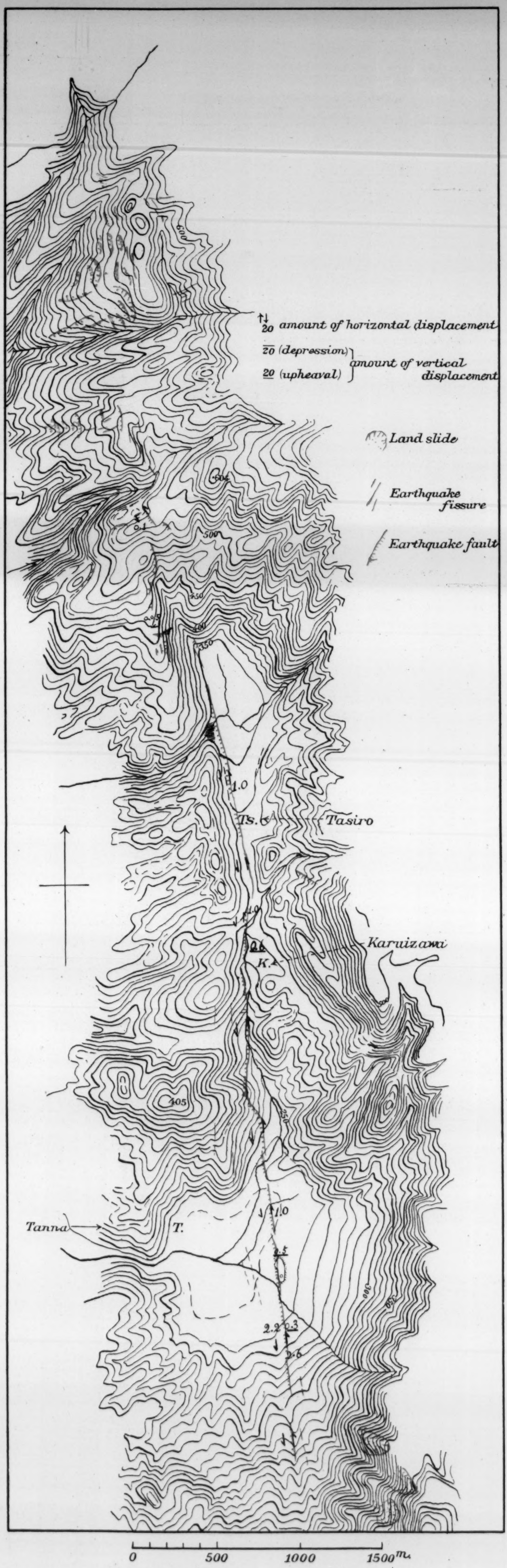

Fig. 12. Map showing the distribution of ground disturbances along the Tanna fault zone (Part 1. North part.)

（震研彙報、第十一號、圖版、大塚）

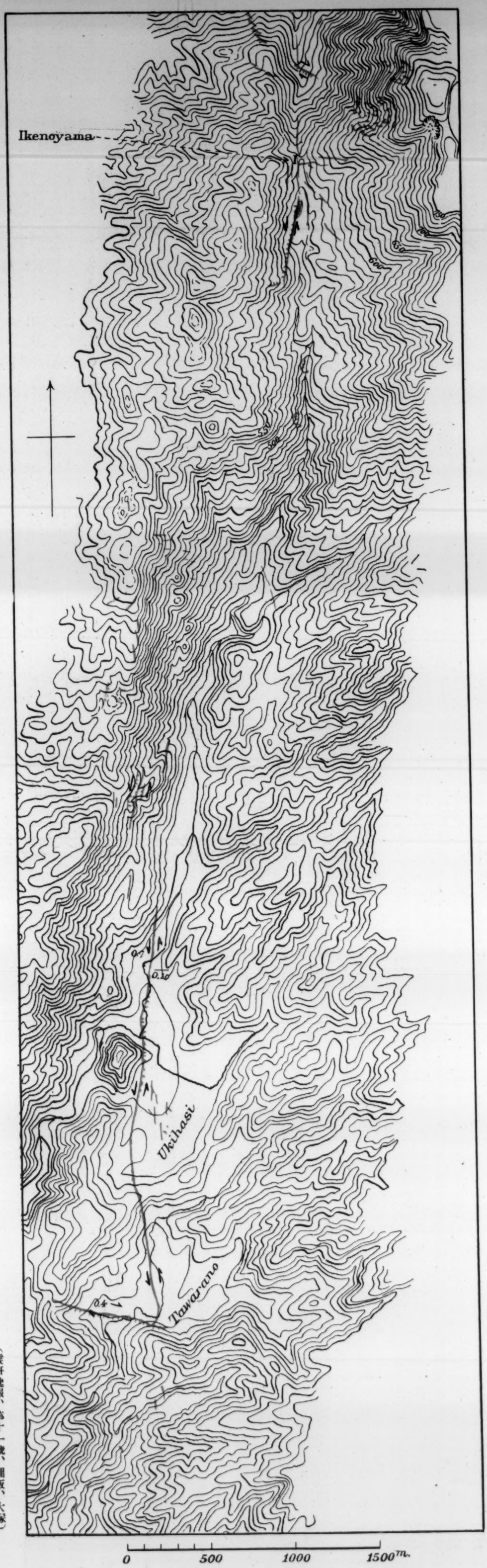

(震研彙報、第十一號、圖版、大塚)

Fig. 13. Map showing the distribution of ground disturbances along the Tanna fault zone (Part. 2. South part).
See Fig. 12.

Fig. 14. Map showing the distribution of ground disturbances near Kadono and Oono. See Fig. 12.

（震研彙報、第十一號、圖版、大塚）

Fig. 14. Map showing the distribution of Recent disturbances near Kadano-saki Cape

Fig. 17. Drowned coast of Mito bay, seen from Wasidu-yama.

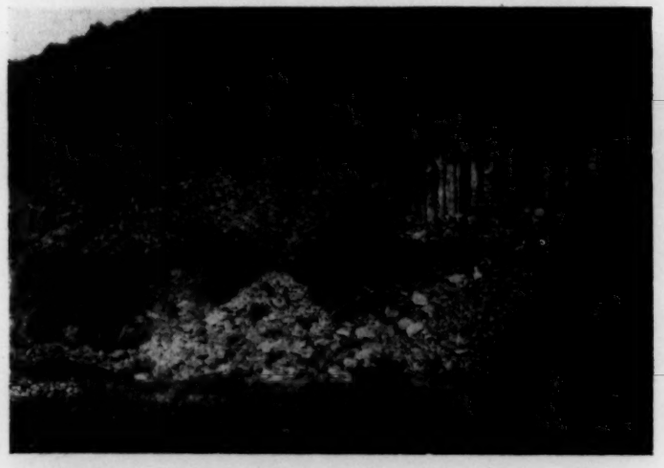

Fig. 18. Columnar joint of Tanakayama lava, nr. Takyo.

Fig. 19. Earthquake rents on the 278 m. ridge about 1500 m. E. of Nirayama.

Fig. 20. Earthquake fissures on the eastern limit of Tanakayama forest.

（震研彙報、第十一號、圖版、大塚）

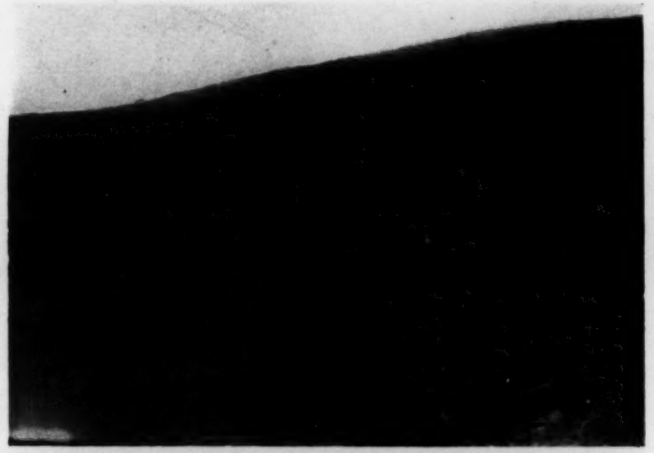

Fig. 21. Earthquake fissures in Tanakayama forest (few hundred m. S. of Fig. 20.)

Fig. 22. Earthquake fissures arranged en echélon, few hundred m. S. of Fig. 21.

Fig. 23. Landslide on the western slope of Kernkol 850 m. E. of Yamanakasinden. (H. Tsuya.)

（震研彙報、第十一號、圖版、大塚）

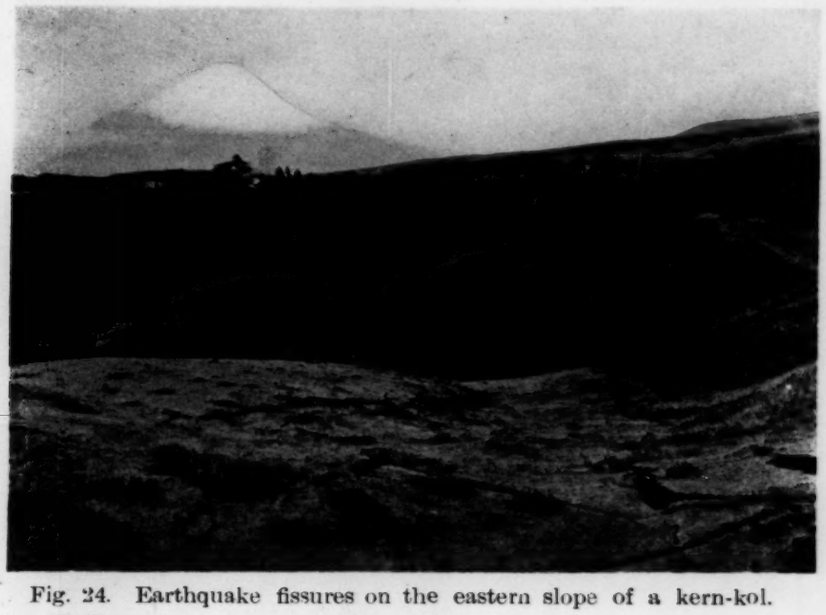

Fig. 24. Earthquake fissures on the eastern slope of a kern-kol. (H. Tsuya.)

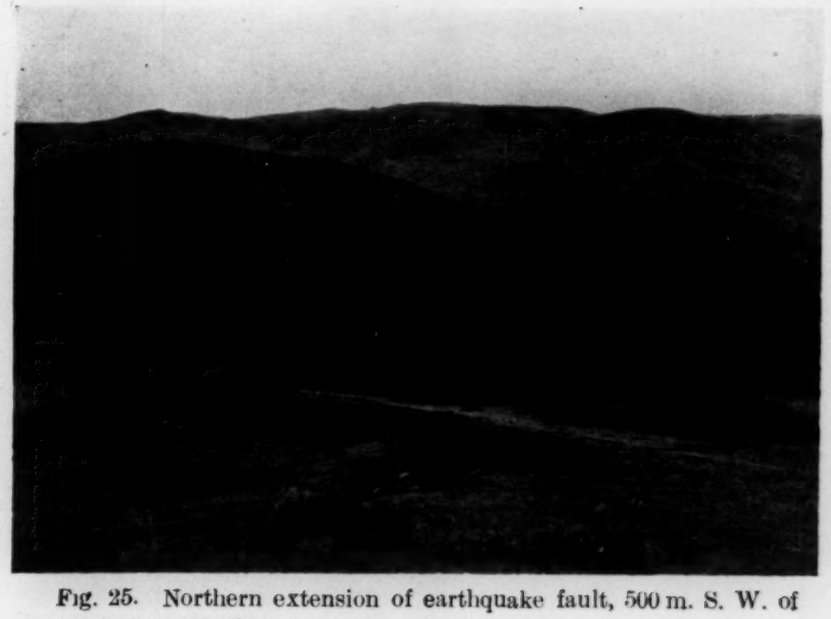

Fig. 25. Northern extension of earthquake fault, 500 m. S. W. of pt. 604 m. (H. Tsuya).

（震研彙報、第十一號、圖版、大塚）

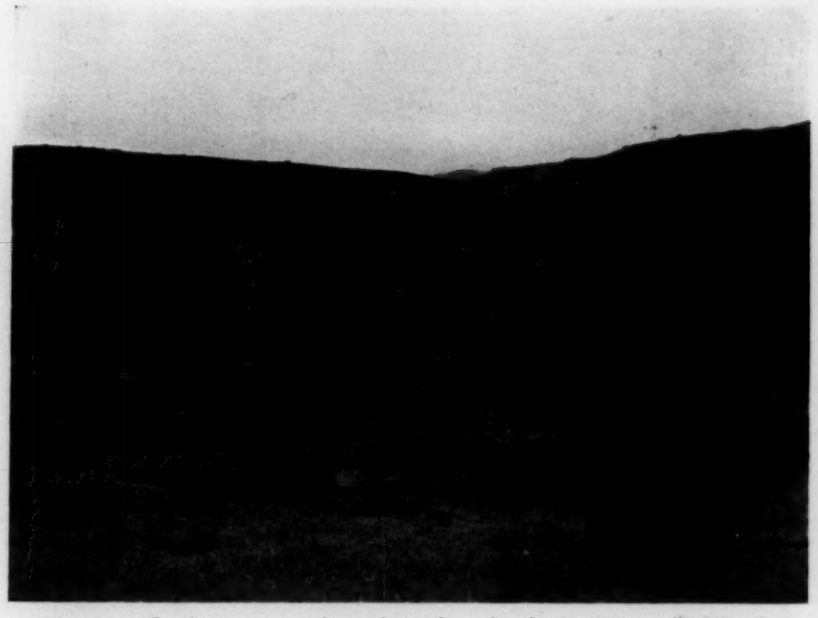

Fig. 26. Northern extension of earthquake fault, 500 m. S. W. of pt. 604 m. left of Fig. 25. (H. Tsuya.)

Fig. 27. Mole-track and plough-shared like ground disturbances on the west slope of the kern-kol 700 m. N. W. W. of pt. 604. (T. Takayama.)

（震研彙報、第十一號、圖版、大塚）

Fig. 28. Water dammed by the earthquake disturbances in Tasiro basin. (H. Tsuya.)

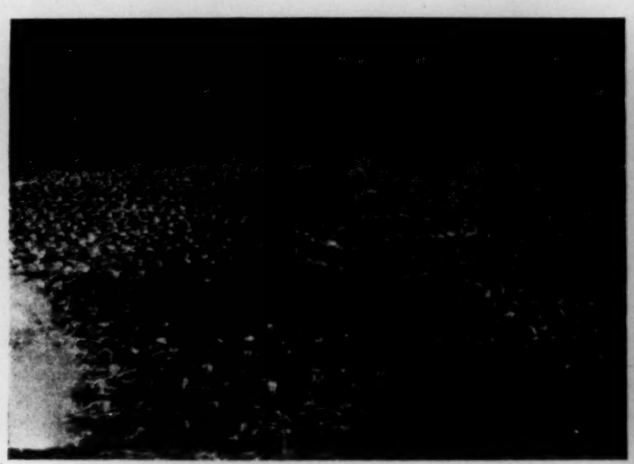

Fig. 29. Horizontal displacement of a rice field dyke.

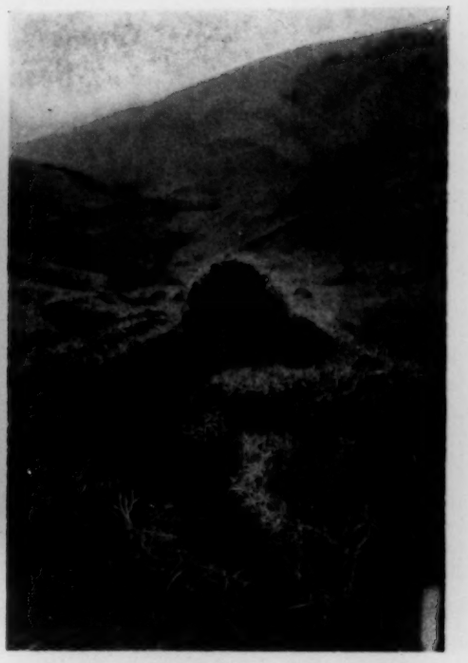

Fig. 30. Moletrack like ground disturbances. Same place as Fig. 27.

（震研彙報、第十一號、圖版、大塚）

（震研彙報、第十一號、圖版、大塚）

Fig. 31. Displaced fence of Tanna reservoir. (H. Tsuya.)

（震研彙報、第十一號、圖版、大塚）

Fig. 32. The horizontal displacement of a small road joining Tanna Nisikata and Takizawa. (H. Tsuya.)

Fig. 33. Mole-track like earthquake fault in Tasiro basin.

Fig. 34. Displaced torii in Tasiro basin.

Fig. 35. Ground disturbances in rice fields in Ukihasi basin. (H.Tsuya.)

Fig. 36, 37. Earthquake faults in the kernbut topography on the eastern steep wall of Tanakayama forest.

（震研彙報、第十一號、圖版、大塚）

Fig 38. Displacement of a small road in Ukihasi basin, Ukihasi central earthquake fault.

Fig. 39. Landslide at Oono.

Fig. 40 Displacement of a rice-field dyke in Tawarano basin.

Fig. 41. Stratified pumice beds near Akô.

（震研彙報、第十一號、圖版、大塚）

Fig. 42. Earthquake fault nr. Kadono. (H. Tsuya.)

Fig. 43. Head of the landslide at Kadiyama. (H. Tsuya.)

Fig 44. Earthquake fault cutting through the Itǫ-Syuzenzi high way, along the Oomi river.

（震研彙報、第十一號、圖版、大塚）

30. *Petrology of Some Lavas of Volcano Asama, Sinano Province, Japan.*

By Hiromichi TSUYA,

Earthquake Research Institute.

(Read April 17, 1933.—Received June 20, 1933.)

Introduction.

This paper presents the results of microscopical and chemical studies on some lavas of Volcano Asama.[1]

Asama, situated 36°24·5′N. and 138°31′E., on the boundary between the two provinces of Sinano[2] and Kôduké[3] in the central part of the Main Island, is one of the most active volcanoes in Japan. Its earliest recorded outburst dates back to 685 A. D. Of its many subsequent eruptions, the most violent was that which took place in August, 1783, when it poured out tremendous mud-and lava-flows, killing 1151 persons who inhabited the adjoining northeast terrane. Since Dec. 1909, its activities have culminated frequently in eruptions of a highly explosive character, but without outpourings of lava-flows. In recent years, since 1927, explosive activities of rather moderate intensity have occasionally been exhibited, the last explosion having taken place in July, 1932. The activity of this volcano last year, from June 1 to Sept. 12, is described in R. Takahasi's paper[4] relating to ground tilts observed during that period at Komoro,[5] a village at the southwest foot of the volcano. During Oct. 17–20, when the writer visited the active crater of the volcano, dense whitish vapor-clouds were issuing from the crater, which is 2000 m. in circumference with a depth of about 200 m., while through rifts in these clouds could be seen a mass of incandescent lava in the crater floor.

This volcano has been the object of study of not a few investigators, whose work however were practically confined to observations of its eruptions. As to its geology and petrology, what have been published thus far are only fragmentary. While studying the Volcano Kusatu-

1) 淺間火山. 2) 信濃國. 3) 上野國.
4) R. TAKAHASI, *Bull. Earthq. Res. Inst.*, 11 (1933), 25.
5) 小諸.

Sirane[6] on the occasion of its last activity in Oct., 1932, the writer had an opportunity of observing Asama and of examining its rocks. Unfortunately his field observations could not be extended beyond a limited area on the northeast side of the volcano, while the microscopic examination covers only six rock-specimens, of which three were collected by the late Dr. Mikio Kawamura. Since nothing like a complete systematic study, geological as well as petrological, of the volcano has yet been feasible, the writer intends here to lay the foundation for more detailed work to follow.

Morphological and Structural Outlines of Asama.

Asama, which rises 2542 m. above sea-level but no more than 1400 m. above the adjoining terranes, is a composite stratified volcano, consisting of triple conides disposed in a cone-in-cone structure. The oldest body, namely the outermost cone, of the volcano is the arcual mountains (2405–2280 m. above sea-level), Kurohuyama-Gippayama-Kengaminé,[7] occupying the western half of the volcano. They represent the outer somma of the present active cone, and is truncated at the top with a ring-wall surrounding a circular caldera about 2000 m. in diameter. This outer somma is built up of numerous layers, alternately accumulated lava-flows and agglomerates of andesitic nature, its stratiformed structure being well exposed on the steep inner slope of the ring-wall. The eastern half of the outer somma cannot be traced at present, being overlain by the central cone Mayékakéyama,[8] whose eruption-centre probably is not in the centre of the caldera, but more to the east of the latter. The crescent-shaped basin called Yunotaira[9] is the atrio between the outer somma on the west and the central cone on the east.

The central cone Mayékakéyama, which is 2521 m. above sea-level, but about 600 m. above the atrio floor, is a truncated cone with outer slopes of about 30°, representing the inner somma of the present active cone which lies in its summit-crater. The arc-shaped ridges—Mayékakéyama and Higasi (east)-mayékakéyama—which run along the west and the east margins respectively of the active cone, are the west and the east segments respectively of the crater-wall of the old summit-crater of the Mayékakéyama cone. The old summit-crater which, encircled with these ridges, must have been about 1000 m. in diameter, is now buried

6) H. TSUYA, *Bull. Earthq. Res. Inst.*, 11 (1933), 82.
7) 黒斑山——牙山——剣ケ峯.
8) 前掛山. 9) 湯ノ平.

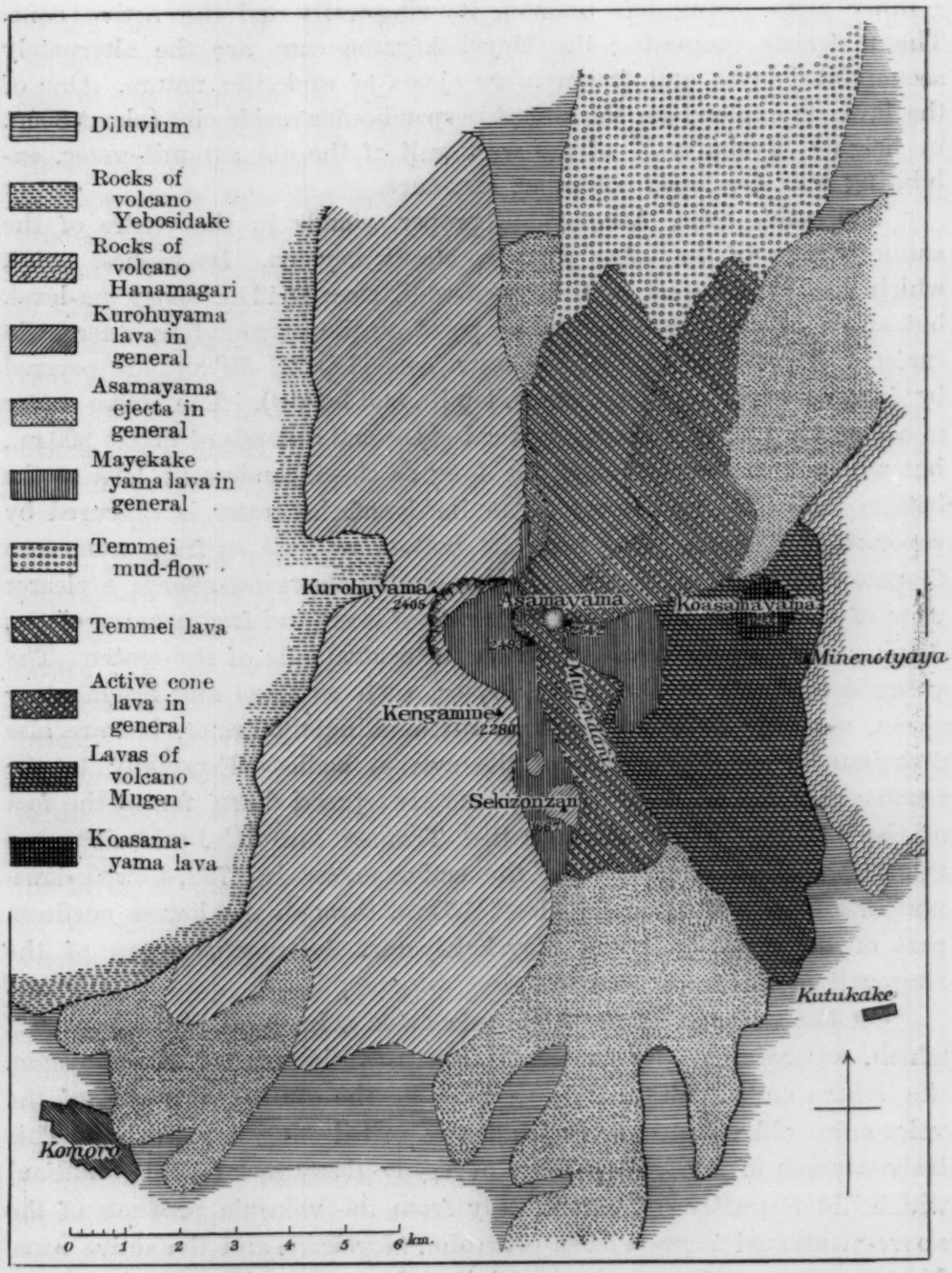

Fig. 1. Geologic sketch-map of Asamayama, based on Kawamura's geologic map.

almost completely under the products of later eruptions that took place in it and formed the present active cone, only shallow crescentic basins

—inner atrio—being left between its ring-walls and the active cone. The materials composing the Mayékakéyama cone are the alternately accumulated lavas and fragmentary ejecta of andesitic nature. One of the lavas is exposed on the almost perpendicular inside cliff (about 80 m. in height), Byôbuiwa,[10] of the west wall of the old summit-crater, exhibiting well-developed columnar structure.

The active cone, Asamayama proper, stands in the centre of the summit-crater of the inner somma, Mayékakéyama. Its highest point, which lies to the east of the crater-wall, rises 2542 m. above sea-level, but about 120 m. above the lowest point on the surrounding inner atrio surface. The outer sides of the active cone slope 25–30° and are covered by fragmentary ejecta (ash, sands, lapilli, and bombs). The active crater is a circular pit with almost vertical sides and a depth of about 200 m., but which is never stationary for long as the incandescent lava at the bottom moves up and down. The inside of the crater is obscured by vapor-clouds, which issue from its bottom as well as from numerous fissures and holes in its walls. Occasionally the wind affords a clearer view of the inside, and shows the strata of lavas and fragmentary ejecta, dipping away in all directions from the central axis of the crater. The volcanic products of the active crater, such as lavas and fragmentary ejecta, not only build up the cone surrounding the crater, but are also distributed over the surface of the somma bodies. Especially to the northeast of the volcano, the products are spread down far to the foot of the volcano. Thus, the so-called Temmei lava (Oni-osidasi)[11] and mud-flow, which erupted from the active crater in 1783, flowed down northward for a distance of about 15 km. through the lowest northern part of the crater-wall and Mayékakéyama, the northern gap of the ring-wall of the inner somma.

On the southern flank of the volcano is a knob called Sekisonzan[12] which, according to Kawamura,[13] is a parasitic cone of Kurohuyama, the outer somma. Besides it, there is in the southeastern part of the volcano an old volcanic body which he called Mugen volcano.[14] This body consists of several lava-flows of highly glassy rock (chiefly obsidian) which differ greatly petrographically from the volcanic products of the above-mentioned three centres—Kurohu, Mayékaké, and the active cone. The lavas are well exposed as precipitous lava-cliffs with columnar joints

10) 屏風岩. 11) 天明熔岩 (鬼押出). 12) 石尊山.
13) M. KAWAMURA, *MS.*, (1911).
14) 無限火山.

on the east wall of the upper course (at an altitude of 2000 m. above sea-level) of the valley Mugenno-tani, which starts from the southern gap of the ring-wall of the inner somma, Mayékakéyama, and runs southeastwards along the southern boundary of Higasi-mayékakéyama. Here they are covered by the volcanic products of Mayékakéyama, while southeastwards they are distributed extensively, being covered by the products of later eruptions of Mayékakéyama and of the active cone. But as to the eruption centre of these lavas and their geological relation to the Kurohuyama outer somma, no direct evidence has been discovered, although Kawamura has suggested that they might be traced to a local vent situated near the upper course (Mugen lava-cliff) of the valley Mugenno-tani, where they formed a massive volcano—Mugen volcano—which now, instead of looking like a volcano, has more the appearance of being a part of the Asama volcano itself.

At the eastern foot of Asama, and 1655 m. above sea-level, or about 200 m. above the surrounding ground, is a dome-shaped hill called Ko-asamayama (little Asama), which is a lava-dome, or tholoide, with sides sloping 35° (average), and having a slight crater-like depression at the centre of its summit. According to Kawamura, with whose conclusions the writer's own observations agree in the main, it forms a sort of parasitic cone, which has come up through the eastern flank of the Mugen volcano. The structure of the dome and its geological relation to the main body of Asama may be seen in the steep sloping sides of the dome. It consists of a single lava very similar, petrographically, to the lavas of the so-called Mugen volcano, rising from the foundation formed of the last-named. The upper parts of the flanks, except the western, of the dome consist of steep lava-cliffs, exhibiting onion-banding, which is a characteristic of the so-called Staukuppe, while their foot are concealed by talus-conoids that surround them. The western flank, where the dome is connected by a saddle to the main body, is gentle in slope. This part and the summit of the dome are covered by loose ejecta (lapilli, scoriae, and bombs) supplied by the present active crater of Asama. From the foregoing facts, there need be no question of the lava-dome Ko-asamayama having a direct structural relation to the Mugen volcano, and that, strictly speaking, it is a parasitic cone of the Mugen volcano, if the latter was a volcano at all, though it is used to be vaguely regarded as a parasitic cone of Asama.

The structural scheme above outlined may be shown in tabular form as follows :

Volcano Asama
- The outer somma—a stratified conide truncated at its top with a ring-wall (Kurohuyama-Gippayama-Kengaminé) surrounding a caldera, with a parasitic cone (Sekison-zan).
- The volcanic body (Mugen volcano) that underlies the inner somma, with a lava-dome (Ko-asamayama) which is considered to have been formed during the development of that body.
- The inner somma (or the central cone of the outer somma)—a stratified conide truncated at its top with a ring-wall (Mayékakéyama and Higasi-mayékakéyama) surrounding an old summit-crater.
- The central cone—a stratified conide having an active crater.

Asama volcano is not old, geologically speaking, its birth dating probably in late Diluvium or later. The foundation on which the volcano rests consists of Neogene Tertiary formations and Diluvial deposits, besides various volcanic rocks, such as hornblende-andesite, pyroxene-andesite, and olivine-pyroxene-andesite and others, which have built up the extinct Diluvial volcanoes, the Yebosidaké[15] volcano group on its west and the Hanamagari (Tuno-otosi)[16] volcano group on its east.

Petrography of Volcano Asama.

Excluding fragmentary ejecta, the rocks of Asama have been divided by Kawamura as follows:

A. Lavas of the outer somma.
   1. Hypersthene-andesite.
   2. Olivine-bearing hypersthene-andesite.
   3. Hypersthene-augite-andesite.
   4. Two-pyroxene-andesite.

B. Lavas of the Mugen volcano.
   5. Obsidian.
   6. Two-pyroxene-andesite.

C. Lavas of the inner somma.
   7. Two-pyroxene-andesite.
   8. Hypersthene-augite-andesite.
   9. Augite-andesite.

D. Lavas of the active cone.

15) 烏帽子岳. 16) 鼻曲山 (角落山).

10. Two-pyroxene-andesite.
11. Olivine-bearing two-pyroxene-andesite.

Of these various rocks that form Asama, the writer examined microscopically and chemically four specimens of an andesitic and two of dacitic nature. Before discussing the petrology of the volcano, the genenal petrographic character of the andesitic and dacitic rocks will be described.

(*A*) *Andesites.*

I. Olivine-bearing two-pyroxene-andesite (one of the Kurohuyama lavas). (Fig. 6)
II. Olivine-bearing two-pyroxene-andesite (Yunotaira lava, an older lava of the Mayekakeyama centre). (Fig. 7)
III. Olivine-bearing hypersthene-augite-andesite (lava of 1783). (Fig. 8)
IV. Olivine-bearing hypersthene-augite-andesite (bread-crust bomb ejected in Sept., 1929). (Fig. 9)

Though each of these has certain distinguishable characters, both megascopic and microscopic, they all resemble one other in their important petrographic characters.

Megascopic Characters.—Megascopically, these rocks are dark gray to black and more or less scoriaceous, with vesicles less than 1·5 mm. in diameter. Phenocrysts of plagioclase, pyroxene, and olivine are scattered through the dark glassy base. Among these phenocrysts, the plagioclase, which is less than 1·5 mm. in diameter, is most dominant; while the olivine, which is less than 1 mm. in diameter, is rare.

Microscopic Characters.—Microscopically, these rocks are porphyritic, with phenocrysts of plagioclase, hypersthene, augite, olivine, and accessory magnetite. These phenocrysts are scattered, with no trace of any regular arrangement, through a dark brown or almost colorless groundmass. As they are present in variable quantities in all the rocks, the structure of the latter varies from nearly dosemic to sempatic. The quantities of the chief constituent minerals were measured volumetrically and their volume percentages calculated as shown in Table I. In the Table the volume percentage of the vesicles in each rock are also shown.

Table I.

Modal Compositions (Vol. %) of the Asama Andesites.

		I	II	III	IV
Phenocrysts	Plagioclase	26·89	28·30	24·58	31·67
	Hypersthene	2·03	3·53	2·25	4·01
	Augite	2·29	3·58	4·08	6·24
	Olivine	tr.	0·10	0·09	0·06
	Magnetite	1·13	0·61	0·68	0·64
Groundmass		67·66	63·88	68·32	57·38
Vesicles		23·00	14·31	19·36	16·96

I. Kurohu lava.
II. Yunotaira lava.
III. Temmei (1783) lava.
IV. Bread-crust bomb ejected in Sept., 1929.

Plagioclase.—The plagioclase phenocrysts which are euhedral and subhedral, are developed in prismatic and nearly equant habit, showing simple and polysynthetic twin-lamellae according to the albite, Carlsbad and pericline laws. Zonal structure due to chemical difference is clearly exhibited. The mode of change of chemical composition in successive zones is not regular. Although the innermost zone is commonly the most calcic and the outermost the most sodic, reversal, or recurrent, zoning is frequently met with. The refractive indices—n_{1D} in (010) or (001)—measured with Tsuboi's dispersion method[17] are shown in the

Table II.

	Plagioclase n_{1D}	Ab%	Hypersthene n_{1D}	Hy%	Augite n_{1D}	Hd%	Olivine β_D	Fay%
I	1·5653–1·5597	29–40	1·6983–1·7046	33–38	1·6964	39	1·6996	23
II	1·5668–1·5613	26–37	1·7016	35	1·6960	38	n. d.	
III	1·5643–1·5574	31–44	1·7032	37	1·6961	38	1·6856	17
IV	1·5662–1·5579	27–43	1·7030	37	1·6960	38	1·7020	25

I. Kurohu lava.
II. Yunotaira lava.
III. Temmei lava.
IV. Bread-crust bomb in Sept., 1929.

17) S. TSUBOI, *Miner. Mag.*, London, 20 (1923), 93.
S. TSUBOI, *Jour. Fac. Sci. Imp. Univ.*, Tôkyô, 1 (1926), 146.

first column of Table II, according to which the mineral is identified as labradorite, averaging $Ab_{35}An_{65}$ in chemical composition. It appears therefore that the plagioclase phenocrysts in the andesites concerned are practically identical in compositions with each other. It is noticeable however that the plagioclase phenocrysts contained in the historic lavas (Temmei lava and 1929 bomb) have sometimes more calcic cores (calcic bytownite as identified by their extinction angles) zonally surrounded by shells of labradorite. The mineral contains numerous minute inclusions of plagioclase, pyroxene, brown glass, and dust material.

Hypersthene.—Hypersthene occurs as euhedral phenocrysts of stout prismatic form measuring 0·5–1·0 mm. along the longest direction. Some regularity appears to exist in the relation between variation in the amounts of the mineral and the order of eruption of the andesite, as shown in Table I. Axial colors observed in thin section are:

X....brownish, Y....yellowish brown, Z....greenish.

The optical plane is always parallel to the c-axis of the mineral. The refractive indices—n_{1D} in (110)—measured with the dispersion method and the approximate chemical compositions determined with the aid of the Tomita diagram[18] are shown in the second column of Table II. A faint zonal structure due to chemical difference is observed in the hypersthene contained in Kurohu lava, the oldest andesite of the four examined specimens. It is clearly exhibited when the mineral flake is immersed in a liquid. The mode of zoning is not regular, the hypersthene with higher and lower refractive indices being alternately developed in successive zones.

Augite.—Augite occurs as euhedral and subhedral phenocrysts averaging 1·0 mm. in diameter. Its amount increases regularly according to the order of eruption of the andesites in which it is contained, the maximum reaching 6·5 vol. % in the latest one (1929 bomb). The mineral is a light greenish brown variety. Sometimes it occurs in a rim around the hypersthene in parallel growth. Twinning after (100) is often met with. Zonal structure due to chemical difference is not observed. Extinction angle $c \wedge Z$ is about 45°. Optic angle is always large. The refractive indices—n_{1D} in (110)—measured with the dispersion method and the approximate chemical composition determined by means of the Tomita diagram are shown in the third column of Table II. Thus, the augite phenocrysts in the four rock-specimens closely agree

18) T. Tomita, *Jour. Geol. Soc.*, Tôkyô, 31 (1924), 364, (in Japanese).

in their important petrographic characters.

Olivine.—Olivine phenocrysts are present in all the four specimens, though very little in amount. They are always unhedral, pale yellowish green or nearly colorless in thin section, and surrounded by minute grains of a monoclinic pyroxene. The principal refractive indices—β_D—measured with the dispersion method and the approximate chemical compositions as determined by the refractive indices are shown in the fourth column of Table II. It is notable that the olivine in the Temmei lava (III) has much lower refractive indices compared with the mineral in the other lavas.

Magnetite.—Magnetite occurs in small amounts as isometrict grains less than 0·3 mm. in diameter.

Groundmass.—The groundmass consists entirely of either brown or colorless glass, except a few feldspar prismoids and pyroxene grains, which however cannot be optically analysed. The refractive index of the glass base in the Temmei lava was measured with the ordinary immersion method and found to be $n_D=1·5240$. This value shows an intermediate basicity of the glass.

Chemical Compositions.—The chemical analyses of the andesites gave the results shown in the first four columns of Table III.

Of the four andesites, according to the C. I. P. W. quantitative system, three (I, II and IV) belong to bandose and one (III) to tonalose. An older analysis (IV′) of a bomb ejected in Dec. 1909, which was made by the Geological Survey and published by Denzo Sato[19] in his report on the eruption of that time, resembles on the whole the four preceding analyses, except in alkalies, showing that the bomb belongs to bandose. It is probable that the total alkalies (1·64%) in the bomb are too low, since S. Tanaka's partial analysis of another bomb ejected in Dec. 1909, showed that the Na_2O and K_2O contents of the bomb are 3·19% and 1·18% respectively. Consequently, the analysis reported by Sato seems to be at fault in these respects.

As is clear from the above table, all the four analysed Asama andesites resemble in bulk composition the rocks of the volcanoes Bandaisan, Tarumaisan, etc. of northeast Japan, all being characterised by normative labradorite. They may thus be classed as typical "bandaite," using Idding's term. While they show certain analogies with the volcanic rocks of the so-called Huzi Volcanic Zone, they differ

19) D. Sato, *Jour. Geogr.*, Tôkyô Geogr. Soc., **22** (1910), 196, (in Japanese).

Table III.

Bulk Compositions of the Asama Andesites.

	I	II	III	IV	IV′
SiO_2	58·39	59·67	62·37	60·24	59·76
Al_2O_3	17·89	16·83	15·90	16·43	16·90
Fe_2O_3	2·45	1·44	1·14	1·54	1·74
FeO	5·33	5·51	4·79	5·26	5·46
MgO	3·30	3·92	3·43	3·92	4·36
CaO	7·23	7·21	6·13	7·07	8·66
Na_2O	3·04	2·81	3·20	3·00	1·05
K_2O	0·71	1·00	1·49	1·16	0·59
H_2O+	0·36	0·28	0·30	0·17	0·13
$-$	0·12	0·13	0·12	0·06	
TiO_2	0·71	0·70	0·66	0·70	1·23
P_2O_5	0·15	0.14	0·13	0·13	tr.
MnO	0·14	0·12	0·11	0·11	0·38
Total	99·82	99·76	99·77	99·79	100·26
Norms.					
Q	15·20	15·92	17·84	15·98	23·84
Or	4·45	6·12	8·90	6·68	3·34
Ab	25·69	23·59	27·26	25·17	8·91
An	32·82	30·22	24·48	28·09	39·78
Di	1·83	3·87	4·12	5·02	2·48
Hy	14·19	15·89	13·63	14·66	16·90
Mt	3·49	2·08	1·62	2·31	2·55
Ap	0·31	0·31	0·31	0·31	tr.
Il	1·37	1·37	1·21	1·37	2·28
C. I. P. W. Symbols	II. 4.″4. 4 (5) Bandose	II. 4.″4. 4 Bandose	II. 4. 3″.4. Tonalose	II. 4. (3) 4. 4 Bandose	II.″4. 4 (5). 4 Bandose

I. Kurohu lava. S. Tanaka anal.
II. Yunotaira lava S. Tanaka anal.
III. Temmei lava. S. Tanaka anal.
IV. Bomb in Sept., 1929. S. Tanaka anal.
IV′. Bomb in Dec., 1909. The Imp. Geol. Surv. anal.

petrographically as well as chemically from late-Diluvium and recent basaltic rocks of the latter, which are characterised either by the dominance of calcic normative plagioclase phenocrysts (calcic bytownite or

anorthite) or by calcic normative plagioclase (bytownite or anorthite), even when these rocks belong to the quardofelic order according to the C. I. P. W. quantitative system.

(*B*) *Dacites.*

V. Hornblende-two-pyroxene-dacite (Mugenno-tani obsidian). (Fig. 10)

VI. Hornblende-two-pyroxene-dacite (Ko-asamayama lava). (Fig. 11)

Of the two dacitic rocks, one (V) occurs at Mugenno-tani in several of the lava-flows without any noticeable layers of fragmentary ejecta between them, and the other (VI) occurs at Ko-asamayama in a single lava, forming a small domical hill of that name. They differ from one another both in megascopic and microscopic features, but agree closely in their important petrographic characters.

Megascopic Characters.—Megascopically, the one (V) is jet-black with glassy luster, and is mediophyric to minophyric with phenocrysts of plagioclase scattered through the black glass base; and the other (VI) is light gray or light brown, more or less vesicular, and is mediophyric with phenocrysts of plagioclase and pyroxene scattered through a dull, somewhat earthy, aphanitic groundmass.

Microscopic Characters.—Microscopically, both of them contain phenocrysts of plagioclase, hornblende, hypersthene, augite, and magnetite. The amounts of these phenocrysts and that of the groundmass through which the phenocrysts are scattered were measured volumetrically, and their volume percentages were calculated as shown in columns V and VI, Table IV.

Table IV.

Modal Compositions (Vol. %) of the Asama Dacites.

		V	VI.
Phenocrysts	Plagioclase	8·78	7·54
	Hornblende	0·25	tr.
	Hypersthene	0·21	0·36
	Augite	0·29	0·02
	Magnetite	0·56	0·56
Groundmass		89·91	91·52
Vesicles		—	10·91

V. Mugenno-tani obsidian. VI. Ko-asamayama lava.

Plagioclase.—The plagioclase phenocrysts are euhedral to subhedral, stout prismatic to equant, and twinned according to the albite, Carlsbad, and pericline laws. Occasionally, two or more individuals of the mineral form a grouped phenocryst. Polysynthetic twinning and zonal structure due to chemical difference are better exhibited in larger phenocrysts than in smaller ones. The refractive indices—n_{1D} in (010) or (001)—measured with the dispersion method and the chemical compositions determined by the refractive indices are shown in the first column of Table V. The mineral contains inclusions of plagioclase, pyroxene, glass, and slender prisms of colorless apatite.

Table V.

	Plagioclase n_{1D}	Ab%	Hornblende n_{2D}	Hypersthene n_{1D}	Hy%	Augite n_{1D}	Hd%
V	1·5600–1·5556	39–48	1·6879	1·6973	33	1·6892	30
VI	1·5590–1·5533	41–51	n. d.	1·6970	33	1·6925	33

V. Mugenno-tani obsidian.
VI. Ko-asamayama lava.

Hornblende.—The hornblende is euhedral, prismatic, and is 0·5–0·1 mm. in the longest direction. The mineral is of a rather pale greenish brown color with the following pleochroism:

X....yellowish green, Y....green, Z... greenish brown.
Absorption: $X<Y<Z$

The hornblende in the Ko-asamayama lava is usually opacitized, while that in the Mugenno-tani obsidian is quite fresh. The larger refractive index—n_{2D}—measured with the cleavage flakes of the mineral is shown in the second column of Table V. $c \wedge Z' = 6·5°$; twinning after (100).

Hypersthene.—The hypersthene is euhedral, prismatic, and is 0·5–0·1 mm. in the longest direction. Occasionally, two or three individuals of the mineral form a glomeroporphyritic phenocrysts associated with plagioclase and augite. It is usually pale greenish brown, and is moderately pleochroic, giving X—pale brown, Y—light yellow, and Z—pale green. Optical plane is parallel to the c-axis of the mineral. The refractive indices—n_{1D} in (110)—measured with the dispersion method and the approximate chemical compositions determined by the Tomita diagram are shown in the third column of Table V. Although the mineral has no inclusions, it is sometimes surrounded by a monoclinic

pyroxene in parallel growth. Hypersthene in the Ko-asamayama lava is often rimmed with opacitic black margin.

Augite.—The augite is euhedral to subhedral, stout prismatic to equant, and is 0·5–0·2 mm. in average diameter. It is pale greenish brown with no pleochroism. Twinning after (100) is sometimes observed. $c \wedge Z = 44{\cdot}5°$; optic angle large. The refractive indices—n_{1D} in (110)—measured with the dispersion method and the approximate chemical compositions determined by the Tomita diagram are shown in the fourth column of Table V.

Magnetite.—The magnetite occurs in isometric form, 0·5–0·1 mm. in diameter.

Groundmass.—The groundmass of the Mugenno-tani obsidian is a colorless glass in thin section, through which microlites are arranged in a flow structure. The refractive index of the glass is 1·4955. The groundmass of the Ko-asamayama lava is colorless to pale brownish gray and is glassy, but it contains, besides small vesicles, feldspar prismoids (oligoclase-andesine according to their extinction angles), pyroxene grains, opacitized hornblende flakes, iron-ore, and a weak double refracting colorless mineral (tridymite ?), the last-named occurring as aggregates of minute anhedral units.

Chemical Compositions.—Chemical analyses of the dacites gave the results shown in Table VI.

According to the C. I. P. W. quantitative system, the two analysed dacites belong to lassenose.

The analysis of the Ko-asamayama lava (VI) shows lower SiO_2 and FeO content and higher Fe_2O_3 and H_2O content, compared with that of the Mugenno-tani obsidian (V), but in other respects they resemble each other. It is probable that analysis VI does not represent very faithfully the composition of the fresh rock, since microscopic examination shows that even the freshest specimen from newly obtained blocks of Ko-asamayama lava undergoes some alteration, as may be inferred from the fact that the hornblende in the rock is almost entirely opacitized. The higher ferric oxide and water content in analysis VI are thus seen to be results of oxidation and hydration of the analysed rock. By recalculation of the two analyses to percentages of the main oxides, exclusive of H_2O, TiO_2, P_2O_5, and MnO, we see that the two resemble each other in all particulars, except in the iron oxides, though the total amount of the last-named in the two analyses is the same.

As is clear from the microscopic description, the dacitic rocks do

not contain quartz phenocrysts, but normatively they are characterized by oligoclase $Ab_{74}An_{26}$ and belong to the persalic class, containing quartz molecules in such quantities that they are classed in the quadofelic order near to quarfelic in the quantitative system. These rocks are, therefore, to be classed as dacite.[20]

Genetical Relationships.

While this is not the place for a general discusssion of the petrology of volcano Asama, a few words may be devoted to the genetical relationship of the rocks whose analyses, optical as well as chemical, have just been given.

From the optical data given in Table II (p. 579) and V (p. 584), the paragenic relations between plagioclases and mafic minerals in the rocks of Asama are graphically represented in Fig. 2. In order to represent here the composition-variations of the mafic minerals, the refractive indices (β_D for olivine, n_{1D} for pyroxene, and n_{2D} for hornblende) have been adopted. The composition of the plagioclases are represented by those of the most sodic parts of the zoned crystals.

Table VI.
Bulk Compositions of the Asama Dacites.

	V	VI
SiO_2	72·01	69·93
Al_2O_3	14·37	14·12
Fe_2O_3	0·73	2·45
FeO	1·81	0·45
MgO	0·57	0·58
CaO	2·56	2·42
Na_2O	4·35	4·04
K_2O	2·39	2·25
H_2O+	0·26	2·00
H_2O-	0·08	0·97
TiO_2	0·41	0·38
P_2O_5	0·07	tr.
MnO	0·08	0·09
Total	99·69	99·68
Norms.		
Q	30·39	31·77
Or	13·91	13·36
Ab	36·70	24·08
An	12·79	11·96
C	—	0·71
Hy	3·65	1·24
Mt	1·16	0·23
Hm	—	2·24
Ap	—	tr.
Il	0·61	0·76
C. I. P. W. Symbols	I.″4. 2″. 4 Lassenose	I. (3) 4. 2″. 4 Lassenose

V. Mugenno-tani obsidian. S. Tanaka anal.
VI. Ko-asamayama lava. S. Tanaka anal.

As will be seen in the figure, the andesites agree so closely in the paragenic relations between either plagioclase and augite or plagioclase

20) It is probable that some of the acid xenoliths, frequently enclosed in recent juvenile ejecta of the volcano, are derived from this dacite.

and hypersthene that they may be considered to represent only one stage in the cooling history of the magma from which they have been derived. The olivine in the Temmei lava (III) is distinctly lower in refractive index than the same mineral contained in the other three lavas (I, II, and IV). Probably the former is a relict mineral, which had ceased to react with the liquid at an earlier stage than the latter. In this connection it is notable that the Temmei lava carries plagioclase phenocrysts in which a calcic bytownite occurs as cores of labradorite.

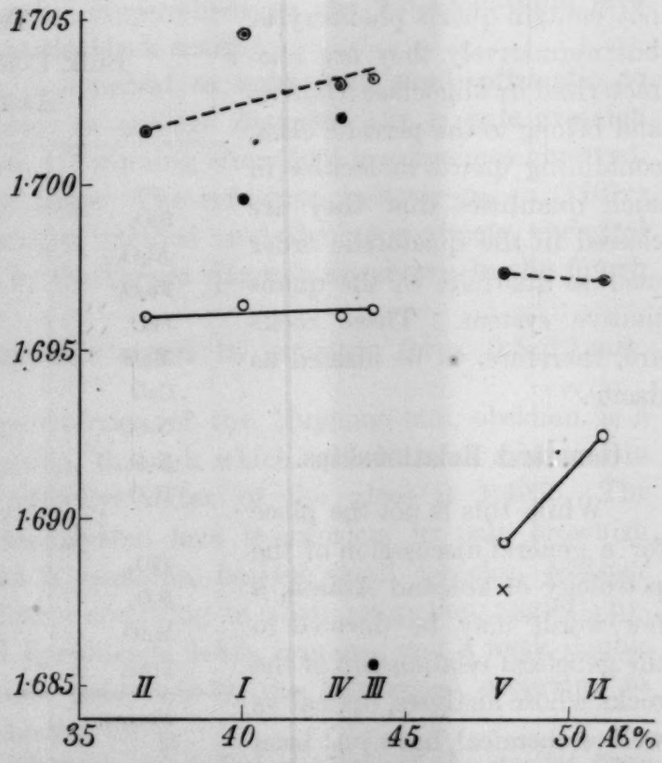

Fig. 2. The actual paragenic relations of plagioclases and mafic minerals (•: olivine, ○: augite, ◉: hypersthene, ×: hornblende) in the volcanic rocks of Asama. I—Kurohu lava; II—Yunotaira lava; III—Temmei lava; IV—Bomb in Sept, 1929; V—Mugenno-tani obsidian; VI—Ko-asamayama lava.

The pyroxene in the dacites are distinctly lower in refractive index than that same minerals in the andesites. It is inferred that the dacites have been derived from a magma partially squeezed out from the parent magma at an earlier stage than that from which the andesites have been derived, if ever there was any genetical relation between the dacites and the andesites.

Since the optical constants of pyroxene vary with the chemical compositions of that mineral, the former may be reflected in the chemical compositions of normative pyroxenes in the rocks in which pyroxenes are the chief mafic minerals, besides plagioclase. Fig. 3 shows the compositions of the normative pyroxenes in the rocks of the Asama volcano. The lime contents in the normative pyroxene increase gradually from I to IV. On the other hand, Table I (p. 579) shows that the amounts

of pyroxene phenocrysts, especially of augite, increase regularly from I to IV. This fact seems consistent with what has been said before, indicating that bulk compositions are greatly affected by the relative amounts of the phenocrystic minerals.

Since the refractive indices of pyroxenes change markedly according to the relative amounts of ferrous oxide and magnesia contained in them, the relation between the ratios of these two oxides held in normative pyroxenes and the compositions of normative plagioclases may be likened to the relation between the refractive indices of modal pyroxenes and the compositions of the modal plagioclases. Fig. 4 shows the former relation of the rocks of Asama. As is seen in the figure, all the andesites in which plagioclase and pyroxenes are the main phenocrystic minerals, agree closely in the compositions of the normative plagioclases as well as in the FeO : MgO ratios of the normative pyroxenes. This fact reflects the actual paragenic

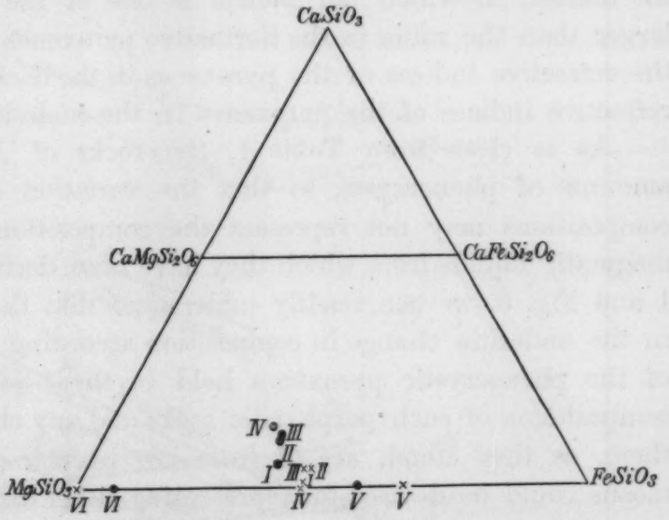

Fig. 3. Compositions of the normative pyroxenes in the rocks of Asama.

●: Normative pyroxene in the bulk composition.
×: Normative pyroxene in the groundmass composition.

I. Kurohu lava. IV. Bomb in Sept., 1929.
II. Yunotaira lava. V. Mugenno-tani obsidian
III. Temmei lava. VI. Ko-asamayama lava.

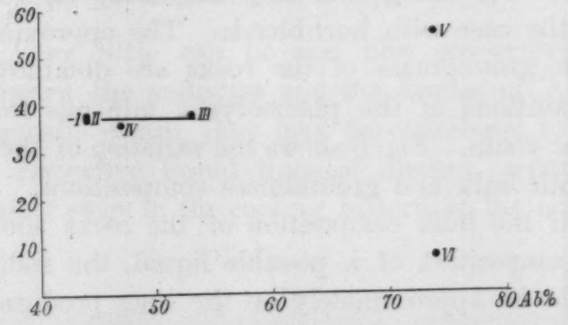

Fig. 4. The relation of normative plagioclase and normative pyroxene in the volcanic rocks of Asama. I—Kurohu lava; II—Yunotaira lava; III—Temmei lava; IV—Bomb in Sept., 1929; V—Mugenno-tani obsidian; VI—Ko-asamayama lava.

relation between the modal plagioclases and the modal pyroxenes held in them (Fig. 2). The FeO : MgO ratios in the normative pyroxenes of the dacites, in which hornblende is one of the chief constituents, are larger than the ratios in the normative pyroxenes of the andesites ; while the refractive indices of the pyroxenes in the dacites are lower than the refractive indices of the pyroxenes in the andesites.

As is clear from Table I, the rocks of Asama contain various amounts of phenocrysts, so that the variation diagram of their bulk compositions may not represent the composition changes of the past magmatic liquids from which they have been derived. Comparing Table I and Fig. 3, we can readily understand that the normative pyroxenes in the andesites change in composition according to the relative amounts of the phenocrystic pyroxenes held in these rocks. Hence, the bulk compositions of such porphyritic rocks and any classification based upon them, as they stand, are of little use in petrogenesis. But, if some means could be devised for representing either directly or indirectly, the compositions of the groundmass of the porphyritic rocks, then the composition change of the liquids from which these rocks have been derived, may be inferred. One means of meeting this requirement is volumetric analysis of the porphyritic rocks.

The approximate chemical compositions of the phenocrystic minerals in the rocks of Asama are known from their optical constants (Tables II and V), though actually they may be very complex, especially is this the case with hornblende. The approximate chemical compositions of the groundmass of the rocks are obtained by subtracting the total compositions of the phenocrystic minerals from the bulk compositions of the rocks. Fig. 5 shows the variation of the Asama rocks with respect to both bulk and groundmass compositions.

If the bulk composition of the rocks should depart but little from the composition of a possible liquid, the indicative points of the rocks should lie approximately on the lines produced in the low silica side of the composition change of the groundmasses. Such a tendency is seen on the curves representing the variation of alumina and alkalies. This fact seems to indicate that the plagioclase phenocrysts remained approximately just where they were formed ; while the mafic minerals are represented by lesser amounts than are possible in rocks formed by the direct congelation of any magmatic liquid.

The indicative points of the dacites show notable departure from the smoothed curves showing the variation of the groundmass composi-

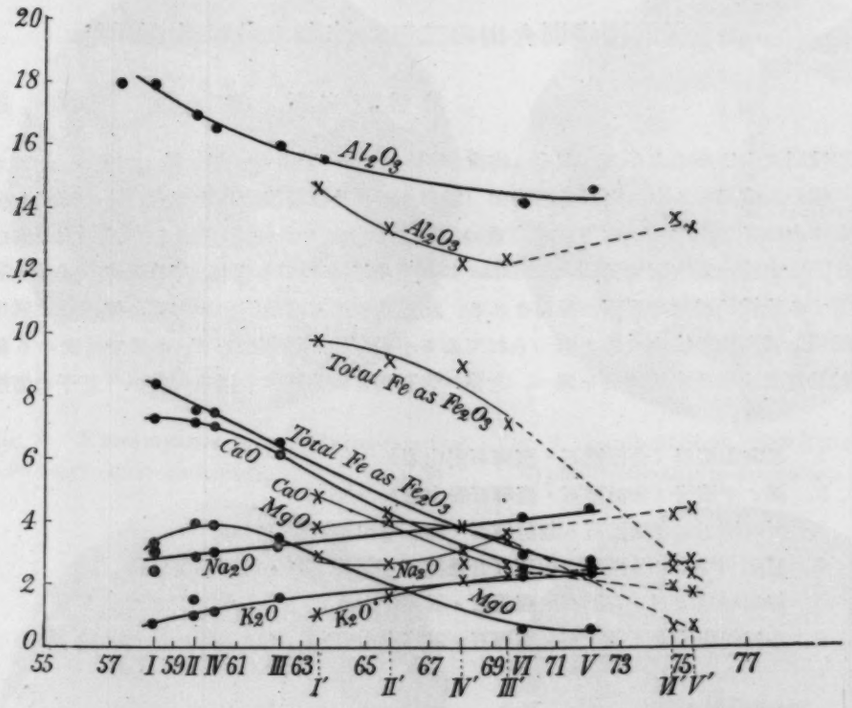

Fig. 5. Variation diagram of the rocks of Asama. Thick lines: bulk compositions; thin lines: groundmass compositions. I—Kurohu lava; II—Yunotaira lava; III—Temmei lava; IV—Bomb in Sept., 1929; V—Mugenno-tani obsidian; VI—Ko-asamayama lava.

tions of the andesites. Very little can be said now concerning the genetical relationship between the andesites and the dacites of Asama, but by assuming a comagmatic origin, they may be considered to have been derived from their respective liquid lines of descent, separating from one another at an early stage in the cooling history of the original common magma.

30. 信濃國淺間火山の二三の熔岩の岩石學的研究

地震研究所 津屋弘達

信濃國淺間火山は外輪山なる黒斑山（海抜 2405 m.）——牙山——剣ヶ峯（2280 m.），其カルデラの東側に偏して噴出せる中央火口丘前掛山（2521 m.）及び前掛山の山頂火口内に噴出し現在活動しつゝある火口丘（2542 m.）より成る三重の所謂 somma volcano である．此火山を構成する岩石は主として中性の安山岩で所謂 bandaite に相當するものであるが，其他に化學成分上石英安山岩に相當する比較的酸性の岩石が見出される．此酸性の岩石は前掛山南東腹の無限谷に露出する黒曜石質熔岩と淺間山の寄生火山と考へられてゐる小淺間山の熔岩である．本文では次の 6 種の岩石の顯微鏡的性質及び化學的性質を述べ，之等の岩石相互の岩石學的關係に就いて若干の考察を加へた．

1. 黒斑山熔岩（含橄欖石・複輝石安山岩）
2. 湯ノ平熔岩（含橄欖石・複輝石安山岩）
3. 天明熔岩（含橄欖石・紫蘇輝石・輝石安山岩）
4. 昭和 4 年 9 月抛出火山彈（含橄欖石・紫蘇輝石・輝石安山岩）
5. 無限谷黒曜石（角閃石・複輝石・石英安山岩）
6. 小淺間山熔岩（角閃石・複輝石・石英安山岩）

Fig. 6. Kurohuyama lava (Olivine-bearing two-pyroxene-andesite). ×35

Fig. 9. Bomb in Sept., 1929 (Olivine-bearing hypersthene-augite-andesite). ×35

Fig. 7. Yunotaira lava (Olivine-bearing two-pyroxene-andesite). ×35

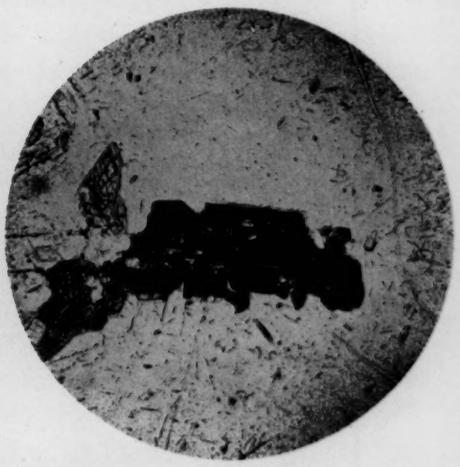

Fig. 10. Mugenno-tani Obsidian (Hornblende-two-pyroxene-dacite). ×35

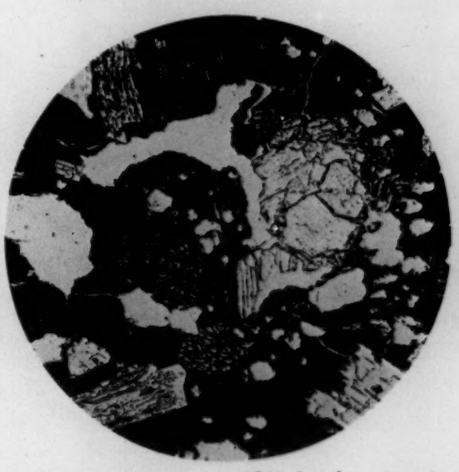

Fig. 8. Temmei lava (Olivine-bearing hypersthene-augite-andesite). ×35

Fig. 11. Ko-asamayama lave (Hornblende-two-pyroxene-dacite). ×35

MICROPHOTOGRAPHS OF THE ROCKS OF ASAMAYAMA.

（震研彙報、第十一號、圖版、津屋）

31. *On the Effects of Discontinuity Surfaces upon the Propagation of Elastic Waves. (II)*

By Genrokuro NISHIMURA and Kiyoshi KANAI,

Earthquake Research Institute.

(Read Sept. 19, 1933.—Received Sept. 20, 1933.)

1. In the preceding paper[1], we studied the initial motion of the free surface of a stratified semi-infinite solid when a dilatational wave of harmonic type is incident upon the bottom surface of the surface layer. In the present paper, taking the multiple reflections of waves at the free and the bottom surfaces of the layer into consideration, we shall study the motion of particles in this stratified semi-infinite solid when a harmonic train of dilatational waves is obliquely incident upon the bottom surface of the layer. We assume, of course as in the preceding paper, that the two solids, *i.e.* the surface layer and the bottom semi-infinite solid, slide over each other without friction at the common boundary. The calculated results show many remarkable facts and it will be of interest to compare them with Professor Sezawa's results, which were obtained from the condition in which the two solids adhered closely at the common boundary. When a dilatational wave of harmonic type of infinite extent is obliquely incident upon the bottom surface of the surface layer, the amplitudes of both vertical and horizontal motions of a particle in the layer vary with the emergency angle of the incident wave, and they are much affected by the thickness of the layer and the wave length (or period and wave velocity) of the incident wave. Therefore the orbital motion of a particle in the layer is generally much affected by the variation of these quantities. When the Poisson's ratio of each of the two media are 1/4 and their densities and rigidities are equal, one of the axes of the elliptic orbits in the layer is always vertical, as in the case of the motion of a particle of water in the surface wave, even if the emergency angle

1) G. NISHIMURA and K. KANAI, "On the Effect of Discontinuity Surfaces upon the Propagation of Elastic Wave. (I)" *Bull. Earthq. Res. Inst.*, 11 (1933).

2) K. SEZAWA and K. KANAI, "Reflection and Refraction of Seismic Waves in a Stratified Body," *Bull. Earthq. Res. Inst.*, 10 (1932).

of the primary wave varies. In this case, moreover, the particle on the bottom surface of the layer always has only vertical motion, while that of the bottom medium on this surface, on the contrary, generally has elliptic motion.

To ascertain the properties of the wave propagation above mentioned, we have calculated numerically the cases in which the emergency angles of the primary wave are 30°, 45° and 60°, the first case having been calculated in detail.

2. When the dilatational wave of harmonic type of infinite extent, which is incident obliquely upon the bottom surface of the surface layer, is expressed by

$$\Delta = \mathfrak{A} e^{i(pt-fx-ry)}, \quad \cdots\cdots\cdots\cdots\cdots\cdots (1)$$

the x- and y- components of displacement u, v corresponding to (1) are

$$\left.\begin{aligned} u &= \frac{if}{h^2}\mathfrak{A} e^{i(pt-fx-ry)}, \\ v &= \frac{ir}{h^2}\mathfrak{A} e^{i(pt-fx-ry)}, \end{aligned}\right\} \quad \cdots\cdots\cdots (2)$$

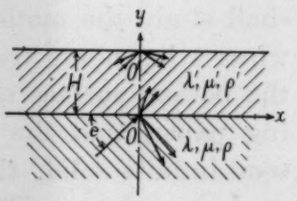

Fig. 1.

where

$$h^2 = \frac{\rho p^2}{\lambda + 2\mu}, \quad r^2 + f^2 = h^2, \quad \cdots\cdots (3)$$

and $p = \dfrac{2\pi}{T}$, ρ and λ, μ are respectively the density and the elastic constants of the lower medium, T being the period of the incident wave (1). (See Fig. 1.)

Now we can easily obtain the following two general wave expressions Δ_1 and 2ϖ which satisfy the wave equations:

$$\Delta_1 = A' e^{i(pt-fx+ry)}, \quad \cdots\cdots\cdots\cdots\cdots (4)$$

$$2\varpi_1 = B' e^{i(pt-fx+sy)}, \quad \cdots\cdots\cdots\cdots\cdots (5)$$

where

$$\left.\begin{aligned} s^2 &= k^2 - f^2, \\ k^2 &= \frac{\rho p^2}{\mu}, \end{aligned}\right\} \quad \cdots\cdots\cdots\cdots\cdots (6)$$

and A', B' are arbitrary constants to be determined. These two waves are necessary to satisfy the boundary conditions at the common boundary $y=0$.

The displacements (u_1, v_1) and (u_2, v_2) corresponding to (4) and (5) are respectively expressed by

$$\left.\begin{aligned} u_1 &= \frac{if}{h^2} A' e^{i(pt-fx+ry)}, \\ v_1 &= -\frac{ir}{h^2} A' e^{i(pt-fx+ry)}, \end{aligned}\right\} \quad \ldots\ldots\ldots\ldots\ldots (7)$$

$$\left.\begin{aligned} u_2 &= \frac{is}{k^2} B' e^{i(pt-fx+sy)}, \\ v_2 &= \frac{if}{k^2} B' e^{i(pt-fx+sy)}. \end{aligned}\right\} \quad \ldots\ldots\ldots\ldots\ldots (8)$$

In the surface layer of which the thickness, density and elastic constants are respectively H, ρ' and λ', μ', there occur multiple reflections of waves at the free surface $y=H$ and the bottom surface $y=0$. To satisfy this condition and the elasticity conditions at these two boundaries, we take the following four waves which of course satisfy the wave equations:

$$\Delta_1' = Ce^{i(pt-fx+r'y)}, \quad \ldots\ldots\ldots\ldots\ldots (9)$$

$$2\varpi_1' = Ee^{i(pt-fx+s'y)}, \quad \ldots\ldots\ldots\ldots\ldots (10)$$

$$\Delta_2' = De^{i(pt-fx-r'y)}, \quad \ldots\ldots\ldots\ldots\ldots (11)$$

$$2\varpi_2' = Fe^{i(pt-fx-s'y)}, \quad \ldots\ldots\ldots\ldots\ldots (12)$$

where

$$\left.\begin{aligned} r'^2 &= h'^2 - f^2, \quad s'^2 = k'^2 - f^2, \\ h'^2 &= \frac{\rho' p^2}{\lambda' + 2\mu'}, \quad k'^2 = \frac{\rho' p^2}{\mu'}. \end{aligned}\right\} \quad \ldots\ldots (13)$$

In these expressions C, D, E and F are arbitrary constants to be determined by the boundary conditions.

The elementary displacement expressions (u_1', v_1) (u_1'', v_1'') and (u_2', v_2') (u_2'', v_2''), corresponding to Δ_1', $2\varpi_1'$, Δ_2' and $2\varpi_2'$, are

$$\left.\begin{aligned} u_1' &= \frac{if}{h'^2} Ce^{i(pt-fx+r'y)}, \\ v_1' &= -\frac{ir'}{h'^2} Ce^{i(pt-fx+r'y)}, \end{aligned}\right\} \quad \ldots\ldots\ldots\ldots\ldots (14)$$

$$\left.\begin{aligned} u_1'' &= \frac{is'}{k'^2} Ee^{i(pt-fx+s'y)}, \\ v_1'' &= \frac{if}{k'^2} Ee^{i(pt-fx+s'y)}, \end{aligned}\right\} \quad \ldots\ldots\ldots\ldots\ldots (15)$$

$$\left.\begin{aligned} u_2' &= \frac{if}{h'^2} De^{i(pt-fx-r'y)}, \\ v_2' &= \frac{ir'}{h'^2} De^{i(pt-fx-r'y)}, \end{aligned}\right\} \quad \cdots\cdots\cdots\cdots\cdots\cdots (16)$$

$$\left.\begin{aligned} u_2'' &= -\frac{is'}{k'^2} Fe^{i(pt-fx-s'y)}, \\ v_2'' &= \frac{if}{k'^2} Fe^{i(pt-fx-s'y)}, \end{aligned}\right\} \quad \cdots\cdots\cdots\cdots\cdots\cdots (17)$$

The boundary conditions in the present study are as follows:[3)]
When $y=H$,

$$\lambda'(\Delta_1'+\Delta_2')+2\mu'\frac{\partial}{\partial y}(v_1'+v_1''+v_2'+v_2'')=0, \quad \cdots\cdots\cdots\cdots (18)$$

$$\frac{\partial}{\partial y}(u_1'+u_1''+u_2'+u_2'')+\frac{\partial}{\partial x}(v_1'+v_1''+v_2'+v_2'')=0. \quad \cdots\cdots (19)$$

When $y=0$,

$$v+v_1+v_2=v_1'+v_1''+v_2'+v_2'', \quad \cdots\cdots\cdots\cdots\cdots\cdots (20)$$

$$\lambda(\Delta+\Delta_1)+2\mu\frac{\partial}{\partial y}(v+v_1+v_2)=\lambda'(\Delta_1'+\Delta_2') + 2\mu'\frac{\partial}{\partial y}(v_1'+v_1''+v_2'+v_2''), \quad \cdots (21)$$

$$\frac{\partial}{\partial y}(u+u_1+u_2)+\frac{\partial}{\partial x}(v+v_1+v_2)=0, \quad \cdots\cdots\cdots\cdots\cdots\cdots (22)$$

$$\frac{\partial}{\partial y}(u_1'+u_1''+u_2'+u_2'')+\frac{\partial}{\partial x}(v_1'+v_1''+v_2'+v_2'')=0. \quad \cdots\cdots (23)$$

From these conditions we obtain the following equations to determine the arbitrary constants:

$$\frac{fr}{h^2}A'-\frac{f^2}{k^2}B'-\frac{fr'}{h'^2}C+\frac{fr'}{h'^2}D+\frac{f^2}{k'^2}E+\frac{f^2}{k'^2}F=\frac{fr}{h^2}\mathfrak{A}, \quad \cdots\cdots\cdots (24)$$

$$\frac{\mu}{\mu'}\frac{(f^2-s^2)}{h^2}A'+\frac{2\mu fs}{\mu' k^2}B'-\frac{(f^2-s'^2)}{h'^2}C-\frac{(f^2-s'^2)}{h'^2}D - \frac{2fs'}{k'^2}E+\frac{2fs'}{k'^2}F=-\frac{\mu}{\mu'}\frac{(f^2-s^2)}{h^2}\mathfrak{A}, \quad \cdots\cdots\cdots (25)$$

$$\frac{2fr}{h^2}A'-\frac{(f^2-s^2)}{k^2}B'=\frac{2fr}{h^2}\mathfrak{A}, \quad \cdots\cdots\cdots\cdots\cdots\cdots (26)$$

3) These conditions are the same as in the preceding paper., *loc. cit.*

$$\frac{2fr'}{h'^2}C-\frac{2fr'}{h'^2}D-\frac{(f^2-s'^2)}{k'^2}E-\frac{(f^2-s'^2)}{k'^2}F=0, \quad \ldots\ldots\ldots\ldots\ldots\ldots(27)$$

$$\frac{(f^2-s'^2)}{h'^2}Ce^{ir'H}+\frac{(f^2-s'^2)}{h'^2}De^{-ir'H}+\frac{2fs'}{k'^2}Ee^{is'H}-\frac{2fs'}{k'^2}Fe^{-is'H}=0, \quad \ldots(28)$$

$$\frac{2fr'}{h'^2}Ce^{ir'H}-\frac{2fr'}{h'^2}De^{-ir'H}-\frac{(f^2-s'^2)}{k'^2}Ee^{is'H}-\frac{(f^2-s'^2)}{k'^2}Fe^{-is'H}=0. \quad \ldots(29)$$

Solving these simultaneous equations, we can obtain the final expressions of A', B', C, D, E and F. Putting these determined expressions of constants in the general expressions of displacements, we can study the behaviour of the particles in the solids.

Let the velocities of dilatational and distortional waves in the lower medium be V_1 and V_2 and those in the surface layer V_1' and V_2', the emergency angle of the dilatational wave incident upon the bottom surface of the layer being e. Then the wave motions of particles in the solids may be studied by the following wave expressions.

For the lower medium :

$$\left.\begin{aligned}
U=\frac{iL\cos e}{2\pi}\Bigg[&\left\{\mathfrak{A}e^{i\left\{\frac{2\pi}{T}t-x\frac{2\pi\cos e}{L}-y\frac{2\pi\sin e}{L}\right\}}+A'e^{i\left\{\frac{2\pi}{T}t-x\frac{2\pi\cos e}{L}+y\frac{2\pi\sin e}{L}\right\}}\right\}\\
&+\frac{V_2^2}{V_1^2}\left(\frac{V_1^2}{V_2^2}\sec^2 e-1\right)^{1/2}B'e^{i\left\{\frac{2\pi}{T}t-x\frac{2\pi\cos e}{L}+y\frac{2\pi\cos e}{L}\left(\frac{V_1^2}{V_2^2}\sec 2e-1\right)^{1/2}\right\}}\Bigg],\\
V=\frac{iL\cos e}{2\pi}\Bigg[&\tan e\left\{\mathfrak{A}e^{i\left\{\frac{2\pi}{T}t-x\frac{2\pi\cos e}{L}-y\frac{2\pi\sin e}{L}\right\}}-A'e^{i\left\{\frac{2\pi}{T}t-x\frac{2\pi\cos e}{L}+y\frac{2\pi\sin e}{L}\right\}}\right\}\\
&+\frac{V_2^2}{V_1^2}B'e^{i\left\{\frac{2\pi}{T}t-x\frac{2\pi\cos e}{L}+y\frac{2\pi\cos e}{L}\left(\frac{V_1^2}{V_2^2}\sec 2e-1\right)^{1/2}\right\}}\Bigg].
\end{aligned}\right\} \quad \ldots\ldots\ldots\ldots\ldots\ldots(30)$$

For the surface layer :

$$\left.\begin{aligned}
U'=\frac{iL\cos e}{2\pi}\Bigg[&\frac{V_1'^2}{V_1^2}\left\{Ce^{i\left\{\frac{2\pi}{T}t-x\frac{2\pi\cos e}{L}+y\frac{2\pi\cos e}{L}\left(\frac{V_1^2}{V_1'^2}\sec 2e-1\right)^{1/2}\right\}}\right.\\
&\left.+De^{i\left\{\frac{2\pi}{T}t-x\frac{2\pi\cos e}{L}-y\frac{2\pi\cos e}{L}\left(\frac{V_1^2}{V_1'^2}\sec 2e-1\right)^{1/2}\right\}}\right\}\\
&+\frac{V_2'^2}{V_1^2}\left(\frac{V_1^2}{V_2'^2}\sec^2 e-1\right)^{1/2}\left\{Ee^{i\left\{\frac{2\pi}{T}t-x\frac{2\pi\cos e}{L}+y\frac{2\pi\cos e}{L}\left(\frac{V_1^2}{V_2'^2}\sec 2e-1\right)^{1/2}\right\}}\right.\\
&\left.-Fe^{i\left\{\frac{2\pi}{T}t-x\frac{2\pi\cos e}{L}-y\frac{2\pi\cos e}{L}\left(\frac{V_1^2}{V_2'^2}\sec 2e-1\right)^{1/2}\right\}}\right\}\Bigg],
\end{aligned}\right\}$$

$$V'=\frac{iL\cos e}{2\pi}\Bigg[\frac{V'^2_1}{V_1^2}\left(\frac{V_1^2}{V'^2_1}\sec^2 e-1\right)^{1/2}\Bigg\{-Ce^{i\left\{\frac{2\pi}{T}t-x\frac{2\pi\cos e}{L}+y\frac{2\pi\cos e}{L}\left(\frac{V_1{}^2}{V'_1{}^2}\sec 2e-1\right)^{1/2}\right\}}$$
$$+De^{i\left\{\frac{2\pi}{T}t-x\frac{2\pi\cos e}{L}-y\frac{2\pi\cos e}{L}\left(\frac{V_1{}^2}{V'_1{}^2}\sec 2e-1\right)^{1/2}\right\}}\Bigg\}$$
$$+\frac{V'^2_2}{V_1^2}\Bigg\{Ee^{i\left\{\frac{2\pi}{T}t-x\frac{2\pi\cos e}{L}+y\frac{2\pi\cos e}{L}\left(\frac{V_1{}^2}{V'_2{}^2}\sec 2e-1\right)^{1/2}\right\}}$$
$$+Fe^{i\left\{\frac{2\pi}{T}t-x\frac{2\pi\cos e}{L}-y\frac{2\pi\cos e}{L}\left(\frac{V_1{}^2}{V'_2{}^2}\sec 2e-1\right)^{1/2}\right\}}\Bigg\}\Bigg], \qquad \ldots\ldots\ldots\ldots\ldots\ldots (31)$$

where A', B', C, D, E and F are expressed by

$$A'\Phi\mathfrak{A}^{-1}=\frac{\mu}{\mu'}\frac{V_1^2}{V'^2_2}\sec^2 e\left(1-\frac{V_1^2}{V'^2_1}\sec^2 e\right)^{1/2}\Bigg\{\left(\frac{V_1^2}{V_2^2}\sec^2 e-2\right)^2$$
$$-4\tan e\left(\frac{V_1^2}{V_2^2}\sec^2 e-1\right)^{1/2}\Bigg\}$$
$$\times\Bigg[-\Bigg\{\left(\frac{V_1^2}{V'^2_2}\sec^2 e-2\right)^2-4\left(1-\frac{V_1^2}{V'^2_1}\sec^2 e\right)^{1/2}\left(1-\frac{V_1^2}{V'^2_2}\sec^2 e\right)^{1/2}\Bigg\}$$
$$\times\Bigg\{e^{\left\{\left(1-\frac{V_1{}^2}{V'_1{}^2}\sec 2e\right)^{1/2}+\left(1-\frac{V_1{}^2}{V'_2{}^2}\sec 2e\right)^{1/2}\right\}\frac{2\pi H}{L}}$$
$$-e^{-\left\{\left(1-\frac{V_1{}^2}{V'_1{}^2}\sec 2e\right)^{1/2}+\left(1-\frac{V_1{}^2}{V'_2{}^2}\sec 2e\right)^{1/2}\right\}\frac{2\pi H}{L}}\Bigg\}$$
$$+\Bigg\{\left(\frac{V_1^2}{V'^2_2}\sec^2 e-2\right)^2+4\left(1-\frac{V_1^2}{V'^2_1}\sec^2 e\right)^{1/2}\left(1-\frac{V_1^2}{V'^2_2}\sec^2 e\right)^{1/2}\Bigg\}$$
$$\times\Bigg\{e^{\left\{\left(1-\frac{V_1{}^2}{V'_1{}^2}\sec 2e\right)^{1/2}-\left(1-\frac{V_1{}^2}{V'_2{}^2}\sec 2e\right)^{1/2}\right\}\frac{2\pi H}{L}}$$
$$-e^{-\left\{\left(1-\frac{V_1{}^2}{V'_2{}^2}\sec 2e\right)^{1/2}-\left(1-\frac{V_1{}^2}{V'_2{}^2}\sec 2e\right)^{1/2}\right\}\frac{2\pi H}{L}}\Bigg\}\Bigg]$$
$$+i\frac{V_1^2}{V_2^2}\sec^2 e\tan e\Bigg[32\left(1-\frac{V_1^2}{V'^2_1}\sec^2 e\right)^{1/2}\left(1-\frac{V_1^2}{V'^2_2}\sec^2 e\right)^{1/2}\left(\frac{V_1^2}{V'^2_2}\sec^2 e-2\right)^2$$
$$+\Bigg\{\left(\frac{V_1^2}{V'^2_2}\sec^2 e-2\right)^2-4\left(1-\frac{V_1^2}{V'^2_1}\sec^2 e\right)^{1/2}\left(1-\frac{V_1^2}{V'^2_2}\sec^2 e\right)^{1/2}\Bigg\}^2$$
$$\times\Bigg\{e^{\left\{\left(1-\frac{V_1{}^2}{V'_1{}^2}\sec 2e\right)^{1/2}+\left(1-\frac{V_1{}^2}{V'_2{}^2}\sec 2e\right)^{1/2}\right\}\frac{2\pi H}{L}}$$
$$+e^{-\left\{\left(1-\frac{V_1{}^2}{V'_1{}^2}\sec 2e\right)^{1/2}+\left(1-\frac{V_1{}^2}{V'_2{}^2}\sec 2e\right)^{1/2}\right\}\frac{2\pi H}{L}}\Bigg\}$$

$$-\left\{\left(\frac{V_1^2}{V'^2_2}\sec^2 e-2\right)^2+4\left(1-\frac{V_1^2}{V'^2_1}\sec^2 e\right)^{1/2}\left(1-\frac{V_1^2}{V'^2_2}\sec^2 e\right)^{1/2}\right\}^2$$
$$\times\left\{e^{\left\{\left(1-\frac{V_1^2}{V'^2_1}\sec 2e\right)^{1/2}-\left(1-\frac{V_1^2}{V'^2_2}\sec 2e\right)^{1/2}\right\}\frac{2\pi H}{L}}\right.$$
$$\left.+e^{-\left\{\left(1-\frac{V_1^2}{V'^2_1}\sec 2e\right)^{1/2}-\left(1-\frac{V_1^2}{V'^2_2}\sec 2e\right)^{1/2}\right\}\frac{2\pi H}{L}}\right\}\Big],$$

.....(32)

$$B'\Phi\mathfrak{A}^{-1}=4\frac{\mu}{\mu'}\frac{V_1^2}{V_2^2}\frac{V_1^2}{V'^2_2}\sec^2 e\tan e\left(1-\frac{V_1^2}{V'^2_1}\sec^2 e\right)^{1/2}\left(\frac{V_1^2}{V_2^2}\sec^2 e-2\right)$$
$$\times\Big[\left\{\left(\frac{V_1^2}{V'^2_2}\sec^2 e-2\right)^2-4\left(1-\frac{V_1^2}{V'^2_1}\sec^2 e\right)^{1/2}\left(1-\frac{V_1^2}{V'^2_2}\sec^2 e\right)^{1/2}\right\}$$
$$\times\left\{e^{\left\{\left(1-\frac{V_1^2}{V'^2_1}\sec 2e\right)^{1/2}+\left(1-\frac{V_1^2}{V'^2_2}\sec 2e\right)^{1/2}\right\}\frac{2\pi H}{L}}\right.$$
$$\left.-e^{-\left\{\left(1-\frac{V_1^2}{V'^2_1}\sec 2e\right)^{1/2}+\left(1-\frac{V_1^2}{V'^2_2}\sec 2e\right)^{1/2}\right\}\frac{2\pi H}{L}}\right\}$$
$$-\left\{\left(\frac{V_1^2}{V'^2_2}\sec^2 e-2\right)^2+4\left(1-\frac{V_1^2}{V'^2_1}\sec^2 e\right)^{1/2}\left(1-\frac{V_1^2}{V'^2_2}\sec^2 e\right)^{1/2}\right\}$$
$$\times\left\{e^{\left\{\left(1-\frac{V_1^2}{V'^2_1}\sec 2e\right)^{1/2}-\left(1-\frac{V_1^2}{V'^2_2}\sec 2e\right)^{1/2}\right\}\frac{2\pi H}{L}}\right.$$
$$\left.-e^{-\left\{\left(1-\frac{V_1^2}{V'^2_1}\sec 2e\right)^{1/2}-\left(1-\frac{V_1^2}{V'^2_2}\sec 2e\right)^{1/2}\right\}\frac{2\pi H}{L}}\right\}\Big],$$

.....(33)

$$C\Phi\mathfrak{A}^{-1}=\frac{2i\mu}{\mu'}\frac{V_1^2}{V_2^2}\frac{V_1^2}{V'^2_1}\sec^2 e\tan e\left(\frac{V_1^2}{V_2^2}\sec^2 e-2\right)\left(\frac{V_1^2}{V'^2_2}\sec^2 e-2\right)$$
$$\times\Big[8\left(1-\frac{V_1^2}{V'^2_1}\sec^2 e\right)^{1/2}\left(1-\frac{V_1^2}{V'^2_2}\sec^2 e\right)^{1/2}$$
$$+\left\{\left(\frac{V_1^2}{V'^2_2}\sec^2 e-2\right)^2-4\left(1-\frac{V_1^2}{V'^2_1}\sec^2 e\right)^{1/2}\left(1-\frac{V_1^2}{V'^2_2}\sec^2 e\right)^{1/2}\right\}$$
$$\times e^{-\left\{\left(1-\frac{V_1^2}{V'^2_1}\sec 2e\right)^{1/2}+\left(1-\frac{V_1^2}{V'^2_2}\sec 2e\right)^{1/2}\right\}\frac{2\pi H}{L}}$$
$$-\left\{\left(\frac{V_1^2}{V'^2_2}\sec^2 e-2\right)^2+4\left(1-\frac{V_1^2}{V'^2_1}\sec^2 e\right)^{1/2}\left(1-\frac{V_1^2}{V'^2_2}\sec^2 e\right)^{1/2}\right\}$$
$$\times e^{-\left\{\left(1-\frac{V_1^2}{V'^2_1}\sec 2e\right)^{1/2}-\left(1-\frac{V_1^2}{V'^2_2}\sec 2e\right)^{1/2}\right\}\frac{2\pi H}{L}}\Big],$$

.....(34)

$$D\Phi\mathfrak{A}^{-1}=\frac{2i\mu}{\mu'}\frac{V_1^2}{V_2^2}\frac{V_1^2}{V_1'^2}\sec^2 e\tan e\left(\frac{V_1^2}{V_2^2}\sec^2 e-2\right)\left(\frac{V_1^2}{V_1'^2}\sec^2 e-2\right)$$
$$\times\left[8\left(1-\frac{V_1^2}{V_1'^2}\sec^2 e\right)^{1/2}\left(1-\frac{V_1^2}{V_2'^2}\sec^2 e\right)^{1/2}\right.$$
$$+\left\{\left(\frac{V_1^2}{V_2'^2}\sec^2 e-2\right)^2-4\left(1-\frac{V_1^2}{V_1'^2}\sec^2 e\right)^{1/2}\left(1-\frac{V_1^2}{V_2'^2}\sec^2 e\right)^{1/2}\right\}$$
$$\times e^{\left\{\left(1-\frac{V_1^2}{V_1'^2}\sec 2e\right)^{1/2}+\left(1-\frac{V_1^2}{V_2'^2}\sec 2e\right)^{1/2}\right\}\frac{2\pi H}{L}}$$
$$-\left\{\left(\frac{V_1^2}{V_2'^2}\sec^2 e-2\right)^2+4\left(1-\frac{V_1^2}{V_1'^2}\sec^2 e\right)^{1/2}\left(1-\frac{V_1^2}{V_2'^2}\sec^2 e\right)^{1/2}\right\}$$
$$\left.\times e^{\left\{\left(1-\frac{V_1^2}{V_1'^2}\sec 2e\right)^{1/2}-\left(1-\frac{V_1^2}{V_2'^2}\sec 2e\right)^{1/2}\right\}\frac{2\pi H}{L}}\right], \quad \ldots\ldots\ldots\ldots(35)$$

$$E\Phi\mathfrak{A}^{-1}=\frac{4\mu}{\mu'}\frac{V_1^2}{V_2^2}\frac{V_1^2}{V_2'^2}\sec^2 e\tan e\left(1-\frac{V_1^2}{V_1'^2}\sec^2 e\right)^{1/2}\left(\frac{V_1^2}{V_2^2}\sec^2 e-2\right)$$
$$\times\left[2\left(\frac{V_1^2}{V_2'^2}\sec^2 e-2\right)^2\right.$$
$$-\left\{\left(\frac{V_1^2}{V_2'^2}\sec^2 e-2\right)^2-4\left(1-\frac{V_1^2}{V_1'^2}\sec^2 e\right)^{1/2}\left(1-\frac{V_1^2}{V_2'^2}\sec^2 e\right)^{1/2}\right\}$$
$$\times e^{-\left\{\left(1-\frac{V_1^2}{V_1'^2}\sec 2e\right)^{1/2}+\left(1-\frac{V_1^2}{V_2'^2}\sec 2e\right)^{1/2}\right\}\frac{2\pi H}{L}}$$
$$-\left\{\left(\frac{V_1^2}{V_2'^2}\sec^2 e-2\right)^2+4\left(1-\frac{V_1^2}{V_1'^2}\sec^2 e\right)^{1/2}\left(1-\frac{V_1^2}{V_2'^2}\sec^2 e\right)^{1/2}\right\}$$
$$\left.\times e^{\left\{\left(1-\frac{V_1^2}{V_1'^2}\sec 2e\right)^{1/2}-\left(1-\frac{V_1^2}{V_2'^2}\sec 2e\right)^{1/2}\right\}\frac{2\pi H}{L}}\right], \quad \ldots\ldots\ldots\ldots(36)$$

$$F\Phi\mathfrak{A}^{-1}=\frac{4\mu}{\mu'}\frac{V_1^2}{V_2^2}\frac{V_1^2}{V_2'^2}\sec^2 e\tan e\left(1-\frac{V_1^2}{V_1'^2}\sec^2 e\right)^{1/2}\left(\frac{V_1^2}{V_2^2}\sec^2 e-2\right)$$
$$\times\left[-2\left(\frac{V_1^2}{V_2'^2}\sec^2 e-2\right)^2\right.$$
$$+\left\{\left(\frac{V_1^2}{V_2'^2}\sec^2 e-2\right)^2-4\left(\mathrm{I}-\frac{V_1^2}{V_1'^2}\sec^2 e\right)^{1/2}\left(1-\frac{V_1^2}{V_2'^2}\sec^2 e\right)^{1/2}\right\}$$
$$\times e^{\left\{\left(1-\frac{V_1^2}{V_1'^2}\sec 2e\right)^{1/2}+\left(1-\frac{V_1^2}{V_2'^2}\sec 2e\right)^{1/2}\right\}\frac{2\pi H}{L}}$$
$$+\left\{\left(\frac{V_1^2}{V_2'^2}\sec^2 e-2\right)^2+4\left(1-\frac{V_1^2}{V_1'^2}\sec^2 e\right)^{1/2}\left(1-\frac{V_1^2}{V_2'^2}\sec^2 e\right)^{1/2}\right\}$$
$$\left.\times e^{-\left\{\left(1-\frac{V_1^2}{V_1'^2}\sec 2e\right)^{1/2}-\left(1-\frac{V_1^2}{V_2'^2}\sec 2e\right)^{1/2}\right\}\frac{2\pi H}{L}}\right], \quad \ldots\ldots\ldots\ldots(37)$$

where

$$\Phi = \frac{\mu}{\mu'}\frac{V_1^2}{V_2'^2}\sec^2 e\left(1-\frac{V_1^2}{V_1'^2}\sec^2 e\right)^{\frac{1}{2}}\left\{\left(\frac{V_1^2}{V_2^2}\sec^2 e-2\right)^2+4\tan e\left(\frac{V_1^2}{V_2^2}\sec^2 e-1\right)^{\frac{1}{2}}\right\}$$

$$\times\left[\left\{\left(\frac{V_1^2}{V_2'^2}\sec^2 e-2\right)^2-4\left(1-\frac{V_1^2}{V_1'^2}\sec^2 e\right)^{\frac{1}{2}}\left(1-\frac{V_1^2}{V_2'^2}\sec^2 e\right)^{\frac{1}{2}}\right\}\right.$$

$$\times\left\{e^{\left\{\left(1-\frac{V_1^2}{V_1'^2}\sec 2e\right)^{\frac{1}{2}}+\left(1-\frac{V_1^2}{V_2'^2}\sec 2e\right)^{\frac{1}{2}}\right\}\frac{2\pi H}{L}}\right.$$

$$\left.-e^{-\left\{\left(1-\frac{V_1^2}{V_1'^2}\sec 2e\right)^{\frac{1}{2}}+\left(1-\frac{V_1^2}{V_2'^2}\sec 2e\right)^{\frac{1}{2}}\right\}\frac{2\pi H}{L}}\right\}$$

$$-\left\{\left(\frac{V_1^2}{V_2'^2}\sec^2 e-2\right)^2+4\left(1-\frac{V_1^2}{V_1'^2}\sec^2 e\right)^{\frac{1}{2}}\left(1-\frac{V_1^2}{V_2'^2}\sec^2 e\right)^{\frac{1}{2}}\right\}$$

$$\times\left\{e^{\left\{\left(1-\frac{V_1^2}{V_1'^2}\sec 2e\right)^{\frac{1}{2}}-\left(1-\frac{V_1^2}{V_2'^2}\sec 2e\right)^{\frac{1}{2}}\right\}\frac{2\pi H}{L}}\right.$$

$$\left.\left.-e^{-\left\{\left(1-\frac{V_1^2}{V_1'^2}\sec 2e\right)^{\frac{1}{2}}-\left(1-\frac{V_1^2}{V_2'^2}\sec 2e\right)^{\frac{1}{2}}\right\}\frac{2\pi H}{L}}\right\}\right]$$

$$+i\frac{V_1^2}{V_2^2}\sec^2 e\tan e\left[32\left(1-\frac{V_1^2}{V_1'^2}\sec^2 e\right)^{\frac{1}{2}}\left(1-\frac{V_1^2}{V_2'^2}\sec^0 e\right)^{\frac{1}{2}}\right.$$

$$\left.\times\left(\frac{V_1^2}{V_2'^2}\sec^2 e-2\right)^2\right.$$

$$+\left\{\left(\frac{V_1^2}{V_2'^2}\sec^2 e-2\right)^2-4\left(1-\frac{V_1^2}{V_1'^2}\sec^2 e\right)^{\frac{1}{2}}\left(1-\frac{V_1^2}{V_2'^2}\sec^2 e\right)^{\frac{1}{2}}\right\}^2$$

$$\times\left\{e^{\left\{\left(1-\frac{V_1^2}{V_1'^2}\sec 2e\right)^{\frac{1}{2}}+\left(1-\frac{V_1^2}{V_2'^2}\sec 2e\right)^{\frac{1}{2}}\right\}\frac{2\pi H}{L}}\right.$$

$$\left.+e^{-\left\{\left(1-\frac{V_1^2}{V_1'^2}\sec 2e\right)^{\frac{1}{2}}+\left(1-\frac{V_1^2}{V_2'^2}\sec 2e\right)^{\frac{1}{2}}\right\}\frac{2\pi H}{L}}\right\}$$

$$-\left\{\left(\frac{V_1^2}{V_2'^2}\sec^2 e-2\right)^2+4\left(1-\frac{V_1^2}{V_1'^2}\sec^2 e\right)^{\frac{1}{2}}\left(1-\frac{V_1^2}{V_2'^2}\sec^2 e\right)^{\frac{1}{2}}\right\}^2$$

$$\times\left\{e^{\left\{\left(1-\frac{V_1^2}{V_1'^2}\sec 2e\right)^{\frac{1}{2}}-\left(1-\frac{V_1^2}{V_2'^2}\sec 2e\right)^{\frac{1}{2}}\right\}\frac{2\pi H}{L}}\right.$$

$$\left.\left.+e^{-\left\{\left(1-\frac{V_1^2}{V_1'^2}\sec 2e\right)^{\frac{1}{2}}-\left(1-\frac{V_1^2}{V_2'^2}\sec 2e\right)^{\frac{1}{2}}\right\}\frac{2\pi H}{L}}\right\}\right].$$

.....(38)

The wave motions in the layer and in the lower medium expressed by (30) and (31) are of course due to the primarily incident dilatational wave such that

$$\left.\begin{aligned} V_0 &= \frac{i\mathfrak{A}L}{2\pi}\cos e\, e^{i\left\{\frac{2\pi}{T}t - x\frac{2\pi\cos e}{L} - y\frac{2\pi\sin e}{L}\right\}}, \\ V_0 &= \frac{i\mathfrak{A}L}{2\pi}\sin e\, e^{i\left\{\frac{2\pi}{T}t - x\frac{2\pi\cos e}{L} - y\frac{2\pi\sin e}{L}\right\}}. \end{aligned}\right\} \quad \cdots\cdots\cdots (39)$$

In expressions (30), (31), and (39) L is the wave length of the harmonic dilatational wave incident upon the bottom surface of the layer.

3. When the Poisson's ratio of each of the solids are 1/4 and both densities are equal, the vibratory motions of particles in the solids due to the incident dilatational wave are found by the following expressions:

For the lower medium:

$$\left.\begin{aligned} U &= \frac{iL\cos e}{2\pi}\left[\left\{\mathfrak{A}e^{i\left\{\frac{2\pi}{T}t - x\frac{2\pi\cos e}{L} - y\frac{2\pi\sin e}{L}\right\}} + A'e^{i\left\{\frac{2\pi}{T}t - x\frac{2\pi\cos e}{L} + y\frac{2\pi\sin e}{L}\right\}}\right\}\right. \\ &\qquad \left. + \frac{1}{3}(3\sec^2 e - 1)^{\frac{1}{2}} B'e^{i\left\{\frac{2\pi}{T}t - x\frac{2\pi\cos e}{L} + y\frac{2\pi\cos e}{L}(3\sec^2 e - 1)^{\frac{1}{2}}\right\}}\right], \\ V &= \frac{iL\cos e}{2\pi}\left[\tan e\left\{\mathfrak{A}e^{i\left\{\frac{2\pi}{T}t - x\frac{2\pi\cos e}{L} - y\frac{2\pi\sin e}{L}\right\}} - A'e^{i\left\{\frac{2\pi}{T}t - x\frac{2\pi\cos e}{L} + y\frac{2\pi\sin e}{L}\right\}}\right\}\right. \\ &\qquad \left. + \frac{1}{3}B'e^{i\left\{\frac{2\pi}{T}t - x\frac{2\pi\cos e}{L} + y\frac{2\pi\cos e}{L}(3\sec^2 e - 1)^{\frac{1}{2}}\right\}}\right]. \end{aligned}\right\} \quad (40)$$

For the surface layer:

$$\left.\begin{aligned} U' &= \frac{iL\cos e}{2\pi}\left[\frac{\mu'}{\mu}\left\{Ce^{i\left\{\frac{2\pi}{T}t - x\frac{2\pi\cos e}{L} + y\frac{2\pi\cos e}{L}\left(\frac{\mu}{\mu'}\sec^2 e - 1\right)^{\frac{1}{2}}\right\}}\right.\right. \\ &\qquad \left. + De^{i\left\{\frac{2\pi}{T}t - x\frac{2\pi\cos e}{L} - y\frac{2\pi\cos e}{L}\left(\frac{\mu}{\mu'}\sec^2 e - 1\right)^{\frac{1}{2}}\right\}}\right\} \\ &\qquad + \frac{\mu'}{3\mu}\left(\frac{3\mu}{\mu'}\sec^2 e - 1\right)^{\frac{1}{2}}\left\{Ee^{i\left\{\frac{2\pi}{T}t - x\frac{2\pi\cos e}{L} + y\frac{2\pi\cos e}{L}\left(\frac{3\mu}{\mu'}\sec^2 e - 1\right)^{\frac{1}{2}}\right\}}\right. \\ &\qquad \left.\left. - Fe^{i\left\{\frac{2\pi}{T}t - x\frac{2\pi\cos e}{L} - y\frac{2\pi\cos e}{L}\left(\frac{3\mu}{\mu'}\sec^2 e - 1\right)^{\frac{1}{2}}\right\}}\right\}\right], \end{aligned}\right\} \quad (41)$$

$$V'=\frac{iL\cos e}{2\pi}\Big[\frac{\mu'}{\mu}\Big(\frac{\mu}{\mu'}\sec^2 e-1\Big)^{\frac{1}{2}}\Big\{-Ce^{i\left\{\frac{2\pi}{T}t-x\frac{2\pi\cos e}{L}+y\frac{2\pi\cos e}{L}\left(\frac{\mu}{\mu'}\sec 2e-1\right)^{\frac{1}{2}}\right\}}$$
$$+De^{\left\{\frac{2\pi}{T}t-x\frac{2\pi\cos e}{L}-y\frac{2\pi\cos e}{L}\left(\frac{\mu}{\mu'}\sec 2e-1\right)^{\frac{1}{2}}\right\}}\Big\}$$
$$+\frac{\mu'}{3\mu}\Big\{Ee^{i\left\{\frac{2\pi}{T}t-x\frac{2\pi\cos e}{L}+y\frac{2\pi\cos e}{L}\left(\frac{3\mu}{\mu'}\sec 2e-1\right)^{\frac{1}{2}}\right\}}$$
$$+Fe^{i\left\{\frac{2\pi}{T}t-x\frac{2\pi\cos e}{L}-y\frac{2\pi\cos e}{L}\left(\frac{3\mu}{\mu'}\sec 2e-1\right)^{\frac{1}{2}}\right\}}\Big\}\Big].$$

In these expressions A', B', C, D, E and F are defined by

$$A'\Phi\mathfrak{A}^{-1}=\frac{\mu^2}{\mu'^2}\Big(1-\frac{\mu}{\mu'}\sec^2 e\Big)^{\frac{1}{2}}\{(3\sec^2 e-2)^2-4\tan e(3\sec^2 e-1)^{\frac{1}{2}}\}$$
$$\times\Big[-\Big\{\Big(\frac{3\mu}{\mu'}\sec^2 e-2\Big)^2-4\Big(1-\frac{\mu}{\mu'}\sec^2 e\Big)^{\frac{1}{2}}\Big(1-\frac{3\mu}{\mu'}\sec^2 e\Big)^{\frac{1}{2}}\Big\}$$
$$\times\Big\{e^{2\pi\cos e\left\{\left(1-\frac{\mu}{\mu'}\sec 2e\right)^{\frac{1}{2}}+\left(1-\frac{3\mu}{\mu'}\sec 2e\right)^{\frac{1}{2}}\right\}\frac{H}{L}}$$
$$-e^{-2\pi\cos e\left\{\left(1-\frac{\mu}{\mu'}\sec 2e\right)^{\frac{1}{2}}+\left(1-\frac{3\mu}{\mu'}\sec 2e\right)^{\frac{1}{2}}\right\}\frac{H}{L}}\Big\}$$
$$+\Big\{\Big(\frac{3\mu}{\mu'}\sec^2 e-2\Big)^2+4\Big(1-\frac{\mu}{\mu'}\sec^2 e\Big)^{\frac{1}{2}}\Big(1-\frac{3\mu}{\mu'}\sec^2 e\Big)^{\frac{1}{2}}\Big\}$$
$$\times\Big\{e^{2\pi\cos e\left\{\left(1-\frac{\mu}{\mu'}\sec 2e\right)^{\frac{1}{2}}-\left(1-\frac{3\mu}{\mu'}\sec 2e\right)^{\frac{1}{2}}\right\}\frac{H}{L}}$$
$$-e^{-2\pi\cos e\left\{\left(1-\frac{\mu}{\mu'}\sec 2e\right)^{\frac{1}{2}}-\left(1-\frac{3\mu}{\mu'}\sec 2e\right)^{\frac{1}{2}}\right\}\frac{H}{L}}\Big\}\Big]$$
$$+i\tan e\Big[32\Big(1-\frac{\mu}{\mu'}\sec^2 e\Big)^{\frac{1}{2}}\Big(1-\frac{3\mu}{\mu'}\sec^2 e\Big)^{\frac{1}{2}}\Big(\frac{3\mu}{\mu'}\sec^2 e-2\Big)^2$$
$$+\Big\{\Big(\frac{3\mu}{\mu'}\sec^2 e-2\Big)^2-4\Big(1-\frac{\mu}{\mu'}\sec^2 e\Big)^{\frac{1}{2}}\Big(1-\frac{3\mu}{\mu'}\sec^2 e\Big)^{\frac{1}{2}}\Big\}^2$$
$$\times\Big\{e^{2\pi\cos e\left\{\left(1-\frac{\mu}{\mu'}\sec 2e\right)^{\frac{1}{2}}+\left(1-\frac{3\mu}{\mu'}\sec 2e\right)^{\frac{1}{2}}\right\}\frac{H}{L}}$$
$$+e^{-2\pi\cos e\left\{\left(1-\frac{\mu}{\mu'}\sec 2e\right)^{\frac{1}{2}}+\left(1-\frac{3\mu}{\mu'}\sec 2e\right)^{\frac{1}{2}}\right\}\frac{H}{L}}\Big\}$$
$$-\Big\{\Big(\frac{3\mu}{\mu'}\sec^2 e-2\Big)^2+4\Big(1-\frac{\mu}{\mu'}\sec^2 e\Big)^{\frac{1}{2}}\Big(1-\frac{3\mu}{\mu'}\sec^2 e\Big)^{\frac{1}{2}}\Big\}^2$$

$$\times\left\{e^{2\pi\cos e\left\{\left(1-\frac{\mu}{\mu'}\sec 2e\right)^{\frac{1}{2}}-\left(1-\frac{3\mu}{\mu'}\sec 2e\right)^{\frac{1}{2}}\right\}\frac{H}{L}}\right.$$

$$\left.+e^{-2\pi\cos e\left\{\left(1-\frac{\mu}{\mu'}\sec 2e\right)^{\frac{1}{2}}-\left(1-\frac{3\mu}{\mu'}\sec 2e\right)^{\frac{1}{2}}\right\}\frac{H}{L}}\right\}\Bigg],$$

.....(42)

$$B'\Phi\mathfrak{A}^{-1}=\frac{12\mu^2}{\mu'^2}\tan e\left(1-\frac{\mu}{\mu'}\sec^2 e\right)^{\frac{1}{2}}(3\sec^2 e-2)$$

$$\times\left[\left\{\left(\frac{3\mu}{\mu'}\sec^2 e-2\right)^2-4\left(1-\frac{\mu}{\mu'}\sec^2 e\right)^{\frac{1}{2}}\left(1-\frac{3\mu}{\mu'}\sec^2 e\right)^{\frac{1}{2}}\right\}\right.$$

$$\times\left\{e^{2\pi\cos e\left\{\left(1-\frac{\mu}{\mu'}\sec 2e\right)^{\frac{1}{2}}+\left(1-\frac{3\mu}{\mu'}\sec 2e\right)^{\frac{1}{2}}\right\}\frac{H}{L}}\right.$$

$$\left.-e^{-2\pi\cos e\left\{\left(1-\frac{\mu}{\mu'}\sec 2e\right)^{\frac{1}{2}}+\left(1-\frac{3\mu}{\mu'}\sec 2e\right)^{\frac{1}{2}}\right\}\frac{H}{L}}\right\}$$

$$-\left\{\left(\frac{3\mu}{\mu'}\sec^2 e-2\right)^2+4\left(1-\frac{\mu}{\mu'}\sec^2 e\right)^{\frac{1}{2}}\left(1-\frac{3\mu}{\mu'}\sec^2 e\right)^{\frac{1}{2}}\right\}$$

$$\times\left\{e^{2\pi\cos e\left\{\left(1-\frac{\mu}{\mu'}\sec 2e\right)^{\frac{1}{2}}-\left(1-\frac{3\mu}{\mu'}\sec 2e\right)^{\frac{1}{2}}\right\}\frac{H}{L}}\right.$$

$$\left.-e^{-2\pi\cos e\left\{\left(1-\frac{\mu}{\mu'}\sec 2e\right)^{\frac{1}{2}}-\left(1-\frac{3\mu}{\mu'}\sec 2e\right)^{\frac{1}{2}}\right\}\frac{H}{L}}\right\}\Bigg],$$

.....(43)

$$C\Phi\mathfrak{A}^{-1}=\frac{2i\mu^2}{\mu'^2}\tan e(3\sec^2-2)\left(\frac{3\mu}{\mu'}\sec^2 e-2\right)$$

$$\times\left[8\left(1-\frac{\mu}{\mu'}\sec^2 e\right)^{\frac{1}{2}}\left(1-\frac{3\mu}{\mu'}\sec^2 e\right)^{\frac{1}{2}}\right.$$

$$+\left\{\left(\frac{3\mu}{\mu'}\sec^2 e-2\right)^2-4\left(1-\frac{\mu}{\mu'}\sec^2 e\right)^{\frac{1}{2}}\left(1-\frac{3\mu}{\mu'}\sec^2 e\right)^{\frac{1}{2}}\right\}$$

$$\times e^{-2\pi\cos e\left\{\left(1-\frac{\mu}{\mu'}\sec 2e\right)^{\frac{1}{2}}+\left(1-\frac{3\mu}{\mu'}\sec 2e\right)^{\frac{1}{2}}\right\}\frac{H}{L}}$$

$$-\left\{\left(\frac{3\mu}{\mu'}\sec^2 e-2\right)^2+4\left(1-\frac{\mu}{\mu'}\sec^2 e\right)^{\frac{1}{2}}\left(1-\frac{3\mu}{\mu'}\sec^2 e\right)^{\frac{1}{2}}\right\}$$

$$\left.\times e^{-2\pi\cos e\left\{\left(1-\frac{\mu}{\mu'}\sec 2e\right)^{\frac{1}{2}}-\left(1-\frac{3\mu}{\mu'}\sec 2e\right)^{\frac{1}{2}}\right\}\frac{H}{L}}\right],$$

.....(44)

$$D\Phi\mathfrak{N}^{-1}=\frac{2i\mu^2}{\mu'^2}\tan e\,(3\sec^2 e-2)\left(\frac{3\mu}{\mu'}\sec^2 e-2\right)$$
$$\times\left[8\left(1-\frac{\mu}{\mu'}\sec^2 e\right)^{\frac{1}{2}}\left(1-\frac{3\mu}{\mu'}\sec^2 e\right)^{\frac{1}{2}}\right.$$
$$+\left\{\left(\frac{3\mu}{\mu'}\sec^2 e-2\right)^2-4\left(1-\frac{\mu}{\mu'}\sec^2 e\right)^{\frac{1}{2}}\left(1-\frac{3\mu}{\mu'}\sec^2 e\right)^{\frac{1}{2}}\right\}$$
$$\times e^{2\pi\cos e\left\{\left(1-\frac{\mu}{\mu'}\sec 2e\right)^{\frac{1}{2}}+\left(1-\frac{3\mu}{\mu'}\sec 2e\right)^{\frac{1}{2}}\right\}\frac{H}{L}}$$
$$\left.-\left\{\left(\frac{3\mu}{\mu'}\sec^2 e-2\right)^2+4\left(1-\frac{\mu}{\mu'}\sec^2 e\right)^{\frac{1}{2}}\left(1-\frac{3\mu}{\mu'}\sec^2 e\right)^{\frac{1}{2}}\right\}\right.$$
$$\left.\times e^{2\pi\cos e\left\{\left(1-\frac{\mu}{\mu'}\sec 2e\right)^{\frac{1}{2}}-\left(1-\frac{3\mu}{\mu'}\sec 2e\right)^{\frac{1}{2}}\right\}\frac{H}{L}}\right],$$

....(45)

$$E\Phi\mathfrak{N}^{-1}=\frac{12\mu^2}{\mu'^2}\tan e\left(1-\frac{\mu}{\mu'}\sec^2 e\right)^{\frac{1}{2}}(3\sec^2 e-2)$$
$$\times\left[2\left(\frac{3\mu}{\mu'}\sec^2 e-2\right)^2\right.$$
$$-\left\{\left(\frac{3\mu}{\mu'}\sec^2 e-2\right)^2-4\left(1-\frac{\mu}{\mu'}\sec^2 e\right)^{\frac{1}{2}}\left(1-\frac{3\mu}{\mu'}\sec^2 e\right)^{\frac{1}{2}}\right\}$$
$$\times e^{-2\pi\cos e\left\{\left(1-\frac{\mu}{\mu'}\sec 2e\right)^{\frac{1}{2}}+\left(1-\frac{3\mu}{\mu'}\sec 2e\right)^{\frac{1}{2}}\right\}\frac{H}{L}}$$
$$-\left\{\left(\frac{3\mu}{\mu'}\sec^2 e-2\right)^2+4\left(1-\frac{\mu}{\mu'}\sec^2 e\right)^{\frac{1}{2}}\left(1-\frac{3\mu}{\mu'}\sec^2 e\right)^{\frac{1}{2}}\right\}$$
$$\left.\times e^{2\pi\cos e\left\{\left(1-\frac{\mu}{\mu'}\sec 2e\right)^{\frac{1}{2}}-\left(1-\frac{3\mu}{\mu'}\sec 2e\right)^{\frac{1}{2}}\right\}\frac{H}{L}}\right],$$

.....(46)

$$F\Phi\mathfrak{N}^{-1}=\frac{12\mu^2}{\mu'^2}\tan e\left(1-\frac{\mu}{\mu'}\sec^2 e\right)^{\frac{1}{2}}(3\sec^2 e-2)$$
$$\times\left[-2\left(\frac{3\mu}{\mu'}\sec^2 e-2\right)^2\right.$$
$$+\left\{\left(\frac{3\mu}{\mu'}\sec^2 e-2\right)^2-4\left(1-\frac{\mu}{\mu'}\sec^2 e\right)^{\frac{1}{2}}\left(1-\frac{3\mu}{\mu'}\sec^2 e\right)^{\frac{1}{2}}\right\}$$
$$\times e^{2\pi\cos e\left\{\left(1-\frac{\mu}{\mu'}\sec 2e\right)^{\frac{1}{2}}+\left(1-\frac{3\mu}{\mu'}\sec 2e\right)^{\frac{1}{2}}\right\}\frac{H}{L}}$$

$$+\left\{\left(\frac{3\mu}{\mu'}\sec^2 e-2\right)^2+4\left(1-\frac{\mu}{\mu'}\sec^2 e\right)^{\frac{1}{2}}\left(1-\frac{3\mu}{\mu'}\sec^2 e\right)^{\frac{1}{2}}\right\}$$
$$\times e^{-2\pi\cos e\left\{\left(1-\frac{\mu}{\mu'}\sec 2e\right)^{\frac{1}{2}}-\left(1-\frac{3\mu}{\mu'}\sec 2e\right)^{\frac{1}{2}}\right\}\frac{H}{L}}\Big],$$

.....(47)

where

$$\Phi=\frac{\mu^2}{\mu'^2}\left(1-\frac{\mu}{\mu'}\sec^2 e\right)^{\frac{1}{2}}\{(3\sec^2 e-2)^2+4\tan e\,(3\sec^2 e-1)^{\frac{1}{2}}\}$$
$$\times\Big[\left\{\left(\frac{3\mu}{\mu'}\sec^2 e-2\right)^2-4\left(1-\frac{\mu}{\mu'}\sec^2 e\right)^{\frac{1}{2}}\left(1-\frac{3\mu}{\mu'}\sec^2 e\right)^{\frac{1}{2}}\right\}$$
$$\times\Big\{e^{2\pi\cos e\left\{\left(1-\frac{\mu}{\mu'}\sec 2e\right)^{\frac{1}{2}}+\left(1-\frac{3\mu}{\mu'}\sec 2e\right)^{\frac{1}{2}}\right\}\frac{H}{L}}$$
$$-e^{-2\pi\cos e\left\{\left(1-\frac{\mu}{\mu'}\sec 2e\right)^{\frac{1}{2}}+\left(1-\frac{3\mu}{\mu'}\sec 2e\right)^{\frac{1}{2}}\right\}\frac{H}{L}}\Big\}$$
$$-\left\{\left(\frac{3\mu}{\mu'}\sec^2 e-2\right)^2+4\left(1-\frac{\mu}{\mu'}\sec^2 e\right)^{\frac{1}{2}}\left(1-\frac{3\mu}{\mu'}\sec^2 e\right)^{\frac{1}{2}}\right\}$$
$$\times\Big\{e^{2\pi\cos e\left\{\left(1-\frac{\mu}{\mu'}\sec 2e\right)^{\frac{1}{2}}-\left(1-\frac{3\mu}{\mu'}\sec 2e\right)^{\frac{1}{2}}\right\}\frac{H}{L}}$$
$$-e^{-2\pi\cos e\left\{\left(1-\frac{\mu}{\mu'}\sec 2e\right)^{\frac{1}{2}}-\left(1-\frac{3\mu}{\mu'}\sec 2e\right)^{\frac{1}{2}}\right\}\frac{H}{L}}\Big\}\Big]$$
$$+i\tan e\Big[32\left(1-\frac{\mu}{\mu'}\sec^2 e\right)^{\frac{1}{2}}\left(1-\frac{3\mu}{\mu'}\sec^2 e\right)^{\frac{1}{2}}\left(\frac{3\mu}{\mu'}\sec^2 e-2\right)^2$$
$$+\left\{\left(\frac{3\mu}{\mu'}\sec^2 e-2\right)^2-4\left(1-\frac{\mu}{\mu'}\sec^2 e\right)^{\frac{1}{2}}\left(1-\frac{3\mu}{\mu'}\sec^2 e\right)^{\frac{1}{2}}\right\}^2$$
$$\times\Big\{e^{2\pi\cos e\left\{\left(1-\frac{\mu}{\mu'}\sec 2e\right)^{\frac{1}{2}}+\left(1-\frac{3\mu}{\mu'}\sec 2e\right)^{\frac{1}{2}}\right\}\frac{H}{L}}$$
$$+e^{-2\pi\cos e\left\{\left(1-\frac{\mu}{\mu'}\sec 2e\right)^{\frac{1}{2}}+\left(1-\frac{3\mu}{\mu'}\sec 2e\right)^{\frac{1}{2}}\right\}\frac{H}{L}}\Big\}$$
$$-\left\{\left(\frac{3\mu}{\mu'}\sec^2 e-2\right)^2+4\left(1-\frac{\mu}{\mu'}\sec^2 e\right)^{\frac{1}{2}}\left(1-\frac{3\mu}{\mu'}\sec^2 e\right)^{\frac{1}{2}}\right\}^2$$
$$\times\Big\{e^{2\pi\cos e\left\{\left(1-\frac{\mu}{\mu'}\sec^2 e\right)^{\frac{1}{2}}-\left(1-\frac{3\mu}{\mu'}\sec 2e\right)^{\frac{1}{2}}\right\}\frac{H}{L}}$$

$$+e^{-2\pi\cos e\left\{\left(1-\frac{\mu}{\mu'}\sec 2e\right)^{\frac{1}{2}}-\left(1-\frac{3\mu}{\mu'}\sec 2e\right)^{\frac{1}{2}}\right\}\frac{H}{L}}\Bigg\}\Bigg].$$

..... (48)

4. When the rigidities and densities of both solids, of each of which the Poisson's ratio are 1/4 respectively, are equal, *i. e.* when $\lambda=\mu$, $\lambda'=\mu'$ and $\mu=\mu'$, $\rho=\rho'$ the expressions of the wave motions of particles in two solids are as follows :—

For the lower medium :

$$U=\frac{iL\cos e}{2\pi}\Bigg[\left\{\mathfrak{A}e^{i\left\{\frac{2\pi}{T}t-x\frac{2\pi\cos e}{L}-y\frac{2\pi\sin e}{L}\right\}}+A'e^{i\left\{\frac{2\pi}{T}t-x\frac{2\pi\cos e}{L}+y\frac{2\pi\sin e}{L}\right\}}\right\}$$
$$+\frac{1}{3}(3\sec^2 e-1)^{\frac{1}{2}}B'e^{i\left\{\frac{2\pi}{T}t-x\frac{2\pi\cos e}{L}+y\frac{2\pi\cos e}{L}(3\sec 2e-1)^{\frac{1}{2}}\right\}}\Bigg],$$

$$V=\frac{iL\cos e}{2\pi}\Bigg[\tan e\left\{\mathfrak{A}e^{i\left\{\frac{2\pi}{T}t-x\frac{2\pi\cos e}{L}-y\frac{2\pi\sin e}{L}\right\}}-A'e^{i\left\{\frac{2\pi}{T}t-x\frac{2\pi\cos e}{L}+y\frac{2\pi\sin e}{L}\right\}}\right\}$$
$$+\frac{1}{3}B'e^{i\left\{\frac{2\pi}{T}t-x\frac{2\pi\cos e}{L}+y\frac{2\pi\cos e}{L}(3\sec 2e-1)^{\frac{1}{2}}\right\}}\Bigg],$$

.....(49)

For the surface layer :

$$U'=\frac{iL\cos e}{2\pi}\Bigg[\left\{Ce^{i\left\{\frac{2\pi}{T}t-x\frac{2\pi\cos e}{L}+y\frac{2\pi\sin e}{L}\right\}}+De^{i\left\{\frac{2\pi}{T}t-x\frac{2\pi\cos e}{L}-y\frac{2\pi\sin e}{L}\right\}}\right\}$$
$$+\frac{1}{3}(3\sec^2 e-1)^{\frac{1}{2}}\left\{Ee^{\left\{\frac{2\pi}{T}t-x\frac{2\pi\cos e}{L}+y\frac{2\pi\cos e}{L}(3\sec 2e-1)^{\frac{1}{2}}\right\}}-Fe^{i\left\{\frac{2\pi}{T}t-x\frac{2\pi\cos e}{L}-y\frac{2\pi\cos e}{L}(3\sec 2e-1)^{\frac{1}{2}}\right\}}\right\}\Bigg],$$

$$V'=\frac{iL\cos e}{2\pi}\Bigg[\tan e\left\{-Ce^{i\left\{\frac{2\pi}{T}t-x\frac{2\pi\cos e}{L}+y\frac{2\pi\sin e}{L}\right\}}+De^{i\left\{\frac{2\pi}{T}t-x\frac{2\pi\cos e}{L}-y\frac{2\pi\sin e}{L}\right\}}\right\}$$
$$+\frac{1}{3}\left\{Ee^{i\left\{\frac{2\pi}{T}t-x\frac{2\pi\cos e}{L}+y\frac{2\pi\cos e}{L}(3\sec 2e-1)^{\frac{1}{2}}\right\}}+Fe^{i\left\{\frac{2\pi}{T}t-x\frac{2\pi\cos e}{L}-y\frac{2\pi\cos e}{L}(3\sec^2 e-1)^{\frac{1}{2}}\right\}}\right\}\Bigg].$$

.....(50)

In these expressions A', B', C, D, E and F are defined by

$$\begin{aligned}A'\Phi\mathfrak{A}^{-1}=&-16\tan e\,(3\sec^2 e-1)^{\frac{1}{2}}(3\sec^2 e-2)^2\\&-\{(3\sec^2 e-2)^2-4\tan e\,(3\sec^2 e-1)^{\frac{1}{2}}\}^2\\&\times e^{-2i\pi\cos e\{\tan e-(3\sec^2 e-1)^{\frac{1}{2}}\}\frac{H}{L}}\\&+\{(3\sec^2 e-2)^2+4\tan e\,(3\sec^2 e-1)^{\frac{1}{2}}\}^2\\&\times\{4\tan e\,(3\sec^2 e-1)^{\frac{1}{2}}e^{2i\pi\cos e\{\tan e+(3\sec^2 e-1)^{\frac{1}{2}}\}\frac{H}{L}}\\&+(3\sec^2 e-2)^2e^{-2i\pi\cos e\{\tan e+(3\sec^2 e-1)^{\frac{1}{2}}\}\frac{H}{L}}\}],\end{aligned}\qquad\cdots\cdots(51)$$

$$\begin{aligned}B'\Phi\mathfrak{A}^{-1}=&6\tan e\,(3\sec^2 e-2)\\&\times[\{(3\sec^2 e-2)^2+4\tan e\,(3\sec^2 e-1)^{\frac{1}{2}}\}\\&\times\{e^{2i\pi\cos e\{\tan e+(3\sec^2 e-1)^{\frac{1}{2}}\}\frac{H}{L}}\\&-e^{-2i\pi\cos e\{\tan e+(3\sec^2 e-1)^{\frac{1}{2}}\}\frac{H}{L}}\}\\&-\{(3\sec^2 e-2)^2-4\tan e\,(3\sec^2 e-1)^{\frac{1}{2}}\}\\&\times\{e^{2i\pi\cos e\{\tan e-(3\sec^2 e-1)^{\frac{1}{2}}\}\frac{H}{L}}\\&-e^{-2i\pi\cos e\{\tan e-(3\sec^2 e-1)^{\frac{1}{2}}\}\frac{H}{L}}\}],\end{aligned}\qquad\cdots\cdots(52)$$

$$\begin{aligned}C\Phi\mathfrak{A}^{-1}=&(3\sec^2 e-2)^2[-8\tan e(3\sec^2 e-1)^{\frac{1}{2}}\\&+\{(3\sec^2 e-2)^2+4\tan e\,(3\sec^2 e-1)^{\frac{1}{2}}\}\\&\times e^{-2i\pi\cos e\{\tan e+(3\sec^2 e-1)^{\frac{1}{2}}\}\frac{H}{L}}\\&-\{(3\sec^2 e-2)^2-4\tan e\,(3\sec^2 e-1)^{\frac{1}{2}}\}\\&\times e^{-2i\pi\cos e\{\tan e-(3\sec^2 e-1)^{\frac{1}{2}}\}\frac{H}{L}}],\end{aligned}\qquad\cdots\cdots(53)$$

$$\begin{aligned}D\Phi\mathfrak{A}^{-1}=&(3\sec^2 e-2)^2[-8\tan e\,(3\sec^2 e-1)^{\frac{1}{2}}\\&+\{(3\sec^2 e-2)^2+4\tan e\,(3\sec^2 e-1)^{\frac{1}{2}}\\&\times e^{2i\pi\cos e\{\tan e+(3\sec^2 e-1)^{\frac{1}{2}}\}\frac{H}{L}}\\&-\{(3\sec^2 e-2)^2-4\tan e\,(3\sec^2 e-1)^{\frac{1}{2}}\}\\&\times e^{2i\pi\cos e\{\tan e-(3\sec^2 e-1)^{\frac{1}{2}}\}\frac{H}{L}}],\end{aligned}\qquad\cdots\cdots(54)$$

$$E\Phi\mathfrak{A}^{-1}=6\tan e(3\sec^2 e-2)[2(3\sec^2 e-2)^2$$
$$-\{(3\sec^2 e-2)^2+4\tan e(3\sec^2 e-1)^{\frac{1}{2}}\}$$
$$\times e^{-2i\pi\cos e[\tan e+(3\sec^2 e-1)^{\frac{1}{2}}]\frac{H}{L}}$$
$$-\{(3\sec^2 e-2)^2-4\tan e(3\sec^2 e-1)^{\frac{1}{2}}\}$$
$$\times e^{2i\pi\cos e[\tan e-(3\sec^2 e-1)^{\frac{1}{2}}]\frac{H}{L}}],$$
$$\ldots\ldots\ldots\ldots\ldots\ldots\ldots\ldots(55)$$

$$F\Phi\mathfrak{A}^{-1}=6\tan e(3\sec^2 e-2)[-2(3\sec^2 e-2)^2$$
$$+\{(3\sec^2 e-2)^2+4\tan e(3\sec^2 e-1)^{\frac{1}{2}}\}$$
$$\times e^{2i\pi\cos e[\tan e+(3\sec^2 e-1)^{\frac{1}{2}}]\frac{H}{L}}$$
$$+\{(3\sec^2 e-2)^2-4\tan e(3\sec^2 e-1)^{\frac{1}{2}}\}$$
$$\times e^{-2i\pi\cos e[\tan e-(3\sec^2 e-1)^{\frac{1}{2}}]\frac{H}{L}},$$
$$\ldots\ldots\ldots\ldots\ldots\ldots\ldots\ldots(56)$$

where

$$\Phi=-16\tan e(3\sec^2 e-1)^{\frac{1}{2}}(3\sec^2 e-2)^2$$
$$+\{(3\sec^2 e-2)^2+4\tan e(3\sec^2 e-1)^{\frac{1}{2}}\}^2 e^{2i\pi\cos e[\tan e+(3\sec^2 e-1)^{\frac{1}{2}}]\frac{H}{L}}$$
$$-\{(3\sec^2 e-2)^2-4\tan e(3\sec^2 e-1)^{\frac{1}{2}}\}$$
$$\times\{(3\sec^2 e-2)^2 e^{2i\pi\cos e[\tan e-(3\sec^2 e-1)^{\frac{1}{2}}]\frac{H}{L}}\}$$
$$-4\tan e(3\sec^2 e-1)^{\frac{1}{2}} e^{-2i\pi\cos e[\tan e-(3\sec^2 e-1)^{\frac{1}{2}}]\frac{H}{L}}.$$
$$\ldots\ldots\ldots\ldots\ldots\ldots\ldots\ldots(57)$$

It will be seen that the wave motions in two solids differ with respect to the amplitude of vibration and the directions of the axes of the orbital motions of particles. Especially at the common boundary $y=0$, the amplitudes of the vibratory motions of particles and the directions of the axes of an elliptic orbit are discontinuous, and this phenomenon cannot be seen when the two solids closely touch each other.

To see the orbital motion of a particle on the free surface we obtain the following expressions of U', V' at $y=H$, when the emergency angles of the primary wave Δ incident upon $y=0$ is respectively 0°, 30°, 45° and 60°.

$$e=0^\circ:\quad \left.\begin{aligned} U'_{y=H}&=0,\\ V'_{y=H}&=0,\end{aligned}\right\} \quad \ldots\ldots\ldots\ldots\ldots(58)$$

corresponding to

$$\left.\begin{aligned} U_{y=0} &= \frac{i\mathfrak{A}L}{2\pi} e^{i\left\{\frac{2\pi}{T}t-x\frac{2\pi}{L}\right\}}, \\ V_{y=0} &= 0, \\ U_0 &= -i\frac{\mathfrak{A}L}{2\pi} e^{i\left\{\frac{2\pi}{T}t-x\frac{2\pi}{L}\right\}}. \end{aligned}\right\} \quad \cdots\cdots\cdots\cdots (59)$$

$e=30°$:

$$\left.\begin{aligned} V'_{y=H} &= \mathfrak{A}L\frac{\sqrt{3}}{4\pi} i\left\{e^{i\left\{\frac{2\pi}{T}t-x\frac{\sqrt{3}\pi}{L}-\pi\frac{H}{L}\right\}}\right. \\ &\qquad \left. -e^{i\left\{\frac{2\pi}{T}t-x\frac{\sqrt{3}\pi}{L}-3\pi\frac{H}{L}\right\}}\right\}, \\ V'_{y=H} &= \mathfrak{A}L\frac{1}{4\pi} i\left\{e^{i\left\{\frac{2\pi}{T}t-x\frac{\sqrt{3}\pi}{L}-\pi\frac{H}{L}\right\}}\right. \\ &\qquad \left. +e^{i\left\{\frac{2\pi}{T}t-x\frac{\sqrt{3}\pi}{L}-3\pi\frac{H}{L}\right\}}\right\}, \end{aligned}\right\} \quad \cdots\cdots\cdots (60)$$

corresponding to

$$\left.\begin{aligned} U_{y=0} &= i\mathfrak{A}L\frac{\sqrt{3}}{4\pi} e^{i\left\{\frac{2\pi}{T}t-x\frac{\sqrt{3}\pi}{L}\right\}}, \\ V_{y=0} &= i\mathfrak{A}L\frac{1}{4\pi} e^{\left\{\frac{2\pi}{T}t-x\frac{\sqrt{3}\pi}{L}\right\}}, \\ U_0 &= -i\mathfrak{A}L\frac{1}{2\pi} e^{i\left\{\frac{2\pi}{T}t-x\frac{\sqrt{3}\pi}{L}\right\}}, \end{aligned}\right\} \quad \cdots\cdots\cdots\cdots\cdots (61)$$

$e=45°$:

$$\left.\begin{aligned} U'_{y=H} &= L\frac{\sqrt{2}}{4\pi} i\left[\left\{Ce^{i\left\{\frac{2\pi}{T}t-x\frac{\sqrt{2}\sqrt{3}\pi}{L}+\sqrt{2}\pi\frac{H}{L}\right\}}+De^{i\left\{\frac{2\pi}{T}t-x\frac{\sqrt{2}\sqrt{3}\pi}{L}-\sqrt{2}\pi\frac{H}{L}\right\}}\right\}\right. \\ &\qquad \left.+\frac{\sqrt{5}}{3}\left\{Ee^{i\left\{\frac{2\pi}{T}t-x\frac{\sqrt{2}\sqrt{3}\pi}{L}+\sqrt{10}\pi\frac{H}{L}\right\}}-Fe^{i\left\{\frac{2\pi}{T}t-x\frac{\sqrt{2}\sqrt{3}\pi}{L}-\sqrt{10}\pi\frac{H}{L}\right\}}\right\}\right], \\ V'_{y=H} &= L\frac{\sqrt{2}}{4\pi} i\left[\left\{-Ce^{i\left\{\frac{2\pi}{T}t-x\frac{\sqrt{2}\sqrt{3}\pi}{L}+\sqrt{2}\pi\frac{H}{L}\right\}}+De^{i\left\{\frac{2\pi}{T}t-x\frac{\sqrt{2}\sqrt{3}\pi}{L}-\sqrt{2}\pi\frac{H}{L}\right\}}\right\}\right. \\ &\qquad \left.+\frac{1}{3}\left\{Ee^{i\left\{\frac{2\pi}{T}t-x\frac{\sqrt{2}\sqrt{3}\pi}{L}+\sqrt{10}\pi\frac{H}{L}\right\}}+Fe^{i\left\{\frac{2\pi}{T}t-x\frac{\sqrt{2}\sqrt{3}\pi}{L}-\sqrt{10}\pi\frac{H}{L}\right\}}\right\}\right], \end{aligned}\right\} \quad (62)$$

where

$$\left.\begin{aligned} C = \mathfrak{A}\Phi^{-1}\left[\left\{-1{\cdot}7889+2{\cdot}4944\cos\left(4{\cdot}5765\frac{\pi H}{L}\right)\right.\right. \\ \left.\left.-0{\cdot}7056\cos\left(1{\cdot}7481\pi\frac{H}{L}\right)\right\}\right. \end{aligned}\right\}$$

$$
\left.\begin{aligned}
&+i\left\{-2{\cdot}4944\sin\left(4{\cdot}5765\,\pi\frac{H}{L}-0{\cdot}7056\sin\left(1{\cdot}7481\,\pi\frac{H}{L}\right)\right\}\right],\\
D=\mathfrak{A}\Phi^{-1}\Big[&\left\{-1{\cdot}7889+2{\cdot}4944\cos\left(4{\cdot}5765\frac{\pi H}{L}\right)\right.\\
&\qquad\left.-0{\cdot}7056\cos\left(1{\cdot}7481\,\pi\frac{H}{L}\right)\right\}\\
&+i\left\{2{\cdot}4944\sin\left(4{\cdot}5764\,\pi\frac{H}{L}\right)+0{\cdot}7056\sin\left(1{\cdot}7481\,\pi\frac{H}{L}\right)\right\}\Big],\\
E=\mathfrak{A}\Phi^{-1}\Big[&\left\{4{\cdot}8-3{\cdot}7416\cos\left(4{\cdot}5765\,\pi\frac{H}{L}\right)\right.\\
&\qquad\left.-1{\cdot}0584\cos\left(1{\cdot}7481\,\pi\frac{H}{L}\right)\right\}\\
&+i\left\{3{\cdot}7416\sin\left(4{\cdot}5765\,\pi\frac{H}{L}\right)+1{\cdot}0584\sin\left(1{\cdot}7481\,\pi\frac{H}{L}\right)\right\}\Big],\\
F=\mathfrak{A}\Phi^{-1}\Big[&\left\{-4{\cdot}8+3{\cdot}7416\cos\left(4{\cdot}5765\,\pi\frac{H}{L}\right)\right.\\
&\qquad\left.+1{\cdot}0584\cos\left(1{\cdot}7481\,\pi\frac{H}{L}\right)\right\}\\
&+i\left\{3{\cdot}7416\sin\left(4{\cdot}5765\,\pi\frac{H}{L}\right)+1{\cdot}0584\sin\left(1{\cdot}7481\,\pi\frac{H}{L}\right)\right\}\Big],
\end{aligned}\right\}\quad(63)
$$

and

$$
\Phi=\left\{-3{\cdot}5777+3{\cdot}8889\cos\left(4{\cdot}5765\,\pi\frac{H}{L}\right)-0{\cdot}31125\cos\left(1{\cdot}7481\,\pi\frac{H}{L}\right)\right\}
+i\left\{3{\cdot}8889\sin\left(4{\cdot}5765\,\pi\frac{H}{L}\right)+1{\cdot}1\sin\left(1{\cdot}7481\,\pi\frac{H}{L}\right)\right\},\quad\ldots.(64)
$$

corresponding to

$$
\left.\begin{aligned}
U_{y=0}&=i\mathfrak{A}L\frac{1}{2\sqrt{2}\pi}e^{i\left\{\frac{2\pi}{T}t-x\frac{\sqrt{2}\pi}{L}\right\}},\\
V_{y=0}&=i\mathfrak{A}L\frac{1}{2\sqrt{2}\pi}e^{i\left\{\frac{2\pi}{T}t-x\frac{\sqrt{2}\pi}{L}\right\}},\\
U_0&=-i\mathfrak{A}L\frac{1}{2\pi}e^{i\left\{\frac{2\pi}{T}t-x\frac{\sqrt{2}\pi}{L}\right\}},
\end{aligned}\right\}\quad\ldots\ldots\quad\ldots\ldots\ldots(65)
$$

$e=60°$:

$$
U'_{y=H}=\mathfrak{A}L\frac{1}{4\pi}i\left[\left\{Ce^{i\left\{\frac{2\pi}{T}t-x\frac{\pi}{L}+\sqrt{3}\pi\frac{H}{L}\right\}}+De^{i\left\{\frac{2\pi}{T}t-x\frac{\pi}{L}-\sqrt{3}\pi\frac{H}{L}\right\}}\right.\right.
$$

$$+\frac{\sqrt{11}}{3}\left\{Ee^{i\left\{\frac{2\pi}{T}t-x\frac{\pi}{L}+\sqrt{11}\pi\frac{H}{L}\right\}}-Fe^{i\left\{\frac{2\pi}{T}t-x\frac{\pi}{L}-\sqrt{11}\pi\frac{H}{L}\right\}}\right\}\Big],$$

$$V'_{y=H}=\mathfrak{A}L\frac{1}{4\pi}i\Big[\sqrt{3}\left\{-Ce^{i\left\{\frac{2\pi}{T}t-x\frac{\pi}{L}+\sqrt{3}\pi\frac{H}{L}\right\}}+De^{i\left\{\frac{2\pi}{T}t-x\frac{\pi}{L}-\sqrt{3}\pi\frac{H}{L}\right\}}\right\} \tag{66}$$

$$+\frac{1}{3}\left\{Ee^{i\left\{\frac{2\pi}{T}t-x\frac{\pi}{L}+\sqrt{11}\pi\frac{H}{L}\right\}}+Fe^{i\left\{\frac{2\pi}{T}t-x\frac{\pi}{L}-\sqrt{11}\pi\frac{H}{L}\right\}}\right\}\Big],$$

where

$$C=\mathfrak{A}\Psi^{-1}\Big[\Big\{-2{\cdot}87225+7{\cdot}68613\cos\Big(5{\cdot}0487\,\pi\frac{H}{L}\Big)-4{\cdot}81388\cos\Big(1{\cdot}5845\,\pi\frac{H}{L}\Big)\Big\}$$

$$+i\Big\{-7{\cdot}68613\sin\Big(5{\cdot}0487\,\pi\frac{H}{L}\Big)-4{\cdot}81388\sin\Big(1{\cdot}5845\,\pi\frac{H}{L}\Big)\Big\}\Big],$$

$$D=\mathfrak{A}\Psi^{-1}\Big[\Big\{-2{\cdot}87225+7{\cdot}68613\cos\Big(5{\cdot}0487\,\pi\frac{H}{L}\Big)-4{\cdot}81388\cos\Big(1{\cdot}5845\,\pi\frac{H}{L}\Big)\Big\}$$

$$+i\Big\{7{\cdot}68613\sin\Big(5{\cdot}0487\,\pi\frac{H}{L}\Big)+4{\cdot}81388\sin\Big(1{\cdot}5845\,\pi\frac{H}{L}\Big)\Big\}\Big], \tag{67}$$

$$E=\mathfrak{A}\Psi^{-1}\Big[\Big\{12{\cdot}99038-7{\cdot}98766\cos\Big(5{\cdot}0487\,\pi\frac{H}{L}\Big)-5{\cdot}00272\cos\Big(1{\cdot}5845\,\pi\frac{H}{L}\Big)\Big\}$$

$$+i\Big\{7{\cdot}98766\sin\Big(5{\cdot}0487\,\pi\frac{H}{L}\Big)+5{\cdot}00272\sin\Big(1{\cdot}5845\,\pi\frac{H}{L}\Big)\Big\}\Big],$$

$$F=\mathfrak{A}\Psi^{-1}\Big[\Big\{-12{\cdot}99038+7{\cdot}98766\cos\Big(5{\cdot}0487\,\pi\frac{H}{L}\Big)+5{\cdot}00272\cos\Big(1{\cdot}5845\,\pi\frac{H}{L}\Big)\Big\}$$

$$+i\Big\{7{\cdot}98766\sin\Big(5{\cdot}0487\,\pi\frac{H}{L}\Big)+5{\cdot}272\sin\Big(1{\cdot}5845\,\pi\frac{H}{L}\Big)\Big\}\Big],$$

and

$$\Psi=\Big\{-5{\cdot}7445+9{\cdot}45225\cos\Big(5{\cdot}0487\,\pi\frac{H}{L}\Big)-3{\cdot}70775\cos\Big(1{\cdot}5845\,\pi\frac{H}{L}\Big)\Big\}$$

$$+i\left\{9{\cdot}45225\sin\left(5{\cdot}0487\,\pi\frac{H}{L}\right)+5{\cdot}92\sin\left(1{\cdot}5845\,\pi\frac{H}{L}\right)\right\}, \quad \ldots(68)$$

corresponding to

$$\left.\begin{aligned} U_{y=0} &= i\mathfrak{A}L\frac{1}{4\pi}e^{i\left\{\frac{2\pi}{T}t-x\frac{\pi}{L}\right\}}, \\ V_{y=0} &= i\mathfrak{A}L\frac{\sqrt{3}}{4\pi}e^{i\left\{\frac{2\pi}{T}t-x\frac{\pi}{L}\right\}}, \\ U_0 &= -i\mathfrak{A}L\frac{1}{2\pi}e^{i\left\{\frac{2\pi}{T}t-x\frac{\pi}{L}\right\}}. \end{aligned}\right\} \quad \ldots\ldots(69)$$

These expressions show that the particle on the free surface has generally elliptic motion, of which one of the axes is always vertical even if the emergency angle of the primary wave varies. The length of the axes, moreover, varies periodically with the ratio of the thickness of the layer and the wave length of the primary wave.

When $e=30°$, the vertical and horizontal displacement on the free surface (60) are written in real forms as follows:

$$\left.\begin{aligned} U'_{y=H} &= -\mathfrak{A}L\frac{\sqrt{3}}{2\pi}\sin\frac{\pi H}{L}\cos\left(\frac{2\pi H}{L}-\frac{2\pi}{T}t+x\frac{\sqrt{3}\pi}{L}\right), \\ V'_{y=H} &= \mathfrak{A}L\frac{1}{2\pi}\cos\frac{\pi H}{L}\sin\left(\frac{2\pi H}{L}-\frac{2\pi}{T}t+x\frac{\sqrt{3}\pi}{L}\right). \end{aligned}\right\} \quad \ldots\ldots(70)$$

The semi-axes of the elliptic motion are respectively

$$\mathfrak{A}L\frac{\sqrt{3}}{2\pi}\sin\left(\pi\frac{H}{L}\right), \quad \ldots\ldots\ldots\ldots\ldots(71)$$

$$\mathfrak{A}L\frac{1}{2\pi}\cos\left(\pi\frac{H}{L}\right). \quad \ldots\ldots\ldots\ldots\ldots(72)$$

When $\frac{H}{L}=0$ or a positive integer, (71) is zero, and $U'_{y=H}=0$.

When $\frac{H}{L}=n+\frac{1}{2}$, where n is an integer, (72) is zero, therefore $U'_{y=H}=0$.

When $\frac{H}{L}=n\pm\frac{1}{6}$, (71) is equal to (72). In this case the particle on the free surface makes a circular orbit of which the radius is $\mathfrak{A}L\frac{\sqrt{3}}{4\pi}$. When $e=30°$, both axes of the elliptic orbit of the surface particle are a circular function of H/L, of which the period is 1/6, one of the

axes of the elliptic orbit being, of course, vertical and the other horizontal.

To find the nature of the orbital motion of the surface when $e=30°$, 45°, and 60°, we calculated the variation of $U'-$ and $V'-$ components with respect to time in the following cases of H/L as shewn in Table I.

Table I.

e	30°	45°	60°
H/L	0, $\frac{1}{10}$, $\frac{1}{8}$, $\frac{1}{5}$, $\frac{1}{2}$, $\frac{4}{5}$, $\frac{5}{6}$, $\frac{9}{10}$, 1,	0, $\frac{1}{10}$, $\frac{1}{5}$, $\frac{1}{2}$, 1,	0, $\frac{1}{2}$, 1,

The calculated results are shewn in the following figures. In these figures, the respective upper curves indicate the variation of $U'-$ and $V'-$ components with respect to time, while the lower ones give the orbit of a certain point on the surface of the layer, U_0 being the amplitude of the primary wave.

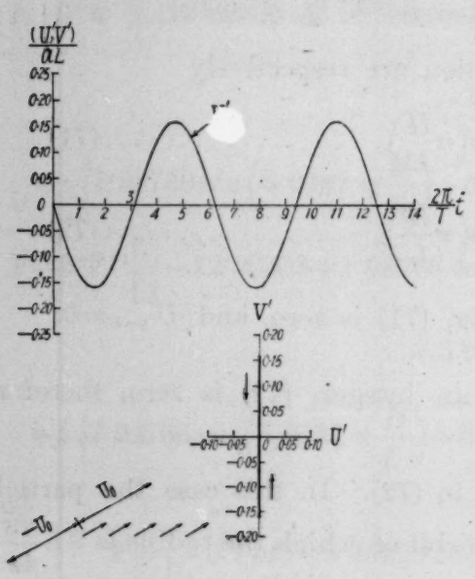

Fig. 2. $\rho=\rho'$, $\lambda=\mu$, $\lambda'=\mu'$, $\mu=\mu'$, $e=30°$, $H/L=0$, $y=H$.

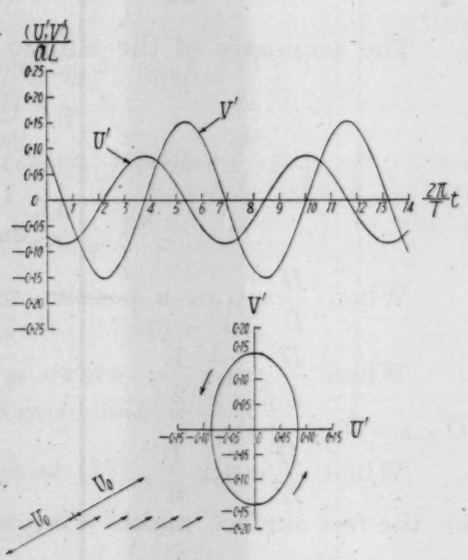

Fig. 3. $\rho=\rho'$, $\lambda=\mu$, $\lambda'=\mu'$, $\mu=\mu'$, $e=30°$, $H/L=1/10$, $y=H$

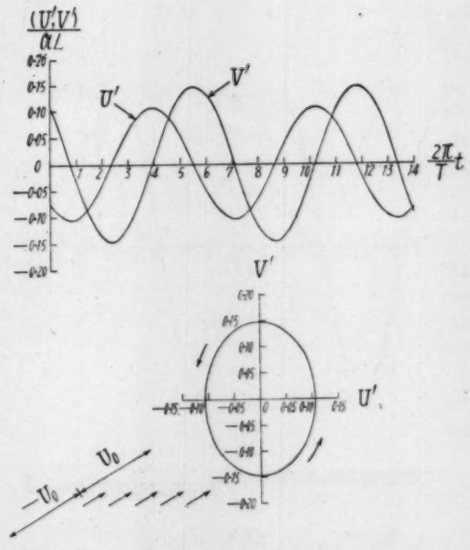

Fig. 4. $\rho=\rho'$, $\lambda=\mu$, $\lambda'=\mu'$, $\mu=\mu'$, $e=30°$, $H/L=1/8$, $y=H$.

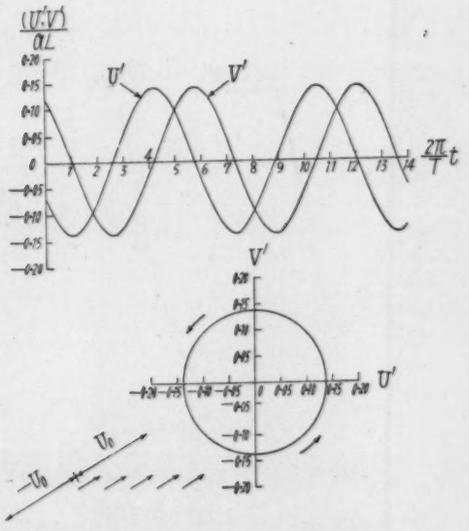

Fig. 5. $\rho=\rho'$, $\lambda=\mu$, $\lambda'=\mu'$, $\mu=\mu'$, $e=30°$, $H/L=1/6$, $y=H$.

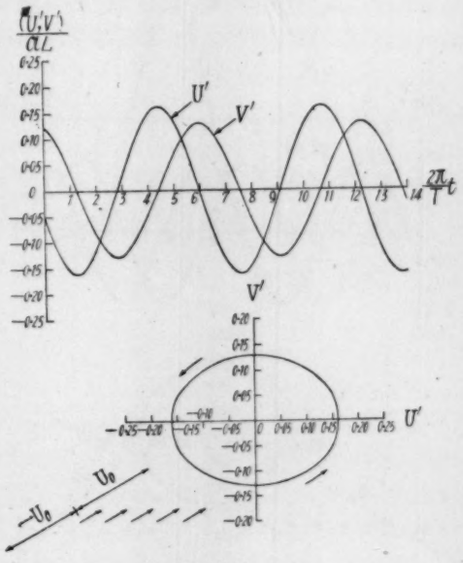

Fig. 6. $\rho=\rho'$, $\lambda=\mu$, $\lambda'=\mu'$, $\mu=\mu'$, $e=30°$, $H/L=1/5$, $y=H$.

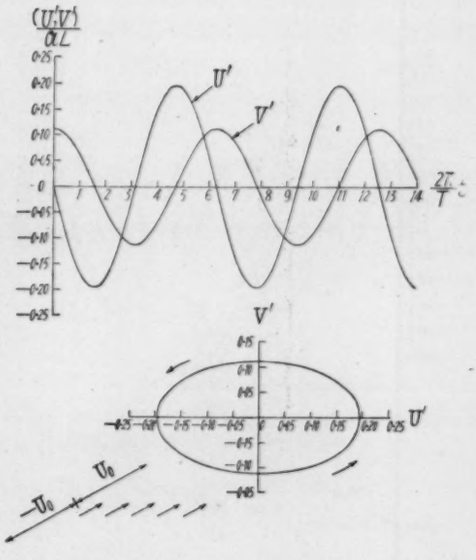

Fig. 7. $\rho=\rho'$, $\lambda=\mu$, $\lambda'=\mu'$, $\mu=\mu'$, $e=30°$, $H/L=1/4$, $y=H$.

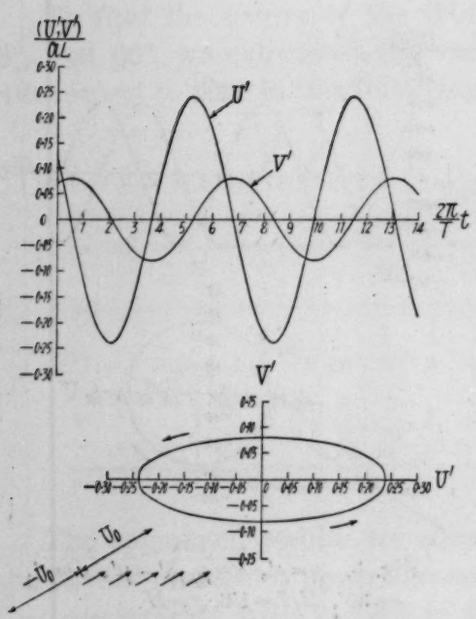

Fig. 8. $\rho=\rho'$, $\lambda=\mu$, $\lambda'=\mu'$, $\mu=\mu'$, $e=30°$, $H/L=1/3$, $y=H$.

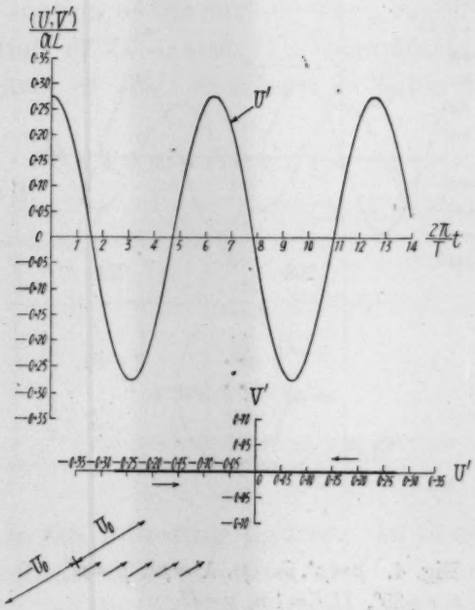

Fig. 9. $\rho=\rho'$, $\lambda=\mu$, $\lambda'=\mu'$, $\mu=\mu'$, $e=30°$, $H/L=1/2$, $y=H$

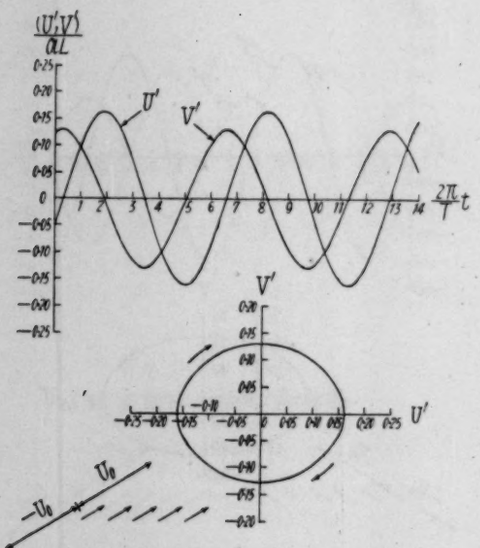

Fig. 10. $\rho=\rho'$, $\lambda=\mu$, $\lambda'=\mu'$, $\mu=\mu'$, $e=30°$, $H/L=4/5$, $y=H$.

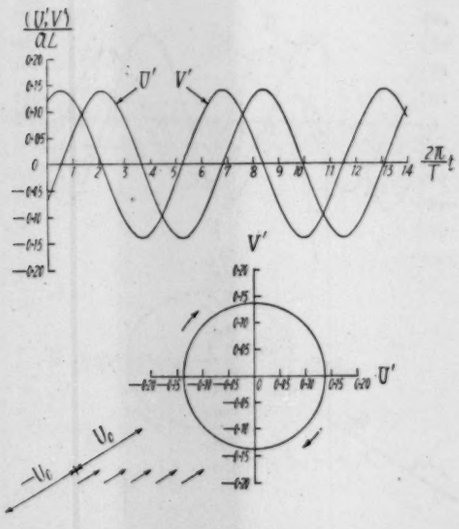

Fig. 11. $\rho=\rho'$, $\lambda=\mu$, $\lambda'=\mu'$, $\mu=\mu'$, $e=30°$, $H/L=5/6$, $y=H$.

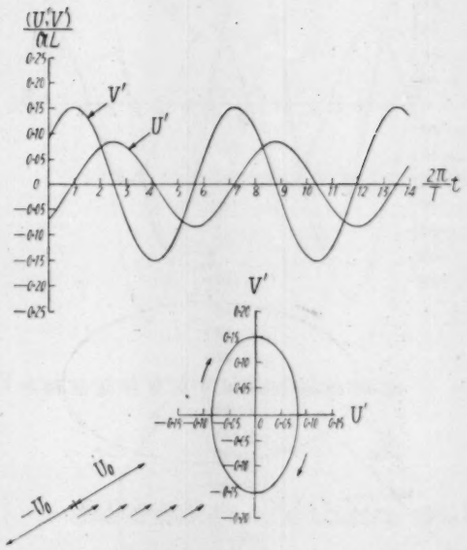

Fig. 12. $\rho=\rho'$, $\lambda=\mu$, $\lambda'=\mu'$, $\mu=\mu'$, $e=30°$, $H/L=9/10$, $y=H$.

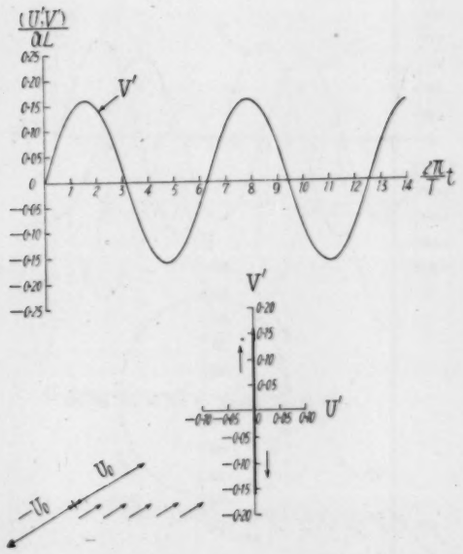

Fig. 13. $\rho=\rho'$, $\lambda=\mu$, $\lambda'=\mu'$, $\mu=\mu$, $e=30°$, $H/L=1$, $y=H$.

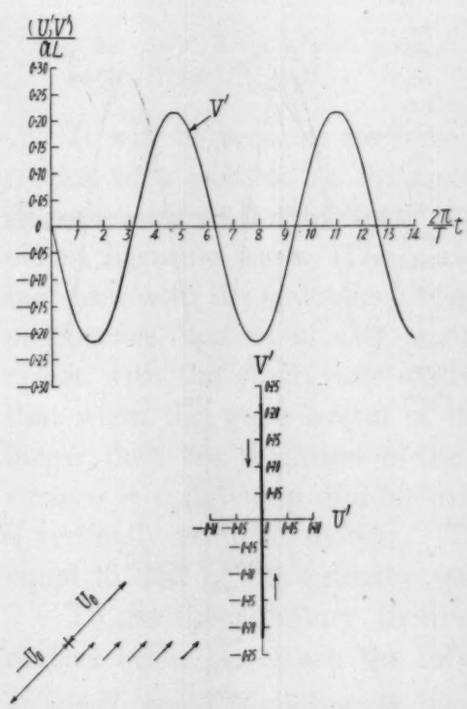

Fig. 14. $\rho=\rho'$, $\lambda=\mu$, $\lambda'=\mu'$, $\mu=\mu'$, $e=45°$, $H/L=0$, $y=H$.

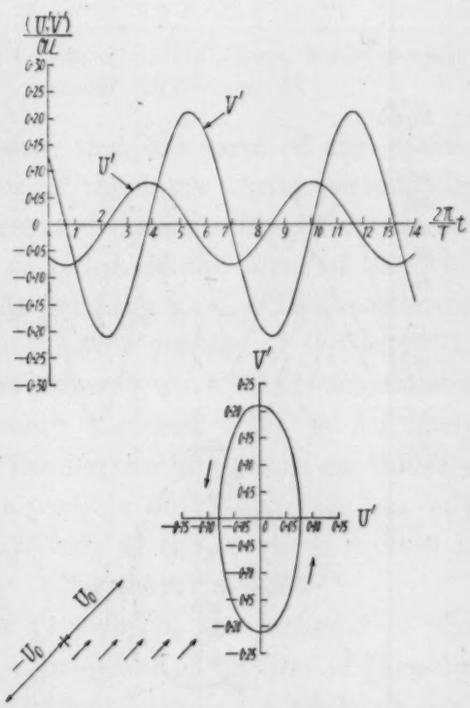

Fig. 15. $\rho=\rho'$, $\lambda=\mu$, $\lambda'=\mu'$, $\mu=\mu'$, $e=45°$, $H/L=1/10$, $y=H$.

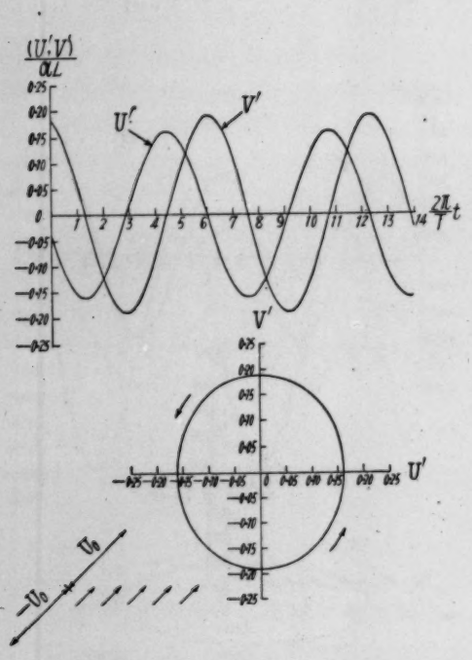

Fig. 16. $\rho=\rho'$, $\lambda=\mu$, $\lambda'=\mu'$, $\mu=\mu'$, $e=45°$, $H/L=1/5$, $y=H$.

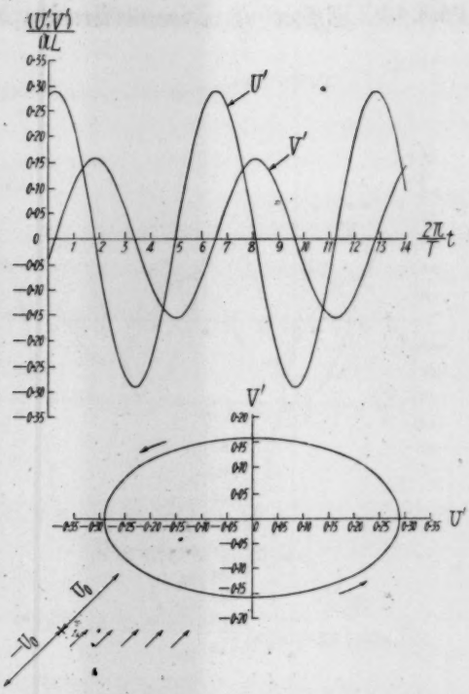

Fig. 17. $\rho=\rho'$, $\lambda=\mu$, $\lambda'=\mu'$, $\mu=\mu'$, $e=45°$, $H/L=1/2$, $y=H$.

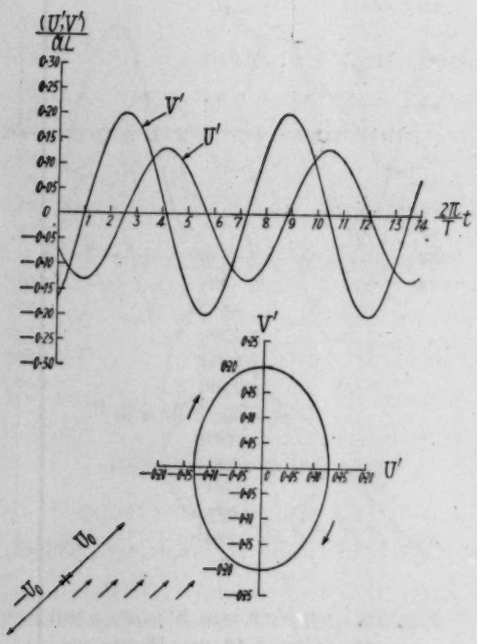

Fig. 18. $\rho=\rho'$, $\lambda=\mu$, $\lambda'=\mu'$, $\mu=\mu'$, $e=45°$, $H/L=1$, $y=H$.

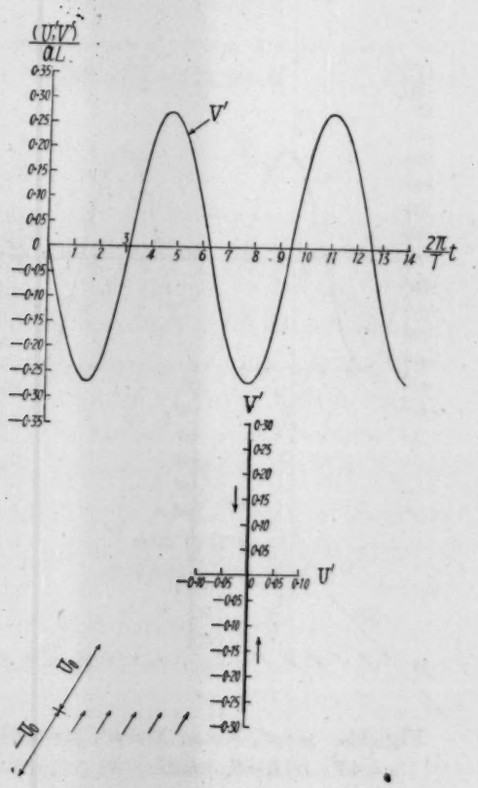

Fig. 19. $\rho=\rho'$, $\lambda=\mu$, $\lambda'=\mu'$, $\mu=\mu'$, $e=60°$, $H/L=0$, $y=H$.

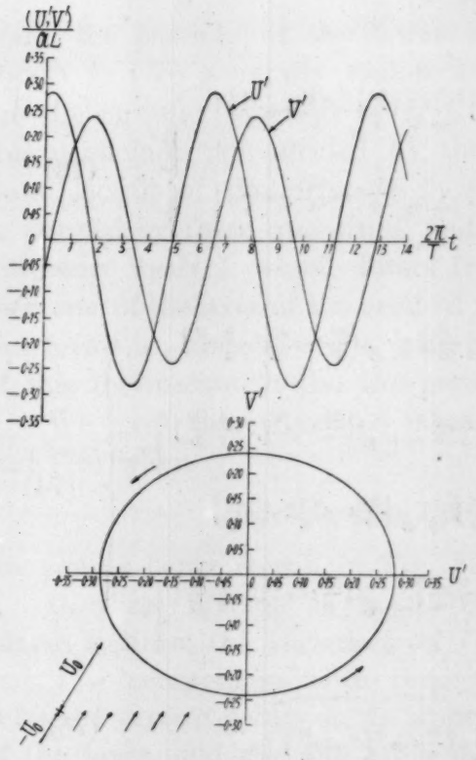

Fig 20. $\rho=\rho'$, $\lambda=\mu$, $\lambda'=\mu'$, $\mu=\mu'$, $e=60°$, $H/L=1/2$, $y=H$.

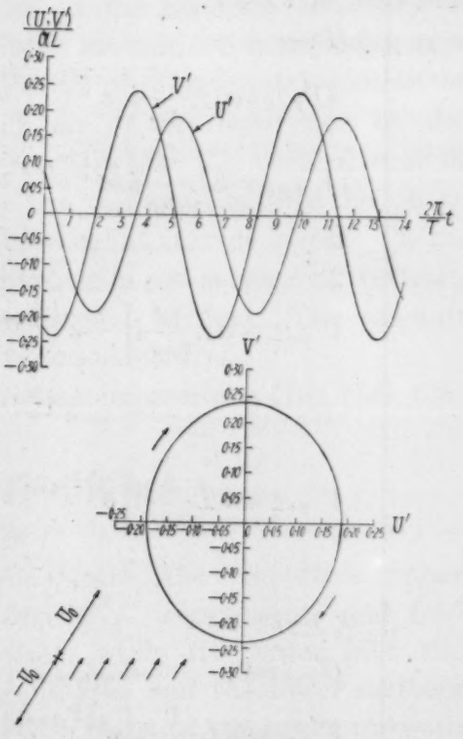

Fig. 21. $\rho=\rho'$, $\lambda=\mu$, $\lambda'=\mu'$ $\mu=\mu'$, $e=60°$, $H/L=1$, $y=H$.

It will be seen, as we have discussed, that the form of the orbital motion of a particle on the free surface of the layer varies periodically with the ratio of the thickness of the layer and the wave length of the incident harminc wave. The period of variation of the form of the orbit increases with the emergency angle of the primary wave. The maximum amplitudes, horizontal and vertical, on the free surface of the layer increase with the emergency angle of the primary wave. It is remarkable that when the wave length of the primary incident wave is infinitely larger than the thickness of the layer, the horizontal motion on the free surface is completely diminished and a particle on that surface has only a vertically periodic motion. The amplitude of this vertical motion is equal to that of the primary wave.

To get the vibratory motion of a particle in the interior of the surface layer, we obtain the following expressions of motion of particles at $y=H$, $y=\frac{1}{2}H$ and $y=0$, together with the expression of the motion of a particle of the lower medium at the common boundary $y=0$ in

the case of $e=30°$.[4]

$y=H$:—

$$\left.\begin{aligned} U'_{y=H} &= \mathfrak{A}L\frac{\sqrt{3}}{4\pi}i\left\{e^{i\left\{\frac{2\pi}{T}t-x\frac{\sqrt{3}\pi}{L}-\pi\frac{H}{L}\right\}}-e^{i\left\{\frac{2\pi}{T}t-x\frac{\sqrt{3}\pi}{L}-3\pi\frac{H}{L}\right\}}\right\}, \\ V'_{y=H} &= \mathfrak{A}L\frac{1}{4\pi}i\left\{e^{i\left\{\frac{2\pi}{T}t-x\frac{\sqrt{3}\pi}{L}-\pi\frac{H}{L}\right\}}+e^{i\left\{\frac{2\pi}{T}t-x\frac{\sqrt{3}\pi}{L}-3\pi\frac{H}{L}\right\}}\right\}, \end{aligned}\right\} \quad \ldots\ldots (73)$$

$y=\frac{H}{2}$:—

$$\left.\begin{aligned} U'_{y=\frac{H}{2}} &= \mathfrak{A}L\frac{\sqrt{3}}{8\pi}i\left[-e^{i\left\{\frac{2\pi}{T}t-x\frac{\sqrt{3}\pi}{L}-\frac{7}{2}\pi\frac{H}{L}\right\}}+e^{i\left\{\frac{2\pi}{T}t-x\frac{\sqrt{3}\pi}{L}-\frac{5}{2}\pi\frac{H}{L}\right\}}\right. \\ &\qquad \left.-e^{i\left\{\frac{2\pi}{T}t-x\frac{\sqrt{3}\pi}{L}-\frac{3}{2}\pi\frac{H}{L}\right\}}+e^{i\left\{\frac{2\pi}{T}t-x\frac{\sqrt{3}\pi}{L}-\frac{1}{2}\pi\frac{H}{L}\right\}}\right], \\ V'_{y=\frac{H}{2}} &= \mathfrak{A}L\frac{1}{8\pi}i\left[e^{i\left\{\frac{2\pi}{T}t-x\frac{\sqrt{3}\pi}{L}-\frac{7}{2}\pi\frac{H}{L}\right\}}+e^{i\left\{\frac{2\pi}{T}t-x\frac{\sqrt{3}\pi}{L}-\frac{5}{2}\pi\frac{H}{L}\right\}}\right. \\ &\qquad \left.+e^{i\left\{\frac{2\pi}{T}t-x\frac{\sqrt{3}\pi}{L}-\frac{3}{2}\pi\frac{H}{L}\right\}}+e^{i\left\{\frac{2\pi}{T}t-x\frac{\sqrt{3}\pi}{L}-\frac{1}{2}\pi\frac{H}{L}\right\}}\right], \end{aligned}\right\} \quad (74)$$

$y=0$:—

$$\left.\begin{aligned} U'_{y=0} &= 0, \\ V'_{y=0} &= \mathfrak{A}L\frac{1}{4\pi}i\left[e^{i\left\{\frac{2\pi}{T}t-x\frac{\sqrt{3}\pi}{L}\right\}}+e^{i\left\{\frac{2\pi}{T}t-x\frac{\sqrt{3}\pi}{L}-4\pi\frac{H}{L}\right\}}\right], \end{aligned}\right\} \quad \ldots\ldots\ldots (75)$$

$y=0$:—

$$\left.\begin{aligned} U_{y=0} &= \mathfrak{A}L\frac{\sqrt{3}}{2\pi}ie^{i\left\{\frac{2\pi}{T}t-x\frac{\sqrt{3}\pi}{L}\right\}}, \\ V_{y=0} &= \mathfrak{A}L\frac{1}{4\pi}i\left[e^{i\left\{\frac{2\pi}{T}t-x\frac{\sqrt{3}\pi}{L}\right\}}+e^{i\left\{\frac{2\pi}{T}t-x\frac{\sqrt{3}\pi}{L}-4\pi\frac{H}{L}\right\}}\right]. \end{aligned}\right\} \quad \ldots\ldots (76)$$

It will be seen that one axis of the orbital motion of a particle in the interior of the surface layer is vertical, and that the amplitudes of the two components U', V' in the surface layer are circular harmonic functions of H/L, and that the period is not equal for the whole space in the interior of the layer. When $y=H$, the period is H/L. When $y=1/2\,H$, it is $2\,H/L$. And when $y=0$ it is $1/2\;H/L$. Therefore the forms of the ellipse of the orbital motion in the layer are generally differ for the whole space. The particle of the layer at the common boundary has only vertical motion and no horizontal, the amplitude of this vertical motion being a circular function of H/L. On the con-

4) When $e=0°$, $U_{y=0}=0$, $V_{y=0}=0$ and $U'_{y=0}=0$, $V'_{y=0}=0$. Therefore there is no motion of particles in the layer, and a particle of the lower medium on the common boundary is at rest. (See (49), (50)).

trary, the particle of the lower medium at the common boundary as shewn in (76) generally makes an elliptic motion, of which the axes are the circular function of H/L. Moreover the horizontal motion of this particle is not affected by the thickness of the layer nor by the wave length of the primary incident wave, while the vertical motion is affected by these quantities, and these two components have the phase difference $4\pi H/L$ which differs from those in the surface layer. Therefore one of the axes of the orbit of this particle is not necessarily vertical, but forms an oblique angle with the horizontal surface. The amount of this inclination is also the periodic function of H/L.

We have also calculated numerically the expressions (73), (74), (75) and (76) when

$$H/L=0,\ 1/8,\ 1/6,\ 1/4,\ 1/3,\ 1/2 \text{ and } 1,$$

the results being shewn in Fig. $22\,a\sim28\,d$.

In these figures, as in the preceding case, the respective upper curves indicate the variations of $U'-$ and $V'-$ components and $U-$ and $V-$ components with respect to time, while the lower give the orbits of certain points on the upper, the middle, and the lower surfaces of the layer, and also the orbit of a certain point of the lower medium on the common boundary $y=0$. U_0 is the amplitude of the primary wave.

The inclination of the axes of the elliptic orbit of a particle of the lower medium on the common boundary $y=0$ to the horizontal plane varies from 0° to 30°, periodically, according to how H/L varies.

When $H/L=0$, *i. e.*, the wave length of the primary wave is very large compared with the thickness of the layer, no horizontal motion is caused in the whole space of the interior of the layer, and the amplitude of the vertical motion is equal to that of the primary wave. In this case the minor axis of the orbit on the common boundary in the lower medium is exactly zero, and the major axis of which the half length is equal to the double amplitudes of the primary wave inclines 30° to the horizontal plane.

When $H/L=1/8$, the inclination of the major axis of the elliptic orbit at $y=0$ in the lower medium is slightly smaller than the emergency angle 30°, and the particle makes an elliptic orbit. In this case, however, the particle on lower boundary of the surface layer has only a vertical motion and no horizontal, while its amplitude is slightly smaller than that of the primary wave.

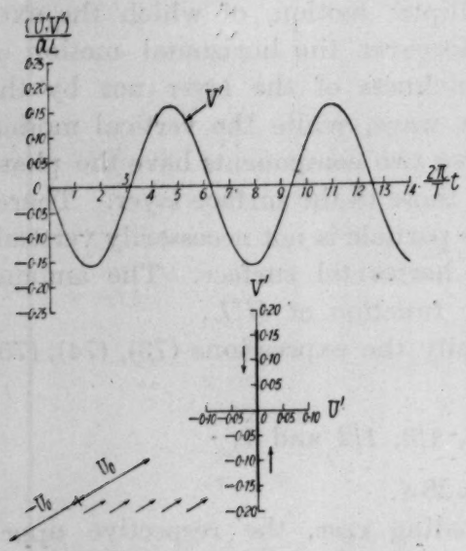

Fig. 22a. $\rho=\rho'$, $\lambda=\mu$, $\lambda'=\mu'$, $\mu=\mu'$, $e=30°$, $H/L=0$, $y=H$.

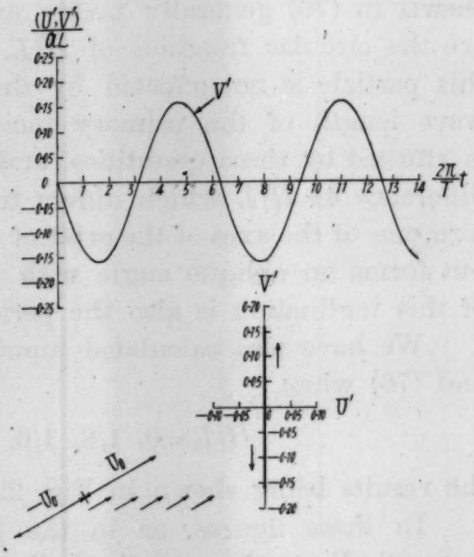

Fig. 22b. $\rho=\rho'$, $\lambda=\mu$, $\lambda'=\mu'$, $\mu=\mu'$, $e=30°$, $H/L=0$, $y=H/2$.

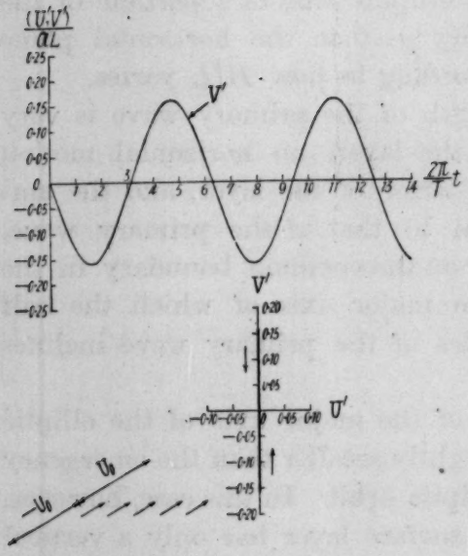

Fig. 22c. $\rho=\rho'$, $\lambda=\mu$, $\lambda'=\mu'$, $\mu=\mu'$, $e=30°$, $H/L=0$, $y=0$.

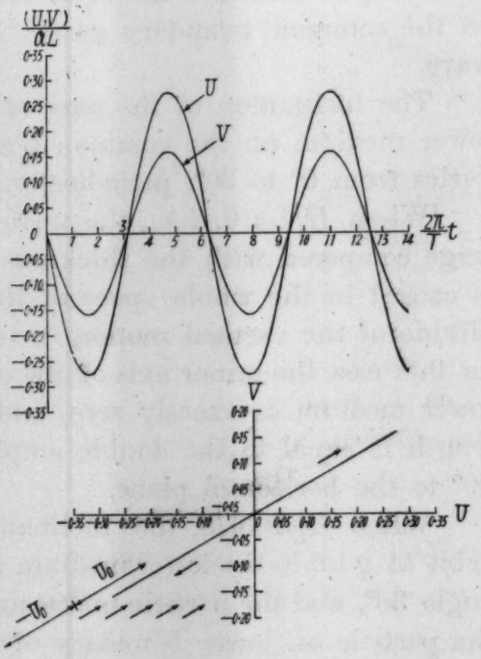

Fig. 22d. $\rho=\rho'$, $\lambda=\mu$, $\lambda'=\mu'$, $\mu=\mu'$, $e=30°$, $H/L=0$, $y=0$.

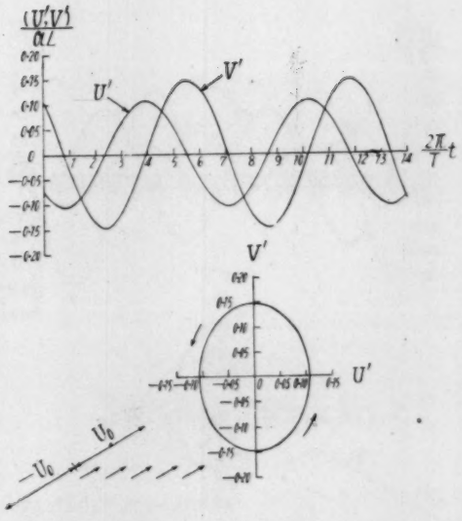

Fig 23a. $\rho=\rho'$, $\lambda=\mu$, $\lambda'=\mu'$, $\mu=\mu'$, $e=30°$, $H/L=1/8$, $y=H$.

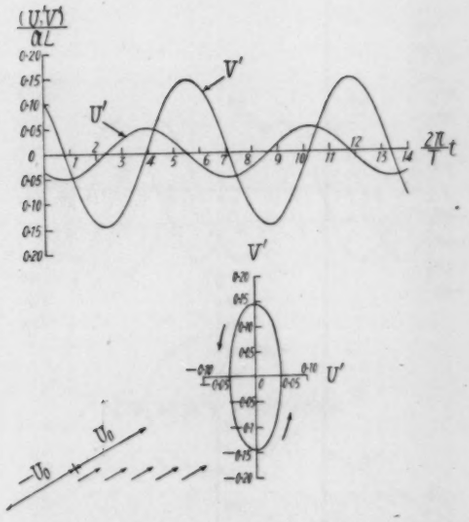

Fig. 23b. $\rho=\rho'$, $\lambda=\mu$, $\lambda'=\mu'$, $\mu=\mu'$, $e=30°$, $H/L=1/8$, $y=H/2$.

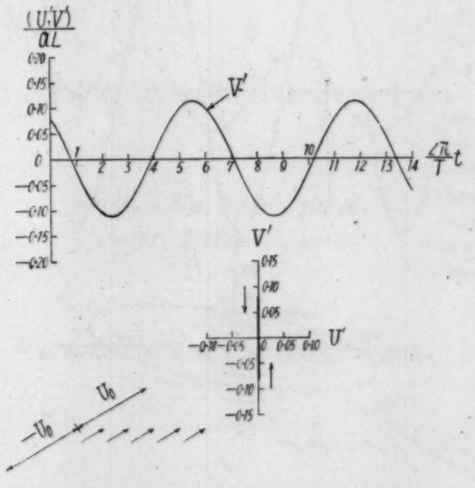

Fig. 23c. $\rho=\rho'$, $\lambda=\mu$, $\lambda'=\mu'$, $\mu=\mu'$, $e=30°$, $H/L=1/8$, $y=0$.

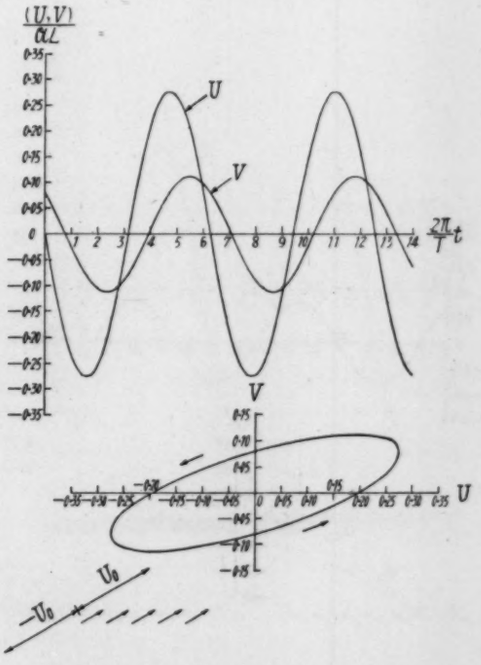

Fig. 23d. $\rho=\rho'$, $\lambda=\mu$, $\lambda'=\mu'$, $\mu=\mu'$, $e=30°$, $H/L=1/8$, $y=0$.

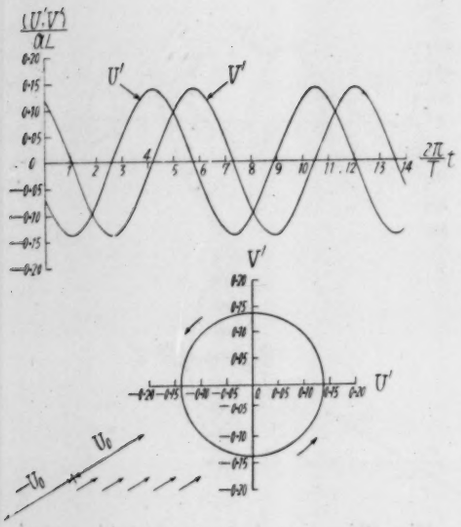

Fig. 24a. $\rho=\rho'$, $\lambda=\mu$, $\lambda'=\mu'$, $\mu=\mu'$, $e=30°$, $H/L=1/6$, $y=H$.

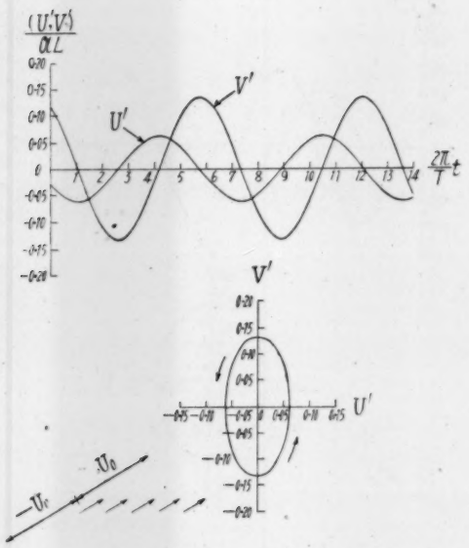

Fig 24b. $\rho=\rho'$, $\lambda=\mu$, $\lambda'=\mu'$, $\mu=\mu'$, $e=30°$, $H/L=1/6$, $y=H/2$.

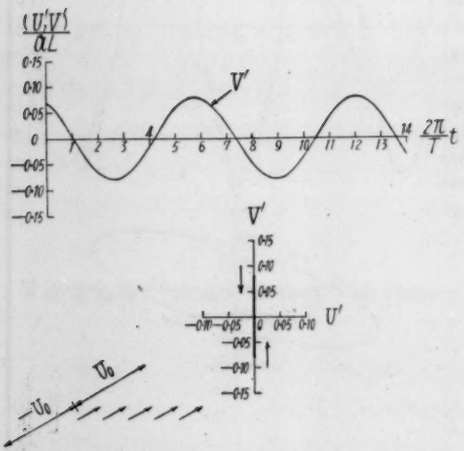

Fig. 24c. $\rho=\rho'$, $\lambda=\mu$, $\lambda'=\mu'$, $\mu=\mu'$, $e=30°$, $H/L=1/6$, $y=0$.

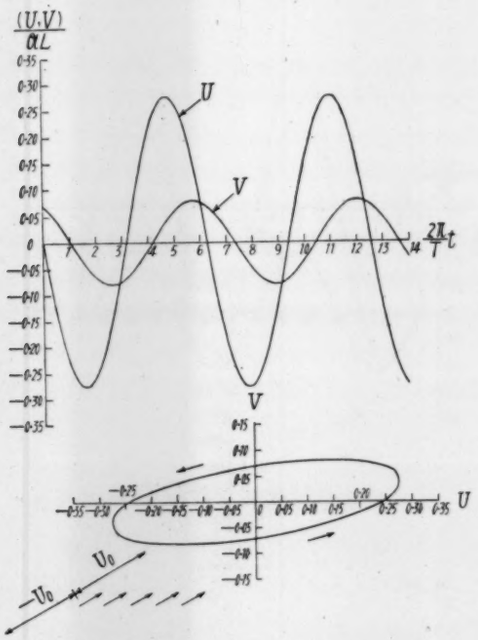

Fig. 24d. $\rho=\rho'$, $\lambda=\mu$, $\lambda'=\mu'$, $\mu=\mu'$, $e=30°$, $H/L=1/6$, $y=0$.

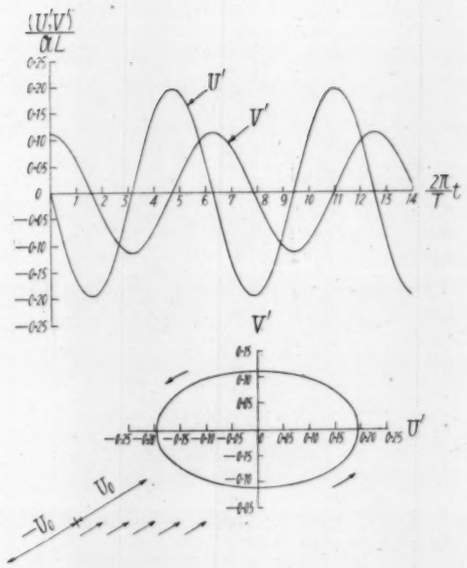

Fig. 25a. $\rho=\rho'$, $\lambda=\mu$ $\lambda'=\mu'$, $\mu=\mu'$, $e=30°$, $H/L=1/4$, $y=H$.

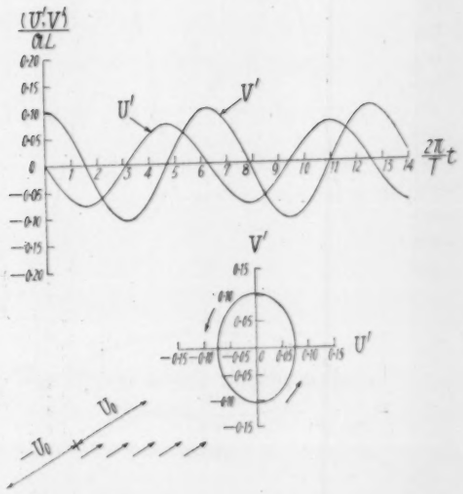

Fig. 25b. $\rho=\rho'$, $\lambda=\mu$, $\lambda'=\mu'$, $\mu=\mu'$, $e=30°$, $H/L=1/4$, $y=H/2$.

$$U'=V'=0.$$

$\rho=\rho'$, $\lambda=\mu$, $\lambda=\mu'$, $\mu=\mu'$, $e=30°$, $H/L=1/4$, $y=0$

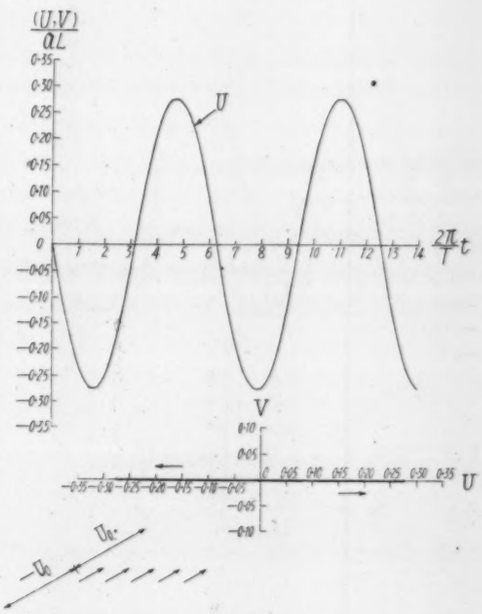

Fig. 25c. $\rho=\rho'$, $\lambda=\mu$, $\lambda'=\mu'$, $\mu=\mu'$, $e=30°$, $H/L=1/4$, $y=0$.

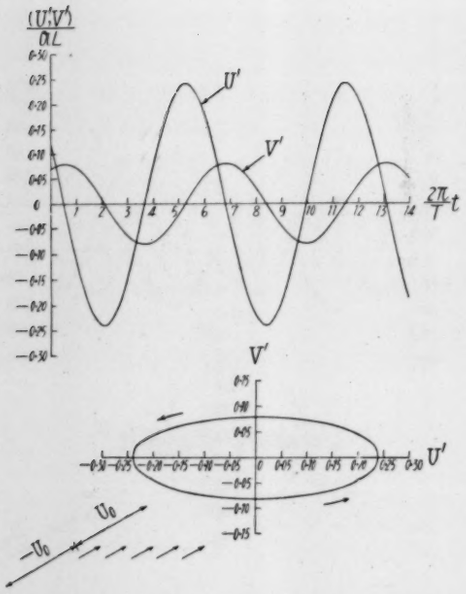

Fig. 26a. $\rho=\rho'$ $\lambda=\mu$, $\lambda'=\mu'$, $\mu=\mu'$, $e=30°$, $H/L=1/3$, $y=H$.

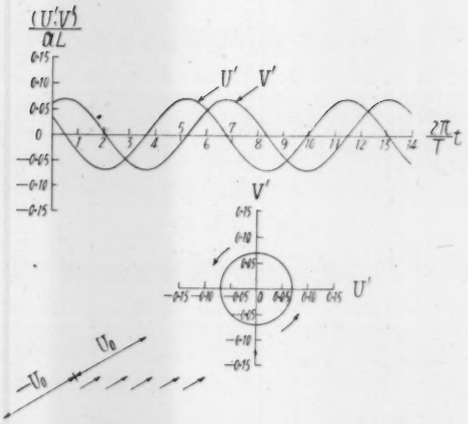

Fig. 26b. $\rho=\rho'$ $\lambda=\mu$, $\lambda'=\mu'$, $\mu=\mu'$, $e=30°$, $H/L=1/3$, $y=H/2$.

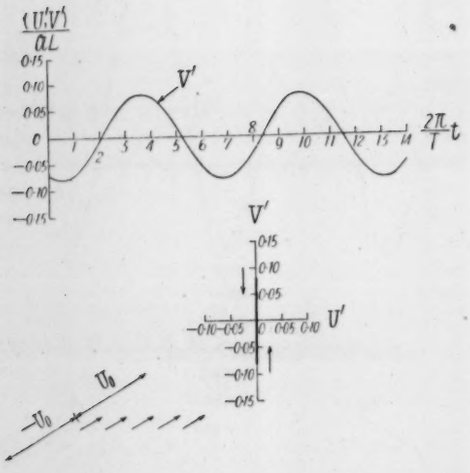

Fig. 26c. $\rho=\rho'$, $\lambda=\mu$, $\lambda'=\mu'$, $\mu=\mu'$, $e=30°$, $H/L=1/3$, $y=0$.

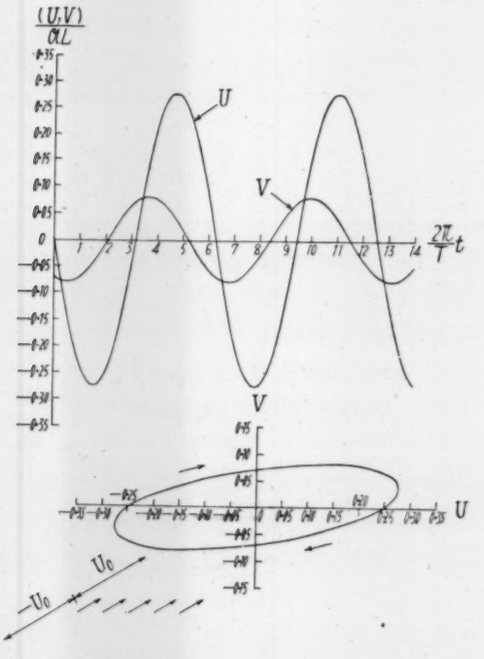

Fig. 26d. $\rho=\rho'$, $\lambda=\mu$, $\lambda'=\mu'$, $\mu=\mu'$, $e=30°$, $H/L=1/3$, $y=0$.

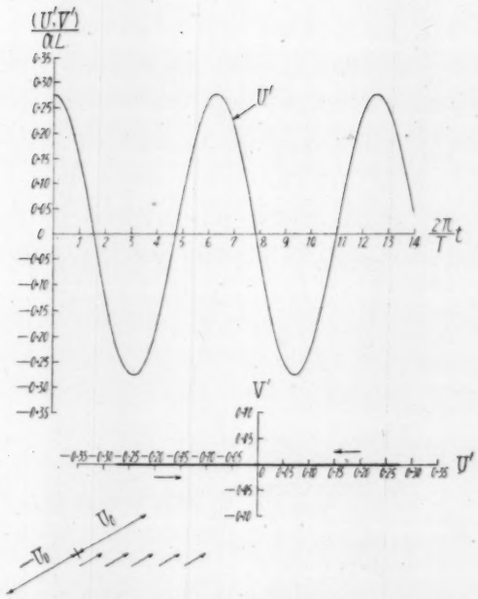

$$U' = V' = 0.$$

$\rho = \rho'$, $\lambda = \mu$, $\lambda' = \mu'$, $\mu = \mu'$,
$e = 30°$. $H/L = 1/2$, $y = H/2$.

Fig. 27a. $\rho = \rho'$, $\lambda = \mu$, $\lambda' = \mu'$, $\mu = \mu'$,
$e = 30°$, $H/L = 1/2$, $y = H$.

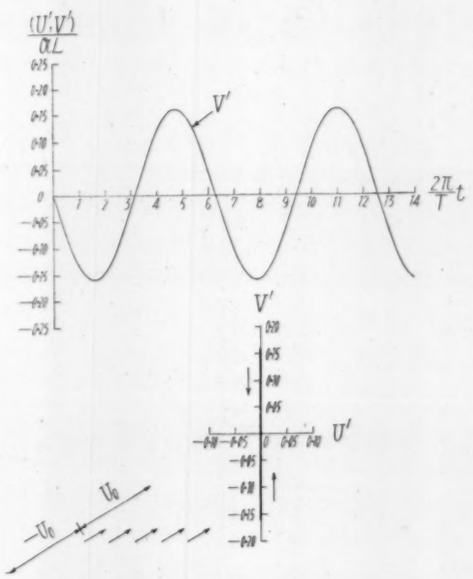

Fig. 27b. $\rho = \rho'$, $\lambda = \mu$ $\lambda' = \mu'$, $\mu = \mu'$,
$e = 30°$ $H/L = 1/2$, $y = 0$.

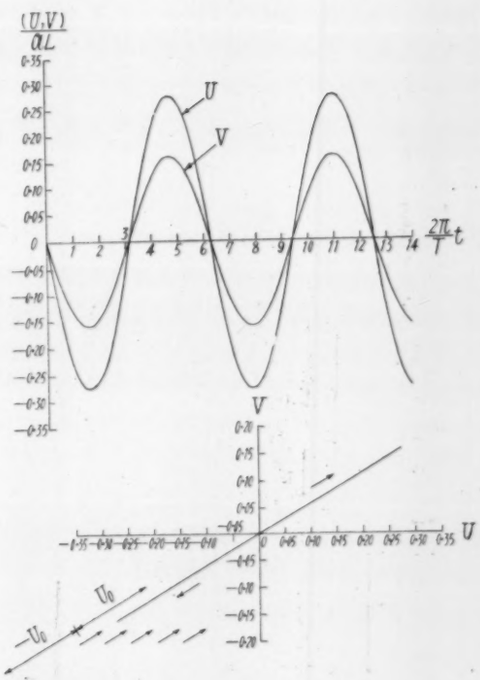

Fig. 27c. $\rho = \rho'$, $\lambda = \mu$, $\lambda' = \mu'$, $\mu = \mu'$,
$e = 30°$, $H/L = 1/2$, $y = 0$.

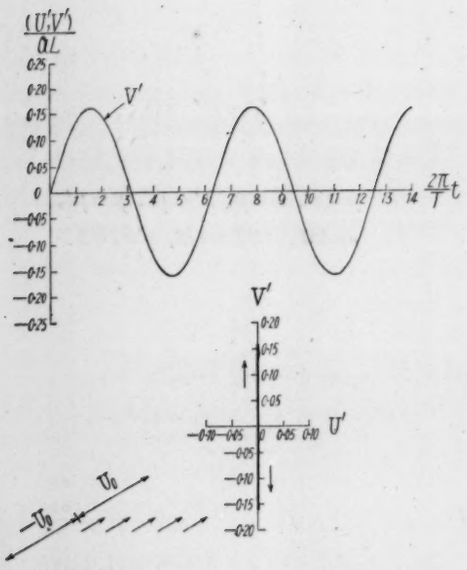

Fig. 28a. $\rho=\rho'$ $\lambda=\mu$, $\lambda'=\mu'$, $\mu=\mu'$, $e=30°$, $H/L=1$, $y=H$.

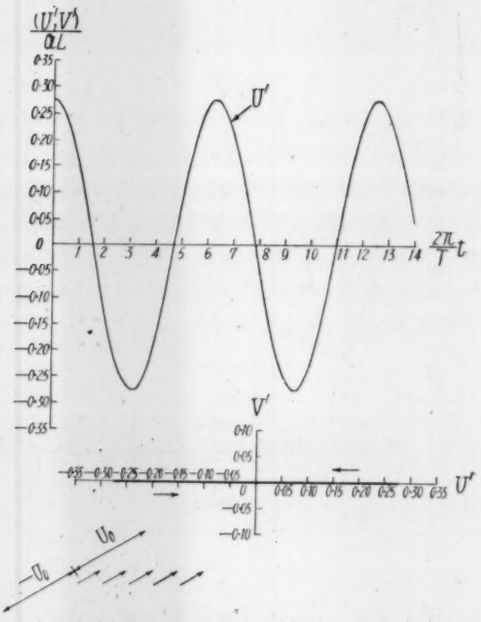

Fig. 28b. $\rho=\rho'$, $\lambda=\mu$, $\lambda'=\mu'$, $\mu=\mu'$, $e=30°$, $H/L=1$, $y=H/2$.

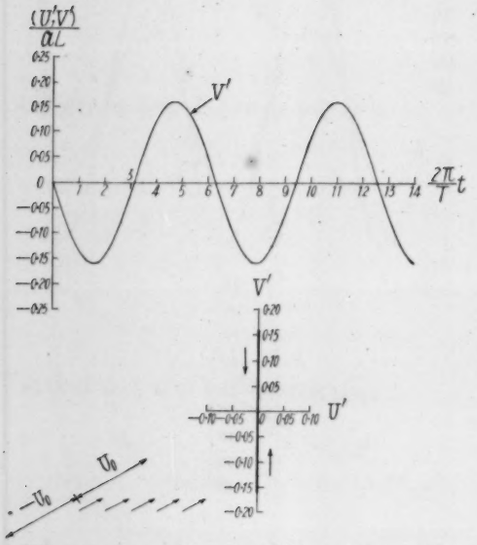

Fig. 28c. $\rho=\rho'$, $\lambda=\mu$, $\lambda'=\mu'$, $\mu=\mu'$, $e=30°$, $H/L=1$, $y=0$.

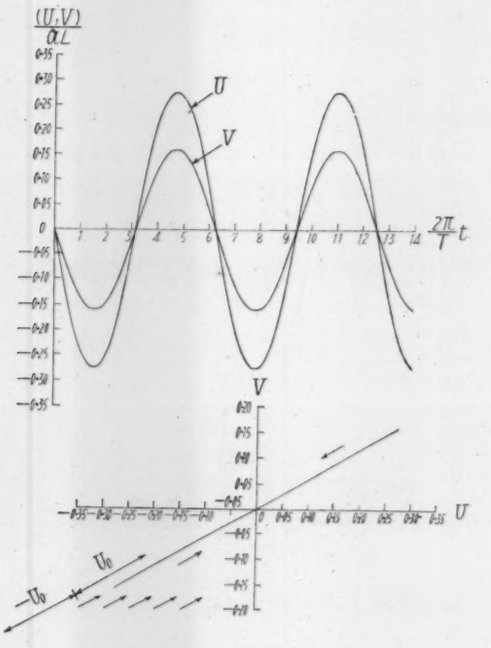

Fig. 28d. $\rho=\rho'$, $\lambda=\mu$, $\lambda'=\mu'$, $\mu=\mu$,' $e=30°$, $H/L=1$, $y=0$.

Generally the particle of the lower medium on the common boundary makes an orbital motion, but the particle of the surface layer on this boundary has only a vertical motion, of which the amplitude is equal to that of the vertical component of the orbital motion of a particle of the lower medium on this common boundary. This is a condition which we cannot obtain from that boundary condition in which the two solids adhere closely at the common boundary.

31. 不連續面が彈性波の傳播に及ぼす影響 (II)

地震研究所 { 西村源六郎
金井清

曩に表面層をもつた半無限彈性體内を傳播する體彈性波がその表面にあたつた時，表面ではどの様な波が起されるかを研究してみたが，その結果は勿論その彈性體内のある點の振動運動を論ずるには不充分なものであつて，單に初動を論ずる時に役立つものである．從つて此の論文ではその表面層の下面に無限につながつた一定の振幅と週期をもつた體彈性波が入射した時，その表層の自由面や内部での分子運動が入射角や入射波の波長或は表面層の厚さによつてどの様な具合になるか卽ち分子運動の振幅や振動軌跡がこれ等の量によつて變化する様子を詳しく檢べてみた．表面層と下の彈性體とが全く彈性係數も密度も等しい様な場合に就て數計算を行ひ又これ等の結果を圖示し，殊に入射角が 30° の場合に就ては詳しく論じてある．次の論文ではこれ等の結果を使つて彈性波成生に關係した今少し深く這入つた研究を發表する考である．

32. *The Most Suitable Formula for the Japanese Gravity Values.*

By Chûji TSUBOI,

Earthquake Research Institute.

(Read Sept. 19, 1933.—Received Sept. 20, 1933.)

Recently, Captain K. Atumi[1] of the Japanese Military Land Survey, after studying the plumb-line deviations at Japanese 68 stations, determined the Geoid undulations throughout the country. As most of the astronomical observations used in his calculations were not made with his precise studies in view, the original observations and, as a consequence the results of the calculations, do not seem to be very accurate. Nevertheless, the conclusions arrived at by him are so remarkable that they must be regarded as indicating something near the truth. His chief conclusions are :—

1. The components of the plumb-line deviation at the Tokyo Astronomical Observatory (Azabu), which is the base station of the Japanese triangulation, are

$$\xi = -9''.46,$$

$$\lambda = +9''.35.$$

2. The semi-major axis of the ellipsoid of revolution that best fits in with Japanese astronomical observations is 6,376,918 m, which is 480 m shorter than that of the Bessel's ellipsoid.

3. The ellipticity of the newly determined ellipsoid is 1/311.

This last conclusion is of special interest, since the large difference in this ellipticity from the normal one of 1/298 seems to indicate certain abnormal subterranean conditions prevailing in the neighbourhood of Japan, noted for its seismic and volcanic activities.

Seeing that it is generally conceded that the ellipticity of the terrestrial ellipsoid can be determined more accurately from gravity observations than from geodetic measurements, the writer intends here to determine the ellipticity of the earth solely from the Japanese gravity values. Gravity measurements in Japan have been and still are

1) A. ATUMI, *Jap. Journ. Astr. Geophys.*, 10 (1933), 307.

made under the supervision of the Imperial Japanese Geodetic Commission. The stations occupied in Hokkaidô, Honsyû, Sikoku, and Kyûsyû, which amount to 122 in all, extend from $\varphi=45°25'$ in the north down to $\varphi=31°28''$ in the south. The Bouguer anomalies at these stations, which have already been published[2], were obtained by comparing the g_0'' at the stations with the values expected from Helmert's formula of 1901, namely,

$$\gamma_0=978{\cdot}030(1+0{\cdot}005302\sin^2\varphi-0{\cdot}000007\sin^2 2\varphi).$$

The anomalies in Japan are generally very large, and range from $+0{\cdot}231$ to $-0{\cdot}043$. The mean value of the anomalies with regard to algebraic sign is $+0{\cdot}049$, while that without it is $0{\cdot}054$. Such large Bouguer anomalies show that the distribution of gravitating masses near Japan differs considerably from what may be expected from the formulas of Helmert and others.

Let us now determine the numerical values of the constants in the equation,

$$\gamma_0=g_\varepsilon(1+B\sin^2\varphi),$$

that best fits in with the Japanese gravity values. The term $\sin^2 2\varphi$ is omitted because no great accuracy is necessary for the purpose of the present calculation, which is only to get an expression for the general gravity distribution in Japan. Now we have 122 observation equations of the form

$$g_0''=g_\varepsilon(1+B\sin^2\varphi)$$

in which g_0'' and φ are observed values, while g_ε and B are unknowns to be determined by calculation. To simplify the calculation, the equation was changed into the form

$$\begin{aligned}(g_0''-979{\cdot}000)&=(g_\varepsilon-979{\cdot}000)+g_\varepsilon B\sin^2\varphi\\&=\Delta g+A\sin^2\varphi,\end{aligned}$$

and the two constants,

$$\begin{cases}\Delta g=g_\varepsilon-979{\cdot}000,\\ A=g_\varepsilon B,\end{cases}$$

were determined by the method of least squares. The normal equations

---

1) *Comptes Rendus d. Séances.* 16^{me} *Conf Gén. d. l'Assoc. Géod. Intern.*, (1911), 252; "Rikwa-Nenpyô," (1930), 311.

by which the constants are to be determined came out as

$$\begin{cases} 122\Delta g + 44{\cdot}170\, A = 115{\cdot}949, \\ 44{\cdot}170\,\Delta g + 16{\cdot}388\, A = 44{\cdot}140. \end{cases}$$

As a solution of this set of equations, we have

$$\begin{cases} \Delta g = -1{\cdot}019, \\ A = 5{\cdot}4392. \end{cases}$$

We have therefore

$$\begin{cases} g_e = 979{\cdot}000 - 1{\cdot}019 = 977{\cdot}981, \\ B = \dfrac{5{\cdot}4392}{977{\cdot}981} = 0{\cdot}005562, \end{cases}$$

whence the final result

$$\gamma_0 = 977{\cdot}981\,(1 + 0{\cdot}005562 \sin^2\varphi).$$

The difference between this and Helmert's formulas is

$$\Delta\gamma = 0{\cdot}049 - 0{\cdot}254 \sin^2\varphi$$

which, as shown in Fig. 1, become zero at latitude $\varphi = 26°3'$. While the difference for the Japanese gravity stations at lower latitudes is not large, it becomes quite appreciable for stations at higher latitudes. The Bouguer anomalies calculated from the new formula became compara-

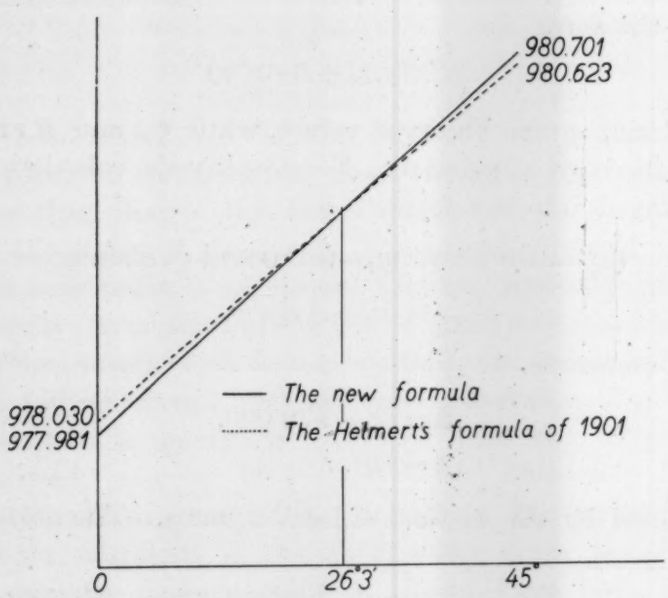

Fig. 1.

tively small and range from +0·153 to −0·088. The mean of the anomalies with regard to sign is 0, while that without regard to it is 0·035. The geographical distribution of Bouguer anomalies as calculated from the new formula is shown in Fig. 2.

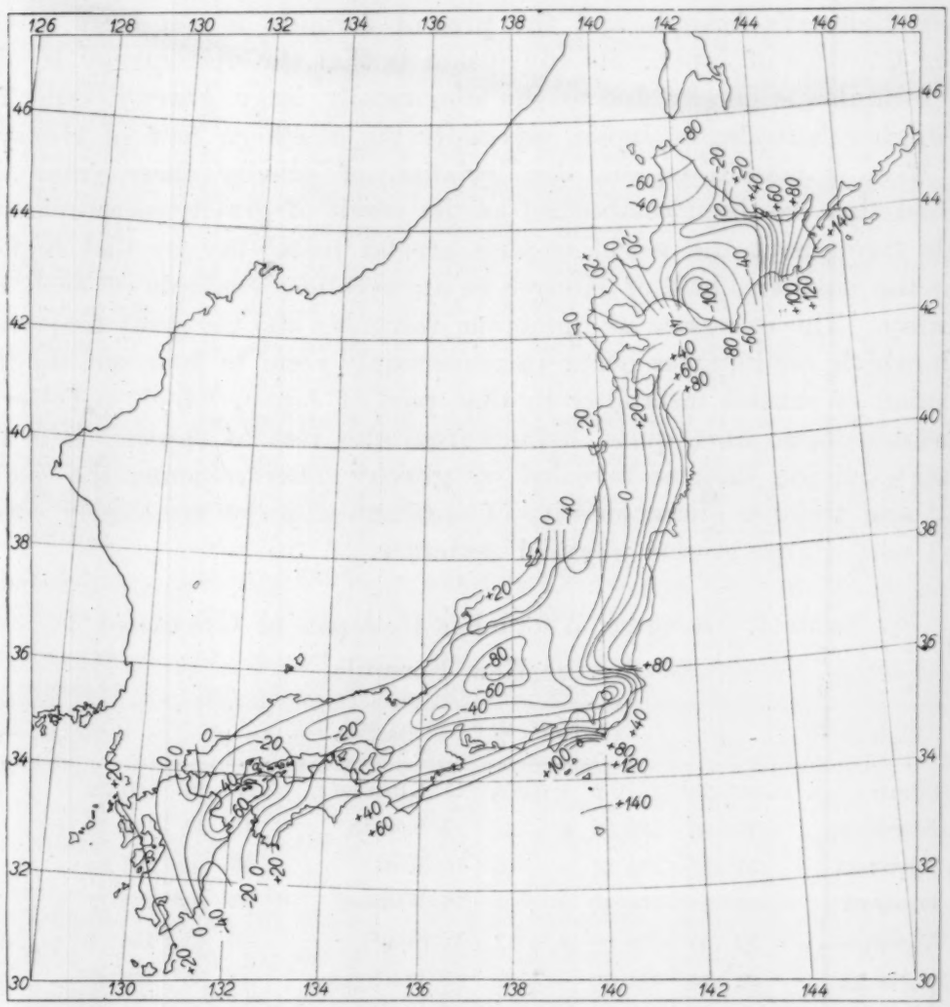

Fig. 2. Bouguer Anomalies as Calculated from the New Formula.

From the well-known relation between coefficient B of $\sin^2\varphi$ in the formula and ellipticity e of the terrestrical ellipsoid

$$B=\frac{5}{2}\frac{\omega^2 a}{g_e}-e$$

we get $e=1/322$. a and ω are the length of the equatorial radius and

the angular velocity of the earth respectively.

Though there is not a small difference between the ellipticity value obtained by Atumi and that obtained by the writer, both are decidedly smaller than the value obtained from gravity measurements made in various parts of the world. Since, as already stated, the difference between Helmert's formula and the present formula is not large in the lower latitudes of Japan, the conclusion is that the discrepancy in the two formulas is chiefly due to the abnormally large gravity value for the higher latitudes of Japan, especially the northern half of Honsyû.

If in a certain region, the deviation of gravity there from the normal that has been established as the result of gravity measurements made throughout the world implies crustal instability in that region, then the northern half of Honsyû is an excellent example of such instability. The existence of numerous volcanoes and the great frequency with which earthquakes occur there certainly seem to bear out the implication of crustal instability in that part of Japan, which is believed to be a tectonic unit, quite distinct from the rest of Japan. It is the writer's opinion that, as revealed by gravity measurements, the geological and tectonic characteristics of northern Honsyû are closely correlated with its particular physical structure.

Table I. Bouguer Anomalies in Japan as Calculated by the New Formula.

Station	φ	λ	$g_0'' - \gamma_0$	Station	φ	λ	$g_0'' - \gamma_0$
1. Sibusi	31° 28′	131° 5′	+ 0.009	13. Kurume	33 19	130 32	− 2
2. Kagosima	31 36	130 32	+ 20	14. Karatu	33 27	129 59	+ 8
3. Miyazaki	31 55	131 24	− 56	15. Kôti	33 34	133 34	0
4. Hitoyosi	32 12	130 46	+ 6	16. Nakatu	33 36	131 11	+ 3
5. Yatusiro	32 31	130 36	+ 11	17. Singû	33 43	136 0	+ 68
6. Nobeoka	32 34	131 39	− 38	18. Matuyama	33 50	132 45	− 56
7. Nagasaki	32 45	129 52	+ 27	19. Orio	33 53	130 42	− 3
8. Kumamoto	32 48	130 43	− 9	20. Tyôhu	34 0	131 0	+ 10
9. Nakamura	32 59	132 55	+ 25	21. Tokuyama	34 4	131 44	− 19
10. Hatizyô-zima	33 6	139 50	+ 154	22. Tokusima	34 5	134 35	− 3
11. Uwazima	33 13	132 35	− 15	23. Yamaguti	34 11	131 29	− 22
12. Ooita	33 15	131 36	− 65	24. Wakayama	34 14	135 11	+ 2

(to be continued.)

Table I. (*continued.*)

Station	φ	λ	$g_0''-\gamma_0$	Station	φ	λ	$g_0''-\gamma_0$
25. Edazima	34 15	132 30	− 32	59. Tyôsi	35 44	140 51	+ 50
26. Marugame	34 18	133 49	+ 9	60. Kawagoe	35 55	139 30	+ 4
27. Hirosima	34 23	132 27	− 37	61. Kamisuwa	36 2	138 8	− 76
28. Yamada	34 30	136 43	+ 2	62. Hukui	36 3	136 15	− 3
29. Hukuyama	34 30	133 23	− 14	63. Tutiura	36 6	140 12	+ 97
30. Okayama	34 39	133 56	− 16	64. Takayama	36 9	137 16	− 64
31. Nara	34 41	135 51	− 6	65. Tukuba	36 13	140 6	+ 60
32. Rendaizi	34 42	138 57	+ 67	66. Matumoto	36 14	137 59	− 88
33. Mikage	34 43	135 15	− 31	67. Matuida	36 19	138 48	− 25
34. Hamamatu	34 43	137 43	+ 12	68 Mito	36 23	140 33	+ 80
35. Oosima	34 45	139 22	+ 112	69. Maebasi	36 24	139 4	− 28
36. Ueno	34 46	136 8	+ 2	70. Ueda	36 24	138 16	− 50
37. Himedi	34 50	134 42	+ 1	71. Kanazawa	36 33	136 42	− 27
38. Hamada	34 54	132 6	+ 7	72. Utunomiya	36 33	139 53	+ 54
39. Okazaki	34 57	137 10	+ 3	73. Nagano	36 40	138 11	− 63
40. Siduoka	34 58	138 23	− 9	74. Toyama	36 40	137 13	− 37
41. Kyôto	35 2	135 47	− 40	75. Nikkô	36 44	139 38	− 18
42. Wada	35 2	140 1	+ 15	76. Ootahara	36 52	140 1	+ 7
43. Tuyama	35 5	134 1	− 23	77. Nanao	37 3	136 58	+ 16
44. Numadu	35 5	138 52	+ 10	78. Taira	37 4	140 53	+ 85
45. Nagoya	35 10	136 53	− 27	79. Takata	37 7	138 16	− 12
46. Oohara	35 15	140 24	+ 27	80. Kuwano	37 23	140 20	+ 27
47. Odawara	35 15	139 9	− 4	81. Nagaoka	37 27	138 53	− 22
48. Hikone	35 16	136 15	− 70	82. Wakamatu	37 30	139 57	− 25
49. Hukutiyama	35 18	135 9	− 15	83. Hukusima	37 45	140 27	+ 16
50. Kamakura	35 19	139 34	− 17	84. Nakamura	37 47	140 55	+ 77
51. Gihu	35 26	136 46	− 48	85. Yonezawa	37 54	140 8	− 8
52. Nakatugawa	35 29	137 32	− 44	86. Niigata	37 55	139 1	− 40
53. Matue	35 30	133 3	+ 2	87. Kawarada	38 1	138 18	+ 31
54. Tottori	35 30	134 14	− 1	88. Yamagata	38 15	140 16	− 7
55. Tiba	35 36	140 9	− 45	89. Sendai	38 15	140 52	+ 50
56. Kôhu	35 39	138 35	− 55	90. Sinzyô	38 45	140 18	− 16
57. Turuga	35 39	136 3	− 49	91. Kesennuma	38 55	141 36	+ 84
58. Tokyo	35 43	139 46	− 30	92. Itinoseki	38 55	141 6	+ 55

(*to be continued.*)

Tabel I. (*continued.*)

Station	φ	λ	$g_0''-\gamma_0$	Station	φ	λ	$g_0''-\gamma_0$
93. Sakata	38 55	139 50	− 41	108. Imoppe	42 34	141 57	− 106
94. Midusawa	39 8	141 8	+ 25	109. Suttu	42 48	140 13	+ 26
95. Yuzawa	39 9	140 30	+ 10	110. Obihiro	42 55	143 12	− 63
96. Tôno	39 18	141 31	+ 60	111. Kusiro	42 58	144 23	+ 103
97. Miyako	39 38	141 58	+ 85	112. Sapporo	43 5	141 20	− 31
98. Akita	39 42	140 7	− 11	113. Nemuro	43 21	145 30	+ 153
99. Marioka	39 42	141 10	+ 32	114. Simohurano	43 21	142 30	− 40
100. Oodate	40 16	140 34	+ 3	115. Asahigawa	43 46	142 22	− 16
101. Hukuoka	40 16	141 19	+ 38	116. Rubesibe	43 47	143 38	− 36
102. Hatinohe	40 31	141 30	+ 87	117. Rumoe	43 56	141 39	− 22
103. Hirosaki	40 36	140 28	− 3	118. Abasiri	44 1	144 1	+ 58
104. Aomori	40 49	140 45	+ 20	119. Monbetu	44 21	143 21	+ 28
105. Hakodate	41 47	140 46	+ 14	120. Nayori	44 22	142 24	− 37
106. Urakawa	42 9	142 45	− 89	121. Esasi	44 57	142 33	− 59
107. Muroran	42 19	140 58	+ 36	122. Wakkanai	45 25	141 41	− 81

32. 日本の重力に最もよく適合する式

地震研究所 坪 井 忠 二

日本に於ける 122 點の重力に最もよく適合する式を定めた. 其の結果は

$$\gamma_0 = 977{\cdot}981(1+0{\cdot}005562\sin^2\varphi)$$

となつた. 之から地球の扁平率を求めると 1/322 となり. 嘗て熱海大尉が日本の鉛直線偏倚から求めた 1/311 と云ふ値と同樣に大變小さい. ヘルメルトの式では扁平率は 1/298 となるが. 此の著しい差は日本の近傍で質量分布の有樣に特徵がある事を示す. 新しい式とヘルメルトの式との差は日本の南半分では餘り著しくないから, 上記の質量の異常は日本の北半分で特に著しいであらう. 地震や火山が日本の北半分に多いのも之と關係がある事と思ふ.

33. *Block Movements of the Earth's Crust in the Kwantô District.*

(*The Crustal-Blocks and Their Movements. Part III.*)

By Naomi MIYABE,

Earthquake Research Institute.

(Read March 20, 1933.—Received Sept. 20, 1933.)

Introduction.

In the preceding investigation[1] on the block movements of the earth's crust, which was made by utilizing data relating to vertical displacements of triangulation points, it was shown that in the Bôsô peninsula the earth's crust, consisting of many blocks, had tilted in various directions. It was also shown that the earth's crust as a whole had deformed, although the mode of this general deformation does not always agree with those of the local constituent crustal blocks. It was also pointed out that in a number of places the boundaries of the crustal blocks thus determined[2] were found to coincide with the tectonic lines or faults that had been traced by Prof. H. Yabe and others of the Geological Institute of the Tôhoku Imperial University.

In this paper the approximate sizes of the blocks in the S. W. Kwantô district that have tilted, and the ways in which they have tilted, are determined by means of vertical displacements of the secondary and tertiary triangulation points that were found to have occurred during the interval 1892–1925[3], and the modes of the block movements thus found are discussed in connection with other geophysical data.

These vertical displacements of triangulation points may consist of two components, namely, the component due to the chronic crustal movements integrated over the time interval between the successive surveys and the other due to the acute crustal movements associated with destructive earthquake, such as, the Kwantô Earthquake of 1923.

1) N. MIYABE, *Bull. Earthq. Res. Inst.*, 9 (1931), 257.

2) The phrase "determining the blocks," used throughout this paper, is a contraction of "Determining the precise tiltings of the blocks, such as the magnitude of tilt, their azimuths of directions, etc."

3) The data are from the Report published by the Military Land Survey (1930).

These two components cannot be separated, *a priori*, without some datum enabling an estimate of the value of either component with sufficient accuracy.

In the district under consideration are nearly 500 triangulation points of second and third order, distributed as shown in Fig. 1, in which the numerals against the triangulation points are the numbers that designate them in the tables throughout this paper.

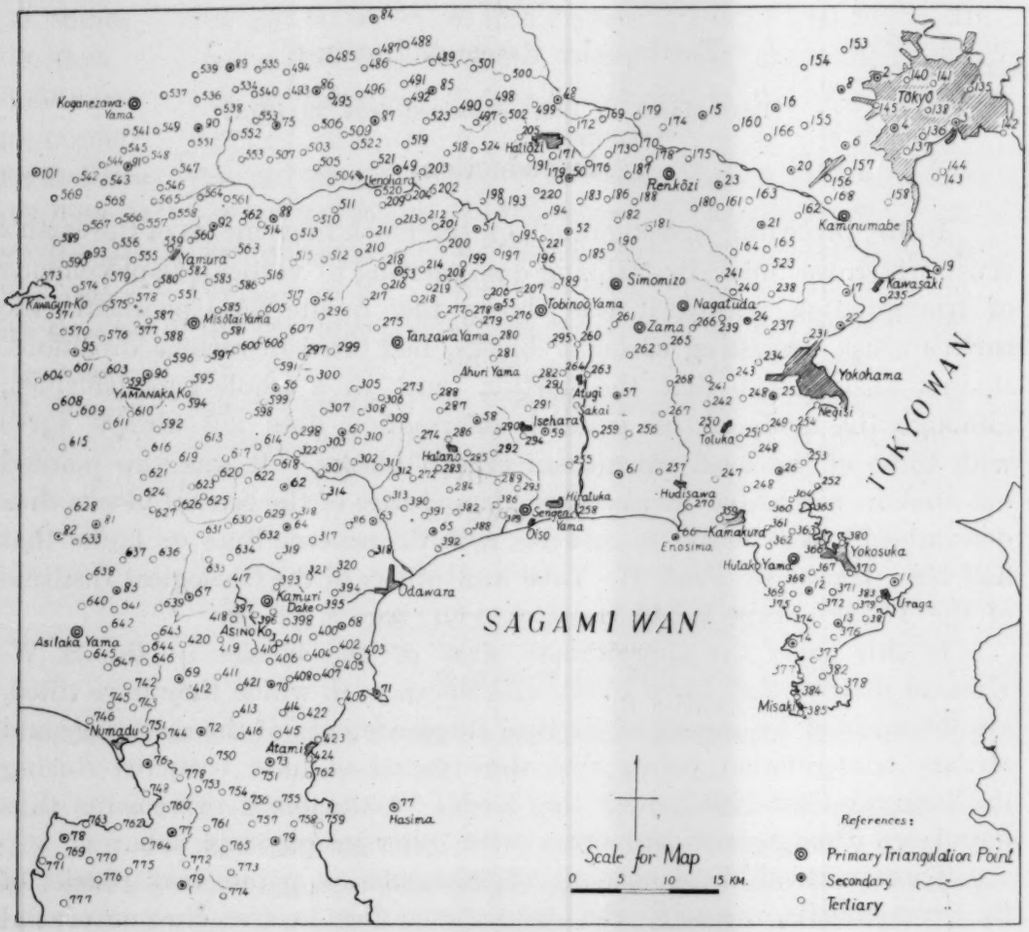

Fig. 1. Geographical distribution of triangulation points.

Determination of the Crustal Blocks.

For determining the approximate sizes of the constituent blocks, together with the magnitude of tilt and the azimuth of direction of tilt of these blocks, a trigonometrical relation

$$\tan\varphi = \tan\varphi_m \cos(\theta - \theta_m) \qquad (1)$$

was used, where $\tan\varphi$ corresponds to the gradient of the vertical movement of the earth's crust in the direction of azimuth θ, the azimuth being measured with reference to N as zero. The angle φ_m, is the magnitude of tilt of the crustal block; in other words, the maximum gradient of the vertical movement measurable on this block, the azimuth of which is θ_m. The value of $\tan\varphi$ is obtained by dividing the differences in the vertical displacements of a pair of triangulation points by the distances separating them as measured on a topographical map on scale 1/50000. The angle θ, which is the azimuth of a line joining a pair of triangulation points, is also measured on the same map.

When relation (1) is satisfied by $\tan\varphi$'s and θ's, calculated from the vertical displacements of different pairs of selected triangulation points, the group of points from which the selection has been made is assumed to be situated on a single block. The magnitude and direction of the block-tilts are determined graphically from the graph, in which $\tan\varphi$ is taken as ordinates and θ as abscissae.

The modes of tilt of 73 blocks were thus determined. The number of triangulation points in these blocks is not all the same; some contain four points and others more than five, as shown in Table I. Those containing only three points are however comparatively few.

Table I

Number of crustal blocks with regard to different mumbers of triangulation points.

Number of Triangulation Points	3	4	5	6	7	8	9
〃 〃 Crustal Blocks	?	33	22	12	4	1	1

Of the values of $\tan\varphi$ and θ thus calculated, those for blocks containing more than five triangulation points are given in Tables II*a*, *b*, ...*q*, *r*, while the graphs used for determining the φ_m and θ_m of these block groups are shown in Figs. 2*a*, *b*, ...*q*, *r*.

Numerous difficulties confront us however when we try to determine the facts in regard to these crustal blocks. They are as follows:

a) The values derived as showing the actual vertical displacements of the triangulation points may contain errors of measurement, of say 1 cm. These errors may to some extent be responsible for the irregular variations in magnitude of the displacements that are superposed on the

Table II $a, b \ldots . p, q, r$.

The numerals in the first column and on the top of each column indicate the triangulation points. Of the two sets of numerals printed close together in the columns, the upper numerals represent the slope of the vertical displacements in 10^{-5} and the lower their directions, the azimuth being referred to N.

a Block 6

From / To	510	505	504	513	88
505	-5.18 1.3	—	....	....	....
504	-2.33 23.8	-6.28 315.0	—	....	....
513	2.62 222.7	-1.27 257.6	4.47 196 3	—	....
88	-1.40 266.9	1.00 236 7	2.91 220.0	-4.70 312.3	—
508	-4.40 302.2	3.04 211.8	1.26 236.8	-5.60 339.3	-5.20 9.5

b Block 7

From / To	551	552	553	554	548
552	-2.02 82.3	—	....	....	....
553	-4 45 107.0	-6.57 161.5	—	....	....
554	-4.56 158 1	-0.86 225.3	-2.59 255.0	—	....
548	2.47 250.2	2.26 255.6	3.68 269.4	4.35 279.8	—
549	4.66 288.5	3.32 274.4	4.52 287.3	5.12 308.8	2.01 17.2

c Block 13

From / To	643	639	67	646	644	641
639	-1·62 2·0	—	....	....	....	....
67	-3·56 40·6	-3·96 73·5	—	....	....	....
646	2·04 211·5	1·91 197·5	2·96 216·8	—	....	....
644	4·50 231·0	2·92 199·5	3·89 223·0	0·54 12·5	—	....
641	4·45 301·0	6·15 263·3	5·21 258·6	2·49 336·0	3·00 321·8	—
83	3·64 317·5	6·10 288·5	5·40 273.0	1·94 342·2	2·25 333·9	00·0 46·0

d Block 15

From / To	293	294	292	289	386	388
294	-12·30 2·6	—	....	....	....	....
292	-11·30 329·7	5·54 237·4	—	....	....	....
289	-4·20 288·7	10·82 207·5	13·20 180·0	—	....	....
386	4·36 240·6	10·80 201·3	11·99 182·1	10·23 184·3	—	....
388	6·19 225·3	9·60 206·0	10·33 196·3	8·50 204·5	7·21 214 8	—
Sengen Ym.	13·90 155·6	13·09 175·3	12·21 152·8	9·96 132 6	6·07 103·2	-1·29 65·8

Table II. (*continued.*)

e Block 20

From / To	360	365	363	362	361
365	-0·40 100·5	—	....	....	....
363	3·62 134·5	6·07 224·3	—	....	....
362	8·46 195·4	5·24 244·5	4·35 257·6	—	....
361	7·57 208·9	2·72 263·0	-0·24 288·2	8·83 5·3	—
359	2·61 252·7	1·58 266·0	-0·2 279·4	-4·11 298·3	0·00 270·4

f Block 30

From / To	278	206	207	55	279
206	1·62 33·8	—	....	....	....
207	3·80 66·2	4·64 90·4	—	....	....
55	5·00 78·1	5·19 134·0	-2·13 232·7	—	....
279	4·67 141·1	1·18 186·0	-2·36 228·5	-2·62 224·0	—
277	-5·71 266·2	-4·17 241·7	-4·50 254·2	-5·30 261·5	-5·95 285·7

g Block 33

From / To	520	519	49	204	211
519	2·42 29·7	—	....	....	....
49	5·76 43·5	-11·53 194·0	—	....	....
204	-14·60 98·3	-11·51 174·5	-10·31 158·0	—	....
211	-6·30 190·3	-4·24 200·6	-1·54 203·6	3·22 224·5	—
209	-15·87 166·5	-5·57 200·6	-1·53 205·7	7·90 251·0	1·56 20·9

h Block 36

From / To	271	290	291	282	276
290	3·12 238·5	—	....	....	....
291	1·2 241·3	-2·50 55·5	—	....	....
282	-9·50 298·8	-7·28 38·0	-11·40 20·1	—	....
276	-10·50 3·2·3	-10·42 6·0	-11·82 348·5	-10·59 332·0	—
295	-10·30 348·5	-7·15 32·6	-9·07 21·5	-6·81 22·8	8·80 119·1

i Block 41

From / To	239	240	24	266	Nagatuda	244
240	-4·90 33·0	—	....	....	....	....
24	1·66 98·8	4·92 159·4	—	....	....	....
266	1·09 247·3	2·87 228·5	0·00 262·2	—	....	....
Nagatuda	-3·29 289·9	0·00 257·3	-2·37 284·5	-5·92 332·9	—	....
244	-4·81 360·0	-2·75 313·3	-4·12 327·0	-3·80 24·7	-1·29 53·5	—
Simomizo	-1·68 288·0	-0·32 274·7	-1·41 285·5	-2·12 297·9	-0·54 287·5	0·28 267·4

Table II. (*continued.*)

j Block 42

To \ From	191	171	173	176	220
171	3·32 78·6	—	....	....	....
173	3·62 85·7	3·73 89·2	—	....	....
176	2·88 97·3	2·53 107·9	−4·78 236·0	—	....
220	−1·14 170·0	−2·66 201·7	−3·90 241·5	−3·53 243·1	—
172	2·62 55·2	1·90 40·8	−3·49 302·3	−1·00 334·0	2·38 29·6

k Block 43

To \ From	221	196	197	195	51
196	8·45 207·5	—	....	....	....
197	3·03 254·8	−2·46 291·6	—	....	....
195	1·04 275·3	−6·50 332·8	−4·90 51·2	—	....
51	−0·57 278·5	−4·20 303·4	−6.03 317·8	−1·70 281·1	—
198	−2·53 300·8	−5·22 312·3	−6·30 342·1	−4·33 315·4	5·26 ·95

l Block 44

To \ From	248	234	254	249	246	251	250	242
234	−2·78 19·8	—	....	....	....	....	....	....
254	−6·90 119·6	0·0 155·0	—	....	....	....	....	....
249	−2·21 136·0	1·54 173·5	4·58 275·3	—	....	....	....	....
246	−0·59 172·0	2·21 185·4	4·38 235·5	3·29 208·3	—	....	....	....
251	+2·34 192·3	2·58 196·8	3·68 258·4	3·20 246·7	0·00 315·0	—	....	....
250	4·27 230·2	3·67 215·9	3·80 268·5	3·64 265·7	2·05 300·7	3·64 289·8	—	....
242	3·15 265·0	3·50 230·8	2·71 285·0	2·16 288·6	0·44 317·5	0·66 319·2	−2·76 350·6	—
241	2·29 301·7	4·01 251·8	2·25 300·4	1·57 307·9	0·12 329·5	0·15 334·7	−1·75 356·5	−0·76 3·0

m Block 47

To \ From	187	188	182	186	50
188	3·13 161·9	—	....	....	....
182	2·32 191·9	1·06 218·0	—	....	....
186	0·68 224·0	−2·08 276·0	−3·21 355·2	—	....
50	−1·28 267·3	−2·16 286·9	−2·75 309·2	−2·18 294·7	—
179	−1·12 265·0	−1·97 283·2	2·57 303·1	−1·90 286·7	0·0 248·9

n Block 56

To \ From	753	761	77	760	76
761	2·78 162·0	—	....	....	....
77	5·32 206·0	4·34 260·7	—	....	....
760	5·42 236·3	1·63 295·3	−2·86 343·8	—	....
76	2·86 296·5	0·53 315·7	−1·38 337·6	−0·58 334·9	—
778	2·28 300·7	1·13 328·5	−3·92 4·6	−4·46 21·1	−3·22 114·7

Table II. (*continued.*)

o Block 62

Triangulation Point / Triangulation Point	394	399	68	395	405	402
399	0·90 135·9	—	....	....	....	....
68	−11·16 166·8	−14·98 277·7	—	....	....	....
395	−11·92 227·2	−5·42 293·1	4·06 307·5	—	....	....
405	7·95 175·5	−13·55 224·3	−4·55 183·0	−4·90 158·0	—	....
402	−8·90 180·5	−13·20 243·0	−4·70 199·8	−5·38 159·2	3·38 333·5	—
404	−12·23 201·0	−13·31 245·8	−10·20 225·8	−14·27 189·9	−9·85 277.2	−13·43 250·4

p Block 63

From / To	591	607	297	300	56
607	5·45 8·5	—	....	....	....
297	−5·52 72·5	−11·14 135·0	—	....	....
300	−8·94 120·5	−9·36 145·5	−7·70 154·5	—	....
56	−3·64 185·8	−4·91 187·0	0·71 216·5	6·87 261·1	—
599	−3·23 199·2	4·43 195·0	0·00 218·6	4·59 251·3	−2·00 224·5

q Block 64

From / To	305	304	308	310	60	322
304	2·95 59·5	—	....	....	....	....
308	13·73 165·4	6·59 203·1	—	....	....	....
310	12·93 177·5	8·78 197·5	11·80 188·2	—	....	....
60	7·10 195·1	9·00 211·0	−0·71 222·4	−21·65 298·7	—	....
322	1·31 221·0	0·34 225·5	−2·99 236·5	−8·96 256·2	−4·11 244·2	—
303	6·01 208·5	3·66 216·5	1·26 226·4	−7·53 256·0	3·07 231·8	−11·27 256·7

Table II. (*continued.*)

r Block 65

To \ From	311	309	312	301	302
309	-10·12 5·8	—	....	....	....
312	20·50 123·2	15·10 168·3	—	....	....
301	-10·20 264·5	-1·73 231·3	-14·59 274·5	—	....
302	-17·24 281·0	-0·78 219·7	-18·77 290·3	3·11 69·3	—
316	5·02 204·2	7·17 197·5	-0·89 204·8	14·80 151·2	12·55 180·8

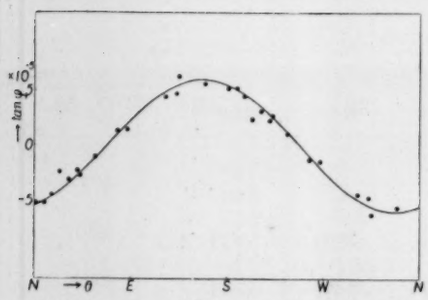

Fig. 2*a*. $\varphi-\theta$ diagram for block 6.

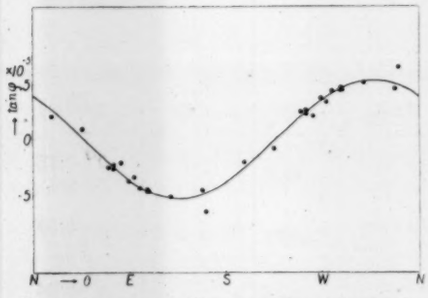

Fig. 2*b*. $\varphi-\theta$ diagram for block 7.

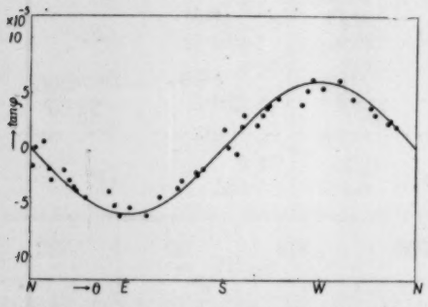

Fig. 2*c*. $\varphi-\theta$ diagram for block 13.

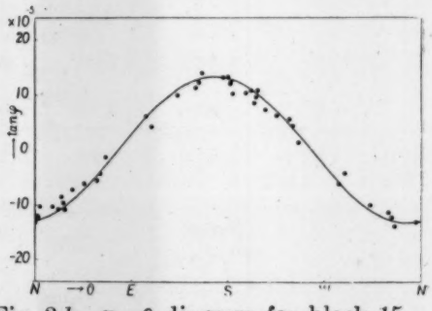

Fig. 2*d*. $\varphi-\theta$ diagram for block 15.

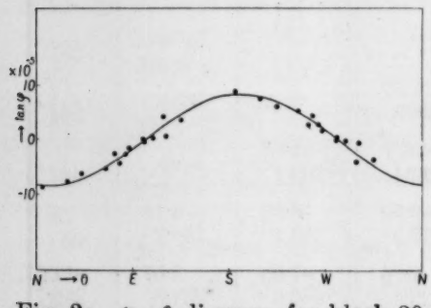

Fig. 2*e*. $\varphi-\theta$ diagram for block 20.

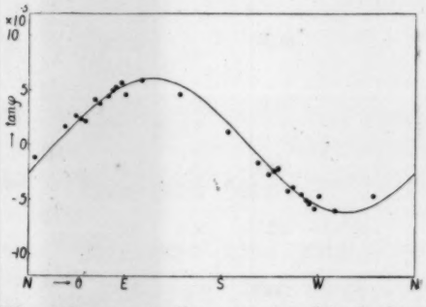

Fig. 2*f*. $\varphi-\theta$ diagram for block 30.

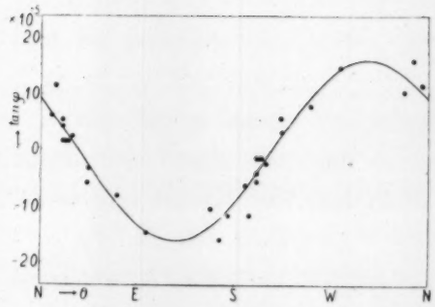

Fig. 2*j*. $\varphi-\theta$ diagram for block 33.

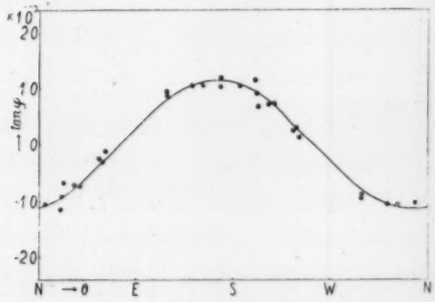

Fig. 2*h*. $\varphi-\theta$ diagram for block 36.

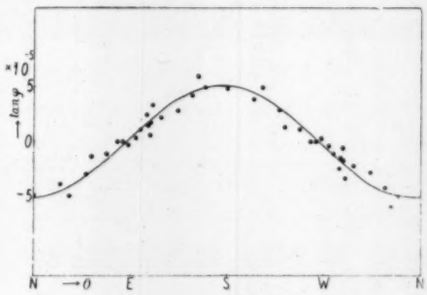

Fig. 2*i*. $\varphi-\theta$ diagram for block 41.

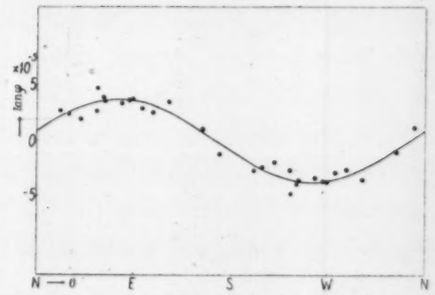

Fig. 2*j*. $\varphi-\theta$ diagram for block 42.

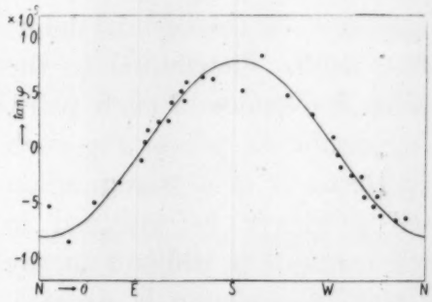

Fig. 2*k*. $\varphi-\theta$ diagram for block 43.

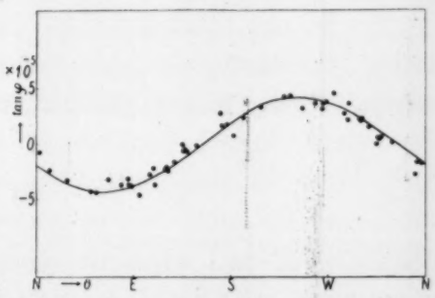

Fig. 2*l*. $\varphi-\theta$ diagram for block 44.

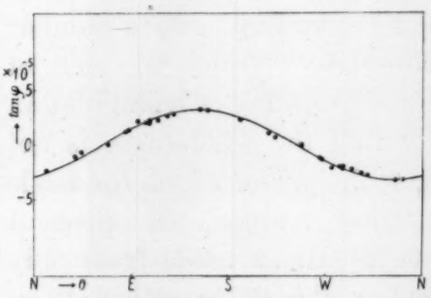

Fig. 2*m*. $\varphi-\theta$ diagram for block 47.

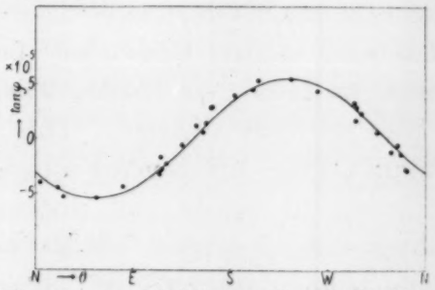

Fig. 2*n*. $\varphi-\theta$ diagram for block 56.

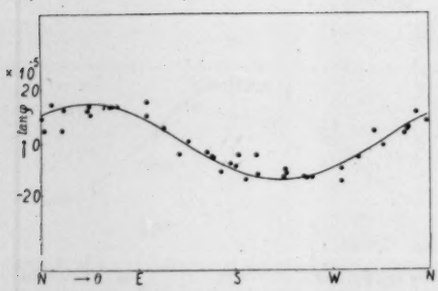

Fig. 2*o*. $\varphi-\theta$ diagram for block 62.

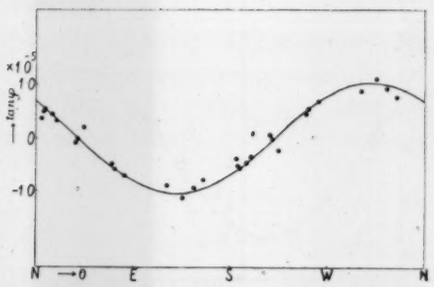

Fig. 2*p*. $\varphi-\theta$ diagram for block 63.

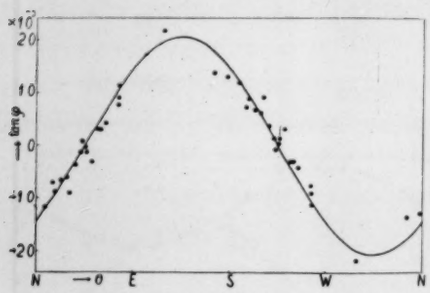

Fig. 2*q*. $\varphi-\theta$ diagram for block 64.

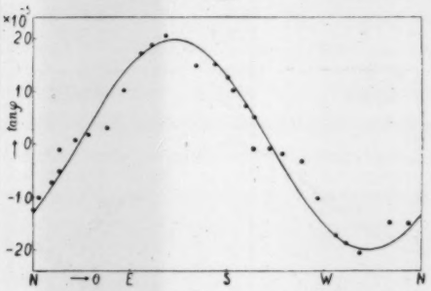

Fig. 2*r*. $\varphi-\theta$ diagram for block 65.

sinusoidal curve representing relation (1); particularly when the actual vertical displacements are small, the fluctuation becomes larger, so that the sinusoidal curve representing relation (1) cannot be clearly determined.

b) In calculating $\tan\varphi$, that is, the gradient of the vertical deformation for different pairs of triangulation points distributed in the district, there is no general rule governing the choice of such pairs. We usually take a number of contiguous triangulation points for such pairs. But as frequently happens, the displacement of a triangulation point may be such that it could with equal propriety be assigned to either one of two adjacent blocks. In such cases, it is difficult to say on which particular block the triangulation point in question is situated.

c) Three points (not lying on a straight line) are necessary and sufficient for determining a plane. Hence, in the present case, by dividing the whole area of the district under consideration into a number of blocks, so that there shall be three triangulation points in each of them, we have $N/3$ blocks, where N is the total number of triangulation points in that district. This way of dividing the whole area is not unique; there are several alternative ways, with each of which the mode of block-tilt comes out differently. For these reasons, all apparent movements of crustal blocks based on determinations made from only three triangulation points have been ignored in this study, although on

occasions when there are no more than three points available, it may not be possible to ignore them. These doubtful blocks are shown in Fig. 3 by the hatched areas: their tilts however are not shown.

d) Even when there are more than four triangulation points, the mode of block-tilt should not be determined if some of them are arranged nearly colinearly.

e) If the surface of the earth's crust is deformed into a curved surface of small curvature, a part of such surface may usually be taken as a block and the present method applied to that part. In that case, however, especially when the triangulation points are widely dispersed, it is not easy to decide whether the triangulation points are situated on an approximate plane or on a sensibly curved surface. Should contiguous blocks happen to be tilted in opposite sense, with nearly equal mean vertical displacements, it is difficult to decide whether these blocks are really separate blocks with a discontinuity between them or whether they are different parts of a smoothly curved surface.

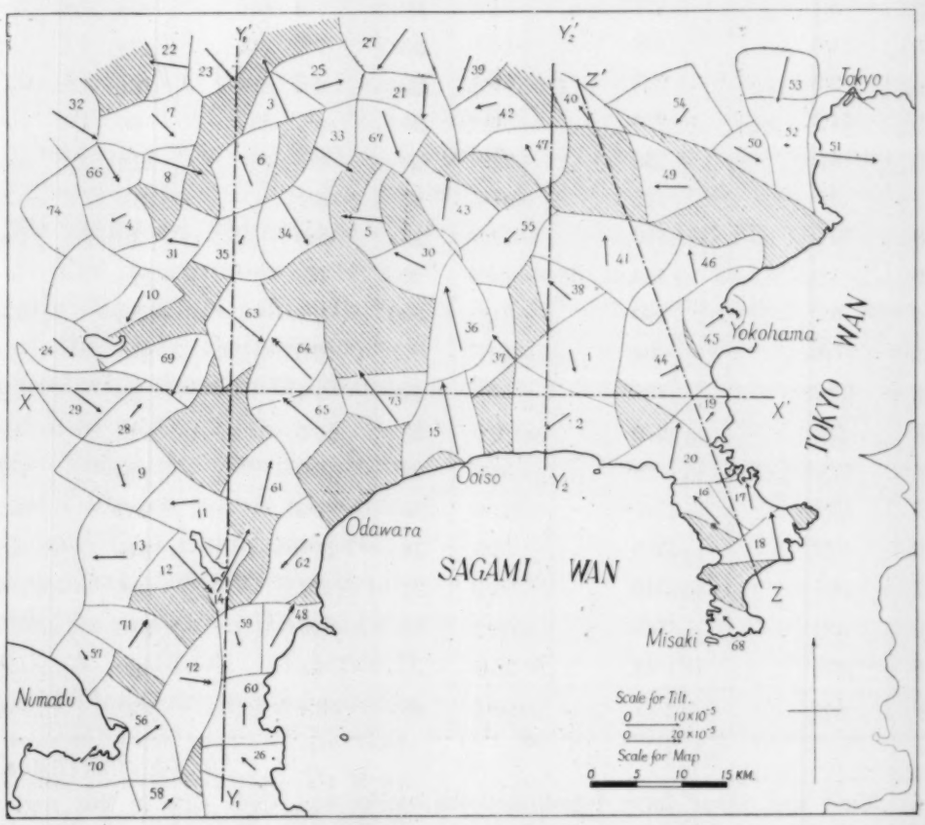

Fig. 3. Crustal blocks and their tilts.

Block Movement.

The crustal blocks and their modes of tilt[4] obtained as results of the present analysis of vertical displacements of triangulation points, are shown in Fig. 3, in which the magnitudes of tilt and their directions are represented by the length and the direction of the arrows. The numerals in Fig. 3 correspond to the numbers of the blocks in Table III, in which are given the numerical values of φ_m and θ_m, together with the mean vertical displacements of the constituent blocks, $\overline{\Delta H}$.

Table III.

Magnitudes and directions of tilts and mean vertical displacements of blocks.

Block	φ_m, Magnitude of Tilt.	ϵ_m, Azimuth of Tilt. referred to N	$\overline{\Delta H}$	Block	φ_m, Magnitude of Tilt.	θ_m, Azimuth of Tilt referred to N	$\overline{\Delta H}$
			cm				cm
1	4.3×10^{-5}	167°	35.0	21	6.3×10^{-5}	184°	−20.2
2	5.1	237	64.0	22	7.0	278	−27.4
3	11.5	336	−44.8	23	7.4	139	−11.0
4	2.9	243	−39.8	24	4.8	131	− 2.0
5	14.2	279	−80.0	25	5.1	75	−20.2
6	6.0	338	−29.5	26	3.1	312	− 9.5
7	5.5	137	−27.7	27	8.7	216	−22.2
8	10.1	109	−52.0	28	3.0	40	−22.6
9	4.2	163	−14.8	29	6.9	128	− 7.4
10	6.2	209	−31.0	30	6.1	295	−49.8
11	5.0	264	−16.0	31	5.5	280	−53.8
12	22.8	137.5	−17.8	32	9.4	122	−17.8
13	0.6	270	0.0	33	16.0	125	−53.8
14	12.5	29.2	52.0	34	9.8	150	−67.2
15	13.3	347.5	127.6	35	1.8	205	−41.6
16	6.8	315	75.5	36	11.4	345	−15.7
17	4.1	348	92.0	37	5.7	316	−20.3
18	8.4	349	106.2	38	5.0	310	0.5
19	2.1	42	28.8	39	6.8	200	−31.5
20	8.4	11	65.4	40	3.1	327	−24.0

(to be continued.)

4) Mutô and Atumi have determined the blocks and their tilts in this region by a different method with practically the same results. See *Bull. Earthq. Res. Inst.*, **7** (1929), 489.

Table III. (*continued.*)

Block	φ_m, Magnitude of Tilt	θ_m, Azimuth of Tilt referred to *N.*	$\overline{\Delta H}$	Block	φ_m, Magnitude Tilt.	θ_m, Azimuth of Tilt referred to *N.*	$\overline{\Delta H}$
			cm				cm
41	$5{\cdot}1\times10^{-5}$	335°	−10.0	58	$2{\cdot}5\times10^{-5}$	45°	−23.5
42	3·7	256	−36·8	59	2·0	165	− 5·0
43	8·0	6	− 56·8	60	4·0	0	1·0
44	4·2	62	20·7	61	16·2	12	7·4
45	$4{\cdot}0_5$	55	12·8	62	14·4	222	17·1
46	5·8	346	+ 0.6	63	10·4	130	−77.5
47	3·2	334	−26·2	64	20·6	315	−67·9
48	16·8	30	− 9·8	65	19·9	310	− 8·7
49	6·0	270	−19·0	66	14·6	150	−34·2
50	5·6	120	−11·5	67	17·0	161	−60·0
51	11·0	97	−21·4	68	2·8	315	115·5
52	$0{\cdot}9_6$	271	−10.5	69	10·8	205	−57·0
53	8·5	194	−16·5	70	4·1	45	0·2
54	3·2	217	−18·5	71	11·4	35	−27·0
55	2·7	225	−36·2	72	11·4	100	−20·8
56	5·5	55	−17·3	73	11·2	323	48·5
57	2·2	145	− 7·6				

We notice in Fig. 3 that

i) The magnitudes of tilt are generally larger in the district west of the river Sagamigawa as compared with those in the district east of that river.

ii) There are several groups of crustal blocks, whose directions of tilt, and to a much less extent, the magnitudes of tilt, practically coincide, as shown in Table IV.

iii) A number of special groups of blocks are located zonally in the northwest part of the district under consideration. In these groups the azimuths of the directions of tilt are almost alike and

Table IV.

Groups of blocks in which the directions of tilts are approximately the same.

Block.	Azimuth of Tilt.	Magnitude of Tilt.
41	355°	$5{\cdot}1\times10^{-5}$
46	346	5·8 〃
16	315	6·8 〃
17	348	4·1 〃
37	316	5·7 〃
38	310	5·0 〃
44	62	4·2 〃
45	55	$4{\cdot}0_5$ 〃
64	315	20·6 〃
65	310	19·9 〃
15	348	13·3 〃
36	345	11·4 〃
73	323	11·2 〃

are directed nearly in opposite sense to those of adjoining groups. These block groups are shown in Table V.

Table V.

Zonal groups of crustal blocks.

Group.	I		II		III		IV	
	Block. Nos.	Azi-muth* of Tilt.	Block Nos.	Azi-muth of Tilt	Block Nos.	Azi-muth of Tilt	Block Nos.	Azi-muth of Tilt.
	5	279	67	161	3	336	23	139
	15	347.5	33	125	6	338	7	137
	30	295	34	150	31	280	8	109
	36	345	63	130			32	122
	64	315					66	150
	65	310						
	73	323						

As may be seen in the above table, the azimuths of the blcko tilt in zones I and III fall in the fourth quadrant, while those in zones II and IV fall in the second. It may also be noticed that block 35, situated between zone II and III, is tilted toward the SW, in direction nearly perpendicular to the direction of tilt of the blocks belonging to zones II and III.

iv) There are several regions where the number of triangulation points is only three or even less. These are shown by the hatched areas in Fig. 3. These regions are frequently found tobe places where the earth's crust had been much disturbed, that is, regions where the value of D is great, D being the quantity that was introduced in the previous paper[5] to represent the degree of disturbance of the earth's crust. These regions are also found to be places where the tectonic lines or faults are more densely distributed. It may however be remarked that areas in which there are less than three triangulation points may possibly consist of blocks that cannot be determined owing to scantiness of points, as for example in the region near Ooyama, north of Ooiso.

v) In the Miura p.eninsula, the blocks and their tilts approximately

* Azimuths of tiltings are referred to N.

5) N. MIYABE, *Bull. Earthq. Res. Inst.*, 9 (1931), 1.

agree with those determined[6] previously from data covering the vertical displacements of bench-marks on the levelling route between Aburatubo and Hudisawa.

The way in which block 74 has tilted deserves notice. It is not shown in Fig. 3. Five triangulation points are situated in this block, one at the centre surrounded by the remaining four, as shown in Fig. 4. Disregarding the vertical displacement data relating to the central triangulation point, the tilt of the block has been determined from data of the four other points, as will be seen from the sine curve of Fig. 5. The vertical displacement of the central point however is too large in amount to agree with the general tilt of the block thus determined. There may be, at least, three ways of interpreting this phenomenon. In the first place, if the vertical displacement of the central point is regarded as due mainly to actual crustal deformation, the earth's crust in this region may be considered to have been deformed into a curved surface, convex upward. Secondly, the vertical displacement of the central point being assumed as above, the crust in this region may be supposed to consist of several minor blocks,[7] the tilts of which are outward from the central point. Thirdly, if the greater part of the amount vertically displaced by the central point be regarded as due to some special local disturbance, just where the central point is situated, the actual amount of vertical displacement of the central point should be reduced so that it shall lie on the same crustal block as that determined by data relating to the four other points. We see however no particular reason why the central point alone should be so greatly disturbed. In order to be able to determine the approximate sizes of the component crustal blocks and the mode of deformation of the earth's crust in the region under consideration, some crucial phenomena should be searched for elsewhere.

The geographical distribution of the mean vertical displacements,

---

6) The blocks in the Miura peninsula were determined by Prof. M. Ishimoto and Mr. R. Takahasi. The result is published in the supplementary volume of Iwanami's "Tisitugaku-Tirigaku-Kôza," (in Japanese).

M. Ishimoto, "Crustal deformations associated with Destructive Earthquakes," Tokyo, 1931, (in Japanese)

7) The term "minor block" or "secondary block" is used for blocks that make up the "primary block," determined in the present investigation from data of the vertical displacements of triangulation points. Several other cases in which the "primary blocks" are considered to consist of several "secondary blocks" will be given later.

Fig. 4. Triangulation points in block 74. The numerical figures in brackets indicate the amounts of vertical displacements in cm.

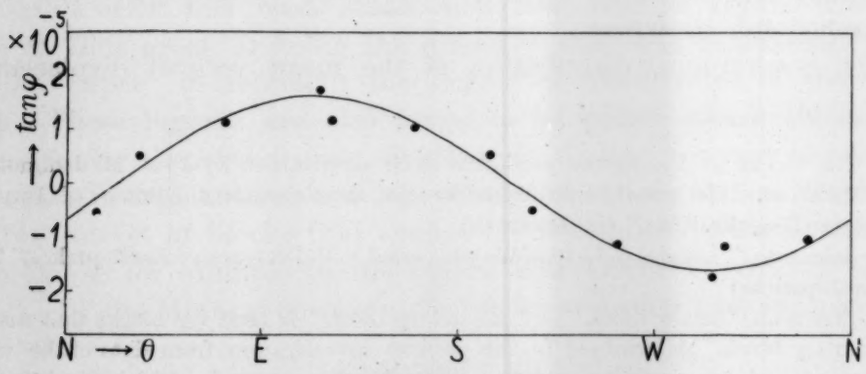

Fig. 5. $\theta-\varphi$ diagram for Block 74.
($\varphi_m = 1.6\times10^{-5}$ $\theta_m = 295°$)

$\overline{\Delta H}$, of the constituent crustal blocks in the Kwantô District is shown in Fig. 6. The mode of deformation of the earth's crust as represented by the mean vertical displacements of these blocks may be regarded as deformations of the earth's crust after the components due to tilt of the constituent crustal blocks have been entirely smoothed out. The following points may be noticed in connection with movements of crustal blocks :

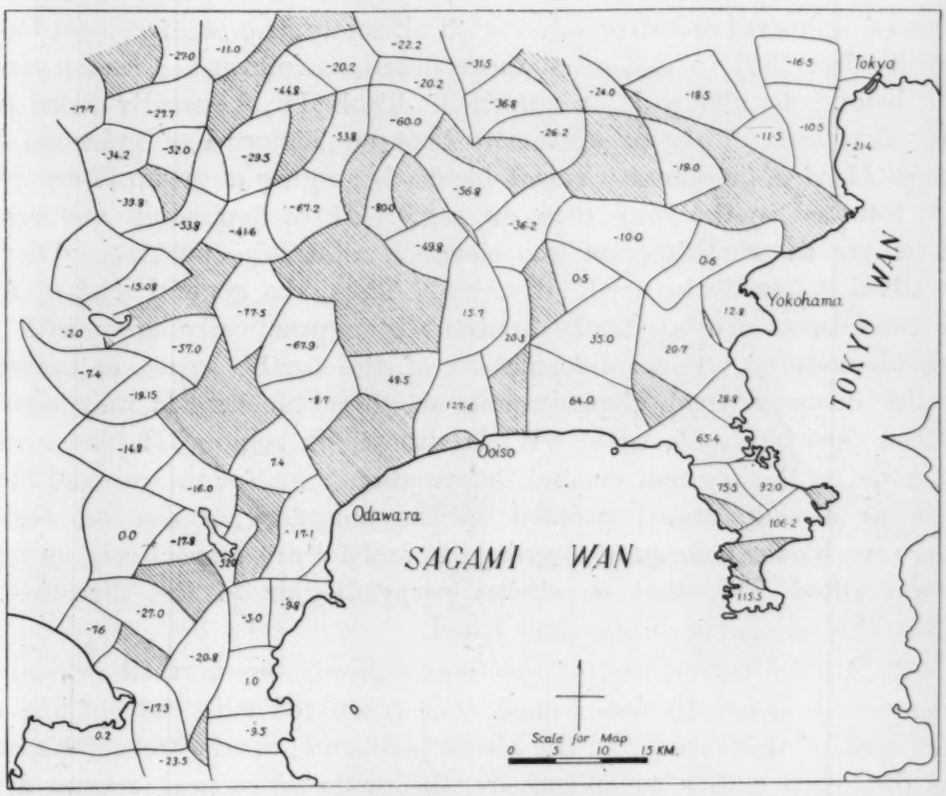

Fig. 6. Distribution of $\overline{\Delta H}$ in cm.

a) Vertical crustal deformation is more conspicuous in the district west of the Sagamigawa than in that east of this river. In the former district, as already mentioned, the amount of tilt of the constituent blocks is also comparatively larger. In the neighbourhood of Ooiso, the earth's crust was conspicuously elevated, while north-west of this elevated region and adjoining it, it was greatly depressed. The difference in the vertical dislocations between these two regions amounted to nearly 2 metres. Moreover, adjoining the greatly depressed region on

its northwest, there is a zonal region where the earth's crust was elevated relative to the adjacent regions. Adjoining this elevated zone is another zone of depression, although the amount of depression is smaller than that in the zones mentioned above. This alternation of zones of upheaval and depression seems to correspond to the zone groups of the crustal blocks, in which blocks belonging to the same group are tilted in the same sense, whereas those belonging to the adjoining group are tilted in reversed sense. The correspondence of zones of upheaval and depression with alternate groups of crustal blocks may be described in somewhat more detail as follows: Crustal blocks that belong to group I, as shown in Table IV, generally titled in a NW direction. They are situated between region I of upheaval and region II of depression. Crustal blocks belonging to group II are generally situated in the zone between region II of depression and region III, where the earth's crust was elevated, relatively speaking. They of are tilted generally in a SE direction. Thus, the general modes of tilt the constituent crustal blocks in this region practically agree with the general mode of vertical deformation of the earth's crust, as indicated by the mean vertical displacements of these blocks. It may also be noticed that block 35, tilted SW, is situated in region III, the anticlinal zone in the vertical crustal deformation. As for this crustal block, it is as already stated situated on the boundary of the two regions where the blocks belonging to groups II and IV are respectively situated. It was tilted SW, that is, almost perpendicular to the direction in which the adjoining blocks had tilted.

b) In the region east of the Sagamigawa, the vertical crustal deformation is generally less conspicuous compared with that of the district west of this river. In the Miura peninsula, where the earth's crust was disturbed rather conspicuously, the mode of vertical crustal deformation is generally a northward tilt, which is in good accord with the tilts of the constituent crustal blocks of this region.

Geological Significances.

The geological structure of the district under consideration were investigated by Prof. H. Yabe and others of the Geological Institute of Tôhoku Imperial University. The trend of the tectonic lines and faults in the geological map[8] of the district is reproduced in Fig. 7. Upon

8) Geological map compiled by S. Shimidzu, Tôhoku Imperial University.

comparing this figure with Fig. 3, which shows the crustal blocks, we notice that in a number of regions, the directions of the boundary lines of the blocks as determined by the present analysis coincide fairly well with the trend of the tectonic lines as traced by the geologists, particularly in the following cases:

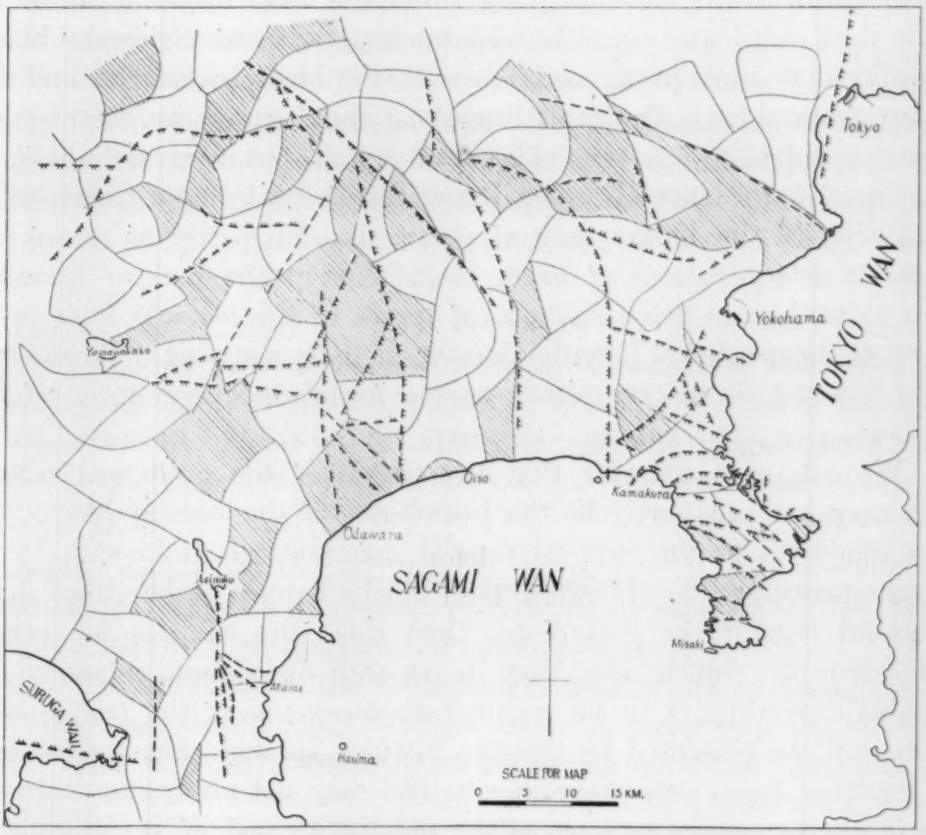

Fig. 7. The blacks and geological faults.

i) The southern boundaries of blocks 50 and 52 coincide with the trend of the tectonic line along the Tamagawa.

ii) The western boundary or block 37 and the eastern boundary of block 2 coincide fairly well with the trend of the tectonic line along the Sagamigawa.

iii) The boundary between blocks 1 and 44 coincide with the tectonic line that extends northward from Hudisawa.

iv) The eastern boundary of block 72 coincides fairly well with the Tanna Fault, a significant feature of the crustal deformation of this

region in connection with the North Idu Earthquake of 1930[9].

v) The western boundary of block 15 nearly coincides with the northward trend of the fault line that forms the western boundary of the Yurugi block[10], and which was traced geologically.

vi) The boundaries of several blocks in the Miura peninsula nearly coincide with the tectonic lines there.

In contrast to the foregoing there are many tectonic lines and faults that in no way coincide with the boundaries of the crustal blocks. Some tectonic lines partly coincide with the block boundaries and then deviate from them. The fault line along the Sagamigawa, for example, coincides with the boundaries of blocks 2 and 37, but it traverses block 35.

These discordances between the trend of the tectonic lines and the boundaries of the blocks may of course be due partly to errors incidental to determinations of block boundaries in the present investigations as well as to determinations of trends of the tectonic lines in the course of the geological investigations or in their mapping. These errors alone however do not completely answer for all the discordances referred to above.

We can next consider that the trends of the geological tectonic lines may not necessarily be the boundaries of the crustal blocks that were subjected to the vertical crustal deformations dealt with in the present investigation. If two crustal blocks happen to be either firmly cemented together or juxtaposed, then since the chances for vertical dislocation are much less than horizontal dislocation, scarcely any sensible discontinuity in the vertical displacements of the triangulation points will be presented by the two blocks. In that case, the trends of the tectonic lines, even were they active, may not always coincide with the block boundaries as long as the present method of investigation is used.

The fact that tectonic lines (geologically determined) may frequently appear to be boundaries of crustal blocks, the principal dislocations of which are horizontal, may justify importance being placed on the investigat-ion of the horizontal above other kinds of deformation of the earth's crust.

---

9) *c.f.*, C. TSUBOI, *Bull. Earthq. Res. Inst.*, **10** (1932), 435.

10) *c.f.*, N. YAMASAKI, *Bull. Imp. Earthq. Invest. Comm.*, No. **100** B (1925), (in Japanese).

Y. ÔTUKA, *Tirigaku-Hyôron*, **6** (1930), (in Japanese).

Horizontal Displacements.

In the district under consideration, the horizontal displacements of the secondary and tertiary triangulation points were also determined from retriangulations made in 1925. As with vertical displacements, the horizontal displacements may also be considered to have two components, one due to chronic and the other to acute crustal movements, neither of which can scarcely be separated from the other.

As has already been pointed out, it is difficult to determine the sizes of the component blocks[11] when the horizontal displacements of the triangulation points constitute the sole datum, although, as Dr. C. Tsuboi has shown[12], sometimes block movements are also conspicuous in the case of horizontal crustal deformations, as in the Tango peninsula.

Indeed in a number of blocks determined in the present investigation by means of vertical displacements, the azimuths of horizontal displacements of the triangulation points on one and the same block are all approximately equal. The azimuths and the magnitudes of the horizontal displacements of the triangulation points on these blocks are given in Table VI.

Before discussing the significance of horizontal displacements of triangulation points in connection with block movements of the earth's crust, the following points should be borne in mind.

a) The azimuths of the horizontal displacements of triangulation points may vary considerably through errors in measuring the displacements. The azimuth θ (referred to N) of the horizontal displacement is calculated by

$$\tan\theta=\frac{u}{v},$$

where v is the northward and u the eastward component of the herizontal displacement. The range of variation of azimuth θ, due to errors of measurement, du and dv, is consequently given by

$$\frac{2d\theta}{\sin 2\theta}=\left(\frac{du}{u}-\frac{dv}{v}\right).$$

---

11) N. Miyabe, *Bull. Earthq. Res. Inst.*, 9 (1931), 1.

12) C. Tsuboi, *Bull. Earthq. Res. Inst.*, 8 (1930), 153.

Table VI.

Blocks in which directions and magnitudes of horizontal displacements of triangulation points are approximately equal.

Block.	Triangulation Point	Horizontal Displacement	Azimuth of Displacement referred to N.
		cm	
17	367	318·1	153°
	380	302·9	151
	370	314·6	154
	371	316·4	155
23	493	94·8	144
	533	106·7	144
	494	85·9	142
	540	88·1	147
20	360	281·5	147
	365	290·0	152
	363	294·8	150
	362	313·2	150
	361	306·5	150
	359	288·2	150
	366	300·4	152
	247	277·5	149
44	248	205·2	150
	234	184·8	152
	254	225·0	151
	249	233·2	152
	246	243·4	151
	251	234·1	150
	250	221·0	150
	242	215·7	149
	241	202·5	148

As the maximum value of $\sin 2\theta$ is 1, by taking 1/10 for $(du/u - dv/v)$, we have for the maximum range of variation

$$d\theta = \frac{1}{20} \fallingdotseq 3°$$

This estimated range of 3° for the variation may be large enough for the upper limit of error. The actual error $(du/u-dv/v)$ may be expected to be 1/100, at most. This estimated variation range of 3° is actually exceeded in most cases. The fluctuation may be due in part to a rotational movement of the crustal block about a vertical axis.

b) Thus, the rotational movements of a crustal block about a vertical axis may produce variation in both azimuth and magnitude of the horizontal displacements of the triangulation points, even though the displacements may be on one and the same block. But, if such movement of crustal blocks really exist, then the distribution of variation in azimuth and magnitude of the horizontal displacements should be systematic, such that they could be expressed in simple form. Assuming that the angular displacements of a block about a vertical axis is γ and that the coordinates of a triangulation point situated on this block are x and y, as referred to the axis of rotation, then the $x-$ and $y-$components of the horizontal displacement of the triangulation point, u and v, due to the rotational movement, may be expressed in the form

$$u=-\gamma y,$$
$$v=\gamma x,$$

whence we have for the azimuth of the horizontal displacement,

$$\tan\theta=\frac{u}{v}=-\frac{y}{x}.$$

In most cases, however, the position of the axis of rotation is not known. We therefore take one of the triangulation points on the same crustal block as a reference point, whose coordinates referred to the axis of rotation and the components of the horizontal displacement are x_0, y_0, u_0, and v_0, respectively. We then have

$$u_0=-\gamma y_0,$$
$$v_0=\gamma x_0,$$

from which the relation between the coordinates and the horizontal displacements is obtained in the form

$$\frac{u-u_0}{v-v_0}=-\frac{y-y_0}{x-x_0}, \qquad (2)$$

where $(x-x_0)$ and $(y-y_0)$ are the coordinates of any triangulation point

as referred to the reference point above defined. They can easily be measured on the topographical map.

The general tendency represented by relation (2) is actually witnessed in several cases. Examples are the groups of triangulation points on blocks 43 and 48, as shown in Figs. 8*a* and 8*b*, in which $(u-u_0)/(v-v_0)$ is taken as the ordinate and z or $(y-y_0)/(x-x_0)$ as the abscissa.

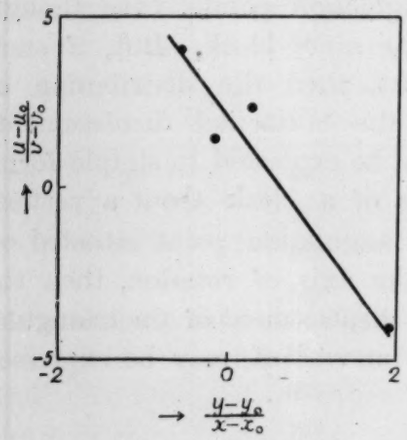

Fig. 8*a*. Relation (3) for block 43.

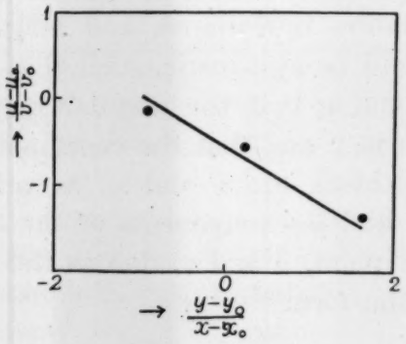

Fig. 8*b*. Relation (3) for block 48.

Moreover, in actual cases we must take into account the effect of areal divergence. The expression for u and v may be modified by adding the terms αx to u und βy to v, where α and β are elongations in the direction of the $x-$ and the $y-$axis. We have therefore instead of relation (2), the relation

$$\frac{u-u_0}{v-v_0}=-\frac{\gamma(y-y_0)-\alpha(x-x_0)}{\gamma(x-x_0)+\beta(y-y_0)}=-\frac{z-\kappa}{1+\kappa' z}, \qquad (3)$$

where $z=(y-y_0)/(x-x_0)$, $\kappa=\alpha/\gamma$ and $\kappa'=\beta/\gamma$. Relation (3) can be transformed, when $\kappa' z$ is smaller than unity, into the form

$$\frac{u-u_0}{v-v_0}=-(z-\kappa)(1-\kappa' z+\kappa'^2 z^2-\ldots.)$$

$$\fallingdotseq \kappa-(1+\kappa\kappa')z+(1+\kappa\kappa')\kappa' z^2. \qquad (3)'$$

The general tendency represented by relation (3′) with respect to the groups of triangulation points on blocks 26 and 63, is shown in Figs. 9*a* and 9*b*, respectively.

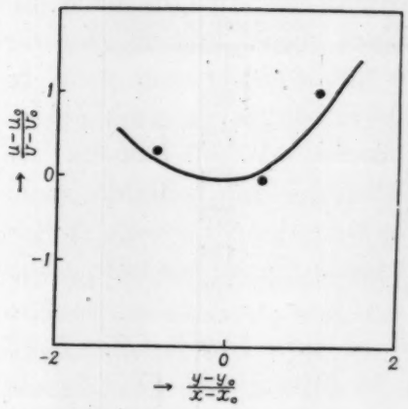

Fig. 9*a*. Relation (3′) for block 26.

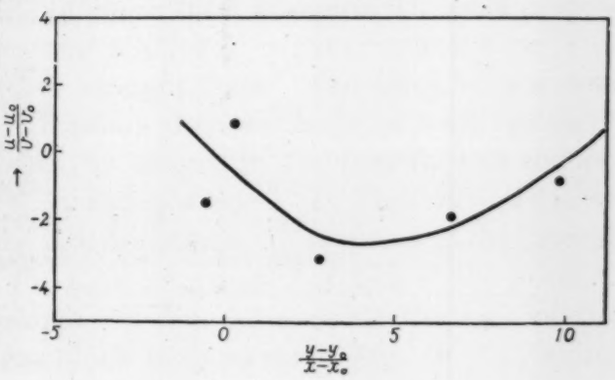

Fig. 9*b*. Relation (3′) for block 63.

At the same time it is well to note also the following facts regarding the horizontal displacements of triangulation points:

i) For several of the blocks, the triangulation points on them have been classified into two or three groups, according to the azimuth of their horizontal displacements. For each of these groups, the azimuths are approximately the same, as shown in Table VII.

Table VII.

Blocks in which the triangulation points are classified into two or more groups according to their horizontal displacements.

Block.	Triangulation Point.	Horizontal Displacements	Azimuth of horizontal displacement.
		cm	
9	631	149·0	91°
	626	149·0	90
	81	77·0	107
	627	83·6	105
	636	109·1	123
39	499	123·4	182
	48	117·2	182
	205	140·1	161
	500	110·6	161

Block.	Triangulation Eoint	Horizontal Displaceements	Azimuth of horizontal displacement.
47	187	146·1	172
	188	140·1	172
	50	133·0	172
	179	142·9	173
	182	143·1	194
	186	146·8	165
49	21	143·6	172
	165	143·1	166
	164	140·1	165
	23	132·2	178
	163	132·5	178

This fact may partly be due to rotational movement of the blocks combined with the particular configuration of the triangulation points and partly to horizontal deformation of the earth's crust within the blocks. But, considering that there are instances in which the surface area of the crustal block is quite large, we may suggest the existence of secondary crustal blocks, whose relative movements in horizontal direction are matters of observation. The groups of triangulation points within the blocks as determined by vertical displacement data, as and shown in Table VII, may thus be significant features pointing to the existence of secondary blocks. The crustal blocks that have been determined by vertical displacement data will hereinafter be called "primary blocks."[13] The assumption of secondary crustal blocks is convenient in our present investigation for elucidating the discordance observed between the boundaries of the primary crustal blocks and the trends of the tectonic lines, referred to in the preceding pages.

ii) Even when the azimuths of the horizontal displacements are nearly equal, their magnitudes in the same block vary in excess of the limits of errors of measurement. This, together with the cases of azimuth-variation referred to above, may justify the suggestion made regarding the probable existence of considerable horizontal deformation in the primary blocks.

iii) By disregarding fluctuations in the azimuth and magnitude of

13) The surface area of the crustal blocks will be discussed later.

the horizontal displacements, the mean horizontal displacements of the primary crustal blocks may be obtained. In Figs. 10 to 13, the profiles of block movements along sections XX', Y_1Y', Y_2Y_2', and ZZ' in Fig. 3 are shown by segments of thin straight lines. The block movements are affected by the mean horizontal displacements of each primary block obtained above (represented by arrows in the figure), and the result is shown by segments of thick straight lines. In Figs. 10 and 11, we notice that the trough along the Sakawagawa is conspicuous in the present crustal deformation, and that the E-W components of tilts of the primary blocks distributed near the trough are directed towards the axis of the trough. In the profile of the block movement in Fig. 10, i.e., along the section in E-W direction, the relative, or differential, horizontal displacements between the crustal blocks are not so marked as those in the N-S direction. Fig. 11 and Fig. 12 show profiles of block movements in N-S direction, while Fig. 13 shows those in NW-SE direction. In the profile of Fig. 11, along the section Y_1Y_1', that is, profile of block movements in the district west of the Sagamigawa, we notice that the azimuths of the block tilts differ considerably with different blocks, and that the amounts of tilt are more or less greater than those shown in Fig. 12, that is the profile of section Y_2Y_2' in the district lying east of the Sagamigawa. It will also be noticed that in the latter profile, the blocks in the district under consideration are tilted on the whole towards the north, all of which are in good accord with the direction of the general tilting of the earth's crust in that district. This tendency of block movements and general crustal deformations is seen to agree in direction more conspicuously in the Miura peninsula, the profile of

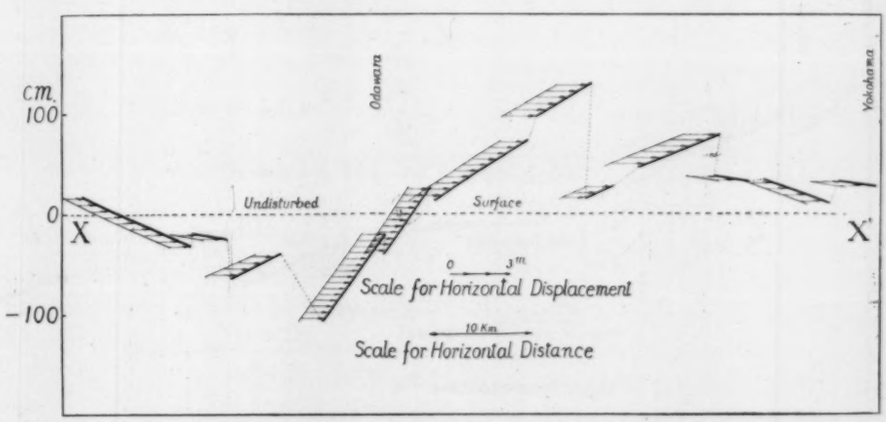

Fig. 10. Profile of the block movements along section XX' in Fig. 3.

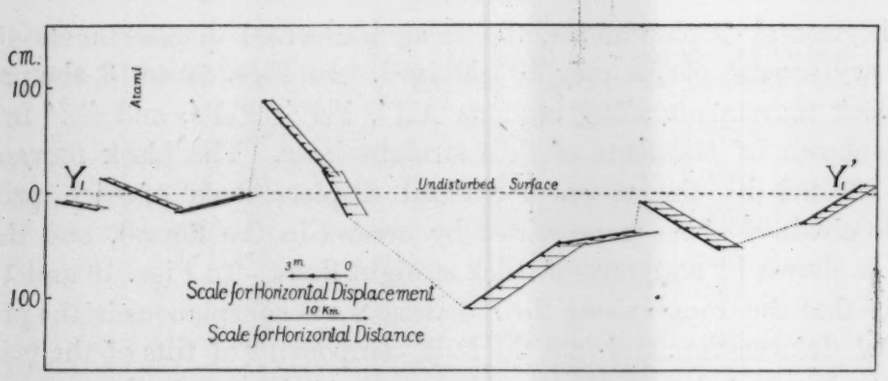

Fig. 11. Profile of the block movements along the section *Y.Y.'* in Fig. 3.

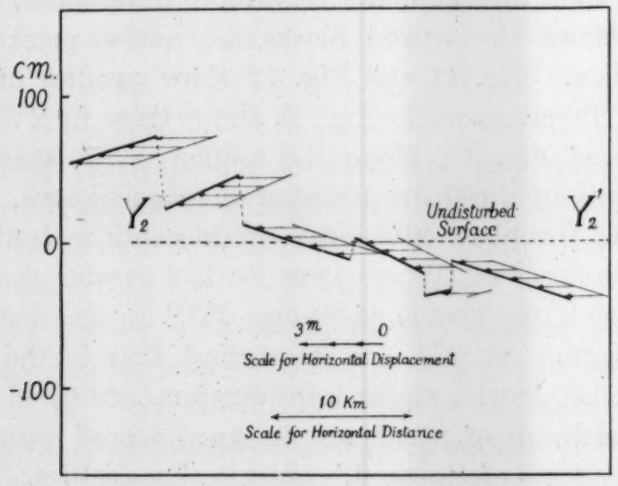

Fig. 12. Profile of the block movements along the section Y_2Y_2 in Fig. 3

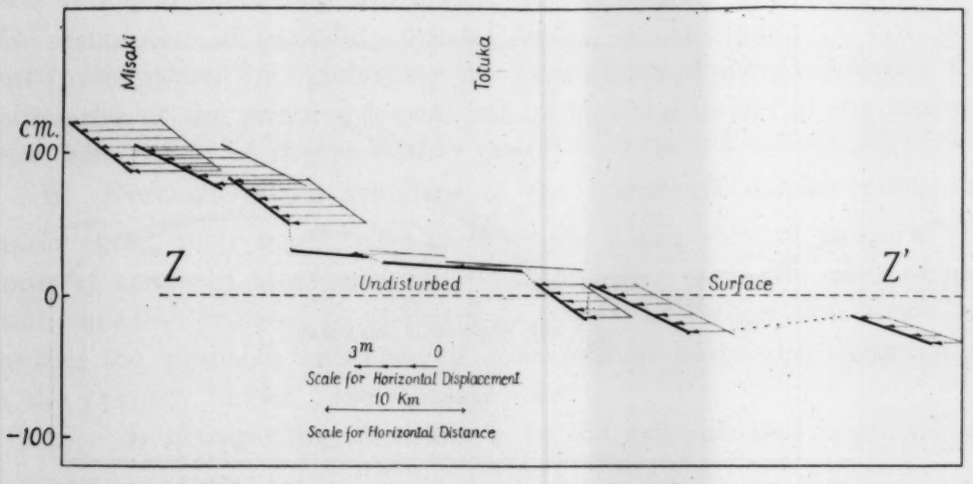

Fig. 13. Profile of the block movements along the section *ZZ'* in Figs. 3.

whose block movements is shown in Fig. 13.

In Figs. 10-13, we notice several gaps and overlaps in the thick straight lines that represent the primary blocks, amounting to several tens of centimetres. These gaps and overlaps may partly be compensated by dilatations and contractions of the earth's crust within the crust blocks. But, in several cases, parts of these gaps and overlaps may be seen as actual dislocations along the boundaries of the adjoining crustal blocks.

Horizontal Deformation Within the Crustal Blocks.

As pointed out above, the earth's crust may be considered to have been deformed horizontally within the constituent crust blocks themselves. In the present chapter, the values representing the horizontal deformation are calculated and their geographical distribution discussed.

The values representing the horizontal deformation inside the blocks are calculated on the assumption that the deformations in each individual primary block are uniform, that is to say, the x- and y-components of the horizontal displacements, u and v, are expressed by linear functions of the coordinates, x and y, in the form[14].

$$u=ax+by+c,$$
$$v=a'x+b'y+c'.$$

The horizontal divergence Δ, rotation ζ, shear s, principal axes of strain γ_1, γ_2, and the angle θ_1 which the direction of γ_1 makes with the x-axis, are expressed in terms of a. b, a', and b', or, $\frac{\partial u}{\partial x}$, $\frac{\partial u}{\partial y}$, $\frac{\partial v}{\partial x}$ and $\frac{\partial v}{\partial y}$, in the following forms:

$$\Delta=a+b'=\frac{\partial u}{\partial x}+\frac{\partial v}{\partial y},$$

$$2\zeta=a'+b=\frac{\partial v}{\partial x}+\frac{\partial u}{\partial y},$$

$$2S=a'+b=\frac{\partial v}{\partial x}+\frac{\partial u}{\partial y},$$

$$\gamma_{\frac{1}{2}}=(a+b')\pm\sqrt{(a-b')^2+(a'+b)^2}$$
$$=\left(\frac{\partial u}{\partial x}+\frac{\partial v}{\partial y}\right)\pm\sqrt{\left(\frac{\partial u}{\partial x}+\frac{\partial v}{\partial y}\right)^2+\left(\frac{\partial v}{\partial x}+\frac{\partial u}{\partial y}\right)^2},$$

$$\tan\theta_1=\frac{\gamma_1-2a}{a^1+b}=\frac{\gamma_1-2\frac{\partial u}{\partial x}}{\frac{\partial v}{\partial x}+\frac{\partial u}{\partial y}}.$$

14) T. Terada and N. Miyabe, *Bull. Earthq. Res. Inst.*, **7** (1929), 223.

On calculating a, b, a', and b' of each constituent block, we have in general the data of the horizontal displacements of n triangulation points, or, n equations for u and as many equations for v, in the form;

$$\begin{aligned} u_1 &= ax_1+by_1+c, & v_1 &= a'x_1+b'y_1+c', \\ u_2 &= ax_2+by_2+c, & v_2 &= a'x_2+b'y_2+c', \\ &\cdots\cdots\cdots & &\cdots\cdots\cdots \\ u_n &= ax_n+by+c, & v_n &= a'x_n+b'y_n+c'. \end{aligned}$$

Eliminating c and c' in $2n$ equations above, we have $\frac{1}{2}n(n-1)$ equations of the form

$$u_k-u_n=a(x_k-x_n)+b(y_k-y_n),$$

and as many equations of similar form, i.e.,

$$v_k-v_n=a'(x_k-x_n)+b'(y_k-y_n),$$

where $k=1, 2, \ldots (n-1)$, and $n=2, 3, \ldots n$. From these equations, a, b. a', and b' are calculated by the method of least squares, as follows;

$$\left.\begin{aligned} a &= \frac{[UX][YY]-[uY][YX]}{[XX][YY]-[XY]^2} \\ b &= \frac{[UX][XY]-[UY][XX]}{[XY]^2-[XX][YY]} \end{aligned}\right\}, \qquad \left.\begin{aligned} a' &= \frac{[VX][YY]-[VY][YX]}{[XX][YY]-[XY]^2} \\ b' &= \frac{[VX][XY]-[VY][XX]}{[XY]^2-[XX][YY]} \end{aligned}\right\},$$

where

$$\begin{aligned} [UX] &= (u_2-u_1)(x_2-x_1)+(u_3-u_1)(x_3-x_1)+\cdots \\ &\quad +(u_n-u_1)(x_n-x_1)+(u_3-u_2)(x_3-x_2)+\cdots+(u_n+u_{n-1})(x_n-x_{n-1}), \\ [UY] &= (u_2-u_1)(y_2-y_1)+(u_3-u_1)(y_3-y_1)+\cdots \\ &\quad +(u_n-u_1)(y_n-y_1)+(u_3-u_2)(y_3-y_2)+\cdots \\ &\quad +(u_n-u_{n-1})(y_n-y_{n-1}), \\ [XX] &= (x_2-x_1)^2+(x_3-x_1)^2+\cdots+(x_n-x_1)^2+(x_3-x_2)^2+(x_n-x_{n-1})^2, \\ [XY] &= (x_2=x_1)(y_2-y_1)+(x_3-x_1xy_3-y_1)+\cdots \\ &\quad +(x_n-x_1)(y_n-y_1)+(x_3-x_2)(y_3-y_2)+\cdots+(x_n-x_{n-1})(y_n-y_{n-1}), \end{aligned}$$

with similar forms for $[VX]$, $[VY]$, and $[YY]$.

Before discussing the horizontal deformation of the earth's crust, it may be said that the amounts of Δ, ζ, and γ are, to a certain extent, affected by any deformation of the base line to which the measured horizontal displacements have been referred and which had been assumed to have been unchanged. Should the base line be changed in length

by dl and in its azimuth by $d\theta$, Tsuboi's[15] corrections must be applied to the components of the horizontal displacements, as follows;

$$u = u' + x.\, dl/l - y.d\theta,$$
$$v = v' + y.dl/l + x.d\theta,$$

where u' and v' are the components of the horizontal displacements obtained on the assumption of an unchanged base line. We then get

$$\frac{\partial u}{\partial x} = \frac{\partial u'}{\partial x} + \frac{dl}{l},$$
$$\frac{\partial u}{\partial y} = \frac{\partial u'}{\partial y} - d\theta,$$
$$\frac{\partial v}{\partial x} = \frac{\partial v'}{\partial x} + d\theta,$$

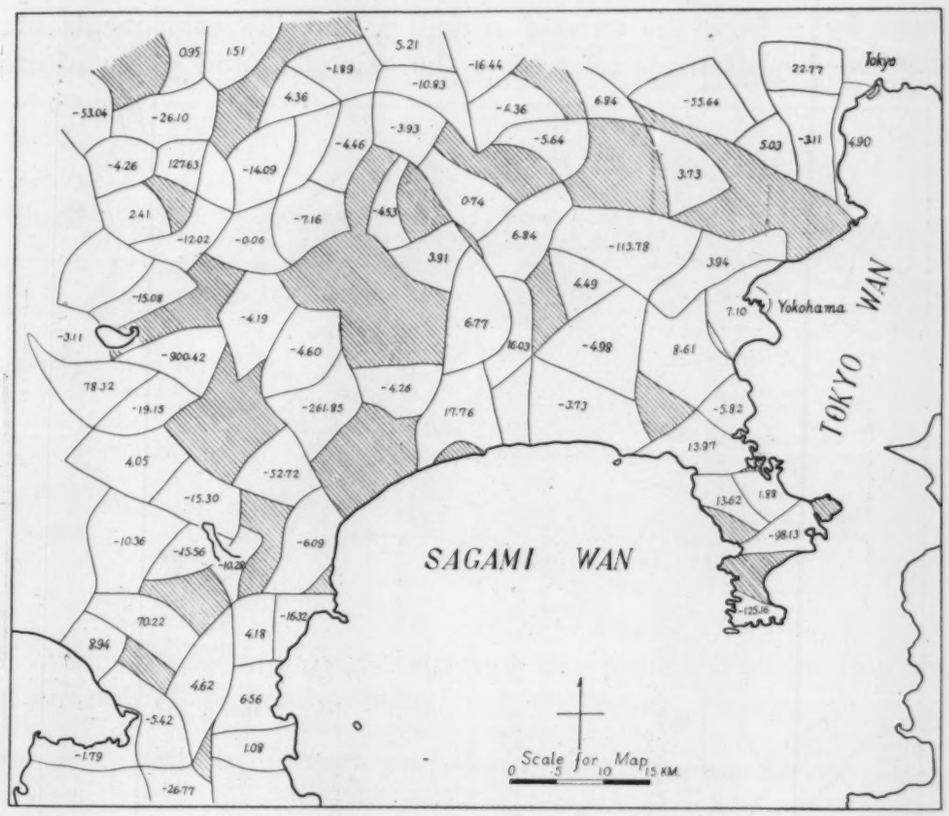

Fig. 14. Geographical distribution of Δ.

15) C. Tsuboi, *Bull. Earthq. Res. Inst., loc. cit.* 7).

$$\frac{\partial u}{\partial y}=\frac{\partial v'}{\partial y}+\frac{dl}{l},$$

whence

$$\Delta=\Delta'+2\frac{dl}{l},$$

$$2\zeta=2\zeta'-2\,d\theta,$$

$$2S''=2S',$$

$$\gamma_1'_2=\gamma_1'_2+2\frac{dl}{l},$$

$$\tan\theta_1=\tan\theta_1',$$

where Δ', ζ', S', $\gamma_1'_2$, and θ_1' are referred to the base line, assumed unchanged. As may be expected from the expression, the amount of S depends on the coordinate axis to which the coordinates and the components of the horizontal displacements of the triangulation points are referred. By letting x' and y' be coordinates referred to another point rotated by ν from the axis of x and y, and the components of the horizontal displacements referred to the axis of x' and y' be u' and v'

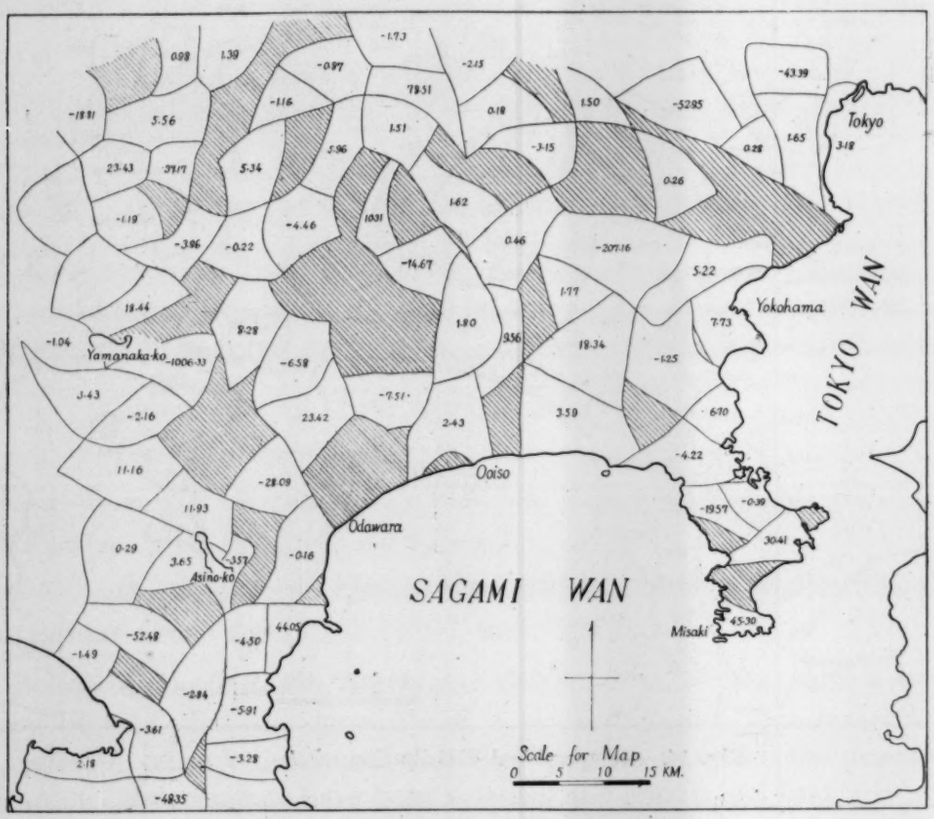

Fig. 15. Geographical distribution of ζ.

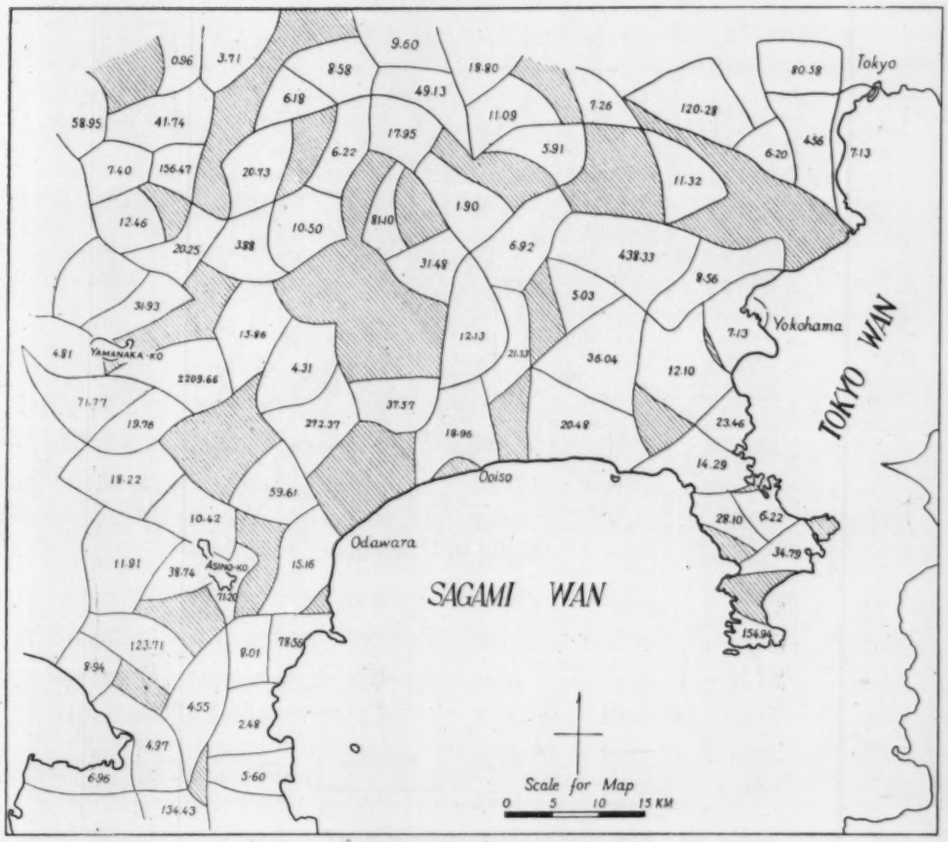

Fig. 16. Geographical distribution of S_m.

respectively, we have

$$2S\left\{\frac{\partial v'}{\partial x'}=\frac{\partial u'}{\partial y'}\right\}=\left(\frac{\partial v}{\partial x}+\frac{\partial u}{\partial y}\right)\cos 2\nu+\left(\frac{\partial v}{\partial y}-\frac{\partial u}{\partial x}\right)\sin 2\nu.$$

From $\dfrac{\partial(2S)}{\partial \nu}=0$, we obtain

$$[\tan 2\nu]_{2S\to\max}=\left(\frac{\partial u}{\partial x}-\frac{\partial v}{\partial y}\right)\Big/\left(\frac{\partial v}{\partial x}+\frac{\partial u}{\partial y}\right),$$

which makes $2S$ maximum. Substituting this value of $\tan 2\nu$ into the above expression, we finally obtain

$$S_{\max}=\sqrt{\left(\frac{\partial v}{\partial x}+\frac{\partial u}{\partial y}\right)^2+\left(\frac{\partial v}{\partial y}-\frac{\partial u}{\partial x}\right)^2}=\frac{1}{2}(\gamma_1-\gamma_2),$$

which is independent of the coordinate axis.

In the present investigation, the geographical distribution of S_m is studied instead of that of S. The geographical distributions of Δ, ζ,

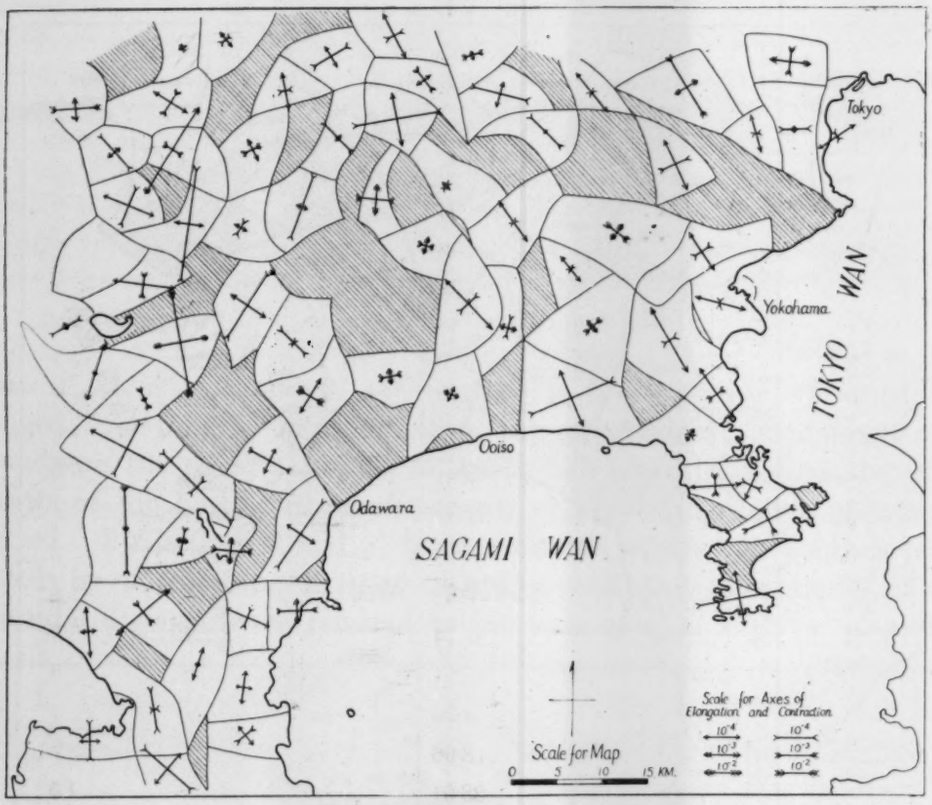

Fig. 17. Geographical distribution of γ_1 and γ_2.

S_m, and γ_1 are shown in Figs. 14, 15, 16, and 17 respectively. The numerical values of Δ, ζ, γ_1, γ_2, θ_1 and S_m, or $\frac{1}{2}(\gamma_1-\gamma_2)$, for each of the primary blocks are given in Table VIII.

In comparing the geographical distribution of Δ and S_m with that of the block tilts, no marked correspondence can be noted.

It may be noticed, however, though not quite markedly, that the majority of the contracted crustal blocks are in the district west of the Sagamigawa, where the block tilts are generally more pronounced than in the other districts.

In comparing the geographical distribution of γ_1 and γ_2 with that of tilts of the crustal blocks, we cannot notice any remarkable general correspondence, though there are several instances of crustal blocks in which the azimuths of the tilts coincide with the directions of the principal axes of contraction, as in blocks 5, 44, 52, 62, and 64, and also those in which the azimuths of the tilts coincide with the directions of

Table VIII.

Δ, ζ, S_m, γ_1, γ_2 and θ_1 of the constituent crustal blocks.

Block	Δ in 10^{-5}	ζ in 10^{-5}	$S_m=\frac{\gamma_1-\gamma_2}{2}$ in 10^{-5}	γ_1 in 10^{-5}	γ_2 in 10^{-5}	θ_1, referred to E, measured counter clockwise.
1	−4·98	18·34	36·04	31·06	−42·02	−48·2
2	−3·73	3·59	20·48	16·75	−24·21	−67·5
3	4·36	−1·16	6·18	10·54	−1·82	−78·6
4	2·41	−1·49	12·46	14·87	−10·05	−22·5
5	−4·53	10·31	81·10	76·57	−85·63	84·3
6	−14·09	5·34	20·73	6·64	−34·82	−64·3
7	−26·10	5·56	41·74	10·64	−62·84	−32·8
8	127·63	37·17	156·47	284.10	−28·84	58·0
9	4·05	11·16	18·22	22·27	−14·17	−26·8
10	−15·08	18·44	31·93	16·85	−47·01	−7·3
11	−15·30	11·93	10·42	−4·88	−25·72	45·0
12	−15·56	3·65	38·74	23·18	−54·30	−10·5
13	−10·36	0·29	11·91	1·57	−22·29	1·8
14	−10·28	−3.57	71·20	60·92	−81·48	85·7
15	−17·76	2·43	18·96	31·74	3·78	−22·7
16	13·62	−19·57	28·01	14·39	41·63	4·5
17	1·88	−0·39	6·22	8·10	−4·34	64·8
18	−98·13	30·41	34·79	−63·34	−132·92	−64·2
19	−5·82	6·70	23·46	17·64	−29·28	−55·5
20	13·97	−4·22	14·29	28·26	−0·32	59·1
21	−10·83	78·51	49·13	38·30	−59·96	37·9
22	0·95	0·98	0·96	1·91	−0·01	23·9
23	1·51	1·39	3·71	5·22	−2.20	−52·4
24	−3·11	−1·04	4·81	1·70	−7·92	−61·0
25	−1·89	−0·87	8·58	6·69	−10·47	−59·5
26	1·08	−3·28	5·60	6·68	−4·52	−49·8
27	5·21	−1·73	9·60	14·31	−3·89	−64·8
28	−19·15	−2·16	19·67	0·52	38·82	25.6
29	78·32	3·48	71·77	155·09	1·55	72·8
30	3·91	−14·67	31·48	35·39	−27·57	74·4
31	−12·02	−3·86	20·25	8·23	−32·27	−8·2$_5$
32	−53·04	−18·81	58·95	5·91	−111·99	−86·2

(to be continued.)

Table VIII. (*continued.*)

Block.	Δ_m in 10^{-5}	ζ in 10^{-5}	$S_m=\frac{\gamma_1-\gamma_2}{2}$ in 10^{-5}	γ_1 in 10^{-5}	γ_2 in 10^{-5}	θ_1, referred to E_1 measured counter clockwise.
33	−4·46	5·96	6·22	1·76	−10·68	−44·5
34	−7·16	−4·46	10·50	3·34	−17·66	−20·5
35	−0·06	−0·22	3·88	3·82	−3·94	−30·8
36	6·77	1·80	12·13	18·90	−5·36	−46·2
37	16·03	9·56	21·33	37·36	−5·30	−15·1
38	4·49	1·77	5·03	9·52	−0·54	−51·6
39	−16·44	−2·15	18·80	2·36	−35·24	−72·4
40	6·34	1·50	7·26	14·10	−0·42	$-52\cdot2_5$
41	−113·78	−207·16	438·33	324·60	−552·06	52·5
42	−4·36	0·18	11·09	6·73	−15·45	74·8
43	0·74	1·62	1·90	2·64	−1·16	43·5
44	8·61	−1·25	12·10	20·71	−3·49	−61·0
45	7·10	7·73	7·13	14·23	−0·03	−14·1
46	3·94	5·22	8·56	12·50	−4·62	−57·3
47	−5·64	−3·15	5·91	0·29	−11·57	44·8
48	−16·32	44·05	78·56	57·24	−89·88	−87·9
49	3·73	0·26	11·32	15·05	−7·59	−65·2
50	5·03	0·28	6·20	11·23	−1·17	−75·0
51	4·90	3·18	7·13	12·03	−2·23	34·6
52	−3·11	1·65	4·56	1·45	−7·67	$-88\cdot0_5$
53	22·77	−43·39	80·58	103·75	−58·21	−6·4
54	−55·64	−52·95	120·28	64·64	−175·92	31·9
55	6·84	0·46	6·92	13·76	−0·08	−54·5
56	−5·42	3·61	4·97	−0·8	−10·02	9·6
57	8·94	−1·49	8·94	13·66	4·22	−84·2
58	−26·77	−48·38	134·43	107·66	−161·20	51·4
59	4·18	−4·50	8·01	12·19	−3·83	−20·9
60	6·56	−5·91	2·48	9·02	4·10	83·8
61	−52·72	−28·09	59·61	6·89	−112·33	63·5
62	−6·09	−0·16	15·16	9·07	−21·24	$-33\cdot1_5$
63	−4·19	8·28	15·86	11·67	−20·05	−33·6
64	−4·60	−0·58	4·31	−0·29	8·91	45·2
65	−261·85	23·42	272·37	10·52	−534·22	58·9

(*to be continued.*)

Table VIII. (*continued.*)

Block	Δ in 10^{-5}	ζ in 10^{-5}	$S_m=\frac{\gamma_1-\gamma_2}{2}$ in 10^{-5}	γ_1 in 10^{-5}	γ_2 in 10^{-5}	θ_1, referred to E, measured counter clockwise.
66	−4·26	−1·79	7·40	3·14	−11.66	$42°_{5}$
67	−3·93	1·51	17·95	15·02	−22·88	−79·1
68	−125·16	45·30	154·94	29·78	280·10	−6·6
69	−900·42	−1006·33	2209·66	1309·24	−3110·08	8·9
70	−1·79	2·18	6·96	5·17	−8·75	2·0
71	70·22	−52·48	123·71	$193·9_3$	−53·49	40·6
72	4·62	−2·84	4·55	$9·1_7$	0·07	72·9
73	−4·26	−7·52	37·57	33·31	−41·83	−79·6

the principal axes of elongation, as in the cases of blocks 4, 6, 13, 23, 26, 40, 63, and 67. The frequency of the values of $(\theta_m-\theta_1)$, the difference between the direction of tilt and the principal axes of elongation that were used in the satistical investigation of the problem, are shown in Fig. 18, in which the sense of tilt is disregarded. In fact, we notice in Fig. 18. that there are three maxima in frequency of $(\theta_m-\theta_1)$, namely, at $(\theta_m-\theta_1)=0°-10°$, $40°-50°$, and $80°-90°$. This shows that there are three different cases in which the supposed relation between the directions of tilt and the principal axes of strain may occur. In the case $(\theta_m-\theta_1)=0°-10°$, the principal axes of elongation approximately agree with the directions of tilt; in the case $(\theta_m-\theta_1)=90°$ (nearly), the principal axes of contraction approximately agree with the directions of tilt; while in case $(\theta_m-\theta_1)=40°-50°$, the directions of the tilts may be regarded as agreeing with those of maximum shears. Thus the geographical distribution of the horizontal deformation within the blocks presents no general characteristics, so that we are led to conclude that the deformation within the blocks are mainly due to local disturbances.

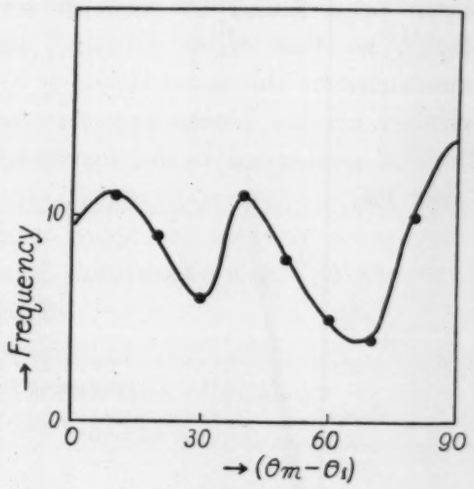

Fig. 18. The Frequency distribution of $(\theta_m-\theta_1)$.

We have already pointed out that the primary crustal blocks may be subdivided into several secondary blocks, and seeing that the triangulation points situated in the respective primary blocks could be divided into two or three groups so far as concerns the azimuths and magnitudes of their horizontal displacements. It may therefore be expected that these secondary block structures will affect to some extent also the values representing the horizontal deformations, such as Δ, S_m, etc. On the other hand, all the blocks may be deformed nearly uniformly under the action of stress, so long as the materials composing them are practically homogeneous and isotropic. But this uniform deformation within the blocks may be limited in extent, which limit when exceeded may result in their breaking up into a number of secondary blocks. After breaking up into these secondary blocks, the deformation may become generally greater and irregular, due to relative movements between the secondary blocks.

The foregoing conceptions, needless to say, cannot easily be verified owing to limitations to our present knowledge. Yet the following facts may perhaps throw some light on the subject. As has been pointed out, the tectonic lines in the district under consideration have in several places been found to coincide with the boundaries of primary crustal blocks, so that these tectonic lines may be regarded as being also boundaries of the secondary blocks. It was also pointed out that the primary crustal blocks are often traversed by these tectonic lines. The effect of geological faults traversing the blocks is shown statistically in Table IX.

Table IX.

Cases	Traversed by fault		No fault	
	$\Delta, S_m > 10^{-4}$	$\Delta, S_m < 10^{-4}$	$\Delta, S_m > 10^{-4}$	$\Delta, S_m < 10^{-4}$
Number of Blocks	15	15	9	34

If the active tectonic lines could be regarded as the boundaries of secondary blocks, the existence of these secondary blocks may affect the horizontal deformations of the primary blocks. As might be expected, in several blocks of this sort, the magnitudes of Δ and S_m are generally considerable, as shown in Table X.

Table X.

Crust of blocks traversed by geological faults, of which Δ's and S_m's are greater than 10×10^{-5}.

Block	Δ	S_m	Block	Δ	S_m
1	-4.98×10^{-5}	36.04×10^{-5}	18	−98.13	34.79
2	−3.48	20.48	19	−5.82	−23.46
5	−4.53	81.10	41	−113.78	438.33
7	−26.10	41.74	58	−26.77	134.43
10	−15.08	31.93	65	−261.85	272.37
14	−10.28	71.20	69	−900.42	2209.66
16	−13.62	28.01	73	−4.26	57.53

But in other crustal blocks of this kind, the horizontal deformations are of the order of magnitude 10^{-4}, as shown in Table XI.

Table XI.

Crustal blocks traversed by geological faults, of which Δ's and S_m's are less than 10×10^{-5}.

Block	Δ	S_m	Block	Δ	S_m
3	4.36×10^{-5}	6.18×10^{-5}	55	6.84	6.92
17	1.88	6.22	56	−5.42	4.97
34	−7.16	10.50	59	4.18	8.21
35	−0.06	3.88	63	−4.19	15.86
44	8.61	12.10	64	−4.60	4.31
45	7.10	7.13	66	−4.26	7.47
46	3.94	8.56	70	−1.79	6.96
51	4.90	7.13			

Moreover, there are several blocks not traversed by any conspicuous tectonic lines, but of which the horizontal deformations are of the order of magnitude 10^{-4}, as given in Table XII.

Table XII.

Crustal blocks traversed by no geological fault, of which Δ's and S_m's are greater than 10×10^{-5}.

Block	Δ	S_m	Block	Δ	S_m
8	127.63×10^{-5}	156.47×10^{-5}	53	22.77×10^{-5}	80.58×10^{-5}
12	−15.56	38.78	54	55.64	120.28
21	−10.83	49.13	61	−52.72	59.61
29	78.78	71.77	71	70.22	123.71
32	−53.04	58.59			

There is much fewer of these blocks than those with horizontal deformations of the order of magnitude 10^{-5}.

While these facts do not of course prove the existence of secondary blocks, as postulated above, they seem at least to suggest their ex istence.

In Fig. 15, which shows the geographical distribution of ζ, we notice several groups of crustal blocks. In all these groups, the rotational deformations of the blocks are in the same sense. These block groups are distributed almost concentrically around the Sagami-wan (Bay)—a fact that recalls the theory of earth vortices, proposed by Prof. S. Fujiwhara,[16] in connection with the mechanism of the 1923 Kwantô earthquake. But present evidences are yet inadequate to support such a theory, since such mode of crustal formation as shown by the geographical distribution of block groups with ζ's of the same sense may be brought about not only by a vortical movement of the earth, but in other ways as well. Horizontal shearing movements of secondary blocks may, besides, produce considerable apparent rotational deformation in the primary blocks, though, within the limits of our present knowledge, it would be difficult to distinguish them from vortical movements.

Statistics covering horizontal deformations of primary blocks show that there is a maximum frequency of horizontal divergence at $4-5\times10^{-5}$ and of shear at $6-7\times10^{-5}$, as shown in Figs. 19 and 20. In both cases, the horizontal deformation within the primary blocks is in general of the order of magnitude little less than 10^{-4}, which may be regarded as the limit of horizontal strain of the earth's crust. A horizontal crustal deformation of the order of magnitude 10^{-5} was found in the crustal deformation of both the rhombic area at Mitaka and in larger

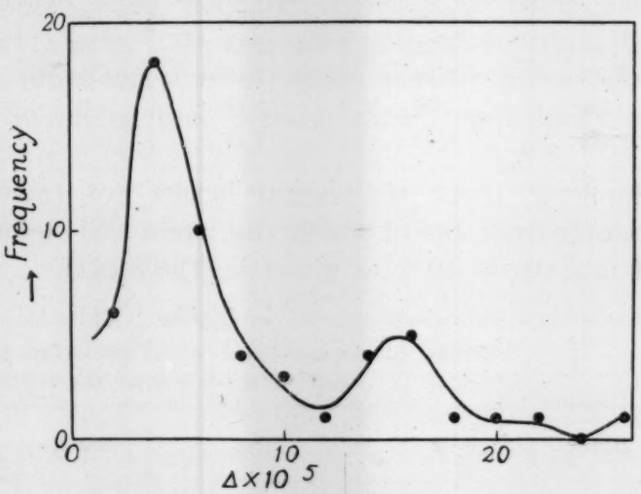

Fig. 19. Frequency distribition of Δ.

16) S. FUJIWHARA and T. TAKAYAMA, *Bull. Earthq. Res. Inst.*, 6 (1928). 149.

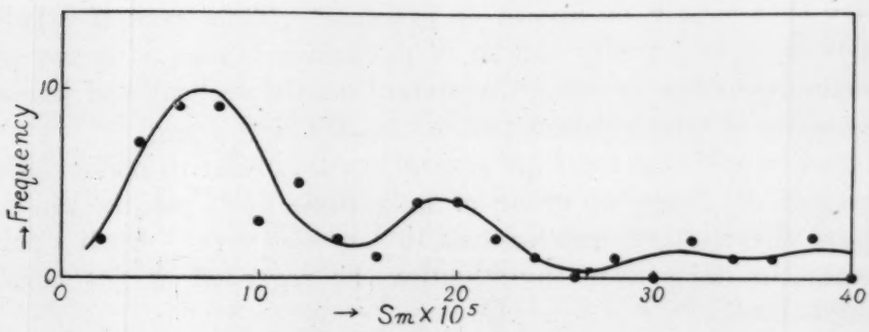

Fig. 20. Frequency distribution of S_m.

areas, such as that which included the Rhombus[17]. A horizontal deformation of this order of magnitude may thus be expected from uniform deformation of the earth's crust. It may then be expected that horizontal deformations greater than 10^{-4} may be accompanied by dislocations. As a matter of fact dislocations that occurred in connection with the Kwantô earthquake of 1923 are found at many places. It is however not easy to say whether they were due to such type of crustal deformations as just referred to or whether they were due to slight local disturbances following the earthquake.[18]

On the other hand, the method of calculating the values representing the horizontal deformation was based on the assumption that deformation in an individual block is uniform throughout. Hence, it may be expected that the numerical values of Δ and S_m thus calculated may generally be of the order of 10^{-4} or less, provided there was no dislocation within the blocks. From this point of view, a crustal block with its Δ or S_m of greater magnitude than 10^{-4} may be regarded as consisting of more than two secondary blocks, the dislocations between these secondary blocks being not necessarily observable. The existence of secondary blocks is thus made probable from a new standpoint. The relative movements between secondary blocks may produce considerable horizontal deformotion Δ within the primary block. The amount of this Δ cannot easily be calculated numerically, as the expression for Δ, due to a horizontal displacement along the boundary of the secondary blocks, contains constants depending upon the position and the trend of a

17) C. Tsuboi, *Proc. Imp. Acad.*, 6 (1930), 367.

18) Cracks may be produced in alluvial plains by gravitational waves in layers of of soils, the possibility of which has been discussed by Dr. T. Matuzawa. T. Matuzawa, *Jap. Journ. Astr. Geophys.*, 3 (1925), 161.

boundary that cannot be known at present.[19] Thus, even if a primary crustal block does actually consist of secondary blocks, it is not practicable to analyse them by using the present data of vertical and horizontal displacements of triangulation points.

It may be said that there are several crustal blocks in which, although the amounts of Δ are of order of magnitude 10^{-5}, yet the amount of maximum shear, S_m, is greater than 10^{-4}, or vice versa. Such a primary block may, in the present investigation, be regarded as not consisting of a single block.

It may also be added that if the crustal deformation is considered to be a secular one—the accumulation during the time interval between successive surveys—dislocations may not be apparent, even if the earth's crust there had deformed conspicuously. This is probably one of the reasons why we cannot find tectonic lines or dislocations marking the boundary lines of secondary blocks.

Crustal Deformations after the Kwantô Earthquake of 1932.

The crustal deformations that occurred after the Kwantô earthquake of 1923 have been determined by vertical displacements of bench marks as revealed by post-seismic revisions of precise levels run a number of times over the district under consideration. These levelling routes are shown in Fig. 21. The various sections of the levelling routes and the dates of the surveys will be found in Table XIII.

It will be noticed upon examining these vertical displacements of bench-marks, that the crustal blocks were still noticeable in the movement that occurred after the earthquake. There are, however, several instances in which the boundaries of previously determined blocks are less marked in the crustal deformations of later intervals.

---

19) If we assume the boundary of secondary blocks along which they have slid horizontally to be a straight line, expressed by $y=ax+b$, Δ due to the relative horizontal displacement ξ along this boundary line is calculated by

$$\Delta=\frac{\xi m(n-m)}{\sqrt{1+a^2}}\left\{\frac{1}{(n-m)(x_1+x_2+\ldots+x_m)-m(x_{m+1}+\ldots+x_n)}\right.$$
$$\left.+\frac{a}{(n-m)(y_1+y_2+\ldots+y_m)-m(y_{m+1}+\ldots+y_n)}\right\}$$

in which m is the number of triangulation points situated on one of the secondary block, and $(n-m)$ those situated on the adjoining block.

Fig. 21. Geographical distribution of levelling routes.

Table XIII.

Dates of surveys of different parts of the levelling routes.

Parts	Atami-Hudisawa	Aburatubo-Tokyo	Sasako-Hatiôzi	Hatiôzi-Yoyohata
I	1884	1896—1898	1884	1884
II	1896	1923 *	1895	1895
III	1923 *	1924 *	1903	1924 *
IV	1926 *	1927 *	1924 *	1930 *
V	1930 *	1930 *	1927 *	
VI			1931 *	

* Surveys after the 1923 earthquake.

Along the levelling route from Hudisawa to Atami, the crustal blocks are still noticeable in the deformation revealed by vertical displacements of benchmarks as deduced from the relevellings made in

October, 1930.

In Fig. 22 are shown the vertical displacements of bench-marks on the route from Hudisawa to Atami, δH_1, δH_2, δH_3, during the time intervals, 1895-1923, 1923-1925, and 1925-1930, respectively. The scale

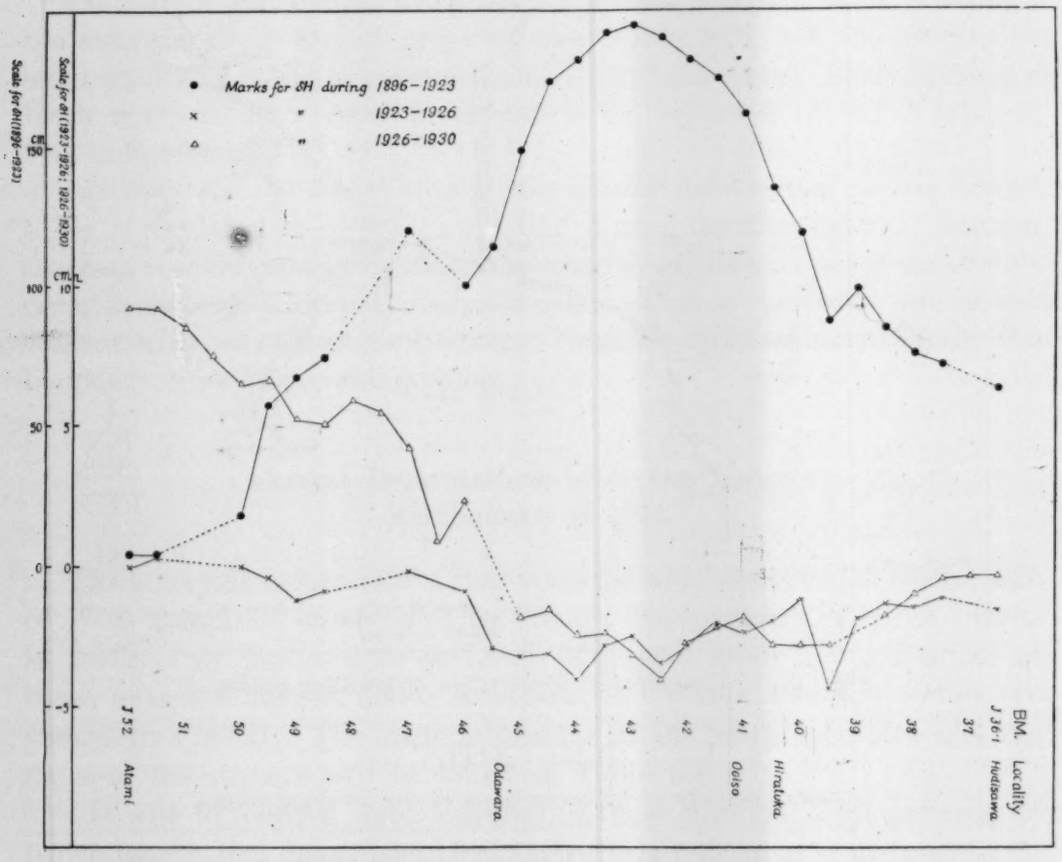

Fig. 22. Vertical displacements of bench-marks along the route between Atami and Hudisawa, for different periods.

for δH_1 is much reduced, compared with those for the later intervals. As shown by these curves, after the Kwantô earthquake the earth's crust as a whole deformed[20] in reverse sense of that found by means of levels re-run soon after the earthquake. The correlations between δH_1 and δH_2 and between δH_2 and δH_3 are shown diagrammactically in Figs 23*a* and *b*. Generally speaking, correlation between δH_1 and δH_2 is negative, while that between δH_2 and δH_3 is positive. And

20) The different types of crustal deformation have been discussed by Tsuboi. C. TSUBOI, *Jap. Journ. Astr. Geophys.*, **10** (1933), 94.

in separate parts of the levelling route divided by boundaries of primary blocks, δH_2 and δH_3 are positively correlated, while δH_2 and δH_1, including components of the acute crustal deformation associated with the Kwantô earthquake, are negatively correlated. Thus in the curves showing the vertical displacements of bench-marks, we notice variations that may largely be due to movements of blocks that were still active during the post-seismic deformations.

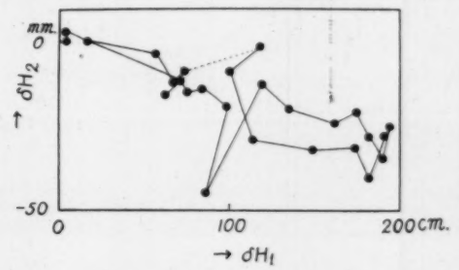

Fig. 23*a*. Diagram showing approxmate negative correlation between δH_1(1896–1923) and δH_2(1923–1926) of the bench-marks situated between Atami and Hudisawa.

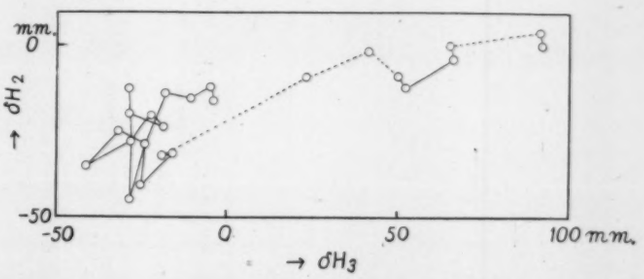

Fig. 23*b*. Diagram showing approximate positive correlation between δH_2(1923–1926) and δH_3(1926–1930) of the same bench-marks as referred to in Fig. 23*a*.

As for crustal deformation shown by vertical displacements of bench-marks on the route from Aburatubo to Takanawa-kita-mati, Tokyo, the block structure appears quite evident in the post seismic deformation of the earth's crust. The vertical displacements of these bench-marks are shown in Fig. 24, the displacements during 1902–1924 being plotted on 1/10 the scale of those for the later periods. In connection with the deformation of the earth's crust in this district, the following points deserve notice:

i) The Miura peninsula as a whole moved up and then down since the great Kwantô earthquake, that is to say, it oscillated with reference to the mainland – a mode of deformation that has been discussed by Tsuboi.[21]

The crustal movement disclosed by changes in heights of bench-marks situated between B. M. 2 and B. M. 5363·1, show however that the earth's crust near the end of the peninsula had tilted continually northward after the earthquake, the direction of this general tilt of the

21) C. Tsuboi, *ibid.*

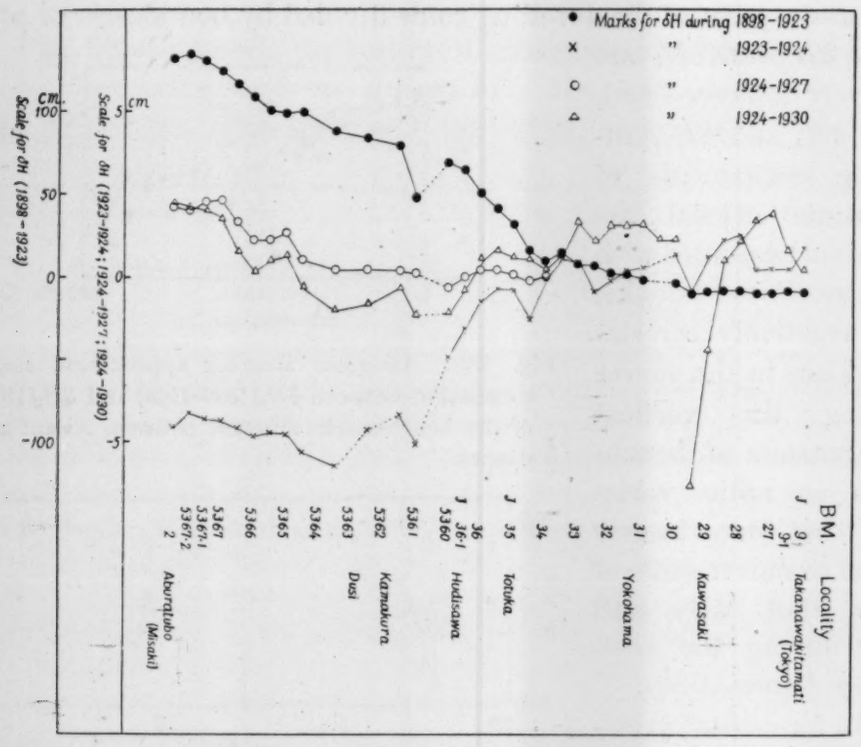

Fig. 24. Vertical displacements of bench-marks along the route between Misaki (Aburatubo) and Tokyo, for different periods.

peninsula approximately agreeing with that of the blocks determined in the preceding chapter.

ii) The curve showing the vertical displacements of bench-marks on the levelling route that passes through block 44 seems to be discontinuous between B.M. 34 and 33·1, which may mean that block 44 consists of secondary blocks, the apparent discontinuity corresponding to the boundary of these secondary blocks.

iii) In the alluvial plain along the river Tamagawa, the crustal blocks had not previously been determined, as the triangulation points are too scattered in this region. In the vertical displacements of bench-marks shown in Fig. 24, however, the blocks are more or less evident, as Prof. Imamura pointed out[22] in his investigation of block movements in connection with the severe earthquake off Haneda in 1926.

The vertical displacements along the levelling route from Hatiôzi to Sasako during the intervals 1903–1924, 1924–1927, and 1927–1930, and those of bench-marks on the Yoyohata—Hatiozi route during

22) A. IMAMURA, *Proc. Imp. Acad.*, **7** (1931), 271.

intervals 1895-1924 and 1924-1930 are shown in Figs. 25 and 26 respectively. In the crustal deformations disclosed by vertical displacements of these bench-marks, however, those that seem to be due to the presence of primary crustal blocks are less pronounced compared with deformations in other districts. Among the deformations that occurred

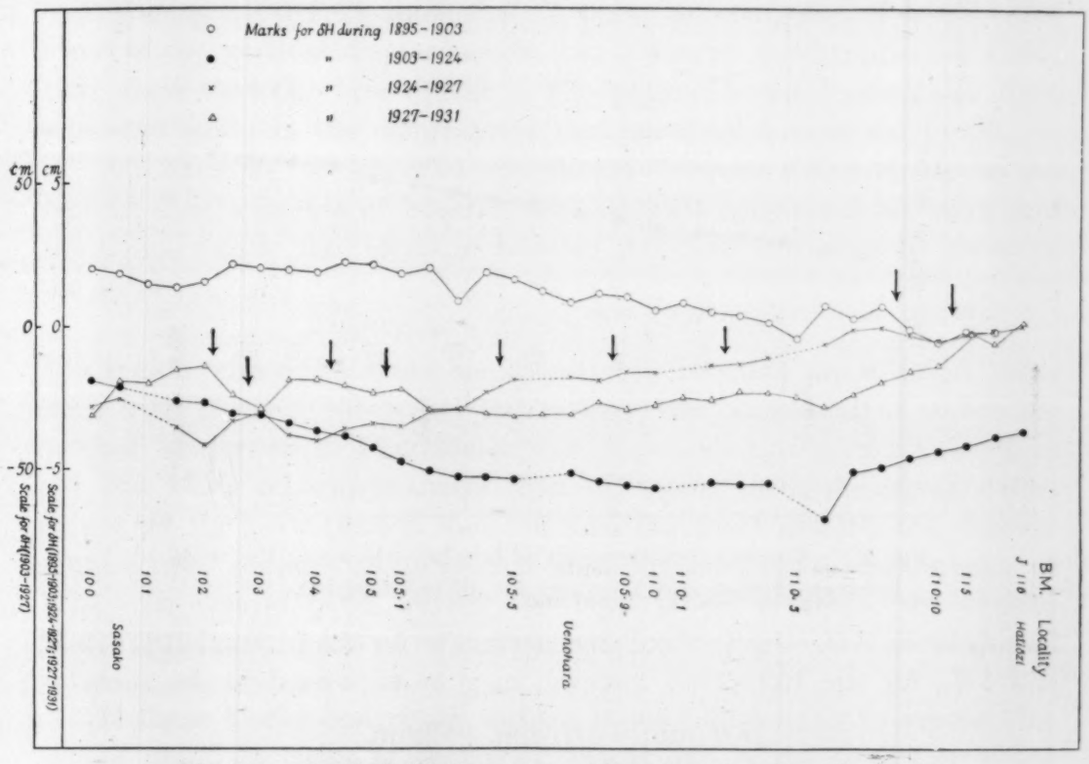

Fig. 25. Vertical displacements of bench-marks along the route between Sasako and Hatiôzi for different periods.

after the earthquake of 1923 is one in which the earth's crust seems to have been deformed in a way suggesting that several adjoining blocks had coalesced into one single block. An example of this is seen in the vertical displacements during different intervals of the bench-mark displacements between B.M. 110·1 and 105·5. The vertical displacements of these bench-marks during the interval 1924–1927 is in positive correlation with those of the same bench-marks for the interval 1927–1930. The two curves just mentioned, showing the vertical displacements for the different time intervals given, coincide when the datum line of the last-mentioned curve is shifted downward about 12mm.[23] The relation there-

23) A similar case was pointed out by Tsuboi in the crustal deformation associated with the North Idu earthquake of 1930.
C. Tsuboi, *Bull. Earthq. Res. Inst.*, 10 (1932), 435.

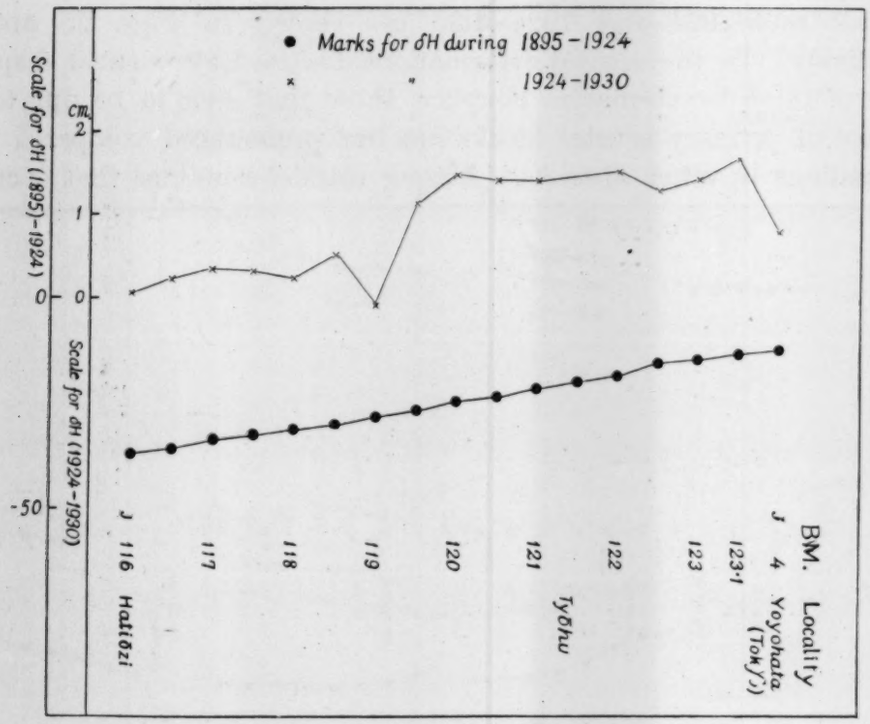

Fig. 26. Vertical displacements of bench-marks along the route between Hatiôzi and Yoyohata for different period.

fore between δH_5, the vertical displacements for the interval 1927–1930, and δH_4, for the 1924-1927 interval, may be expressed in the form

$$\delta H_4 \text{mm.} = \delta H_5 \text{mm.} + 12\text{mm.}$$

On the other hand, the earth's crust along this levelling route, between B.M. 110·1 and 105·6, is divided into those two crustal blocks that were previously determined by using the data of vertical displacements of triangulation point. However, as shown in Fig. 25, the boundaries of these blocks are not apparent from the vertical displacements of bench-marks. This may of course be due partly to the manner in which the constituent blocks had tilted; or expressed in another way, the particular way in which the blocks had tilted happened to be favourable for producing the discontinuities in the vertical displacements, which may be considered to be due to the different ways in which the blocks had tilted. In short, in whatever way the constituent blocks may have tilted, so far as the correlation between the vertical displacements of these bench-marks due to the different time intervals is concerned, the earth's crust of this part of the levelling route, in its postseismic move-

ments, behaved as if it were a single or united block.

Another example of a coalesced block is shown by the crustal deformation in the region where are B.M. 110·8 to 110·2. This region is presumed to be a single block, judging from the vertical displacements of triangulation points. But the vertical displacements of bench-marks in it during 1903–1924 show that it may be composed of two blocks, whereas the vertical displacements that occurred during interval 1924–1927 show that they are united. The region, however, seems to have separated again in the deformation that occurred during 1927–1930.

An example of negative correlation between δH_4 and δH_5 is the vertical displacements of bench-marks situated between B.M. 105·4 and 105·1, in which the relation between δH_4 and δH_5 may be given in the form

$$\delta H_5\text{mm.} = -8\text{mm.} - 0{\cdot}7 \times \delta H_4\text{mm.}$$

The region where the above mentioned bench-marks are situated coincides with block 6, previously determined, the boundaries of which are marked by arrows in Fig. 25.

The block movements were thus still going on in the crustal deformation of the later periods that followed the great disturbance, due to acute crustal movements associated with the destructive earthquake of 1923. In several cases during the later period however, the crustal blocks apparently behaved as if they were adhering to or had coalesced with the adjoining blocks.

If these blocks had really united, it may be possible to express this fact of union in terms of degree of disturbance in the earth's crust for the corresponding time interval, though to do so may not be an easy task. In the following pages, therefore, the time variations of the degree of crustal deformations are discussed.

In order to express the degree of disturbance in the earth's crust, attempts were at first made to investigate statistically the distribution of the absolute values of gradients of the rates of vertical displacements along these levelling routes.

In Fig. 27 are plotted the frequencies of the absolute values of $\Delta\left(\frac{\delta H}{\delta t}\right)$, that is the gradients of the rates of vertical dispalcements of benchmarks between Aburatubo and Takanawa-kita-mati. It might be expected that where the earth's crust had only been slightly deformed, the curve would lie very close to the axis of the ordinates, thus showing the usual frequency distribution of errors of measurements. If, on the

other-hand, the earth's crust was much disturbed, the frequency curves

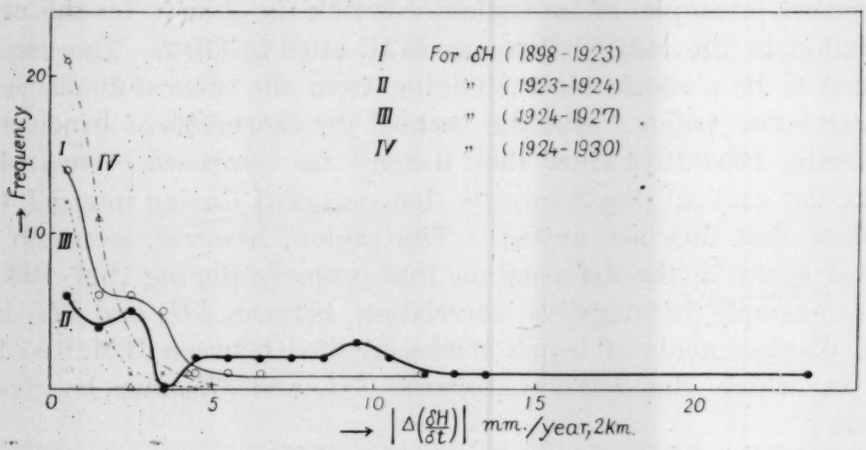

Fig. 27. Frequency of $\left|\Delta\left(\frac{\delta H}{\delta H}\right)\right|$ along the route.

of the absolute values of $\left|\Delta\left(\frac{\delta H}{\delta t}\right)\right|$ may be expected to be flattened and to deviate considerably from the theoretical curve representing the frequency distribution of errors. In Fig. 27, curve I, showing the the frequency distribution of $\left|\Delta\left(\frac{\delta H}{\delta t}\right)\right|$ for the interval 1895–1923 is much more flattened than those for the later intervals, if we except the curve for the interval 1923–1927. The flatness of curve I may be due mainly to the disturbance associated with the destructive earthquake of 1923. Curve II in Fig. 27, which is the frequency curve of $\left|\Delta\left(\frac{\delta H}{\delta t}\right)\right|$ for the interval 1923–1927, is more flattened than curve I. This fact may show, on one hand, that crustal deformation had continued for quite a long while after the destructive earthquake, and on the other hand, that the crustal deformation for interval 1895–1923 may include those due to chronic earth movements.

Another possibility in connection with the foregoing facts is that the crustal deformation due to movements tending to counterbalance the disturbances associated with the destructive earthquake has been going on in the post-seismic periods, with loosneing of the bonds joining adjacent blocks as the result of disturbance due to the acute crustal deformation at the time of the destructive earthquake. The frequency curve showing the gradients of the vertical displacements rates of the bench-marks lying between Aburatubo and Tokyo are plotted again in

Fig. 28, their signs being taken into account. The result in Fig. 28 shows that the frequency maximum has deviated a little to the negative side and that the negative side of the slope of the curve, representing the vertical displacements during the interval 1923–1927, is gentler compared with a similar curve obtained for the vertical displacements of the same bench-marks during the interval 1895–1923.

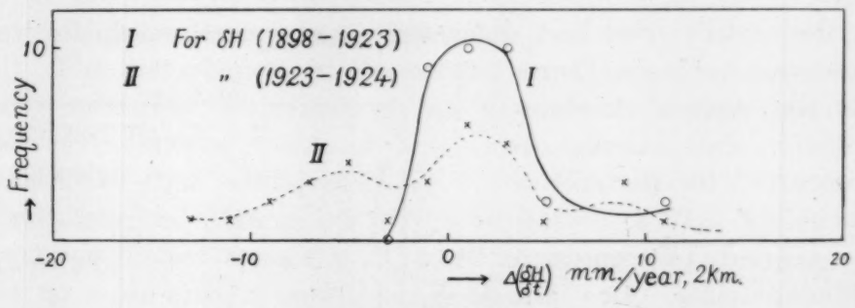

Fig. 28. Frequency of $\Delta\left(\frac{\delta H}{\delta H}\right)$ along the route between Aburatubo and Tokyo.

Curves showing the frequency distribution of $\left|\Delta\left(\frac{\delta H}{\delta t}\right)\right|$ for vertical displacements of bench-marks on the lines of levels from Hudisawa to Atami and from Hatiôzi to Sasako are shown in Figs. 29 and 30 respectively.

In Fig. 29, the curves corresponding to the vertical displacements for the interval, including the destructive earthquake of 1923, is for obvious reasons flat when compared with curves for later intervals.

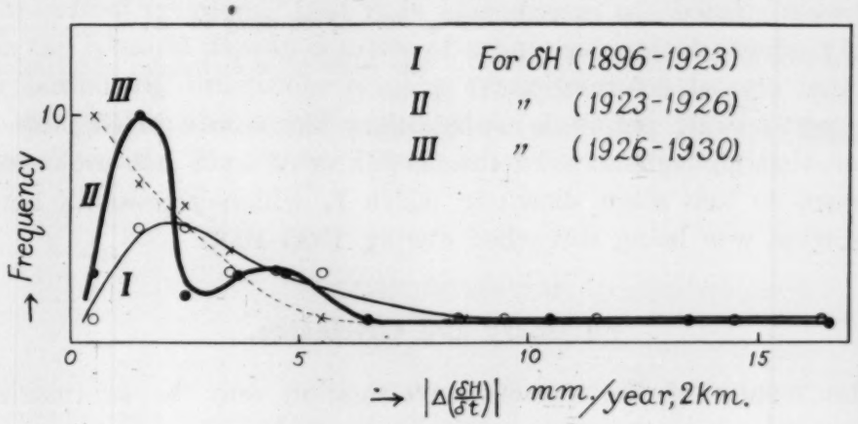

Fig. 29. Frequency of $\left|\Delta\left(\frac{\delta H}{\delta H}\right)\right|$ along the route between Atami and Hudisawa.

In Fig. 30, curve I represents the vertical displacements that occurred during the interval 1895–1903. During this interval no destructive earthquake had occurred in the neighbourhood of this district that might have been accompanied by conspicuous crustal deformations, hence Curve I is very close to the axis of ordinates. The crustal deformation during this time interval was consequently very slight. In comparison with Curve I, Curves II, III and IV are much more flattened, that is, the earth's crust had deformed much more markedly in the later intervals. Curve II represents the vertical displacements during that interval in which occurred the destructive earthquake of 1923, while curves III and IV represent the displacements for the post-seismic periods. Curve III is somewhat flatter than curve IV, whereas curve IV more or less resembles curve I. The case of curve III is similar to that of the vertical displacements of the bench-marks on the route from Aburatubo to Tokyo. The tendency of curve III to change in the post-seismic period to curve IV may show to a certain extent that crustal deformation in the post-seismic period is subsiding. The curves in Fig. 29 show however that disturbances in the earth's crust have not yet ceased by any means to that stage shown in curve I, which represents how the earth's crust was being disturbed during 1895–1903.

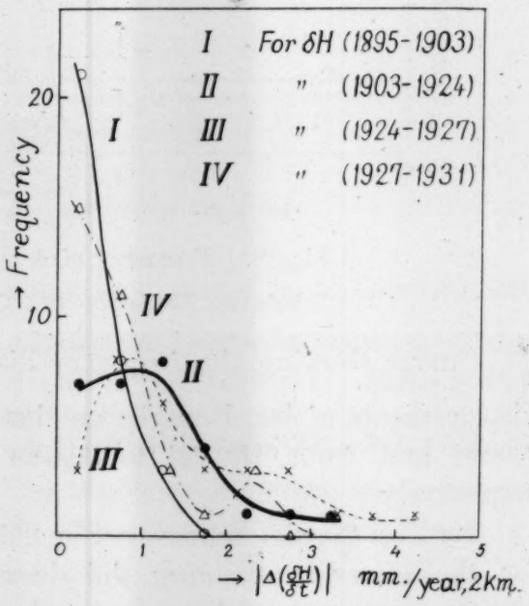

Fig. 30. Frequency of $\left|\Delta\left(\frac{\delta H}{\delta t}\right)\right|$ along the route between Sasako and Hatiozi.

Summary and Conclusion.

The results of the present investigation may be summarized as follows:

i) The approximate sizes of the crustal blocks are determined together with the magnitudes and the azimuths of their tilts. The

earth's crust in the SW Kwantô is believed to consist of these blocks.

ii) The horizontal deformations within each of these blocks are calculated by using data relating to the horizontal displacements of secondary and tertiary triangulation points. In several of these blocks, the horizontal deformations thus calculated greatly exceed magnitude 10^{-4}, whence it is suggested that the primary crustal blocks, as deduced from the data of vertical displacements of triangulation points, may be composed of several secondary blocks.

iii) The disturbances in the earth's crust as a whole seem to have gradually subsided. Evidences of this to a certain extent may be seen in the vertical displacements of bench-marks that were measured after the destructive 1923 earthquake.

The horizontal dimensions of the crustal blocks are about 10 km., as may be estimated from Fig. 3, while those of the secondary blocks may be no more than 2 or 3 kilometres.

In the previous investigation of crustal deformation in Honzyô and Hukagawa, Tokyo,[24] where the bench-marks are more packed together, we notice some tilted blocks with horizontal dimensions of 2 or 3 kilometres.

Thus, from data relating to vertical displacements of triangulation points and bench-marks, we find the existence of crustal blocks with horizontal dimensions of from 10 to 1 km.

The possible block structure of the earth's crust in the Kwantô district and its significance was discussed by Prof. T. Terada[25] from his study on the propagation of seismic waves.

The writer concludes that it is plausible to assume that the earth's crust in the Kwantô district consists of a large number of crustal blocks, having horizontal dimensions ranging from 10 to 1 km.

In conclusion, the writer wishes to express his sincere thanks to Professor Torahiko Terada for his kind advice and guidance.

---

24) N. Miyabe, *Prof. Imp. Acad.*, 8 (1932), 417.
Bull. Earthq. Res. Inst., 10 (1932), 844.

25) T. Terada, *Tirigaku-Hyôron*, 1 (1925), 841, (in Japanese)

35. 關東地方に於ける地塊運動

地震研究所 宮部直巳

大正十二年の關東地震後測量された三角點の垂直變動を用ひ，地塊の大體の大いさ，傾斜とその方向とを定めてみると，相模野を中心とする關東地方西南部は大體第三圖に示すやうな地塊より成ることが知られる．

是等の各地塊の中での水平の變形を，各三角點の水平移動量を用ゐて計算してみると多くは 10^{-5} 乃至 10^{-4} の程度の大いさとなる．併し中には非常に大なるものもあり．地塊内に於いて單に一樣な變形をなしたものとは考へられないやうな場合もある．是等の事實はさきに定められた地塊が，更に多くの小地塊より成ると考へるのに都合がよいやうに思はれる．

地震後數回行はれた水準測量の結果についても尙，地塊運動の痕跡が認められる．

關東地方の地殻が多くの地塊より成るといふことは，既に寺田教授によつても論ぜられた所であるが本研究の結果によつても大體水平方向に數粁乃至十粁程の擴がりを有する地殻より成ると考へて差支ないやうである．

34. *Earth-tilts observed at Mt. Tukuba, Japan.*

By Win INOUYE,

Earthquake Research Institute.

(Read June 20, 1933.- Received Sept. 20, 1933.)

1. Introduction. In his previous note[1] the author reported the earth-tilts that were observed at Mt. Tukuba during the three years and nine months from December 23, 1927, to September 30, 1931, of which this note is a continuation. It deals mostly with observations made between the last-mentioned date and April 9, this year.

The observations were made by a pair of Ishimoto all-silica tiltmeters, installed in a room of uniform temperature built on solid granite foundation. As the period of each horizontal pendulum was adjusted to fifteen seconds, a deflection of 1 cm on a photographic record corresponds to a tilt of 1 second of arc.

The earth-tilts were separated into two kinds, those that fluctuated in a period of about one or two weeks and those that did so in longer periods, the same as was done in the previous note. The variations in the air temperature at Mt. Tukuba were also divided into two kinds, the short and the long period, in the same way as in the previous note.

2. Short period fluctuations. The two components of the short period fluctuations in the earth-tilts and also the short period fluctuations in the air temperature for the period now under consideration are shown in Fig. 1.

As pointed out in the previous note, it will be seen from the figure that the fluctuations of each component of the tilts fairly resemble those of the air temperature. To illustrate this, the relation between the two phenomena during Sept. 11 to Oct. 11, 1931, are shown in Figs. 2 and 3. In these figures the abcissae represent the air temperatures and the corresponding ordinates the components of the earthtilts. As will be seen from these figures, these relations are rather complicated.

The vectors representing the resultants of the short period fluctuations of the tilts are also very complicated. Witness the vector diagrams

1) W. INOUYE, *Bull. Earthq. Res. Inst.*, **10** (1932), 130.

Air Temperature
5°
4
3
2
1
0
9·7
10·1
10·7
11·1
11·7
12·1
12·7
1·1
1·7
2·1
2·7
3·1
3·7
4·1
4·7
5·1
5·7
6·1
6·7
7·1
7·7
8·1
8·7
9·1
9·7
10·1
10·7
11·1
11·7
12·1
12·7
1·1
1·7
2·1
2·7
3·1
3·7
4·1
Earth-tilts
N.W.
S.E.
S.W.
N.E.

Fig. 1.

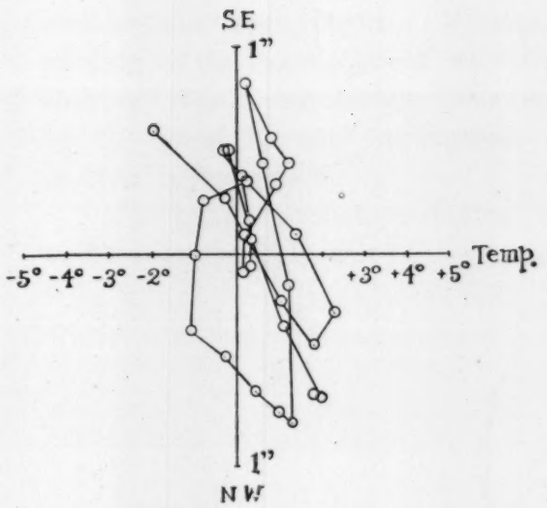

Fig. 2.

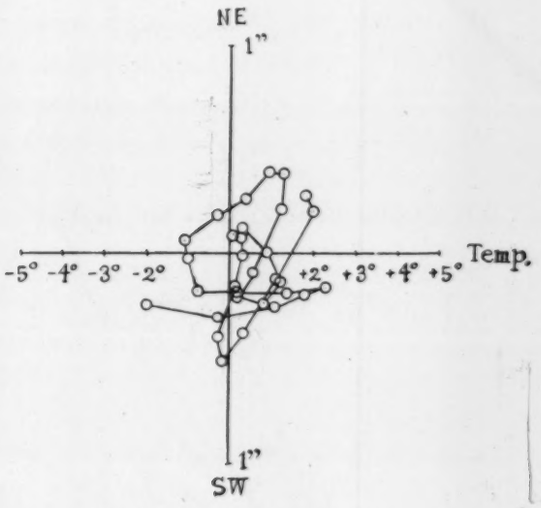

Fig. 3.

representing the earth-tilts during the periods from Sept. 7 to Oct. 13 and from Oct. 13 to Nov. 30, 1931, illustrated in Figs. 4 and 5.

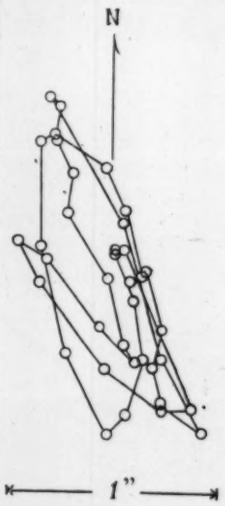

Fig. 4.

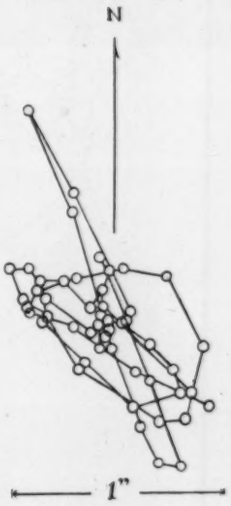

Fig. 5.

3. Secular and seasonal variations. The slow variations in the earth-tilts expressed in two components (as in the previous note) and those in the air temperature are shown in Fig. 6. From the resultant of the two component earth-tilts, a vector diagram was obtained as illustrated in Fig. 7. As stated in the previous note, it will be seen from these figures, that the earth-tilts exhibit secular and seasonal variations, both of which were disturbed several times by tilt-storms.

We notice further that these variations lessen with time since these

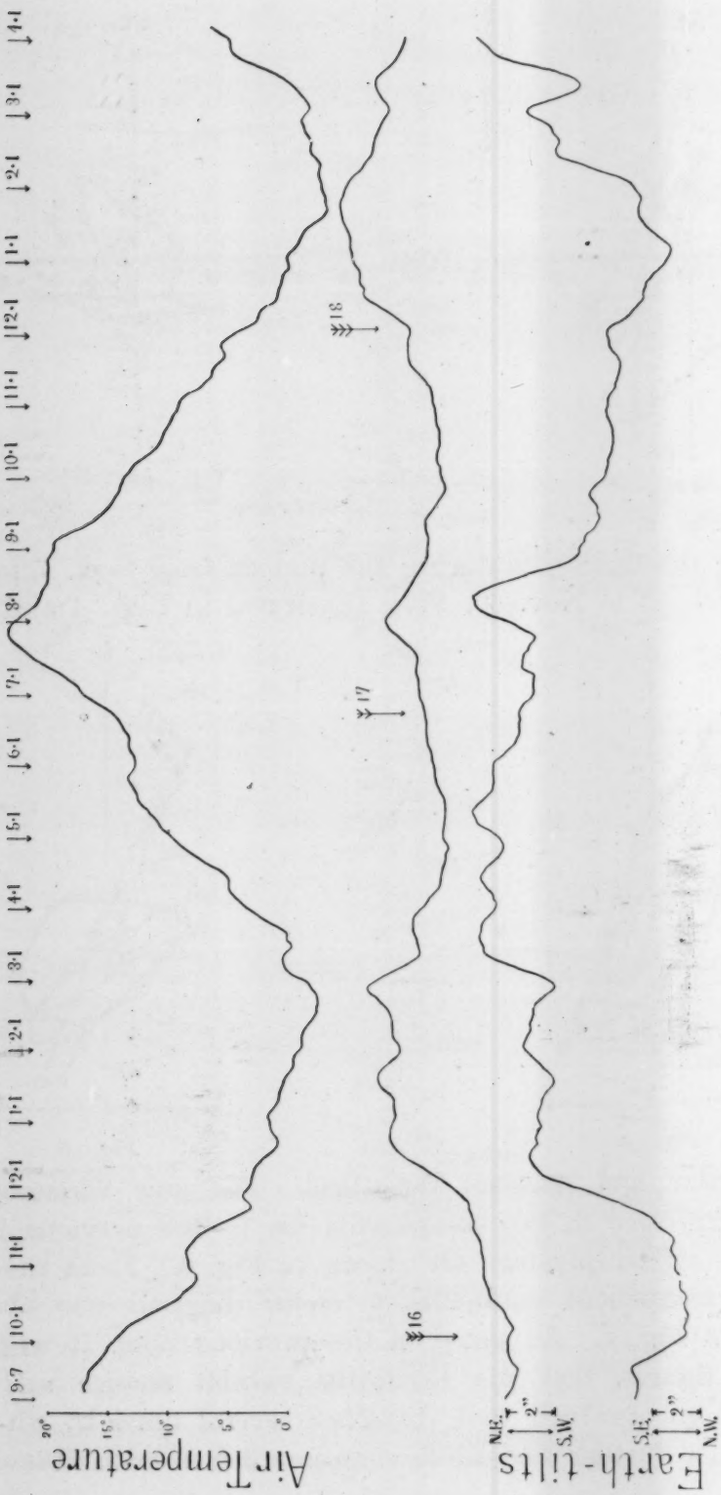
Air Temperature
20°
15°
10°
5°
0°
9·7
10·0
10·1
11·1
12·1
11·1
10·1
9·1
8·1
7·1
6·1
5·1
4·1
3·1
2·1
1·1
12·1
11·1
10·1
9·1
8·1
7·1
6·1
5·1
4·1
3·1
2·1
1·1
16
17
18
Earth-tilts
N.E.
2"
S.W.
S.E.
2"
N.W.

Fig. 6.

observations were begun. Whether these phenomena are caused by settling of the foundation on which the instruments are set up or whether they are due to secular recovery of the earth's crust since its disturbance by the great Kwantô earthquake of Sept. 1, 1923, is a problem for further investigation.

The secular variation during the period of observation amounted to 21 seconds, N.E.-wards.

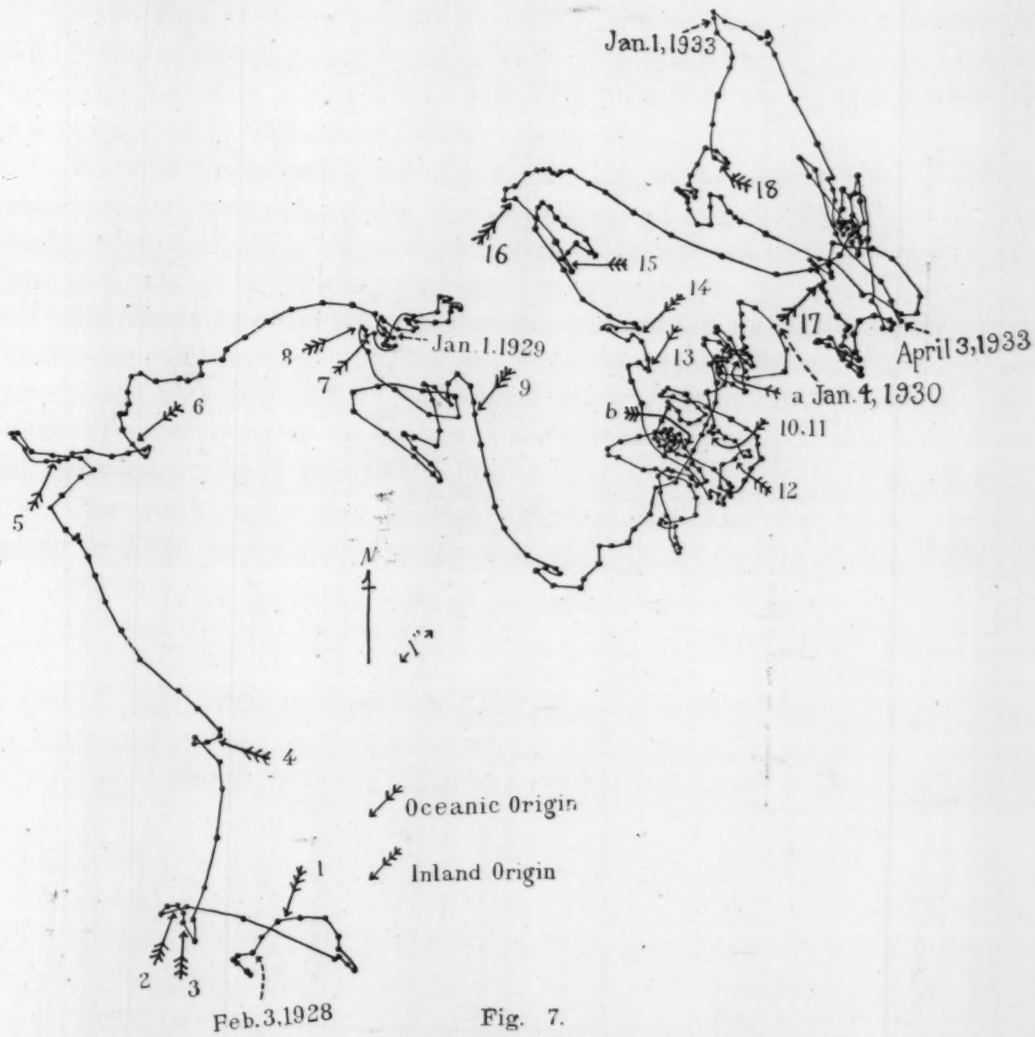

Fig. 7.

4. Earth-tilts and earthquakes. As already stated, the secular changes in the earth-tilts frequently underwent irregular fluctuations of fairly long periods. These fluctuations of earth-tilt may be called "tilt-storms".

With only one exception, the periods of these tilt-storms usually lasted from one to four months. The exceptional period lasted fifteen months, from Dec. 3, 1929 to Feb. 28, 1931.

Excluding the last-mentioned exceptional period, the author tried to find some possible relation between the earth-tilts and the moderate

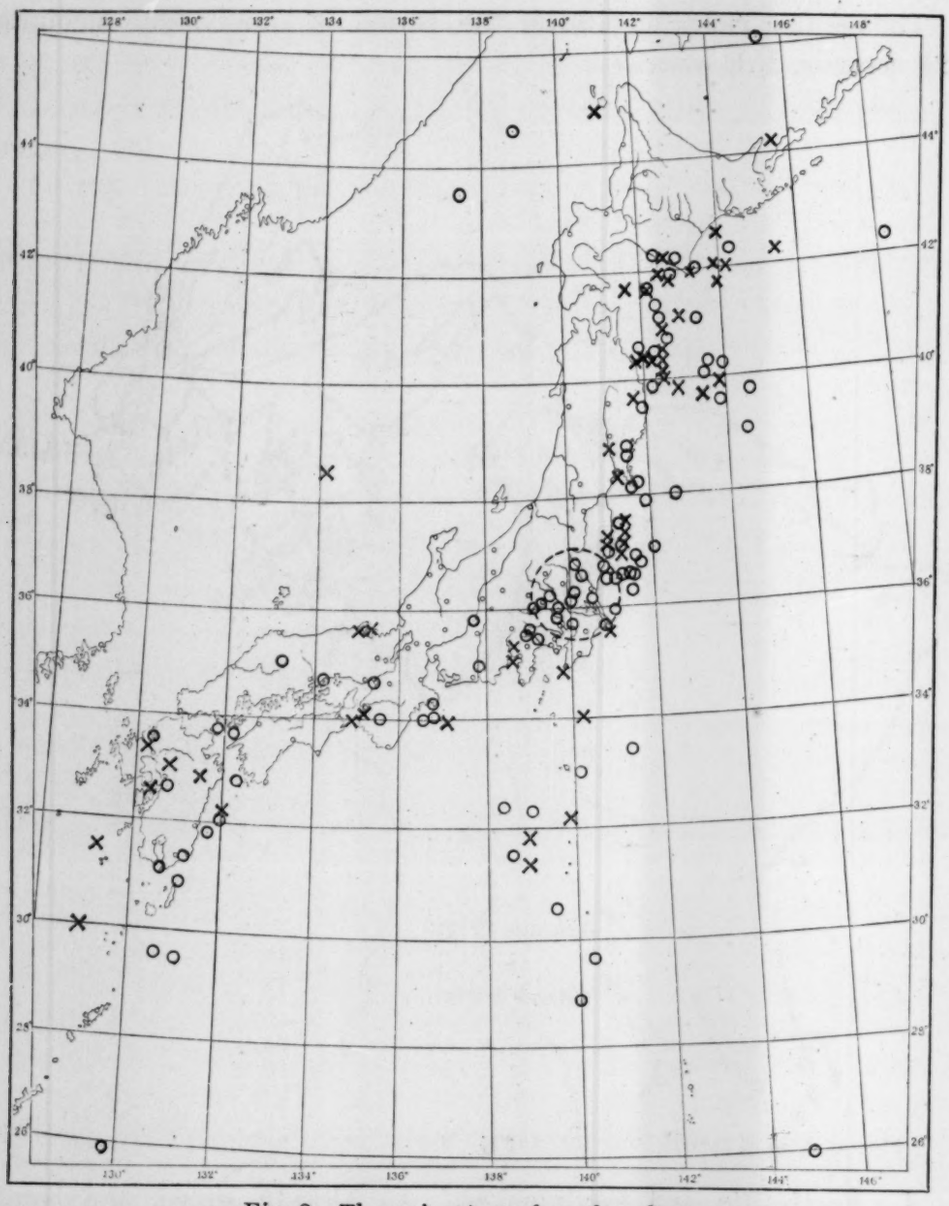

Fig. 8. The epicenters of earthquakes.

○....Those that occurred during the periods of tilt-storms, and
×... those that occurred during the periods without them.
The larger circle has its center at Mt. Tukuba, the radius being 90 km.

earthquakes that originated in and about the main island of Japan. These earthquakes were divided into two groups according to whether they occurred during the periods of tilt-storms or not. The epicenters of these earthquokes, with marks distingushing the two groups, are plotted in Fig. 8.

Now, since the total period of the tilt-storms amounted to about 770 days, while that of the period without them was about 670 days, it follows that if there were no relation connecting the tilt-storms at Mt. Tukuba and the earthquakes that originated in a certain region, these earthquakes might occur with equal probability in the period of tilt-storms as in the other period.

As will be seen in the figure, in the region about Mt. Tukuba earthquakes occurred mostly in the periods of tilt-storms, while in the regions beyond they occurred regardless almost of the tilt-storms at Mt. Tukuba.

To illustrate this, the author has selected the moderate earthquakes that were reported by the Central Meteorological Observatory as having originated within a distance of about 90 km from Mt. Tukuba. The data concerning these earthquakes are given in Table I, and the dates of their occurrences plotted in Fig. 7.

The earthquakes that originated about Mt. Tukuba, at all events, seem to have some definite connection with the tilt-storms at Mt. Tukuba.

Table I.

No.	Date	Time of occurrence	Epicentre	
			λ	φ
		h m	°	°
1	1928 II 12	6 10	140·0	36·1
2	„ III 23	10 21	139·8	36·0
3	„ IV 13	1 36	140·1	36·2
4	„ V 21	1 29	140·1	35·6
5	„ VIII 27	3 11	141·1	36·4
6	„ X 5	15 58	139·6	36·1
7	1929 IV 18	3 33	140·9	36·3
8	„ IV 23	23 16	140·0	36·1
9	„ VIII 16	22 21	140·2	36·5
10	1930 V 1	9 58	140·8	35·7
11	„ V 1	13 20	140·8	35·7
12	„ VI 1	2 58	140·4	36·4
13	1931 VI 9	14 07	140·9	36·5
14	„ VI 17	21 09	139·4	35·6
15	„ IX 21	11 20	139·3	36·0
16	„ X 3	2 36	139·3	36·0
17	1932 VI 22	9 36	141·1	35·9
18	„ XII 2	2 41	140·5	36·4

Table II_1. The Values of the Earth-tilts.

N.E.—S.W. (N.E.—ward is taken positive.) The unit is 0·1 second of arc.

Month / Day	1931 IX	X	XI	XII	Month / Day	1931 IX	X	XI	XII
1	4	0	10	16	16	− 8	6	10	37
2	1	0	10	17	17	− 6	4	11	39
3	1	− 2	10	18	18	− 4	3	12	42
4	1	− 3	10	20	19	− 5	2	13	44
5	1	− 5	9	21	20	− 4	5	16	45
6	0	− 5	6	22	21	− 3	6	18	47
7	0	− 4	8	24	22	− 2	8	17	48
8	1	− 4	10	25	23	− 5	9	14	49
9	1	− 5	10	27	24	− 5	10	10	49
10	2	− 4	10	28	25	− 3	9	15	49
11	2	− 4	10	30	26	− 3	8	12	49
12	− 1	− 1	12	31	27	2	8	13	48
13	− 3	0	11	33	28	4	8	14	49
14	− 9	7	12	34	29	2	10	15	45
15	−10	7	11	35	30	2	9	16	44
					31		9		43

Table II_2. N. E.—S. W.

Month / Day	1932 I	II	III	IV	V	VI	VII	VIII	XI	X	XI	XII
1	43	41	60	36	23	29	32	50	30	24	28	38
2	47	43	58	34	24	27	30	49	30	24	27	38
3	47	43	57	34	23	27	34	47	30	25	27	39
4	47	42	54	32	26	27	36	47	30	26	27	40
5	46	45	48	29	27	27	38	46	30	28	28	39
6	46	45	39	27	28	26	38	45	30	27	28	38
7	46	46	35	26	28	28	36	44	30	26	27	38
8	46	46	33	26	26	32	35	42	30	26	27	38
9	42	49	34	27	23	33	35	41	30	25	30	41
10	42	49	36	28	22	32	34	41	31	26	32	45
11	46	47	38	27	22	32	35	40	31	27	33	49
12	48	49	36	27	21	32	34	39	32	26	31	54
13	47	49	36	26	21	33	34	36	34	25	30	54
14	46	45	31	27	22	33	35	37	32	26	31	54
15	45	43	31	26	22	32	35	38	32	26	33	54
16	44	43	32	24	24	31	35	38	32	26	35	57
17	46	43	34	23	25	30	35	38	31	25	36	60
18	52	44	36	24	24	30	35	38	28	25	38	60
19	58	46	37	24	26	30	35	37	26	25	40	61
20	60	47	36	24	26	31	35	36	25	27	40	60
21	60	48	36	24	26	31	34	35	24	26	42	57
22	58	51	38	25	25	32	34	34	22	25	42	56
23	55	56	38	25	26	33	37	32	21	25	42	56
24	53	55	38	25	26	32	40	31	23	24	40	56
25	51	55	38	22	28	32	43	31	22	25	39	54
26	48	57	41	21	27	33	45	32	23	27	37	55
27	44	58	41	23	29	35	47	31	24	29	32	58
28	40	60	37	23	30	35	49	30	23	30	32	60
29	41	60	34	21	30	34	50	28	24	29	34	59
30	39		36	23	30	32	51	28	24	27	36	59
31	39		36		29		51	30		27		60

Table II_3. N. E.—S. W.

Day \ Month	1933 I	II	III	IV	Day \ Month	1933 I	II	III	IV
1	61	64	44	40	16	64	49	54	
2	61	62	44	40	17	65	49	54	
3	61	61	44	40	18	67	50	50	
4	62	60	44	38	19	67	51	47	
5	63	60	45	37	20	68	50	47	
6	63	61	43	36	21	67	55	45	
7	62	61	44	35	22	67	57	44	
8	61	60	45	35	23	66	54	44	
9	59	57	47	36	24	64	51	43	
10	60	54	47	37	25	63	48	40	
11	61	51	50		26	64	46	39	
12	62	50	53		27	64	46	39	
13	61	51	53		28	65	45	40	
14	60	53	54		29	66		40	
15	62	52	56		30	64		40	
					31	65		40	

Table II_4. S. E.—N. W.

(S. E.—ward is taken positive.)

Day \ Month	1931 IX	X	XI	XII	Day \ Month	1931 XI	X	XI	XII
1	4	−26	−21	8	16	2	−30	−21	37
2	5	−26	−20	13	17	− 1	−24	−19	38
3	4	−25	−15	18	18	1	−21	−17	35
4	2	−20	−17	17	19	− 3	−16	−17	35
5	− 7	−20	−16	22	20	− 5	−20	−14	39
6	− 1	−21	−19	27	21	0	−18	−11	40
7	− 1	−26	−24	31	22	− 1	−26	− 9	40
8	− 5	−32	−23	29	23	− 3	−25	1	38
9	− 2	−27	−22	30	24	− 3	−25	− 3	39
10	−10	−21	−22	30	25	− 3	−23	− 6	39
11	−12	−19	−18	39	26	− 1	−24	− 6	37
12	−10	−18	−14	41	27	−20	−22	− 5	36
13	−10	−18	−13	48	28	−25	−21	− 4	34
14	− 2	−40	−15	47	29	−25	−22	− 2	34
15	3	−33	−22	41	30	−23	−22	3	33
					31		−20		35

Table II_5. S. E.—N. W.

Day \ Month	1932 I	II	III	VI	V	VI	VII	VIII	IX	X	XI	XII
1	37	42	23	53	44	62	45	53	18	7	8	6
2	35	40	23	54	58	54	39	54	11	6	8	6
3	33	42	23	51	53	54	28	55	15	6	2	3
4	34	42	25	50	51	54	29	56	16	12	6	2
5	37	39	29	49	51	52	28	60	17	2	0	3
6	39	41	38	51	53	54	33	55	21	3	1	4
7	38	41	53	53	61	50	34	61	25	5	7	5
8	36	43	62	56	69	43	39	67	24	5	9	1
9	39	38	60	53	67	41	41	63	18	7	3	− 7
10	37	38	59	53	70	42	39	58	11	4	− 1	− 8
11	37	39	59	62	65	42	44	61	13	8	− 2	− 8
12	33	39	60	66	67	43	41	65	11	6	4	−14
13	28	38	51	61	64	39	39	66	0	5	4	−10
14	29	39	61	61	64	43	41	60	− 5	5	2	−11
15	29	37	56	63	59	37	46	61	− 4	7	1	− 8
16	32	33	57	57	59	44	51	66	3	5	0	− 7
17	32	39	59	58	62	46	51	59	8	0	− 1	− 8
18	29	39	56	65	55	47	41	54	15	0	− 3	− 8
19	27	39	56	59	51	44	34	48	16	3	− 2	− 9
20	32	40	62	51	53	43	35	41	18	0	4	− 9
21	30	38	61	50	53	46	36	36	19	4	2	− 4
22	27	36	61	48	53	43	38	36	22	6	3	− 6
23	30	34	62	52	56	43	33	28	19	5	1	− 7
24	29	38	66	52	52	42	33	25	11	4	2	−14
25	28	38	65	49	51	38	34	20	11	6	3	−14
26	31	30	58	52	53	38	36	26	5	7	2	−12
27	33	22	53	50	49	39	37	24	10	7	12	−13
28	43	23	55	48	55	43	39	22	12	6	14	−15
29	45	24	55	43	58	47	37	14	9	8	12	−12
30	45		54	50	53	42	36	12	10	10	7	−15
31	44		55		59		44	12		9		−23

Table II_6. S. E.—N. W.

Day \ Month	1933 I	II	III	VI	Day \ Month	1933 I	II	III	IV
1	−27	− 5	43	55	16	− 3	39	3	
2	−25	− 2	45	55	17	− 2	39	7	
3	−25	0	42	55	18	− 7	39	19	
4	−18	2	40	62	19	− 6	25	27	
5	−19	1	39	56	20	− 7	12	37	
6	−19	0	43	59	21	− 5	11	37	
7	−21	− 2	35	65	22	− 6	8	48	
8	−20	3	40	66	23	− 9	15	47	
9	−16	17	29	64	24	−11	24	47	
10	−16	21	28	64	25	− 6	30	51	
11	−15	31	16		26	−10	37	51	
12	−17	35	8		27	− 8	38	49	
13	−12	27	10		28	− 8	42	51	
14	−11	25	0		29	− 9		57	
15	− 7	32	− 3		30	−10		61	
					31	− 9		60	

34. 筑波山に於ける傾斜變化觀測報告

地震研究所　井　上　宇　胤

筑波山に於ては，昭和三年一月から地表面の傾斜變化觀測が行はれて居るが，昭和六年十一月迄の觀測結果の報告は前の論文に掲載して置きましたから，此處では主にそれ以後昭和八年四月上旬迄の結果を取扱つてあります．觀測結果の取扱方及び其れから得られた結果は殆ど前報告と同樣であります．

日本各地に發生した地震を筑波山に於ける傾斜嵐の時期に發生したものと，然らざるものとに分けて見ると，少くとも筑波山附近の地震は明かに傾斜嵐に關係ある事を知りました．

35. *On Barometric Gradients at Times of Earthquakes, in Japan (2nd paper).*

By Win Inouye and Yoshi Inaba,

Earthquake Research Institute.

(Read Dec. 20, 1932.—Received Sept. 20, 1933.)

1. Introduction.

In an earlier note,[1] one of the authors discussed the question of barometric gradients at times of earthquakes, in Japan, for which purpose Japan was divided into eleven regions. Earthquakes of the Kwantô district were however excluded, because of the too complicated nature of the geotectonic structure of the Kwantô, compared with the somewhat necessarily rough and ready character of the investigation.

In attacking the problem for the second time, we included the Kwantô earthquakes with the primary object of confirming one of the results obtained in our previous studies, namely,—"The azimuthal distribution of barometric gradients at times of earthquakes that have originated in a certain region differed from time to time. This phenomenon seems to have some correlation with the occurrence of severe earthquakes in or about that particular district."

For our data we used the earthquakes listed in the Table[2] of Japanese strong earthquakes, edited since 1912 by T. Ishikawa of the Central Meteorological Observatory, Tokyo. We took from the monthly report of the Central Meteorological Observatory, barometric pressures of the hours nearest to those of the earthquakes from three neighbouring meteorological stations, each station forming the vertex of a right-angled triangle, and then found the barometric gradient by combining a properly selected pair of differences of barometric pressures.

2. We shall, first of all, examine some examples taken from the previous investigation.

a) The first example is the barometric gradients at times of earthquakes that originated in the Iwaki Sea.

We divided the whole period into three, the early the middle, and

1) W. Inouye, *Bull. Earthq. Res. Inst.*, 10 (1932), 55.

2) *Kensin-dihô*, 2 (1926).

the last. The barometric gradients at times of earthquakes, treated separately in three periods, are shown respectively in Figs 1, 2, and 3.

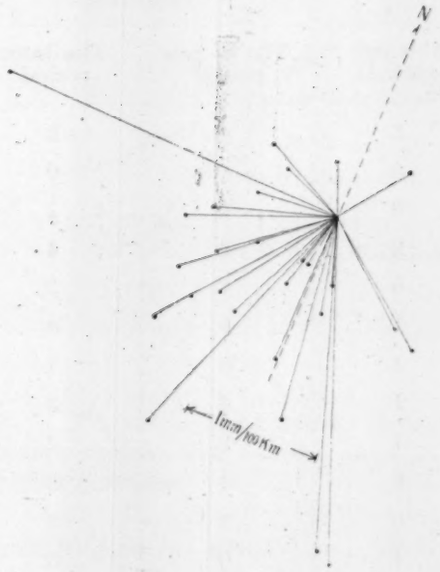

Fig. 1. The barometric gradients in the early period. The vectors point to higher pressures.

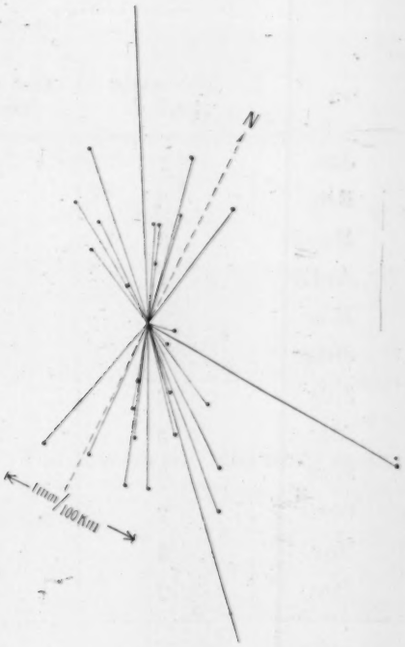

Fig. 2. The barometric gradients in the middle period. The vectors point to higher pressures.

The barometric gradients of the early period, namely, since the beginning of the period to Aug. 28, 1916, diverged a good deal, although they had a tendency to be directed S. W.-ward. Contrary to this, however, during the period between the occurrence of the fairly strong earthquake of Aug. 28, 1916, that originated in the same district and that of the great Kwantô earthquake of Sept. 1, 1923, the barometric gradients were directed towards comparatively narrow sectors, N. W.-ward and S. E.-ward. In the last period, after the great Kwantô earthquake, the barometric gradients dispersed again as in the early period.

From the monthly earthquake frequencies for each period listed in Table I, we

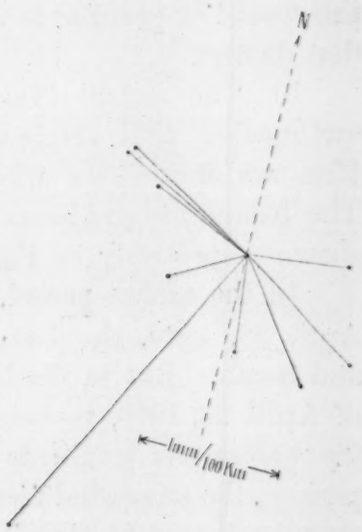

Fig. 3. The barometric gradients in the last period. The vectors point to higher pressures.

Table I.

	The Iwaki Sea.			The South-Eastern Sea of Hokkaidô.	
	The early period.	The middle period.	The last period.	The earlier period.	The later period.
Jan.	1	4	2	4	2
Feb.	3	7	0	4	0
March	3	0	0	7	1
April	1	3	2	2	4
May	1	3	0	2	3
June	4	5	1	0	6
July	3	1	1	5	1
Aug.	3	0	1	4	3
Sept.	0	3	1	3	4
Oct.	2	0	0	1	3
Nov.	3	1	0	1	2
Dec.	2	2	1	0	3

notice that they are fairly dispersed in time, so that the differences in the general features of the barometric gradients at times of earthquakes in each period may not be due to any particular seasonal characteristic that would be peculiar to the barometric gradients at ordinary times over that district.

b) The second example is the barometric gradients at times of earthquakes that originated in the South-Western sea of Hokkaidô. Here we divided the whole period into two, the earlier and the later. The barometric gradients at times of earthquakes in the two periods are shown respectively in Figs. 4 and 5.

In the earlier period, that is, since the beginning of the period to April 23, 1920, the barometric gradients were mostly directed North and South. But in the later period, that is, since the severe earthquake of April 23, 1920, that occurred in the district to the end of the period, the barometric gradients were directed South ward. To enable comparison, the azimuthal frequencies of the barometric gradients that existed over the district at six o'clock every morning for the period of one year, beginning April 1, 1928, are shown in Fig. 6. As will be seen from the figure, the barometric gradients at ordinary times dispersed fairly

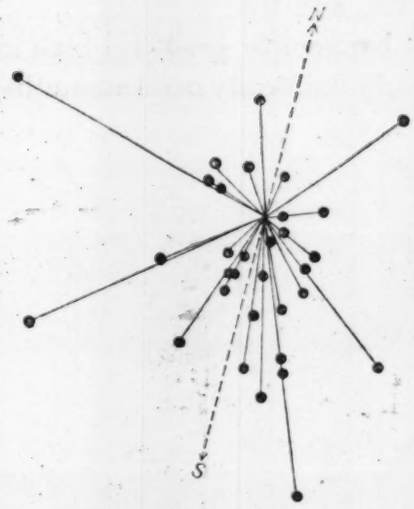

Fig. 4. The barometric gradients in the earlier period. The vectors point to higher pressures.

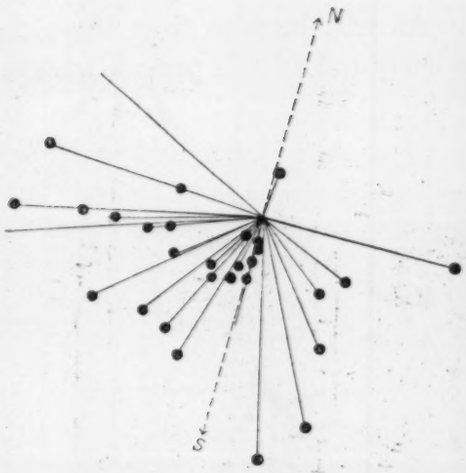

Fig. 5. The barometric gradients in the later period. The vectors point to higher pressures.

uniformly in all azimuths. Moreover, the monthly earthquake frequencies for each period are given in Table I, from which it will be seen that the frequencies underwent no important seasonal fluctuations.

3. We shall next consider the barometric gradients at the times when the earthquakes originated in the Kwantô district.

To find the barometric gradients over this district the barometric pressures at Tokyo, Mito, and Maebasi were used. In this case, considering the time of occurrence of the great Kwantô earthquake, we divided the whole period into three, the early (since the beginning of 1912 to the end of 1916), the middle (since the beginning of 1917 to Sept. 30, 1923) and the last (since Oct. 1, 1923 to the end of 1925). We further subdivided each period into warm and cold.

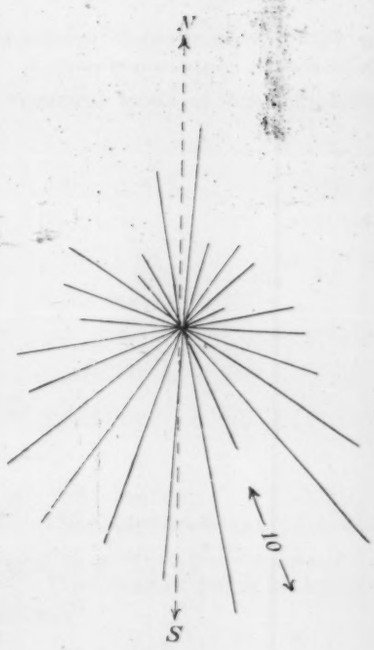

Fig. 6.

The barometric gradients at times of earthquakes in the three periods, the season of each of which have been divided into warm and

cold, are shown in Figs. 7 a, 7 b, 8 a, 8 b, 9 a, and 9 b.

As will be seen from these figures, the barometric gradients both in the early and middle periods were scattered fairly uniformly in all azimuths,

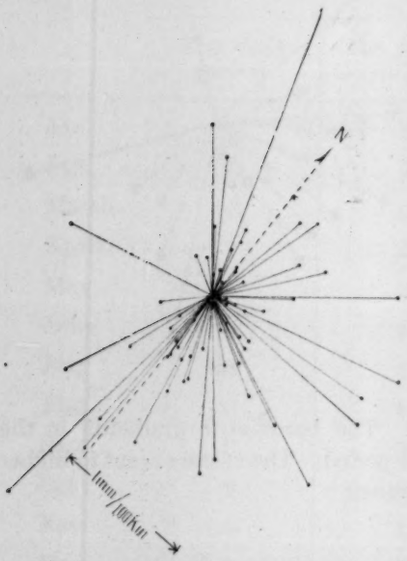

Fig. 7a. The barometric gradients in cold season of the early period. The vectors point to lower pressures.

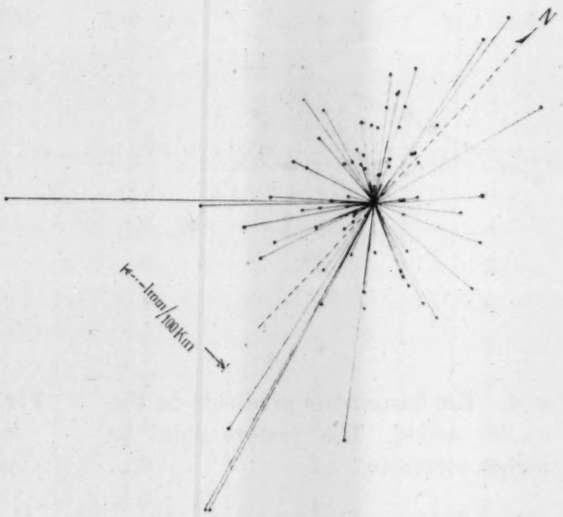

Fig. 7b. The barometric gradients in warm season of the early period. The vectors were directed to lower pressures.

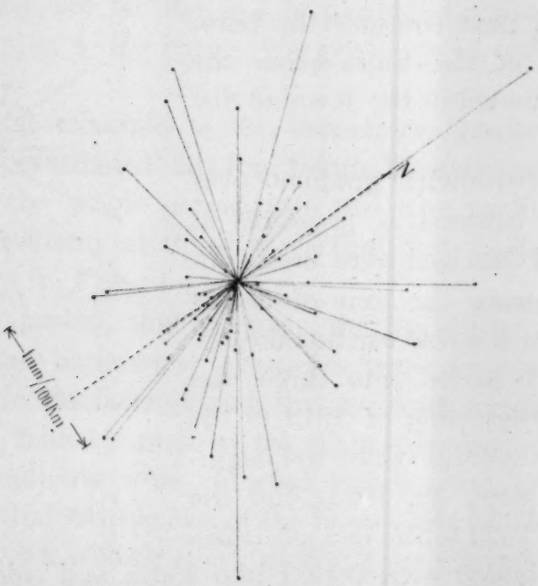

Fig. 8a. The barometric gradients in cold season of the middle period. The vectors point to lower pressures.

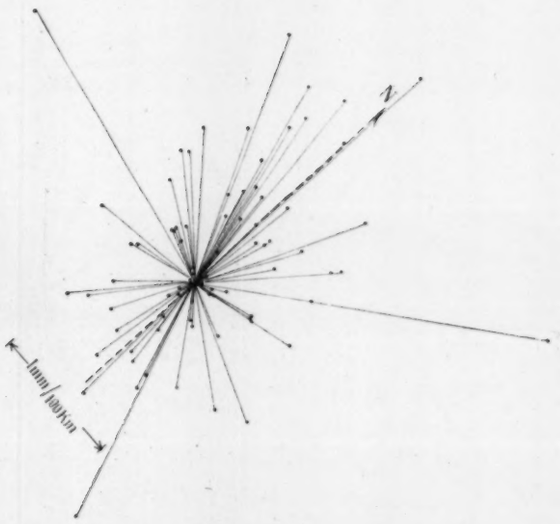

Fig. 8b. The barometric gradients in the warm season of the middle period. The vectors point to lower pressures.

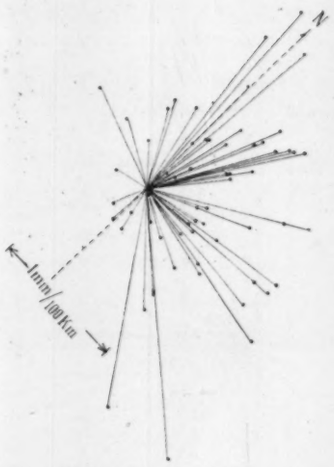

Fig. 9a. The barometric gradients in the cold season of the last period. The vectors point to lower pressures.

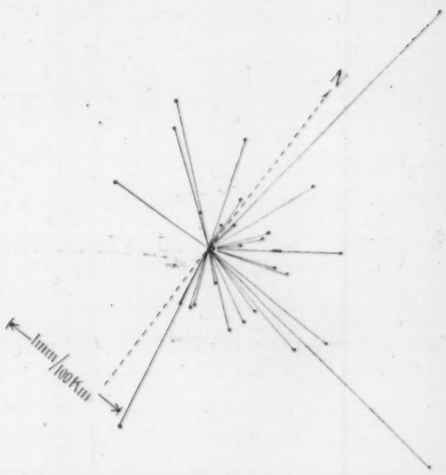

Fig. 9b. The barometric gradients in the warm season of the last period. The vectors point to lower pressures.

while those in the last period were somewhat polarized. For reference, the barometric gradients at 6 a.m. and 6 p.m. for every day during 1929 are shown respectively in Figs. 10, 11, 12, and 13.

Next, the vectors representing barometric gradients at times of earthquakes were plotted at the epicenters of the corresponding earth-

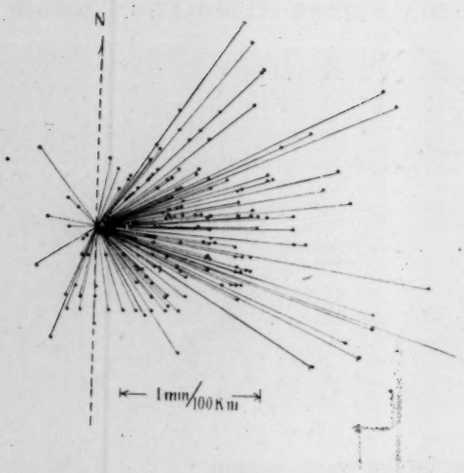

Fig. 10. The barometric gradients in Winter. The vectors point to lower pressures.

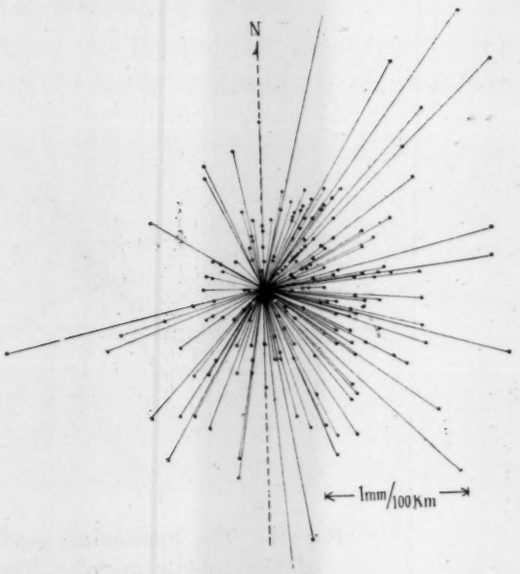

Fig. 11. The barometric gradients in Spring. The vectors point to lower pressures.

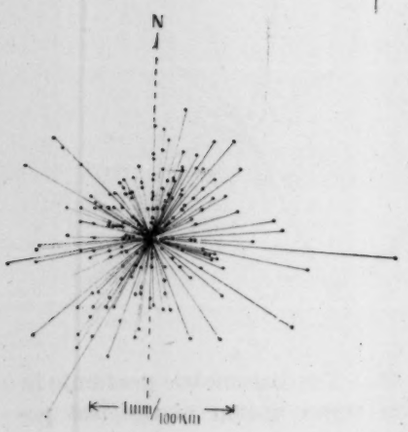

Fig. 12. The barometric gradients in Summer. The vectors point to lower pressures.

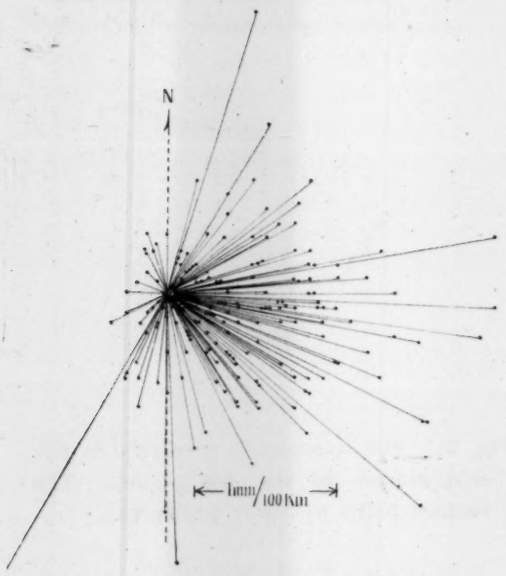

Fig. 13. The barometric gradients in Autumn. The vectors point to lower pressures.

quakes. These are shown in Figs. 14, 15, and 16, the three periods being considered separately.

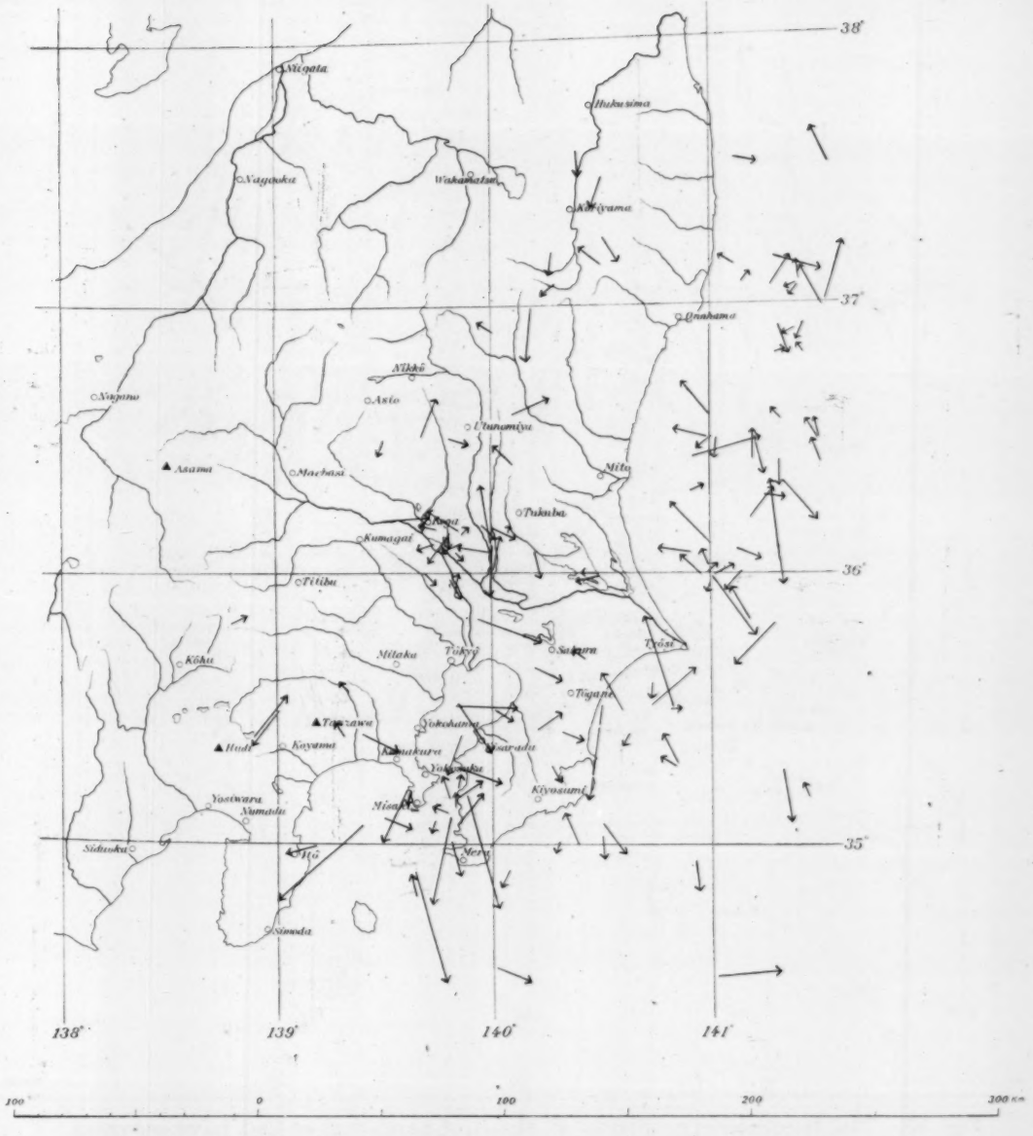

Fig. 14. The barometric gradients at times of earthquakes that have occurred in the early period. The vectors point to lower pressures.

As will be seen from these figures, the vectors in the early and middle periods were directed almost haphazardly, whereas among vectors of the last period we see something approaching systematic distribution.

4. The order of magnitude of the barometric gradients in question is 1 mm in mercury per 100 km. It is highly questionable whether the

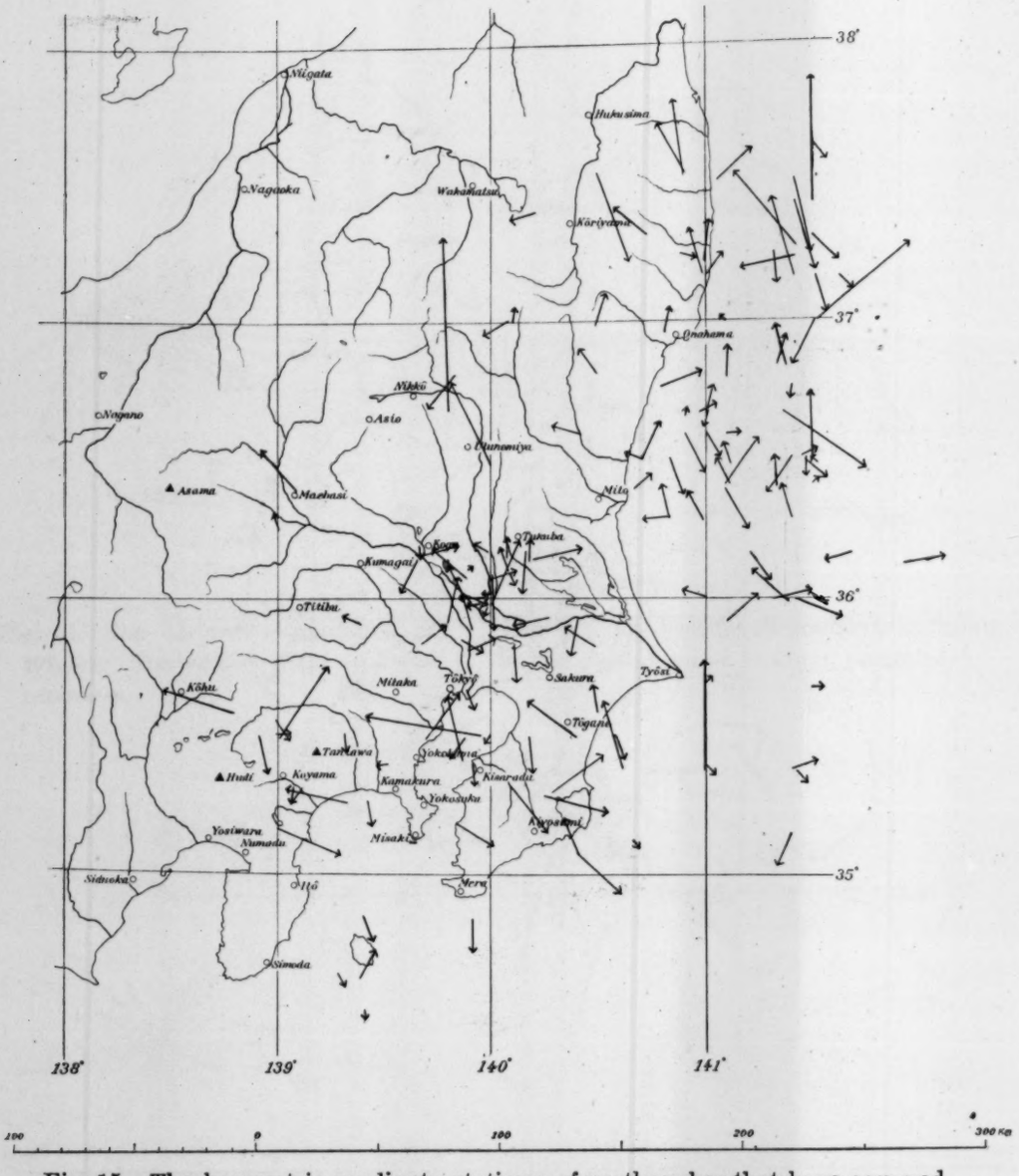

Fig. 15. The barometric gradients at times of earthquakes that have occurred in the middle period. The vectors point to lower pressures.

barometric gradient at times of earthquakes really do act as a secondary cause of the earthquake.

It may be suggested at all events that when a severe earthquake originate in a certain district, the barometric gradients at times of earthquakes which occurred in or neighbourhood that district may differ in its general features according to whether it is before or after the severe earthquake.

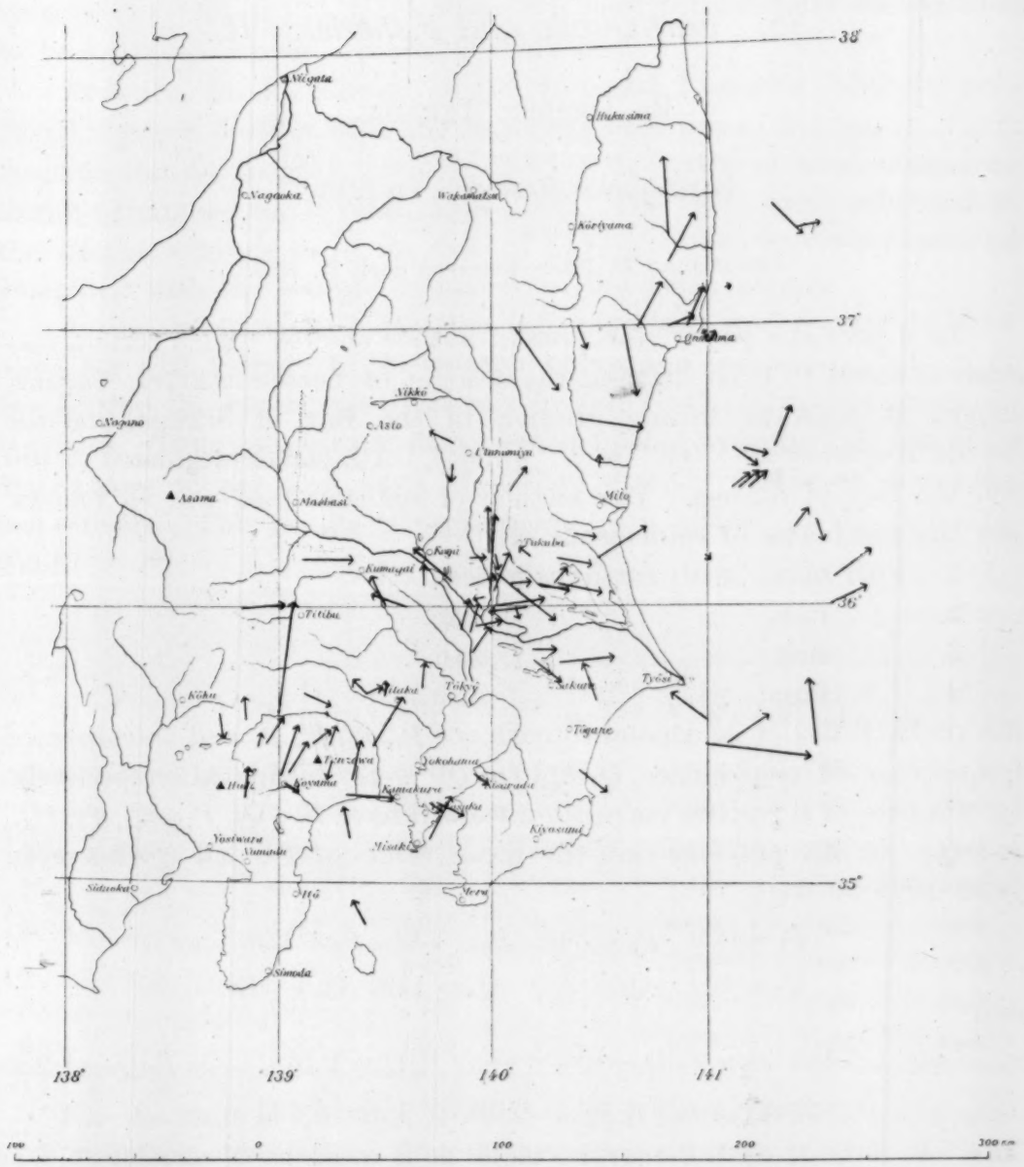

Fig. 16. The barometric gradients at times of earthquakes that have occurred in the last period. The vectors point to lower pressures.

35. 地震發生前の氣壓勾配に就いて（第二報）

地震研究所 { 井上宇胤 / 稻葉佳

本邦の二三の地方に於ける地震發生前の氣壓勾配の大勢が，其の地方或は附近に發生した大地震に前後して變化した事を調査してあります．

36. *Earthquake and Fisheries. II.*

By Torahiko TERADA,

Earthquake Research Institute.

(Read June 20, 1933.—Received Sept. 19, 1933.)

In a previous paper[1] the present author showed that a certain correlation seems to exist between the amount of horse-mackerel, *Caranx*, caught at Sigedera fishing ground, in the Bay of Suruga, and the decade frequency of "felt" and "unfelt" earthquakes originated in Idu and the Bay of Suruga. The method of statistics used was as follows. For the four cases of coincidence of

1. Fish max. with earthquake max.
2. „ min. „ „ min.
3. „ max. „ „ min.
4. „ min. „ „ max.

the probabilities of accidental coincidence P_1, P_2, P_3, P_4 and the observed frequencies of coincidence Q_1, Q_2, Q_3, Q_4 were calculated respectively. In the case of a positive correlation we will have $P_1<Q_1$, $P_2<Q_2$, $P_3>Q_3$, $P_4>Q_4$. In the previous case the mean values of P's and Q's for seven years 1924–30 were

$$P_1=\cdot059 \quad P_2=\cdot340 \quad P_3=\cdot139 \quad P_4=\cdot139$$
$$Q_1=\cdot081 \quad Q_2=\cdot359 \quad Q_3=\cdot119 \quad Q_4=\cdot113$$

and

$$r_1=P_1/Q_1=\cdot7285 \quad r_2=P_2/Q_2=\cdot9472 \quad r_3=P_3/Q_3=1\cdot168 \quad r_4=P_4/Q_4=1\cdot230$$
$$R=(r_1+r_2)/(r_3+r_4)=0\cdot6985 \quad 1/R=1\cdot432.$$

The last ratio R or $1/R$ may be taken as a measure of correlation, i. e.

for a positive correlation $R<1$ or $1/R>1$

for a negative correlation $R>1$ or $1/R<1$.

The criterion for the magnitude of $|1-R|$ or $|1-1/R|$ for ensuring the reality of correlation is at present unknown, but referring to the case of *Caranx* in Sigedera the existence of some real correlation seems to be sufficiently ensured by the remarkable parallelism which exists between the curves for the earthquakes and fishery data. Thus, the

1) T. TERADA, *Proc. Imp. Acad.*, 8 (1932), 83; *Bull. Earthq Res. Inst.*, 10 (1932), 393.

value of $|1-R|$ or $|1-1/R|$ above 0·5 may provisionally be regarded to be an indication of a probable correlation.

Recently, Dr. K. Kimura of the Imperial Fisheries Institute published a paper dealing with the fisheries in the Bay of Suruga, in which is given the th roughly revised data of the catch of *mezi*, immature tunny (*Thunnus*) for 9 years, 1924–1932. The data were subjected to the similar analysis as in the case of *Caranx* in the previous paper and compared with the seismic frequency in the same manner.

As, in the previous paper, the fish curve for *mezi* seemed to show some lag with respect to the seismic curve, the comparison was made by shifting the two curves relatively by different intervals of successive ten days. Thus the seismic data were compared with the fish data of 10 days before, of the same days, of 10 days after,.... and of 60 days after respectively. The results of comparison are shown in the following Table.

Table I.

	$r_1=\frac{P_1}{Q_1}$	$r_2=\frac{P_2}{Q_2}$	$r_3=\frac{P_3}{Q_3}$	$r_4=\frac{P_4}{Q_4}$	$R=\frac{r_1+r_2}{r_3+r_4}$	$\frac{1}{R}=\frac{r_3+r_4}{r_1+r_2}$
10 days before	1·375	0·902	1·067	1·211	1·000	1·000
Corresp. day	1·056	1·095	1·162	0·838	1·076	0·930
10 day after	0·915	1·011	0·935	1·121	0·937	1·067
20 „ „	0·845	0·958	1·238	1·108	0·769	1·301
30 „ „	1·687	1·056	0·777	0·875	1·662	0·602
40 „ „	0·809	0·935	1·088	1·550	0·661	1·513
50 „ „	1·013	1·293	1·038	0·875	1·205	0·830
60 „ „	1·000	1·032	0·946	0·870	1·064	0·894

For the shift of 30 days, R shows a high value of 1·66, i. e. a sensible *negative* correlation. For 20 days and 40 days of shift $R=0·77$ and 0·66 respectively, i. e., suggesting some slight positive correlation. Assuming, however, the provisional criterion above mentioned, we may say that the influence of earthquakes upon *mezi* fishery lags after the earthquakes by about one month and appears as a negative effect in diminishing the amount of catch of this kind of fishes.

The relation between earthquakes and fisheries, even if such thing may exist, can by no means be a simple one. Before we may arrive at

1) K. Kimura, *Bull. Jap. Soc. Sci. Fisheries*, 1 (1933), 221.

any reliable conclusion, we must first of all accumulate available data as far as possible. The present note may be of some interest, as affording an example of different cases of similar statistical comparisons, which must be made for preparing the road for a more systematic study.[1)]

The best thanks of the author is due to Dr. K. Kimura for his kindness in placing the valuable data for the author's disposal and also to Mr. Tetu Watanabe for the aid given in the course of the statistical investigation.

---

36. 地震と漁獲（第二報）

地震研究所 寺田寅彦

駿河灣東北部に於ける鰺の漁獲高と同方面に於ける地震頻度との間に若干の正相關あることは既に報告した通である．其の報告中に，メジと地震との關係に就ては，鰺の場合程明瞭でないが，併し地震の效果が數十日おくれて正相關として現はれるらしいといふことを述べて置いた．其後水產試驗場の木村喜之助氏から九年間のメジ漁獲高の詳しい調査材料を示教されたので，其材料に就て前回同樣の統計方法を適用して見た．メジの場合には曲線だけから見た相關が極めて不判明で，しかも，地震の效果が數十日後の漁獲に現はれるかも知れないといふ可能性があるので，地震曲線に對して漁獲曲線を種々にずらして見て，二つの曲線の相關を調べた．其結果は餘り明瞭でないが，兎も角も現在の材料の示す處では，地震の效果が約三十日後に負相關として漁獲高の上に現はれるらしく見える．勿論此れだけでは何等確實な決論は出來ないが，併し，少くも，鰺とメジとで，全然ちがつた關係を示すといふ點だけでも幾分の興味があると思はれるから，統計の結果を玆に記錄して後日の參考に供する次第である．

---

1) The relation between earthquakes and fisheries seems to have become a subject of the more serious investigations than it was at the time when the previous paper of the present author was written, in view of Prof. S. Hatai's interesting research on the responses of catfish to earthquakes (Proc. Imp. Acad, **8** 1932, 375) and also of Mr. Y. Suyehiro's recent research on some anomalous phenomena observed with respect to some kinds of fishes caught at the time of the recent earthquake in Sanriku which caused a disastrous sea-waves (*Dôbutugaku-Zassi*, **45** (1933), 245.)

37. *Construction d'un sismographe accélérométrique pour la composante verticale*

par Mishio ISHIMOTO,

Institut de Recherches sur les Tremblements de terre.

(Reçu le 18, Septembre, 1933.)

Introduction.

Il y a quelques années, nous avons publié un mémoire[1] sur la construction d'un sismographe accélérométrique pour la composante horizontale. Cet appareil comporte principalement une paire de pendules dont la période propre demeure assez petite en comparaison avec celle des secousses sismiques. Dernièrement nous avons réalisé un autre appareil qui energistre aussi accélérométriquement les secousses sismiques pour la composante verticale.

Evidement le fait que la gravité dans la composante verticale, nous empêche de construire un appareil de grande sensibilité, spécialement pour le type ordinaire. On veut avoir un pendule de grande période suspendu à un ressort qui sert en même temps à compenser le poids du pendule. De telles conditions d'équilibre sont assez délicates et le pendule sort souvent en dehors de sa limite de compensation avec le changement de la force élastique du ressort résultant des variations de la température de l'air.

A l'égard du sismographe accélérométrique, cependant, la compensation de gravité n'est pas difficile à obtenir du fait que la période propre du pendule est assez petite. Après avoir construit un appareil sans obstacle, nous l'avons installé dans une pièce souterraine du notre Institut. Quoiqu'il y ait eu certains changements de température pendant une longue période d'observation, le pendule a gardé sa position à peu près constante et nous n'avons fait aucun reglage pour le ramener à sa position initiale.

Nous avons exécuté tout d'abord plusieurs sortes d'étalonnages. Parmi eux il était presque impossible de réaliser un mécanisme de l'oscillation sinusoïdale dans la direction verticale. Les systèmes d'oscillation d'une

1) M. ISHIMOTO, *Bull. Eyrthq. Res. Inst.*, 9 (1931), 316.

plate-forme constrainte dans la direction verticale ne sont pas utilisables pour notre but: il y a toujours une superposition des petites périodes d'oscillation à l'oscillation fondamentale. Les oscillations de petite période superposées ont généralement des valeurs de grande accélération et elles nous empêchent de distinguer l'oscillation en question. Nous avons réussi enfin en adoptant une planche de bois: elle est tenue rigidement par une de ses extrémités et l'appareil a été placé sur l'autre extrémité. L'appareil exécute une oscillation sinusoïdale dans la direction vertical simplement sous une force restitutive de la flexion de la planche.

En tout cas, le sismograph accélérométrique pour la composante verticale n'est pas difficile à réaliser en comparaison avec celui du type ordinaire. Il y a, cependant, la question de l'amortisseur. D'abord nous avons utilisé la viscosité de l'huile pour amortir l'oscillation: mais trouvant que l'air est le médium d'amortissement dont la viscosité reste presque constante dans le domaine de la température naturelle, c'est lui que nous avons adopté définitivement.

Récemment, nous avons construit un appareil pour observer spécialement les bruits sismiques fréquents autour de la station de Tukuba.[2] Donc, la période d'oscillation du pendule est tenue assez petite. Nous avons exécuté d'ailleurs plusieurs sortes d'étalonnages pour examiner les caractéristiques de cet appareil avec les oscillations dans la composante verticale.

Constructoin de l'appareil.

La construction de cet appareil a été réalisée suivant des dimensions à peu près semblables à celles de l'appareil pour la composante horizontale. La masse du pendule est de 15 kg; la période propre du pendule était reglée à 0,070 s., mais elle est devenue un peu plus grande par suite de l'attachement de leviers qui servent à amplifier le mouvement du pendule. Ils forment une série de trois leviers avec les mêmes rapports d'amplification que dans l'autre appareil. Donc, le déplacement du centre de gravité du pendule est amplifié géométriquement 215

2) A Tukuba, il y a une station sismologique attachée à notre Institut. M. Inouyé a déjà étudié la nature des secousses sismiques de cet endroit avec le sismographe accélérométrique de la composante horizontale. [*Bull.* 11 (1933), 69.] Il est très remarquable que les secousses sont accompagnées par des bruits qui ont une relation étroite avec les secousses de la composante verticale. Nous voulons, en effet, les étudier avec le sismographe accélérométrique de la composante verticale.

fois à l'extrémité de la plume. D'après ces données, nous pouvons calculer sa sensibilité approximative avec la formule :

$$\xi = \frac{T_0^2}{4\pi^2} \times \text{accélération} \times \text{amplification}$$

où T_0 corespond à la période d'un pendule dont la masse est concentrée au centre de gravité et nous le calculions comme 0,067 s. Ainsi un millimètre de la déviation à la pointe de la plume correspond à 4,12 gal de l'accélération. L'aspect général de cet appareil est donné schématiquement dans la Fig. 1. et sa photographie à la Fig. 2 dans la dernière planche.

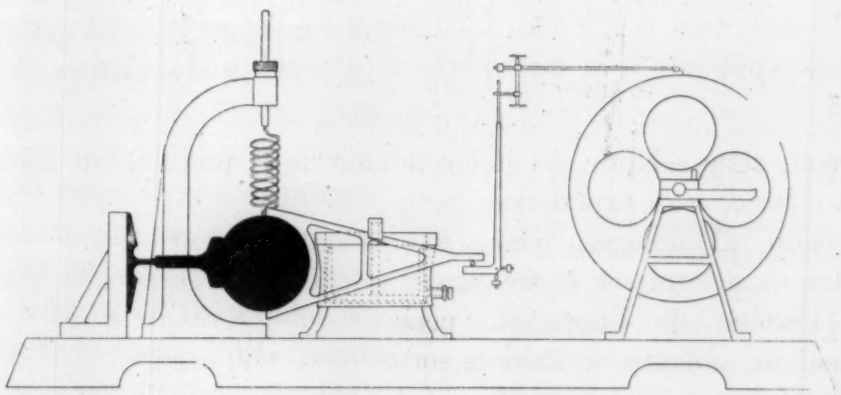

Fig. 1. Le sismographe accélérométrique resprésenté schématiquement.

Nous avons mis un amortisseur d'air au pendule pour empêcher son oscillation propre. C'est le procédé que nous avions déjà adopté et que nous avons décrit dans un des mémoires précédents.[3] Sa construction est un peu difficile pour avoir 0,1 mm de paroi entre les deux pièces, mais certainement il apporte des bons résultats. Nous pouvons avoir un état convenable d'amortissement avec le reglage du robinet permettant de faire communiquer l'air de la chambre avec celui du dehors. Quoique la viscosité de l'air soit assez petite en comparaison avec celle de l'huile, elle a l'avantage de ne pas changer beaucoup avec les variations thermiques. Conséquemment, il n'est pas nécessaire d'inspecter temps en temps les conditions de l'amortisseur. La résistance due au frottement solide à l'extrémité de la plume, ainsi qu'aux pivots des leviers n'est pas évitable tant que nous employons le système d'energistrement mécanique. Mais elle ne dépasse pas la valeur de 0,4 dyne d'après

3) M. Ishimoto, *Bull. Earthq. Res. Inst.*, 9 (1933), 113.

ce que nous avons expérimenté déjà.[4] La plume est prête à se déplacer pour 0,006 gal d'accélération.

Etalonnages.

Nous avons exécuté plusieurs sortes d'étalonnages pour déterminer les caractéristiques de cet appareil.

1° Nous avons posé des poids les uns après les autres sur la masse du pendule. Les déviations inscrites par la plume étaient toujours proportinnelles aux poids. Nous n'avons pas réussi, cependant, dans la détermination absolue de la sensibilité : parce que le point d'application de la force n'est pas certain dans tous les cas.

2° Nous avons donné une inclinaison θ à l'appareil. La diminution de gravité appliquée à la masse sera représenté par la relation suivante:

$$g\,(1-\cos\theta)$$

Evidement, cette relation est indépendante de la position du centre de gravité. Donc, cette expérience a beaucoup d'avantages pour permettre de déterminer la sensibilité absolue de l'appareil. Les résultats obtenus à l'aide de cet étalonnage sont montrés dans la Fig. 3. Un millimètre de déviation de la plume correspond à 4,1 gal de l'accélération.

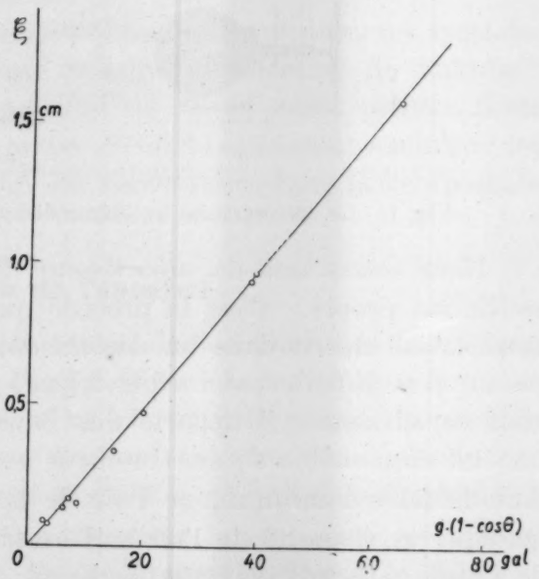

Fig. 3. Courbe d'étalonnage obetenue faisant incliner l'appareil.

3° Nous avons placé un fil élastique de caoutchouc dont une extrémité est attachée à la masse du pendule et dont l'autre est animée d'un mouvement sinusoïdal d'amplitude constante et de différentes périodes. Nous avons ainsi facilement obtenu une série de courbes d'étalonnage suivant le degré d'amortissement du pendule. Avec cette expérience nous avons pu déterminer la période propre d'oscillation du pendule chargé des leviers d'amplification. (Fig. 4) D'un

4) M. Ishimoto, *loc. cit.*

autre côté, nous avons déterminé la période libre d'oscillation dans les mêmes conditions : les deux résultats obtenus sont 0,081 s.

4° Pour l'exécution de l'étalonnage dynamique nous avons utilisé une planche en bois dont une extrémité est tenue rigidement et dont l'autre est libre. En posant l'appareil sur l'extrémité libre, nous faisons osciller le système. Sa période propre d'oscillation depend d'une part du paramètre élastique et des dimensions de la planche, d'autre part de la masse de l'appareil. Nous avons fait varier la période propre d'oscillation de ce système en changeant la position de l'appareil en partant de l'extrémité de la planche. Nous avons ainsi réussi à réalises diverses périodes. Pour enregistrer le déplacement vertical de la masse, nous avons pris un fil, dont une extrémité est attachée au sol et l'autre à une plume glissante. Comme la longueur du fil est constante, le mouvement vertical de la planche correspondant à la position de l'appareil est représenté par le glissement de la plume. Les deux inscriptions faites à la fois sur un tambour tournant sont représentées à la Fig. 5. Nous avons comparé l'amplitude d'oscillation (a) et la déviation maxima de la plume de l'appareil (ξ_{max}) pour chaque période. Naturellement cette expérience pourra se vérifier en supposant qu'une relation soit représentée par

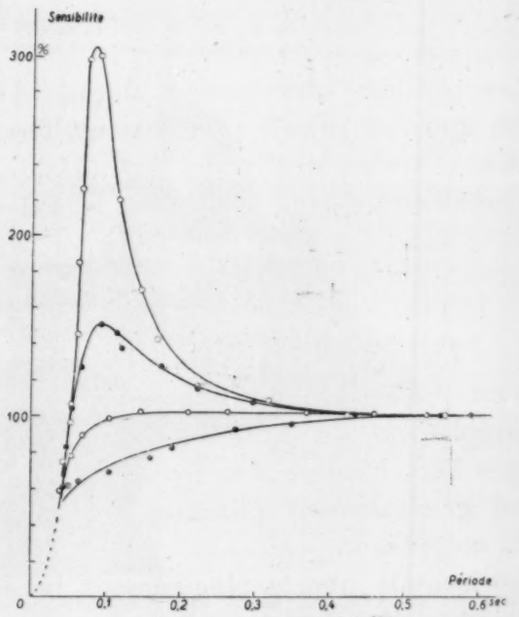

Fig. 4. Courbe d'étalonnage obtenue faisant appliquer la force de différente période à la masse.

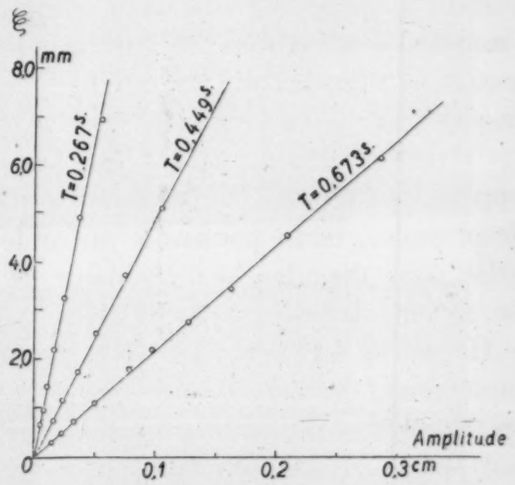

Fig. 6. Courbe d'étalonnage obtenue faisant osciller l'appareil dans la direction verticale.

$$\xi_{max} = \frac{4\pi^2 a}{T^2}$$

Les résultats obtenus sont donnés dans la Fig. 6 : qui nous montre que cet appareil inscrit parfaitement l'oscillation en valeur de son accélération et qu'un millimètre de déviation de plume corespond à 4,1 gal de l'accélération pour toutes les périodes expérimentées.

Enregistrements obtenus.

Les enregistrements obtenus par les appareils accélérométriques sont présentés depuis deux ans dans "Le Rapport Sismométrique" du supplement du Bulletin de notre Institut. Nous remarquons surtout que l'accélération des secousses sismiques de la composante horizontale est généralement plusieurs fois plus grande que celle des secousses de la composante verticale. Il est tout à fait visible dans la composante horizontale que le changement brusque de l'amplitude des secousses à la phase-S à lieu pour tous les séismes. Cela est expliqué par la raison que la trajectoire du rayon sismique arrive perpendiculaire à la surface terrestre suivant la dimunition de sa vitesse quand il approche de la surface. Dans la composante verticale, au contraire, le changement de l'amplitude n'est pas distinct entre les secousses préliminaires et les secousses principales : ce fait est aussi simple résultat des conditions de la surface.

Le mouvement initial des secousses sismiques enregistré par cet appareil est assez clair et nous pouvons distinguer tout de suite une des deux ondes, onde poussante ou onde tirante : cette distinction est très utile pour discuter le mécanisme de la production des ondes sismiques au foyer. T. Suzuki[5] a déjà comparé les deux enregistrements obtenus à Hongô (Tôkyô) par les deux sortes de sismographe et conclu que le mouvement initial des secousses est considéré comme une onde ayant les propriétés d'un choc tandis que les ondes dans le train de secousses ont les propriétés sinusoïdales.

Avec les observations de Hongô nous pouvons relever 0,2 s. de période prédominante dans les secousses de la composante verticale, tandis que nous avons 0,3 s. dans la composante horizontal, Cette discordance est due probablement aux deux différents modes d'oscillation propre de la couche superficielle. Si ces deux périodes correspondent aux deux

5) Il l'a parlé à la 82^{me} séance de notre Institut.

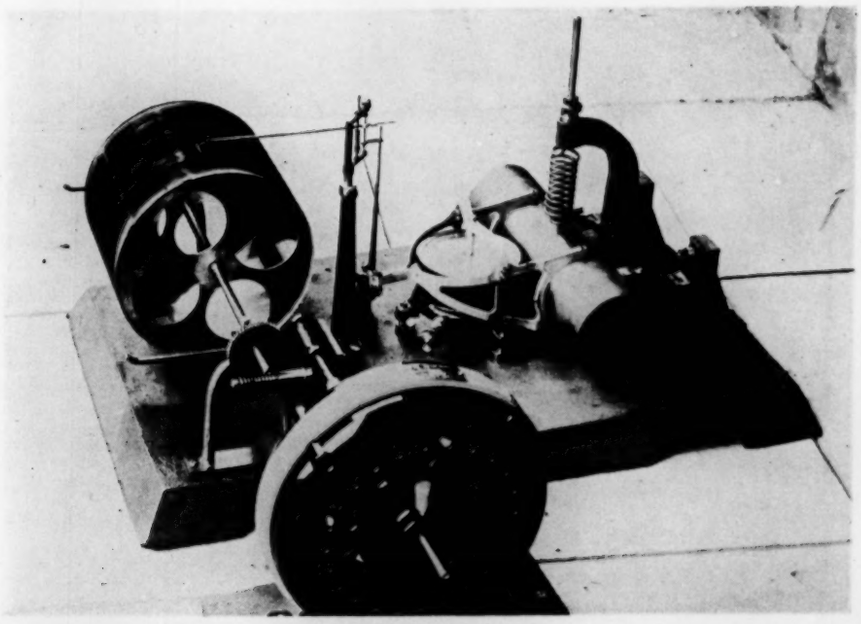

Fig. 2. Photographie du sismographe accélérométrique de la composante verticale.

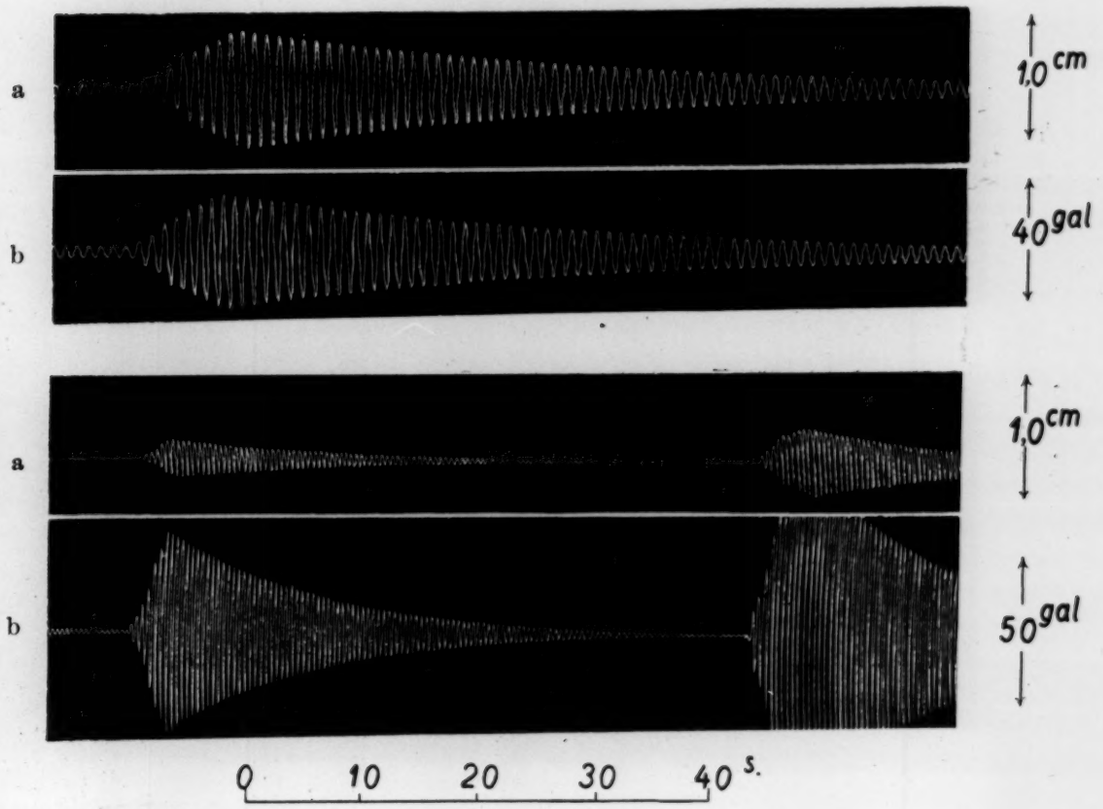

(震研彙報、第十一號、圖版、石本)

Fig. 5. a) Les enregistrements des oscillations verticales de planche.
b) Les mouvements de la pointe de plume de l'appareil correspondant aux oscillations.

différentes vitesses dans la couche, il est certainement possible de déterminer le rapport de Poisson pour ce milieu solide. Mais en général le rapport de deux période n'est pas si constant pour touts les séismes que nous n'osons pas ici discuter ce paramètre élastique.

En tout cas, l'appareil que nous avons construit enregistre très bien les secousses sismiques. Nous voulons continuer les observations accélérométriques et éclaircir les propriétés des seceusses sismiques.

---

37. 上下成分加速度地震計の製作.

地震研究所 石本巳四雄

上下成分の變位地震計は製作上，觀測上大なる困難を伴ふが，加速度地震計は其の困難が比較的少ない．此れは周期が小であつて安定であるからである．

構造は第一圖，及び第二圖に示してある．重錘の質量は 15 kg. 振子の周期は 0·08 秒，幾何倍率は 215 である．

感度試驗は次の四種類の方法によつて行はれた．

1. 既知質量を重錘上に附置.
2. 器械に傾斜を與ふ.
3. 振幅は一定，周期の異る力を重錘に與ふ.
4. 器械を上下方向に正絃運動せしむ.

以上の試驗結果よりして針先の變位 1 mm は，4·1 gal に相當する事が判明した．

此の地震計によつて得られた地震記象は「地震觀測報告」中の所載のものであるが，特に初動の性質に關しては鈴木理學士の研究がある．

---

38. *Contraction of the Japanese Islands since the Middle Neogene (advance paper).*

By Yanosuke ÔTUKA,

Earthquake Research Institute.

(Read Sept. 19, 1933—Received Sept. 20, 1933)

It was long unknown what kind of structural characteristics are exposed in the Japanese Tertiary strata. Recently however our knowledge of Tertiary geologic structures has been greatly enriched, thanks to the studies of a number of Japanese investigators, especially in Northeast Japan by such oil-geologists as Prof. T. Iki, I. Ômura, Y. Chitani, Y. Iizuka and others, and also in Southwest Japan by Prof. J. Makiyama, the members of the Imperial Geological Survey, and the writer. Yet in spite of all this increased knowledge, the question as to how the Japanese Tertiary strata had contracted or shrunk since their deposition remained unanswered. Under these circumstances the writer tried to ascertain to what extent the Middle Neogene strata had contracted during the late Tertiary disturbances in Japan—information indispensable to the study of Japanese post-Miocene tectonic history. So the writer has measured and drawn a map showing how the contractions are distributed in the Middle Neogene strata as deduced from available data. The extent of the Middle Neogene strata that had deformed since the Middle Neogene was measured by referring to the geologic maps and sections contained in twenty-five selected papers consulted in this study and listed at the end of this paper.

It will be seen from fig. 1, that the Fossa Magna divides the Japanese arc into two parts, Northeast and Southwest Japan. The contraction is much greater in the western half of Northeast Japan and in the Fossa Magna than in Southwest Japan.

As will be seen from Fig. 2, which shows the contraction along the Japanese arc, the contraction in Northeast Japan is small, while the Fossa Magna is a very contracted region, as previously inferred by the writer[1]. Fig. 3 shows however that in the western half of Northeast Japan the contraction is large and in the eastern half small.

1) Y. ÔTUKA, *Bull. Earthq. Res. Inst.*, 9 (1931), 340-352.

As shown in Fig. 1, the small contractions are limited to the old land masses like Southwest Japan, and the Kitakami and Abukuma mountainlands. The contractions are found mostly in the zone from the west half of Northeast Japan to the Fossa Magna. This characteristic distribution of large contractions shows that in post-Middle Neogene this zone was more plastic than the other old land masses just mentioned.

It was held until now that the present general configuration of the Japanese arc had practically been formed by late Tertiary movements. But as will be seen from these figures, the general trend of structural lines and that of lines of equal $\frac{F-L}{F}$ and $\frac{F-L}{F}\cdot\cos\alpha$ do not coincide with the trend of the Japanese arc. It may then be said that the structural characteristics of the Middle Neogene Tertiary strata, which were deformed during the late Tertiary crustal movements, are quite independent of the present configuration of the Japanese arc. The Japanese arc must then have been formed after the Tertiary probably during Pleistocene. The late Tertiary movement was only a prelude to the formation of the Japanese arc.

The following is the way in which the writer did the calculating and mapping:

1. Made the geologic structural map.
2. Determined the general trend of structural lines of the Japanese Neogene Tertiary.
3. Drew the geologic sections at right angles to the general trend of the structural lines.
4. Measured horizontal length (L) of the geologic section.
5. Measured length (F) of the middle Neogene strata along the folded structure along the length of the geologic section.
6. Calculated $\frac{F-L}{F}$ for each geologic section. Fig. 1 shows the distribution of $\frac{F-L}{F}$.
7. Determined the center of the Japanese arc (C) after N. Kumagai,[2] joining "C" and the middle point (Mn.) of every geologic section with straight lines.
8. Measured angle α between line C-Mn and the general trend line of the structural lines.
9. Calculated $\frac{F-L}{F}\cdot\cos\alpha$ and $\frac{F-L}{F}\cdot\sin\alpha$.

2) N. Kumagai, Tigaku Ronsô, (1930), 471-502.

Figs. 2 and 3 show the distribution of these two values. The following table gives the numerical value of each reference.

	$\frac{F-L}{F}$	α	$\frac{F-L}{F}\cdot\sin\alpha$	$\frac{F-L}{F}\cdot\cos\alpha$
1) Daisyaka (Daishaka)	·133	19°	·044	·128
2) Kosaka	·102	18	·032	·089
3) Kitahukuoka	·015	5	·001	·015
4) Gozyônome	·102	20	·036	·088
5) Iwayadô	·015	3	·001	·015
6) Honzyô	·082	18	·026	·079
7) Yamagata	·080	13	·017	·075
8) Zyôban (Jôban)	·035	25·5	·015	·032
9) Niitu	·297	14	·071	·287
10) Maki	·339	12	·071	·330
11) Tyôsi (Chôshi)	·015	19	·005	·014
12) Takasaki	·062	66	·054	·024
13) Atuki	·035	55	·029	·020
14) Bôsô	·015	35	·009	·012
15) Bôsô	·355	42	·237	364
16) Sinano (Shinano)	·285	37	·172	·228
17) Sinano	·211	67	·196	·087
18) Asigara	·615	47	·450	·420
19) Noto	·030	3	·008	·030
20) Mino	·015	?	·015	·015
21) Enasan	·035	?	·035	·035
22) Enasan	·035	?	·035	·035
23) Husimi (Fushimi)	·035	15	·009	·034
24) Tuyama	·015	?	·015	·015
25) Tosa	·015	44	·010	·011
26) Hyûga	·015	61	·013	·007
27) Kakegawa	·035	67	·032	·014

1929 Y. Iizuka: Geol. Topog. Map Oil Fiel. Jap. Emp., "Daishaka" sheet.
1930 K. Kinoshita: 1:75,000 Geol. Sheet Map, "Kosaka" sheet.
1833 Y. Otuka: Geology nr. Kitahukuoka etc. Jour. Geol. Soc. Tokyo, **40**, 475.
1919–17 R. Oda: Geol. Top. Map Oil Fiel. Jap. Emp., "Gojonome, Akita" sheets.
1928 F. Saito: Tert. Form. West. Marg. Kitakami Plateau, Jour. Goegr. **39**, 462.
1921 Y. Chitani: Geol. Top. Map. Oil. Fiel. Jap. Emp., "Honjo, Akita" sheet.
1928 Y. Iizuka: Geol. Top. Map Oil Fiel. Jap. Emp. "Sinjo. Yamagata" sheet.
1928 K. Watanabe: Spec. Geol. Map., Joban Coal Fiel. sec. 11.
1904 S. Otsuka: Geol. Top. Map. Oil Fiel. Jap. Emp., "Niitsu, Echigo" sheet.
1931 I. Oomura: "Oil Geology," Iwanami Koza.
1926 S. Yamane: 1:75,000 Geol. Sheet. Map, "Choshi" sheet.
1932 T. Murakoshi: Geology nr. Takasaki, Ms.
1932 K. Suzuki: Pliocene nr. Atuki, Kanagawa Prf. Jour. Geol. Soc. Tokyo, **39**, 461.
1933 Y. Otuka: Geology nr. Kururi, Ms.
1933 Y. Otuka: Geology nr. Kiyosumi, Ms.

1931 Y. Ôtuka: Early Pliocene etc. Bull. Earthq. Res. Inst. 9, 3.
1931 F. Homma: Geology of Mid. Sinano, Geologic Map.
1933 T. Onoyama: Tertiary nr. Kanazawa City and Isurugi. Chikyu, 19, 4.
1927 N. Kiyono and K. Ishii: 1:75,000., Geol. Sheet. Map, "Tajimi" sheet.
1929 K. Ishii: 1:75,000, Geol. Sheet. Map, "Enasan" sheet.
1931 K. Ishii: 1:75,000, Geol. Sheet. Map, "Fushimi" sheet.
1929 T. Suzuki: 1:75,000, Geol. Sheet. Map, "Muroto" sheet.
1930 T. Suzuki: 1:75,000, Geol. Sheet. Map, "Kochi" sheet.
1930 Y. Ôtuka: Geologic Problems nr. the Town of Takanabe etc. Geogr. Rev. Japan, 6, 7.
1931 J. Makiyama: Stratigraphy of the Kakegawa Pliocenes etc. Mem. Col. Sci. Kyoto Imp. Univ. ser. B, VII, 1.

---

38. 新第三紀中期以來の日本島の收縮.

地震研究所　大塚彌之助

文獻及び野外調査により日本の各地に發達する中部新第三系の地質構造を調べ，收縮度を求めた．先づ地質構造の一般走向と之に直角な方向に截つたと考へられるところの地質斷面圖とを求めた．そして水平長さ L の地質斷面圖中に於ける褶曲又は傾斜した中部新第三系の地層の元來の長さ F を水平層準に就いて測定し，$\frac{F-L}{F}$ を求めた．假に $\frac{F-L}{F}$ を收縮度と呼ぶ．收縮度の分布圖は第1圖a,bに示す通りで，東北日本の西部からフオツサマグナ地方へかけて，收縮度の大きい地域がある．

第2,3兩圖は日本の島弧に平行な方向と直角な方向とに收縮度を分けてみせた圖である．α は熊谷助教授の北海道を含めた日本島弧の中心と考へられたものを假に中心として，或る調査地と中心とを結ぶ半徑と一般走向とのなす角を示してゐる．

第2圖は日本島弧に沿へる收縮度を示すもので，東北日本と西南日本とがフオツサマグナ地方で境されてゐること，フオツサマグナの收縮度がかなり大きいのに，東北日本と西南日本とが極めて小さいことがわかる．之によると油田第三系は弧に沿うては餘り收縮してゐないこととなる．

第3圖は日本島弧を日本海側及び太平洋側から挾んで起るやうな收縮度を示してゐて，この圖によると東北日本の西半では收縮度が著しく大きい．殊に新潟地方では大きく．併しこの圖でも東北日本の東半，西南日本の收縮度は他地方に比して著しく小さい．

上記のやうに收縮度の小さいところは北上山地，阿武隈山地，西南日本と言ふ樣な古い地質系統からなつてゐる地方で，收縮度の大きい地方は之等の古い岩石からなる地域に比して遙に可塑性を持つてゐたらしい．

從來日本群島は第三紀末地殼運動でその概形が作られたと考へられてゐたが，之等の圖によつて日本島弧が全く新第三系の地質構造と無關係なことがわかつた．故に日本島弧の概形の形成は恐らく第四紀中に完成されたものであらうと考へることができる．

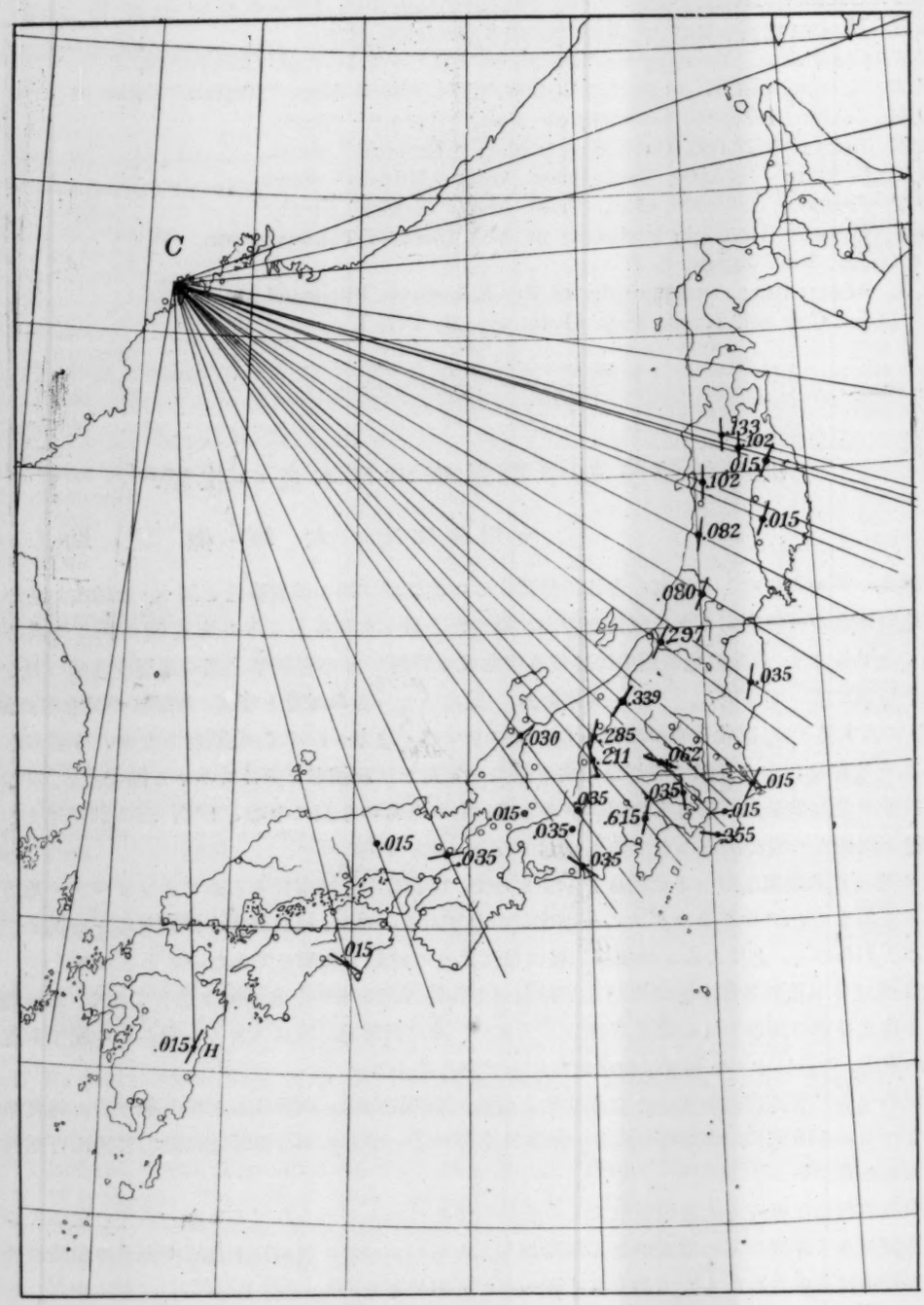

Fig. 1a. General trend of structural lines and $\frac{F-L}{F}$.

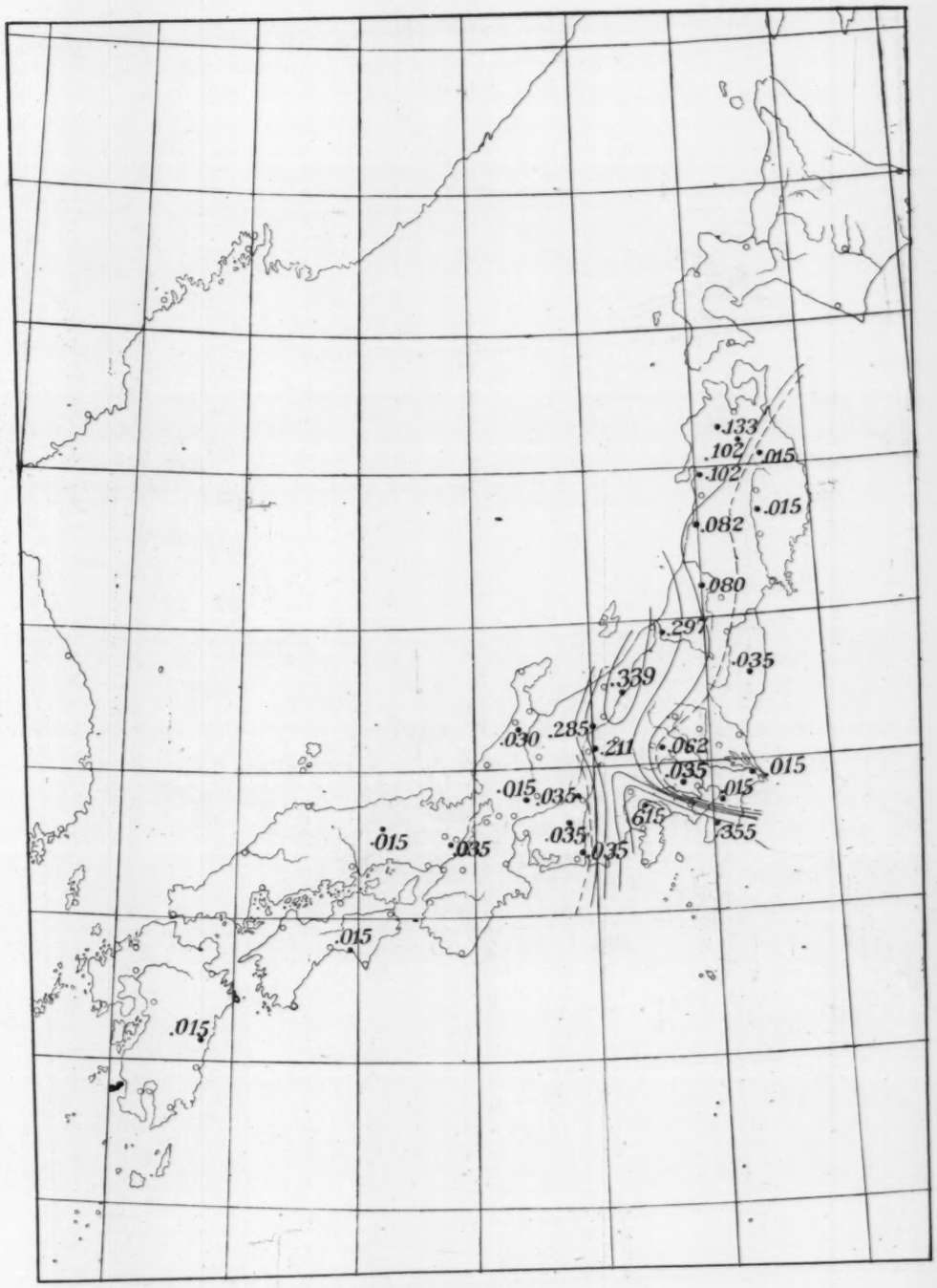

Fig. 1b. Lines of Equal $\frac{F-L}{F}$.

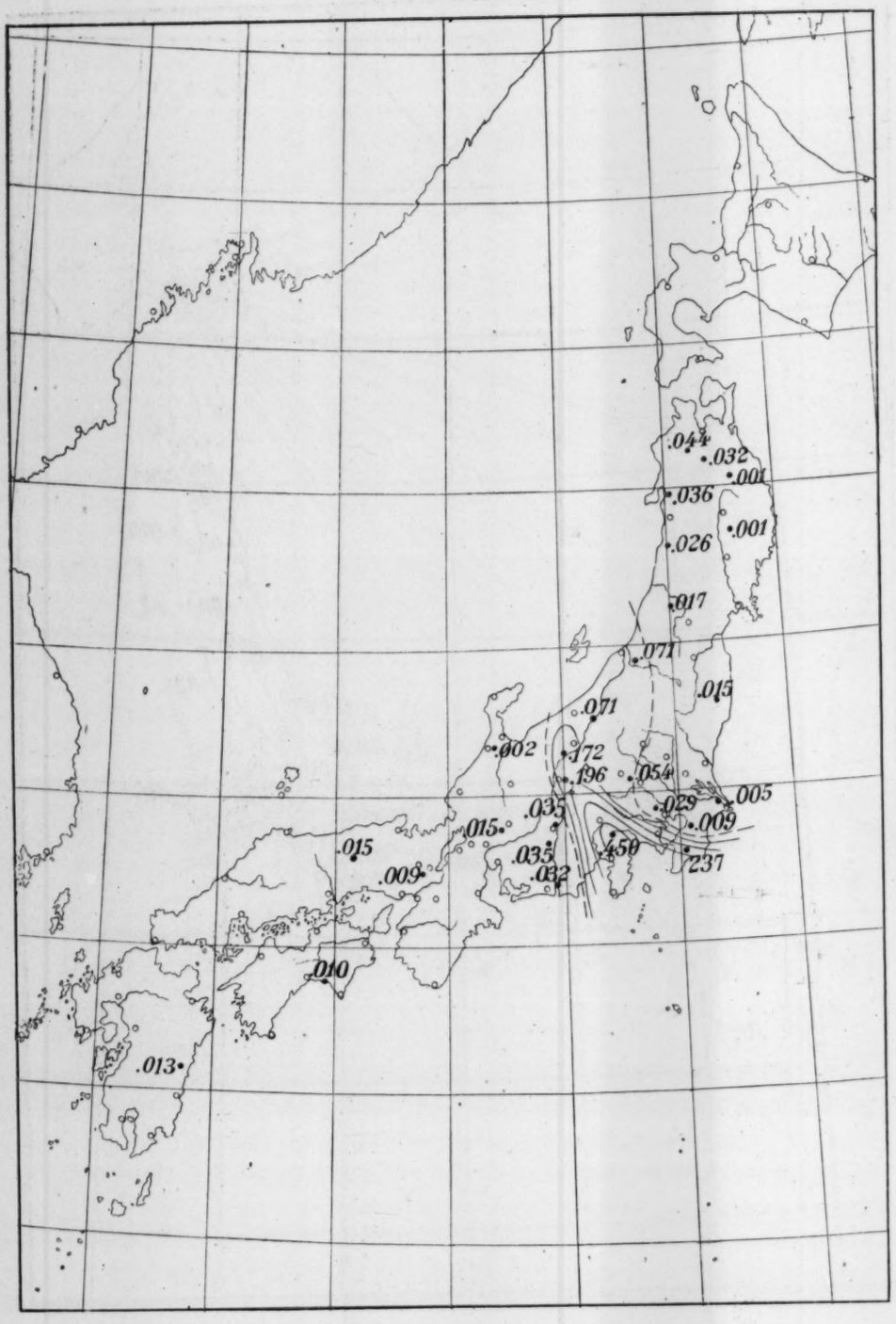

Fig. 2. Lines of Equal $\frac{F-L}{F} \cdot \sin \alpha$

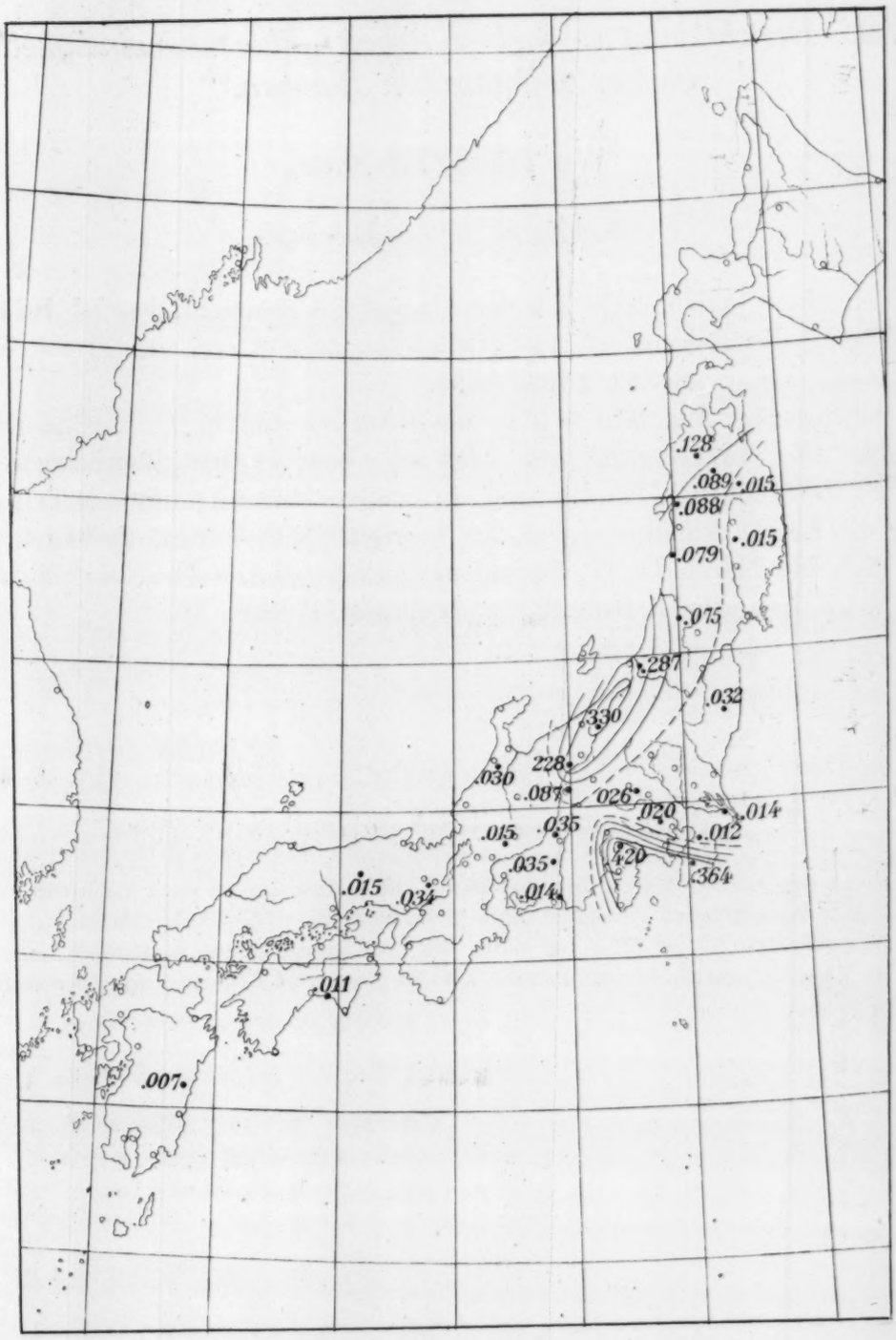

Fig. 3. Lines of Equal $\frac{F-L}{F}.\cos\alpha$

39. *Berichtigung zu meiner Arbeit „Fluggeschwindigkeit einiger vulkanischen Bomben.*[1]*“*

Von Takeo MATUZAWA,

(Eingegangen 20. September 1933.)

In dieser Arbeit habe ich das Ungeschick gemacht, dass ich bei der Ableitung der Barometerformel (Seite 330, Zeile 2 von unten) ρ in der Klammer stehen bleiben lassen habe.

$R\beta$ beträgt ungefähr 0·15 g, was beim konstanten β unveränderlich bleibt. Die Hinzufügung von $-R\beta$ zu g bewirkt aber glücklicherweise keinen bedenklichen Einfluss auf die weitere Ausführung, weil Teil $R\beta$ nur die zweite Annäherung in der Bewegungsgleichungen bedeutet.

Ich bin Herrn Dr. T. Suzuki zu meinem besten Dank verpflichtet für seine freundliche Bemerkung zu diesem Fehler.

---

39. Kwazandan no Hikôsokudo Ronbun no Teisei.

. Kono Ronbun de Takasa to Kûki-Mitudo tono Kwankei wo dasu Toki (330 Peizi, sita kara 2 Gyôme) ρ wo Kakko no Naka e okiwasureta.

Sitagatte kono Kô no Eikyô wa motto ôkii node aruga, korewa motomoto Naosi no Ue no Naosi de arukara korewo habuita koto ni yotte sono Saki no Keisan niwa taisita Eikyô ga nai.

---

1 T. MATUZAWA, *Bull. Earthq. Res. Inst.*, 11 (1933), 327–346.

——所　報——

○談話會記事

第七十七回談話會（昭和七年十二月廿日）

1. 伊豆湯河原—箱根町間地質調査報告　久野久
1. 伊豆綱代層の地質並に岩石に就て　久野久
1. 振動知覺の限界測定　石本巳四雄・大塚實
1. 北上川に就て　寺田寅彦
1. 地磁氣分布と日本の構造（第二報）　寺田寅彦
1. 人爲地震動に依る架構の震動實驗　谷口忠
1. 地殻内部に異物質がある場合の應力釣合（其の二）　西村源六郎・高山威雄
1. 不連續面が彈性波の傳播に及ぼす影響（其の一）　西村源六郎
1. 建築物の實際の耐震力に就て　物部長穂
1. 日本に於ける地震の分布に就て　山口生知
1. 地震前の氣壓勾配に就て（其二）　井上宇胤
1. 大正十三年より昭和六年までの東京有感地震　小平孝雄

第七十八回談話會（昭和八年一月十七日）

1. 日本群島沿岸海底地形　田山利三郎
1. 四國に於ける山崩れの方向性　寺田寅彦
1. 日本のゼオイドに就て　寺田寅彦
1. 興津・串本間の地殻の垂直變動に就て　宮部直巳
1. 地殻内部に異物質がある場合の應力釣合（其の三）　西村源六郎・高山威雄
1. 地震初動分布と其れに伴つた地形變動　石本巳四雄
1. 大地震の區域は地球上に廻轉するか　長岡半太郎
1. 大地震と緯度變化に付き（前回の續き）　長岡半太郎

第七十九回談話會（昭和八年二月廿一日）

1. 古河より白河に至る水準線の改測に就て　梅本豐吉
1. 仙臺近傍最近地質時代の地殻運動　田山利三郎
1. 或火山彈の飛行速度　松澤武雄
1. 噴火の際のガス壓力　松澤武雄

1. 地球に一つの層がある場合の地表に於けるレーリー波の振幅に就て	鈴木武雄
1. 日本に於ける地震の分布に就て（續報）	山口生知
1. 地震初動に關した二三の統計的問題（第一報）	福富孝治
1. 北上山地西緣の新第三系の構造	大塚彌之助
1. 地球廻轉週期に及ぼす噴火の影響	長岡半太郎

○ 出　　張

1. 昭和七年十二月六日地震事項取調の爲め靜岡縣下へ出張	那須信治
1. 昭和七年十二月六日地中電流測定の爲め千葉縣下へ出張	高橋龍太郎
1. 昭和七年十二月十五日地質取調の爲め靜岡縣下へ出張	大塚彌之助
1. 昭和七年十二月十六日地質取調の爲め靜岡縣下へ出張	坪井誠太郎
1. 昭和八年一月九日地殼變動取調の爲め靜岡縣下へ出張	坪井忠二
1. 昭和八年三月三日地震事項取調の爲め岩手縣下へ出張	高橋龍太郎
1. 昭和八年三月三日地震事項取調の爲め岩手縣下へ出張	那須信治
1. 昭和八年三月六日地震事項取調の爲め岩手・青森兩縣下へ出張	齊田時太郎
1. 昭和八年三月六日地震事項取調の爲め岩手・青森兩縣下へ出張	大塚彌之助

——所　報——

○談　話　會

第八十回談話會（昭和八年三月二十日）

1. 高壓過熱水蒸氣の珪酸及珪酸鹽に對する作用	白井俊明
1. 地球物理學的に見たる日本の構造	坪井忠二
1. 富士山の側火山列に就て	藤原咲平
1. 地球の剛性は一定せるか	長岡半太郎
1. 緯度變化と噴火との關係	長岡半太郎
1. 三陸地震津浪と災害豫防	今村明恒
1. 關東地方に於ける地塊運動	宮部直巳
1. 地震波の勢力，其の他に就て	河角廣
1. 不連續面が彈性波の傳播に及ぼす影響（其の二）	西村源六郎 金井清
1. 三月三日の三陸津浪調査概報	那須信治 高橋龍太郎 大塚彌之助 齊田時太郎
1. 三陸地方津浪被害調査	濱田稔

第八十一回談話會（昭和八年四月十八日）

1. 東京市内に於ける最近の土地の變動	宮部直巳
1. 淺間火山の二三の熔岩に就いて	津屋弘達
1. 宮城・福島兩縣下に於ける津浪調査概報	宮部直巳
1. 三陸津浪（廣田灣，大船渡灣其他）	西村源六郎 高山威雄
1. 三陸津浪調査（續報）	高橋龍太郎
1. 津浪被害に關する一考察	石本巳四雄

第八十二回談話會（昭和八年五月十六日）

1. ゲオイドが三軸橢圓體である事實から生ずる噴火と地震	長岡半太郎
1. 水準測量に就いて	坪井忠二
1. 伊東地方の水準測量	坪井忠二
1. 統計に因る地震豫知の不確定度	寺田寅彦
1. 加速度地震計と變位地震計による初動の比較	鈴木武夫
1. 三陸津浪の發光現象に就て	武者金吉
1. 三陸津浪〔其二〕（綾里灣，氣仙沼灣）	西村源六郎 高山威雄

1. 釜石町津浪被害に就て　石本巳四雄・萩原尊禮
1. 三月三日北海道津浪調査報告　那須信治

○出　張

1. 昭和八年三月十四日地震事項取調の爲め宮城岩手兩縣下へ出張　武者金吉
1. 昭和八年三月十七日地震，津浪事項取調の爲め茨城福島宮城及千葉四縣へ出張　宮部直巳
1. 昭和八年三月十八日地震，津浪事項取調の爲め宮城縣下へ出張　高橋龍太郎
1. 昭和八年三月十八日地震，津浪事項取調の爲め北海道へ出張　那須信治
1. 昭和八年三月二十四日地震，津浪事項取調の爲め宮城岩手兩縣へ出張　西村源六郎
1. 昭和八年三月二十四日地震，津浪事項取調の爲め宮城岩手兩縣へ出張　高山威雄
1. 昭和八年三月二十九日地震事項取調の爲め長野縣下へ出張　齊田時太郎
1. 昭和八年三月三十日地震，津浪事項取調の爲め宮城縣下へ出張　坪井忠二
1. 昭和八年三月三十日地震，津浪事項取調の爲め宮城岩手兩縣下へ出張　高橋龍太郎
1. 昭和八年三月三十日地震，津浪事項取調の爲め宮城縣下へ出張　松澤武雄
1. 昭和八年三月三十日地震，津浪事項取調の爲め宮城縣下へ出張　石本巳四雄
1. 昭和八年四月一日地震，津浪事項取調の爲め宮城縣下へ出張　木村一治
1. 昭和八年四月八日地震，津浪事項取調の爲め岩手縣下へ出張　齊田時太郎
1. 昭和八年四月八日地震，津浪事項取調の爲め岩手縣下へ出張　石本巳四雄
1. 昭和八年四月八日地震，津浪事項取調の爲め岩手縣下へ出張　木村一治
1. 昭和八年四月二十一日淺間火山觀測に關する用務の爲め長野縣下へ出張　石本巳四雄
1. 昭和八年四月二十一日淺間火山觀測に關する用務の爲め長野縣下へ出張　齊田時太郎
1. 昭和八年四月二十二日地質取調の爲め靜岡縣下へ出張　大塚彌之助
1. 昭和八年四月二十四日津浪事項取調の爲め宮城岩手兩縣下へ出張　石本巳四雄
1. 昭和八年四月二十四日津浪事項取調の爲め宮城岩手兩縣下へ出張　萩原尊禮
1. 昭和八年四月二十六日津浪事項取調の爲め宮城下へ出張　高橋龍太郎
1. 昭和八年四月二十六日津浪事項取調の爲め宮城岩手兩縣下へ出張　大塚彌之助
1. 昭和八年五月九日津浪事項取調の爲め岩手縣下へ出張　那須信治
1. 昭和八年五月十七日地質取調の爲め東京府下大島へ出張　津屋弘達
1. 昭和八年五月十八日津浪事項取調の爲め岩手縣下へ出張　井上宇胤
1. 昭和八年五月十八日津浪事項取調の爲め岩手縣下へ出張　那須信治
1. 昭和八年五月二十九日學術上取調の爲め京都府下へ出張　坪井忠二
1. 昭和八年六月七日淺間火山觀測用務の爲め長野縣下へ出張　齊田時太郎

——所　　報——

○談　話　會

第八十三回談話會（昭和八年六月二十日）

1. 筑波山に於ける傾斜變化觀測報告（其四）　井上宇胤
1. 地震と漁獲（第二報）　寺田寅彦
1. 津浪の光現象に就て　寺田寅彦
1. 富士川口以南の地質構造　大塚彌之助
1. 三陸海岸の地形と津浪被害　大塚彌之助
1. 不連續面が彈性波の傳播に及ぼす影響（其の三）　西村源六郎・金井清
1. 三陸津浪調査（第三報）「氣仙沼以南」　高橋龍太郎
1. 三陸地方港灣の形と津浪の高さとの關係　山口生知
1. 土地の高低と津浪の被害　那須信治

第八十四回談話會（昭和八年七月四日）

1. 仙臺にて觀察されたる斷層の一特例　矢部長克
1. 港灣の深さに及ぼす主風の影響　中野猿人
1. 地震波の走時に關する二三の問題　河角廣
1. 昭和六年二月二十日日本海北部の深發地震の調査（第一報）　河角廣・吉山良一
1. 水中爆發による薄板の彈性破損　西村源六郎
1. 風の爲め起される脈動に關係した問題（其の一）　西村源六郎
1. 三軸楕圓體ゲオイドの原因　長岡半太郎
1. 太平洋底の割れ目と大地震帶との關係　白井俊明
1. 須佐に於ける津浪　松澤武雄・神原健・水上武
1. 津浪の勢力と土木工事の被害　松尾春雄
1. 三月三日津浪發生機巧に就て　石本巳四雄

第八十五回談話會（昭和八年九月十九日）

1. 土地の高低と津浪の被害　那須信治
1. 日本の重力に就て　坪井忠二
1. 船舶に於ける重力測定の可能性　坪井忠二
1. 燒ヶ嶽火山の活動　小平孝雄
1. 不連續面が彈性波の傳播に及ぼす影響　西村源六郎・金井清

1. 三月三日の三陸津浪に伴つた音響に就て（其の四）　井上宇胤
1. 無線通信法を利用せる重力比較測定の實驗に就て　木村一治
1. 日本島の收縮（豫報）　大塚彌之助
1. 富士・大島線に就て　長岡半太郎・白井俊明

○出　張

1. 昭和八年六月二十六日淺間火山觀測に關する用務の爲め長野縣下へ出張　齋田時太郎
1. 昭和八年六月二十八日津浪事項取調の爲め宮城岩手兩縣下へ出張　那須信治
1. 昭和八年六月二十九日津浪事項取調の爲め宮城岩手兩縣下へ出張　小平孝雄
1. 昭和八年七月十三日箱根火山地質調査の爲め靜岡神奈川兩縣下へ出張　久野久
1. 昭和八年七月十五日津浪事項調査の爲め岩手縣下へ出張　高橋龍太郎
1. 昭和八年七月十八日淺間火山觀測に關する用務の爲め長野縣下へ出張　石本巳四雄
1. 昭和八年七月二十六日地質取調の爲め千葉縣下へ出張　大塚彌之助
1. 昭和八年七月三十一日地殼變動取調の爲め東京府下及千葉縣下へ出張　宮部直巳
1. 昭和八年八月九日地震事項取調の爲め長野縣下へ出張　那須信治
1. 昭和八年八月二十五日地震事項取調の爲め長野縣下へ出張　那須信治
1. 昭和八年八月二十五日地震事項取調の爲め長野縣下へ出張　坪井忠二
1. 昭和八年九月八日地震事項取調の爲め長野縣下へ出張　高橋龍太郎
1. 昭和八年九月十九日地震事項取調の爲め長野縣下へ出張　那須信治

——所　報——

○談 話 會

第八十六回談話會（昭和八年十月十六日）

1. 檢潮儀記錄による三陸津浪研究概報	宮部直巳
1. 東京市内水準測量の結果	宮部直巳
1. 風の影響による海水面の異常なる上昇	宮部直巳
1. 三陸强震の前に觀察されたる魚の異常生態（豫報）	武者金吉
1. 三陸津浪の發光現象（第二報）	武者金吉
1. 昭和八年九月二十一日の能登地震踏査報告	鈴木武夫 大塚彌之助
1. 淺間火山の構造と最近の活動狀況	津屋弘逵
1. 風によつて起される脈動に關係した問題（其の二）	西村源六郎
1. 不連續面が彈性波の傳播に及ぼす影響（其の五）	西村源六郎 金井清
1. 地上及地中の振動比較（豫報）	井上宇胤
1. 丹後但馬の地震に就きて 1. ホツサ・マグナと日本アルプスに就きて	長岡半太郎 白井俊明

第八十七回談話會（昭和八年十一月廿一日）

1. 破壞の進行に關する一實驗（豫報）	岸上冬彥
1. 相模灣底の變化に就て	寺田寅彥
1. 地震動の分解	石本巳四雄 木村一治
1. 大船渡・綾里・門ノ濱三灣の潮汐の副振動（概報）	高橋龍太郎
1. 三陸沿岸に於ける過去の津浪に就て	今村明恒
1. 不連續面が彈性波の傳播に及ぼす影響（其の六）	西村源六郎 金井清
1. 草津白根山の活動狀況	津屋弘逵
1. 草津白根山の二三の熔岩に就て	津屋弘逵
1. 淺間山最近の活動狀況について	那須信治

○出　　張

1. 昭和八年九月二十二日淺間火山觀測並に調査の爲め長野群馬兩縣下へ出張	石本巳四雄
1. 昭和八年九月二十二日地震事項取調の爲め富山石川兩縣下へ出張	大塚彌之助
1. 昭和八年九月二十二日地震事項取調の爲め富山石川兩縣下へ出張	鈴木武夫
1. 昭和八年十月十一日淺間火山取調の爲め長野縣下へ出張	津屋弘逵
1. 昭和八年十月二十四日學術上取調の爲め廣島縣下へ出張	石本巳四雄

第十一號索引

頁

福富孝治　(28) 地震初動に關した二三の統計的問題(英文) …… 510

萩原尊禮　(2) 固體摩擦の振動倍率に及ぼす影響(英文) …… 14

稻葉佳・井上宇胤；井上宇胤・稻葉佳　參照

井上宇胤　(6) 筑波山に於ける加速度地震計に依る地震觀測報告(英文) …… 69

井上宇胤　(34) 筑波山に於ける傾斜變化觀測報告(英文) …… 693

井上宇胤・稻葉佳　(35) 地震發生前の氣壓勾配に就いて(第二報)(英文) …… 704

石本巳四雄　(14) 地殼變動と震源に於ける地震波發生(佛文) …… 254

石本巳四雄　(37) 上下成分加速度地震計の製作(佛文) …… 717

石本巳四雄・大塚實　(8) 振動の知覺限界測定(佛文) …… 113

金井清・西村源六郎；西村源六郎・金井清　參照

金井清・西村源六郎・高山威雄；西村源六郎・高山威雄・金井清　參照

川畑幸夫・武藤勝彥；武藤勝彥・川畑幸夫　參照

河角　廣　(24) 地震波の傳播（第二報）發震機巧，地殼構造と地震波の振幅に就て(英文) …… 403

岸上冬彥　(4) 和歌山縣に於ける土地潛動の測定(英文) …… 38

小平孝雄　(20) 關東地方の地震(英文) …… 350

久野　久　(22) 本邦火山岩の石基に產する珪酸鑛物に就いて(英文) …… 382

久野　久　(23) 伊豆網代產玄武岩に就いて(豫報)(英文) …… 391

松澤武雄　(18) 或火山彈の飛行速度(獨文) …… 329

松澤武雄　(19) 噴火の時のガスの壓力(獨文) …… 347

松澤武雄　(39) 火山彈の飛行速度の訂正(獨文) …… 732

宮部直巳　(16) 興津・串本間に於ける地殼の變動(英文) …… 278

宮部直巳　(33) 關東地方に於ける地塊運動(英文) …… 639

武藤勝彥・川畑幸夫　(17) 濃尾震災地及び其の他の地方に於ける檢測水準測量の調査(邦文) …… 315

西村源六郎・金井清　(10) 不連續面が彈性波の傳播に及ぼす影響(I)(英文) …… 123

西村源六郎・金井清　(31) 不連續面が彈性波の傳播に及ぼす影響(II)(英文) …… 595

西村源六郎・高山威雄　(12) 重力の働ける半無限彈性體內に存在する球狀填充物

附近の應力(I)(英文)…… 196
西村源六郎・高山威雄　(13) 重力の働ける半無限彈性體內に存在する圓形塡充物附近の應力(I)(英文)…… 229
西村源六郎・高山威雄・金井清　(25) 重力の働ける半無限彈性體內に存在する圓形塡充物附近の應力(II)(英文)…… 454
大塚實・石本巳四雄；石本巳四雄・大塚實　參照
大塚彌之助　(29) 北伊豆の地形及び地質構造と昭和五年十一月二十六日伊豆地震の際にその地域に生じた地變及び地殼變形との關係(英文)…… 530
大塚彌之助　(38) 中部新三紀以來の日本島の收縮(英文)…… 724
鈴木武夫　(11) 表面層のある場合の表面に於けるレーリー波の振幅(英文)…… 187
高橋龍太郎　(3) 淺間山麓に於ける地表傾斜變化の觀測(英文)…… 25
高山威雄・西村源六郎；西村源六郎・高山威雄　參照
高山威雄・西村源六郎・金井清；西村源六郎・高山威雄・金井清　參照
田丸卓郎　(21) 加速度地震計の製作及び研究(邦文)…… 362
寺田寅彥　(36) 地震と漁獲(第二報)(英文)…… 714
坪井忠二　(15) 地殼の强さに就いて(英文)…… 275
坪井忠二　(26) 伊豆伊東地方に於ける地殼の垂直移動(英文)…… 488
坪井忠二　(32) 日本の重力に最もよく適合する式(英文)…… 632
津屋弘逵　(7) 昭和7年10月草津白根山の爆發(英文)…… 82
津屋弘逵　(30) 信濃國淺間火山の二三の熔岩の岩石學的研究(英文)…… 575
山口生知　(5) 地震の時間的及び空間的分布に就いて(英文)…… 46
山口生知　(27) 日本に於ける地震の分布(英文)…… 500
吉山良一　(1) 等方不均一球內の一點より起る彈性波(第一報)(英文)…… 1
陸地測量部　(9) 東京市及其の附近と板橋町・富士見村間一等水準線檢測成果報告(邦文)…… 122

Index to Vol. XI.

Page

FUKUTOMI, T. (28) Some Statistical Problems concerning Initial Earthquake Motion. (The First Report). (in English) 510

HAGIWARA, T. (2) Influence of Solid Friction on Dynamical Magnification. (in English) 14

INABA, Y. and INOUYE, W.; *See* INOUYE, W. and INABA, Y.

INOUYE, W. (6) Observations of Near Earthquakes on Mt. Tukuba with an Ishimoto Acceleration Seismograph. (in English) 69

INOUYE, W. (34) Earth-tilts observed at Mt. Tukuba, Japan. (in English) 693

INOUYE, W. and INABA, Y. (35) On Barometric Gradients at Times of Earthquakes, in Japan (2nd paper). (in English) 704

ISHIMOTO, M. (14) La déformation de la croûte terrestre et la production des ondes sismique au foyer. (en français) 254

ISHIMOTO, M. (37) Construction d'un sismographe accélérométrique pour la composante verticale. (en français) 717

ISHIMOTO, M. et OOTUKA, M. (8) Determination de la limite perceptible des secousses. (en français) 113

KANAI, K. and NISHIMURA, G.; *See* NISHIMURA, G. and KANAI, K.

KANAI, K., NISHIMURA, G. and TAKAYAMA, T.; *See* NISHIMURA, G., TAKAYAMA, T. and KANAI, K.

KAWABATA, Y. and MUTO, K.; *See* MUTO, K. and KAWABATA, Y.

KAWASUMI, H. (24) Study of Propagation of Seismic Waves. (The second paper). (in English) 403

KISHINOUYE, F. (4) Measurement of a Land-creep in Wakayama Prefecture. (in English) 38

KODAIRA, T. (20) Earthquakes of the Kwantô District. (in English) 350

KUNO, H. (22) On Silica Minerals occurring in the Groundmass of Common Japanese Volcanic Rocks. (in English) 382

KUNO, H. (23) Preliminary Note on Basalt from Aziro, Idu. (in English) 391

MATUZAWA, T. (18) Fluggeschwindigkeit einiger vulkanischen Bomben. (in deutsch) 329
MATUZAWA, T. (19) Gasdruck bei einigen vulkanischen Ausbrüchen in Japan. (in deutsch) 347
MATUZAWA, T. (39) Berichtigung zu meiner Arbeit „Fluggeschwindigkeit einiger vulkanischen Bomben". (in deutsch) 732
MIYABE, N. (16) The Crust Deformations in the District between Okitu and Kusimoto, along the Pacific Coast of the Main Island of Japan. (in English) 278
MIYABE, N. (33) Block Movements of the Earth's Crust in the Kwantô District. (The Crustal-Blocks and Their Movements. Part III.) (in English) 639
MUTO, K. and KAWABATA, Y. (17) Vertical Displacements of Bench Marks in the Nôbi and other Districts. (in Japanese) 315
NISHIMURA, G. and KANAI, K. (10) On the Effects of Discontinuity Surfaces upon the Propagation of Elastic Wave. (I). (in English) 123
NISHIMURA, G. and KANAI, K (31) On the Effects of Discontinuity Surfaces upon the Propagation of Elastic Waves. (II). (in English) 595
NISHIMURA, G. and TAKAYAMA, T. (12) On Stresses in the Interior and in the Vicinity of a Spherical Inclusion in a Gravitating Semi-infinite Elastic Solid. (I). (in English) 196
NISHIMURA, G. and TAKAYAMA, T. (13) On Stresses in the Interior and in the Vicinity of a Horizontal Cylindrical Inclusion in a Gravitating Semi-infinite Elastic Solid. (I). (in English) 229
NISHIMURA, G., TAKAYAMA, T. and KANAI, K. (25) On Stresses in the Interior and in the Vicinity of a Horizontal Cylindrical Inclusion of Circular Section in a Gravitating Semi-infinite Elastic Solid. (II). (in English) 454
OOTUKA, M. and ISHIMOTO, M.; *See* ISHIMOTO, M. and OOTUKA, M.
ÔTUKA, Y. (29) The Geomorphology and Geology of Northern Idu Peninsula, the Earthquake Fissures of Nov. 26, 1930, and the Pre- and Post-Seismic Crust Deformations. (in English) 530
ÔTUKA, Y. (38) Contraction of the Japanese Islands since the Middle

Neogene (advanced paper). (in English) 724
Suzuki, T. (11) Amplitude of Rayleigh Waves on the Surface of a Stratified Medium. (in English) 187
Takahasi, R. (3) Tilt of the Earth's Crust observed at the Asama Volcano. (in English)..... ... 25
Takayama, T. and Nishimura, G.; *See* Nishimura, G. and Takayama, T.
Takayama, T., Kanai, K. and Nishimura, G.; *See* Nishimura, G., Takayama, T. and Kanai, K.
Tamaru, T. (21) The Construction and Study of an Acceleration Seismograph. (in Japanese) 362
Terada, T. (36) Earthquake and Fisheries. II. (in English) 714
Tsuboi, C. (15) Notes on the Mechanical Strength of the Earth's Crust. (in English) 275
Tsuboi, C. (26) Vertical Crustal Displacement in the Seismic Region of Itô, on the East Coast of the Idu Peninsula. (in English)..... 488
Tsuboi, C. (32) The Most Suitable Formula for the Japanese Gravity Values. (in English) 632
Tsuya, H. (7) Explosive Activity of Volcano Kusatu-Siranê in October, 1932. (in English) 82
Tsuya, H. (30) Petrology of Some Lavas of Volcano Asama, Sinano Province, Japan. (in English) 575
Yamaguti, S. (5) On Time and Space Distribution of Earthquakes. (in English) 46
Yamaguti, S. (27) Distribution of Earthquakes in Japan. (in English)..... 500
Yosiyama, R. (1) Elastic Waves from a Point in an Isotropic Heterogeneous Sphere. Part I. (in English) 1
Land Survey Department (9) Relative Vertical Displacements of Bench Marks along Routes in Tôkyô and the Environs and from Itabasi to Huzimi. (in Japanese) 122

附近の應力(I)(英文)……196
西村源六郎・高山威雄　(13) 重力の働ける半無限彈性體內に存在する圓形填充物附近の應力(I)(英文)……229
西村源六郎・高山威雄・金井清　(25) 重力の働ける半無限彈性體內に存在する圓形填充物附近の應力(II)(英文)……454
大塚實・石本巳四雄；石本巳四雄・大塚實　參照
大塚彌之助　(29) 北伊豆の地形及び地質構造と昭和五年十一月二十六日伊豆地震の際にその地域に生じた地變及び地殼變形との關係(英文)……530
大塚彌之助　(38) 中部新三紀以來の日本島の收縮(英文)……724
鈴木武夫　(11) 表面層のある場合の表面に於けるレーリー波の振幅(英文)……187
高橋龍太郎　(3) 淺間山麓に於ける地表傾斜變化の觀測(英文)……25
高山威雄・西村源六郎；西村源六郎・高山威雄　參照
高山威雄・西村源六郎・金井清；西村源六郎・高山威雄・金井清　參照
田丸卓郎　(21) 加速度地震計の製作及び研究(邦文)……362
寺田寅彥　(36) 地震と漁獲(第二報)(英文)……714
坪井忠二　(15) 地殼の强さに就いて(英文)……275
坪井忠二　(26) 伊豆伊東地方に於ける地殼の垂直移動(英文)……488
坪井忠二　(32) 日本の重力に最もよく適合する式(英文)……632
津屋弘逵　(7) 昭和7年10月草津白根山の爆發(英文)……82
津屋弘逵　(30) 信濃國淺間火山の二三の熔岩の岩石學的研究(英文)……575
山口生知　(5) 地震の時間的及び空間的分布に就いて(英文)……46
山口生知　(27) 日本に於ける地震の分布(英文)……500
吉山良一　(1) 等方不均一球內の一點より起る彈性波(第一報)(英文)……1
陸地測量部　(9) 東京市及其の附近と板橋町・富士見村間一等水準線檢測成果報告(邦文)……122

Index to Vol. XI.

Page

FUKUTOMI, T. (28) Some Statistical Problems concerning Initial Earthquake Motion. (The First Report). (in English) 510

HAGIWARA, T. (2) Influence of Solid Friction on Dynamical Magnification. (in English) 14

INABA, Y. and INOUYE, W.; *See* INOUYE, W. and INABA, Y.

INOUYE, W. (6) Observations of Near Earthquakes on Mt. Tukuba with an Ishimoto Acceleration Seismograph. (in English) 69

INOUYE, W. (34) Earth-tilts observed at Mt. Tukuba, Japan. (in English) 693

INOUYE, W. and INABA, Y. (35) On Barometric Gradients at Times of Earthqua'-es, in Japan (2nd paper). (in English) 704

ISHIMOTO, M. (14) La déformation de la croûte terrestre et la production des ondes sismique au foyer. (en français) 254

ISHIMOTO, M. (37) Construction d'un sismographe accélérométrique pour la composante verticale. (en français) 717

ISHIMOTO, M. et OOTUKA, M. (8) Determination de la limite perceptible des secousses. (en français) 113

KANAI, K. and NISHIMURA, G.; *See* NISHIMURA, G. and KANAI, K.

KANAI, K., NISHIMURA, G. and TAKAYAMA, T.; *See* NISHIMURA, G., TAKAYAMA, T. and KANAI. K.

KAWABATA, Y. and MUTO, K.; *See* MUTO, K. and KAWABATA, Y.

KAWASUMI, H. (24) Study of Propagation of Seismic Waves. (The second paper). (in English) 403

KISHINOUYE, F. (4) Measurement of a Land-creep in Wakayama Prefecture. (in English) 38

KODAIRA, T. (20) Earthquakes of the Kwantô District. (in English) 350

KUNO, H. (22) On Silica Minerals occurring in the Groundmass of Common Japanese Volcanic Rocks. (in English) 382

KUNO, H. (23) Preliminary Note on Basalt from Aziro, Idu. (in English) 391

MATUZAWA, T. (18) Fluggeschwindigkeit einiger vulkanischen Bomben. (in deutsch) 329
MATUZAWA, T. (19) Gasdruck bei einigen vulkanischen Ausbrüchen in Japan. (in deutsch) 347
MATUZAWA, T. (39) Berichtigung zu meiner Arbeit „Fluggeschwindigkeit einiger vulkanischen Bomben". (in deutsch) 732
MIYABE, N. (16) The Crust Deformations in the District between Okitu and Kusimoto, along the Pacific Coast of the Main Island of Japan. (in English) 278
MIYABE, N. (33) Block Movements of the Earth's Crust in the Kwantô District. (The Crustal-Blocks and Their Movements. Part III.) (in English) 639
MUTO, K. and KAWABATA, Y. (17) Vertical Displacements of Bench Marks in the Nôbi and other Districts. (in Japanese) 315
NISHIMURA, G. and KANAI, K. (10) On the Effects of Discontinuity Surfaces upon the Propagation of Elastic Wave. (I). (in English) 123
NISHIMURA, G. and KANAI, K (31) On the Effects of Discontinuity Surfaces upon the Propagation of Elastic Waves. (II). (in English) 595
NISHIMURA, G. and TAKAYAMA, T. (12) On Stresses in the Interior and in the Vicinity of a Spherical Inclusion in a Gravitating Semi-infinite Elastic Solid. (I). (in English) 196
NISHIMURA, G. and TAKAYAMA, T. (13) On Stresses in the Interior and in the Vicinity of a Horizontal Cylindrical Inclusion in a Gravitating Semi-infinite Elastic Solid. (I). (in English) 229
NISHIMURA, G., TAKAYAMA, T. and KANAI, K. (25) On Stresses in the Interior and in the Vicinity of a Horizontal Cylindrical Inclusion of Circular Section in a Gravitating Semi-infinite Elastic Solid. (II). (in English) 454
OOTUKA, M. and ISHIMOTO, M.; *See* ISHIMOTO, M. and OOTUKA, M.
ÔTUKA, Y. (29) The Geomorphology and Geology of Northern Idu Peninsula, the Earthquake Fissures of Nov. 26, 1930, and the Pre- and Post-Seismic Crust Deformations. (in English) 530
ÔTUKA, Y. (38) Contraction of the Japanese Islands since the Middle

Neogene (advanced paper). (in English) 724
Suzuki, T. (11) Amplitude of Rayleigh Waves on the Surface of a Stratified Medium. (in English) 187
Takahasi, R. (3) Tilt of the Earth's Crust observed at the Asama Volcano. (in English)..... ... 25
Takayama, T. and Nishimura, G.; *See* Nishimura, G. and Takayama, T.
Takayama, T., Kanai, K. and Nishimura, G.; *See* Nishimura, G., Takayama, T. and Kanai, K.
Tamaru, T. (21) The Construction and Study of an Acceleration Seismograph. (in Japanese) 362
Terada, T. (36) Earthquake and Fisheries. II. (in English) 714
Tsuboi, C. (15) Notes on the Mechanical Strength of the Earth's Crust. (in English) 275
Tsuboi, C. (26) Vertical Crustal Displacement in the Seismic Region of Itô, on the East Coast of the Idu Peninsula. (in English)..... 488
Tsuboi, C. (32) The Most Suitable Formula for the Japanese Gravity Values. (in English) 632
Tsuya, H. (7) Explosive Activity of Volcano Kusatu-Sirané in October, 1932. (in English) 82
Tsuya, H. (30) Petrology of Some Lavas of Volcano Asama, Sinano Province, Japan. (in English) 575
Yamaguti, S. (5) On Time and Space Distribution of Earthquakes. (in English) 46
Yamaguti, S. (27) Distribution of Earthquakes in Japan. (in English)..... 500
Yosiyama, R. (1) Elastic Waves from a Point in an Isotropic Heterogeneous Sphere. Part I. (in English) 1
Land Survey Department (9) Relative Vertical Displacements of Bench Marks along Routes in Tôkyô and the Environs and from Itabasi to Huzimi. (in Japanese) 122